NASA Conference Publication 2171

The Universe at Ultraviolet Wavelengths

The First Two Years of International Ultraviolet Explorer

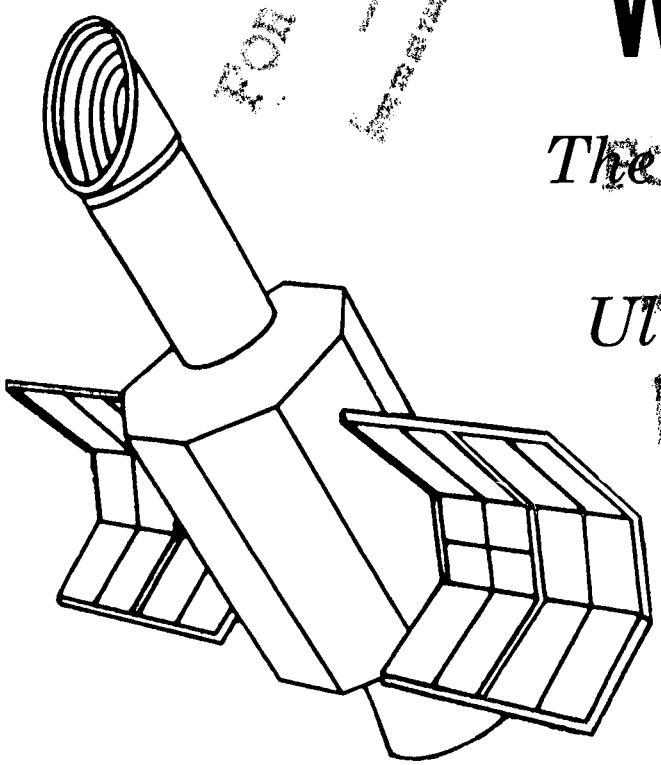

Proceedings of a symposium held at NASA Goddard Space Flight Center Greenbelt, Maryland May 7-9, 1980

NASA

NASA Conference Publication 2171

The Universe at Ultraviolet Wavelengths

The First Two Years of International Ultraviolet Explorer

Robert D. Chapman, *Editor*
Goddard Space Flight Center
Greenbelt, Maryland

Proceedings of a symposium held at
NASA Goddard Space Flight Center
Greenbelt, Maryland
May 7-9, 1980

NASA
National Aeronautics
and Space Administration

Scientific and Technical
Information Branch

1981

PREFACE

On May 7-9, 1980 a symposium was held at the Goddard Space Flight Center to celebrate the first two years of operation of the International Ultraviolet Explorer. This volume contains the papers presented at that meeting. The broad range of topics represented by the subdivisions within the volume attests to the versatility of the highly successful IUE mission.

The overall Symposium Chairperson was Albert Boggess, III; the Scientific Program Chairperson was Anne B. Underhill; and, the Local Arrangements Chairperson was Jaylee Mead. The Organizing Committee consisted of Albert Boggess, Anne Underhill, Jaylee Mead, David S. Leckrone, Stephen P. Maran and Robert D. Chapman.

We wish to express our thanks to the individuals who chaired the sessions, and to the invited speakers who ably reviewed the contributions of IUE to the many sub-disciplines of astronomy.

The papers are presented here as submitted by each speaker with a minimum of editing.

Robert D. Chapman
Editor

CONTENTS

PART IV
BINARY STARS AND HIGHLY-EVOLVED OBJECTS

PART VII
DATA REDUCTION

INTRODUCTION

OUTLOOK FOR ULTRAVIOLET ASTRONOMY

Erika Böhm-Vitense
University of Washington

INTRODUCTION

When Anne asked me whether I would be willing to give this summary and outlook, I was somewhat reluctant because I do not know much about galactic and extragalactic astronomy. Anne replied "Erika, it's all the same physics." This is of course the assumption on which we all base our studies, so I could not object.

When I met Bob Wilson here in March and I mentioned this talk, he said "Oh, that is always nice, because you can put in all your research that you did not have a chance to talk about before."

So I will emphasize the common physics in all or at least most of the IUE studies, and try to give an outlook based on what we have learned so far. I will concentrate on those topics for which I feel I can contribute something to the discussion rather than speculate freely on topics about which I do not know much or to repeat what has been said already in the review talks.

I am sure my forecasts will be generally wrong because the most fascinating research is always stimulated by discoveries that were not predicted.

COMMON PHYSICS OF IUE STUDIES

In our IUE observations we are dealing with wavelengths longward of 1100Å, which means we are using photons corresponding to transitions with energy differences up to 11eV.

Energy differences ΔE enter into astrophysical problems generally by means of a factor $e^{-\Delta E/kT}$ which is most sensitive to changes in ΔE and ΔT for $\Delta E/kT>>1$. This, however, usually leads to small intensities. In most cases the best choice is to observe effects for which $\Delta E/kT$ lies between 1 and 10 which gives good temperature discrimination and still measurable intensities. For $\Delta E \approx 10$eV this leads to temperatures between 10^4 and 10^5K, which is the temperature range with which most of us are dealing.

The solar system observers do not have to worry about intensities and therefore can deal with lower temperatures. Also investigations of interstellar matter may deal with lower T since absorption of hot background radiation is studied.

Most IUE studies deal with gases that are optically thin in the continuum. Since we are dealing with $\Delta E \sim 10kT$ the energy loss of optically thick

gases would be too large for the gas to stay hot except if the energy source is directly attached to the gas and increases with increasing temperature as is the case for the stars. For most other objects the available energy is fixed by external sources like stellar radiation, gravitational energies, shockwaves, magnetohydrodynamic effects or possibly cosmic rays. Therefore, generally only optically thin objects can stay hot.

This means nearly all our observations are dealing with non-thermodynamic equilibrium conditions. For the interpretation of the observations we all have to solve statistical equilibrium equations. We should all struggle with the radiative transfer equations. So far mainly stellar astronomers have been brave enough to tackle the full problem. People studying gaseous nebulae in the visual where most lines are optically thin have tried to circumvent the radiative transfer problem by introducing Menzel's cases ABC, thus eliminating the optically thick lines. IUE now leads to the observation of those optically thick lines in the ultraviolet for instance in planetary nebulae or in the bulges of Seyfert galaxies. So now astronomers working on these objects will have to struggle with the radiative transfer problem also.

Every one of us, of course, has a special topic and aim of his or her study, but it seems that the problem of temperature determination, chemical abundance determination, and, above all, the question about the energy sources for the high temperature regions are important in most of the studies. In the following discussion I will, therefore, concentrate on these questions.

After these general remarks let me go into the specific questions. I apologize that I have to be selective and scanty because of time limits.

STELLAR ASTRONOMY

Since I consider myself to be a stellar astronomer I hope you will forgive me if I emphasize this field even though it is by many colleagues considered to be old-fashioned. It is still the backbone of much galactic and extragalactic research.

O AND B STARS

T_{eff} Determinations

For O stars $\Delta E/kT$ reaches values of about 2 for $\lambda \sim 1100$Å as compared to ~ 0.5 in the visual region. The IUE spectral region therefore offers a much better opportunity to determine effective temperatures for O and B stars (Underhill[1] 1980) though there is still some discussion with respect to the calibration of the T_{eff} scale. With these UV studies we will now be able to distinguish much better between different T_{eff} and correspondingly between different stellar masses and evolutionary time scales than before. This is, of course, quite important for a better understanding of the early chemical evolution of our own and of other galaxies, which therefore in the future will become more transparent.

Stellar Winds

The discovery of strong, highly ionized, high velocity winds in O and BO stars (Morton[2] 1967, Morton et al.[3] 1969) was a big surprise. These winds are still a field of intensive study, especially their source of energy. If during its lifetime on the main sequence a massive star loses about 10% of its mass (Conti[4] 1978) with roughly 3 times the escape velocity (Abbott[5] 1978) we find that the kinetic energy of the lost mass is comparable to the total gravitational energy but to less than 1% of its total luminosity (see also McCray and Snow[6] 1979).

It seems that it is generally agreed upon that the winds are accelerated by radiation (Lucy and Solomon[7] 1970, Castor, Abbott and Klein[8] 1975). Once the high velocities are reached only about 1% of the kinetic energy has to go into turbulence (for a possible mechanism see for instance Nelson and Hearn[9] 1978) and then dissipated into heat to create temperatures around 3.10^5K, which are necessary to ionize OV (Lamers and Snow[10] 1978). Of course Anne Underhill suggested magnetic fields to do the heating and Sreenivasan discussed in London, Ontario, the possibility that differential rotation could cause turbulence and heating. Joe Cassinelli discussed the possibility that X-rays could cause the ionization and actual heating would not be necessary.

From the compilation of Lamers and Snow (1978) we see that at spectral type BO a steep decrease of wind velocity is observed. Joe Cassinelli pointed out that for temperatures less than 30,000K the scattering or absorbing ions may disappear. I would like to suggest that at these temperatures also the photons which can be absorbed or scattered disappear.

In Figure 1 the energy needed per cm^2 for the strong winds, namely 0.1% of the flux or $10^{-3} \cdot \sigma T_{eff}^4$ is plotted as a function of T_{eff}. In the same figure we have also plotted as a function of T_{eff} the flux F_λ per 50Å at different wavelengths according to Kurucz et al.[11] (1974).

Only for radiation shortward of the Lyman continuum edge at 912Å do we see a steep change in the flux for T_{eff} around 30,000K. It therefore appears that the driving force for the wind must be sought for $\lambda<912$Å, possibly the HeI lines. Unfortunately this wavelength region is almost impossible to observe, except perhaps with IUE if we think about wavelengths longward of 540Å.

Continuing observations of massive stars with different ages will probably tell us how the winds and mass loss change when the stars evolve off the main sequence, and what will be the final mass of evolved massive stars. This will determine the time scale for the final evolution and therefore the timescale for the expected enrichment of the interstellar medium by heavy elements which determines the chemical evolution of galaxies.

STUDIES OF A STARS

Normal A Stars

Some really old-fashioned astronomers like me still study continuous energy distributions in ordinary main sequence A stars. With $\Delta E/kT$ about 5 to 10 IUE observations offer an excellent opportunity to determine effective temperatures in A and F stars. The observed discontinuity at 1700Å enables us to determine metal abundances as well (Böhm-Vitense[13] 1980a, de Boer, this volume[12]) by comparison with available model energy distributions (Kurucz 1979).

Am and Ap Stars

As we saw earlier, some of the rapidly rotating stars show more energy for $\lambda<1530$Å than the slowly rotating stars. I consider this observation important since it may hold the key to understanding the difference between Am stars and normal A stars. It may also hold the key to the understanding of the heating of the outer layers of the O stars if it is due to effects of differential rotation. Future studies will hopefully help to understand the influence of rotation on convection, turbulence, and energy distributions of late A and early F stars.

Monitoring the T_{eff} of the Ap stars during their rotational cycle may tell us about the influence of magnetic forces on the stratification of the outer layers of these stars where magnetic forces could be important.

STARS OF SPECTRAL TYPE F AND LATER

Chromospheric and Transition Layer Emission

The study of classical stellar chromospheres, transition layers and coronae in F,G,K and M stars and the relation to mass loss in late type stars has been an exciting field in the last years. We have confirmed that the boundary line for classical chromospheres follows the Cepheid instability strip, and marks the line where efficient hydrogen convection stops (Böhm-Vitense and Dettman[14] 1980). The exact position within the instability strip is still being studied (Parsons[15] 1980). We expect to learn a lot about the interaction of pulsation and convection from these studies.

We have also learned where on the cool end of the HR diagram the hot transition layer emission terminates (Linsky and Haisch[16] 1979) presumably due to deep reaching stellar winds (Mullan[17] 1978), though we are still looking for an energetic driving mechanism. The influence of Lyα has been discussed by Haisch et al.[18] (1980). X-ray studies of the cool giants and supergiants will show whether these stars actually do not have a transition layer and corona or whether the temperature gradient in the transition layer is too steep to give measurable emission. Vaiana[19] (1980) reports strong X-ray emission of M stars, which may however only refer to very young M stars. The X-ray observations will give us the coronal temperatures and thereby the boundary

condition with which we can determine the stratification of the transition layer uniquely. Without it we do not know whether a low-emission line flux of high-excitation lines is due to the absence of high temperature regions, to a steep temperature gradient or to a low electron density.

In any case the complicated structures of the Mg II k_2 emission cores with several shortward shifted absorption components indicate outstreaming material in low temperature high luminosity stars (Stencel et al.[20] 1980). Future studies of late type stars of all luminosity classes will clarify the relation between the termination of the transition layer emission, the presence of the X-rays and the mass outflow visible in the Mg II lines.

The Energy Source for Heating the Transition Layer and Corona

The energy source for the heating of the transition layers and coronae and the energy balance is still a topic of very active research. As pointed out earlier, we feel that the weak or absent transition layer emission of old stars tells us that other than acoustic wave heating must be important for the high layers. Magnetic and magnetohydrodynamic effects will have to be considered. We shall then expect a correlation between rotation and transition layer emission, since magnetic field strengths, due to dynamo generation, are expected to decrease with decreasing rotation. Ayres and Linsky[21] (1980) find a positive correlation between X-ray emission and rotation for G and K stars in binaries. Our studies of the correlation between transition layer emission and rotation shows different results for different spectral types. In Figure 2 we see that the F0 stars η Lep (v_r sin i = 0 km/sec), γ Dor v_r sin i = 106 km/sec) and δ Hor (v_r sin i = 190 km/sec) all show the same weak emission. In order to understand this we must ask why do single stars rotate rapidly? Either they are young and have not had time to slow down in spite of corona and stellar wind, or they have evolved into a region with convection and corona only recently, as seems to be the case for α Tri and 31 Com. In these cases they will have strong transition layer emission. On the other hand, they may also be rapid rotators because they do not have strong convection and therefore do not have a hot corona and stellar wind and therefore have not slowed down as may be the case for F0 stars right at the boundary for the onset of convection like γ Dor, δ Hor and β Cae. With this in mind our Figure 2 does perhaps not contradict a positive correlation between rotation and transition layer emission. Further studies are needed to improve the statistics and decide whether we have a positive correlation or not.

The study of stars with known ages will be very helpful to follow the evolution of chromospheric and transition layer emission with increasing age of the stars. Unfortunately even main sequence F and G stars in clusters are rather faint, except in the Hyades. Perhaps IUE II will help.

Energy Balance and Coronal Temperatures

There has been an extensive discussion in the literature whether the minimum flux corona is indeed the stable form of spherically symmetric coronae as proposed by Hearn[22] 1975.

For any equilibrium stratification we must require that

$$\text{div } F = \text{div } F_{rad} + \text{div } F_{mech} + \text{div } F_{cond} + \text{div } F_{wind} = -\frac{dQ}{dt} = 0 \quad (1)$$

where Q is the enthalpy, F_{rad} = radiative flux, F_{cond} = conductive flux, F_{wind} = energy flux of stellar wind, F_{mech} = sum of energy fluxes which heat the transition layer and corona.

Hearn only considers the $\int \text{div } F\ r^2\ dr$ over the corona.

Let us use the following abbreviations:

$$F_t = \int_{\text{corona}} \text{div } F\ r^2\ dr = F_1 + F_m \text{ with} \quad (2)$$

$$F_1 = \int_{\text{corona}} (\text{div } F_{rad} + \text{div } F_{cond} + \text{div } F_{wind})\ r^2\ dr \quad (3)$$

$$F_m = \int_{\text{corona}} (\text{div } F_{mech})\ r^2\ dr, \quad F_m < 0 \text{ means heat input} \quad (4)$$

$F_m > 0$ means heat loss

For equilibrium $F_1 = -F_m$.

Hearn showed that for a given n_e the F_1 has a minimum for some $T=T_{min}$. He believes T_{min} to be the temperature of a stable corona.

For stability we must require $\frac{dF_t}{dT} > 0$, then a $\Delta T>0$ will lead to cooling and vice versa. Now $\frac{dF_1}{dT} < 0$ for $T < T_{min}$ as Antiochos and Underwood[23] emphasize. $\frac{dF_t}{dT} > 0$ can then only occur if $\frac{dF_m}{dT} > 0$ for $T<T_{min}$. This shows that the minimum flux corona can be stable only for a positive temperature dependence of the energy input for $T<T_{min}$: For $\Delta T<0$ we need to put in more energy in order to make up for the increased losses in order to achieve some heating. Figure 3 illustrates the situation.

Usually it is assumed that F_m is determined by the conditions in the deeper layers. We therefore expect F_m to be independent of the coronal temperature. In this case T_{min} is not the temperature of a stable corona but rather a lower limit for the coronal temperature.

If on the other hand the coronal heating is due to currents in the corona as suggested by Vaiana and Rossner[24] (1978) then the stability at $T = T_{min}$ will depend on the temperature dependence of such current heating.

In any case the actual temperature must be determined from $F_m = -F_1$. (See also Mangeney and Souffrin[25] 1977).

Following Unsöld's[26] (1955) arguments Hearn's conclusion that the pressure at the base of the corona is determined only by the amount of the mechanical energy input is confirmed in the sense that the energy input into the upper chromosphere determines the pressure at the base of the transition region.

Future detailed studies of chromospheric, transition layer and coronal X-ray emission will enable us to determine the stratification in these layers uniquely and thereby derive div F_{mech} = -div F_1 as a function of height. We will then better understand the details of the heating mechanisms. For a true description of the corona we will have to take into account, though, the none spherical geometry as was emphasized by Vaiana and Rossner[24] (1978).

THE WILSON BAPPU EFFECT

The discovery by Wilson and Bappu[27] (1957) of the increasing width of the Ca II K_2 emission with increasing luminosity has stimulated much research. A similar effect is observed for the Mg II h_2 and k_2 emissions. The surprising fact is that the widths of the lines appears to be independent of T_{eff} and Z. Figure 4 shows a compilation of the available data from Stencel et al.[20] 1980 and from our observations. A very slight decrease is found for lower metal abundances.

This effect has caused a long-lasting debate concerning its origin. Wilson[28] 1972 favored an explanation by an increasing Doppler width. Ayres[29] explains the increasing width by an increasing optical depth in the damping wings of the lines.

For the Mg II lines we can now observe both the h_2 and k_2 lines. For pure optically thin Doppler broadening the two lines should have the same width. For optically thick Doppler broadened lines the k_2 line should be wider by a minute fraction. If the widths are determined by the damping wings the ratio should be about 1.4. The total emission in the lines could also be used in a similar way. Unfortunately on the IUE spectra the measurement of the h_2 line is rather inaccurate since it appears at the ends of the echelle orders. There is a lot of scattering in the measurements but in the average the h_2 line is narrower by a factor 1.4±0.5. It is not quite clear whether the ratio is intensity dependent.

Perhaps it will be possible in the future to get a more reliable calibration even for the low counts at the ends of the echelle orders so that h_2 could be measured more accurately. Then this debate could be settled.

OLD STARS

Chemical Abundances

In our opinion the detection of the radial velocity variations for all Ba II stars (McClure[30] et al. 1980) and the actual observation of the white dwarf companion of ζ Cap (Böhm-Vitense[31] 1980b) is quite important since it

opens up the possibility that many abundance anomalies observed in old stars could be due to mass exchange in binaries. McClure et al. pointed out that in relatively open globular clusters like ω Cen might perhaps have binaries. The strong emission lines in the ζ Cap system probably indicate excess hot gas in the system and the strong h_3 and k_3 Mg II absorption lines seem to show excess circumstellar, cool, low-density gas. Future observations of stars with peculiar abundances will help to clarify how many of these peculiarities can be related to white dwarf companions. X-ray observations may decide whether mass exchange is taking place now and in which direction it is going.

X-ray Source in Sirius B

The UV studies of the Sirius system so far have not been able to solve the problem of the X-ray source for Sirius B. Perhaps mass exchange could be an explanation. The question remains, is there gas in the system that could be accreted by the white dwarf? We have looked for signs of it. After the correction of the Sirius B spectrum for the IUE calibration error explained by A. Holm[32] (1979), we still find some humps in the light tail seen perpendicular to the direction of dispersion, which we believe is mainly due to scattered light of Sirius A. Figure 5 shows some of the cross sections through the spectrum at different wavelengths. The points shown are averages over 5 wavelengths. While for the long wavelengths the tail looks smooth with little scatter, we see humps for pixels, 11 or 12 at other wavelengths, some of which are close to carbon lines. The profiles shown were all normalized to FN = 2000 at pixel No. 8 where the Sirius A tail starts. The actual counts in Figures 5b-d are lower by about a factor 2 as compared to Figure 5a. Can we believe the hump at pixels No. 9 and 12 for these wavelengths? Is there emission in the carbon lines around Sirius B? Additional spectra can perhaps answer this question.

Generally the study of mass exchange in close binaries especially in connection with nova or nova-like outbursts have been and probably will continue to be an active field of research. The flux in the ultraviolet emission lines will tell us how much energy is liberated in the exchange process which gives us a handle on the amount of mass transfer.

YOUNG STARS

With the detection of the bright ultraviolet continua in T Tauri stars (Imhoff[33] 1980) we have at least learned that we do not yet understand what is happening during the birth of a star. The bright ultraviolet continuum of Herbig Haro object No. 1 is, however an even more extreme case (Ortolani and D'Odorico[34]). Figure 6 shows a short wavelength region $4^h.5$ exposure of Herbig Haro object No. 1 which was taken by Karl-Heinz Böhm and myself with the help of Fred Bruhweiler. This object has a visual magnitude of about 16, with most of the light coming from emission lines. There is also an estimated 2^m extinction around 1500Å.

Ortolani and D'Odorico find that the relative energy distribution corresponds to a blackbody with $T \gtrsim 40{,}000K$.

We suspect that all Herbig Haro objects have strong ultraviolet continua. This is not predicted by the currently favored hypothesis that the emission is due to shock wave excitation.

In HH 24A the visual continuum was found to be strongly polarized (Schmidt and Miller[35] (1979), Strom et al.[36] (1974)). Is the UV continuum of HH objects also strongly polarized? IUE will not be able to tell us. Could the UV continuum be due to Rayleight scattering? If so, why do we never see the original lightsource? The main problem is, however, to get enough intensity unless the light source is imbedded in the Herbig Haro object. In that case the Herbig Haro object would be expected to be a strong infrared source, which it is not.

Further studies will clarify whether all HH objects have strong UV continua, and how the energy distributions differ for different objects. The relation between the UV energy distributions and the emission line intensities may help to clarify the energy sources for these objects and their relation to star births.

THE INTERSTELLAR MEDIUM

THE GALACTIC HALO

While the Copernicus satellite permitted to observe interstellar lines in the IUE wavelength region even at higher resolution than IUE, IUE has increased the distance range of observations considerably. The most exciting observation in this field is in my mind the confirmation of the existence of high-temperature gas in the galactic halo (Savage[37] 1979) which had been suspected a long time ago (Spitzer[38] 1956). Possibly hot halo gas was also seen in the Magellanic Clouds, Savage[37]. Future observations of extragalactic objects in the local group may show whether hot halos are present in all of the systems or how the presence-or absence-is related to other properties of the galaxies.

The most interesting problem is again the energy source for the heating. Is the galactic halo being heated randomly by supernova explosions as already discussed by Spitzer? This could explain the inhomogeneities of the halo gas. Could the high temperature have survived from the collapse of the galaxy? Spitzer estimated that for $T \gtrsim 10^6$ K the cooling times would be long enough. The inhomogeneities would then be explained by the cooling instability of the hot gas.

If current galactic models are correct (Tinsley and Larson[39] (1978)) which require continuous instreaming of material in order to keep the metal abundance Z of the galaxy from increasing, then it seems the inflowing halo gas will have to be heated more or less continuously unless the intergalactic gas is already hot. If so then due to the cooling instability clouds could condense from the hot gas while cooling and could fall into the plane.

If appropriate background objects can be found, the investigation of the distribution of the hot gas within the halo, especially as a function of galactic latitude and distance, will help us to identify the energy source.

SUPERNOVA REMNANTS

The possibility to study distant hot stars has permitted us to observe galactic supernova remnants, thus giving us a chance to actually study their chemical abundances and test directly our hypothesis of heavy element enrichment of the interstellar gas by supernova explosions, which up to now was difficult to observe.

EXTRAGALACTIC RESEARCH

GALAXIES IN THE LOCAL GROUP

Since I am not an expert in extragalactic research I am not sure whether I should say anything about this field. I will be very brief. As Anne said, basically the same kind of studies discussed so far can be and are being done in extragalactic objects of our local group, except that we are limited to the study of the brightest objects. Since we can overlook the whole extragalactic systems, we are better off than for our own galaxy if we want to study, for instance, variations of chemical abundances as a function of position within the system. The distribution of stellar birthplaces and their properties can also be studied better in extragalactic systems since we are not bothered quite that much by interstellar dust. A simulation of the early stages of chemical evolution of our own galaxy may be witnessed now in the LMC. As stated above for the young massive objects UV observations permit much better temperature and thereby mass and age discrimination. The dependence of mass loss on Z can be studied by comparing the winds of the massive stars in the LMC and SMC with those of stars in our own galaxy. The changes in stellar evolution due to different degrees of mass loss can be observed directly.

Interstellar lines of hot, possibly halo gas have been detected in the LMC (Savage[37] 1980). The overall velocity field of this gas can be studied better in the LMC than in our galaxy and may give us information about the global infall or outstreaming of the hot gas.

ACTIVE GALAXIES

Theoretical studies of energetic shockwaves and the expected UV emission spectra as well as studies of the interaction of relativistic particles with interstellar gas and dust will probably bring us closer to the understanding of the phenomena observed in the nuclei of active galaxies like the Seyfert galaxies. This may ultimately lead to an understanding of quasars and their luminosity function and distances.

REFERENCES

1. Underhill, A. 1980, Monthly Notices R.A.S. 189, 601.

2. Morton, D. C. 1967, Ap. J., 203, 386.

3. Morton, D. C., Jenkins, E. B., Brooks, N. 1969, Ap. J., 155, 879.

4. Conti, P. 1978, Ann. Rev. of Astr. and Astrophys., 16, 371.

5. Abbott, D. 1978, Ap. J., 225, 893.

6. McCray, R. and Snow, T. P. 1979, Annual Rev. Astr. Astrophys., 17, 213.

7. Lucy, L. B., and Solomon, P. M. 1970, Ap. J., 159, 879.

8. Castor, J. I., Abbott, D. C., and Klein, R. I. 1975, Ap. J., 195, 157.

9. Nelson, G. D. and Hearn, A. G. 1978, Astr. Astrophys., 65, 223.

10. Lamers, H. J., and Snow, T. P. 1978, Ap. J., 219, 504.

11. Kurucz, R. L., and Peytremann, E., and Avrett, E. H. 1974. Blanketed Model Atmospheres of Early Type Stars. Smithsonian Institution.

12. Kurucz, R. L. 1979, Ap. J. Suppl., 40, 1.

13. Böhm-Vitense, E. 1980a, Ap. J. submitted for publication.

14. Böhm-Vitense, E., and Dettmann, T. 1980, Ap. J.

15. Parsons, S. 1980, Ap. J., in press.

16. Linsky, J. L., and Haisch, B. M. 1979, Ap. J. Letters, 29, L27.

17. Mullan, D. J. 1978, Ap. J., 226, 151.

18. Haisch, B. M., Linsky, J. L. and Basri, G. S. 1980, Ap. J. 235, 519.

19. Vaiana, G. S. 1980, preprint.

20. Stencel, R. E., Mullan, D. J., Linsky, J. L., Basri, G. S., Worden, S. P. 1980, Ap. J. Suppl, in press.

21. Ayres, T. R., and Linsky, J. L. 1980, preprint.

22. Hearn, A. G. 1975, Astr. and Astrophys., 40, 277.

23. Antiochos, S. K., and Underwood, J. H. 1978, Astr. and Astrophys. 68, L19.

24. Vaiana, G. S., and Rossner, R. 1978, Annual Review of Inst. and Astrophys., 16, 393.

25. Mangeney, A. and Souffrin, P. 1979, Astr. & Astrophys. 78, 36.

26. Unsöld, A. 1955, In Physik d. Sternatmosphären. 1955, Springer Verlag. p. 671.

27. Wilson, O. C., and Bappu, M. K. V. 1957, Ap. J., 125, 661.

28. Wilson, O. C. 1972, in Stellar Chromospheres, National Aeronautics and Space Administration, NASA SP-317, p. 305.

29. Ayres, T. R. 1979, Ap. J., 228, 509.

30. McClure, R. D., Fletcher, J. M., Nemec, J. M. 1980, Ap. J. Letters, in press.

31. Böhm-Vitense, E. 1980b, Ap. J. Letters, in press.

32. Holm, A. 1979, IUE Newsletter No. 8.

33. Imhoff, C. 1980, preprint.

34. Ortolani, S., and D'Odorico. 1980, Astr. Astrophys., 83, L8.

35. Schmidt, G. D. and Miller, J. S. 1979, Ap. J. Letters, 234, L191.

36. Strom, K. M., Strom, S. E., and Kinman, T. D. 1974, Ap. J. Letters, 191, L93.

37. Savage, B. D., and de Boer, K. S. 1979, Ap. J. Letters, 230, L77.

38. Spitzer, L. 1956, Ap. J., 124, 20.

39. Tinsley, B. M., and Larson, R. B. 1978, Ap. J., 221, 554.

40. Boyarchuk, A. A. and Kopilov, I. M. 1964, A general catalogue of rotational velocities.

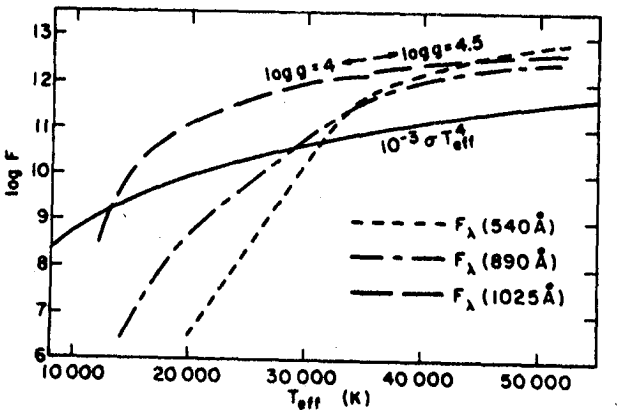

Figure 1: The kinetic energy fed per cm^2 and second into the high velocity wind of O stars, i.e. about $10^{-3}\ \sigma\ T_{eff}^4$, is shown as a function of T_{eff}. For comparison we have also plotted for main sequence stars the radiative energy contained in 50Å bands at different wavelengths (according to Kurucz and Peytremann[11] 1972). Only for λ <912Å does this radiative flux decrease rapidly for T_{eff} < 30,000 K. (For T_{eff} > 35,000 K no models with log g = 4. were available, so models with log g = 4.5 were used instead).

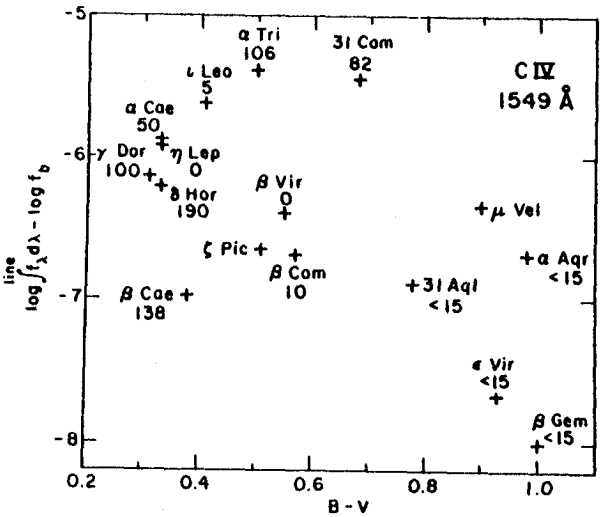

Figure 2: The ratios of the observed emission line flux in the C IV lines at 1549Å to the total flux f_b are plotted as a function of B-V for the stars observed by us. The numbers give the rotational velocities v_r sin i in Km/sec (Boyarchuck and Kopilov[40] 1964). The rather rapidly rotating stars α Tri and 31 Com show more emission than do the slowly rotating stars β Vir, β Com and 31 Aql. However, the rapidly rotating stars γ Dor, δ Hor and β Cae, show less emission than the slowly rotating stars α Cae and η Lep. The latter stars all have B-V<0.40 and are therefore rather close to the boundary line for the onset of convection and chromospheric emission.

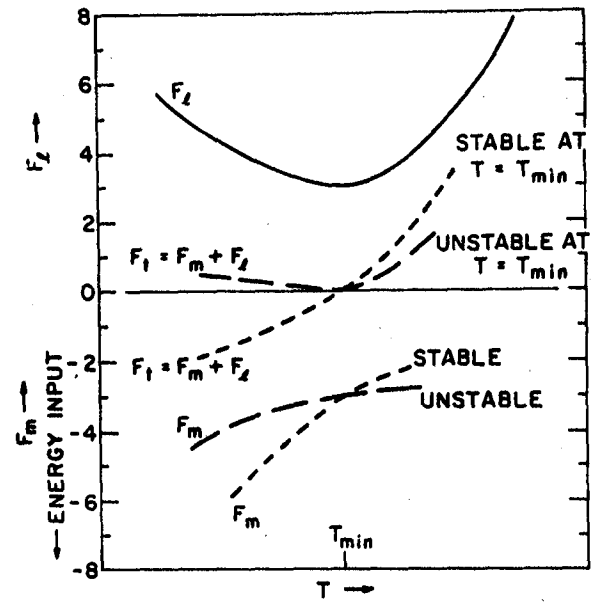

Figure 3: Illustrates the requirements for a stable corona. For a given temperature dependence of the coronal energy losses F_l with a minimum at $T = T_{min}$ the corona may be stable or unstable depending on the temperature-dependence of the energy input $F_l = -F_m$. For a steep increase of F_m with temperature the corona will be stable, possibly even for $T<T_{min}$. For F_m temperature independent or only slightly increasing with T the corona could be unstable even for $T>T$ min.

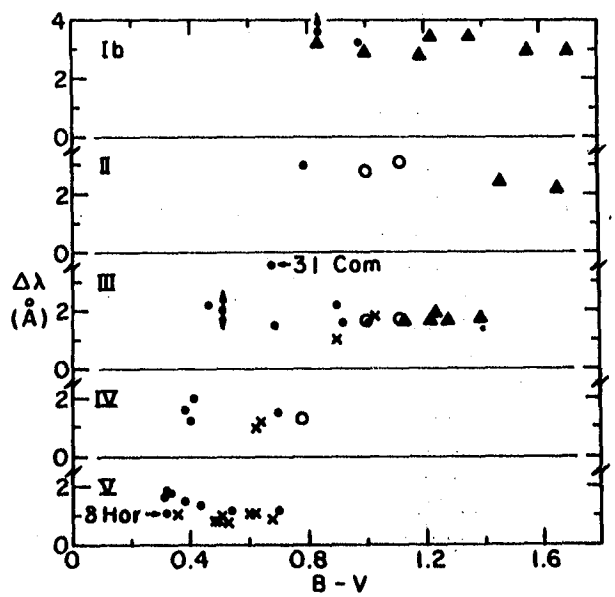

Figure 4: The width at the base of the Mg II k_2 emission lines is plotted as a function of B-V for stars of different luminosity classes. Triangles refer to data given by Stencel et al.[20] 1980. Dots refer to normal metal abundance stars observed by us, x refer to metal deficient stars and open circles to Ba stars or the super metal-rich star 31 Aql. It is obvious that the width is independent of B-V, it decreases slightly with decreasing metal abundance.

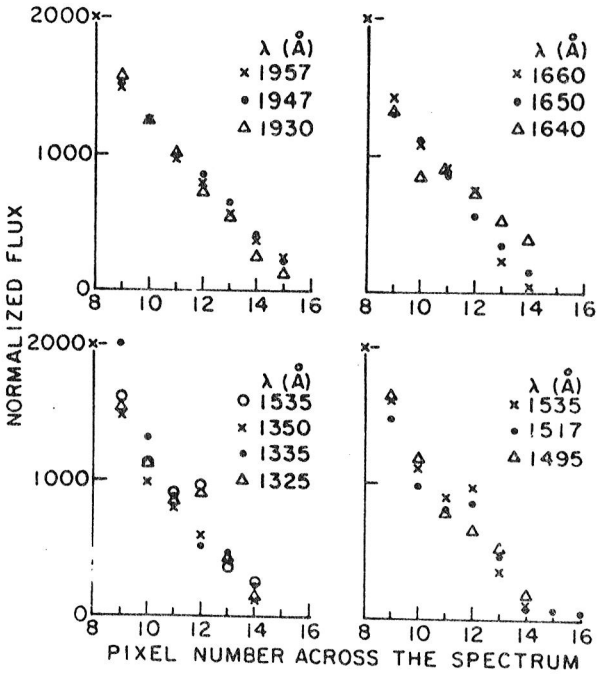

Figure 5: The intensity distribution in the spectrum of Sirius B perpendicular to the direction of dispersion is shown for different wavelengths λ. All cross sections were normalized to the same flux numbers at pixel No. 8. (The intensity maximum is always a pixel No. 6). For wavelengths around 1950Å a smooth distribution is seen attributed to scattered light from Sirius A. At shorter wavelengths humps may occur at pixels No. 9 and 12, shown here for the wavelengths near the CI, CII, and CIV lines. We do not know how to decide whether these humps are just accidental or whether there is a glow in these and other lines in the region around Sirius B.

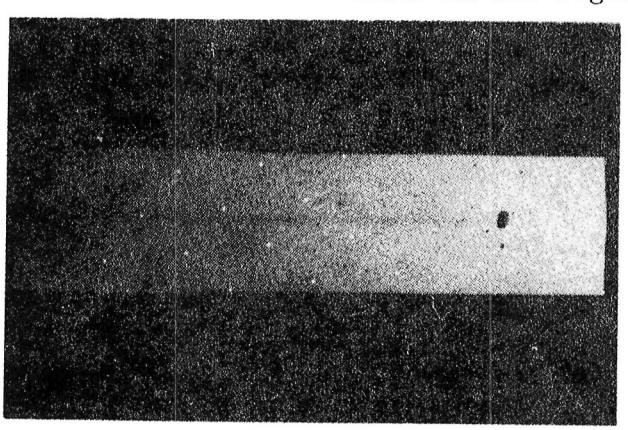

Figure 6: A $4^h.5$ exposure of the short wavelength spectrum of Herbig Haro No. 1 ($m_v = 16^m.0$). The geocoronal Lyα covers up Lyα of the object. A continuum is visible. In addition weak emission lines of CIII (1909Å), CIV (1549Å), CII (1335Å) and CI (1657Å) can be seen. Faint lines at 1945Å, at 1818Å (SiII), 1751Å (NIII), 1640Å (HeII), 1400Å (SiIV) and 1302Å (OI) may be present.

I. THE SOLAR SYSTEM

NEW INSIGHT INTO THE PHYSICAL STATE OF SOLAR SYSTEM OBJECTS*

P. D. Feldman
Physics Department
Johns Hopkins University
Baltimore, Md. 21218

ABSTRACT

The application of IUE to observations of solar system objects is summarized and a brief survey of new discoveries made during the first two years of IUE operation is given.

INTRODUCTION

The successful launch and operation of an earth-orbiting ultraviolet telescope facility such as IUE provides a new tool to the planetary astronomer with many features not available in earlier satellite observatories. The use of IUE for solar system observations in the first two years of operation has been directed at a wide variety of problems concerning planets, satellites, asteroids and comets. We present here a brief overview of some of the discoveries in this area made to date, with particular emphasis on the utilization of some of the unique capabilities of IUE. More detailed discussion of some recent results can be found elsewhere in the symposium proceedings.

There are several advantages to using IUE for solar system observations. Perhaps the most important is the ability to make synoptic observations over a rather long baseline in time in order to determine the response of a planetary atmosphere to the variability in the solar ultraviolet or particle output or to study the large-scale weather pattern in the lower atmosphere of a planet. This type of information is not obtained from the ultraviolet "snapshot" taken by rocket experiments or planetary flybys, and in the case of HI Lα observations of Jupiter, discrepant brightness values obtained by a variety of rocket and flyby experiments during a 10-year period were only recently recognized as being indicative of a true temporal variability (ref. 1). IUE also allows for spatial imaging in the ultraviolet with $\approx$5" resolution using the large spectrograph apertures, and larger scale spatial features can be mapped by offsets of the apertures. The wide spectral range of the IUE spectrographs and the dual dispersion capability allows for comprehensive, simultaneous observations of a large number of related species in a planetary atmosphere, and provide vital, correlative information to complement ultraviolet instruments on planetary flybys and probes such as Voyager or Pioneer Venus Orbiter. Finally, we note the opportunity to increase our knowledge of the ultraviolet spectra of comets many-fold and in a systematic manner to study their time evolution over a large range of

* Work supported by NASA grant NSG-5393.

heliocentric distance. Two moderately active comets have been observed to date (Seargent, 1978m and Bradfield, 1979ℓ) and it is to be hoped that a giant comet like Bennett (1970II) or West (1976VI) might make an apparition during the lifetime of IUE.

There are observing difficulties encountered when using IUE for solar system objects due to the original design of the satellite to allow for observations of the entire range of astronomical objects and these will be mentioned briefly to indicate the problems faced in observing these targets. These include saturation of the Fine Error Sensor (FES) on nearly all of the planets; the need for an accurate spacecraft-centered ephemeris for moving targets; long-wavelength scattered light in the short wavelength spectrograph camera due to the use of a non-solar blind photocathode; and the 45° solar avoidance cone which constrains observations of Venus and comets. Despite these difficulties, the first two years of IUE have witnessed many new discoveries that have made IUE a primary tool in solar system research.

BRIEF SURVEY OF RESULTS TO DATE

The results presented here are not meant to be a complete summary of all solar system observations but rather a sampling of highlights which illustrate the utility of IUE for these studies. Reference is made only to work that has been published or submitted for publication or is included in this symposium.

Saturn

The traditional method of determining the composition of a planetary atmosphere is illustrated by the detection of acetylene (C_2H_2) in absorption in the spectrum of reflected sunlight near 1750 Å from Saturn (ref. 2). Acetylene was previously identified in the far-infrared spectrum of Jupiter and also appears in IUE spectra of Jupiter (ref. 3). For both planets, the relative abundance of C_2H_2 is determined and found to be consistent with recent photochemical models. Saturn also has been found to exhibit an asymmetrical distribution of HI Lα emission similar to what is observed for Jupiter (ref. 4).

Jupiter

The spatial imaging capability of IUE is beautifully illustrated by the photowrite images of aurora in the north and south polar regions of Jupiter given by Clarke et al. in this volume (ref. 5). In this case three exposures were taken with the large aperture of the short-wavelength spectrograph on the center of the planet and offset by ~20" towards each of the poles. Enhanced emission of HI Lα and strong emission in the Lyman bands of H_2 near 1600 Å is seen in the polar regions but not near the equator or at mid-latitudes. The spectrum of the Jovian aurora is very similar to that observed by Voyager (ref. 6), and provides a means of remotely monitoring the magnetospheric activity of Jupiter with time. Jupiter also exhibits an asymmetry in HI Lα emission near the equator which has also been observed by Voyager and by a rocket experiment (ref. 1). The longitudinal variation and

temporal behavior of this bulge has been studied by IUE (ref. 4).

One of the most exciting discoveries of the Voyager flybys is the intense volcanic activity of the satellite Io. Ultraviolet observations of the plasma torus associated with Io (ref. 6) show it to be composed of ions of sulfur and oxygen and the ion temperature and density can be deduced from the relative intensities of lines of different stages of ionization, such as SII and SIII which are observable with the IUE short-wavelength spectrograph (ref. 7). The surface of Io shows marked variation in ultraviolet albedo with phase, presumably due to differences in SO_2 frost on the surface in areas of recent volcanic activity.

Mars

IUE observations of Mars have focussed on the seasonal variability of atmospheric ozone first detected by the Mariner 9 orbiter (ref. 8).

Venus

Due to the constraint of a 45° solar avoidance cone, Venus can be observed only during a short period around the time of greatest elongation at which time the disk is roughly half illuminated. Because of its proximity to earth, tracking of Venus by the satellite is extremely difficult and the FES is hopelessly saturated. Orientation of the spectrograph slits on the illuminated half of the disk is accomplished by minimizing the extent of spill-over in the FES camera. High dispersion observations of the bright side have been used to determine the abundance of SO_2 in the Cytheran atmosphere (ref. 9) and to help identify Lα induced fluorescence of CO fourth positive bands as an additional source of emission in low resolution spectra of the atomic oxygen multiplets at 1304 and 1356 Å (ref. 10).

By offsetting from the illuminated portion of the disk to the dark side, low dispersion spectra of the nightglow, first observed by photometers on Mariner 5 and more recently by the ultraviolet spectrometer on Pioneer Venus Orbiter, were obtained. Although severely contaminated by scattered light from the illuminated side of the disk, these spectra were used to identify the nightglow emissions as the δ-band system of nitric oxide produced by the radiative attachment of nitrogen and oxygen atoms (ref. 11). This identification was subsequently verified by the Pioneer Venus Orbiter UVS which was then able to use these emissions to study the transport of atomic nitrogen across the terminator to the night side (ref. 12).

Comets

Two moderately active comets, Seargent (1978m) (ref. 13) and Bradfield (1979ℓ) (ref. 14), have been observed by IUE, the latter over an extended 7 week period in January and February 1980 during which time the comet's heliocentric distance varied from 0.71 a.u. to 1.53 a.u. Spectra of Comet Bradfield taken over a period of several weeks are found to be very similar to the spectra of Comet Seargent (ref. 13) and earlier rocket spectra of Comet West (1976 VI) (ref. 15). This similarity suggests a common composition for these comets and although the sample of comets observed to date in the ultraviolet is quite small, future observations of comets by IUE and

other orbiting observatories should provide a suitable statistical basis for understanding the composition and origin of these objects.

Several new discoveries have emerged from preliminary analyses of the Comet Bradfield spectra. These include the identification of CS as either a parent molecule or as the daughter of an extremely short-lived parent based on the point-like spatial distribution of the CS emission at 2576 Å (obtained at a resolution of ~1000 km) (ref. 16); the identification of the [OI] ^1S-^3P transition at 2972 Å, probably produced by direct photodissociation of H_2O; a still unexplained anomalous distribution of band intensities in the CO^+ first negative system; and a determination of the water production rate with heliocentric distance that strongly disagrees with earlier such determinations (ref. 17). High dispersion observations have been used to study the fluorescent pumping of the very strong OH bands near 3090 Å (ref. 18) and the spatial variation of various species observed at low dispersion provides a comparison for photochemical models of the coma.

CONCLUSION

The success of IUE for solar system observations illustrates the benefits obtained by complementing the direct exploration of the planets with earth-orbit observations in the ultraviolet and points the way for strong consideration of planetary and cometary spectroscopy in the requirements for the next generation of orbiting observatories.

REFERENCES

1. Clarke, J. T.; Weaver, H. A.; Feldman, P. D.; Moos, H. W.; Fastie, W. G.; and Opal, C. B.: Spatial Imaging of Hydrogen Lyman-α Emission from Jupiter, Astrophys. J., 240, 1980 (in press).

2. Moos, H. W.; and Clarke, J. T.: Detection of Acetylene in the Saturnian Atmosphere using the IUE Satellite, Astrophys. J. (Letters), 229, L107-L108, 1979.

3. Owen, T.; et al.: Observations of the Spectrum of Jupiter from 1500 to 2000 Å with the IUE, Astrophys. J. (Letters), 236, L39-L42, 1980.

4. Clarke, J. T.; and Moos, H. W.: Spatial Imaging of UV Emission from Jupiter and Saturn, The Universe in Ultraviolet Wavelengths: The First Two Years of IUE, NASA CP-2171, 1980: this compilation.

5. Clarke, J. T.; Moos, H. W.; Atreya, S. K.; and Lane, A. L.: Observations of Polar Aurora on Jupiter, The Universe in Ultraviolet Wavelengths: The First Two Years of IUE, NASA CP-2171, 1980: this compilation.

6. Broadfoot, A. L.; et al.: Extreme Ultraviolet Observations from Voyager 1 Encounter with Jupiter, Science, 204, 979-982, 1979.

7. Moos, H. W.; Clarke, J. T.; Atreya, S. K.; and Lane, A. L.: Observations of the Io Plasma Torus, The Universe in Ultraviolet Wavelengths: The First Two Years of IUE, NASA CP-2171, 1980: this compilation.

8. Conway, R. R.; Durrance, S. T.; Barth, C. A.; and Lane, A. L.: Seasonal Observations of Mars, The Universe in Ultraviolet Wavelengths: The First Two Years of IUE, NASA CP-2171, 1980: this compilation.

9. Conway, R. R.; McCoy, R. P.; Barth, C. A.; and Lane, A. L.: IUE Detection of Sulfur Dioxide in the Atmosphere of Venus, Geophys. Res. Letters, 6, 629-631, 1979.

10. Durrance, S. T.; Conway, R. R.; Barth, C. A.; and Lane, A. L.: High Resolution Observation of the Venus Dayglow Spectrum 1250-1430 Å, The Universe in Ultraviolet Wavelengths: The First Two Years of IUE, NASA CP-2171, 1980: this compilation.

11. Feldman, P. D.; Moos, H. W.; Clarke, J. T.; and Lane, A. L.: Identification of the UV Nightglow from Venus, Nature, 279, 221-222, 1979.

12. Stewart, A. I.; and Barth, C. A.: Ultraviolet Night Airglow of Venus, Science, 205, 59-62, 1979.

13. Jackson, W. M.; et al.: The Ultraviolet Spectrum of Comet Seargent 1978m, Astron. Astrophys., 73, L7-L9, 1979.

14. Feldman, P. D.; et al.: IUE Observations of the Ultraviolet Spectrum of Comet Bradfield (1979ℓ), Nature, 1980 (in press).

15. Feldman, P. D.; and Brune, W. H.: Carbon Production in Comet West 1975n, Astrophys. J. (Letters), 209, L45-L48, 1976.

16. Jackson, W. M.; Halpern, J.; Feldman, P. D.; and Rahe, J.: The Analysis of IUE Observations of CS in Comet Bradfield (1979ℓ), The Universe in Ultraviolet Wavelengths: The First Two Years of IUE, NASA CP-2171, 1980: this compilation.

17. Weaver, H. A.; Feldman, P. D.; and Festou, M. C.: Water Production Models for Comet Bradfield (1979ℓ), The Universe in Ultraviolet Wavelengths: The First Two Years of IUE, NASA CP-2171, 1980: this compilation.

18. A'Hearn, M. F.; Schleicher, D. G.; Donn, B.; and Jackson, W.: Fluorescence Equilibrium in the Ultraviolet Spectra of Comets Seargent (1978m) and Bradfield (1979ℓ), The Universe in Ultraviolet Wavelengths; The First Two Years of IUE, NASA CP-2171, 1980: this compilation.

HIGH-RESOLUTION OBSERVATION OF THE VENUS DAYGLOW SPECTRUM 1250-1430 Å

Samuel T. Durrance, Robert R. Conway, Charles A. Barth

Department of Astro-Geophysics and
Laboratory for Atmospheric and Space Physics
University of Colorado, Boulder, Colorado 80309

and

A. L. Lane

Jet Propulsion Laboratory
California Institute of Technology
Pasadena, California 91103

ABSTRACT

The spectrum of the dayglow of Venus between 1250 and 1430 Å has been measured in high-resolution with the International Ultraviolet Explorer. Seven exposures which were made with the short wavelength camera in the high-dispersion mode using the large aperture were combined to give a total exposure time of 309 min. The atomic oxygen lines at 1302.2, 1304.9, 1306.0, and 1355.6 Å are present. In addition, the (14,3) and (14,4) bands of the carbon monoxide fourth positive system at 1317 and 1354 Å respectively are identified. These bands are compared with synthetic spectra, showing the excitation mechanism to be fluorescent scattering of solar Lyman alpha radiation.

INTRODUCTION

From April to August of 1979 the Pioneer Venus Orbiter Ultraviolet Spectrometer obtained spectra of the Venus dayglow at a resolution of 13 Å. Figure 1 shows a portion of a sum of 480 of these spectra which were obtained at illumination, emission, and phase angles less than 60°. The data are shown as the solid curve. The identification in these data of carbon monoxide fourth positive bands (CO4+) in the (14,v") progression resolved some long-standing uncertainties in the interpretation of the Venus dayglow (Durrance, et al., 1980). A synthetic spectrum of this progression is shown as the dotted curve. A prominent unblended feature in this spectrum was identified as the CO4+ (14,5) band at 1392 Å. The (14,3) and (14,4) bands at 1317 and 1354 Å are blended with atomic oxygen (OI) 1304 and 1356 Å lines, and were identified through inference.

We present here a high-resolution spectrum of the Venus dayglow in which the atomic oxygen and carbon monoxide features are resolved. The spectrum was obtained from observations made with the International Ultraviolet Explorer satellite (IUE) at a resolution of about 0.4 Å. It is also shown that the theory of the excitation mechanism as scattering of solar Lyman alpha is consistent with the shape of the observed CO4+ bands.

OBSERVATIONS

Venus is a particularly difficult object to observe with IUE. It is outside the restricted region around the sun only near its greatest elongation when its visual magnitude is about -4. This extreme brightness saturates the Fine Error Sensor (FES) tracking system so that it is not possible to automatically track during an observation or to point precisely at a location on the disk.

Tracking is accomplished by calculating the drift rate of the planet with respect to the stars in spacecraft-centered coordinates and converting these to spacecraft gyro rates. The precise location of the planet is then determined by minimizing the figure of scattered light in the FES image after the crescent of Venus is placed over the large entrance aperture of the spectrometer. The image of Venus is only slightly larger than the aperture so a substantial reduction in the reflected light for the FES camera is seen. It is estimated that the center-of-light can be found with this technique to an accuracy of about ± 2 arc sec.

On April 12, 1980, during the time of Eastern elongation, a series of 7 exposures were made with the short wavelength camera in the high-dispersion mode using the large aperture. Exposure times varied from 20 to 60 min. with a total exposure time of 309 min. To minimize the effects of drift during each observation, the exposure was stopped periodically while the scattered light figure in the FES image was recentered and then the exposure was continued. Also for some of these observations the large aperture was offset toward the bright limb in order to enhance the airglow intensity relative to that of the disk.

A large background is present in these spectra as can be seen in Figure 2 which shows a portion of the sum of the gross spectra for all 7 observations. Altogether 7 overlapping echelle orders are shown which cover the region from 1280 to 1380 Å. The data shown here have been smoothed with a 9-point running average and are overplotted with the estimated background which was determined as follows: Since the spectrum is expected to have no continuum, or at most a very weak one, the spectra are assumed to consist only of emission lines plus a large background. Order 107 was assumed to consist of background only which was determined as a 25-point smooth of the data, after the removal of any reseaux. This background was then used to mask out the emission lines in order 106; that is, the background for order 106 was then determined as a 25-point smooth of the data excluding any points which were higher than the background of order 107 by an amount that was determined visually. This process was then repeated for successive orders, each time using the background of the adjacent order to form a mask.

THEORY AND DISCUSSION

Since carbon monoxide is present in the Venus upper atmosphere (Niemann et al., 1979), fluorescent scattering of solar radiation is a plausible excitation mechanism to explain its airglow emissions (Barth, 1969). In particular Kassal (1976) has shown that the scattering of solar Lyman alpha by the CO4+ (14,0) band is comparable to or greater than the scattering by the rest of that system for CO column densities $\sim 10^{17} cm^{-2}$.

A high-resolution synthetic spectrum of the CO4+ (14,v") progression which assumes fluorescent scattering of solar Lyman alpha as the excitation mechanism has been produced. The details of this spectral synthesis are given in an earlier paper (Durrance et al., 1980) and will not be included here.

The data minus the fitted background are shown in Figure 3. The OI 1302.2, 1304.9, 1306.0, and 1355.6 lines are resolved and easily visible in this spectrum. A reseau at the position of the 1302.2 line has been removed so the relative intensity of this line is not accurately indicated here. A synthetic spectrum of the CO4+ (14,3) and (14,4) bands is shown plotted below the data and is offset for clarity. They are both resolved although the (14,4) band is not completely separated from the OI 1355.6 line. The agreement in position, shape, and relative intensity is quite good.

Agreement between theory and data is shown with more detail for the (14,4) band in Figure 4. The high-resolution synthetic spectrum has been degraded to 0.4 Å resolution using a rectangular slit function to agree with the data. The atomic line, using the same procedure for degrading the resolution, is also included for comparison. In this figure the data have been filtered with a low pass filter and the synthetic spectrum is normalized to the data. It can be seen here that the agreement between theory and data is quite good although there does appear to be a small discrepancy in the intensities of the satellite branches.

CONCLUSIONS

With IUE it has been possible to obtain high-resolution spectra of the Venus dayglow in the 1250-1430 Å range which resolve the CO4+ (14,3) and (14,4) bands from the OI 1304 and 1356 Å lines. Comparison of these CO bands with synthetic spectra confirms the conclusion that they arise as a result of the fluorescent scattering of solar Lyman alpha.

REFERENCES

Barth, C.A., "Planetary Ultraviolet Spectroscopy", Appl. Opt., 8, 1295-1304, 1969.

Durrance, S.T., C.A. Barth, and A.I.F. Stewart, "Pioneer Venus Observations of the Venus Dayglow Spectrum 1250-1430 Å", J. Geophys. Res., 7, 222-224, 1980.

Kassal, T.T., "Scattering of Solar Lyman-Alpha by the (14,0) Band of CO", J. Geophys. Res., 81, 1411-1412, 1976.

Neimann, H.B., R.E. Hartle, W.T. Kasprzuk, N.W. Spencer, D.M. Hunten and G.R. Carigan, "Venus Upper Atmosphere Neutral Composition: Preliminary Results from the Pioneer Venus Orbiter", Science, 203, 770-772, 1979.

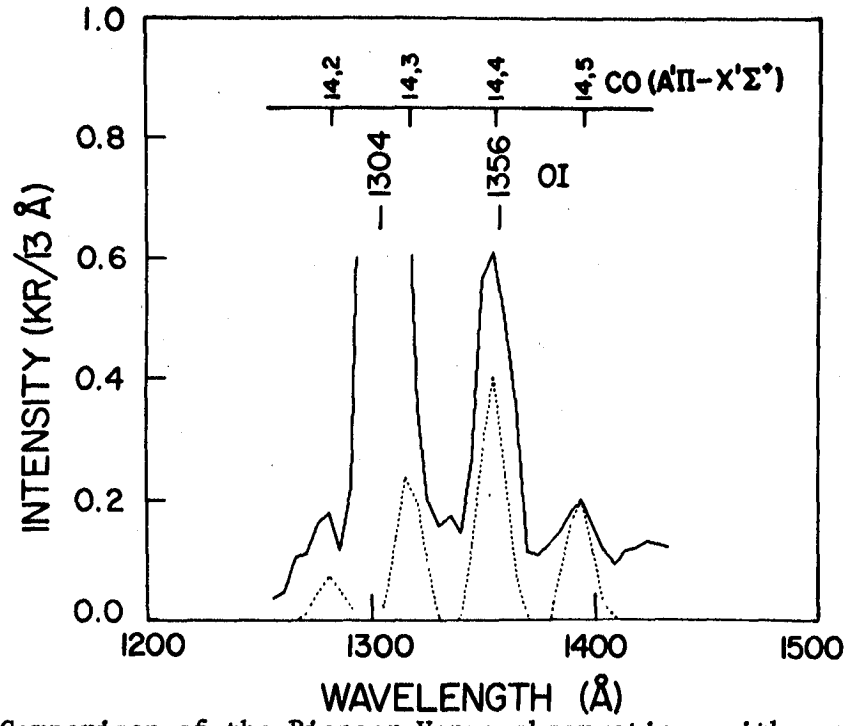

Figure 1. Comparison of the Pioneer Venus observations with a synthetic spectrum of the CO4+ (14,v") progression. The solid curve is the observations, which were obtained at illumination and emission angles less than 60°, and the dotted curve is the synthetic spectrum degraded to 13 Å resolution.

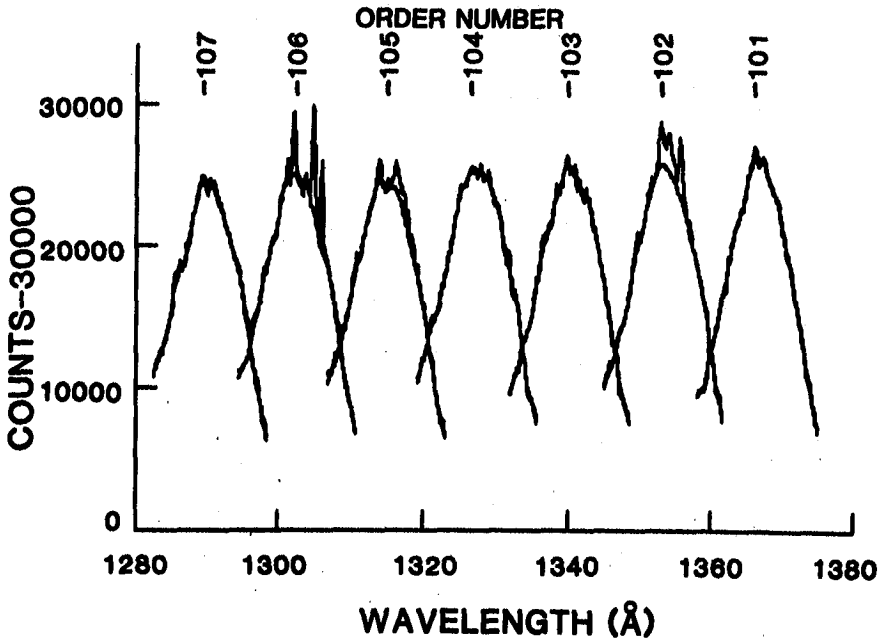

Figure 2. IUE spectrum of the Venus dayglow 1280-1380 Å. This is a sum of 7 different observations for a total exposure time of 309 min., using the short wavelength camera in the high-dispersion mode with the large aperture. The fitted background is shown as the smooth curve.

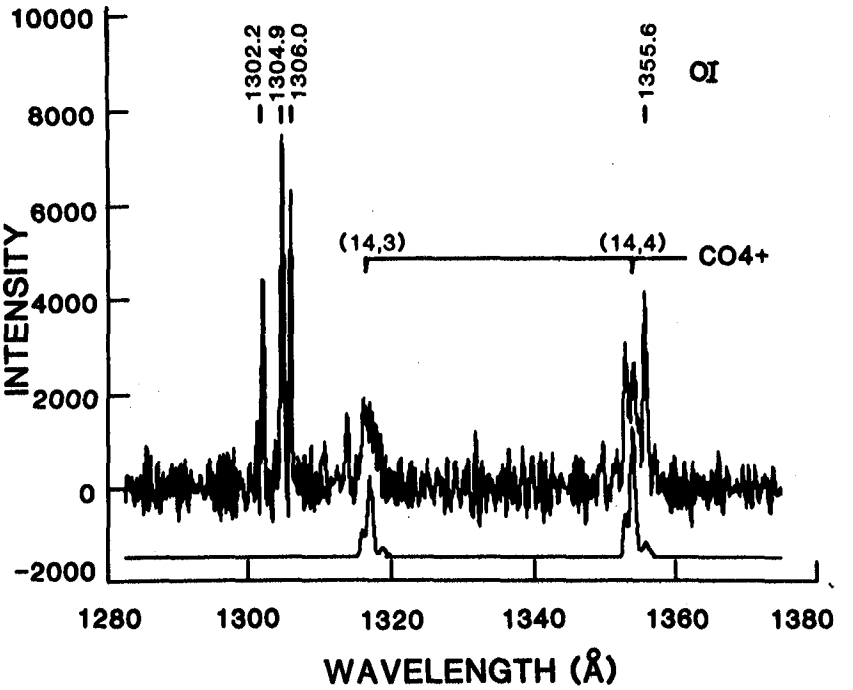

Figure 3. Comparison of the CO4+ (14,v") progression with the observations. The jagged curve is the data minus background. The solid curve is the synthetic spectrum degraded to 0.4 Å resolution and offset for clarity.

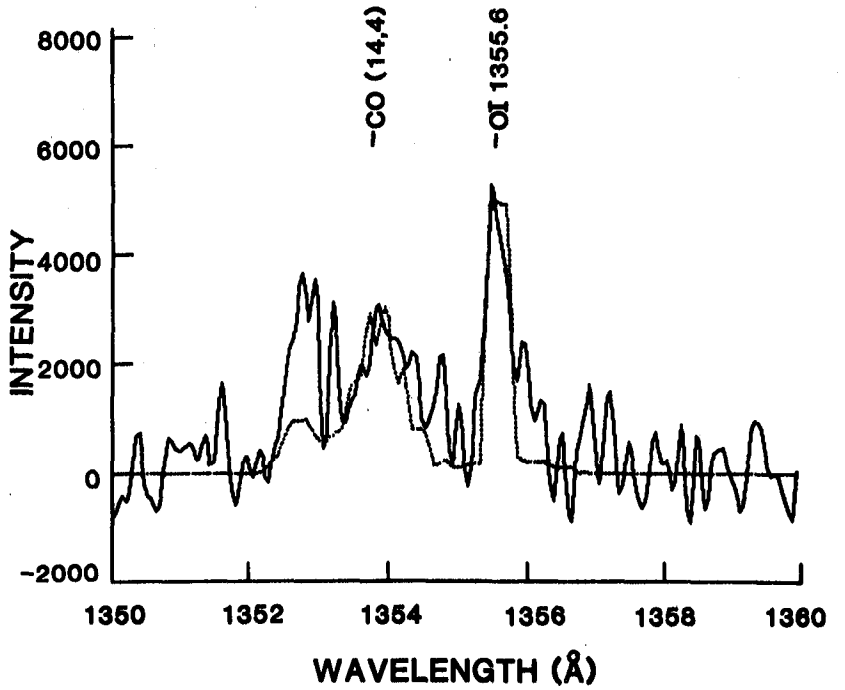

Figure 4. Comparison of the synthetic spectrum of the CO4+ (14,4) band and the OI 1355.6 line with the observations. The solid curve is the data and the dotted curve is the theory.

SEASONAL OBSERVATIONS OF MARS

Robert R. Conway, Samuel T. Durrance, and Charles A. Barth

Department of Astro-Geophysics and
Laboratory for Atmospheric and Space Physics,
University of Colorado, Boulder, CO 80309

A.L. Lane

Jet Propulsion Laboratory,
California Institute of Technology,
Pasadena, CA 91103

ABSTRACT

IUE has detected the Hartley bands of ozone in the spectrum of Mars. Seasonal observations show a variation in the north consistent with the measurements of Mariner 9. New observations during Martian late fall in the south were made.

INTRODUCTION

Ozone was discovered on Mars by the ultraviolet spectrometer on board the Mariner 7 spacecraft (Barth and Hord, 1971), and was subsequently measured extensively from the Mariner 9 orbiter (Barth et al., 1973; Lane et al., 1973; Barth and Dick, 1974; Wehrbein, 1979). Those measurements demonstrated variations in both its vertical and global distribution. The total ozone amount was found to be a maximum during winter over the north pole but slowly decreased throughout the spring. In the south it was absent during the Martian midsummer season but appeared again in late summer. Daily variations were also observed and were occasionally associated with the presence of clouds. The general conclusion of these observations was that ozone is present when the Mars atmosphere is cold and dry. The photochemical theory of ozone, which considers the role of water vapor, supports this conclusion.

The Mariner measurements were restricted to northern winter-spring, and southern summer. In this report we describe a technique of using the IUE satellite to observe ozone on Mars, and present the results of a preliminary analysis on some of the data acquired.

TECHNIQUE

Ozone is detected by observing its absorption of sunlight in the wavelength region from 2100 to 2800 Å where the Hartley bands have a peak cross section of $1 \times 10^{-17} cm^2$. Because of its restricted global distribution on Mars, a successful detection with IUE depends on the ability to restrict the instrument's field of view to that region of the planet where ozone is present. As shown in Figure 1, the angular diameter of the planet as seen from earth has varied between 5 and 13.8 arc sec since April of 1979. The optimum observing time is at opposition when the 3 arc sec small aperture includes only about 5% of the bright disk. Ideally the small aperture would be

placed over the winter pole where Mariner found ozone to be most abundant. However Figure 1 shows that the aspect of Mars also varies considerably, with the sub-Earth point moving between $\pm 25^{\circ}$ latitude. During the February opposition the northern hemisphere faced the Earth and provided the opportunity to observe the northern mid to late spring. Under these same conditions Mariner observed between 5 and 10 μ-atm. of ozone (1μ-atm. = 2.68×10^{-15} molecules cm^{-3}).

The drift rate of Mars with respect to the stars and its position were calculated in spacecraft-centered coordinates. Even though Mars had a maximum magnitude of -0.3 it was possible to track using the center-of-light lock after placing the planet in the large aperture. The pattern of scattered light in the Fine-Error-Sensor (FES) image was monitored to verify the tracking. During an observing session a pattern of five exposures were made as shown in Figure 2. Displacements were made in ecliptic coordinates by first slewing the spacecraft 4.5 arc sec in the desired direction from the center-of-light point and then moving directly to the small aperture. The orientation of Mars shown in Figure 2 is for March 15, 1980. In January, before the opposition, the terminator was to the west of the planet and its north pole was 10 deg closer to ecliptic north. Between January and April the phase angle varied between -30 and +30 deg.

Observations were made on September 25, 1979 and on January 23, March 15, and April 8, 1980 with exposure times varying from 9 to 75 sec. These exposures were made with the long wavelength camera in low resolution using both the large and small apertures. For the observations with the small aperture a 10 sec exposure gave good signal without saturation.

OBSERVATIONS

From the set of observations made in the pattern shown in Figure 2, the relative reflectance of the various regions of Mars was calculated as follows. The center-of-light observation from each session was taken to represent the equatorial region and was used as the standard spectrum. Each of the other four observations were divided by this spectrum and the ratio was normalized to unity in the 3000 Å region. The extracted net spectra computed by the IUE data processing operation were used.

Figures 3 and 4 show the relative reflectance spectra for the wavelength region from 2400 to 3000 Å. In each figure the ratio for the northern region is on the right and that for the southern region is on the left. The data were smoothed by an 11-point running average before the ratio was calculated. In all of the southern ratios and in the northern ratio for January, the smooth curve plotted over the data is the absorption spectrum of ozone normalized to the data.

On the basis of this analysis, we conclude that these observations have detected ozone in the Mars atmosphere. The observations of the northern region in January and March occurred when the Martian seasons were mid and late spring respectively. They show a positive detection in midspring and

the absence of ozone in late spring. This is the same behavior observed by Mariner 9 over the north pole. The observations of the southern region are for Martian mid to late fall. These IUE observations contain new information since Mariner 9 did not observe the south during those seasons.

REFERENCES

1. Barth, C.A. and C.W. Hord (1971). Science, 173, 197.
2. Barth, C.A., et al. (1973). Science, 179, 795.
3. Lane, A.L., et al. (1973). Icarus, 18, 102.
4. Barth, C.A. and M.L. Dick (1974). Icarus, 22, 205.
5. Wehrbein, W.M. et al. (1979). Icarus, 38, 288.

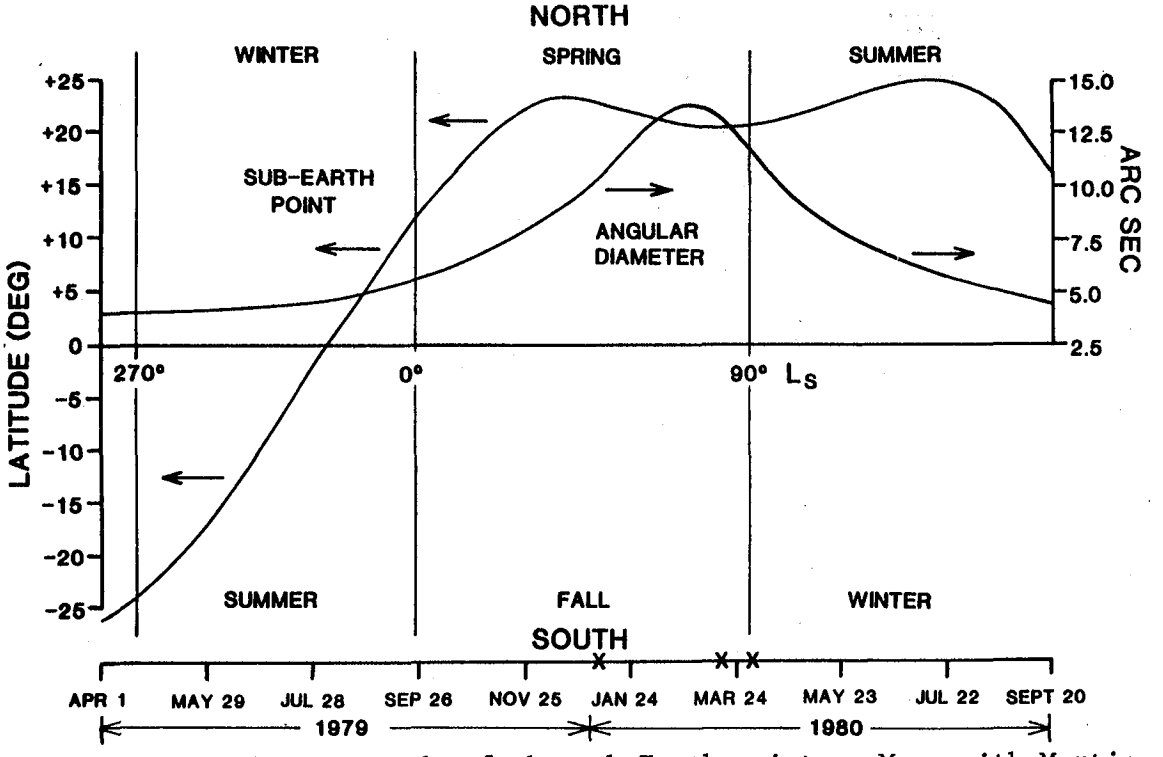

1. Variation of the latitude of the sub-Earth point on Mars with Martian season from April of 1979 through September of 1980. The apparent angular diameter of Mars is also shown.

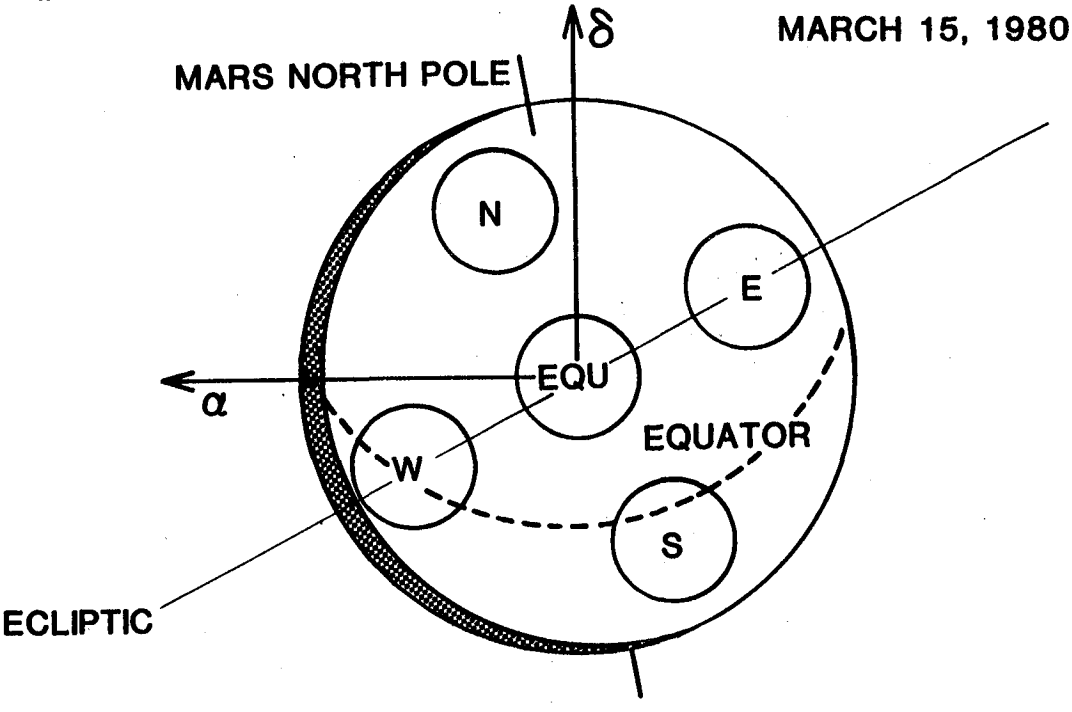

2. Aspect of Mars as viewed from Earth on March 15, 1980. Small circles indicate locations of small aperture for each of five exposures.

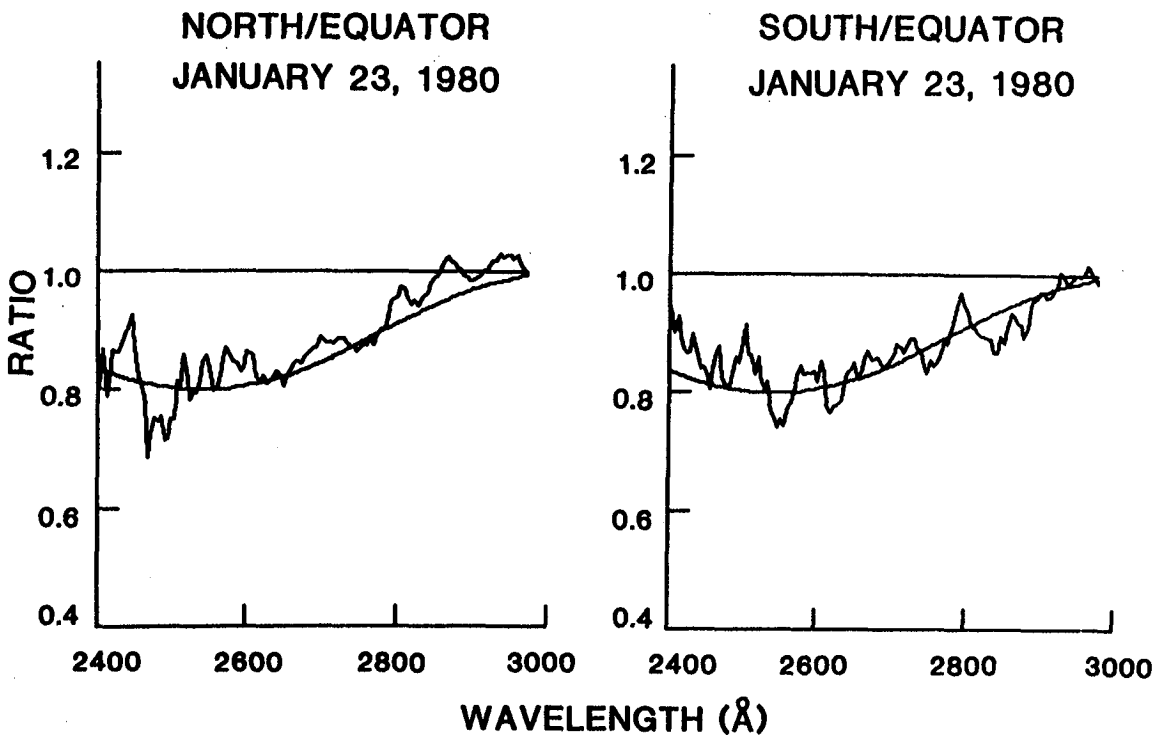

3. Ratio of north and south observations to equatorial observation for January 23, 1980 session. Smooth curve is ozone absorption spectrum.

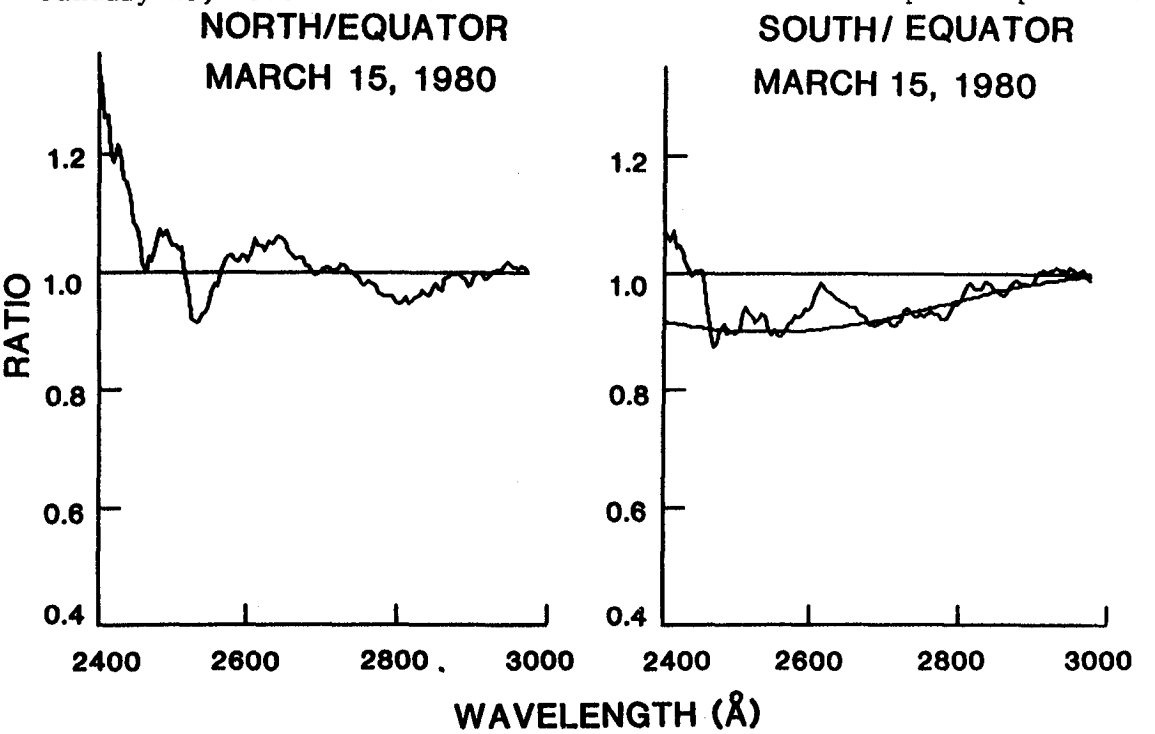

4. Ratio of north and south observations to equatorial observations for March 15, 1980 session. Smooth curve is ozone absorption spectrum.

SPATIAL IMAGING OF UV EMISSION FROM JUPITER AND SATURN

J. T. Clarke and H. W. Moos
Physics Department, The Johns Hopkins University, Baltimore, MD 21218

Spatial imaging with the IUE can be accomplished both by moving one of the apertures in a series of exposures and within the large aperture in a single exposure. The image of the field of view subtended by the large aperture is focussed directly onto the detector camera face at each wavelength; since the spatial resolution of the instrument is 5 - 6 arc sec and the aperture extends 23.0 by 10.3 arc sec, imaging both parallel and perpendicular to dispersion is possible in a single exposure. The correction for the sensitivity variation along the slit at 1216 Å has been obtained from exposures of diffuse geocoronal H Ly α emission. Details of this technique will be presented in a separate paper (ref. 1) in the data reduction session of this symposium. Fig. 1 shows the relative size of the aperture superimposed on the apparent discs of Jupiter and Saturn in typical observations.

By moving the planet image 10 - 20 arc sec along the major axis of the aperture (which is constrained to point roughly north-south) maps of the discs of these planets are obtained with 6 arc sec spatial resolution.

The spatial imaging properties of the telescope are illustrated in the photowrite image of one exposure (SWP 5307) of Jupiter (Fig. 2); the aperture was positioned half on and half off the south pole of the planet in this exposure. The H Ly α (1216 Å) emission shows clearly the outline of that portion of the aperture positioned on the Jovian disc; the remainder of the aperture is dimly illuminated by geocoronal Ly α emission, and the sharp drop in planetary emission at the edge of the planet shows up clearly at Ly α. Furthermore, it happens that longer wavelength grating-scattered light extends along the dispersion line past the Ly α image and drops off rapidly perpendicular to dispersion at the edge of the planet, providing a check on the north-south positioning of the aperture on the planet.

As an example of this north-south scanning at Ly α, Fig. 3 shows the north-south distribution of the Lyα emission from Jupiter derived from three exposures taken on 10 December 1978. The apparent limb darkening and equatorial bulge in emission have also been observed by the Voyager flybys (ref. 2) and a recent sounding rocket (ref. 3). The limb darkening is real, i.e. more than would be produced by the spatial resolution of the instrument on a uniformly emitting disc. The equatorial hot spot is also localized longitudinally: note that the second exposure (taken $\sim 40°$ longitude away from the first) appears to match up to a lower equatorial level of emission. Jupiter rotates with a 10 hour period, and these exposures can be repeated approximately every 50 minutes, providing a longitudinal separation of about 30° between exposures.

A single large aperture SWP exposure of Saturn is shown in Fig. 4. The long wavelength continuum is solar radiation Rayleigh-scattered by H_2 in

Saturn's upper atmosphere. The Rayleigh-scattering cross section increases as λ^4 toward shorter wavelengths, and some absorbers must be present in the planet's upper atmosphere to produce the observed drop in emission. The spectrum of the banded structure $\sim$ 1650 - 1850 Å is plotted in Fig. 5 and shown to correspond to a series of absorption bands of C_2H_2. The presence of this molecular species in Saturn's atmosphere was discovered using the IUE. Note also the north-south asymmetry in both continuum emission and the grating-scattered light in Fig. 5. The northern half of Saturn was occulted by the rings in this observation (as drawn in Fig. 1). The north-south ratio of emission (i.e. on the rings to off the rings) appears to be roughly constant with wavelength, indicating simple extinction by ring particles rather than scattering by gas around the rings.

REFERENCES

1. Clarke, J. T. and Moos, H. W.: Extracting Spatial Information from Large Aperture Exposures of Diffuse Sources. GSFC IUE Symposium, NASA CP-2171, 1980.

2. Broadfoot, A. L. et al.: EUV Observations from Voyager I Encounter with Jupiter. Science, vol. 204, 1979, p. 979.

3. Clarke, J. T., Weaver, H. A., Feldman, P. D., Moos, H. W., Fastie, W. G., and Opal, C. B.: Spatial Imaging of Hydrogen Lyman α Emission from Jupiter. Astrophys. J., in press, 1980.

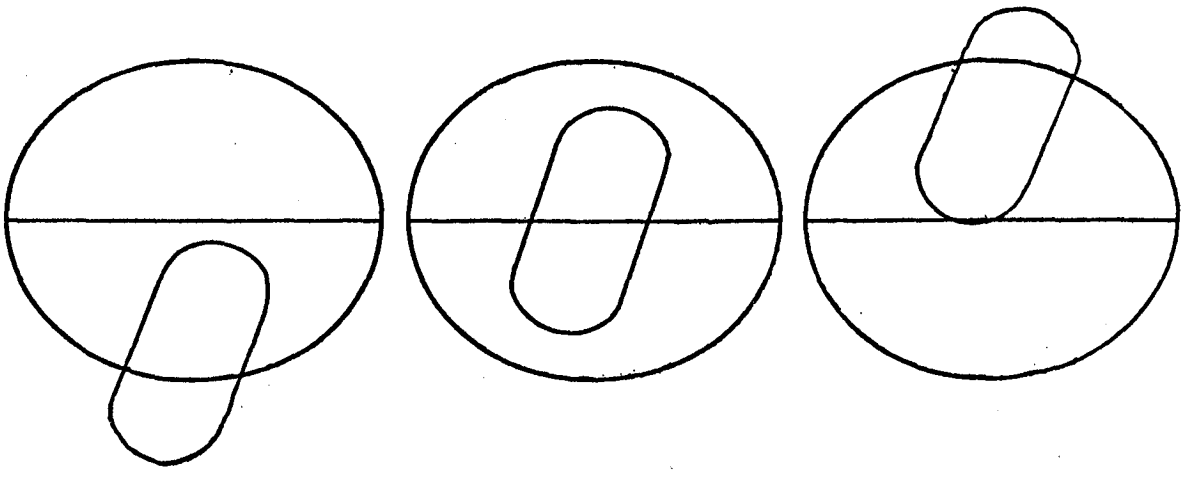

JUPITER

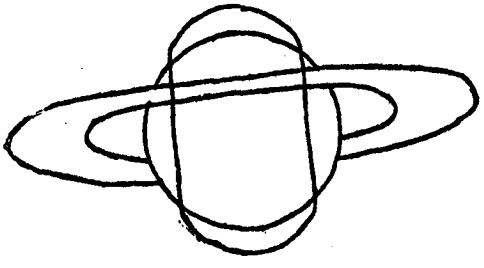

SATURN

Figure 1

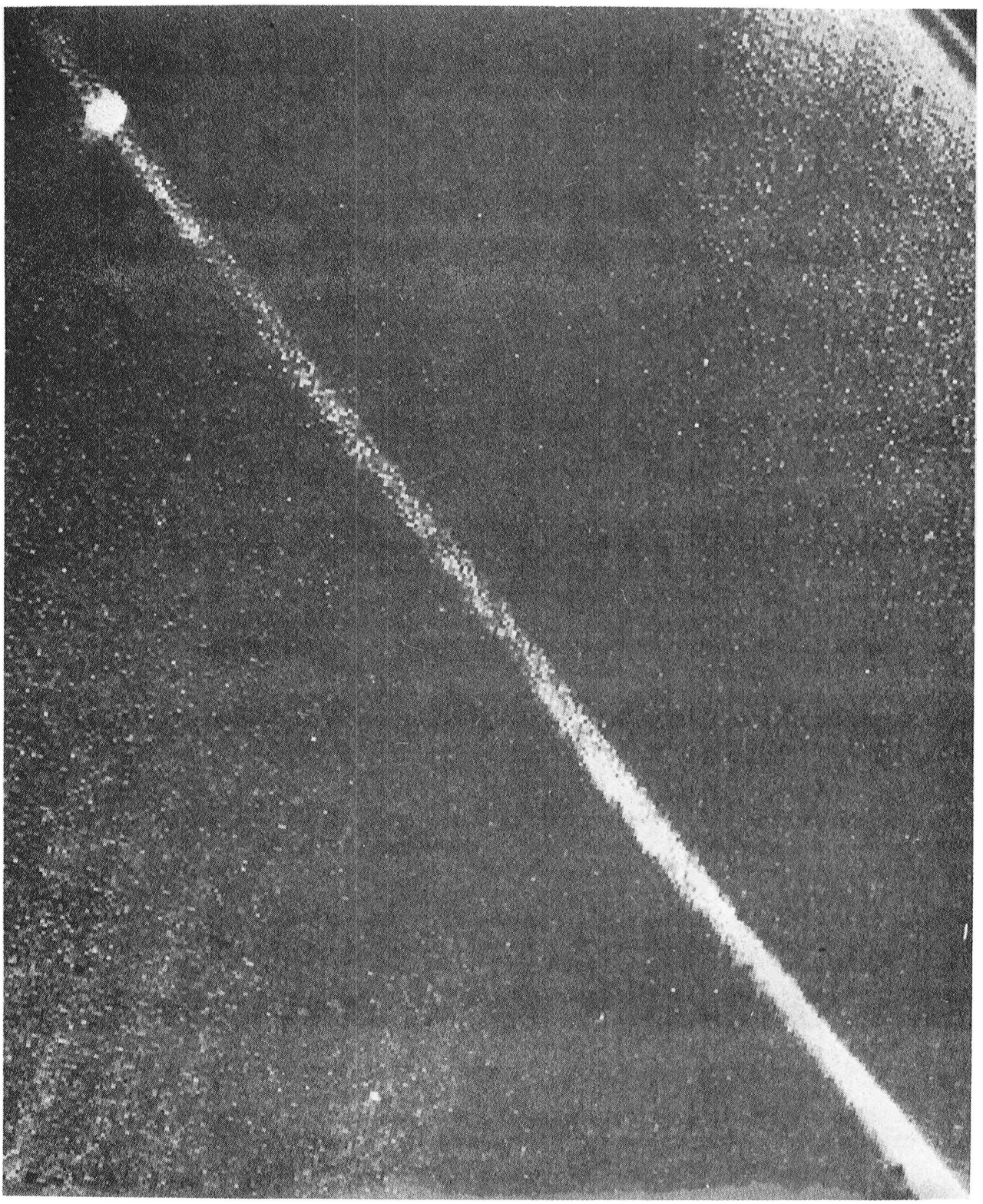

Figure 2

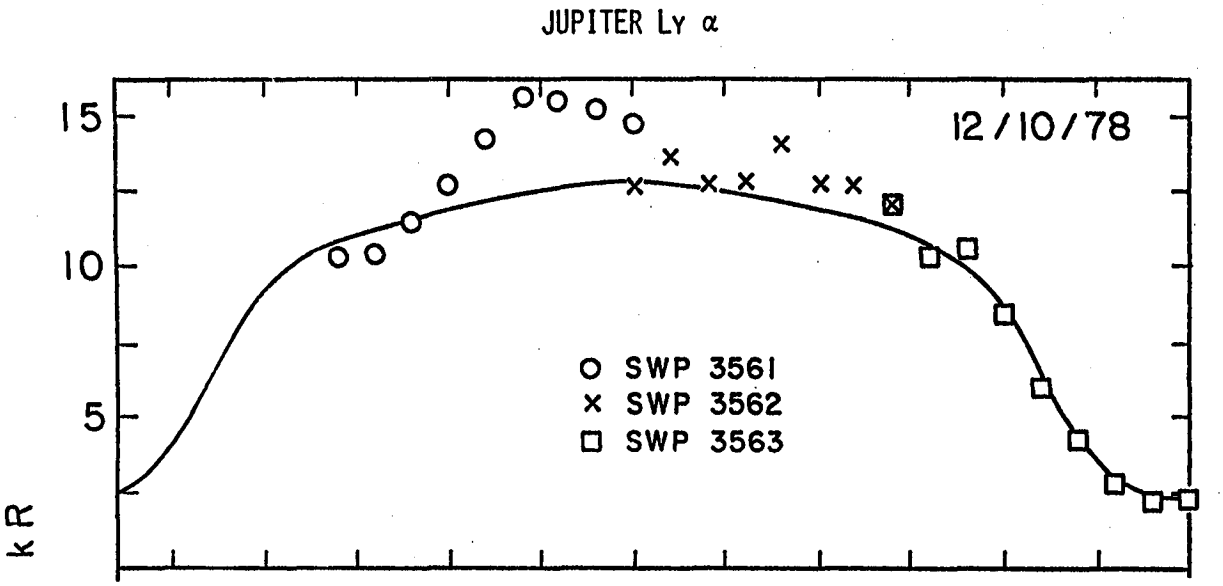

Figure 3

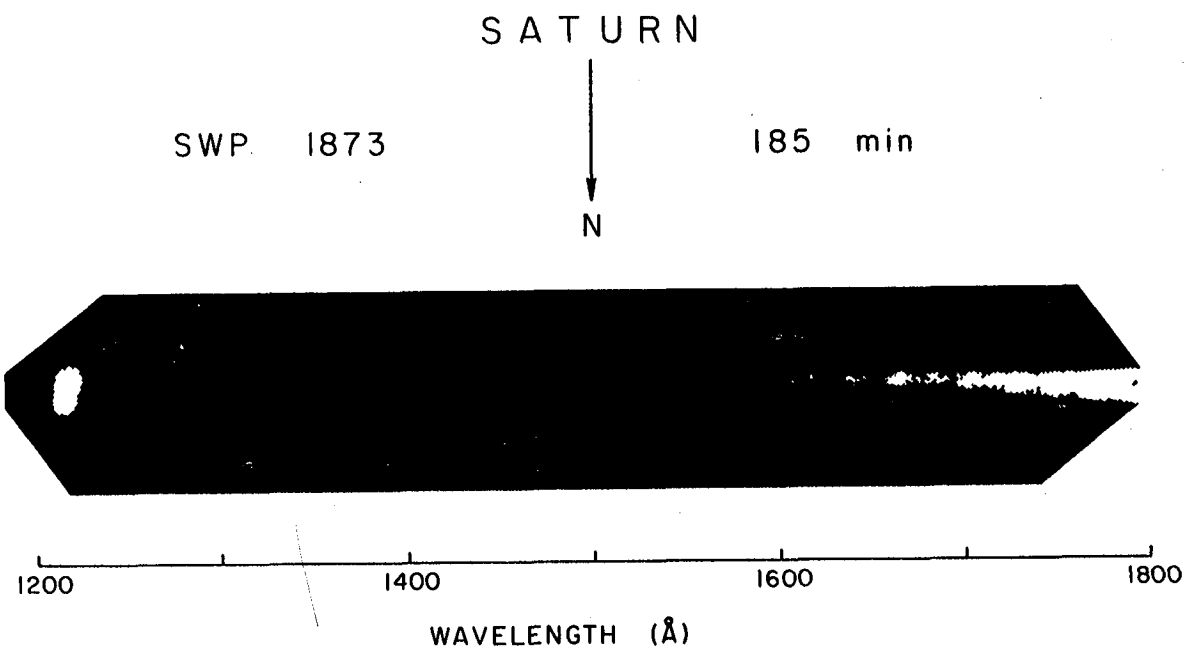

Figure 4

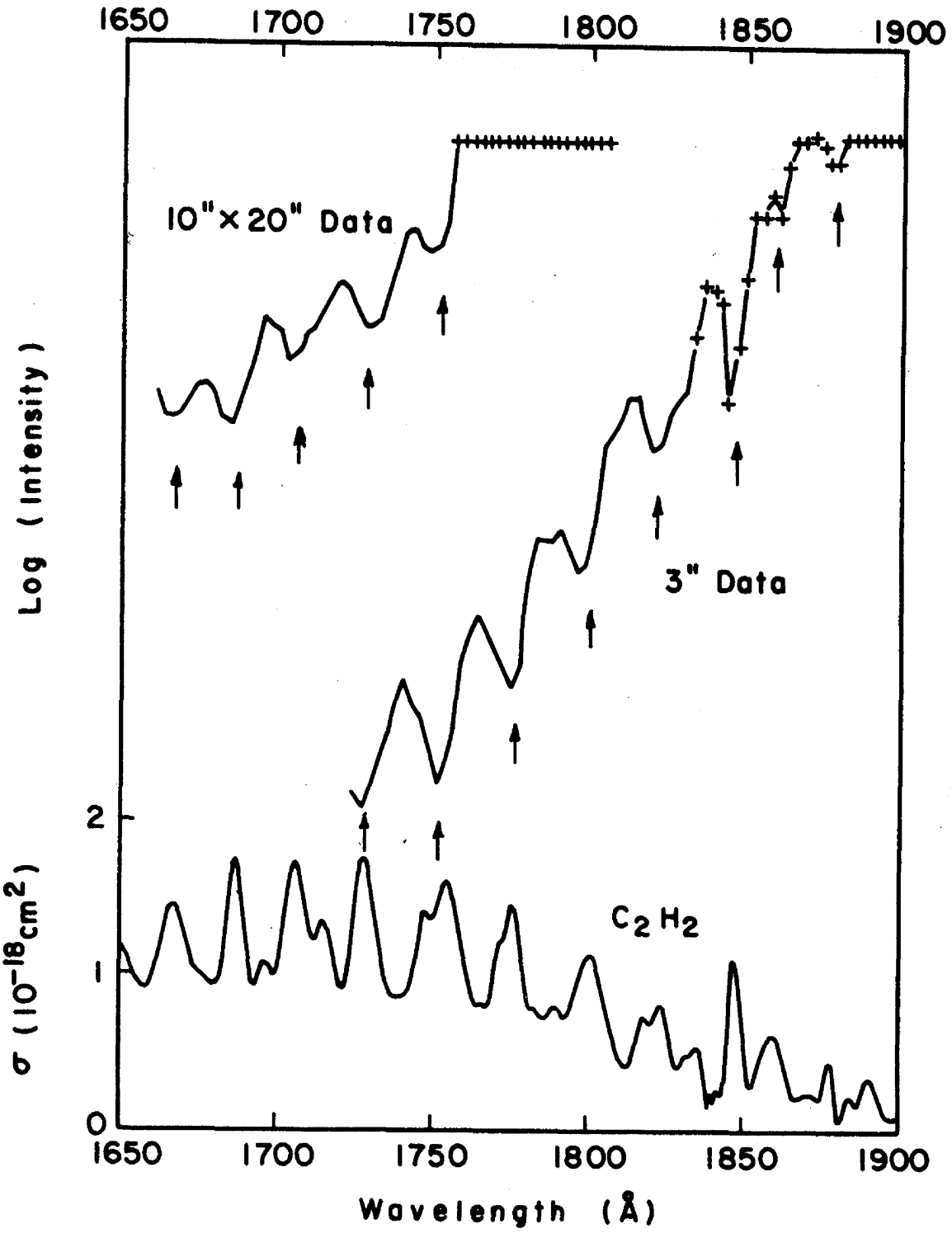
1650
1700
1750
1800
1850
1900
10"×20" Data
3" Data
Log (Intensity)
σ (10⁻¹⁸cm²)
C₂H₂
2
1
0
1650
1700
1750
1800
1850
1900
Wavelength (Å)

Figure 5

OBSERVATIONS OF POLAR AURORA ON JUPITER

J. T. Clarke and H. W. Moos
Physics Department, The Johns Hopkins University, Baltimore, MD 21218

S. K. Atreya
Department of Atmospheric & Oceanic Science
University of Michigan, Ann Arbor, MI 48109

A. L. Lane
Jet Propulsion Laboratory, California Institute of Technology
Pasadena, California 91103

ABSTRACT

North-south spatial maps of Jupiter were obtained with the SWP camera in IUE observations on 10 December 1978, 19 May 1979, and 7 June 1979. Bright auroral emissions were detected from the north and south polar regions at H Ly α (1216 Å) and in the H_2 Lyman bands (1250-1608 Å) on 19 May 1979; yet no enhanced polar emission was detected on the other days. The relationship between the IUE observing geometry and the geometry of the Jovian magnetosphere will be discussed.

The discovery more than a decade ago of radio emission from Jupiter, which appeared to be modulated both by the rotation of the planet and the orbital position of the moon Io, opened the door for speculation on the distribution of charged particles in the probably Jovian magnetic field and the possibility of polar aurora on Jupiter. Searches for visible and radio-frequency auroral emissions have been hampered by poor sensitivity and spatial resolution, respectively. Sounding rocket and Earth-satellite (Copernicus) ultraviolet observations tentatively identified H_2 Lyman band emission (ref. 1,2) and an H Ly α hot spot (ref. 3), each of which was expected to result from charged particle excitation of H and H_2 in Jupiter's upper atmosphere. The Voyager flybys (ref. 4) positively identified polar auroral emissions both in the visible and at H Ly α and the H_2 Lyman and Werner bands in the ultraviolet. We will describe here a north-south mapping of Jupiter, performed with the IUE SWP camera under low dispersion, which shows strong polar brightening at H Ly α (1216 Å) and in the H_2 Lyman and Werner bands (1150 - 1608 Å).

The photowrite images of three spectra of Jupiter's south pole, central region, and north pole, taken 19 May 1979, are shown in Fig. 1. North-south imaging in this method of mapping has been described in the previous paper (ref. 5). The central spectrum shows the expected bright Ly α line and progressively stronger Rayleigh-scattered continuum at longer wavelengths. In addition, the polar spectra show marked emission features at 1608 Å

and around 1570 Å. These emissions appear at the edge of the grating-scattered light from the respective northern and southern edges of the planet, and have been identified as H_2 Lyman band emission. Fig. 2 shows the whole-slit spectra from the three exposures, and the Lyman-band emission appears in the polar images well above the level of continuum seen in the equatorial spectrum.

The north-south distribution of the Ly α emission derived from these three exposures is shown in Fig. 3, along with the positions of the aperture on the planet. A pronounced brightening appears at both poles, trailing off away from the planet to the level of background geocoronal emission (1-2 kR). The north-south width of the 1216 Å and 1608 Å features is 5 - 7 arc sec at both poles. This is comparable to the 6 arc sec instrumental resolution, hence the north-south extent of the Jovian auroral oval is not measureable. However, the polar Ly α brightening in SWP 5309 of the north pole shows a marked east-west asymmetry, indicating that the emitting region was smaller than the 10 arc sec aperture width. This asymmetry may be explained either by a point source aurora or by a diffuse source partially filling the aperture. The south pole emission appears diffuse east-west.

It is estimated that emission 1/8 the measured brightness at 1608 Å in these exposures could be detected with the IUE in a 15 min. exposure. The potential thus exists for monitoring these aurora as a function of both the orbital position of Io and the 10° tilt of Jupiter's magnetic pole toward or away from the Earth.

REFERENCES

1. Rottman, G. J., Moos, H. W. and Freer, C. S.: The Far-Ultraviolet Spectrum of Jupiter. Astrophys. J., vol. 184, 1973, p. L89.

2. Giles, J. W., Moos, H. W. and McKinney, W. R.: The Far-Ultraviolet (1200 - 1900 Å) Spectrum of Jupiter Obtained with a Rocket-Borne Multichannel Spectrometer. J. Geophys. Res., vol. 81, 1976, p. 5797.

3. Atreya, S. K., Yung, Y. L., Donahue, T. M. and Barker, E. S.: Search for Jovian Auroral Hot Spots. Astrophys.J., vol. 218, 1977, p. L83.

4. Broadfoot, A. L. et al.: EUV Observations from Voyager I Encounter with Jupiter. Science, vol. 204, 1979, p. 979.

5. Clarke, J. T. and Moos, H. W.: Spatial Imaging of UV Emission from Jupiter and Saturn. GSFC IUE Symposium, NASA CP-2171, 1980: this compilation.

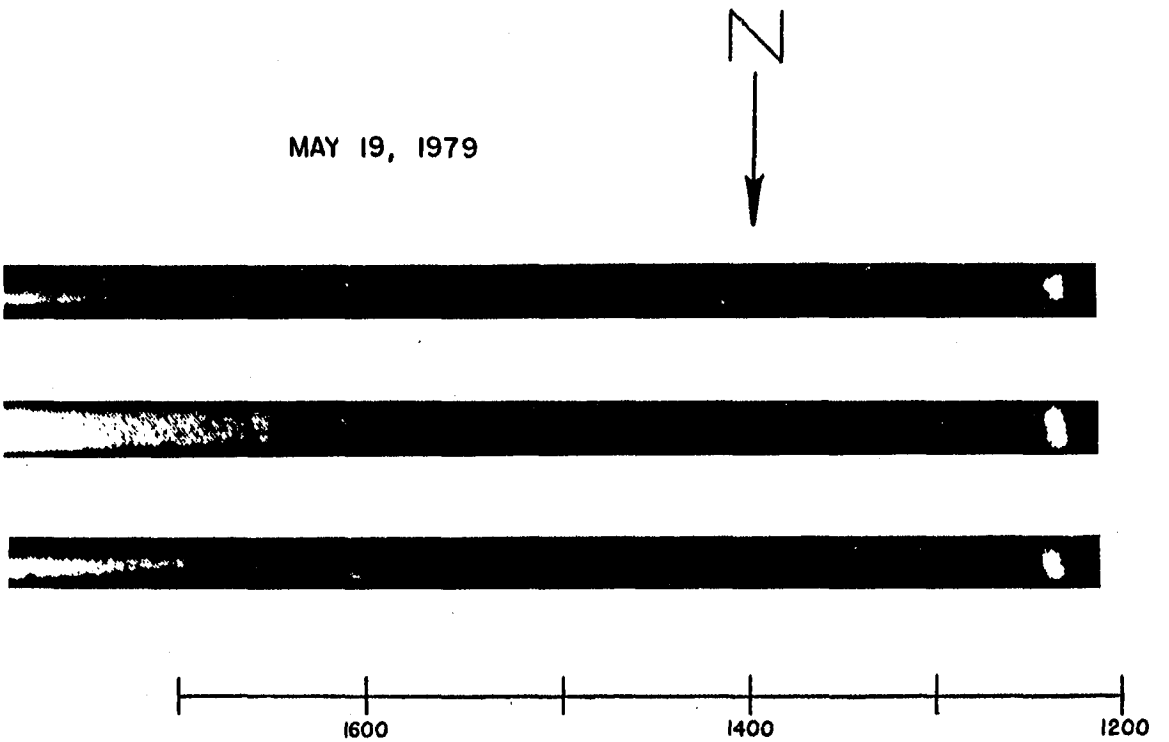

Figure 1

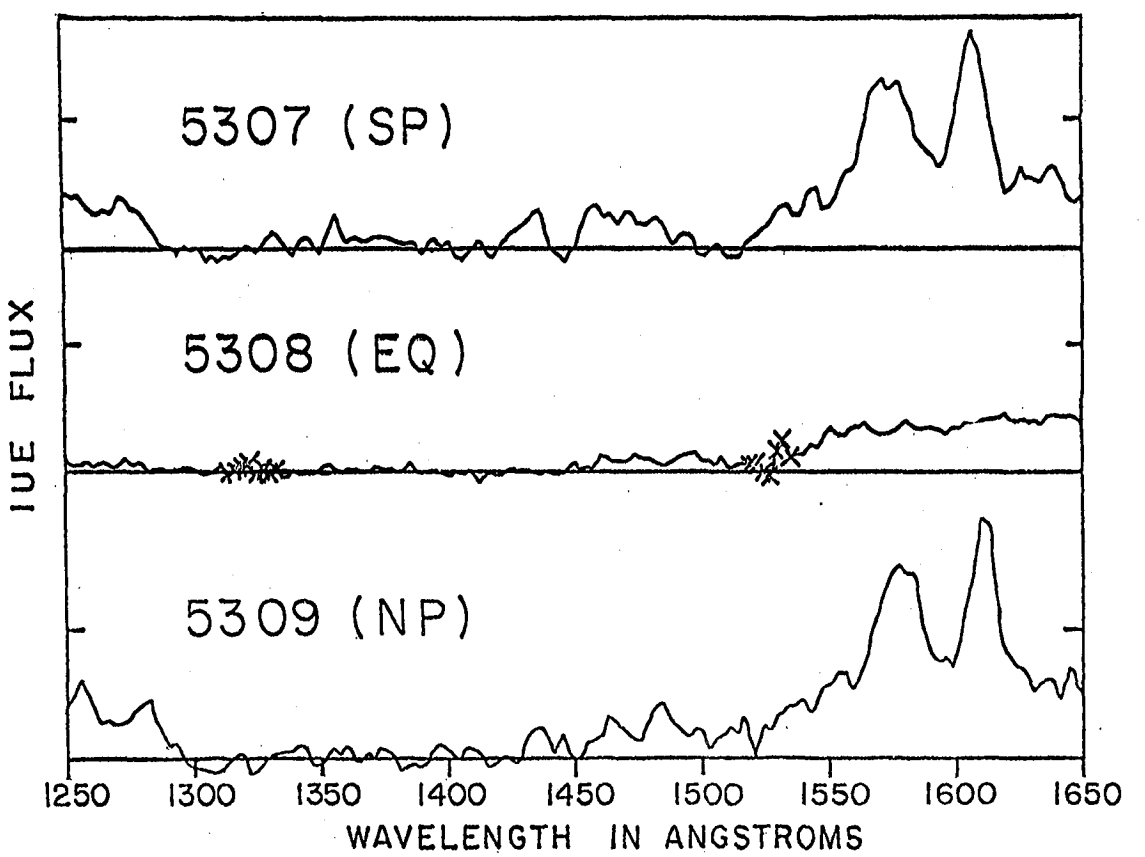

Figure 2

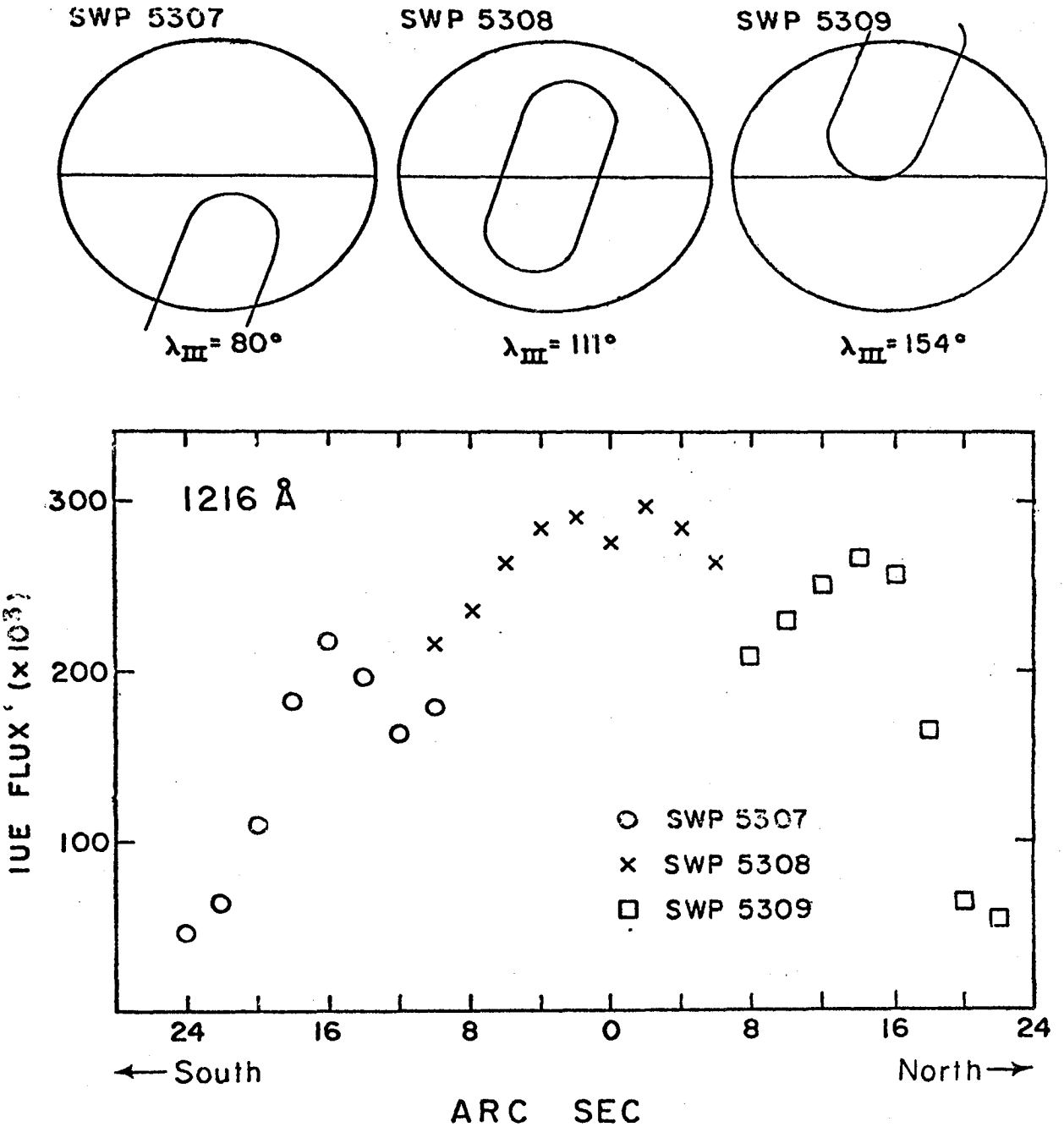
SWP 5307
SWP 5308
SWP 5309
λIII= 80°
λIII= 111°
λIII= 154°
1216 Å
IUE FLUX (×10³)
300
200
100
SWP 5307
SWP 5308
SWP 5309
24
16
8
0
8
16
24
South
North
ARC SEC

Figure 3

OBSERVATIONS OF THE Io PLASMA TORUS

H. W. Moos and J. T. Clarke
Physics Department, The Johns Hopkins University, Baltimore, MD 21218

S. K. Atreya
Department of Atmospheric & Oceanic Science
University of Michigan, Ann Arbor, MI 48109

A. L. Lane
Jet Propulsion Laboratory, California Institute of Technology
Pasadena, California 91103

ABSTRACT

The short wavelength spectrograph on the IUE satellite has been used to obtain spectra of the plasma torus near the orbit of Io about Jupiter. Three exposures of about 8 hours each taken in March and May 1979 show emission features due to SII, SIII, and OIII. The absence of features at other wavelengths permits upper limits to be set on other species in the torus.

INTRODUCTION

It is now known that ionic species are trapped in the orbital path of Io. The basic picture is that atoms ejected from the satellite are ionized and thus trapped on Jovian magnetic field lines. The field lines move with the 10 hour planetary rotational period, spreading the ions into a toroidal-like cloud along the orbital path. The only identified ionic emissions are those of sulfur and oxygen. However, a number of species have strong lines in the spectral region covered by the short wavelength spectrograph. For this reason, three observations of the Io torus were made near the times of the Voyager 1 and Voyager 2 flybys (5 March and 10 July 1979).

OBSERVATION DETAILS

Large aperture, low dispersion spectra of the torus were taken with the SWP camera on 1 March 1979, 3 March 1979 and 19 May 1979 (SWP 4448, 4463, 5302). The aperture, aligned approximately perpendicular to the orbital plane, was pointed between 3 and 6 R_J. The exposure times were 520, 445 and 440 minutes respectively.

Due to the long exposure times, the spectra contained in addition to readout noise, noise spikes due to fast particle hits, radioactive spots or blemishes on the camera face and geometry correcting reseaux marks. Running a median filter perpendicular to the dispersion direction before adding the line by line spectra was found to significantly reduce these noise spikes. The photometric error in SWP data during this time period has been corrected using the standard algorithim (IUE Newsletter #8). The three spectra were then summed to produce Fig. 1.

To determine the baseline and noise signal, the averages and standard deviations were computed for the 1278 - 1376 Å, 1426 - 1651 Å, and 1776 - 1951 Å wavelength regions. The baseline varied (3121, 883 and 5030 FN respectively). The standard deviation was approximately constant with an average value of 3163 FN.

DISCUSSION

Fig. 1 shows the sum of the three observations. The features at 1256 Å and 1198 Å are identified as SIIλ 1257 and SIIIλ 1199. The 1729 Å feature has not been identified. There is a persistent blemish which produces a hit like feature near this wavelength in lengthy SWP exposures; however when this is removed either by hand or by a median filter perpendicular to the dispersion, the feature remains in the torus spectra. In addition, all three photowrite images show a distinct image of the entrance aperture indicating that the 1729 Å feature is real. The feature at 1664 Å is identified as OIIIλ 1664. However, the peak is only 10% above the 3σ noise level. Therefore, although statistically significant the identification must be considered marginal. Although the apparent peak at 1397 Å is close to the expected SIVλ 1406, it may be due to a shift in the background level near this point. In any case, a statistically significant signal does not exist at 1406 Å.

Table 1 lists a series of ionic species, in order of decreasing cosmic abundance, with strong emission lines in this spectral region. The measured brightness of the three identified species are listed. For the other species the upper limit to the brightness was determined from three times the standard deviation and the spectrograph sensitivity.

To estimate the number densities, a simple homogenous torus model similar to that used by Broadfoot et al (ref. 1) was used. (In this case the torus was centered on the orbit rather than the magnetic equator.) Although it is likely that the emission structure was quite complex, these IUE spectra were averaged over most of a rotational period; thus, the simple model may be appropriate. The number densities were computed using an electron density of 2×10^3 cm^{-3} (ref. 2) an electron temperature or 10 eV and an average path length of 7.3 R_J. Also shown in Table 1 are the number densities reported by the Voyager 1 UVS group. These values are based on short wavelength transitions observed by the Voyager 1 extreme ultraviolet spectrograph and a model similar to ours (ref. 1). The most serious discrepancy is in the case of OIII where the IUE value is one sixth the Voyager value. The uncertainties in the number densities depend directly on those of the excitation coefficients used. A more detailed discussion of the data analysis and the sources of the excitation rates will be published at a later date.

We thank the IUE Observatory staff for their aid in the acquisition and reduction of the data. This work has been supported by a grant from NASA.

REFERENCES

1. Broadfoot, A. L. et al 1979 Science 204, 979.

2. Bridge, H. S. et al 1979 Science 204, 987.

Table 1

OBSERVED IONIC SPECIES AND UPPER LIMITS

Species	λ (Å)	Brightness (Rayleighs)	IUE number density cm^{-3}	Voyager 1 number density† (cm^{-3})
O III *	1664	12 *	140	850
C II	1335	6.7	4.2	
C III	1909	8.5	8.6	
N III	1750	9.4	50	
N IV	1485	10	18	
Si II	1264	6.7	2.0	
Si III	1892	8.5	7.9	
Si IV	1395	7.9	1.1	
S II *	1257	43 *	140	
S III *	1199	30 - 60 *	160 - 320	95
S IV	1406	8.2	49	55
Al II	1671	11	0.22	
Al III	1856	8.4	0.72	
Ca II	1839	8.4	47	
P II	1308	6.4	12	
P III	1344	6.7	17	

† Reference 1

* Observed: The brightness value is a measured one rather than an upper limit.

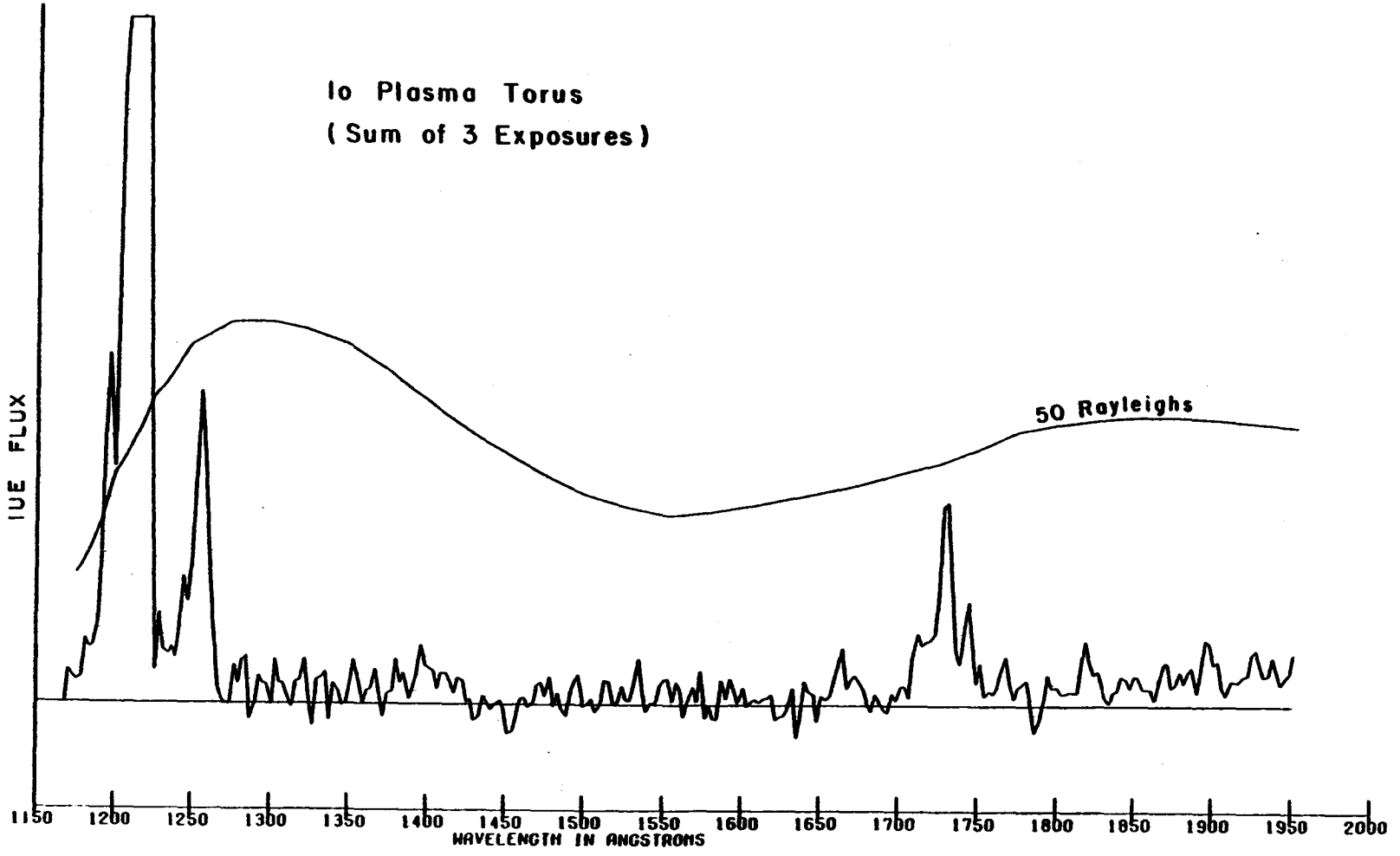
Io Plasma Torus
(Sum of 3 Exposures)
50 Rayleighs
IUE FLUX
1150
1200
1250
1300
1350
1400
1450
1500
1550
1600
1650
1700
1750
1800
1850
1900
1950
2000
WAVELENGTH IN ANGSTROMS

Figure 1

ANALYSIS OF IUE OBSERVATIONS OF CS IN COMET BRADFIELD (1979 1)

W. M. Jackson and J. Halpern
Howard University
Washington, DC 20059

P. D. Feldman
Johns Hopkins University
Baltimore, MD 21218

J. Rahe
Laboratory for Astronomy and Solar Physics
Goddard Space Flight Center
Greenbelt, MD 20771

ABSTRACT

The CS high-resolution and low-resolution IUE data obtained on Comet Bradfield (1979 1) have been analyzed. The high resolution rotational band profiles can be fitted with theoretical band profiles which are derived using a Boltzmann temperature of 70 K. A very rapid variation with heliocentric distance, for the CS brightness has been found. The implications of these results for models of the coma along with the origin of the CS species are discussed.

INTRODUCTION

The first sulfur containing radical discovered in comets was observed in Comet West (1976 VI) during the rocket observations of Smith and Casswell (ref. 1). These initial results were later confirmed by IUE observations of Comet Seargent (1978 m) (ref. 2) and Comet Bradfield (1979 1) (ref. 3). The gas emission rate from Comet Bradfield (1979 1) was sufficient so that, contrary to the previous observations, high-resolution spectra of CS could be measured. Low-resolution spectra of the comet were obtained with the large aperture at different heliocentric distances and these spectra show that the CS emission appears as a point source.

OBSERVATIONS

The details of the IUE satellite instrumentation have previously been described (ref. 4) so that only the observational procedure will be outlined in this section. Several long wavelength high-resolution spectra were taken at various times using the large (10" x 20") aperture of the spectrograph. The comet was tracked on the center of its maximum brightness using the fine error sensor of the IUE. In all of the high-resolution spectra the photo-

write images showed a darkening in the region of the CS bands but only two exposures were obtained which exhibit sufficient signal to noise ratios so that useful data could be extracted from the tape. The CS bands actually occur in two different orders in the spectrum, one of which occurs near the center of the camera and the other near the edge. The quality of the CS image near the edge of the camera is severely degraded by the variation in the grating efficiency across its blaze. Nevertheless, some indication of the presence of the CS band was obtained.

One of the two high-resolution spectra that were analyzed is shown in Figure 1. The data have been averaged using a five point running mean. The spectrum clearly shows two peaks corresponding to the Q and R branches of the $X^1\Sigma \rightarrow A^1\Pi$ transition in CS. The overall width of both bands is greater than 0.2nm which is a factor of two to three times greater than the quoted instrumental bandwidth for an extended object. The actual instrumental bandwidth is probably less than the quoted value of 0.08nm since as Figure 2 shows the CS emission does not completely fill the large aperture of the spectrograph. This increases the effective resolution of the instrument because the CS emission serves as a narrower slit.

HIGH RESOLUTION THEORETICAL PROFILES

In order to interpret the observed band profiles, theoretical band profiles based upon the known CS spectrum and rotational line factors as given in Herzberg (ref. 5) were calculated. The observed CS spectrum at 257.5nm is a $X^1\Sigma \rightarrow A^1\Pi$ transition and thus shows P, Q and R branches. Because of the small rotational constant of CS, the lines are closely spaced, especially in the Q branch, where many lines are bunched together near the origin. The R and Q branches have heads at 257.60 and 257.77nm, respectively while the P branch shows no head.

A perturbation exists in the CS spectrum at the J=15 level in the 0-0 band. This was neglected in the present calculations of the rotational line factors (ref. 5) since it is unlikely to lead to a serious error in the fitting of the rotational profile. Only one or two lines at relatively high values of J, will be affected by this perturbation so that only one or two lines in the total spectrum will be distorted.

It was assumed that the rotational energy could be described in terms of a Boltzmann temperature. Spectral profiles were built up using a Lorentzian form for each individual line, the width of which equalled the slit width of the IUE spectrometer. The actual profiles were constructed on a PDP-11/03 computer with a VT 55 graphic display terminal. Theoretical profiles were calculated using a Lorentzian bandwidth varying from 0.001nm to 0.08nm. The best fit for the shape, wavelength and relative heights of the Q and R bandheads occurred when a HWHM bandwidth of 0.02nm was used. This is in reasonable agreement with the low-resolution results which show that HWHM of the intensity peak for the observed CS (0-0) band fills only ½ of the long side of

the large aperture, corresponding to a true HWHM bandwidth of 0.02nm.

Figure 3 illustrates the comparison between the computed and observed spectra using a 0.02nm HWHM bandwidth for the three Boltzmann temperatures of 70, 80 and 90K. The points are the average value of the two runs and they are plotted with error bars which represent the average error between the runs. It is clear that the 80 K temperature gives the best fit to the observed data in terms of shape, peak wavelengths, and the relative heights of the observed rotational band. The fact that the observed data fits a Boltzmann temperature at 80 K implies that for the CS molecule there are enough collisions to support a "temperature". Infra-red radiative decay is not fast enough to allow the molecule to completely relax to its lowest rotational level, which is in complete contrast to all other cometary molecules which have allowed infra-red transitions. The "temperature" that is observed probably results from a competition between collisional pumping and radiative decay and thus does not correspond to any physical temperature associated with the nucleus or the coma. More detailed modeling which includes radiative decay will be required if a physically meaningful temperature is to be extracted.

LOW-RESOLUTION ANALYSIS

A preliminary analysis of the low dispersion exposures at three different heliocentric distances is given in Table 1. Here, the brightness of the CS (0,0) band is averaged over a 10" x 15" aperture for comparison with model calculations. As the image of this feature is nearly point-like, no median filtering was applied. Also, no correction was made for the reseau mark that appears in the image and so the results given may be slightly in error. The production rate given in the table is derived by integrating the output of a Haser model over the given aperture size, and since the image is point-like, is extremely sensitive to the variation in geocentric distance. The model assumes a CS parent with a lifetime of 100 sec (at 1 a.u.), an outflow velocity of 1 km sec^{-1} and a g-factor for the (0,0) band of 7×10^{-4} photons sec^{-1} mol^{-1} at 1 a.u. The variation of production rate with heliocentric distance is very rapid, of the order of r^{-6}-r^{-7}, considerably faster than the variation for OH over the same period (ref. 8). Although the difference may well be real, one must use caution in applying a radial outflow model in this case as the parent scale length is within the collision region around the nucleus while the model is collisionless.

The most likely candidate as a parent for CS is the CS_2 molecule. This molecule is known to produce (ref. 6) CS via the following reactions

1. $CS_2\ (X^1\Sigma^+g) + h\nu \rightarrow CS(X^1\Sigma^+) + S(^3P)$

2. $\rightarrow CS(X^1\Sigma^+) + S(^1D)$

in the 190nm region. Recent work (ref. 7) suggests that at 193nm the CS is

produced vibrationally excited to $v'' \leq 7$ and that the branching ratios for reactions (1) and (2) are 20% and 80%, respectively. The absorption coefficient for this band has been measured (ref. 9). When it is combined with the higher solar flux (ref. 10) in this region, one can compute a photochemical lifetime at 1AU of 103 sec. At the largest observed heliocentric distance and with a 1km/sec outflow velocity this corresponds to a scale length of 88 km, well below the resolution of the present observations.

DISCUSSION

The CS molecule is the first diatomic molecule with an allowed infrared transitions that shows any evidence that it has retained memory of the temperature at which it was formed. In light of the fact that CS is produced via photodissociation in high vibrational levels (ref. 7) it is likely that the observed "temperatures" are the result of radiative cascade from these higher levels. Thus one needs a detailed knowledge of the photodissociation dynamics to include the effect of these cascade processes in any radiative equilibrium model of the coma of the comet. Only when this is done will one be able to evaluate how collisions can contribute to the observed temperatures.

The photodissociation model of CS_2 can also explain the presence of S atoms in the comet since these atoms are the products of the photodissociation of both CS_2 and CS. Most of the S atoms are produced in the ^1D state which has a radiative lifetime (ref. 11) of 25 sec. However, because of this short lifetime and the relatively low sulfur abundance it is unlikely that ^1D atoms can be detected directly as in the case of carbon (the ^1D-^1P transition at 193.1nm) where the lifetime of the ^1D state is 3200 sec (ref. 12). It is possible that resonance fluorescence mechanism may excite the ($^1S \rightarrow {}^1D$) transition at 7725Å since this transition has a lifetime of only 0.47 sec (ref. 11) and the analogous D atom transition has already been observed.

CONCLUSION

The detailed analysis of both the high- and low-resolution CS data obtained during the observation of Comet Bradfield (1979 1) suggests that this radical is produced by photodissociation of CS_2. The heliocentric variation of the CS brightness is consistent with this conclusion along with the presence of S atoms in comets. Further analysis of the data may reveal how important collisions are in the inner part of the coma.

ACKNOWLEDGEMENTS

The authors are grateful for the complete cooperation they received from

the IUE observatory staff. W. M. Jackson would like to acknowledge the helpful conversations with M. A'Hearn and the support of the Planetary Atmospheres Program of NASA under grant number NSG 5071. The work at Johns Hopkins University was supported by NASA grant NSG-5393.

REFERENCES

1. Smith, A. M., and Casswell L., submitted to Astrohys. J. (1980).

2. Jackson, W. M., Rahe, J., Donn, B., Smith, A. M., Keller, H. U., Benvenuti, P., Delsemme, A. H., and Owen, T., Astron. Astrophys., 73, L 7 (1978).

3. Feldman, P. D., Weaver, H. A., Festou, M. C., A'Hearn, M. F., Jackson, W. M., Donn, B., Rahe, J., Smith, A. M., and Benvenuti, P., accepted for publication, Nature (1980).

4. Boggess, A. et al. Nature, 275, 377-385 (1978).

5. Herzberg, G., Diatomic Molecules, D. Van Nostrand, New York, (1950), 128.

6. Filseth, S. V., Advances in Photochemistry, 10, John Wiley and Sons, (1977) 1.

7. Yang, S. C., Freedman, A., Kawasaki, M., and Bersohn, R., J. Chem. Phys., 72, 4058 (1980).

8. Weaver, H. A.; Feldman, P. D.; and Festou, M. C.: Water Production Models for Comet Bradfield (19791). The Universe in Ultraviolet Wavelengths: The First Two Years of IUE. NASA CP-2171, 1980: this compilation.

9. Rabalais, J. W., McDonald, J. M., Scherr, V., and McGlynn, S. P. Chem. Rev., 71, 73 (1971).

10. Huebner, W. F., and Carpenter, C. W. Los Alamos report LA-8085-MS 1979.

11. Okabe, H., Photochemistry of Small Molecules, John Wiley and Sons (1978) 156.

TABLE 1

Heliocentric Variation of the Average Brightness of the CS (0,0) Band

Heliocentric Distance, r (a.u.)	Geocentric Distance, Δ(a.u.)	Average Brightness (kR)	Derived CS Production Rate (sec^{-1})
0,71	0.615	2.1	$1x10^{26}$
0.80	0.40	1.2	$5x10^{25}$
0.925	0.20	2.6	$1.6x10^{25}$

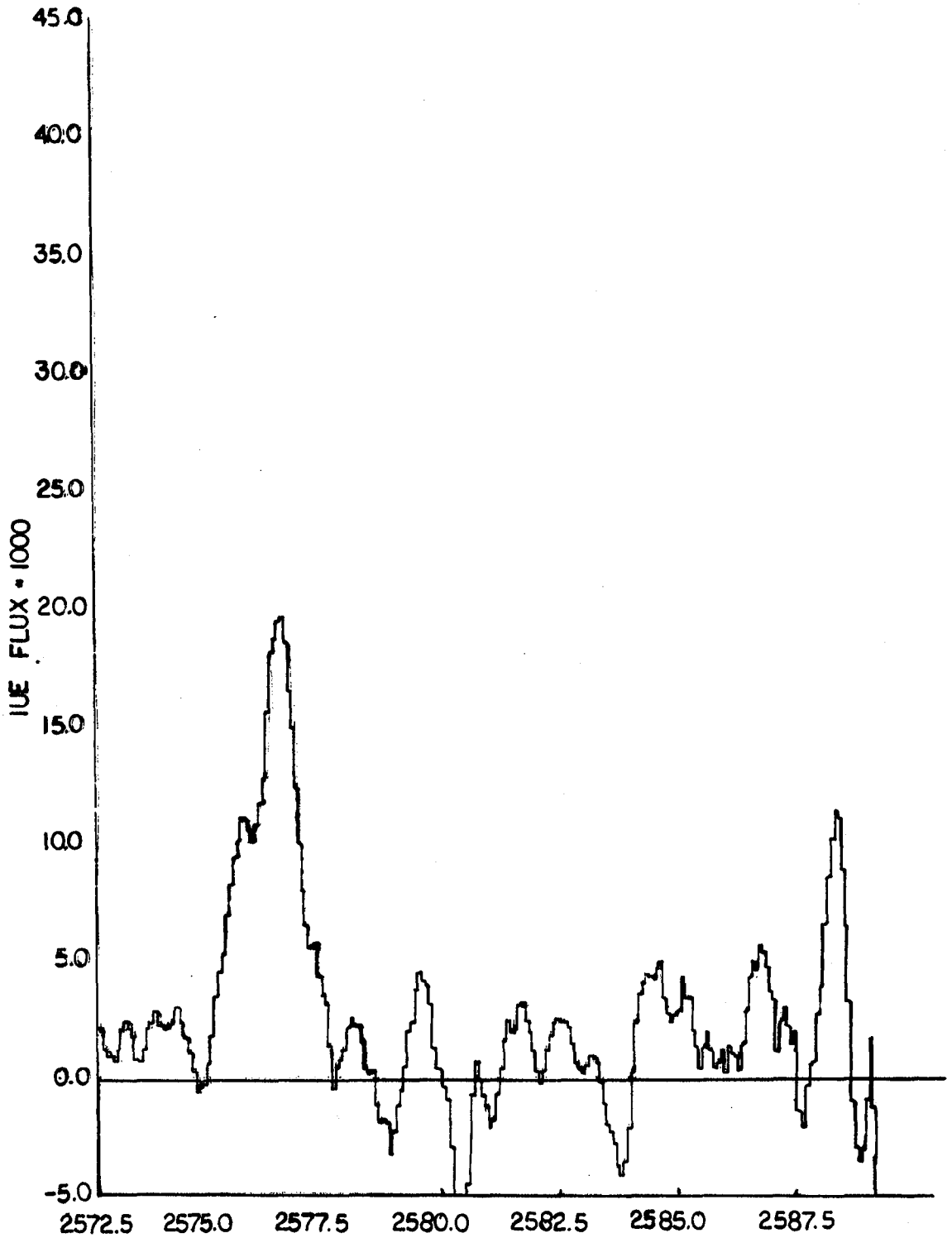

Figure 1.

High-resolution IUE Spectra of Comet Bradfield (1979 1) in the CS region.

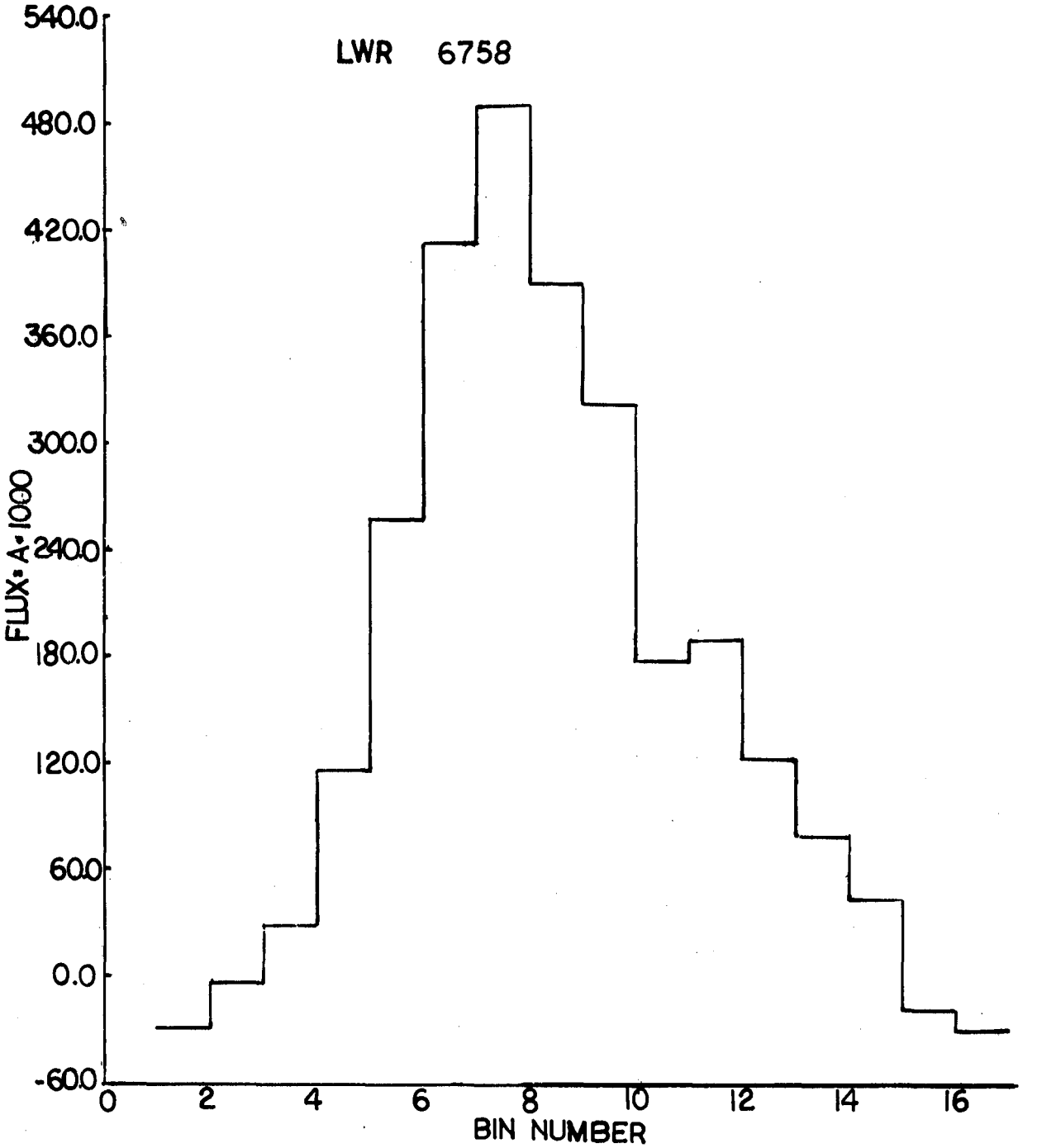

Figure 2.

Spatial profile of low-resolution spectra of CS scanned along the long dimension of the slit.

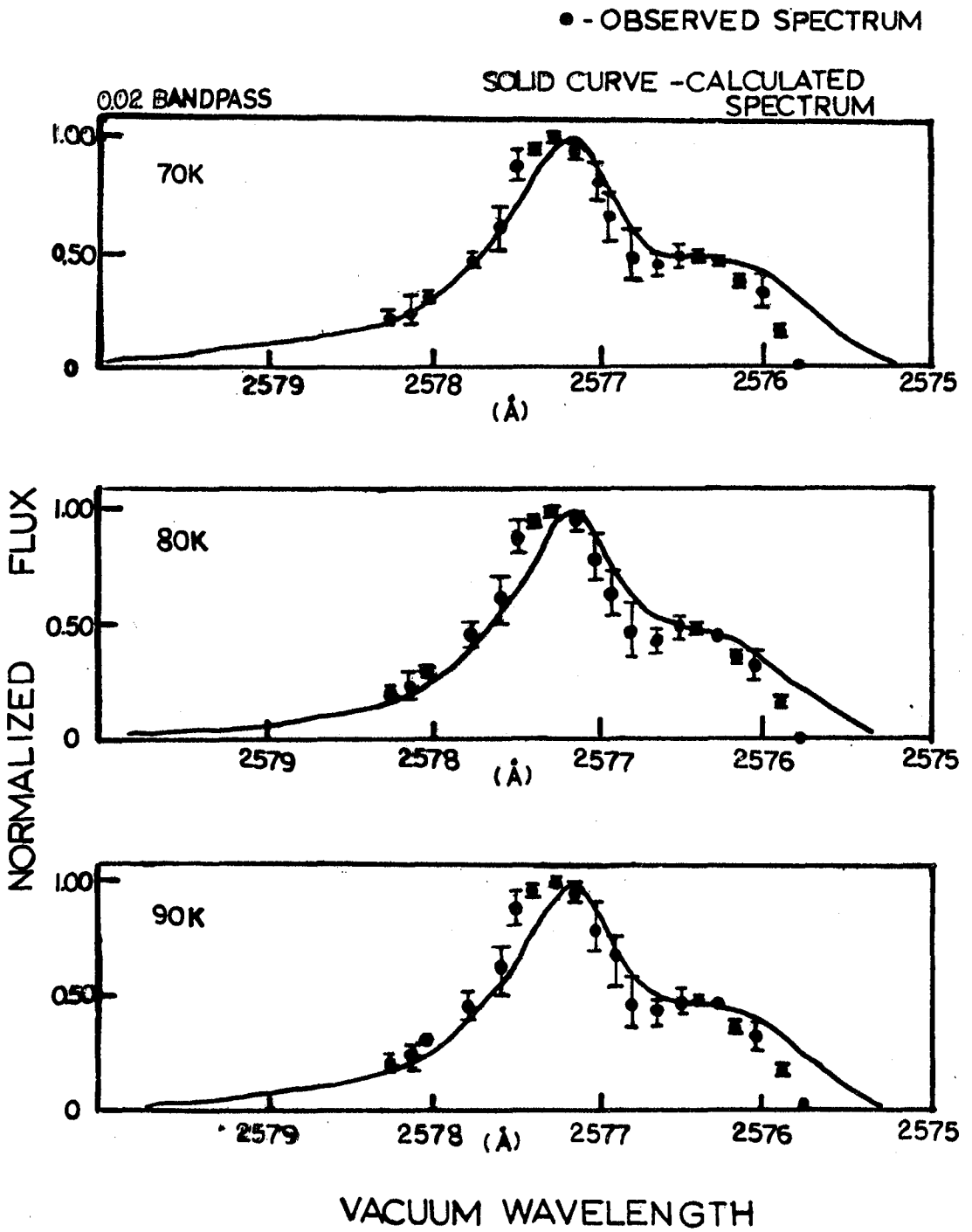

Figure 3.

Comparison between observed and theoretical CS band profiles for 0.02nm HWHM bandpass and at temperatures of 70, 80, and 90 K.

WATER PRODUCTION MODELS FOR COMET BRADFIELD (1979ℓ)*

H. A. Weaver and P. D. Feldman
Physics Department
Johns Hopkins University
Baltimore, Md. 21218

M. C. Festou
Space Physics Research Laboratory
University of Michigan
Ann Arbor, MI. 48109

ABSTRACT

IUE observations of Comet Bradfield (1979ℓ) made from 10 January 1980 to 3 March 1980 permit a detailed study of water production for this comet. Brightness measurements are presented for all three water dissociation products, H, O, and OH, and comparisons are made with model predictions. The heliocentric variation of the water production rate is derived.

INTRODUCTION

Recent observations of Comet Bradfield (1979ℓ) have convincingly demonstrated the advantages of the IUE for the study of comets. In particular, these IUE observations allow an in-depth study of the production of water, the presumed primary constituent of the cometary nucleus, as all three water dissociation products, H, O, and OH, were observed simultaneously. The excellent pointing capability of the instrument and the ability to obtain spatial imaging within the 10" x 20" aperture allowed us to map the brightness across the coma for each species at a resolution of ~1000 km, thus facilitating comparisons with model predictions. Comet Bradfield was observed at least once a week from 10 January 1980 to 3 March 1980 enabling us to follow the variation in the water production rate as the comet's heliocentric distance increased from 0.71 a.u. to 1.53 a.u. This provided another important insight into the nature of cometary phenomena.

MODEL

A radial outflow model (ref. 1) was used to interpret the data and to calculate water production rates. This is a spherically symmetric model which assumes that all species flow radially outward from the nucleus with a constant speed. The outflow velocities and characteristic lifetimes against destruction for the given atoms or molecules are the input parameters and the model then gives the density of the species as a function of distance from

*Work supported by NASA grant NSG-5393.

the nucleus. Densities are converted to column densities which are then related to surface brightness, assuming resonant scattering or resonance fluorescence to be the only important excitation mechanism for ultraviolet emission.

Figure 1 shows a comparison of model and observation for OH. The labels A and B refer to the same model but using different input parameters for v_{H_2O} and τ_{OH}. A more exact model (ref. 2), taking into account the spatial distribution of the dissociation fragments, gives essentially the same fit to the data. The derived OH production rate, Q_{OH}, depends on the chosen input parameters. It was obtained from the absolute OH brightness measurement using an excitation factor for resonance fluorescence (g-factor) calculated by A'Hearn et al. (ref. 3). Unfortunately, brightness data at projected distances $>10^5$ km are needed to choose between the two curves shown.

DISCUSSION

The study of the OH (and presemably H_2O) production rate vs. heliocentric distance shown in Fig. 2 produced some interesting and rather surprising results. It is usually assumed that this variation has an r^{-2} dependence, based on the concept that the comet's absorption of solar radiation controls the vaporization of gas from the nucleus. Our result that the production rate decreases as $r^{-3.7}$ is in disagreement with this assumption and is also quite different from the results derived from OAO-2 observations of Comets Bennett (1970 II) and Tago-Sato-Kosaka (1969 IX) (refs. 4, 5).

While the OH emission is optically thin, this is not the case for the Lyα emission of atomic hydrogen. An approximate radiative transfer calculation is used (ref. 6) to relate the measured surface brightness to column density for comparison with the model. Since our measurements are confined to regions relatively close to the nucleus we neglect radiation pressure. The data, shown in Fig. 3, are in reasonably good agreement with predictions based on the derived Q_{OH} values.

In principle we can use oxygen to distinguish between models A and B because O will be twice as abundant when τ_{OH} is half as large. However, the oxygen problem is complicated by other factors. First, it is difficult to calculate an accurate g-factor as the cometary absorption wavelength is doppler-shifted into a steeply-sloped portion of the corresponding solar line (ref. 7). Also, since the absorption takes place from a ^3P term, it is necessary to know the relative populations of the fine structure levels of the ground state. Finally, it appears that the oxygen emission is barely optically thick.

Nevertheless, some qualitative information about the source of the oxygen may be obtained from an examination of the spatial variation of the oxygen, both from offset exposures and from variation within the aperture itself. Oxygen produced from a second dissociation:

$$H_2O + h\nu \rightarrow OH + H$$

$$OH + h\nu \rightarrow O + H$$

leads to an integrated column density which is independent of projected distance near the nucleus. The data, however, show a variation in brightness near the nucleus indicating a direct dissociation source of oxygen. Two possibilities immediately come to mind. Oxygen in the ground state may be produced from direct photodissociation of H_2O via the reactions:

$$H_2O + h\nu \rightarrow O[(^1D) \text{ or } (^1S)] + H_2$$

$$O[(^1D) \text{ or } (^1S)] \rightarrow O(^3P) + h\nu.$$

The presence in our spectra of the "trans-auroral" oxygen line at 2972 Å suggests that such a process may play a role in oxygen production. If this photodissociation channel operates at a 10% efficiency level (ref. 2) (with 90% of the H_2O dissociating into OH + H) then the agreement between model predictions and the data is much better than for the case when only a second dissociation is considered (see Fig. 4). The other possibility is a source of O which is <u>not</u> water. Likely candidates are CO and CO_2. An estimate of their importance may be obtained by reference to the carbon emission lines also present in the spectrum.

CONCLUSION

The data presented here represent a small sub-set of all the Comet Bradfield observations containing spatial information about the water dissociation products. Continuation of this analysis with the remaining data should serve to place further constraints on water production models for comets.

REFERENCES

1. Haser, L.: Distribution d'intensité dans la tête d'une comète. Bull. Acad. Roy. Belgique, 43, 740-750, 1957.

2. Festou, M.: The Density Distribution of Neutral Compounds in Cometary Atmospheres II. Production Rate and Lifetime of OH Radicals in Comet Kobayashi-Berger-Milon (1975 IX). Submitted to Astron. and Astrophys., 1980.

3. A'Hearn, M. F.; Schleicher, D. G.; Donn, B.; and Jackson, W.: Fluorescence Equilibrium in the Ultraviolet Spectra of Comets Seargent (1978m) and Bradfield (1979ℓ). The Universe in Ultraviolet Wavelengths: The First Two Years of IUE. NASA CP- , 1980. (Paper of this compilation).

4. Keller, H. U.; and Lillie, C. F.: The Scale Length of OH and the Production Rates of H and OH in Comet Bennett (1970 II): Astron. and Astrophys., 34, 187-196, 1974.

5. Keller, H. U.; and Lillie, C. F.: Hydrogen and Hydroxyl Production Rates of Comet Tago-Sato-Kosaka (1969 IX). Astron. and Astrophys., 62, 143-147, 1978.

6. Festou, M.; et al.: Lyman-alpha Observations of Comet Kobayashi-Berger-Milon (1975 IX) with Copernicus, Astrophys. J., 232, 318-328, 1979.

7. Feldman, P. D.; Opal, C. B.; Meier, R. R.; and Nicolas, K. R.: Far Ultraviolet Excitation Processes in Comets. The Study of Comets, ed. B. Donn et al. NASA SP-393, 773-795, 1976.

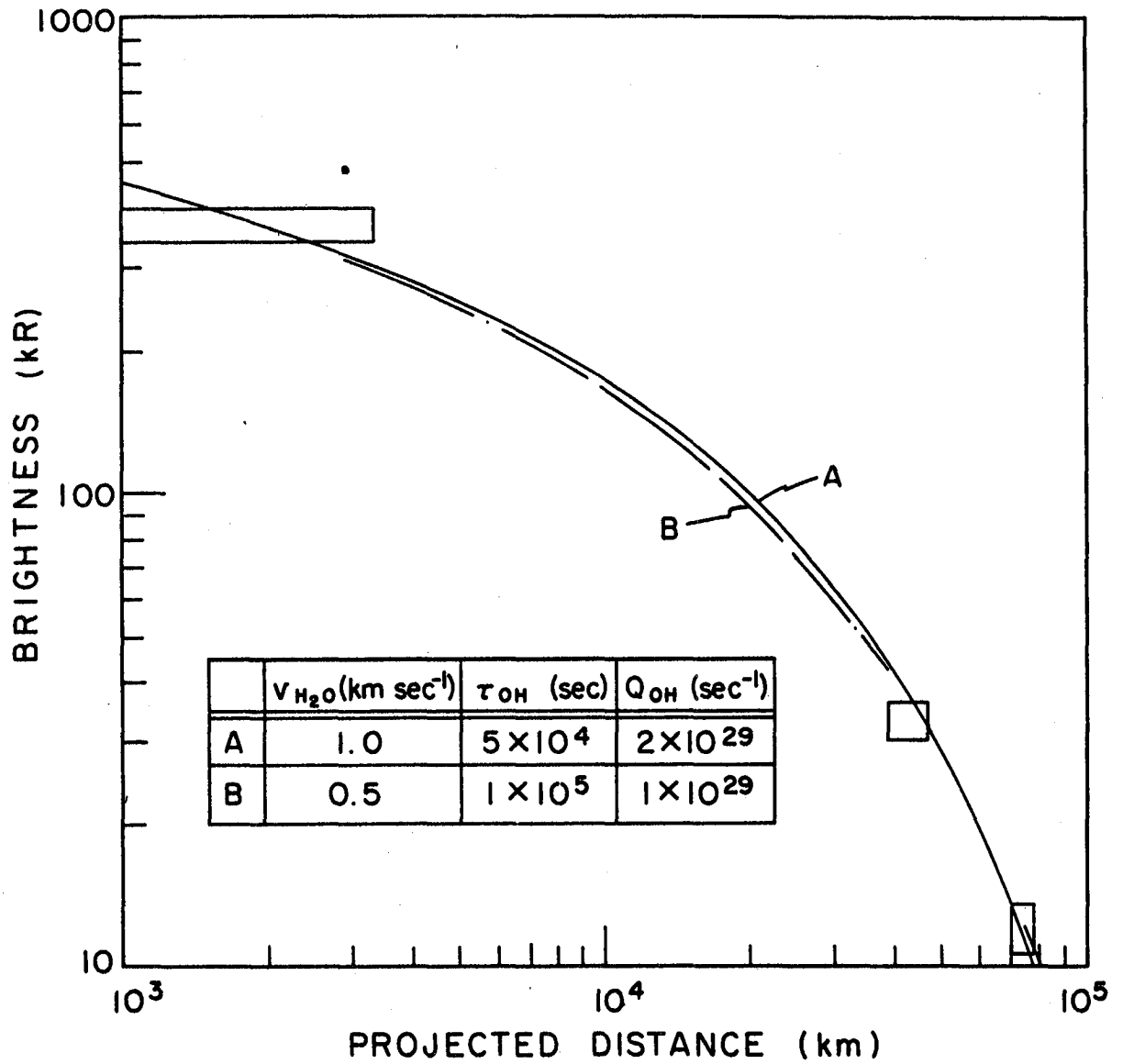

Fig. 1. Comparison of the OH (0,0) band brightness profile with a radial outflow model using the parameters defined in the insert. Data from three exposures are shown as rectangular boxes, the horizontal size being the projected length of the spectrograph slit on the comet and the vertical size the measurement uncertainty.

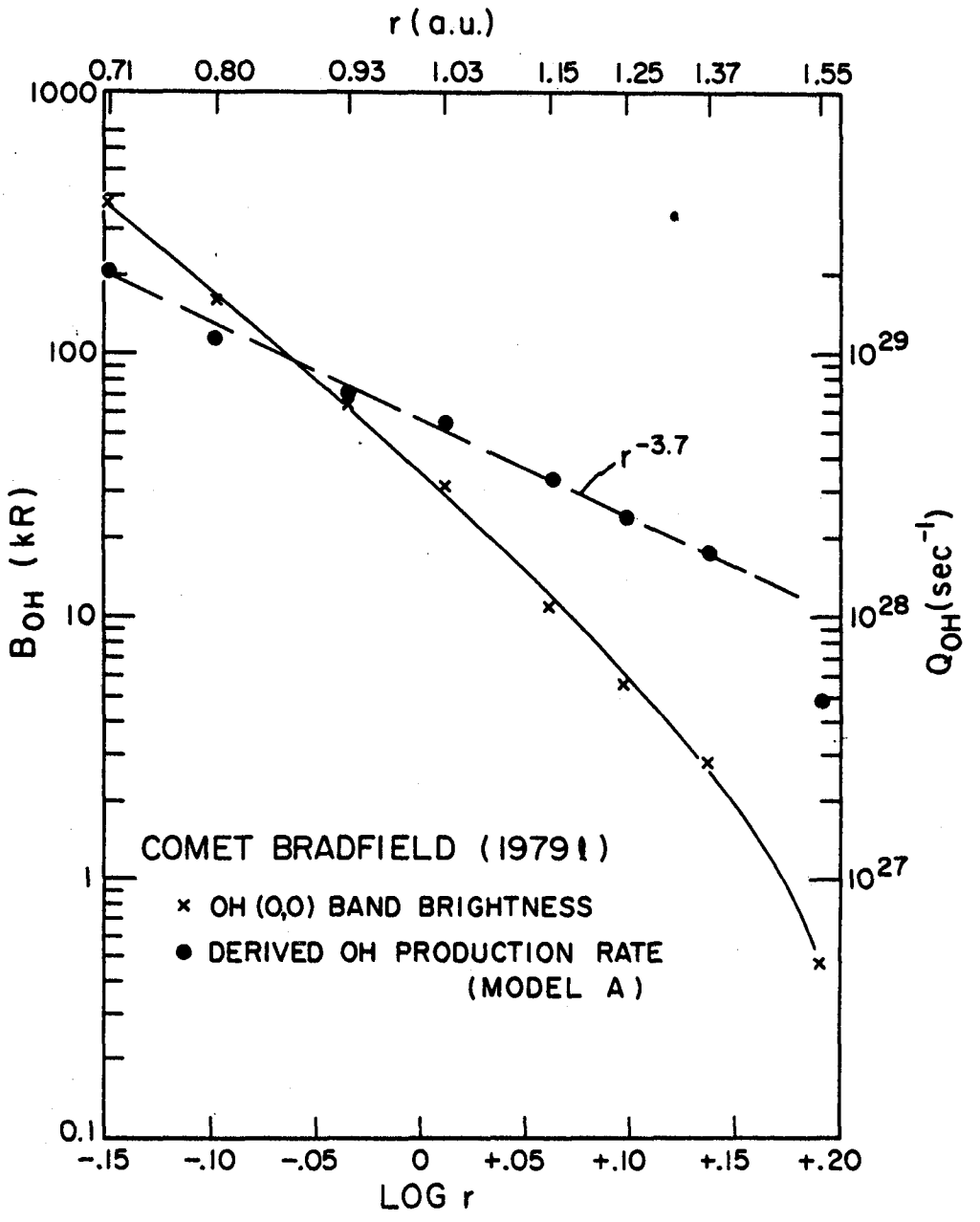

Fig. 2. Brightness of the OH (0,0) band as a function of heliocentric distance. Also shown is the derived OH production rate using model A. Model B reduces the production rate by a factor of two for each measurement but leaves the slope unchanged.

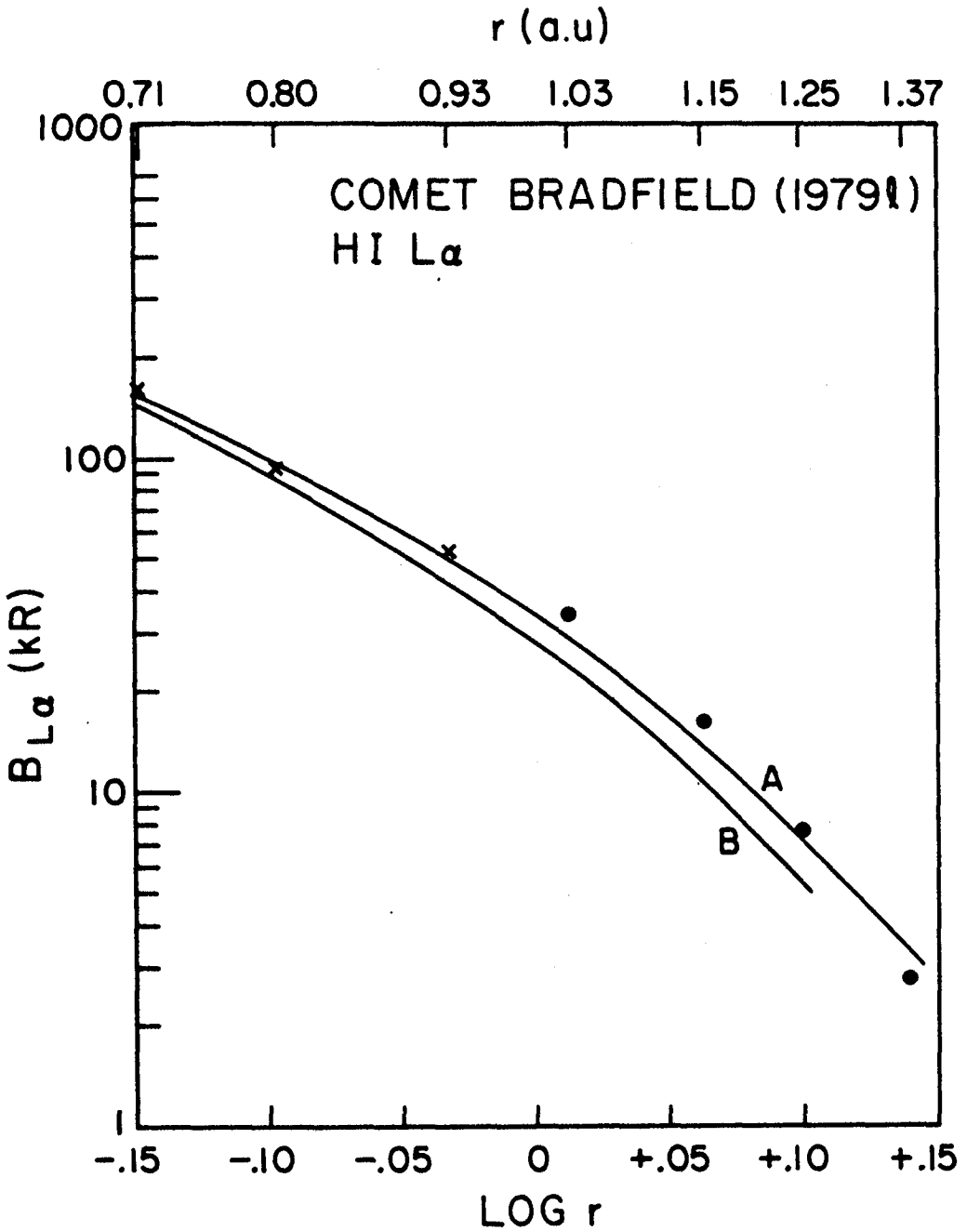

Fig. 3. The two curves show the predicted HI Lα brightness as a function of heliocentric distance using models A and B and H_2O production rates derived from the OH measurements. The plotted points represent the measured values. The dots include a subtraction of geocoronal Lα while the x's do not.

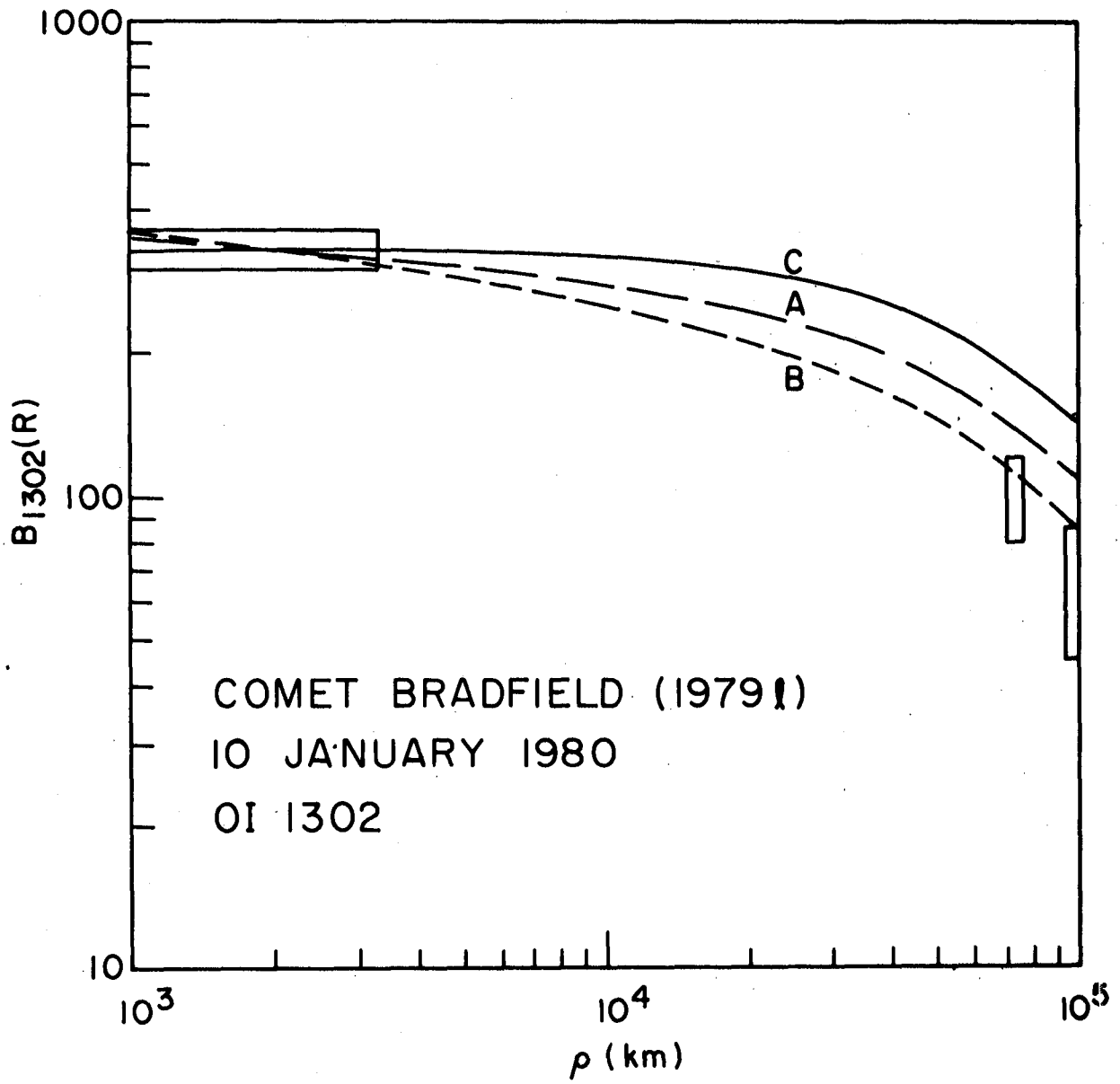

Fig. 4. Comparison of the O(1302 Å) brightness profile with model predictions. All three curves have been normalized to the observed average brightness obtained with the aperture centered on the nucleus. Curves A and B are the same as in Fig. 1 and assume a 10% branching ratio for direct production of O. Curve C is for zero branching and is the same for both models.

FLUORESCENCE EQUILIBRIUM IN THE ULTRAVIOLET SPECTRA OF COMETS SEARGENT (1978m) AND BRADFIELD (1979ℓ)

Michael F. A'Hearn and David G. Schleicher
University of Maryland

Bertram Donn, Goddard Space Flight Center

William M. Jackson, Howard University

ABSTRACT

We have carried out detailed fluorescence calculations for OH including the Swings effect. These calculations have been used to reproduce the high resolution spectra of Comets Seargent and Bradfield taken with IUE. There does not seem to be any evidence of a need for an additional population of thermalized OH radicals as suggested by some other investigators. The calculations also provide the OH fluorescence efficiencies (g factors), as a function of heliocentric radial velocity, which are needed to derive OH abundances from measured fluxes. A close examination of the spectra shows no sign of the corresponding emission bands of OD allowing us to place upper limits on the ratio N(OD)/N(OH). Preliminary attempts to reproduce the CO^+ band structure by fluorescence will also be discussed.

INTRODUCTION

As remarked by the previous speakers, derivation of abundances and production rates in comets usually assumes that the species being studied is in fluorescent equilibrium. With the exception of a few cases, this assumption has been studied and found to be true for most species observed in the optical. The assumption is much less well tested in the ultraviolet. In order to validate the assumption of fluorescent equilibrium, one must be able to reproduce all aspects of the observed spectrum. In this talk, we will consider two species, both of which have been studied to some extent previously, OH and CO^+. The observational data consist of several post-perihelion spectra of Comet Seargent (1978m) taken at $r_H \sim .9$ AU and $\dot{r}_H = +34$ km/sec plus very many spectra of Comet Bradfield (1979ℓ) taken at $0.7 \text{ AU} \leq r_H \leq 1.5$ AU and $24 \text{ km/s} < \dot{r}_H < 28$ km/s. The spectra of Comet Seargent have been described briefly by Jackson et al.[1] and those of Comet Bradfield by Feldman et al.[2]

OH The OH radical has been studied at both high and low resolution. Three bands have been observed: the 0-0 band at λλ 3080-90, the 1-1 band at λλ 3130-3150, and the 1-0 band at λλ 2800-2850. From ground-based observations of the 0-0 band, it has long been known that these bands exhibit a large Swings effect. This alone proves that fluorescence plays an important role in the equilibrium of OH but not necessarily that fluorescence is the only important mechanism.

We have carried out an extensive calculation of the fluorescence equilibrium of OH, including the Swings effect. For the calculations we have included 3 vibrational levels and 5 rotational levels in each electronic state, as well as the Λ-doubling of the levels. For the solar flux we have used the atlas of Kohl, Parkinson, and Kurucz[3] while the oscillator strengths for the various transitions have been taken from a variety of sources. The calculations predict both the integrated intensities of the bands and their detailed structure as a function of heliocentric distance and heliocentric radial velocity. (Details of the calculations will be presented elsewhere.)

The relative intensities of the 1-0, 1-1, and 0-0 bands are predicted to be 1:1:8:50 at the radial velocities of the Bradfield observations. This is in good agreement (10%) with the observed low-dispersion spectra. The 0-0 and 1-0 bands have also been examined at high resolution. Figure 1 shows the 0-0 band of Comet Bradfield at r_H = 0.71 AU and $\dot{r}_H$ = 24.0 km/sec. The dashed vertical lines represent the strengths of the lines as calculated for pure fluorescence equilibrium and then multiplied by the wavelength dependence of the long wave low dispersion camera. Because this band is near the edge of the camera response, there is almost 40% variation in sensitivity across the band. Clearly the agreement between theory and observation is excellent in this case. The fact that the longest wavelength theoretical lines are too strong by 10 to 15% may be due to either the use of the low dispersion sensitivity curve in the high-dispersion mode or to errors in the ripple-correction of the observed spectrum. This particular discrepancy does not appear to be due to a defect in the theory. Four lines are marked A through D since the ratios A/B and C/D exhibit the Swings effect most strikingly.

To investigate optical depth effects, we have used the column densities of OH derived from the low dispersion spectra combined with the theoretical calculation which predicts that, for this radial velocity, nearly all of the OH radicals are approximately evenly split between the 2 Λ-doubled components of the ground state ($^2\Pi_{3/2}$, J = 3/2, K = 1). The effective cross-section at the line center also depends on the velocity dispersion of the OH radicals. If we assume a velocity dispersion of 1 km/sec, we derive an optical depth at the line center of order unity for either of the strong lines arising from the ground state. These lines are the ones labelled A and B in Figure 1. The optical depth in any other lines should be significantly lower. Because the theoretical predictions (which assume negligible optical depth) agree so well with the observations we conclude that the velocity dispersion is sufficiently higher than the 1 km/sec assumed above that the line center optical depth is much less than unity.

The dramatic Swings effect is shown by comparing Figure 1 with Figure 2, which is the spectrum of Comet Seargent obtained at r_H = 0.93 AU and $\dot{r}_H$ = +34.0 km/sec. According to theory, the change in heliocentric distance should have only very small effects on the spectrum so that the large differences are due to the change in radial velocity from +24 to +34 km/s. Note particularly the ratios A/B and C/D in the two figures. The theoretical calculations for Comet Seargent do not agree with observation as well as in the case of Comet Bradfield although we still have agreement within about 25% on all lines. Differences between the two cases include: 1. somewhat different IUE data processing, 2. Comet Seargent was somewhat brighter and at

greater heliocentric distance so that optical depth effects may be noticeable, 3. the difference in the relative populations of the 2 Λ-doubled levels of the ground state may allow collisional effects to appear. At present, however, we feel that the agreement is good enough that further processes, although possibly significant, can not be justified on the basis of this data alone.

To further test the fluorescence predictions we have examined the 1-0 band in Comet Bradfield as shown in Figure 3 which is taken from the same spectrum as Figure 1. Because the 1-0 band has only .02 the intensity of the 0-0 band, the signal-to-noise ratio in Figure 2 is considerably worse than in Figure 1. Nevertheless, the agreement between theory and observation is excellent. Furthermore, we have extracted one emission line from 2 adjacent orders, as shown in the figure, and it tends to confirm our hypothesis that the echelle ripple correction is the cause of the discrepancy at the long-wavelength end of Figure 1. Note that in Figure 3, there has been no correction for the spectral sensitivity of the IUE spectrograph system because the low-disperion system varies in sensitivity by only 2% across Figure 3.

Another aspect of the OH spectrum is the study of the isotopically shifted bands expected from O^2H. A careful examination of the spectrum of Comet Seargent shows no trace of the O^2H bands and, assuming that both forms are in fluorescent equilibrium, this allows us to set an upper limit on the column density ratio $N(O^2H)/N(O^1H) \leq .01$. Much longer exposures on Comet Bradfield, not yet analyzed, will provide us greatly improved sensitivity for this determination.

Summarizing our work on OH, we feel that pure fluorescence equilibrium adequately describes the data thus far obtained. We now move to another species for which we will derive exactly the opposite conclusion.

$\underline{CO^+}$ The First Negative system of CO^+ ($B^2\,E^+ - X^2\,E^+$) was identified in rocket spectra of Comet West by Feldman and Brune[3] and by Smith et al. (private communication). The spectra showed the $\Delta V = +1$, 0, -1, and -2 sequences. The IUE spectra of both Comets Seargent and Bradfield, however, show a completely different structure for the CO^+ bands. Because these bands are weak compared to those of OH, we have studied them only in low resolution spectra. Figure 4 shows the relevant portion of a low resolution spectrum of Comet Bradfield. The origins of many of the CO^+ bands are also shown.

Krishna-Swamy[4] has carried out a fluorescence calcuation for CO^+ to predict the relative intensities of the different bands and according to his predictions the $\Delta V = 0$ sequence should be the strongest sequence. This is what was observed in Comet West but appears not to be true for Comets Seargent and Bradfield, in both of which the $\Delta V = 0$ sequence is entirely absent. Because Krishna-Swamy gave only relative band strengths with no calibration to absolute number of molecules and because he used a solar atlas which, at these wavelengths, seems to have serious systematic errors, we have begun our own calculations of CO^+ fluorescence in an attempt to explain our anomalous data. For a preliminary calculation we have omitted the Swings effect (as did Krishna-Swamy) because the rapid acceleration of CO^+ ions should smear out the heliocentric radial velocities enough that the Swings

effect is negligible. Also for our preliminary calculations, which serve mainly to provide an absolute scale for the fluorescence efficiency, we have omitted B-A (Baldet Johnson) and A-X (Comet Tail) Systems. We derive somewhat different intensity ratios than did Krishna-Swamy, but we still find that the $\Delta V = 0$ sequence should be as strong as the $\Delta V = -1$ sequence.

In order to investigate the possibility of optical depth effects, suggested as a possibility in our paper describing the original Bradfield results (Feldman et al. 1980), we have assumed that the feature at λ 2310 is indeed the $\Delta V = -1$ sequence of CO^+ and that it is fluorescently pumped. This yields a column density of CO^+ only 1% of that of OH in Comet Bradfield. This in turn implies that the optical depth in the $\Delta V = 0$ sequence of CO^+ is less than that of OH, probably a few tenths. If the velocity dispersion of CO^+ is significantly greater than 1 km/sec, as one would expect, then the optical depth is negligible. Optical depths, therefore, can not explain the anomalous intensities.

One other significant difference between these observations and those of Comet West is that IUE observes only a small region near the nucleus while the rocket spectra of Comet West sampled most of the coma. If these spectral features are indeed CO^+, then possibly we are seeing highly vibrationally excited bands (e.g., 4-4 and 5-5) which might be due either to collisions or to direct production of CO^+ in excited states. Even these hypotheses are difficult to accept because they must completely overwhelm the fluorescence mechanism. In any case, it is clear that these emission features are not due to CO^+ in fluorescent equilibrium.

NOTE ADDED IN PRESS

Further analysis by A'Hearn and Feldman suggests that the "CO^+" bands are, in fact, not due to CO^+. The feature at λ 2310 is due to the Mulliken bands of singlet C_2, while the feature at λ 2430 is due to Lyman alpha in second order.

REFERENCES

1. Jackson, W. M. and many others: 1979 Astron. & Astrophys. 73, L7.

2. Feldman, P. D. and many others: 1980 Nature (in press).

3. Kohl, J. L., W. H. Parkinson, and R. L. Kurucz: 1978 "Center and Limb Solar Spectrum in High Spectral Resolution 225.2 nm to 319.6 nm" (Harvard-Smithsonian Center for Astrophysics).

4. Feldman, P. D. and W. H. Brune: 1976 Ap.J. 209, L45.

5. Krishna-Swamy, K.S.: 1979 Ap. J. 227, 1082.

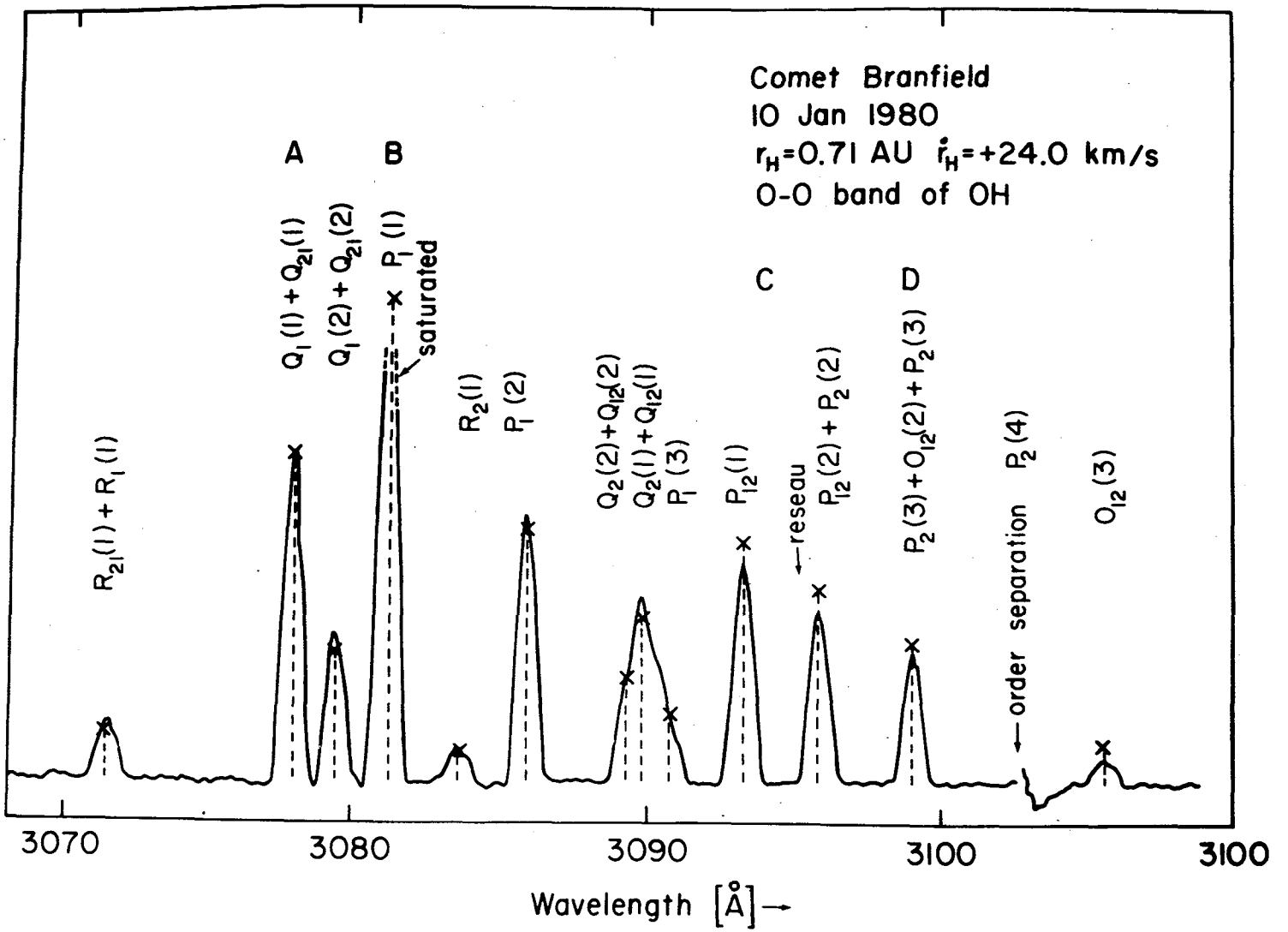

Fig. 1: High-dispersion spectrum of O-O band of OH in Comet Bradfield. Dashed vertical lines are the theoretical line intensities based on pure fluorescence equilibrium. Compare the line ratios A/B and C/D in this figure and Figure 2.

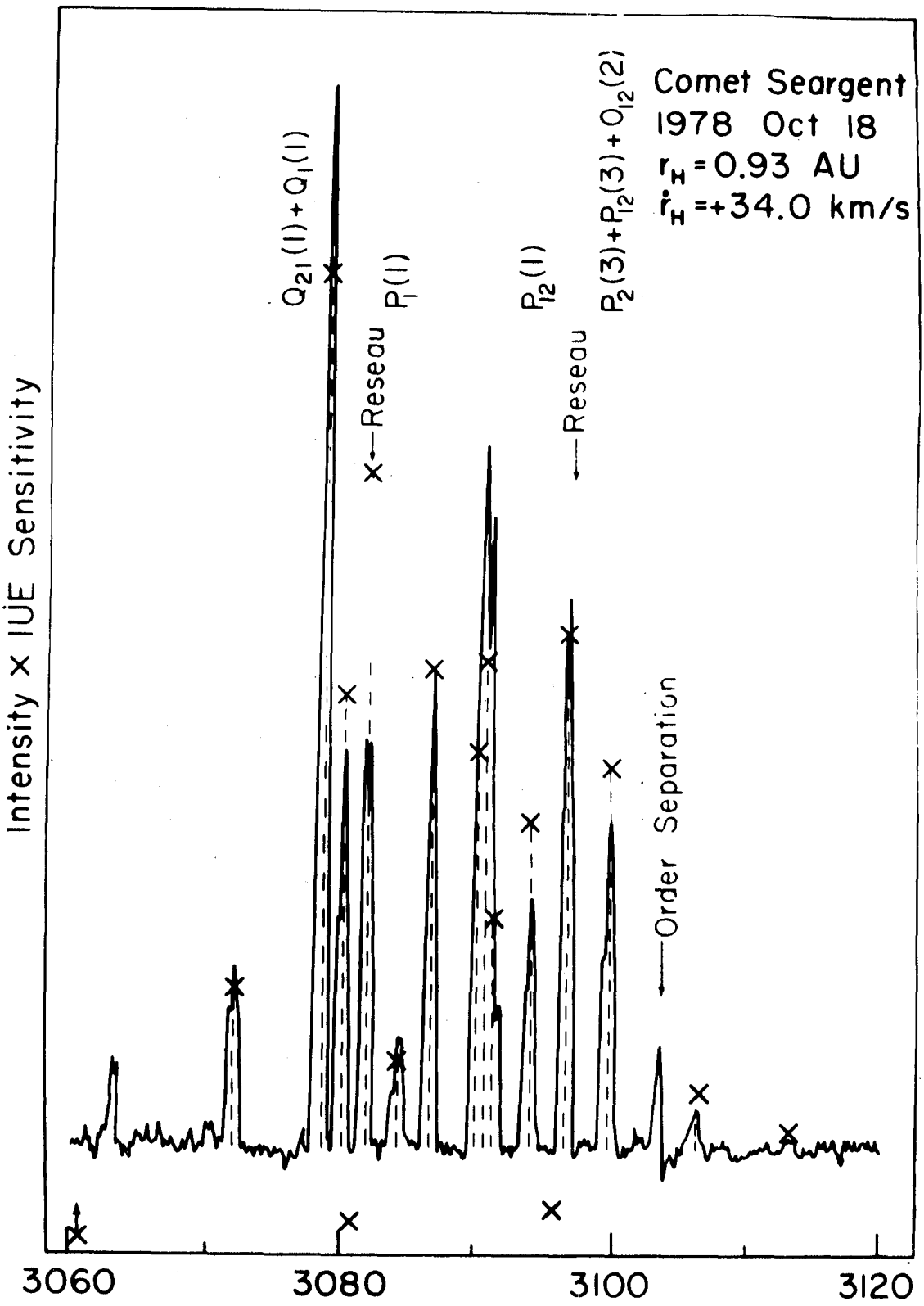

Fig. 2: High-dispersion spectrum of 0-0 band of OH in Comet Seargent.

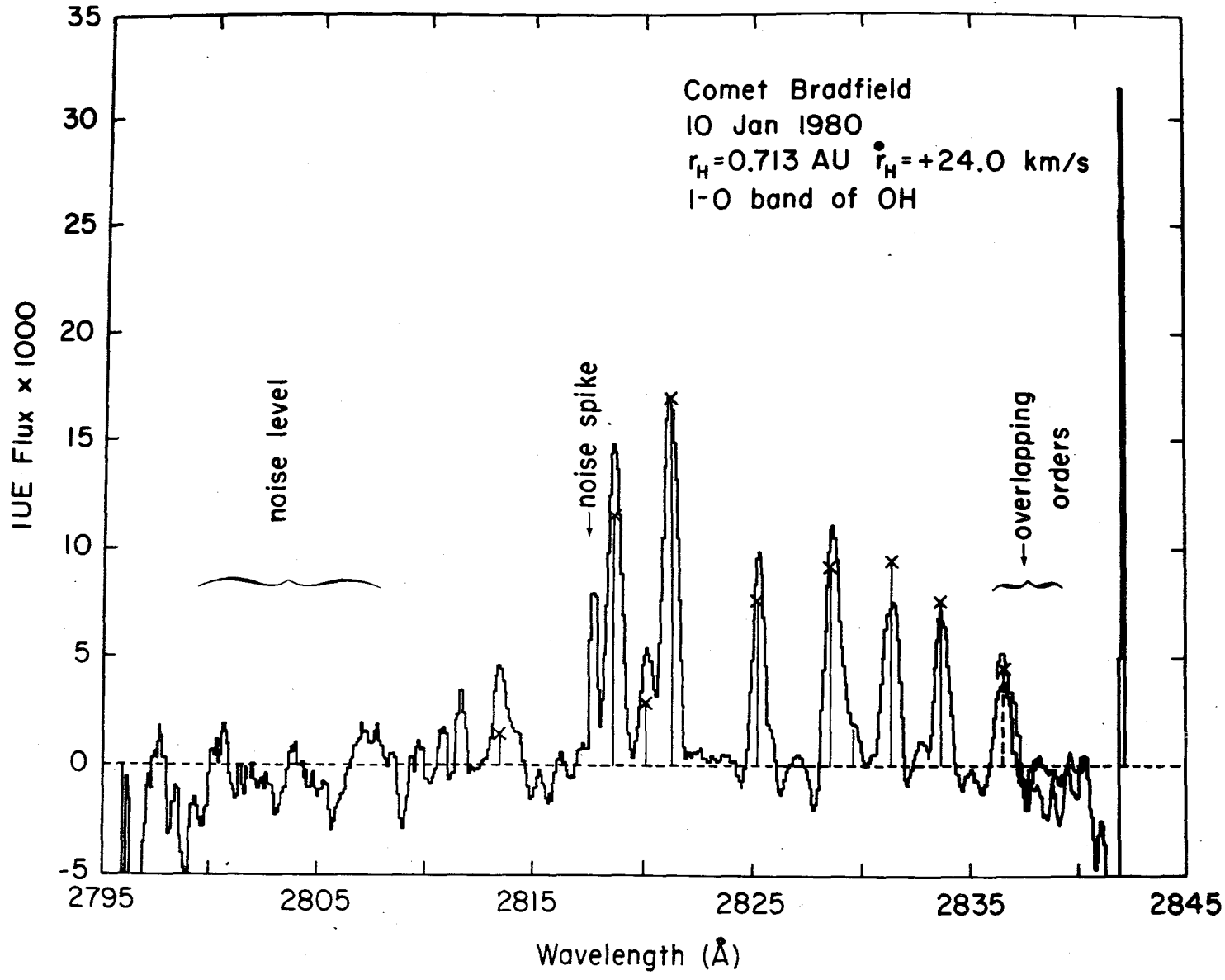

Fig. 3: High-dispersion spectrum of 1-0 band of OH in Comet Bradfield. Taken from same exposure as Figure 1.

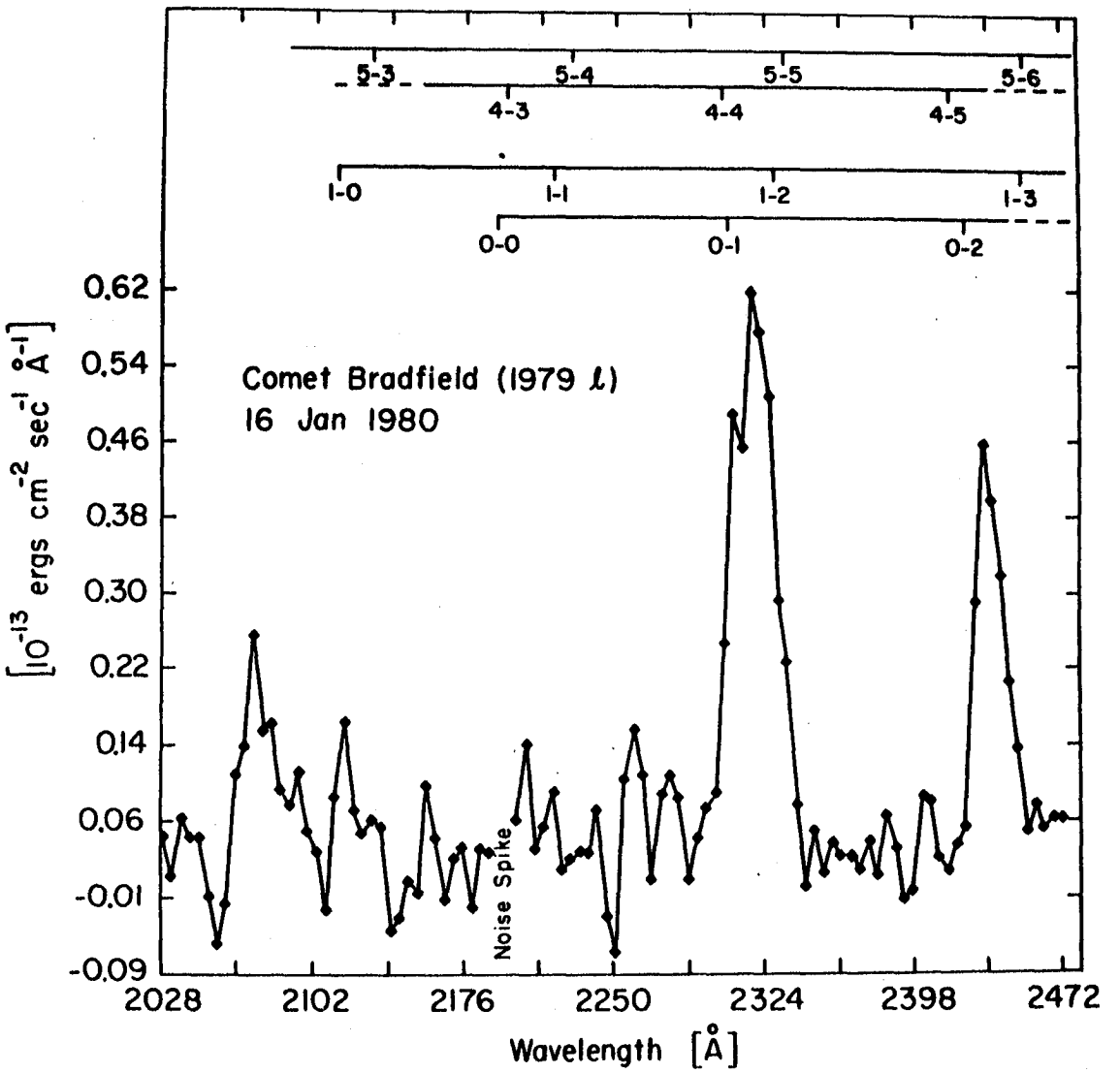

Fig. 4: Low-dispersion spectrum of Comet Bradfield in the region of the CO^+ bands. Origins of various CO^+ bands are indicated.

OBSERVATIONS OF URANUS WITH THE INTERNATIONAL ULTRAVIOLET EXPLORER

John Caldwell, Tobias Owen, A. R. Rivolo, V. Moore
Earth and Space Sciences Department
S.U.N.Y. at Stony Brook
Stony Brook, NY 11794

P. S. Butterworth
University of Leicester
Leicester, United Kingdom

G. E. Hunt
Department of Physics and Astronomy
University College London
London, United Kingdom

ABSTRACT

Published reports of infrared spectrophotometry of Uranus (ref. 1) disagree concerning the presence or absence of a high altitude (stratospheric) haze layer in the atmosphere of Uranus. An analysis of broadband ultraviolet photometry from the ANS by Savage, Cochran and Wesselius 1980, favors a stratospheric haze, and further suggests a decrease in albedo from 2200 Å to 1800 Å. The latter phenomenon is important because many molecules of planetary interest have strong, broad, electronic transitions below 2000 Å, and observations here could provide an important means of studying trace constituents. IUE observations of Uranus are not inconsistent with a stratospheric haze, but would equally well match a clear stratosphere model if a plausible modification of standard solar photometric properties is allowed. Exposures of up to 5 hours of the SWP on board IUE indicate that the reflectivity of Uranus is flat from 2200 to 1800 Å, in conflict with Savage et al. The observations from the two satellites were made 5 years apart, and Uranus is known to be changing in other spectral regions (ref. 2). However, we conclude there is no basis for modelling trace constituents of the Uranian stratosphere at this season. This research is supported in part by NASA grant NSG 5250 at Stony Brook.

REFERENCES

1. Price, 1978, Icarus 35, 93; Fink and Larson, 1979, Astrophys. J. 233, 1021.

2. Klein and Turegan, 1978, Astrophys. J. 224, L31.

Observation of Outer Planets at Lyman Alpha

Jon Darius
Astronomy Division, ESTEC

K.H. Fricke
Physikalisches Institut der Universitat Bonn

DARIUS : In your SWP spectra, did you make any attempt to rescue Uranian photons from geocoronal and interplanetary Lyman alpha?

CALDWELL: We haven't tried that.

DARIUS : In that case you may be interested to learn

Three weeks ago at the IUE ground station near Madrid we carried out a triple planetary observation in one IUE shift to measure the Ly-α reflectivity of Jupiter, Saturn, and Uranus. The exposures were planned to take account of the light travel times, Sun to planet and planet to Earth, in order to assess the response of the three atmospheres to essentially the same incident solar flux. Automatically eliminated are all additional uncertainties introduced when different instruments are used for such a comparative measurement.

Jupiter and Saturn were observed at the centres of their discs in the large aperture of the SWP camera at low resolution. With an angular diameter of 38".7, Jupiter completely filled the large aperture and tracking was checked using an ephemeris for Ganymede (J3) in the (x,y) co-ordinate system of the Fine Error Sensor (FES). Saturn (17".4) effectively filled 70% of the large aperture, and any deviation from the applied drift rate could be checked by the FES counts. The disc of Uranus (3".8) was centered in the small aperture and a simultaneous exposure carried out in the SWP large aperture to facilitate correction for non-planetary Lyman α emissions.

Integrated flux numbers $\int FN d\lambda$ were obtained from the line-by-line spectrum by fitting a Gaussian bell curve with a low order polynomial as background estimate. This method effectively removes isolated hot spots and the scattered light in the dispersion direction. Interpolation in the mean sensitivity table of Bohlin et al., (1980) yield 1.82×10^{-3} photons cm^{-2} $\AA^{-1} FN^{-1}$ at Lyman α. If we apply this calibration and combine the photon statistical error with the error in $\int FN d\lambda$, we obtain the first line in Table 1.

Now the contaminating sky signal at Lyman α (large aperture) can be subtracted from the Uranus+sky signal (small aperture) by scaling up by the ratio of the exposure times and scaling down by the ratio of solid angles subtended by the two aperatures. The former is uncontroversial; but whereas the official value of the latter, ω_{LA}/ω_{SA}, is 26.5 ± 3.7 based on pre-flight

measurements (Bohlin et al. 1980), independent in-flight evidence from six images of geocoronal Lyman α (Ojanguren 1979), lend credence to a ratio of 31.7 ± 1.5 for the energy received in the two apertures. The succeeding argument will be invalidated should this contention prove incorrect.

For the sake of a preliminary analysis, without prejudice to application of a better model for the interplanetary and geocoronal hydrogen in due course, we take the ratio of interplanetary to geocoronal Lyman α emissions to be 7:3 (IUE being near apogee) and assume that we shall have overestimated the contaminating interplanetary emission by 20% at Uranus, by 40% at Saturn, and by 70% at Jupiter - granted that the geocoronal contribution remains constant in each case. These figures include a geometric correction for planetary position with respect to the upwind direction. The configurations of the outer planets, the brightest satellites, and the large-aperture orientation on April 14 does not compel us to correct for additional non-planetary signal.

The column emission rates at the planets (in kiloRayleighs) in Table 1 are derived in the usual fashion after dividing the corrected fluxes by the size of the aperture and the length of exposure. An upward adjustment has been applied for the estimated line-of-sight absorption by neutral hydrogen and for the center-to-limb variation on the planet. Allowing for the inverse-square sun-planet distance falloff of the illuminating solar flux and normalizing to Jupiter, we obtain the relative Ly-α reflectivities in the last line of Table 1. (We draw attention also to the apparent drop in the Ly-α brightness of Jupiter from its March 1979 (Broadfoot et al., 1979) value back to the 1978 Copernicus level (Cochran and Barker 1979), and shall comment elsewhere.)

Within the errors, it could not be claimed on the basis of these recent IUE observations that the albedos of Jupiter and Saturn at Ly-α substantially differ; indeed, prior studies support a normal $1/r^2$ dependence (Weiser et al. 1977). On the other hand, the relative albedo of Uranus is so high as to disarm though not quell suspicion that it can be explained by errors inherent in our presently naive model. (One issue to be satisfactorily resolved, of course, is the disagreement over the correct aperture ratio. Bohlin (1980) has commented that the official large-aperture area may have been over-estimated, in which case we contend that the small aperture must be further diminished.) Assuming the high reflectivity to be real, one may be able to account for it in several ways. The possibility that it reflects a fluctuation in incoming solar flux is fortunately excluded by the way the present observations were conducted.

The observational geometry was such, that at Jupiter and Saturn the centre of IUE field of view lies in the planets' equatorial, but for Uranus in high northern latitudes. As the phase angle are small, the same is essentially true for the solar illumination direction. Production of neutral hydrogen atoms will proceed via solar EUV ionization with follow up ion molecule reactions. The total production rates at the planets will scale with the inverse squared distance from the Sun. For the rapidly rotating planets the global average is one fourth of the total production rate. This implies that with the present viewing geometry for Uranus the average production rate

on the sunlit hemisphere will be relatively enhanced over the scaled average production rates of Jupiter and Saturn, unless rapid interhemispherical convection exists. Additionally, the eddy diffusion coefficient, which controls the downflow of the dissociated H-atoms to the recombination altitude, (Wallace and Hunten, 1973) may vary with latitude as it is known to do in the terrestrial atmosphere. Both processes may lead to a greater reservoir of H scatterers above the absorbing methane layer, and correspondingly contribute to the observed high Ly-α albedo. Brown (1976) has reported radio emissions, which possibly originated at Uranus. If the direction was indeed correctly identified, this observation would imply the existence of a magnetic field and hence magnetosphere at Uranus, from which particles may precipitate and cause greatly enhanced Ly-α emissions in the auroral zones (see e.g. Figure 5 of Broadfoot et al., 1979). If the Uranian dipole is approximately aligned with the spin axis, one complete auroral zone was in the central part of the IUE field of view during our observation. Such additional emissions besides resonantly scattered solar photons would greatly help to explain the large observed Uranian Ly-α albedo.

Albedo measurements of Uranus by Savage et al. (1980) using ANS reveal a suspected decline below 2000 Å which may require the presence of both aerosol particles and an additional absorbing agent (micron-size particles or gaseous compounds like CS_2 of PH_3). In the far ultraviolet, however, the potential depressive effect of the former becomes negligible.

In any case, new IUE measurements (Caldwell et al. 1980) do not support the 20% shortward albedo drop inferred from the uncertain ANS measurement at 1800 Å and moreover do not necessarily require an absorption stratospheric haze. Further study of relative brightness among the outer planets is in progress.

REFERENCES

Bohlin, R.C., 1980, private communication.

Bohlin, R.C., A.V. Holm, B.D. Savage, M.A.J. Snijders and W.M. Sparks 1980, Astron. Astrophys., in press.

Broadfoot, A.L. et al. 1979, Science 204, 982.

Brown, L.W. 1976, Astrophys. J. 207, L209.

Caldwell, J., Owen, T., Rivilo, A.R., Moore, V., Butterworth, P.S. and Hunt, G.E. 1980, this symposium.

Cochran, W.D. & Barker, E.S. 1979, Astrophys. J. 234, L151.

Ojanguren, O. 1980, thesis, Universidad Central de Madrid.

Savage, B.D., Cochran, W.D. & Wesselius, P.R. 1980, Astrophys. J. 237, in press.

Wallace, L. & Hunten, D.M. 1973, Astrophys. J. 182, 1013.

Weiser, H., Vitz, R.C. & Moos, H.W. 1977, Science 195, 755.

Table 1

Lyman Alpha Measurements of Jupiter, Saturn, and Uranus

	Jupiter	Saturn	Uranus
Observed signal (photons cm^{-2})	1072 ± 44	1792 ± 58	148 ± 12
Contaminating emission (photons cm^{-2})	85	740	94
Column emission rate at planet (kR)	9.3	3.6	1.9
Relative reflectivity for Ly-α	1.0	1.2	2.7

DISCUSSION

CALDWELL: I am not too surprised by your results; they may be explicable in terms of the presence of methane vapour in the upper atmospheres of Jupiter and Saturn suspected to be absent in Uranus.

Michalitsianos: What are the strongest bands of OH molecular emission, and at what wavelengths do they occur? What references are appropriate for molecular data?

P. Feldman: The (0,0) band at 3065-3090Å is the strongest feature in a cometary spectrum. The molecular spectrum at high resolution was measured at Johns Hopkins in 1947 by Dicke and Crosswhite and published in 1961 in J. Mol. Spectroscopy.

Maran: Is there any thermodynamic problem with CS as a parent molecule in the cometary nucleus?

P. Feldman: I don't believe so.

P. Feldman: Why is the other line in the O I 1356 doublet not apparent in the spectrum shown?

Durrance: The transition probability for the other member of the doublet at 1358.5 Å is almost an order of magnitude smaller than this one.

Maran: If Mariner 9 were still operating, would IUE tell you anything about ozone on Mars that Mariner 9 could not?

Conway: The contribution of IUE is to observe the variation of ozone during seasons, especially in the south, not observed by Mariner 9.

P. Feldman: Is the Lyman α bulge on Saturn associated with the rings?

Clarke: This feature may be associated with either the rings, the atmosphere of Titan, or the atmosphere of Saturn. However, the rings appear to present the most likely source.

Maran: What was the limit on the Lα surface brightness when you <u>didn't</u> detect polar aurora?

Clarke: The central Lα brightness on December 10, 1980 was 14 kR, including ~2 kR of geocoronal background.

Roman: Do the discrepancies between the densities derived from IUE and from Voyager indicate a variation in the short time between the observations or inaccuracies in the measurements?

Moos: The reason for the difference is not clear at the present time. I do not believe that it is due to temporal variations in the torus.

Maran: Is CS_2 stable in the solid state in the cometary nucleus?

W. Jackson: Yes.

W. Jackson: Did you put a variable OH photochemical lifetime in your model?

Weaver: No; we assume the same lifetime for all values of heliocenturi distance. This should be adequate since the variation in heliocenturi velocity was not large.

Benvenuti: How long was the exposure you used to observe the O I profile? Did you check the stability of the Comet nucleus within the large aperture?

Weaver: Two hours. The drift during the exposure appeared to be only a few arc seconds. The S I image appears nearly pointlike and this argues for a small drift.

Dubin: Festou derived a lifetime of OH from the radial distribution of DH from the nucleus while you indicated a lifetime between 1×10^5 and 5×10^4 sec. Can you state a more precise value for the lifetime?

Weaver: The derived lifetime depends on the choice of H_2O outflow velocity which is not well known. For a velocity of 1 km s^{-1} the lifetime is 5×10^4 sec, while for $=0.5$ km s^{-1} the lifetime is 1×10^5 sec. Observations at projected distances greater than 10^5 km should allow us to choose between these two.

II. O–A STARS

NEW INSIGHT INTO THE PHYSICS OF ATMOSPHERES OF EARLY TYPE STARS

Henny J.G.L.M. Lamers

Space Research Laboratory
Astronomical Institute
Utrecht/The Netherlands

ABSTRACT

The insight into the physics of atmospheres of early type stars obtained from IUE observations is discussed. The paper is concentrated on the phenomenon of mass loss and stellar winds from hot stars, since many of the IUE observations of early type stars were directed to that problem. The mass loss rate of early type stars increases by about a factor of 10^2 to 10^3 during their evolution. This seems incompatible with the radiation-driven wind models and may require another explanation for the mass loss from early type stars. The winds of early type stars are strongly variable and the stars may go through active phases. Eclipses in binary systems by the stellar winds can be used to probe the winds. A few highly interesting future IUE studies are suggested.

I. INTRODUCTION

Ultraviolet astronomy has changed our ideas about early type stars (O,B,A) rather drastically. About fifteen years ago there was a general tendency to believe that the atmospheres of these stars were reasonably well understood. Although there were still quantitative discrepancies between observed and predicted spectral features, the physical processes in the atmospheres were considered to be well known. In a way, the atmospheres of hot stars were very simple: a they were in hydrostatic equilibrium, b and in radiative equilibrium, convection not being important c the opacities are mainly due to simple atoms.

Although these physical assumptions were simple, the actual calculation of stellar atmospheres was still difficult, because of two complicating factors: firstly, the large radiative intensities and the small particle densities made it necessary to consider deviations from thermodynamic equilibrium (non-LTE) in the calculation of the continuum and line opacities. And secondly, the effect of line-blanketing in the ultraviolet could change the temperature stratification of the atmospheres by back-warming. At about that time Mihalas and colleagues started the calculation of non-LTE models, while Morton and co-workers calculated the first line-blanketed model atmospheres for hot stars. It would be just a matter of time and bigger computers to bring the theory and observations into agreement.

There were a few stars (and very few astronomers) that did not fit this general scheme: e.g. the Wolf-Rayet stars with their strong emission lines and large outflow velocities; the star P Cygni with its characteristic line profiles (P Cygni profiles) indicating mass ejection; the shell stars with their narrow shortward shifted absorption lines; the magnetic Ap-stars and the metallic Am-stars with their peculiar abundances. It was obvious that for these stars additional physical processes had to be

taken into account, such as mass-ejection or magnetic fields. However, as these kinds of stars were rather extreme, their existence did not shake the general belief that the atmospheres of early type stars are in principle very simple and not very exciting.

The physical reason for this was, of course, the fact that the visual spectrum only shows us the tail of the energy distribution curves for the early type stars. Since the radiation in this tail is not very sensitive to the physical processes in the atmospheres, most of the interesting properties of early type stars remained hidden for the ground-based astronomers by the Earth's atmosphere. It is in this respect not surprising that UV astronomy in general and the Copernicus and IUE observations in particular have changed our insight into the structure and evolution of early type stars.

In this paper I will concentrate on the new knowledge obtained by IUE, extending the many interesting results obtained by the Copernicus satellite, on the structure and stability of early type stellar atmospheres.

II. MASS LOSS IN THE HR-DIAGRAM

The first high-resolution UV observations of Morton and his colleagues (e.g. Morton, 1967) showed that early type supergiants are ejecting mass with a velocity of about 2000 km/s at a rate of about 10^{-6} $M_\odot$/yr. The Copernicus satellite has extended these observations to a large number of stars (Snow and Morton, 1976; Lamers and Snow, 1978), indicating that all early type stars with $M_{bol} < -6$ ($L > 2\ 10^4\ L_\odot$) are losing mass at a rate high enough to be observable ($\dot{M} > 10^{-9} - 10^{-10}$ $M_\odot$/yr). Stars with lower luminosity only lose mass if their rotational velocity is large enough ($v \sin i > 200$ km/s) (Snow and Marlborough, 1976; Lamers and Snow, 1978).

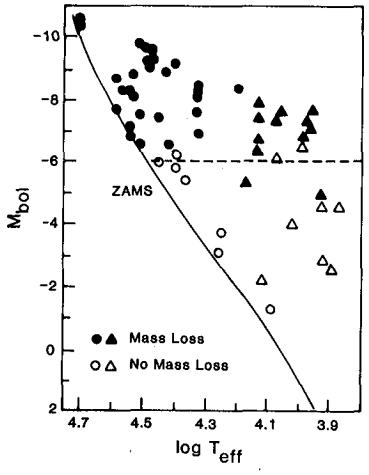

Figure 1

The distribution of stars with and without observable mass loss in the HR diagram. Circles: Snow and Morton (1976) Copernicus; Triangles: Lamers et al. (1980a); IUE.

The Copernicus observations left a gap in the hot part of the HR diagram unobserved; the region of $T_{eff} < 20\ 000$ K and $M_{bol} > -6$ occupied

by stars of types B3 and later, and luminosity classes III, II and Ib. Lamers et al. (1980a) have filled in this gap with IUE observations of 22 stars of spectral types B5 to F0. The search for mass loss indicators in the UV resonance lines (P Cygni profiles or extended violet absorption wings) is summarized in Figure 1. This figure shows that the limit of observable mass loss occurs at $M_{bol} \simeq -6$ over the entire range of $7500 < T_{eff} < 40\,000$ K. If we remember that the evolutionary tracks of massive stars are approximately horizontal in the HR diagram, this implies that stars which do not lose mass at the main sequence ($M_{bol} > -6$) will not lose mass in the hydrogen shell-burning phase either. Stars which do suffer mass loss on the main sequence will continue to do so in the hydrogen shell-burning phase.

The fate of rapidly rotating stars of $M_{bol} > -6$ at the main sequence is still uncertain. They may lose mass during the hydrogen core burning, but when the star expands with conservation of angular momentum in each layer, the rotation-induced mass loss may stop. IUE observations of slightly evolved B-stars are required to answer this question.

Apart from the region in the HR diagram shown in Figure 1, mass loss also occurs in very hot highly evolved stars like some O-subdwarfs and central stars of planetary nebulae. These will be discussed by Heap (these proceedings).

III. MASS LOSS RATES

The most extended set of mass loss rates for early type stars prior to IUE was from Barlow and Cohen (1977) based on the infrared excess of 44 luminous O, B and A stars, ranging in temperature from 8500 to 50000 K. The rates derived by these authors show a correlation with luminosity: $\dot{M} \propto L^{1.15}$. These observations provided a very strong argument in favor of the radiation-driven wind theory from Castor et al. (1975) which predicted $\dot{M} \propto L^{1/\alpha}$ with $\alpha \simeq 0.80$ and a very weak dependence on gravity. However, the stars studied by Barlow and Cohen were only supergiants and there was some indication that at least one main sequence star (τ Sco, BO V) had a much smaller rate.

Recent IUE observations of main sequence O-stars have changed this picture drastically. A combination of the mass loss rates from evolved O and Of stars (Lamers et al., 1980b) with those of unevolved O V stars (Conti and Garmany, 1980) shows very clearly that the mass loss rate is not a simple function of luminosity, but that it increases drastically from O V, through O III or O(f) to O f stars (Figure 2). The rates for O (f) and O f stars are about a factor 30 and 100 respectively, larger than those for O V stars of the same luminosity. The rates for WR-star of the same luminosity are about a factor 10 larger than for the O f stars. Remembering that the evolutionary tracks are approximately horizontal in the HR diagram, we can express this behavior in terms of evolution. The stars with initial mass $M > 15\ M_\odot$ ($M_{bol} < -6$) have a small mass loss rate near the main sequence. The mass loss rate increases very strongly by about a factor 100 during the hydrogen core-burning phase to the hydrogen shell-burning phase. The Wolf-Rayet stars, which supposedly represent an even later stage of evolution, (Conti, 1976) have again higher rates. So the mass loss rate increases during the stellar evolution by as much as a factor 10^2 or 10^3, whereas the luminosity hardly changes.

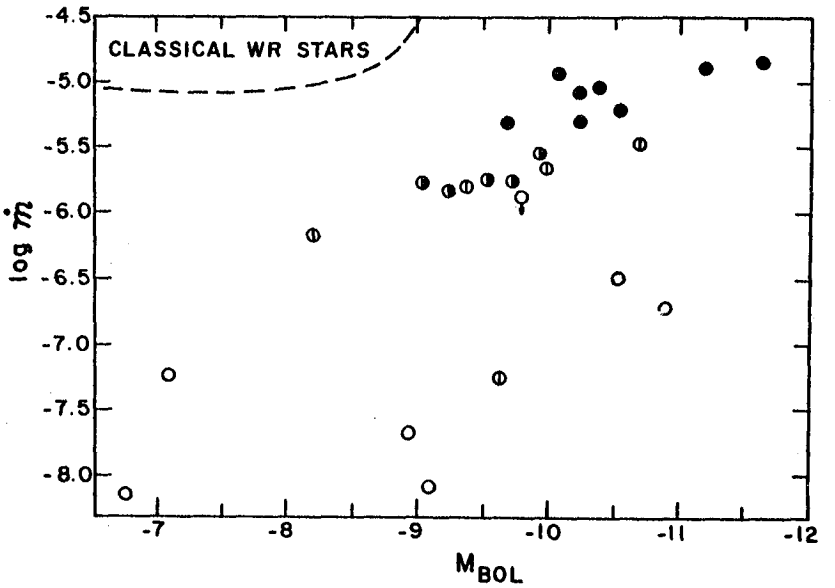

Figure 2

Mass loss rates from O-stars. Notice the large range of $\dot{M}$ for constant luminosity (Conti and Garmany, 1980).

Obviously, the luminosity is not the main parameter which determines the mass loss rate, contrary to the predictions of the radiation-driven models. This suggests very strongly that we may have to look for an alternative mass loss mechanism which should be closely connected to the evolution stage of the star and thus its interior structure.

IV. THE ACCELERATION OF THE STELLAR WIND

Whatever the mechanism may be that determines the mass loss rate from a star, the large outflow velocities which have been observed in the UV resonance lines are most likely due to radiative acceleration (e.g. Cassinelli et al., 1978). One way to determine the acceleration is to measure the terminal velocity, v_∞, reached in the wind at a large distance from the star. (This should not be confused, as is often done, with the edge velocity, v_{edge}, measured from the extension of the violet wings of the UV resonance lines: for stars with a small mass loss rate v_{edge} can be much smaller than v_∞).

The most extensive study of terminal velocities, prior to IUE, was made by Abbott (1978), who found $v_\infty \simeq 3 \times v_{escape}$. This agreed very well with the radiation-driven wind models, which predict $v_\infty = (\alpha/1-\alpha)^{1/2} v_{escape}$ if $\alpha \simeq 0.90$. The IUE observations of late-B and -A type supergiants show that the ratio v_∞/v_{esc} decreases towards the cooler stars, and reaches a value of about 0.5 for A type supergiants (Lamers et al., 1980a, Figure 3). This indicates that the radiation pressure is much smaller in the winds of A-stars than in O-stars, as might have been expected. In this respect it is interesting to notice that the mass loss rates of A-supergiants are also much less than those of O-stars of the same luminosity (Praderie et al., 1980).

Radiation pressure may not be the only mechanism which accelerates stellar winds, as it may be insufficient to explain the large velocities

of the WR stars. For example, Willis et al. (1979) derived a mass loss rate of 1.1 x 10^{-4} $M_\odot$/yr and v_∞ = 1600 km/s for the WR star γ Velorum

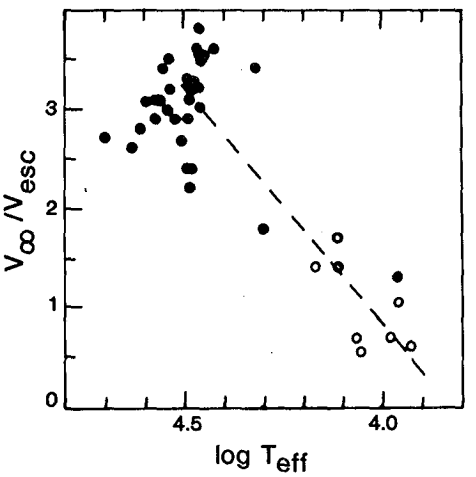

Figure 3

The ratio between the terminal velocity and the escape velocity decreases with decreasing effective temperature. Dots: Abbott (1978), Circles: Lamers et al. (1980a).

(WC8 + 09I) from IUE observations. The momentum of the wind is $\dot{M}v_\infty$ = 1.1 x 10^{30} erg/cm s. The total momentum of the radiation is L/c = 1.3 x 10^{28} erg/cm s. So the momentum of the wind is about 90 times as large as the momentum of the radiation. Unless each photon can be scattered a large number of times in opposite parts of the stellar winds (bouncing back and forward between the front and rear end of the wind) the radiation pressure is largely insufficient to explain the large wind velocity.

This suggests that not only do we have to look for another mass loss mechanism for hot stars (see III), but also for an additional mechanism to accelerate the winds, at least in WR stars.

V. THE HEATING OF STELLAR ENVELOPES

The Copernicus observations have shown that the stellar winds are superionized, i.e. the degree of ionization is higher than can be accounted for by a wind in radiative equilibrium with the photospheric flux. In particular Snow and Morton (1976) and Lamers and Snow (1978) have shown that there is a one-to-one correlation between superionization and mass loss (including the Be-stars), suggesting that the two phenomena are in some way connected to each other. The origin of this superionization is unknown, but its presence indicates that somewhere above the photosphere, the stellar gas is heated considerably. The heating may occur in the subsonic part of the envelope, giving rise to a thin hot corona ($\Delta R \simeq 0.1\ R_*$, $T \simeq 5 \times 10^6$; Cassinelli et al., 1978); in the trans-sonic region of the wind (Cannon and Thomas, 1977); or in the extended supersonic part of the wind, producing either a homogeneous warm wind ($T \simeq 2 \times 10^5$ K; Lamers and Morton, 1976) or an inhomogeneous wind with hot bow shocks of high density and high velocity blobs ($T \simeq 10^6$ K; Lucy and White, 1980).

The recent observations of x-ray fluxes from hot stars by the Einstein Observatory (Long and White, 1980) suggests that the temperature should be in the range of 10^6 - 10^7 K and that the hot region is not located deep in the wind, as predicted by the thin coronal model.

The IUE observations have given two very interesting results in this respect. Firstly, Underhill (1980) found two narrow emission peaks in the spectrum of the AO supergiant HR 1040 at the wavelength of the two C IV

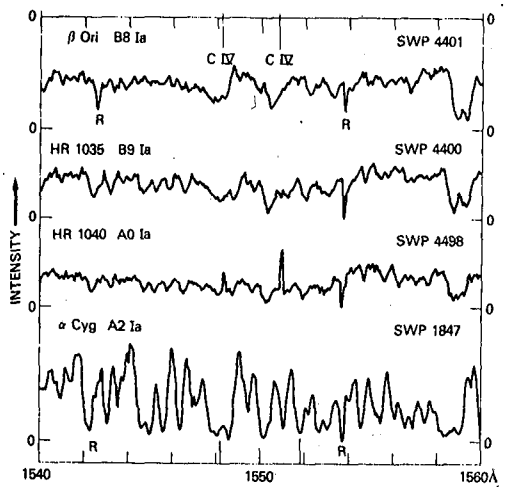

Figure 4

The C IV resonance lines (λ 1548.19, 1550.76) in the IUE spectra of four supergiants. Notice the C IV emission peaks in the spectrum of HR 1040 (AO Ia) (Underhill, 1980).

lines. These were not found in the IUE spectrum of the same star observed by Praderie et al. (1980). If the two peaks are real (and not due to particle noise) their presence indicates the existence of a variable chromospheric activity in the winds of supergiants of types as late as AO.

Secondly, the IUE observations of the two extreme supergiants P Cyg (B1 Ia) and ζ^1Sco(B1 Ia - 0) which have a mass loss rate of about 2 x 10^{-5} $M_\odot$/yr show the presence of narrow absorption features or P Cygni profiles of low ions (Fe II, Al II, Mg II) in the wind (Hutchings, 1979; Cassatella et al., 1979; Wolf and Appenzeller, 1979). Although the winds of early type supergiants are generally superionized, the winds of extreme supergiants with very large mass loss rates have a low degree of ionization. This behavior might be explained by assuming that the dissipation of nonthermal energy in the stellar envelopes is not sufficient to heat the very dense winds of extreme supergiants because of the high radiative cooling rate. This situation resembles the presence of low ionization stages such as Fe II in the spectra of early type shell stars.

VI. VARIABLE STELLAR WINDS

The envelopes of early type stars are variable on timescales of hours-to-years. The best tracer of variability in the visual spectrum is the H_α line and variations in the H_α profiles have been reported for various kinds of early type stars, such as supergiants and Be-stars (Snow et al., 1980; Stalio et al., 1979; Doazan et al., 1980). Apart from the

Be-stars the changes in the profiles are usually not very drastic, but the timescale of about one hour is surprisingly short. The UV resonance line profiles observed by Copernicus and BUSS also showed large variations on timescales of hours-to-months (York et al., 1977; Snow et al., 1980; Lamers et al., 1978). On the basis of these observations I proposed that mass loss is not a stationary process in early type stars, but that it occurs in "puffs": sudden ejections of gas from the star (not necessarily spherically symmetric) which are accelerated by radiation pressure. A similar process may occur in variable Be-stars during their active phases, in which case the puffs might be spherically or rotationally symmetric.

The IUE observations have provided a few very interesting examples which demonstrate how strong the variations can be. Heck et al. (1980) have identified six components in a number of UV resonance lines in ζ^1Sco on June 21, 1979, which they attribute to the occurrence of a large number of puffs. On September 13, 1979, most of the components had disappeared.

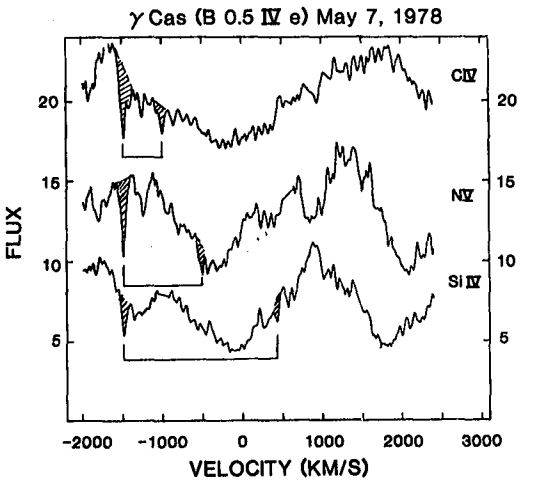

Figure 5

The UV resonance lines of C IV, N V and Si IV in the IUE spectrum of γ Cas (B0.1 IV e). Notice the narrow absorption components at -1500 km/s (Henrichs et al., 1980).

It is interesting to note that the time of highest puff-activity coincides with a sharp drop in visual brightness of about 0.15 magnitude.

A different, but possibly correlated, type of variation has been observed in the IUE spectrum of γ Cas (B0.5 IVe). In six out of ten IUE spectra obtained from this star the lines of N V, C IV and Si IV have sharp absorption components at about -1500 km/s (Doazan et al., 1980; Henrichs et al., 1980, Figure 5). The appearance and disappearance of these components suggest that puffs or shells are ejected very frequently from this star. Because of their large outflow velocities (possibly due to radiative acceleration) the narrow components can only be observed for about one week. (For an alternative explanation see Thomas et al., these proceedings.)

These kind of observations show that mass loss may be a highly nonstationary phenomenon in early type stars and that at least several

kinds of stars go through active phases. This again suggests that mass loss cannot be due to radiation pressure only.

VII. PROBING THE STELLAR WINDS IN BINARIES

A few late type giants and supergiants, such as ζ Aur, have an early type comparison which can be used to probe the envelope of the late type star, by studying the spectrum of the B-star when it moves behind the extended envelope. The same approach can be used for the study of a few early type binary systems.

Willis et al. (1979) has obtained IUE spectra of the Wolf-Rayet binary γ Velorum (WC8 + 09I) in six different phases of the binary period. Although this system is not an eclipsing binary in the visual spectrum, the winds of both stars are so extended that eclipse effects can be seen in many UV lines. As an example we show in Figure 6 the ratio of two IUE spectra at $1500 \lesssim \lambda \lesssim 1900$ Å, between phase 0.51 (when the O-star was behind the envelope of the WR star) and phase 0.1. The many absorption features in this ratio-spectrum show the presence of the corresponding absorbing ions in the wind of the WR star. By studying the phase dependent

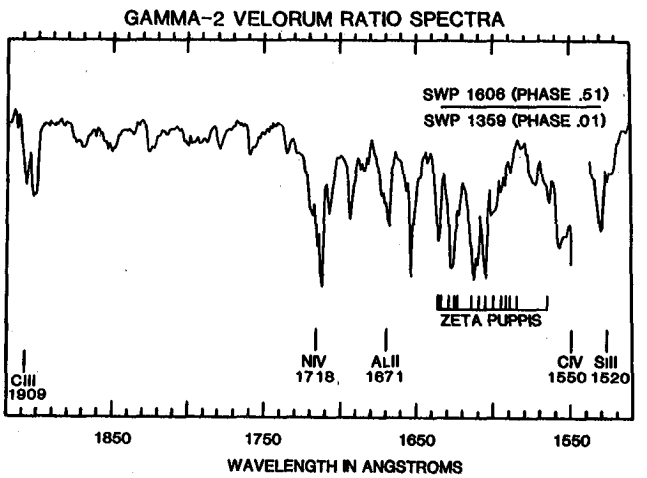

Figure 6

The ratio of two IUE spectra of the WR binary γ Velorum (WC8 + 09 I). The absorption lines are due to eclipse of the O-star by the wind of the WR star at phase 0.51 (Willis et al., 1979).

behavior of lines of high and low excitation and ionization Willis et al. demonstrated that the wind of the WC star is highly ionized but that the degree of excitation is low ($T_{exc.} \simeq 10\,000$K). This may be due to the same mechanism which cools the winds of the high mass loss supergiants ζ^1Sco and P Cyg.

A careful study of the UV-line eclipses in a few early type binaries with a wind would be extremely useful in determining the variation of density, velocity and ionization in the stellar winds.

VIII. EARLY TYPE STARS IN OTHER GALAXIES

The brightest early type stars in the LMC and SMC can be observed

with IUE. Since the metal abundance in both galaxies is smaller than in our galaxy, a differential study of stars in the LMC/SMC compared to galactic stars of the same temperature and luminosity will demonstrate the effect of metal abundances on stellar winds. The radiation pressure forces which presumably accelerate the winds of luminous OB stars are largely due to line opacities of CNO ions (Lamers and Morton, 1976). If the mass loss were due to radiation pressure, stars with smaller CNO abundances are expected to have smaller mass loss rates. If the mass loss is due to some other mechanism (see III) and the radiation pressure only acts in accelerating the wind, we might expect that the mass loss rates are the same in LMC/SMC stars and galactic stars, but that the wind velocities of the SMC/LMC stars are smaller than those of similar galactic stars.

Hutchings (1980) has studied the IUE low resolution spectra of 7 LMC supergiants and he found evidence that the radial velocities at minimum intensity in the lines are about 0.7 times as large as those in corresponding galactic stars. This, however, does not necessarily imply that the wind velocities in the LMC stars are smaller. The theoretical P Cygni profiles calculated by Castor and Lamers (1979) showed that a decrease in line opacity (e.g. due to a smaller abundance of the observed ion) will reduce the velocity at the line minimum, even if the wind velocity does not change at all. Nevertheless, these first IUE observations of the LMC/SMC stars are interesting since they demonstrate that differences with galactic stars do exist. A careful study of the UV lines combined with a study of H_α to estimate the mass loss rates independently, might turn out to be very valuable for our understanding of the mass loss phenomenon.

IX. CONCLUSIONS

I have concentrated on the subject of mass loss and stellar winds from early type stars. There are two reasons for this: firstly, I think that this is the most important problem in the study of early type stars as it may change our concepts on the structure of stellar atmospheres and evolution of massive stars, and secondly, this is a subject to which many IUE studies were directed and where IUE observations have made a very important contribution.

Let me summarize the new insights which we have gained from the IUE observations:

a The mass loss rate of an early type star with $L > 2 \times 10^4 L_\odot$ increases drastically during its evolution. It may increase by about a factor 30 from the zero age main sequence to the hydrogen shell burning phase, and another factor of 10 when it becomes a WR star. This rapid increase seems to be incompatible with the radiation-driven wind theory and may require another mass loss mechanism which should be closely related to the stellar evolution phase.

b The terminal velocities in late-B and -A supergiants are considerably smaller than those of O-stars, indicating a less efficient acceleration mechanism. The momentum of the stellar winds of WR stars is about 10^2 times larger than the momentum of the radiation. This suggests that, at least in WR stars, the acceleration is produced by a mechanism much more efficient than radiation pressure.

c The presence of hot gas in the stellar winds as first suggested by the UV lines from high ionization stages such as N V and O VI, is confirmed by the observed x-ray fluxes. The winds of the extreme B-supergiants with $\dot{M} \simeq 2 \times 10^5 M_\odot/yr$ and the dense shells of shell stars, however, have low ionization and excitation temperatures.

d The winds of early type stars are variable on a time scale of hours-to-years. The observations of a few early supergiants and of Be-stars show that stars may go through active phases in which puffs or shells are ejected frequently. For one star, ζ^1Sco, the active phase was found to coincide with a decrease in visual magnitude.

The examples which I have given are in a way extremes in terms of variability or mass loss. It is possible that we can explain the physics of the more normal mass losing stars by ignoring these extremes. I am afraid, however, that this is not very likely.

P.S. Based on our present knowledge, I can suggest a few IUE studies which would be most valuable in providing insight into the physics of mass loss from hot stars: 1: the study of few binary systems in which the wind can be probed by eclipses in the UV lines; 2: the study of the variability of a few stars in detail in UV, visual and x-rays; 3: the study of mass loss and wind velocities of similar stars (same L and T_{eff}) with different abundances.

REFERENCES

Abbott, D.C. 1978, Ap.J. 225, 893.

Barlow, M.J. and M. Cohen. 1977, Ap.J. 213, 737.

Cannon, C.J. and R.N. Thomas. 1977, Ap.J. 211, 910.

Cassatella, A., F. Beeckmans, P. Benvenutti, J. Clavel, A. Heck, H.J.G.L.M. Lamers, F. Macchetto, M. Penston, P.L. Selvelli and D. Stickland. 1979, Astron.Ap. 79, 223.

Cassinelli, J.P., J.I. Castor and H.J.G.L.M. Lamers. 1978, P.A.S.P. 90, 496.

Cassinelli, J.P., G. Olson and R. Stalio. 1978, Ap.J. 220, 573.

Castor, J.I., D.C. Abbott and R.I. Klein. 1975, Ap.J 195, 157.

Castor, J.I. and H.J.G.L.M. Lamers. 1979, Ap.J.Suppl. 39, 481.

Conti, P.S. 1976, Proc. 20th Liege Internat. Astroph. Coll., Mem. Roy. Soy. Liege, 9, 193.

Conti, P.S. and C.D. Garmany. 1980, Ap.J. (in press).

Doazan, V., L.V. Kuhi and R.N. Thomas. 1980, Ap.J. (letters) 235, L17.

Doazan, V., P. Selvelli, R. Stalio and R.N. Thomas. 1980 in "The Second European IUE Conference: (in press).

Heck, A., G. Burki, L. Bianchi, A. Cassatella and J. Clavel. 1980, Astron.Ap. (in press).

Henrichs, H.F., G. Hammerschlag-Hensberge and H.J.G.L.M. Lamers. 1980, in "The Second European IUE Conference" (in Press).

Hutchings, J.B. 1979, Ap.J. 233, 913.

Hutchings, J.B. 1980, Ap.J. (in press).

Lamers, H.J.G.L.M., C. de Jager, F.M. Macchettto, and F. Praderie. 1980a, Astron.Ap. (in preparation).

Lamers, H.J.G.L.M., F. Paerels and C. De Loore. 1980b, Astron.Ap. (in press).

Lamers, H.J.G.L.M. and T.P. Snow. 1978, Ap.J. 219, 504.

Lamers, H.J.G.L.M., R. Stalio, and Y. Kondo. 1978, Ap.J. 223, 207.

Long, K.S. and R.L. White. 1980, Ap.J. (in press).

Lucy, L.B. and R.L. White. 1980, Ap.J. (in press).

Morton, D.C. 1967, Ap.J., 145, 1017.

Praderie, F., A. Talavera and H.J.G.L.M. Lamers. 1980, Astron.Ap. (in press).

Snow, T.P. and J.M. Marlborough. 1976, Ap.J. (letters), 203, 287.

Snow, T.P. and D.C. Morton. 1976, Ap.J.Suppl. 32 429.

Snow, T.P., G.A. Wegner and P.B. Kunasz. 1980, Ap.J. (in press).

Stalio, R., L. Rusconi, G. Sedmak, C. Arpigny, Y. Georgelin and B. Rocca. 1979, Astron.Ap. 77, L10.

Underhill, A.B. 1980, Ap.J. (letters) 235, L149.

Willis, A.J., R. Wilson, F. Macchetto, F. Beeckmans, K.A. van der Hucht and D.J. Stickland. 1979, in "The First Year of I.U.E., University College London, ed. A.J. Willis.

Wolf, B. and I. Appenzeller. 1979, Astron.Ap. 78, 15.

York, D.G., A. Vidal Madjar, C. Laurent and R. Bonnet. 1977, Ap.J. (letters) 213, L61.

IUE OBSERVATIONS OF YOUNG VARIABLES

Gösta F. Gahm

Stockholm Observatory, S-133 00 Saltsjöbaden

Sweden

ABSTRACT

New insight to the physics and behavior of young variables have been provided by observations with the IUE satellite. These results are briefly reviewed.

INTRODUCTION

A number of far-UV spectrograms of young variable stars have become available through observations with the IUE satellite. Several T Tauri stars and Herbig type Be- and Ae-stars in dark nebulae have been observed and to my knowledge spectrograms of a total of 17 stars, which have been considered to be very young pre-main-sequence stars, are now collected. In many of these cases only part of the spectral region available at the IUE is covered and there are examples where large spectral regions are severely underexposed. With a few exceptions the stars have been observed with the low resolution cameras, providing spectral resolutions of 6 to 7 Å.

Most of the observations lack simultaneous photoelectric and/or spectroscopic observations over the visible and infrared spectral regions. Furthermore, at the initial period of IUE observations, the observers selected primarily objects with very intensive emission line spectra in the visible region. For these stars it is usually extremely difficult to make any precise statements on the dimensions and energy distribution of the star itself and also to derive the value of interstellar extinction and to discuss the influence of possible circumstellar extinction. It is therefore clear that we need much more observations of young variables before their physical properties can be overviewed in more detail.

Nevertheless, the IUE observations have given a completely new insight to the physics and behavior of very young stars, and in the following I will try to extract some of the new information obtained. This review is based

on the observations of RU Lup by Gahm et al. (1979), S CrA by Appenzeller and Wolf (1979), T Tau, GW Ori and V 380 Ori by Gondhalekar et al. (1979), RW Aur by Imhoff and Giampapa (1980) and by Cram et al. (1980), DR Tau, CoD - 35°10525 and AS 205 by Appenzeller et al. (1980) in addition to our unpublished observations of RU Lup and DI Cep (G. Gahm, R. Liseau) and of HR 5999 (A. Casatella, G. Gahm, R. Viotti).

MAIN OBSERVED CHARACTERISTICS

The far-UV spectrograms have revealed the presence of very hot and intensive regions around the stars. The ion of highest ionization stage observed in emission is N V at λ1238 Å, requiring some 200 000 K to form. This line is present on DR Tau, CoD - 35°10525 and RU Lup. For this latter star we (Gahm, Liseau and Fredga, unpublished) have set an upper limit to the absolute flux of coronal lines (forming at $\sim 10^6$K) of $< 3\times10^6$ the solar value.

All T Tauri stars show C IV at λ1548, 1550 Å in emission and in addition the spectral region from λ1150 Å to λ1900 Å is as a rule rich in emission lines of Si IV, Si III, Si II, C III, C II, C I, O I and a number of Fe II lines. Hence, the emitting regions around T Tauri stars cover a large range in temperatures - from 7000 K to at least 200 000 K.

The spectral region from λ1900 Å to λ3300 Å is in some cases dominated by emission lines and in others by absorption lines although the Mg II lines at λ2796, 2803 as a rule are in very strong emission. The particular wavelength at which a transition from essentially an absorption line spectrum to essentially an emission line spectrum occurs is very different from star to star. V 380 Ori of spectral type A 1 is the star of earliest spectral type observed and has an absorption line spectrum all the way down to at least λ1200 Å. RW Aur on the other hand start to show emission lines shortward of 3300 Å (Gahm, 1970). Of course, the critical wavelength of the transition may very well be variable with time.

The emission lines or absorption lines are seen against a continuous emission extending over the entire spectrum. With the exceptions of the stars of earliest spectral type V 380 Ori and HR 5999 (A7 III:e) this continuum is a strong excess continuum over the expected photospheric contribution. So far, there has been no reason to call upon any other emitting process than Balmer continuous emission in the emitting volume around the stars in order to explain the far-UV excess (Gahm et al., 1979; Appenzeller et al., 1980). In the case of RU Lup one has to consider Balmer emission from the hottest as well as the coolest regions.

THE PHYSICS OF INDIVIDUAL STARS

So far, rather little of detailed analysis of the far-UV spectra of the young variables has appeared. The IUE spectra provide information on

emission line fluxes and equivalent widths of relatively strong lines only and no information on line profiles, with the exception of the Mg II lines of RW Aur (Imhoff, private communication).

Observations over the visible spectral regions have been obtained simultaneously with the IUE observations for DI Cep (Gahm and Malmort, under preparation); CoD - $35^{o}10525$ and AS 205 (Appenzeller et al. 1980) and HR 5999 (Co-operative project organized by P.S. Thé). We therefore have information on the observed energy distribution from λ1150 Å to λ5500 Å (for HR 5999 up to 4.7 μ) for several stars. In the near future we therefore expect presentations of the separate energy distributions of the stars and their emitting envelopes as well as discussions on the separate contributions of circumstellar and interstellar extinction. It is premature at this point to make any statements on these results.

The emission lines can be used as probes into the physical state of the emitting volumes. The diagnostic procedure was developed by Pottasch (1963) and has been used by Cram et al. (1980) to model the emitting volumes around RW Aur and RU Lup. The basic assumption is that both the ionization and the excitation equilibrium of the radiating ions are controled by local conditions. In short, the ionization equilibrium of different ions provides an estimate of the average temperature and also interval in temperature where the emission originates. From the observed fluxes of different lines of different ions the total surface flux is determined after corrections for distance, extinction and dimensions of the star. The emission measure, $\int N_e^2 dh$, is then plotted against electron temperature, T_e, and the resulting relation can be compared to solar values.

In the following we will proceed in a similar but somewhat different way for line fluxes observed for RU Lup during June, 1979 when the far-UV flux of the star was large. According to Gahm et al. (1974) and Gahm et al. (1979) the total visual absorption to RU Lup is $0.3 < A_v < 1.0$. The observed fluxes of different lines forming at different characteristic temperatures (T_{max}) are given in Table 1 where the total line luminosity L_{line} has been computed with an E(B-V) = 0.2 with an average "normal" reddening law according to Savage and Mathis (1979). The last column gives the volume emission measure VN_e^2 computed with the same numerical figures as used by Cram et al. (1980).

The results are given in Fig. 1 where the curve represents the corresponding solar values increased by a factor of 10^6. Also given as crosses are the corresponding volume emission measures of RW Aur from Cram et al. (1980).

The general result, then, is that when treated in this way, the line emission on T Tauri stars behaves very similarly to what is seen on the sun, only that the total emission on these (rather extreme!) T Tauri stars are several orders of magnitude larger than on the sun. Whether this is an indication that the T Tauri envelopes are maintained by similar physical processes that operate on the sun is a question which remains to be explored.

If we had information on N_e for the different temperature zones it would be possible to obtain some idea of the geometrical extent of these zones. For RU Lup Gahm et al. (1974) derived $N_e = 3 \times 10^{11}$ cm^{-3} for lines forming at 10^4 K and lower. For higher temperatures, between 5×10^4 to 10^5 K, the density-sensitive ratios Si III λ1892/C III λ1980 and Si IV λ1403/C III λ1908 can be used (Cook and Nicolas, 1979; Doschek et al., 1978). For RU Lup we obtain $N_e = 2 \times 10^{10}$ for this temperature zone. These simple tools lead to relatively extensive emitting volumes around the stars.

A very important result realized by Cram et al. (1980) from considerations like these is that the suggestion that the 10^5 K plasma in the solar chromosphere-corona transition zone is not directly heated by the local deposition of mechanical energy, but rather indirectly heated by thermal conduction from the 2×10^6 K solar corona, does not apply to T Tauri stars and that "direct, in situ, heating of the 10^5 K plasma must occur".

STATISTICAL RELATIONS

As a complement to the efforts of modelling the physical structure of individual stars we could try to find statistical relations between different observed properties of the 11 stars for which far-UV information exists and in this way hopefully learn something about the nature of young objects. We are presently treating released IUE spectra of such stars in a homogenous way but in the following presentation we must rely also on published or in-print flux-calibrated spectrograms that have been reduced according to somewhat different schemes. Since more accurate comparisons must await a full treatment, I will only give the general results as follows.

1. It is very difficult to find any relation between the appearance of the visible spectrum and any property of the far-UV spectrum. For instance, the absolute C IV flux, as corrected for interstellar extinction and distance (which are uncertain in many cases) does not correlate in any particular way with degree of emission in the visible spectral region, nor does it correlate with degree of ultraviolet or infrared excess.

2. The critical wavelength, λ_{crit}, at which the spectrum changes from an absorption line spectrum to an emission line spectrum was taken by Appenzeller et al. (1980) to be related to the envelope density. This seems to be a reasonable suggestion but I have not been able to find any relation between λ_{crit} and the density-sensitive Si III to C III ratios discussed above. No other relation is apparent such as to the degree of self-absorption in the hydrogen lines or to emission line profiles in general.

3. The character of the light variations and the corresponding amplitudes as given by Herbig and Rao (1972) do not relate in any obvious way to observed characteristics in the far-UV spectrum.

Quite clearly, it will be easier to demonstrate possible relations when

more stars are observed. In particular, we need a larger sample of stars for which distances and interstellar extinction can be treated accurately. However, line ratios in the far-UV are relatively independent of these parameters and I find it rather alarming that ratios of lines of for instance C IV, III, II and I do not relate to any other observed property of the star. The intensity ratios of C IV λ1550 Å to Si IV λ1403 Å is very similar from star to star and they fall in the same range as given by Doschek et al. (1978) for coronal hole, quiet sun, solar flares and several late-type stars. Their suggestion that the differential emission measure as derived from the ions in these temperature zones is independent of atmospheric conditions and dependent only on atomic properties of the plasma will then include the rather extreme emitters considered here.

The ratio of Si III λ1892/C III λ1908 is sensitive to density and is plotted as ordinate in Fig. 2. Estimates of the corresponding electron densities are also given. In the left part of the diagram this ratio is plotted against emission class as defined by Herbig (1962). With the notable exception of DI Cep there seems to be a trend such that stars with weak emission line spectra in the visible region have envelope zones at $4x10^4$ to 10^5 K of lower densities than those with strong emission line spectra. The relation holds also when the ratios are plotted against equivalent widths of the Fe II emission at λ4924 Å (as taken from Cohen and Kuhi, 1980 and this work), again with the embarrasing exception of D I Cep.

However, the important result is not whether this trend exists or not but rather that in spite of the fact that the objects show such an enormous range in observed parameters like in the degree of emission (the luminosity of the C IV lines ranges over a factor of 100), in emission line widths and profiles, in degree of excess emission and type of variability, the density in the region producing line emission at $5x10^4$ to 10^5 K does not differ by more than a factor of 2 or so from the average values, provided that the density scale as given by Cook and Nicolas (1979) is applicable to the T Tauri stars.

If this is true one could start to outline some very interesting implications. However, I find the small range in implied densities very alarming because this is exactly what could happen if the lines were optically thick. In this case the Si III/C III ratio does not provide a useful tool for the physics of T Tauri stars.

THE CAUSE OF THE LIGHT VARIATIONS

The far-UV spectrograms of young variables may provide important information on the cause of the brightness variations with time. The only star that has been followed by repeated far-UV observations with the IUE and ground-based observations over the visible spectral region is HR 5999 (Thé et al. in preparation). The star stayed, however, close to maximum brightness during all IUE observations. This demonstrates the difficulty in having a simultaneous infrared, visible and far-UV coverage of a single star at different brightness levels. Another attempt directed to follow the variations of

DI Cep failed due to bad weather conditions at the ground-based station (Gahm and Malmort in 1978).

We have observed RU Lup on three occasions using the Short Wavelength Prime Camera with an entrance slit of 10x20 sec. on May 18, 1978 and June 17 and 19, 1979. Large variations have occured in the far-UV flux of the star. In spite of this the general appearance of the three spectrograms is very much the same on all three occasions. In fact, if one plots the peak line intensities of lines of different ions divided by the smoothed intensity level of the background continuum as done in Fig. 3 one finds that the line-to-continuum fluxes (ℓ/c) have not changed at all, while the total flux level have changed by a factor 3.5 from May 18 to June 19. In Fig. 3 I/<I> represents ℓ/c and for the continuum flux the May 18 spectrogram is set to 1.0.

Now, if the variations are due to violent structural or physical changes in the emitting envelope one needs a rather delicate balance in VN_e^2 throughout the whole region with the different temperature zones. It would mean that the source depths of the different temperature zones change in a rather delicate way as to maintain the general form of the curve presented in Fig. 1 and also to effect strong and weak lines in similar ways. We note that the Si III λ1892 line increased its ℓ/c significantly on June 17, 1979 when the star had intermediate brightness.

A very simple and direct way of explaining this type of variations results if we assume that the dominant cause of the variations is opacity changes in a circumstellar dust layer in the line-of-sight to the star. This interpretation for the variations of RU Lup was also favoured by Gahm et al. (1974) based on photometric and spectroscopic observations at visible wavelengths.

On other stars the dominant cause of the light variations may obviously be intrinsic and all efforts to follow the stars repeatedly, preferably also over visible and infrared wavelengths, should be encouraged.

REFERENCES

Appenzeller, I., Wolf, B.: 1979, Astron.Astrophys. 75, 164.

Appenzeller, I., Chavarria, C., Krautter, J., Mundt, R., Wolf, B.: 1980, Astron.Astrophys. (in press).

Cohen, M., Kuhi, L.V.: 1980, Astrophys,J. Suppl. 41, 743.

Cook, J.W., Nicolas, K.R.: 1979, Astrophys.J. 229, 1163.

Cram, L.E., Giampapa, M.S., Imhoff, C.I.: 1980, Astrophys.J. (in press).

Doschek, G.A., Feldman, U., Mariska, J.T., Linsky, J.L.: 1978, Astrophys.J. Letters 226, L 35.

Gahm, G.F.: 1970, Astrophys.J. 160, 117.

Gahm, G.F., Nordh, H.L., Olofsson, S.G., Carlborg, N.C.J.: 1974, Astron. Astrophys. 33, 339.

Gahm, G.F., Nordh, H.L., Olofsson, S.G.: 1975, Icarus 24, 372.

Gahm, G.F., Fredga, K., Liseau, R., Dravins, D.: 1979, Astron.Astrophys. 73, L 4.

Gondahalekar, P.M., Penston, M.V., Wilson, R.: 1979, The first year of IUE, NASA/ESA/SRC Symp. at Univ.College London, p. 109.

Herbig, G.H.: 1962, Advances Astron.Astrophys. 1, 47.

Herbig, G.H., Rao, N.K.: 1972, Astrophys.J. 174, 401.

Imhoff, C.L., Giampapa, M.S.: 1980, Astrophys.J. Letters (in press).

Pottasch, S.R.: 1963, Astrophys.J. 137, 945.

Savage, B.D., Mathis, J.S.: 1979, Ann. Rev.Astron. Astrophys. 17, 73.

TABLE 1. VOLUME EMISSION MEASURES OF RU LUP

Line	λ (Å)	T_{max} (^oK)	Observed flux (erg/cm^2s)	L_{line} (erg/s)	VN_e^2
C II	1335	20 000	2.0×10^{-12}	2.6×10^{31}	5.9×10^{55}
C IV	1549	110 000	5.5×10^{-12}	6.6×10^{31}	7.2×10^{54}
Si II	1526	15 000	9.2×10^{-13}	1.1×10^{31}	8.4×10^{57}
Si IV	1400	79 000	2.2×10^{-12}	2.7×10^{31}	4.3×10^{55}
N V	1240	200 000	7.0×10^{-13}	1.1×10^{31}	9.4×10^{54}

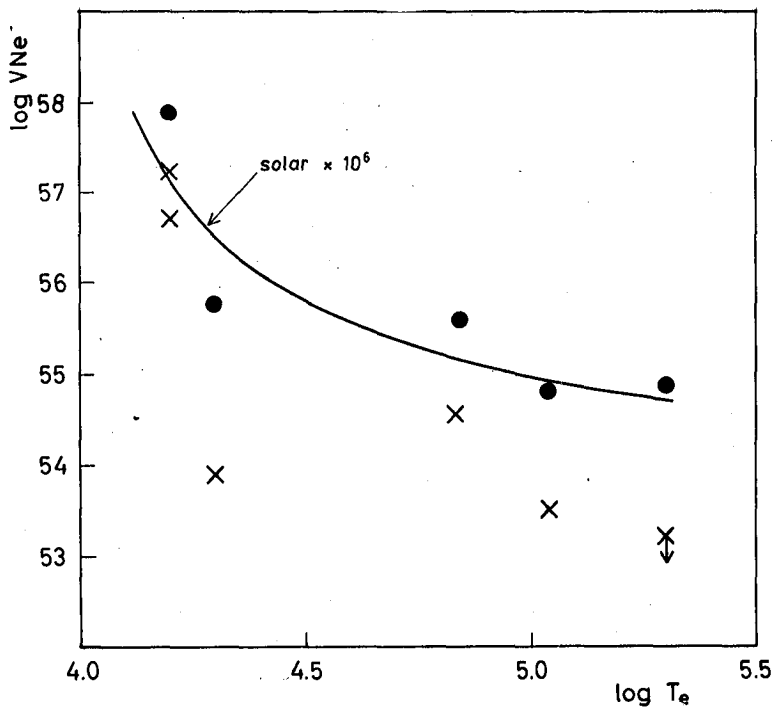

Fig. 1. Logarithmic volume emission measure as a function of logarithmic electron temperature for RU Lupi (filled circles) and RW Aur (crosses).

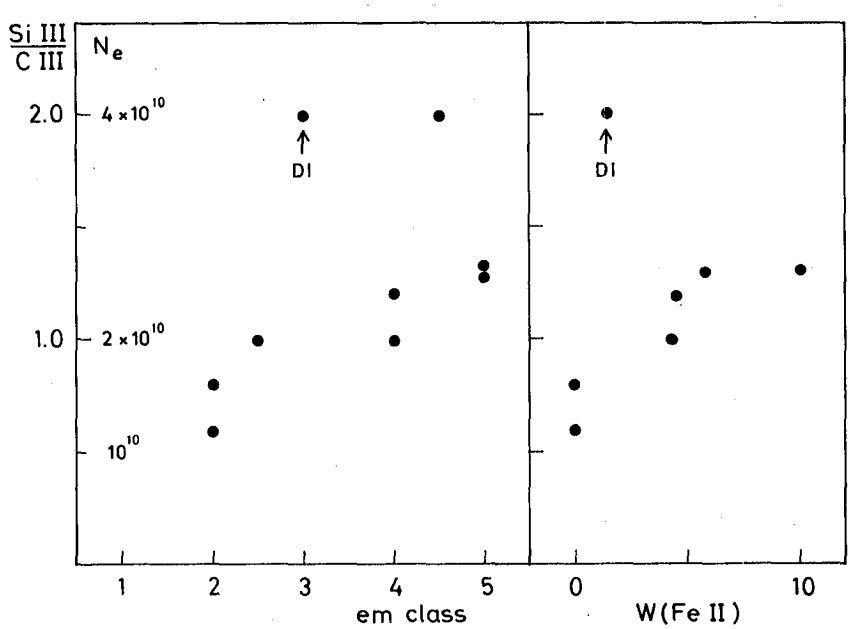

Fig. 2. The ratio of Si III λ1892 to C III λ1908 with corresponding electron densities N_e as function of emission class and the equivalent width of Fe II λ4924. DI marks the position of DI Cephei.

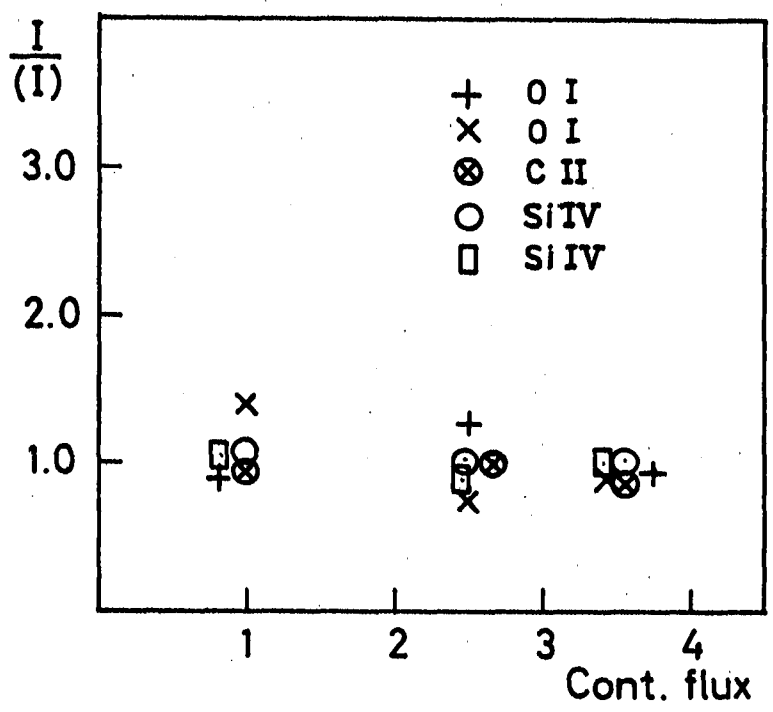

Fig. 3. Normalized intensities of lines of different ions as function of continuous excess flux at far UV wavelengths.

MASS-LOSS RATES FROM EARLY-TYPE STARS*

Peter S. Conti and Catharine D. Garmany
Joint Institute for Laboratory Astrophysics
University of Colorado and National Bureau of Standards

ABSTRACT

We have derived mass loss rates for a number of unevolved O-type stars and a few WN stars from high dispersion IUE spectra of their P Cygni profiles. When combined with other published mass loss rates, we find that the relationship between log $\dot{m}$ and M_{BOL} is a broad band rather than a linear relation, suggesting that the line radiation driven wind theory may not be sufficient to explain mass loss. The mass loss rates for the WN stars, while more uncertain, confirm that these stars lose mass about 100 times faster than O-stars.

INTRODUCTION

It has been known for many years that early-type stars are losing mass. The first evidence came from rocket UV observations of P Cygni profiles of resonance lines (1), and later determinations of mass loss have come from infrared studies (2), emission lines in the visible (3) and radio observations (4). The observed mass loss has been attributed to UV line radiation pressure (5). In this theory, the mass loss should be proportional to the stellar luminosity, and indeed, observations of O supergiants and Of stars support this. However, our initial IUE observations of five main sequence stars resulted in mass loss rates much lower than the predicted values (6). It is important to find the reason for such a difference, not only for its bearing on theories of mass loss from these stars, but also because stellar evolutionary calculations are affected (7). Our understanding of the atmosphere of early-type stars has been further complicated by the recent Einstein Observatory observations that many of these stars are X-ray sources (8). We have observed an additional 16 main sequence O-stars during the second year of IUE, and have confirmed our earlier finding: at a given luminosity stars are observed to have mass loss rates which differ by a factor of 30.

APPEARANCE OF THE SPECTRA

In the O-type stars, the P Cygni profile of the C IV λ1548 and N V λ1232 resonance doublets are the most consistent indicators of mass loss. Among the earliest spectral types the C IV line is characterized by a sharp blue absorption edge and a terminal velocity greater than 3400 km s^{-1}. At

*This work supported by NASA under grant number NAS5-22833.

later spectral types, the blue edge of the profile becomes less steep and the terminal velocity decreases. However, as illustrated in Figure 1, the degree of line saturation is not related to the bolometric magnitude of the star.

In general, the same description that applies to C IV also applies to the N V line, although blending with Lyman α makes the determination of a terminal velocity uncertain. Both of these lines are fully saturated in the WN stars.

The appearance of the N IV λ1718 line is strongly temperature dependent. In the latest O-type stars it is photospheric, but with increasing effective temperature it develops a blue wing and eventually appears as a P Cygni profile, although the blue edge never reaches the terminal velocity of the strong resonance lines. All of the WN stars show an unsaturated P Cygni profile whose blue edge reaches the same terminal velocity as the other lines.

The Si IV λ1393 resonance doublet is photospheric in all of the main sequence O-stars, but it becomes a saturated P Cygni profile in the O supergiants and late WN7 and WN8 stars. See Figure 2.

MODEL FITTING

We have found mass loss rates for the stars by comparing their P Cygni lines with the model profiles computed by Castor and Lamers (9) and modified by Olson (unpublished) to include nonlocal radiative coupling for doublet profiles. The line profile in an expanding atmosphere is determined by the mass loss rate, the velocity law, the ion abundance, the stellar radius, and atomic parameters. Castor and Lamers have parameterized their models according to the total optical depth and the assumed velocity law, and each observed line profile is then fit by these parameters. The mass loss rate is then derivable from the profile parameters, the terminal velocity, the stellar radius, and the fractional abundance of the absorbing ion. We have used this approach, which is also discussed by Conti and Garmany (6) and applied to a few stars observed during the first year of IUE. One of the most difficult assumptions in this method is the ionization fraction. When two or more nonsaturated P Cygni profiles are seen in the same star, the relative ionization fractions can be computed, and compared with calculated fractions for a given temperature and density, which has been our approach. All of the O-stars are cluster members with well-established bolometric magnitudes. We have adopted Conti's (10) temperature scale in our determination of ionization balance and stellar radii.

RESULTS

We have derived mass loss rates for 16 O-type stars of luminosity class V or III. The rates range from 10^{-6} $M_\odot$ yr^{-1} to 2×10^{-9} $M_\odot$ yr^{-1}, and the rates are not linearly related to stellar luminosity as predicted by the line radiation driven wind theory. In Figure 3 we show log $\dot{m}$ vs. M_{BOL} for

the stars we observed, as well as stars with mass loss rates derived by other methods. For a given M_{BOL}, the rates differ by as much as a factor of 30. The higher rates may be associated with stars which have left the ZAMS but are still burning hydrogen in their core.

We have also calculated mass loss rates for several WN stars, which are shown in Figure 3. The method used was the same as for the O-stars, although the greater uncertainty in the temperatures, ionization fractions, and luminosities make an error estimate difficult. However, we note that our values are similar to those found from observations by Willis (private communication).

These results will be reported elsewhere in more detail.

REFERENCES

1. Morton, D. C.: 1967, Astrophys. J. 150, 535.
2. Barlow, M. J. and Cohen, M.: 1977, Astrophys. J. 213, 737.
3. Conti, P. S. and Frost, S. A.: 1977, Astrophys. J. 212, 728.
4. Abbott, D. C., Bieging, J. H., Churchwell, E. and Cassinelli, J. P.: 1980, Astrophys. J. (in press).
5. Castor, J. I., Abbott, D. C. and Klein, R. K.: 1975, Astrophys. J. 195, 157.
6. Conti, P. S. and Garmany, C. D.: 1980, Astrophys. J. (in press).
7. Chiosi, C., Nasi, E. and Sreenivassan, S. R.: 1978, Astron. Astrophys. 63, 103.
8. Harnden et al.: 1979, Astrophys. J. 234, L51.
9. Castor, J. I. and Lamers, H.J.G.L.M.: 1979, Astrophys. J. Suppl. 39, 481.
10. Conti, P. S.: 1976, Mem. Soc. Roy. Sci. Liege 9, 193.

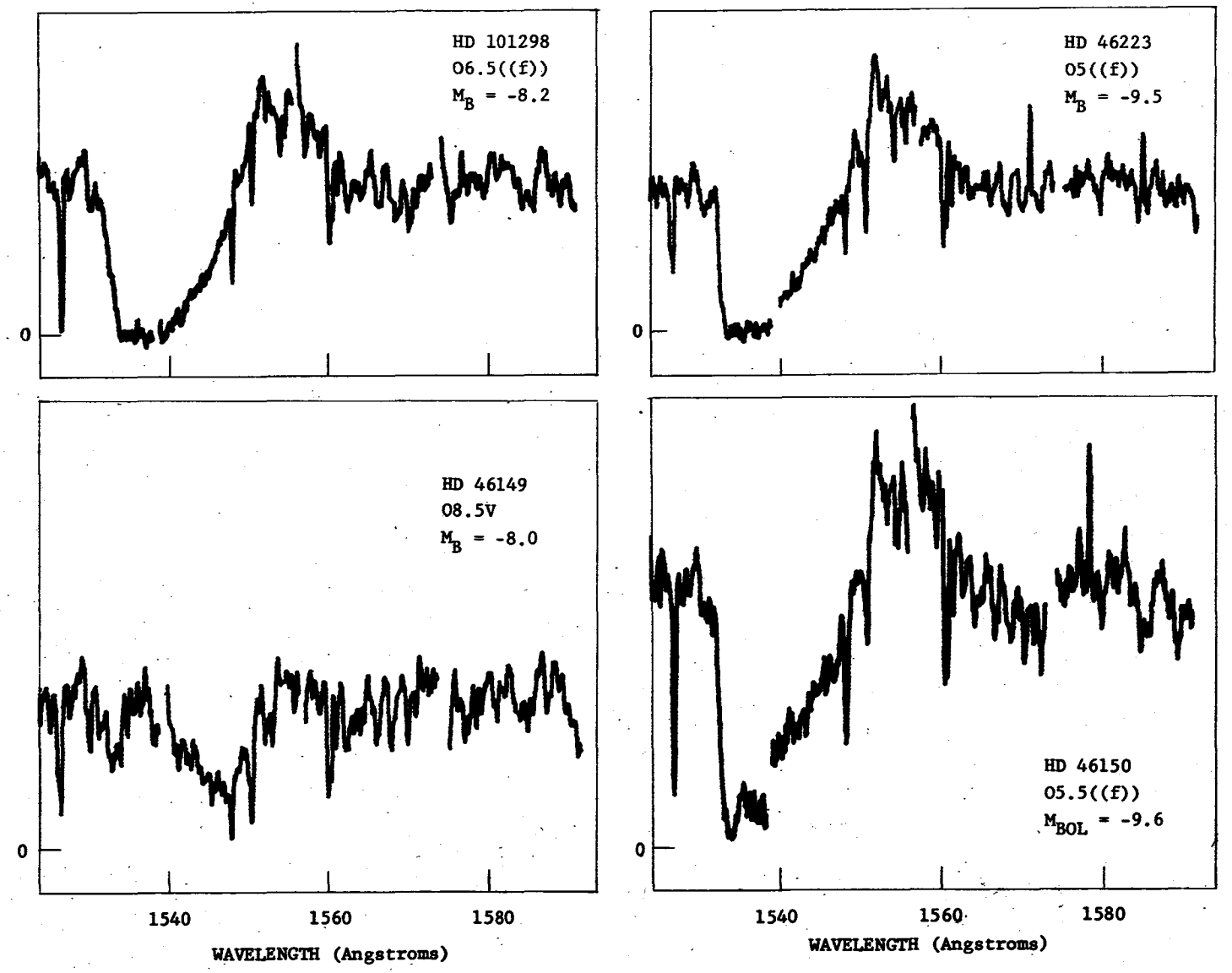

Fig. 1: Line profiles of C IV λ1548,1550 in four O-type stars. IUE observations taken with the SWP camera in October 1979.

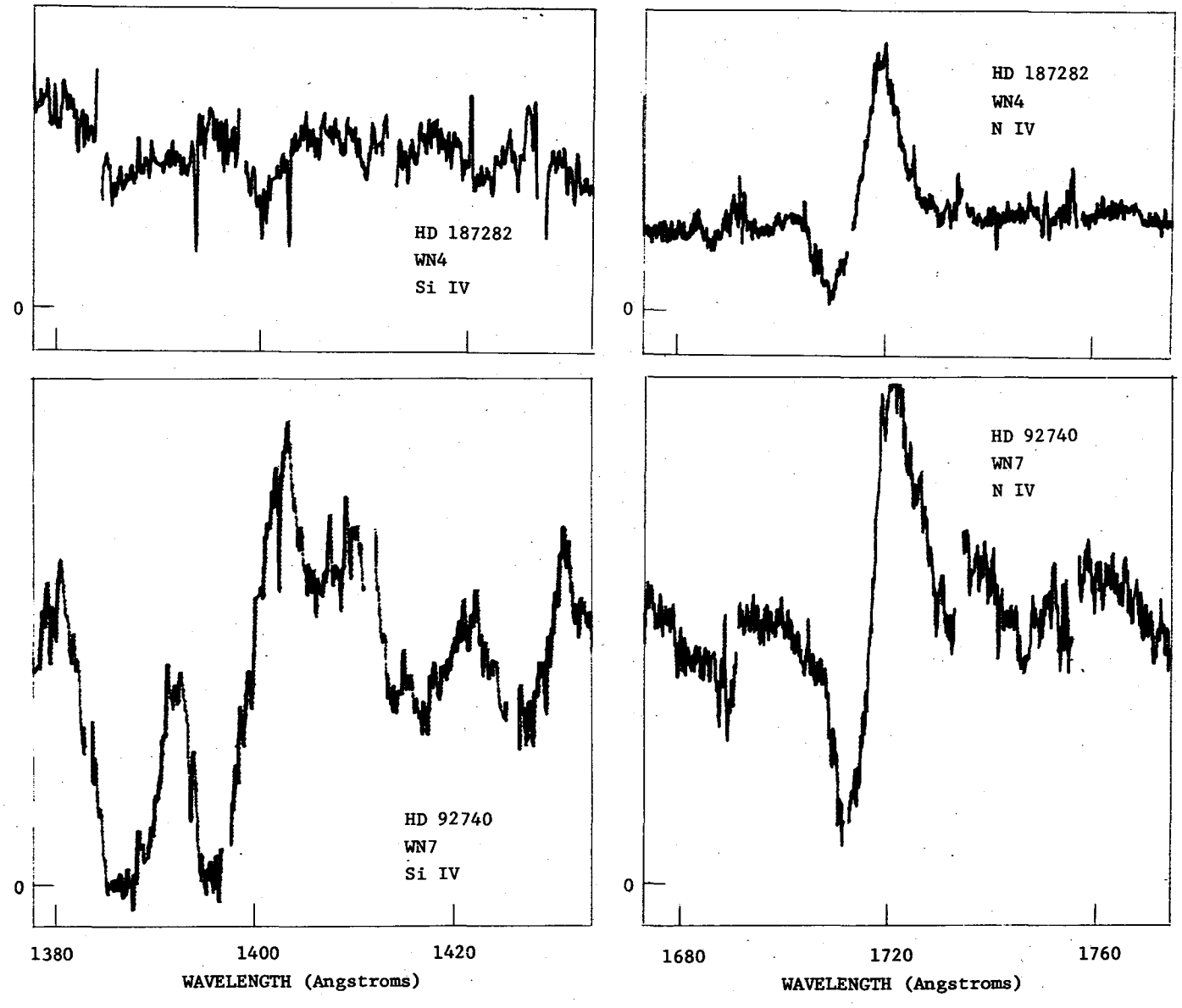

Fig. 2: Line profiles of Si IV λ1393,1402 and N IV λ1718 in a WN4 and WN7 star.

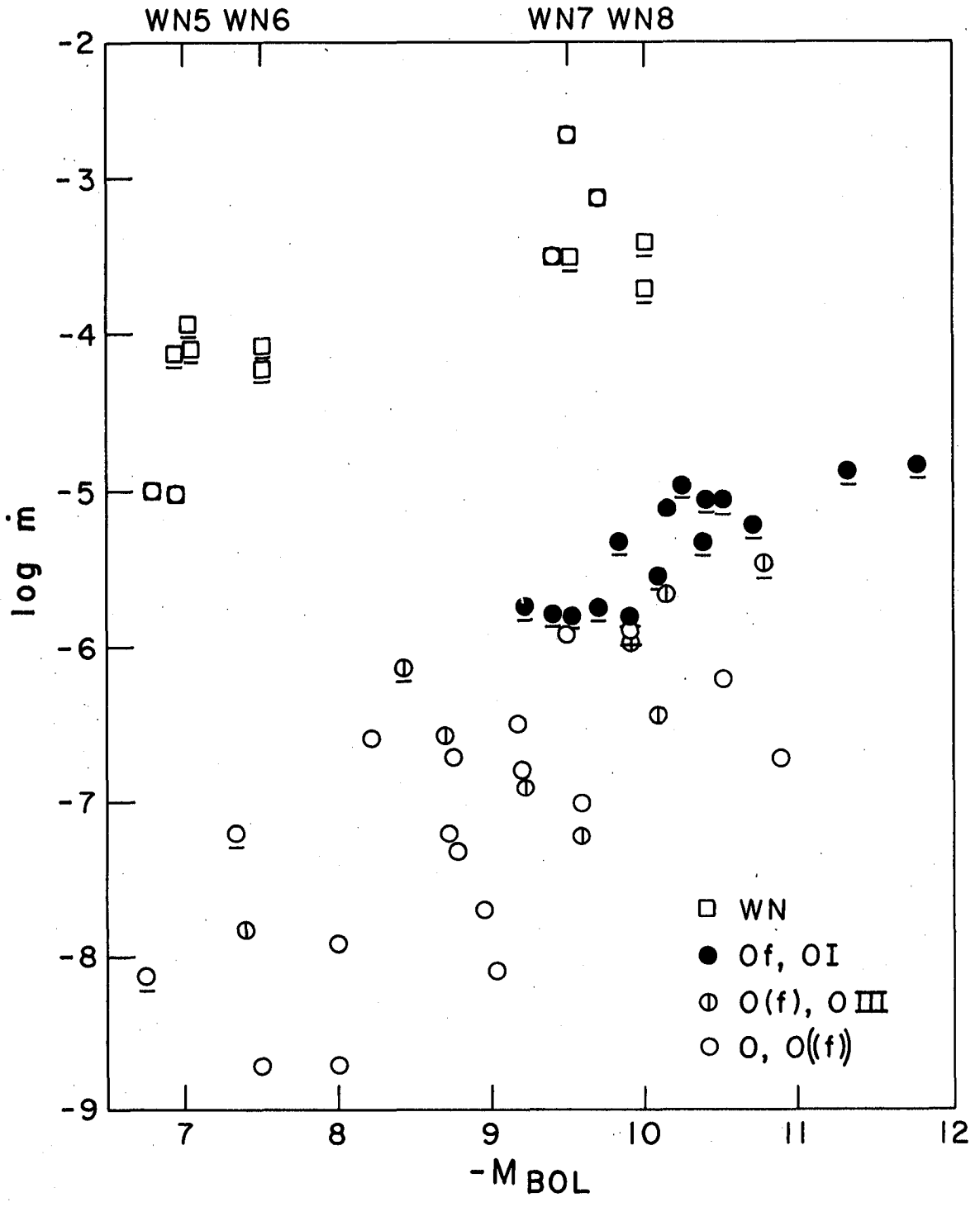

Fig. 3: Mass loss, log $\dot{m}$, vs $-M_{BOL}$ for various early-type stars. Rates measured by other methods are underlined, our new determinations are not.

IUE OBSERVATIONS OF VARIABILITY IN WINDS FROM HOT STARS

C.A. Grady and Theodore P. Snow, Jr.
LASP, University of Colorado at Boulder

ABSTRACT

Observations of variability in stellar winds or envelopes provide an important probe of their dynamics. For this purpose a number of O, B, Be, and Wolf-Rayet stars have been repeatedly observed with the IUE satellite in high-resolution mode. In the course of analysis, instrumental and data handling effects were found to introduce spurious variability in many of our spectra. Software has therefore been developed to partially compensate for these effects, but limitations remain on the type of variability that can be identified from IUE spectra. With these contraints, preliminary results of multiple observations of two OB stars, one Wolf-Rayet star, and a Be star are discussed.

TEXT

Observations of variability in stellar winds or envelopes provide an important probe of their dynamics. IUE, with its ability to simultaneously sample large portions of the ultraviolet spectrum, can potentially enable one to relate temporal variations in one spectral feature to other lines. Ultimately this may yield a spatial as well as spectral probe of the outer atmospheres of hot stars. Before any such analysis can be undertaken, however, it is essential to determine the type and amplitude of variability which can be measured from IUE high-resolution spectra.

Reduction and analysis of IUE high-resolution data for temporal variability is complicated by a number of instrumental and data handling effects which can introduce sufficient spurious variability into the spectra to swamp any real stellar variability. These effects and programming to partially compensate for them developed on the PDP 11/34 of LASP/University of Colorado using the Interactive Data Language are discussed by Grady (1). Limitations do remain on the amplitude of line profile variations that IUE is capable of detecting in high resolution. For example, in order to compensate for differing exposure times and positioning of the target star in the spectrograph slit, all of our data has been normalized to the continuum = 1. As a result, it is impossible to monitor changes in continuum level. Thus, our effort has been concentrated on changes in profile shape and relative intensity in a number of lines known to indicate mass loss. (2)

It is then necessary to determine the changes in relative flux which can be confidently attributed to the star, rather than the instrument and subsequent data handling. One of the stars in our variability search, α Cam (HD 30614, O9.5Iab) showed no evidence of any change in its P Cygni profiles to the limits imposed by noise in the data when observed nearly continuously for three days in September, 1978, for a total of 75 exposures, when reobserved once a month later, and again in January of 1979. For this reason, this

star has been chosen to determine the noise limits in different parts of the SWP spectrum. Only SWP spectra are considered in this paper, as we are still awaiting our reprocessed LWR spectra. Table 1 gives the limits on change in relative flux level as a percentage of the zero to continuum level. To be confident that the change in flux level is stellar, rather than instrumental or processing-induced, the further constraint has been imposed that the change in the flux level must be sustained over a 0.1Å interval. Changes over smaller intervals may be real, but a detailed examination of gross and background records for each image would be essential in order to determine whether or not this is the case.

OBSERVATIONS

Even with these conditions, three stars surveyed to date show clear evidence of temporal variations in their P Cygni profiles. Analysis is still in the preliminary stages for all three. They are κ Cas (B1Ia, HD 2905), 59 Cygni (Be, HD 200120) and γ^2 vel (WC8 + 09I, HD 68273).

κ Cas was observed as part of a cooperative program with H.J.G.L.M. Lamers, C. deJaeger, and F. Machetto. It was observed for 29 hours in alternation with α Cam on Sept. 9-10, 1978. A total of 26 SWP high-resolution exposures were made during this time with exposure times of 6-10 minutes. All profiles were constant to within the limits of detection. On Oct. 12, 1978 a single exposure of κ Cas was obtained. The fully-saturated P Cygni profiles showed no changes in shape or relative intensity beyond the noise limits. The two unsaturated profiles, CII λ1335, and AlIII λ1854, λ1862 did show noticeable changes. The CII P Cygni profile appears slightly broader in the October spectrum than in the Sept. data. It was not possible to measure the edge velocity for this line as the profile lacks a sharp short wavelength absorption edge. The changes in the AlIII profile are much larger. In the September observations only the AlIII λ1854 line has a well developed Type I P Cygni profile (see Fig. 1). A saturated emission feature is present at the wavelength expected for the λ1862 emission. Weak absorption is present shortward of this feature. In the October observation both AlIII components are clearly present, although the λ1862 line suffers from an instrumentally saturated emission peak. The emission part of the λ1854 profile appears to be about the same as in September. Likewise, the edge velocity, as measured from the λ1854 line, appears to be constant. The striking changes in the absorption component occurs at the red side of the absorption feature, in the velocity range -(410-710) ±20km/sec.

59 Cygni was observed in cooperation with V. Doazan, R.N. Thomas, L. Kuhi, and J.M. Marlborough. Data has been processed at LASP only for observations made in June and September of 1979. Data handling problems have prevented analysis of all ions with the exception of CIV λ1548.188, λ1550.762. (See Fig. 2) In June, 1979 the doublet is blended together in absorption. The profile appears to be saturated. By September, however, both components are clearly visible. How this correlates with changes in other orders is not yet known. A cursory examination of SiIV λ1400 indicates that no such drastic changes occurred for that ion.

γ^2 vel was observed as part of a collaborative program involving K.A. van der Hucht, A. Willis, F. Machetto, R. Wilson, and D. Stickland with some of the data analysis taking place at C.U. We have processed CIII λ1176, SiIII λ1206, NV λ1240, CII λ1335, SiIV λ1400 (Fig. 3), CIV λ1550 (Fig. 4), and NIV λ1718. All of the ions surveyed show some changes in the shape of the absorption part of the P Cygni profile. More dramatically, all show decreased emission at phase 0.53 of the binary orbit. At this phase the Wolf-Rayet star is in front as seen from Earth. With data covering only one orbital period it is impossible to be certain that this decrease is related, but the data are rather suggestive.

CONCLUSIONS

Despite the limits on the amplitude and type of temporal variability that can be confidently detected using IUE in high-resolution mode, it is possible to observe significant time variations in the P Cygni profiles of hot stars.

REFERENCES

1. Grady, C.A.: Problems and Programming for Analysis of IUE High-Resolution Data for Variability. The Universe in Ultraviolet Wavelengths: The First Two Years of IUE. NASA CP-2171, 1980: this compilation.
2. Snow, T.P. Jr. and Morton, D.C.: Ap J Supp Ser, vol. 32, 1976, pp. 429-465.
3. Niemelä, V.S. and Sahade, J.: The Orbital Elements of γ^2 Velorum, preprint Sept. 1979.

TABLE 1

Ion	Wavelength	Noise (as % of continuum level)
CIII	1175.67	∿100
SiIII	1206.51	∿ 60
NV	1240	$35^{\pm}4$
SiIV	1398	$20^{\pm}3$
CIV	1549	$19^{\pm}2$
NIV	1718.551	$15^{\pm}2$

Percentage change in flux level which must be exceeded in a given P Cygni profile to be confident that any variations are stellar rather than instrumental. In all cases the data has been normalized to continuum = 1.

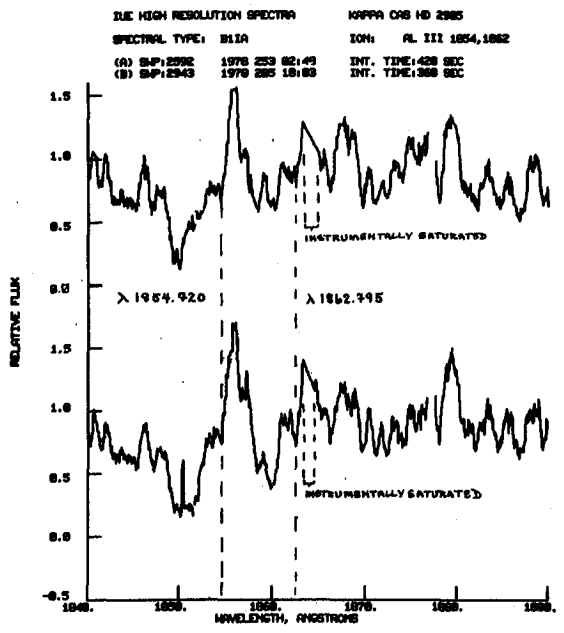

Fig. 1. κ Cas observed (upper spectrum) Sept. 9, 1978 and (lower spectrum) Oct. 12, 1978 in AlIII λλ1854, 1862. Note the change in the absorption.

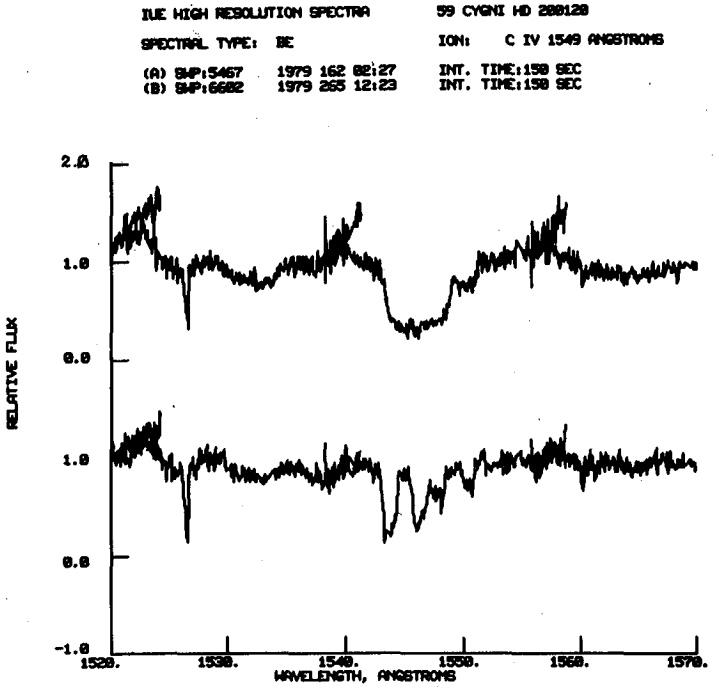

Fig. 2. 59 Cygni observed (upper spectrum) June 10, 1979 and (lower spectrum) Sept., 1979 in CIV.

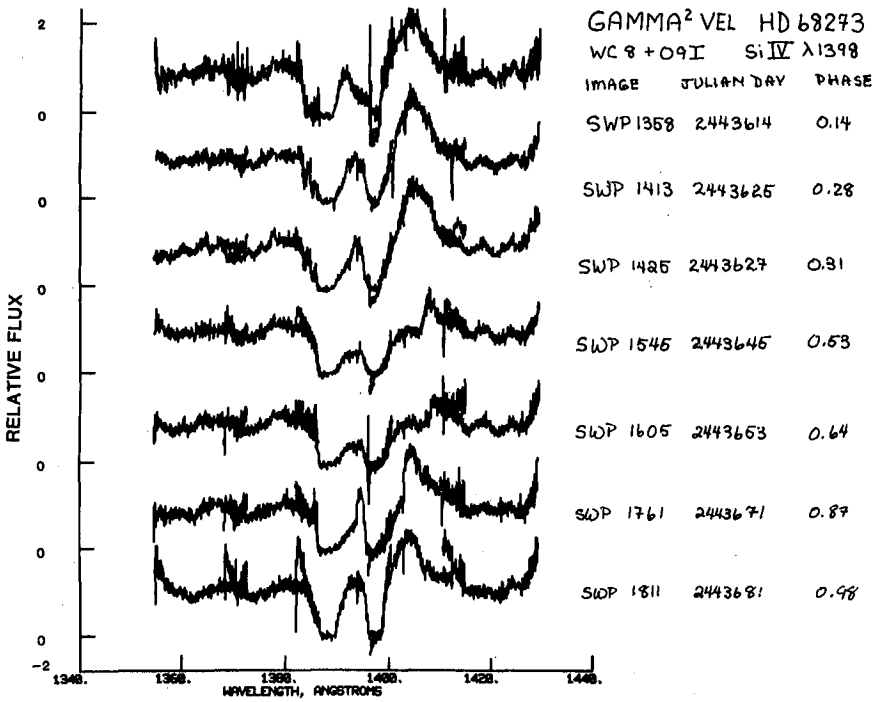

Fig. 3. γ^2vel: Observations at different phases in 1978 of SiIV λ1398. Phases calculated from (3).

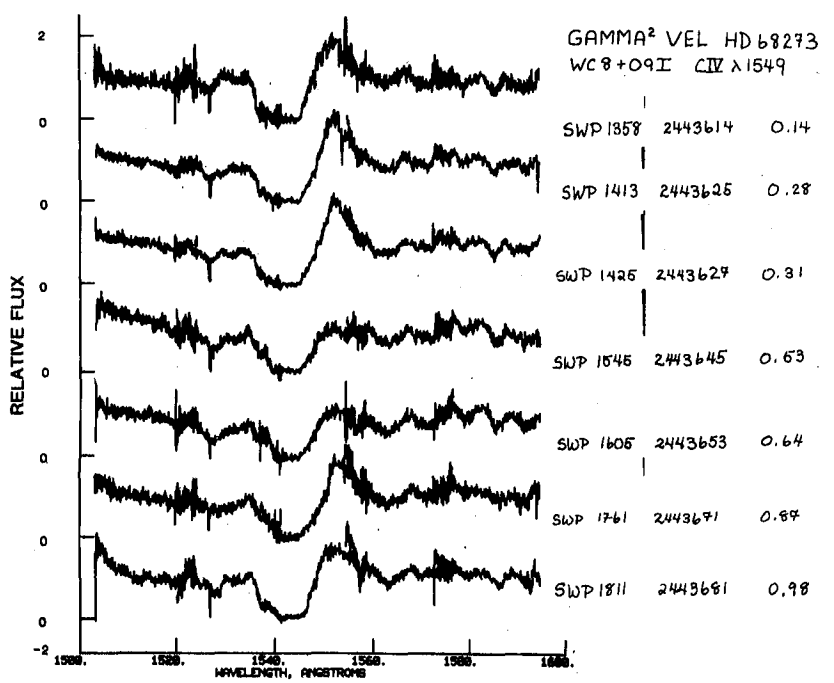

Fig. 4. γ^2vel: Observations at different phases in 1978 of CIV λ1549.

ANOMALOUS IONIZATION SEEN IN THE SPECTRA OF B SUPERGIANTS

Joseph P. Cassinelli and David C. Abbott

Washburn Observatory
Madison, WI 53706

ABSTRACT

An IUE survey of B supergiants has been conducted to study the persistence with spectral type of the ultraviolet resonance lines of N V, C IV, and Si IV. N V is seen as late as B2.5Ia, C IV until B6Ia and Si IV throughout the range from B1.5 to B9. This is in fairly good agreement with the Auger ionization model of Cassinelli and Olson (1979). The terminal velocities are derived for the 20 stars in the sample and it is found that the ratio v_T/v_{esc} decreases monotonically with spectral type from the value of 3.0 that it has in the O spectral range to the value 1.0 at B9Ia.

INTRODUCTION

Unexpectedly high ionization stages such as O VI were seen in the Copernicus spectra of O stars (Snow and Morton, 1976). Several possible explanations were considered by Cassinelli, Lamers and Castor (1978). X-ray emission has now been discovered from O stars by observations from the Einstein satellite (Harnden et al. 1979, Seward et al. 1979, Long and White 1980), and it is now clear that there is some very hot gas in the outer atmospheres of the stars. The x-ray emission is sufficient to produce the ionization anamolies in the cool outflow by the Auger mechanism as had been proposed by Cassinelli and Olson (1979). In this process, a total of two electrons are ejected from C, N or O following the K shell absorption of an x-ray photon. (Weisheit 1974). Thus if the dominant stage of ionization in the outflow is O IV a trace amount ($\sim 10^{-3}$) of O VI is produced, which is sufficient to explain the P Cygni lines seen in the UV spectra. As O IV should be an abundant ion stage (>10%) for stars as late as BO.5Ia (Teff = 29000) O VI should persist to that spectral type and no further. Morton (1979) carried out a careful study of Copernicus spectra of early B supergiants and found that O VI does persist to BO.5 and is absent at B1Ia.

In a similar fashion N V should persist as long as N III is a dominant ion stage and C IV as long as C II is a dominant ion stage in the cool parts of the wind. To give further test of the Auger ionization model we have carried out a survey of 20 B supergiants in every spectral class from B1.5 to B9Ia.

OBSERVATIONAL RESULTS

Figure 1 shows the spectra at N V 1239, 1243Å for 11 of the B supergiants from B1.5 to B5. The line is clearly present from B1.5 to B2Ia but disappears at later spectral types. At the bottom of the array of spectra is shown the results of theoretical calculations of absorption line strengths expected in a 20,000 K star at $N_e = 10^{11}$ cm^{-3}. These were calculated using

f values from Kurucz and Peytremann (1975) supplemented by more recent work by Abbott (1978), Morton (1978) and others. LTE populations were used in the calculation of the line strength, and the plotted line segments are proportional to the logarithm of the strength. After accounting for these background lines, we concluded that N V is present only as far as B2.5Ia where, using the calibration of Underhill et al. 1979, T_{eff} = 20400. As usual terminal velocities of the winds, v_T, can be derived for each line from the maximal shortward displacement of the absorption feature.

Figure 2 shows the spectra of all 20 supergiants in our survey in the region of the C IV doublet 1548, 1551Å. For the earlier stars the line displays the broad strong P Cygni profile familiar in O stellar spectra. The line becomes progressively weaker for the later spectral types. After consideration of the calculated strengths of the photospheric lines, we concluded that C IV in the wind could be traced as far as B6Ia at which the effective temperature is about 12000Å. In an earlier IUE survey Underhill (1979) noted the presence of C IV as late as B5Ia. The theoretical photospheric line strengths at the bottom of the figure were calculated as before, but now using 15000 K for the left panel and 10000 K for the right panel. Again terminal velocities are derived from each line.

Figure 3 shows the Si IV doublet 1394, 1403Å region of the spectrum. The line clearly persists beyond either N V or C IV and continues throughout the sequence to B9Ia. (If the wind were in radiative equilibrium and not subject to x-radiation it would disappear at B3Ia.)

The spectrum of θ Ara shows distinctive structures in the resonance lines of N V, C IV and Si IV. There is an apparent contribution from the lines at zero velocity displacement. This roughly symmetric contribution could perhaps have been produced in a "transition region" between the photosphere and x-ray forming region.

DISCUSSION

The run of "terminal" velocities, derived for the three ions, versus spectral type is shown in Figure 4. For Si IV the velocity is determined from the stronger component at 1393Å. Indicated in this Figure is the result that N V persists to B2.5Ia and C IV to B6Ia. These are in rather good agreement with what is expected if N V is produced from N III and C IV is produced from C II by the Auger mechanism. (Cassinelli and Olson 1979). The persistence of Si IV can also be explained by the Auger mechanism but as the ion Si II has more than 10 electrons the analysis is more complicated (Weisheit 1976). The ion could eject from 2 to 4 electrons following L or K shell absorption of x-radiation. In any case it is not surprising that it should persist to later spectral types than does C IV.

Also shown in Figure 4 is the escape speed at the photosphere versus spectral type. These were derived from the data on cluster membership distances, effective temperatures (Barlow and Cohen 1977) and masses derived from theoretical evolutionary tracks (Chiosi et al. 1978), in the manner described in the terminal velocity survey of Abbott (1978). In that paper Abbott derived the ratios of v_T/v_{esc} for 36 stars, all but one of spectral

type B_1 or earlier plus some Wolf Rayet stars. He found $v_T/v_{esc} = 3.0$. IUE spectra of other O-type stars also show a $v_T/v_{esc} = 3.0$ scaling (Garmany 1980). This relation does not hold for B supergiants as is seen from Figure 4. The terminal velocity decreases monotonically from $\sim 2.7\ v_{esc}$ at B1.5Ia to $1.0\ v_{esc}$ at B9Ia. The A2Ia star, α Cyg, also has $v_T = 1.0\ v_{esc}$.

Thus, there is a continuous relation between v_T and v_{esc} extending from the earliest O stars to the latest B supergiants. The reason for the decreasing value of v_T/v_{esc} in the later type stars is not clear. The effective temperature, gravity and rotational velocity are all properties which decrease monotonically from early O-stars to late B supergiants.

The decrease in v_T/v_{esc} does not conflict with the line driven wind theory of Castor, Abbott and Klein (1975). As discussed by Abbott (1978), that theory predicts $v_T = [\alpha/(1-\alpha)]^{1/2}\ v_{esc}$ where α is a numerical constant which is determined by the mixture of optically thick and optically thin lines. If all the lines are optically thick α=1, and if all the lines are thin α=0.0. In this model $\alpha = 0.9$ gives $v_T/v_{esc} = 3.0$, and α=0.5 gives $v_T/v_{esc} = 1.0$. The result of Figure 4 therefore may indicate that the ionization balance changes in B supergiants from a radiation force dominated by a few very strong lines to a force produced from lines which are more numerous but weaker.

The x-ray emission of early type supergiants also changes in character at around B1.5Ia. Vaiana et al. (1980) notes that essentially every O star observed by Einstein is an x-ray source. However in the Einstein survey of O and B supergiants Cassinelli et al. (1980) have found that there is a change at B1.5. All objects at B1.5I and earlier were detected with $L_x \approx 10^{-7.5}\ L_{Bol}$ whereas limits on x-ray luminosities beyond B1.5Ia were lower than $10^{-8.0}\ L_{Bol}$. Thus there is reason for pursuing further studies of the anomalous ionization in B supergiants. It may be the best diagnostic for studying the coronae or hot flow instabilities now available.

REFERENCES

Abbott, D.C. 1978a, J. Phys. B: Atom. Molec. Phys. 11, 3479.
Abbott, D.C. 1978b, Ap.J., 225, 893.
Barlow, M.J., Cohen, M. 1977, Ap.J., 213, 737
Cassinelli, J.P., Castor, J.I., Lamers, H.J.G.L.M. 1978, P.A.S.P., 90, 496.
Cassinelli, J.P., and Olson, G.L. 1979, Ap.J., 229, 304.
Cassinelli, J.P., Waldron, W.L., Vaiana, G., Rosner, R. 1979, in prep.
Castor, J.I., Abbott, D.C. and Klein, R.I. 1975, Ap.J., 195, 157.
Chiosi, C., Nasi, E. and Sreenivasan, S.R. 1978, Astr. Ap., 63, 103.
Garmany, K. 1980, private comm.
Harnden, F.R., Branduardi, G., Elvis, M., Gorenstein, P., Grindlay, J., Pye, J.P., Rosner, R., Topka, K., and Viana, G.S. 1979, Ap.J. (Letters), 234, L51.
Kurucz, R.L., Peytremann, E. 1975, SAO Sp. Rpt. 362. Smithsonian Inst. Washington, D.C.
Lamers, H.J.G.L.M., Snow, T.P. 1978, Ap.J., 219, 504.
Long, K.S. and White, R.L. 1980, Columbia Astro. Lab. Contribution No. 183.
Morton, D.C. 1978, Ap.J., 222, 863.

Morton, D.C. 1979, M.N.R.A.S., 189, 57.
Snow, T.P. and Morton, D.C. 1976, Ap.J. Suppl., 32, 429.
Seward, F.D., Forman, W.R., Giacconi, R., Griffiths, R.E., Harnden, F.R., Jones, C. and Pye, J.P. 1979, Ap.J., 234, L51.
Underhill, A.B. 1980, Ap.J., 235, 149.
Underhill, A.B., Divan, L., Prevot-Burnichan, M.L. and Doazan, V. 1979, M.N.R.A.S., 189.
Vaiana, G. et al. 1980, submitted to Ap.J.
Weisheit, J.C. 1974, Ap.J., 190, 735.

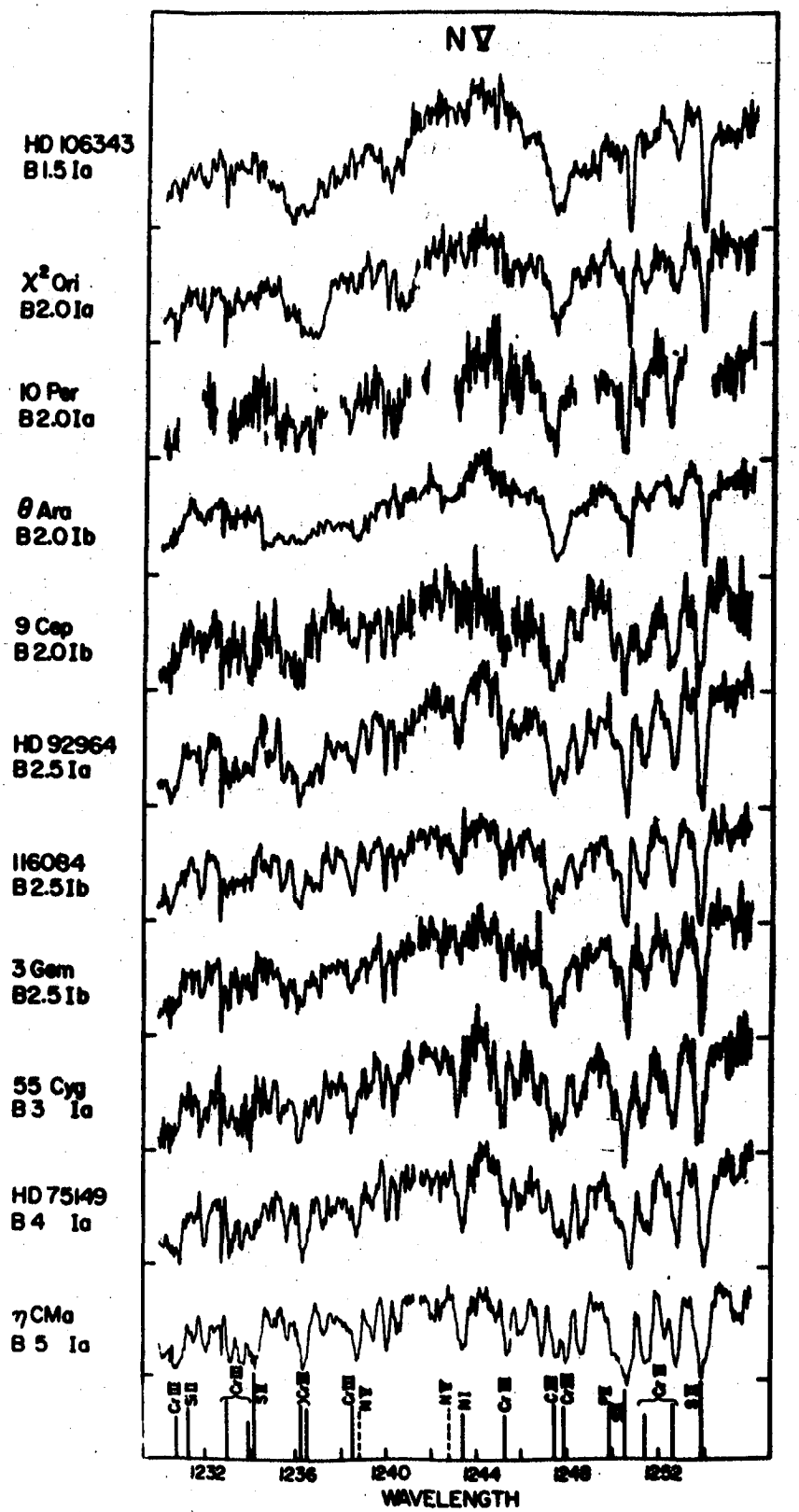

Fig. 1: The spectral region near 1240Å in B supergiants from B1.5 to B5. The major photospheric and interstellar lines in the region are identified at the bottom. The predicted relative strength of these spectral lines is indicated by the length of the line segment. Lines whose opacity was not calculated (usually interstellar) are indicated by dashed lines.

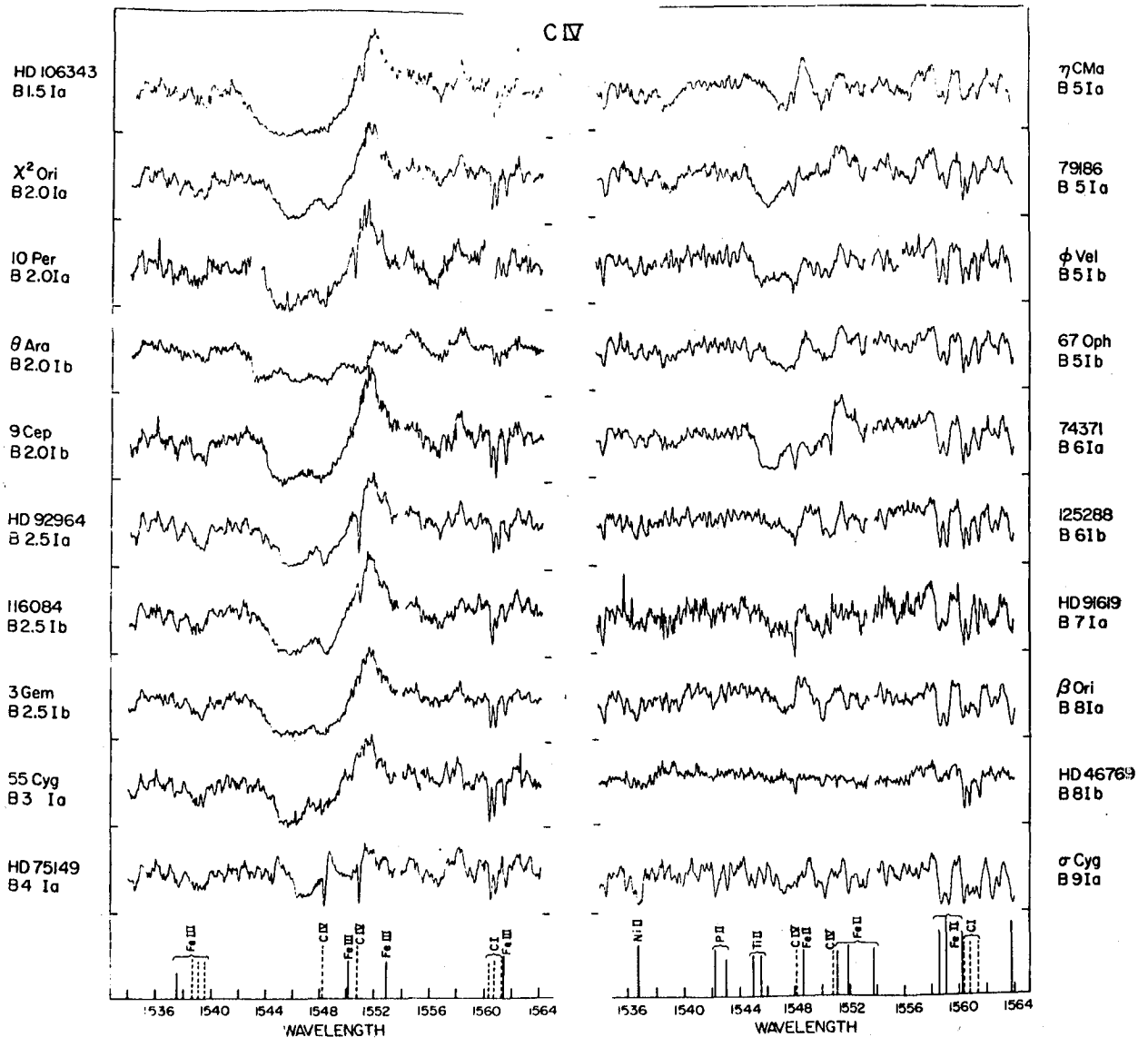

Fig. 2: The spectral region near 1550Å in B supergiants from B1.5 to B9.

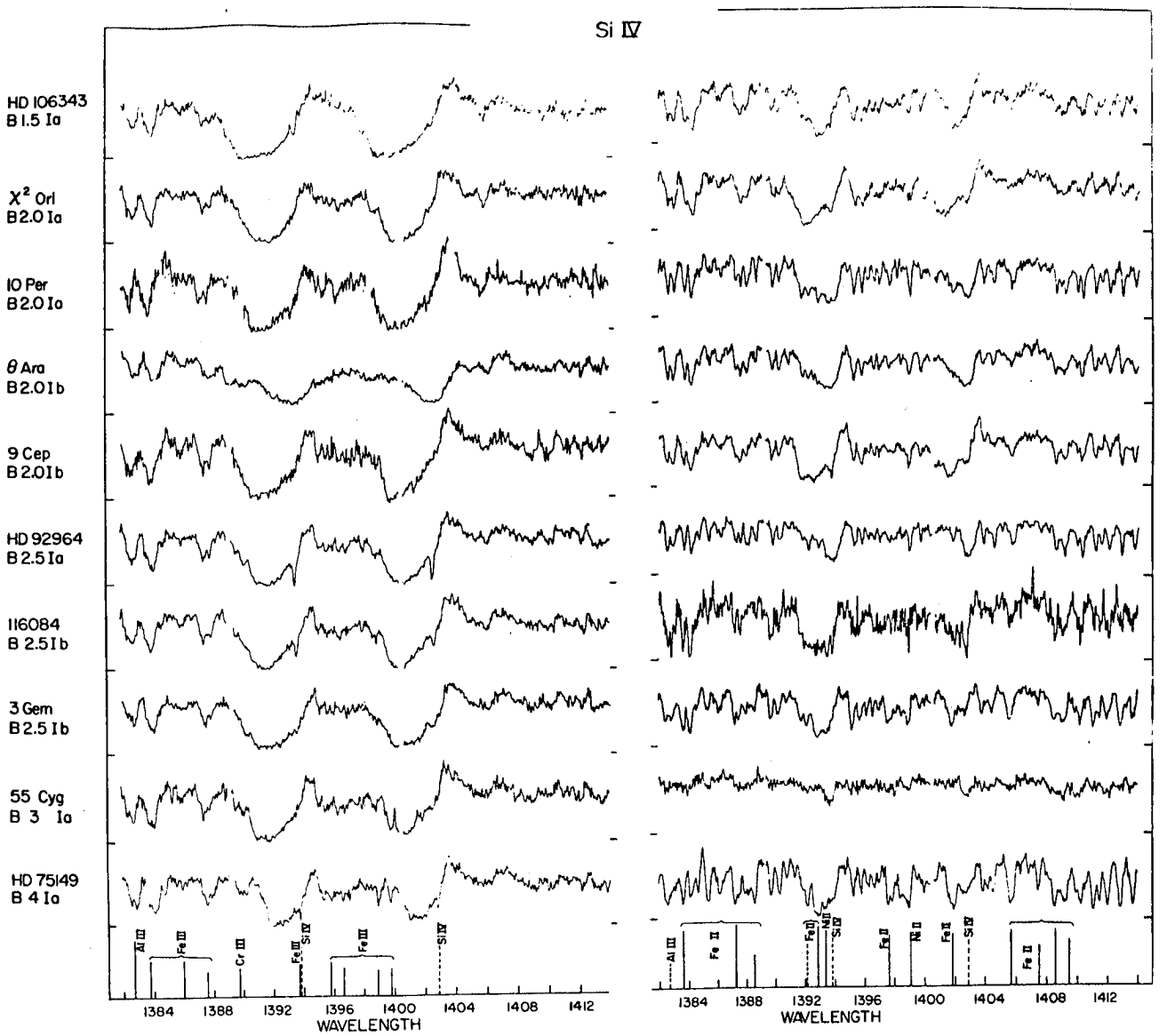

Fig. 3: The spectral region near 1400Å for B supergiants from B1.5 to B9.

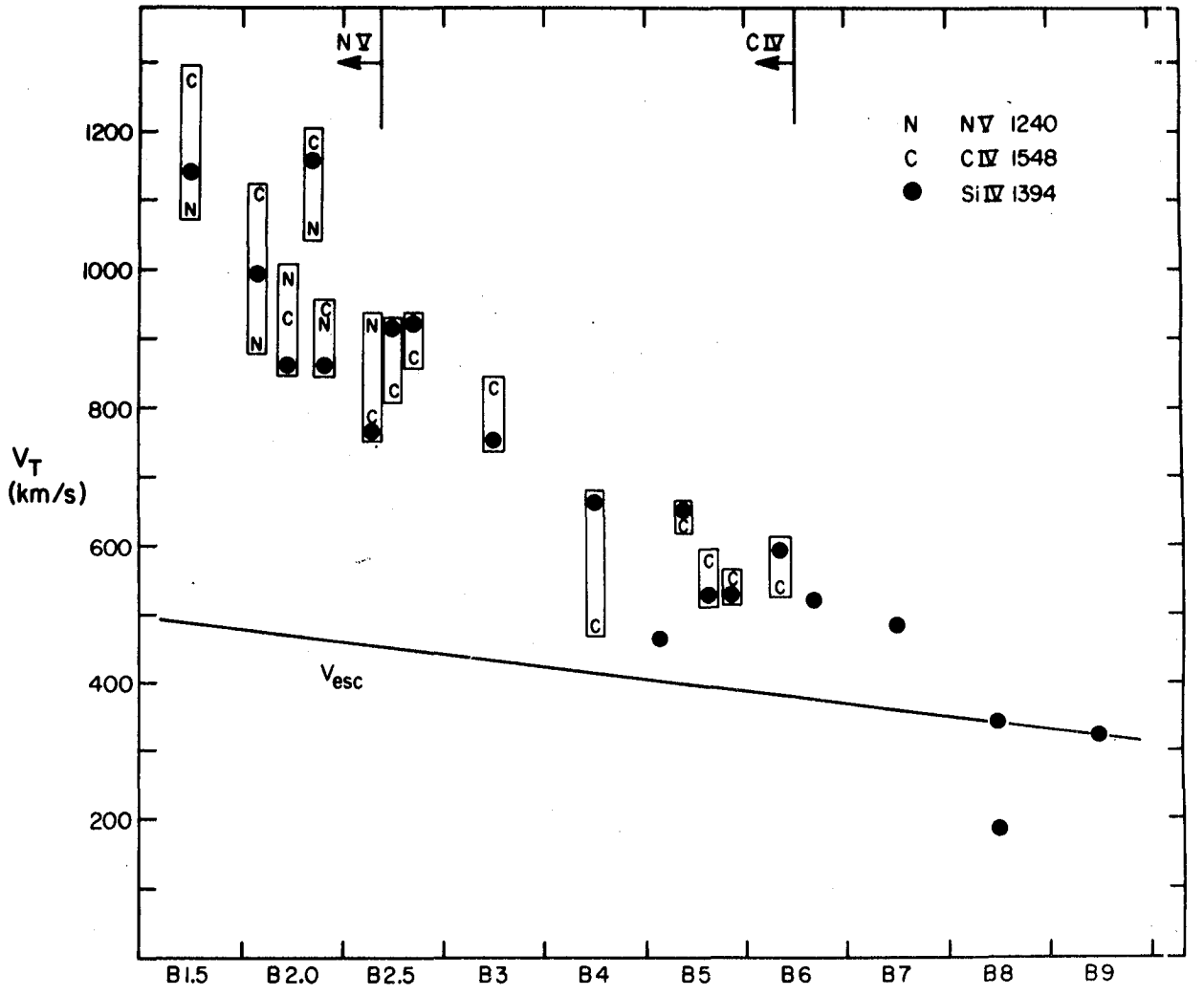

Fig. 4: Terminal velocities v_T derived from the resonance lines of N V, C IV and Si IV 1394. A box surrounds the measurements of one star in those cases in which more than one of the lines appears in the spectrum. Also shown in the run of escape speed for the supergiants of spectral type B1.5 to B9.

ABSOLUTE ENERGY CURVES FROM LATE B-TYPE SUPERGIANTS

Anne B. Underhill
Laboratory for Astronomy and Solar Physics
Goddard Space Flight Center

ABSTRACT

Absolute energy curves for six late B and early A-type supergiants have been determined from IUE data and from other ultraviolet and ground-based photometry. Effective temperatures and angular diameters are presented as well as estimates of the outflow velocity of the wind. All six stars show a strong Balmer continuum in emission; the Ia supergiants also show an infrared excess which reaches into the visible range. Evidence is found for the presence of a warm mantle as well as for wind from the Ia stars.

INTRODUCTION

From ultraviolet spectra it has become clear that O stars and early B stars have an outer atmosphere or mantle in which at least some of the gas is heated to temperatures of the order of 10^5 K and where a rapidly flowing wind is generated. The purpose of this investigation is to see what the evidence is for a mantle for the late B supergiants. The material in the mantle of an O or early B star is seen best by means of the ultraviolet absorption and emission resonance lines.

There is evidence that the mantles of late B and early A stars are seen most easily by means of the continuous spectrum. For instance, Berger et al. (1) showed that the continua of supergiant A stars longward of 5000 Å are usually red, relative to what is seen for main-sequence A stars of the same subtype, and Barlow and Cohen (2) have found that the late B and early A Ia supergiants tend to have a small infrared excess.

The continuous spectrum from the photosphere of an early-type star, that is from the boundary layer of the interior model of the star, can usually be well represented by the predicted spectrum from one of the LTE line-blanketed model atmospheres of Kurucz (3), see Underhill et al. (4). Therefore, comparing the energy distributions of supergiants with the predicted continuous spectra of Kurucz will show whether additional continuous radiation, generated in the mantle of the star, is present or not. Figures 1, 2 and 3 present such comparisons for six B/A supergiants. Solutions for effective temperature and angular diameter have been made for these stars using the methods of Underhill et al. (4) and of Underhill (5) and the results are given in Table 1. The absolute fluxes plotted in the figures have been corrected for interstellar extinction. The adopted values of E(B-V) can be seen to be about correct because no residual effect of the broad interstellar absorption ban centered at 2175 Å is evident in the plotted energy distributions. The relatively sharp dip near 2250 Å is due to blended absorption lines of Cr III formed in the mantle.

DISCUSSION

All of the supergiants studied here show excess emission in the Balmer continuum. In some cases this emission is strong; its presence is the reason why Underhill et al. (4) found that for supergiants the Chalonge and Divan values of D were smaller than the values predicted by means of model atmospheres. All of the Ia supergiants show an infrared excess extending into the visible range. The observations of Barlow and Cohen (2) permit one to trace this excess to longer wavelengths. The wavelength of the "turn-over point" of the infrared excess emission of HD 21291 and 21389 indicates that the electron temperature in the part of the mantle from which the infrared excess originates is near 23000 K.

The effective temperatures given in Table 1 are about correct because the intensity of the stellar light at wavelengths shortward of 1500 Å relative to that at wavelengths near 4100 Å is correctly represented by models having effective temperatures similar to the values given in Table 1. The amount of far ultraviolet light relative to that in the visible is a sensitive indicator of effective temperature for these stars. Near 4100 Å there should be no distortion of the continuum by excess emission due to the gas in the mantle and the Balmer continuous emission from the mantle should be very weak at 1500 Å.

The winds of these six B and A supergiants are easily visible only in the Mg II resonance lines. The terminal velocity estimated from the position of the shortward edge of the Mg II absorption profiles is given in Table 1. These stars do not show P-Cygni-type emission in Mg II.

The mantles of the B/A supergiants appear to be cool, $T_e \approx 23000$ K, but hotter than the effective temperature of the star, and to contain gas flowing at about 250 km s^{-1}. The star HD 21389 sporadically shows sharp C IV resonance lines in emission (Underhill (6)). None of these stars shows obvious absorption in the resonance lines of Si IV and C IV, but all show the resonance lines of Al III and C II as well as those of Al II and Si II.

The IUE observations used in this work were obtained with the skilled and gracious assistance of the IUE Resident Astronomers and Telescope Operators at the Goddard Space Flight Center.

REFERENCES

(1) Berger, J., Chalonge, D., Divan, L. and Fringant, A. M. 1956, Ann. Astrophys., 19, 267.
(2) Barlow, M. J. and Cohen, M. 1977, Ap.J, 213, 737.
(3) Kurucz, R. L. 1979, Ap.J. Suppl., 40, 1.
(4) Underhill, A. B., Divan, L., Prévot-Burnichon, M. L. and Doazan, V. M.N.R.A.S., 189, 601.
(5) Underhill, A. B. 1979, Ap.J, 234, 528.
(6) Underhill, A. B. 1980, Ap.J, 235, L149.

Table 1
Effective Temperatures, Radii, Luminosities
and Terminal Velocities of B/A Supergiants

Name	Spectral Type	E(B-V) mag	T_{eff} K	Θ 10^{-4} arc sec
53 Cas	B8 Ib	0.41	11600	3.62
β Ori	B8 Ia	0.04	11800	26.67
HD 21291	B9 Ia	0.41	10300[a]	7.27
η Leo	A0 Ib	0.02	9400	6.90
HD 21389	A0 Ia	0.54	9900[a]	8.05
α Cyg	A2 Ia	0.03	8600[a]	21.07

Name	d[b] kpc	$\frac{R}{R_\odot}$	log $\frac{L}{L_\odot}$	v_∞(Mg II) km s^{-1}
53 Cas	0.93	36	4.33	0[c]
β Ori	0.228	65	4.87	262
HD 21291	1.03	80	4.87	235
η Leo	0.54	40	4.05	>70[d]
HD 21389	1.00	87	4.82	240
α Cyg	0.45	102	4.71	278

[a]Allowance has been made for an infrared excess.

[b]From an adopted M_V.

[c]No sign of a wind in Mg II.

[d]Displacement of the deepest point of the Mg II resonance lines.

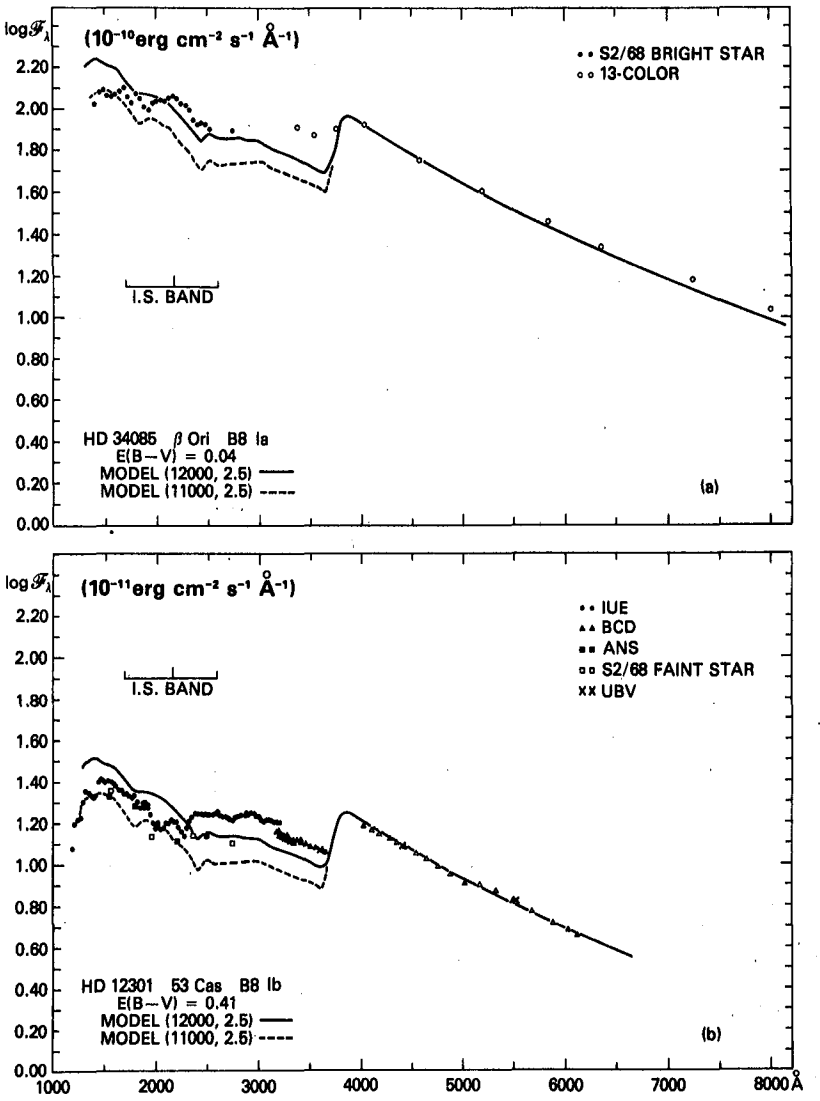

Fig. 1 - The energy curves, corrected for interstellar extinction, of the B8 supergiants 53 Cas and β Ori. The sources of photometric data are indicated in the figure.

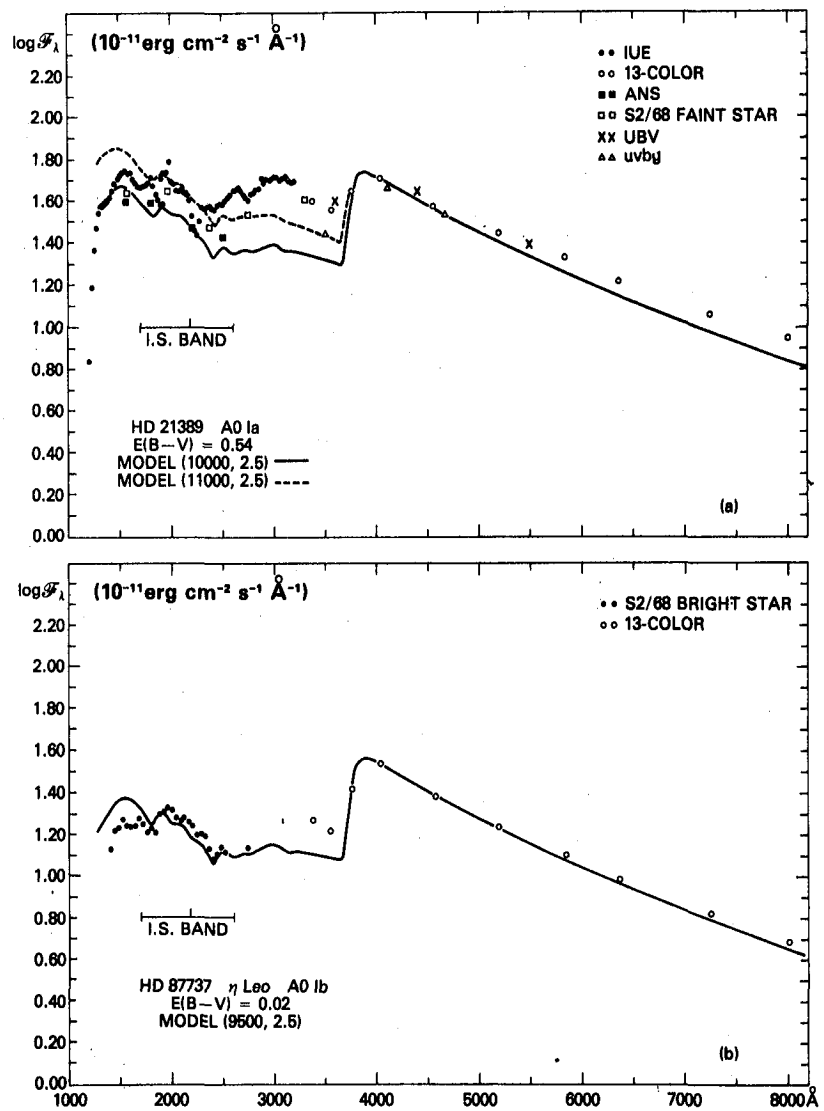

Fig. 2 - The energy curves, corrected for interstellar extinction, of the A0 supergiants η Leo and HD 21389. The sources of photometric data are indicated in the figure.

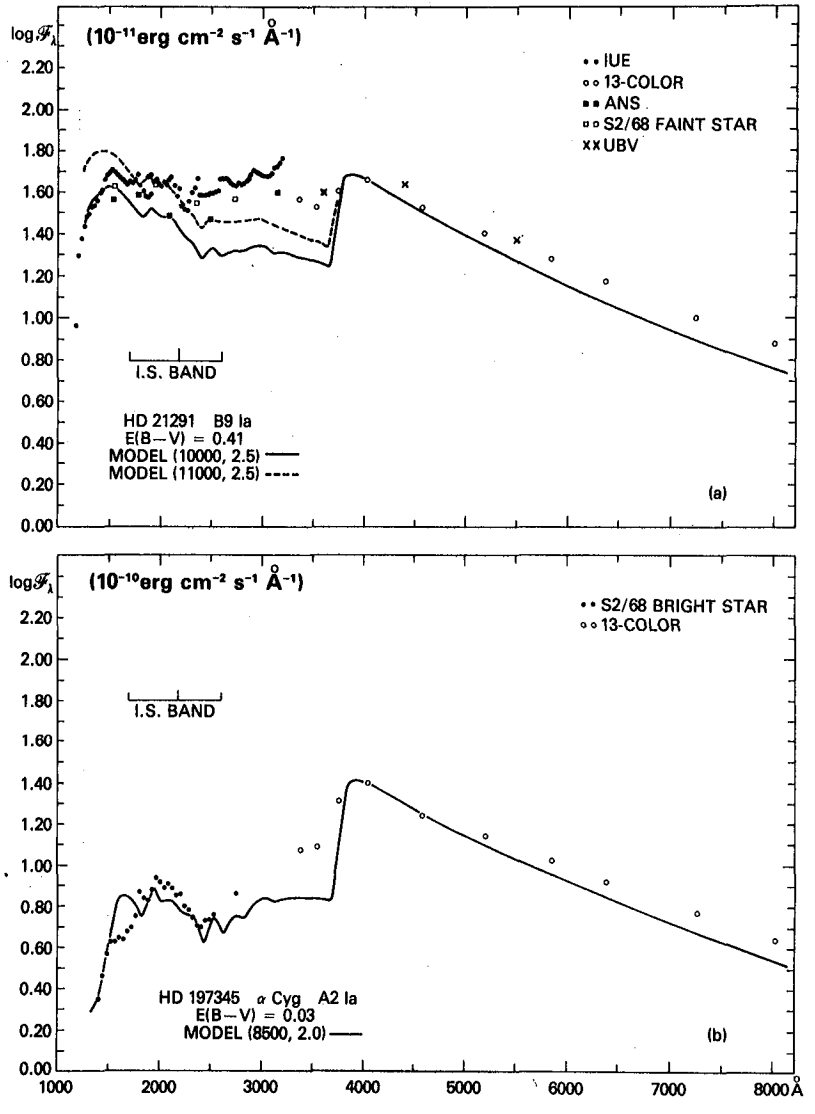

Fig. 3 - The energy curves, corrected for interstellar extinction, of HD 21291, B9 Ia, and α Cyg, A2 Ia. The sources of photometric data are indicated in the figure.

IUE AND GROUND-BASED OBSERVATIONS OF MASS-LOSS IN THE MAGELLANIC CLOUDS

F. Macchetto
ESA, ESTEC
Noordwijk Netherlands

P. Benvenuti
ESA, VILSPA
Madrid, Spain

S. D'Odorico
ESO
Geneva, Switzerland

N. Panagia
Istituto di Radioastronomia
Bologna, Italy

ABSTRACT

Ground-based and IUE observations of hot stars in the Large and Small Magellanic Clouds have been carried out to investigate the mass-loss process in these objects and to search for differences with galactic hot stars. Preliminary results show that in a large proportion of the stars observed the mass-loss process is taking place. A mechanism for acceleration of the wind in OB stars is proposed.

INTRODUCTION

This study of hot stars in the Large and Small Magellanic Clouds was carried out in order to:

(a) investigate in detail the mass-loss process in hot stars;

(b) investigate possible differences in the mass-loss characteristics due to chemical composition differences;

(c) investigate whether there exist broad differences between the mass-loss process as it occurs in the three galaxies, namely the two Magellanic Clouds and our own.

This paper presents some general results of the study. In particular a mechanism that accounts naturally for the acceleration of winds in hot stars is proposed.

OBSERVATIONS

Photometric observations were carried out with the ESO 50 cm photometric telescope in La Sillar, in September 1979. The diaphragm used was 15 arc sec in diameter. The U, B, V and Hβ photometric results shown in Table 1 are the

average of three or four nights of observations. Night-to-night deviations were at most one or two tenths of a magnitude in V. The photometric standards used were taken from the E-region standards for U, B, V and Hβ photometric list of Crawford and Mander [1]. The values shown in brackets are not our own data. Spectroscopic observations were carried out in September 1979 (indicated S) and January 1980 (J) with the ESO 1.52 m telescope and Boller & Chivens spectrograph. In September the dispersion used was 114 Å/mm. Recording was with a two-stage EMI intensifier tube and III a-J baked plates. In January the dispersion was 60 Å/mm. Recording was with a three-stage EMI intensifier tube and III a-J baked plates. The spectrum was widened in both cases.

While only two spectra per star could be obtained in September, at least three sets of spectra, each with three different exposure times, were obtained in January. This will allow us to establish if spectral variability occurs with a period of four months and also with a shorter period of about one week.

Observations were carried out with IUE in January (J) of those stars that had not already been studied by other investigators. These were obtained at the same time as the ground-based observations from La Silla. Use of the archived IUE observations will be made as this material becomes available.

An additional set of stars was observed at the end of March with IUE. The IUE observations were made in the low dispersion mode in all cases.

RESULTS

Although the analysis of the data is still in a preliminary phase, some general results can already be indicated.

A significant fraction of the stars observed show mass-loss, as indicated for example by broad Hα emission or by P Cygni type profiles in the UV lines. These stars have been identified with an asterisk in the column "mass-loss" of Table 1.

As an illustration of the results obtained, Figures 1, 2, 3 and 4 show the spectrum of the star HD 35343 (SK 94). This star is classified as Bep in the Sanduleak catalogue and shows a large number of emission and absorption lines.

The most prominent emission lines in the visible part of the spectrum are those of the Balmer series of Hydrogen of which Hα, Hβ and Hγ are shown in Figures 1, 2 and 3 respectively. The profiles of the three lines appear to be asymmetric. It is not clear if this is due to the contamination by absorption lines of other atoms in the blue side of each of the lines or if these are real P Cygni-like profiles. The halfwidth at zero intensity measured towards the red wing is 40 Å for Hα corresponding to an expansion velocity for the wind of Vexp = 2057 Km/s. The equivalent values for Hβ are 24 Å corresponding to 1580 Km/s and for Hβ the width is 12 Å corresponding to 830 Km/s. Other emission lines in the visible are those of SII 6521 and 6386, SiII 6371 and 5915, FeIII 6323, HeII 6310 (weak) 4686 (strong) and 4200 (strong), [OIII] 50006 and 4958, SiIII 4532 and 4567 and SIII 4478.

In the ultraviolet region the following lines are found in emission: NII 1758 and 1748, HeII 1640, CIV 1550 and 1549, SiIV 1394 and 1403 and NV 1239 and 1243. The wind velocity as measured from both the HeII and CIV profiles turns out to be 1550 Km/s which is significantly lower than that measured from Hα. This may be due to the depletion of hard-ionizing photons which restrict the presence of CIV to regions closer to the star.

DISCUSSION

It appears that in a broad sense the properties of the mass-loss process in the hot stars of the Magellanic Clouds and those of our own galaxy are very similar, although differences of detail, as already shown by Hutchins[2], can be seen and will be further investigated.

Of particular interest is the confirmation of weak correlation found for galactic OB stars (Panagia and Macchetto[3]) between the terminal velocity and the effective temperature (Figure 4). A similar correlation between terminal velocity and excitation class has been found by Willis[4] for WN stars. In both cases the higher the effective temperature the higher is the terminal velocity. In addition for all high temperature (or excitation) stars the momentum carried by the mass-loss (MV_∞) exceeds the momentum that the stellar radiation can release to the wind through single scattering, ϕ Lc (where ϕ is some effective efficiency factor, usually of the order of 0.1). Clearly a more efficient process is needed to account for the wind acceleration - this can be provided by multiple scattering of hard UV photons in the range - 200 to 500 Å (Panagia and Macchetto[3]). The process can be described qualitatively as follows. In the interval 200-500 Å the number of expected atomic and ionic lines is very large (a hundred or so) so that the average separation between subsequent lines is of the order of $c\Delta\lambda/\lambda \simeq 1000$ Km/s. Therefore, when a photon in this range is re-emitted in the backward direction (after being absorbed at a given position of the envelope) it can be absorbed at the opposite side of the envelope by a line transition which is shifted to the red by about $c\delta\lambda/\lambda \simeq 2v$ relative to the transition which had produced the first absorption. This process can be repeated several times (typically 5 to 20) until the photon eventually either excapes in the outward direction or hits the star and is thermalised. Therefore, the efficiency of this process is mainly determined by geometry and only marginally by both mass-loss rate and chemical abundances. With this mechanism the momentum given to the wind can amount to several times (5-20) L (200-500 Å/c, which is just what is needed to explain the acceleration of the wind in OB stars, and possibly in WR stars too (Panagia and Macchetto[3]).

In addition, since the acceleration due to multiple scattering is most efficient at some distance from the stellar surface (typically 2 to 4 stellar radii) the wind velocity is expected to present a gradual rise with radius and to approach the terminal value quite far from the star. This also agrees well with observations.

REFERENCES

1. Crawford, D. L. and Mander, J., 1966, Astron. J., 71, 114.

2. Hutchins, J. B., 1980, Astrophys. J., 235, 413.

3. Panagia, N., and Macchetto, F., in preparation.

4. Willis, A., 1980, Proc. Second European IUE Conf., 25-28 March 1980, Tübingen.

Table 1

Star	Spectral type	V	B - V	U - B	Hβ	Spectrum Visible	IUE	Mass-loss
Large Magellanic Cloud								
HD 32228	09.5 + W	10.789	-0.170	-0.906	2.679	S/J	J	*
38282	WN6	11.177	-0.144	-0.872	2.256	S		
HDE 268605	09.7 IB	11.355	-0.137	-0.964	2.644	S		
268743	06	11.643	-0.172	-0.906	2.331	S		
269090	BO I	11.682	-0.075	-0.929	2.558	S		
269333	B1	11.260	-0.158	-0.825	2.467	S/J		*
269357	06	12.123	-0.249	-1.024	2.269	S		
269445	OBf	11.459	0.242	-0.805	2.163	S/J		*
269546	B4	9.921	-0.064	-0.751	2.548		J	
269676	04-5	11.510	-0.193	-0.908	2.516	S/J		*
269698	04 If	11.877	-0.156	-0.932	2.579	S/J		*
269810	03IF	12.269	-0.232	-1.004	2.643	S/J		*
269828	08	11.181	0.007	-0.791	2.557	S/J		*
269858	OI	11.094	-0.067	-0.900	2.212	S		
269891	BO.7	11.449	0.149	-0.701	2.450	S		
269896	ON 9.7	11.363	-0.018	-0.866	2.475	S		
269936	BO.7	11.202	-0.041	-0.829	2.524	S		
270952	06 IAF	12.018	-0.192	-0.998	2.443	S/J		*
271213	B3 IA	12.261	-0.105	-0.708	2.737	S		
No photometry								
HD 34664	BEP	(11.83)	-	-	-	J	J	*
35343	PEC	(9.8)	-	-	-	J	J	*
HED 269748	WR	(12.8)	-	-	-	J	J	*
Small Magellanic Cloud								
HD 4862	OB	10.768	1.099	0.917	2.624			
5045	OB	11.077	-0.047	-0.872	2.487	S/J		*
5030	B6 I	11.229	0.080	-0.473	2.513	S/J		*
BBBB1, SK31	OB	11.146	-0.020	-0.740	2.549	S		
HD 5291	OB	10.858	0.062	0.618	2.511	S		
5980	OB + W N3	11.967	-0.231	-1.004	2.458	S/J		*
46531	OB	11.798	-0.164	-0.863	2.565	S/J		*

S = September 1979
J = January 1980

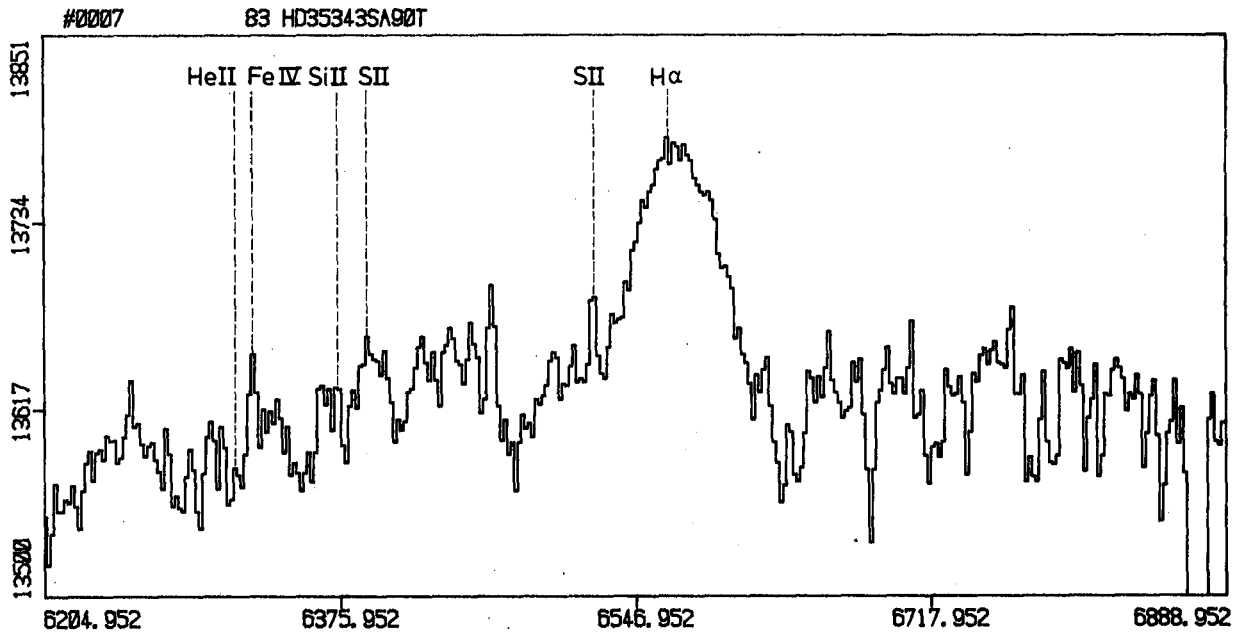

Figure 1

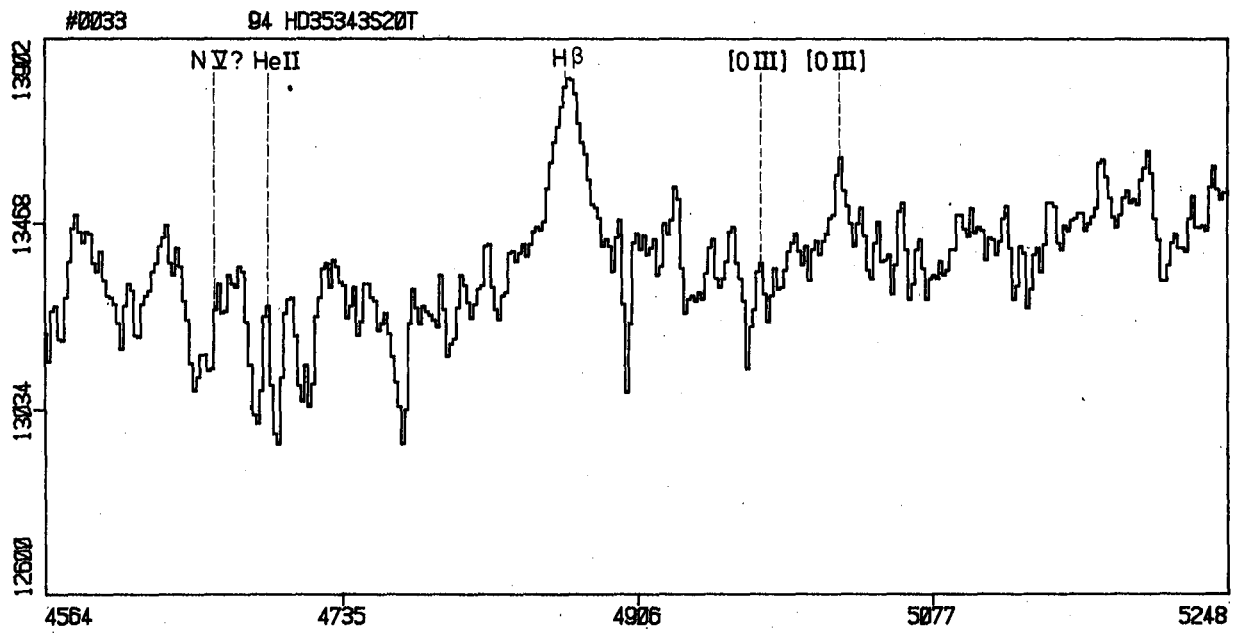

Figure 2

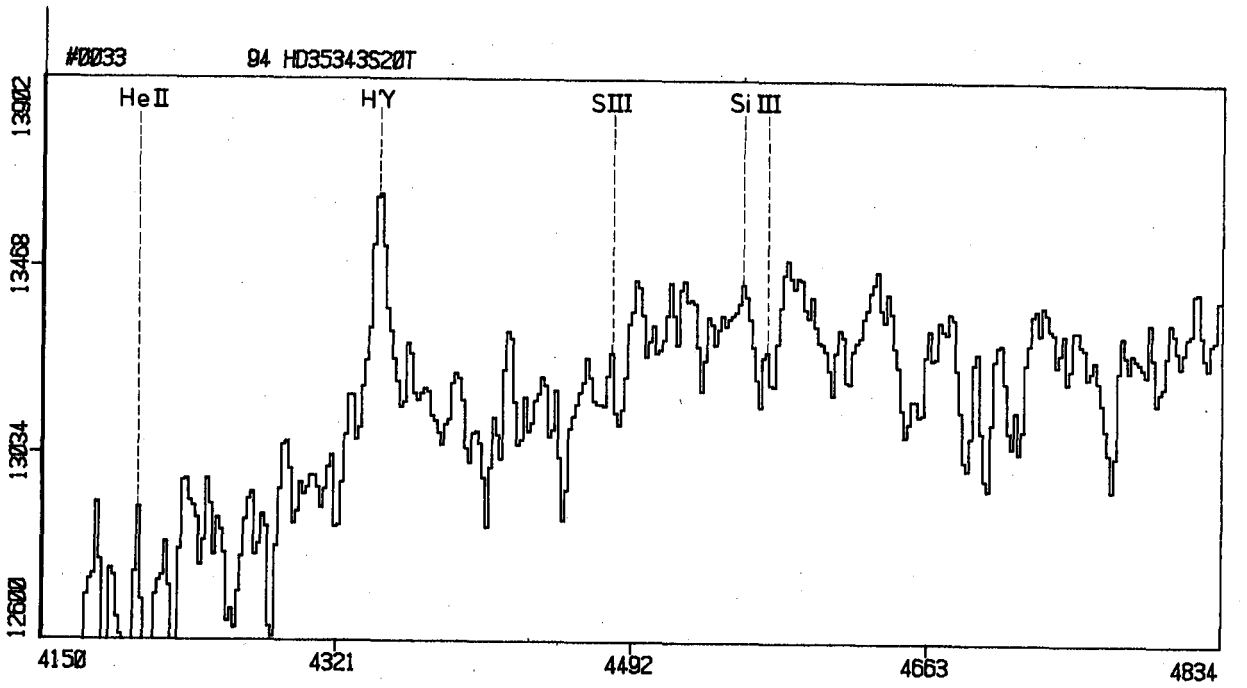
#0033
94 HD35343S20T
HeII
HY
SIII
SiIII
13002
13468
13034
12600
4150
4321
4492
4663
4834

Figure 3

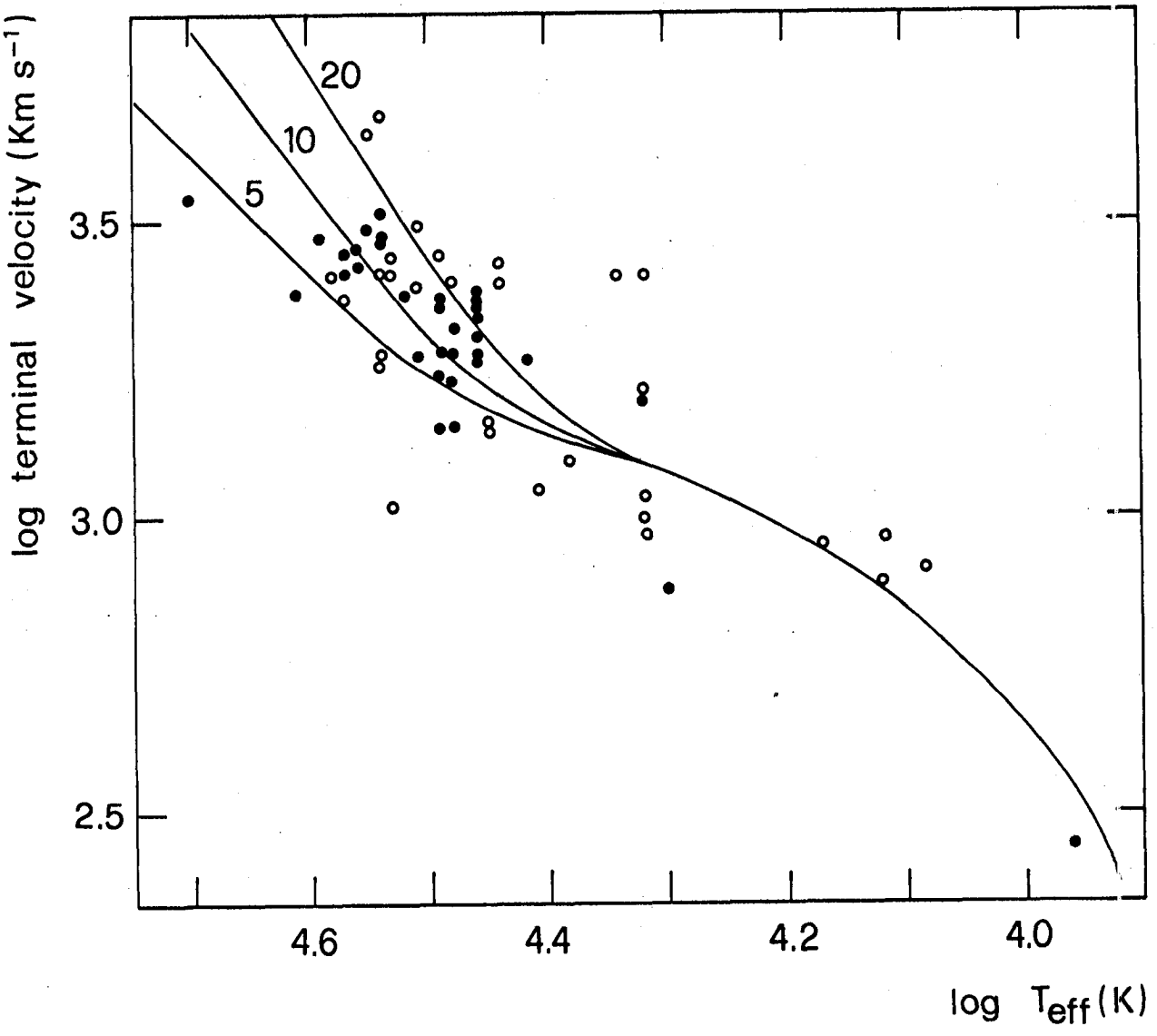
log terminal velocity (Km s^{-1})
3.5
3.0
2.5
20
10
5
4.6
4.4
4.2
4.0
log T_{eff} (K)

Figure 4

PROPOSED THREE-PHASE MODELING OF Be STARS FROM COMBINED UV AND VISUAL OBSERVATIONS

V. Doazan, R. Stalio, and R. N. Thomas

Observatoire de Paris, Osservatorio Astronomico di Trieste,
Institut d'Astrophysique, Paris

ABSTRACT : FarUV observations of the behavior of (wind-velocity, superionization) values as a function of the phase of the (Be, B-shell, B-normal) pattern established by visual observations for γ Cas and 59 Cyg are translated into a crude atmospheric model for the Be phase and several kinds of mass-flux variability across the three phases.

I. INTRODUCTION :

In the visual spectral region, one finds it possible to establish quite homogeneous classes of normal stars, based on their continuum, the overall strengths of some lines, and the wings of most lines. Such features characterize a photosphere, defined as an atmospheric region which can be modeled from values of (gravity, total radiative-flux $\equiv$ effective temperature) under those thermodynamic constraints accompanying the condition that the star be a closed, thermal system. Those anomalous features, and those stars in which such anomalous features are strong, which cannot be modeled under the preceeding two-dimensional, (closed, thermal) description are labeled peculiar ; and their origins are attributed to the existence of atmospheric regions lying above the photosphere, within which the thermodynamic constraints accompanying the (closed, thermal) description are not imposed. Prior to observations made in the farUV,x-ray, farIR, and radio spectral regions,our knowledge of such outer atmospheric regions came almost wholly from such peculiar stars, including the Sun because of its peculiarly-close location, which enables detection of anomalous features with only small amplitudes.Indeed, there has been strong confusion as to whether many normal stars do not have such outer atmospheric regions, or whether they are simply too small to be detected under present observational techniques in such stars.

In the farUV and x-ray spectral regions, such homogeneity within visually-defined (luminosity, spectrum) class is very often replaced, among both normal and peculiar stars, by strong individuality and variability in the observed spectral features ; which implies that such two-dimensional specification of a star is insufficient, observationally and thermodynamically. These same features of individuality and variability are shown in the visual spectral regions of most peculiar stars, as is the additional feature of gradualness, or the existence of all degrees of peculiarity between very large and very small.Such gradualness should be contrasted to any belief that peculiarity is an abruptly-occuring characteristic. All this suggests that peculiar stars differ from normal stars only in having larger amplitudes of those parameters which must be adjoined to the "normal", two-dimensional, set in order to describe the "anomalous" phenomena in the visual, and the "normal" phenomena in the farUV, x-ray, farIR, and radio regions, and to model those outer atmospheric regions

where such phenomena arise. This suggests that a combination of visual spectral features of peculiar stars and pan-spectral features of both peculiar and normal stars can be used, empirically : first, to map out the structure of those exo-photospheric regions ; then, to identify those additional, independent parameters and modified thermodynamic constraints that are necessary and sufficient to model such structure.

The present paper summarizes such a combination of recent farUV observations with visual observations extending over almost a century for one type of peculiar star : the Be/shell. We find that the apparently different "objects" --- Be, B-shell, B-normal --- are actually just three different temporal phases of one kind of object, with passage between phases occuring in time incomparably shorter than evolutionary. By linking such phase-changes, and implied atmospheric structure, to different levels of mass-flux occuring at different times in a given star, while noting that the maximum superionization level in the farUV region does not appear to change, we identify both additional parameters and modified thermodynamic restraints and character. We note that 30 % of main-sequence B stars show, at a given epoch, either the Be or B-shell phase spectra. Some portion of the remaining B-normal stars must correspond to the third, B-normal, phase, with temporarily-low mass-flux amplitudes, even though some B-normal stars may have too small potential-amplitudes to ever show such phase-changes. Thus, peculiarity and variability seem essential aspects of main-sequence B stars ; and their existence is evidently important in understanding stellar structure and evolution. We suggest the same situation holds throughout the HR diagram, for other ("peculiar", "normal") pairs; and that such investigations as the present should be extended to them.

II. OBSERVATIONS :

1. Visual evidence for 3-phase representation :

Many astronomers regard Be and B-shell spectra as characterizing similar, but not identical, objects ; it is not always accepted that they may well be only different time-phases of the same kind of object, corresponding to different phase-values of those thermodynamic parameters needed to describe exo-photospheric structure. However, there are sufficient examples in the literature of stars passing variously between Be, B-shell, and B-normal spectra in all directions (Ref. 1). In the stars 59 Cyg (B1.5Ve) and γ Cas (B0.5IVe), each of which has been studied over almost a century, we find a remarkable similarity in pattern of such change,over the last 70 years,differing only in epoch. Each has been characterized by long,relatively-quiet periods, with relatively-short periods of spectacular change (about 7 years, for each). During these latter, each star showed two short B-shell phases, which occur between two strong Be phases, with the whole episode ending in a phase which would be B-normal under low resolution, and is at most a very weak Be phase under high resolution,with any emission limited very feebly to Hα. Fig. 1 exhibits this history.

Thus the visual spectrum shows in each of two stars : (1) Balmer emission lines that can be produced only by atmospheres extended several radii,with displacements of emission lines, or of absorption cores, corresponding to less than 100 kms^{-1}.Conclusions from line-widths are uncertain because of difficulty

in separating electron-scattering, rotation, expansion effects ; (2) Sub-ionized FeII, etc lines, in both emission and absorption, again showing velocities $\lesssim$ 100 kms^{-1} ; (3)Both these features appearing and disappearing in times ranging from weeks to years. We have collected other examples of such behavior, some similar, some different, in passage between different phases (Ref. 1). The important point is that this behavior of 59 Cyg and γ Cas is not exceptional.

2. FarUV characteristics in various phases of Fig. 1 :

a) 59 Cyg (B1.5Ve) : Snow and Marlborough (Ref. 2) made farUV observations with Copernicus in 1972, apparently just at the end of a long Be phase or just before a shell-phase ; and in 1975, just after a shell-phase and the beginning of a rise to a strong emission phase. In 1972, the strongest NV absorption component is violet displaced $\lesssim$ 50 kms^{-1}, with a faint component at about -300 kms^{-1}. In 1975, they report only one component, at about -180 kms^{-1}. SiIV echoes this behavior ; and the lines are highly asymmetric.

We (Ref. 3) obtained IUE results in December 1978 and June 1979, during a feeble, but rising Be phase ; Rogerson, Snow, Marlborough and ourselves obtained Copernicus observations monthly between July and October 1979. In December 1978, the deepest portion of the NV resonance line is shifted by -750 kms^{-1} ; in June, it is shifted by -400 kms^{-1}. The following monthly observations show shifts varying with no pattern, but always in the range -400 to -800 kms^{-1}. Fig. 2 shows all these data for NV. In December 1978 and June 1979, the CIV resonance lines follow the velocity shifts of NV ; while the SiIV resonance lines show no shifts larger than -100 kms^{-1} and are quasi-symmetric. The striking thing is the absence, for NV and CIV, of the small velocity shifts; and for SiIV, of the large, during 1978-79 ; by contrast to the 1972 behavior.

b) γ Cas (BO.5IVe) : Hammershlag-Hensberge (Ref. 4), on the basis of IUE observations showing narrow, violet-displaced, additional (to an almost undisplaced component) components in the NV, CIV, SiIV lines in March 1979, as contrasted to April-May 1978, alerted that γ Cas might be entering a new shell phase. It is clear, from Fig. 1, that when these stars enter a "shell-phase", events happen quickly.

We obtained IUE observations at VILSPA-Madrid in October 1979, as well as visual spectra in October, November, December 1979 and February and April 1980, at the Haute-Provence Observatory. A comparison of these visual spectra with those taken regularly over the last 20 years shows no change, other than the well-known V/R variation of the Hα and Hβ emission peaks, and small changes in the emission intensity. Thus we conclude that the narrow absorption components observed in the farUV by Hammerschlag-Hensberge do not correspond to a new shell phase at this moment ; they correspond simply to the double-component mass-flow pattern in a well-defined Be-phase (Ref. 5).

Our IUE observations confirm the existence of the narrow, violet-displaced components observed in NV, CIV, SiIV by Hammerschlag-Hensberge (Ref.9) In conjunction with the 59 Cyg results, these data are very interesting, as regards conditions on the long-term variability cycle. These γ Cas data, taken at "quiet and moderately strong" Be phase, show two velocity components (Fig. 3) -- or two concentrations of absorbing atoms -- for each of SiIV, CIV, NV ; one,

the largest, at about -100, -200 kms^{-1} ; the smaller, at about -1400 kms^{-1}. By contrast to 59 Cyg, observed at increasing emission phase, we observe no ionization-velocity correlation : just this apparent ionization-height gradient. These results should be compared with the cited 1972 observations of 59 Cyg, at the end of a long emission phase or at the beginning of the second shell phase. There, also, no ionization-velocity correlation was noted ; but there, also, one observed a faint, high velocity component in the NV and SiIV lines at about -300 kms^{-1} ; while the strong absorption component lay at about -50 kms^{-1} or less.

III. CONCLUSIONS :

. We suggest the following tentative model :

1. From γ Cas in 1978-79 and 59 Cyg in 1972 : reasonably strong Be emission phases : The two absorption components in all highly-ionized lines refer to chromosphere-coronal transition, and postcoronal, atmospheric regions. The lack of such ions at intermediate velocities corresponds to the presence of a corona sufficiently-hot to suppress such ions. The coronal-level x-ray emission from γ Cas substantiates this picture.

Thus, in the well developed Be phase, we have evidence for an atmospheric structure in which : (i) a radiative flux under quasi-thermal conditions provides a photosphere ; (ii) a nonradiative flux provides a heating supplemental to radiative, resulting in an outward increase, then decrease, of T_e ; (iii) a matter-flux provides a flow accelerating outward through sub-thermal, trans-thermal, and superthermal ranges, and an associated density decrease much flatter than photospheric. These are the characteristics of the atmosphere of an (open, non-thermal) system (Ref. 6). The T_e, flow-velocity, and density distributions are given in Fig. 4 : adopting the Mihalas photospheric model (Ref. 7) of a B0.5IVe star as starting point for T_e, density ; a mass-flux of 10^{-8} $M_\odot y^{-1}$ to locate starting point for trans-thermal flow, and maximum beginning height of chromosphere ; an x-ray indication of 10^6 K corona ; and the observed (V, ionization) values of γ Cas for pre- and post-corona. We have only relative locations in height, no absolute scales. Note that a mass-flux range from 10^{-7} to 10^{-9} corresponds to 3.10^{11} - 3.10^9 range in particle concentrations at beginning of trans-thermic flow.

2. From the Balmer and metal-shell observations : From the T_e values in Fig. 4, we see that Balmer emission can be produced in the photosphere-chromosphere, and in those postcoronal regions cooler than where the farUV lines arise. The sub-ionized metals, such as FeII, can arise only in the latter region. The velocities associated with the Balmer and sub-ionized emission require, then, a deceleration in the far post-coronal regions ; these are indicated by dotted lines in Fig. 4. Such deceleration must come from interaction with the ISM, apparently closer than the ~ 0.1psc distances associated with such interactions in the usual literature (Ref. 8) ; but the problem is open.

3. Variability in mass-flux : IF we associate variability in mass-flux velocities with that in mass-flux itself, we identify three kinds of such variability ; (a) That corresponding to small fluctuations in the developed Be phase, where the velocity of the two maximum concentrations of absorbing superionized species does not change significantly, only the size of the concentration (ie density of the wind) ; (b) That corresponding to variations in the phase of

increasing from small to large Be emission, where both velocity of maximum superionization concentration and its size change significantly ; (c) That corresponding to different phases, where the velocity changes very strongly ; for example, between the 1972 and 1978-79 phases of 59 Cyg. These aspects of variability are evidently critical in understanding the variability of atmospheric structure between the B-normal, Be, and B-shell phases. The size of the mass-flux evidently plays a crucial role ; but the interactions between mass-flux size, the ability of the nonradiative flux to heat a particular atmospheric region, and of the radiative flux to provide further acceleration to whatever maximum velocity is reached are equally important. To clarify these problems, empirically, we clearly need observations in farUV, x-ray, farIR and radio, very frequently during such rapidly-changing epochs as the 7-year ones shown by γ Cas and 59 Cyg.

4. The densities in Fig. 4 are too small to produce the observed Hα emission during a strong Be phase. Since densities increase as F_M : either we increase $F_M \geq 10^{-6}$ in the strong Be phase ; or we abandon a density fixed by a continuous flow in the postcoronal regions, substituting for part of that region a reservoir, with boundaries fixed by interaction with the ISM, filled by a variable mass-flux, enhanced during the beginning and increasing Be phases.

REFERENCES :

1. Doazan, V., Underhill, A. B. 1981 in preparation
2. Snow, T. P., Marlborough, J. M. 1980 Astrophys. J. 235, 85
3. Doazan, V., Kuhi, L. V., Thomas, R. N. 1980 Astrophys. J. 235, L17
4. Hammerschlag-Hensberge, G. 1979 IAU Circ 339
5. Doazan, V., Selvelli, P., Stalio, R., Thomas, R. N. 1980, 2nd IUE-ESA Symp.
6. Heidmann, N., Thomas, R. N. 1980 Astron. Astrophys. in press
7. Mihalas, D. 1972 NCAR-TN/STR-76
8. Dyson, J. E., de Vries, J. 1972, Astron. Astrophys. 20, 233
9. Henrichs, H. F., Hammerschlag-Henberge, C., Lamers, H. J., 1980, 2nd IUE-ESA Symp.

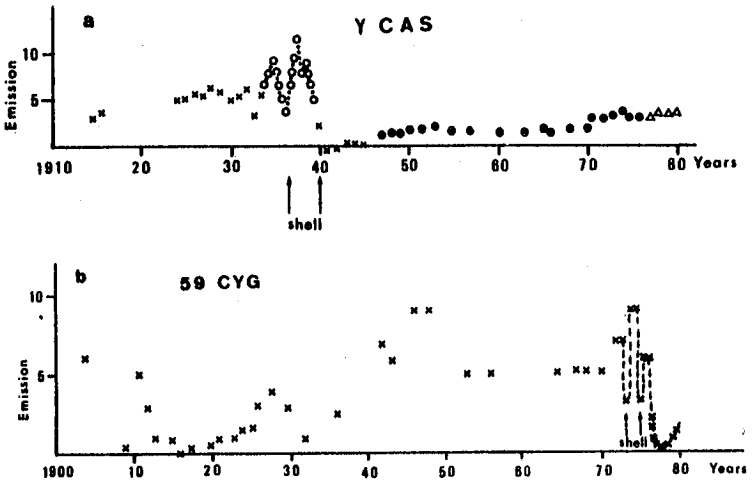

FIG. 1 : Long-term variations of γ Cas (1a) and 59 Cyg (1b) in the visual, Ref. 5. Ordinates : arbitrary-scaled Balmer line emission.

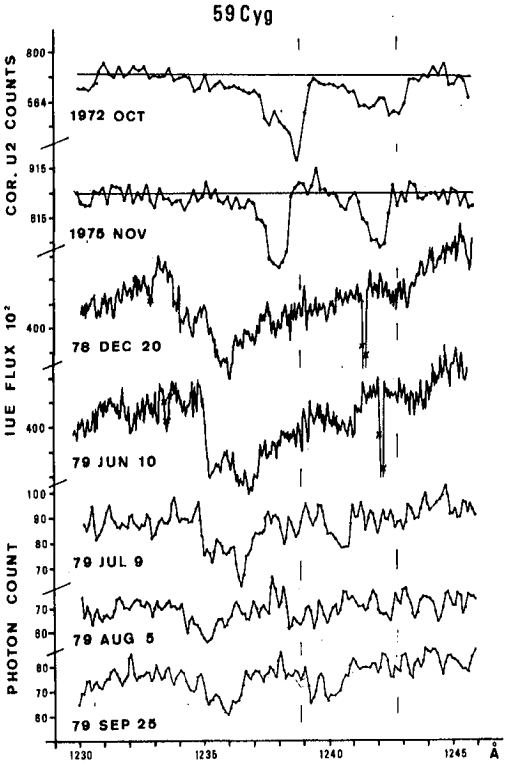

FIG. 2 : NV resonance lines in 59 Cyg : 1972, 1975, Copernicus, Ref. 2 ; December'78, June'79, IUE, Ref. 3 and this paper ; July-September'79, Copernicus. Solid lines are laboratory λ ; crosses are reseau.

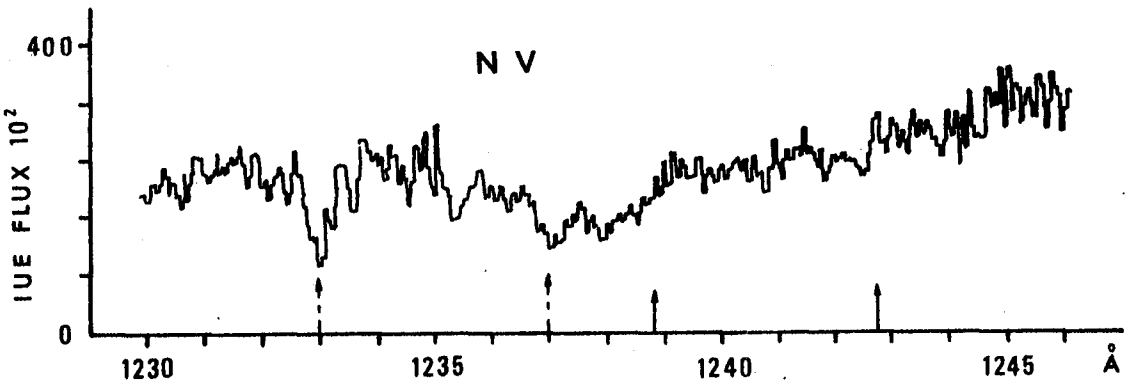

FIG. 3 : NV resonance lines in γ Cas, Ref. 5. Solid arrows are laboratory λ, crosses are reseau marks. Ordinates : 10^2 IUE flux counts.

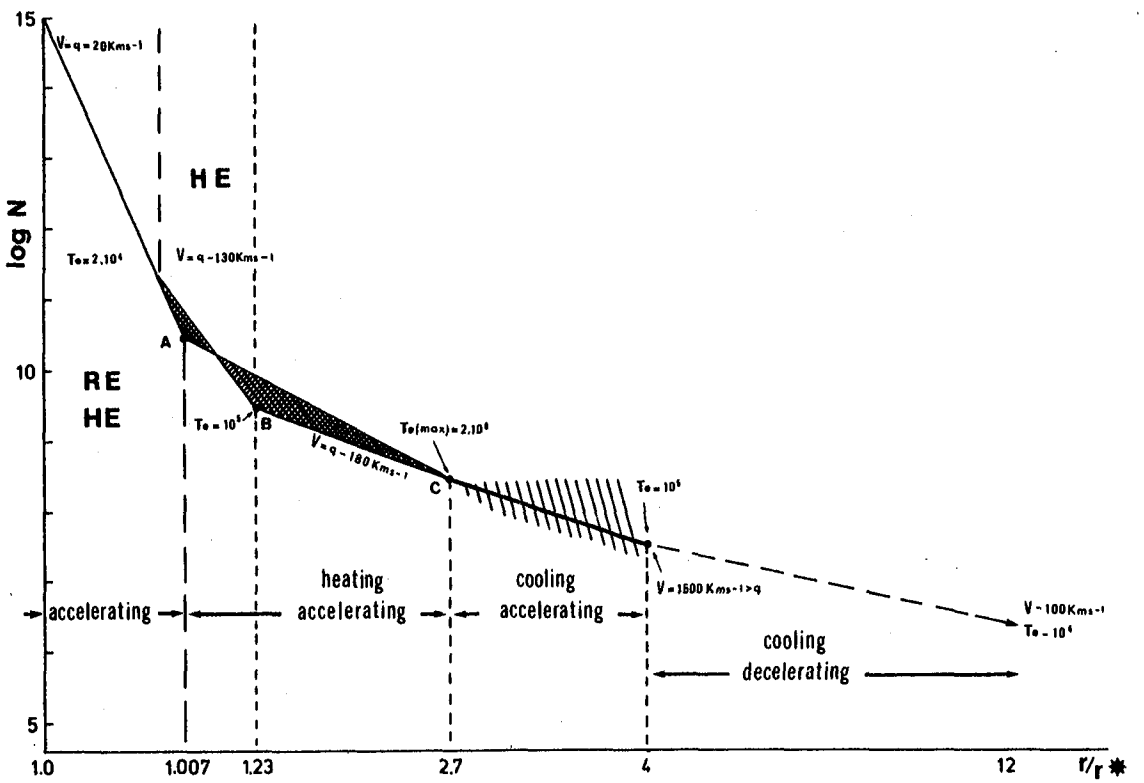

FIG. 4 : Schematic γ Cas atmosphere for $F_M = 10^{-8} M_\odot y^{-1}$. Flow becomes transonic at thermal points : A, if no preheating ; B, if preheating ; cross-hatched area shows uncertainty in preheating : and supersonic in region of T_e(max), beginning at C. Single-hatched area shows uncertainty on cooling and acceleration/deceleration.

OBSERVATIONS OF THE GAS STREAM IN THE MASS TRANSFER BINARY HR 2142[1]

Geraldine J. Peters
Department of Astronomy
University of Southern California
Los Angeles, CA 90007

ABSTRACT

The mass transfer binary system HR 2142 has been observed at selected phases with the high resolution spectrograph on IUE. The observations were scheduled throughout the interval $0.91 < \phi < 0.00$ in order to permit us to view the light of the primary star through the gas stream as it presents different orientations to our line of sight. Numerous UV lines formed in the gas stream have been identified. The strengths and velocity variations displayed by these lines are compared with those observed in the ground-based spectral region. As part of a preliminary analysis of the IUE data, column densities and velocities from Si III (4), Si IV (1), and Ti III (1) are used to deduce electron densities in the gas stream as well as its thickness. Possible evidence for stratification in the gas stream is presented.

INTRODUCTION

HR 2142 (HD 41335) is a 5th magnitude Be star which is also a mass transfer binary system (references 1 and 2). With a period of 80.86 days and a systemic mass of about 15 $M_\odot$, it is a high mass counterpart of the familiar Algol type binary system.

In order to investigate the physical properties of the gas stream, a series of high resolution IUE observations were completed throughout the phase interval $0.91 < \phi < 0.00$, when we view the light of the primary star through the gas stream. The journal of the observations is presented in table I. The phase, ϕ, which is listed for each observation, is obtained from a recent orbit solution for this single lined spectroscopic binary system (reference 2). According to this solution, if the period is fixed at $80\overset{d}{.}86$, $K = 9.4$ km s^{-1}, $V_o = 24.1$ km s^{-1}, and conjunction occurred on JD 2441990.6. Also included in table I is a list of phases based solely upon spectroscopic observations (reference 1) in which $\Phi_s = 0.0$ when the Balmer gas stream lines peak in strength.

In this paper, a preliminary analysis of the IUE data is presented. Phase dependent observations of features in the spectral region $\lambda\lambda 1295 - 1310$ [which contains Si III (4), Si II (3), and Ti III (1)] and the Si IV resonance lines are analyzed and compared with earlier ground-based and Copernicus ultraviolet observations.

[1]This project is being supported, in part, by NASA grant NSG 5422.

ABOUT THE MODEL

Details about the model for HR 2142 can be found in references 1 - 4. In figure 1, we show the model which has been developed over the past seven years from both ground-based and Copernicus ultraviolet observations. The phase interval over which the IUE observations were made is indicated. Some features of the model which are shown in figure 1 are: 1) the presence of a well-defined gas stream and counter stream which apparently have large inclinations with respect to the line of centers in the system; 2) the existence of an extended, rotating, low-density ($N_e \simeq 10^{10}$ cm^{-3}) accretion disk positioned about the primary star; and 3) the existence of an overall stellar wind from the primary star and/or the disk which appears to be enhanced at $\phi = 0.5$. Since the system does not undergo an eclipse and the projected rotational velocity of the primary is high (about 400 km s^{-1}, reference 5), we assume that the inclination of the system is about 70°. Therefore, the physical parameters we deduce for the gas stream pertain to relatively high latitudes. Since the spectral type for the primary is B1IV, the total mass in the system is about 15 $M_\odot$.

DESCRIPTION OF THE OBSERVATIONS

In figures 2 and 3, we show the phase dependent spectral variations observed in two selected regions. Between λλ1295 and 1310 we observe lines of Si III (4), Si II (3), Ti III (1), and O I (2). The O I line is entirely an interstellar feature and is used as an aid in calibrating the wavelength scale. Si II 1304 is a blend of interstellar and gas stream lines. Superimposed on broader photospheric features are sharper lines of Si III (4) and Ti III (1) which are formed in the gas stream. In figure 3, it can be seen that the SiIV resonance lines have gas stream components which are redshifted by about 100 km s^{-1} relative to the centers of the photospheric lines.

From an inspection of figures 2 and 3, it can be seen that the sharp, shell-type absorption lines which are formed in the gas stream are already present in the earliest spectrum taken at $\phi = 0.91$. In fact, the strongest members of Si III (4), as well as other gas stream features seen in other spectral regions, are saturated at this phase! The gas stream lines peak in strength between $0.95 < \phi < 0.96$. However, the intensities of the gas stream lines decline rapidly after $\phi = 0.96$. It should be noted, though, that the intrinsically stronger features persist at conjunction.

From $\phi = 0.91$ through 0.96, the gas stream lines show a positive velocity shift (50 - 100 km s^{-1}) relative to the photosphere of the primary star. However, at conjunction, the gas stream lines which remain appear to be at rest relative to the photosphere.

The ultraviolet observations described above are compatible with earlier ground-based and Copernicus UV observations of this star. In the visible spectrum, the Balmer gas stream features reach maximum strength at $\phi = 0.96$ but disappear completely at conjunction. Furthermore, the Balmer features show a large velocity shift (80 km s^{-1}, reference 1) relative to the photosphere at $\phi = 0.92$ but this shift decreases to zero by conjunction. Copernicus observations (references 3 and 4) revealed that gas stream lines of

C II, N II, Si III, S III, and Fe III were present at conjunction whereas weaker lines of Si II and S II were absent. The latter study did show that all of the gas stream lines in the ultraviolet were weaker at conjunction but it also revealed that the profiles of the lines are complex and contain multiple components. One of these components is a highly saturated feature which remains relatively fixed in velocity from $\phi = 0.90$ through $\phi = 0.96$. The other components are unsaturated and show more positive velocities. The total equivalent width for the unsaturated components is comparable to that of the main component. At conjunction, the strengths of the higher velocity components are much reduced. We now believe that the velocity variations displayed by the gas stream lines can be understood in terms of the variable multiple components.

The most numerous gas stream features in the UV spectrum of HR 2142 are lines of Fe III. Lines of C I, C III, N I, N III, O I, O III, and Fe II are not observed. Ultimately, all of the gas stream lines which can be identified and reliably measured will be analyzed to refine the model for the gas stream. However, in view of the complexity already observed in the gas stream lines (reference 4), the preliminary analysis of the IUE data presented in this paper is restricted to lines which are unsaturated and presumably unblended with other features.

ANALYSIS

The fact that Fe II gas stream lines are not observed suggests that the temperature in the gas stream is above 18,000°K. From the ratio of Fe III 1032/1130 (reference 4), we conclude that the temperature in the gas stream is close to 19,000°K. Therefore, in the analysis presented below, we adopt a gas stream temperature of 19,000°K.

As stated in the last section, the complex nature of the gas stream lines renders any analysis of saturated features highly uncertain. Although the Fe III lines are the most numerous gas stream lines, all of these features which have reliable f-values are quite saturated. Upon inspection of the data, it was determined that Ti III (1) 1296 was especially suitable for analysis.

As seen in figure 2, Ti III λ1295.88 begins to show at $\phi = 0.92$. By $\phi = 0.96$, it has reached a maximum strength of 0.2 A. Other stronger members of this multiplet are blended with Si III (4) $\lambda\lambda$1295 and 1299. The Ti III features appear to have disappeared completely by $\phi = 0.98$. For the analysis of the line strength, the f-value was obtained from Wiese and Fuhr (reference 6) while the partition functions for Ti were computed from data in Drawin and Felenbok (reference 7). The column density from Ti III 1296 observed at $\phi = 0.96$ is 1.8×10^{14} cm^{-2}. The column density for Ti III becomes 10^{15} cm^{-2}. If $T \simeq 19{,}000$°K and $N_e \simeq 10^{12}$ cm^{-3}, then Ti III/Ti = 5×10^{-3}. Since hydrogen is 10^7 times more abundant than Ti, the Ti III 1296 observation implies a hydrogen column density of 2×10^{24} cm^{-2} at a phase of 0.96. Therefore, with a density about 10^{12} cm^{-3}, a path length of 10 to 20 $R_\odot$ (or 1 - 2 R_*) is implied. This result is compatible with the theoretical calculations for the structures of gas streams by Lubow and Shu (reference 8). Finally, it should be emphasized that such large column densities persist for a very short inter-

val of time ($0.93 < \phi < 0.96$). Densities are at least ten times lower outside of the above stated phase interval.

The Si IV gas stream lines (figure 3) are also unsaturated and, therefore, suitable for analysis. The column density of Si IV is 3×10^{13} cm^{-2} at a phase of 0.96. At $\phi = 0.91$, it is half of this value while at conjunction the column density is reduced by two-thirds. If the temperature in the Si IV region is about 19,000°K and the electron density is between $10^{11} - 10^{13}$ cm^{-3}, then most of the silicon must be triply ionized. Since the abundance ratio between hydrogen and silicon is 3×10^{4}, a hydrogen column density of about 10^{18} cm^{-2} is implied. Therefore, either a low electron density or a small path length is implied. Neither are compatible with analyses of other spectral features formed in the gas stream. The low column density from the Si IV lines suggests that these features are formed in a different portion of the gas stream than are the lines of Ti III, Fe III, and the Balmer lines. Perhaps it should be noted that the Si IV lines show a larger velocity shift (about 120 km s^{-1}) relative to the photosphere than do the above mentioned lines as well as the gas stream lines of Si III.

The weaker, unblended members of Si III (4) were also analyzed. These lines suggested a Si III column density of 5×10^{14} cm^{-2}. If the path length is about 10 $R_{\odot}$, an electron density of 10^{11} cm^{-3} is implied for the Si III region. Some of the Si III lines remain saturated throughout the interval of the observations. The velocities from the Si III lines are compatible with those from the Balmer lines.

In this paper, a preliminary analysis of the IUE observations has been presented. Ultimately, the analysis of the saturated lines as well as the acquisition of additional observations should allow us to develop a detailed model for the mass flow in the system.

REFERENCES

1. Peters, G. J.: Evidence for the Existence of Mass-Exchange Binary Be Stars from Periodic Spectral Variations. Be and Shell Stars, ed. A Slettebak (Holland: Reidel), 1976, pp. 417-428.

2. Peters, G. J.: Mass Flow in the Binary System HR 2142: I. Analysis of Ground Based Spectrograms. Astrophys. Journ., 1980, submitted.

3. Polidan, R. S., and Peters, G. J.: Ultraviolet Observations of Close Binary Stars. Close Binary Stars, ed. M. Plavec and R. K. Ulrich, 1980, in press.

4. Peters, G. J., and Polidan, R. S. Mass Flow in the Binary System HR 2142: II. nalysis of the Ultraviolet Fe III Features. Astrophys. Journ., 1980, submitted.

5. Slettebak, A.: Be Stars as Rotating Stars: Observations. Be and Shell Stars, ed. A. Slettebak (Holland: Reidel), 1976, pp. 123-136.

6. Wiese, W. L., and Fuhr, . Atomic Transition Probabilities for Scandium and Titanium. Journ. Phys. and Chem. Ref. Data, vol. 4, p. 263.

7. Drawin, H. W., and Felenbok, P.: Data for Plasmas in Local Thermodynamic Equilibrium (Paris:Gauthier-Villars), 1965.

8. Lubow, S. H., and Shu, F. H.: Gas Dynamics of Semidetached Binaries. Astrophys.Journ., vol. 198, pp. 383-406

TABLE I - JOURNAL OF IUE OBSERVATIONS OF HR 2142

Image No.	Date (U.T.)	Julian Date (244+)	Phase (ϕ)	Phase (Φ_s)
SWP 8596	1980 March 30	4328.51	0.91	0.95
SWP 8597	1980 March 30	4328.55	0.91	0.95
SWP 8604	1980 March 30	4329.21	0.92	0.96
SWP 8616	1980 March 31	4330.14	0.93	0.97
SWP 6962	1979 October 23	4169.99	0.95	0.99
SWP 8637	1980 April 2	4332.50	0.96	0.00
SWP 6996	1979 October 25	4172.03	0.98	0.02
SWP 7007	1979 October 27	4173.78	0.00	0.04

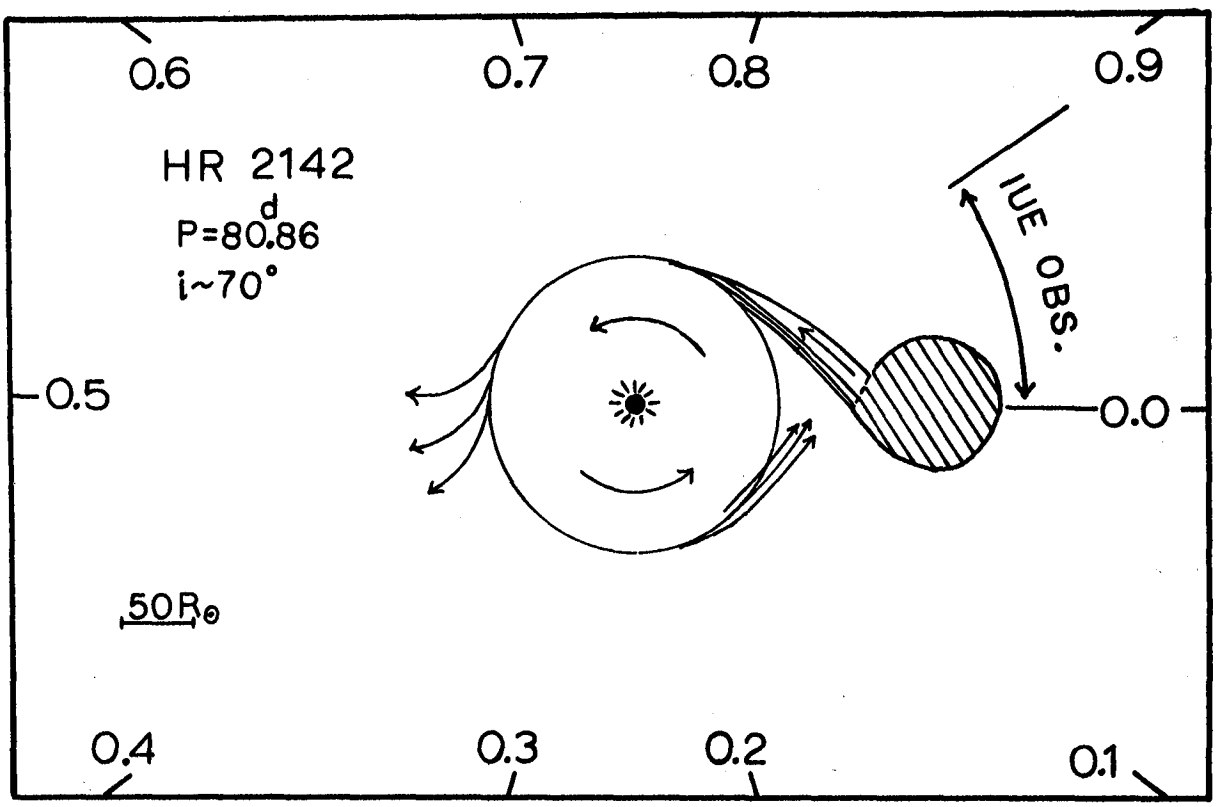

Figure 1: A model for the binary HR 2142. The interval in phase during which the IUE observations were obtained is indicated.

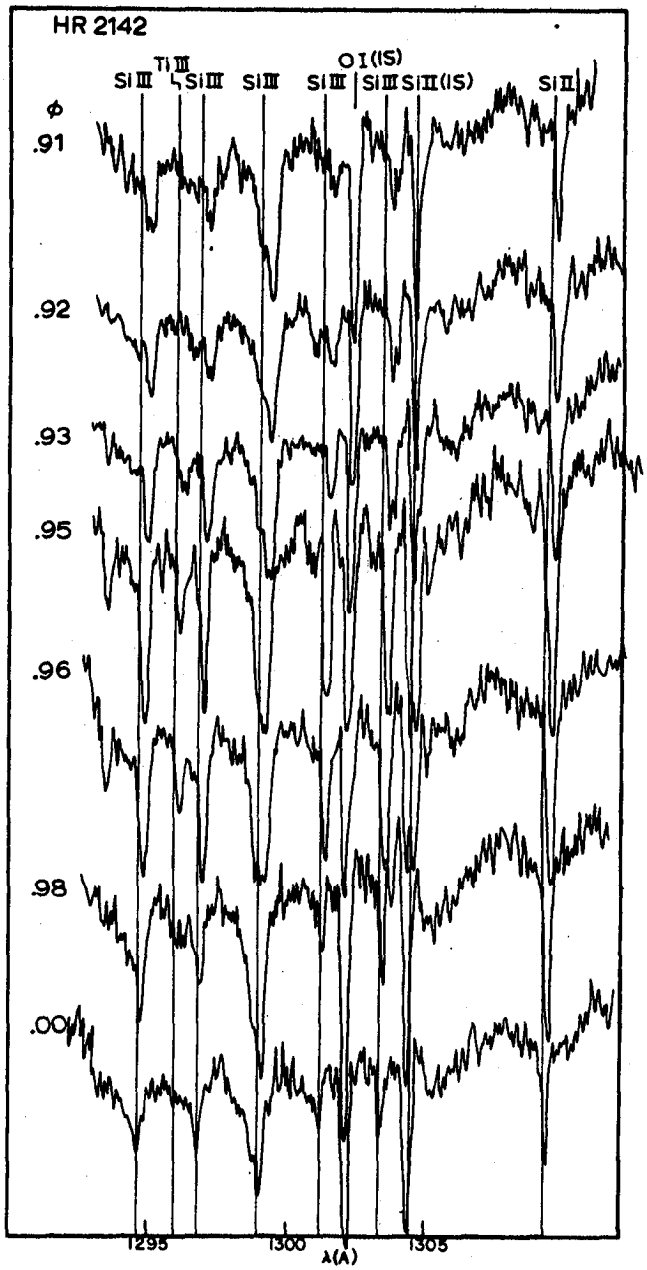

Figure 2: Phase dependent spectral variations in the strengths of the gas stream lines observed between $0.91 < \phi < 0.00$. The major features are labeled and the vertical lines indicate the locations of the corresponding photospheric lines.

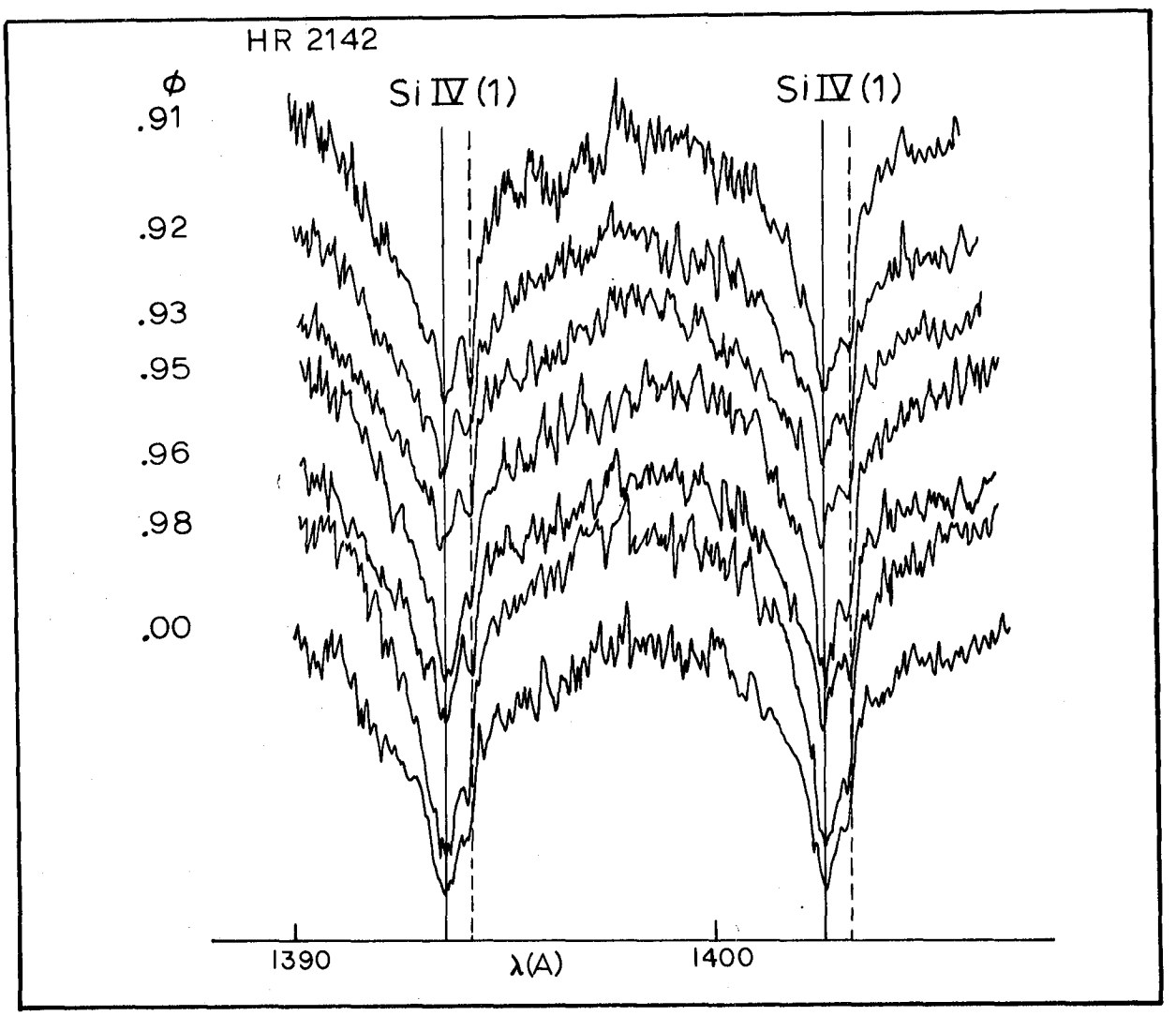

Figure 3: Phase dependent spectral variations in Si IV (1). The vertical dashed lines indicate the location of the gas stream component.

THE UV RESONANCE LINES OF THREE HOT Ap STARS HD 133029, HD 175362 and HD 219749

Karl D. Rakos
Institute for Astronomy
Vienna, Austria

SUMMARY:

High resolution spectra of the Ap stars HD 133929, HD 175329 and HD 219749 have been obtained during two 16 hour shifts with the IUE satellite at Goddard Space Flight Center. Stellar wind, extended atmosphere in rigid corotation with the stellar surface and the influence of the strong magnetic field on the upper part of the atmosphere would explain the shape and the strength of the resonance lines. The resonance lines of HD 175362 in particular show very peculiar behavior. The necessary driving forces for the expanding envelope are not compatible with the diffusion theory of the Ap atmospheres.

INTRODUCTION AND OBSERVATIONS:

HD 175362 belongs to the group of helium-weak stars building an extension of the Ap stars toward higher temperatures. The oblique-rotator model for the star has been published recently by Hensler, 1979. References to other investigations concerning HD 175362 can be found in his paper. Bonsack (1977) made a detailed study of HD 133029 yielding the following results: vsin i = 21 km/s, period of rotation of 2^d89, T_{eff} = 11375 K, B9p (log g = 4.0). Temperature estimates have been carried out by Adelman (preprint 1979). HD 219749 has probably a higher temperature but the same spectral type. The rotation period is 2^d60.

Stimulated by the discovery of mass loss in the B9p star Alpha And (Rakos et al. 1979), the attempt was made to obtain high resolution observations in UV for other hot Ap stars. Very good high resolution short wavelength spectra of each star have been used for this investigation. IUE data reduction was carried out with the Tololo-Vienna interactive image processing system. According to the low value of v.sin i the spectral lines are in general narrow, but nevertheless there are very few lines without strong blends.

Highly ionized atoms Si IV, C IV, N V and N IV (Figure 1) are present showing strong absorption with extended blue wings and emission in the line cores. The emission features have velocities of expansion as high as 150 km/s. Much higher expansion velocity is connected with the broad absorption wings of this lines.

The Si IV doublet 1393.755 and 1402.769 is very strong in HD 175362. The first line shows strong reversal component in the core. From the blue edge of this emission the expansion velocity of 100 km/s and from the envelope absorption component 560 km/s can be derived. The second line seems to have even stronger blue-shifted (150 - 170 km/s) emission. Also a general expansion velocity of 500 km/s can be measured from the blue absorption line wing.

This doublet is very faint and blended by other lines in HD 133029. The C IV doublet 1548.195 and 1550.768 shows very similar behavior. The lines are less pronounced than the Si IV resonance doublet, 4 lines due to Fe III mask possible absorptions due to a wind or the emission components. At least the first line of C IV suggests an expansion velocity in the range of 600 km/s. The star HD 133029 and especially HD 219749 have visible C IV resonance doublets with certain blue-shifted wings.

The N V resonance doublet 1238.810 and 1242.800 in the spectrum of HD 175362 is very strong and the lines are broad. The first line has an undisplaced emission component and the blue-shifted absorption core at -170 km/s. The line wings are very broad allowing expansion velocities of more than 700 km/s. The second line of the doublet is unfortunately contaminated with a reseau mark. A strong emission is shifted bluewards slightly and broad line wings are present.

The spectrum of HD 133029 is underexposed at 1230Å. HD 219749 shows defintely very broad absorption and a terminal velocity of 500 km/s A probable emission can be allocated within the absosrption wing with an expansion velocity of -360 km/s.

Finally, in the spectrum of HD 175362 the N IV intercombination line from the ground state 1486.496 may be present as a very wide absorption feature completely on the blue side of the unshifted line position. The maximum of the expansion velocity derived from this feature approaches 1200 km/s. The same line is even sronger but less shallow in the other two stars. The low resolution spectra have pronounced absorption features in the same place. The presence of the emission features is uncertain.

The discussed lines demonstrate a hot expanding shell, stellar wind, and mass loss, an unexpected new characteristic of magnetic stars.

The mass loss is also confirmed by the other resonance lines of Si III and Si II. The Si III 1206.510 line is strong and broad in HD 175362 with an extended blue wind and the maximum expansion velocity of 600 km/s. The Si II (3) 1309.274 line is not a resonance line, but it originates from the fine structure level of the ground term. Such lines tend to behave like resonance transitions in the lower density part of stellar atmosphere, where neither the photon flux nor the

particle density is high enough to populate the excited levels. The line is strong broad and symmetrical in the spectrum of HD 175362. The Doppler velocity of ± 340 km/s can be derived from the profile. The resonance line of the same multiplet 1304.369 is unfortunately on the edge of the detector field and therefore of very low quality. The 1309.274 line is also strong and broad in HD 219749 and HD 133029. In the spectrum of HD 175362 the second Si II resonance line at 1526.719 shows a narrow interstellar feature in the core, which has very broad, shallow, and symmetric wings. The photospheric Si II line of the same multiplet (UV 2) 1533.445 is visible but fainter by a factor of two. According to their gf values the intensities should be reversed. The same situation also holds for the resonance line Si II 1260.418 and the fine structure level line 1264.737.

HD 133029 and HD 219749 have very strong 1526.719 and 1533.445 lines. The first line has strong blue wings, showing a terminal velocity in the range of -500 km/s.

Also the resonance lines of Si II 1190.418 and 1193.284 in the spectrum of HD 175362 are remarkable. The first line seems to show core reversal and emission in the blue and red wings with a very moderate velocity of ±120 km/s. The second line is stronger and probably symmetric, it is unfortunately on the edge of the detector field.

The doublet Ti III 1295.897 and 1298.706 in the spectrum of HD 175362 contains broad, rather symmetric lines with emission in the cores of both lines. Likewise, S II and C II resonance lines confirm the expansion velocity in the order of 600 km/s in HD 175362. S II 1250.500 is very strong line, somewhat disturbed by the reseau mark on the detector. It is also present in HD 219749 with a similar velocity distribution. The doublet C II 1334.515 and 1335.703 is one of the strongest absorption features (except Lyman Alpha) in the spectrum of HD 175362. The asymmetry in the blue wing is strongly indicated.

C II lines are also visible in the other two stars. The first line of the doublet in HD 219749 has a blue shift of -70 km/s and a wide shallow blue wing with the terminal velocity of -400 km/s. HD 133029 has also an extended blue wing of the unshifted 1334.515 line with the same velocity distribution.

The resonance lines of neutral atoms are very narrow, as opposed to the broad features produced by ions. A very good example in HD 175362 is N I at 1199.55. The line is very similar to two other lines; N I 1200.218 and 1200.707. The same is true for O I 1355.605 and Cl I 1379.528 in all three stars.

DISCUSSION OF THE RESULTS:

Stellar wind and mass loss in the atmosphere of a peculiar magnetic star is an unexpected phenomenon. It poses a serious problem for the explanation of abundance anomalies by diffusion. The whole stellar

atmosphere would not be quiet enough for diffusion processes to operate, even if the expanding envelope is restricted to the outermost regions of the stellar atmosphere. The second question concerns the driving forces for the expanding envelope. Also the reason for the measured abundance anomalies located at the opposite magnetic poles should be explained.

First, discussion should be pointed to the question of the stellar luminosity class. HD 175362 is classifed as B8p IV according to its visual spectrum. According to the Snow-Jenkins Catalogue (1977), Si III 1206.510 is not visible in B8 III stars. It is strong in the spectrum type earlier than B5 III or B4 V, but also in B8 Ia. This line is strong in HD 175362 and at least suggests an unusual character of the upper part of the atmosphere. Supergiant structure is also supported by the energy distribution in the low dispersion spectrum. The Ultraviolet Bright-Star Spectrophotometric Catalogue (ESA SR 27) has been used for comparison. HD 175362 has a similar spectrum as the stars HD 34085 B8 Ia, HD 202850 B9Iab, and HD 212593 B9 I. Also the presence of C II multiplet no. 11 at 1323.9 of photospheric origin suggests the supergiant structure. These lines are missing in the spectra of the main sequence stars of type B8 V, but they are quite strong for spectrum type B8 Ia. The same is true for the multiplet no. 4 of C III around 1176Å - as a comparison see Beta Orionis A B8 Ia (Snow-Jenkins, 1977). Two other stars, HD 133029 and HD 219749 are "standard" Ap stars without any strong indication for giant structure, except for stellar wind.

Besides the recent detection of a magnetic field in Canopus (F0 Ib), Rakos et al. (1976), the present results confirm that strong magnetic fields in stars are widely independent of the stellar type and, therefore fossil in origin.

It is reasonable to suppose a rigid corotation of closed magnetic lines of force within a distance of a few stellar diameters from the stellar surface. At larger distances the lines remain open, as do the magnetic lines of the solar magnetic sector structure in the neighborhood of our planet (see figure 2). The ionized atoms will be forced and accelerated along these lines, spinning with the frequency ω and semidiameter according the magnetic field β, charge q, and the mass m of the ion.

$$r = \frac{m\ c\ v_t}{q\ B} \qquad\qquad w = \frac{q\ B}{m\ c}$$

The resulting speed v_t depends on the distance from the stellar surface and the efficiency of the rigid rotation and the corresponding centrifugal forces. For $R_* = 6\ R$, and the period of rotation of 3^d67, the equatorial rotational velocity will be 83 km/s. In a distance of only 7 R_* the velocity of 600 km/s could be achieved.

In general, the v_t is given by the following equation

$$v_t = \frac{2 \pi R \; R_*}{P \; 86400 \; R}$$

(P is the rotational period in days, usually known for Ap stars.) The escape velocity v_e is given by

$$v_e = 617.7 \; (M*/M \;)^{1/2} \; / \; (R*/R \;)^{1/2} \quad km/s$$

For the condition $v_t = v_e$ we can get the "escape radius" R_e

$$R_e/R \; = (12.2 \; P)^{2/3} \; (M*/M \;)^{1/3}.$$

For HD 175362 and the assumption $M* = 3 \; M$ we get the following result:

$$R_e = 18 \; R \quad \text{and} \quad v_e = 252 \; km/s.$$

For a larger stellar diameter, according to the proposed spectral type, this velocity can be produced within the extended stellar atmosphere. Ions with high spinning speeds in the line of sight over the stellar surface, accelerated along the magnetic line of force by rigid corotation of the atmosphere, would explain broad symmetric absorptions in the wings of the resonance lines and the absence of such broad features for neutral atoms.

Finally, instead of diffusion, some kind of magnetohydrodynamic separation process should be investigated. In general, the magnetic field and its direction, systematic motion of the gas in the deeper region of the stellar interior, the atomic mass and the charge set the path for the motion of each ion - similar to the mass spectrograph principle. As soon as the specific ions are guided to the surface of the star, the abundance anomaly is formed. Slight changes in the stellar structure may result in the large abundance anomalies. From this point of view the magnetic stars are a permanent challenge for the theorist.

I am grateful to the IUE Observatory staff for the assistance which they have given me in obtaining my spectra.

REFERENCES:

Bonsack, W. K. 1977. Astron. and Astrophys. 59, 195.
Hensler, G. 1979. Astron. and Astrophys. 74, 284.
Rakos, K. D., Jenkner, H., Wood, H. J. 1979. Astron. and Astrophys., in print.
Rakos, K. D., Schermann, A., Weiss, W. W., Wood, H. J. 1976. Astron. and Astrophys. 56, 453.
Snow, T. P., Jenkins, E. B. 1977. Astrophys. J. Suppl. 33, 269.

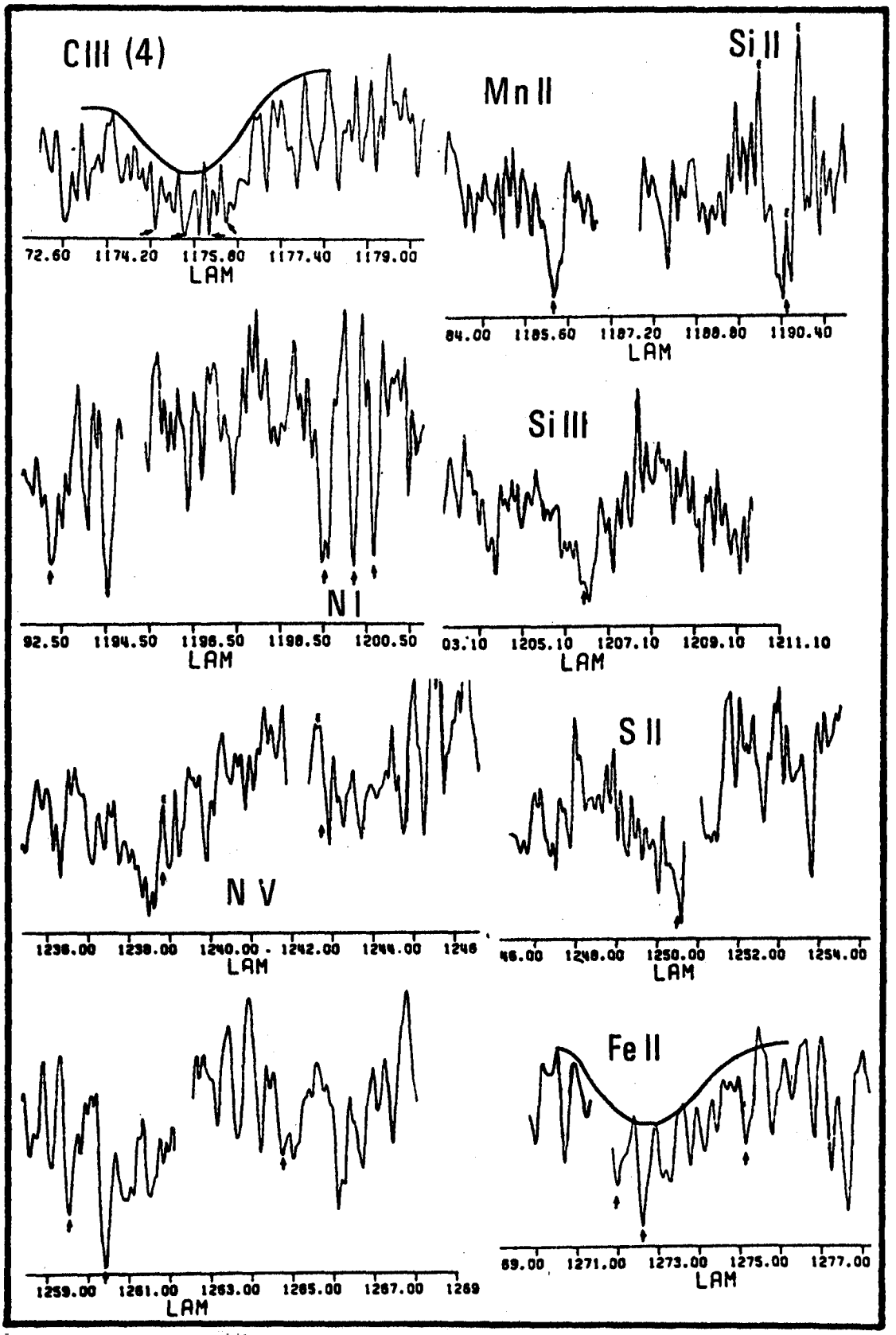

Figure 1. The UV resonance lines in the spectrum of HD 175362.

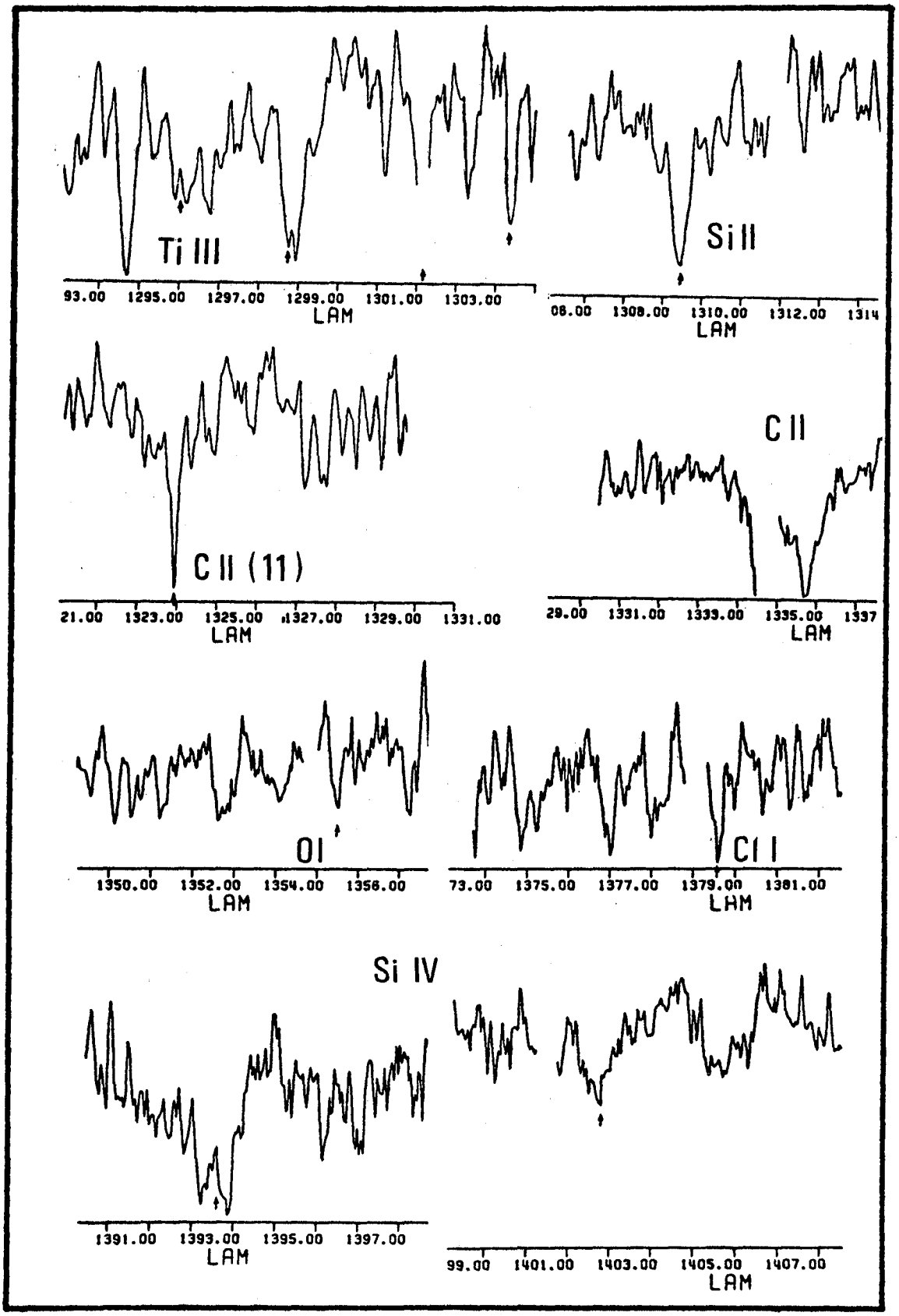

Figure 1. cont.

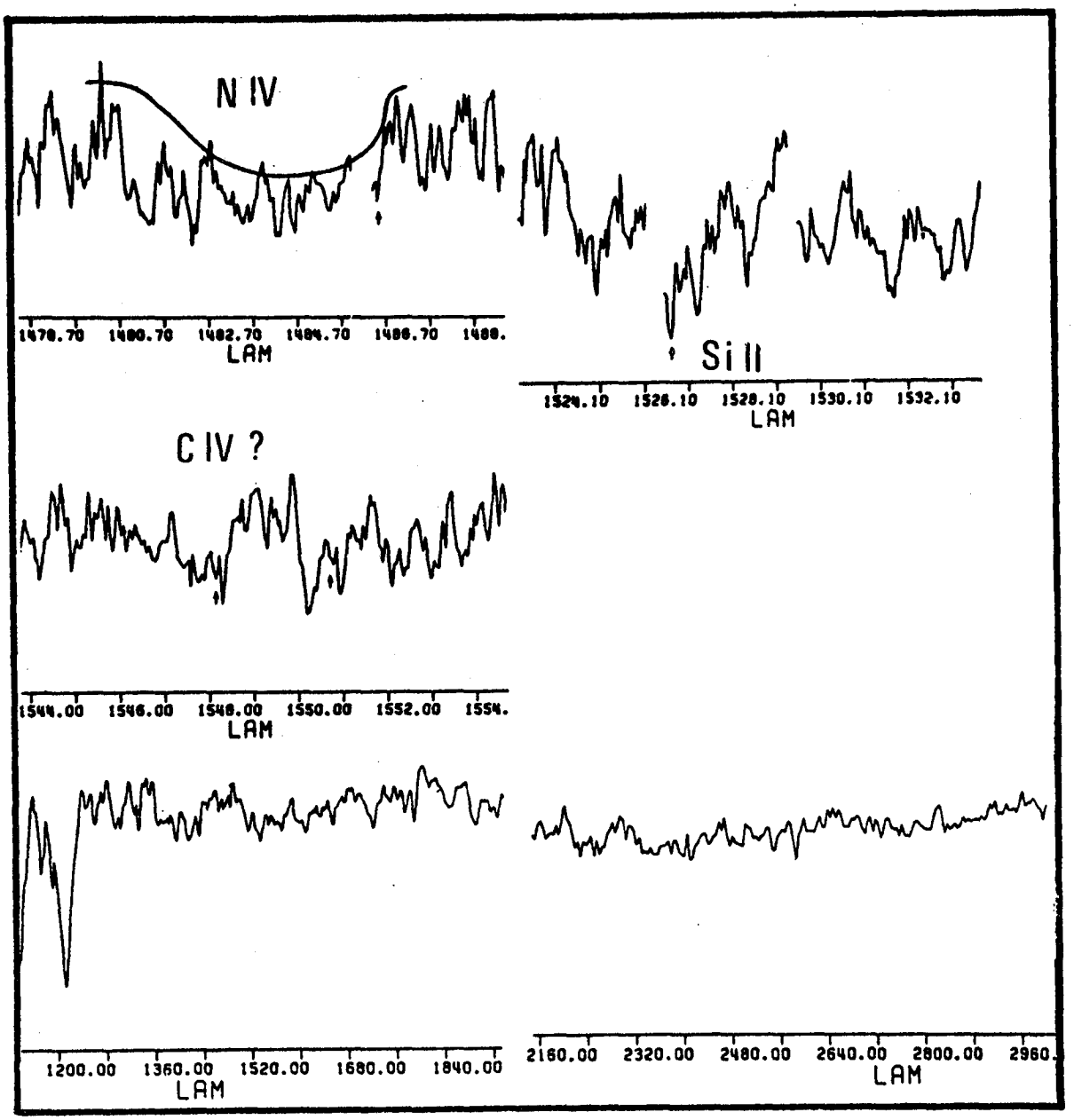

Figure 1. cont.

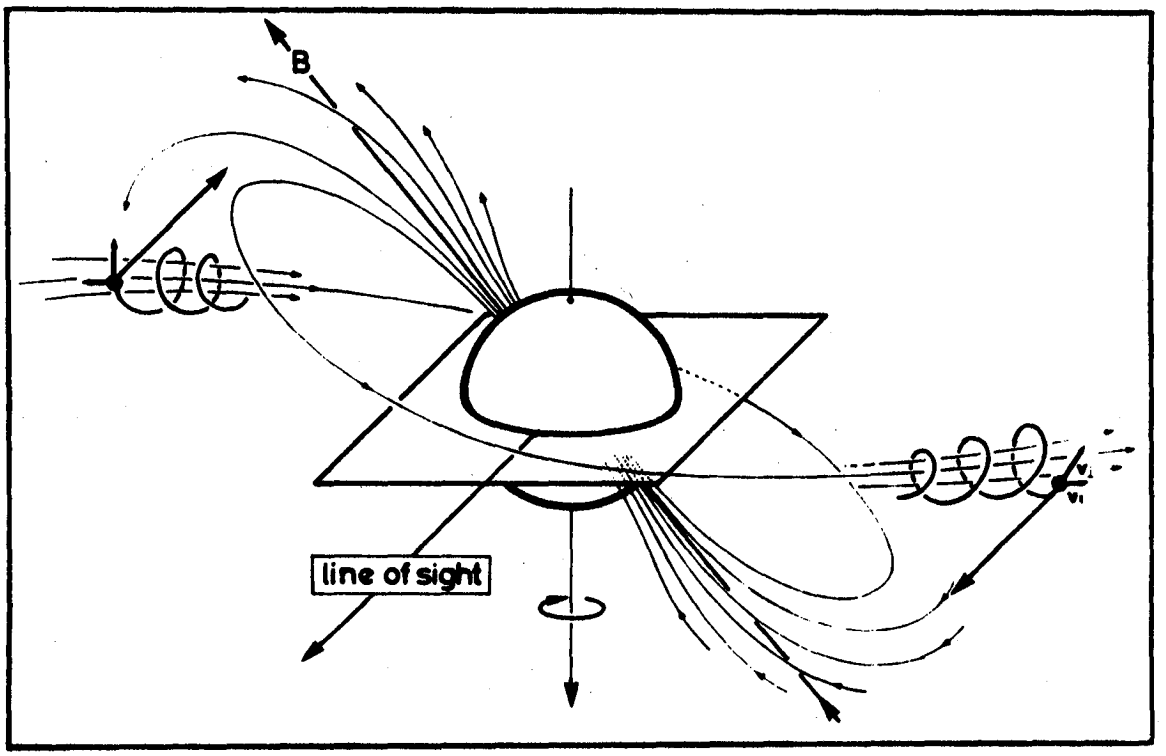

Figure 2. Spinning ions in the line of sight over the stellar surface.

VARIATIONS IN THE UV SPECTRUM OF a CENTAURI

Richard P. Fahey
Laboratory for Astronomy and Solar Physics

ABSTRACT

Equivalent width and central depth measurements of the ultraviolet absorption lines from the spectrum of the He I variable star a Cen [HD 125823] are presented. The measurements are from 53 short-wavelength, and 45 long-wavelength, high-resolution spectrographs taken with the International Ultraviolet Explorer (IUE) satellite over a 25 day period during July and August of 1978. Central depth measurements were of lines of Cr III, Mn III, V III, C III, Si II, and S II seen in the region between 1245 and 1255 Å. Equivalent widths are of the three He I 2^3S - n^3P^o transitions found at 2945, 2829 and 2764 Å.

The period for cyclic intensity variations in He I is determined using a four-parameter, least-squares fit to a sinusoid. The IUE observations match both a period of 8.8163 ± 0.0003 days and a previously unreported period of 9.2532 ± 0.0003 days with equal minima for the least-squares fit. The phase of Cr III maximum relative to He I maximum is found to be 0.53 cycles for the IUE observations.

HE I INTENSITY VARIATIONS

Intensity changes in the spectrum of the B3 V He I variable a Cen are cyclic, with a period of roughly 8.8 days (Norris, 1971; Underhill et al., 1975). For the present study, 45 LWR and 53 SWP spectra of a Cen were obtained over a 25 day interval. From these, intensity variations in He I and in Cr III lines have been measured.

In this section two major points are discussed; (1) the measurement by equivalent width and central depth of the energy absorbed from the continuum flux of a Cen by lines of He I, and (2) the determination of the period of variation of the intensity of these lines.

THE LINES MEASURED

Among the absorption lines in the visible spectrum of a Cen, those from the He I $^3P^o$ states (e.g. 2^3P^o - n^3D) show especially strong cyclic intensity changes. In the range of IUE wavelength sensitivity, no members of these

multiplets exist. However, the members of the 2^3S - n^3P^o multiplets from n = 5 through n = 9 are seen. Since these are also triplet helium transitions, they were expected to vary in strength in phase with the $^3P^o$ lines observed at visible wavelengths.

In July and August of 1978, 45 long wavelength spectra of a Cen were taken at uneven time intervals over a 23-day period. Well defined lines from the 2^3S - n^3P^o series can be seen in them at 2945, 2829, 2764, 2724 and 2696 Å. No study of the line 2^3S - 4^3P^o at 3188 Å is possible because the flux in the order of the IUE echellograms containing it is too weak.

QUANTITIES MEASURED

The He I lines at 2945, 2829 and 2764 Å were strong enough, and their profiles clear enough, that equivalent width measurements were appropriate to search for intensity variations in them. Measurements of the central depth of 2829 Å were also made so that the sensitivity of the two methods could be compared.

RESULTS OF MEASUREMENT

The equivalent widths of the lines 2945, 2829 and 2764 Å, as well as the central depths of the line 2829 Å, were measured. Because the width of each line varies with time, the calculation of equivalent width was always performed between the same two wavelengths for each line.

Each of the He I lines measured from the IUE spectra is from the same series in $^3P^o$ transitions, thus, their average gives more information about the time variations in a Cen than any individual line does. Figure 1 gives a plot of the weighted average of all five measurements of He I lines observed by IUE versus time.

A four-parameter, least-squares fit to a sinusoid using the variable metric method of Fletcher and Powell (1963) was applied to the 45 measurements of the He I triplet series of a Cen seen with IUE.

The period determined is twofold: 8.8164 ± 0.0003 days and 9.2530 ± 0.0003 days with roughly equal fit (i.e. the sample variance and its gradient on the hypersurface are almost the same in both cases).

Because the exposure time for IUE observations was about 90 seconds for each spectrogram, it should be possible to detect cyclic changes on the order of hours or minutes. A search of the IUE He I line strength measurements for a short-time variations from 0.01 days to 1 day leads to no probable period.

REGION FROM 1245 Å to 1255 Å

Observations of the spectrum of a Cen with the Copernicus Satellite in 1975 and 1977 confirmed the fact that regions rich in Cr III, V III or Mn III absorption lines showed intensity variations consistent with the cyclic behavior of He I strength. This section presents the results of intensity measurements for 5 individual lines in 53 IUE spectrograms and a least squares fit to a four parameter sine curve for these and previously discussed lines.

IMPORTANCE OF THIS REGION

Three factors contributed to the choice of the 10 Å spectral range centered on 1250 Å for this study. First, of the two spectral regions surveyed with Copernicus in 1977, only this one is accessible to IUE. Second, the earlier study of a Cen with Copernicus in 1975 covered the entire range from 1000 Å to 1400 Å and showed no region within the range of IUE to vary more strongly than that around 1250 Å. Third, the complete multiplet Cr III (6) is identifiable.

RESULTS OF MEASUREMENTS

The absorption lines examined in the range 1245 - 1255 Å are from heavier elements than the helium discussed before. Thus, they are much less Doppler broadened due to thermal effects. Further, there are many more strong lines at these wavelengths, so many of the lines of interest are blended. In such cases, an appropriate measure of intensity is central depth.

The region from 1245 to 1255 Å was divided into three sectors for the purpose of drawing constant reference lines for each of the spectra. Examples of these lines for one sector are given in Fig. 2 which shows the spectrum at maximum and minimum absorption. These plots include the measured wavelength of each feature for which the central depth was measured.

It is worth noting that the entire region from 1245 to 1255 Å shows large, cyclic changes in flux. There are many lines from Cr III, V III and Mn III in this range that are not as strong or well-identified as those measured in this investigation. These may be contributing to the total flux change in this region as they have been observed to do in many sectors of the Copernicus spectra of the same star at these and other wavelengths.

The least squares fit to a sine curve for the Cr III lines not only gives the period of intensity changes, but also the phase relative to He I strength variations. Two give the following results

1. Cr III alone (53 data points)--The best fit to a four parameter sine curve is 9.2536 ± 0.0003 days. A second minimum in the sample variance with essentially the same value and gradient

indicates a period of 8.8160 ± 0.0003 days. The phase leads that of He I by 0.53 ± 0.01 cycles in both cases.

2. Cr III and He I from IUE (98 data points)--Here again two periods are indicated. The most probable is 9.2534 ± 0.0003 days, while the other is 8.8161 ± 0.0003 days. The Cr III data have been shifted by 0.53 cycles to allow the search for a single-period least-squares fit. The last two figures (Figs. 3,4) show the fit of a sine wave of period 9.25 days and one of 8.82 days to the combined He I and Cr III observations from IUE.

REFERENCES

1. Davidon, W. C.: Variable Metric Method for Minimization, A. E. C. Research and Development Report, ANL-5990(Rev.), 1959.

2. Fletcher, R. and Powerr, M. J. D.: Computer Journal, 6, 163, 1963.

3. Kelley, R. L. and Palumbo, L. J.: Atomic and Ionic Emission Lines Below 2000 Å - Hydrogen through Krypton, Wash., D. C., NRL report 7599, 1973.

4. Norris, J.: Nature, 219, 1342, 1968.

5. Norris, J.: Ap. J. Suppl, 23, 213, 1971.

6. Underhill, A. B., Fahey, R. P. and Klinglesmith, D. A.: Ap. J., 197, 393, 1975.

7. _____: Ap. J., 199, 120, 1975b.

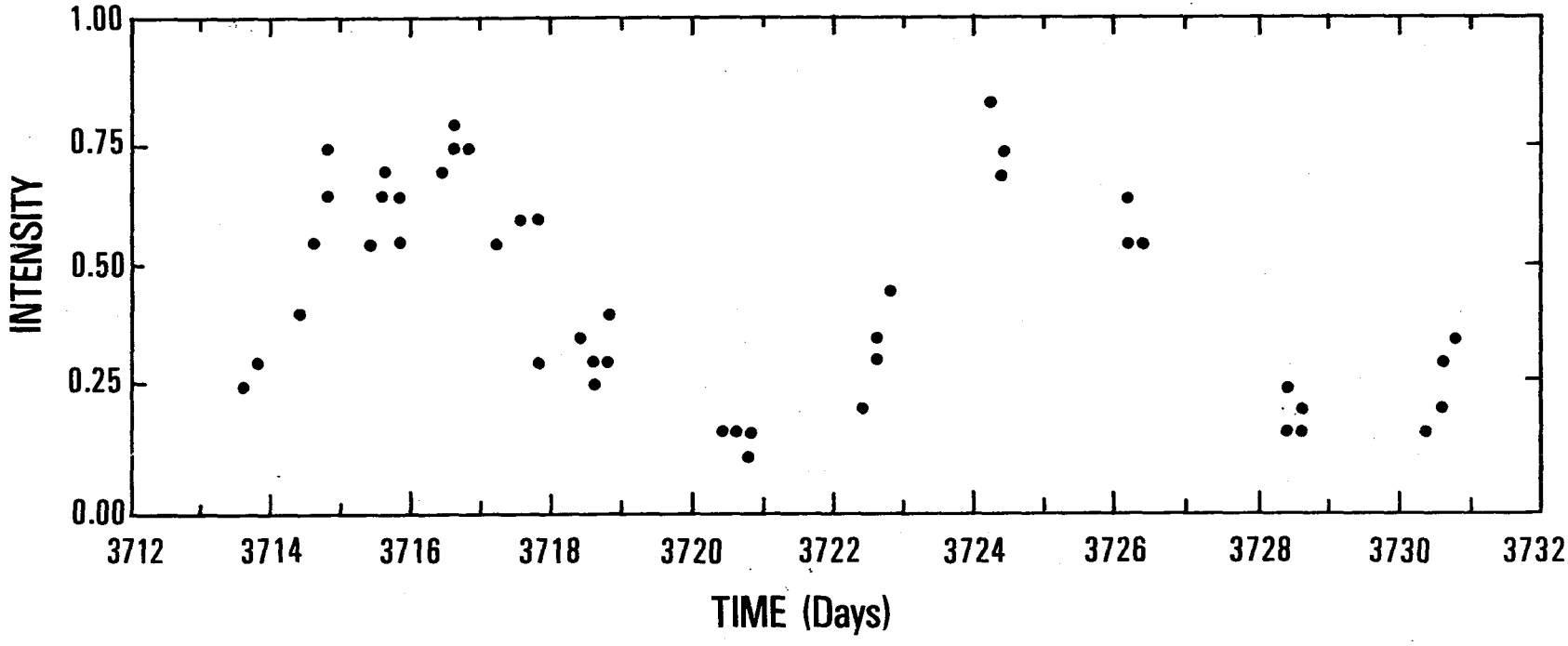

Fig. 1 - AVERAGE (After normalization) OF INTENSITY OF ALL IUE
He I LINES MEASURED vs. TIME

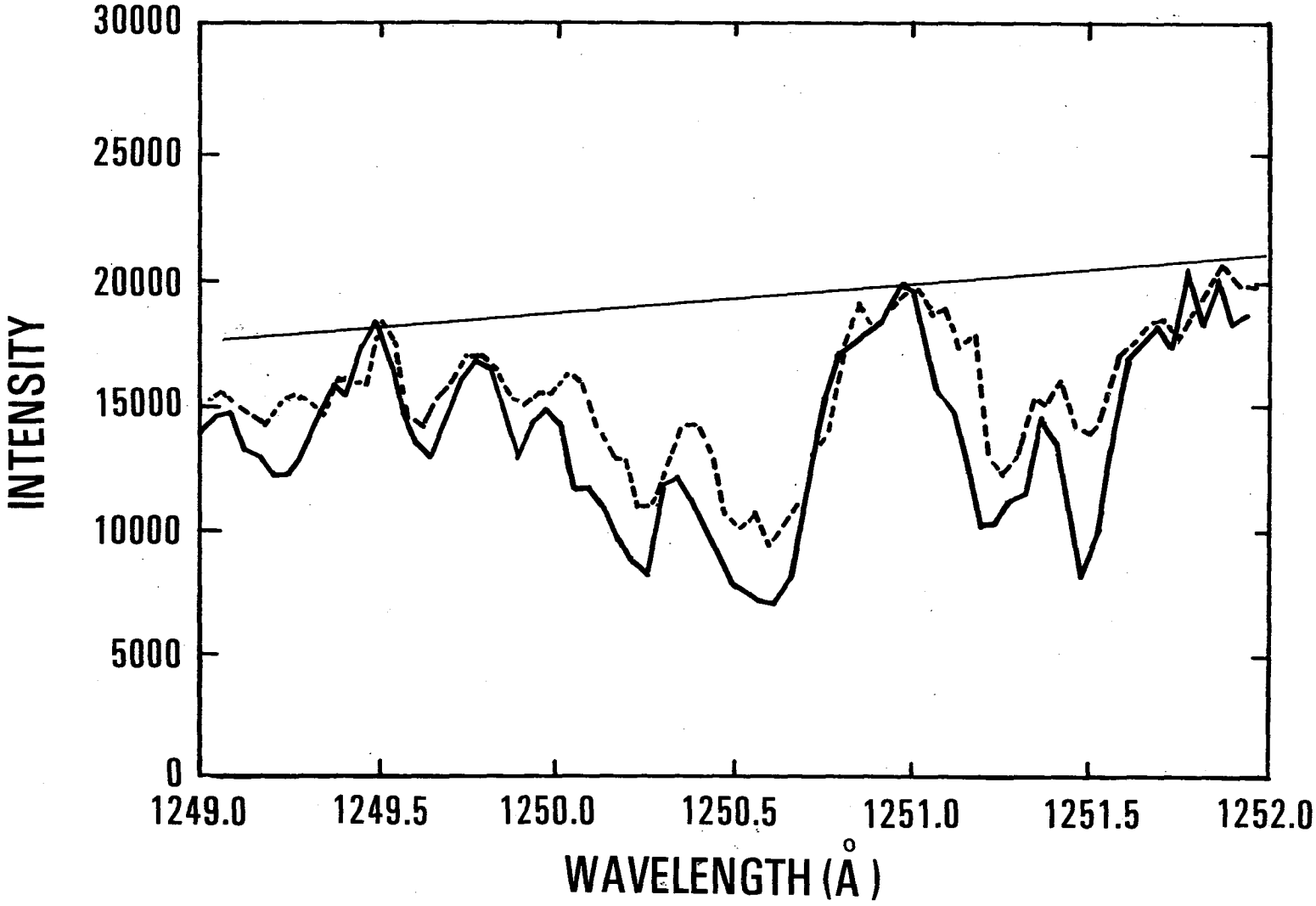

Fig. 2 - REGION BETWEEN 1249 and 1252 Å at
He I MAXIMUM (Dashed) and MINIMUM (Solid)

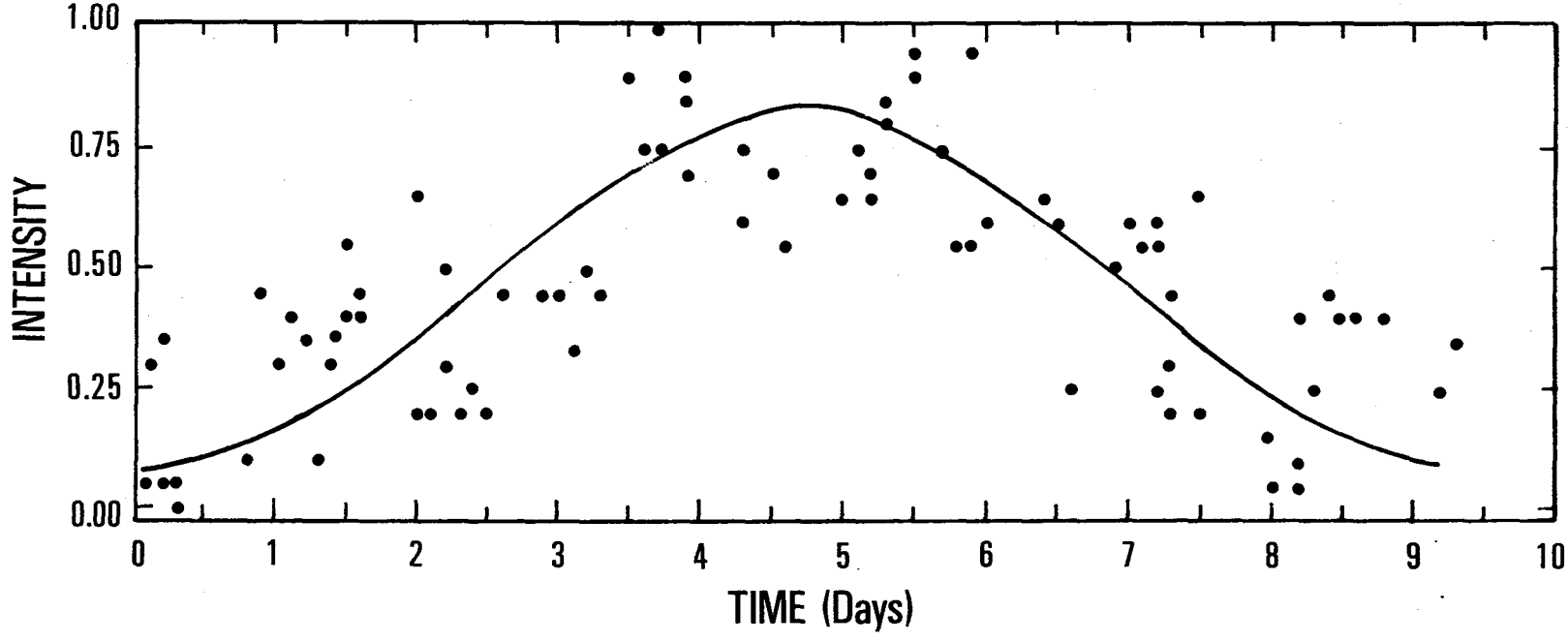

Fig. 3 - INTENSITY OF He I NAD Cr III (Shifted by 0.53 period) (Dots)
FROM IUE OBSERVATIONS AND A SINE CURVE
OF PERIOD 9.253 DAYS vs. TIME

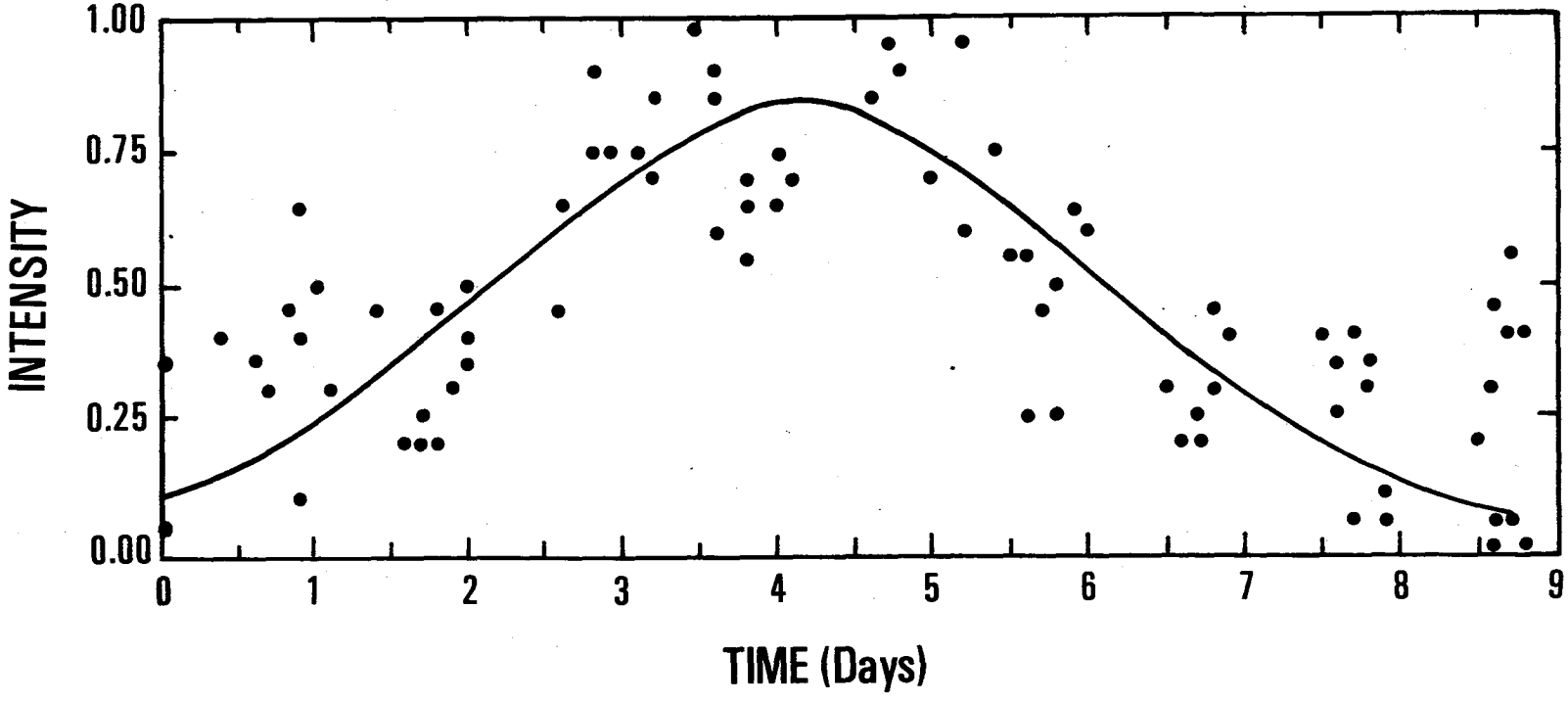

Fig. 4 - INTENSITY OF He I AND Cr III (Shifted by 0.53 period) (Dots)
AND A SINE CURVE OF PERIOD 8.8163 DAYS vs. TIME

THE ULTRAVIOLET VARIABILITY OF THE T TAURI STAR RW AURIGAE[1]

Catherine L. Imhoff[2] and Mark S. Giampapa[2]
Steward Observatory, University of Arizona

ABSTRACT

Between 1978 and 1979 the visible brightness of RW Aurigae increased by $0^m.9$. During this time (a) CIV and SiIV increased by factors of 2 to 4 while the lower ionization lines remained unchanged, (b) the fluorescent OI line increased by a factor of 8, (c) the shell spectrum changed from emission to absorption, and (d) the ultraviolet continuum brightened by $2^m.3$. On a time scale of a week the continuum varied by as much as $0^m.8$ but the MgII emission lines showed no variability over 10%. We hypothesize an active chromosphere, transition region, and envelope cooled by mass loss in order to explain the ultraviolet observations of RW Aur.

INTRODUCTION

A large portion of our IUE observing program has been devoted to an extensive study of RW Aurigae, a well-known T Tauri star with strong emission characteristics. Our two main objectives have been (a) to obtain the best possible data for the star, utilizing multiple observations in order to generate a spectrum with good signal-to-noise across a broad wavelength range and attempting high dispersion observations, and (b) to study the star's variability in the ultraviolet continuum and emission lines.

The results of our first set of observations have been reported in our first paper (ref. 1). A complete discussion of all our observations of RW Aur is in preparation. In this paper we present a preliminary discussion of these results, concentrating on the ultraviolet variability of the star.

RW Aur has been observed during two periods, the first during July 30 to 31, 1978, and the second over April 2 to 9, 1979. The individual observations are separated by intervals as short as half a day and as long as nine months. The observations during the latter period are more extensive, but for both runs long and short wavelength observations were made. Between July 1978 and April 1979 the star brightened from $V=11^m.5$ to $10^m.6$, according to the IUE fine error sensor. Variability in the ultraviolet spectrum was seen in the short wavelength emission lines, the shell lines at longer wavelengths, and the

[1]This research is supported by the National Aeronautics and Space Administration through grant NSG 5235 to the University of Arizona.

[2]Guest Observer, International Ultraviolet Explorer

ultraviolet continuum.

RESULTS

The short wavelength spectrum of RW Aur exhibits a number of emission lines, including HI, CI, CII, CIII, CIV, NIV, OI, SiI, SiII, SiIII, and SiIV. Figure 1 depicts the spectrum as seen in 1979. Between our 1978 and 1979 observations the lower ionization lines (except for OI) remained at essentially the same flux levels. However the highly ionized lines increased in strength, CIV by a factor of 2.1 and SiIV by 3.8. NV 1240 and HeII 1640 are not observed in RW Aur. The enhancement of the higher temperature lines indicates a change in the structure of the star's emission region (thought to be either a chromosphere or shocked zone) that is reminiscent of the changes seen in solar and stellar flares. The OI 1304 emission lines are also seen to strengthen by over a factor of 8. Since these lines are fluorescent with Lyman-β, the variability signals a change in the flux and/or line profile of the Lyman-β line.

How do the emission fluxes for RW Aur compare to solar and stellar chromospheric fluxes? To make this comparison we convert the observed fluxes to surface fluxes corrected for extinction. As for many T Tauri stars, the spectral type of RW Aur and the amount and nature of the extinction affecting it are uncertain. We have therefore considered two cases which should embrace the most likely parameters describing RW Aur: the "liberal" Case I, a G5 star affected by $1^m.69$ of visual extinction characterized by R=6 and the θ Orionis extinction law, and the "conservative" Case II, a K2 star affected by $0^m.17$ of normal extinction. The two cases yield different radii (2.6 and 3.0 $R_\odot$) for the star but the largest difference in the derived surface fluxes comes from the assumptions about the extinction. We find that even in the conservative Case II, the surface fluxes for RW Aur exceed the quiet solar chromospheric fluxes (ref. 2) by a factor of about 2000. Thus the surface fluxes for RW Aur exceed those of the active chromosphere dwarfs (ref. 3) and even the RS CVn stars (ref. 2). Figure 2 has been adapted from Dupree's (ref. 4) figure 6 to show RW Aur compared to a number of other stars. Conservative Case II is depicted; Case I yields surface fluxes a factor of 8 higher.

In stars with active chromospheres, one sees both an increase of the emission line surface fluxes over the solar values and an additional enhancement of the high temperature SiIV, CIV, and NV lines, as well as HeII (thought to be due to recombination after X-ray ionization). In RW Aur we see very high surface fluxes but an apparent weakening of the higher temperature lines. CIV is weaker than SiIV, while for NV and HeII we can only set upper limits. There are also curious deviations in the weakness of CII and the strength of SiII.

These results are in general repeated in IUE observations of other T Tauri stars (ref. 5,6,7,8). We note the following general behavior: (a) CII is weak compared to other lines. CIV 1550/CII 1335 ranges from 2.0 to over 6; the ratio is 1.3 in the quiet Sun. (b) CIV is weakened in the strong

emission stars. CIV 1550/SiIV 1400 is around the solar value of 2.3 and higher for weak emission stars but only 0.9 in S CrA, RU Lup, and RW Aur. (c) HeII 1640 and NV 1240 have been detected only in the weak and moderate emission stars. (d) The density sensitive ratio CIII] 1909/SiIII 1892 decreases from 2.3 in T Tauri to 0.1 for RW Aur. This reflects an increase in electron density from under 10^8 cm^{-3} to 4 x 10^{10} cm^{-3}, if calculated curves (ref. 9) may be applied to these stars. According to these indicators, RW Aur is the most extreme T Tauri star that has thus far been observed with IUE.

We are currently exploring a possible explanation of the behavior of the T Tauri stars in the ultraviolet. We hypothesize an active chromosphere that is affected by mass loss. The mass loss is greatest in the strong emission stars such as RW Aur. It cools the chromosphere-corona sufficiently that T_{max} in RW Aur is only 80,000 K; the density increases and follows an r^{-2} distribution (ref. 10). The existence of such a low T_{max} may produce two regions of intermediate temperature, the traditional transition region and an outer extended region, both of which may contribute to the fluxes of lines such as CI, SiI, SiII, FeII, and HI. Further evidence for a temperature turn-over comes from a derived temperature of 5000 K or less at 5 R_* for the fluorescent FeI lines in RW Aur (ref. 11). For stars with smaller amounts of mass loss, the deviation from normal chromospheric structure is smaller.

We obtained several short exposures of RW Aur in order to determine the MgII emission line flux. The observed emission lines are the strongest in RW Aur of several T Tauri stars surveyed; only a 3 minute exposure was required. Four different images obtained in 1979 yield an observed flux of 1.55 x 10^{-11} erg cm^{-2} s^{-1}, with agreement to 10%. Thus we have no evidence for variability of the MgII lines over 10% in a week's time span.

The great strength of the MgII lines encouraged us to attempt high dispersion observations of the lines; a 3 hour exposure was sufficient (figure 3). Each line is extremely broad (7 Å full width) with a deep central reversal at line center. The interpretation of the line profiles seen in T Tauri stars is a wide-open question; we defer a discussion of these lines to a later paper. We are planning to make additional high-resolution observations of the MgII lines this fall simultaneously with ground-based high-resolution data obtained for the Balmer lines, NaI D, and CaIIH and K.

The MgII lines are surrounded by numerous low excitation lines of FeII, CrII, and MnII. In some T Tauri stars observed with IUE these lines are in absorption, others in emission. The long wavelength ultraviolet spectrum of RW Aur, however, changed from emission in 1978 to absorption in 1979. It is difficult to understand this behavior unless it is due to an extended shell. In fact one may ascribe the change from emission to absorption as related to the brightening of the star. One might consider that any line produced in a shell around the star is the combination of an absorption component produced by the gas in the line of sight to the star and an emission component from the extended shell. At low resolution, the line

appears in absorption or emission depending upon the geometric extent of the shell, the brightness of the star, the strength of the absorption lines and the strength of the emission. If the brightness of the star increases, the absorption contribution is enhanced over the emission (assumed unaffected by the variability). If this is so, one may expect absorption to predominate when the star is bright, emission when it is faint. The large range of variability in the ultraviolet indicates that this behavior can be seen most easily in this wavelength range.

A confirmation of the shell nature of the absorption lines comes (surprisingly) from one of our high resolution spectra of the MgII lines. In a 7 hour exposure the ultraviolet continuum is well enough exposed to show individual absorption lines. Although the signal-to-noise is only about 5, the lines are broad (1 Å) and dip to zero residual intensity making them easily visible. The source of the ultraviolet excess is therefore interior to the shell. We have performed line identifications over the wavelength range 2600 to 3100 Å. Numerous lines of low excitation multiplets have been identified, including MgI(1), TiII(1), VII(1,2,3), CrII(5,6,7,8,11), MnII(1,5,18,19), and FeII(1,60,61,62,63,64,78).

The ultraviolet continuum from 2000 to 3300 Å showed variations on all observed time scales. Between 1978 and 1979 the ultraviolet continuum at 3050 Å rose by $2^m.3$; at the same time the visual brightness increased by $0^m.9$. During the 1979 run, a variation of $0^m.4$ was seen in half a day and $0^m.8$ in a week. The tendency for variability to increase at shorter wavelengths in T Tauri stars is thus continued into the ultraviolet.

A composite energy distribution for RW Aur was formed from several exposures of different durations. Good signal-to-noise was thus obtained over a range from 2000 to 3300 Å. The 2200 Å graphite feature is definitely weak or absent. No more than a few tenths of a magnitude of visual extinction may be present if the extinction law is normal. If larger amounts of extinction are present then the extinction law must be peculiar, perhaps resembling that found for θ Ori. Both Case I and Case II discussed above are consistent with these results. In both of these assumed cases the energy distribution of the ultraviolet excess may be determined. As noted in our first paper, the resemblence to Balmer bound-free emission is unmistakable.

CONCLUSIONS

In summary we may state that the ultraviolet variability of RW Aur has exhibited the following behavior as the star brightened: (a) The high temperature lines of CIV and SiIV increased by factors of 2 to 4 while the lower ionization lines remained unchanged. (b) The fluorescent OI lines increased by over a factor of 8. (c) The shell spectrum at longer wavelengths changed from emission to absorption. (d) The ultraviolet continuum increased by $2^m.3$ and varied by smaller amounts on shorter time scales. In addition the MgII emission line fluxes did not vary by over 10% in one week. We hypothesize an active chromosphere and transition region affected by mass loss to

explain the ultraviolet observations of RW Aur. It is clear that the variability of the T Tauri stars in the ultraviolet can provide valuable information on the nature of these stars.

REFERENCES

1. Imhoff, C. L., and Giampapa, M. S. 1980, Ap. J. (Letters), in press.

2. Linsky, J. L., et al. 1978, Nature, 275, 389.

3. Hartmann, L., Davis, R., Dupree, A. K., Raymond, J., Schmidtke, P. C., and Wing, R. F. 1979, Ap. J. (Letters), 233, L69.

4. Dupree, A. K. 1979, preprint.

5. Gondhalekar, P. M., Penston, M. V., and Wilson, R. 1979, The First Year of IUE (ed. A. J. Willis), p. 109.

6. Gahm, G. F., Fredga, K., Liseau, R., and Dravins, D. 1979, Astr. Ap., 73, L4.

7. Appenzeller, I., and Wolf, B. 1979, Astr. Ap., 75, 164.

8. Appenzeller, I., Chavarria, C., Krautter, J., Mundt, R., and Wolf, B. 1980, preprint.

9. Doschek, G. A., Feldman, U., Mariska, J. T., and Linsky, J. L. 1978, Ap. J. (Letters), 226, L35.

10. Heidmann, N., and Thomas, R. N. 1979, preprint.

11. Willson, L. A. 1975, Ap. J., 197, 365.

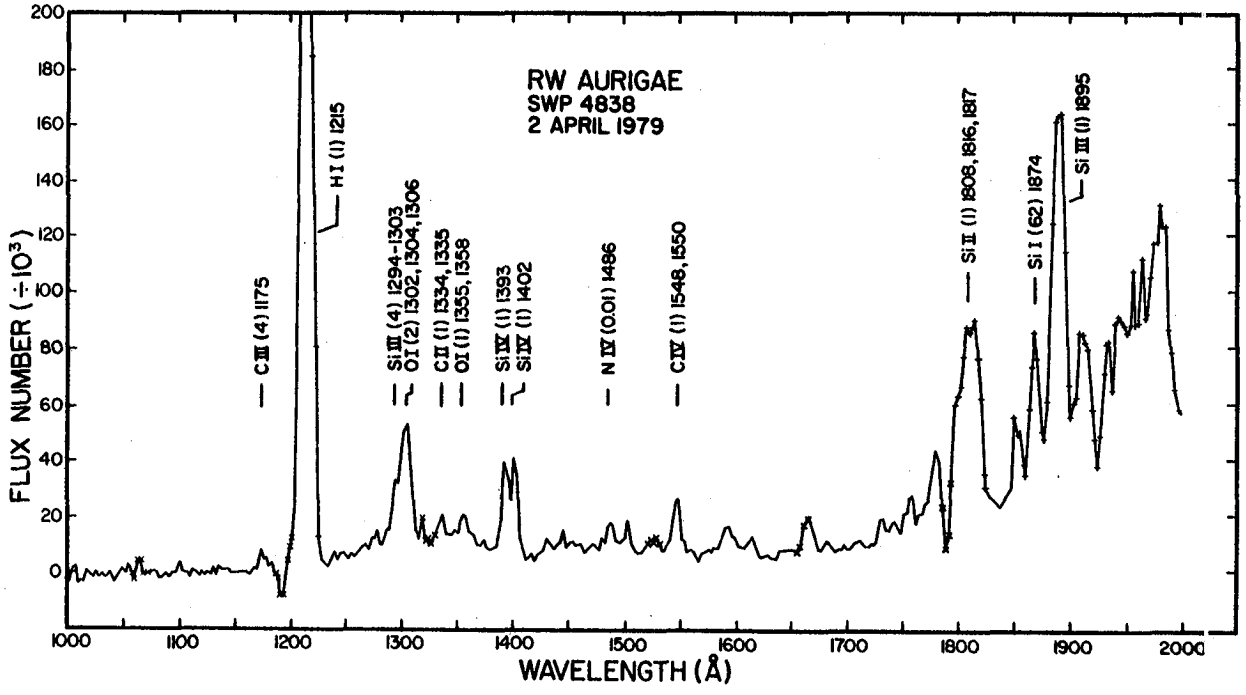

Figure 1. - The short wavelength ultraviolet spectrum of RW Aurigae obtained in 1979. IUE relative intensity is plotted against wavelength. The crosses denote the presence of reseaux, while the plusses indicate saturated pixels.

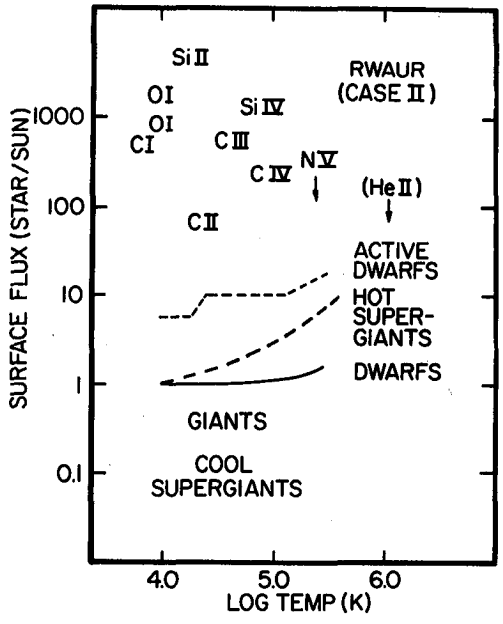

Figure 2. - Comparison of the surface fluxes for RW Aurigae (for Case II) with other stars. Individual ultraviolet lines are indicated. Only upper limits for NV and HeII can be given.

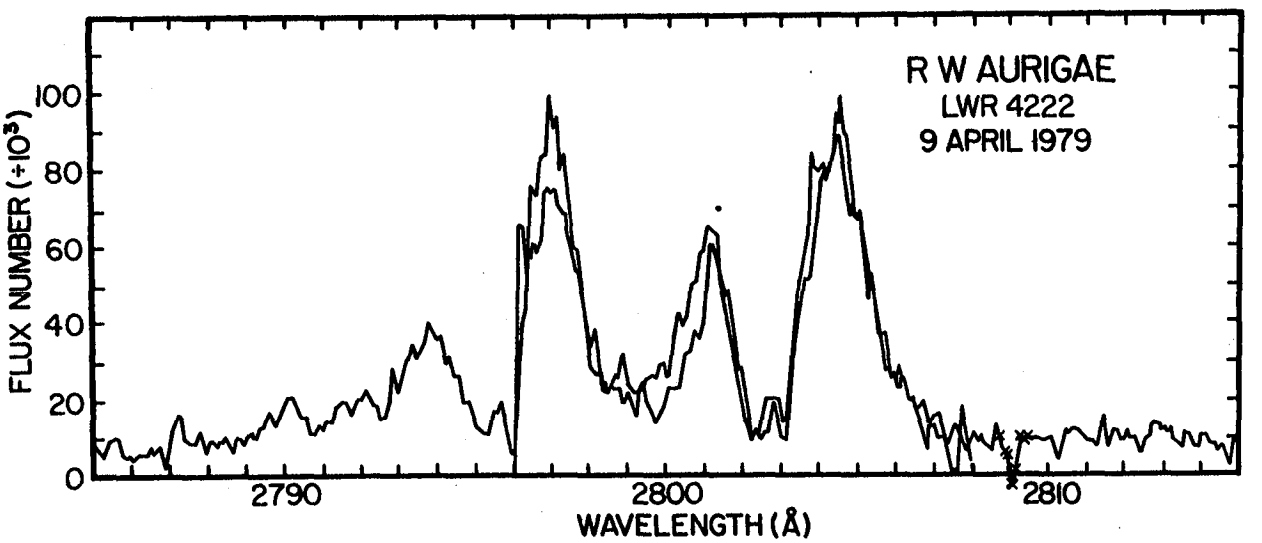

Figure 3. - The MgII lines observed with high resolution. Low resolution observations set a flux scale of 1 FU = 4.22×10^{-14} erg cm^{-2} s^{-1} $Å^{-1}$.

IUE OBSERVATIONS OF BLUE HALO HIGH LUMINOSITY STARS*

Margherita Hack, Margarita L. Franco and Roberto Stalio

Astronomical Observatory, Trieste, Italy

ABSTRACT

Two high luminosity population II blue stars of high galactic latitude, BD+33°2642 and HD 137569 have been observed at high resolution. The stellar spectra show the effect of mass loss in BD+33°2642 and abnormally weak metallic lines in HD 137569. The interstellar lines in the direction of BD+33°2642, which lies at a height $z \gtrsim 6.2$ kpc from the galactic plane, are split into two components. No high ionization stages are found at the low velocity component; nor can they be detected in the higher velocity clouds, because of mixing with the corresponding stellar/circumstellar lines.

INTRODUCTION

Various classes and subclasses of blue halo stars of population II and old disk population have recently been described and discussed (ref.s 1 and 2). Three large groups, which include all subclasses, are generally recognized to be important: the horizontal branch (HB) stars, the subdwarfs, the high luminosity (HL) population II-B stars. This last group is formed of stars which lie several magnitudes above the HB stars. Bernard 29, in the globular cluster M 13, BD+33°2642 and HD 137569 are commonly thought to belong to the HL-population II-B-star group.

Here we report on the high resolution IUE observations of BD+33°2642 and HD 137569. The spectrum of BD+33°2642 (only SWP observations, exposure time 4.7 hours) will be discussed more extensively since it presents the effects of mass-loss in the high-

* Based on observations by the International Ultraviolet Explorer (IUE) collected at the Villafranca Satellite Tracking Station of the European Space Agency. This work was partly supported by a CNR-Italy contract.

ly ionized resonance lines of C IV, Si III and Si IV, and intriguing evidence for the presence of high ionization stages in the interstellar lines. The basic data for the two stars are presented in Table 1.

THE STELLAR SPECTRA

The main results emerging from a study of BD+33°2642 made by Stalio and Franco (ref. 6) are:

1) the effective temperature, on the basis of the spectral energy distribution, is found to be about 18000 K, lower than the temperature determined from the line spectrum (ref. 4) by about 5000 K. Discrepancies between temperatures determined from the continuum and line spectrum are also found in population I early-type supergiants (see e.g. ref. 7) but seem not to be so great. They are generally ascribed to the different depths of formation of the two spectra,

2) the carbon spectrum appears less ionized than in ζ Sco, whose UV spectrum has been used for comparison. This result is probably due to combined effects of a lower effective temperature and lower carbon abundance,

3) the photospheric turbulence is small: it has been calculated to be 2.3 km s^{-1} from a curve of growth of Fe III lines. This value is in agreement with the visual data, but in conflict with the observations of population I stars having similar effective temperature and gravity (ref. 8),

4) the star has a stellar wind revealed by the displaced lines of C IV, Si III and Si IV (figure 1). The terminal velocity is estimated to be -520 km s^{-1} from the steep blue edge of the Si III resonance profile. A lower limit for the mass-loss is calculated to be 4.7×10^{-8} $M_\odot$ yr^{-1}.

HD 137569, on the contrary, does not show clear evidence for mass flux: the most prominent features in the UV, the resonance lines of C II, have large symmetrical wings. The remaining spectrum consists of abnormally weak metallic lines of Mg II, Si III and Fe III, multiplet 34. The ultraviolet flux distribution is that of a B3 supergiant with no reddening. The anomalous B-V colour index, and the variable radial velocities reported in ref. 5, support the idea that the star is part of a binary system.

THE INTERSTELLAR SPECTRA

If we consider both stars as having low mass (ref. 2) typical of population II objects, their height from the galactic plane is 6.2 kpc for BD+33°2642 and 0.8 kpc for HD 137569. By virtue of its distance, BD+33°2642 can provide information on the high ionization galactic halo gas. The interstellar spectrum is split into two components at about -35 and -105 km s^{-1}. All measurable lines are presented in table 2. High ionization stages, C IV and Si IV, seem to be present (figure 1) at the stellar velocity, thus suggesting that they might come from gas formed around the star.

The interstellar spectrum is very well measurable in HD 137569 due to the weakness of stellar lines. All usually observed interstellar lines are present at about zero velocity. There might be evidence of weak Si IV components at 0 and -100 km s^{-1}.

CONCLUSIONS

We have studied two stars of the group of HL-population II-B objects, whose cinematical and evolutionary situation is rather controversial. BD+33°2642 is likely to be a population II object, similar to the globular cluster giant Bernard 29; it has a large amount of mass loss for its low mass, and, besides abundances, presents differences with population I stars of the same spectral class in the size of the photospheric turbulent motions, which are smaller, and in the amount of discrepancies between the effective temperature determined from the continuum and line spectrum. HD 137569 has a simpler UV spectrum than BD+33°2642: it shows abnormally weak metallic lines and no evidences of high ionization stages and mass flux, unlike all known early type stars of low gravity.

For both stars the reddening, as deduced from the interstellar bump at 2175 Å, is low. The radial velocities of the interstellar gas in the line of sight of BD+33°2642 are at -35 and -105 km s^{-1}; no high ionization stages are found in the low velocity cloud; nor can they be detected in the higher velocity cloud, because of mixing with the corresponding stellar/circumstellar lines.

REFERENCES

1. Newell,E.B.:1973, Astrophys. J. Suppl. 26, 7
2. Greenstein,J.L., Sargent,A.I.:1974, Astrophys.J.Suppl. 28, 157
3. Blanco,V.M.,Demars,S.,Douglass,G.G.Fitzgerald,M.P.: Publ.of the United States Naval Observatory, 2nd series,Vol.21
4. Traving,G.:1962, Astrophys. J. 135, 439
5. Danziger,I.J.,Jura,M.A.:1970, Astrophys. J. 161, 997
6. Stalio,R.,Franco,M.L.:1980, Astron.Astrophys., in press
7. Stalio,R.,Selvelli,P.L.,Crivellari,L.: 1977, Astron.Astrophys. 60, 109
8. Lamers,H.J.G.L.M.,DeLoore,C.:1975, in Physique des Mouvements dans les Atmosphères Stellaires, Ed. R.Cayrel and M.Steinberg, CNRS France,P.453
9. Rogerson,J.B.Jr.,Upson,W.L.:1977, Astrophys.J.Suppl. 35, 37

TABLE 1 : The Basic Data.

	BD+33°2642	HD 137569	
Spectral Type	B2	B5	
V	10.8	7.86	ref. 3
B-V	-0.14	0.24	ref. 3
l"	52°	21°	
b"	+51°	+52°	
Radial Velocity	-95 km s^{-1}	variable; -30 km s^{-1} in our spectrum	
T_{eff}	22900 °K	12000 °K	ref. 4 / ref. 5
log g	2.3	2.3	ref. 4 / ref. 5
M_V	-3.9	-2.6	based on masses of 0.66 $M_\odot$

TABLE 2 : Radial velocities of the interstellar lines on the wavelength scale of the star rest frame, BD+33°2642.

Ion	λ (A)	Vel (km s^{-1})	Vel (km s^{-1})	Ion	λ (A)	Vel (km s^{-1})	Vel (km s^{-1})
C I	1656.928	-	-103	Si II	1260.418	-42	-101
	1657.380	-	-113		1264.730	-	-103
	1657.907	-	-118		1265.023	-	-102
	1328.833	-20	-110		1304.369	-40	- 98
	1277.240	-29	-		1526.719	-33	- 72
C II	1334.530	-20	-110		1533.445	-	-112
	1335.700	-23	-102	Si III	1206.510	-	- 90*
C IV	1548.202	-	- 87*	Si IV	1393.755	-	- 90*
	1550.774	-	- 81*		1402.769	-	- 85*
N I	1199.549	-15;-55	-	S II	1250.586	-35	-106
	1200.224	-34	-		1253.812	-29	-100
	1200.711	-5;-43	-		1259.520	-30	-102
O I	1302.170	-36	- 98	Fe II	1608.456	-28	- 84
Mg I	2026.405	-	- 82	Ni II	1741.560	-31	-117:
A III	1670.786	-41	- 95		1751.920	-22	-
Al III	1854.720	-	-106*		1773.960	-42	-
	1862.795	-	-102*	Zn II	2026.097	-27	-105
Si II	1193.284	-36	- 87				
	1194.497	-	- 90				

* also photospheric contributions

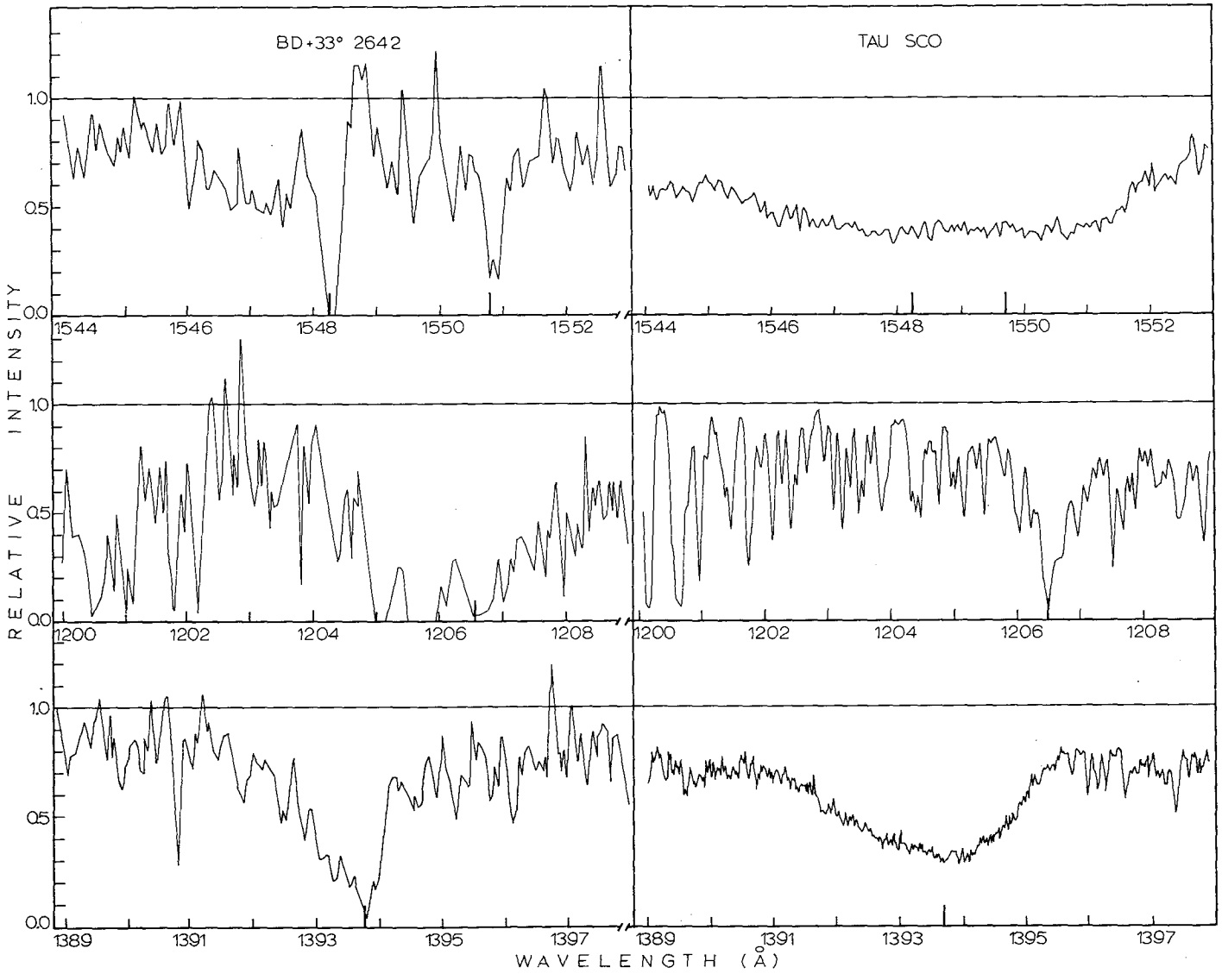

Fig. 1. Resonance line profiles of the C IV doublet (top), of Si III 1206.52 (middle) and of Si IV 1393.73 (bottom) compared with the same lines observed in Sco (ref. 9).

THE EMISSION/ABSORPTION FE II SPECTRUM OF HD 45677

R. Stalio and P.L. Selvelli
Astronomical Observatory of Trieste
Italy

ABSTRACT

The complex behavior of the Emission/Absorption spectrum of Fe II is analyzed. The far UV spectrum is characterized almost solely by absorption lines, while, in the near UV, strong emissions are predominant. Radiative excitation from the ground to the highest levels ($\chi \simeq 10$ eV) with re-emission in the near UV, visible and I.R. seems to be the main mechanism capable of explaining the observed spectral features.

THE EMISSION/ABSORPTION SCHEME

The emission-line star HD 45677 (a short summary of its main observed characteristics is presented in Table 1) shows a Fe II spectrum which appears as (1) sharp in absorption with typical Be-shell-phase profiles; (2) sharp in emission in its forbidden components, (3) wider in emission, sometimes with sharp absorption on the blue wing. This variety of profiles is present throughout the different spectral ranges observed: the passage from shell-phase-like profiles to emission is gradual as one moves from the ultraviolet below 2000 Å to longer wavelengths. There is probably a "null" region, around 2100 Å, where absorptions and emissions are balanced. Above 2300 Å the lines are in emission, but the strongest ones show a reversal on the blue wing. In the visual this characteristic is enhanced, the emission appearing as split into two components. All forbidden Fe II lines are in the visual-near IR ranges. The usually expected inter/circumstellar Fe II absorptions are observed between 2300 and 2600 Å superimposed on the corresponding stellar emissions.

The only important exception to the above scheme is due to multiplet UV 191, in emission at about 1786 Å. Figure 1 illustrates some of the behaviors described above.

Ni shows the same behavior, the passage from absorptions to emissions being observed in a more restricted wavelength range from 1200 to 1750 Å. Other emission lines in the ultraviolet spectrum are OI at λ1305 and the Mg II resonance doublets. At λ1641.2 there is also an unidentified strong emission that was incorrectly attributed to He II: it cannot be He II because the wavelength displacement is too large and its presence would be in contradiction with the generally low ionization character of the emission spectrum.

II. THE GROTRIAN DIAGRAM

We restrict the analysis to that portion of the energy level diagram formed by the term systems of the quadruplets and of the sextets. The extension to the doublets follows naturally. Octets are unimportant. One must recall that deviations from LS coupling can be important for Fe II, so that intercombination transitions must be taken into account.

If we consider only the sextets, we see from Figure 2 that transitions between the ground term a^6D and the closest ones a^6S (multiplet 7F), z^6D° (multiplet UV1), z^6F° (UV2), z^6P° (UV3) correspond to actually observed emission lines. On the contrary, as the excitation potential of the upper terms increases, we observe the transitions a^6D-y^6P° and a^6D-x^6P° in absorption. The terms y^6P° and x^6P° emit to the metastable term a^6S (multiplet UV 191), which in turn emits to the a^6D. Trnasitions from the ground to higher energy terms, as for example a^6D-w^6P° (EP high=11.30 eV, multiplet UV18) fall below the wavelength range of IUE. As the correlated downward transition to a^6S is not observed either in emission or in absorption, we guess that there is not enough flux reaching the region of formation of Fe II lines to cause excitation above about 10 eV. Partial support for this idea comes from a comparison of the transition probabilities and the observed line strengths. The oscillator strengths for the transitions a^6S-x^6P° and a^6S-w^6P° are comparable; conversely only the lines of the lower energy transition (multiplet 191) are seen in emission. Thus the situation can be represented by a simple three-level-atom scheme, the levels being the terms a^6D, a^6S and either y^6P° or x^6P°: we observe high frequency quanta being transformed into low frequency quanta through radiative processes occurring in diluted radiation fields. The high energy quanta are radiated in the Balmer continuum of the B2 stellar photosphere. Part of these quanta have energy sufficient to excite Fe II until about 10 eV; not more, because the flux of a B2 star falls down steeply shortward of Ly α.

A similar three-level-atom scheme holds for the quadruplets and doublets. A partial energy transition scheme for the quadruplets is given in Figure 2b. All the levels of the lowest even terms are excited to high energy levels ($\Delta E > 7$eV) of the permitted odd terms. These last emit to the metastable levels around 3 eV, which in turn emit to the lowest even terms via forbidden transitions observed in the visual-near IR range.

NI shows the same behavior for the $2p^3\ ^2D^\circ$, $2p^3\ ^2P^\circ$ and $3S^2P$ terms, the lower term $2p^3\ ^2P^\circ$ being excited to $3S^2P$, 8.3 eV above.

The three-level-atom scheme, however, explains only partially the observed emissions. It is not very evident what is the source of excitation of the odd-term-z-levels. In Figure 2a we see, for example, that two strong emissions (the multiplets UV3 and V42) depart from z^6P°, despite the fact that there is no evident way of feeding it. The emissions corresponding to the transition z^6P°-e^6D are, in fact, too weak; intercombination transitions do not seem to play any role in this case. Also for the quadruplets and doublets the z levels behave in this way. We have not yet, carefully checked the influence of intercombinations in these cases.

III. CONCLUSIONS

It is still too early to draw definite conclusions from our observations. HD 45677 is not a very common object, although the features that we have briefly described in Table 1 and called "stellar" are characteristic of all early-type stars: the profiles of the "sensitive" lines give evidence of motions, and there is mild superionization (NV seems to be absent) indicating chromospheric-coronal regions.

The unusualness lies in the cool "metallic" line spectrum, essentially Fe II. The concomitant presence of absorption lines in the far-UV, permitted emissions in the near UV and permitted-forbidden emissions in the visible and near-IR suggests a simple explanation in terms of resonance fluorescence from the ground terms under conditions of diluted radiation and matter density.

However, the difficulty of explaining a number of emission line strengths, as for example that of multiplets UV3 and V42, makes us reluctant to assume the resonance fluorescence mechanism as the only possible one: there might be other mechanisms, like pumping from other ions, which produce part of the observed emission spectrum.

In our case it is possible that a clue towards a better understanding of the odd-term-z-level excitation will come from IUE observations with a high signal-over-noise ratio in that region that we have called "null", around 2100 Å.

TABLE 1

m_V = 8.5-9.5	Presently fading in light
Spectral type: B2	From visual and UV spectral energy distribution. IR excess.
E (B-V): 0.15	From the "bump" at λ2175.
IUE high resolution observations:	2xLWR: the emission strength has declined from the first (Sept 1978) to the second observation (March 1979); 1xSWP (March 1979).
IUE "stellar" absorption spectrum:	C IV and Si IV are the highest ionization states definitely present; undisplaced resonance lines observed; FWHM 250 and 40 km s^{-1} respectively. Al III resonance doublet and Fe III (multiplet 34) with abrupt rising of the blue wing to the continuum.
IUE emission spectrum:	described in the text.

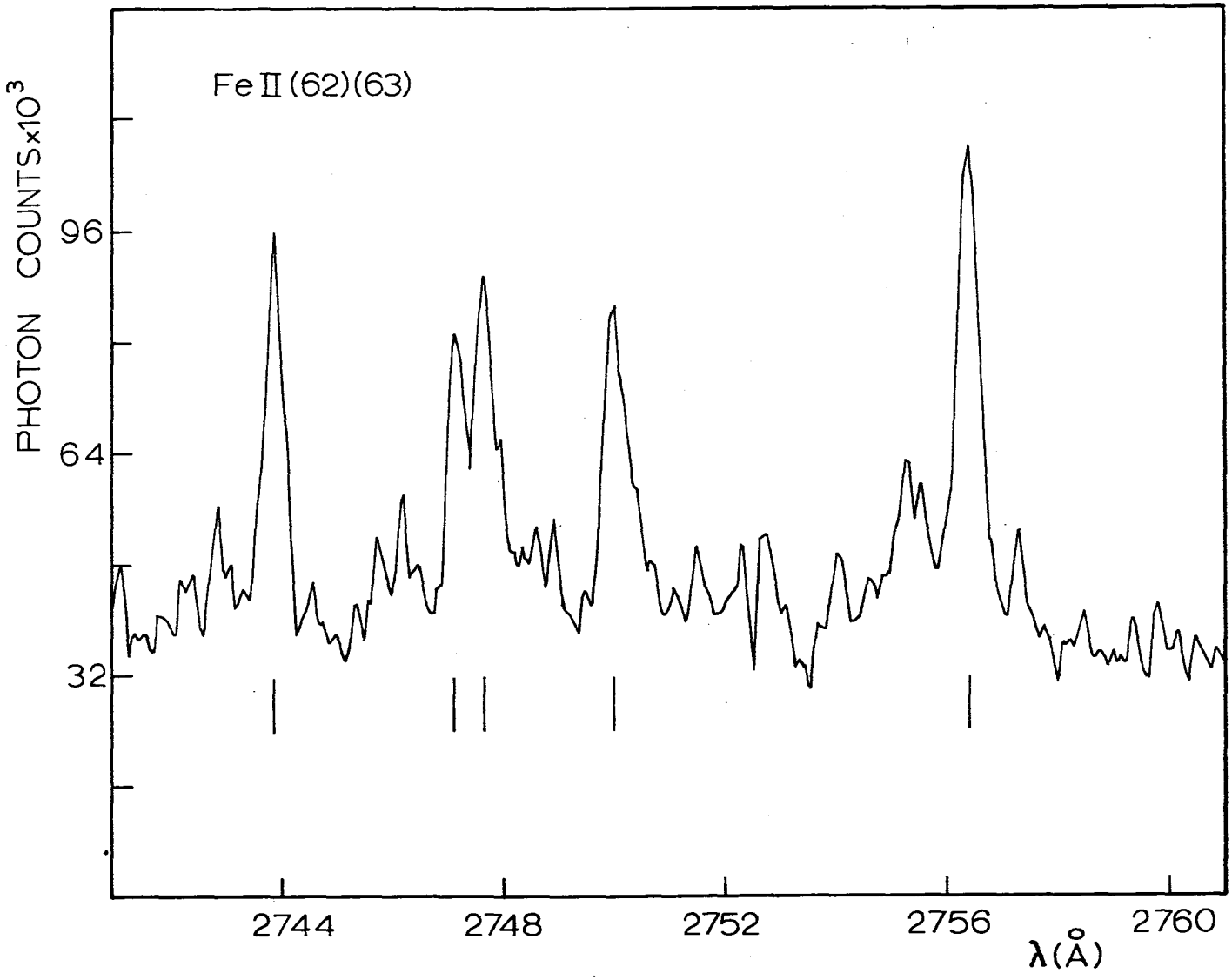
Fe II (62)(63)
PHOTON COUNTS x10³
96
64
32
2744
2748
2752
2756
2760
λ(Å)

Figure 1

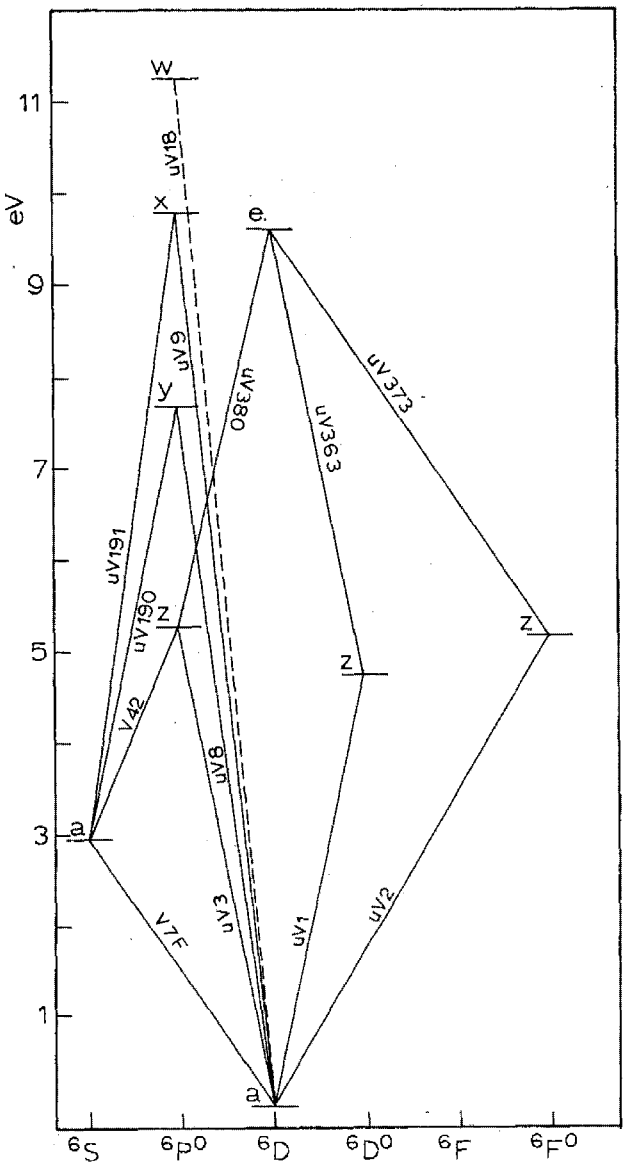
eV
11
9
7
5
3
1
W
X
Y
Z
a
e
uV18
uV9
uV191
uV190
V42
uV8
uV3
V7F
uV380
uV363
uV373
uV1
uV2
Z
Z
Z
a
6S
6P0
6D
6D0
6F
6F0

Figure 2a

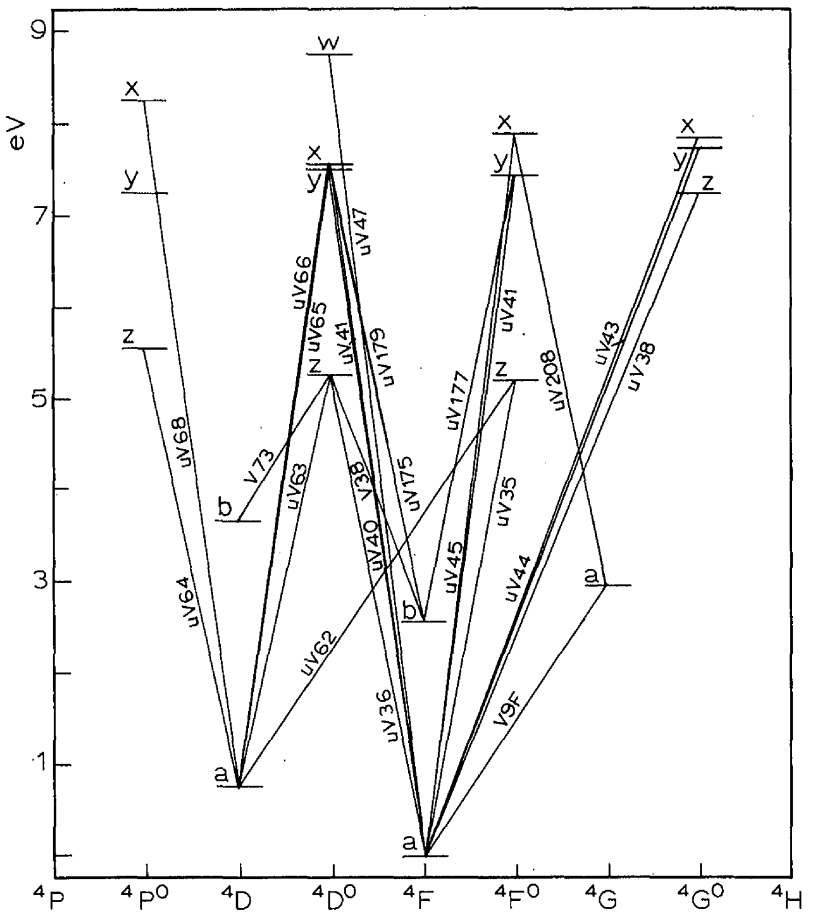
eV
9
7
5
3
1
w
x
y
z
a
b
uV66
uV65
uV41
uV47
uV179
uV68
uV73
uV63
uV38
uV40
uV64
uV62
uV36
uV175
uV177
uV45
uV41
uV35
uV208
uV44
uV43
uV38
V9F
4P
4P0
4D
4D0
4F
4F0
4G
4G0
4H

Figure 2b

THE DETECTION OF COMPANION STARS TO THE CEPHEID VARIABLES ETA AQUILAE AND T MONOCEROTIS

John T. Mariska, G.A. Doschek, and U. Feldman
E.O. Hulburt Center for Space Research
Naval Research Laboratory

ABSTRACT

We have obtained ultraviolet spectra with IUE of the classical Cepheid variables η Aql and T Mon at several phases in their periods. For η Aql significant ultraviolet emission is detected at wavelengths less than 1600 Å, where little flux is expected from classical Cepheids. Furthermore, the emission at wavelengths less than about 1600 Å does not vary with phase. Comparison with model atmosphere flux distributions shows that the nonvariable emission is consistent with the flux expected from a main-sequence companion star with an effective temperature of about 9500 K (A0 V - A1 V). For T Mon a nonvarying component to the ultraviolet emission is observed for wavelengths less than about 2600 Å. Comparison with model atmosphere flux distributions suggests that the companion has an effective temperature of around 10,000 K (A0) and is near the main sequence.

INTRODUCTION AND OBSERVATIONS

Classical Cepheids are a major element in the determination of galactic and extragalactic distances. Thus determinations of their masses and absolute magnitudes are of considerable interest. One method for determining these properties is to study binary systems containing Cepheids. We report evidence here that the classical Cepheids η Aql and T Mon have companion stars.

As part of a program to study classical Cepheids with IUE, we obtained spectra of η Aql and T Mon on several days in 1979. All of the spectra were obtained at low resolution. Exposures were made in both the long and short wavelength cameras and with both the large and small apertures. Figures 1 and 2 show samples of the calibrated spectra at several different phases for η Aql and T Mon, respectively.

Examination of the spectra in figures 1 and 2 shows a number of interesting features. In both cases at short wavelengths (below 1600 Å in figure 1 and below 2000 Å in figure 2) the magnitude of the flux and its spectral distribution are clearly incompatible with the F or G type spectrum expected for a Cepheid. Only at longer wavelengths does the continuum flux increase with increasing wavelength as would be expected

for a Cepheid. Furthermore, only at longer wavelengths does the flux vary with phase, as expected for a Cepheid. For both stars the features pointed out above are seen in all of the spectra we have obtained, including those taken with the small aperture. Thus the source of the radiation must be within 1.5 arc sec of the two Cepheids. We therefore suggest that the features of the spectra presented in figures 1 and 2 indicate that η Aql and T Mon have early type companion stars.

ANALYSIS AND DISCUSSION

To determine accurately the characteristics of the companion stars, we have compared the observed flux at the Earth in the wavelength range of IUE with predicted fluxes from a series of stellar atmosphere models calculated by Kurucz (ref. 1). Each set of model atmosphere fluxes was reddened using published color excesses for the Cepheids. To reduce the contribution from the Cepheid, the models were fit to the data at the phase closest to minimum light. Further details on the model fits are presented elsewhere (refs. 2 and 3).

For η Aql the best fit was found for a model with an effective temperature of about 9500 K. For T Mon the best fit was for a model with an effective temperature of 10,000 K. Figures 3 and 4 show the data near minimum light, the best fit model fluxes, and fluxes for models with effective temperatures that bracket the best fit values for η Aql and T Mon, respectively. In both cases the agreement of the model fluxes with the observations is good in the region of the spectrum where the flux is due only to the companion and interstellar reddening is not a major problem.

If we assume that the companion stars are at the distance of the Cepheids, then we can use the observed ultraviolet flux to estimate the radius of the stars and hence their luminosity class. The radius is given by the expression $(R/d)^2 \pi F_\lambda = f_\lambda$, where R is the radius of the star, d is the distance to the star, F_λ is the surface flux at the star, and f_λ is the flux measured at the Earth, corrected for interstellar absorption. Following this procedure, we find radii for the companion stars of η Aql and T Mon of 2.2 $R_\odot$ and 7.4 $R_\odot$, respectively. Further details of the determination are given elsewhere (refs. 2 and 3). The radii determinations indicate that the companion star to η Aql is an A0 V to A1 V star, while the companion star to T Mon is an A0 III star.

The detection in the ultraviolet of companion stars to Cepheid variables could provide a valuable method for checking the period-luminosity relation. So far with IUE we have observed 6 classical Cepheids, two of which have companions. Pel (ref. 4) has estimated that at least 25% of all Cepheids are binaries. As our understanding of normal stars in the ultraviolet region of the spectrum improves, these companions to Cepheids could prove to be a new check on the period-luminosity relation.

REFERENCES

1. Kurucz, R.L. 1979, Ap. J. Suppl., 40, 1.

2. Mariska, J.T., Doschek, G.A., and Feldman, U. 1980, Ap. J. (Letters), 238, in press.

3. Mariska, J.T., Doschek, G.A., and Feldman, U. 1980, Ap. J., submitted.

4. Pel, J.W. 1978, Astr. Ap., 62, 75.

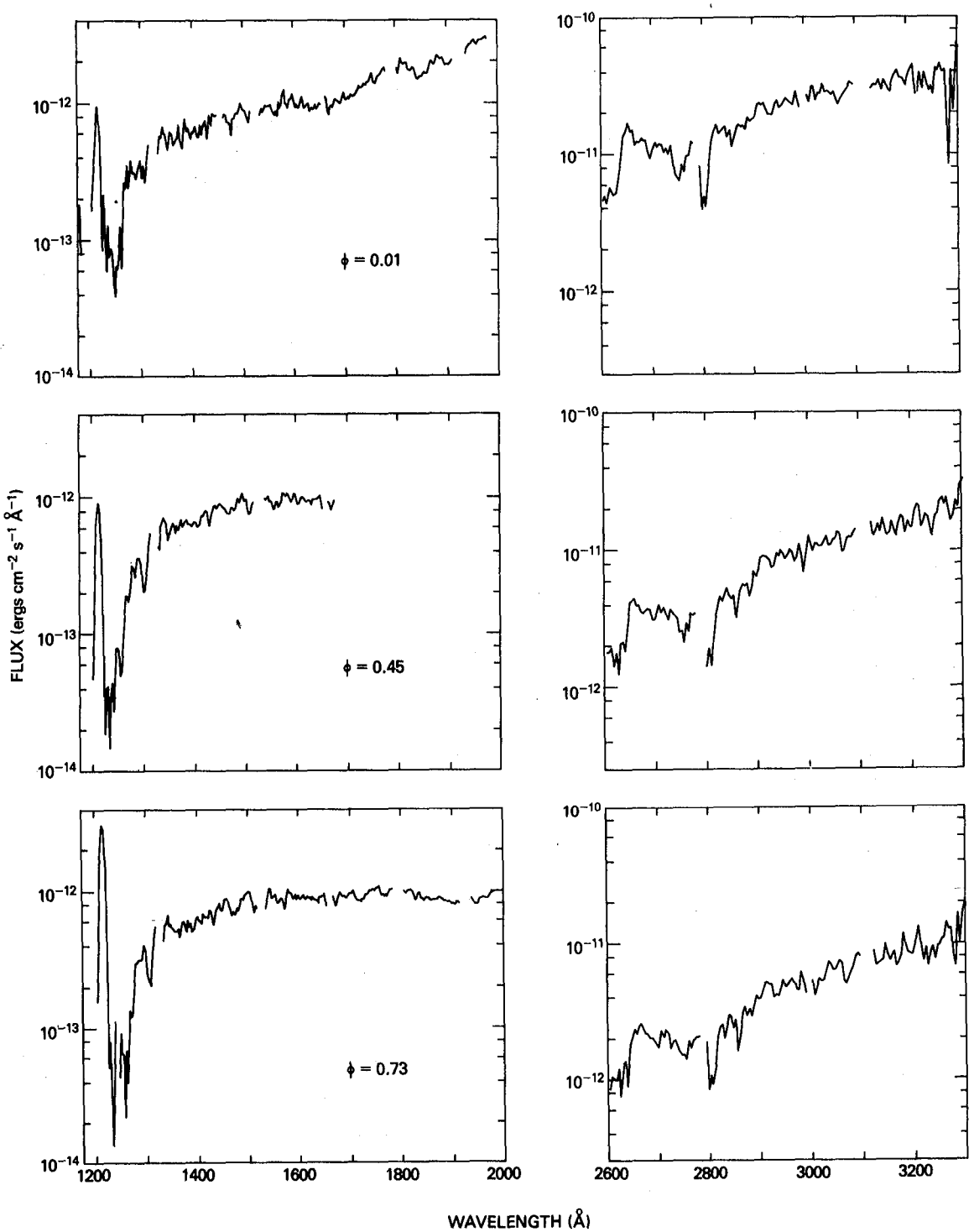

Figure 1. Low-dispersion short and long wavelength spectra in absolute flux units of η Aql at 3 phases in the 7.18 day period.

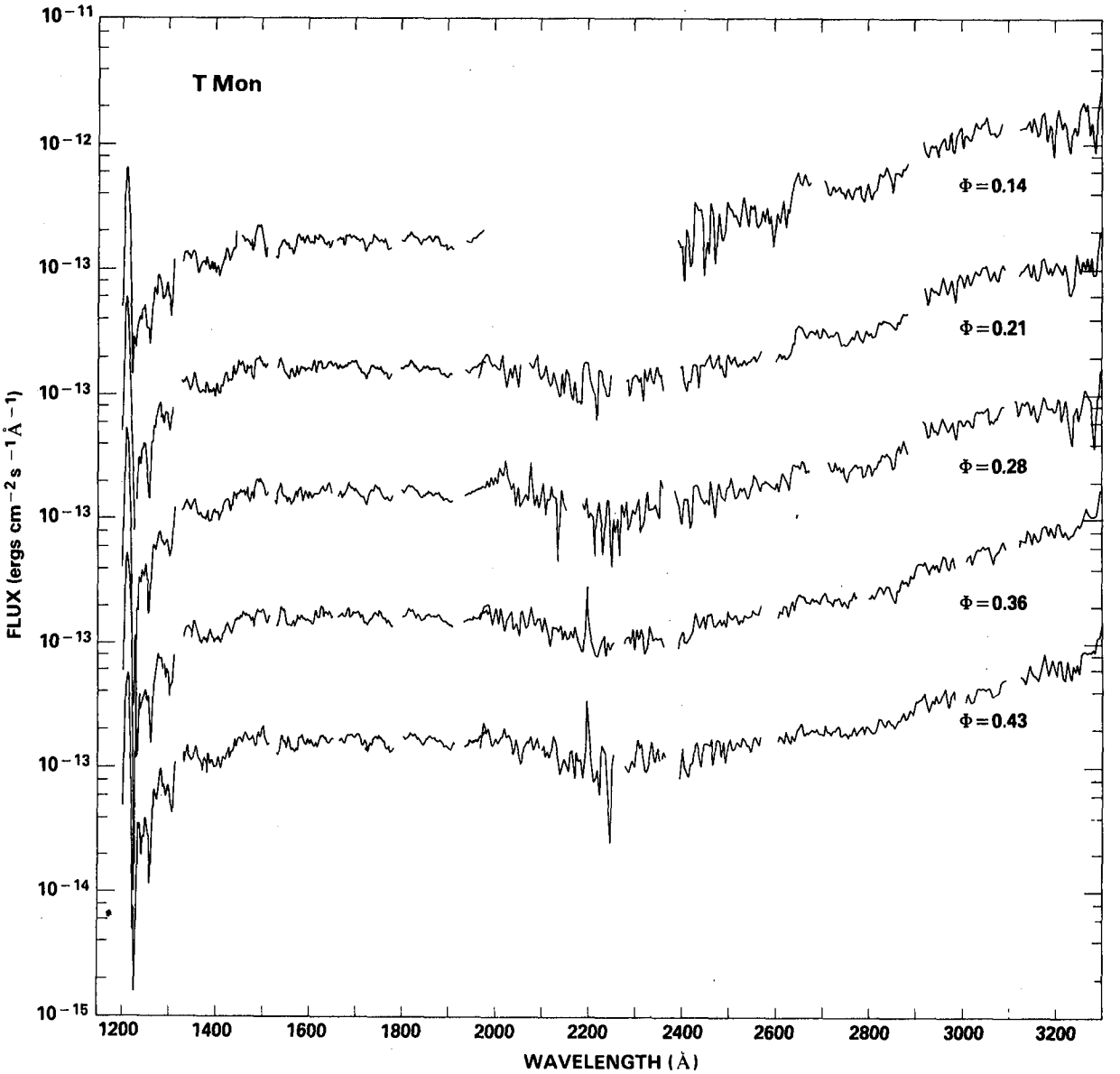

Figure 2. Low-dispersion short and long wavelength spectra of T Mon at 5 phases in the 27 day period. The ordinate for each spectrum has been displaced from the one above it by a factor of ten.

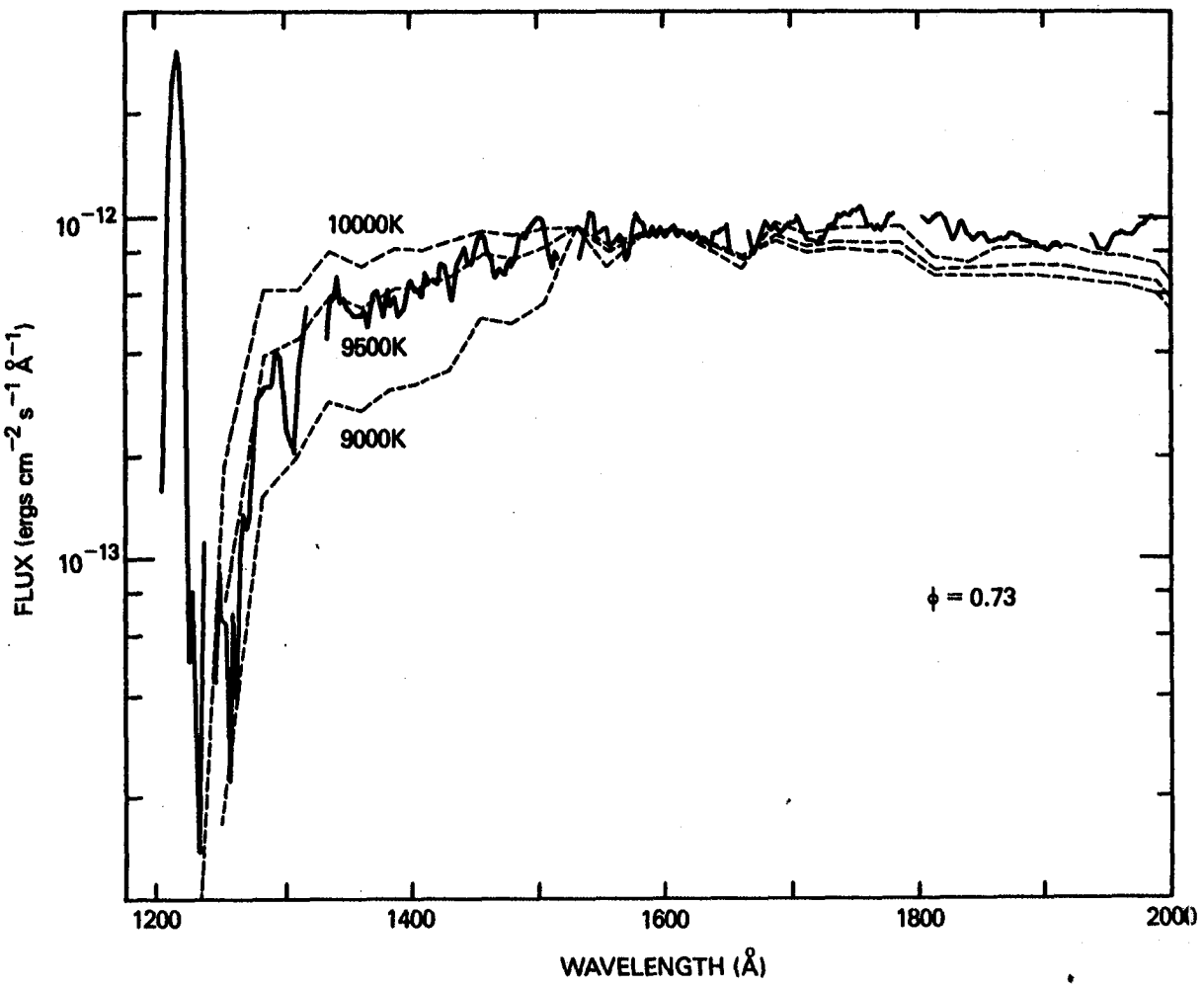

Figure 3. A comparison of the absolute flux distribution at the Earth for η Aql at phase 0.73 with reddened flux distributions from model atmospheres by Kurucz. The models have been adjusted to fit the data at 1600 Å.

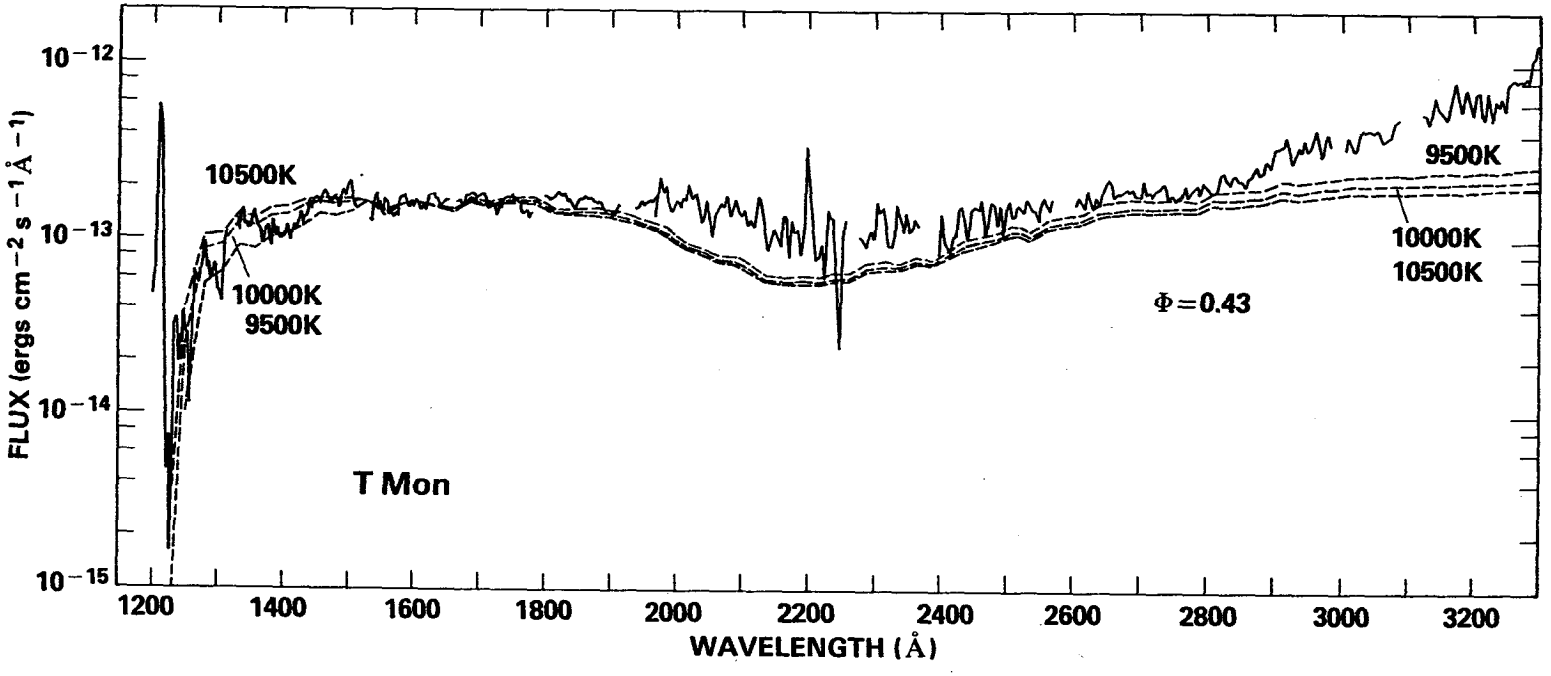

Figure 4. A comparison of the absolute flux distribution at the Earth for T Mon at phase 0.43 with reddened flux distributions from model atmospheres by Kurucz. The models have been adjusted to fit the data at 1600 Å.

LINE STRENGTH VARIATIONS IN β CEPHEI

David Fischel and Warren M. Sparks

Goddard Space Flight Center

ABSTRACT

The line strength variations of the resonance line of C IV (1550Å, 2s ^{2}S - ^{2}P) observed by OAO-II have been confirmed by IUE observations. In addition, the NV resonance line (1204Å, 2s ^{2}S - ^{2}P), the Si III line (1206Å, 3p ^{1}P - ^{1}D, multiplet 11) and the Si IV resonance line (1395Å, 3s ^{2}S - ^{2}P) all vary in line strength essentially in phase with the C IV variation. The (preliminary) period of the variation is 6.02/12.04 days.

INTRODUCTION

Observations of β Cephei taken by OAO-II in 1971 revealed a mysterious variation in the C IV doublet at 1550Å (ref. 1). The doublet appeared to disappear totally, but this was an effect of the coarse resolution of OAO-2, since each line clearly appears in all of the IUE observations. IUE observations were taken October 10, 1978 (day 285) and February 24 to March 10, 1979 (days 55-71). The variations detected by OAO-II have been confirmed and other strong lines have been observed to emulate the C IV variation.

OBSERVATIONS

The October 10, 1978 spectra were exposed for 20 seconds. Since the 1550Å region is in a valley of low spectral sensitivity, the February - March exposures were incrementally increased to 50 seconds, and then decreased to 20 seconds. In this manner, the observations around February 26, 1979 provide the most reliable equivalent widths of C IV and, yet, the spectra could be searched for variations in other lines.

One scan on October 10, 1978 was lost due to confusion of the star tracker by the apparent visual companion located at 250°, 13.5 arsec distant with $\Delta m = 4.7$ mag. (references 2 and 3). Subsequent observations used an offset in the star tracker reference point to compensate for the apparent companion when it was in the field-of-view.

DATA REDUCTION

The data has been photometrically corrected with the new intensity transfer function. The relative net flux for order 89 (which contains 1550Å) was obtained by estimating the background flux at the edge of the order, subtracting it from the gross spectrum and applying the $(1+ax^2)\ \mathrm{sinc}^2 x$ correction with a = Ø.Ø1. When each line of the doublet appeared clearly singular, each line's equivalent width was measured separately and added together. Since the lines blend together as their strength increases, such cases necessitated measuring a single equivalent width covering both lines.

Table I lists the IUE exposure number for the short wavelength prime camera (SWP), the observation midpoint time, and the total equivalent width. Figure 1 illustrates the variation of the C IV line strength over a 6.Ø2 day period. (Zero time has been arbitrarily selected as day zero of 1978). If the data were plotted for a 12.Ø4 day period, the crosses would appear between phases zero and Ø.5, and the circles would appear between phases Ø.5 and one. Visual inspection of the distribution of crosses and circles clearly shows the nearly perfect similarity. If this similarity did not exist, one would choose the 12.Ø4 day period as the more likely period.

Figure 2 illustrates the variation observed in the C IV doublet. At minimum strength (ϕ = Ø.94), the lines are clearly separable and their strengths are in the expected 2:1 ratio. As their strengths increase, the weaker (blue) component increases more rapidly than the red component, and extends its absorption further to the blue than the red component extends to the red. Furthermore, even at maximum strength (ϕ = Ø.41), the region between the lines is never completely absorbed.

It is not yet clear whether this strong variation of the blue component is enhanced by the presence of other absorption lines varying in strength or not. Additionally, at some phases (e.g. ϕ = Ø.23), the red wing of the blue component exhibits a very sharp rise. Figure 3 illustrates the same effects in the N V 1240Å doublet. This doublet does virtually disappear at minimum strength (ϕ = Ø.94). Both components first appear to the blue side of their rest wavelengths. At maximum strength (ϕ = Ø.41), both components are near their rest wavelengths, and then shift redward as the phase progresses. A similar effect occurs in

the C IV lines, but it is much less obvious. Since the N V is a well separated doublet there is no blending between the components, and the effects are more dramatic than in C IV.

The Si III singlet at 1204Å and the SI IV doublet at 1395Å also show the same periodic line strength variation. Weaker lines do not exhibit any strong 6.02 day variation.

CONCLUSIONS

The OAO-II observations have been confirmed by the IUE observations which provide much better data for theoretical analysis. The 6.02 or 12.04 day variation appears in the strongest lines of C IV, N V, Si III, and Si IV and unusual line profiles are observed. Whatever mechanism causes these variations, it is most effective in the outermost layers of the stellar atmosphere. The previously hypothesized tidal distortion by an unseen binary companion for either P = 12.04d, $\varepsilon = 0$ or P = 6.02, $\varepsilon = 1/2$ does not explain the wavelength shifting. If a tidal distortion occurred, one would see both bulges, one contributing to the blue and one to the red wing. Pending further analysis which awaits receipt of the remainder of the processed data from the IUE observatory, we conclude that the mechanism must be pulsational with a 6.02 day period.

REFERENCES

1. Fischel, D. and Sparks, W. M.: Ultraviolet Observations of β Canis Majoris and β Cephei in Scientific Results from the Orbiting Astronomical Observatory (OAO-2), NASA SP-310, 1971, pp 475-478.

2. Burnham, S. W.: A General Catalogue at Double Stars, part II, Carnegie Institution of Washington, 1908, pg 945.

3. Hoffleit, D.: Catalog of Bright Stars Yale University Observatory, 1964, pg 336.

TABLE I

SWP	Date GMT	W
2428	285:08:14:40	2.980
2929	285:08:49:50	3.290
2930	285:08:18:00	2.890
2931	285:09:45:36	3.059
2932	285:10:13:05	3.915
2933	285:10:40:10	3.451
2934	285:11:08:30	3.663
2935	285:11:36:08	3.626
2937	285:12:31:47	3.066
2938	285:13:00:12	3.292
4361	55:05:20:12	1.533
4362	55:05:48:35	1.315
4370	55:17:16:53	0.878
4384	56:23:07:32	0.951
4386	57:00:06:26	1.313
4387	57:00:35:02	1.802
4395	57:05:52:44	1.579
4405	58:04:22:35	2.631
4418	58:23:01:14	3.093
4452	61:02:56:22	1.636
4453	61:03:31:55	1.882
4458	62:02:32:44	1.678
4459	62:03:03:20	1.538
4460	62:03:33:05	1.479
4468	63:02:45:56	2.124
4481	63:20:46:40	2.570
4502	64:23:22:11	3.173
4511	65:22:36:10	2.505
4532	67:00:31:57	1.667
4533	67:01:57:30	1.542
4550	67:22:10:12	1.197
4551	67:22:38:28	1.387
4552	67:23:08:40	1.464
4554	68:01:57:02	0.879
4555	68:03:30:59	0.856
4576	69:20:20:25	2.055
4595	70:21:05:43	3.581
4596	70:22:00:44	3.439
4597	70:22:55:11	3.769
4598	70:23:49:55	3.382
4599	71:00:44:50	3.345

4600	71:01:34:06	3.392
4601	71:02:33:19	3.956
4602	71:03:27:30	3.913
4609	71:20:44:46	3.066

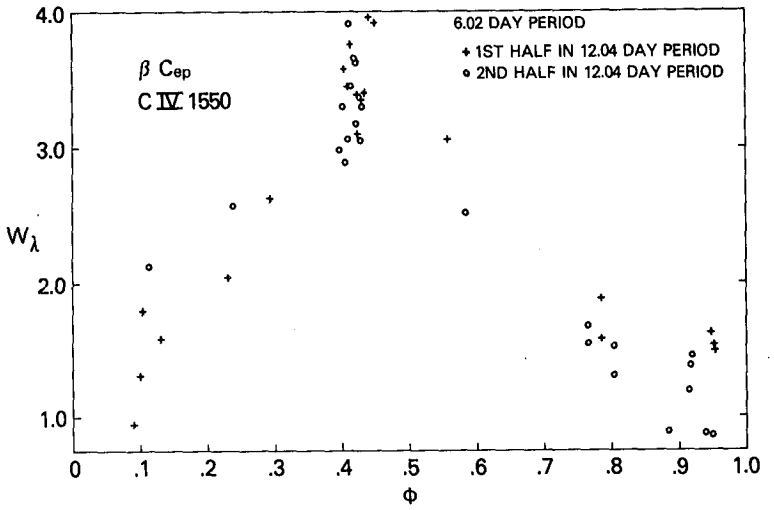

Figure 1

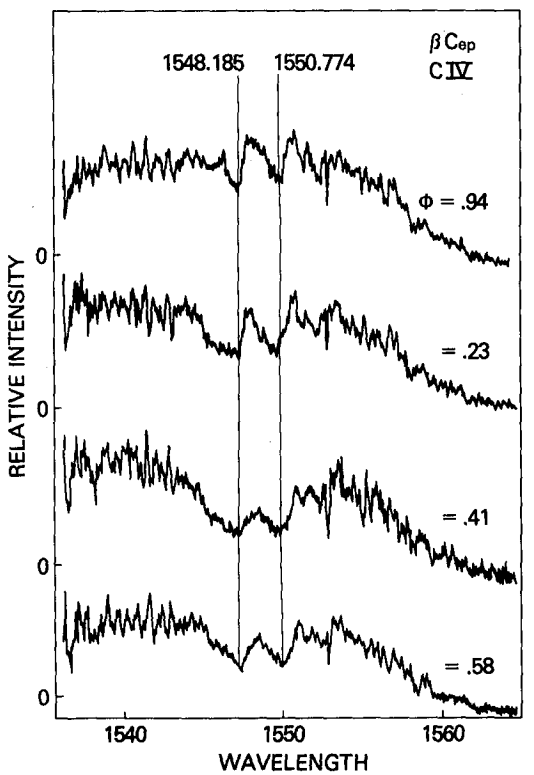

Figure 2

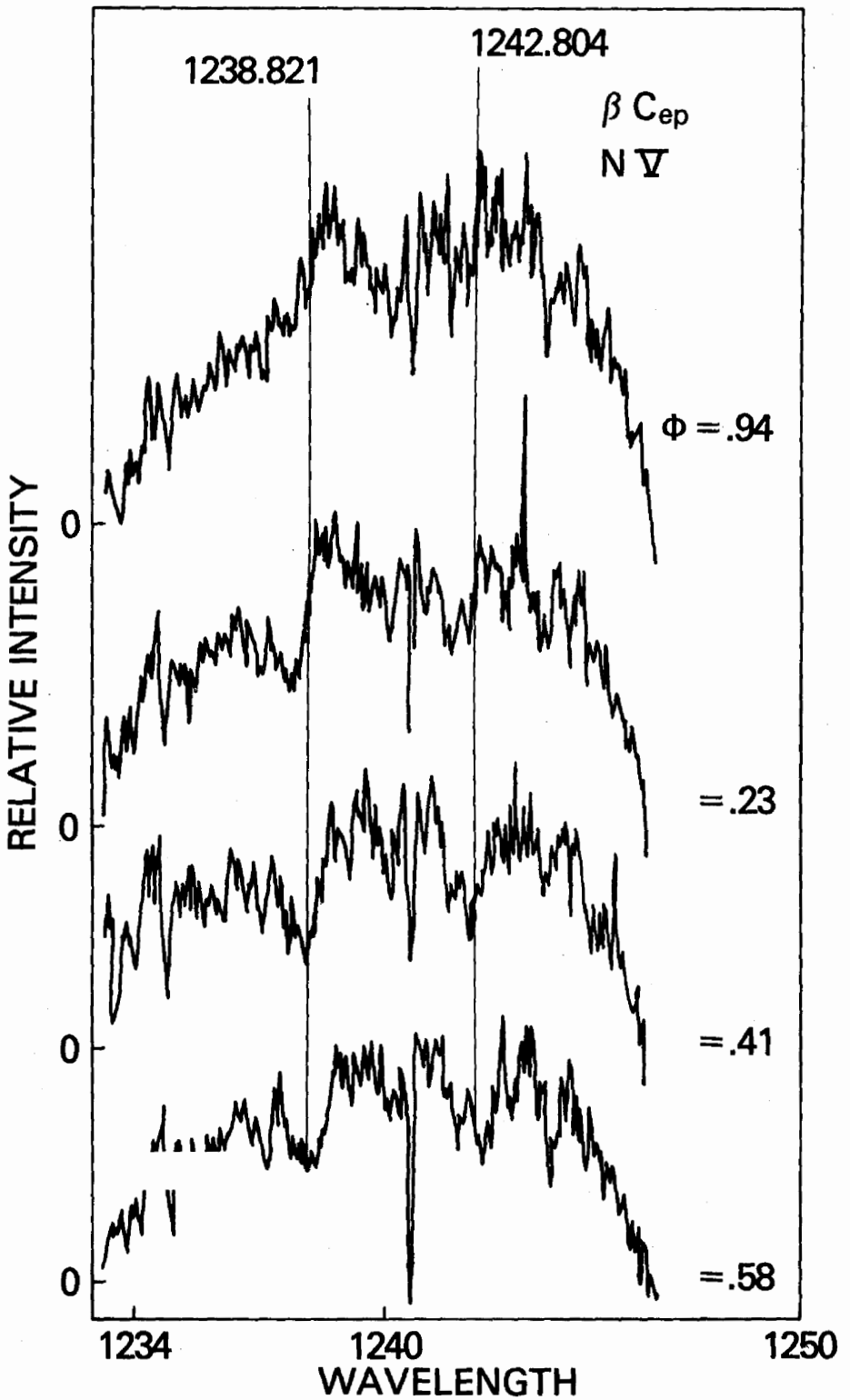
1238.821
1242.804
β Cep
N V
Φ = .94
= .23
= .41
= .58
RELATIVE INTENSITY
0
0
0
0
1234
1240
1250
WAVELENGTH

Figure 3

COMMENTS ON THE ORIGIN OF HEATING IN THE MANTLES OF EARLY-TYPE STARS

Anne B. Underhill
Laboratory for Astronomy and Solar Physics
Goddard Space Flight Center

ABSTRACT

It is shown that quiescent heating by magneto-dynamic effects can produce a range in injected non-radiative energy that is probably adequate to account for the range in physical properties that is observed for the mantles of early-type supergiants.

INTRODUCTION

The properties of B-type Ia supergiants are summarized in Table 1. The question arises of why there is such a large change in level of ionization and outflow velocity in the mantle (that is, in the outer atmosphere of the star where the effects of the deposition of non-radiative energy are apparent) when the change in effective temperature is by a factor of only 2.6.

Table 1.
Properties of the B Ia Supergiants

Property	09.5/B0	B3/B5	B9/A0
T_{eff}(K)	26000	14000	10000
Radius ($R_\odot$)	36	56	85
v_∞(km s^{-1})	1900	600	250
Diff. vel (km s^{-1})	$\leqslant$40	$\leqslant$25	$\leqslant$15
Wind profile seen	O VI, N V, C IV, Si IV	C IV ?, Si IV Al III, C II	Mg II, C II Si IV ?, Al III ?
Wind profile not seen	Al III, C II, Al II, Fe II, Mg II	O VI, N V, Al III, Fe II, Mg II	O VI, N V, C IV, Al II, Fe II
Typical stars	α Cam, 15 Sgr ϵ Ori, κ Ori	o^2 CMa η CMa	HD 21291 HD 21389

DISCUSSION

Important points concerning the heating of stellar mantles by quiescent magneto-dynamic processes have been summarized by Stencel and Ionson (1) and applied by them to late-type stars. Their formulas are equally valid for early-type stars. In the case of B supergiants, one can consider that all the Ia supergiants originate from about the same place on the ZAMS. Thus these stars probably have about the same initial magnetic field. Substitution into Stencel and Ionson's formulas of values for the stellar radius and for the density and temperature in the mantle appropriate for B supergiants shows that β is probably significantly less than unity and that the magnetic Reynolds number is large. Consequently, magnetic heating will dominate over possible heating from mechanical waves. Also it follows that the initial magnetic field will have dissipated by very little during the time taken by the star to evolve from the ZAMS to being a B Ia supergiant.

Let us assume that the magnetic field in the mantle at a point at radius R has the value and shape of a dipole field, and that the typical size of a coronal loop, R_L, is proportional to the radius of the photosphere. Then the rate of heating by quiescent magnetic processes per unit volume in the mantle, $Q_{quiescent}$, will vary as $\rho^{\frac{1}{2}} v^2 \vec{B}_{initial} R^{-4}$. Substitution of typical values for ρ(about the same for all B supergiants), v, the typical differential velocity in the mantle (probably turbulence due to rotation), and stellar radius shows that if $Q_{quiescent}$ is 1.0 for O9/B0 supergiants, it will be 0.067 for B3/B5 supergiants and 0.0045 for B9/A0 supergiants.

Consideration of these numbers and of observed details of B-type supergiant spectra as well as recognition of the fact that supergiants are formed initially with small magnetic fields suggests:

1. that the mantles of luminous early-type stars are inhomogeneous;
2. that the mantles are probably heated by magnetic energy, quiescent heating occurring in magnetic-loop structures which may be relatively small;
3. that outflow is started by magnetic events and accelerated by radiation pressure;
4. that impulsive magneto-dynamic heating may occur locally.

These four conclusions will account for the observed variability of the light and spectra from Ia supergiants as well as for the main characteristics of the ultraviolet spectra of B supergiants.

The full text of this paper has been submitted to the Astrophysical Journal Letters for publication.

REFERENCE

(1) Stencel, R. E. and Ionson, J. A. 1979, Pub. Astron. Soc. Pac., 91 451.

Hartmann: Several authors have shown that the radiation pressure force in the wind is unstable to perturbations, so that you may not need to invoke perturbations in the stellar core.

Also, I don't believe that the Castor, Abbott, and Klein force calculations extend to A stars. Therefore, law will depend on effective temperature. Thus, one cannot expect that the scaling $V_\infty/Vesc \approx 3$ necessarily holds for all stars, and so your contradiction of the low terminal velocities in A stars may not be correct.

Aller: Those of us who try to derive abundances from stellar spectra would like to have stars for which we can trust model atmosphere. Earlier work on LMC supergiants (for practical reasons) utilized the very brightest stars where atmospheres are unstable. Is there a limit on luminosity below which we can be pretty sure the stellar atmosphere models may be trusted? In our work on LMC supergiants Ross, O'Mara, Bruce Peterson, and I selected <u>less</u> luminous stars in hopes we would escape the difficulty.

Lamers: $M_{bol} = -6$ seems a good cut-off below which you should be safe, except for the very rapidly rotating stars.

Peimbert: What is known about mass loss rates from stars in the Magellanic Clouds? What are the predictions by the different mass loss mechanisms proposed?

Lamers: The mass loss rates of the Magellanic Cloud stars are not well known, but a first differential study by Hutchings, based on low resolution spectra, suggests that the wind velocities and the rates may be smaller than for Galactic stars.

If the wind is due to radiation pressure, one expects that the rates are smaller in the Magellanic Cloud stars, because the C, N, O abundances are smaller and the radiation pressure comes mainly from the CNO lines. If the mass loss is <u>driven</u> by some other mechanism but <u>accelerated</u> by radiation pressure, one expects about the same mass loss rates but smaller wind velocities.

Stencel: You indicated a correlation between mass loss rates and v sin i. Given the current scenario for cool stars requiring rotation to power dynamos to produce magnetic fields which influence the outer atmosphere (chromosphere and corona), and speculation that reconnection in coronal polar plumes is the site of the solar wind origin, do you think this dynamo mechanism could be important in hot stars?

Lamers: The connection between rotation and a dynamo mechanism for creating magnetic fields in hot stars is possible. However, the chromo-

spheric activity in late-type stars is correlated with rotation and convection for the generation of magnetic flux tubes. In hot stars the convection layer is either absent or very thin.

Darius: Perhaps I could comment that the ratio of terminal to escape velocity deviates from Abbott's relation not only for lower temperatures but for lower luminosities at the same high temperatures as the luminous OB stars. In particular, in the anomalous cases of mass loss found in two hot subdwarfs, the ratio runs therefore higher than the value expected from the radiatively driven model and confirmed by Abbott for more luminous mass-losers.

Imhoff: I would just like to comment that the density-sensitive ratio Si III/C III] is about 10 in RW aur, which falls outside the range you have in your diagram. I find the range in the ratio is higher than you've indicated.

Plavec: I notice that you made a comment that all the excess continuum can be explained in terms of hydrogen free-bound emission. I think that a considerable contribution must be due to hydrogen free-free emission, since the continuum and veiling are seen right across the Balmer jump all the way up to about 4,000 Å.

Gahm: The free-free emission is certainly a dominant feature at blue wavelengths. However, for the wavelengths looked at with the IUE, the free-bound emission dominates.

Hartmann: Can you comment on the presence or absence of HE II 1640 Å in T TAU Stars?

Imhoff: Some "weak-lined" stars show relatively weak 1640 Å emission. The strong-lined stars like RW AUR and RV LUP show no evidence for 1640 Å.

Gahm: Yes, in RV Lupi He II 868 Å is present in emission, but it is very weak.

Underhill: I wish to emphasize the point implicit in some of your illustrations that stars at the same point in the HR diagram (same T_{eff} and R), and therefore at same stage of evolution, of ten show different spectra from their mantles. A very striking case is for WN7 stars which fall exactly on the same spot as E Ari (BO Ia). The striking parts of their line spectra are very different, but their continuous spectra are very similar. This is because the continuous spectrum is formed in the photosphere which is similar in both stars, but the characteristic lines are formed in the mantles which are different.

Lamers: The ionization balance in the winds of early type stars can vary drastically from star to star. From a study of Copernicus spectra of 25 stars we found that the Si IV/N V ratio strongly decreases with increasing T_{eff} for T_{eff} >30000K, whereas the O VI/N V ratio is independent of T_{eff}, but depends on the density in the wind: O VI/N V

decreases as the density increases (Gathier, Lamers and Snow, 1980, Astron. Astrophys., in press).

Wallerstein: What do the WC stars show for mass loss?

Conti: The analysis of WC spectra is difficult and complicated; we have not yet completed our analysis.

Rumpl: Did I understand you to say that some of the mass loss rates were derived on the basis of one line?

Conti: In most cases two lines, e.g., O IV and C IV were used, but there were a few where the mass loss rates were based on one line, e.g., N IV in WN stars. However, as noted earlier, the derived ionization structure was similar for most of the stars.

Hartmann: How do the mass loss rates derived from radio techniques compare with your rates?

Conti: Generally they agree within a factor of two or three. One star, 9 SGR, is discrepant by a factor of 40. There may be some source confusion in the radio measurement, but otherwise there is no real problem in understanding this.

Conti: Would you please comment on the variability reports for α CAM?

Grady: Large scale line profile variability was reported for αCAM in the first IUE conference, in April of 1979. At this time we were working with old ITF data and the net, ripple-corrected, extracted spectra, provided by GSFC and VILSPA. We have since discovered that the background extraction procedure is faulty and in fact, that the large scale line profile variability in αCAM was totally spurious and due to changes in the background extraction. We have yet to check for changes in terminal velocity measurements.

Lamers: The additional components that you see in θAra may not be exceptional for early type supergiants. In a study of the Copernicus spectra of 25 stars, we found that in almost all stars there are narrow components ($\Delta v \simeq 200$ km s) superimposed on the P Cygni profiles. These occur typically at $V \simeq 0.70\ V_\infty$ (Lamers, Gathier and Snow, 1980, Astron. Astrophys., in press). Is it possible that the components that you see in Ara might be the same features, but only stronger?

Cassinelli: We have called the lines in θAra "transition region lines" because they appear at zero velocity displacement. Similar lines are seen in several of the Ib supergiants at around B5. Because of the lack of velocity shift, I think these are different from the features you have discussed.

Linsky: Have you noticed any correlation of x-ray luminosity and mass loss rates in O stars and early B supergiants?

Cassinelli: Mass loss rates in early B supergiants are poorly known. For the O-type stars there is no obvious simple correlation. But there is considerable attenuation of x-rays by the wind and L_α may be 10^{35} -10^{36} egs/sec before attenuation, compared to $L_x \approx 10^{32}$ egs/s observed. Thus, any intrinsic correlation can be easily masked by uncertain attenuations in different stars.

Aller: If you take the observed x-ray fluxes for these O stars, how well does the predicted $N(O^{+3})/N(O^{+5})$ agree with the observed values of this ratio? In other words, does the mechanism work well when you put in the numbers?

Cassinelli: Yes, for the O stars the Auger mechanism seems to suffice quantitatively. That is the x-rays flux that actually reaches the outermost layers of the wind where $\upsilon \simeq \upsilon_\infty$ (and is subject to no further attenuation on travelling to earth) is sufficient to convert enough O^{+3} to O^{+5} to explain the observed profile.

Hartmann: Are you concerned that you are really observing the terminal velocity in the cooler stars when the lines are weak?

Cassinelli: There may be some problem. However, it doesn't surprise me that the velocities decrease with decreasing effective temperature even in the context of radiatively driven wind theory.

Lamers: Is your efficiency for transferring momentum from the radiation to the wind large enough to explain the acceleration of the very thick winds of Wolf-Rayet stars?

Macchetto: In the case of the Wolf-Rayet stars, the larger rates of mass-loss increases the efficiency of transfer of momentum from the radiation field to the wind through three effects: a) as the opacity of each line increases, the number of scatterings per photon is also increased, b) the number of lines which become available are also increased, and c) the spectral interval from which photons become available to be scattered is increased towards longer wavelengths and therefore the increase in the total flux is considerable.

Underhill: You speak of sufficient flux in the range 200 to 500 Å for driving the wind of stars like ζ^1 Sco. How do you know that sufficient flux is available? I doubt it unless your stars are of types near O5.

Macchetto: The single scattering mechanism is capable of accelerating winds up to velocities of between 500-1000 km/s. This mechanism can account for the wind acceleration of all B type stars ($T_{eff} \leq 20000°K$). Therfore the expressed low flux shortwaved of 500 Å does not present any problem. For hotter stars, the multiple scattering mechanism becomes increasingly important, and can easily accelerate the winds to velocities as large as 3000-4000 km/s.

Linsky: Since the infrared excesses imply a large amount of material at 22,000K, have you computed L_α and C II emission fluxes and, in the case of L_α, whether they are observable through the interstellar medium?

Underhill: All the B supergiants do indeed show C II 1335Å emission in the low and high dispersion IUE data. L_α emission is not seen presumably due to interstellar absorption. I have not computed any fluxes.

Lamers: The mass loss rates for A-type supergiants derived by Barlow and Cohen from infrared excess are about a factor 30 larger than those derived from the UV spectra (Lamers, et al., 1978, Ap. J. 223, 207; Praderie et al., 1980, Atron. Astrophys., in press). Can you comment on these large rates derived from the IR-excess?

Underhill: I consider Barlow and Cohen's calculations to be based on an inappropriate theory and to be of no relevance for the late B supergiants.

Holm: Systematic errors are known to exist in the low dispersion which produce discrepancies between the SWP and the LWR spectra of the order of 70%. Moreover, longward of 3200 Å the reproducibility of the spectra is lower than over most of the wavelength range of the instrument. Dr. R. Bohlin and I are attempting to derive an improved calibration to be published in the next IUE newsletter.

Underhill: I have not used IUE low-dispersion spectra longward of 3200 Å. The fluxes which I do find in the range 1200 to 3200 Å agree reasonably well with the available ANS and S2/68 faint star photometry.

Plavec: When you go, in the LWR camera, from 2,000 Å longwards, at which wavelength do you first encounter the Balmer emission?

Underhill: Balmer continuum emission becomes significant from about 2100 Å longward.

Plavec: I noticed on my LWR spectra, even those of standard main-sequence stars, that I get increased flux--something like a mild "Balmer emission," which I suspect must be due to incorrect calibration, i.e., it must be spurious.

Underhill: A. V. Holm tells me that the intensity calibration of the LWR camera is uncertain longward of 3200 Å: it may contain small errors in the range 3000 to 3200 Å.

Underhill: I am doubtful of some of the identifications you have made. In many late B stars and in Si stars there is a broad strong absorption feature near 1485 Å which can plausibly be identified as a Si II line whose upper level can autoionize.

Rakos: I cannot exclude this possibility but Si II lines are of moderate strength.

Lien: Have there been any non-periodic flare events, given the limitations of the SWP camera?

Fahey: Not in the region studied, but there is some evidence in some of the material which has not been analyzed on detail.

Underhill: Did you see any "wind profiles" in the ultraviolet spectrum of a Centauri?

Fahey: Yes, there was evidence of emission on many spectra (especially LWR) and often the HE I lines around 2945 Å showed a P Cygni profile.

Stencel: 1) The Mg II profile is amazing. A sample of 50 late-type stars indicates general agreement with the Wilson-Bappu/ Weiler-Oegerle correlations of line width to absolute magnitude, to $\pm 0^m.7$. But, forcing RW Aur on this correlation leads to $M_v \sim -12^m$. I gather Kuhi already noted this for the CA II H+K lines. Basri (1980 U of Colo. Dissertation) has found the lowest gravity cool stars may have transfer effects which excessively broaden the Mg II emission core. 2) The Mg II profile appears to represent outflow. 3. Rutten, Cram & Lites have modeled Fe II emission in the solar spectrum and find that it can be pumped by UV photons from the lower photosphere. By analogy, Fe II emission in T Tauris could arise from a hot, sub-envelope source. Changes from absorption to emission due to density variations.

Savage: Have you considered the effect of interstellar line absorption on the emission line fluxes? It is quite common for interstellar absorption by species like C II λ1335 or Si II λ1260 to be total over velocity widths of about 50 to 60 km s^{-1}.

Imhoff: We have no estimates at present.

Plavec: Emission spectra of binary stars of the W Serpentis type also show striking differences in line intensities compared to typical chromospheres. Then the stars show mass outflow but the kinetic and ionization energies for the emission lines probably ultimately comes from accretion. I noticed that in your SWP spectra a sudden rise of the continuum flux for λ>1750 A. I have observed the same phenomenon, and eclipse observations of β Lyrae suggest that it is due to an accumulation of Fe III emission lines. Do your T Tauri observations suggest that the material flows in or out?

Imhoff: There is no indication either way in the ultraviolet observations, aside from interpretations of the high resolution Mg II lines. Other data suggests mass loss but the observations are not simply interpreted.

Gahm: Did the ratio of Si III to C III line intensities change with time?

Imhoff: The ratio is roughly C III]/Si III=0.1 in both observations but the quality of the data doesn't allow us to see variability of under a factor of 2.

Gahm: You mentioned that the absolute flux of versions mission lines increased with increasing brightness of the star. Were there also changes in the equivalent width of the lines?

Imhoff: We have not yet determined the fluxes for the weak continuum seen at short wavelengths, so we have no equivalent width estimates.

Gahm: Comment on the question of infall or outflow. In the case of RW Aur the absorption lines RW are seen on the Balmer continuum from 3300 to 3750 Å are violetshifted on all spectrograms I've looked at.

Imhoff: RW Aur is probably one of the clearer cases of mass loss, but the situation for T Tauri stars in general is not clear.

Böhm-Vitense: Would it be possible that the apparently weak emission in the h_3 absorption in Mg II could actually be left over between two absorption components, the longward component being due to interstellar absorption and the shortward component being the intrinsic circumstellar line?

Imhoff: Yes, in fact J. Linsky suggested also when I first showed him the line profile that the "emission" would be leftover between two absorption components.

de Boer: I would like to comment that the interstellar lines you detected are of negative radial velocity, in the same sense as galactic rotation would produce. Your star is at $l \approx 60°$ and $b \approx 50°$, equal to but of opposite sign as, the direction of the Small Magellanic Cloud. The absorption pattern has very similar radial velocities, but with opposite sign, as detected toward the SMC (Savage and de Boer, this symposium and submitted to Ap.J.). You cannot exclude that C IV is interstellar in deed, at large 2, due to a gaseous galactic halo.

Stalio: No, in fact, I cannot. If C IV is intersteleon, it is unfortunate that it has the same radial velocity as the star. On the other side one must take into account that there are two rather well-separated groups of interstellar lines at velocities different from the star velocity.

III. F–M STARS

AN IUE'S EYE VIEW OF COOL-STAR OUTER ATMOSPHERES

Tom Ayres†
Joint Institute for Laboratory Astrophysics
University of Colorado and National Bureau of Standards

I. INTRODUCTION

One of nature's curiosities is that cool stars have hot outer atmospheres. In fact, some cool stars have hotter plasma in their coronal exteriors than in their fusion-powered interiors.

The study of exotic atmospheric phenomena in stars was limited until recently to our own Sun. The Sun is a fairly mundane sort of star, as stars go, although the solar surface confronts us with a myriad of constantly changing fine structure that tax the theorist's ingenuity to explain.

The Sun has taught us that the chromosphere and corona are powered by the deposition of mechanical energy. The remarkable temperature inversions in the solar outer atmosphere arising from the dissipation of comparatively small amounts of heat are likely the result of thermal instabilities driven by the inefficiency of the plasma radiative cooling at low densities. The nature of the heating mechanism remains elusive, however, although magnetic fields are thought to play a central role.

Somewhat more than two years ago, the study of cool-star chromospheres and coronae gained a measure of respectability with the advent of the International Ultraviolet Explorer. For the first time, large numbers of cool stars could be observed in the ultraviolet with enough sensitivity to detect the faint emission features formed in the chromosphere ($T \cong 6 \times 10^3$ K) and hotter layers ($T \lesssim 2 \times 10^5$ K) of the outer atmosphere. A year and a half ago, the Einstein soft X-ray telescope was orbited, and almost immediately began detecting coronal emission from ordinary late-type stars. Together, these complementary instruments have provided a remarkable picture of the occurrence of chromospheres and coronae in the HR diagram that is very different from that anticipated by stellar theorists (Vaiana 1980; Linsky 1980).

A few months ago, the Solar Maximum Mission was launched to study solar chromospheric activity at the height of the sunspot cycle.

The detailed morphological and dynamical study of solar active regions by SMM very likely will be a key to understanding many aspects of stellar activity that are seen so vividly with IUE and Einstein. Nevertheless,

†This work is supported in part by NASA under grants NAS5-23274 and NGL-06-003-057 to the University of Colorado.

there is much we cannot learn if we study the Sun in isolation. In particular, the Sun confronts us with an unchanging set of fundamental stellar parameters; surface gravity, effective temperature, chemical composition, age, rotation rate, and so forth. Variations in the gross structure of chromospheres and coronae in stars with very different fundamental properties can, in principle, provide important clues to the nature of outer atmospheric phenomena that studies of the Sun cannot. For example, we might suspect that stellar magnetic fields are the driving force behind the physical structuring and plasma heating in stellar coronae, if the Skylab S-054 soft X-ray images of the solar corona are a useful guide (Vaiana and Rosner 1978), but the origin of the Sun's magnetic field is only poorly understood, and will likely not be explained in the basis of solar observations alone, no matter how detailed.

We must therefore temper the morphological and dynamical picture that solar physicists will provide of our nearby G2 V star with gross surveys of chromosphere-corona properties in a wide range of cool stars, in addition to more comprehensive studies of particularly interesting objects. (I am told that Otto Struve once commented that at least one in five stars is remarkable [e.g. Stencel et al., these proceedings], so there should be no lack of suitable candidates for the latter studies!)

It is in the spirit of the solar-stellar connection, and the supplementing of gross survey results with detailed studies of individual stars, that I present my review.

Because of space limitations I cannot begin to cover all of the IUE studies of cool stars that have been undertaken by the many groups and individuals who are active in this field. (To those authors whose work I do not mention, my apologies.)

Instead, I will focus on three separate topics that together demonstrate the power of IUE for probing the occurrence of chromospheres and coronae in the cool half of the HR diagram, and perhaps also shed some light on the reasons why stellar outer atmospheres behave in the peculiar ways they do.

I summarize the three topics as follows:

First, I will describe how the IUE is used in practice to deduce the physical properties of stellar outer atmospheres. I will discuss the sorts of information that one can extract from low-dispersion and echelle-mode spectra with the SWP and LWR cameras. I will illustrate the discussion with spectra of two bright binary systems, α Centauri (G2 V + K1 V) and Capella (G6 III + F9 III). In fact, the comparison of these two systems with the Sun has revealed unexpected clues to the nature of the chromosphere-corona phenomena. (Harking back to Otto Struve's comment, there should be at least one remarkable star in that group of five, and there is!)

Second, I will describe the several IUE surveys of stellar Mg II emission that are now available. The Mg II h and k resonance lines are important radiative cooling agents in stellar chromospheres, and have provided the first empirical confrontation with a proposed chromospheric heating

mechanism, namely acoustic waves. In addition, the correlations of Mg II emission core shape parameters with stellar luminosity -- the Wilson-Bappu relation for the FWHM for example -- provide useful clues to systematic trends of chromospheric structure with changing stellar properties, especially surface gravity. I will discuss what the stars that obey the Wilson-Bappu effect seem to be telling us about chromospheric conditions, and equally important, how the stars that don't obey the Wilson-Bappu relation fit into the overall picture.

Last, I will summarize some of the recent low-dispersion surveys of cool-star emission in the 1150 Å-2000 Å short wavelength region. Several of the strong emission features found in that region -- C II 1335 Å and C IV 1550 Å for example -- are formed in the thin, 10^5 K transition region (TR) interface between the multi-million degree corona and the 6000 K chromosphere. I will describe the evidence that the cool half of the HR diagram is divided into zones where the TR emission is prominent, and zones where the hot lines tend to be very weak or below detection thresholds. I will present preliminary correlation diagrams comparing the chromospheric emission in the Mg II doublet with the hotter lines of the SWP region, and demonstrate that stars with weak transition regions have weak chromospheres as well. Finally I will speculate on the nature of the chromospheric heating mechanism that is suggested by the Mg II correlations,and review an evolutionary scenario to explain the weakening of cool-star outer atmospheres in the red giant branch.

II. ULTRAVIOLET SPECTROSCOPY WITH IUE

IUE offers the stellar spectroscopist two complementary observing modes: (1) low dispersion, for which no information concerning detailed line profiles or velocities is available, but the resolution is adequate to separate important emission features from each other and from background continua; and (2) the echelle mode, which can provide detailed line profiles with a resolution of somewhat better than 30 km s^{-1}, and individual line positions to within several km s^{-1}. The echelle mode does sacrifice sensitivity for increased resolving power, consequently only a few bright cool stars are accessible, even with long exposures (at short wavelengths). Nevertheless, comparatively faint stars are observed routinely in the Lα region with the low dispersion mode (and at the 2800 Å Mg II resonance lines with the LWR echelle mode).

A. LOW DISPERSION MODE, SHORT WAVELENGTH REGION

Figure 1 compares IUE short wavelength spectra of the nearby solar-type dwarfs of α Centauri (G2 V + K1 V) with an irradiance spectrum of the Sun that has been degraded to the 6 Å FWHM resolution of the low dispersion mode. The solar data were obtained during a moderately active portion of the sunspot cycle (Mount, Rottman and Timothy 1980).

The spectra illustrated in Figure 1, and in several of the subsequent figures, are normalized fluxes. That is, the absolute monochromatic fluxes measured at the Earth have been divided by the stellar bolometric luminosity,

also as measured at the Earth. (The resulting monochromatic units are $Å^{-1}$.) Normalized fluxes are a fair way to compare the chromospheric emission of stars having very different surface areas (dwarfs and giants, for example), and essentially represent the fraction of the stellar irradiance budget that is provided by the particular emission spectra. Normalized fluxes are independent of often uncertain stellar distances, although they are sensitive to bolometric corrections, which can be quite large for K and M stars.

One sees in Figure 1 that the two α Centauri dwarfs are very similar to each other and to the Sun in their ultraviolet emission properties. Both α Cen A and B exhibit all of the important transition region and chromospheric lines seen in the solar short wavelength spectrum (O I 1305 Å, C II 1334 Å, Si IV 1400 Å, C IV 1550 Å, Si II 1815 Å). In fact, the normalized line strengths of α Cen A and B are quantitatively similar to the solar values (Ayres and Linsky 1980a).

The presence of TR emission in both α Centauri dwarfs is proxy evidence that these solar-type stars possess multi-million degree coronae analogous to that of the Sun. In fact, both components of α Centauri have been resolved recently as coronal soft X-ray sources by the High Resolution Imager on Einstein (Golub et al. 1980).

Figure 2 depicts the ultraviolet emission spectrum of another binary system, Capella (α Aurigae A; G6 III + F9 III). Capella has a much shorter orbital period than α Centauri (0.3^y versus 80^y), and the two giants are too close to each other to be separately observed by IUE or Einstein. Consequently, only the composite emission spectrum is obtainable.

While Capella exhibits essentially the same emission features that are prominent in the solar spectrum, the normalized line strengths, particularly of the 10^5 K transition region features, are considerably larger, and several of the line ratios, O I 1305 Å/C II 1335 Å and C I 1660 Å/C IV 1550 Å for example, are quite different. Like the α Centauri system, Capella has been detected as a prominent coronal soft X-ray source by HEAO-1 and Einstein (Cash et al. 1978, Holt et al. 1979).

Given SWP spectra such as those illustrated in Figures 1 and 2, one can determine straightforwardly integrated line strengths, line ratios, and continuum intensity distributions.

Emission line strengths indicate the amount of material present over the temperature range where the particular atom or ion is most abundant. In addition, many of the prominent high temperature emission features accessible to IUE in the Lα region, namely the Si IV, C IV and N V doublets, are important radiative coolants between about 6×10^4 and 2×10^5 K. Consequently, the strengths of these features are an indirect probe of the plasma energy budget in the transition region.

Like the emission line strengths, line ratios play an important role in diagnosing the physical conditions in stellar outer atmospheres. The most common application of line ratios is to estimate transition region densities (Doschek et al. 1978b). In principle, intensity ratios of spectral features

that are formed under similar plasma thermal conditions, but which have different sensitivity to local density — "permitted" and "forbidden" transitions, for example — can be used to deduce the spatially averaged pressures in the atmospheric structures responsible for the ultraviolet emission. However, many obstacles remain in the practical application of density sensitive line ratios (Raymond and Dupree 1978; Baliunas and Butler 1980), particularly because most of the numerical simulations of the response of line ratios to density have been specialized to solar transition region structures (Doschek et al. 1978a). Nevertheless, the density diagnostic line ratio techniques offer essentially the only way to estimate transition region pressures in other stars that is comparatively free of geometrical considerations (the situation of a patchy TR brightness distribution, for example).

The question of transition region pressures is an important one, because it bears directly on the nature of the heating mechanism. The classical (preSkylab) picture of the solar transition region was of a geometrically thin interface between the hot corona and cool chromosphere that supported a large conductive heat flux driven by the steep temperature gradient (Withbroe 1977). The heat conducted from the corona downward into the cooler and denser chromospheric layers was an important energy loss channel that, in concert with high temperature radiative emission, served to stabilize the coronal plasma thermally. When the conductive flux through the transition region is dissipated entirely by radiative cooling, the gas pressure in the TR is proportional to the conductive flux itself (for a plane parallel nondivergent geometry, see e.g., Rosner, Tucker and Vaiana 1978).

Since the conductive flux is proportional to the temperature gradient, and since the emission strength of an optically thin resonance line of an abundant ion in the TR is roughly proportional to the square of the gas pressure divided by the local temperature gradient, then the TR emission should be directly proportional to the gas pressure (e.g., Haisch and Linsky 1976). Consequently, if stellar TRs obey the conductive heating hypothesis, then the stellar TR pressures should scale directly from solar values as the ratio of the stellar and solar surface fluxes of permitted TR lines (Haisch and Linsky 1976). Alternatively, if stellar transition regions are heated by a nonconductive process — magnetic reconnection in situ, for example — then the same surface flux could be provided at considerably lower pressures simply by a flatter temperature gradient In fact, empirical studies of the temperature gradient at the 10^5 K level of the solar TR, by means of emission measure analyses, have revealed that the likely conductive flux in those and deeper layers is insufficient to balance the measured radiative losses, consequently an additional heating agent seems to be required (Withbroe 1977). Furthermore, Noyes (1974) has proposed a semiempirical TR model to explain the intense emission in 10^5 K lines observed in sunspot plumes (Foukal et al. 1974), that is characterized by a much flatter temperature gradient than is predicted by the conductive heating model. It is therefore premature to suppose that all stellar transition regions are a product of conductive heating (e.g., Baliunas et al. 1979), until reliable, independent pressure estimates are available to test that contention in a wide variety of late-type stars.

A third useful aspects of the IUE low dispersion spectra of cool stars is the continuum emission distribution longward of 1500 Å. Radiation in

that spectral region is produced in the stellar outer photosphere, and is a sensitive diagnostic for the stellar effective temperature. For example, the substantial drop in normalized continuum emission levels near 1800 Å between α Cen A and α Cen B is the result of only a 500 K difference in effective temperature. On the other hand, the close similarity in the normalized continuum emission strengths of α Cen A and the Sun indicates that the two G dwarfs have very nearly the same effective temperature. [In several respects, α Cen A and the Sun are twins of each other (Flannery and Ayres 1978).] Finally, the continuum emission levels in the composite low dispersion spectrum of Capella are significantly larger than solar. The ultraviolet continuum enhancement implies that the hotter secondary, which dominates the short wavelength emission of the system, is very likely a late F giant.

In addition to its usefulness as a temperature diagnostic, the short wavelength continuum emission can signal the presence of previously unrecognized stellar companions. For example, Mariska, Doschek and Feldman (1980) have discovered a hot-star companion to the classical cepheid η Aquilae on the basis of an anomalously bright emission signature in the region shortward of 1600 Å that did not vary with the cepheid pulsation period.

B. ECHELLE MODE, LONG WAVELENGTH REGION

Useful as the low dispersion mode is, the stellar spectroscopist should feel somewhat uncomfortable that it does not provide many of the basic pieces of information that are central to atmospheric structure analyses. Principal among these are line shapes and velocities. Fortunately, the IUE echelle modes can provide such information for a wide range of cool stars longward of 2500 Å, and for the few brightest shortward of 2000 Å.

i) Line Shapes

Emission line profiles contain an enormous amount of information concerning plasma conditions in — and the geometry of — the line-forming region.

When a feature is optically thin, one can estimate the amplitude of nonthermal broadening velocities in the layers where the emission originates. For example, Athay and White (1978,1979) and Bruner (1978) have applied this technique to high-quality solar C IV profiles, obtained with the OSO-8 UV spectrometer, to set limits on the possible acoustic wave flux passing through the 10^5 K layers

When a line is optically thick and develops a centrally reversed emission core, one can estimate the optical path length required to produce the central reversal. The line optical depth and total emission can then be used to estimate the plasma density and geometry of the emitting structures. Lites, Hansen and Shine (1980) have applied such an approach to self-reversed C IV profiles observed in an active region near the solar limb by OSO-8.

Some emission features, the 2803 Å h and 2796 Å k resonance lines of Mg II for example, are very optically thick in stellar chromospheres. In

fact, the Mg II features are effectively thick (see Hummer and Stewart 1966) as well. Very optically thick lines that are effectively thick in the chromosphere, and which possess extensive Lorentzian damping wings (H I 1216 Å Lα and the H and K resonance lines of Ca II are other examples) are valuable thermal structure diagnostics (Ayres 1975; Basri et al. 1979). The outer edges of the emission features, beyond the narrow Doppler-dominated core, and the damping wings of these lines carry, in principle, a faithful mapping of the outer atmospheric thermal structure from the middle chromosphere down to the deep photosphere (in the case of Mg II and Ca II). For example, the k_1 profile minimum features are formed near the temperature minimum region at the photosphere-chromosphere interface, while the k_2 emission peaks are formed in the hotter layers of the middle chromosphere, where the Mg II cores first become effectively thick.

The left-hand panel of Figure 3 compares echelle-mode profiles of Mg II k from α Cen A and B. The ordinate is normalized flux, $f_\lambda/\ell bol$, in the same units as Figures 1 and 2.

First, note that the Mg II emission cores are overwhelmingly brighter than any of the chromospheric or transition region features of the short wavelength spectrum (even Lα). Since the Mg II features are important radiative coolants in the stellar chromosphere, one sees that the chromospheric energy budget must be considerably larger than that of the overlying transition region.

Second, note that the inner damping wings of the α Cen A k profile are brighter than the α Cen B k wings. This difference is a reflection of the 500 K photospheric temperature difference of the two dwarf stars, and is analogous to the behavior of the UV continuum emission seen in Figure 1. However, the contrast is amplified near 1800 Å compared with 2800 Å owing to the exponential character of the ultraviolet Planck function.

Despite the cooler photospheric emission, the α Cen B k core is brighter than that of α Cen A (in normalized flux). Consequently the α Cen B chromosphere likely occupies a larger fraction of the overall stellar energy budget than that of α Cen A. A similar difference is seen in the Lα region (Fig. 1), where the α Cen B TR emission features are somewhat brighter than those of α Cen A.

Finally, note that the k-line emission core of α Cen B is narrower at the top, and has a smaller FWHM, than that of α Cen A, although the emission features are more nearly the same width at their bases. The broadening of the k-line FWHM with increasing absolute visual luminosity (α Cen A is $1^m.3$ brighter than α Cen B in M_V) is a well-known correlation that was first recognized in the near ultraviolet Ca II H and K resonance lines by Wilson and Bappu (1957). The existence of such a simple correlation has provided chromospheric theorists with a tantalizing challenge, whose resolution remains controversial even after two decades of study. I will return to the Wilson-Bappu effect, and its bearing on chromospheric structure, later in the review.

ii) Profile Asymmetries and Velocities

Besides the fundamental emission core shape parameters, high resolution observations of the h and k features offer further possibilities for deducing chromospheric structure. For example, under certain circumstances, asymmetries in the emission cores can indicate gross material inflows or outflows (Stencel and Mullan 1980). Furthermore, absorption features superimposed on the intrinsic stellar emission profile can be used to probe the properties of circumstellar (Hartmann, Dupree and Raymond 1979; Stencel et al. 1980) and interstellar matter (Böhm-Vitense 1980a) along the line of sight. Finally, emission centroid velocities and gross asymmetries in the profiles can be used to isolate the component emission in certain moderate and short-period binary systems. Although the separation of the companion stars on the sky may be too small to allow the component spectra to be observed individually, often the projected orbital velocity amplitudes are sufficiently large to permit at least partial resolution of the component spectra by the Doppler effect. This technique is particularly useful in practice, because the closer the two companions are to one another, the faster the orbital motions, and the easier it is to separate the individual spectra (if the orbit is favorably inclined in the line of sight). Furthermore, there is a well-known correlation between orbital period and chromospheric activity levels in cool-type spectroscopic binaries, in the sense that the shortest period systems ($P < 10^d$ RS CVns, for example) tend to exhibit the brightest optical emission lines (Ca II and Hα; see e.g., Young and Koniges 1977), and the strongest coronal soft X-ray emission (Walter, Charles and Bowyer 1978). Nature has indeed been kind to provide a class of interesting close-binary systems that are possible to study with a small aperture instrument such as IUE.

The right-hand panels of Figure 3 illustrate some of these notions more quantitatively.

I have depicted profiles of the Capella Mg II k emission at two orbital phases when the primary and secondary have the maximum, and opposite, radial velocity separations. In both panels the radial velocity scale is relative to the system center-of-mass velocity, and the positions of the primary's and secondary's velocity zeros at each orbital phase are indicated by arrows. The substantial asymmetry in the K-line emission produced by the F-giant secondary is readily apparent. Note also that the Mg II emission envelope of the giant stars is considerably broader than that of the α Centauri dwarfs, as required by the Wilson-Bappu relation.

What appears to be k_3 central reversal in the G-star component of the composite emission profile (bottom, right-hand frame of Fig. 3) is very likely mostly interstellar Mg II absorption. In particular, the deep self reversal in the primary k emission core (Aa) is absent in the upper frame when the primary is to the red of the system center of mass, but an absorption feature is present at the same velocity (-10 km s^{-1} relative to the Capella COM) as the "k_3" feature in the bottom frame. The presence of a strong interstellar Mg II absorption feature is not unexpected, since a prominent interstellar D I Lα absorption is seen against the intrinsic stellar Lα emission (Dupree, Baliunas and Shipman 1977; Ayres and Linsky 1980b).

Nevertheless, the presence of such a strong absorption feature in the center of the k line of a nearby star ($d \cong 13$ pc) is somewhat disconcerting. In particular, the k_2 emission peak separation plays an important role in some theoretical interpretation of the Wilson-Bappu effect, and the red-violet k_2 emission asymmetry has been invoked as a spectral anemometer to measure stellar wind flows (e.g. Stencel and Mullan 1980). However, as Böhm-Vitense (1980a) has shown recently in a systematic survey of interstellar Mg II absorption, in stars more distant from the Sun than a few tens of parsecs, much of the k_3 self reversal and the k_2 peak asymmetry may be an artifact of the interstellar absorption component. In fact, the presence of a saturated interstellar absorption core displaced somewhat from the stellar radial velocity may explain why some supergiants, 56 Peg (KO Ibp) for example, exhibit opposite k_2 peak asymmetries in Mg II and Ca II (Stencel et al. 1980), despite the fact that the two sets of resonance lines are formed at essentially the same levels of the stellar chromosphere, and presumably under nearly similar conditions of temperature, density and macroscopic flow velocity (cf. Basri 1979). (Note, however, that purely circumstellar absorption can produce the same result [see Stencel et al., these proceedings].)

C. ECHELLE-MODE, SHORT WAVELENGTH REGION: THE CAPELLA DICHOTOMY

One has seen from the comparison of low-dispersion, short wavelength spectra that the Capella system is considerably more active than the solar-type stars of α Centauri or the Sun itself. One anticipates that echelle-mode studies of Capella in the short wavelength region might reveal clues to the particular properties of the chromospherically active giant system that sets it apart from the quiescent main sequence stars.

Figure 4 compares the stronger member of the C IV doublet, 1548 Å, and the weakest component of the Si II triplet, 1808 Å, in α Centauri A and Capella. The Capella profiles were taken at one of the orbital velocity crossings when the contributions from the G primary and F secondary are superimposed in velocity.

Note that the α Centauri A profiles are narrower than their Capella counterparts, in fact close to the echelle-mode resolution of $\cong 25$ km s^{-1}. The α Centauri profiles are also considerably fainter than the Capella emission features, as anticipated from the low dispersion spectra.

The enhanced width of C IV 1548 Å, in particular, is likely an artifact of an optically thick emitting region, in contrast to the solar TR which usually is regarded as optically thin in C IV (but see Lites et al. 1980). If the principal broadening mechanism is Doppler in character, either thermal or small-scale velocity fields, an optically thick emitting region can produce a profile that is a factor of $\alpha \cong (\ell n\ \tau_{\ell c})^{1/2}$ wider than the intrinsic Doppler width, where $\tau_{\ell c} >> 1$ is the line center optical thickness of the layer. The scale factor α is a very slowly varying function of $\tau_{\ell c}$, and could provide at least factor of 2 width enhancements for the strongest TR lines of Capella. However, the saturation phenomenon (also called "opacity broadening") is not a convincing explanation for the enhanced Si II 1808 Å width of Capella, since the Si II feature is already optically thick in the solar chromosphere (Tripp, Athay and Peterson 1978), and presumably also in

α Cen A. On the other hand, the Si II feature is likely not thick enough that the Lorentzian wings of the profile function can significantly influence the emission line shape (the wing effect is likely important for the Mg II h and k cores, however). Consequently, the enhanced Si II width in Capella must be explained either by an increase in the intrinsic chromospheric Doppler width, or by an extrinsic Doppler broadening mechanism such as macroscopic flow patterns or rotation.

In short, the significant differences between the gross emission line strengths of Capella and α Centauri A are continued in the details of the individual line shapes. The comparison of line shapes has not directly helped us understand the fundamental differences between the giant stars and the solar-type dwarfs. Nevertheless, the comparison has provided us with at least one potentially useful clue: the transition region of Capella is very likely optically much thicker than the solar TR. (This suggests in fact that the Capella TR is not heat-conduction dominated, since the optical thickness $\tau \sim P/[dT/dh]$ of the conductive equilibrium TR is independent of the TR pressure P, since $[dT/dh] \sim F_{cond} \sim P$, and τ therefore should be the same in Capella as in the Sun.)

An even more important — and unexpected — clue to the nature of the giant-dwarf emission dichotomy was revealed by short wavelength echelle-mode observations of Capella at different orbital phases.

Figure 5 compares several prominent emission features of the Capella short wavelength spectrum at two orbital phases. The profiles in the left-hand panel were taken at one of the orbital velocity crossings when the two stars have the same projected radial velocity, and their spectra are superimposed. The profiles in the right-hand panel were taken near one of the elongations when the F-type secondary is shifted to the red of the system center-of-mass velocity, and the G-type primary is shifted to the blue. The velocity separation is of order 50 km s^{-1}. The zero-points of the individual stellar velocity scales at the two orbital phases are indicated by arrows.

The emission profiles are arranged from bottom to top in a sequence of increasing temperature of formation. The bottom-most and top-most profiles are composites of two or more features that are formed at similar temperatures and have similar line shapes (Si IV 1394,1403 Å + C IV 1548,51 Å, for example). The features were superimposed on a common velocity scale to enhance the signal-to-noise of systematic velocity patterns.

The profiles in the left-hand panel are all comparatively symmetric and the composite Si IV + C IV line shape has essentially the same velocity centroid as the chromospheric O I and Si II features. (The dotted curves are the long wavelength edges of the emission profiles reflected about the system COM velocity to illustrate the symmetry of the line shapes. The error bars within each profile are estimated emission bisectors.) The lack of significant differential shifts between the TR features and the chromospheric lines at the velocity crossing suggests that there are no substantial systematic flows of material at the 10^5 K level in Capella — a wind for example — compared with the cooler chromospheric layers (Ayres and Linsky 1980b). This result is contrary to interpretations of low S/N Copernicus spectra of

Capella (Dupree 1975, 1976), which indicated the presence of a $\cong 30$ km s^{-1} accelerating outflow at and above the 10^5 K level.

The right-hand panel illustrates the most surprising result of the Capella study (Ayres and Linsky 1980b): while the chromospheric features (O, I, Si II) taken near one of the elongations in the orbit are asymmetric, indicating contributions from both the G primary and F secondary, the high temperature composite profile remains comparatively symmetric, and shifts bodily to the red following the radial velocity motion of the secondary, exclusively. The straightforward interpretation of this curious behavior is that most of the high temperature emission from the Capella system is produced by the F-type secondary, rather than by the somewhat more massive and luminous primary. This result is contrary to the presumption of most previous work on the Capella system that the G-star is the major ultraviolet emitter (e.g. Dupree 1975; Haisch and Linsky 1976). In fact, symmetrizing the long wavelength emission edges of the elongation profiles about the secondary's velocity indicates that the bulk of the low temperature, chromospheric emission is produced by the F-star as well.

In short, the Capella-α Centauri emission dichotomy has resolved itself into an emission dichotomy between the Capella giants themselves. This is a promising simplification because the evolved giants are obviously very different from the main sequence dwarfs, but the Capella stars are very similar to one another in their fundamental stellar properties: mass, temperature, luminosity, chemical composition, age, and so forth.

The only fundamental property that is very different between the Capella siblings, and is a plausible candidate to explain the emission dichotomy, is rotation (Ayres and Linsky 1980b). The Capella primary is a sharp-lined, slow-rotating giant, while the secondary has a diffuse spectrum and presumably is a fast rotator. The rotation dichotomy itself is likely a result of the somewhat more advanced evolutionary state of the primary compared with that of the secondary owing to the small mass difference (Iben 1965).

D. THE ROTATION-ACTIVITY CONNECTION

Rotation is a plausible candidate to explain the Capella ultraviolet emission dichotomy, if the chromospheric activity of cool stars is intimately related to surface concentrations of magnetic fields, as certainly appears to be the case for the Sun (Vaiana and Rosner 1978). If the decay of surface fields is responsible for the heating of the outer atmosphere, the fields must be replenished continually for the chromosphere and corona to persist over evolutionary timescales. A likely replenishment mechanism is dynamo action (Parker 1955, 1970), and the dynamo is more vigorous in fast rotating convective stars than in slow rotators. Indeed, the chromospherically most active of cool stars are those in short-period binary systems (the RS CVns, for example; Hall 1978), where tidal friction forces the two companions into rapid, synchronous rotation (Zahn 1977). Furthermore, Bopp and Fekel (1977) have argued that rotation, rather than binarity per se, is responsible for the BY Draconis flare star "syndrome" among dwarf M stars. Finally, the recent Einstein survey of coronal soft X-ray emission (Vaiana 1980; Vaiana et al. 1980) has revealed that the brightest cool-star sources, as a class, are the

F-type stars. These tend to be fast rotators compared with single G, K and M stars, very likely because the F stars are young (see e.g. Skumanich 1972).

Ironically, the corona itself is thought to be responsible for the spin-down of single stars as they age. In particular, a weak coronal breeze, such as the solar wind, that is magnetically coupled to the stellar photosphere out to many radii, can shed angular momentum effectively (Durney 1972). If the magnetic braking by a coronal breeze is positively correlated to the chromospheric activity level, then the corona is, in a sense, a self-defeating entity. However, short-period binary systems need not suffer the coronal decay of single stars, owing to the large reservoir of angular momentum in their orbits to maintain the component rotation rates through tidal coupling.

Finally, the rotation-activity connection has an intriguing, practical consequence. Soft X-ray and EUV images of the Sun have revealed that active regions are composed of discrete structures, namely magnetic loops (Rosner, Tucker and Vaiana 1978). If the analogous loop systems on an active star extend an appreciable fraction of the stellar radius above the photosphere, and if the loops corotate with the phtospheric plasma, one might expect enhanced broadening of TR (and coronal) emission features, compared with chromospheric or photospheric line profiles. Furthermore, if a particularly active -- or flaring -- loop system happens to be near one of the equatorial limbs, one might find an emission enhancement in the wing of the C IV 1548 Å profile, for example, that corresponds to the projected rotational velocity of the active region at the time of observation. Again nature has provided a simple way to obtain crude spatial information concerning structures on the surface of another star. All one requires is moderate spectral resolution, which is certainly more appealing from a practical standpoint than the alternative: direct imaging with kilometer-aperture telescopes!

III. MG II h AND k: CHROMOSPHERIC COOLING AND WIDTH-LUMINOSITY CORRELATIONS

Turning aside from stellar transition regions for the moment, I would like to discuss Mg II emission in more detail, particularly with regard to chromospheric radiative losses, and the origin of the Wilson-Bappu relations.

A. CHROMOSPHERIC COOLING BY MG II h AND k

Mg II h and k are important radiative cooling agents in stellar chromospheres (Linsky and Ayres 1978). Calibrated measurements of the integrated core emission of these lines provide a more-or-less direct probe of chromospheric energy budgets. In fact, comparisons of pre-IUE Mg II fluxes with the predictions of chromospheric heating by acoustic waves constituted the first direct test of a proposed theoretical chromosphere formation mechanism (Linsky and Ayres 1978).

The important result from the early Mg II work was that when expressed in the form $f_{Mg\ II}/\ell_{bol}$, the stellar emission fluxes showed a wide range of variation at a given spectral type and luminosity class, but no clear correlation with surface gravity. The empirical result was diametrically opposite to the predictions of the acoustic heating scenario. The latter required

rather uniform chromospheric heating (and consequently also uniform Mg II cooling) at a given spectral type and luminosity class, because only convection zone parameters -- T_{eff} and g -- ultimately determined the acoustic flux production. Furthermore, the acoustic theory predicted a large systematic increase in the heating with decreasing surface gravity (e.g. Ulmschneider et al. 1977). Some attempts have been made recently to rectify the substantial discordances between the acoustic heating theory and the semiempirical chromospheric cooling estimates (Schmitz and Ulmschneider 1979; Böhm 1980), but the fundamental disagreement remains (Linsky 1980). The failure of the acoustic heating scenario to explain the formation of stellar chromospheres is no surprise to solar physicists, given the overwhelming empirical evidence that the structure of the solar outer atmosphere is intimately related to magnetic fields (Skumanich, Smythe and Frazier 1975; Vaiana and Rosner 1978), which are not even considered in the conventional acoustic heating treatments.

In any event, IUE has provided a greatly expanded data set to test proposed chromospheric heating mechanisms. For example, Basri and Linsky (1979) and Stencel et al. (1980) have presented diagrams analogous to that of Linsky and Ayres, but based on the more homogeneous and better calibrated IUE spectra. Furthermore, Böhm-Vitense and Dettmann (1980) recently have published an extensive survey of F and late-A stars to probe the occurrence of classical chromospheres in the HR diagram. Mg II fluxes for additional stars are available elsewhere (e.g. Hartmann, Dupree and Raymond 1980; Pagel and Wilkins 1979).

I have combined these several IUE studies of Mg II emission on a common diagram in Figure 6. The "bubbles" represent mean $f_{MG\ II}/\ell_{bol}$ ratios in each of the spectral type/luminosity class bins for which data are available. Often, only one star falls in a bin, but in some cases, particularly in the K-giant region, as many as ten stars are represented by a single bubble. The small filled circles refer to stars for which Mg II emission was not detected (these data are taken from the Böhm-Vitense and Dettmann study). The dashed circles are Mg II flux ratios based on the Copernicus work of Weiler and Oegerle (1979) as quoted by Basri and Linsky. The Copernicus fluxes are very uncertain compared with the IUE measurements. I have included them only to fill out regions of the bubble diagram where IUE measurements were not available.

The Mg II bubblegram illustrates three important characteristics of the occurrence of chromospheres in the HR diagram.

First, there is an abrupt onset of detectable chromospheric emission in the early F stars that coincides with the beginnings of vigorous convective activity (see Böhm-Vitense and Dettmann for details).

Second, there is no large systematic trend of increasing $f_{Mg\ II}/\ell_{bol}$ ratios with increasing luminosity, although the variation of flux ratios within a given bin (not illustrated in Fig. 6 explicitly) can be an order of magnitude or more. For example, the active G8 dwarf ξ Boo A has a Mg II flux ratio (Basri and Linsky 1979) some twenty times that estimated from the Pagel and Wilkins (1979) h and k profiles of the G8 dwarf τ Ceti. Therefore, the

new IUE Mg II spectra confirm the tentative results of the earlier Linsky and Ayres study.

Third, the stars in the red giant branch (KO III and later) appear to exhibit somewhat weaker chromospheric Mg II emission ratios than the dwarfs or supergiants of similar spectral type (see also Stencel et al. 1980). This is in fact the same region of the HR diagram where Linsky and Haisch (1978) identified an abrupt drop in transition region emission, which they interpreted as a weakening, or disappearance altogether, of solar-like coronae. Incidentally, the Linsky-Haisch division corresponds to the onset of strong stellar winds in the red giants ($\dot{M} \cong 10^{-8}$ $M_\odot$ yr^{-1} compared with $\dot{M} \cong 10^{-14}$ for the solar "breeze"), and has been characterized as a corona-wind boundary (Haisch, Linsky and Basri 1980).

I will return to the question of the origins of the structure seen in the Mg II bubblegram at the conclusion of the review.

B. THE WILSON-BAPPU RELATIONS

Because the Ca II H and K and Mg II h and k transitions are so similar in their atomic properties, it is not surprising that the systematic increase of H and K emission core FWHMs with increasing stellar luminosity -- the well-known Wilson-Bappu effect -- is seen in the Mg II features as well (Moos et al. 1974; McClintock et al. 1975; Dupree 1976). The study of the Wilson-Bappu effect is somewhat easier in the Mg II lines than in Ca II since the former always exhibit much larger core-wing contrasts than the latter. Furthermore, a large (and still growing) sample of high-quality Mg II line shapes has been obtained by one instrument, namely IUE. A homogeneous data set is an essential ingredient for determining systematic trends in line profile shapes.

Although the conventional Wilson-Bappu effect refers solely to the broadening of the emission core FWHM (Lutz 1970), other characteristic profile features, such as the K_1 minimum separation and K_2 peak separation (see Fig. 7), also obey qualitatively the same width-luminosity correlations as the FWHM (Ayres, Linsky and Shine 1975; Cram, Krikorian and Jefferies 1979). Curiously, though, the Mg II and Ca II profiles of solar active regions, which exhibit 5-10x enhanced chromospheric emission compared with "quiet" regions, are broader at the base (WK_1), but narrower at the emission peaks (WK_2), while the FWHM is essentially unchanged (Shine and Linsky 1972). In fact, the constancy of the Ca II FWHM among stars of similar absolute visual magnitude, but very different chromospheric activity levels, allows the Wilson-Bappu effect to be a reliable luminosity indicator, on the one hand, but a headache for theoretical modelers, on the other (see e.g. Böhm-Vitense 1980b).

The simple dependence of the K (and k) FWHMs on stellar luminosities, and little else, suggests that the fundamental correlation is in terms of stellar surface gravity (e.g. Lutz and Pagel 1979).

i) Doppler versus Damping Control

There are essentially two kinds arguments to explain why the Ca II and Mg II FWHMs broaden with decreasing surface gravity. The first class of arguments assumes that the emission core shapes are controlled entirely by nonthermal Doppler broadening, and the widening of the emission profiles with decreasing surface gravity simply reflects a systematic increase of chromospheric nonthermal velocities with increasing stellar luminosity. The second class of arguments assumes that the outer edges of the emission core are at least partially controlled by the Lorentzian damping wings, and that the overall broadening of the emission profile is caused by a physical thickening of the stellar chromosphere with decreasing surface gravity. [Previous work on both aspects is summarized by Ayres (1979).]

The Doppler hypothesis would seem to be plausible if, for example, the Mg II emission cores were broadened by acoustic waves having roughly the same flux in dwarf and giant stars. Since the acoustic flux is proportional to the square of the disturbance amplitude v and to the material density ρ, one would expect v to increase with decreasing surface gravity to compensate for the substantial drop in ρ. However, in the supergiant stars, which have very wide Mg II emission profiles, nonthermal velocities greatly in excess of the chromospheric sound speed would be required to explain the observed broadening (Basri 1979). It is not clear how this "shocking" result could be attained in a real stellar chromosphere. Furthermore, it is difficult to reconcile the k_1 width-luminosity relation in the Doppler context, since the profile minimum features are formed well beyond the chromospheric Doppler core (Engvold and Rygh 1978). Finally, the narrowing of the K_2 emission peak separation in solar plages compared with quiet Sun profiles, but relatively unchanged FWHM, are difficult to understand in the pure Doppler picture, unless the nonthermal broadening decreases rapidly with altitude in active regions, contrary to semiempirical chromospheric models (Shine and Linsky 1974).

The second class of Wilson-Bappu explanations, based on the hypothesis of damping wing control in the outer emission core, relies on a physical thickening of stellar chromospheres as surface gravity decreases. In the damping wings, the monochromatic opacity is a slowly varying function of wavelength displacement ($\kappa_{\Delta\lambda} \sim \Delta\lambda^{-2}$), at least compared with that of the Doppler core ($\kappa_{\Delta\lambda} \sim \exp -(\Delta\lambda/\Delta\lambda_D)^2$). As a result, there is a one-to-one correspondence between wavelength displacements in the profile and atmospheric column densities, in the sense that the intensity at a particular $\Delta\lambda$ is a mapping of the emissivity $\eta(T)$ at monochromatic optical depth $\tau_{\Delta\lambda} \cong 1$ (i.e. an Eddington-Barbier relation; see e.g. Ayres 1979). For example, the temperature minimum at the photosphere-chromosphere interface would be mapped onto an intensity minimum (i.e. K_1) at a wavelength displacement from line center $\Delta\lambda_*$ such that the monochromatic optical depth down to the location of the T_{min} in mass column density, m_* (g cm^{-2}), is of order unity. If T_{min} is shifted to larger column densities, then $\Delta\lambda_*$ will increase as well ($\Delta\lambda_* \sim m_*^{1/2}$). The correspondence between structure in the atmospheric emissivity, which is characterized in terms of the line source function S_ℓ, and features in the emergent profile is illustrated in Figure 7.

The notion that stellar chromospheres might physically thicken in column density with decreasing surface gravity is appealing, particularly because stellar photospheres exhibit just that behavior (at least when they are in hydrostatic equilibrium), owing to the pressure sensitivity of the dominant continuous opacity source, H^- (e.g. Ayres et al. 1975). In fact, Lutz, Furenlid and Lutz (1973) have invoked the photospheric thickening mechanism to explain the gross broadening of the photospheric wings of Ca II H and K with increasing stellar luminosity. It remains, then, to find a mechanism to similarly thicken stellar chromospheres.

There are in fact several possibilities (e.g. Thomas 1973), but I will summarize here only the one proposed by Ayres (1979), if only because I have read that paper somewhat more carefully than the others.

ii) Chromospheric Scaling Laws

In that study, I proposed a set of simple scaling laws for the thickness and mean electron density of stellar chromospheres as functions of, primarily, surface gravity g and an activity scale parameter $\tilde{F}$. The latter indicates by how much a given stellar chromosphere deviates from the gravity-independent mean heating trend I adopted from the Linsky-Ayres Mg II study (see §IIIA, above). For example, $\tilde{F} = I$ for the quiet Sun, while $\tilde{F} \cong 5$ for a medium strength plage.

The scaling laws are predicated on the notion that the initial temperature inversion at the base of the chromosphere is caused by an instability in the low temperature plasma cooling when a source of mechanical heating is present. The thermal instability is driven by the dependence of the plasma radiative cooling (ergs cm^{-2} g^{-1}) on the electron density, and the fact that the electron density itself depends strongly on temperature only between about 5×10^3 K and 8×10^3 K, while for lower and higher temperatures n_e is directly proportional to the hydrogen density n_H. For example, at low temperatures ($T < 5 \times 10^3$ K), electrons are provided by the first ionizations of the abundant metals Fe, Si and Mg (Vernazza, Avrett and Loeser 1976), consequently $n_e \cong 10^{-4}\ n_H$, where the proportionality constant is the collective abundance of those metals. Similarly, above 8×10^3 K, hydrogen is essentially fully ionized, consequently $n_e \cong n_H$. In either regime, the electron density, and therefore also the radiative cooling, is inextricably bound to the rapid outward decrease of the hydrogen density in a hydrostatic stellar atmosphere.

If the atmospheric energy balance is dominated by radiative emission and absorption (radiative equilibrium), the rapid outward decline of the plasma cooling when n_e is proportional to n_H is of little consequence because the radiative heating rate also declines in proportion to the electron density. A balance can thereby be struck between the radiative heating and cooling at comparatively low temperatures ($T < 5000$ K). However, if the atmosphere supports a small mechanical heat deposition, in addition to the radiative absorption, that does not fall off with height as n_H or faster, then at some altitude the mechanical deposition will become comparable to the radiative heating. The combined energy input will then exceed the plasma's ability to cool itself at low temperature, in the face of the rapid outward decline of

the electron density. A thermal instability will ensue, and the plasma will heat up until partial ionization of hydrogen liberates enough additional electrons that the radiative cooling function can balance the mechanical heat input. In the regime of partial ionization of hydrogen, the electron density is at least temporarily divorced from the outward decrease of the hydrogen density. For example, the electron density can remain constant with height while n_H decreases by four orders of magnitude, as long as the temperature rises slowly outward. The atmospheric layers in which the electron density is relatively unchanged and the temperature rises smoothly outward over a four order of magnitude decrease in the gas pressure is what I would characterize as the classical chromosphere. However, once the temperature reaches 8000 K what I would characterize as the electron density is again inextricably tied to the outward hydrostatic decrease of the hydrogen density, and a second thermal instability and temperature inversion -- the transition region -- is possible.

In short, I propose that the gross structure of stellar chromospheres is a simple consequence of the trifurcated character of the n_e/n_H ratio for $T < 10^4$ K, and the sensitivity of the plasma cooling to the electron density.

If one assumes that the energy deposition per gram of material in the chromosphere is constant with height, and that the total heat deposition is the same in a dwarf and a giant star of similar activity levels (namely, the same $f_{Mg\ II}/\ell_{bol}$ ratios at a given T_{eff}), then it is easy to show that the chromosphere of the low gravity giant must be thicker in column density than that of the high gravity dwarf. However, the dwarf star chromosphere requires a larger mean electron density than that of the giant star to ensure that the total radiative cooling will be the same. If one considers two stars of similar surface gravity but different activity levels, one finds that the chromosphere must thicken in the active star, and the mean electron density must increase as well.

The simple chromospheric scaling laws I proposed have profound implications for the Wilson-Bappu effect, if the characteristic profile features -- the K_1 minima and K_2 emission peaks -- are at least partially controlled by the Lorentzian damping wings.

For example, the K_1 minimum feature separation broadens with increasing chromospheric thickness, because the monochromatic optical depths down to the temperature minimum increase in proportion to the column density. Furthermore, the K_2 emission peak separation widens with decreasing mean electron density because the line source function thermalizes to the chromospheric Planck function at larger line-center optical depths, and consequently is mapped onto emission maxima further away from line center. (Note, the so-called thermalization depth, or scattering length, Λ depends inversely on the collisional destruction probability ε, which itself is proportional to n_e. In a chromospheric having an outward temperature rise, Λ is the line-center optical depth at which the source function S_ℓ is a maximum [see Fig. 7]. The maximum of the source function is mapped onto the line profile as a pair of emission peaks in a completely analogous way to the mapping of the source function minimum at T_{min} onto the K_1 intensity minima.)

Consequently, both the K_1 and K_2 feature separations should broaden with decreasing surface gravity, in fact with the same $g^{-1/4}$ behavior. One would therefore expect that profile positions between K_1 and K_2, the FWHM in particular, would show a similar $g^{-1/4}$ gravity dependence.

For stars of similar surface gravity but different activity levels, the situation is somewhat changed. The K_1 feature separation widens with increasing activity as the chromosphere becomes thicker. However, the K_2 peak separation becomes narrower with increasing activity because the larger mean electron density in the active chromosphere forces the line source function to thermalize at shallower optical depths, and consequently to be mapped onto K_2 peaks that are closer to line center. In fact, the K_1 broadening and K_2 narrowing have equal, but opposite, dependences on the activity scale factor $\widetilde{F}$. Consequently, one expects the FWHM to be relatively independent of activity. These behaviors are illustrated schematically in Figure 8.

Although my arguments are perhaps overly simplistic, they do make definite predictions that can be tested.

iii) Confrontation with IUE Observations

The major parameter dependence of the derived width-luminosity scaling laws is the broadening of the K_1 feature separation with decreasing surface gravity, namely $\Delta\lambda_{K1} \sim g^{-1/4}$. What is true for Ca II K_1 is equally true for Mg II k_1.

Figure 9 compares measured Mg II k_1 widths (Basri and Linsky 1980; Stencel et al. 1980) with estimated stellar surface gravities. Since the theoretical k_1 widths also depend on the activity parameter $\widetilde{F}$, stellar metallicity and effective temperature, I have applied appropriate corrections determined from the original scaling laws (Ayres 1979) to isolate the gravity dependence (see also Linsky et al. 1979). The activity parameter is straightforward to derive from measured $f_{Mg\ II}/\ell_{bol}$ ratios, and is usually the largest component of the correction. The adjustments for T_{eff} and nonsolar metallicity are less secure, but are small in most cases. More important, any errors introduced by uncertainties in the k_1 adjustments pale beside the uncertainties in the stellar surface gravities themselves.

Two sets of data are represented in Figure 9. The open and filled circles and open squares depict stars for which both high-quality Mg II k and Ca II K line shape parameters are available, and for which reasonable surface gravity estimates could be found (see Basri and Linsky, and Stencel et al. for details). These data will appear in subsequent diagrams that compare the k and K lines against each other. (I have separated the stars crudely into dwarfs [V], giants [IV,III] and supergiants [II,I].) The pluses represent additional gaints and supergiants from the Stencel, et al. lists for which Mg II k line shape parameters and surface gravity estimates are available, but no Ca II information. I have included these stars in the diagram to give a better impression of the true scatter of the data.

The four-pointed open circles refer to quiet and active Sun profiles of k obtained with the French experiment on OSO-8 (courtesy P. Lemaire; see

Chapman 1980). The plage k_1 separation is larger than that of the quiet Sun, but when corrected for an activity enhancement of $\widetilde{F} = 5$, it actually falls somewhat below the quiet Sun width. (Notice that I have plotted the adjusted k_1 widths in km s^{-1} to partially mollify the Doppler broadening enthusiasts.)

Finally, I have drawn a line with slope -1/4 through the quiet Sun point to illustrate the gravity dependence expected from the simple scaling laws.

It is clear from the figure that while the stars appear to obey a gross trend of increasing k_1 width with decreasing surface gravity compatible with the scaling laws, there is a great deal of scatter, and the lowest gravity stars appear to deviate significantly from the expected relation. Analogous studies of the Ca II K_1 width-luminosity correlation have proposed a gravity dependence closer to -1/5 than -1/4 (e.g. Cram et al. 1979), and a somewhat flatter relation would appear to be appropriate for Mg II k_1 here as well. The departure of the supergiants from the proposed relation is not unexpected, because a subtlety in the k-wing formation process -- partial coherent scattering (e.g. Ayres 1975) -- was glossed over in the derivation of the scaling laws. The density-sensitive coherent scattering effects become increasingly important the lower the surface gravity, and work in the direction of producing a narrower k_1 separation than if the wing scattering were completely noncoherent (see Basri 1979).

iv) The Stars that Don't Obey the Wilson-Bappu Effect

In any event, it is not clear whether the Mg II Wilson-Bappu relation is relevant to the supergiants in the first place. For example, α Ori (M2 Iab) and β Dra (G2 II) have similar Mg II FWHMs, yet the former is some 4 magnitudes brighter in M_V. Furthermore, ζ Cyg (G8 IIIp) is somewhat more luminous in absolute visual magnitude than β Dra, yet has a Mg II FWHM only half as large, and in fact comparable to that of α Ser (K2 III) which is 2 1/2 magnitudes fainter than ζ Cyg in M_V.

Incidentally, another class of stars that do not obey the Wilson-Bappu relations are the short-period eclipsing binaries (e.g. Young and Koniges 1977). In such systems, the Ca II and Mg II FWHMs are correlated with the emission core strength, contrary to a central tenet of the Wilson-Bappu effect that the FWHM is independent of chromospheric activity levels. However, the Ca II and Mg II features of such systems are broadened by the rapid synchronous rotation of the binary companions (at least for the eclipsing systems, which are viewed edge on). The violation of the Wilson-Bappu relation in these cases is simply an expression of a stronger driving force, namely the rotation-activity connection. (This is also a situation in which the Doppler advocates are correct, although the broadening is extrinsic rather than intrinsic.)

v) Mg II k_1 Versus Ca II K_1

Figure 10 compares Mg II k_1 separations with the corresponding K_1 widths in the available sample of dwarfs, giants and supergiants. Ca II

data were taken from the recent surveys by Linsky et al. (1979) and Cram et al. (1979).

The scaling laws predict that the k_1/K_1 width ratio should depend only on atomic parameters and the Mg/Ca abundance ratio. For solar abundances (Mg/Ca $\cong$ 15), the W_{k1}/W_{K1} ratio (when the W's are in Å) should be 2.5. On the other hand, if the minimum features are formed in the Doppler core, it is easy to show that the expected width ratio is about 0.75. The empirical relation in Figure 10 lies comfortably between the alternative predictions.

To explain the apparent discrepancy in terms of the scaling laws requires either a Mg/Ca abundance ratio roughly half of the accepted solar value, which seems unlikely, or a mechanism that would selectively narrow the Mg II k_1 separation relative to Ca II K_1. One possibility is the difficulty of defining the location of the relatively flat k_1 minima in typical IUE LWR echelle spectra, particularly because the Mg II wings are significantly more distorted by atomic line blanketing than are the Ca II inner wings. However, the high-resolution OSO-8 Mg II profiles from the quiet and active Sun exhibit the same overall discrepancy, and the solar k_1 and K_1 feature separations are far less ambiguous than typical stellar data. A more plausible differential broadening possibility is the coherent scattering phenomenon mentioned previously. Coherent scattering has a stronger influence on the Mg II wings compared with those of Ca II, owing primarily to the existence of the subordinate infrared triplet in Ca II which introduces an additional source of noncoherence in the photon scattering and redistribution process that is not available to Mg II h and k (e.g. Ayres 1975).

If one were feeling particularly charitable, one would use the solar width ratios to "calibrate" the magnitude of the differential coherent narrowing effect, namely $Wk_1/WK_1 \cong 1.5$-2.0, and conclude that the remaining stellar width ratios were reasonably consistent with the revised prediction. It is encouraging that the largest deviations from the original prediction occur for the supergiants where chromospheric densities are lowest and the coherence effects largest, while the smallest deviations occur for the high gravity dwarfs where the coherence effects should be least.

vi) Mg II k_2 Versus Ca II K_2

Figure 11 compares Mg II emission peak separations with those of Ca II. The prediction of the Damping hypothesis is depicted as a dotted line, while that of the Doppler hypothesis is depicted as a dashed line. (A height-independent chromospheric Doppler width is assumed for both cases: Yes, the K_2 separation in the Damping picture does depend on the non-thermal broadening, through its effect on the line-center optical depth scale, but only as $v^{1/2}$.)

Although the empirical data appear to be in better agreement with the Damping hypothesis, the comparison is somewhat more ambiguous than that for the K_1 features. Unlike the profile minima, the Ca II and Mg II emission peaks are formed at different heights in the chromosphere. In principle, if the broadening velocity is larger in the k_2 forming region than in the K_2 layers, the Doppler prediction would be increased. Furthermore, the presence

of saturated interstellar Mg II absorption components in the emission core potentially could produce a spuriously large empirical k_2 separation.

vii) Summary

I have presented the Mg II width-luminosity correlations to illustrate several points. First, the Damping hypothesis provides a viable alternative to the conventional Doppler arguments, that mimics quite naturally several aspects of the Wilson-Bappu relations which the Doppler theories are hard-pressed to explain. Second, the comparision of empirical line widths to the predictions of chromospheric scaling laws, for example, is hampered not so much by the poor quality of the measured profiles (which previously was the case), but rather by a lack of reliable stellar parameters, particularly surface gravity. Finally, the optically thick emission cores of Ca II K and Mg II k contain a great deal of information concerning the gross structure of stellar chromospheres that is only just beginning to be tapped.

IV. EMPIRICAL CORRELATIONS AMONG CHROMOSPHERIC, TRANSITION REGION AND CORONAL EMISSION

The final topics I will address are empirical correlations among chromospheric, transition region and coronal emission, and the implications of these correlations for understanding the occurence of chromospheres and coronae in the HR diagram.

As mentioned previously, in the first year of IUE Linsky and Haisch (1978) discovered an apparent division in the HR diagram between stars that tend to exhibit solar-like transition region emission (i.e. C IV 1550 Å) and stars for which the 10^5 K lines are very weak or below detection thresholds. However, stars in the latter category often appear to have prominent chromospheric emission spectra (e.g. O I and Si II). The Linsky-Haisch work generated considerable controversy, particularly concerning whether the division, which the authors characterize as a corona-wind boundary (Haisch et al. 1980), is "sharp" or "fuzzy" (e.g. Dupree and Hartmann 1980). Indeed, Hartmann, Dupree and Raymond (1980) found two hydrid cases of G-type supergiants (α and β Aqr) for which a strong chromospheric wind appears to coexist with hotter, TR-like material. These examples suggest (e.g. Linsky 1980) a multi-component situation analogous to that of the solar outer atmosphere where the structures that emit TR and coronal radiation (the closed magnetic loop systems of active regions) are physically distinct from the structures that produce much of the solar wind (coronal holes, which are regions of diverging magnetic fields).

It is worthwile, then, to reexamine the question of TR boundary lines in the HR diagram, and correlations between TR and chromospheric emission in general, in light of the much larger sample of ultraviolet spectra available today.

A. EMPIRICAL EMISSION CORRELATIONS

The observations I will summarize below are described in more detail by Ayres, Marstad and Linsky (1980). Some ultraviolet data have been taken from other surveys, for example that by Böhm-Vitense and Dettmann (1980) for many of the F stars, and Hartmann et al. (1980) for 3 G-K supergiants. The stellar soft X-ray

measurements are partly from the HEAO-1 experiment and partly from preliminary results of Einstein IPC imaging that were kindly made available through a collaborative observing program with the CFA Stellar Survey team (see e.g. Ayres et al. 1980 for details).

Figure 12 compares the normalized emission strengths of prominent chromospheric and transition region emission lines, and broad-band soft X-ray fluxes (0.15-4.5 keV) as functions of normalized Mg II fluxes. The stars are separated crudely according to spectral type (i.e. warm or cool) and luminosity class (i.e. dwarfs or giants). No finer separation is practical at this stage owing to the limited sample. The four-pointed open circles refer to measurements of the quiet and active Sun as described by Ayres et al. (1980).

Beginning with the chromospheric O I triplet (1305 Å) in the upper left-hand panel of Figure 12, one sees that the O I flux ratios are well-correlated with Mg II, and that the slope of the correlation is roughly unity. However, the giant stars tend to have systematically larger O I fluxes at a given Mg II flux level than the dwarf stars. I conclude that O I is a genuinely "chromospheric" diagnostic, but that the mean atmospheric density plays an important role in setting the overall strength of the oxygen emission. Such a link is plausible because the O I triplet lines are thought to be strongly pumped by H I Lβ, through a Bowen fluorescence mechanism, and the pumping should increase substantially with decreasing chromospheric density (Haisch et al. 1977).

The upper middle panel illustrates the comparison between the Si II triplet (~1815 Å) and Mg II. Here again one finds a close correlation between the two chromospheric features, although the overall emission levels in Si II are a factor of ≅30 smaller. The weakness of Si II relative to Mg II is a reflection of the dominant role played by h and k in the chromospheric radiative cooling.

The top right-hand panel compares the C II doublet (1335 Å) with Mg II. Once again the correlation is strong, at least among the cooler dwarfs and giants, although the slope of the correlation appears to be steeper than for the purely chromospheric O I and Si II features. Curiously, the F stars deviate substantially from the mean trend, in the sense that their C II emission is enhanced relative to Mg II. Since C II is formed in the lower portion of the transition region, it is not surprising that the correlation with Mg II does not have unit slope. Presumably one is seeing the differences between an optically thick layer (the upper chromosphere) and an optically thin layer (the TR) that are at essentially the same gas pressure (e.g. Haisch and Linsky 1976). The fact that a correlation exists at all is compelling evidence that the TR and chromosphere are physically linked in some way, presumably by magnetic fields or a common heating mechanism.

The lower left-hand panel compares the He II Balmer α line (1640 Å) and Mg II. Again one finds an excellent correlation, but apparently of even steeper slope than that of C II. Although He II is formed at only somewhat hotter levels of the TR than C II, photoionization of helium by coronal radiation fields is thought to play an important role in the He I-He II ionization balance (Avrett, Vernazza and Linsky 1976). In fact, Hartmann et al. (1980) have proposed that the He II flux is an indirect diagnostic for the level of coronal soft X-ray emission, namely $F_X \cong 50\ f_{He\ II}$. Some support for that suggestion is found in the steep slope of the He II-Mg correlation (but see below).

The middle, bottom panel compares the summed fluxes of Si IV 1400 Å, C IV 1550 Å and N V 1240 Å with Mg II. The three transition region doublets are formed over a temperature range of 0.6-2 x 10^5 K, and the sum is usually dominated by C IV (10^5 K). Here, one finds a very similar behavior to that of C II. The cooler stars exhibit a good correlation of the hot line flux with Mg II, having a steeper than unit slope, while the F stars deviate systematically from the mean trend. Furthermore, even for the most active stars of the sample (the RS CVn systems HR 1099 and UX Ari), the summed TR fluxes are at least an order of magnitude smaller than the corresponding Mg II fluxes. This dichotomy implies that the chromospheric energy budget in "normal" stars is always considerably larger than that of the overlying TR.

The final panel compares coronal soft X-ray emission levels with Mg II. (A larger, and more systematic, study of X-ray-Mg II correlations is currently in progress [Zwaan 1980]). Again a rough correspondence of increasing X-ray flux with increasing Mg II flux is apparent, although the slope is steeper than any of the previous correlations. However, several of the stars for which only upper limits are available (primarily G-K supergiants) seem to fall well below the mean trend, which is based largely on G-K dwarfs and G giants. For example, the upper limit that falls below the lower edge of the diagram refers to the bright K2 giant Arcturus. That nondetection should be compared with the detection of the K1 giant β Gem (the filled circle immediately above the "3") at normalized flux levels an order of magnitude higher despite the somewhat smaller Mg II flux ratio. It is likely not coincidental that the stars which were not detected in the collaborative mini-survey all show evidence for stellar winds and circumstellar envelopes.

Curiously, the soft X-ray flux levels in the brightest coronal sources exceed the corresponding Mg II fluxes. In those stars, the coronal energy budget must be comparable or larger than that of the chromosphere, whereas in the quiescent dwarf stars, such as the Sun, the coronal energy budget is only a small fraction of the chromospheric budget.

Finally, one sees that the He II-soft X-ray scaling proposed by Hartmann et al. (1980) is incompatible with the measured flux levels, except perhaps for the brightest of the coronal sources. For example, Hartmann et al. predicted that α Aqr (G2 II) would have a soft X-ray flux in the 1/4-keV band of order 7 x 10^{-12} ergs cm^{-2} s^{-1} at the Earth based on the measured He II flux of ≅2 x 10^{-13}. However, the 3σ upper limit for the entire 0.15-4.5 keV Einstein IPC band is only 2 x 10^{-13}, which is considerably smaller than the predicted flux. A similar situation exists for β Aqr, where the measured He II flux is comparable to the Einstein upper limit, whereas the soft X-ray flux should be a factor of ≅50 larger according to the Hartmann et al. prescription. There are at least two ways to resolve the dilemma.

First, circumstellar material surrounding both α Aqr and β Aqr may heavily attentuate the intrinsic coronal soft X-rays, consequently the upper limits measured at the Earth may have little meaning. However, note that the Sun exhibits only 4-7 times enhanced soft X-ray emission relative to He II in both quiet and active regions, contrary to the factor of $\cong$50 expected. Even if circumstellar obscuration is viable for the supergiants, one would still have to find an additional mechanism to explain the solar discrepancy.

A second, more plausible, possibility is that the He II emission strength is itself overestimated, especially in the stars having weak coronae. This possibility is attractive because the "He II" feature is actually a blend of He II and Fe II. Consequently, the intrinsically steep He II-Mg II correlation predicted by the Hartmann et al. prescription (namely $f_{\text{He II}} \cong 0.02 f_X \sim f_{\text{Mg II}}^3$) may be significantly diluted by a $f_{\text{Fe II}} \sim f_{\text{Mg II}}^1$ contribution at moderate and low $f_{\text{Mg II}}/\ell_{\text{bol}}$ levels. Note that the Fe II component is at least 30% of the total He II emission in the Sun (Kohl 1977). The composite relation might then mimic the empirical He II-Mg II slope of 2.

In any event the possibility of either mechanism -- circumstellar obscuration or Fe II contamination -- urges caution in the practical application of the Hartmann et al. He II-soft X-ray scaling prescription.

B. IS THE CORONA-WIND BOUNDARY REAL?

The apparent correlations among chromospheric, TR and coronal emission imply that transition regions and coronae do not completely die out to the right of the Linsky-Haisch boundary. Nevertheless, the weakening of transition regions and coronae in the red giant branch is a real phenomenon that is seen clearly even in the chromospheric Mg II emission (Fig. 6). The Linsky-Haisch boundary appeared to be "sharp" in the early IUE spectra for two reasons. First, the TR emission falls off rapidly with decreasing chromospheric activity levels, and the giants to the right of the dividing line generally have weak chromospheres. Second, the red giant ultraviolet spectra are dominated by chromospheric O I emission that is considerably enhanced relative to that of dwarf stars having comparable Mg II activity levels (Fig. 12). If one obtains low dispersion short wavelength spectra of dwarf and giant stars to optimally expose the brightest emission feature (aside from Lα), namely O I 1305 Å, then one would in effect be selectively underexposing at C IV in the giants compared with the dwarfs, by a factor of five or so. Since the IUE vidicons have a limited dynamic range, the factor of five in exposure can make the difference between "signal" and "noise" at C IV.

In short, the weakening of transition regions and coronae in the red giant branch is genuine, but appears "abrupt" primarily because of two selection effects: (1) The steep contrast between TR and Mg II emission; and (2) underexposures in the Lα region of giant stars driven by the selective enhancement of O I emission.

C. ON THE OCCURRENCE OF CHROMOSPHERES AND CORONAE IN LATE-TYPE STARS

The fact that coronal and TR emission are well-correlated with Mg II flux levels, at least in the cool stars for which all three have been detected,

suggests to me that chromospheres and coronae must be physically associated. However, the steepness of the soft X-ray correlation, and to some extent also that of the TR emission, suggests to me that the chromospheric and coronal heating mechanisms are quite different. The latter notion is strengthened by the discordant behavior of the F-stars in TR emission, and by the K giants and G-K supergiants in soft X-rays. The F-stars appear to support rather prominent TRs and coronae (e.g. Vaiana 1980), but comparatively weak chromospheres, while the cool giants and supergiants appear to be deficient in coronal material compared with dwarf stars of similar chromospheric Mg II emission.

I will now outline a speculative picture to tie together these disparate notions.

The detailed studies of the Sun during the Skylab era have strongly implicated magnetic fields as the fundamental building block in the solar outer atmosphere (Vaiana and Rosner 1978). The fields are responsible for the physical structuring of the coronal plasma and likely also for the heating.

If the solar corona and TR are heated by a magnetic agency, is it not reasonable that the chromosphere might be similarly heated, especially given the close correspondence of chromospheric brightness with mean magnetic field strength (Skumanich et al. 1975)? Actually, the answer is probably no, for the following reasons. The thermal energy density in the corona is much smaller than the magnetic energy density, consequently the dissipation of only a small fraction of the available coronal field, by reconnection for example, is required to balance coronal energy losses by radiation and backconduction to the chromosphere. On the other hand, the thermal energy density in the chromosphere is more nearly comparable to that of the magnetic field, consequently large volumes of field would have to be converted to heat on short timescales in order to power the large radiative losses in Mg II h and k and maintain the chromospheric temperature inversion.

An intriguing alternative to an in situ field dissipation mechanism for heating the chromosphere, is if the small-scale magnetic flux tubes thought to exist in the photosphere (Chapman 1980) serve simply as conduits of acoustic wave energy into the outer atmosphere. Magnetic flux tubes could, in principle, operate as acoustic wave guides owing to the reduced radiative damping of acoustic modes that results from the decreased gas pressures inside the tubes. (The gas pressures are lower owing to the large internal magnetic pressures.) Since the wave damping is proportional to the square of the gas pressure while the wave flux is directly proportional to the pressure, a potentially much larger absolute flux of wave energy could survive photospheric passage inside the tubes than in the unmagnetized plasma surrounding the tubes. In this picture, stellar chromospheres and coronae would be confined entirely to the interiors of magnetic flux tubes, but the heating mechanism in the distinct atmospheric layers would be quite different. Consequently, chromospheric and coronal emission levels should be grossly correlated, because the different atmospheric layers are physically associated through the agency of the magnetic field, yet the correlation need not have unit slope because the heat deposition mechanisms are distinct.

In this scenario, the weakening of chromospheres toward the early F stars is explained by a decrease in the acoustic wave flux as the stellar outer envelope becomes less convective. However, the TR and corona need not weaken correspondingly, since they are powered by the magnetic field directly. In particular, the rapid rotation of the F stars likely compensates somewhat for the reduced convective motions in the dynamo replenishment of surface fields. Alternatively, the F star chromospheres may be systematically thinner than those of cool stars owing to the enhanced photoionization of neutral hydrogen in the outer atmosphere by Balmer continuum radiation. The photoionization effect would strongly decouple the n_e/n_H ratio from its intrinsic temperature sensitivity, thereby removing the ionization "safety-valve" for the plasma cooling function that may be responsible for the extraordinary thickness (in pressure) of chromospheres in cooler stars.

The existence of the "corona-wind" boundary in the HR diagram is also understandable in the acoustic/magnetic scenario: A quirk of nature has allowed stars with very different main sequence heritages to evolve into nearly the same region of the HR diagram (Ayres 1980). Figure 13 depicts the phenomenon.

The heavy dashed curve represents the corona-wind boundary proposed by Linsky and Haisch. Evolutionary tracks for $1M_\odot$ (right-hand track) and $3M_\odot$ stars connect the Zero Age Main Sequence and the giant branch. Also included are contours of constant stellar radius, and arrows that indicate the general flow of stellar evolution in the two major regions which feed stars into the giant branch. Simple consideration of stellar statistics suggests that most of the comparatively numerous K giants must have evolved from main sequence stars only slightly more massive than the Sun. On the other hand, the less numerous G giants must evolve typically from $\cong 3M_\odot$ A-type or B-type stars. Consequently, the K giants tend to be old ($\gtrsim 10^9$ yr) and have evolved vertically in the HR diagram from relatively slowly rotating progenitors (F-G dwarfs). On the other hand, the G giants tend to be young ($\lesssim 10^8$ yr), and have evolved more nearly along the lines of constant radius from rapidly rotating progenitors (B-A dwarfs).

The substantial evolutionary expansion, advanced age, and slow-rotating predecessors of the K giants virtually guarantee that they too will be slow rotators. (In fact, the development of a massive chromospheric wind would rapidly shed any vestige of rotational angular momentum that had survived to that evolutionary stage.) Similarly, the modest evolutionary expansion and rapid-rotating precedessors of the youthful G giants virtually guarantee that they will be fast rotators (certainly compared with the K giants). The apparent weakening of chromospheric and coronal emission in the red giant branch, is then simply an artifact of comparing young magnetically active stars having vigorous dynamos to the left of the boundary with old, magnetically dying stars to the right. Chromospheres are considerably more visible in the K giants than are coronae, because the major component of the chromospheric heating, namely acoustic waves, is still active, despite the decay of the surface magnetic fields which are the sole coronal energy source.

The case of the supergiants is somewhat different from that of the giants. The supergiants have evolved horizontally in the HR diagram from very massive ($\gtrsim 10 M_\odot$) progenitors and must be quite young (10^6-10^7 yr). These stars have suffered enormous evolutionary expansion and are likely slow rotators as a result. Dynamo action must be comparatively weak in the supergiants once they have cooled sufficiently to develop convective envelopes. Nevertheless, because such stars are so young, one would anticipate that some of the primordial fields from the protostellar collapse would have survived dissipative processes over the relatively brief main sequence lifetime of the massive progenitor, and would therefore be available during the supergiant phase to form chromospheres and coronae by the scenario I have outlined above. Since the corona is a field-dissipative mechanism itself, and since the dynamo replenishment action is likely to be nil, one would expect to find a general weakening of the mean coronal emission levels with increasing age (toward cooler spectral types), and a peaking of chromospheric emission toward the early G supergiants where the rising acoustic flux production encounters the failing mean surface magnetic field levels.

D. CONCLUSION

I can only hope that the insight and impetus that the first and second years of IUE have given to the study of cool-star outer atmospheres will continue unabated into the third and future years.

REFERENCES

Athay, R. G. 1976, The Solar Chromosphere and Corona: Quiet Sun, (Boston: D. Reidel).

Athay, R. G. and White, O. R. 1978, Ap. J., 226, 1135.

_____. 1979, Ap. J. Suppl., 39, 333.

Avrett, E. H., Vernazza, J. E. and Linsky, J. L. 1976, Ap. J. (Letters), 207, L199.

Ayres, T. R. 1975, Ap. J., 201, 799.

_____. 1979, Ap. J., 228, 509.

_____. 1980, in Proceedings of "Cool Stars, Stellar Systems and the Sun," ed. A. K. Dupree, SAO Special Report, in press.

Ayres, T. R. and Linsky, J. L. 1980a, Ap. J., 235, 76.

_____. 1980b, Ap. J. (in press).

Ayres, T. R., Linsky, J. L. and Shine, R. A. 1975, Ap. J. (Letters), 195, L121.

Ayres, T. R., Marstad, N. and Linsky, J. L. 1980, in preparation.

Baliunas, S. L., Avrett, E. H., Hartmann, L. W. and Dupree, A. K. 1979, Ap. J. (Letters), 233, L129.

Baliunas, S. L. and Butler, S. E. 1980, Ap. J. (in press).

Basri, G. S. 1979, Ph.D. Thesis, Univ. of Colorado, Boulder, Colorado.

Basri, G. S. and Linsky, J. L. 1980, Ap. J., 234, 1023.

Basri, G. S., Linsky, J. L., Bartoe, J.-D. F., Brueckner, G. E. and Van Hoosier, M. E. 1979, Ap. J., 230, 924.

Bohm, H. U. 1980, preprint.

Böhm-Vitense, E. 1980a, preprint.

_____. 1980b, in Stellar Turbulence, eds. D. F. Gray and J. L. Linsky (New York: Springer-Verlag), p. 300.
Böhm-Vitense, E. and Dettmann, T. 1980, Ap. J., 236, 560.
Bopp, B. W. and Fekel, F., Jr. 1977, A. J., 82, 490.
Bruner, E. C., Jr. 1978, Ap. J., 226, 1140.
Cash, W., Bowyer, S., Charles, P., Lampton, M., Garmire, G. and Riegler, G. 1978, Ap. J. (Letters), 223, L21.
Chapman, G. A. 1980, in Proceedings "Skylab Series C Workshop: Active Regions," ed. F. Q. Orrall, (in press).
Cram, L. E., Krikorian, R. and Jefferies, J. T. 1979, Astr. Ap., 71, 14.
Doschek, G. A., Feldman, U., Bhatia, A. K. and Mason, H. E. 1978b, Ap. J., 226, 1129.
Doschek, G. A., Feldman, U., Mariska, J. T. and Linsky, J. L. 1978a, Ap. J. (Letters), 226, L35.
Dupree, A. K. 1975, Ap. J. (Letters), 200, L27.
_____. 1976, in Physique des mouvements dans les atmospheres stellaires, ed. Cayrel and Steinberg (Paris: CNRS), p. 439.
Dupree, A. K., Baliunas, S. L. and Shipman, H. 1977, Ap. J., 218, 361.
Dupree, A. K. and Hartmann, L. 1980, in Stellar Turbulence, eds. D. F. Gray and J. L. Linsky (New York: Springer-Verlag), p. 279.
Durney, B. R. 1972, The Solar Wind, NASA Report, ed. Sonett, Coleman and Wilcox.
Engvold, O. and Rygh, B. O. 1978, Astr. Ap., 70, 399.
Flannery, B. P. and Ayres, T. R. 1978, Ap. J., 221, 175.
Foukal, P. V., Huber, M. C. E., Noyes, R. W., Reeves, E. M., Schmahl, E. J., Timothy, J. G., Vernazza, J. E. and Withbroe, G. L. 1974, Ap. J. (Letters), 193, L143.
Golub, L., Harnden, F. R., Rosner, R., Topka, K. and Vaiana, G. S. 1980, B.A.A.S., 11, 775.
Hall, D. S. 1976, in Multiple Periodic Variable Stars, ed. W. S. Fitch (Dordrecht: D. Reidel), p. 287.
_____. 1978, A. J., 83, 1469.
Haisch, B. M. and Linsky, J. L. 1976, Ap. J. (Letters), 205, L39.
Haisch, B. M., Linsky, J. L. and Basri, G. S. 1980, Ap. J., 235, 519.
Haisch, B. M., Linsky, J. L., Weinstein, A. and Shine, R. A. 1977, Ap. J., 214, 785.
Hartmann, L., Dupree, A. K. and Raymond, J. C. 1980, Ap. J. (Letters) (in press).
Holt, S. S., White, N. E., Becker, R. H., Boldt, E. A., Mushotzky, R. F., Serlemitsos, P. J. and Smith, B. W. 1979, Ap. J. (Letters), 234, L65.
Hummer, D. G. and Stewart, J. C. 1966, Ap. J., 146, 290.
Iben, I., Jr. 1965, Ap. J., 142, 1447.
_____. 1967, Ann. Rev. Astr. Ap., 5, 571.
Kohl, J. H. 1977, Ap. J., 211, 958.
Linsky, J. L. 1980, in Proceedings Jan. 1980 HEAO-AAS Meeting (in press).
Linsky, J. L. and Ayres, T. R. 1978, Ap. J., 220, 619.
Linsky, J. L. and Haisch, B. M. 1978, Ap. J. (Letters), 229, L27.
Linsky, J. L., Worden, S. P., McClintock, W. and Robertson, R. M. 1979, Ap. J. Suppl., 41, 47.
Lites, B. W., Hansen, E. R. and Shine, R. A. 1980, Ap. J., 236, 280.
Lutz, T. E. 1970, A. J., 75, 1007.
Lutz, T. E. and Pagel, B. E. J. 1979, preprint.

Lutz, T. E., Furenlid, I. and Lutz, J. H. 1973, Ap. J., 184, 787.
Mariska, J. T., Doschek, G. A. and Feldman, U. 1980, Ap. J. (Letters) (in press).
McClintock, W., Henry, R. C., Moos, H. W. and Linsky, J. L. 1975, Ap. J. 202, 733.
Moos, H. W., Linsky, J. L., Henry, R. C. and McClintock, W. 1974, Ap. J. (Letters), 188, L93.
Mount, G. H., Rottman, G. and Timothy, J. G. 1980, preprint.
Noyes, R. W. 1974, contribution to IAU Symposium No. 27, Cambridge, Mass.
Nugent, J. and Garmire, G. 1978, Ap. J. (Letters), 226, L83.
Pagel, B. E. J. and Wilkins, D. R. 1979, preprint.
Parker, E. N. 1955, Ap. J., 122, 293.
_____. 1970, Ann. Rev. Astr. Ap., 8, 1.
Raymond, J. C. and Dupree, A. K. 1978, Ap. J., 222, 379.
Rosner, R., Tucker, W. H. and Vaiana, G. S. 1978, Ap. J., 220, 643.
Schmitz, F. and Ulmschneider, P. 1980, Astr. Ap. (in press).
Shine, R. A. and Linsky, J. L. 1972, Solar Phys., 25, 357.
_____. 1974, Solar Phys., 39, 49.
Skumanich, A. 1972, Ap. J., 171, 565.
Skumanich, A., Smythe, C. and Frazier, E. N. 1975, Ap. J., 200, 747.
Stencel, R. E. and Mullan, D. J. 1980, Ap. J. (in press).
Stencel, R. E., Mullan, D. J., Linsky, J. L., Basri, G. S. and Worden S. P. 1980, Ap. J. (in press).
Thomas, R. N. 1973, Astr. Ap., 29, 297.
Tripp, D. A., Athay, R. G. and Peterson, V. L. 1978, Ap. J., 220, 314.
Ulmschneider, P., Schmitz, F., Renzini, A., Cacciari, C., Kalkofen, W. and Kurucz, R. L. 1977, Astr. Ap., 61, 515.
Vaiana, G. S. 1980, in Proceedings Jan. 1980 HEAO-AAS Meeting (in press).
Vaiana, G. S. and Rosner, R. 1978, Ann. Rev. Astr. Ap., 16, 393.
Vaiana, G. S., et al. 1980, preprint.
Vernazza, J. E., Avrett, E. H. and Loeser, R. 1976, Ap. J. Suppl., 30, 1.
Walter, F. M., Cash, W., Charles, P. A. and Bowyer, C. S. 1980, Ap. J., 236, 212.
Walter, F. M., Charles, P. A. and Bowyer, C. S. 1978, A. J., 83, 1539.
Weiler, E. J. and Oegerle, W. R. 1979, Ap. J. Suppl., 39, 537.
Wilson, O. C. and Bappu, M. K. V. 1957, Ap. J., 125, 661.
Withbroe, G. L. 1977, in Proceedings of the OSO-8 Workshop (Boulder: University of Colorado Press), p. 2.
Withbroe, G. L. and Noyes, R. W. 1977, Ann. Rev. Astr. Ap., 15, 363.
Young, A. and Koniges, A. 1977, Ap. J., 211, 836.
Zahn, J. P. 1977, Astr. Ap., 57, 383.
Zwaan, C. 1980, in Proceedings, "Cool Stars, Stellar Systems and The Sun," ed. A. K. Dupree, SAO Special Report (in press).

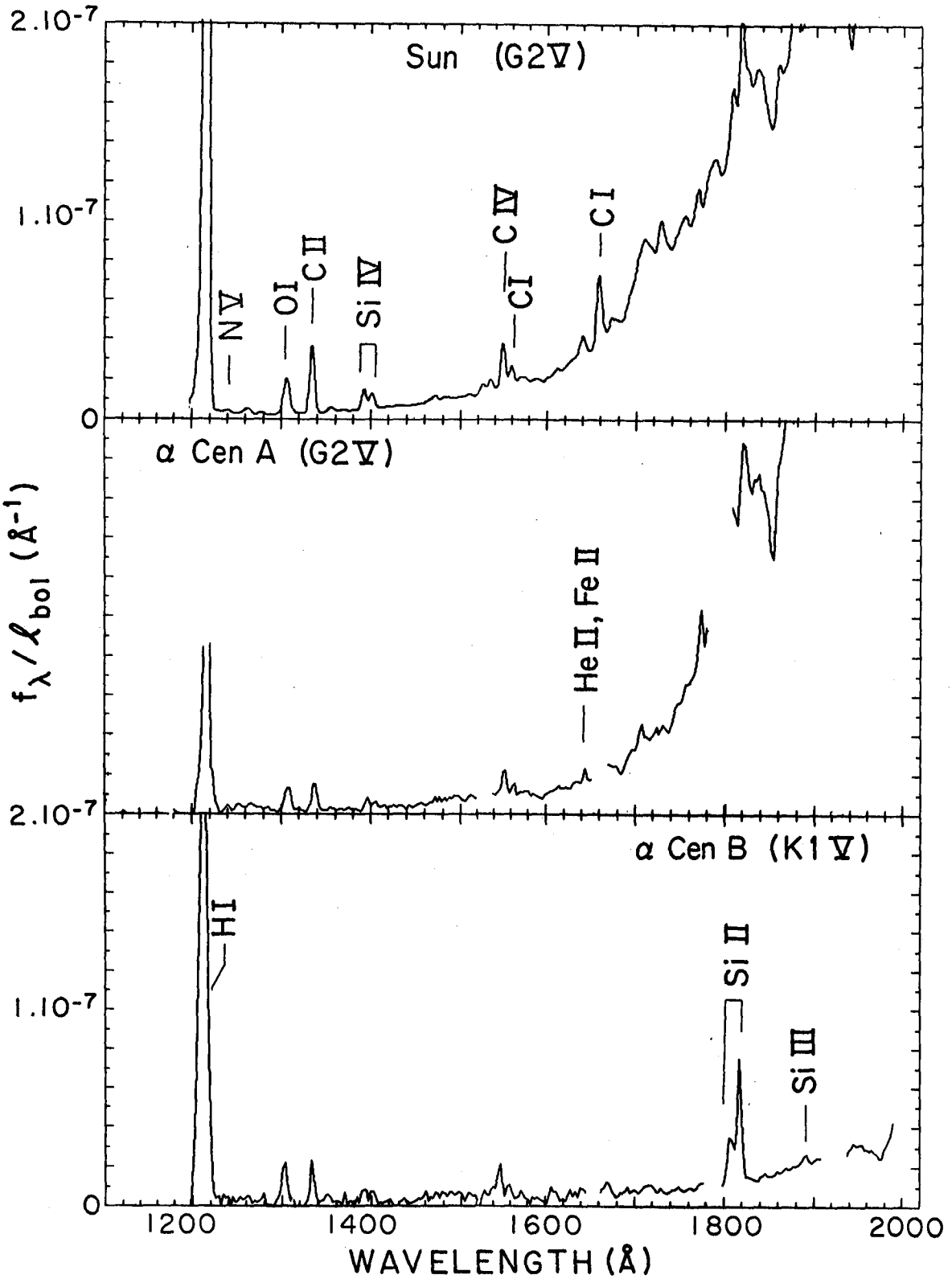

Fig. 1. Short wavelength, low dispersion IUE ultraviolet spectra of α Centauri A and B compared with the solar spectrum (as IUE would see it). Gaps in the stellar spectra are regions affected by saturation or reseau marks.

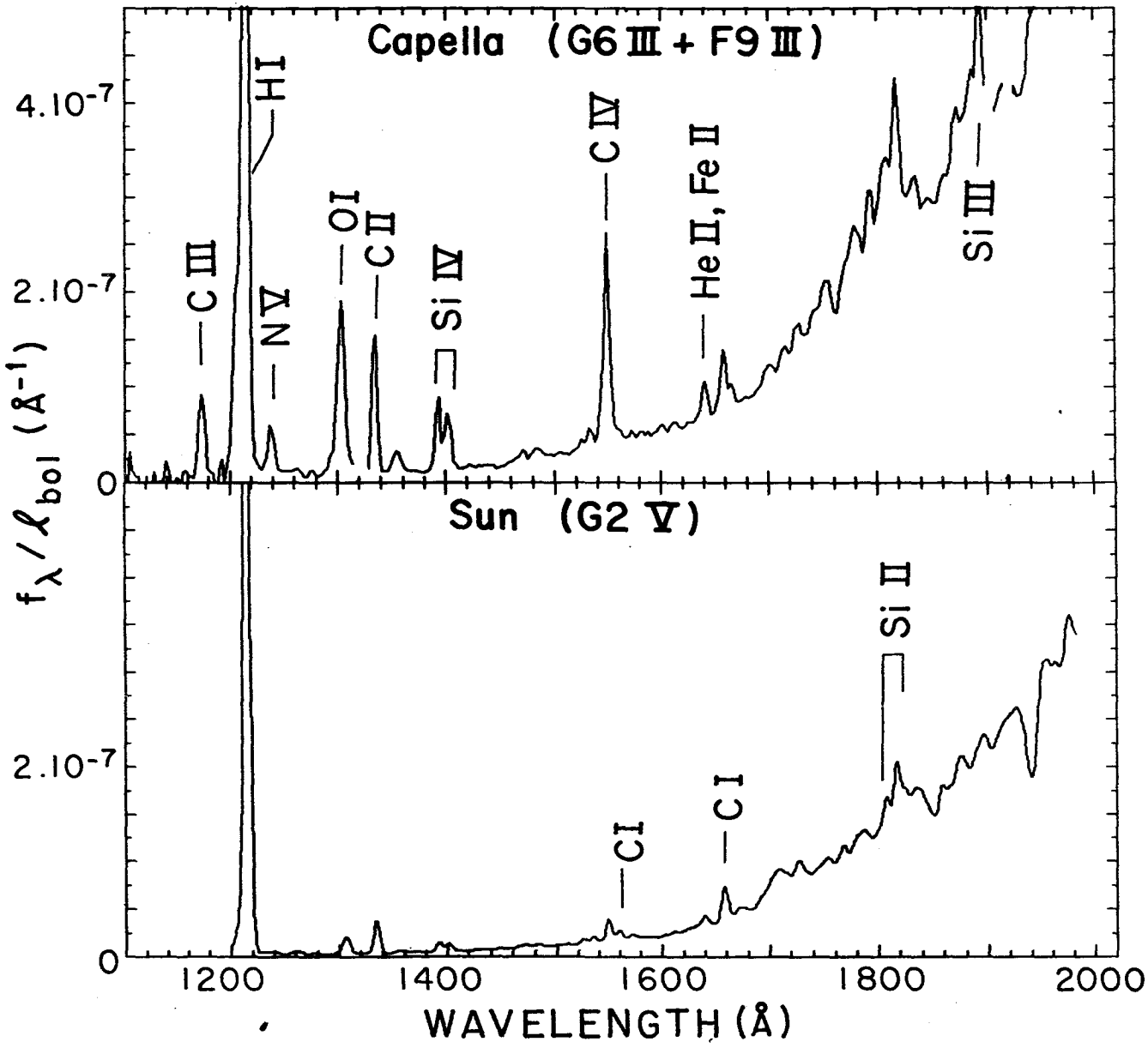

Fig. 2. Same as Figure 1 for Capella.

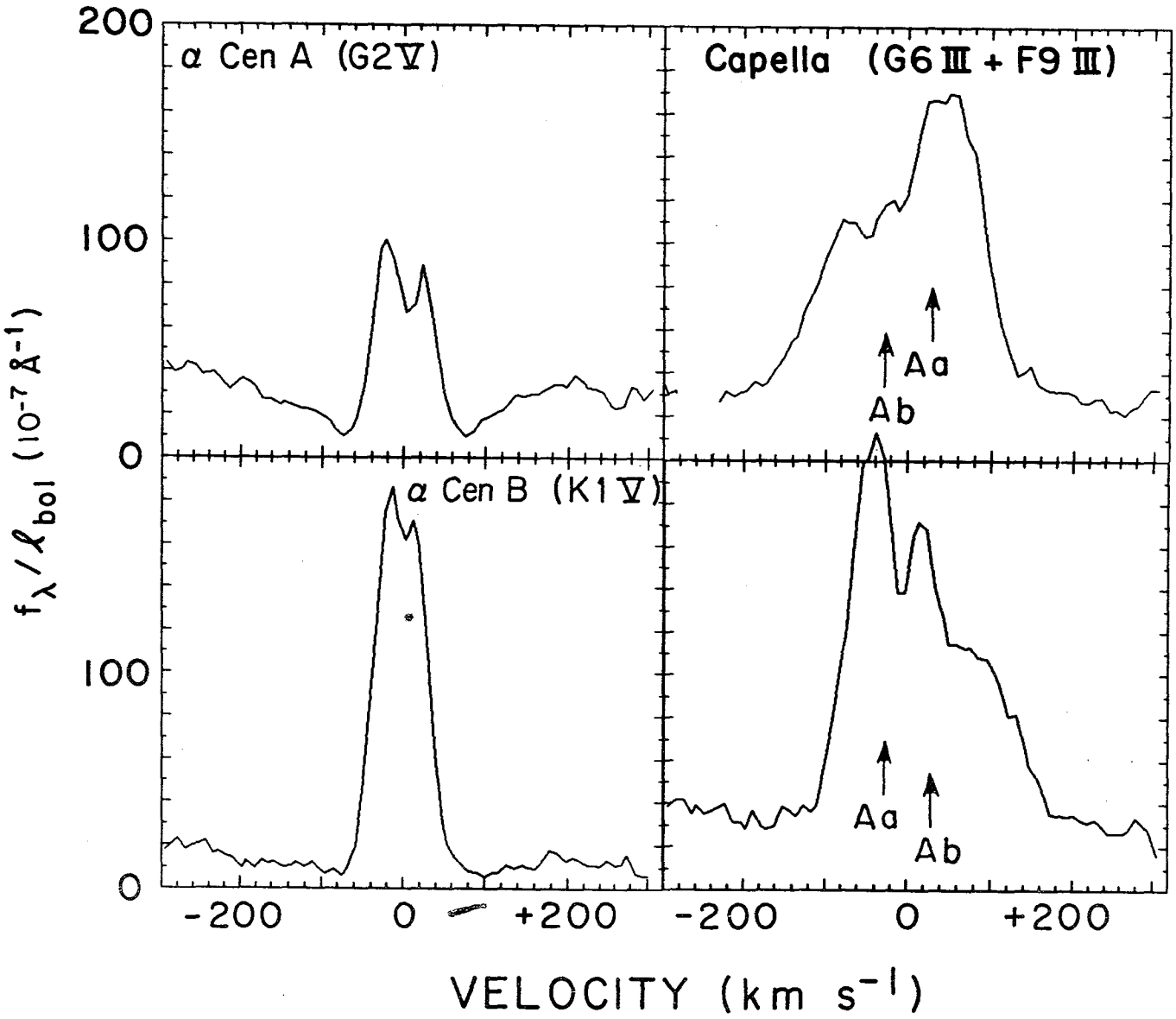

Fig. 3. LWR echelle-mode profiles of Mg II k (2796 Å) in α Centauri A and B, and Capella (orbital phase 26^d, top panel; phase 81^d, bottom panel).

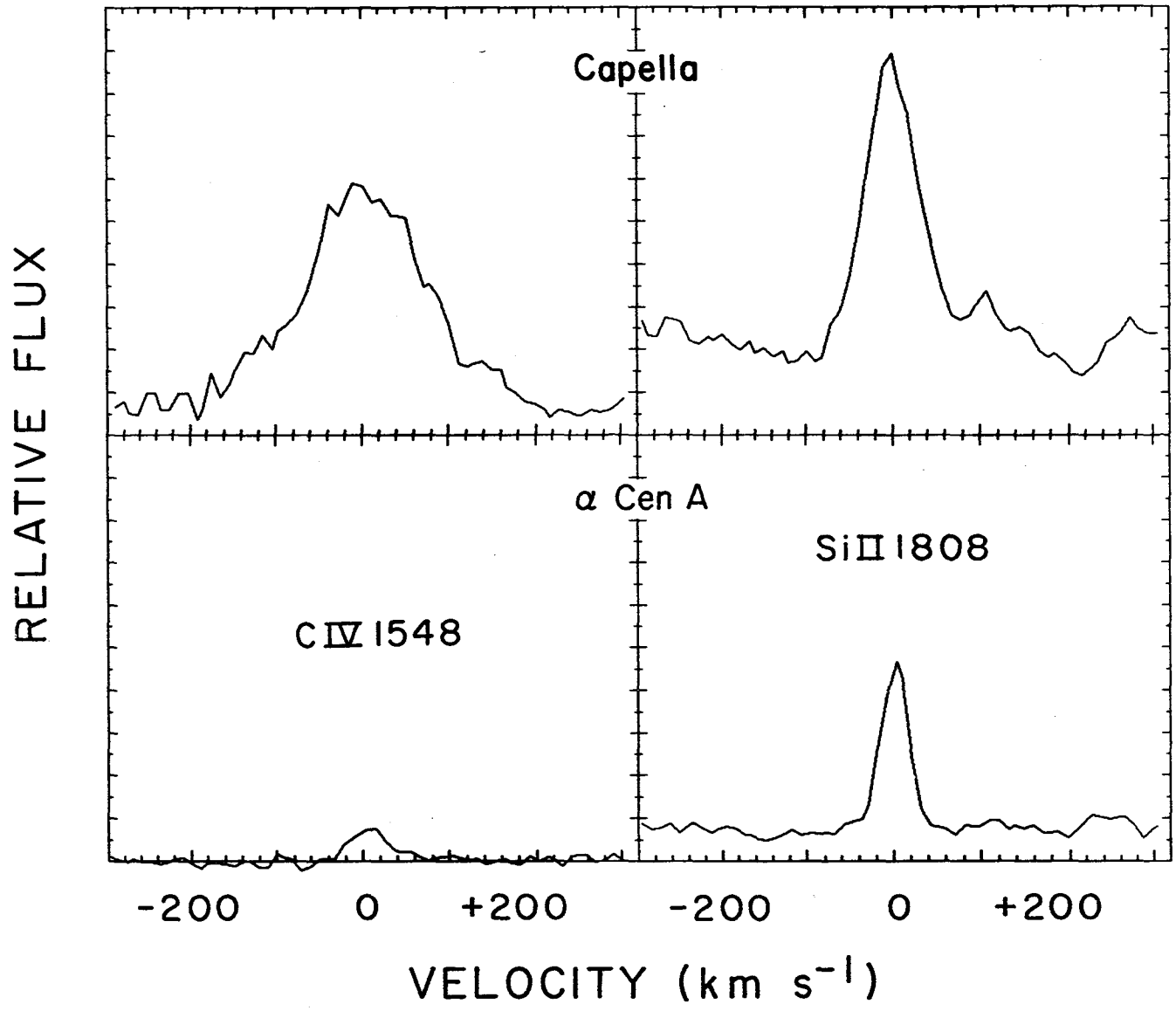

Fig. 4. Comparison of SWP echelle-mode profiles of C IV 1548 Å and Si II 1808 Å in α Centauri A and Capella.

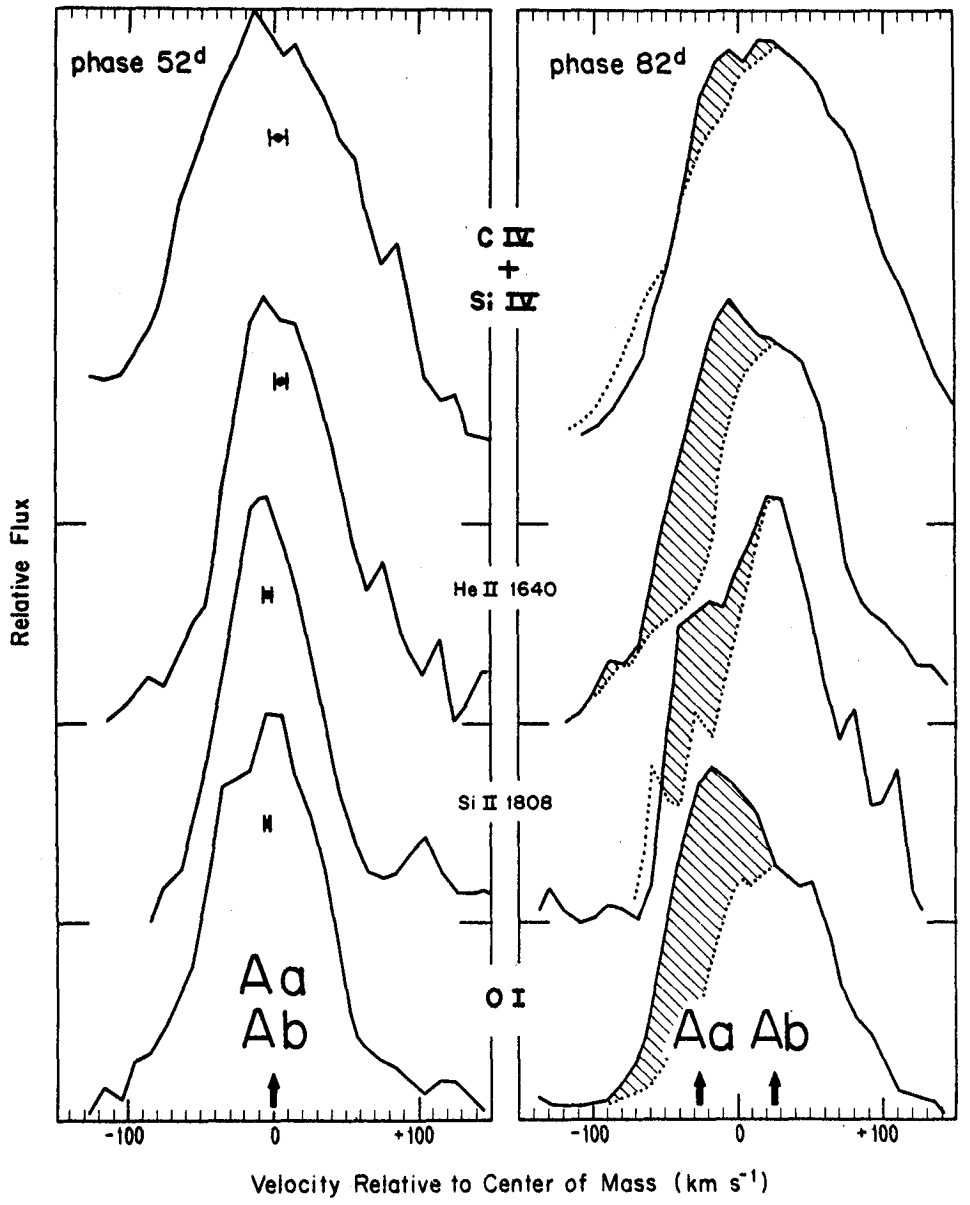

Fig. 5. Comparison of Capella chromospheric and transition region line profiles at two orbital phases: velocity crossing, left-hand panel; near elongation, right-hand panel. The COM velocities of the G-type primary (Aa) and F-type secondary (Ab) at each phase are indicated by arrows. (Courtesy Astrophysical Journal.)

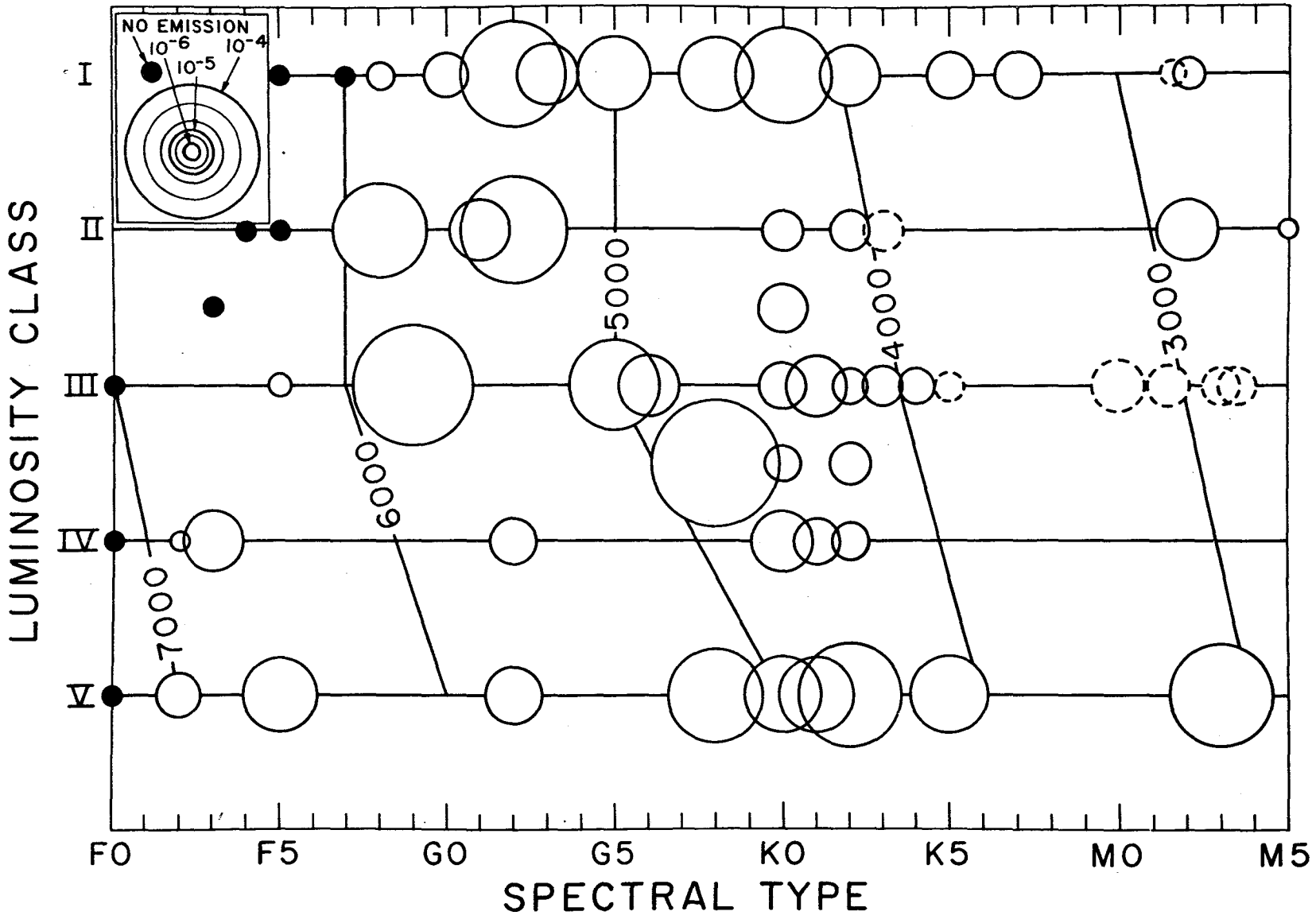

Fig. 6. Bubblegram of chromospheric radiative losses in Mg II h and k. Area of each bubble is proportional to the average value of $f_{\text{Mg II}}/\ell_{\text{bol}}$ in the particular spectral-type/luminosity-class bin. See legend, upper left-hand corner.

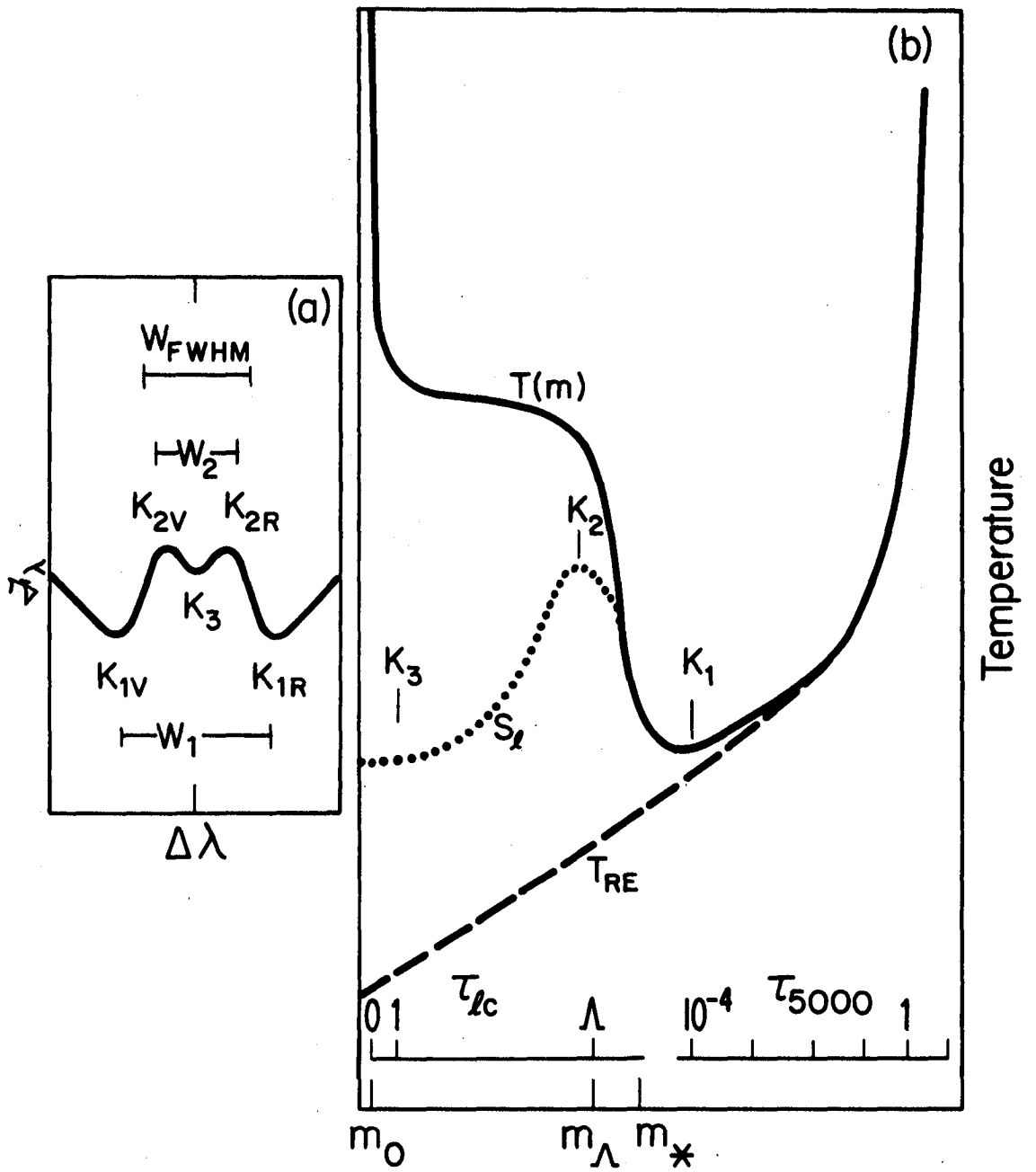

Fig. 7. Correspondence of atmospheric thermal structure (right-hand panel) to emission structure in Mg II k or Ca II K line profile. For example, the minimum temperature region at the top of the photosphere is mapped onto an intensity minimum in the line profile ("K_1"). The displacement of K_1 from line center is governed by the depth of the temperature minimum in mass column density, m_* (g cm^{-2}). If m_* increases, so does $\Delta\lambda_{K_1}$. (Courtesy Astrophysical Journal.)

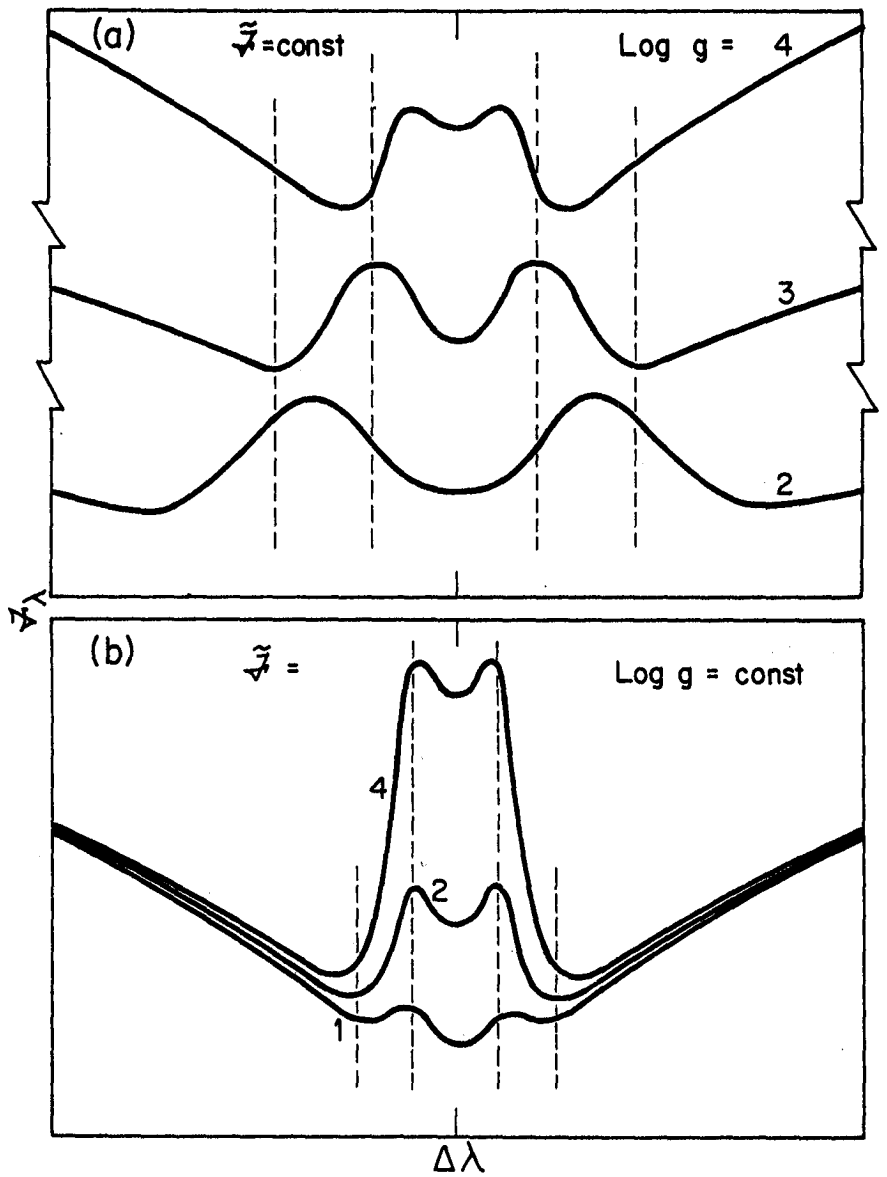

Fig. 8. Schematic depiction of Ca II K and Mg II k profile behavior with changing surface gravity (top panel) and chromospheric activity (bottom panel) as predicted by scaling laws. The intensity scale in the top panel is arbitrary for each profile. In particular, all three emission features should have similar integrated core surface fluxes. Note that the K_1 minimum feature separation broadens both with decreasing surface gravity and increasing chromospheric activity, while the K_2 separation broadens with decreasing surface gravity but becomes narrower with increasing activity. (Courtesy Astrophysical Journal.)

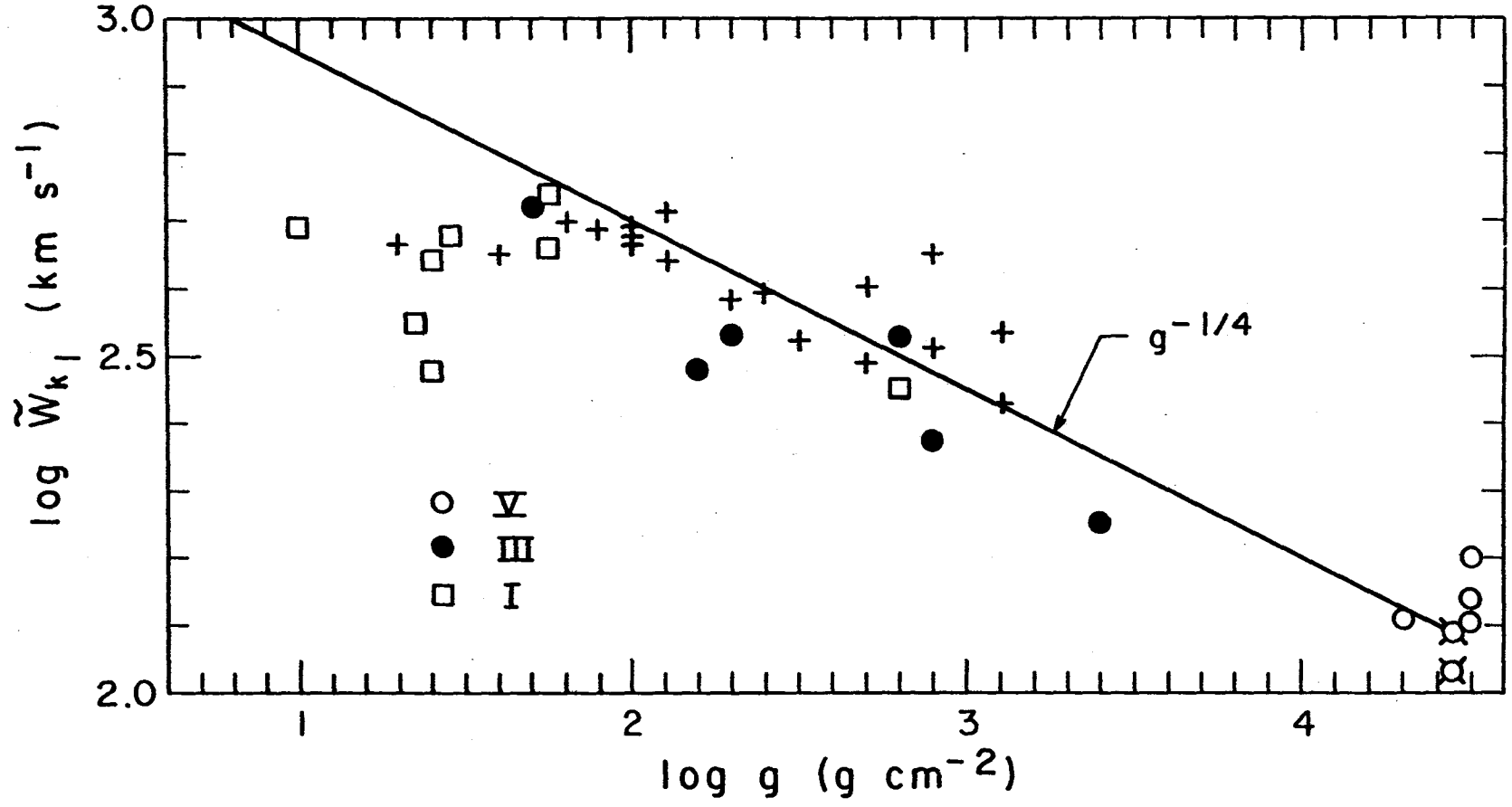

Fig. 9. Comparison of adjusted k_1 widths (see text) with estimated surface gravities. The $g^{-1/4}$ relation predicted by the scaling laws is illustrated by the solid curve that passes through the quiet Sun point.

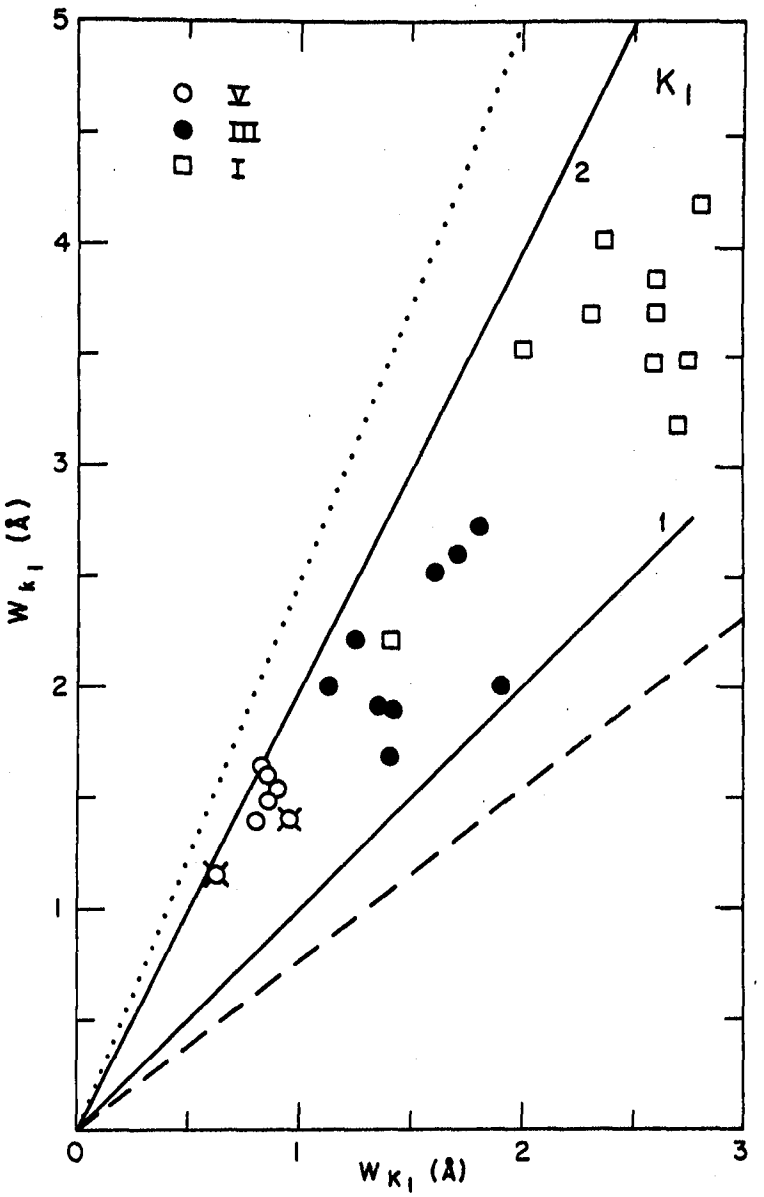

Fig. 10. Comparison of Mg II k_1 and Ca II K_1 separations for the available sample of dwarfs, giants and supergiants. The dotted curve depicts the 2.5 relation expected from the chromospheric scaling laws and "Damping" hypothesis, while the dashed curve is the relation expected if the minimum features were formed entirely in the Doppler core. Partial coherent scattering effects, which were not considered explicitly in the derivation of the scaling laws, would tend to reduce the 2.5 prediction somewhat. The decrease would be largest for the supergiants where the PCS effects are most pronounced.

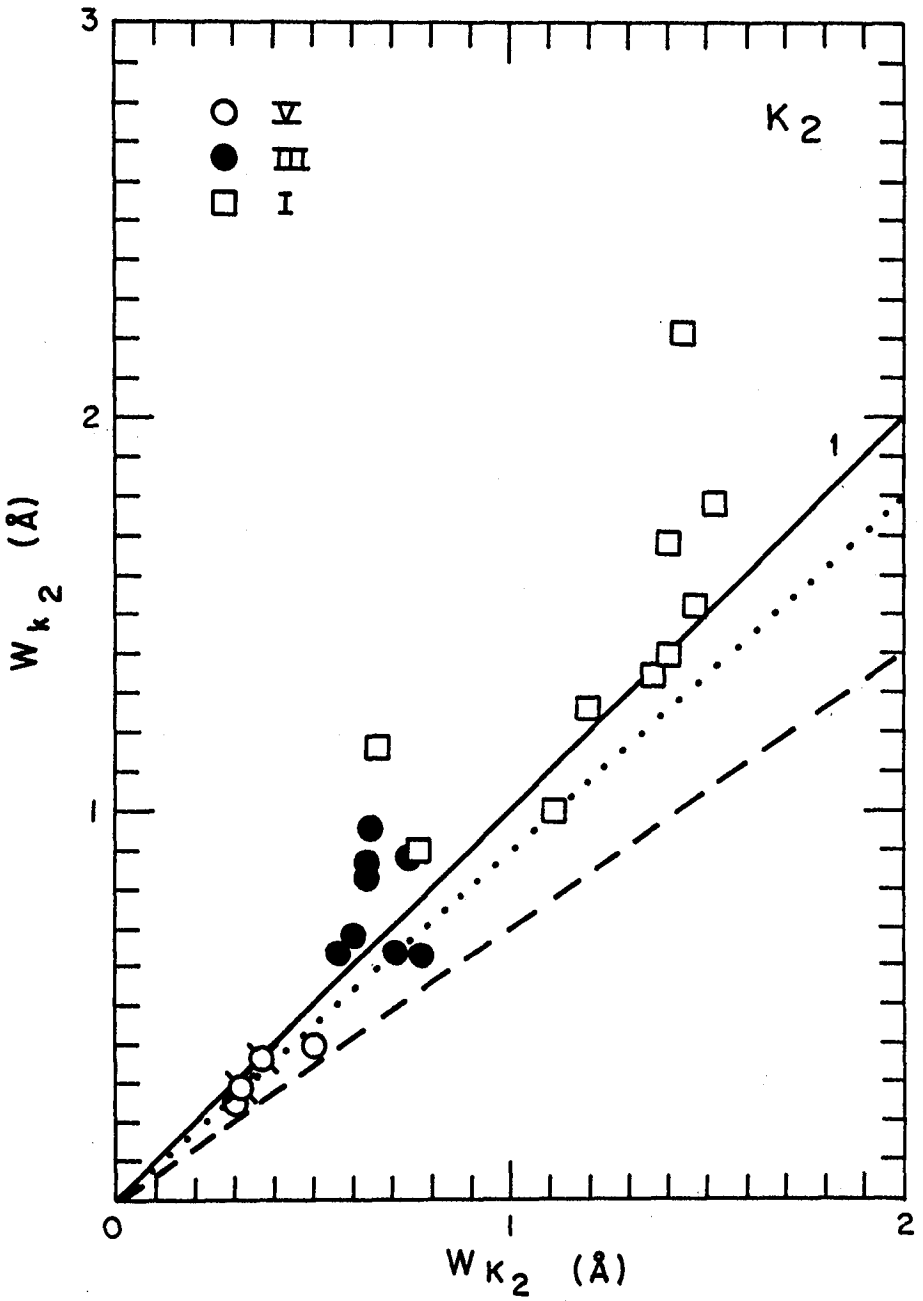

Fig. 11. Same as Figure 10 but for the k_2 and K_2 peak separation. The Damping (dotted curve) and Doppler (dashed curve) predictions are based on a depth-independent chromospheric broadening velocity. Both predictions would be increased if the nonthermal broadening in the middle chromosphere rises outwards. In addition, some of the measured k_2 widths may be overestimates of the true separations owing to the influence of interstellar and circumstellar absorption components in the k emission core.

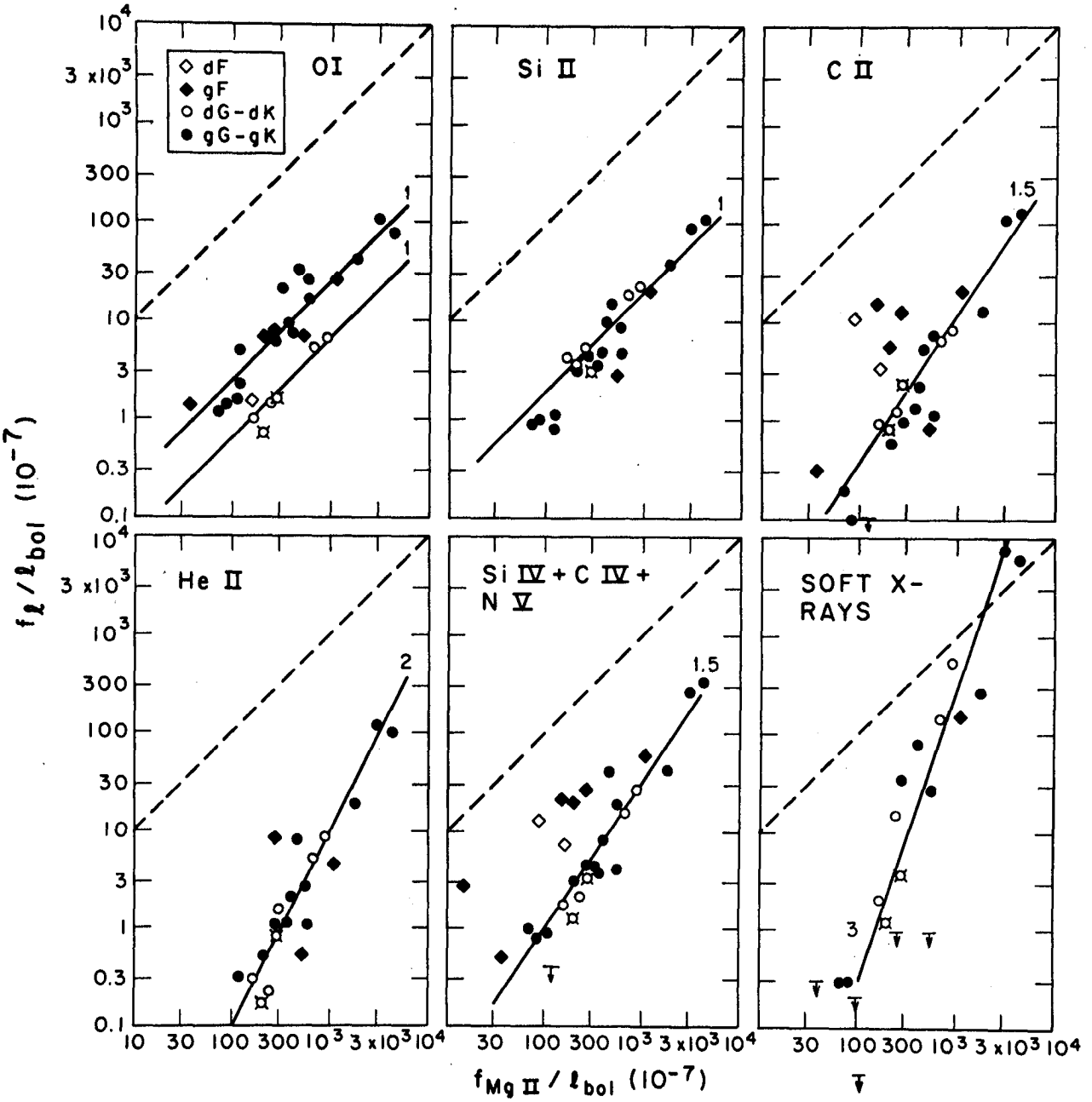

Fig. 12. Correlogram for chromospheric, transition region and coronal emission. The individual normalized fluxes are plotted against the normalized Mg II emission strength. The dashed curves in each panel are for $f_\ell / \ell_{bol} \equiv f_{Mg\ II} / \ell_{bol}$. Note that the Mg II emission is always considerably larger than that of the prominent features of the short wavelength spectrum. The solid curves are not fits to the data, but merely indicate the approximate slope of the individual correlations. (Courtesy Astrophysical Journal.)

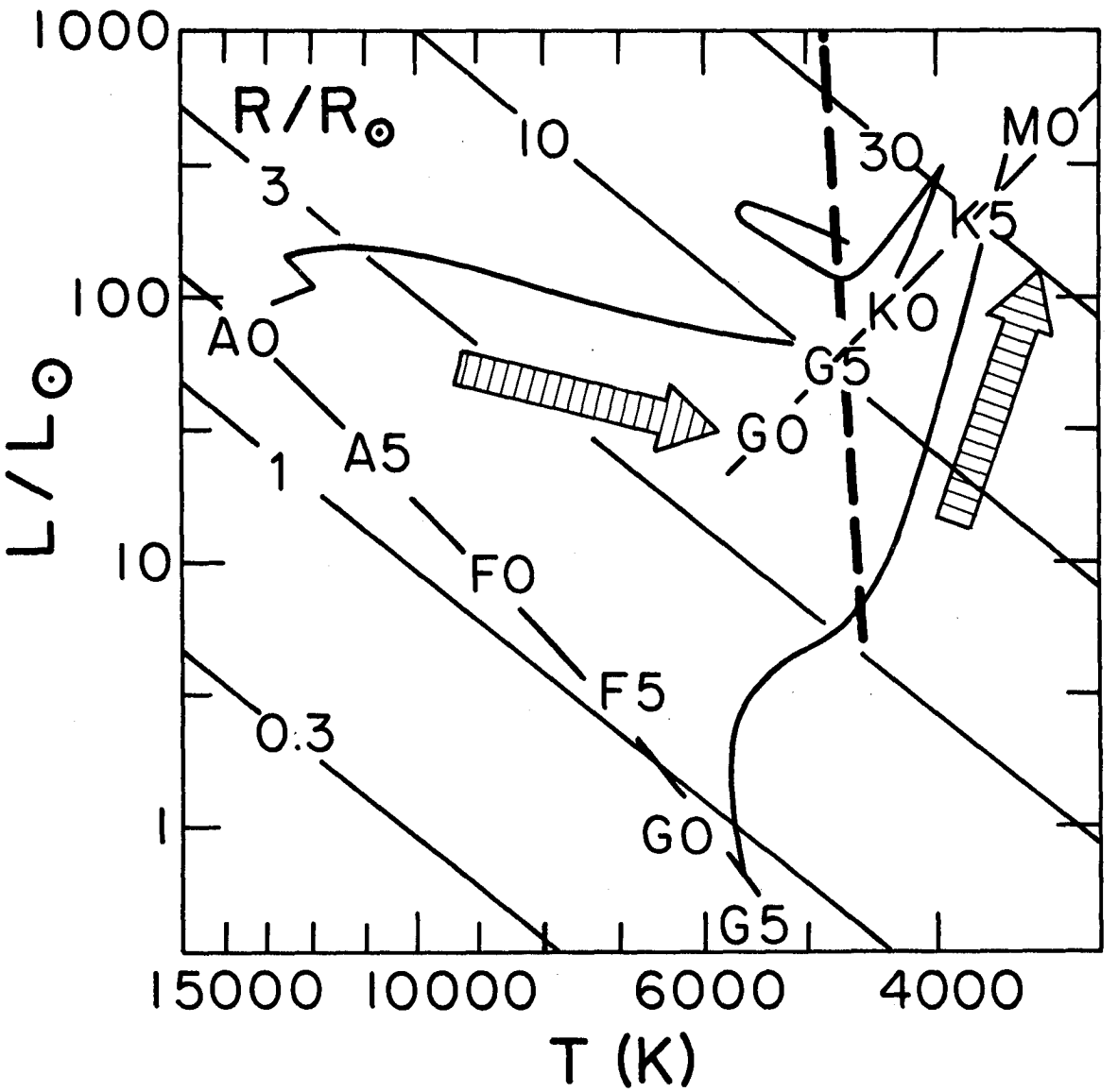

Fig. 13. A simple evolutionary scenario to explain the weakening of coronae and chromospheres, in the red giant branch. The heavy dashed curve is the corona-wind boundary proposed by Linsky and Haisch. The thin curves are evolutionary tracks (Iben 1967) for 1 $M_\odot$ (right-hand track) and 3 $M_\odot$ stars. The arrows indicate the general flow of evolution into the G and K giant regions. Spectral types are given for the Zero Age Main Sequence and in the yellow (F-G) and red (K-M) giant branches.

THE Mg II h and k LINES IN A SAMPLE OF dMe AND dM STARS[1]

Mark S. Giampapa[3]
Steward Observatory, University of Arizona

P. L. Bornmann[3]
Department of Astro-Geophysics, University of Colorado

T. R. Ayres and J. L. Linsky[2,3]
Joint Institute for Laboratory Astrophysics
University of Colorado and National Bureau of Standards

S. P. Worden[3]
Department of Astronomy, University of California, Los Angeles

ABSTRACT

We present observed Mg II h and k line fluxes for a sample of 4 dMe and 3 dM stars obtained with the IUE satellite in the long wavelength, low dispersion mode. The observed fluxes are converted to stellar surface flux units and the importance of chromospheric non-radiative heating in this sample of M dwarf stars is intercompared. In addition, we compare the net chromospheric radiative losses due to the Ca II H and K lines in those stars in the sample for which calibrated Ca II H and K line data exist. Moreover, we estimate active region filling factors which likely give rise to the observed optical and ultraviolet chromospheric emission. Finally, we briefly discuss the implications of the results for homogeneous, single-component stellar model chromospheres analyses.

INTRODUCTION

The resonance lines of Ca II and Mg II, designated as the H and K and h and k lines, respectively, are valuable diagnostics of stellar chromospheric properties. The dominant role of the H and K lines in model chromospheres analyses has been due to their accessibility to earth-based observation

[1]This research is supported in part by the National Aeronautics and Space Administration through grants NAS 5-23274 to the University of Colorado and to the Air Force Geophysics Laboratory.

[2]Staff Member, Quantum Physics Division, National Bureau of Standards.

[3]Guest Observer, International Ultraviolet Explorer.

(ref. 1 and references therein). However, with the advent of the International Ultraviolet Explorer (IUE) satellite, the resonance lines of Mg II are now available for theoretical analysis. The height of formation of the h and k lines is somewhat greater than the height of formation of the Ca II H and K resonance lines. Furthermore, Mg II can be represented with a simple atomic model. Hence the radiative transfer can be solved more accurately to yield more reliable results. In the following we will offer a brief quantitative assessment of low dispersion Mg II h and k line observations of dMe and dM stars.

RESULTS

The stars observed, their spectral types and the Mg II (h + k) line fluxes at the earth are given in the first three columns of table I[4]. The spectral types are taken from reference 2 except for 61 Cyg B. The spectral type for this star is given in reference 3. The relations between stellar angular diameter and (V-R) color (refs. 4, 5) convert the observed flux to surface flux. The (V-R) color index for each star follows from reference 6 (the (V-R) color for AT Mic is not available). The ratio of the Mg II (h+k) stellar surface flux to the same quantity for the mean Sun is listed in column 4 of table I. This ratio is based upon the mean solar value of the Mg II h and k line flux given in reference 7. The importance of chromospheric non-radiative heating in this sample of M dwarf stars considered here can be readily intercompared through the ratio

$$R_{hk} = F(\text{Mg II h+k})/\sigma T_{eff}^{4},$$

where R_{hk} represents the chromospheric radiative losses in the h and k lines normalized to the total stellar surface flux. We assume that the radiative equilibrium contribution to the h and k line fluxes is negligible in these cool dwarfs. The values of R_{hk} are listed in column 5 of table I. The effective temperatures for GL 380 and GL 411 are taken from reference 8. The values of T_{eff} for EQ Vir and YZ CMi are taken from reference 9. The effective temperature of 61 Cyg B is taken from reference 10 while that for UV Ceti is estimated from its spectral type and reference 11. Values of R_{HK}, the analogous quantity for the Ca II H and K lines, are taken from reference 8 and listed in column 6 of table I (the R_{HK} value for 61 Cyg B follows from reference 10 while the R_{HK} values for EQ Vir and YZ CMi given in reference 8 have been modified to reflect the new T_{eff} measurements presented in reference 9). Finally, we list in column 7 of table I the ratio of the Mg II (h+k) line fluxes to the Ca II (H+K) line fluxes. Omitted entries in table I indicate that the particular value is not available.

DISCUSSION

The values of the ratio F(Mg II h+k)/$F_{\odot}$(Mg II h+k) are less than unity, with the exception of the most active star (as defined by the R_{hk} values), EQ Vir. The values of R_{hk} for the dMe stars are basically an order of magnitude greater than for the dM stars. Furthermore, F(Mg II h+k)/$F_{\odot}$(Mg II h+k)

[4]The observed Mg II fluxes for YZ CMi and UV Ceti have been kindly provided by K. G. Carpenter and R. F. Wing in advance of publication.

increases with increasing R_{hk}. In addition, the ratio F(Mg II h+k)/F(Ca II H+K) is greater than unity (with the exception of GL 380) for the sample considered here. Thus the Mg II resonance lines generally play a more important role in the overall chromospheric energy balance in dMe and dM stars than do the Ca II H and K resonance lines. However, there is an important caveat that must be noted: the Mg II data and the Ca II data discussed in this investigation were not acquired simultaneously. Thus the emergence and decay of stellar surface activity combined with the rotational modulation of these features are likely to cause variations in the observed net chromospheric radiative losses. Therefore data sets obtained at widely separated times of observation cannot be confidently compared on a star-by-star basis (with the possible exceptions of the "most active" and the "least active" stars). We can, however, partially circumvent this difficulty by comparing the mean values of physical quantities for a particular sample of stars. Since the degree of chromospheric activity among stars in a given sample is uncorrelated, the mean values of physical quantities will remain relatively constant. We thus find the mean value of the ratio F(Mg II)/F(Ca II) to be 2.85. This is similar to the mean solar value of 2.5 (ref. 10). The mean values of R_{hk} and R_{HK} are $\overline{R_{hk}} = 8.6$ (-5) and $\overline{R_{HK}} = 3.3$ (-5). The ratio $\overline{R_{hk}}/\overline{R_{HK}}$ is 2.6 which is even closer to the solar value of 2.5. Thus we conclude that the mechanism which determines the relative contributions of certain spectral lines to the energy balance in the chromosphere must be similar in the late-type, main sequence dwarf stars.

An approach to account for the degree of chromospheric emission in M dwarf stars is to assume that the dM and dMe stars fundamentally differ from each other in terms of the fractional area of their surface which is covered by active (plage) regions. The active region filling factor can be crudely estimated according to the following expression (ref. 12)

$$F = A\,F_a + (1-A)\,F_Q, \qquad (1)$$

where A is the dimensionless ratio of the area of the active region to the area of the visible quiet stellar surface. The symbols F_a and F_Q represent the Mg II h and k line surface flux for an active and quiet region, respectively. The underlying assumptions which lead to equation (1) are given in reference 12. The values of A based upon the Mg II h and k fluxes presented in this investigation are given in column 2 of table II. We also list in column 3 of table II the values of A given in reference 12. These filling factors are based upon the Ca II H and K line data presented in reference 8. In order to compute the relative active region filling factors it was necessary to arbitrarily define $A \equiv 1$ for EQ Vir and $A \equiv 0$ for GL 411 (ref. 12). Excluding these extreme values, we find the mean values A (Mg II) = 0.15 and A (Ca II) = 0.07. Of course the small size of the sample renders a comparison of these two estimates of active region filling factors less meaningful. However, it is interesting to note that model chromospheres deduced from the Ca II K-line profiles of reference 8 underpredict the Mg II k-line flux by an order of magnitude or more for a subset of the dMe and dM stars discussed in this investigation (ref. 13). In summary, the apparently discrepant mean active region filling factors derived from the Ca II H and K and the Mg II h and k lines combined with the failure of model chromospheres to reconcile two overlapping chromospheric spectral features suggest that single-component, homogeneous model atmospheres are not physically realistic representations of

M dwarf stars.

The stellar chromospheric emission features probably arise from plage regions which are, in turn, composed of magnetic flux tubes. A schematic model of a magnetic flux tube is presented in figure 1. The levels h_1 and h_2 represent the heights of formation of the Ca II K-line and the Mg II k-line, respectively. We consider a flux tube in hydrostatic equilibrium. Therefore

$$P_{ext}(h) = P_g(h) + [B(h)]^2/8\pi,$$

where $P_{ext}(h)$ is the external (field-free) gas pressure at height h, $P_g(h)$ is the internal gas pressure and B(h) is the internal magnetic field strength, also at height h. We ignore turbulent pressure in this preliminary analysis. At the levels h_1 and h_2 we have

$$P_1^{ext} = P_1^{g} + B_1^{2}/8\pi,$$

$$P_2^{ext} = P_2^{g} + B_2^{2}/8\pi.$$

Now $P_2^{ext} < P_1^{ext}$ by the constraint of hydrostatic equilibrium. But $B_2 < B_1$ in a flux tube characterized by diverging field lines (see fig. 1). Thus it is possible for $P_2{}^g > P_1{}^g$, which would lead to enhanced Mg II k-line emission. The condition $P_2{}^g > P_1{}^g$ occurs if the inequality

$$B_1^{2} - B_2^{2} > 8\pi\ (P_1^{ext} - P_2^{ext})$$

is fulfilled. An alternative way to conceptualize the problem is to note that the emission area (filling factor) for the k line, A_2, is greater than the emission area for the Ca II K line, A_1, as shown schematically in figure 1. Of course a proper analysis of the chromospheric line spectrum in a magnetic flux tube requires a two-dimensional radiative transfer calculation since the flux tube is in radiative exchange with its surroundings. Moreover, the importance of lateral turbulent heat exchange will change along a flux tube as the field decreases with height (refs. 14, 15).

CONCLUSIONS

The Mg II h and k line data and the transition region line data from IUE combined with Balmer line and H and K line data for the dMe and dM stars offer us the unique opportunity to construct self-consistent stellar model chromospheres. We further suggest that multi-component model atmospheres are more realistic physical representations of stellar chromospheres. In particular, we hypothesize that a detailed consideration of the line spectrum arising from magnetic flux tubes is required in order to reconcile various chromospheric spectral line diagnostics.

REFERENCES

1. Linsky, J. L.: Ann. Rev. Astron. Ap., in press, 1980.

2. Kunkel, W. E.: Variable Stars and Stellar Evolution, ed. V. E. Sherwood and L. Plant (Dordrecht: Reidel), 1975.

3. Kelch, W. L., Linsky, J. L. and Worden, S. P.: Ap. J., 229, 700, 1979.

4. Barnes, T. G. and Evans, D. S.: M.N.R.A.S., 174, 489, 1976.

5. Barnes, T. G., Evans, D. S. and Parsons, S. B.: M.N.R.A.S., 174, 503, 1976.

6. Veeder, G. J.: A. J., 79, 1056, 1974.

7. Linsky, J. L. and Ayres, T. R.: Ap. J., 220, 619, 1978.

8. Giampapa, M. S., Worden, S. P., Schneeberger, T. J. and Cram, L. E.: Ap. J., in press, 1980.

9. Pettersen, B. R.: Astron. Ap., in press, 1980.

10. Linsky, J. L., Worden, S. P., McClintock, W. and Robertson, R. M.: Ap. J. (Supplement), 41, 47, 1979.

11. Allen, C. W.: Astrophysical Quantities (London: Athlone Press), 1976.

12. Giampapa, M. S.: S.A.O. Spec. Pub., "Proceedings of the Conference on Cool Stars, The Sun and Stellar Systems," in press, 1980.

13. Giampapa, M. S.: Ph.D. Dissertation, University of Arizona, 1980.

14. Zwaan, C.: Mem. S. A. It., p. 525, 1977.

15. Zwaan, C.: Solar Phys., 60, 213, 1978.

TABLE I. - SUMMARY OF IUE Mg II (h+k) OBSERVATIONS

Star	Spectral Type	f*(Mg II)	F*(Mg II)	$\frac{F}{F_\odot}$(Mg II)	R_{hk}	R_{HK}	F(Mg II)/F(Ca II)
EQ Vir	dK5e	1.36 (-12)	2.67 (6)	2.12	1.71 (-4)	1.2 (-4)	1.43
61 Cyg B	dM0	6.52 (-12)	3.10 (5)	0.25	2.92 (-5)	8.2 (-6)	2.67
GL 380	dM0	8.19 (-13)	4.95 (4)	0.04	3.97 (-6)	1.0 (-5)	0.38
GL 411	dM2	5.79 (-13)	3.33 (4)	0.03	4.39 (-6)	1.4 (-6)	3.06
AT Mic	dM4.5e	3.94 (-12)	----	----	----	----	----
YZ CMi	dM5.5e	1.26 (-12)	9.37 (5)	0.75	1.68 (-4)	2.5 (-5)	6.72
UV Ceti	dM6e	6.41 (-13)	4.00 (5)	0.32	1.40 (-4)	----	----

* Units: ergs - cm^{-2} - s^{-1}

TABLE II. - ACTIVE REGION FILLING FACTORS

STAR	A (Mg II)	A (Ca II)
EQ Vir	≡ 1.0	≡ 1.0
61 Cyg B	0.10	0.065
GL 380	0.01	0.07
GL 411	≡ 0.0	≡ 0.0
AT Mic	---	---
YZ CMi	0.34	0.07
UV Ceti	0.14	---

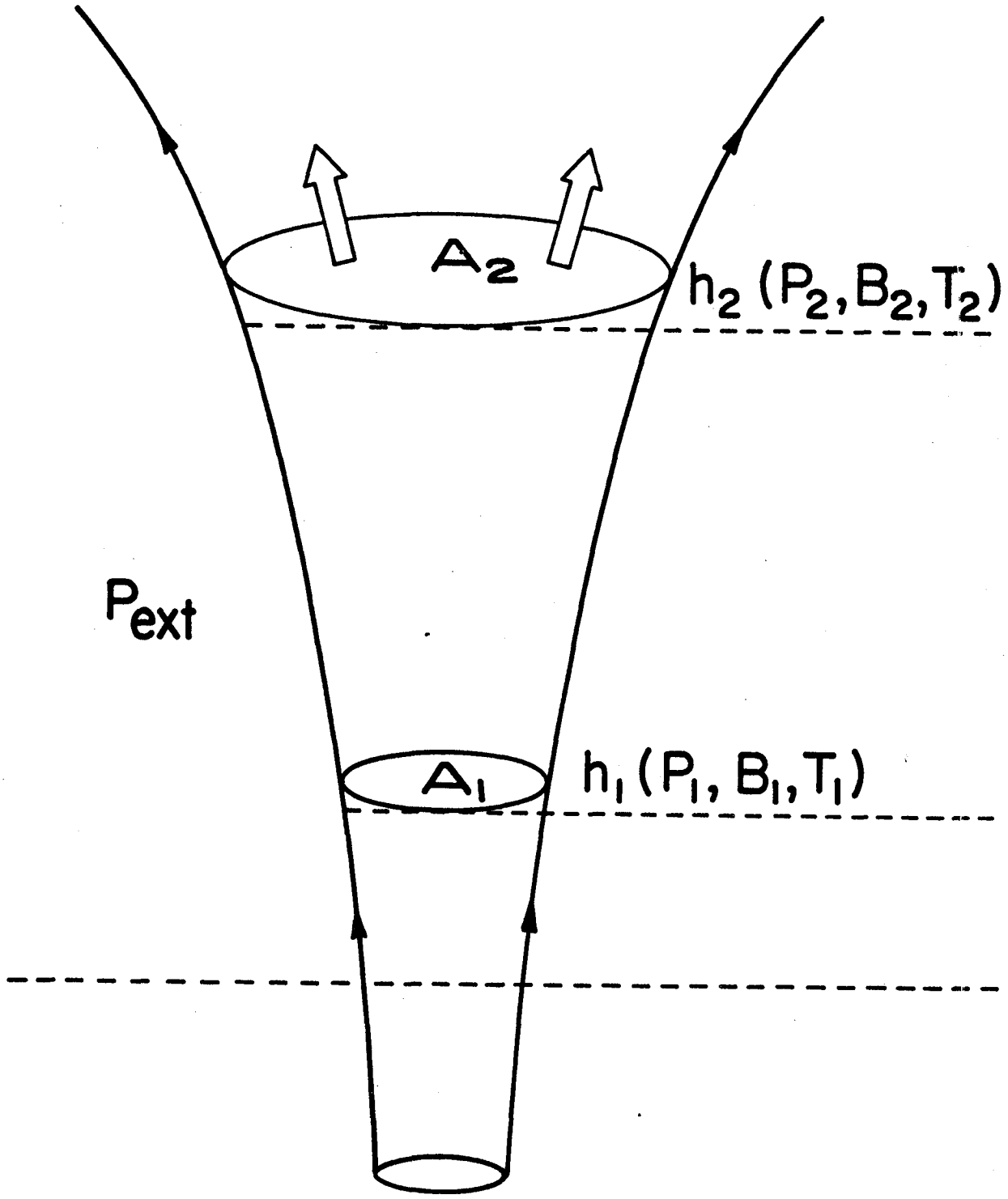

Figure 1. - Schematic model of a magnetic flux tube.

IUE SPECTRA OF F AND LATE A STARS[1]

Jeffrey L. Linsky[2,3] and Norman C. Marstad
Joint Institute for Laboratory Astrophysics
National Bureau of Standards and University of Colorado

ABSTRACT

We report on IUE spectra of α CMi (F5 IV-V), β Cas (F2 IV), α Car (F0 Ib), and γ Boo (A7 III) in the context of the question as to whether chromospheres disappear in the early F-late A portions of the HR diagram. Both α CMi (Procyon) and β Cas show bright emission line spectra indicative of chromospheres and transition regions, but neither α Car (Canopus) nor γ Boo show any evidence of emission in their SWP spectra or at the Mg II lines, despite very deep exposures. These results are consistent with those recently published by Böhm-Vitense and Dettmann. We note that α CMi has emission line fluxes roughly 6 times those of the quiet Sun, but the rapidly rotating δ Scuti-type variable β Cas has surface fluxes 10-50 times those of the quiet Sun. Upper limits on emission line fluxes for α Car are 4-20 times those of the quiet Sun and for γ Boo are 15-80 times the quiet Sun. We conclude that the apparent absence of emission lines in the spectra of α Car and γ Boo should not be interpreted as due to the absence of nonradiatively heated outer atmospheres in stars hotter than spectral type F0, but rather to our inability to see emission lines with IUE against a background of scattered light and a bright photospheric absorption line spectrum either in low or high dispersion.

INTRODUCTION

We consider here the important question of whether the outer atmospheres of stars change in a fundamental way near spectral type F0 as convection zones become thin and carry little flux with increasing stellar effective temperature. The earliest-type stars with Ca II H and K line emission noted by Wilson (1966) in his 10 Å mm^{-1} photographic survey are at spectral type F5. These data, together with the empirical result that stellar rotational velocities decrease rapidly in the middle F stars (e.g. Kraft 1967) and the theoretical result that acoustic wave heating (the presumed chromospheric heating source) should decrease rapidly in the early F-type stars, led many authors to conclude that chromospheres disappear in the middle F stars. Subsequently, using higher dispersion spectra, Warner (1966,1968) found weak

---

[1]This work was supported by NASA through grants NAS5-23274 and NGL-06-003-057 to the University of Colorado.

[2]Staff Member, Quantum Physics Division, National Bureau of Standards.

[3]Guest Observer with the International Ultraviolet Explorer (IUE) satellite.

Ca II emission in Canopus (F0 Ib) and γ Vir N (F0 V), and Le Contel et al. (1970) reported occasional Ca II emission in the δ-Scuti-type star γ Boo (A7 III). Freire (1979) and Freire et al. (1977,1978) have searched for emission in the Ca II lines and ultraviolet C II and Si II lines in Vega (A0 V) and two other early A-type stars without success.

Böhm-Vitense and Dettmann (1980) have observed 21 F- and 13 A-type stars with IUE. They find that chromospheric emission lines begin to appear at $(B-V) \gtrsim 0.32$ (about spectral type F0) on the main sequence, but at the Cepheid instability strip for the more luminous stars. Our observations confirm their identification of an empirical dividing line for the appearance of chromospheric emission lines in the Hertzsprung-Russell (HR) diagram, but we feel that the data cannot determine whether chromospheres disappear in this region of the HR diagram.

OBSERVATIONS

We summarize the stellar parameters and our IUE observations in Tables 1 and 2. Since our goal was to search for emission features superimposed on a bright background consisting of the stellar ultraviolet absorption line spectrum and scattered near ultraviolet light, we obtained several exposures including very long exposures in which the long wavelength portions of the spectra are heavily overexposed.

The composite low dispersion spectra (deleting saturated pixels) are presented in Figure 1 in absolute flux units at Earth. The calibration factors used are those described by Turnrose et al. (1980) and Cassatella et al. (1980), except that the small aperture α CMi spectra were calibrated using the low dispersion fluxes of the strong C II λ1335 and C IV λ1550 doublets cited by Brown and Jordan (1980). These data imply that the transmission of the small aperture for our α CMi observations was 0.33. Since the α CMi spectra were obtained with the small aperture, we are able to measure fluxes in the Si III λ1206 and Lα features accurately.

Clearly both α CMi and β Cas exhibit bright emission lines due to chromospheric ions (O I, C I) and ions (C II, C III, C IV, Si IV, N V) formed at temperatures of $20\text{-}200 \times 10^3$ K, perhaps in geometrically thin regions analogous to the solar transition region. However, neither α Car nor γ Boo show any of these emission lines in the low dispersion data. A high dispersion SWP spectrum of α Car also shows no evidence for any emission features.

High dispersion spectra of the Mg II features in β Cas, α Car, and γ Boo are shown in Figure 2. These spectra show no clear evidence of Mg II emission, despite the very long exposure times to bring up the line cores to typically 150 DN. Böhm-Vitense and Dettmann (1980) call attention to a strong correlation between Mg II emission and the appearance of chromospheric emission lines in the SWP images. We feel that the apparent absence of Mg II emission in β Cas is probably due to rotational smearing of a weak emission feature in the core of an absorption line. Emission features appear in the 1200-1600 region of this star despite rotation smearing, because the contrast between the emission line flux and 6 Å of continuum is large. We find no

evidence for Mg II emission in α Car (see Fig. 2), although Evans et al. (1975) identify emission features in their Copernicus V2 spectrum of the star. We feel that our data have higher signal-to-noise and higher spectral resolution than their data. Thus we feel that the absence of Mg II emission in our data is real. Also interstellar absorption features in the cores of the Mg II lines can suggest double emission features which may not be present.

We list in Table 3 observed fluxes at Earth and probable identifications of emission features we consider to be real. Also given are flux upper limits for α Car and γ Boo. These are estimated as roughly equal to the flux in adjacent "emission" features with widths comparable to emission lines in β Cas and measured above a curved line drawn through the low points in the spectra. These "emission" features are probably stretches of continuum between absorption lines. Thus the "noise" in the α Car and γ Boo spectra is not true noise but rather the up and down character of absorption line spectra. Our estimates of emission line flux upper limits thus refer to the maximum emission line flux that could be confused with the absorption line spectrum and thus not identified as an emission line.

The observed fluxes were then converted to stellar surface fluxes using the Barnes-Evans relation for stellar angular diameters (cf. Linsky et al. 1979). The derived angular diameters and ratios of surface flux to flux observed at Earth are given in Table 1. Listed in Table 4 are quiet Sun surface fluxes cited by Linsky et al. (1978) and the ratios of stellar surface fluxes to quiet Sun surface fluxes.

DISCUSSION

The α CMi surface fluxes are about a factor of 6 times larger than the quiet Sun, whereas those of β Cas are typically 30 times larger than the quiet Sun. Brown and Jordan (1980) estimate transition region pressures for α CMi consistent with pressures at the top of the chromospheric model derived by Ayres et al. (1974). Since transition region surface fluxes in solar plages are typically 10 times the quiet Sun, the nonradiative heating rates in the outer atmosphere of β Cas exceed those of solar plages by a factor of 3. We know that chromospheric nonradiative heating rates are well correlated with stellar rotational velocities for stars of similar spectral type (e.g. Kraft 1967, Skumanich 1972), and there is growing evidence of a correlation between nonradiative heating rates in transition regions and coronae as well (Ayres and Linsky 1980, Linsky 1980). The significant increase in emission line surface fluxes from α CMi to β Cas is consistent with this picture. An alternative explanation for the large heating rate in the outer atmosphere of β Cas is dissipation of shock waves excited by the stellar oscillations.

We feel that the upper limits on the surface fluxes for emission lines in α Car and γ Boo are significant. For example, if one added emission lines with surface fluxes comparable to those of α CMi to the observed spectrum of α Car, these emission lines would be extremely hard to detect against the bright absorption line spectrum of α Car. Similarly, emission lines with surface brightnesses even as large as those of β Cas would be undetectable

against the bright absorption line spectrum of γ Boo. Thus, with IUE we are unable to determine whether or not chromospheres and transition regions cease to exist as one proceeds from the early F to hotter stars. All we can say is that our data and those of Böhm-Vitense and Dettmann (1980) show that chromospheres and transition regions cease to appear spectroscopically in the ultraviolet as observed with an instrument like IUE.

It is important to recognize the instrumental and astrophysical reasons behind the latter statement. The instrumental limitations of IUE are its limited signal-to-noise, sensitivity of the short wavelength cameras to scattered long wavelength light, halation in the image converters, and the potential for SEC Vidicon damage when oversaturating the long wavelength portion of an image to bring up the relatively weak short wavelength portion of the spectrum. As a result, we would caution future observers against taking even deeper exposures of early F- and late A-type stars, and we expect that deeper exposures would not be productive in any case. The High Resolution Spectrograph (HRS) now being built for Space Telescope (Brandt et al. 1979) will not have many of the limitations of IUE as it will include a solar blind, photon-counting detector capable of very high signal-to-noise, large dynamic range, and up to 1.2×10^5 resolution. With this instrument we expect that chromospheric emission lines will be detected in the late A-type stars until at some spectral type we will run into the fundamental astrophysical limitation of detecting weak emission features against a very bright photospheric absorption line spectrum.

Finally, we expect that most stars hotter than spectral type F0 probably contain nonradiatively heated outer atmospheres. This is based on the detection by Einstein of X-rays from many types of hot stars including O-type and WR stars, the A-type dwarfs Sirius A and Vega, and α Car (Vaiana et al. 1980). Also, Underhill (1980) has presented evidence for nonradiatively heated outer atmospheres (mantles) for O, B, and A-type supergiants. Thus nonradiatively heated outer atmospheres can be produced even in the absence of deep convection zones. Linsky (1980) and Underhill (1980) argue that magnetic fields, both remnant and dynamo regenerated, are responsible for nonradiative heating in most if not all stars.

We wish to thank Dr. A. Boggess and the staff of the IUE Observatory for their assistance in the acquisition and reduction of these data. We also wish to thank Dr. C. Jordan for permission to use her IUE fluxes of α CMi prior to publication.

REFERENCES

Ayres, T. R. and Linsky, J. L. 1980, Ap. J., in press.
Ayres, T. R., Linsky, J. L., and Shine, R. A. 1974, Ap. J., 192, 93.
Böhm-Vitense, E. and Dettmann, T. 1980, Ap. J., 236, 560.
Brandt, J. C. et al. 1979, SPIE, 172, 254.
Brown, A. and Jordan, C. 1980, in Proc. Second Year of IUE, Tubingen, in press.
Cassatella, A., Holm, A., Ponz, D., and Schiffer, F. H. 1980, NASA IUE Newsletter, No. 8, p. 1.

Evans, R. G., Jordan, C., and Wilson, R. 1975, M.N.R.A.S., 172, 585.
Freire, R. 1979, Astr. Ap., 78, 148.
Freire, R., Czarny, J., Felenbok, P., and Praderie, F. 1977, Astr. Ap., 61, 785.
_____. 1978, Astr. Ap., 68, 89.
Johnson, H. L., Mitchell, R. I., Iriarte, B., and Wisniewski, W. Z. 1966, Comm. Lunar Planetary Lab., 4, 99.
Kraft, R. P. 1967, Ap. J., 150, 551.
Le Contel, J. M., Praderie, F., Bijaoui, A., Dantel, M., and Sareyan, J. P. 1970, Astr. Ap., 8, 159.
Linsky, J. L. 1980, Proc. Workshop on Cool Stars, Stellar Systems and the Sun, S.A.O. Special Report, in press.
Linsky, J. L. et al. 1978, Nature, 275, 389.
Linsky, J. L., Worden, S. P., McClintock, W., and Robertson, R. M. 1979, Ap. J. Suppl., 41, 47.
Skumanich, A. 1972, Ap. J., 171, 565.
Turnrose, B., Bohlin, R., and Harvel, C. 1980, NASA IUE Newsletter, No. 8, p. 28.
Uesugi, A. and Fukuda, I. 1970, Cont. Inst. Ap. and Kwasan Obs., Univ. of Kyoto, No. 189.
Underhill, A. B. 1980, preprint.
Vaiana, G. et al. 1980, submitted to Ap. J.
Warner, B. 1966, Observatory, 86, 82.
_____. 1968, Observatory, 88, 217.
Wilson, O. C. 1966, Science, 151, 1487.

Table 1

STELLAR PARAMETERS

Star	HD	Spectral Type	V[a]	V-R[a]	Ang. Dia. (milliarcsec)	F/f[b]	v sin i[c] (km s^{-1})
α CMi	61421	F5 IV-V	0.37	0.42	5.94	4.82(15)	6
β Cas	432	F2 IV	2.27	0.31	1.99	4.29(16)	72
α Car	45348	F0 Ib	-0.75	0.24	6.97	3.50(15)	0
γ Boo	127762	A7 III	3.02	0.14	1.01	1.67(17)	145

[a]From Johnson et al. (1966).

[b]Ratio of surface flux to flux observed at Earth.

[c]Rotational velocities from Uesugi and Fukuda (1970).

Table 2
SUMMARY OF IUE OBSERVATIONS

Star	Spectral Type	IUE Image	Exp. Time (Min.)	Aperture[a]	Dispersion[b]
α CMi	F5 IV-V	SWP 1306	30	S	L
		SWP 1317	30	S	HI
		SWP 1318	6	S	L
		SWP 1319	10	S	L
		SWP 1320	20	S	L
β Cas	F2 IV	SWP 2372	26	L	L
		SWP 2373	6.5	L	L
		LWR 2156	11	L	HI
α Car	F0 Ib	SWP 2302	30	L	HI
		SWP 5439	1	L	L
		LWR 2083	0.67	L	HI
		LWR 4703	3	L	HI
γ Boo	A7 III	SWP 2395	24	L	L
		LWR 2172	16	L	HI

[a]S = small, L = large.

[b]L = low, HI = high.

Table 3
SUMMARY OF OBSERVED FLUXES[a]

Wavelength	Ion	α CMi	β Cas	α Car[c]	γ Boo[c]
1175	C III		1.1(-12)		
1206	Si III	3.5(-12)			
1216	H I[b]	4.1(-11)	1.6(-11)	<8(-12)	
1239	N V	1.5(-12)	3.2(-13)	<5(-12)	<2(-13)
1253	S II?		3.9(-13)		
1273	C I	2.8(-12)	4.4(-13):		
1304	O I	3.1(-12)	2.3(-12)	<5(-12)	<4(-13)
1316		6.9(-13):	3.5(-13):		
1335	C II	7.5(-12)	2.0(-12)	<5(-12)	<4(-13)
1354	O I	1.2(-12):	5.5(-13)		
1371	O V	1.0(-12):			
1394	Si IV	1.1(-12)	7.3(-13)	<5(-12)	<4(-13)
1403	Si IV+O IV	6.6(-13)	1.1(-12)	<5(-12)	<4(-13)
1440		2.0(-12):			
1466	C I	3.8(-12)			
1549	C IV	1.1(-11)	4.7(-12)	<1(-11)	<8(-13)

[a]Fluxes at Earth (ergs cm^{-2} s^{-1}).
[b]Uncorrected for interstellar absorption.
[c]Upper limits.

Table 4

STELLAR SURFACE FLUXES AND STELLAR/QUIET SUN SURFACE FLUX RATIOS

Feature	Quiet[a] Sun	α CMi[b]		β Cas		α Car[c]		γ Boo[c]	
		SF	SF/QS	SF	SF/QS	SF	SF/QS	SF	SF/QS
N V 1239	8.6(2)	7.2(3)	8	1.4(4)	16	<1.8(4)	<21	<3.3(4)	<38
C IV 1550	5.8(3)	5.3(4)	9	1.8(5)	31	<3.5(4)	<6	<1.3(5)	<22
Si IV 1394	1.7(3)	5.3(3)	3	3.1(4)	18	<1.8(4)	<11	<6.7(4)	<39
Si IV+O IV 1403	9.4(2)	3.2(3)	3	4.6(4)	49	<1.8(4)	<19	<6.7(4)	<71
C III 1175	1.6(3)			4.5(4)	28				
Si III 1206	3.4(3)	1.7(4)	5						
C II 1335	4.6(3)	3.6(4)	8	8.6(4)	19	<1.8(4)	<4	<6.7(4)	<15
O I 1304	4.0(3)	1.5(4)	4	1.4(5)	35	<1.8(4)	<5	<6.7(4)	<17
O I 1355	3.2(2)	5.8(3):	18:	2.4(4)	75				
H I 1216	2.1(5)	2.0(5)[d]	1	6.9(5)[d]	3	<2.8(4)[d]	<0.1		

[a]Quiet Sun fluxes cited by Linsky et al. (1978). Units ergs cm^{-2} s^{-1}.

[b]Absolute flux calibration by comparison with C II λ1335 and C IV λ1549 low dispersion fluxes in Brown and Jordan (1980).

[c]Upper limits estimated as equal to typical "noise" features in the spectra, which are probably sections of continuum between absorption features.

[d]Uncorrected for interstellar absorption.

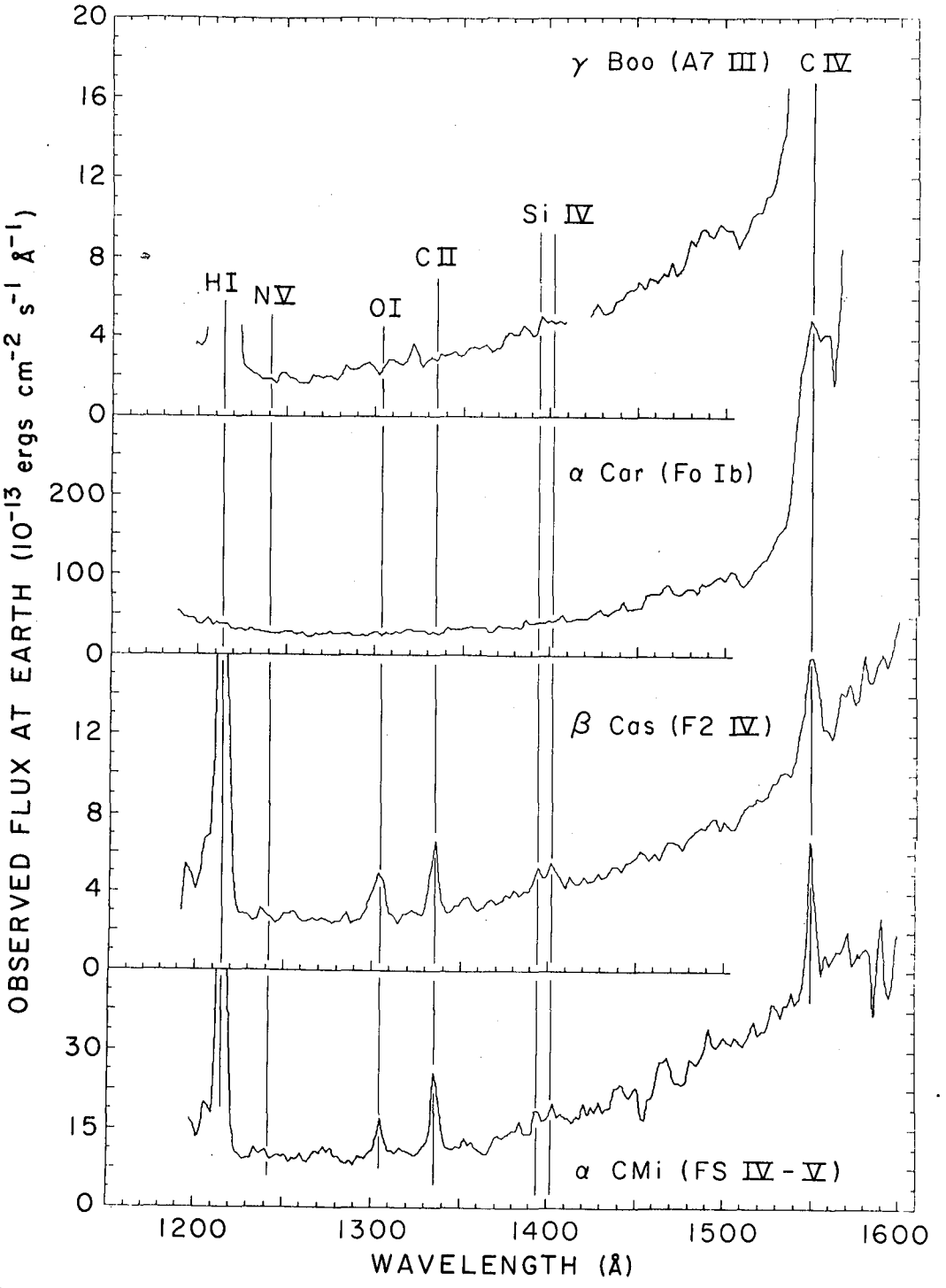

Fig. 1. Composite low dispersion spectra in absolute flux units at Earth. Vertical lines indicate the location of important emission lines that are present in the spectra of β cas and α CMi but absent in the spectra of γ Boo and α Car. These spectra are saturated beyond about 1600 Å, and scattered light is probably a major contributor to the apparent continua.

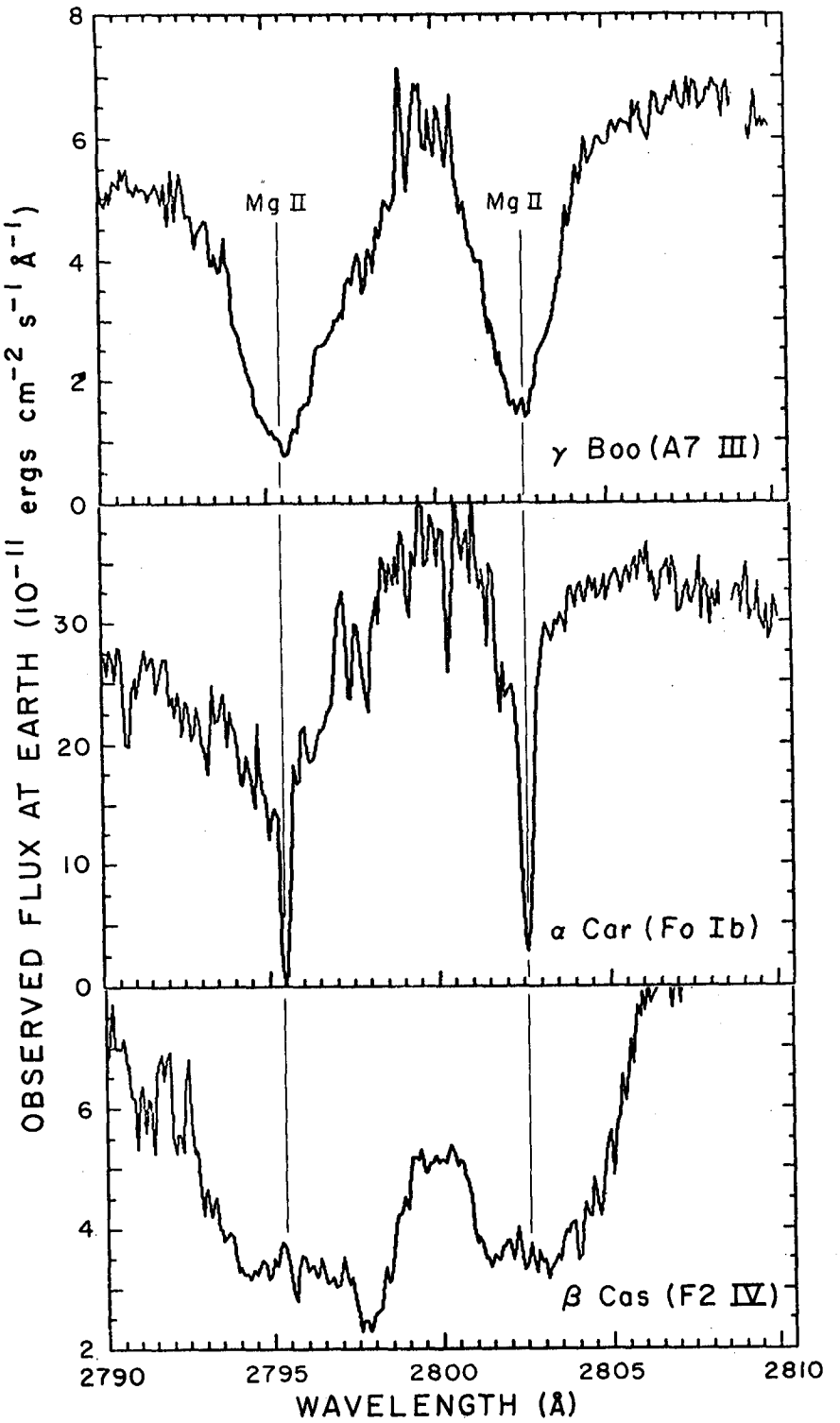

Fig. 2. High dispersion spectra in absolute flux units at Earth, obtained by merging the two echelle orders containing the Mg II lines. Despite the deep exposures used to bring up the cores of the Mg II lines, there are no apparent emission features. The deep absorption features in the Mg II lines of α Car are interstellar.

THE STRUCTURE OF CHROMOSPHERES AROUND LATE-TYPE GIANTS AND SUPERGIANTS

A. Brown, M. Ferraz and C. Jordan

Department of Theoretical Physics
Oxford University, 1 Keble Road
Oxford, OX1 3NP, England

ABSTRACT

Observations α Tau (K5III) and β Gru (M2II) made at high resolution have been used to confirm line identifications of features blended at low resolution. The high resolution spectra allow selected pairs of lines to be used to find the electron density, N_e, and the opacity, τ. These can be used together with the emission measure to place constraints on the structure of the atmosphere. The line formation processes are briefly discussed. Photo-excitation by strong lines appears to be important in these late-type atmospheres.

INTRODUCTION

Previous observations made with the IUE satellite have shown that giants and supergiants later than about K2 do not have significant emission in lines which in the sun would be formed in the chromosphere-corona transition region (Refs 1-5). Instead, the observed spectra are dominated by lines formed at $T_e < 2 \times 10^4$ K. In particular strong OI resonance line emission is observed, which in the sun and α Boo has been shown (Ref. 6,7) to be produced via H Ly β excitation to a higher OI level.

High-resolution spectra have now been obtained of α Tau (K5III) and β Gru (M2II) in order to study line fluxes and profiles and also to confirm identifications of lines blended at low resolution. These spectra show that the strong OI lines themselves excite lines of SI (uv 9) (Ref. 8), and confirm the importance of SI as a contributor to other features in late-type stars, as noted previously for α Ori (M2 Ib) (Ref. 2). A line at 1641.2A is attributed to OI pumped by the OI resonance lines.

In this paper methods of determining the opacity, and electron density in addition to the usual emission measure are presented. The mechanisms by which particular emission lines are excited are briefly discussed.

OBSERVATIONS

The dates, exposure times and resolution of spectra used in the analyses are given in Table 1. All were obtained using the large slot. The observations were made at the ESA VILSPA Satellite Tracking Station with the assistance of the Resident Astronomers.

The low-resolution spectra and samples of the high-resolution spectra have been previously published (Refs. 1, 8) and are not illustrated here. The

GPHOT image provided by VILSPA is the basis of the further data reduction in which spectra can be summed and overexposed pixels removed. An algorithm provided by Gondhalekar was used to correct for the error in the original intensity transfer function for the SWP camera. The flux calibration used is that provided by Bohlin and Snijders (Ref. 9) and by Cassatella and Selvelli (Ref. 10).

METHODS OF ANALYSIS

The quantity usually derived from absolute line flux is the emission measure, $\int N_e^2\, dh$. For lines of neutral and singly ionized atoms the contribution function may be broad, and the region of formation not clearly defined. Also, below $T_e \sim 2 \times 10^4$ K, where hydrogen is not fully ionized, the relevant quantity is $\int N_e N_H\, dh$. Thus it is preferable to find $\int N_e N_H g(T)\, dh$, where $g(T)$ is the temperature dependent part of the contribution function, as a function of temperature, and build up a self-consistent model by using several lines and independent determinations of N_e and τ ($\alpha \int N_H\, dh$).

The electron density N_e may in late-type giants and supergiants be found from the relative intensity of lines within the $2s^2 2p^2\ ^2P\text{-}2s2p^3\ ^4P$ multiplet of CII around 2325A. The transition probabilities have been calculated (Ref. 11) but cross-sections are available only by extrapolating data for OIV (Ref. 12) and NIII (Ref. 13). These approximate values lead to critical densities in the range 4×10^8 cm^{-3} to 6×10^7 cm^{-3}. With more accurate cross-sections the ratio of the CII multiplets at 1335Å and 2325Å may be used to determine T_e, providing collisional excitation is the dominant mechanism.

The opacity may be determined from the relative intensities of lines from a common upper level, where one of the lines is optically thin (Ref. 14). Using a simple probability of escape approach the ratio of the fluxes F, in two such lines is given by

$$F_1/F_2 = \lambda_2 b_1 q_1 / \lambda_1 b_2 q_2 \qquad (1)$$

where λ is the wavelength, b is the branching ratio, and q is the probability of escape, which is 1 for an optically thin line. Then since for a Gaussian line profile (Ref. 15),

$$q = 1 - \mathrm{erf}\left((\ln \tau_o)\ 1/2\right) \qquad (2)$$

where τ_o is the opacity at line centre, q and then τ_o can be found. The total opacity $\tau = 2\ \tau_o$ is given by

$$\tau = 1.2 \times 10^{-14}\ \lambda(A) f_{12} M^{1/2} \int \frac{N_E}{N_H} \frac{N_1}{N_{ion}} \frac{N_{ion}}{N_E} \frac{N_H}{T_i}\, 1/2\ ds \qquad (3)$$

where f_{12} is the absorption oscillator strength, M is the atomic weight, N_E, N_1, N_{ion} and N_H are the number densities of the element, lower level, ion (or atom) and hydrogen, respectively. T_i is the temperature corre-

sponding to the Doppler width of the line. Although some approximations are necessary initially, the quantity $\int N_H\, ds$ can be determined, providing checks on models such as that by Kelch et al. (Ref. 16) for α Tau. Table 2 gives some examples of pairs of lines which can be useful. The method may also be applied to numerous lines of FeII above 2000Å. The oscillator strengths required for CI are given in Ref. 14; for OI values by Garstang (Ref. 17) have been used; for SI values are tabulated by Wiese et al. (Ref. 18).

It should be noted that the analysis of emission line fluxes and profiles in these late-type stars may be complicated by the long ionization and recombination times expected at $T_e < 2\times10^4$ K and densities of $<10^9$ cm^{-3}; times of 10^3-10^4s are estimated for neutral and singly ionized species.

RESULTS

The present paper emphasizes methods since further work on the atomic models and atomic data is required before quantitative analyses are possible. Some preliminary results are given below.

In α Tau the OI 1304/1641 ratio leads to $\int N_H\, ds \sim 8 \times 10^{21}$ cm^{-2}, and the CI 1657.4/1994 ratio to $\int N_H\, ds < 6 \times 10^{21}$ cm^{-2}, assuming all the population to be in the ground term. The SI lines at 1296.17Å and 1302.87Å have approximately the same intensity indicating $\tau > 1$ in these lines, and giving $\int N_H\, ds > 2 \times 10^{19}$ cm^{-2}. These values of $6\text{-}8\times10^{21}$ are larger than expected from the model of the chromosphere of α Tau based on the MgII and CaII lines (Ref. 16). Also the absolute flux of the CII 2326Å line leads to an emission measure of $\sim 10^{28}$ cm^{-5} at 10^4K, again an order of magnitude larger than predicted. However, the CII 1335Å line is observed to be weaker than expected from CII 2325Å and improved excitation cross-sections are required before drawing definite conclusions regarding the temperature of formation. The SiII lines at 1808Å and 1817Å indicate other problems with the atomic model or cross-sections. They give an emission measure a further order of magnitude greater than found from CII 2326Å. It has been pointed out than in the sun the ^{2}D level can be excited predominantly from the metastable ^{4}P level rather than the ^{2}P level (Ref. 19). Cross-section calculations by Roberts (Ref. 20) supported this suggestion. However in α Tau and β Gru where $N_e<10^9$ cm^{-3}, the ^{4}P level does not acquire sufficient population for this explanation of the strength of ^{2}P-^{2}D to be appropriate. Either the cross-section for ^{2}P-^{2}D is still underestimated or other processes such as recombination or ionization are populating the metastable level. The absence of SiIII at 1892Å suggests however that the population of SiIII is low.

Simple estimates show that the OI emission in α Tau is too strong to be accounted for by collisional excitation or recombination but that the H Ly β excitation process could provide sufficient emission as in α Boo (Ref. 7).

Similar results are derived for β Gru. The opacity for OI is even larger, giving $\int N_H\, ds \sim 3\times10^{22}$cm^{-2}. The SI lines provide limits of $10^{19} < \int N_H\, ds < 4\times10^{22}$cm^{-2}. The CII 2325Å/1335 ratio again suggests a low

T_e or an overestimate of the 2325Å emission measure. The SiII 1808, 1817 lines require an emission measure an order of magnitude larger than that for CII 2325Å. For β Gru the CII $^2P-^4P$ line ratios can be used to determine N_e, giving a value of $\sim 10^8$ cm^{-3}.

The relative intensities of the FeII lines above 2000Å allow some general conclusions to be drawn. Although the FeI (mult. 44) lines pumped by the MgII emission (Refs. 21, 22) are observed in both α Tau and β Gru these lines are apparently not broad enough to pump FeII uv 32 or uv 373. Mult. uv 32 is present and its strength can be attributed to pumping by uv 1 which has an opacity of $\sim 10^3$. There is similar interlocking between the other multiplets observed. In β Gru uv 399, which terminates on the upper level of uv 63 is particularly strong, and the population of the upper and lower levels of uv 399 are comparable, indicating a selective population mechanism. It has been pointed out previously (Ref. 1) that H Ly α can excite levels in the 5p configuration of FeII, the classifications of which have been extended by Johansson (Ref. 23). These 5p levels can then decay to the 5s levels giving rise to uv 399 and similar multiplets. (Penston has privately pointed out the strength of uv 399 in RR Tel. and suggested recombination as a cause). Johansson found that charge exchange with NeII is important for FeI → FeII in laboratory sources. Since the FeII multiplets are important not only for stellar spectra but also for quasars and Seyfert galaxies it is of interest to investigate these possibililes further.

Finally, the possible role of H Ly α in photo-exciting (or effectively ionizing) high levels of SI is pointed out. The relative strengths of the SI 1425 and 1475 multiplets do not appear to be consistent with collisional excitation, using f-values and solar relative intensities as a guide to the cross-sections. The strong lines of SI observed ie. mult. uv 3, uv 2, uv 1, and uv 9 originate from the lowest terms formed by recombination from the three possible SII parents. The strength of the SI emission suggests a recombination or cascade spectrum following photo-ionization (or excitation) by radiation around H Ly β.

REFERENCES

1. Brown, A., Jordan, C., and Wilson, R. 1979 Proc. Symp. 'The First Year of IUE' (Ed. Willis) 232.

2. Carpenter, K.G. and Wing, R.F. 1979 Bull. Am. Astr. Soc. 11, 419.

3. Dupree, A.K., Black, J.H., Davis, R.J., Hartmann, L., Raymond, J.C. 1979 Proc. Symp. 'The First Year of IUE' (Ed. Willis) 217.

4. Dupree, A.K. 1979 'Highlights of Astronomy, 1979' In Press.

5. Linsky, J.L. and Haisch, B.M. 1979 Astrophys. J. Letts. 229, L27.

6. Shine, R.A., Lites, B.W., Chipman, E.G., Roussel-Dupre, D., Bruner, E.C., Rottman, G.R., Orrall, F.Q., Athay, R.G. and White, O.R. 1976 Bull. AAS, 8, 331.

7. Haisch, B.M., Linsky, J.L., Weinstein, A. and Shine, R.A. 1977 Astrophys. J. 214, 785.

8. Brown, A. and Jordan, C. 1980 Mon. Not. R. astr. Soc. In Press.

9. Bohlin, R.C. and Snijders, M.A.H. 1978 SRC IUE Newsletter No. 2.

10. Cassatella, A. and Selvelli, P.L. 1979 SRC IUE Newletter No. 4.

11. Dankwort, W. and Trefftz, E. 1978 Astron. and Astrophys. 65, 93.

12. Flower, D.R. and Nussbaumer, H. 1975 Astron. and Astrophys. 45, 145.

13. Nussbaumer, H. and Storey, P.J. 1979 Astron. and Astrophys. 71, L5.

14. Jordan, C. 1967 Sol. Phys. 2, 441.

15. Zanstra, H. 1949 Bull. Astron. Inst. Neth. 11, 1.

16. Kelch, W.L., Linsky, J.L., Basri, G.S., Chiu, H-Y., Chang, S-H., Maran, S.P., Furenlid, I. 1978 Astrophys. J. 220, 962.

17. Garstang, R.H. 1961 Proc. Camb. Phil. Soc. 57, 115.

18. Wiese, W.L., Smith, M.W. and Miles, B.M. 1969 'Atomic Transition Probabilities', Vol. II, NSROS-NBS 22, (US. Govt. Printing Office, Washington, D.C.).

19. Jordan, C. 1969 Astrophys. J. 156. 49.

20. Roberts, D.E. 1970 J. Phys. B. 3, 676.

21. Van der Hucht, K.A., Stencel, R.E., Haisch, B.M. and Kondo, Y. 1979 Astron. and Astrophys. Suppl. 36, 377.

22. Gahm, G.F. 1974 Astron. and Astrophys. Suppl 18, 259.

23. Johansson, S. 1979 Physica Scripta 18, 217.

Table 1

Spectra Obtained

Star	Type	Date	Exposure Time (min)	Resolution	Camera
α Tau	K5III	78/9/29	20	LO	SWP
		78/10/1	40	LO	SWP
		79/1/25	90	LO	SWP
		79/1/27	150	LO	SWP
		79/9/29	390	HI	SWP
		78/1/10	10	LO	LWR
		79/9/29	10	HI	LWR
β Gru	M2II	79/10/1	175	LO	SWP
		79/10/7	370	HI	SWP
		79/10/1	20	HI	LWR

Table 2

Opacity Sensitive Line Sets

Atom	Transition	ΔJ	λ(A)
CI	$2p^2\ ^3P\text{-}2p3s\ ^3P^\circ$	2-1	1658.1
		1-1	1657.4
		0-1	1657.9
	$2p^2\ ^1D\text{-}2p3s\ ^3P^\circ$	2-1	1993.6
	$2p^2\ ^3P\text{-}2p3s\ ^1P^\circ$	2-1	1614.5
		1-1	1613.8
		0-1	1613.4
	$2p^2\ ^1D\text{-}2p3s\ ^1P^\circ$	2-1	1930.9
OI	$2p^4\ ^3P\text{-}2p^33s\ ^3S^\circ$	2-1	1302.17
		1-1	1304.86
		0-1	1306.03
	$2p^4\ ^1D\text{-}2p^33s\ ^3S^\circ$	2-1	1641.30
SI	$3p^4\ ^3P\text{-}3p^34s''\ ^3P^\circ$	2-1	1296.17
		1-1	1302.87
	$3p^4\ ^3P\text{-}3p^34s\ ^3S^\circ$	2-1	1807.34
		1-1	1820.36
		0-1	1826.26

THE CHROMOSPHERIC AND TRANSITION LAYER EMISSION OF STARS WITH DIFFERENT METAL ABUNDANCES

Erika Böhm-Vitense[1)]
University of Washington

ABSTRACT

We report preliminary results on observations of chromospheric and transition layer emission of stars with different metal abundances. Metal deficient stars generally show reduced emission in the Mg II resonance lines and also in the other chromospheric and transition layer emission lines. This is interpreted as showing that energy fluxes other than acoustic fluxes must at least be co-responsible for the coronal and transition layer heating.

INTRODUCTION

Let me state in the beginning that this is not the final word on the subject matter but rather a progress report. We are continuing our observations.

To date we have looked at 13 metal poor stars of varying metal abundances and at one super metal rich star 31 Aql. By means of this study we want to get information about the heating mechanisms for the chromospheres, the transition layers and the coronae.

If only acoustic flux is responsible for the heating, we expect very little difference for population I and population II stars. The noise generation in the convection zones should be nearly the same since the convective velocities are hardly influenced by the metal abundances (Böhm-Vitense[1)] 1971).

[1)] Guest Investigator with the International Ultraviolet Explorer satellite, which is sponsored and operated by the National Aeronautics and Space Administration, by the Science Research Council of the United Kingdom and by the European Space Agency.

Under NASA Contract No. NSG 5398

If, however, we observe that the heating in the chromospheres and transition layers is different for metal poor stars then some other mechanism must be responsible for it. Judging from solar observations we would assume that it is the magnetic field. This may decay with increasing age of the stars.

THE OBSERVATIONS

GENERAL DESCRIPTION

13 metal deficient stars were observed up to now, excluding the two metal poor horizontal branch stars HD 109995 and HD 161817 which did not show any signs of chromospheric emission. Since for a given electron density and temperature the line emission is proportional to the metal abundance Z we purposely selected mainly stars of moderate metal deficiency.

A comparable number of normal metal abundance stars was also observed.

For most stars we have studied the cores of the Mg II resonance lines as well as the short wavelength chromospheric and transition layer emission line spectrum.

THE EMISSION IN THE MG RESONANCE LINES

In order to determine the absolute fluxes we used the absolute calibration of Castella and Selvelli[2] (1980) for the high resolution spectra, which gave somewhat lower values than a calibration of our measured average intensity at 2740±50Å by the absolute intensities measured by Thompson[3] et al. 1978 for λ~2740Å.

The results of our measurements for the k_2 emission line fluxes are displayed in Figure 1 where we have plotted the ratio RF of the flux in the Mg II k_2 line to the total flux σT_{eff}^4. We find generally lower Mg II emission for the metal deficient stars analoguous to the decreased Ca II K_2 emission. The reduction is about a factor three, surprisingly independently of the amount of metal deficiency.

THE SHORT WAVELENGTH EMISSION LINES

We have restricted this discussion to the intensities of the carbon lines at 1657Å(CI), 1335Å(C II) and 1549Å(C IV), which span nearly the whole range of temperatures observed.

The results of our measurements are given in Figures 2-4. We have not seen with certainty any shortwave emission lines in any of the metal deficient stars except some emission in the CI 1657Å line which often appears as a broad

feature. We do not quite know what we see. We have tried to estimate upper limits from little humps that may be real or not, or from looking at the noise of the tracings and estimate how large the intensity could be without being recognized as a line.

Unfortunately the upper limits are not as low as we would like them to be. We have to take still longer exposures of the brightest of the metal deficient stars.

We do not consider for the moment the 1657Å lines for HD 140283 and μ Cas, since we do not really know what they are. From the figures it is then clear that the higher the necessary temperature for the line emission, the steeper is the intensity decrease of the line with decreasing temperature. One gets the impression that the normal metal abundance stars break up into two branches. The high intensity branch being mainly populated by stars with some peculiarity. 31 Aql which appears to be super-metal rich, but is a high velocity star, does not know on which branch it belongs. The branches, though not very obvious, are still somewhat preserved on Figures 3 and 4.

We also see that the metal poor stars show less emission than the normal metal abundance stars. Again the reduction of the intensity is present for low metal deficiency as well as for large metal deficiencies.

Even for slight metal deficiencies we do not see with certainty any emission lines.

THEORETICAL IMPLICATIONS

The fact that the intensity reduction of the emission lines in metal deficient stars is not correlated with the degree of metal deficiency tells us that it is not a direct effect of the reduced metal abundance but rather due to a common property of all metal deficient stars which presumably is their large age. Since apparently metal enrichment happened fast the ages of all metal poor stars and the oldest normal metal abundance stars do not differ very much. We therefore conclude that the reduced chromospheric emission of metal poor stars tells us that the energy input into the chromospheres decreases with increasing age of the stars. Since the convection and therefore the acoustic flux do not change with time there must be an important additional energy input mechanism which does change with time. Solar observations suggest that it is the magnetic field even though the details of the heating mechanisms are not yet well understood. With increasing age of the stars rotation and with it the magnetic fields of the stars may decay (Kippenhahn[4] 1972).

We might ask is this conclusion not drawn too hastily? Could not the same amount of energy be fed into the outer layers of the stars, and we would not see the radiation because of the lower metal abundances or because of stratification differences like a lower electron density in the chromosphere and transition layer or a steeper temperature gradient?

If the same amount of energy is fed into the outer layers then the energy balance requires that it must come out somewhere. If it would come out as a stellar wind we might not see it. This wind would then have to be stronger than for stars with transition layer emission. A stronger wind however requires either higher coronal densities and/or higher temperatures. Both would lead to higher X-ray emission than for normal metal abundance stars, which is not observed. As Dr. Vaiana[5] (1980) points out, the X-ray emission of metal deficient stars is at the lower end of the observed X-ray flux distribution for stars.

A steep temperature gradient in the transition zone could lead to a large conductive heat transport back into the chromosphere, but since Mg II and Ca II emission is weak we do not see it being radiated away from the chromosphere either.

It then appears that less energy input into chromosphere, transition layer and corona is required for old stars, telling us that magnetic fields are important for the heating.

REFERENCES

1. Böhm-Vitense, E. 1971; Astron. and Astrophys. 14, 390.

2. Castella, A. and Selvelli, P. L. 1980, preprint.

3. Thompson, G. I., Nandy, K., Jamar, C., Monfils, A., Houziaux, L., Carnochan, D. J., and Wilson, R. 1978: Catalogue of Stellar Ultraviolet fluxes. The Science Research Council 1978.

4. Kippenhahn, R. 1973: In "Stellar Chromospheres", National Aeronautics and Space Administration.

5. Vaiana, G. 1980, Private communication.

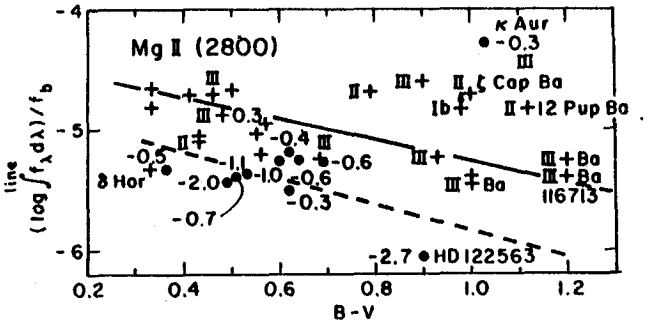

Figure 1: The Mg II (2795) k_2 emission line intensities $\int F_\lambda d\lambda$ divided by the bolometric flux F_b are plotted as a function of B-V for the stars. x mark stars with normal metal abundances or apparently super metal rich stars. Dots mark metal deficient stars. The log Z-log $Z_\odot$ values are given at the points. Luminosity classes are also indicated.

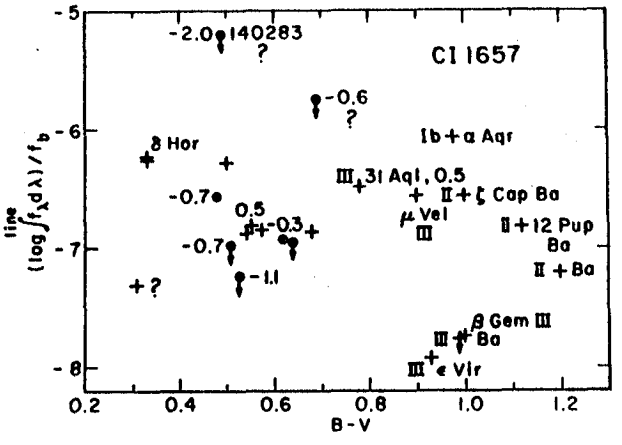

Figure 2: The emission line surface fluxes in the CI line at 1657Å divided by the total flux σT_{eff}^4 are plotted as a function of B-V of the stars. Notation as in Figure 1.

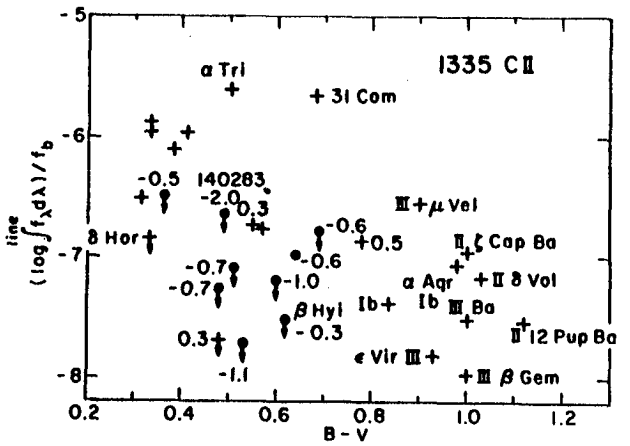

Figure 3: The emission line surface fluxes in the C II lines at 1335Å divided by the bolometric flux σT_{eff}^4 are plotted as a function of B-V. Notations as in Figures 1 and 2.

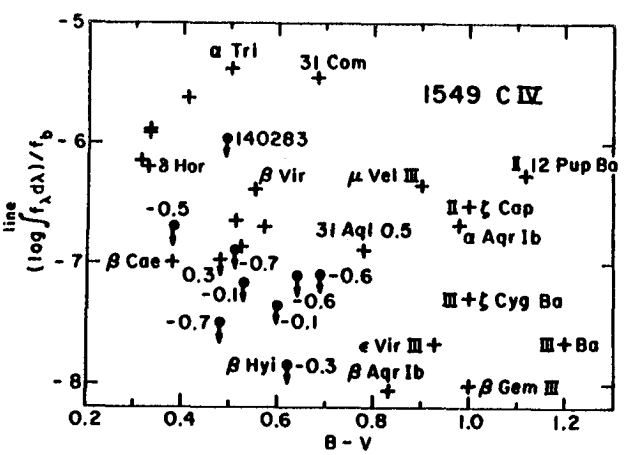

Figure 4: The emission line surface fluxes in the C IV lines at 1549Å divided by σT_{eff}^4 are plotted as a function of B-V. Notation as in Figures 1-3.

UV CHROMOSPHERIC AND CIRCUMSTELLAR DIAGNOSTIC FEATURES AMONG F SUPERGIANT STARS

Robert E. Stencel
Joint Institute for Laboratory Astrophysics
University of Colorado and National Bureau of Standards

Simon P. Worden
Sacramento Peak Observatory, AURA & S.A.M.S.O./U.S. Air Force

and

Mark S. Giampapa
Steward Observatory, University of Arizona

INTRODUCTION

We undertook a survey of F supergiant stars to evaluate the extension of chromospheric and circumstellar (CS) characteristics commonly observed in the slightly cooler G, K and M supergiant spectra. In the optical regions, the usual diagnostic spectral features are swamped by the brighter photospheric light in F stars. Therefore, an ultraviolet survey was elected since UV features of Mg II and Fe II might persist in revealing outer atmosphere phenomena even among F supergiants. Our survey encompassed spectral types F0 to G0, and luminosity classes Ib, Ia and Ia-0.

PROFILE TYPES

Four generic types emerged from our limited survey -- two indicative of chromospheres, one strictly photospheric and one indicative of CS envelopes (Figure 1).

CHROMOSPHERIC PROFILES

Optical and UV observations of the Sun and other G, K and M stars have revealed that the emission cores of the Ca II "H&K" (3933,3968 Å), and Mg II "h&k" (2795,2802 Å) resonance lines are valuable indicators of the existence of and conditions in stellar chromospheres. Such lines are very optically thick at line center and collisionally coupled to the excitation temperature (T_e) in the stellar atmosphere to heights above the temperature minimum and into the chromospheric temperature rise [cf. Stencel et al. (1)].

Doubly reversed emission is seen in the F8 Ib and G0 Ib stars surveyed, including γ Cyg, α UMi and β Aqr. However, the F8 profiles are strikingly different from the G0 type, despite a very small difference in T_e. β Aqr shows a strong longward dominated emission with substantial CS absorption superposed on the shortward emission component. In contrast, γ Cyg and α UMi show far weaker doubly reversed central emission features. In γ Cyg

it is difficult to be certain that the shortward emission component is not affected by CS absorption. Böhm-Vitense and Parsons have described γ Cyg as lacking in Mg II emission, suggesting to us that chromospheric or CS variability is at play, possibly as has been now seen for α Aqr (G2 Ib).

Among more luminous late F supergiants we find another Mg II profile type, characterized by δ CMa (F8 Ia), which shows strong shortward emission near line center, but no longward emission. This profile type is reminiscent of an inverse P Cygni profile and has been seen also in HD 96918 (G0 Ia-0) and ρ Cas (F8p Ia), where it is even more pronounced. To avoid the difficulties of invoking global chromospheric collapse (inverse of the standard P Cygni explanation), we could explain the appearance of such profiles by noting an excess longward absorption component, perhaps due to large scale downflows along the edges of giant cells (as seen in the solar network). This could obscure the longward emission and leave us with the observed inverse P Cygni profile. It is noteworthy that we find this chromospheric profile type only for stars of the highest intrinsic luminosity.

PHOTOSPHERIC PROFILES

As we look to F stars of warmer T_e, evidence in Mg II for chromospheric emission vanishes, presumably due to the increasing degree of ionization. For spectral types F0 to F5 we find repeatedly a smooth broad absorption feature with strongly damped line wings and a narrow Doppler core of essentially zero residual intensity. Examples of this include α Car (F0 Ib), ν Aql (F2 IB) and α Per (F5 Ib), all objects of comparable M_V. Among objects of greater intrinsic luminosity we find a hybrid profile -- strong damping line wings with a boxy, non-Doppler core. This boxy dark core is probably CS in origin and is seen in 1^1 Sco (F2 Ia), HD 74180 (F2 Ia) and in 89 Her (F2 Ia), except that 89 Her also reveals a trace of longward emission next to the CS absorption at line center. Again we find a distinct luminosity difference in the Mg II profiles.

CIRCUMSTELLAR PROFILES

Finally we detected one object which may provide the link between strong mass-losing stars like α Cyg (A2 Ia) and β Aqr (G0 Ib) in having qualitatively similar Mg II profiles. α Lep (F0 Ib) was found to have a pair of strong CS components shifted by -1.24 and -1.73 Å from line center. No chromospheric emission is obvious, although strong interstellar absorption at line center could obscure this. This CS structure suggests a substantial envelope and extensive mass loss. Alternately, one might identify the region between CS and line center absorptions as due to emission, but rather arcane radiative transfer effects might be required to verify such a picture. Success in CS profile modeling of αCYG by Kunasz should help to clarify the meaning of the α Lep profile.

THE OUTER ATMOSPHERES OF F SUPERGIANTS

With the IUE observations of our survey, it is possible to make some general comments regarding the atmospheric structure of F supergiant stars.

DETECTION OF CHROMOSPHERES

We have obtained high dispersion Ca II K line spectra for many of the stars in our UV study and find in general that outer atmospheric structure is far more apparent in the Mg II k line than in Ca II K. Hence the necessity for UV observations in this area is now clear. Deep exposures of the Ca II K line center for δ CMa and α Lep revealed only photospheric absorption without a hint of the striking profile structure seen in Mg II k. This occurs because the abundances and ionizations are different, but the general lack of significant chromospheric emission in Ca II K and Mg II k places strong constraints on the geometric extent of chromospheres since radiative losses in these lines (dominant sinks for G, K and M chromospheres) are minimal. Either the losses are confined to resonance lines of higher ions (hot chromospheres) or the chromospheres are "thin." Additional far UV and EUV observations will clarify this matter.

FAILURE OF THE WILSON-BAPPU EFFECTS

One of the aims of our survey was to determine the usefulness of the emission line width-to-luminosity correlation in use for the G-M stars in both the Ca II and Mg II lines [Wilson and Bappu (2), Weiler and Oegerle (3)]. In Table 1 we collect relevant information on our survey stars and present measured widths and infer M_V where possible. Inspection reveals that only the F8-G0 Ia-0 stars are even approximated in this way. We conclude that the Wilson-Bappu and Weiler-Oegerle correlations are probably not suitable for stars earlier than G0, because of significant physical differences in emission core formation as compared to cooler stars. We have already noted the striking difference between F8 and G0 Ib stars despite the small change in T_e. Some combinations of rotation, pulsation, evolution and magneto-acoustic effects makes the respective chromospheric signatures quite different. Whereas the wing emission lines of Ca II [Stencel (4)] are useful among F-M stars in evincing mass loss and indicating M_V, we found no comparable features in the Mg II line wings among F supergiants.

VELOCITY FIELDS

Where Mg II emission cores are seen, asymmetries can be interpreted as indicative of globally averaged motions. The near symmetric profiles of γ Cyg and α UMi suggest that inflow and outflow roughly cancel -- as they would in large scale convection-like motions. The inverse P Cygni profile of the F8 Ia-0 stars is more difficult to understand, but could arise from extensive network-like structures which are the sites of material downflow, vis-a-vis the Sun. A height dependent ionization transition could help accomplish this, i.e., hot (Mg III) matter wells up at the centers of large cells and cools (Mg II) as it begins its descent along the cell boundaries (the network). The alternative explanation for an inverse P Cygni profile, that of a collapsing envelope, might have its place in the evolutionary scenario for such volatile objects, but it is difficult to reconcile with other indicators for substantial stellar winds and mass loss, especially for ρ Cas.

Where CS core absorption is seen, assuming one can disentangle the interstellar component, the width and/or displacements from line center argue for significant stellar winds, mass loss and CS envelopes. As has been described by Lamers et al. (5) for α Cyg, stars like α Lep may provide additional evidence for the sporadic, non-continuous or "puffy" mass loss since we clearly detect a pair of outward moving shells.

FUTURE RESEARCH

With the limited time available for our survey, we did not have the opportunity to explore the SWP (1200-2000 Å) region of F supergiant spectra, nor the detailed comparison between Cepheid and non-Cepheid objects in this region of the HRD. Because of increasing continuum brightness, it will probably be difficult to clearly identify emission lines arising from any analog of the solar 'transition region' (TR: 100,000 to 250,000 K), or from cooler coronal hole outflow sites (CH: <25,000 K). Representative lines would include: TR -- N V 1240 Å, Si IV blend at 1400 Å and C IV 1550 Å; CH -- O I 1300 Å. Again, Böhm-Vitense and Parsons have surveyed similar stars and hopefully will describe their findings at this conference and elsewhere. A comprehensive survey would clarify the distribution of chromospheres, TR, coronae and CS material among the F supergiants.

We thank A. Boggess and his dedicated staff for assistance in obtaining and analyzing data under program LFBSW, as well as for contractual support. Mg II region spectral plots of stars mentioned herein will be available on request for a limited time from the first author.

REFERENCES

1. Stencel, R., Mullan, D., Linsky, J., Basri, G., and Worden, S. "The Outer Atmospheres of Cool Stars. VII. High Resolution, Absolute Flux Profiles of the Mg II h & k Lines in Stars of Spectral Types F8 to M5," 1980 Astrophys. J. Suppl., in press.

2. Wilson, O. and Bappu, V. "H and K Emission in Late-Type Stars: Dependence of Line Width on Luminosity," 1957 Astrophys. J. 125, 661.

3. Weiler, E. and Oegerle, W. "A COPERNICUS Survey of Mg II Emission in Late-Type Stars," 1979 Astrophys. J. Suppl. 39, 537.

4. Stencel, R. "Extensions of the Wilson-Bappu Effect Among Very Luminous Stars," 1978 IAU Colloquium 80: The Hertzsprung-Russell Diagram, ed. A. Davis-Philip and D. Hayes (D. Reidel, Dordrecht), p. 59.

5. Lamers, H., Stalio, R., and Kondo, Y. "A Study of Mass Loss from the Mid-UV Spectrum of α Cyg, β Ori and ϵ Leo," 1978 Astrophys. J. 223, 949.

TABLE 1. - Comparison of Mg II k and Ca II K in F Supergiants

Star	Sp. Type	LWR#[a]	Exp.	M_v [b]	Mg II k Profile	Mg II k W_o [c]	Mg II k $M_v(k)$ [d]	Ca II K Profile	Ca II K W_o [c]	Ca II K $M_v(K)$ [e]	UV Fe II Emission?
α Car	F0 Ib	4703	3	-4.8	No em.	--	--	No obs.			No
α Lep	F0 Ib	5021	16	-4.5	CS&IS	1.2CS	--	No em.+CS	1.0a	--	No
ν Aql	F2 Ib	5015	70	-4.7	Wk.em?	--	--	No em.	0.9CS?	--	No
ι^1 Sco	F2 Ia	5046	25	-8.4	CS core	1.4CS	--	No em.	1.1CS?	--	No
HD 74180	F2 Ia	5043	60	-8.4	CS core	1.0CS	--	No. obs.			No
89 Her	F2 Ia	5047	100	-8.4	CS+em?	2.1CS	--	CS+w.e.*	2.2CS	--	Yes
α Per	F5 Ib	5018	14	-4.6	No em.	--	--	Wk. em.	1.5e?	-2.8	No
δ CMa	F8 Ia	5020	20	-7.5	Inv. P Cyg	2.3HW	-5.9	No em.	0.3core	--	Weak?
α UMi	F8 Ib	5017	15	-4.6	DR em.	1.8	+0.3	No em.	0.6core	--	No
γ Cyg	F8 Ib	5016	25	-4.6	DR em+CS?	2.3	-1.3	No em.+w.e.	0.6core	--	No
ρ Cas	F8p Ia	5014	447	-9:	Inv. P Cyg	2.1HW	-5.3	CS+w.e.	1.8CS	--	Yes
HD 96918	G0 Ia0	4702	75	-9:	Inv. P Cyg	2.9HW	-7.4	No obs.			Yes
β Aqr	G0 Ib	4446	18	-4.5	DR em.+CS	3.8	-4.6	Wk.em.	2.0	-4.7	No

[a] Large aperture, high dispersion; exposure time in minutes.

[b] Data from Patterson and Neff, 1979 Astrophys. J. Suppl. 41, 215.

[c] Emission base width ($\Delta\lambda_{k\ 1}$), half width (HW) or CS absorption width, in Å.

[d] $M_v(k) = -15.15 \log W_o(\text{km/sec}) + 34^m.93$.

[e] $M_v(K) = -15.0 \log W (\text{km/sec}) + 28^m.0$.

* Wing emission lines, cf. Stencel 1977 Astrophys. J. 215, 176.

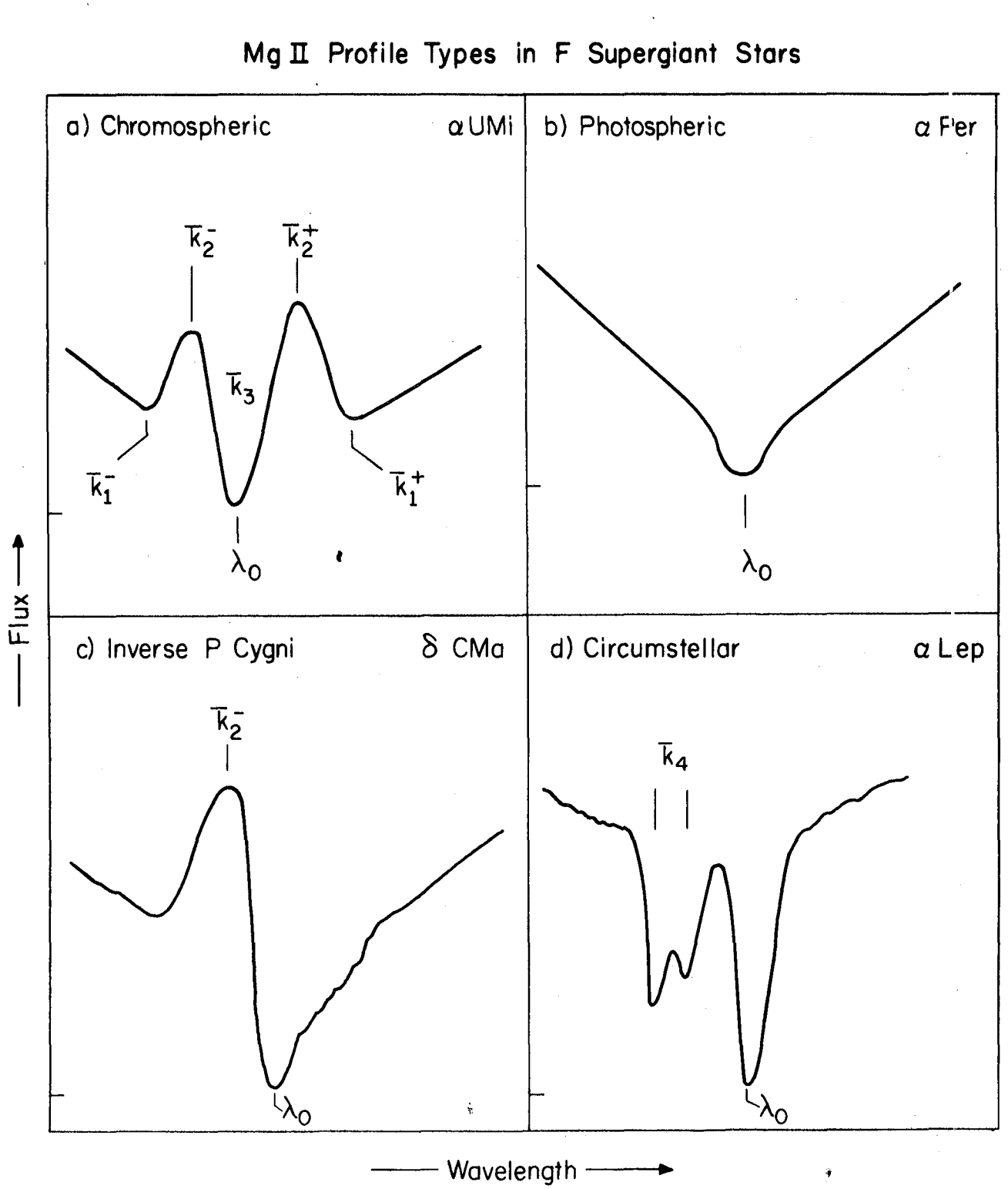
Mg II Profile Types in F Supergiant Stars
a) Chromospheric
α UMi
b) Photospheric
α Per
c) Inverse P Cygni
δ CMa
d) Circumstellar
α Lep
Flux
Wavelength

Figure 1

HIGH RESOLUTION ABSOLUTE FLUX PROFILES OF THE MG II h & k LINES IN EVOLVED F8 TO M5 STARS

Robert E. Stencel[1]
Joint Institute for Laboratory Astrophysics
University of Colorado and National Bureau of Standards

Dermott J. Mullan[1]
Bartol Research Foundation, University of Delaware

Gibor S. Basri
Department of Astronomy, University of California at Berkeley

Jeffrey L. Linsky[1,2]
Joint Institute for Laboratory Astrophysics
University of Colorado and National Bureau of Standards

"One in Five Stars is Remarkable" -- O. Struve

INTRODUCTION

We present the central results of a survey of the Mg II resonance line emission in a sample of over 50 evolved late-type stars, including spectral-luminosity types F8-M5 and Ia-IV. Observed and surface fluxes have been derived and correlations noted. The major findings include: a) Mg II k emission core asymmetry transition near K1 III, analogous to that known for Ca II K; b) a small gravity and temperature dependence of the Mg II chromospheric radiative loss rate. These results and others are fully discussed in a report in press in the Astrophysical Journal Supplement Series [Stencel et al. (1)], encompassing IUE second year programs CCBDM, CMBRS and LFBSW.

MESSAGES IN THE MG II PROFILES

We posit that asymmetry in the doubly-reversed emission core of collisionally-dominated resonance lines (e.g. Mg II k, Ca II K) can be used to infer chromospheric velocity fields, once the interstellar component is accounted for. We recognize the uniqueness problems of inhomogeneous atmospheres with arbitrary relative motions. However, the thrust of the observed asymmetry transitions and Occam's Razor provide us with some degree of confidence in the interpretation we choose.

A SHORT HISTORY LESSON

A fascinating observational connection between chromospheric velocity fields, mass loss and the existence of stellar coronae has developed over the past few years. The extensive high dispersion work on cool stars by Olin

[1]Guest Observer with the International Ultraviolet Explorer (IUE) satellite.
[2]Staff Member, Quantum Physics Division, National Bureau of Standards.

Wilson has been re-surveyed by Reimers (2) and Stencel (3) who discussed evidence for mass loss in Ca II K_4 features and the occurrence of Ca II "wing emission" features, respectively, in the Hertzsprung-Russell Diagram (HRD). Both found evidence for mass loss above a locus in the HRD running between mid-K giants and early-G supergiants. Stencel (4) also pointed out that the Ca II K core emission asymmetry was K_2R* dominated above a similar locus. Contemporaneously, Mullan (5) described his seminal STL (supersonic transition locus) theory which predicts a significant increase in mass loss rate for stars above a locus similar to that just described observationally. In addition to velocity information, temperature information has been added by Linsky and Haisch (6) and Vaiana et al. (7) who looked for high excitation (100,000 K) UV lines, and soft X-ray flux, respectively, and found that stars cooler and more luminous than K1 III rarely exhibit evidence for outer atmosphere material much hotter than about 20,000 K. The anti-correlation of coronae and strong mass loss seemed established. The analogy with solar coronal holes and active region loops was irresistible. But the simplicity of the scenario may also prove to be its downfall, as we shall see shortly.

STUDY OF THE MG II EMISSION ASYMMETRY

We undertook a survey of cool stars to establish whether Mg II might exhibit an asymmetry bifurcation in the HRD comparable to that known for Ca II K. Our initial sample of over 40 late-type stars (G and K, luminosity classes II, III and IV) showed that a rough segregation does exist along the lines of that seen for Ca II [Stencel and Mullan (8)]. However, the asymmetry locus was "fuzzy" with several discrepant stars on either side of the dividing line. Initially we considered these discrepancies as due to small number statistics, but careful analysis of the strength of interstellar (IS) Mg II absorption by Böhm-Vitense has clarified the situation. IS Mg II column densities are much larger than Ca II and result in superposition of non-negligible IS absorption features on the intrinsic chromospheric Mg II emission profile, even for stars closer than 100 pc. When we screen our asymmetry data to remove IS effects (accept only $S/L > 1$ for $v_r > 0$, and $S/L < 1$ for $v_r < 0$) the resulting 19 stars show a very clear asymmetry segregation as is seen for Ca II K, but now occurring among slightly warmer stars (K1 III rather than K3 III). See Figure 1a. We compare these transition loci in Figure 1b and note a plausible scenario emerging vis-a-vis the STL theory; as a star evolves from the main sequence, it retains a corona until it reaches the early K giants where it crosses the temperature dividing line (TDL) due to the encroachment of the sonic point of the stellar wind into the upper chromosphere, disrupting the global corona. As stellar evolution to the right in the HRD continues, the stellar wind appears first as outflow in the Mg II core-forming regions, and then in the deeper Ca II core-forming layers. Finally as the mass loss becomes substantial and sustained, circumstellar (CS) features begin to appear in the cores of neutral optical lines.

---

*We adopt the conventions that K_2R or R refers to the K line long wavelength peak and K_2V or V refers to the K line short wavelength peak. The corresponding features in the Mg II k line are L and S, respectively.

CORONA - MASS LOSS ANTI-CORRELATION?

Despite the appeal of such scenarios, re-evaluation of theory and new data give us pause. The foundations of the STL theory have been challenged by Holzer (9). A larger sample of IS effect-free Mg II profiles would be desirable. Recent correlation studies between Mg II and C IV 1550 Å flux by Ayres and Marstad (10) -- see paper by Ayres in these proceedings -- reveal a strong functional dependence between fluxes in these two lines. The sense of the correlation is that for a ten-fold decrease in Mg II surface flux for a given T_{eff}, a 30-40 fold decrease occurs in C IV surface flux in normal cool stars. Since, as we will shortly discuss, Mg II surface flux ratioed to bolometric flux decreases with decreasing T_{eff} across the TDL of Figure 1b (cf. Fig. 2), C IV flux would rapidly vary across a similar range in T_{eff}. Given detection sensitivities, C IV might appear to be present on one side of the TDL and absent on the other. In addition, hotter material might be confined to magnetic flux tubes in the chromosphere and corona, while the cooler outflowing matter might follow magnetic open regions between loop structures (analogous to coronal holes). The point is that for different T_{eff}, log g combinations, as well as age, rotation, chemical composition, pulsation and whatever, the filling factors for either temperature regime could vary significantly, as is evidenced by the observations. Thus, cool stars showing strong mass loss might also possess small patches of coronal plasma. This surface detail study may prove to be the major use for UV spectra of cool stars. Hartmann et al. (11) argue that Alpha Aqr (G2 Ib) may be a good example of this, as C IV is bright but obvious CS absorption features are seen in Ca II K and Mg II k. The lack of soft X-rays in this case could be due to self-absorption in the CS envelope (10). Additional "hybrid" stars like Alpha Aqr are also found among the K giants, and possibly all along the STL locus (third year IUE work in progress). If the Mg II-C IV-soft X-ray correlations are valid, then all stars are "hybrid" in possessing both coronal and mass loss features to varying degrees, and the usefulness of the term "hybrid" becomes very limited.

TALES FROM THE SUPERGIANTS

Late-type supergiants are too often considered in aggregate as cool mass losing stars with few other individualizing characteristics. Our Mg II survey has revealed some differences in kind between stars with T_{eff} differences as small as a few hundred degrees K. Also, we find a 3 to 4 times greater chromospheric radiative loss rate in Mg II emission for cool supergiants than is typical for higher gravity cool giants of similar T_{eff}.

MG II PROFILE DIFFERENCES

At least four distinct profile types are seen among F8-M5 Ib supergiants. F8 supergiants like Gamma Cyg and Alpha UMi show weak doubly-reversed Mg II emission cores. G0-G5 supergiants (Beta Aqr, Alpha Aqr, 9 Peg) exhibit very strong emission with S>>L and substantial CS absorption at -125 km/sec. The G5-K5 supergiants also show strong emission with S>L but with more moderate strength CS absorption shifted generally less than -50 km/sec (Xi Pup, Epsilon Peg, Lambda Vel). Finally, the coolest supergiants we have surveyed

(M2-M5: Alpha Ori and Alpha Her) again show strong Mg II emission with a strong CS or selective absorption (Fe, Mn?) feature superimposed on the k_2 emission component. The Mg II surface flux ratioed to bolometric flux (σT_{eff}^4) appears to peak at spectral type G0 and fall off steeply toward F8, and only gradually toward M5 (Fig. 2).

EVIDENCE FOR ACOUSTIC HEATING?

Following Linsky and Ayres (13), we define the chromospheric radiative loss rate in Mg II h & k, R_{hk}, as the ratio between integrated surface flux of the h & k emission, divided by bolometric flux of the star (see also Ayres, proceedings of this conference). In Figure 2 we present derived R_{hk} values for the sample of cool stars we obtained during second year IUE programs and note that the supergiants tend to lie a factor 3 or 4 above giants and bright giants with comparable T_{eff}. Proponents of acoustic wave heating of stellar chromospheres have computed several orders of magnitude difference in acoustic flux over a similar range of gravity and temperature, in contrast to our observational findings. However, Ulmschneider (private communication) notes that first-order corrections to the acoustic heating theory greatly reduce this predicted gravity dependence, toward the observed amount. This matter deserves further attention. We were able to find the small gravity dependence in R_{hk} because of the uniformity of the data used, in contrast to previous studies by Linsky and Ayres (13) and Basri and Linsky (14), which relied on UV data of varying resolution and signal-to-noise.

THE PROBLEM WITH 56 PEG

Our survey has defined observationally a subgroup of stars falling between Mg II and Ca II asymmetry dividing lines that challenges our supposed understanding of emission line formation and chromospheric velocity fields. 56 Peg-type stars have the unique defining property of discrepant asymmetries between Ca II K (V/R > 1) and Mg II k (S/L < 1). 56 Peg (K0 Ib-IIp) is the archetype, and Sigma Oph (K3 II), Alpha Boo (K2 III) and Gamma Aql (K3 II) are examples. Stencel and Mullan (8) first called attention to 56 Peg by virtue of the nearly 4 magnitude discrepancy between M_V(Ca K) = -1.6, and M_V(Mg k) = -5.3. SWP spectra of some of these show substantial C IV emission line flux, indicative of a hot outer atmosphere. A more complete report on 56 Peg itself is in preparation [Basri et al. (15)], but we wished to provide a status report at this time.

SEMI-EMPIRICAL MODELING

In terms of the STL theory, 56 Peg-type stars have outer atmospheres in which the supersonic stellar wind penetrates only into the upper chromosphere where Mg II is formed, but not as deep as where Ca II is formed. We have begun to derive semi-empirical models to match the surface flux and asymmetries in various UV lines, using the computation methods of Basri and Linsky (16) for Ca II and Mg II, and of Lites and Cook (17) for C II, III and IV. To date, experiments with meso-scale waves [Basri and Linsky (16)] are promising, but far from adequate. To produce the asymmetries observed, we need

to increase the physical segregation in height of formation between the k_3 and K_3 features. One way of accomplishing this spread in the respective optical depth scales is to assume a Mg/Ca abundance ratio much different from solar. Alternately, CS Mg II could be more pronounced than for Ca II due to STL effects in the upper chromosphere.

INTERPRETATIONS

Waves or global pulsations remain a possible mechanism for production of the discrepant asymmetries in this portion of the HRD, since the Pop. II Cepheid-like RV Tau irregular variables frequently are assigned spectral types like early K, class II. For 56 Peg itself, profile variability has not yet been observed in the Ca II K line over several years of monitoring, but additional Mg II k observations are being pursued. Photospheric analysis does not support an unusual Mg/Ca ratio. If the asymmetry loci are as statistically significant as we believe they are, then a non-negligible fraction of the HRD, early to mid K giants and early K bright giants, exhibit an unusual atmospheric structure characterized by fine structure in chromospheric velocity fields, and selective CS absorption. These might be expected to show Ca II K variability and sporadic mass loss as reported by Chiu et al. (18) for Arcturus.

We thank Al Boggess and his dedicated staff for assistance in obtaining and analyzing the data discussed here, as well as for support under contracts NAS5-23274 to the Univ. of Colo. and NAS5-25762 to Bartol Research Foundation.

REFERENCES

1. Stencel, R., Mullan, D., Linsky, J., Basri, G. and Worden, S. "The Outer Atmospheres of Cool Stars. VII. High Resolution Absolute Flux Profiles of the Mg II h & k Lines in Stars of Spectral Types F8 to M5" 1980 Astrophys. J. Suppl., in press.
2. Reimers, D. "Observational Evidence for Mass Loss from K Giants and G & K Supergiants" 1977 Astron. and Astrophys. 57, 395.
3. Stencel, R. "Emission Lines in the Wings of Ca II H & K. II. Dependence of Line Widths on Luminosity" 1977 Astrophys. J. 215, 176.
4. Stencel, R. "The Ca II V/R Ratio and Mass Loss" 1978 Astrophys. J. 223, L37.
5. Mullan, D. "Supersonic Stellar Winds and Rapid Mass Loss in Cool Stars" 1978 Astrophys. J. 226, 151.
6. Linsky, J. and Haisch, B. "Outer Atmospheres of Cool Stars. I. The Sharp Division into Solar-Type and Non-Solar Type Stars" 1979 Astrophys. J. 229, L27.
7. Vaiana, G. and 25 co-authors "The HEAO-2 Stellar Coronae Survey" 1980 Preprint.
8. Stencel, R. and Mullan, D. "Detection of Mass Loss in Stellar Chromospheres" 1980 Astrophys. J. 238, in press (15 May).
9. Holzer, T. "The Theory of Solar and Stellar Winds" 1980 Proceedings of the Cool Star Workshop, S.A.O. Special Report, in press.
10. Ayres, T. and Marstad, N. 1980, in preparation.

11. Hartmann, L., Dupree, A. and Raymond, J. "Hybrid Atmospheres and Winds in Supergiant Stars" 1980 Astrophys. J. (Letters) 236, L143.
12. Linsky, J., Worden, S., McClintock, W. and Robertson, R. "Stellar Model Chromospheres. X. High Resolution, Absolute Flux Profiles of the Ca II H & K Lines in Stars of Spectral Type F0-M2" 1979 Astrophys. J. Suppl. 41, 47.
13. Linsky, J. and Ayres, T. "Stellar Model Chromospheres. VI. Empirical Estimates of the Chromospheric Radiative Loss Rates of Late-Type Stars" 1978 Astrophys. J. 220, 619.
14. Basri, G. and Linsky, J. "Outer Atmospheres of Cool Stars. II. Mg II Flux Profiles and Chromospheric Radiative Loss Rates" 1979 Astrophys. J. 234, 1023.
15. Basri, G., Stencel, R. and Linsky, J. "Stellar Model Chromospheres. XIII. The Peculiar Outer Atmosphere of 56 Peg (K0 Ibp)" 1980 Astrophys. J., in preparation.
16. Basri, G. and Linsky, J. "Outer Atmospheres of Cool Stars. VIII. Chromospheric Models for the Supergiants Beta Dra, Epsilon Gem and Alpha Ori" 1980, in preparation.
17. Lites, B. and Cook, J. "A Semi-Empirical Model of the Upper Flare Chromosphere" 1979 Astrophys. J. 228, 598.
18. Chiu, H.-Y., Adams, P., Linsky, J., Basri, G., Maran, S. and Hobbs, R. "Variable Mass Loss from Arcturus and the Hypothesis of Giant Convection Cells" 1977 Astrophys. J. 211, 453.

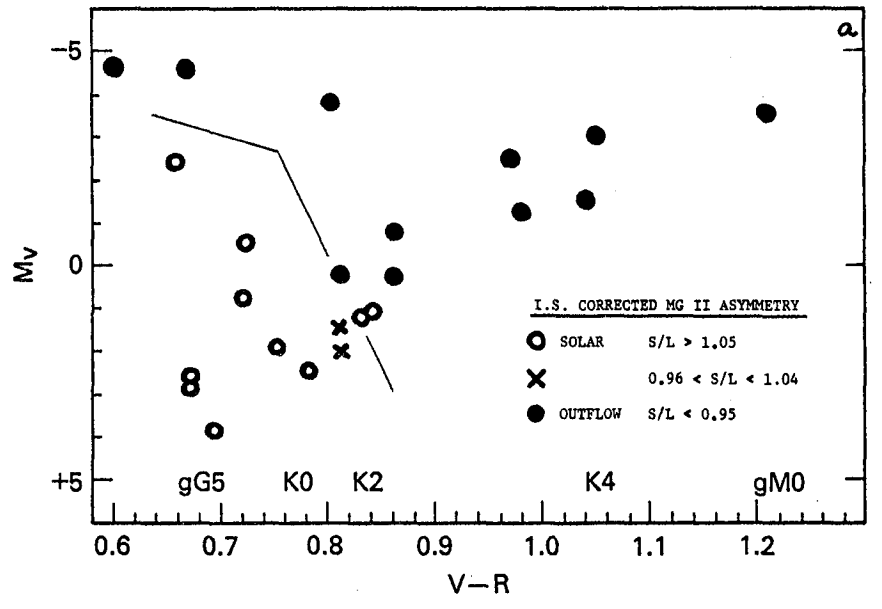

Fig. 1a. Mg II core emission asymmetry, k_2-/k_2+, or S/L, on a color-magnitude diagram for late-type stars. This sample accounts for the effect of overlying interstellar Mg II.

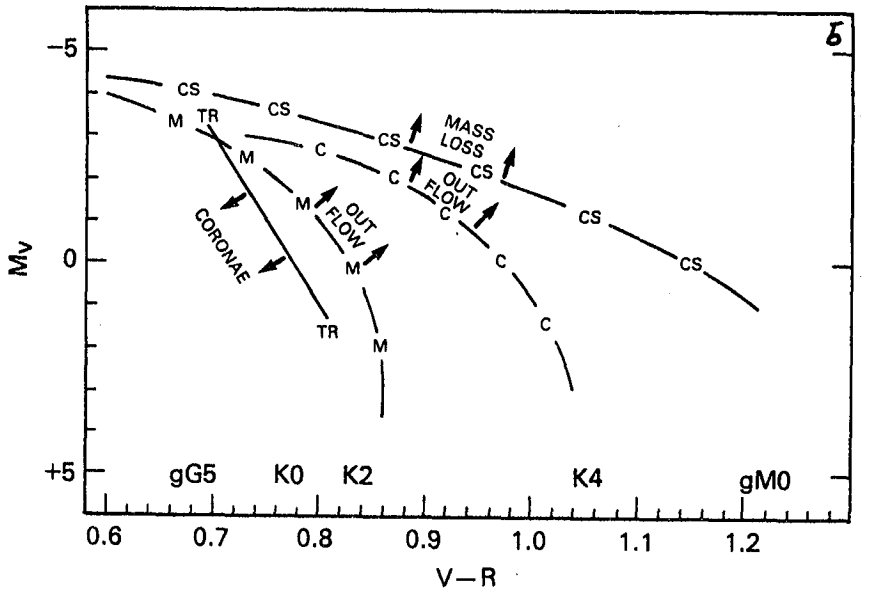

Fig. 1b. Collected transition loci in the HRD. Cf. reference 8.

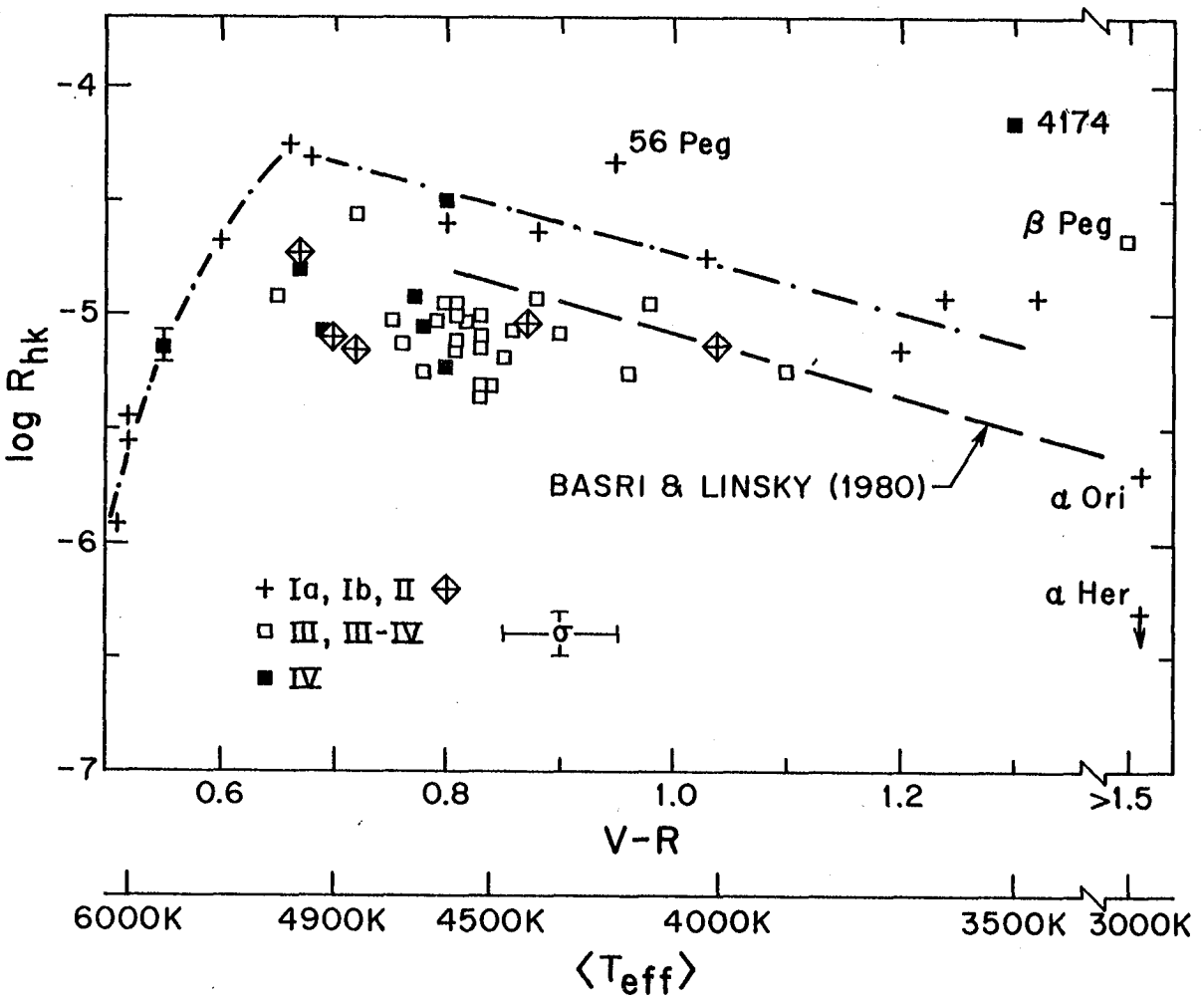

Fig. 2. Chromospheric radiative loss rate in Mg II, R_{hk}, which is the ratio of integrated Mg II h and k surface flux to total bolometric luminosity, as a function of V-R photometric color. See text for discussion.

IUE - ULTRAVIOLET AND OPTICAL CHROMOSPHERIC STUDIES OF LATE-TYPE GIANTS IN THE HYADES CLUSTER*

S. L. Baliunas, L. Hartmann, and A. K. Dupree
Harvard-Smithsonian Center for Astrophysics

ABSTRACT

We present ultraviolet and optical observations of four bright, late-type giants in the Hyades cluster detected with IUE in order to study chromospheric and coronal activity in stars of the same age. Two of the giants, 77 Tau and γ Tau, clearly exhibit emission in the high-temperature ions such as N V, C IV, and Si IV at levels several times larger than the upper limits for the other two giants, δ Tau and ϵ Tau. Comparison of the Mg II h and k fluxes and the Ca II K emission strengths shows that 77 Tau and γ Tau have larger chromospheric radiative losses than δ Tau, ϵ Tau, and β Gem, a field giant which also displays low upper limits to emission from high-temperature ions. Coronal X-ray emission has been detected from the *Einstein* Observatory (HEAO-2) in 77 Tau and δ Tau. Obviously both 77 Tau and δ Tau have hot coronae, but the surface flux in X-rays is an order of magnitude brighter in 77 Tau than in δ Tau.

The Hyades giants are similar in age, temperature, gravity, and metallicity; none are known to be close binaries. Thus, our results indicate that another parameter determines the amount of chromospheric and coronal emission in late-type giants.

INTRODUCTION

The study of stars in the galactic cluster nearest the Sun, the Hyades, presents a unique opportunity to explore chromospheric and coronal emission in late-type stars. For the cluster stars, which are coeval, certain parameters which are thought to affect the chromospheric emissions can be controlled.

The Hyades cluster is several hundred million years old and the main sequence stars are younger on the average than corresponding main sequence field dwarfs in the solar neighborhood. Among the optically brightest members of the cluster are four stars near spectral type KO III. In addition to similar effective temperatures, gravities, and metallicities, their ages are all alike. The

* Supported in part by NASA grants NSG 5370 to the Harvard College Observatory and NAG-5-5 to the Smithsonian Astrophysical Observatory

photospheric similarity of these stars is borne out in detailed analyses of spectroscopic and photometric observations (ref. 1, 2). The cluster giants occupy similar positions in the H-R diagram. We have also chosen to compare the four Hyades giants with β Gem (KO III), a field star with photospheric properties resembling those of the Hyades giants, with the possible exception of a somewhat lower, more solar metallicity (ref. 2).

OBSERVATIONS

We observed both the optical Ca II K and ultraviolet Mg II h and k chromospheric emission cores in these giants (Figure 1). The optical data here are high-resolution echelle spectra obtained at Mt. Hopkins with the image-intensified, photon-counting Reticon array (ref.3). The spectral resolution is approximately 40 mÅ. From these Ca II K profiles we have measured the normalized emission in excess of a quadratic baseline fit to the bottom of the photospheric absorption core. The Ca II K cores show a factor of three range in this normalized emission. The two Hyades giants 77 θ^1 Tau and γ Tau both show stronger Ca II emission than δ and ϵ Tau. For comparison, the field giant β Gem has a Ca II emission strength comparable to those of ϵ and δ Tau.

The Mg II h and k profiles were obtained at high-resolution with IUE. The scales have been adjusted to allow the intercomparison of surface fluxes between the Hyades and β Gem. The fluxes of the Mg II chromospheric emission cores behave similarly to those of Ca II K: the surface fluxes of the integrated emissions have a range of about a factor of two. Again, the Hyades giants 77 Tau and γ Tau are brightest in Mg II, while δ Tau and ϵ Tau, along with β Gem, have lower integrated surface fluxes.

The low-dispersion, short-wavelength IUE spectra also show this same trend in the solar transition-region emissions. The lines formed above a temperature of about 20,000 K, such as C II, C IV, Si IV, and N V are clearly visible in 77 Tau and γ Tau (Figure 2). The surface fluxes are higher, by factors of 2-5, than detections or upper limits of non-detection for the same lines in δ Tau, ϵ Tau, and β Gem. For 77 Tau and γ Tau, which show stronger chromospheric Ca II and Mg II emissions, the surface fluxes of the transition-region lines are enhanced. The stars δ Tau, ϵ Tau, and β Gem are weak in both the high-temperature transition-region lines and in the chromospheric Ca II and Mg II emissions.

DISCUSSION

Several interesting conclusions can be drawn from these data:

(1) The solar transition-region fluxes are strongest in 77 Tau and γ Tau, compared to δ Tau, ϵ Tau, and β Gem. This is correlated with the strength of the Ca II and Mg II emissions. Thus, the surface fluxes of the transition-region lines are enhanced as the chromospheric mechanical energy deposition increases, as evidenced in the increased radiative losses observed in Mg II and Ca II. This result has also been found in late-type dwarfs (ref. 4).

(2) The Hyades giants δ Tau and 77 Tau have been detected, with the *Einstein Observatory*, as X-ray sources (ref. 5), while ϵ and γ Tau have not yet been observed. The X-ray surface flux of 77 Tau is about a factor of 10 larger than in δ Tau; the C IV emission is about 6 times higher in surface flux in 77 Tau compared to the upper limit in δ Tau. Thus, the X-ray emission strength is correlated with the strengths of the high-temperature transition-region lines and the larger Mg II and Ca II chromospheric radiative losses. The weak-chromosphere stars ϵ Tau and δ Tau presumably also have solar-like transition regions, but at a level below our detection limit in the IUE spectra. The ultraviolet and optical spectra may be used to predict the level of X-ray activity from these stars. On the basis of our spectra, we predict X-ray emission from γ Tau at a level comparable to that of 77 Tau, while ϵ Tau will show a lower X-ray luminosity, similar to that of δ Tau.

(3) The Hyades giants are located in a region of the H-R diagram in the vicinity of the onset of mass-loss indicators. For example, the Mg II and Ca II profiles can show a violet-to-red emission-peak asymmetry with V < R, the violet peak depressed relative to the red. For stars which show this asymmetry, often outflows and mass-loss may be inferred (ref. 6).

However, in the Hyades spectra V/R asymmetries of Mg II and Ca II chromospheric emission cores are not simply related to the strength of chromospheric and coronal emission. In fact, Mg II asymmetries showing V < R (corresponding to outflows) occur here for the more chromospherically active stars. Additionally, the Ca II K profiles all show V > R, which can be opposite the Mg II asymmetry. As an explanation for the apparent inconsistency in the Ca II and Mg II asymmetries, variability may be invoked because the optical and ultraviolet spectra are not simultaneous. However, we have monitored the Ca II profiles in these stars over 6 months and we observed no changes in the shapes or the strengths of the line profiles. No changes are present, either, in two sets of ultraviolet spectra of the Hyades giants over the past year.

(4) Finally, chromospheric scaling laws which predict Ca II and Mg II fluxes as the basis of effective temperature and gravity alone (ref. 7, 8) are insufficient to explain the wide range of emissions among these Hyades giants which are all similar in effective temperatures, gravity, chemical composition, and age.

SUMMARY

The study of the Hyades giants, with extremely similar photospheres, has pointed out that chromospheric and coronal emission from these giants can be quite dissimilar. Present predictors of chromospheric emissions, which depend simply upon location in the H-R diagram, are insufficient to explain the wide range of chromospheric emissions observed here. Among the Hyades giants, large age differences may be ruled out as a cause of the range of chromospheric strengths. Additionally, none of these giants are known to be situated in close binary systems. Another parameter, such as rotation, may well be important for refining theories that predict the chromospheric emissions from these giants. Further, the ultraviolet and optical chromospheric data presented here may be used to predict the X-ray luminosity from these giants.

Stencel: Your Mg II profiles are fascinating. The X-ray source 77 Tau seems to have no central reversal. Assuming interstellar Mg II doesn't obscure the intrinsic information, what do you make of the "discrepant" asymmetries between Ca II K and Mg II K in these Hyades giants?

Baliunas: The interstellar contribution to Mg II profiles is an inconsistent explanation for the asymmetries. The radial velocities of these stars are all within a few km/sec, and the assumption of homogeneous cloud projected across the Hyades would produce similar Mg II asymmetries. Here, however, the asymmetry of Mg II in ϵ Tau is clearly opposite from the remaining Hyades giants. Differential flow velocites between the K_3 and k_3 line-forming regions may be a possible explanation.

Garrison: These four giants do have slightly different visual classifications, ranging from G8.5 III to K1 III. I'm sorry that I don't remember which is which, but it would be interesting to know if the emission line differences are in the same sequential sense.

Baliunas: Let us list the photospheric data for the Hyades giants as given by, say, Ref. 2.:

Star	T_{eff}	Spectral Type	log g
γ Tau	4900	K0 III	2.3
δ Tau	5000	K0 III	2.8
ϵ Tau	5000	K0 III	2.8
77 θ^1 Tau	5000	K0 III	3.0

The largest discrepancy here is that of γ Tau *vs.* 77 Tau. In fact, for these two stars with the largest range in temperature and gravity, the chromospheric emissions are quite similar. We should look elsewhere for an explanation of the spread in emissions.

REFERENCES

1. Chaffee, F. H., Jr., Carbon, D. F., and Strom, S. E.: *Ap. J.*, 166, 593, 1971.

2. Lambert, D. L., Dominy, J. F., and Siverten, S.: *Ap. J.*, 235, 114, 1980.

3. Baliunas, S. L.: Ph.D. Thesis, Harvard University, 1979.

4. Hartmann, L., Davis, R., Dupree, A. K., Raymond, J., Schmidtke, P. C., and Wing, R. F.: *Ap. J. (Letters)*, 233, L69, 1979.

5. Stern, R., Underwood, J. H., Zolcinski, M.C. and Antiochos, S.: *Cool Stars, Stellar Systems, and the Sun*, (ed. A. K. Dupree), Smithsonian Special Report, 1980, in press.

6. Stencel, R. and Mullan D. J.: *Ap. J.*, 237, in press.

7. Ayres, T. R., and Linsky, J. L.: *Ap. J.*, 200, 660, 1975.

8. Kelch, W. L., Linsky, J. L., Basri, G. S., Chiu, H.-Y., Chang, S.-H., Maran, S. P., and Furenlid, I.: *Ap. J.*, 220, 962, 1978.

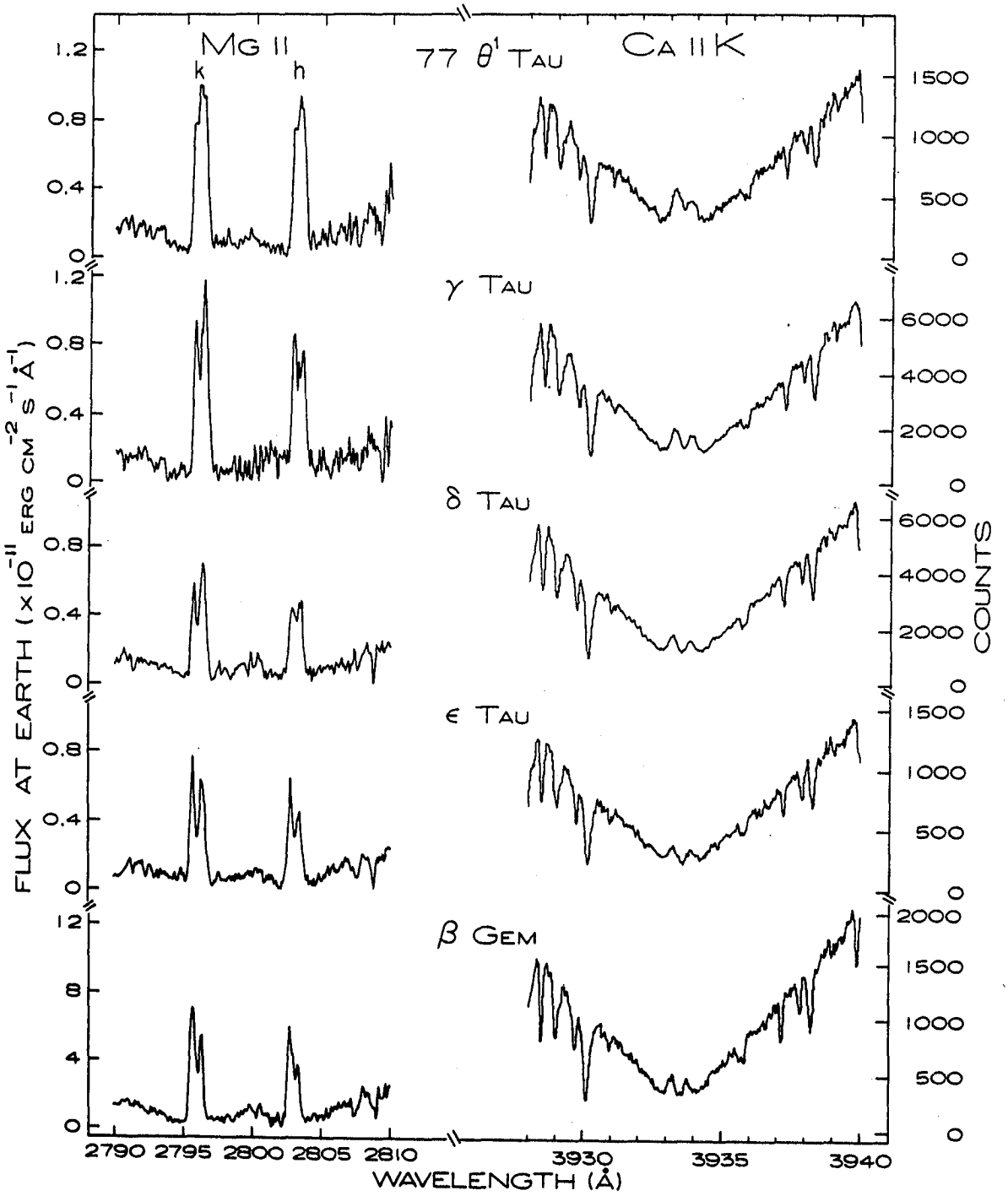

Figure 1. -- Mg II h and k (left) and Ca II K (right) profiles of the four Hyades giants 77 Tau, γ Tau, δ Tau, ϵ Tau, and the field giant β Gem. The observed fluxes at the earth have been determined by the calibration given in ref. 3. The chromospheric emission strengths are largest in 77 Tau and γ Tau.

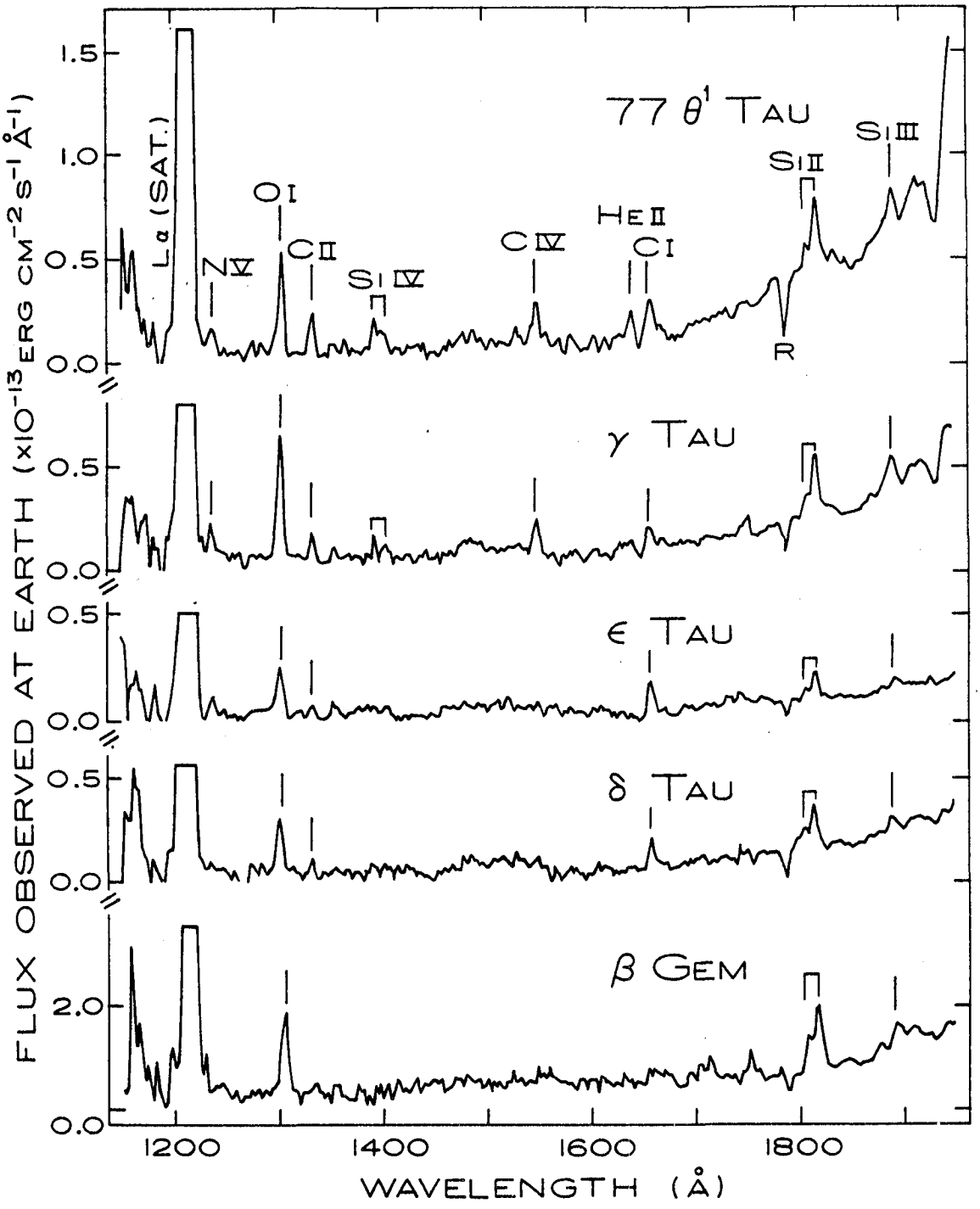

Figure 2. -- IUE short-wavelength, low-resolution spectra of the four Hyades giants and the field star β Gem. The high-temperature, solar-transition region lines are clearly present in 77 Tau and γ Tau. The enhancement of the ultraviolet emissions is correlated with the strong Ca II and Mg II chromospheric emissions in these stars.

IUE ULTRAVIOLET OBSERVATIONS OF W UMa STARS*

A. K. Dupree and S. Preston
Harvard-Smithsonian Center for Astrophysics

ABSTRACT

Four W UMa eclipsing binary systems have been observed with IUE: 44 Boo, VW Cep, W UMa, and ϵ CrA. They generally show large surface fluxes of high temperature lines (C II, C IV, N V, Si IV) which may result from the high rotational velocities forced by synchronous rotation. High dispersion spectra of the 44 Boo system in the Mg II line enable the individual stellar components to be identified. The line widths and phase variations are consistent with the optically determined spectroscopic orbit. Circumstellar absorption of Mg II may be present at selected phases.

INTRODUCTION

The W UMa systems are eclipsing binaries composed of late-type dwarf stars with an orbital period of less than one day. Their high spatial frequency means such a configuration is an important phase in the main sequence evolutionary process. The two components of these systems are of unequal mass implying that mass transfer has undoubtedly played a role in the evolution of these systems. There are indications of sudden changes in orbital periods over a few months as well. Light wave effects are found in some systems suggestive of stellar surface activity.

Early results from IUE (ref. 1, ref. 2) showed that these systems are rich sources of ultraviolet emission and suggested that binaries of shorter orbital period had a higher surface flux of UV lines than those of longer period. Most recently the discovery from HEAO-1 (ref. 3) that one member of this class is an X-ray source and the subsequent detection of many of these systems with the *Einstein* Observatory (ref. 4) show that these stars contain extensive coronae as well.

Much theoretical work has been done on structural models for these systems. It is generally thought that a large flux of energy is transferred from the more massive primary to the secondary star. Models suggest that the components share a common envelope in which transfer of energy from primary to secondary must occur by the action of circulation currents in a manner similar to convection.

Since we believe that convection plays a crucial role in generating solar chromospheric activity, we might well expect enhancement over single stars. These binaries are rapidly rotating and enhancement and concentration of magnetic fields must occur. This may well lead also to increased heating and radiative losses. In addition, one structural theory - the thermal relaxation

*Supported in part by NASA grants NSG 5370 to the Harvard College Observatory and NAG-5-5 to the Smithsonian Astrophysical Observatory

oscillation theory - (ref. 5, 6) predicts phases of mass exchange between components. So in the ultraviolet we might search for the spectroscopic signatures of circumstellar material and mass flow.

These W UMa systems are valuable objects with which to investigate coronal structure, stellar surface activity, and the dynamics of mass transfer or mass loss. It is also important to pursue the effect of rotation on chromospheric structure. It has long been known that the Ca K flux is enhanced in binary systems and apparently the extension of such enhancement is found in high chromospheric and coronal regions as well.

OBSERVATIONS - LOW DISPERSION

IUE spectra have been obtained of several W UMa type systems listed in Table 1. Short wavelength spectra (figure 1) exhibit the typical spectral features of high temperature chromospheric and transition region lines, namely O I, C II, Si IV, C IV, and N V. In ϵ CrA, the strong continuous emission at long wavelengths results from the high effective temperature of the components. Similar continuous emission is found in the system 44 Boo. This is a visual binary with one component being the W UMa system (G2 V) and the other an F4 V star. The continuum in this case arises from the F dwarf which is only ~ 2" away from the W UMa system at present and hence unresolvable with IUE. The strong He II (λ1640) line is notable in all of these systems. Its presence underscores the X-ray detections as the λ1640 transition can be increased through photoionization of He I by X-rays followed by recombination (ref. 7).

Surface fluxes in the emission lines (figure 2) are substantially higher than those found in the quiet solar spectrum and display an increasing enhancement with temperature of formation. Although the enhancement is more than an order of magnitude higher, this behavior is similar to that found in solar active regions suggesting a structure dominated by a constant conductive flux. Since we assume that the flux is homogeneously distributed over the stellar surface, these values may well be a lower limit to the true surface flux above active areas.

The surface flux of the C IV transition (λ1550) is a convenient index of enhancement and radiative losses in the stellar atmosphere at temperatures of 2×10^5 K. Inspection of the relation between emergent flux and stellar rotational velocity (figure 3) shows a clear correlation. The four W UMa systems have velocities $\geq$ 100 km s^{-1}, and exhibit the highest surface flux in the C IV line. Both the velocities and fluxes are higher than those of the RS CVn systems included for comparison. The correlation suggests a continuity in the effect of rotation upon the radiative losses; however there are still substantial variations in fluxes at a given rotational velocity. Some of this variation may result from activity on the stellar surface similar to that found for λ And (ref. 8) in which the ultraviolet flux correlates with the V light modulation. The extreme values found for ϵ CrA may be associated with the earlier spectral type of the system or the larger mass ratio (ref. 9) between the components.

OBSERVATIONS - HIGH DISPERSION

The system 44 Boo has been observed at various epochs with high dispersion at long wavelengths (figure 4). In this figure, the continuum and photospheric lines arise in the F dwarf companion and the central emission reversal from the W UMa component. The sample spectra at four phases show the variation of individual profiles with phase; the central emission reversal shows the orbital motion of the members of the W UMa system with an amplitude in agreement with the optical spectroscopic orbit (ref. 10, ref. 11). The breadth of each emission component at elongation (phase 0.28) is consistent with the rotational velocity expected from synchronous motion, namely $\pm$ 1.5 Å and $\pm$ 1.1 Å for the primary and secondary star respectively. The flux ratio is consistent with the surface area presented at elongation and supports a relatively uniform distribution of surface flux. There are phase changes in the profile from epoch to epoch; the flux attributed to the primary star remains approximately constant, whereas the secondary appears to fluctuate by 10 to 20% in the Mg II k line flux. This seems reasonable if the secondary is merely the recipient of the luminosity generated principally on the primary star.

There is a suggestion of absorption features in the Mg II k profile that have a variable velocity of about -100 km s^{-1}; these appear to be present at various epochs and may indicate the presence of circumstellar material in the system. Confirmation of this, and in particular its appearance with orbital phase, suggests that mass transfer occurs between the components of contact systems.

REFERENCES

1. Dupree, A. K.; Black, J. H.; Davis, R. J.; Hartmann, L.; and Raymond, J. C.: *Chromospheres and Coronae of Late-Type Stars.* in *The First Year of IUE*, A. J. Willis, ed., University College London, p. 217.

2. Dupree, A. K.; Hartmann, L.; and Raymond, J. C.: *Ultraviolet Spectroscopy of Binary Systems.* in I.A.U. Symp. No 88, Close Binary Systems, in press.

3. Carroll, R. W.; Cruddace, R. G.; Friedman, H.; Byram, E. T.; Wood, K.; Meekins, J.; Yentis, D.; Share, G. H.; and Chubb, T. A.: *Astrophys. J. Lett.*, 235, L77, 1980.

4. Cruddace, R. G.; Dupree, A. K.; Carroll, R. W.; Friedman, H.; Byram, E. T.; and Wood, K.: *Bull. A.A.S.*, 11, 721, 1979.

5. Lucy, L. B.: *Astrophys. J.*, 205, 208.

6. Flannery, B. P.: *Astrophys. J.*, 205, 217.

7. Hartmann, L.; Davis, R.; Dupree, A. K.; Raymond, J.; Schmidtke, P. C.; and Wing, R. F.: *Astrophys. J. Lett.*, 233, L69.

8. Baliunas, S. L.; and Dupree, A. K.: *Ultraviolet and Optical Chromospheric Activity in λ Andromedae: Evidence for Starspots and Active Regions in Cool Stars, Stellar Systems and the Sun*, A. K. Dupree, ed., Smithsonian Special Report, in press.

9. Tapia, S.; and Whelan, J.: *Astrophys. J.*, 200, 98, 1975.

10. Popper, D. M.: *Astrophys. J.*, 97, 394, 1943.

11. Stoeckley, T.; and Carroll, R.: in preparation.

12. Ayres, T.; and Linsky, J.: 1980, preprint.

13. Batten, A. H.; Fletcher, J. M.; and Mann, P. J.: *Pub. D.A.O.*, 15, 121, 1978.

TABLE 1

Observations and Parameters of W UMa Systems

System	Spectrum	Period (days)	Image*	Phase	Exposure (minutes)	References
44 Boo	G2, F4 (primary)	0.268	Average of 9 SWP	Many	23 to 45	11
			LWR 3197	0.28	25	
			LWR 5834	1.00	19	
			LWR 5836	0.40	15	
			LWR 5838	0.78	15	
VW Cep	G2	0.278	SWP 6534	0.84-0.46	150	11
W UMa	F8	0.334	SWP 6881	0.45	75	13
ϵ CrA	F0	0.591	SWP 6830	0.79	2	9
			SWP 6831	0.85	40	

* All exposures were made using the Large Aperture.

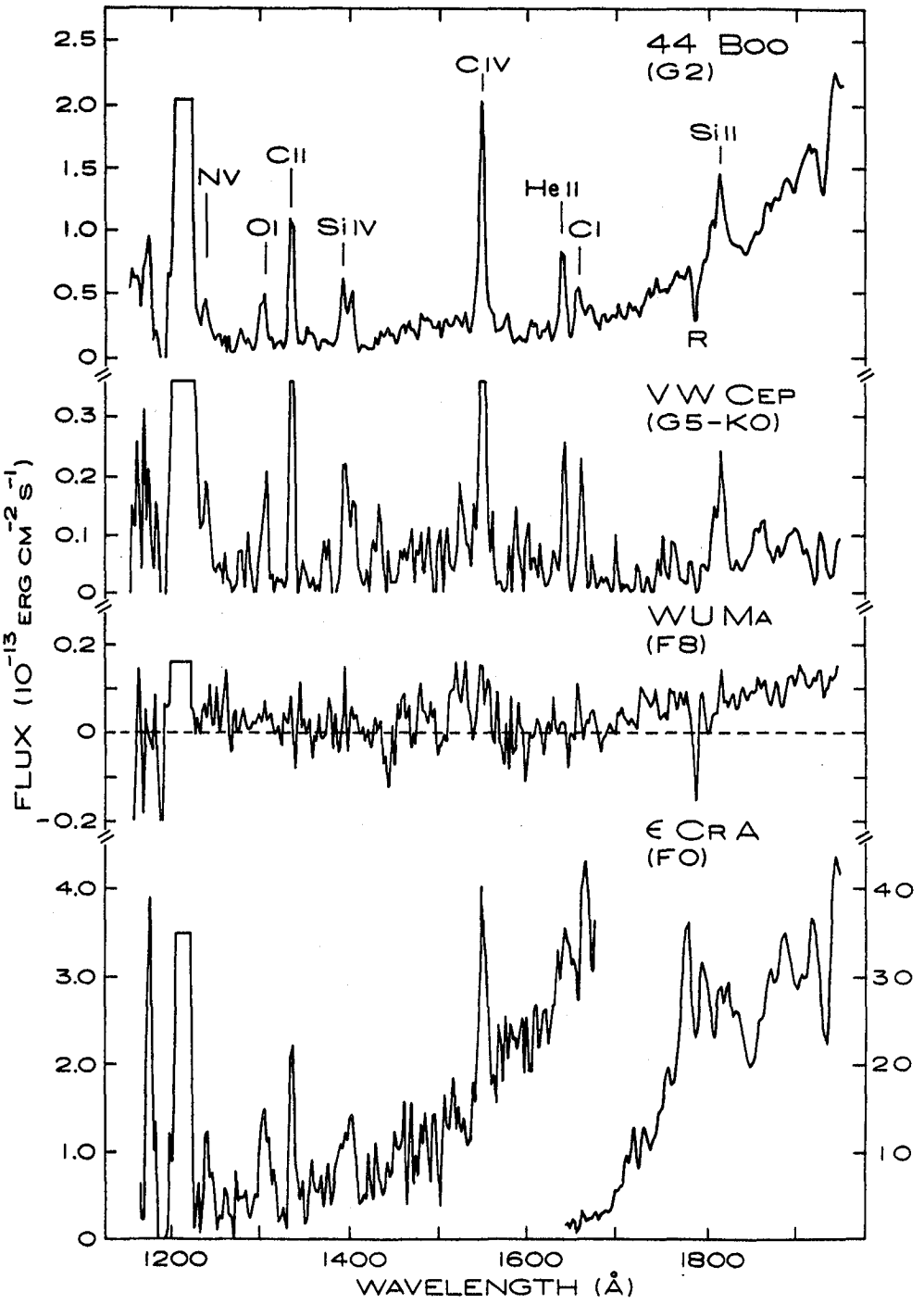

Figure 1. Short wavelength spectra of 4 W UMa systems. The spectrum of 44 Boo represents an average of 6 images. The spectrum of W UMa is underexposed **and serves only to provide an upper limit to the C IV lines at λ1550 Å. The spectrum of ε CrA is a composite of a long exposure (40 min.) to detect the high temperature lines at short wavelengths and a shorter exposure (20 min.) to measure the continuum near λ1800.**

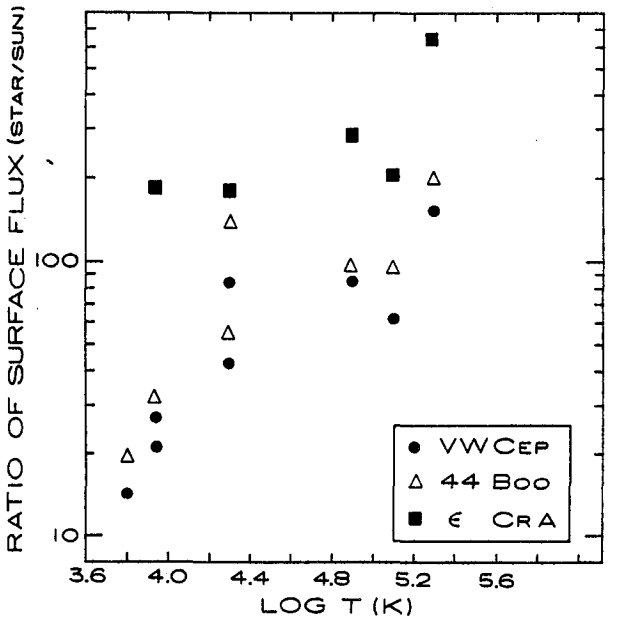

Figure 2. The ratio of surface flux in selected emission lines to that in the quiet Sun. All three systems show a similar pattern of enhancement which is generally the highest found to date in late-type stars.

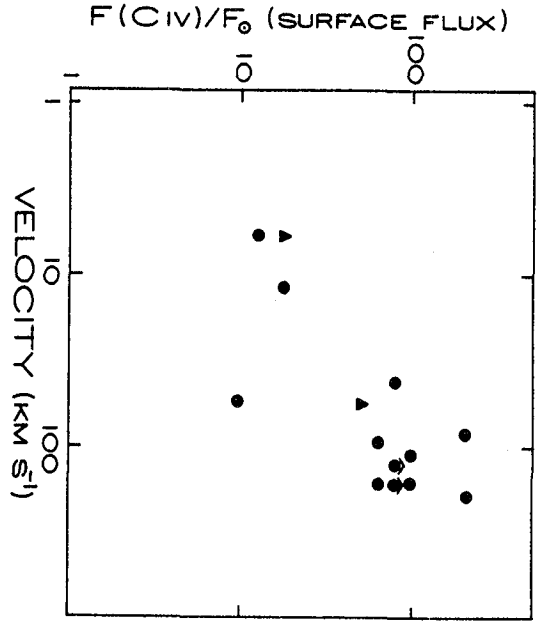

Figure 3. The surface flux in the C IV (λ1550) transition as a function of velocity of the components for several binary systems. Synchronous rotation was assumed for those systems with orbital period less than 5 days. The four W UMa systems have $V \gtrsim 100$ km s^{-1}. Upper limits for the components of W UMa itself are shown. Several RS CVn systems are also included. The triangles indicate the position for Capella with attribution of the total flux to the secondary (ref. 12) or to the primary star.

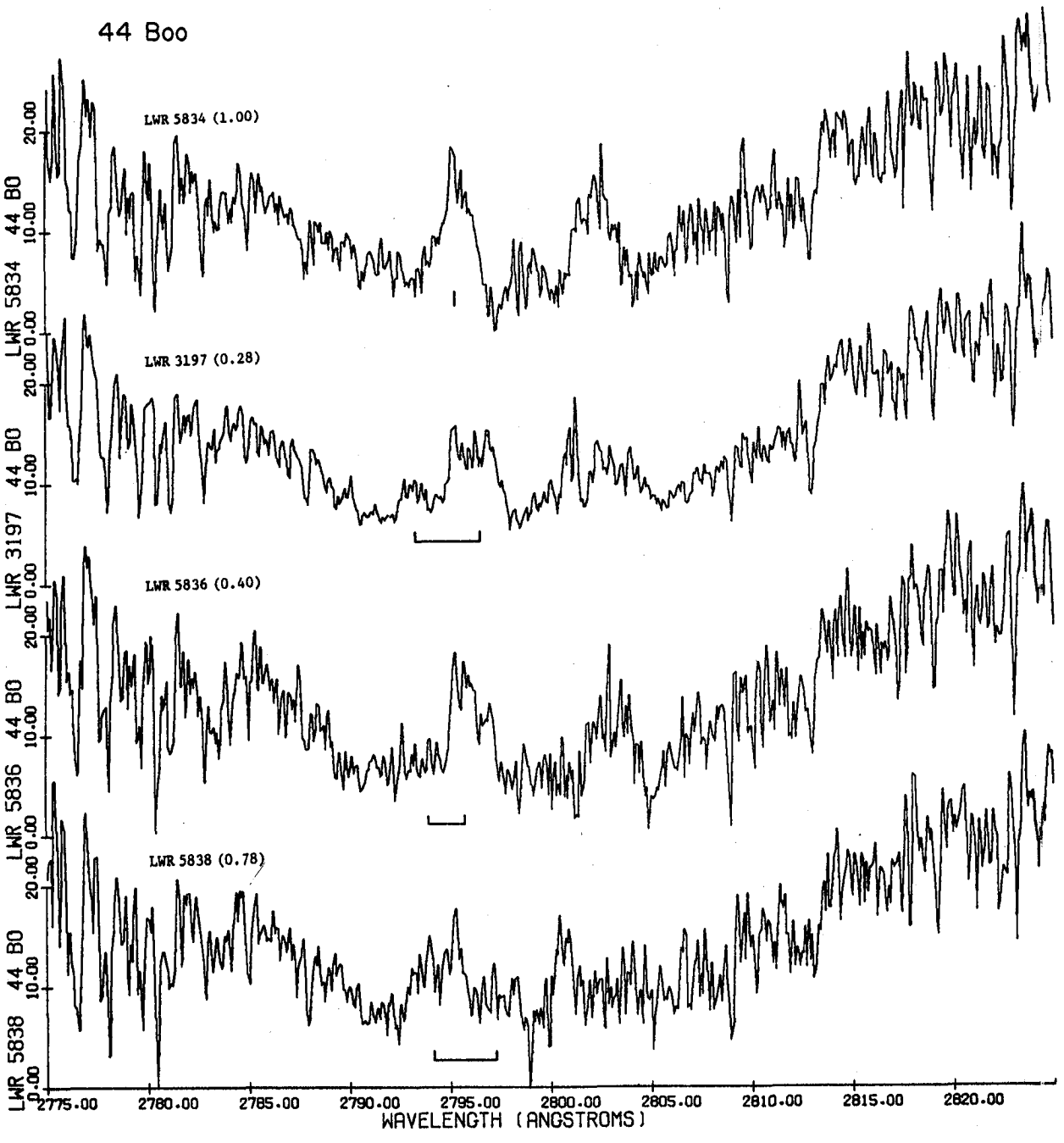

Figure 4. Samples from the high dispersion observations of the Mg II spectral region in 44 Boo. The F4 V component contributes the narrow photospheric absorption lines. The emission cores show the phase dependent behavior expected from the optically determined spectroscopic velocity curve (ref. 10, ref. 11) marked by the solid lines. At phase 0.28 the primary star has the maximum redshift; at phase 0.78 the primary star is approaching.

NOTES ON THE EARLY-TYPE COMPONENTS OF W Cep, o Cet, CH Cyg, AR Mon, and BL Tel

Robert F. Wing and Kenneth G. Carpenter
Astronomy Department, The Ohio State University

ABSTRACT

Low-resolution IUE spectra in both spectral regions have been used to clarify the nature of the warmer components of several binary systems. W Cep, the primary of which is a luminous K-type supergiant, shows an ultraviolet absorption spectrum of type B0 or B1; this system is heavily reddened. The hot companion of Mira (o Cet) is surprisingly faint in the short-wavelength region, but it excites a rich emission spectrum from the surrounding gas. The ultraviolet-active M7 giant CH Cyg is shown to be a binary with a hot companion. This system has also been observed at high resolution and shows variable Fe II emission and well-separated circumstellar and interstellar absorptions within the broad Mg II emission profiles. The eclipsing binaries AR Mon and BL Tel are shown not to have hot companions.

INTRODUCTION

Ultraviolet spectroscopy can add an important dimension to the study of binary stars. In many cases, a hot secondary component whose presence can only be indirectly inferred from optical observations can be accurately classified in the ultraviolet. In other cases it may be important merely to be able to show that no hot component exists. Furthermore, the presence of strong transitions of many abundant ions makes the ultraviolet especially suitable for studying the interactions between components of a binary system, which may take the form of emission from a surrounding nebula or absorption from a circumstellar shell.

RESULTS

W Cephei

This semi-regular variable is a luminous K-type supergiant with a hot companion which fills in the spectrum shortward of about 4000 Å. The system has been classified K0ep Ia + O? (Bidelman 1954; Cowley 1969) and has been discussed with the VV Cephei stars (whose primaries are mostly of type M) by Cowley (1969). Since no lines are clearly seen in the near-ultraviolet spectrum of the companion, satellite observations in the far ultraviolet are needed to determine its spectral class.

Exposure times of 15 and 30 min were used to record the long- and short-wavelength regions, respectively, at low resolution. The energy distribution

is strongly affected by interstellar reddening, and the 2200 Å feature is prominent. The spectrum of the hot component is featureless in the long-wavelength region but filled with strong absorption lines below 2000 Å. The strongest of these are the doublets of Si IV and C IV near 1400 and 1550 Å, respectively; their relative and absolute strengths indicate a spectral type of B0 or B1. This result should be considered preliminary for two reasons: we have not yet secured an adequate set of spectra of spectral-type standard stars; and the contributions of interstellar lines to the observed absorptions cannot be determined at the resolution employed.

o Cet (Mira)

Mira is a close visual binary whose companion was first discovered spectroscopically (Joy 1926). When the red variable is near minimum light, the companion dominates the spectrum below 4000 Å. Its near-ultraviolet spectrum, however, is not classifiable, as it shows only broad hydrogen lines with P Cygni profiles. The companion is sometimes called an O star, sometimes a B star; in any case its faintness compared to the M giant primary indicates that it lies below the main sequence. The companion undergoes both slow and rapid variations (see Yamashita et al. 1978) and has been named VZ Cet.

Normal (i.e. single) Mira variables show a wide variety of emission lines in the optical region and hence might be expected to contribute some features in the ultraviolet. However, our IUE exposures on R Leo, R LMi, and R Hya do not show any definite features except the Mg II doublet at 2800 Å. We were expecting, therefore, that the ultraviolet spectrum of Mira itself would be essentially that of the companion. This is indeed the case in the long-wavelength region, where the spectrum is continuous with superimposed Mg II emission. The short-wavelength spectrum, however, is not that of a star but that of a nebula.

The spectrum of Mira from 1200 to 1950 Å is shown in Figure 1. Many strong emission lines are present, while the continuum from the hot star is relatively weak and surprisingly red. This 60-min exposure was made on January 28, 1980 when the primary was a bit past maximum light (the Fine Error Sensor registered a visual magnitude of 4.4). Since the long-wavelength region was well exposed in only 5 min, one might have expected the continuum of the hot star to be greatly overexposed in one hour in the short-wavelength region. Either the companion is not as hot as usually thought, or it is strongly reddened by circumstellar or interstellar material.

Most of the emission lines in Figure 1 are readily identifiable with the strongest transitions of abundant ions. What is remarkable is the wide range of excitation present. All the lines normally seen in high-excitation nebulae (N V, Si IV, C IV, He II, etc.) are there, but in addition there are strong lines of O I, C I, and Si II, which characterize the low-excitation chromospheres of K and M giants. Clearly there exists a wide range of temperature in the gas producing the emission. We note also that the semi-forbidden lines of O III], C III], Si III], and probably N III] are quite strong, indicating that at least some of the emitting gas is at low density.

Since it is likely that the primary star is losing mass with each annual cycle of its light variation and that this material fills a large volume of space around both stars, it is easy to see how a wide range of temperature and density could arise. Nearly all of the circumstellar gas can be illuminated by the hot star, and this radiation is most intense near the hot star while the density is probably highest in the immediate vicinity of the cool primary star.

Models of the Mira system will have to account for the relatively red color of the hot companion and its faintness in the short-wavelength region. It does not seem likely that it is as cool as it looks if it can excite the nebula so effectively. The great strength of the emission lines would tend to argue against interstellar absorption, or absorption from a dust shell surrounding the entire system, as the mechanism responsible for suppressing the spectrum of the hot star. At the same time, absorption occurring closer to the hot star would reduce its efficacy in exciting the emission spectrum, and in any case it is hard to understand how grains of any kind could exist near the hot star. A quantitative study of the relative emission line strengths might show whether or not they suffer selective absorption.

CH Cygni

This semiregular variable of type M7 III has gone through several episodes of "activity" — notably in 1963, 1967, and 1977 — during which the near-ultraviolet spectrum has become covered by a hot continuum, and emission lines of relatively low excitation (mainly Fe II) have appeared throughout the optical region. Both single-star and binary models have been proposed for CH Cyg. Recently, Yamashita and Maehara (1979) have detected changes in the photospheric radial velocity of the M star and have suggested that it is a binary system with a period of 5750 days (about 16 years) and a velocity semi-amplitude of 6.8 km/sec.

The spectrum obtained with IUE in the short-wavelength region leaves no doubt that a hot secondary star is present. Not only is the spectrum very bright (the optimum exposure time proved to be 5 min for low-resolution SWP images) but also the spectrum contains absorption lines of C IV, Si IV, etc. which presumably arise in the photosphere of the hot star. A spectral classification should be possible when more standards have been collected. The most conspicuous feature in the short-wavelength region, however, is one that does not belong in the spectrum of a hot star at all — a very strong emission line of O I! Since this line at 1300 Å can be pumped by Lyβ photons (Bowen 1947), it seems that CH Cyg must represent an unusually favorable case for the operation of this fluorescence mechanism, with the hot star supplying the Lyβ photons and the cool star supplying the neutral gas. On the other hand, the absence of detectable Lyα emission may make it hard to maintain that an adequate supply of Lyβ photons is available.

In the long-wavelength region, after overexposing the spectrum in 2 min at low resolution, we took subsequent exposures at high resolution (optimum exposure time 40 min). Three plates were obtained, separated by intervals of several months; all show a large number of rather weak emission lines, but on

the most recent plate the Fe II emission is decidedly weaker than on the other two. Sections of two of these spectra are shown in Figure 2. The upper panel, which covers the interval from 2600 to 2650 Å, shows that the Fe II lines of multiplet (1) were much stronger in May 1979 than in January 1980. The lower panel covers the region from 2750 to 2800 Å on the same two dates and includes the 2795 Å line of Mg II. This line is broad and strong in emission and contains two distinct absorption components separated by 110 km/sec; the other member of the Mg II doublet at 2802 Å has a similar profile. Since the systemic velocity of CH Cyg is -58 km/sec (Yamashita and Maehara 1979), the longward absorption component has nearly zero velocity and is probably interstellar, while the shortward component is produced in a circumstellar shell that is expanding outward at about 50 km/sec with respect to the star. A similar expansion velocity was observed at the K line of Ca II by Yamashita and Maehara. On the other hand, the Hα profile, recently studied by Anderson, Oliversen and Nordsieck (1980), is very different, with only a single absorption component dividing the emission into nearly equal parts. In that case no interstellar line is involved, and the absorption feature is at approximately the center-of-mass velocity — perhaps, as suggested by Yamashita and Maehara, because the Balmer absorption is associated with the circumstellar shell of the hot star, which in recent years has been in front of the M giant and moving across the line of sight.

AR Monocerotis

This 21-day eclipsing binary has a spectral type of K0 II; no evidence of the secondary star is seen spectroscopically. The secondary must be a fairly large star because the primary eclipses are about 0.8 mag deep (Payne-Gaposchkin 1944). The strange thing about this system is that the primary eclipse occurs when, according to the radial-velocity curve, the K star is in front (Sahade and Cesco 1944).

To check the possibility that the companion might be of relatively early type, AR Mon was observed at low resolution with exposures of 30 and 90 min in the long- and short-wavelength regions. The spectrum seems normal for an early K giant, with chromospheric emission lines of Mg II and O I and transition-region lines of C II, C IV, and N V. A weak continuum was recorded down to about 1700 Å, and its color is approximately normal for a K star. We conclude that the companion is no hotter than type G and probably is cooler than the primary.

BL Telescopii

This 778-day eclipsing system has many peculiarities. Although the primary has been classified as an F8 supergiant (Cousins and Feast 1954), the system has a large radial velocity, high galactic latitude, and appreciable proper motion. The primary eclipses are 2.0 mag deep, and the spectroscopic orbit (Wing 1963) indicates that the secondary must be at least as massive as 2 $M_\odot$.

At minimum light, weak TiO features have sometimes been recorded in the

red, and this suggests that the companion is an M star (Cousins and Feast 1954). On the other hand, Feast (1966) has offered the suggestion that the TiO features are produced near the limb of the F supergiant and that the eclipses are caused by a dense H II region ionized by, and surrounding, a hot subdwarf secondary.

We have observed BL Tel both outside eclipse (1979 February 11) and in eclipse (1979 May 26). Readings taken with the Fine Error Sensor indicate that the eclipse was 1.3 mag deep visually at the time of our second observation, while the fluxes at representative wavelengths in the ultraviolet showed changes of 1.0 to 1.5 mag. The spectrum seen in the ultraviolet is that of an F star, with a strong absorption feature due to the Mg II doublet and weaker absorptions as far shortward as 1700 Å. No chromospheric emission was recorded, and no significant changes in the spectrum (other than its intensity) occurred as a result of the eclipse. It would appear that spectroscopic evidence of the companion should be sought not in the ultraviolet but in the infrared.

REFERENCES

Anderson, C. M., Oliversen, N. A., and Nordsieck, K. H. (1980). *Wisconsin Astrophysics* No. 105 (preprint).

Bidelman, W. P. (1954). *Astrophys. J. Suppl.*, 1, 218.

Bowen, I. S. (1947). *Publ. Astron. Soc. Pacific*, 59, 196.

Cousins, A. W. J., and Feast, M. W. (1954). *Observatory*, 74, 88.

Cowley, A. P. (1969). *Publ. Astron. Soc. Pacific*, 81, 297.

Feast, M. W. (1966). *Monthly Notices Roy. Astron. Soc.*, 135, 287.

Joy, A. H. (1926). *Astrophys. J.*, 63, 281.

Payne-Gaposchkin, C. (1944). *Astrophys. J.*, 100, 251.

Sahade, J., and Cesco, C. U. (1944). *Astrophys. J.*, 100, 374.

Wing, R. F. (1963). *Monthly Notices Roy. Astron. Soc.*, 125, 189.

Yamashita, Y., Ichimura, K., Shimizu, Y., and Nakagiri, M. (1978). *Tokyo Astron. Bull.*, 2nd series, No. 254.

Yamashita, Y., and Maehara, H. (1979). *Publ. Astron. Soc. Japan*, 31, 307.

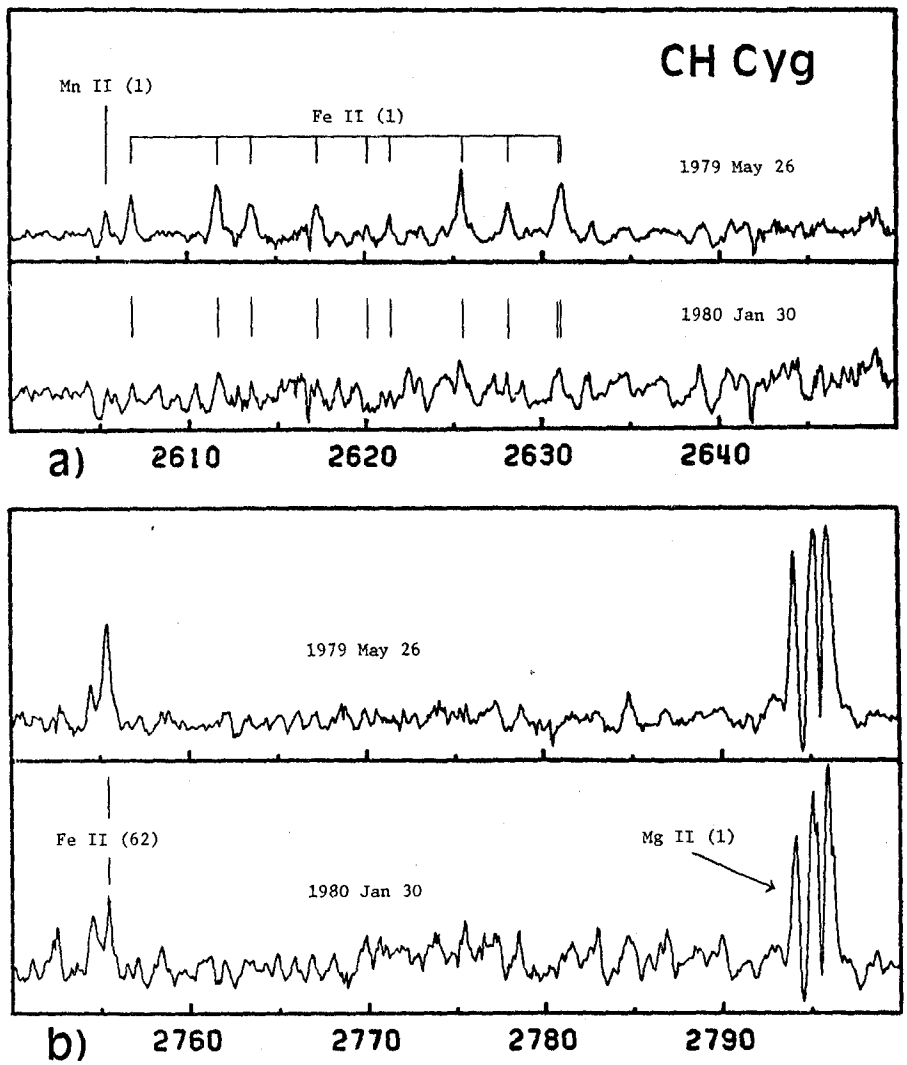

Figure 1.--The spectrum of Mira (o Cet) in the short-wavelength region. The continuous spectrum from the hot companion is surprisingly faint and is probably obscured. The rich emission-line spectrum shows a wide range of excitation and probably arises in a large volume of gas which surrounds the entire system and is illuminated by the hot secondary. The Lyα line is largely geocoronal, but a stellar component comparable in strength to O I λ1300 is also present. The feature near 1500 Å marked with an 'X' is spurious. In the long-wavelength region, the spectrum is dominated by the continuum of the hot star with superimposed Mg II emission.

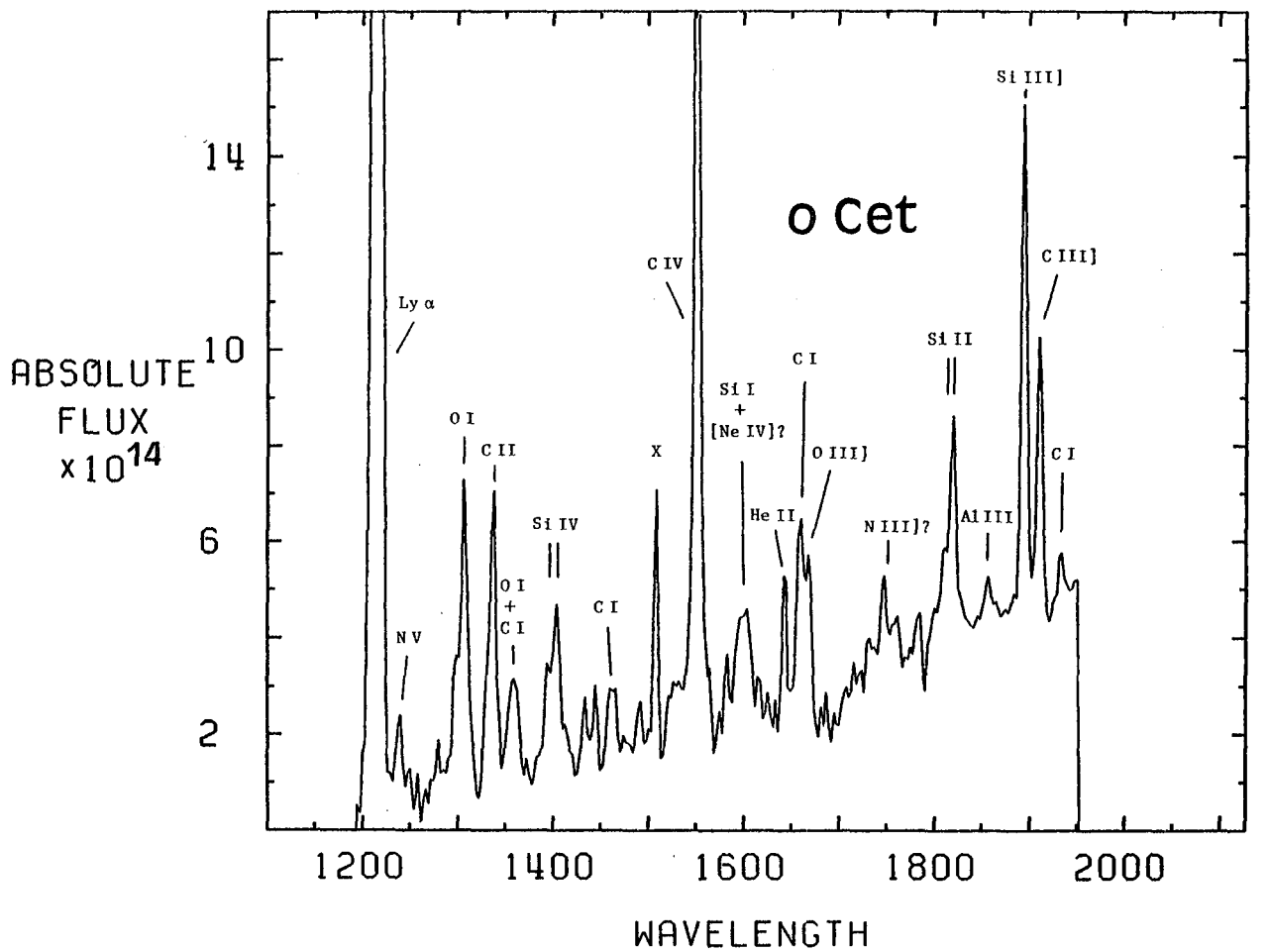

Figure 2.--Segments of high-resolution spectra of CH Cyg obtained on two different dates. (a) The region 2600 - 2650 Å, showing emission lines of Fe II and Mn II which were stronger on May 26, 1979 than on January 30, 1980. (b) The region 2750 - 2800 Å containing the 2795 Å line of Mg II, which shows both interstellar and circumstellar absorption components.

IUE OBSERVATIONS AND INTERPRETATION OF THE SYMBIOTIC STAR RW HYA

M. Kafatos
Department of Physics
George Mason University
Fairfax, Virginia

A. G. Michalitsianos
and R. W. Hobbs
Laboratory for Astronomy and Solar Physics
NASA/Goddard Space Flight Center
Greenbelt, Maryland

ABSTRACT

IUE observations of the high excitation symbiotic star RW Hya (gM2 + pec) have been obtained. Analysis of the intense UV continuum observed between 1100 Å to 2000 Å suggests this star is a binary system in which the secondary is identified as a hot subdwarf with $T_{eff} \sim 10^5$ K. We deduce a distance to the system of $\sim$ 1000 pc. The UV spectrum consists of mainly semi-forbidden and allowed transition lines of which the CIV (1548 Å, 1550 Å) emission lines are particularly strong, and UV continuum at both shorter and longer wavelengths. Strong forbidden lines seem to be absent suggesting the presence of a nebula of high densities, in the approximate range 10^8 - 10^9 cm^{-3}. Tidal interaction between the red giant primary and the hot subdwarf is suggested as a likely means to form the observed nebula. RW Hya is suggested as a possible source of soft X-ray emission from material accreting onto the surface of the hot subdwarf. Detection of such emission with HEAO-B ("Einstein") would give us information if this accretion is taking place via Roche lobe overflow or via capture from a stellar wind emitted by the primary. A general discussion of elemental and ionic abundances in the nebula is also presented.

INTRODUCTION

RW Hydrae consists of a star of gM2 spectral type with lines in the visual characteristic of higher temperatures than would be expected for a late type giant; Merrill (ref. 1) observed H, He I, He II, [O III], [Ne III], and [Fe V], [Fe VII]. A 376 day orbital period was determined from radial velocity observations of emission and absorption lines by Merrill (ref. 1).

Our IUE results confirm the binary hypothesis of Merrill. The star system consists of the late type giant and a hot companion which we classify as a central star of a planetary nebula. The two stars are immersed in a dense nebula which gives off intense allowed and semi-forbidden lines, the strongest ones being the C IV doublet. IUE is particularly useful in observing late type stars that have composite spectra, since the luminosity of the primary M giant does not overwhelm the emission from the companion in the far UV.

UV OBSERVATIONS

Ultraviolet observations were obtained of RW Hya on July 29 and September 1 1979 over the wavelength range 1100 A to 3200 A using exclusively the 10" x 20" large aperture of the IUE spectrometer. Virtually no change was seen in the spectrum observed during the two observing sessions. In Figure 1a,b we show the short and long wavelength observations of RW Hya. Ly α 1216 Å is observed in absorption. The C IV lines are so strong that subsequent exposures of 30 seconds obtained on September 1 saturated one pixel! High dispersion ($\sim$ 0.1 Å resolution) spectra obtained on September 1 in the short wavelength region revealed a number of allowed and semi-forbidden lines. We have identified 39 lines in the spectrum of RW Hya and have possible candidates for 12 others. In Table I we show line identifications and fluxes for the strongest IUE features. Other numerous lines of the ions in Table I were also observed (e.g the CIII 1174.9 - 1175.8 Å lines, the O I] 1355.6 Å line etc.). Moreover, we identified lines of the (43) and (68) multiplets of Fe II, the Si II 1808 + 1817 Å lines and the Al III 1854.7, 1862.8 Å lines. Twelve possible lines that we observed are a number of Fe II features, a Si III feature and some forbidden [Ne III] ,[Ne IV],[O II],[O III] lines. These are very tentative identifications and we are very skeptical whether in fact any forbidden line was seen. In contrast to the short wavelength region which is rich in lines we only detected definite lines CII], Mg II and O III in the long wavelength region (see Figure 1 and Table I). The short wavelength continuum drops as the Rayleigh-Jeans black body tail of a hot star emission would be expected. Beyond about 2000 Å, F_λ is essentially constant with wavelength.

DATA ANALYSIS

From equivalent width measurements of the Ly α absorption line we obtain a column density of H I in our line of sight N_H I$\sim 6.4 \times 10^{18}$ cm^{-2}. Using the interstellar extinction relationship (ref. 2), we find E(B-V) $\sim 1.3 \times 10^{-3}$. This low value of extinction is consistent with the 1200 Å to 1700 Å Rayleigh-Jeans excellent fit to the observed continuum. We estimate a lower limit to the temperature of the hot component $T_2 \sim 50{,}000$ K (if, for example, the star had a temperature of 30,000 K, the black body maximum would be in the 1000 Å region of the spectrum and would not follow the observed Rayleigh-Jeans tail).

We estimate the absolute magnitude of the primary as $M_V \sim 0.0$, although it could be slightly smaller. From the observed apparent magnitude of $m_V \sim 10$, we obtain a distance of $\sim$1000 pc and a height above the galactic plane of $\sim$ 600 pc. The corresponding stellar parameters are $M_{bol} \sim -2.2$, $\log L_*/L_\odot \sim 2.8$ and $\log R_*/R_\odot \sim 1.9$.

The apparent magnitude of the secondary was obtained from the observed Rayleigh-Jeans tail, $m_V \sim 14.75$, and therefore the secondary is much fainter than the primary in the visible. We estimate an upper limit to its temperature $T_2 \sim 200{,}000$ K in order not to violate the Eddington limit for a star of 1 $M_\odot$. The stellar parameters for an intermediate temperature T_2 = 100,000 K are $M_{bol} \sim -3.0$, $\log L_*/L_\odot \sim 3.1$ and $\log R_*/R_\odot \sim -0.9$. Such a star is in the middle of

the central star of planetary nebula region (ref. 3).

Between 2000 Å and 3200 Å the continuum contribution by the companion is assumed negligible in comparison to the nebular continuum. We attribute the continuum in this range to Balmer recombination for reasons that will be made evident further in the text. At 2400 Å the measured continuum flux is $F_\lambda \sim 5\times10^{-13}$ ergs cm^{-2} s^{-1} A^{-1} and yields a relation for continuum emission for an ionized nebula which is (ref. 3)

$$n_e^2 \, (L/L_o)^3 \, D_{1000}^{-2} \sim 3.45 \times 10^{18} cm^{-6} \qquad (1)$$

where n_e is the electron density in the nebula and L the linear size of the nebula scaled to $L_o \equiv a_o$, a_o is the semi-major axis of the elliptical orbit for a mass ratio of the two stars $M_1/M_2 \sim 2$, $M_2 \sim 1\ M_\odot$ and an assumed orbital period $\sim$ 376 days (ref. 1). On the other hand, from the Stromgren sphere relation we have

$$n_e^2 \, (L/L_o)^3 \sim 1.26 \times 10^{19} \, N_{47} \, cm^{-6} \qquad (2)$$

where N_{47} is the number of ionizing photons emitted per sec in units of 10^{47} s^{-1}. Accordingly, taking the distance to the system as $D_{1000} = 1$, we require $N_{47} \sim 0.3$ and therefore $T_2 \lesssim 100{,}000$ K.

The strength of all the observed lines is proportional to $n_e^2 \, L^3$ since collisional de-excitation would have to be negligible because of the existence of the semi-forbidden lines. The estimated upper limit to the electron density would then be $\sim 10^9$ cm^{-3}. Using the atomic data (ref. 3,4,5,6) we computed the theoretical line strengths. Taking all the ions present, one may estimate the elemental abundances for different nebular temperatures, T_e. We find the most reasonable abundances for $T_e \sim 12{,}500$ K, otherwise some elements are too overabundant or too underabundant with respect to the solar values. Using a number of arguments involving the absence of forbidden lines in the UV, the presence of the forbidden lines observed in the visible (ref. 1), the C III / C III] ratio, the ratios of lines in the O IV] multiplet and the absence of the two photon continuum, we estimate the approximate range of the densities in the nebula to be 10^8 - 10^9 cm^{-3} and the corresponding range of linear sizes 3×10^{14} - 6.5×10^{13} cm. We obtain reasonable ionic abundances from the observed line fluxes, with one exception, He III being underabundant by a factor of 10. It may very well be that the temperature of the secondary is in the low part of the range we estimated, $T_2 \lesssim 50{,}000$ K. The observed flat continuum above 2000 Å would then have to be due to something other than photoionization by the hot companion.

The low excitation lines of O I, Si II, Mg II and Fe II may be originating from different regions than the compact, ionized nebula. A cool chromosphere is possible, although the various possibilities cannot be distinguished.

TIDAL INTERACTION

It is interesting to note that for $n_e \sim 10^9 cm^{-3}$, the size of the nebula

would only be about five times the primary radius. Using an escape velocity from the primary of 100 km s^{-1} we estimate the steady state mass loss from the primary required to be 6×10^{-6} $M_\odot$ yr^{-1} for $n_e \sim 10^8$ cm^{-3} and 3×10^{-6} $M_\odot$ yr^{-1} for $n_e \sim 10^9$ cm^{-3}. These rates seem to be high for the primary in the general region of the H - R Diagram (ref. 7), which we would have expected to be less than $\sim 3 \times 10^{-7}$ $M_\odot$ yr^{-1}. It is interesting to note that the symbiotic star GX 1+4 seen to emit X-rays (ref. 8) has a nebula with radius and density similar to that of RW Hya. Its luminosity, however, at X-rays is high, $\sim 4 \times 10^{37}$ ergs s^{-1}. HEAO-2 ("Einstein") observations of RW Hya would be very useful. If Roche lobe overflow-a likely possibility-is occurring, we expect an X-ray luminosity of RW Hya comparable to GX 1+4; if capture from a stellar wind is occurring, more modest X-ray luminosities would be observed ($\sim 10^{34}$ ergs s^{-1}).

REFERENCES

1. Merrill, P. W. 1950, Astrophys. J., 111, 484.

2. Savage, B. D., and Mathis, J. S. 1979, Ann. Rev. Astr. and Astrophys., 17, 73.

3. Osterbrock, D. E. 1974, Astrophysics of Gaseous Nebulae (W. H. Freeman & Co.-San Francisco).

4. _____. 1963, Plan. Sp. Sc., 11, 621.

5. _____. 1970, Astrophys. J., 160, 25.

6. Kafatos, M., and Lynch, J. P. 1980, Astrophys. J. Suppl., April issue.

7. Cassinelli, J. P. 1979, Ann. Rev. Astr. and Astrophys., 17, 275.

8. Davidsen, A., Malina, R., and Bowyer, S. 1977, Astrophys. J., 211, 866.

TABLE 1.- LINE IDENTIFICATION AND FLUXES

Ionic Transition	Wavelength (A)	Wavelength of IUE Feature (A)	Flux (ergs cm^{-2} s^{-1})
S V]	1199.180	1199.200	1.56×10^{-12}
N V	1238.82+1242.8	1238.836+1242.82	2.73×10^{-11}
O I	1302.169 etc.	1302.468 etc.	1.83×10^{-11}
Si IV	1393.755	1393.930	5.08×10^{-11}
O IV]	1399.774	1399.810	
O IV]	1401.156	1401.198	
Si IV	1402.770	1402.928	
S IV] + O IV]	1404.770+1404.81	1404.770	
S IV]	1406.000	1406.084	
O IV]	1407.386	1407.414	
N IV]	1486.496	1486.512	5.59×10^{-11}
C IV	1548.185+1550.77	1548.448+1550.97	3.89×10^{-10}
He II	1640.332	1640.412	2.07×10^{-11}
O III]	1660.803	1160.914	4.10×10^{-11}
O III]	1666.153	1666.248	
N III]	1748.610	1748.840	8.27×10^{-12}
N III]	1749.674	1749.794	
N III]	1752.160	1752.378	
N III]	1753.986	1754.164	
Si III]	1892.030	1892.172	4.27×10^{-12}
C III]	1908.734	1908.922	5.76×10^{-11}
C II]	2325+2327+2328	2332.4	2.43×10^{-11}
Mg II	2796+2803	2799.4	1.00×10^{-11}
O III	3047	3040.0	9.70×10^{-12}
O III	3193	3141.6	2.62×10^{-11}

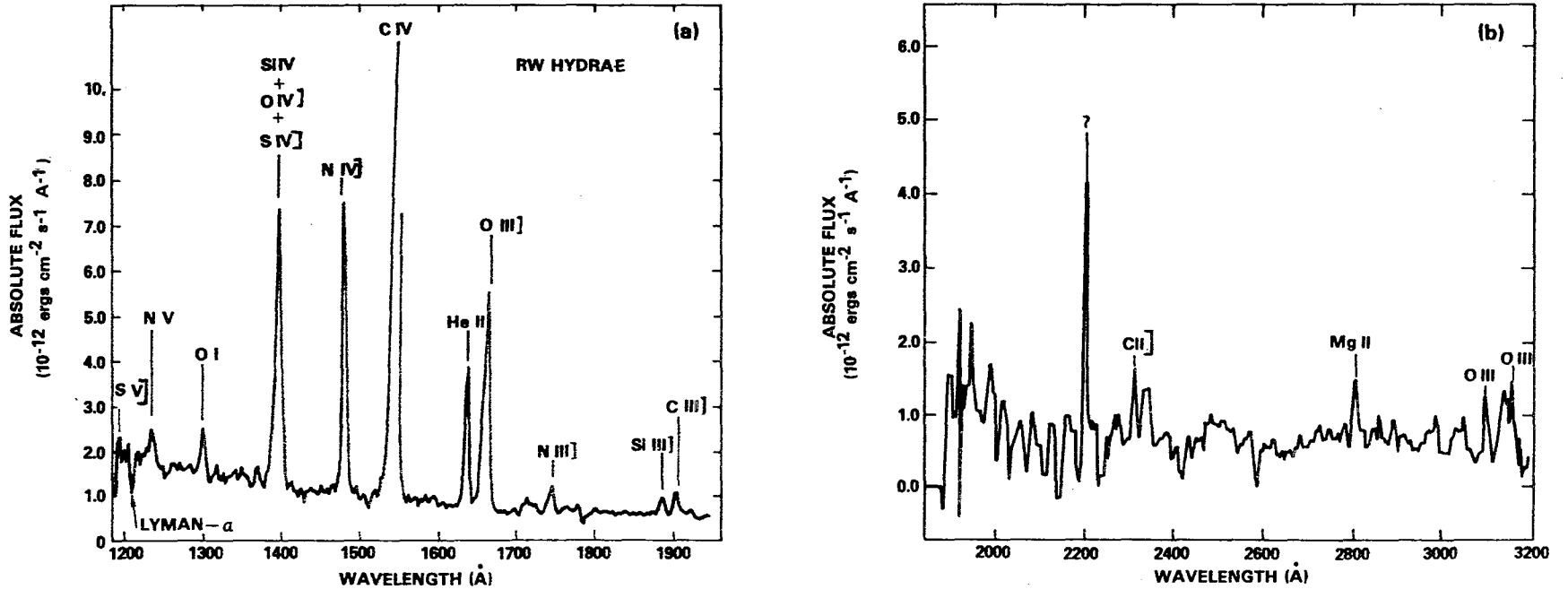
(a)
RW HYDRAE
ABSOLUTE FLUX
(10^-12 ergs cm^-2 s^-1 A^-1)
WAVELENGTH (Å)
LYMAN−α
S V]
N V
O I
Si IV
+
O IV]
+
S IV]
N IV]
C IV
He II
O III]
N III]
Si III]
C III]
(b)
ABSOLUTE FLUX
(10^-12 ergs cm^-2 s^-1 A^-1)
WAVELENGTH (Å)
?
C II]
Mg II
O III
O III

FIG. 1.

IUE OBSERVATIONS OF CIRCUMSTELLAR EMISSION FROM THE LATE TYPE VARIABLE R AQR (M7 + pec)

Robert W. Hobbs and A.G. Michalitsianos
Laboratory for Astronomy and Solar Physics
NASA-Goddard Space Flight Center

M. Kafatos
George Mason University

ABSTRACT

As part of a program to observe circumstellar emission from late type stars, IUE observations of R Aqr (M7 + pec) have been obtained in low dispersion. Strong permitted, semi-forbidden and forbidden emission lines are seen, superimposed on a bright ultraviolet continuum. We deduce that the strong emission line spectrum that involves C III], C IV, Si III], [O II] and [O III] probably arises from a dense compact nebula the size of which is comparable to the orbital radius of the binary system of which R Aqr is the primary star. The low excitation emission lines of Fe II, Mg II, O I and Si II probably arise in the chromosphere ($T \sim 10{,}000$ K) of the R Aqr. The secondary is probably a white dwarf, comparable to or somewhat brighter than the sun, since such a star can produce enough ionizing photons to excite the continuum and emission line spectrum and yet be sufficiently faint as to escape detection by direct observation. We attribute the UV continuum to Balmer recombination from the dense nebula and not to blackbody emission from the hot companion.

I. Data, Analysis, and Introduction

Ultraviolet spectra (Figures 1 and 2) of the late type star R Aqr (M7 + pec) have been obtained with the International Ultraviolet Explorer (IUE) and reveal intense emission lines and continuum. This is consistent with earlier optical observations of Merrill[1, 2, 3] which indicate that the system consists of hot stellar companion and a relatively cool late type star. In low dispersion the spectrum between 1200 Å to 3200 Å shows strong permitted emission lines of C IV (1548 Å, 1550 Å), Si III (1883 Å, 1892 Å), C III (1907 Å, 1909 Å) and Mg II (2796 Å, 2803 Å), forbidden emission lines of O II (2470 Å) and probably [O III] (2321 Å). The UV observations are thus consistent with lines of [O III] (4929 Å, 5007 Å) observed in the optical spectra of Merrill[3] and [O II] (3726 Å, 3729 Å) of Ilovaisky and Spinrad[4].

The strong lines of He II, C II, C IV , O I, O III , O IV, S II, Si IV and Fe II are evident in the spectrum. The identification of N V and Si II 1304 Å, 1309 Å is ambiguous because other lower excitation lines of nitrogen are not present, and similarly for silicon, Si II 1265 Å is not observed. A number of Fe II features in various multiplets are also identified.

In addition to the bright emission line spectrum there is a general ultraviolet continuum, the intensity of which appears independent of wavelength over the spectral range observed. We attribute the origin of this continuum to hydrogen recombination rather than H I two-photon emission.

Of particular interest in our observations is the distinct lack of a stellar UV continuum that should be present if an O or B type main sequence star is the source of excitation in the nebula, as has been suggested by Merrill[3]. We conclude that the continuum observed most likely originates not from a stellar source, but from a low excitation nebula with an electron temperature $T \sim 15{,}000$ K and characteristic size 10^{15} cm. The source excitation is a sub-luminous central planetary nebula star or bright white dwarf of $T_* \geq 50{,}000$ K, whose orbit about the primary M7 star is comparable to the size of the ionized nebula, i.e. $10^{14} - 10^{15}$ cm. The details of our conclusions are discussed in the following sections.

The low excitation lines of Fe II and Mg II have been previously observed in the spectra of single late type stars by Carpenter and Wing [5], and the presence of the above lines as well as O I and Si II lines in the UV spectrum of R Aqr argues strongly for a cool chromosphere $T_* \sim 10{,}000$K for the primary M7 star[6]. However, we assume from our analysis that other high excitation lines observed in our data do not arise from the companion directly. We attribute the formation of the majority of strong lines to a compact nebula that is excited by emission from the hot companion.

The observed continuum flux can be used to obtain the general parameters of the nebula. These parameters can then be checked against those derived from our analysis of the continuum spectrum. For that purpose we have used the combined strengths of C II (2325, 2327, 2328 Å), C IV (1548, 1551 Å), C III] (1907, 1909 Å), [O II] (2470 Å), [O III] (2321 Å) and O IV] (1400, 1401, 1405, 1407 Å). We have selected these lines because they consist of various ion species, they are the strongest features in the spectrum, and because there is little ambiguity in identification. However, it is not clear if the 1402 Å feature is due entirely to O IV], and what portion of the broad 2328 Å feature is due to [O III] or C II.

The observed continuum is essentially flat and rises slightly toward long wavelengths. The continuum, therefore, cannot be due to a star since a stellar continuum would vary with wavelength by more than an order of magnitude over the spectral range observed. Balmer recombination and H I two-photon emission arising from a nebula are possible mechanisms to explain this continuum. However, shortward of 3200 Å the two-photon continuum of hydrogen will dominate if the densities are sufficiently low ($\lesssim 10^4$ cm^{-3}), and will produce a prominent peak in intensity around 1400 Å (Bohlin, Harrington and Stecker[7]); this peak is not observed in our data, and we conclude that the two-photon process is not the dominant mechanism. On the other hand, the Balmer recombination continuum depends only weakly on temperature for T~15,000 K and the expected flux varies only by a factor of

two between 1200 to 3200 Å. We conclude that this mechanism dominates and that the densities involved must be $\gtrsim 10^5$ cm^{-3}, since densities appreciably lower than this value would result in a conspicuous two-photon continuum peak around 1400 Å. Given this lower limit in density we can calculate a corresponding upper limit for the diameter of an ionized nebula responsible for the observed flux, $\sim 5 \times 10^{14}$ cm.

A further argument in support of a nebula with this characteristic size and density as that found above can also be made from observations of emission lines in the visible by Merrill[3]. Merrill[3] determined an orbital period for the hot companion of approximately 27 years from radial velocity measurements. The corresponding size of the semi-major axis for an elliptical orbit with this period is 1.7×10^{14} to 2.1×10^{14} cm, for a mass ratio of the primary and secondary of 1:1 and 3:1, respectively (assuming one solar mass for the secondary). If the ionized nebula was appreciably larger than the separation of the stars one would not expect to observe substantial variations in line strengths. However, Ilovaisky and Spinrad[4] have compared their visual spectral data of R Aqr to earlier observations of Merrill and found no evidence for a hot stellar companion whatsoever. From this they suggest the emission properties of the spectrum are probably time-dependent. Merrill[3] also found that the apparent position of the nebular emission appears to vary with time. Accordingly, this is consistent with our model that suggests the ionized nebula is comparable in scale to the size of the binary orbit. At a distance of 260 pc a central ionized cloud of scale size $L = 2 \times 10^{14}$ and electron density of $n_e = 1.5 \times 10^7$ cm^{-3} is sufficient to explain the observed recombination continuum.

The densities we obtained above from observations of the UV continuum can also be roughly checked by the [O III] line strengths observed by Merrill[3] who found that the 4363 Å line is unusually strong, and that prior to 1934 "the ratio of its intensity of 4959 Å is equaled or exceeded in only one other nebula, IC 4997". The intensity of the hydrogen lines relative to those of [O III] R Aqr is similar to that observed in most planetary nebulae, Hβ being about equal to 4959 Å prior to 1922. After this time the hot component started to dominate the spectrum for a few years reaching a maximum in 1933-34[8]. From Aller and Liller[9] we estimate the intensity ratio of the 4363 Å to 5007 Å and 4959Å i.e. I(4363 Å)/I(4959 Å, 5007 Å) 0.1 for the planetary nebula IC 4997 observed in 1922. Based upon the observations of IC 4997 (Aller and Liller[9] and the statement of Merrill [3] concerning the similarity of this ratio of R Aqr to that of IC 4997 prior to 1934 (i.e. 1922), it follows that the strength of the 4363 A line agrees with densities $10^6 \lesssim n_e \lesssim 10^8$ cm^{-3} for temperatures $3 \times 10^4 \lesssim T \lesssim 8 \times 10^3$, respectively (Kafatos and Lynch[10].

Moreover, as deduced from our continuum measurements the nebular density cannot be more than $\sim 10^8$ cm^{-3} since the [O II] and O[III] lines would be suppressed, and the 4363 Å line would be even stronger. Additionally, if densities were much higher the nebula would be comparable in extent to the size of the primary M7 star, which is unrealistic on physical grounds. It follows that the nebular parameters from the foregoing arguments are in the

range $10^5 \lesssim n_e \lesssim 10^8$ cm^{-3}, $10^{14} \lesssim L \lesssim 10^{15}$ cm, and $10^4 \lesssim T \lesssim 3 \times 10^4$ K. We adopt a model $n_e \lesssim 10^7$ cm^{-3}, $L \sim 2 \times 10^{14}$ cm and $T \sim 15{,}000$ K.

b.) Emission Lines

We have also deduced the nebular parameters and the relative ionic abundances by two different methods, i) by using the carbon line strengths, ii) by using the oxygen line strengths. We have assumed that the scale size of the nebula is $L \sim 2 \times 10^{14}$ cm; although the general trend of our results appears somewhat insensitive to this parameter, we have assumed normal cosmic abundances for the various elements under consideration[11].

i) carbon line strengths (model A)

The semi-forbidden lines of C II and C III and the allowed lines of C IV can be used with one another to find the product $n^2 L^3$ [12, 13, 14, 15]. It is essential that we identify the 2328 Å feature as C II], otherwise no self-consistent model can be constructed using the carbon lines (even if the [O III] were present it would not be more than 0.1 of the total intensity of the feature). The results of this calculation are shown in Table 1 (Model A). The ionic abundance N(O II) and N(O III) can then be obtained (the latter is an upper limit since some O IV could also be present). We can also obtain the ionic abundance of He III from the 1640 Å line using this carbon line strength analysis. However, the ionic abundance of the He III is found to be large in this case and all of the helium would have to be doubly ionized. We have deduced the H-α (6563 Å) and [O III] 5007 Å) as well as the flux of the continuum in Table 1 (Model A). Although Model A is not unique it does indicate a general trend in our data. Reasonable ionic abundances for the oxygen ions can be obtained if we use the carbon line strengths to $n^2 L^3$. However, the densities would have to be generally lower than might be suggested by the strong [O III] 4363 Å line observed by Merrill[3]. Additionally, the computed flux level of the continuum from Model A is too low to explain our data.

ii) oxygen line strengths

Assuming the 2328 A feature is mainly due to [O III] and the 1402 Å feature is mainly O IV], one can obtain values of n_e and T[10]. Since collisional depopulation becomes important above 10^6 cm^{-3}, the forbidden lines values of n_e obtained from a single temperature are not unique, but are relatively insensitive to temperature. A typical case is shown in Table 1 for T = 15,000 K and L = 2×10^{14} cm (Case B). The continuum deduced from the line strengths of oxygen agree well with the observed continuum. Moreover, the deduced ionic abundance of He III agrees with the ionic abundance of O III (helium is essentially singly ionized, whereas oxygen is mostly doubly ionized).

On the other hand, if we use the cosmic abundances of carbon in this analysis, the line strengths should be a factor of ~50 larger than what is observed. The only alternative is to assume that atomic carbon is under-

abundant by a factor ~50 in the ionized nebula. The depletion of carbon could be the result of the precipitation of carbon into grains. The relatively low abundance deduced in our analysis appears generally to be the case since this result will not change even if parameters in Table 1 are varied (say the temperature is varied between 10,000 K to 15,000 K). At this point, however, it is not possible to distinguish between either Models A or B. It suffices here to say that Model B appears more attractive since it does account for the continuum.

It is of interest to note that the values of the nebular parameters deduced in our analysis, i.e. $L = 2 \times 10^{14}$ cm, $n_e \sim 10^5 - 10^7$ cm^{-3} and $T \sim 15{,}000$ K agree with the general parameters for nebular emission in symbiotic stars of[16].

The compact nebula could be entirely the result of mass loss from the primary star. Applying the equation of continuity and estimating the escape speed of the M7 giant to be 24 km s^{-1}, that was obtained using the period-density relation for a period = 387 days and an assumed stellar mass of $1M_\odot$ to $3M_\odot$, we find $M = 10^{-7} M_\odot yr^{-1}$ for a nebula of radius $r \equiv L/2$ 10^{14} cm and density $n_e \sim 1.3 \times 10^7$ cm^{-3}. This mass loss rate is probably a lower limit since, as will be shown later on, the hot companion is too faint to ionize the entire nebula. It is also unlikely that all the material lost by the star is still ionized.

c.) properties of the stellar companion

We have already seen that the observed continuum cannot be due to a star and most likely arises from a nebula. However, since we have assumed that the source of nebular excitation is a sub-luminous white dwarf, the nebular continuum flux observed of 10^{-13} ergs cm^{-2} s^{-1} A^{-1} places an upper limit of flux that is contributed by the companion. In Table 2 we show the stellar parameters for the unseen companion if its flux contribution in the continuum is this upper limit.

In the first column of Table 2 we assume a temperature for the hot companion. The second column gives the corresponding stellar radius if the continuum at the detector is 10^{-13} ergs cm^{-2} s^{-1} A^{-1} at 1200 Å. The third column gives the luminosity in solar units. Columns 4 and 6 give the absolute flux and apparent visual magnitudes, respectively. The last column indicates the number of ionizing photons $N_i(s^{-1})$ emitted by the star.

This upper limit of continuum flux suggests a star whose apparent magnitude is too faint to be observed today. However, in 1934 it attained $m_v \sim 8$ magnitudes. In order for it to be observable today the continuum would have to be 10^4 times greater. The 1934 event appears, therefore, to have been en eruption of the hot companion that was not sufficiently strong to be classified a nova. It is possible that this eruption was triggered by mass transfer from the primary to the secondary.

We also note that the companion can ionize the dense nebula in the system. The stellar temperatures required are in the approximate range of 10^5 to 1.5 x 10^5 K, although temperatures as low as 5 x 10^4 K could be assumed if the density of the nebula was slightly lower than that shown in Model B. It is most likely the case that the compact ionized nebula is "ionization" bound rather than "density" bound and therefore, the mass rate for the primary of 10^{-7} $M_\odot$ yr^{-1} is likely a lower limit. We also find that nebular temperatures greater than 15,000 K are required, otherwise the density implied by the analysis based on the oxygen line strengths would be high, and a much brighter star would be required to ionize the nebula.

We find that the nebular parameters deduced from our oxygen line analysis, $n_e \sim 10^7$ cm^{-3}, 1.5 x $10^4 \leqslant T \leqslant$ 2.5 x 10^{14} cm, and the companion 5 x $10^4 \lesssim T \lesssim$ 1.5 x 10^5 K, 0.7 $\lesssim L_* \lesssim$ 7L can account for the nebular continuum, explain the observed emission lines, and provide sufficiently low stellar luminosity that the companion could not be seen directly.

III. Summary

The UV emission observed in our data and the forbidden line emission observed by Merrill[3] and Ilovaisky and Spinrad[4] are most likely the result of the excitation of a nebula by a white dwarf. If an O or B type main sequence star is postulated as the excitation source of the nebula, such a model could not reconcile the continuum properties of the ultraviolet spectrum. Accordingly, our model is constrained to adopt a model in which a bright white dwarf (few $L_\odot$) is the companion to the M7 giant. The fact that a white dwarf is capable of supplying enough ionizing photons to excite the emission lines observed further strengthens this interpretation. We can summarize the general properties of our model as follows: R Aqr is a symbiotic star system that most likely consists of an M7 primary and white dwarf companion. The 27 year period we have adopted from Merrill[3] for the companion star is such that for reasonable mass ratios of 1:1 and 1:2 (assuming the dwarf to be a $1M_\odot$) the physical separation of the stars is a few x 10^{14} cm, which is also the approximate dimensions of the ionized nebula. The faint hot companion star is itself not sufficiently luminous to be observable directly. Its presence, however, is manifested in the ionizing effects which it has on its immediate surroundings, which create a low excitation nebula. Further observations in the radio, visible and ultraviolet would be useful in monitoring the time-dependence of the different emitting regions.

REFERENCES

1. Merrill, P.W., 1921, Astrophys. J., 53, 375.
2. _____. 1935, ibid, 81, 312.
3. _____. 1950, ibid, 112, 514
4. Ilovaisky, S.A. and Spinrad, H. 1966, Pub. Ast. Soc. Pacific, 78, 527.
5. Carpenter, K.G. and Wing, R.F. 1979, Bull. Am Ast. Soc., 11, 419.
6. Linsky, J.L. 1979, Bull. Am. Phys. Soc., 24, 771.

7. Bohlin, R.C., Harrington, J.P. and Stecker, T.P., 1978, Astrophys. J., 212, 575.
8. Mattei, J.A. 1979, J. Roy. Ast. Soc. Canada, in print.
9. Aller, L.H. and Liller, W. 1966, M.N.R.A.S., 132, 337.
10. Kafatos, M. and Lynch, J.P. 1979, Astrophys. J., submitted.
11. Cameron, A.G.W. 1973, Space Sci. Rev., 15, 121.
12. Osterbrock, D.E. 1963, Pla. Space Sci., 11, 621.
13. _____. 1970, Astrophys. J. 160, 25.
14. _____. 1974, Astrophysics of Gaseous Nebulae (W.H. Freeman & Co., San Francisco).
15. Bely, O. 1966, Proc. Phys. Soc., 88, 587.
16. Boyarchuck, A.A. 1975, Variable Stars and Stellar Evolution, eds. Sherwood, V.E. and Plaut, L. (D. Reidel Pub. Co.-Holland), 377.

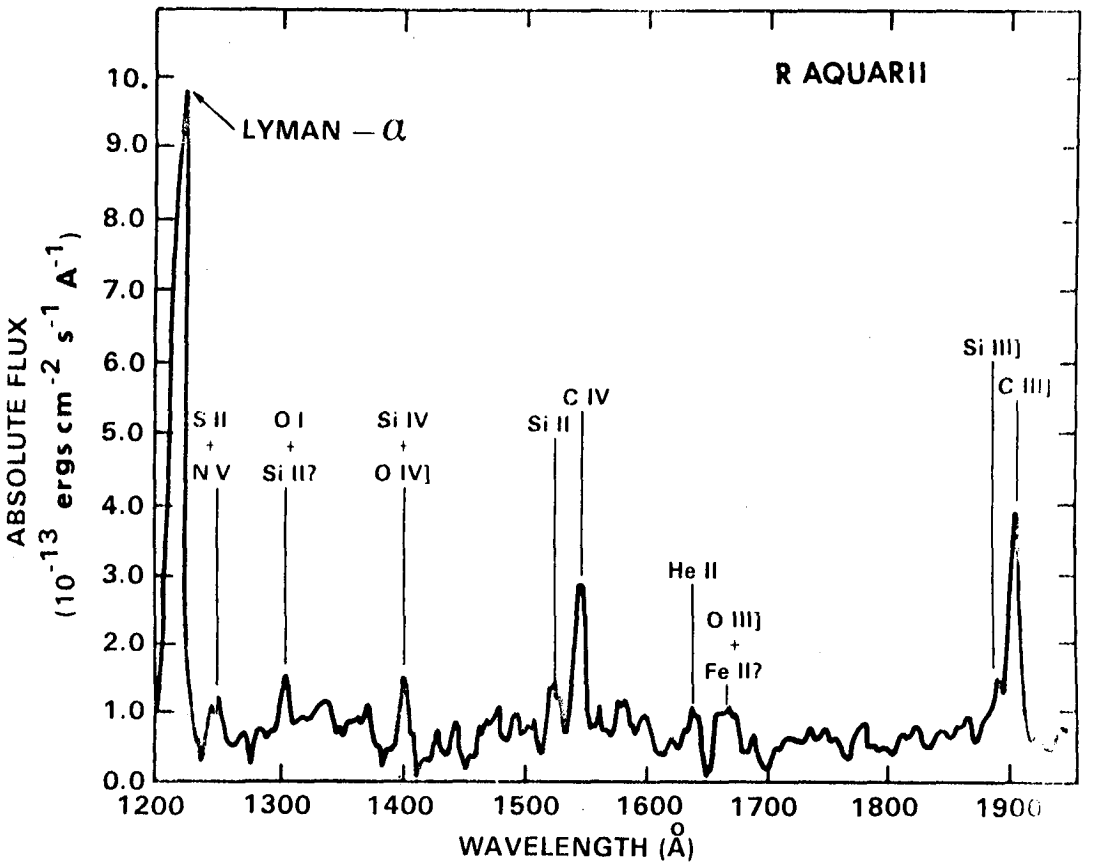

Figure 1:
Low dispersion (~ 6 A resolution) spectrum of R Aqr obtained on July 25, 1979 in the wavelength range 1200 Å to 2000 Å using the large aperture (10" x 20") of the IUE spectrometer. The exposure time on the SEC Vidicon camera was 10 minutes. The Lyman-α line at 1216 Å has a combined intensity of the geocoronal and stellar Lyman-α emission. The spectrum is deconvolved and geometrically and photoelectrically corrected. The absolute flux scale is accurate to a factor two using the standard IUE reduction program.

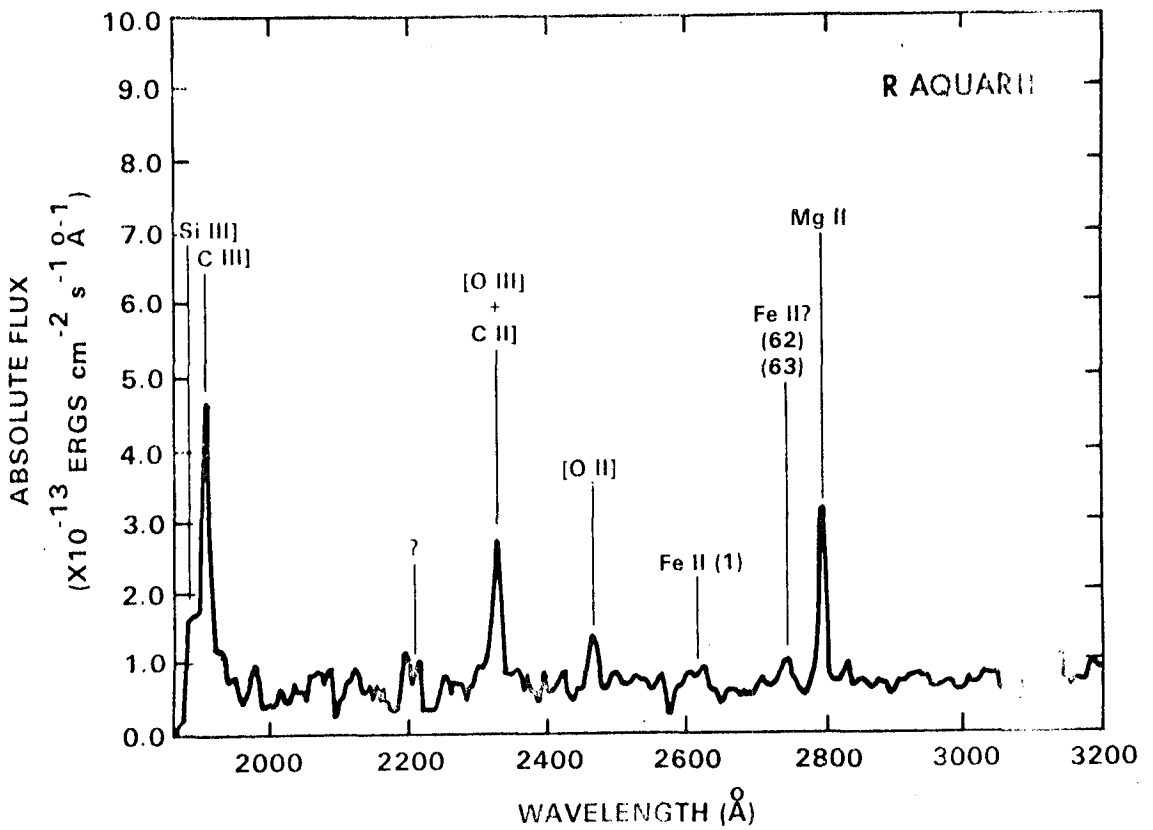

Figure 2:
Low dispersion spectrum of R Aqr between 2000 Å and 3200 Å obtained with the large aperture on IUE. Exposure time was 20 minutes. The feature identified with a question mark is probably an artifact in the detector. The continuum level is seen to rise slightly toward long wavelengths.

TABLE 1

Nebular Parameters

$L = 2 \times 10^{14}$ cm, $T = 15{,}000$K

Case A Carbon Line Analysis		Case B Oxygen Line Analysis	
$n_e^2 L^3 (cm^{-3})$	4.4×10^{55}	$n_e^2 L^3 (cm^{-3})$	1.25×10^{57}
N(C II)	0.53	N(O II)	0.06
N(C III)	0.32	N(O III)	0.86
N(C IV)	0.15	N(O IV)	0.08
$n_e (cm^{-3})$	2.3×10^{6}	$n_e (cm^{-3})$	1.25×10^{7}
N(O II)	0.81	N(C II)*	0.09
N(O III)	0.19	N(C III)*	0.55
N(He III)	1	N(C IV)*	0.36
Flux (H-α) 6563A (ergs cm^{-2} s^{-1})	1.2×10^{-12}	N(He III)	0.02
Flux [O III] 5007A (ergs cm^{-2} s^{-1})	1.5×10^{-12}	Flux (H-α) (ergs cm^{-2} s^{-1})	3.3×10^{-11}
$F_{Continuum}$(2000A) (ergs cm^{-2} s^{-1} A^{-1})	10^{-15}	Flux [O III] 5007A (ergs cm^{-2} s^{-1})	5.5×10^{-11}
		$F_{Continuum}$(2000A) (ergs cm^{-2} s^{-1})	2.0×10^{-14}

*see discussion in text

TABLE 2

HOT COMPANION

$T_*(K)$	$R_*/R_\odot$	$L_*/L_\odot$	M_V	m_v	$N_i(s^{-1})$
1.5×10^5	4.1×10^{-3}	7.4	12	19.1	4.3×10^{44}
10^5	5.6×10^{-3}	2.8	11.4	18.5	2.0×10^{44}
5.0×10^4	1.2×10^{-2}	0.75	10.1	17.2	5.0×10^{43}

T_* : stellar temperature

R_* : stellar radius

L_* : stellar luminosity

M_V : absoulte visual magnitude

m_v : apparent visual magnitude

N_i : number of ionizing photons emitted by companion

IUE OBSERVATIONS OF TWO LATE TYPE STARS BX MON (M4 + pec) AND TV GEM (M1 Iab)

A.G. Michalitsianos
R.W. Hobbs
Laboratory for Astronomy and Solar Physics
NASA Goddard Space Flight Center
Greenbelt, MD

M. Kafatos
Department of Physics
George Mason University
Fairfax, Virginia

ABSTRACT

IUE observations of two late type stars BX Mon and TV Gem have been obtained that reveal the emission properties in the ultraviolet of sub-luminous companions. Analysis of the continuum emission observed from BX Mon suggests the companion is a middle A III star. High excitation emission lines observed between 1200 Å and 2000 Å (C IV, Si III], C III]) that generally do not typify emission observed in either late M type variables or A type stars are also detected. It is suggested that these strong high-excitation lines arise in a large volume of gas heated by non-radiation processes that could be the result of tidal interaction and mass exchange in the binary system. In contrast to stars such as BX Mon that are observed in the visible to have emission lines superimposed on the strong absorption of the M giant, the luminous M1 supergiant TV Gem shows unexpected intense UV continuum throughout the sensitivity range of IUE. The UV spectrum of TV Gem is characterized by intense continuum with broad absorption features detected in the short wavelength range. Our analysis shows that the companion could be a B9 or A1 III-IV star, although a fully self-consistent model including the observed color index has as yet not been fully developed. Alternate suggestions are presented for explaining the UV continuum in terms of an accretion disk in association with TV Gem.

INTRODUCTION

IUE observations of two late type giants BX Mon (M4 + pec) and TV Gem (M1 Iab) were obtained that reveal strong emission continuum. BX Mon was selected for IUE observations because earlier ground-based spectra obtained by Minkowski showed broad emission in Hα, Hγ, and H: that are superimposed on a strong absorption spectrum[1]. As such, the visible spectrum suggests the presence of a hot companion that is not sufficiently luminous to dominate the integrated light of the binary system. Following the observations of Minkowski further work by other observers was not pursued, leaving only sparse references in the literature that collectively indicate this star could possibly be an intense source of ultraviolet emission, and possibly a symbiotic system. Our UV observations, however, indicate that the companion is most likely a middle A luminosity III-IV star. The general appearance of the UV spectrum from BX Mon is not representative of UV spectrum observed in

classic symbiotics, which suggests that BX Mon most likely does not undergo tidal interaction or mass exchange with its companion to the same extent as currently envisaged for symbiotic stars. This follows because the ultraviolet spectrum in the long wavelength range (2000 Å to 3200 Å) is dominated by blackbody emission continuum that can be explained by an A main sequence star, and accordingly, does not typify the general models presently considered for symbiotic stars that have as companions white dwarfs or central stars of planetary nebulae. However, the high excitation lines in emission that are observed suggest a large volume of gas is present that is not heated by photo-excitation processes.

On the other hand, the detection of strong ultraviolet continuum from TV Gem is unexpected because earlier ground-based spectral classification observations suggest this star is only a normal M type supergiant [3,4]. Similarly, photometric observations of TV Gem[5,6] do not show a blue excess in the continuum, which is a result consistent with earlier spectral data obtained from ground-based observations.

Low dispersion UV spectra obtained in both short and long wavelength cameras show strong continuum throughout the IUE spectral range. The continuum is for the most part featureless with the exception of a number of broad absorption features in the short wavelength spectrum. These features might be identified with Si, Al and Fe absorption found in early B or A luminosity II-III stars[7]. However, a fully self-consistent model that explains our UV spectra and earlier ground-based photometric observations of TV Gem has as yet not been fully developed. We discuss the details concerning our observations and analysis of both stars in the sections that follow.

BX Mon: Observations and Analysis

Mayall[8] determined the intrinsic light period of BX Mon = H.V. 10446 of 1380 days; that designates this star as the longest recorded intrinsic variable. It is listed in the Catalogue of Emission Line Stars of Bidelman[1]. IUE observations of BX Mon were obtained on 31 August 1979 in low dispersion (~ 6 Å spectral resolution) using 60 minute exposures in both the short and long wavelength cameras and the large (10" x 20") entrance aperture of the IUE spectrometer. The FES white light monitor obtained a visual magnitude ~11, which places the luminosity of the primary star near maximum light at the time of these observations. The observed extremes in m_v are 11 to 13 magnitudes[8]. IUE spectra in high dispersion are not possible owing to the unreasonably long exposures required to achieve adequate signal-to-noise.

The short wavelength spectral range exhibits both continuum and line emission. Between 1200 Å and 2000 Å the spectrum is characterized by O I (1302 Å), C IV (1548, Å 1550 Å), Si III] (1892 Å) and C III] (1906 Å) emission (Figure 1). The absolute line fluxes measured for the strongest emission lines are shown in Table 1, and were obtained using the data reduction routines in FORTH developed by Drs. Klinglesmith and Fahey at NASA/GSFC. The long wavelength spectral range (2000 Å to 32000 Å) is

generally dominated by the continuum of the hot companion. The absorption feature at 2800 Å due to Mg II (2800 Å) is found typically in 8000 K to 10,000 K A type main sequence stars[12].

The continuum of the hot companion in the long wavelength range was found to be best approximated by line blanketed continuum models that correspond to A type luminosity class III stars around 9000 K[9]. As such, we adopt an A4 or A5 III star as the companion to BX Mon. From the observed continuum distribution with blanketing, we deduce an $E_{B-V} \sim +0.25$ for the interstellar absorption[11]. A lower limit of distance can be approximated if we suppose that the A type companion has a visual magnitude sufficiently less than the primary at minimum so that it does not dominate the integrated light of the system. Accordingly, as an upper limit we assume $m_V \gtrsim 14$, whose corresponding absolute magnitude M_V from Allen (ref. 12) is $M_V = +2.5$, appropriate for an A4 type III star. A lower limit of distance $d \sim 1400$ pc is obtained assuming these conditions.

The high-excitation lines emission observed in the 1200 Å and 2000 Å range are, however, more difficult to explain in terms of emission from either an M4 or A main sequence star. It is unlikely that the high excitation line emission such as C IV (1548 Å, 1550 Å) is explained by a late A type star because the appearance of such lines is inconsistent with UV spectra of A1 V to A7 IV-V stars obtained by OAO-2[12]. Analysis of Ca II K line core emission in A1 V to A7 IV-V stars suggests also that chromospheric emission is minimal for these spectral types[13]. Chromospheric emission from the cool M4 giant atmosphere is also unlikely because IUE spectra obtained of late type M variables and Mira variables and even M supergiants suggest only a warm chromosphere ($T_{chromosphere} \sim 10{,}000$ K) is present[14, 15]; that is not sufficiently ionizing to produce the observed line emission.

It is likely that mass loss commonly associated with late type M stars[16] forms a circumstellar shell around the binary system. Photoexcitation and recombination processes are not appropriate here for exciting circumstellar material because middle A type main sequence stars cannot provide sufficient UV ionizing photons in the circumstellar envelope volume ($r \gtrsim 10^{15}$ cm) to explain the observed excitation. As such, invoking a form of mechanical heating through shock waves, tidal interaction or possibly strong stellar magnetic fields provides speculative ideas for model development. More spectra in the visual, UV are required to develop a general model that encompasses all aspects of emission from this interesting object.

UV Observations of TV Gen = HD42475

IUE observations of TV Gem were obtained in low dispersion using 10 minute exposures in both short and long wavelength cameras on November 25, 1979. Observations were repeated in the same manner on January 16, 1980, with essentially similar results. The spectrum is characterized by strong continuum that is devoid of emission lines but which has broad absorption features in the short wavelength spectral range (Figure 2). The absorptions features observed are centered at 1400 Å, 1540 Å, 1604 Å. The low resolution of ~6 Å makes precise identification of these absorption features

difficult. The feature centered around 1400 Å is possibly explained by the presence of Si IV lines that appear blended in low dispersion spectra. Si IV 1400 Å absorption would typify middle B type main sequence stars[17] as we have found by examining low resolution spectra from OAO-2 of early standard stars. The features identified in Figure 2 persist even if the spectra from different observing dates are averaged together, supporting the view that these features are real and not detector noise.

Broad features, centered at 1540 Å and 1604 Å, that are $\Delta\lambda \sim 40$ Å and $\Delta\lambda \sim 20$ Å in width, respectively, are also observed. The feature at 1604 Å is possibly explained as Fe III (1601 Å, 1611 Å, UV118) or Al III (1600 - 1612 Å) observed in early O and B stars. Generally, B5 to B7 V stars exhibit weak absorption due to Si IV and C IV[17]. As seen here the features at 1400 Å and 1604 Å would be consistent with this interpretation. However, the feature at 1540 Å cannot be attributed to C IV because its measured wavelength (even in low resolution) is too far removed from the rest wavelengths of the resonance doublets (1548 Å, 1550 Å). It could, however, be possibly attributed to Fe III.

Observations that were kindly made available to us by Dr. J.B. Oke using the multi-channel scanner of the 200-inch telescope confirms the existence of large excess continuum in the near UV between 3500 Å and 3200 Å. The visible spectrum is characterized by normal M1 or M0 type I supergiant emission in which TiO bands dominate the absorption. Early spectral classification work has classified TV Gem as a normal M1 supergiant. Emission in the hydrogen lines, ionized and neutral species are not observed [22], although this star is noteworthy for having particularly weak Ca II H and K emission[22].

Comparing the general properties of the UV continuum in the short wavelength range with OAO-2 spectra of standard early type stars, we find that the continuum might be explained if the companion is a B9 - A1 (III-IV) star. An O or B supergiant is immediately ruled out because such a star would be sufficiently luminous that earlier spectral classification observations [20, 21] would have detected its presence. On the other extreme, a bright white dwarf or central star of a planetary nebula is also ruled out because the expected UV continuum flux based on stellar parameters[12] would be $\sim 10^2$ times less than observed for a star at 1400 pc.

Based on the adopted distance to TV Gem, a B9 III-IV star would have an apparent magnitude uncorrected for absorption $m_V = 10.35$ (absorption corrected $m_V = 9.15$), and corresponding absolute magnitude $M_V = -2.8$ and bolometric magnitude $M_{bol} = 3.4$. Similarly, an A1 III - IV type would have $m_V = 9.8$ uncorrected for absorption (absorption corrected $m_V = -2.8$) and $M_{bol} = -3.1$.

If we postulate the existence of a B9 or A1 III - IV type star the difference in apparent magnitude between the two stars is 2 to 3 magnitudes. Although the M1 supergiant is brighter than a B9 or A1 star by approximately 3 magnitudes, one would expect that some level of flux contribution to the photometric color of the M1 be made by an early companion, especially in the

blue band. For TV Gem B-V = +2.30 [23] and B-V = +2.25[24], that is consistent with typical photometric colors of normal M1 supergiants. For comparison an M1 supergiant similar to TV Gem such as α Sco (M1 Iab + B), but known to have an early companion, has a B-V = +1.82 [24]. The difference in magnitudes between primary and secondary in α Sco is $\Delta M \sim 4$. Accordingly, the B-V color index of TV Gem does not indicate an abnormally high level of blue continuum but in fact suggests a color typical of only a cool star, even though the estimated magnitude difference between primary and secondary is $\Delta M \sim 3$. The B-V in TV Gem should in fact be even smaller than that measured for α Sco on the basis of this analysis.

An observational test to determine if in fact an early companion is associated with TV Gem would consist of a UBV monitoring program. TV Gem has a variable designation SRc and as such has irregular excursions in luminosity that occur on timescales of 182 days. If the companion is assumed to have constant brightness, the B-V color index of TV Gem should become smaller as the M supergiant approaches minimum light. If a correlation is established between color and brightness in the manner described here, this would argue in favor of the presence of an early companion star.

An alternative explanation of our IUE data might be found if we consider the presence of a high energy source in close proximity to the extended envelope of the M1 supergiant. If $F\lambda \alpha \lambda^{\circ}$ or even $F\lambda \alpha \lambda^{-1}$, then $F_{\nu} \alpha \nu^{-2}$. This frequency dependence is similar to the properties of the high energy spectrum in soft X-rays observed in well known X-ray sources. Emission from an accretion disc onto a compact object may thus explain the strong UV continuum. This interpretation immediately explains the general absence of blue excess in the spectrum of TV Gem and an absence of strong or weak emission lines. As such, an accretion disk could form from the material exchanged from the extended envelope of the primary that falls on a condensed object that would heat infalling material to temperatures in the 10^6 K range. Observations in the visual, UV and X-rays are required to further discern the properties of the companion to TV Gem.

REFERENCES

1. Bidelman, W.P., 1954, Astrophys. J. Supp., 1, 175.
2. Michalitsianos, A.G., Kafatos, M., Hobbs, R.W. and Maran, S.P., 1980, Nature, 284, 148.
3. Keenan, P.C. 1942, Astrophys. J., 95, 461.
4. Morgan, W.W. and Keenan, P.C., 1873, Ann. Rev. Astro. and Astrophys., 11, 29.
5. Humphreys, R.M. 1970, Astron. J., 75, 602.
6. Lee, T., 1970, Astrophys. Jr., 162, 217.
7. Nandy, K., 1976, Highlights of Astronomy (D. Reidel Publ. Co.-Holland), 4, Part II, 289.
8. Mayall, M.W., 1940, H.C.O. Bull., 913, 8.
9. Kurucz, R.L., 1979, Astrophys. J. Supp. 40, 1.
10. Panek, R.J., 1977, Ap. J., 216, 747.

11. Spitzer, L., 1978, Physical Processes in the Interstellar Medium (New York: John Wiley & Sons).
12. Allen, C.W., 1973, Astrophysical Quantities.
13. Freire, R., Czarny, J., Felenbok, P. and Praderie, F., 1977, Astron. and Astrophys, 617, 85.
14. Kafatos, M., Michalitsianos, A.G. and Hobbs, R.W., 1980, Astron. and Astrophysics, submitted.
15. Carpenter, K.G. and Wing, R.F., 1980, private communication.
16. Goldberg, L., 1980, Q.J. R. Astr. Soc., 20, 361.
17. Nandy, K., 1976, Highlights of Astronomy (D. Reidel Pub. Co.-Dordrecht), 4, Part II, 289.
18. Code, A.D., 1976, Highlights of Astronomy (D. Reidel Pub. Co.-Dordrecht), 4, Part II, 325.
19. Keenan, P.C., 1942, Ap. J., 95, 461.
20. Morgan, W.W. and Keenan, P.C., 1973, An. Rev. Astr. and Astrophysics, 11, 29.
21. Jennings, M.C. and Dyck, H.M., 1972, Ap. J., 177, 427.
22. Humphreys, R.M., 1970, Astro. J., 75, 602.
23. Lee, T., 1970, Astrophys. J., 162, 217.

Table 1

ABSOLUTE LINE INTENSITIES

($\times 10^{-13}$ ergs cm^{-2} s^{-1})

Ion	Laboratory λ(A)	BX Mon
N V	1239, 1243	0.6
O I+Si II	1302, 1309	1.8
O V	1371	0.1
Si IV + O IV]	1394, 1401 1403, 1407	0.2
N IV]	1487	
C IV	1548, 1550	1.2
[Ne IV]	1575	0.2
He II	1640	0.7
O III]	1661, 1666	0.7
N III]	1749, 1750, 1752, 1754	1.1
Si III]	1892	0.5
C III]	1907, 1909	0.5

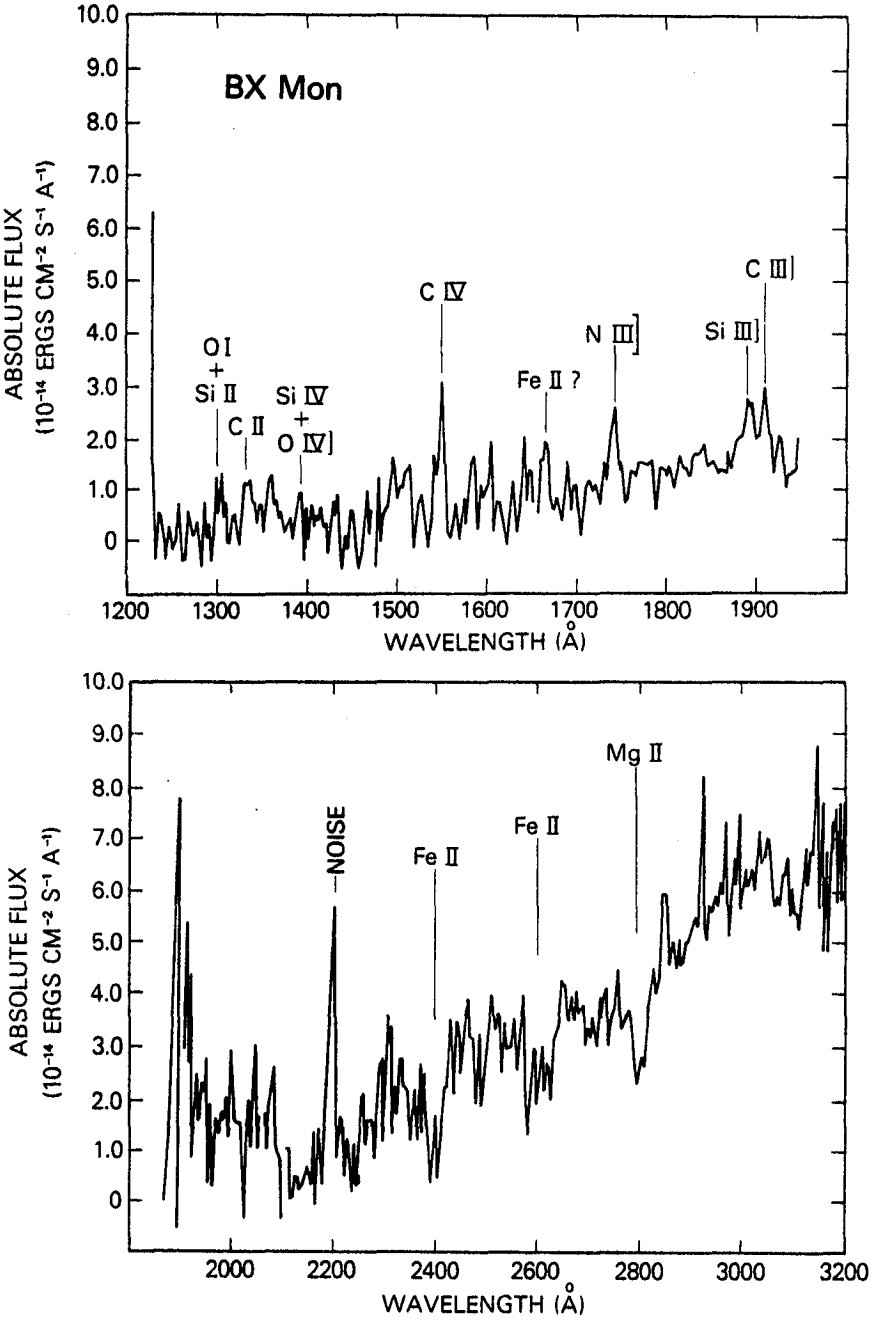

Figure 1
IUE low dispersion spectrum of BX Mon obtained using the 10" x 20" entrance aperture. Exposures of 60 minutes were used in both long and short wavelength cameras. Continuum and absorption features in the LWR range are explained by a middle A main sequence star. High excitation emission lines dominate the short wavelength range.

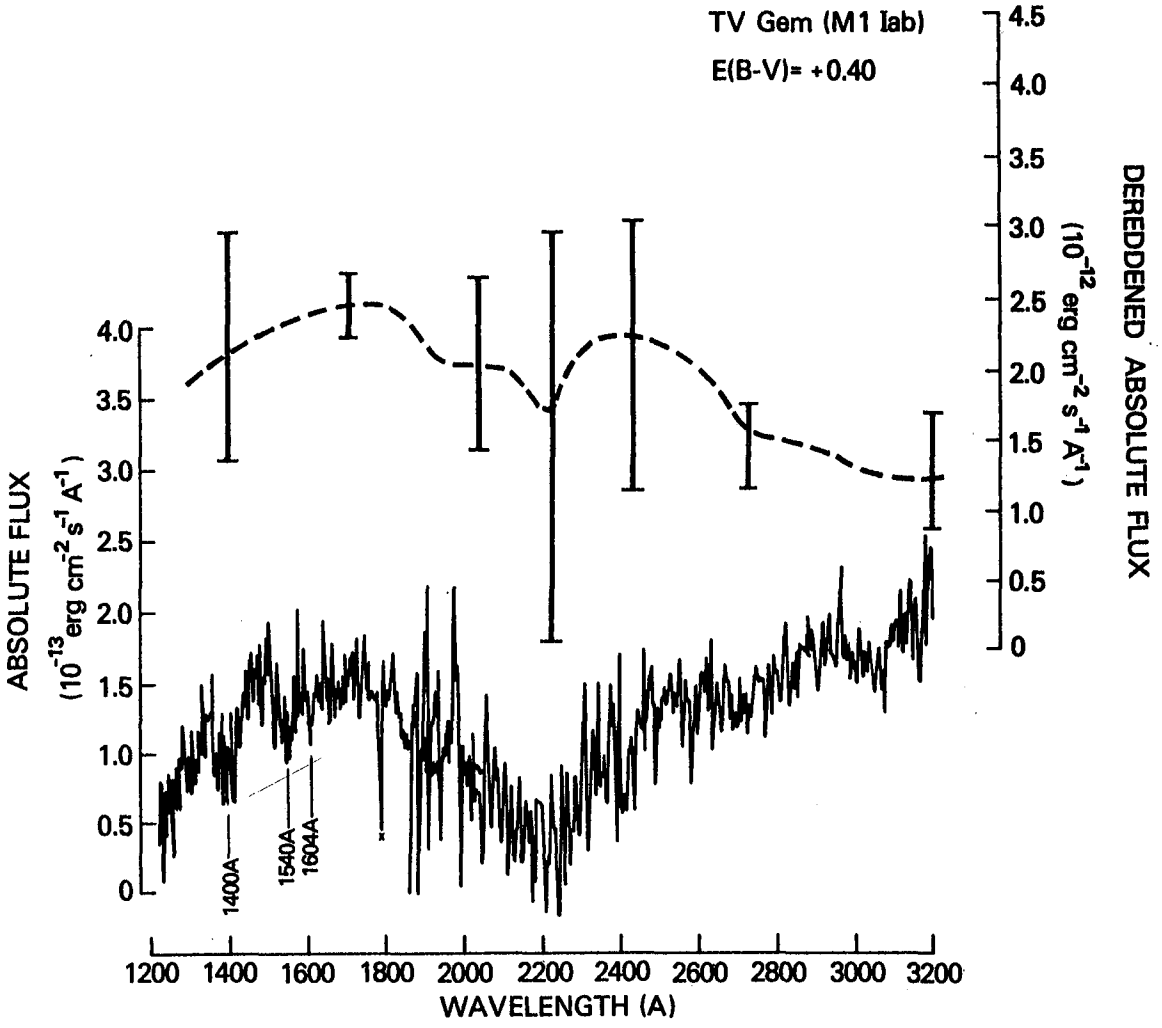

Figure 2
UV spectrum of TV Gem between 1200Å and 3200Å obtained in low dispersion using 10 minute exposures. Continuum dereddened (dashed line) by applying an E_{B-V} = +0.40 to the observed continuum. The error bars denote the uncertainty of the dereddened continuum if we consider the extreme uncertainty of the measured continuum level.

THE 1979 ECLIPSE OF ZETA AURIGAE

Robert D. Chapman
Laboratory for Astronomy and Solar Physics
Goddard Space Flight Center
Greenbelt, MD 20771

ABSTRACT

Observations of the system ζ Aurigae made around primary eclipse are described, and their significance is discussed in a preliminary fashion.

THE OBSERVATIONS

High-dispersion, long- and short-wavelength spectra of the atmospheric eclipsing binary star system ζ Aurigae (K2II + B8V) have been obtained during a total of ten observing sessions between September 15, 1979 and March 31, 1980. Dates of observations, corresponding to numbered positions in Figure 1 are: (1) Sept. 15, (2) Nov. 1, (3) Nov. 13, (4) Nov. 15, (5) Nov. 18, (6) Nov. 22, (7) Dec. 16, (8) Jan. 29, (9) Feb. 29, (10) Mar. 31. The spectrum obtained on Sept. 15 resembles the spectrum of a single late B-star (e.g. the B6V star σ Eri). Atmospheric effects are present and increasing in strength between Nov. 1 and Nov. 18. To a first approximation, the spectrum changes appear to be an increase in strength and number of absorption lines with changes in the undisturbed continuum being small. This point requires further study, however. On Nov. 22, the B star had passed second contact, and the spectrum of the system was a pure emission line spectrum. At mid-eclipse, on Dec. 16 the spectrum had changed but little from its appearance on Nov. 22. The egress spectra obtained in 1980 are not significantly different in appearance from the ingress spectra. A study of differences in detail is being undertaken now. Figure 2 shows the behavior of the Fe II resonance lines in three spectra.

Ionic spectra which are increasing in strength during the ingress atmospheric phases of the eclipse include: Al II, Al III, Cr II, Mn II, Fe I (?), Fe II, Fe III, Co II and Ni II. The Fe I identification remains in doubt since only multiplet UV7 has been identified so far.

DISCUSSION

The analysis of the ζ Aurigae spectra are still being carried out, and these remarks should be considered preliminary. The volume of data to be digested turns out to be quite large, and final conclusions will not be available for some time.

First, there is no evidence for the chromosphere of the K supergiant in our spectra--except possibly in the Mg II resonance lines. Estimates, based on observations of single late type supergiants by other IUE observers, led us to conclude that the exposure times required to obtain high dispersion spectra at mid-eclipse were in excess of 30 hours. In fact, good exposures were obtained in 2-3 hours. Furthermore, as mentioned earlier, the spectrum changed only slightly in the month from second contact to mid-eclipse, indicating that the physical conditions in the emitting plasma did not change significantly in the time period. We conclude that the emitting plasma is illuminated by the B star even at mid-eclipse. Thus, the emission probably arises in an extensive circumstellar shell which would appear as a bright "halo" around the supergiant.

In addition to the lines due to once ionized metals, both C IV and Si IV lines are present in the spectra. The C IV lines are typical of the two ions, (see Figure 3). Each of the C IV lines consist of a narrow line, near the rest wavelength, and a redward shifted broad line. The narrow line remains unchanged through the sequence of spectra, while the broad line increases in strength into the eclipse, and decreases in strength through egress, though its strength during egress is greater than during ingress. The narrow, constant component of each line is probably interstellar, while the broad component may be formed in a shock wave where the winds from the two stars interact. Highly turbulent motion in the shock wave can account for the breadth of the line profiles. We will continue to follow the system around its orbit to test this hypothesis.

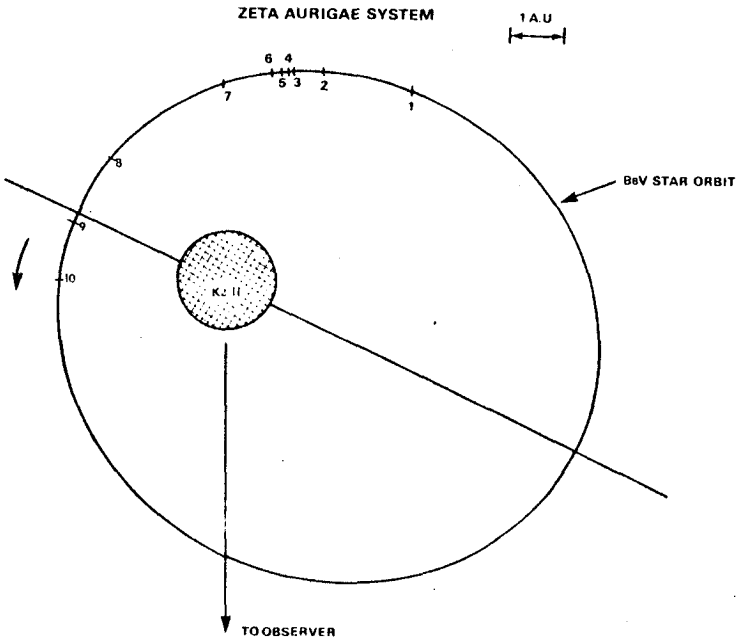

Figure 1

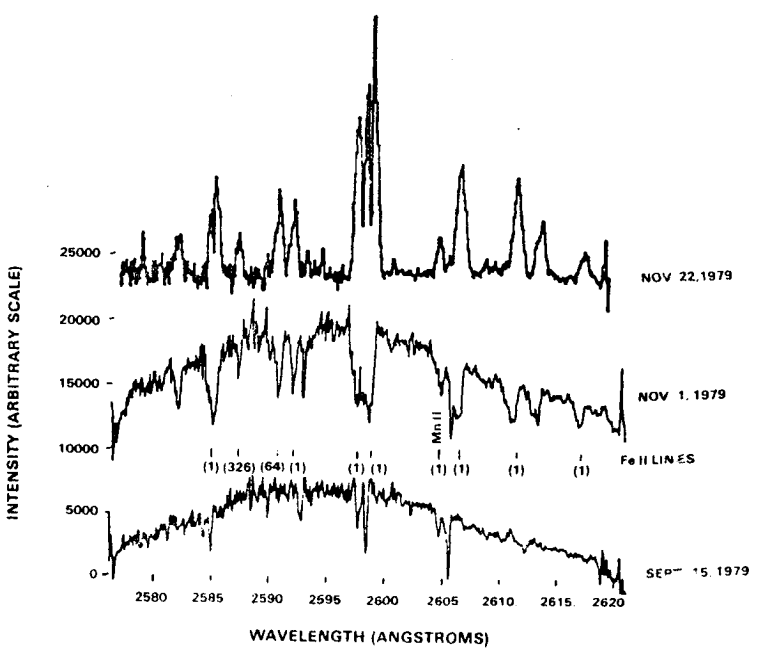

Figure 2

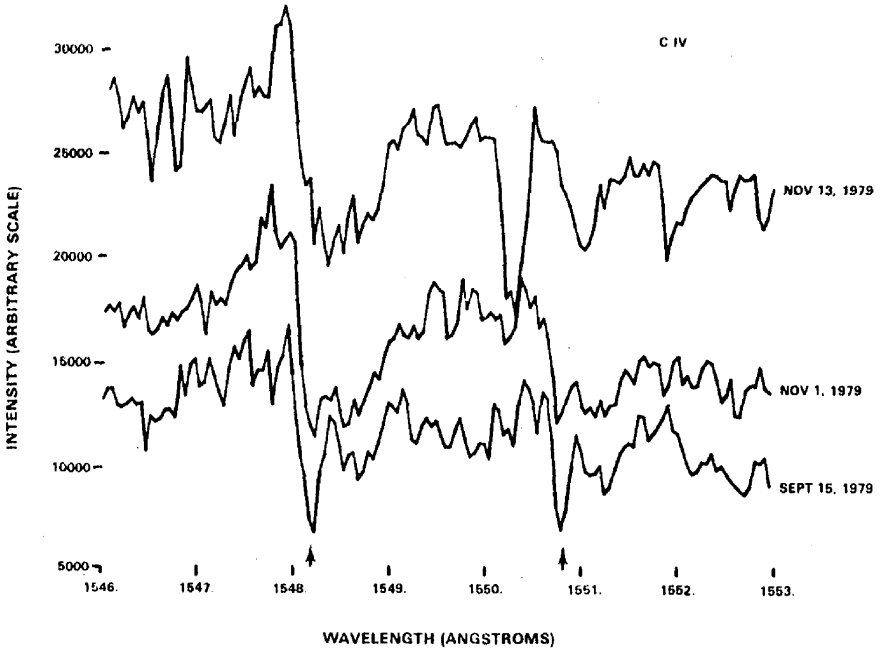
C IV
30000
25000
20000
15000
10000
5000
INTENSITY (ARBITRARY SCALE)
NOV 13, 1979
NOV 1, 1979
SEPT 15, 1979
1546.
1547.
1548.
1549.
1550.
1551.
1552.
1553.
WAVELENGTH (ANGSTROMS)

Figure 3

VISIBLE-BAND AND IUE OBSERVATIONS OF μ SAGITTARII

J. D. Dorren
Biruni Observatory, Shiraz, Iran

E. F. Guinan and E. M. Sion
Villanova University, Villanova, Pennsylvania 19085

ABSTRACT

Hα and u band photometry and IUE spectra of the binary system μ Sagittarii are discussed. An estimate of mass-loss is made from the observed P Cygni profiles. There are indications of pulsation in the supergiant B8 component.

We present Hα intermediate and narrow-band and u photometry, and IUE observations of the bright (V = +3.86) variable star μ Sagittarii (HR 6812, HD 166937, ADS 1169A), spectral classification B8 Iap.

Spectroscopic observations (ref. 1) suggest that it is a single-line spectroscopic binary of period 180.45 days with a highly eccentric (e = 0.4) orbit and with a mass function of $f(m) = 2.64 M_{\odot}$, indicating massive components. The relative orbit is shown in figure 1 in which the supergiant component is at superior conjunction, defining 0.0 phase. Morgan and Elvey (ref. 2) reported an eclipse of the B8 supergiant lasting about 20 days with a depth of ~ 0.14 mag in V and constant light lasting ~ 11 days. The phase of minimum light coincided with the spectroscopic phase of superior conjunction of the B8 star.

No further photoelectric observations were available until those of Dorren and Guinan (ref. 3) at Biruni and Villanova Observatories, near the expected time of superior and inferior conjunctions of the B8 Ia component. Following Copernicus and IUE observations by Plavec and Polidan (refs. 4, 5), in which a UV flux excess indicated the presence of a component hotter than the B8 star, photometric observations in Hα intermediate and narrow-band and u filters made by Dorren at Biruni in June 1979 near the expected time of eclipse of the B8 star revealed light variations similar to those found by Morgan and Elvey, suggesting an eclipse lasting about 20 days with depths of ~ 0.14 mag at λ6585 and ~ 0.16 mag at λ3500. Observations at Villanova were made by Dorren and Guinan during September and October 1979 at λ6585 to investigate the possible eclipse of the unseen component. A decrease in light of about 0.08 mag was observed with minimum light occurring at orbital phase 0.57, calculated from the revised ephemeris:

$$T\,(\mathrm{Min}) = \mathrm{JD}2444035.0 + 180.^{d}55 \cdot E$$

which corresponds to the time of light minimum observed near the expected superior

conjunction of the B8 supergiant component. The phase (0.57) at which the above minimum occurs is consistent with the published values of e and ω. However, observations made in April and May 1980 starting at orbital phase 0.75 reveal departures from the expected outside-eclipse light variation and suggest the presence of minima near phases 0.75 and 0.83. A re-evaluation of the photometric data indicates the possibility of a $\sim$26 day quasi-sinusoidal light variation with an amplitude of about $0^m.10$. This 26 day light variation is of the order of magnitude expected for the radial pulsation of the B8 supergiant star (ref. 6). It is interesting to note that there is evidence for pulsation in β Orionis, which is of the identical spectral type (ref. 7). A check star, 16 Sgr was observed on 6 nights; no variation above the level of 0.015 mag was found, indicating that the comparison star 15 Sgr is not the source of the variations. The situation is further complicated by the fact that in an orbit of such high eccentricity and with a supergiant component of radius $\gtrsim 70 R_\odot$, most of the light variation near zero orbital phase would be caused by the tidal distortion of the B8 star (see fig. 1), while an eclipse of the unseen component would be responsible for the light variation at phase 0.57, if the orbital inclination is sufficiently high for eclipses to occur.

The λ6585 light curve is shown in figure 2, together with the Hα index, formed in the usual way. The index is about 0.1 mag more negative than typical values for stars of the same spectral type, indicating strong Hα emission which, however, shows little phase dependence.

Two IUE high-dispersion long and short wave and 4 low-dispersion long and short wave IUE spectra were obtained by Guinan and Sion on 1979 September 24 UT near the expected time of the eclipse of the unseen component. The flux distribution, de-reddened using $E_{B-V} = 0.3$ derived from the λ2200 feature (ref. 8) is shown in figure 3 together with fluxes at B and V wavelengths (ref. 9), and in the infrared out to 10 μ (ref. 10). A fit using a model atmosphere of Kurucz (ref. 11) with blanketing included for the filtered wavelengths, corresponding to a temperature of $T_{eff} =$ 11,000°K and log g = 2.0, appropriate for a B8 supergiant, is also shown. The agreement is good and there is no indication of flux due to a hotter component, suggesting that if the system does contain such a component, it was either eclipsed at the time of the IUE observations, or the smaller component contributes little to the total light of the system. A better fit to the data could be obtained by assuming $T_{eff} = 11,500$°K and log g = 2.0 using the Kurucz model. It is interesting to note the strong deviations from black body behaviour in ultraviolet wavelengths exhibited by a star of a temperature appropriate for the B8 Ia spectral type. The Copernicus spectra* show the presence of a hot component at orbital phases 0.9 and 0.26 and its absence at phase 0.5. Skylab UV observations at phase 0.7 (ref. 12) indicate a maximum flux level of $\sim 1.7 \times 10^{-10}$ ergs cm^{-2}sec^{-1}Å^{-1} at λ1800, a factor of $\sim$6 below the observations shown in figure 3.

The UV spectrum of μ Sgr is extremely rich in absorption lines. Those of Fe II are most numerous, and the Mg II h and k lines are particularly prominent. Lines of

* Polidan, R.S., private communication

Fe I, Si II, Al III, Mg I, He I, He II and Lyman α have also been identified. P Cygni profiles of Si IV and C IV with blue-shifted absorption components are also present, indicating mass loss, and are shown in figure 4. From the measured terminal velocity, $v_\infty \sim 200$ km/sec, obtained from the shortward edge of the absorption profile, an upper limit of $\dot{M}_{max} = 1.0 \times 10^{-5} M_\odot/yr$ for the mass loss rate is found using the relation (ref. 13):

$$\dot{M}_{max} = \left(\frac{L}{cv_\infty}\right) = 7 \times 10^{-12} \left(\frac{L}{L_\odot}\right)\left(\frac{3000}{v_\infty}\right) M_\odot/yr$$

where c is the velocity of light and the total luminosity, L, of the B8 star is $\sim 3.7 \times 10^{38}$ ergs/sec if an absolute bolometric magnitude of ~ -7.7 is assumed. Such a rate would only be achieved if there were a complete transfer of photon momentum in a single scattering. Thus the mass loss estimate that we obtained is consistent with the value of $1.1 \times 10^{-6} M_\odot/yr$ obtained by Barlow and Cohen (ref. 10) from IR observations.

The presence of a $9^m.9$ B3 companion of μSgr, if assumed to be a main-sequence star, provides a second estimate of the B8 star's luminosity, yielding a value close to the above, and hence a distance to the system of ~ 1 kpc.

Photoelectric observations of μSgr are continuing in an effort to improve our understanding of this unusual binary system. A more detailed study will be published with Plavec and Polidan.

REFERENCES

1. Ichinohe, N.: Astrophys. J., vol. 26, 1907, p. 157.

2. Morgan, W.W. and Elvey, C.T.: Astrophys. J., vol. 88, 1938, p. 110.

3. Dorren, J.D. and Guinan, E.F.: IAU Circ. No. 3410, 1979.

4. Plavec, M. and Polidan, R.S.: IAU Circ. No. 3333, 1979.

5. Plavec, M.: Interacting Binary Systems. The Universe at Ultraviolet Wavelengths: The First Two Years of IUE. NASA CP-2171, 1980: this compilation.

6. Ledoux, P. and Walraven, Th.: Handbuch der Astrophysik, ed. S. Flügge, vol. 51, 1958, p. 572.

7. Chentsov, E.L. and Snezhko, L.I.: Soviet. Astr., vol. 15, 1971, p. 429.

8. Nandy, K., Thompson, G.I., Jamar, C., Monfils, A. and Wilson, R.: Astron. and Astrophys., vol. 44, 1975, p. 195.

9. Tüg, H., White, N.M. and Lockwood, G.W.: Astron. and Astrophys., vol. 61, 1977, p. 679.

10. Barlow, M.J. and Cohen, M.: Astrophys. J., vol. 213, 1977, p. 737.

11. Kurucz, R.L.: Astrophys. J. Suppl., vol. 40, 1979, p. 1.

12. Henize, K.G., Wray, J.D., Parsons, S.B. and Benedict, G.F.: NASA Reference Publication 1031, 1979.

13. Mihalas, D.: Stellar Atmospheres, 1978 (Second Edition, W.H. Freeman and Co.)

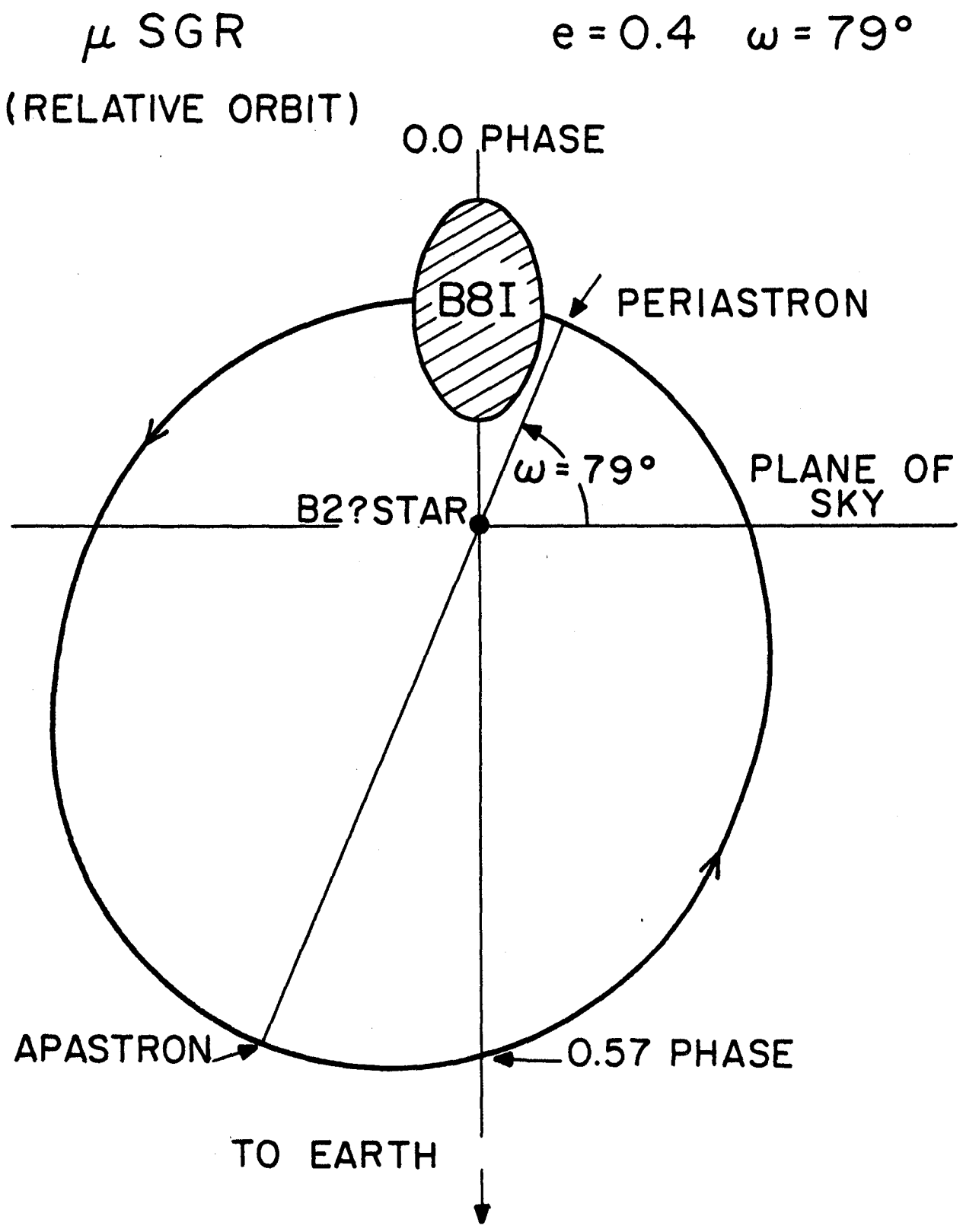

Fig. 1: The relative orbit of μ Sagittarii, approximately to scale

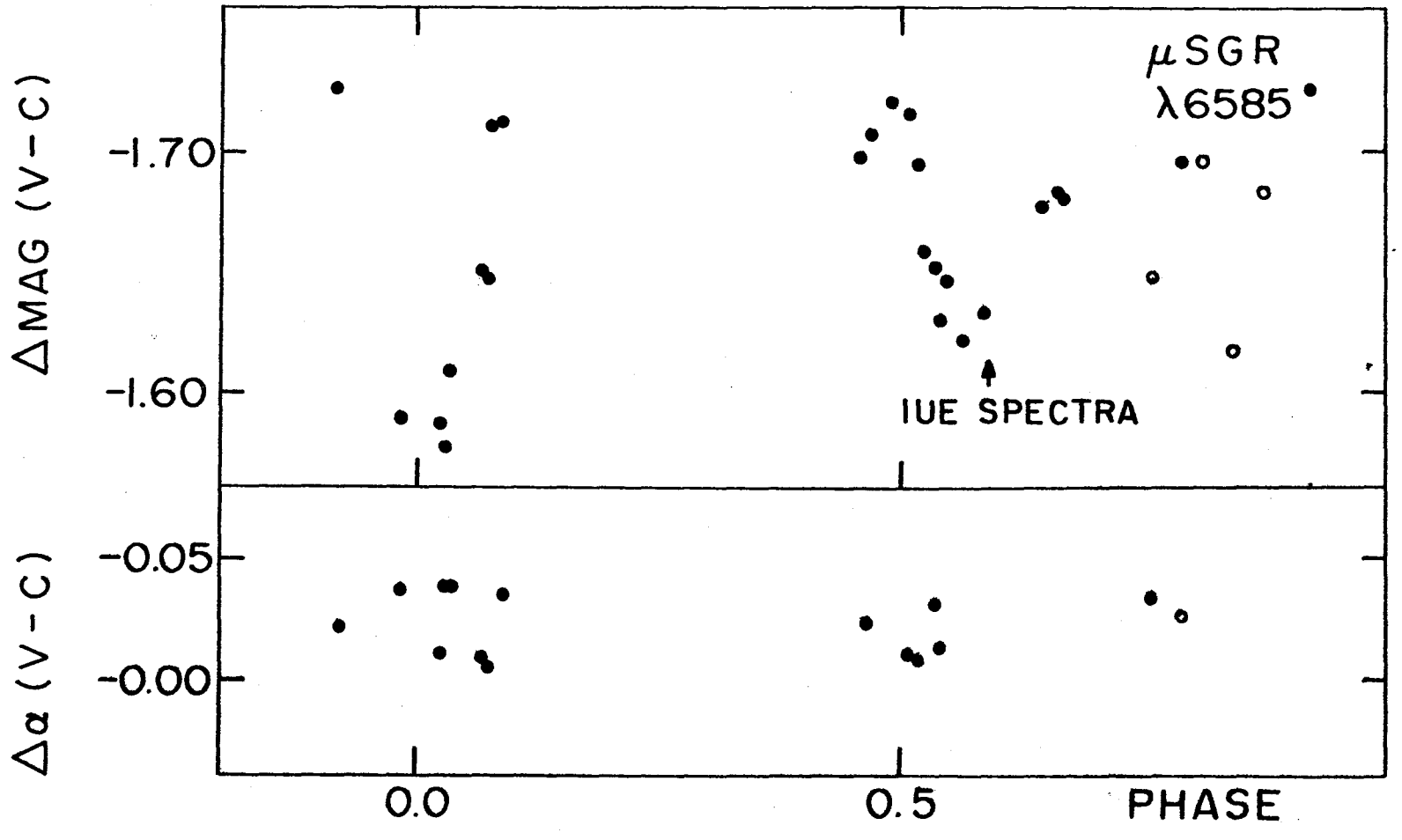

Fig. 2: λ6585 intermediate-band light curve and differential α-index, as a function of orbital phase.

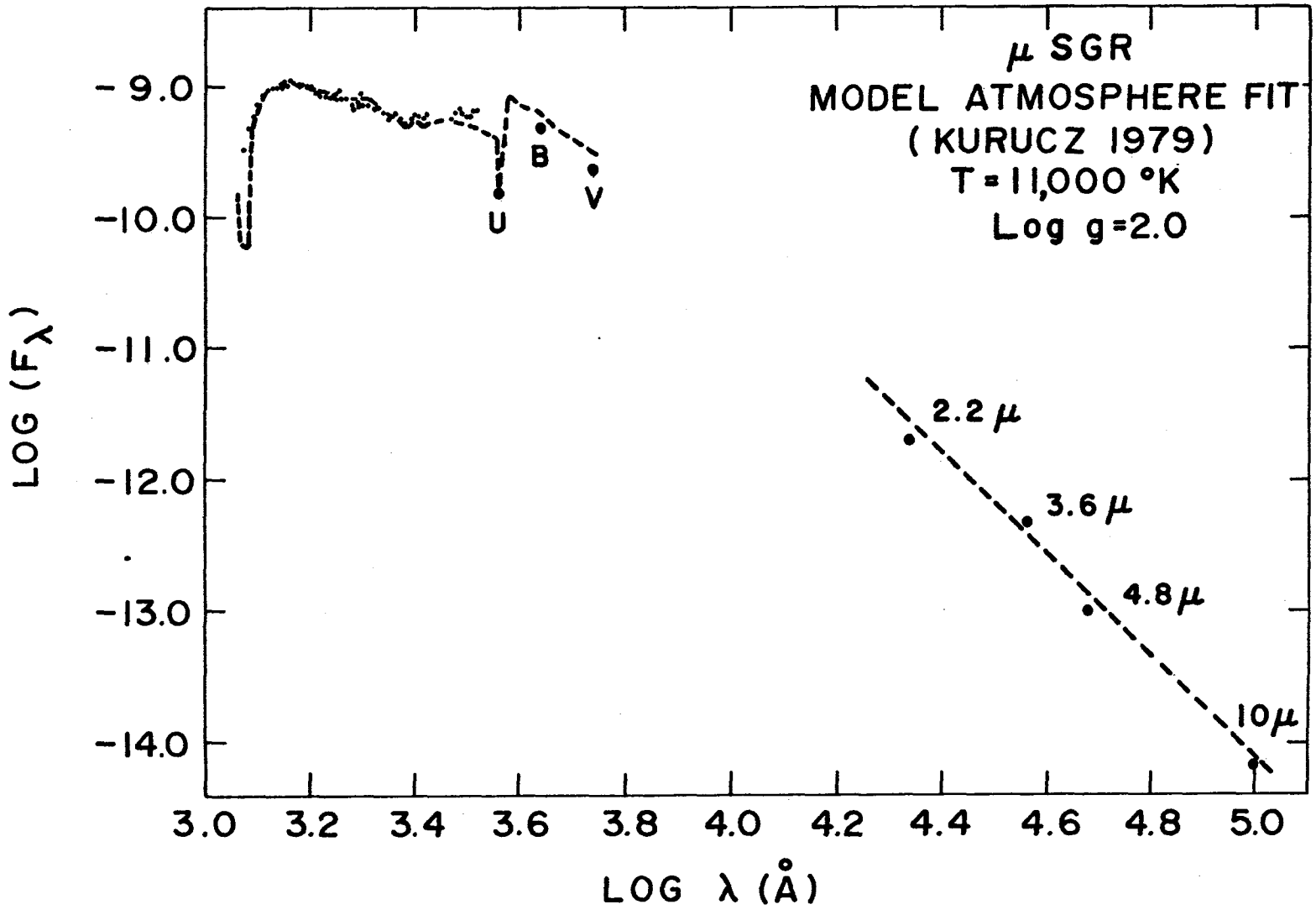

Fig. 3: Absolute flux (in ergs. cm^{-2}. sec^{-1}. $Å^{-1}$) as a function of wavelength, from 0.1 to 10 μ. The broken line is a fit using a Kurucz model atmosphere with T_{eff} = 11,000°K and log g = 2.0

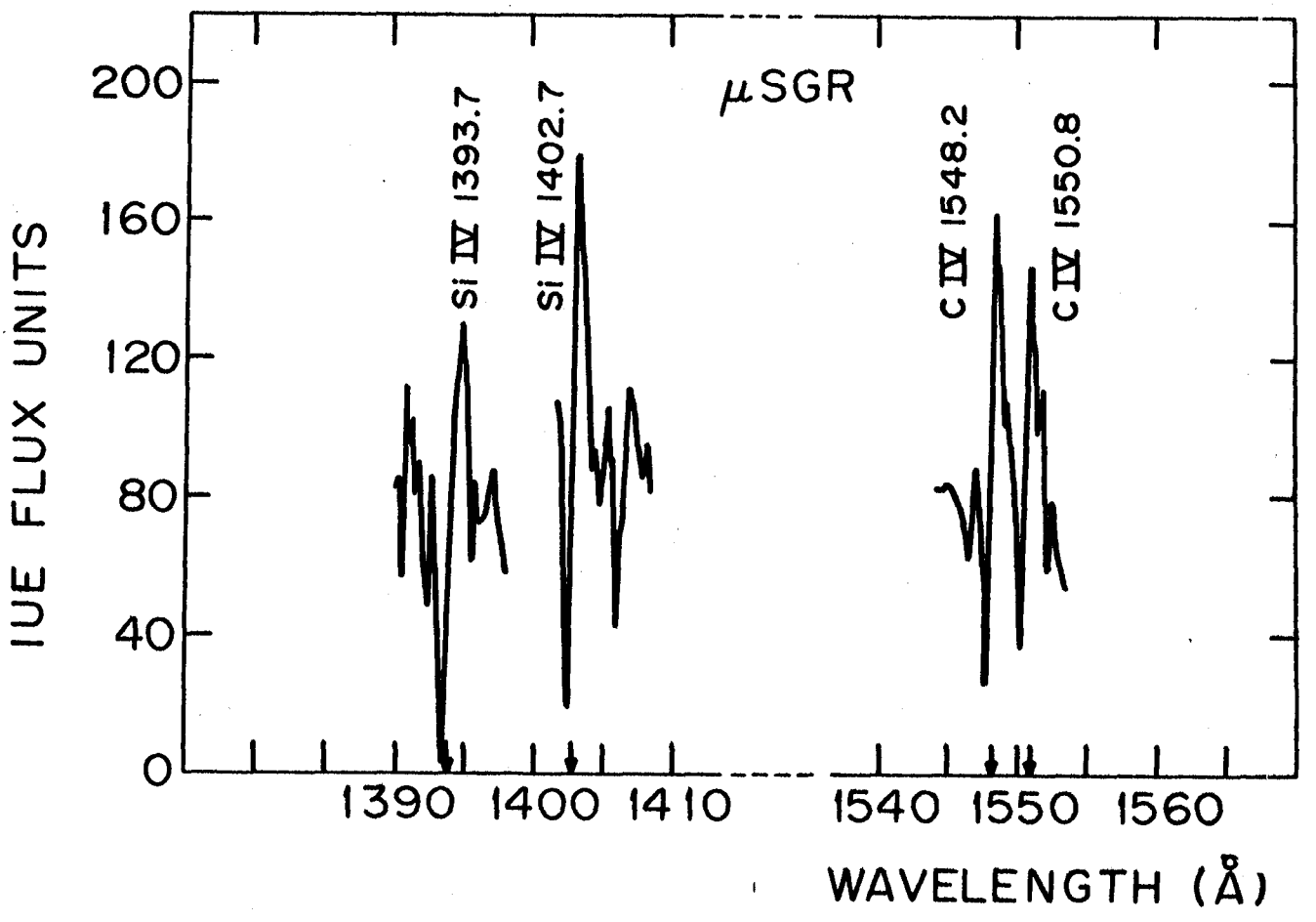

Fig. 4: P Cygni profiles of Si IV and C IV. The arrows indicate the positions of the rest wavelengths.

DISCUSSION - PART III

Dupree: In the Capella system, it is somewhat puzzling that the surface flux of N V is ~100 times the solar flux when attributed to the B component and yet your evaluation (Ayres and Linsky, 1980 preprint) of the rotational velocity is 40 km s^{-1} for Capella B. Such large surface fluxes have been found in late type systems, but only in stars with 3 to 4 times this rotational velocity.

Stencel: Your solar-like ratio of Mg II k to Ca II K (2.5) is interesting in light of a ratio nearer unity for supergiants where strong circumstellar absorption could hide preferentially Mg II emission. But GL 380 showed 0.4 for the ratio--is it known for strong flaring?

Giampapa: GL 380 is not known for flaring, although it has a high R_{HK} value and H absorption, indicating a "strong" chromosphere. The other point is that the Ca II and Mg II data were not obtained simultaneously. Due to change in stellar surface features, the comparison of line ratios for lines observed at different times can be deceptive.

Jordan: What are the underlying assumptions in your expression for the area of active regions?

Giampapa: 1) The star with the largest R_{hk} (or R_{HK}) value is assumed to have $A \equiv 1$; the star with the smallest is assumed to have $A \equiv 0$; 2) the character of an active region is the same for all the stars, and 3) the center-to-limb behavior of the Mg II lines (or Ca II lines) is ignored. The resulting filling factor is a relative value, not an absolute measurement.

Böhm-Vitense: I agree that on the main sequence we cannot say with certainty whether an A9 V star has less chromospheric emission than observed for F0 V star, however, I feel sure that an F2 II star has much less emission line flux than an F2 V star, otherwise we would have seen it.

Linsky: It is clear that the ultraviolet continuum flux is rising rapidly for stars earlier than F0 and that the surface fluxes of chromospheric and transition region emission lines vary from star to star due to rotational velocity, magnetic fields, and perhaps luminosity differences. For these reasons, our inability to "see" an emission line spectrum against the ultraviolet continuum will not be a precise line in the H-R diagram but rather a diffuse line which may well depend on luminosity.

Hartmann: We have seen a 40 km s^{-1} shift between S I and O I in α TrA (K4 III). Will the possibility of wind expansion affect the escape probability of your optical depth method?

Jordan: Yes. This is just an initial exploration of the problem.

Linsky: There is likely an interstellar absorption component to the α Tau O I 1302,4,6 lines. Since the radial velocity of α Tau is

≈50 km/s, would not the observed asymmetry and self-reversal of these lines be due to interstellar absorption rather than be intrinsic to the star itself (due to velocity gradients)?

Jordan: Probably both effects occur.

Linsky: Do you see any lines formed at temperatures hotter than C II in αTau, and how certain is your identification of the C II λ1335 multiplet?

Jordan: We find no emission lines hotter than C II in αTau. We believe that the identification of C II 1335 is real because the C II λ1335/C II λ2334 ratio is temperature dependent and indicates a temperature of 7000K. If the 1335 feature is a blend, then the ratio would indicate an even cooler temperature.

Ahmad: There is no reason to expect the coronal temperature to be higher in the presence of a stellar wind. In the case of the sun, in fact, the corona is cooler where there is a solar wind. Presumably energy that would have otherwise been thermalized has become kinetic energy of the wind.

Underhill: Following a remark by Thomas regarding selecting 2 parameters by which to characterize models of the outer atmosphere, it seems to me to be unprofitable to model the outer atmosphere of a star by deliberately taking the mass flux and the local temperature as separable and independent free parameters. The temperature and rate of outflow of matter are the results of some physical process which is occurring. Both are most likely determined by one physical process and they are unlikely to be independent of each other. Suitable parameters are the absolute value of the local magnetic field and the amplitude of local differential motions. These together put into the equations of physics probably will determine the local rate of mass outflow and the local electron temperature. Integration over the surface of the star will result in a model of what we see.

Underhill: Do any of these F supergiants have an IR excess in the 1 to 10 μm region? That might be the wavelength region where the extra non-radiative energy which you mention is finally radiated.

Stencel: IR excess around the most luminous F supergiants would not surprise me since objects like ρ Cas are known to undergo shell episodes (Sargent, 1962) and probably have massive stellar winds. The non-radiative cooling is not occurring in mid-UV emission lines, so if there is any, it might come out in the IR, presuming weak far-UV emission (Parsons, 1979).

Mullan: The velocity dividing line discovered by Stencel and Mullan is Mg II asymmetry data coincides with the Linsky-Haisch temperature dividing line. Selection effects discussed by Ayres are not relevant in our sample because the Mg II emission shows no gradients in intensity where we see asymmetry gradient. I conclude that cool coronal and rapid mass

loss are correlated. Hence, rapid coronal mass loss is driven by a non-thermal mechanism in late type giants.

Stencel: Certainly possible. Although we can make a preliminary correction to the effect of Mg II interstellar absorption on the stellar emission asymmetry, selection effects may be important in the current sample. The anisotropy of the local ISM dictates that a more complete sky survey be performed, with cool stars.

Böhm-Vitense: I do not think that there is a discrepancy with convection theory. The stars actually will not produce as much acoustic noise as your graph indicates. In those calculations it is usually not considered that for early F supergiants the convection zones become thinner than the size of the assumed mixing length and that therefore a smaller mixing length should be chosen which leads to a thinner convection zone, etc. until a radiative equilibrium zone with very low convective velocities is obtained.

Stencel: Yes, the calculations of Ulmschneider and modifications by Bohn (1980) involve several simplifying assumptions. The thinness of F star "Mg II and Ca II Chromospheres" will be dictated by the larger photospheric temperatures, compared to G stars, by virtue of higher ionization.

Plavec: Can you say a little bit more about the hot component in CH Cygni?

Wing: I think the type must be O or very early B, but we haven't really attempted a classification yet because we don't have an adequate grid of standard stars. Anyway, there's no doubt that it's a star. Also, it's so bright that I would guess that it's on or close to the main sequence, rather than sub-luminous.

Guinan: Did you detect any variations in the spectra of CH Cyg with time?

Wing: We observed CH Cygni three times at high resolution in the long-wavelength region on 1979 February 12, 1979 May 26, and 1980 January 30. We did not notice any change in magnitude, but the Fe II emission was definitely weaker on the third plate than on the other two.

Garrison: What was the phase of Mira?

Wing: The spectrum shown was taken in January 1980, when the primary was about two months past maximum light.

Keyes: Our ground-based spectrophotometric scanner observations from Lick show that the He II λ4686, if present, is quite weak, as are the Bowen fluorescence O III lines around 3300 Å. However, the He I lines typical of symbiotic stars, e.g., $\lambda\lambda$6678, 5876, 4471 and others are easily detected. Therefore, it seems that a temperature for the hot subdwarf was obtained assuming that the nebular continuum we see at long wavelengths is due to photoionization. However, we should point out that

Merrill saw [Fe VII] emission and very likely even a 100,000 K star cannot ionize Fe VI. Quite possibly, x-ray emission from the region close to the subdwarf is responsible for the Fe VI ionization as well as the nebular continuum (accretion disk).

Sion: What is the outburst history of RW Hya? If, as it seems from your spectra, the hot component is a white dwarf or degenerate star, the accretion rate you quote could allow steady nuclear burning which could produce both your estimated x-ray luminosity and the observed UV continuum.

Kafatos: As far as I know, this object has not shown any outbursts. It is very similar in the line identifiable to CI Cygni.

Underhill: Many Fe V lines are seen in the spectra of O4, O5 stars. Do you see any Fe I near 1400 Å?

Kafatos: The only strong lines near 1400 Å are the Si IV, O IV], S IV] multiplets. If any Fe lines are there, they are weak.

Wallerstein: The historic light curve of R Aqr by Mattei and Allen shows that when the hot source was bright the long period variable was suppressed at maximum. Such a phenomenon could be due to a single star, rather than a binary system, in which magnetic activity excites the chromosphere during an outburst. The maximum of the long period variable component could be suppressed when the magnetic field prevents the LPV pulsation.

Keyes: Concerning the observed arc minute scale shell just mentioned by Slovak. Could this be the result of past outburst history, perhaps planetary nebulae shell-like ejection by the star that now appears as a hot subdwarf? Maybe someone who is more familiar with this system and planetary nebular evolution could comment.

Kafatos: Very possibly so.

Sion: I should like to point out that according to calculations by B. Paczynski and myself, if the accretion rate onto the white dwarf exceeds 10^{-7} Mo/yr., the white dwarf will evolve into a red giant structure on a very short time scale, which will produce a shell interacting strongly with the red giant companion in a symbiotic system.

Wing: The values you quoted for B-V and E(B-V) for TY Gem suggest that the color excess is based on 'normal' colors for the M supergiant. If the hot star contributes to B, the reddening may be somewhat larger, as suggested by your 2200 Å feature. I can't help remarking on the similarity of BX Mon to o Cet, the spectrum of which I showed earlier today. In both cases, the hot star is surprisingly red, and faint in the short-wavelength region, considering its effectiveness in exciting a bright, high-excitation nebular.

Bolton: You used the phrase "tidal interactions" when discussing possible sources of energy input for the UV spectrum. Is this a catch phrase or do you have a specific physical model in mind?

Michalitsianos: It is a catch phrase; very little is known about the physical properties of BX Mon, i.e., the orbit of the hot companion observed here with IUE is not known. As such, models developed for this star system at this point can only be speculative. I can say, however, that the high excitation emission lines that are observed are not produced by photo-excitation of the A III-IV stars because such a star does not produce sufficient ionizing photons.

Rakos: Bx Mon also shows interstellar absorption in the region of 2200 Å. Have you corrected the observations for this absorption?

Michalitsianos: Yes, Bx Mon exhibits interstellar absorption as indicated by the broad depression of the continuum at λ2200 Å. The long wavelength continuum 2000-3200Å shown in this viewgraph does not have interstellar reddening removed, although we have done so when we lifted the line blanketed continuum for a A III-IV, 9000K main-sequence star hour models of Kurucz.

Slovak: How great a disparity is there between the observed (de-reddened) IUE data as compared to the extrapolation of the M1ab optical flux distribution into the ultraviolet at λ = 2000 Å?

Michalitsianos: The hot companion to TV Gem contributes approximately 60% of the total emission continuum at λ3000Å. The continuum energy distribution is declining very rapidly from the M0-M1 Iab supergiant, and its contribution in the IUE spectral range is negligible in comparison to the hot companion in this system.

Kafatos: I would like to say that we had an "Einstein" observing program accepted and hopefully these x-ray observations will help us decide whether the UV continuum is due to a late B type star or an accretion disk.

Guinan: Have you compared your IUE spectra of ζ Aur with those published for 32 Cygni by Stencel?

Chapman: No.

IV. BINARY STARS AND HIGHLY EVOLVED OBJECTS

THE IMPACT OF IUE ON BINARY STAR STUDIES

Mirek J. Plavec
Department of Astronomy, University of California, Los Angeles

ABSTRACT

Every class of binary stars can be profitably studied with IUE, and for most of them, such observations are of fundamental importance, and have already yielded extremely valuable results or new surprising facts. Some of the classes are discussed in this review.

Atmospheric structure and wind complexes can now be studied, in binaries with supergiant components, much farther out in resonance lines of abundant elements. A hot component was discovered in μ Sagittarii, and will probably enable us to study the atmosphere of the B8 Ia supergiant. A B-type companion to the F2 Ia supergiant in ε Aurigae was found. A significant portion of the spectrum of the secondary component in β Lyrae was isolated. A whole class of objects was discovered with the IUE (the W Serpentis stars), bearing resemblance to β Lyrae. The radiation from these objects is probably largely produced in the process of accretion. Strong emission lines with P Cygni profiles suggest mass outflow driven by an induced stellar wind. A hot companion of the helium-rich star υ Sagittarii was also discovered. We know now, thanks to IUE, that many if not all symbiotic stars are binaries, in which the hot component is probably a hot subdwarf. Valuable studies of the energy distribution and of gas streams in Algols are also reported.

INTRODUCTION

I would like to claim that the two years of existence of IUE opened a new epoch in the studies of binary stars. Although the inevitable delay between observation and publication makes me unaware of many important results, what I know already demonstrates the enormous impact of IUE. The day when there will be no IUE or when we get no more time on it, will put us back by decades, and will be analogous to Galileo Galilei giving up his telescope and going back to Tycho Brahe's quadrants. Thus I should actually start and conclude my talk by first thanking every one and all of those who contributed to the success of the mission, and then immediately by asking: When do we start talking seriously about IUE 2, 3 , ...n?

One proof of the enormous impact of IUE will be the fact that I will not be able to cover some important types of binary stars. My talk should be considered as a supplement to the excellent review talk given last year by Dupree (ref. 1). She talked mostly about binary stars with active chromospheres, i.e. the RS CVn stars and W UMa stars, also about X-ray binaries. I must also relegate the important topic of the cataclysmic variables and novae to other speakers at this symposium. Also, I can only mention here the increasing discoveries of blue companions to supergiants and Cepheids (ref. 31). They promise better determination of properties; however, they may imply much more.

ζ AURIGAE AND VV CEPHEI STARS

Continuum observations in the ultraviolet are particularly important for binary systems in which one component is a hot star, much smaller in size than its mate. A classical example are the systems ζ Aurigae, 31 Cygni, 32 Cygni, and VV Cephei. The optical spectrum is completely dominated by a red supergiant, spectral type approximately K4 Ib for the first three, and M2 Ia for VV Cep. Hopelessly blended with the numerous deep metallic lines and/or molecular bands of the supergiant are the few lines signalling the presence of a B star: the Balmer lines and occasionally one or two He I lines. In VV Cep, the only signature of the hot component are (presumably) co-moving emission components of the Balmer Hα and Hβ lines. No wonder, then, that both the geometrical properties, masses etc. as well as the nature of the hot companions are poorly known.

These supergiant systems are famous because of the atmospheric eclipses: as the hot star travels behind the enormously extended atmosphere of the supergiant, the attenuated gases leave their imprints in the spectrum, and we can study individual layers in the atmosphere of a late-type supergiant. Orbital periods are very long, typically several years, so the eclipses are rare. The system with the longest period (20 years) among them, VV Cephei, was fortunately emerging out of eclipse in 1978-79, thereby providing a unique opportunity for IUE observers. Hagen et al. (ref. 2), Faraggiana and Selvelli (ref. 3, 4) and Dupree et al. (ref. 1) have already presented first reports on the sequence of changes in the emerging B spectrum. The system with the best determined elements, ζ Aurigae, had an eclipse at the end of 1979. I am confident that it was also adequately covered.

Far ultraviolet observations of the atmospheric eclipses are not mere supplements to optical data. Since many strong resonance lines are observable in the UV, the outermost atmospheric strata can be traced out much farther into space, and valuable data on stellar winds can be assembled. This also implies that such observations are not restricted to the phases adjacent to the eclipses. Thus, Stencel, Bernat and Kondo (ref. 5) have succesfully studied 31 and 32 Cygni outside eclipse. The B star is of course not a passive test particle: it directly influences the supergiant atmosphere by its ionizing radiation. The system of 32 Cygni, poorly known from optical studies, is becoming a most interesting case, since the stars are closer together and the B star appears to move relatively deep in the outer layers of its mate. Stencel et al. (ref. 5) find a hot turbulent region near the B star, and a cooler, calmer, but faster moving wind farther out of the system. The spectrum is very rich in prominent emission lines with P Cygni profiles.

I would like to emphasize that the atmospheric eclipses should not be our only concern and interest in the supergiant systems. The supergiant stage of stellar evolution is short, so each such system provides a sensitive test of our theories of single star evolution or of double star evolution -- whichever prevails. Because of larger separations, the above-mentioned systems are more likely to follow the single star precept, but we will not be sure until the hot components are adequately observed. Are they really normal main sequence stars? Are their masses compatible with the observed differential evolution in the system? Only refined far UV studies can tell.

μ SAGITTARII

One more question comes to mind in connection with the supergiant systems: Is the combination of a K-M supergiant and a B main-sequence star the only possible? Does nature discriminate against other combinations, or is it merely observational selection? Our most recent discovery in μ Sagittarii speaks in favor of the observational bias. μ Sagittarii is a luminous and fairly hot supergiant, B8 Ia. It is a 4th magnitude star in spite of a 1 mag. interstellar extinction. It has long been known as a single-line spectroscopic binary with a period of almost exactly half a year. I was most enticed by its large mass function, f(m) = 2.64. If the mass of the supergiant lies between 10 and 20 solar masses, as is reasonable to assume, then the invisible component must have 8 - 13 solar masses. When our search at Lick Observatory for a red component failed, we started observations in the far UV, using first Copernicus and then IUE. When a few lines suggesting a hot component showed on Copernicus spectra and the IUE short-wavelength spectrum appeared composite, some predictions could be made. Fortunately, the system is eclipsing. Elvey detected a shallow eclipse in 1938, but this must be the secondary eclipse, with the hot component in front. Therefore I predicted (ref. 6) that there must occur another and deeper eclipse in September 1979. The eclipse was indeed observed by Polidan with Copernicus, and by Guinan et al. optically and with the IUE.

Fig. 1 shows my August 1978 spectrum compared with Guinan's eclipse spectrum from September 1979. Their subtraction provides the beautiful spectrum shown in Fig. 2. This, then, is a newly discovered star, hot and bright, yet never before seen or even suspected. I think Fig. 2 is a tribute to the photometric qualities of IUE: we don't get a field of scattered points, but rather a nice, well-defined spectrum. From the steep slope of the continuum, and also from the absorption lines present, we conclude that the star is quite hot, about 40,000 K, and is probably an O star. Because of its mass, it should be a main-sequnce object. Yet, again, let's be cautious until good radial velocities in the UV are obtainable and made. We will then have also a very valuable mass determination of a B8 Ia supergiant. If the companion does not have the characteristics we anticipate, we may also have another evolutionary puzzle.

The importance of this discovery may be more far-reaching. Polidan found additional absorption lines in the combined spectrum about a month before the September 1979 eclipse: therefore we may well have another atmospheric eclipse, but this time we will probe the outer atmosphere of a much hotter supergiant than in the "classical" ζ Aurigae stars. The B8 Ia supergiant in μ Sgr is known to have a pronounced stellar wind: here is the opportunity to study the wind complex.

ε AURIGAE

Also unique among the supergiant systems is ε Aurigae, in which we see an F2 Ia supergiant periodically eclipsed every 27 years by -- well, by something! The eclipse appears total but cannot be total since the same F2 spectrum remains. The depth of the eclipse appears to be essentially independent of the wavelength. Many exotic models have been invented ad hoc to explain

the nature of the mysterious invisible body, including of course an accreting black hole (which is still possible). Hack (ref. 7) suggested in 1961 that the eclipse is caused by a very extended atmosphere of a B star, which itself is not directly involved in the eclipses. Shortly after the successful launch of IUE, Hack and Selvelli (ref. 8) announced that they had indeed discovered a B star spectrum in the far UV. They find that the star has a temperature of about 15,000 K, radius only about 2 $R_\odot$, and bolometric magnitude 7 mag. lower than the F supergiant. The star appears to be either at, or more likely somewhat below, the main sequence.

Thus, possibly, we now know the components in ε Aurigae. However, considerable puzzle remains. The eclipse model postulates a huge ionized envelope, some 850 $R_\odot$ in radius around the B star, to act as a neutral semi-transparent screen. No other ordinary and modest B5 V star is known to have such an entourage. Hack and Selvelli suggest that perhaps the envelope was produced in a nova outburst of the hot star. However, postnovae do not look like B5 V stars. Moreover, what would be then the role of the F star? Just an accidental silent witness? More likely the supergiant plays a vital role in the system, perhaps as the ultimate source of the circumstellar material. Huang's (ref. 9) plausible idea of the eclipse being caused by a flat disk seen edge-on can be supplemented by the assumption that the disk is formed by accretion on the B star of the material flowing from the F star. This idea, already suggested by Morris (ref. 10) runs into the difficulty that the F star, although large (probably about 175 $R_\odot$), is still very much smaller than its critical Roche lobe. Perhaps we do not understand all the ways a supergiant can lose mass efficiently.

Although my remark will probably not apply to ε Aurigae, I would like to caution that a thick disk can considerably obscure the light of the central star, but also that accretion can produce B-type continua simulating a genuine star. In any case, I bet that the next eclipse, due to start in 1982, will confront us with many surprises in ε Aurigae -- if only we have an ultraviolet telescope then to watch the surprises.

β LYRAE AND THE W SERPENTIS STARS

I would now like to elaborate on my last remark by discussing the group of interacting binaries which I named the W Serpentis stars. It includes β Lyrae, SX Cas, RX Cas, W Crucis, V 367 Cygni, AR Pavonis, and W Serpentis. These are eclipsing binaries of intermediate periods (13 to 605 days), long known for puzzling anomalies and discrepancies in their light- and radial velocity curves. β Lyrae was observed by Hack et al. (ref. 11, 12) with Copernicus, and found to have a unique spectrum in the far UV, essentially a set of strong emission lines. Optical observations also signal unusual properties. The only visible spectrum is B8 II, but the corresponding star is less massive than the other one which displays a continuum (since we observe two fairly deep eclipses) but no recognizable spectral lines. Again, special models were invoked, with or without a black hole, with the plausible justification that an extraordinary phenomenon calls for an extraordinary model.

Unique objects are undesirable. Almost in all cases, some vital information is not accessible, and cannot be replaced by inference from related objects

if these do not exist. Fortunately, we now know that β Lyrae is not a unique object. Within one short run in August 1978, R. H. Koch and myself found six binaries that have the same type of emission-line spectra in the far UV. This was not an accidental discovery. An important characteristic of the W Serpentis objects is the presence of emission lines (usually Balmer lines, in W Ser also He I, Fe II) in the optical spectra, which are incompatible with the optical continuum, belonging to a star too cool (A - G) to excite the emissions. It was therefore natural to search for a hotter source in the ultraviolet with the IUE. What we found (ref. 13) actually created more problems than it solved, but also showed that these systems are of considerable importance for our understanding of binary star evolution, in particular for understanding of accretion.

AR Pavonis appears to be a system showing the characteristics of both the W Ser stars and the symbiotic variables, and displays emissions of both types. For the other five stars, the far UV spectrum of W Serpentis shown in Fig. 3 is fairly representative. We observe strong emission lines of fairly highly ionized elements (N V, C IV, Si IV, Si III, Fe III, Al III, etc.) superposed on a relatively hot continuum. To trace this continuum is not easy because of the many emission lines, as well as deep depressions caused by severely blended strong absorptions. In W Ser, SX Cas, and β Lyr the estimated temperature of this continuum is, within about 1,000 K, approximately 11,500 K. The optically observed spectrum in β Lyrae (B8 II) corresponds to this temperature, but the observed hotter components in SX Cas (A6 III) and W Ser (F5 II) are much cooler than that. Only shortward of about 4,000 Å, our scans made at Lick Observatory with the IDS scanner indicate a weak contribution apparently coming from the hotter source seen in the UV. The ultraviolet continuum must therefore come from a region much smaller than the observed stellar surfaces.

Where in the system is the hot region located? Observations of the primary eclipse of SX Cas in February 1979 gave the answer. Optically, the eclipse is total. As my Lick scans confirm, the ordinarily seen A6 III disappears completely and is replaced by the spectrum of the cooler component, G5 III. At the same time, the UV hot continuum disappears as well, while the emission line spectrum is virtually unaffected (Fig. 4). Thus the hot source coincides with the hotter component in the system. W Ser, SX Cas, RX Cas, and β Lyrae are known to display unusually large period fluctuations and some other symptoms of rapid mass transfer. I suggest that the observed UV phenomena are associated with accretion. The hotter stars seen optically are the gainers in this process. Matter flows toward them from the secondary star, which presumably fills is critical Roche lobe. In an ordinary, short-period Algol semi-detached system (such as U Sge, U Cep), the stream impacts directly on the surface of the gainer. The W Ser systems have larger dimensions, so that the gainer is a smaller target, and the on-flowing material carries too much angular momentum. Therefore an accretion disk forms first (Fig. 5) and only its viscosity can eventually bring the gas particles inward to the surface of the accreting star. Thus we have an analogy to the accretion disks in the cataclysmic variables, but in the W Ser stars the accretion occurs on non-degenerate stars. We can scale the available models for cataclysmic variables (ref. 14) to estimate what kind of phenomena we will get in our case (ref. 15, 16). Most gravitational energy is released as a rule in a thin boundary layer between the disk and the surface of the accreting star, and I suggest that this

is the source of the UV continuum. In cataclysmic variables, the gainer is a white dwarf, so that this boundary lies at the bottom of a deep potential well, and soft X-ray emission is most likely to be emitted by it. For our main-sequence gainers, the potential well is much shallower, and the boundary layer will radiate most in the ultraviolet. In SX Cas, the observed temperature of the UV continuum requires a mass transfer rate of about 2×10^{-6} $M_\odot$/year, a plausible number which can easily be surpassed in other systems if the "case B" mass transfer is assumed. A preliminary estimate of the semi-thickness of the boundary layer indicates that it is about 0.06 of the radius of the A6 III gainer. However, more spherically symmetrical, albeit less dense clouds of gas must surround the gainer, since the observed A6 III spectrum is actually a shell spectrum, i.e. the absorption lines are formed in an extended atmosphere. In the model I am considering, the gainer has a radius of 6 $R_\odot$, and the accretion disk could in principle extend as far as some 30 $R_\odot$. There is no evidence, however, that a uniform, optically thick disk extends to any such distance, although some material is probably there and occasionally acts as a semi-transparent screen during secondary eclipses, which were in the past reported to be unusually long, but of variable duration. It is, however, also true that scaling up the models for cataclysmic binaries leads to a disk which is always geometrically quite thin perpendicularly to the orbital plane, with a maximum thickness of about only 1/10 of the star's radius; seen edge-on, such a disk would hardly cause more than a perturbation of the eclipse light curve. With the IDS scanner of the Lick Observatory, we also observed an "ultraviolet excess" of light shortward of 4000 Å at the time when the UV continuum was eclipsed. I think this radiation may come from a "warm spot" formed at a place where the in-coming stream meets a denser accumulation of matter in the outer parts of the disk. This would then be an analogy of the famous "hot spot" observed in the cataclysmic variables, but on a more modest scale, because of the shallowness of the corresponding potential well and low density of the disk.

Now, let us ask the important question: How different is β Lyrae from, say, SX Cas? I can see two important but not fundamental differences. Firstly, the accretion disk in β Lyrae is really optically thick to a large distance from its center of gravity, and actually simulates a star (perhaps it is also geometrically much thicker than some theorists are willing to permit). All this may be due simply to a higher rate of mass transfer, which may well be two orders of magnitude larger than in SX Cas, i.e. 10^{-4} $M_\odot$/y or thereabouts. Secondly, β Lyrae has an unusually hot and bright loser, which is a B8 II star. The integrated spectrum of the individual segments of the accretion disk cannot be assigned one definite temperature, but each spectral region can well be represented by one value of temperature -- and this temperature happens to be (accidentally) very close to that of the B8 II star probably everywhere in the accessible spectral range (ref. 12). The B8 II star appears to dominate the spectrum everywhere and the eclipses are only partial. Yet the case for the detection of the spectrum of the secondary (which may contain, in addition to the disk, also the genuine contribution of the accreting star if it is not completely hidden in the disk) is not hopeless, and some progress has already been made. Fig. 6 shows two spectra of β Lyrae, the lower taken during a secondary eclipse (i.e. the eclipse of the disk by the B8 II star). We notice a substantial reduction in the flux everywhere except in the region about 1700 - 2200 Å, which behaves as if there were no

eclipse. The only reasonable explanation I have is that this region of the spectrum is dominated by overlapping emission lines of Fe III, which are formed well outside the eclipsed space. If we now subtract the two spectra, we get (Fig. 7) a fairly well-defined flat spectrum corresponding to a temperature near 10,700 K. I think this is the very first look anyone ever had at the spectrum of the mysterious secondary object in β Lyrae.

Perhaps we will also soon be able to better understand the mysterious absence of the absorption lines of the secondary from the spectrum of β Lyrae, a mystery augmented by the fact that this object is more massive than the visible B8 star. We know now that probably everywhere in the accessible spectrum, the continuum temperature of the disk is about the same, or only slightly lower, than the effective temperature of the B8 star. Thus the "effective spectral type" along the spectrum is always about B8 - A1. The very few strong lines appropriate for such a spectral type in the optical region must be badly blended with the same lines from the B8 star, and often, as in the case of the Balmer and He I lines, contaminated by emission on top of that. However, in the far ultraviolet many more lines are available, and I hope that our high-dispersion observations at the primary eclipse, planned for this summer, may well bring us a positive identification. The lines may, of course, be seriously washed out by the differential Keplerian rotation of the disk.

The strong emission lines observed in β Lyrae and all the W Serpentis stars remain a puzzle. As we saw in SX Cas (and also W Ser), their intensity is not significantly altered at any phase of the eclipse of the gainer. I wish we had the same coverage for secondary eclipses, and the rest of the orbital phases. Without this direct evidence, it is tempting to associate the emissions with the loser, which in SX Cas and RX Cas is a G giant. Since the observed emissions are indeed similar to those seen for example in Capella, a chromospheric origin appears the most simple and plausible explanation. Yet there are serious objections to this hypothesis. The power radiated in the emission lines in SX Cas is several solar luminosities, i.e. much larger than in Capella or in the considerably more powerful chromospheric emitters such as are the RS CVn stars (ref. 1, 17). Again, the N V line competes in strength with the C IV line or is stronger, while in giant chromospheres and in all parts of the transition region in the Sun, the C IV line is much stronger (ref. 18). And then, while it is easy to identify the potential carriers of the chromospheres in systems with G-type secondaries, where is this star in β Lyrae and V 367 Cygni?

Perhaps the most decisive argument comes from high-dispersion observations of β Lyrae. All emission lines are found to have pronounced P Cygni profiles (Fig. 8), although the low-dispersion spectra hardly show any indication of this (Fig. 9) -- which is a serious warning. The absorption components indicate an outflow at a velocity of about 150 km/s. Absence of most intercombination lines suggest a fairly high density of the line-forming region, $N_e \simeq 3 \times 10^{12}$ cm^3. The presence of fairly pronounced absorption components demands a fairly large depth of the formation region, and lack of eclipses suggests that this region is far outside the space actually swept by the two components. Radial velocity observations in β Lyrae with Copernicus (ref. 11,12) show that the emission lines, with a very few possible exceptions, do not participate in the orbital motion of either component. I think that both

the kinetic energy of this stellar wind as well as the ionization energy are ultimately derived from the gravitational energy released during accretion, but the actual mechanism of conversion is not clear. Is ionization maintained by a flux of soft X rays, generated in shocks near the gainer? Or is the ionization collisional? The amount of energy involved is not negligible, and the process must affect the evolution of the system: The line emitting region seems to have fairly high density ($N_e = 3 \times 10^{12}$ cm^{-3}), it must be fairly thick to produce the absorption components, and its radius must also be quite large, as it probably lies outside the binary system. If the outflow is isotropic, fairly large mass loss from the system is indicated.

In order to test the isotropy of the outflow, I attempted to find non-eclipsing counterparts of the W Serpentis stars. The picture of the system may actually be less complex when it is not viewed edge-on, with all the accreting material obscuring the view of the accreting star. It may indeed be true that the gainer is easier to see, but the consequence appears to be that the emission lines are much less conspicuous against a stronger continuous background. The problem is also: how to find the non-eclipsing counterparts? I examined Be stars and shell stars with spectral peculiarities. The stars KX And (HD 218393), HD 51480, and HD 72754 were indeed found to have UV continua (including deep absorptions) quite similar to that of SX Cas. At least some emissions are weakly present (ref. 19). The last one of the three was reported to be similar to β Lyrae by Thackeray and Hutchings (ref. 20). The former two yield a good support to the claim made by myself and my collaborators (Harmanec, Křiž, Peters, Polidan - ref. 21) that a good model for Be and shell stars is that of an interacting binary system.

υ SAGITTARII

Another bizarre object is ν Sagittarii, a single-line spectroscopic binary with a period of 138 days. Its spectrum is famous for being extremely helium-rich and hydrogen-poor. A similar but much milder overabundance of helium with respect to hydrogen has been suspected in β Lyrae, and a certain degree of similarity indeed exists between these two objects. The invisible companion to the helium-rich star in υ Sagittarii was detected with the IUE (Duvignau et al., ref. 22; Hack et al., ref. 23), and is probably an O9 V star. Rather surprisingly, the UV spectrum shows no emission lines. Possibly the period of rapid mass transfer is definitely over in this system.

SYMBIOTIC STARS

This is a group of objects for which, in spite of considerable effort, non-controversial models were simply not possible without far ultraviolet observations. In the optical region, one observes a late-type continuum with superposed emission lines (H, He I, He II, C III, N III, some forbidden lines), which require a radiation source much, much hotter than the M or K star whose absorption spectrum is seen. Single and binary star models were proposed, and indeed both types may still apply, since the group is probably not homogeneous. However, the spectra I saw (AG Peg, AR Pav -- ref. 24, 25) and those described in literature (R Aqr, RW Hya -- ref. 26) fully justify their inclusion in my talk, since these stars are binaries. Z And (ref. 27) can almost certainly be added. This in itself solves a fundamental problem that

worried astrophysicists for decades.

An inspection of Fig. 1 in the paper by Keyes and Plavec in this volume shows why the dilemma was practically insolvable without UV spectroscopy: in the optical region, the hot component contributes virtually no radiation. The small "ultraviolet excess", and veiling of absorption lines observed shortward of about 5000 Å, is more likely due to free-free (and farther shortward to bound-free) radiation of hydrogen than to the hot component itself. (Incidentally, the figure I referred to is another testimony to the very good photometric performance of the IUE spectrographs. The diagram combines fluxes measured by the IDS scanner at the 120-inch Shane telescope of the Lick Observatory with those obtained with the IUE: they match without any artificial adjustment.)

In the symbiotics, the late-type component is an M or K giant, not a supergiant as in the ζ Aurigae stars. Yet it dominates the optical spectrum, since the hot component is most likely a subdwarf, well below the main sequence. Bath (ref. 28) suggested that the UV continua may actually be due to the narrow accretion transition regions on ordinary stars, described here in the section on the W Serpentis stars. I think there is good evidence that the hot components are genuine hot subdwarfs; I believe that they may be products of case B mass transfer, and that the symbiotics are systems in which a little bit of cosmic justice takes place and the companion, which initially stole part of its mate's mass, is returning it back. Whether the subdwarf can accomodate it is questionable. In AG Pegasi, Keyes and myself find a similarity between the hot star and a WR nucleus of a planetary nebula. However, in the past century, the outflow from this star resembled rather an extremely slow nova. Yet it is likely that the ultimate source of activity is the M2 III companion. That star seems now to be much smaller than its Roche lobe. Apparently we do not understand a lot in this case, but when we eventually will, we may know much more about subdwarfs, planetary nebulae, and novae.

THE ALGOLS

In the large class of the semi-detached binaries of the Algol type, the optical spectrum is dominated by the hotter, main-sequence component, but a certain degree of contamination (small in short period systems like U Sge and U Cep, large in longer-period ones like AW Peg and V 356 Sgr) does exist, due to the presence of the subgiant or giant, later-type loser. The IUE observations made so far by me and others will yield a more reliable determination of effective temperatures. Yet a more far-reaching program is conceivable. If the high-dispersion spectra are good enough to permit spectrum synthesis, one could profitably study the abundances and decide if they are anomalous. At the end of mass transfer, the loser's outer layers contain material partly processed inside the star. Will it be transferred to the gainer, or dispersed into space? We need this information badly in order to decide how much matter is transferred and how much escapes from the system.

Some more direct evidence on this topic is already being obtained from detailed studies of line profiles, which enable us to study gas streaming in the system (Kondo et al., ref. 29; Peters and Polidan, ref. 30). They claim that little is accreted; rather, the gas escapes or falls back on the loser.

CONCLUSIONS

Although the IUE satellite has been operating for two years only, and the bulk of results and discoveries is still not accessible, it is already obvious that studies of all kinds of close binaries will profit considerably. I have surveyed only a limited number of types of interacting binaries. I have devoted a fairly large amount of available space to such exotic objects like β Lyrae, ε Aurigae, υ Sagittarii, W Serpentis, AG Pegasi, and AR Pavonis. I do not think that they are bizarre oddities far outside the mainstream of astrophysical research. On the contrary: each of them is trying to tell us something very important about the fundamental problems of stellar structure and evolution.

Let me formulate just a few of these problems.

(1) Do stellar black holes exist at all? If they do, do they play any significant role in stellar population -- or are they just bizarre freaks? β Lyrae, ε Aurigae, and υ Sagittarii were often in the past invoked as possible systems harboring a black hole. This hypothesis is all but abandoned now, but we should be quite sure.

(2) How are extremely helium-rich, hydrogen-poor atmospheres produced in binary systems? β Lyrae and, above all, υ Sagittarii hold clues to the answer. Mass loss should bring He-rich material to the surface, but the theory does not predict any such extreme helium overabundance as has been reported for υ Sagittarii.

(3) How are the subdwarfs in symbiotic stars related to cataclysmic variables? What actually determines that a star flares up as a dwarf nova (like Z And) or as a slow nova (like AG Peg)? Why is the subdwarf in AG Pegasi similar to the WR nuclei of planetary nebulae, and if it is, why did it flare up in the past century as a nova? How is a planetary nebula formed in a binary system? And why are all nuclei of planetary nebulae of the WN type, not WC (but AG Peg does not seem to be a pure WN)?

(4) The supergiant in ε Aur and the giant in AG Peg are much smaller than their respective Roche lobes, and Reimers' formula gives a small rate of mass loss through stellar wind, too. Yet they appear to be the ultimate sources of all the activity and circumstellar mass. Where are we wrong?

(5) A fundamental problem of evolution with mass transfer in interacting binaries: How do the gainers accrete mass? Do they really swell all the way to their respective Roche lobes, as current theories postulate? Or can they reject the surplus material and drive it out of the system? How is it done? By exceeding locally the Eddington limit? Or does an instability occur, due to rapid rotation of the gainer? The W Serpentis stars, and β Lyrae in particular, promise all the answers.

After years of considerable effort, analyses based on optical data could not yield answers to our queries about the exotic systems, and in many cases a dead end was reached. IUE opened new horizons in a very dramatic way. We have now many more facts, and still more are within our reach. We should not retreat now. We need continued ultraviolet observations, perhaps even more refined: we need spectrograms calibrated both for spectrophotometry and for radial velocity work, and at sufficiently high dispersion.

REFERENCES

1. Close Binary Stars: Observations and Interpretation. (Ed.: M.J. Plavec, D. M. Popper, R.K. Ulrich), Reidel, 1980.
   Dupree, A.K., Hartmann, L., and Raymond, J.C.: Ultraviolet Spectroscopy of Binary Systems, p. 39.

2. Hagen, W., Black, J.H., Dupree, A.K., and Holm, A.V.: Astrophys. J., 1980, in press.

3. Faraggiana, R. and Selvelli, P.L.: Astron. Astrophys. 76, L 18, 1979.

4. Faraggiana, R.: The UV spectrum of VV Cep. 1980, Ref. 1, p. 549.

5. Stencel, R.E., Kondo, Y., and Bernat, A.P.: Ultraviolet Observations of 31 Cygni and 32 Cygni. 1980, Ref. 1, p. 555.

6. Plavec, M.J.: Two Bright Eclipsing Binaries in Sagittarius. Info. Bull. Var. Stars No. 1598, 1979.

7. Hack, M.: A new explanation of the binary system ε Aurigae. Mem. Soc. Astro. Ital. Vol. 32, No. 4, 1961.

8. Hack, M. and Selvelli, P.L.: IUE observations of the eclipsing binary Epsilon Aurigae. Nature Vol. 276, p. 376, 1978.

9. Huang, S.S.: An interpretation of ε Aurigae. Astrophys. J. 141, 976, 1965

10. Morris, S.C.: The masses and dimensions of ε Aurigae. Astron. J. 70, 685, 1965.

11. Hack, M., Hutchings, J.B., Kondo, Y., McCluskey, G.E., Plavec, M., and Polidan, R.S.: The ultraviolet spectrum of Beta Lyrae. Astrophys. J. 198, 453, 1975.

12. Hack, M., Hutchings, J.B., Kondo, Y., and McCluskey, G.E.: The ultraviolet spectrum of Beta Lyrae, III. Astrophys. J. Suppl. 34, 565, 1977.

13. Plavec, M.J. and Koch, R.H.: Detection of emission lines of hot plasma in five peculiar eclipsing systems. Info. Bull. Variable Stars No. 1482, 1978.

14. Pringle, J.E.: Soft X-ray emission from dwarf novae. Mon. Not. R.A.S. 178, 195, 1977.

15. Plavec, M.J.: IUE observations of long-period eclipsing binaries: A study of accretion onto non-degenerate stars. 1980, Ref. 1, p. 251.

16. Bath, G.T.: Cataclysmic variables, Hubble-Sandage variables, and η Carinae 1980, Ref. 1, p. 155.

17. Linsky, J.L., et al.: IUE observations of cool stars. Nature Vol 275, p. 389, 1978.

18. Doschek, G.A., Feldman, U., Mariska, J.T., and Linsky, J.L.: Electron densities in stellar atmospheres determined from IUE spectra. Astrophys. J. Lett. 226, L 35, 1978.

19. Plavec, M.J.: The shell star HD 218393 as an interacting binary. Bull. Amer. Astron. Soc. 11, 648, 1979.

20. Thackeray, A.D.: A spectroscopic reconnaissance of new β Lyrae system HD 72754. Mon. Not. R.A.S. 154, 103, 1971.

21. Many articles in "Be and Shell Stars", (ed. A. Slettebak), Reidel, 1976.

22. Duvignau, H., Friedjung, M., and Hack, M.: The ultraviolet spectrum of υ Sagittarii. Astron. Astrophys. 71, 310, 1979.

23. Hack, M., Flora, U., and Santin, P.: IUE observations of two peculiar binary systems, Beta Lyrae and Upsilon Sagittarii. 1980, Ref. 1, p. 271.

24. Keyes, C.D. and Plavec, M.J.: The symbiotic binary system AG Pegasi. 1980, Ref. 1, p. 535.

25. Keyes, C.D. and Plavec, M.J.: The symbiotic star AG Pegasi studied and compared with AR Pavonis. Bull. Amer. Astron. Soc. 11, 731.

26. Michalitsianos, A.G., Kafatos, M., Hobbs, R.W., and Maran, S.P.: IUE observations of the hot components in two symbiotic stars. Nature Vol. 284, p. 148, 1980.

27. Friedjung, M.: IUE observations of Z Andromedae. 1980, Ref. 1, p. 543.

28. Bath, G.T.: Symbiotic stars - a binary model with supercritical accretion. Mon. Not. R. A. S. 178, 203, 1977.

29. Kondo, Y., McCluskey, G.E., and Stencel, R.E.: IUE ultraviolet spectra of the interacting binary U Cephei. 1980, Ref. 1, p. 237.

30. Polidan, R.S. and Peters, G.J.: Ultraviolet observations of close binary stars. 1980, Ref. 1, p. 293.

31. Mariska, J.T., Doschek, G.A., and Feldman, U.: Discovery of a blue companion to η Aquilae. Astrophys. J. Lett., 1980, in press.

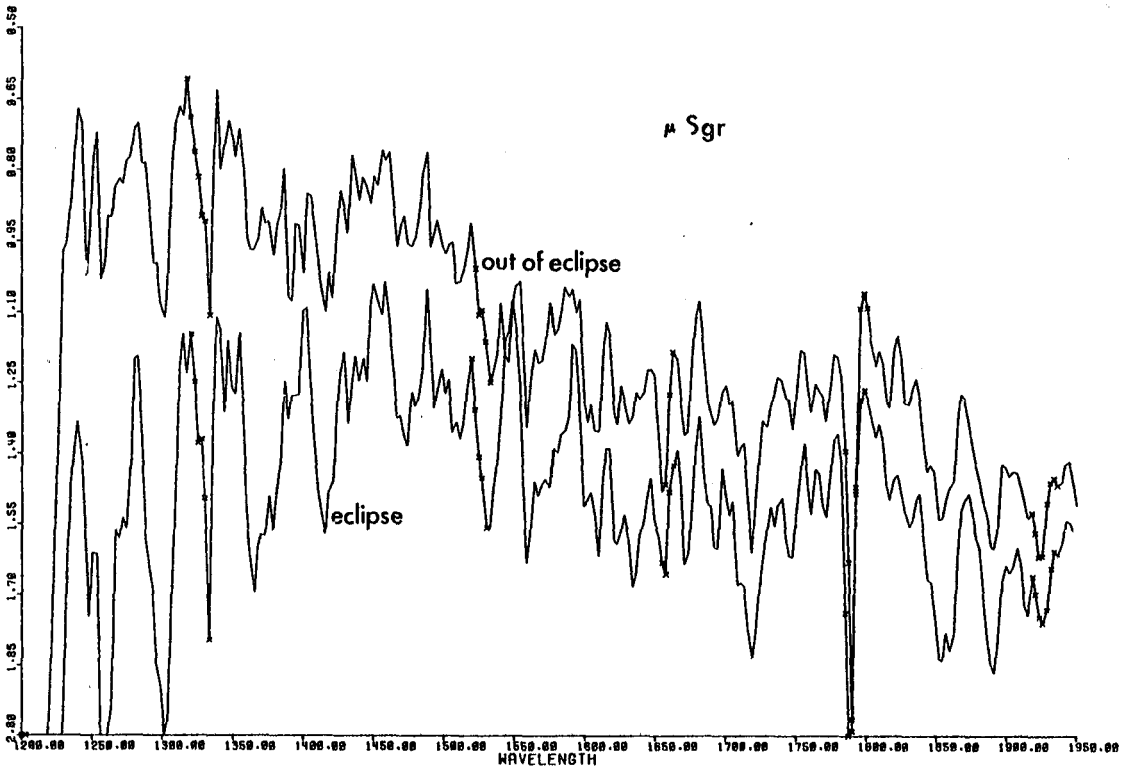

Fig. 1.: IUE spectra of μ Sagittarii taken at primary eclipse and outside it.

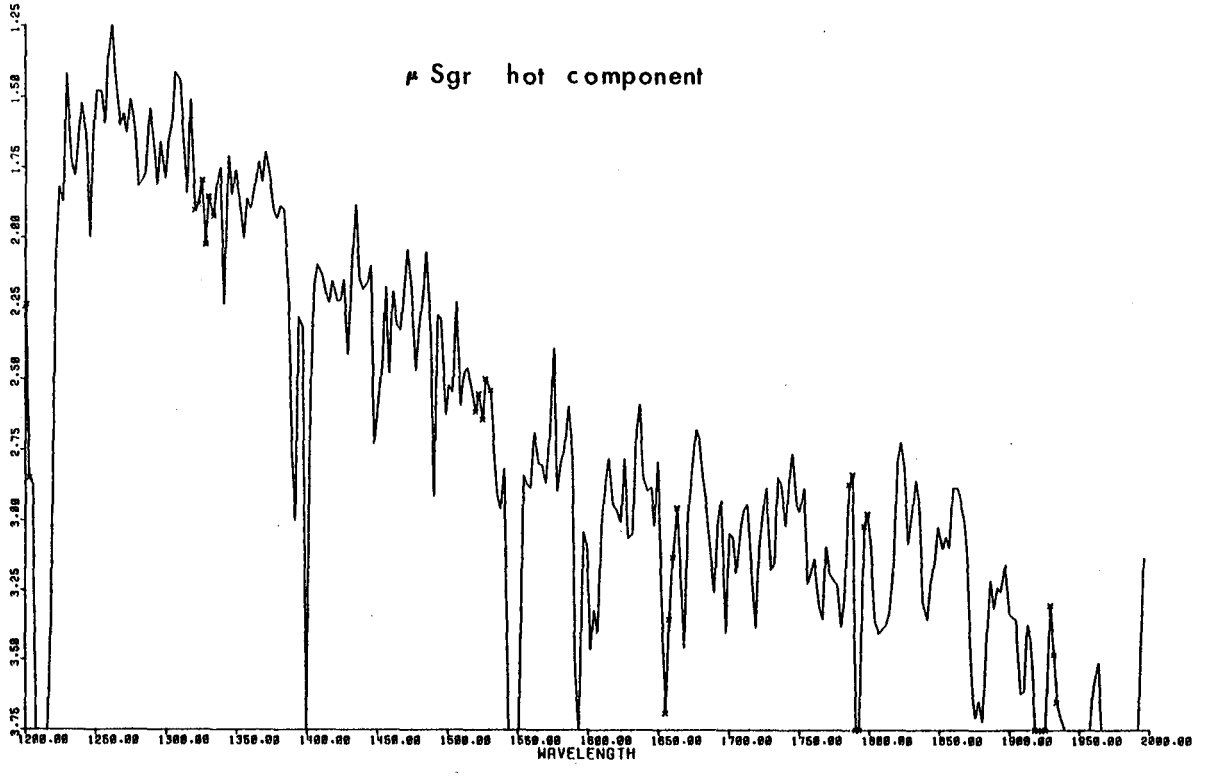

Fig. 2.: Reconstructed spectrum of the hot component in μ Sagittarii.

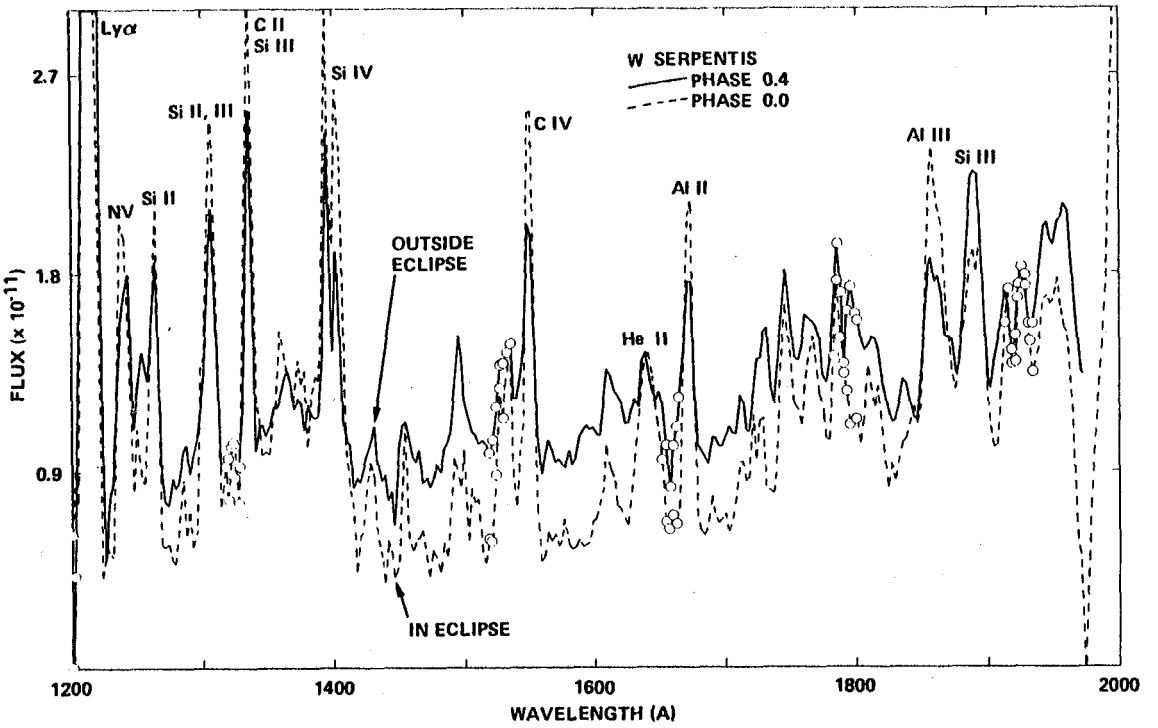

Fig. 3.: Far ultraviolet spectrum of W Serpentis.

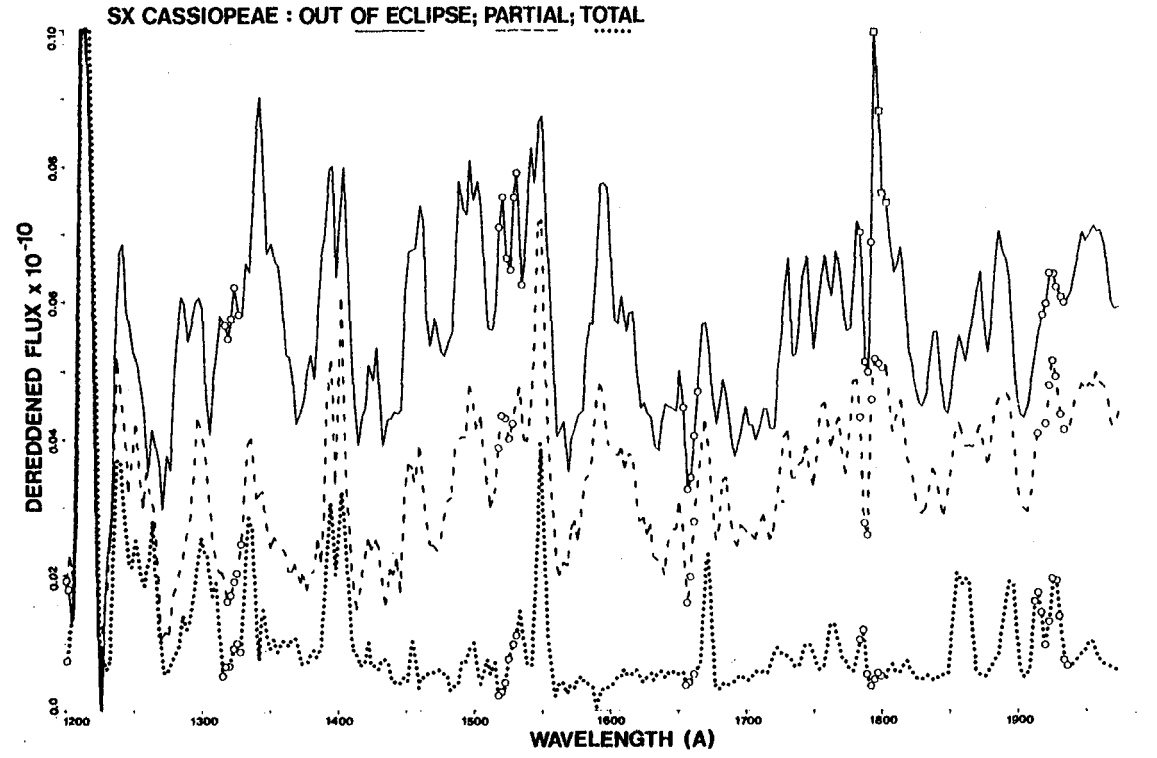

Fig. 4.: Far ultraviolet spectra of SX Cassiopeae taken during totality, during partial eclipse, and outside eclipse.

Fig. 5.: A schematic model of the system SX Cassiopeae showing disk accretion.

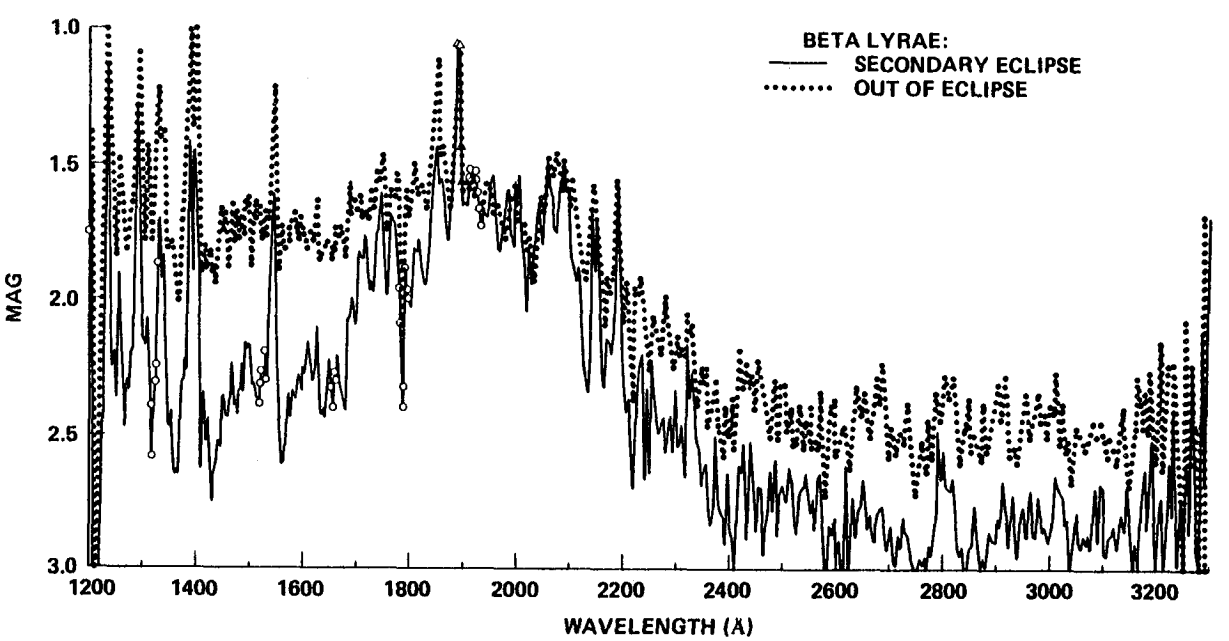

Fig. 6.: Ultraviolet spectra of β Lyrae, taken in secondary eclipse and outside eclipse.

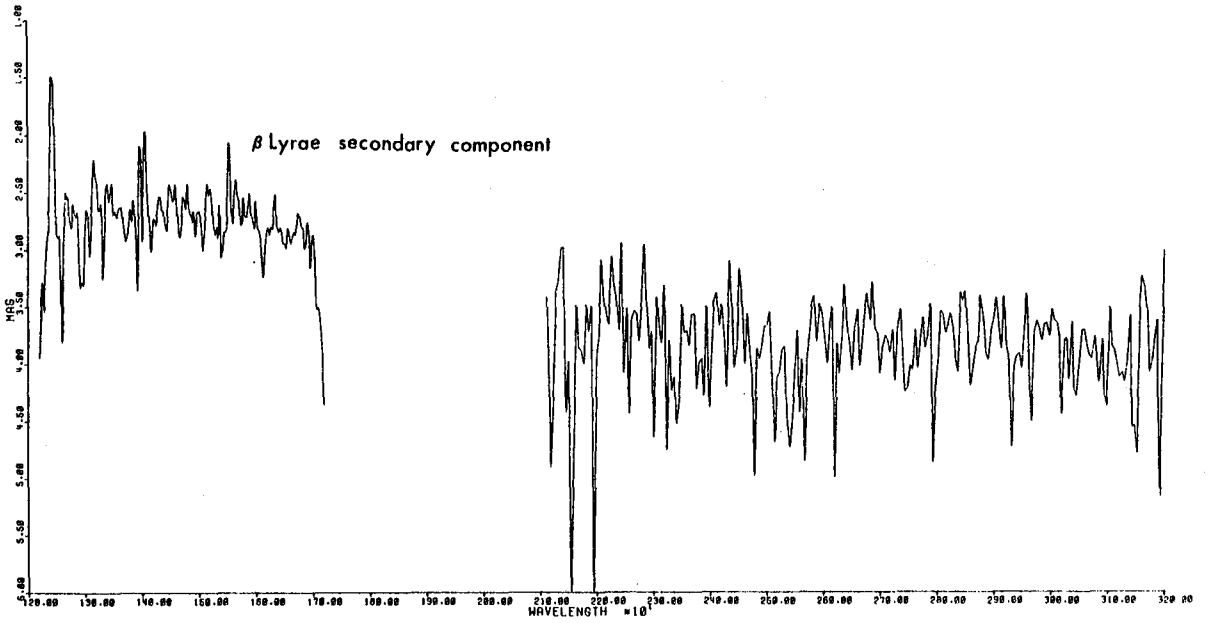

Fig. 7.: Reconstructed spectrum of the secondary component in β Lyrae.

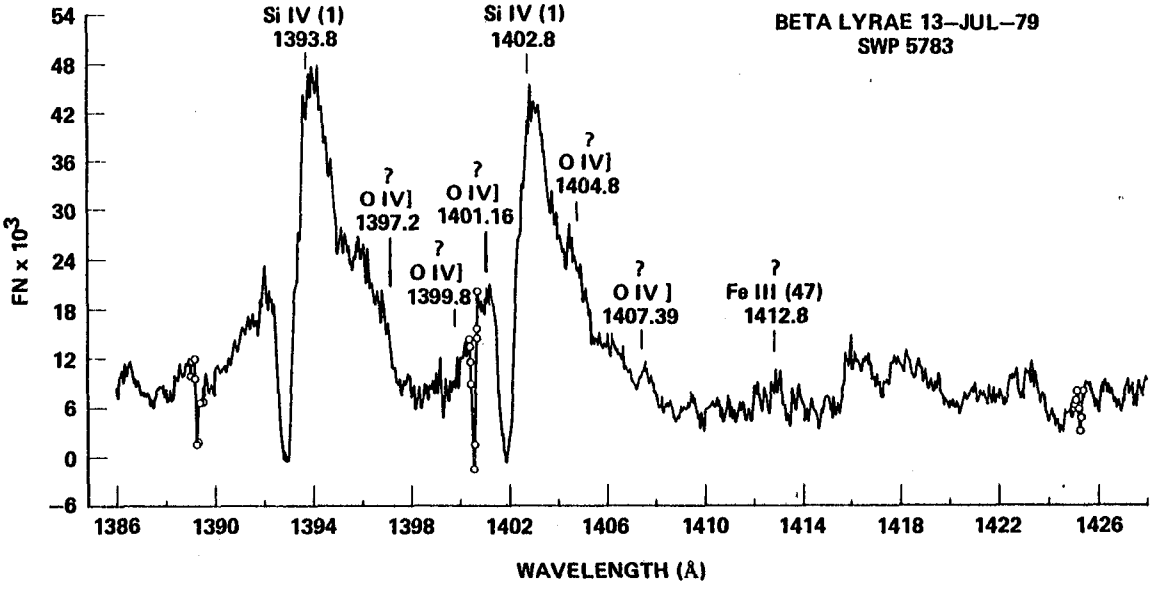

Fig. 8.: High-dispersion spectra of β Lyrae show P Cygni profiles of emission lines.

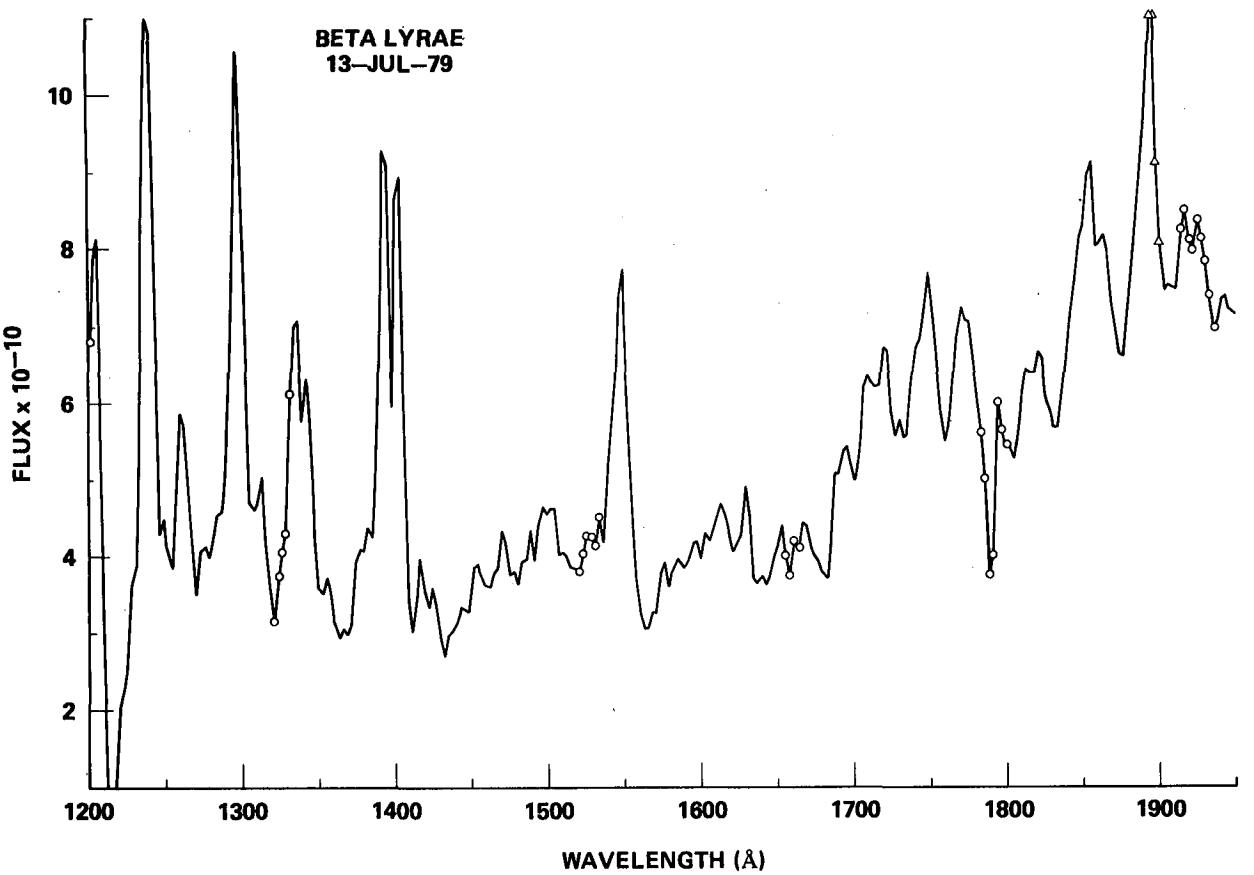

Fig. 9.: Low dispersion spectrum of β Lyrae shows virtually no trace of the P Cygni character of the emissions.

HIGHLY-EVOLVED STARS

Sara R. Heap
Laboratory for Astronomy and Solar Physics
Goddard Space Flight Center

1. INTRODUCTION

According to current theories of stellar evolution, any star will eventually exhaust all its sources of energy, and become some kind of compact object--a degenerate dwarf, neutron star, or black hole. A low-mass red giant slowly loses its outer envelope, while its core continues to contract, and it ultimately becomes a degenerate dwarf. A higher-mass red giant undergoes a supernova event, in which the core collapses while the outer layers explode. For a star of intermediate mass, the explosion is powerful enough to drive off the envelope, and the core becomes a neutron star. For a massive star, however, the explosion is not strong enough to eject the whole envelope, and the star as a whole collapses further to form a black hole.

These three end-products of stellar evolution--the degenerate dwarf, neutron star, and black hole--and their immediate precursors manifest themselves in the optical region of the spectrum in a wide variety of species (Table 1), which I've classified according to whether they are isolated stars (i.e. single or non-interacting), components of close interacting binaries, or members of a globular cluster.

Table I

Optical Appearance of Highly-Evolved Stars

	Observable Species		
Compact Object	Isolated	Interacting Binary	Globular Cluster
Black Hole		X-Ray Binary	?
Neutron Star	Pulsar ↑SN	X-Ray Binary	?
Degenerate Dwarf	White Dwarf ↑ Planetary Sub-dwarf	Cataclysmic Variable AM Her Object Sco X-1 Like Object	

Isolated Stars

While isolated black holes, by definition, are unobservable, isolated neutron stars reveal themselves as pulsars, and isolated degenerate stars are visible as white dwarfs. Their immediate precursors are believed to be the central stars of planetary nebulae and other hot "sub-dwarfs".

Interacting Binaries

The compact objects manifest themselves most spectacularly, if indirectly, as components of close, interacting binaries. Although the compact component is usually invisible, it makes its presence unmistakably clear in accreting material supplied by a nearby "normal" companion, which for one reason or another (stellar wind, rotational ejection, Roche-lobe overflow) is losing mass. In the process of infall to the compact object, gravitational energy is released, some of which goes into radiation. It is not surprising, then, that all these classes of interacting binaries involving compact objects have among them at least some objects which are known to be X-ray sources. Cyg X-1 is, perhaps, the most promising black-hole candidate. So far, there are at least 14 binaries having neutron-star companions known. There are several types of binaries containing degenerate dwarfs of which I have listed only a few. One type is the cataclysmic variables (novae, dwarf novae and recurrent novae) in which the compact companion is a non-magnetic or weakly magnetic degenerate dwarf. Another type, of which AM Her is the most spectacular example, is the binaries which contain a highly magnetic degenerate dwarf.

Globular Clusters

We may consider globular clusters as a class of "highly evolved" stars not only because they contain stars which have exhausted or are close to exhausting their nuclear fuels but also because they are highly evolved dynamically, with relaxation leading to very dense central regions. It is now known that globular clusters are a class of objects in which x-ray emission is two orders of magnitude more probable than for the galaxy as a whole (ref. 1). Why this should be so is unclear, but this finding has led to suggestions of massive black-holes accreting stellar debris (ref. 2) and formation of binaries by capture of field stars (ref. 1) in the dense central regions.

All these objects are of great interest, not only because they define the end-points of stellar evolution, but also because they represent extreme physical conditions not accessible in a terrestrial laboratory. As a rule, however, these objects are faint optically, either due to low intrinsic luminosity or interstellar extinction, and until 1978 they were observed in the ultraviolet only with medium or wide-band filters, if at all. The IUE, however, has made it possible to obtain ultraviolet spectra of these objects, sometimes even at high dispersion. The most promising black hole candidate, Cyg X-1, has been observed by IUE with full phase coverage. The IUE has also observed the Crab pulsar; and I believe that Benvenuti will be reporting the results later in this symposium. The IUE has been used to obtain ultraviolet phase coverage of six x-ray binaries believed to contain neutron-star companions, and it has observed dozens of degenerate and pre-degenerate stars.

Because studies of highly evolved stars with the IUE have been so extensive, this review can only describe a few selected topics. The appendix to this review, however, contains a list of published observations up until the time of this review.

2. PRE-DEGENERATE HOT STARS

Elemental Abundances

Beyond the statement that subluminous, blue stars are highly-evolved solar-mass stars in the process of becoming white dwarfs, the evolutionary status of these stars is not well understood; nor is it understood even to what extent these objects form a homogeneous group. Part of the problem is that their physical parameters, particularly surface chemical compositions, have not been determined. Analyses of IUE spectra, which contain strong lines of important elements such as He, C, N and Si, however, are now proving useful in defining the parameters for these stars. The lion's share of the work has been carried by the Kiel astronomers (ref. 3-6), who have performed non-LTE analyses of IUE spectra of hot sub-dwarfs. Their results for three sdO stars are shown in Table II. Note that in all three stars, helium is enriched, the carbon-to-nitrogen abundance ratio is very low, but the silicon abundance is normal. As the Kiel group points out, the normal abundance of silicon, which should well represent the "metals", rules out gravitational settling of heavy elements. However, the overabundance of nitrogen and helium and the depletion of carbon indicate prior processing by the CNO-cycle.

Table II

Compositions of 3 sdO Stars
(from Gruschinske, Hunger, Kudritzki, Simon,
Kiel University [ref. 3-6])

	Abundances Relative to Sun			
	He	C	N	Si
HD 49798	2.8	0.4	25	1.4
HD 127493	3.0	0.02	8	1.4
BD +75°325	3.0	0.4	12	1.1

Stellar Winds

One of the first discoveries made with the IUE (ref. 7) was that the UV spectra of some hot, subluminous stars have P Cygni lines, indicating high-velocity mass-loss very much like that inferred in young OB stars. Subsequent analyses of the profiles of these lines, as obtained from high-dispersion IUE spectra, have confirmed the detailed similarities of winds in these two groups of stars, which are at opposite extremes of stellar evolution. It is

now clear that these hot, subluminous stars serve as an excellent laboratory for studying the properties of high-velocity winds, because they provide a broad range of stellar parameters, like effective temperature or escape velocity, to correlate with wind characteristics. Figure 1 shows a temperature-gravity plot of some subluminous O stars which have been observed by IUE. Note that most of these stars undergoing high-velocity mass loss fall in a well-defined region bounded by particular $\mathcal{L}/\mathcal{M}$ ratios. These boundaries are the same as those for young massive O stars (cf. ref. 8). Also as with young O stars, there is a general trend of increasing terminal velocity of the wind with stellar escape velocity. These similarities suggest that mass-loss in hot stars is an atmospheric phenomenon, totally unrelated to interior structure, which of course must be very different for young OB stars and these old, subluminous stars. The correlation of the presence of the wind with $\mathcal{L}/\mathcal{M}$ and the correlation of terminal to escape velocity are consistent with radiation-driven mass loss (cf. ref. 9).

There is one outstanding exception to the empirical criterion above for the presence of a wind. This exception is the central star of NGC 2392, whose visual spectrum indicates an O6f spectral type but whose ultraviolet spectrum is continuous. I have been pondering this fact for two years now and still have no good explanation.

The wind of one particular star, the nucleus of NG 6543, has been studied intensively. The spectral type of the central star is midway between Of and WR. Analysis of high-dispersion profiles of the wind lines (shown in Figure 2) indicates a rate of mass loss, $\dot{M} \approx 7 \times 10^{-7} M_\odot$/yr., which exceeds the theoretical maximum mass-loss rate given by radiation-driven winds. Analysis of the profiles as obtained from low-dispersion spectra via a clever technique devised by Castor, Lutz and Seaton (ref. 10) yields similar results for this central star. I mention this technique, since it was developed specifically for IUE low-dispersion spectra, and should prove exceedingly useful for studying winds in stars too faint for high-dispersion spectroscopy.

3. DEGENERATE STARS

X-Ray Emission in White Dwarfs

About five years ago, it was discovered (ref. 1) that Sirius B, the white-dwarf component of Sirius, is a soft x-ray source. One explanation (ref. 12, 13) was that soft x-ray radiation produced in the deep photosphere could escape from a metal-deficient atmosphere and would yield the observed fluxes, provided that the effective temperature exceeds 32000°K. Another explanation was that coronal emission from an envelope surrounding Sirius A or Sirius B provides the observed x-rays. These possibilities are ruled out by Böhm-Vitense et al.'s (ref. 14) IUE observations which show that (1) the UV absolute flux distribution yields an effective temperature of only 26,000°K which is too low for the production of soft x-rays, and (2) no emission lines indicative of a chromosphere or corona are present in the UV spectrum of either Sirius A or Sirius B, at least at low dispersion. Escape of deep photospheric emission does appear to be valid, however, for another hot white dwarf, HZ 43, which is the brightest ultra-soft-x-ray source in the sky. Oke and

Greenstein's (ref. 13) IUE observations showed that its $T_{eff} \approx 60000°K$, making it one of the hottest white dwarfs known.

The Nature of Cataclysmic Variables (Novae, Recurrent Novae, Dwarf Novae)

It is generally believed that cataclysmic variables are close binaries in which the red component fills its Roche-lobe and transfers matter, via an accretion disk, onto a white dwarf (ref. 16). The nature of the outburst differs among the cataclysmic variables: in novae and recurrent novae, the outburst is associated with unstable nuclear burning of hydrogen-rich material accreted on the surface of the white dwarf, while in dwarf novae, the outburst is associated with a sudden increase in mass transfer from the red dwarf.

Observations during the first two years of operation of the IUE have yielded a great wealth of data concerning cataclysmic variables, including observations of several novae at outburst. Rather than reviewing all these data, I shall use studies of Nova Cyg 1978 and the dwarf nova, Ex Hya, as examples of IUE investigations. Later on in this symposium, we shall be hearing more on cataclysmic variables (Lambert et al. "Old Novae"; Hartmann and Raymond, "Cataclysmic Variables"; Fabbiano et al., "Accreting Degenerate Dwarfs").

Nova Cygni 1978

Nova Cyg 1978 is the first nova for which detailed ultraviolet observations have been obtained, and it is a tribute to the flexibility of IUE operations, that it could start observing this fast nova within a day after it reached (visual) maximum. Figure 3 shows the development of the far-ultraviolet spectrum of Nova Cyg (ref. 17) from its initial absorption-line phase to its nebular phase six months later. Once in the nebular phase, the great strength of the nitrogen lines, NV λ1240, NIV] λ1486, NIII] λ1751, becomes apparent. Seaton (ref. 18) has made a preliminary abundance analysis of the nebula and finds a nitrogen-to-carbon abundance ratio of two, that is, nearly seven times the solar ratio. This enrichment of nitrogen implies that some of the ejected material has undergone hydrogen burning by the CNO cycle, as predicted by the nuclear-runaway theory (ref. 19). Also consistent with the nuclear-runaway theory is the finding of near-constancy of the bolometric luminosity during visual decline (ref. 20).

Ex Hya

Ex Hya is a dwarf nova having a binary period of 99 minutes and an interval between outbursts of about 15 months. It also happens to be a soft x-ray source. Figure 4 shows the flux distribution of Ex Hya during quiescence as obtained by simultaneous IUE and ground-based observations (ref. 21). It is immediately apparent from this figure how crucial IUE observations are in extending spectral coverage of dwarf novae into the region of maximum flux, and hence, in making adequate comparisons with theoretical flux distributions. Bath, Whelan, and Pringle (ref. 21) find that the observed flux distribution of Ex Hya is consistent with that of an optically thick accretion disk. This fit is a fruitful comparison with theory, in that important physical properties may then be derived, including

the rate of mass transfer, $\dot{M} \approx 1 \times 10^{-9}$ $M_\odot$ per year, as well as physical and geometrical properties of the disk ($R_{disk} \gtrsim 50\ R_*$, T_{disk} ($R = 1.36\ R_*$) = 34800°K, T_{disk} ($r \gtrsim 50\ R_*$) = 3700°K) and the white dwarf ($T_* = 70000$°K). From a comparison of the soft x-ray flux with the estimated bolametric flux, Bath et al. infer that the x-ray flux is generated in the "boundary layer" where disk material skids to a landing on the stellar surface.

Accretion Onto Magnetic White Dwarfs - AM Her

Earlier I mentioned that there appear to be two types of accreting degenerate dwarfs - the non-magnetic or weakly magnetic stars, to which most of the cataclysmic variables belong, and the highly magnetic degenerate dwarfs, of which AM Her is a spectacular example. In the case of AM Her, the picture of accretion is one in which material flows from the red dwarf onto the magnetosphere of the white dwarf and spirals in to the stellar surface at the magnetic poles. The predicted spectrum of accretion (ref. 22) onto magnetic degenerate dwarfs differs from that of non-magnetic dwarfs in the presence of strong ultraviolet cyclotron radiation associated with strong magnetic fields. Intense UV emission, however, is not observed in AM Her, according to Raymond et al. (ref. 23), a finding which presents a severe difficulty for the theory of polar accretion. Later on in this symposium, we shall be hearing from Dr. Chanmugan more about this discrepancy and possible resolutions.

4. X-RAY BINARIES

In the past two years, an international team of IUE observers has succeeded in observing all known x-ray binaries within the limits of sensitivity of the IUE. The appendix summarizes the IUE data obtained on massive x-ray binaries and low-mass x-ray binaries. The distinction among x-ray binaries according to the mass of the optical primary is also a distinction in source of accreted material: in the massive x-ray binaries, the primary generally loses mass via a high-velocity wind, while in the low-mass binaries, the primary generally loses mass through overflow of its Roche lobe. IUE observations have proved to be essential in clarifying the properties of the wind of the massive x-ray binaries, and they have proved most useful in identifying the component mechanisms of x-ray emission of low-mass x-ray binaries, and hence, in clarifying the process of accretion onto the compact object.

Massive X-Ray Binaries

Perhaps the most outstanding achievement of the IUE observers in studying massive x-ray binaries has been the detection of phase-dependent variations in the profiles of unsaturated wind lines such as the Si IV or C IV resonance doublets. This phase dependence is evident even in low-dispersion spectra of Cyg X-1, SMC X-1 and LMC X-4 (ref. 24), but it shows up most markedly in the high-dispersion spectra of Vela X-1 (ref. 25). Figure 5 shows how the profiles of the Si IV wind lines vary with binary phase. This variation was first predicted by Hatchett and McCray (ref. 26) as a consequence of ionization of the wind in the vicinity of the compact object. McCray's prediction as applied to Vela X-1 is illustrated in Figure 6. In

the vicinity of the x-ray source, material is so highly ionized that there are no ions capable of scattering stellar photons. Hence at $\phi = 0.5$, when the highly ionized cavity lies in front of the primary, the high-velocity shoulder of the absorption component disappears, while the emission component is relatively unaffected. Conversely, at $\phi = 0.0$, when the ionization cavity lies behind the primary, the absorption component is unaffected, but the emission component, arising partly in material receding from the observer, is diminished. This is, indeed, what is actually observed.

5. GLOBULAR CLUSTERS

The IUE has proved useful both in detecting and in locating ultraviolet-emitting sources in globular clusters. So far, six globular clusters, including three known x-ray emitters, have been observed with the IUE (ref. 27). In general, the UV spectra of globulars indicate a mixed stellar content: the near-UV emission arises from late-type horizontal-branch stars and giants, while the far-uv emission usually arises from blue horizontal-branch stars. The ultraviolet properties of blue horizontal-branch stars, both those in clusters and field stars, will be described later on in this symposium by Dr. deBoer.

Dupree et al. (ref. 27) find that in the metal-poor globulars (which are expected to have blue horizontal-branch stars) the ultraviolet surface brightness becomes more centrally concentrated toward shorter wavelengths, a finding which suggests that blue horizontal-branch stars are segregated toward the center. If this concentration is the effect of segregation by mass, it may be an indication that these stars are binary (ref. 28). If so, this would be strong support of the binary origin of x-ray emission in globular clusters.

One of the clusters studied is the metal-rich cluster, NGC 6624, which is also an x-ray burster. The IUE observations indicate a point-source of far-UV emission. Since NGC 6624 is a metal-rich cluster, it is unlikely that this source is a blue horizontal-branch star. Instead, Dupree et al. suggest it may be the x-ray source itself.

6. SUMMARY AND ACKNOWLEDGEMENTS

Although it must be apparent from this review, let me list explicitly some of the ways in which the IUE has proved useful in studying highly-evolved stars. We have seen how important high-dispersion spectra are for abundance analyses of the sdO stars and for studies of the wind from the central star of NGC 6543 and the wind from the O-type component of Vela X-1. We have seen how important low-dispersion spectra are for absolute spectrophotometry of the dwarf nova, Ex Hya. We have seen how important angular resolution is for detecting and locating UV-sources in globular clusters. Finally, we have seen how important operational flexibility is in documenting the behavior of Nova Cyg 1978 at outburst. This is a nice set of features to have on an ultraviolet satellite, features which should assure continued fruitful research on highly-evolved stars in the future.

In closing, I would like to thank all those who sent me reports on their investigations of highly-evolved stars with the IUE. It is on these reports that this review is based.

REFERENCES

1. Clark, G.W. 1975. Ap. J. 199, L143.

2. Bahcall, J.N. and Ostriker, J.P. 1975, Nature 256, 23.

3. Simon, K.P., Gruschinske, J., Hunger, K., and Kudritzki, R.P. 1980, in The Second Year of IUE, Tubingen

4. Gruschinske, J., Hunger, K., Kudritzki, R.P., and Simon, K.P., 1980, in The Second Year of IUE, Tubingen.

5. Kudritzki, R.P., Gruschinske, J., Hunger, K., and Simon, K.P., 1980, in The Second Year of IUE, Tubingen.

6. Baschek, B. 1980, in The Second Year of IUE, Tubingen.

7. Heap, S.R., et al. 1978, Nature 275, 385.

8. Snow, T.P. and Morton, D.C. 1976, Ap. J. Suppl. 32, 429.

9. Castor, J.I., Abbott, D.C., and Klein, R.I., 1975, Ap. J. 195, 157.

10. Castor, J.I., Lutz, J., and Seaton, M.J. 1980 preprint (UV Spectra of Planetary Nebulae. III. Mass Loss from the Central Star of NGC 6543")

11. Mewe, R., Heise, J., Gronenschild, E.H.B.M., Brinkman, A.C., Schrijver, J., den Boggenende, A.J.F., 1975, Ap. J. 202, L67.

12. Shipman, H.L., 1976, Ap. J. 206, L67.

13. Shipman, H.L., Margon, B., Bowyer, S., Lampton, M., Paresce, F., Stern, R. 1977, Ap. J. 213, L25.

14. Böhm-Vitense, E., Dettmann, T. and Kapranidis, S., 1979, preprint ("On the Energy Distribution in Sirius B").

15. Greenstein, J.L. and Oke, J.B. 1979, Ap. J. 229, L141.

16. Kraft, R.P. 1962, Ap. J. 135, 408.

17. Sparks, W.M., Wu, C-C, Holm, A.V. and Schiffer, F.H., 1979, in Highlights in Astronomy, Volume 5.

18. Seaton, M.J., 1980, Invited Talk ("Spectra of Gaseous Nebulae") in The Second Year of IUE, Tubingen.

19. Sparks, W.M., Starrfield, S., Truran, J.W. 1976, Ap. J. 208, 819.

20. Stickland, D., Penn, C.J., Seaton, M.J., Snijders, M.A.J., Storey, P.J., Kitchen, C.R., 1979, preprint.

21. Bath, G.T., Pringle, J.E., and Whelan, J.A.J. 1980, M.N.R.A.S. 190, 185.

22. Lamb, D.Q., and Masters, R. 1979, submitted to Ap. J. (Letters).

23. Raymond, J. et al. 1979, Ap. J. 230, L95.

24. Hammerschlag-Hensberge, G., 1980, Invited Talk ("IUE Observations of X-Ray Binaries"), in The Second Year of IUE, Tubingen.

25. Dupree, A.K., et al. 1980, to appear in Ap. J. June issue.

26. Hatchett, S.P. and McCray, R.A., 1977, Ap. J. 211, 552.

27. Dupree, A.K., Hartmann, L., Black, J.H., Davis, R.J., Matilsky, T.A., Raymond, J.C., and Gursky, H. 1979, submitted to Ap. J. (Letters).

28. Hartmann, L., Invited Paper, "NATO Advanced Study Institute on Galactic X-Ray Sources", Cape Sounion, Greece (in press, J. Wiley, 1980).

APPENDIX

INFORMAL BIBLIOGRAPHY OF STUDIES OF HIGHLY-EVOLVED STARS WITH THE IUE

The following appendix lists reports of IUE observations of highly-evolved stars. Many of these reports were presented either at this symposium or at the IUE Symposium at Tubingen in March, 1980. In the following bibliography, the former papers are referenced as "This Volume," while the latter are referenced as "IUE 2", which is shorthand for "The Second European IUE Conference," which will be published and made available from: Scientific and Technical Publications Branch, ESTEC, Postbus 299, 2200 AG Noordwijk, The Netherlands.

HOT SUBLUMINOUS STARS

SdO Stars

BD +75° 325	Kudritzki et al. (1980), IUE2
HD 49798	Gruschinske et al. (1980), IUE2
HD 127493	Simon et al. (1980), IUE2
HD 149382	Baschek, Scholz, and Kudritzki (1980), IUE2
HD 205805	Baschek, Scholz, and Kudritzki (1980), IUE2
BD +37° 442	Rossi, Viotti, Darius, and D'Antona (1980), IUE2
BD +37° 1977	D'Antona, Rossi, and Viotti (1980), IUE2
BD +48° 1777	D'Antona, Rossi, and Viotti (1980), IUE2

Helium - Rich Stars

BD -9° 4395	Heber and Schönbern (1980), IUE2
BD +10° 2179	Heber and Schönbern (1980), IUE2

Halo Stars

Feige 86	Hack (1979) A&A 75, L4 Hack (1980) A&A 81, L1
HD 192273	Bromage et al. (1980), IUE2 Hack and Stalio (1980), This Volume.

Central Stars of Planetary Nebulae

NGC 6826	Heap (1979), in Mass Loss and Ev of O Type Stars
Abell 78	
— — —	Pottasch and Gauthier (1980), This Volume.

Horizontal - Branch Stars

de Boer (1980), This Volume

WHITE DWARFS

Sirius B	DA	Böhm-Vitense et al. (1979) Ap. J. 232, L189
HZ Her	DA	Greenstein and Oke (1979), Ap. J. 229, L141
HZ 21	DO	Greenstein and Oke (1979), Ap. J. 229, L141
G 186-31	DA	Greenstein and Oke (1979), Ap. J. 229, L141
G 261-43	DA	Greenstein and Oke (1979), Ap. J. 229, L141
LP 145-141	C_2	Weidemann et al. (1980) A&A 83, L13
WD Companions to BaII Stars		Böhm-Vitense (1980) This Volume

AM Her-LIKE OBJECTS

AM Her	Raymond et al. (1979), Ap. J. 230, L95 Tanzi et al. (1980), A&A 83, 270 Chanmugan (1980), This Volume Fabbiano, Steiner, et al. (1980), This Volume
AN UMa	Hartman (1980), This Volume
2A0311-227	Hartman (1980), This Volume

CATACLYSMIC VARIABLES

Novae	Outburst	Reference
Nova Cyg	1978	Sparks, Wu, Holm, and Schiffer (1979), Highlights in Ast. Vol. 5 Casatella et al. (1979), A&A 74, L18 Stickland et al. (1979), Preprint Seaton (1980), IUE2 ("Gaseous Nebulae")
HR Del	1967	Hutchings (1979), PASP 91, 661 Duerbeck et al. (1980), IUE2 Delcina - Hacyan et al. (1980), IUE2 Duerbeck and Seitter (1980), IUE2
RR Pic	1967	Duerbeck et al. (1980), IUE2 Duerbeck and Seitter (1980), IUE2
DQ Her		Hartmann (1980), This Volume
V603 Agl. (old Novae)	1918	Duerbeck et al. (1980), IUE2 Lambert et al. (1980), This Volume
Recurrent Novae		
U Sco	1979	Sparks et al. (1979), in Highlights of Ast., Vol. 5
WZ Sge	1978	Holm et al. (1979), in Close Binary Systems, (IAU Symp 88) Freidjung et al. (1980), IUE2
T CrB	1946	Duerbeck et al. (1980), IUE2 Duerbeck and Seitter (1980), IUE2
Dwarf Novae		
SS Cygni		Heap et al. (1978), Nature 275, 385 Fabbiano, Steiner et al. (1980), This Volume
RU Peg		Duerbeck and Seitter (1980), IUE2
BV Cen EX Hya VW Hyi		Bath, Pringle, and Whelan (1980), MNRAS 190, 185.

X-RAY BINARIES (Reviewed by Hammeschlag - Hensberge (1980) IUE2)

Massive X-Ray Binaries

HD 153919	=	1700-37	06.5f	Dupree et al. (1978), Nature 275, 400
HD 77581	=	Vela X-1	B0.5Ib	Dupree et al. (1980), in press (Ap. J., June 1980)
HD 226868	=	Cyg X-1		Treves et al. (1980), in press (Ap. J., June 1980)
				Dupree et al. (1978), Nature 275, 400
Sk 160	=	SMC X-1	BØI	Bonnet - Bidaud et al. (1980), in press (A&A)
PH-Sk	=	LMC X-4	08III	Bonnet - Bidaud et al. (1980), in press (A&A)
X Per	=	0352 +30	09.5IV-Ve	Hammerschlag - Hensberge et al. (1980), in press (A&A)
He 715	=	1145-61	B1Ve	Hammerschlag - Hensberge et al. (1980), in press (A&A)
LSI +61°303				Hutchings (1979), PASP 91, 657
HD 152667	=	1653-46		Hutchings and Dupree (1980), in press (Ap. J.)

Low-Mass Binaries

V 818 Sco	=	Sco X-1	Willis et al. (1980), in press (Ap. J., June 1980)
V 1341 Cyg	=	Cyg X-2	Maraschi et al. (1980), preprint
HZ Her	=	Her X-1 A-F	Gursky et al. (1980), in press (Ap. J., June 1980)
			Dupree et al. (1978), Nature 275, 400
AM Her	=	1814 +49 Mag WD	Raymond et al. (1979), Ap. J. 230, L95
			Tanzi et al. (1980), A&A 83, 270
			Chanmugan (1980), This Volume.

PULSARS-SN

Crab Pulsar	Benvenuti et al. (1980), This Volume
SN1979 in M100	Panagia (1980), This Volume

GLOBULAR CLUSTERS

M 15	x-ray	Dupree et al. (1979), Ap. J. 230, L89
NGC 1851	x-ray	Hartman (1980), in press, ("Galactic X-Ray Sources", J. Wiley, 1980)
NGC 6624	x-ray, metal-rich	
47 Tuc	metal-rich	
M92		
NGC 6752		

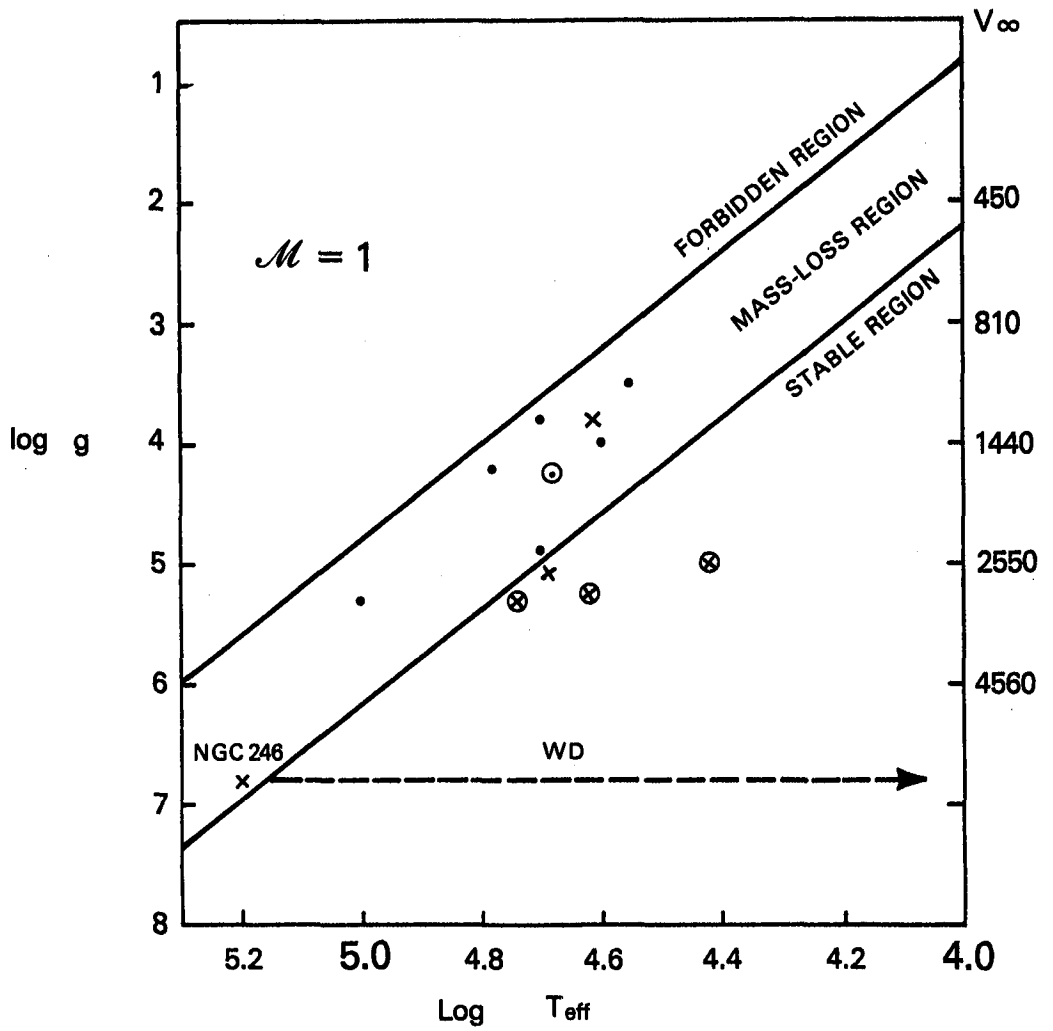

Figure 1. Temperature-Gravity Diagram for Hot, Subluminous Stars Observed with the IUE. The right-hand ordinate is the terminal velocity of the wind predicted for a one-solar-mass star. Stars whose UV-spectra show P Cygni profiles indicating a high velocity wind are denoted by dots, while those showing no evidence for a wind are denoted by crosses. Those stars for which the atmospheric parameters have been estimated by a full non-LTE analysis (ref. 3-6) are denoted by circles. The boundary line to the forbidden region is the Eddington limit for a one solar-mass star. The boundary line to the stable region is an extrapolation of the boundary found for young OB stars (ref. 8).

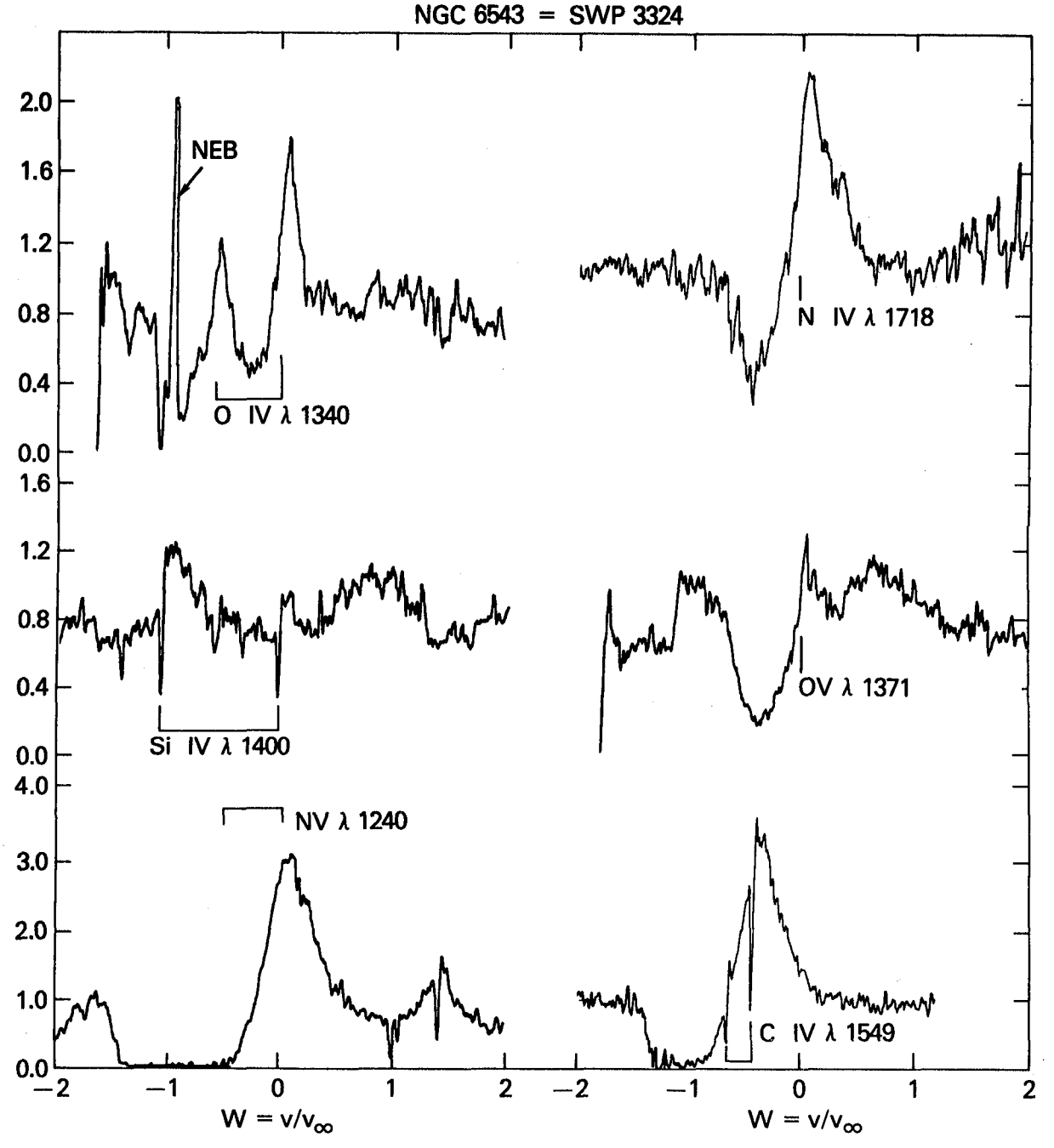

Figure 2. Wind Profiles in the Spectrum of the Central Star of NGC 6543. The image from which these normalized profiles were derived has been reprocessed to correct for earlier ITF errors.

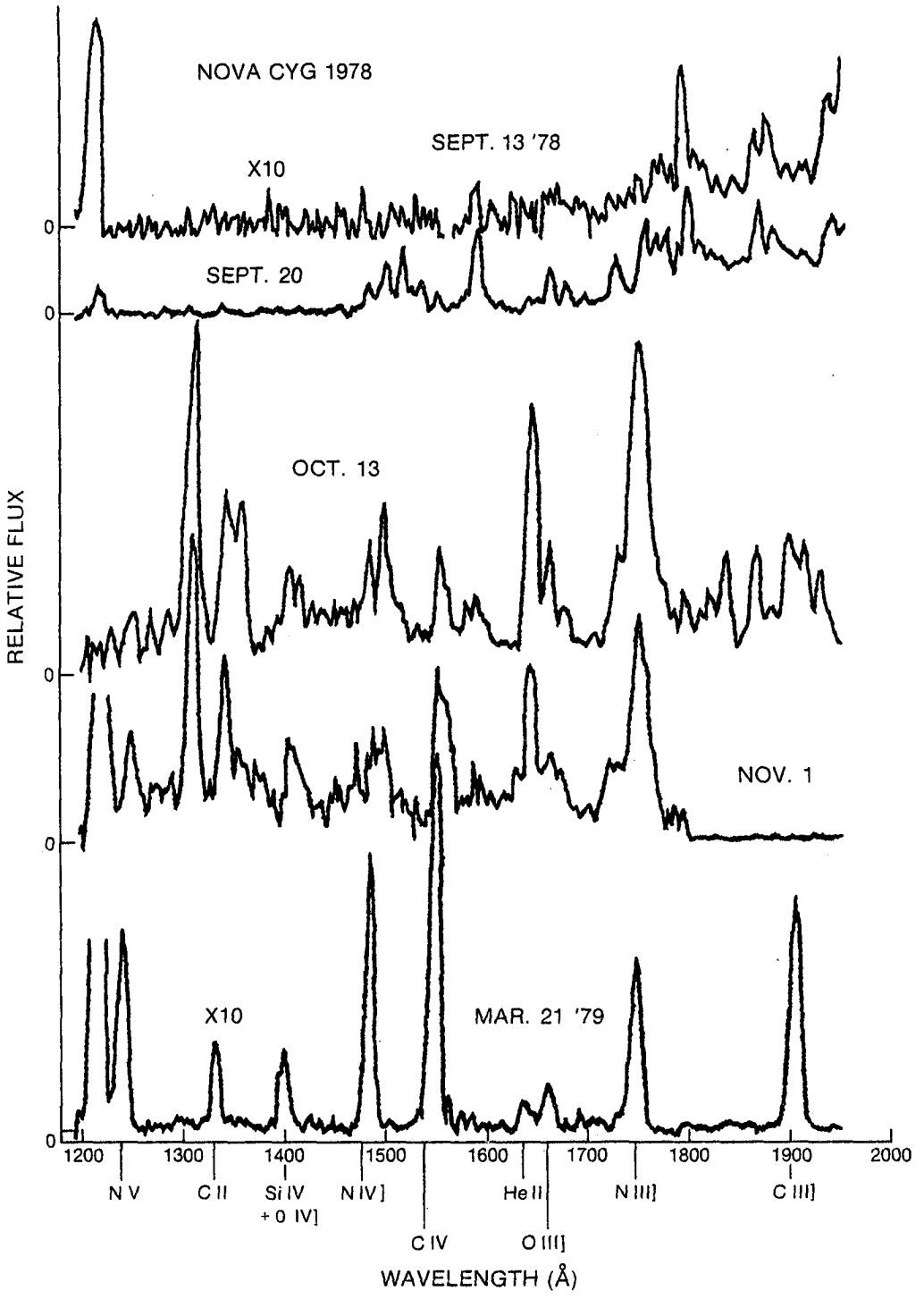

Figure 3. Development of the Far-UV Spectrum of Nova Cyg 1978 (reproduced from ref. 17).

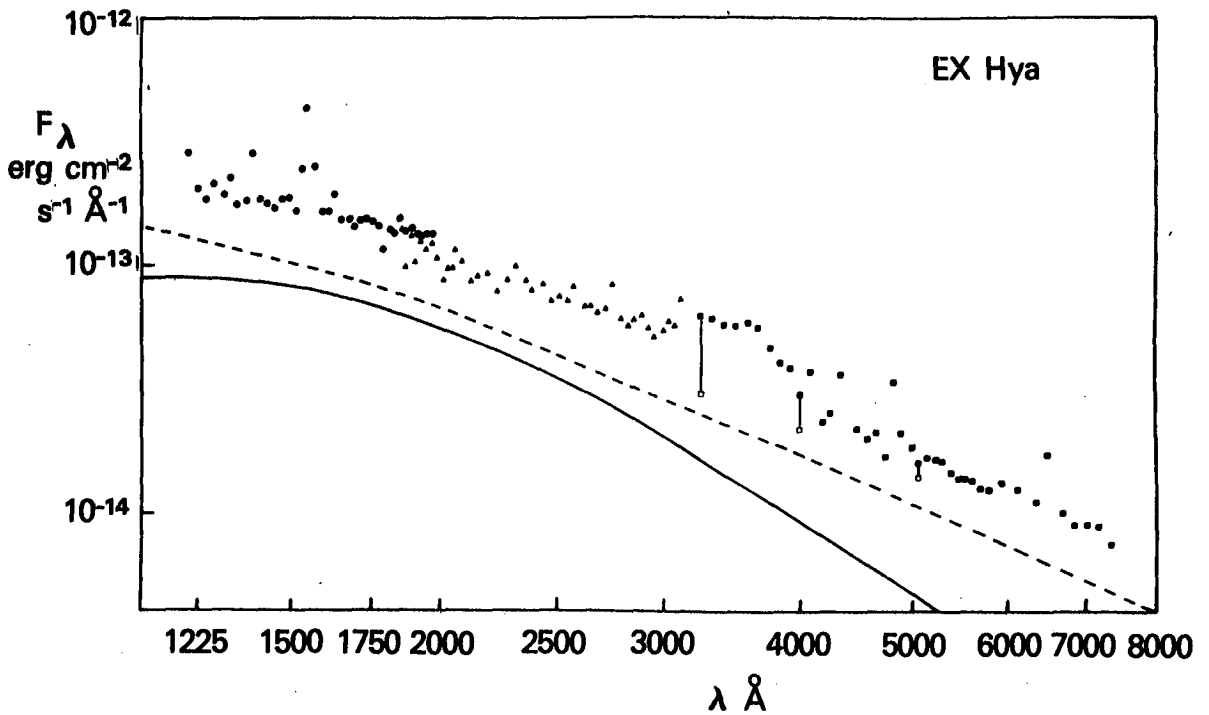

FIG. 4 THE SPECTRUM OF EX Hya OBSERVED IN QUIESCENCE. THE CIRCLES ARE SHORTWAVE, AND THE TRIANGLES LONGWAVE, OBSERVATIONS WITH IUE. THE FILLED SQUARES ARE AAT OBSERVATIONS CORRECTED FOR ATMOSPHERIC EXTINCTION. THE MAGNITUDE OF THE CORRECTION IS INDICATED BY THE OPEN SQUARES. THE SOLID LINE IS THE BEST FIT BLACK BODY TO THE ULTRAVIOLET DATA CORRESPONDING TO T = 24 000K. THE DASHED LINE IS THE BEST FIT ACCRETION DISC SPECTRUM DISCUSSED IN THE TEXT. BOTH THESE LINES HAVE BEEN DISPLACED DOWNWARDS SO THAT THEY DO NOT INTERFERE WITH THE DATA POINTS.

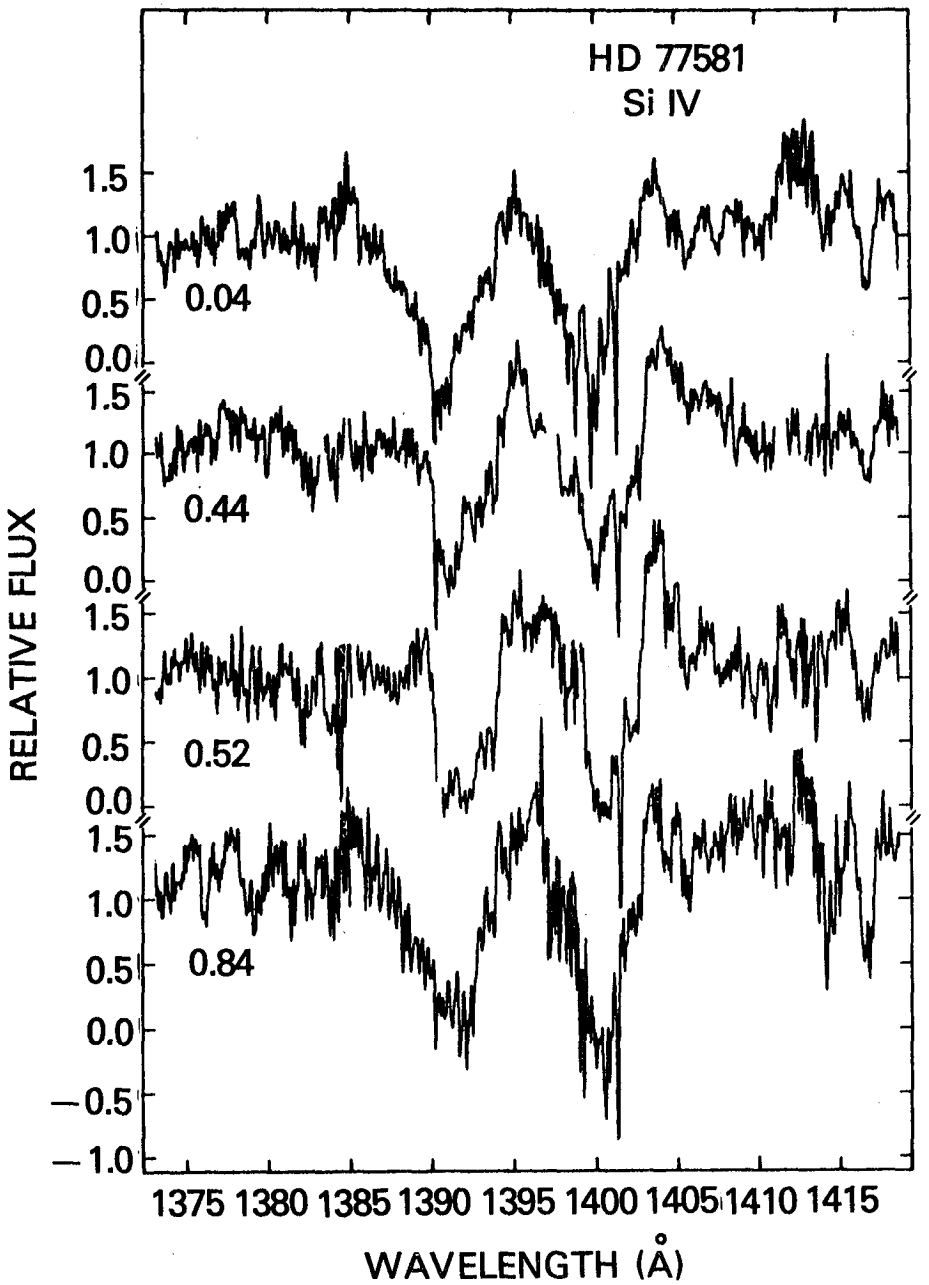

Figure 5. Si IV lines as a function of phase from high dispersion spectra. Note the substantial changes in the blue wing of both lines, and the appearance of a high velocity absorption feature at phase 0.52 (reproduced from ref. 25).

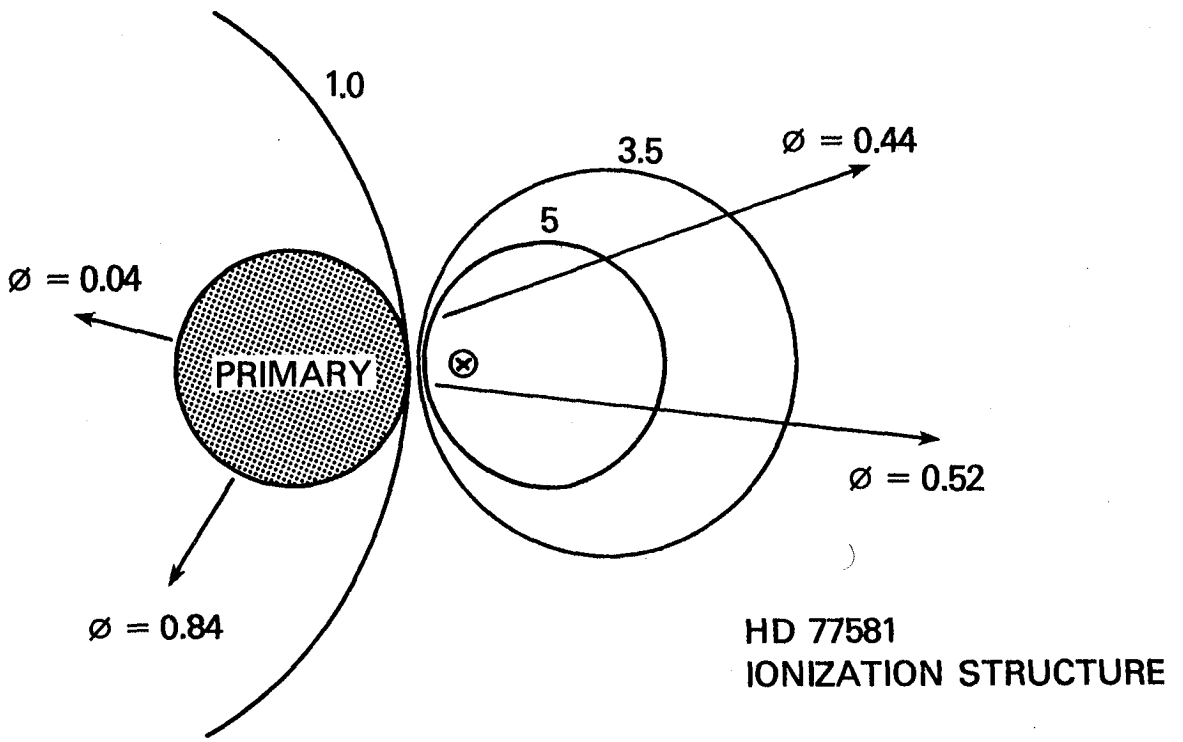

Figure 6. Predicted ionization surfaces for q = 3.5 and q = 5; within these spheres, it is assumed that an ion is missing from the volume to the right of the q = 1 locus (reproduced from ref. 25).

IUE SPECTRA OF A FLARE IN HR 5110:

A FLARING RS CVn OR ALGOL SYSTEM?[1]

Theodore Simon and Jeffrey L. Linsky[2,3]
Joint Institute for Laboratory Astrophysics
National Bureau of Standards and University of Colorado

Francis H. Schiffer III[4]
Computer Sciences Corporation

ABSTRACT

Ultraviolet spectra of the RS CVn-type binary system HR 5110 have been obtained with IUE on May 31, 1979 during a period of intense radio flaring of this star. High temperature transition region lines are present, but are not enhanced above observed quiescent strengths. The similarities of HR 5110 to the Algol system, AS Eri, suggest that the 1979 May-June flare may involve mass exchange rather than annihilation of coronal magnetic fields.

INTRODUCTION

We report here on IUE spectra of the close binary system HR 5110 (=HD 118216) obtained during a radio flare and subsequently during a presumably quiescent period. HR 5110 consists of an F2 IV primary and a G-K star secondary in a nearly circular orbit of period $2^d.61$ and mean separation 0.05 a.u. (1); the system is viewed nearly pole-on. Hall (2) includes HR 5110 in his list of RS CVn variables. The other stars in this group are close binaries with periods of 1-14 days, typically consisting of a chromospherically-active KO IV star with intense Ca II H-K emission, and an F-G IV-V star, which is usually the brighter optical component but whose chromospheric emission lines are normally the weaker. Photometric light curves of RS CVn systems exhibit a unique quasi-sinusoidal distortion wave or "wave of darkening," which Eaton and Hall (3) have modeled in terms of dark starspots covering a large fraction of one hemisphere of the K subgiant star. Many RS CVn systems are strong sources of soft X-rays (4-6), with coronal temperatures near 10^7 K, and have been observed to flare at radio wavelengths (7,8). These nonthermal microwave bursts are most likely due to gyro-synchrotron emission (9,10). Ultraviolet observations of the RS CVn-systems HR 1099,

[1]This work was supported by NASA through grants NAS5-23274 and NGL-06-003-057 to the University of Colorado.

[2]Staff Member, Quantum Physics Division, National Bureau of Standards.

[3]Guest Observer with the International Ultraviolet Explorer (IUE) satellite.

[4]Resident Astronomer, IUE Observatory.

λ And, and Capella, obtained early during the IUE mission (11), revealed bright emission lines indicative of hot chromospheres ($T = 4\text{-}20 \times 10^3$ K) and transition regions ($T = 20\text{-}250 \times 10^3$ K). Quiescent chromospheric models to explain these IUE observations have been discussed by Simon and Linsky (12) for HR 1099 and UX Ari, and by Baliunas et al. (13) for λ And and Capella. Simon, Linsky and Schiffer (14) have also presented IUE observations obtained during a flare of UX Ari and, guided by solar coronal loop models, have proposed an interacting magnetic loop model for major flare events in RS CVn binaries.

HR 5110 is an unusual RS CVn-type system in several respects. The mass ratios of RS CVn's are typically within 30% of unity, and the more massive component is also the cooler, more highly evolved star (2,15). In HR 5110, however, the F star primary is clearly the more massive, since Conti (1) found $m_2/m_1 = 0.28 \pm 0.08$. He also concluded that the secondary of HR 5110 fills its Roche lobe, unlike the majority of RS CVn systems which are classified as detached binaries. Thus, HR 5110 resembles mass-exchange Algol systems, which also exhibit weak X-ray emission (16) and sporadic radio bursts (17,18). The photometric light curve of HR 5110 (19) shows evidence of a small reflection effect ($0^m.01$ in V), but no distortion wave. The apparent absence of a distortion wave could be due to the low inclination of the system, assuming starspots to be concentrated along equatorial regions of the secondary, and to the relatively small contribution of the secondary to the total light of the system in the V band.

OBSERVATIONS

We observed HR 5110 initially on 1979 May 31 at 17^hUT as a target of opportunity observation with IUE after notification by Paul Feldman that a major radio flare was underway in the system. Feldman (20) measured a 10.76 GHz flux of 0.425 Jy on May 29 at 8^h26^mUT with continued flaring activity in the range 0.20-0.35 Jy over the next two days. Our IUE observations thus occurred during a period of intense radio flaring. On February 1, 1980 comparison spectra were taken at the identical orbital phase when the system was presumably quiescent. The circumstances of the observations are given in Table 1. By convention, orbital phase 0.5 corresponds to conjunction with the F star in front of the secondary.

The two SWP spectra have been calibrated in absolute flux units at Earth using the standard IUE calibration factors and the latest ITF. Longward of about 1700 Å both SWP spectra are saturated due to the rapidly rising photospheric flux of the F2 IV primary. The HR 5110 emission line spectrum looks qualitatively similar to spectra of β Cas, a rapidly-rotating F2 IV single star discussed by Linsky and Marstad (21), and the RS CVn binary UX Ari (12), if allowance is made for the weak underlying continuum of the cooler stars (G5 + K0 IV) in the UX Ari system.

Integrated fluxes of the strongest emission features present in these spectra are listed in Table 2. Probable identifications of the ions responsible for the emission features are given in order of their estimated relative importance. In proposing identifications, we have been guided by line

lists for the solar limb spectrum (22) and Capella (23). The line strengths are presented in the form of surface fluxes, assuming that all of the flux originates from the cooler star, for which we compute an angular diameter of 0.45 milliarcsec from the Barnes-Evans relation (24). We comment on this assumption later. At a distance of 52 pc from the Sun, the secondary has a radius of 2.6 $R_\odot$ and therefore fills its Roche lobe (1); for simplicity, we ignore geometrical distortion of the secondary. For comparison with the HR 5110 data, Table 2 also presents surface fluxes for β Cas, UX Ari in both quiescent and flare states, and the quiet Sun.

DISCUSSION

The first conclusion that can be drawn directly from inspection of Table 2 is that the accurately measured strong lines (e.g., those of N V, C II, O I, C IV, and He II) are fainter in the "flare" spectrum than in the "nonflare" spectrum. While this may appear surprising, it is important to realize that image SWP 5415 was obtained almost 2 1/2 days after the radio flare was first detected. HR 1099 was observed on 1978 March 1, also long after the onset of a major radio flare, and the ultraviolet emission lines showed no enhancement over quiescent values (11,12). By contrast, IUE spectra of the January 1, 1979 flare of UX Ari (14) were obtained only 26 hours after the initial detection of the radio flare, while the radio flare was still active, and showed a factor of 5.5 enhancement of the UV line strengths

These three examples suggest that the time scales of radio and UV flares in RS CVn systems may be quite different. Since the intense radio flux and the enhanced ultraviolet line emission may originate at different heights in the stellar atmosphere and since solar flares exhibit strong radio emission long after the ultraviolet aspects of the flare are completed, it is not implausible that stellar radio flares would be of longer duration than the associated UV flare events. We therefore conclude that both SWP 5415 and SWP 7834 represent quiescent conditions, and that the different flux levels observed are representative of normal time variations in the activity of the system.

The HR 5110 "flare" differs from the earlier UX Ari flare in another significant detail. In the high dispersion UX Ari flare spectra, we observed prominent asymmetries in the profiles of the Mg II resonance lines at 2800 Å, corresponding to Doppler velocities of 475 km s^{-1}, and we interpreted those asymmetries as evidence for gas flowing along a magnetic flux tube coupling the primary and secondary stars. No similar line asymmetries appear in the HR 5110 spectra, although mass transfer taking place at velocities less than 150 km s^{-1} might be impossible to detect because of the ~13° inclination of the system.

IDENTIFICATION OF THE ACTIVE STAR

A critical question is: Which star in the HR 5110 system contributes most of the flux seen in the bright UV emission lines? It is not possible to answer this question directly because the maximum radial velocity separation between the component stars is only 43.7 km s^{-1}, so the high dispersion mode

of IUE and an accurate absolute wavelength scale would be needed to identify the emitting star on the basis of line splitting or absolute wavelength displacement. This approach was followed in our analysis of the UX Ari system (12), where the maximum velocity difference is 126 km s^{-1}. On the basis of Doppler shifts of the Mg II lines, we identified the K0 IV star as the dominant contributor in this system. Some caution is warranted because Ayres and Linsky (23) show that the Ca II H-K emission features and the transition region lines of the Capella system are contributed by the G6 III primary and F9 III secondary, respectively. However, the circumstance leading to this dichotomy for the Capella system, viz. a factor of 10 difference in rotational velocities of the primary and secondary, does not seem to be repeated in the short-period synchronously rotating RS CVn binaries.

Circumstantial evidence for associating the secondary in HR 5110 with the strong UV emission lines comes from a comparison of the derived surface fluxes with those measured in β Cas (F2 IV) and UX Ari (G5 V + K0 IV). We choose β Cas as a comparison star because it has the same spectral type as the HR 5110 primary and is a very rapid rotator like HR 5110 (25). Despite its early spectral type, β Cas exhibits a chromospheric and transition region emission line spectrum. We assume that the existence of a chromosphere and a transition region in this star is due to the effectiveness of rapid rotation in producing a strong hydromagnetic dynamo even though the stellar convection zone is thin.

Comparing the surface fluxes listed in Table 2, we see that the emission lines of HR 5110 are a factor of 10 brighter than the corresponding lines in β Cas. If for stars of the same spectral type the rotational velocity is the dominant variable determining outer atmosphere heating (23), we conclude that the F2 IV star in HR 5110 contributes no more than ~10% to the observed emission line flux. Furthermore, the closer agreement between the surface fluxes of HR 5110 and UX Ari, assuming that the cooler stars in both cases are the dominant emitters, suggests that the secondary in HR 5110 is the more likely source of the observed line emission.

RS CVn OR ALGOL?

Although different time scales for radio and UV flares may account for our failure to observe an enhancement of the emission lines of HR 5110 in May, 1979 we now briefly consider an alternative explanation: namely, that radio flares in this system are the result of episodic mass transfer from the secondary to the primary, instead of magnetic field annihilation processes in large coronal loops, as we proposed for UX Ari (14). We note, however, that chromospheric models based on the IUE fluxes for HR 5110 would yield approximately the same surface pressures (0.7-1.1 dyn cm^{-2}) as derived earlier for UX Ari, and so the hydrostatic coronal loop model of Rosner, Tucker, and Vaiana (25) would predict loop dimensions comparable to the separation (~10 R_o) of the components in this system.

To summarize, we have repeated Conti's (1) analysis of UBVRI photometry of HR 5110, supplemented with new JHKLM data that we have obtained at Kitt Peak. For this purpose, we required that the radius of the secondary be the same as the Roche lobe (2.6 R_o, see Ref. 1), we adopted a parallax of 0".019,

and we used the Barnes-Evans relation. With these assumptions, the observed spectral energy distribution, 3600 Å-5 μm, can be matched by a composite spectrum, F2 IV + G5 IV, except for a small ($0^m.3$) infrared excess which might be due to intrasystem material (e.g., a circumstellar ring). The magnitude difference between the components is $\Delta V = V_G - V_F = 1^m.15$, while the absolute bolometric magnitudes for the primary and secondary are $M_{bol} = +1.60$ and $M_{bol} = +2.65$, respectively. In this calculation, the secondary is twice as luminous as found by Conti.

We now compute the luminosity ratio L_x/L_{bol}, where L_x is the X-ray luminosity. Ayres and Linsky (23) have shown that this ratio is correlated with equatorial rotation velocity: the more rapid the rotation, the larger the ratio, and hence the more active the chromosphere-corona. The range of L_x/L_{bol} values for RS CVn binaries is $5 \times 10^{-4} - 2 \times 10^{-3}$, with a corresponding spread of 20-80 km s^{-1} in rotational velocity.

Assuming synchronous rotation, we calculate v_{eq}=49 km s^{-1} for the G5 IV secondary in HR 5110 (but v sin i=10 km s^{-1}). For this rotational velocity, we then expect $L_x/L_{bol} \geq 5 \times 10^{-4}$. The observed $L_x = 3.0 \pm 0.9 \times 10^{30}$ ergs s^{-1} (4) and our estimated L_{bol}, however, yield $L_x/L_{bol} = 1 \times 10^{-4}$, which is a factor of 5 below typical values for RS CVn systems. An upper limit on this ratio, based on the implicit uncertainties, would still place HR 5110 at least a factor of 2 below the least active of the remaining RS CVn binaries.

Despite the large UV fluxes observed for HR 5110, this calculation suggests that the RS CVn designation for this system may be misleading and that the interacting coronal loop model may not apply to flare episodes of this star. In view of its Algol-like characteristics, the most attractive alternative is mass exchange from the cool secondary to the F2 primary through the inner Lagrangian point (26). Only a modest flow of material ($\sim 5 \times 10^{16}$ g s^{-1}) is required to account for the radio, ultraviolet, and X-ray power observed. HR 5110 closely resembles the Algol system AS Eri (27), which consists of an A3 V primary of mass 1.9 $M_\odot$ and a cool secondary of mass 0.2 $M_\odot$, which fills its Roche lobe. The secondary of AS Eri appears to be collapsing to the white-dwarf state (28), and we speculate that the same evolutionary picture may apply to HR 5110 and other RS CVn-type systems.

We wish to thank Dr. A. Boggess, Dr. C.-C. Wu, and the staff of the IUE Observatory for their assistance in the acquisition and reduction of these data.

REFERENCES

1. Conti, P. S.: 1967, Astrophys. J. 149, 629.
2. Hall, D. S.: 1976, in Multiple Periodic Phenomena in Variable Stars, Part I, ed. W. S. Fitch (Dordrecht: Reidel), p. 287.
3. Eaton, J. A. and Hall, D. S.: 1979, Astrophys. J. 227, 907.
4. Walter, F. M., Cash, W., Charles, P. A. and Bowyer, C. S.: 1980, Astrophys. J. 236, 212.
5. Walter, F., Charles, P. and Bowyer, S.: 1978, Astrophys. J. (Letters) 225, L119.

6. Swank, J.: 1979, in Highlights in Astronomy, 5, in press.
7. Gibson, D. M., Hjellming, R. M. and Owen, F. N.: 1975, Astrophys. J. (Letters) 200, L99.
8. Mutel, R. L. and Weisberg, J. M.: 1978, Astron. J. 83, 1499.
9. Spangler, S. R.: 1977, Astron. J. 82, 169.
10. Owen, R. N., Jones, T. W. and Gibson, G. M.: 1976, Astrophys. J. 210, L27.
11. Linsky, J. L., et al.: 1978, Nature, 275, 389.
12. Simon, T. and Linsky, J. L.: 1980, Astrophys. J., in press.
13. Baliunas, S. L., Avrett, E. H., Hartmann, L. and Dupree, A. K.: 1979, Astrophys. J. (Letters) 233, L129.
14. Simon, T., Linsky, J. L. and Schiffer, F. H. III: 1980, Astrophys. J., in press.
15. Popper, D. M. and Ulrich, R. K.: 1977, Astrophys. J. (Letters) 212, L131.
16. Schnopper, H. W., et al.: 1976, Astrophys. J. (Letters) 210, L75.
17. Wade, C. M. and Hjellming, R. M.: 1972, Nature 235, 270.
18. Hjellming, R. M., Webster, E. and Balick, B.: 1972, Astrophys. J. (Letters) 178, L139.
19. Hall, D. S., et al.: 1978, IAU Bull. on Variable Stars, No. 1459.
20. Feldman, P. A.: 1979, IAU Circular, No. 3366.
21. Linsky, J. L. and Marstad, N. C.: In this volume.
22. Burton, W. M. and Ridgeley, A.: 1970, Solar Phys. 14, 3.
23. Ayres, T. R. and Linsky, J. L.: 1980, Astrophys. J., in press.
24. Barnes, T. G. and Evans, D. S.: 1974, M.N.R.A.S. 174, 489.
25. Rosner, R., Tucker, W. H. and Vaiana, G. S.: 1978, Astrophys. J. 220, 643.
26. Jones, T. W. and Woolf, N. J.: 1973, Astrophys. J. 179, 869.
27. Popper, D. M.: 1973, Astrophys. J. 185, 265.
28. Refsdal, S., Roth, M. L. and Weigert, A.: 1974, Astron. & Astrophys. 36, 113.

Table 1

Summary of IUE Observations of HR 5110[a]

IUE Image	Dispersion	Exposure (min)	Date (JD 2440000+)	Orbital Phase[b]	Comment
SWP 5415	Low	30	4025.2003	0.6412	"Flare"
LWR 4652	High	10	4025.2192	0.6484	"Flare"
LWR 6838	High	10	4270.7214	0.5963	"Nonflare"
SWP 7834	Low	25	4270.7361	0.6019	"Nonflare"

[a]All observations were made through the 10" × 20" large aperture.

[b]Phases computed from ephemeris given in Ref. 19.

Table 2

Comparison of Line Surface Fluxes (ergs cm^{-2} s^{-1})

Line or Multiplet	HR 5110[a]		UX Ari[b]		β Cas[c]	Quiet Sun[d]
	Flare	Quiet	Flare	Quiet		
C III 1175 Å	7.1(5)	1.1(6)	1.2(6)	2.0(5)	4.5(4)	1.6(3)
N V 1239 Å	4.1(5)	8.4(5)	1.2(6)	1.9(5)	1.4(4)	8.6(2)
O I 1304 Å	1.2(6)	1.5(6)	1.3(6)	4.4(5)	1.4(5)	4.0(3)
C II 1335 Å	1.1(6)	1.4(6)		4.4(5)	8.6(4)	4.6(3)
Si IV 1394 Å	2.2(5)	7.2(5)	7.0(5)	1.3(5)	3.1(4)	1.7(3)
Si IV+O IV 1403 Å	5.9(5)	5.0(5)	6.5(5)	1.2(5)	4.6(4)	7.9(2)
C IV 1549 Å	1.7(6)	2.2(6)		6.5(5)	1.8(5)	5.8(3)
C I 1561 Å	1.4(5)	1.9(5)			2.0(4)	2.0(3)
He II 1640 Å	7.2(5)	1.1(6)		3.5(5)		1.3(3)
C I 1657 Å	3.5(5)	9.2(5)				5.3(3)
Mg II 2796 Å	1.9(7)	2.1(7)	1.7(7)	6.8(6)		6.8(5)
Mg II 2803 Å	1.7(7)	1.7(7)	1.4(7)	5.8(6)		5.3(5)

[a]Assuming all the emission comes from the secondary with an angular diameter of 0.45 milliarcsec. If the emission is assumed to come from the F star only (angular diameter of 0.53 milliarcsec), then all surface fluxes should be divided by factor of 1.4.

[b]Assuming all the emission comes from the K0 IV star whose angular diameter is 0.62 milliarcsec. Data from Refs. 12 and 14.

[c]Assuming an angular diameter of 2.0 milliarcsec. Data from Ref. 21.

[d]Quiet Sun fluxes cited in Ref. 11.

ANALYSIS OF THE SYMBIOTIC STAR AG PEGASI

Charles D. Keyes and Mirek J. Plavec
Department of Astronomy, University of California, Los Angeles

ABSTRACT

High and low dispersion IUE data are analyzed in conjunction with coincident ground-based spectrophotometric scans and supplementary infrared photometry of the symbiotic object AG Pegasi. The IUE observations yield an improved value of E(B-V) = 0.12. The two stellar components are easily recognized in the spectra. The cool component may be an M1.7 III star and the hot component appears to have T_{eff} of approximately 30000 K. The emission lines observed in the ultraviolet indicate two or three distinct emitting regions. Nebular component ultraviolet intercombination lines suggest an electron density of several times 10^{10} cm^{-3}.

INTRODUCTION

AG Pegasi (HD 207757) is a well-known symbiotic star, although it does not display the irregular outbursts that are typical of most symbiotics. It brightened only once, over 100 years ago, and has been declining ever since. The important work of Hutchings, Cowley, and Redman (ref. 1) describes the spectral peculiarities and changes which have interested many ground-based investigators over the years. The first satellite ultraviolet observation, and first direct evidence of a hot star in the system, was the broad-band OAO-2 photometry of Gallagher et al (ref. 2).

AG Pegasi was observed with IUE in August and November, 1978 by MJP. Both high and low dispersion SWP images and only low dispersion LWR images were obtained. Coincident ground-based spectrum scans of high photometric accuracy were made in the 3200-7000 Å region with the Cassegrain Image Dissector Scanner (IDS) on the Lick 3-meter Shane telescope in August, 1978 by CDK. Figure 1 shows the combined observed spectrum of AG Peg. It is quite gratifying to note that the three IDS scans and two IUE images match extremely well with no artificial shifting imposed. It should also be noted that all SWP IUE images have been corrected for the image processing error originally present in the data.

We have re-evaluated the interstellar reddening of AG Peg with the extinction curve of Seaton (ref. 3) and found the color excess to be E(B-V) = 0.12 ± 0.03 from the 2200 Å extinction feature. The larger value of 0.2 obtained by Gallagher et al. is probably due to the very strong emission lines contaminating their broad-band photometry shortward of 2000 Å.

The observations show clearly the presence of both a hot and a cool component in the system. The IUE spectra are dominated by a

number of extremely strong emission lines and a bright continuum that rises steadily toward shorter wavelengths. The IDS spectra show that the decline of the ultraviolet continuum continues to approximately 4300 Å where the continuum begins a steady rise to the red.

THE COOL COMPONENT

Infrared photometry of AG Pegasi has been published by Szkody (ref. 4) and Swings and Allen (ref. 5). We have previously (ref. 6) obtained a value of $f_e = 5.5 \pm 0.8 \times 10^{-8}$ ergs-cm^{-2}sec^{-1} for the total observed continuous flux of the cool component (corrected for interstellar extinction). This result was based upon an integration of the published photometry and upon an independent extrapolation of our Lick spectrophotometry. Colors obtained from the Szkody magnitudes were also used to determine the spectral type of the cool component in the system of Lee (ref. 7). On the assumption that the luminosity class is III, the colors formally indicate a classification of M1.7 III. Comparison of our Lick scans with standard stars 104 Her (M1 III) and 2 Peg (M3 III) shows that AG Peg is intermediate between them and suggests that the cool component may be normal. The effective temperature, according to Lee, is 3570 K.

Consistently throughout this presentation we shall express the distance d in kpc and the stellar parameters in solar units. The general formula

$$R = 5.89 \times 10^{12}\ T^{-2}\ d\ f^{0.5} \qquad (1)$$

leads to the following relations for the cool component:

$$R_c = (108 \pm 9)d \qquad L_c = (1720 \pm 260)d^2 \qquad MBOL_c = (-3.3 \pm 0.2) + 5 \log d \qquad (2)$$

If the cool component really is luminosity class III, then using the calibration of Lee, $MBOL_c = -1.9$, $R = 56\ R_\odot$, and $d = 0.5$ kpc. If the luminosity class is II, $MBOL_c = -3.8$, $R = 134\ R_\odot$, and $d = 1.24$ kpc ($z = 0.6$ kpc below the galactic plane), and, even in this case, the star would be substantially smaller than its critical Roche lobe, estimated by Hutchings et al to be 285 $R_\odot$.

THE HOT COMPONENT

The total continuum flux (corrected for extinction) between 1200 and 3200 Å is $f_h = 1.26 \times 10^{-8}$ erg-cm^{-2}sec^{-1}. (The emission lines, incidentally, contribute an additional 27 percent.) This observed continuum is most likely a combination of a true stellar continuum and the continuous radiation of a nebular H II region.

The hot component spectrum is clearly contaminated by that of the cool component longward of 4300 Å. We have attempted to remove the cool component contamination by subtracting a scan of the M1 III standard 2 Peg from AG Peg in the 3400-5500 Å region. The scans were normalized and were virtually identical in the 5300-5500 Å interval where the hot component contributes negligibly to AG Peg. Figure 2 shows the resultant

energy distribution of the hot component plus hydrogen nebula compared with the Kurucz (ref. 8) model atmosphere energy distributions that provide the two best fits. By fitting the energy distributions we determine from (1)

$$T = 25000 \quad R_h = 1.34\ d \quad L_h = 635\ d^2 \quad MBOL_h = -1.94 - 5 \log d \qquad (3)$$

$$T = 30000 \quad R_h = 1.0\ d \quad L_h = 730\ d^2 \quad MBOL_h = -2.40 - 5 \log d \qquad (4).$$

For the surface gravitational acceleration we get

$$\log g = 4.4 - 2 \log d \qquad (5)$$

if we assume the hot object mass is not too different from one solar mass (ref. 1). A subdwarf is indicated, despite the model log g. Indeed, the Wolf-Rayet character of some of the ultraviolet emission features (see next section) implies a wind blowing outward from the hot component and that some sort of extended region of line formation must exist. Moreover, model atmosphere calculations of hot stars with extended atmospheres have shown that the resultant energy distributions tend to resemble those of cooler, less extended atmospheres (ref. 9). Therefore, it would be quite surprising if a standard, plane-parallel, LTE, high surface gravity, normal composition atmosphere represented well this subdwarf.

Note that there is a modest flux excess in the 3000-4000 Å region that grows more pronounced as models hotter than 30000 K are tried. This excess is doubtlessly due in part to continuous Balmer emission, the overlapping of high Balmer lines, and perhaps free-free emission. We are currently attempting to adequately combine emission from a hydrogen nebula with individual stellar models in the hope of producing a better fit.

As a result of the Wolf-Rayet character of some lines, we also compared the ultraviolet energy distribution of AG Peg with the TD-1 observations of several Wolf-Rayet stars by Willis and Wilson (ref. 10) in the 1350-2550 Å region. Their one WN5 (HD 50896) and one of two WN6 (HD 192163) stars displayed continua clearly steeper than that of AG Peg. The remaining WN6 star (HD 191765), for which Willis and Wilson find a surprisingly similar temperature to HD 192163, provided a better, though not perfect, match in this spectral region. Willis and Wilson determined a Zanstra temperature, based upon the 1640 Å He II equivalent width and a grid of Kurucz model atmospheres, of 29200 K for HD 191765. Using the tabulations of Willis and Wilson we determine the He II 1640 Zanstra temperature for AG Peg to be 31900 K. We should note that the 1640 equivalent width in AG Peg is considerably stronger than that of either WN6 star in the Willis and Wilson sample.

THE EMISSION LINES

Emissions of N V, C IV, Si IV, and lower ions of these elements are present in the IUE spectra. No O IV is seen, although the O III 1663 Å doublet and several of the Bowen flourescent lines are visible.

A quite well-developed recombination spectrum of He II is also present. The high dispersion IUE spectra show that the line profiles are quite complex and that many lines have two or three components.

One component comes from a highly ionized region near the hot object and shows broad P Cygni profiles of a Wolf-Rayet character. The N V resonance doublet at 1239 and 1242 Å and the permitted N IV 1718 line show this structure. The N IV] intercombination line at 1486 Å (Fig. 3) displays both the broad Wolf-Rayet structure and a sharp, nebular component (FWHM = 0.3 Å) which apparently is formed in a more distant, quiescent region.

All the other intercombination lines, C III] 1909 Å , Si III] 1892 Å , and the N III] 1750 Å group, display only the sharp, nebular component. The resonance doublet of C IV at 1548 and 1550 Å (Fig. 4) shows the nebular emission component and several narrow, blue-shifted absorptions superposed on a broad 1550 emission. The 1548 component is quite weak, probably due to a broad P Cygni absorption of the 1550 line.

An analysis of the line strengths of the N III] 1750 multiplet indicates that the electron density in the N III] region must be between 1×10^{10} cm^{-3} and 5×10^{10} cm^{-3}. The presence of the C III] 1909 Å line, the absence of C III 1906 Å, and evaluation of critical densities for collisional de-excitation of the relevant energy levels are consistent with this result. Maximum densities implied by the other intercombination lines are also all less than approximately 10^{11}.

COMMENTS

The symbiotic stars are a group of objects where, in spite of considerable effort, non-controversial models were not possible before the advent of IUE (and perhaps not after). In the optical spectrum, a late type continuum is observed on which are superposed emission lines (H, He I, He II, C III, N III, and some forbidden lines), which require a radiation source much hotter than the K or M type giant whose absorption spectrum is visible. Single- and binary-star models were proposed, and both may have some validity, since the group may very well be heterogeneous. An inspection of Fig. 1 shows why the dilemma was practically unsolvable without ultraviolet spectroscopy. In the optical region, the hot component is virtually unobservable, having a much smaller radiating surface. In fact, the small "ultraviolet excess" and "absorption line veiling" contaminating the late-type spectrum shortward of about 5000 Å seems to be due to free-free and bound-free radiation of hydrogen, naturally excited by the hot component, but testifying only indirectly to its presence. For AG Peg, we find the radius of the hot subdwarf on the order of 1 $R_\odot$, effective temperature probably about 30000 K , while the mass may be 1 - 2 $M_\odot$. The profiles of the emission lines are composite, and the broadest components suggest a similarity between the hot star and the WR nuclei of planetary nebulae. In the past century, the outflow of mass from AG Peg had the character of an extremely slow nova. The red giant component

is probably not merely a passive companion; more likely, it triggered the activity and is the ultimate source of much of the material. Yet it appears now to be much smaller than its Roche limit - a rather vexing dilemma.

One of the current problems is the actual temperature of the hot component. Michalitsianos et al. (ref. 11) believe that the hot component temperature in RW Hydrae must be above 10^5 K, and explain that the continuum longward of about 2000 Å is due to a hydrogen cloud. Since AG Pegasi closely resembles the Wolf-Rayet spectra for which Willis and Wilson postulate temperatures only on the order of 30000 K, we think that such a temperature is sufficient to explain both the ultraviolet continuum and the strength of the He II lines, and that the hydrogen cloud contributes only modestly in the vicinity of the Balmer jump in AG Pegasi.

REFERENCES

1. Hutchings, J.B., Cowley, A.P., and Redman, R.O.: Mass Transfer in the Symbiotic Binary AG Pegasi. Astrophys. J., 201, 404, 1975.

2. Gallagher, J.S., Holm, A.V., Anderson, C.M., and Webbink, R.F.: Ultraviolet Photometry from the Orbiting Astronomical Observatory. XXXIII. The Symbiotic Star AG Pegasi. Astrophys. J., 229, 994, 1979.

3. Seaton, M.J.: Interstellar Extinction in the UV. Mon. Not. R.A.S., 187, 73P, 1979.

4. Szkody, P.: Infrared Photometry of Dwarf Novae and Possibly Related Objects. Astrophys. J., 217, 140, 1977.

5. Swings, J.-P. and Allen, D.A.: Photometry of Symbiotic and VV Cephei Stars in the Near Infrared. Publ. Astron. Soc. Pac., 84, 523, 1972.

6. Close Binary Stars: Observations and Interpretation. (Ed. M.J. Plavec, D.M. Popper, R.K. Ulrich), Reidel, 1980.
   Keyes, C.D. and Plavec, M.J.: The symbiotic binary system AG Pegasi. 1980, p.535.

7. Lee, T.A.: Photometry of High-Luminosity M-Type Stars. Astrophys. J., 162, 217, 1970.

8. Kurucz, R.L.: Model Atmospheres for G, F, A, B, and O Stars. Astrophys. J. Supp., 40, 1, 1979.

9. Cassinelli, J.P.: The Continuous Energy Distribution from Stars with Hot Extended Atmospheres. Astrophys. Lett., 8, 105, 1971.

10. Willis, A.J. and Wilson, R.: Ultraviolet Observations of nine Wolf-Rayet Stars. Mon. Not. R.A.S., 182, 559, 1978.

11. Michalitsianos, A.G., Kafatos, M., Hobbs, R.W., and Maran, S.P.: IUE observations of the hot components in two symbiotic stars. Nature, 284, 148, 1980.

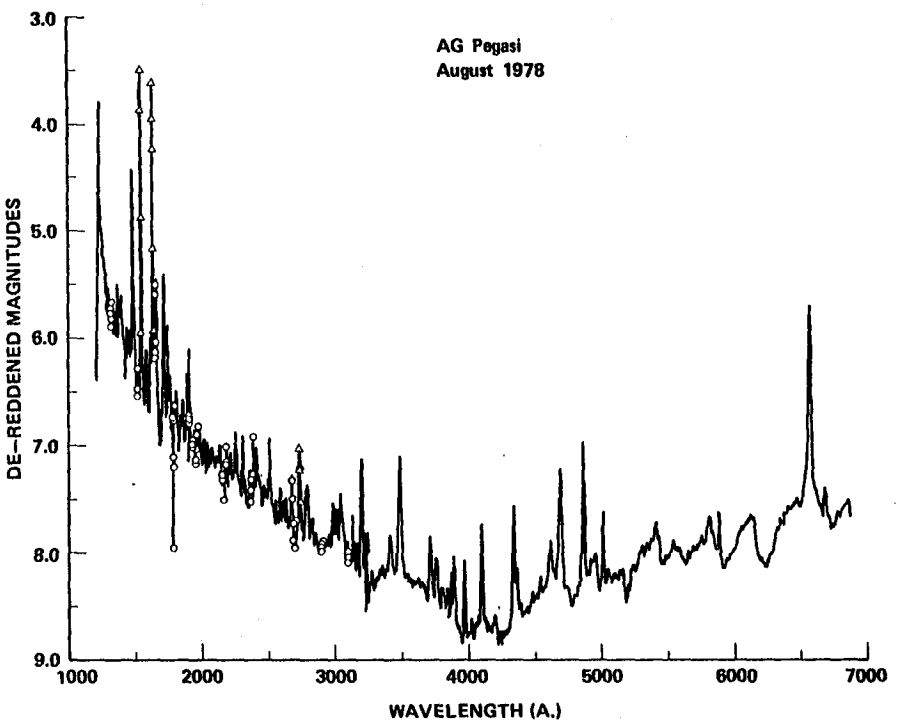

Fig. 1.: Spectrum of AG Pegasi, 1200-7000 Å. Circles mark reseau contamination, triangles are saturated pixels.

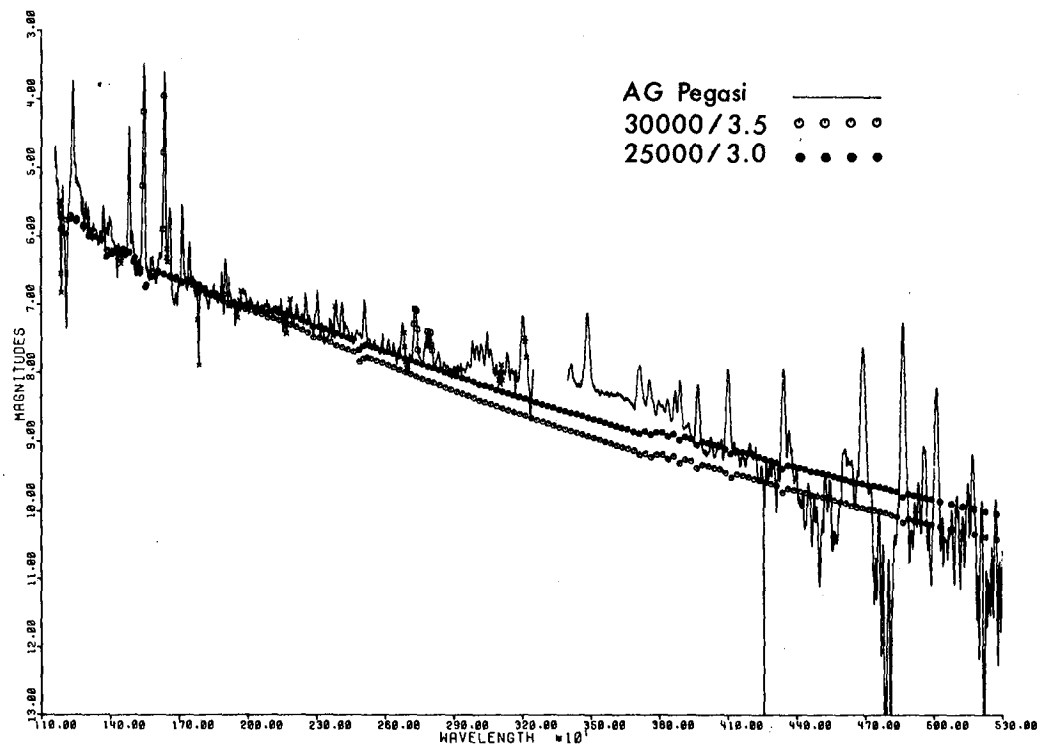

Fig. 2.: Spectrum of hot component and hydrogen nebula only compared with best two Kurucz atmosphere fits for AG Peg.

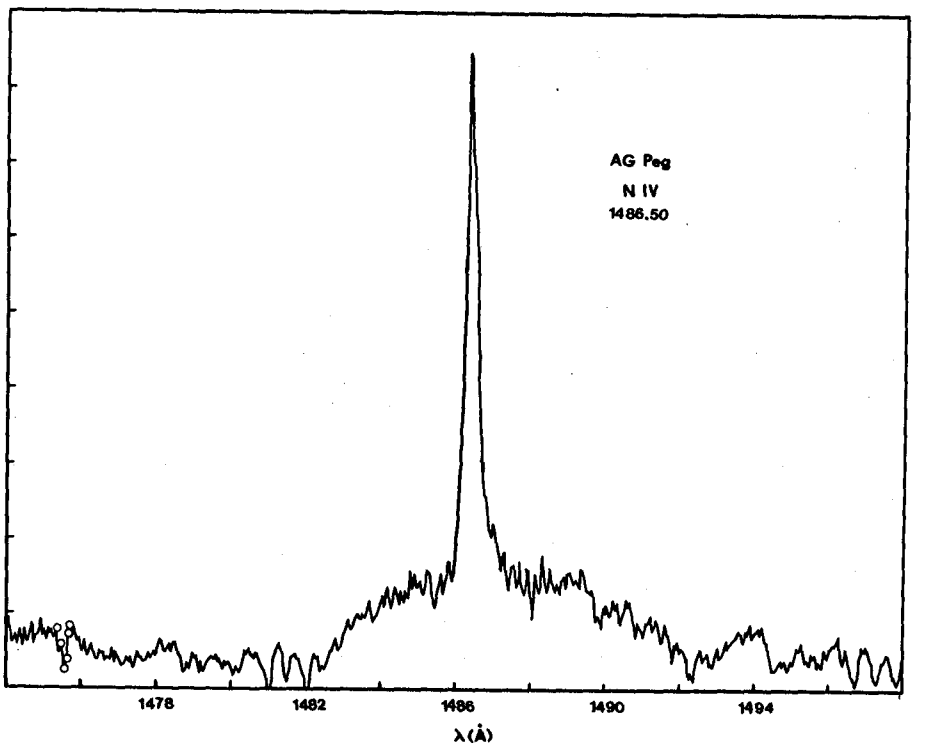

Fig. 3.: The N IV] 1486 line in AG Pegasi.

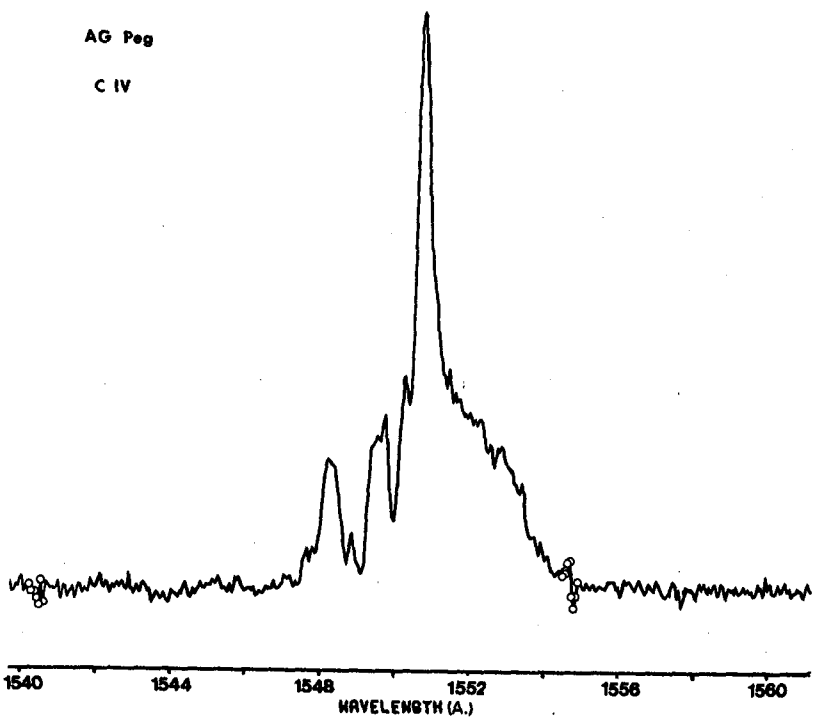

Fig. 4.: The C IV 1548, 1550 resonance doublet in AG Pegasi.

IUE OBSERVATIONS OF SYMBIOTIC STARS

Jorge Sahade
Instituto de Astronomía y Física del Espacio
and CONICET, Buenos Aires, Argentina

Estela Brandi
Observatorio Astronómico, La Plata, Argentina

ABSTRACT

The IUE observations suggest that the symbiotic stars can be placed in two broad groups. One of the groups is characterized by strong, narrow emissions arising from a wide range of excitation energies, while the other one typically shows a strong continuum with absorption lines and very few or no emissions at all. Both broad groups appear to suggest that we are dealing with binary systems and that they probably differ in the characteristics and extent of the chromosphere-corona formation that is present in the system.

Twenty stars that are listed among the symbiotic stars were observed with the IUE in December, 1978/January, 1979 and in July, 1979, mostly in the low dispersion arrangement, except for 17 Leporis and AX Monocerotis, which were also observed with high dispersion.

The aim of the program was to ascertain:

1) whether or not the belief that all symbiotic stars are binaries is sustained by the UV observations;

2) whether or not the behavior of the whole group is similar in the UV;

3) whether or not there were any detectable changes in the UV spectra between the two observing epochs.

The stars that were observed are:

R Aquarii [1]	WY Geminorum# [2]	AR Pavonis*# [1]
Z Andromedae [1]	RW Hydrae [1]	AG Pegasi* [1]
T Coronae Borealis* [1]	17 Leporis* [2]	AX Persei [1]
BF Cygni# [1]	AX Monocerotis*# [2]	RX Puppis# [1]
CH Cygni [2]	BX Monocerotis# [2]	RR Telescopii# [1]
CI Cygni# [1]	RS Ophiuchi# [2]	WY Velorum [2]
V1016 Cygni# [1]		HD 4174 [1]

The five objects definitely known to be binaries are indicated on the list with an asterisk, while the symbol # stands for observations made only on one of the two epochs.

The examination of the UV spectra of the twenty stars disclosed that they can be placed in two broad groups. The first group is characterized by the presence of numerous narrow emission lines that arise from a wide range of excitation energies, from 6000°K (Mg II) to 10^5 °K (N V). The strong emissions in the short wavelength range are of resonance and intercombination lines and of transitions that correspond to higher excitation, like He II 1640. The lines normally present are

C III]	1909
Si III	1892
N III]	1749
O III]	1666
He II	1640
C IV	1548, 1551
N IV]	1486
Si IV	1394, 1403
C II	1335
N V	1239, 1243

but, of course, the relative intensities are not the same on all the stars that we would place in our first group.

The SWP images were secured with exposure times short enough so that the emission lines would not become saturated. Therefore, our material in the short wavelength mode is not suitable for the detection of a hot continuum,

if present; however, such a continuum is clearly visible in the case of AR Pav.

In the IUE long-wavelength range, the group normally displays strong Mg II in emission; however, in the case of AG Peg, no Mg II is observed on our images. The Mg II resonance doublet appears to be variable in Z And and in WY Vel, and, in the context of this fact, we should mention here that in the spectroscopic binary μ^1 Scorpii Sahade and van der Hucht (ref. 1) found that Mg II is also strongly variable and concluded that the variation may perhaps be correlated with variations in Balmer emission.

The second broad group shows typically no emissions except of Mg II in WY Vel and in CH Cyg, and of O I 1303 in CH Cyg. The images secured for the stars in this group show a continuum spectrum which does not correspond to a late type star. In the cases of WY Vel and WY Gem the resonance lines that are present in emission in the first group, appear in absorption, reminding us of the behavior of Be stars in the ultraviolet.

If we consider the first broad group, we can conclude that

1) the resonance lines must be formed in a region of low density where collisional excitation is at work and is characterized by a large range in excitation temperatures; this suggests that the objects have some sort of a chromosphere-corona formation that may perhaps be linked to the late-type star;

2) although our SWP material, except in the case of AR Pav, does not show evidence for an early-type continuum, the presence of high-excitation lines, like He II 1640, and the presence of a continuum on the LWR images point towards the existence of a hot source and, thus, support the hypothesis that we are dealing with binary systems.

The behavior of our second group appears to support the same conclusion and, therefore, the validity of the binary hypothesis for the symbiotic stars is generally valid for our large sample. The difference in spectral behavior in the two groups should then be related to the characteristics and extent of the chromosphere-corona formation.

On the list of the observed objects which is given ut supra, we have indicated with number "1" those that belong in our group 1, and with number "2" those that belong in our group 2.

No correlation is possible to establish between what we have learned from the IUE material and what we know about the symbiotic stars from investigations made in other wavelengths. Only simultaneous photometric and spectral observations in a wide range of wavelengths, taken at appropriate times, could help us understand whether or not the two broad groups are actually related to the phase in the nova-like behavior, and, therefore, to arrive to a more definite picture of the structure -and evolution- of the extended envelopes in the symbiotic stars. The whole thing may even have a bearing on Linsky and Haisch's (ref. 2) finding of solar and non-solar type stars.

The analysis of the low-dispersion spectra will be published in detail elsewhere, and the results from the high dispersion material will form a subsequent paper.

REFERENCES

1. Sahade, J. and van der Hucht, K.A.: Ultraviolet Observations of β Persei, μ^1 Scorpii and γ_2 Velorum. Astrophysics and Space Science, in press, 1980.
2. Linsky, J.L. and Haisch, B.M.: Outer Atmospheres of Cool Stars.I. The Sharp Division into Solar-Type and Non-Solar-Type Stars. Astrophysical Journal Letters, vol. 229, April 1, 1979, pp. L27-L32.

THE WHITE DWARF COMPANION OF THE Ba II STAR ζ CAP

Erika Böhm-Vitense
University of Washington

ABSTRACT

The Ba II star ζ Cap has a white dwarf companion. Its T_{eff} is determined to be 22000K, its mass $M \sim 1 M_{\odot}$. The importance of this finding for the explanation of abundance peculiarities is discussed.

During the course of observing chromospheric and transition layer emission of stars with different chemical abundances we also observed the Ba II class 2 star ζ Cap (G5 IIp). Figure 1 shows the tracing which we obtained at the computer screen at the IUE observatory. The intensity increases again for λ<1500A. We even see a slight intensity increase shortward of Ly α, indicating a faint B star spectrum. The energy distribution obtained after correcting for the instrumental sensitivity is seen in Figure 2. For comparison we have also plotted the energy distributions for the G8 III standard star ε Vir and for the weak Ba II star ζ Cyg (G8 IIp). These spectra are all normalized to the same visual magnitude. The intensity for λ<1500A increases with increasing Ba II anomaly of the star. For ζ Cap we see the superposition of the normal G8 II star spectrum (for λ ≥1600Å), the cool chromospheric emission line spectrum (1500<λ<1600Å), some intense emission lines from regions with temperatures around 100,000K, (CIV, NV), and the additional faint B type stellar spectrum (for λ<1500Å).

An estimate of the absolute magnitude shows immediately that the B star must be a white dwarf. Interpreting the decrease of the intensity for λ<1300Å as the Ly α wing we can determine the relation between T_{eff} and log g (g = gravitational acceleration) which will produce such a Ly α profile. From the calculation by Wesemael[1] et al. (1979) we find a log g, T_{eff} relation shown by the solid line in Figure 3.

If we know the absolute magnitude of ζ Cap we know the distance and the absolute flux for the companion ζ Cap B at 1300Å which gives a relation between the radius R and T_{eff}. For white dwarfs the radius determines the mass $M_{\odot}$ of the white dwarf and thereby also the gravitational acceleration g. We have used the Hamada, Salpeter [2] (1961) relation M(R) for helium white dwarfs. The spectroscopists (Kemper[3] 1975, Sneden and Smith [4] 1980) tell me that M_V = -3 for ζ Cap.

With this value we find a relation between T_{eff} and log g as shown by the dashed line for M_V = -3. The intersection with the solid line determines the best value for T_{eff} and log g (M) leading to T_{eff} = 22000K and M = 0.98$M_{\odot}$. For lower absolute brightness, i.e. a smaller distance of ζ Cap A, ζ Cap B has to be smaller and more massive. The ζ Cap companion is then very similar to Sirius B.

This observation seems to be especially important in view of the findings of McClure et al.[5] (1980) who observed radial velocity variations of all strong Ba II stars. They are now checking on the weak Ba II stars. For two of the systems they could determine mass functions which indicate masses of 1 to 2 $M_\odot$ for the invisible companions. They concluded that these had to be white dwarfs. Since all Ba II stars appear to have companions they concluded that the Ba anomaly is due to mass exchange between binaries rather than to mixing in the star. In fact, the strong emission lines seen in the ζ Cap system make it probable that some mass exchange is still going on. The question then arises how much of the peculiar abundances seen in red giants of both populations is due to mass exchange and how much due to actual mixing?

Whether ζ Cyg also has a white dwarf companion is not quite clear; we need to study the data more carefully. If it has one, it must be of lower temperature, probably around 14000K, but of similar mass.

These are the two brightest Ba II stars. We have since observed Ba II stars ~2.5 magnitudes fainter. So far none of them has a possible companion bright enough to be clearly recognizable on 4^h exposure spectra. We are still studying the data. Details of this study will be published in the Ap.J. Letters.

REFERENCES

1. Wesemael, F., Auer, L.H., van Horn, H.M., and Savedoff, M.R. 1979, preprint.

2. Hamada, T., and Salpeter, E.E. 1961, Ap.J., 134, 683.

3. Kemper, E. 1975, P.A.S.P. 87, 537.

4. Sneden, C. and Smith, V. 1980, preprint.

5. McClure, R.D., Fletcher, J.M., Nemec, J.M. 1980, Ap.J. Letters, in press.

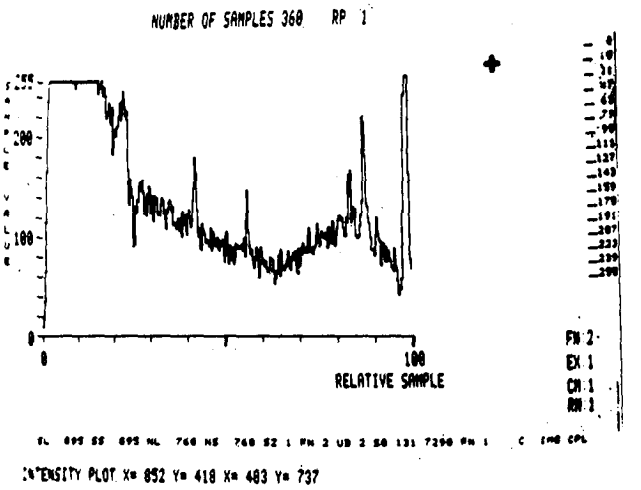

Figure 1: The short wavelength spectrum of the Ba II star ζ Cap as seen on the computer screen at the IUE observatory. The increase in intensity for λ<1500Å is attributed to a white dwarf companion. The intensity increase shortward of Ly α indicates rather high temperatures for the companion.

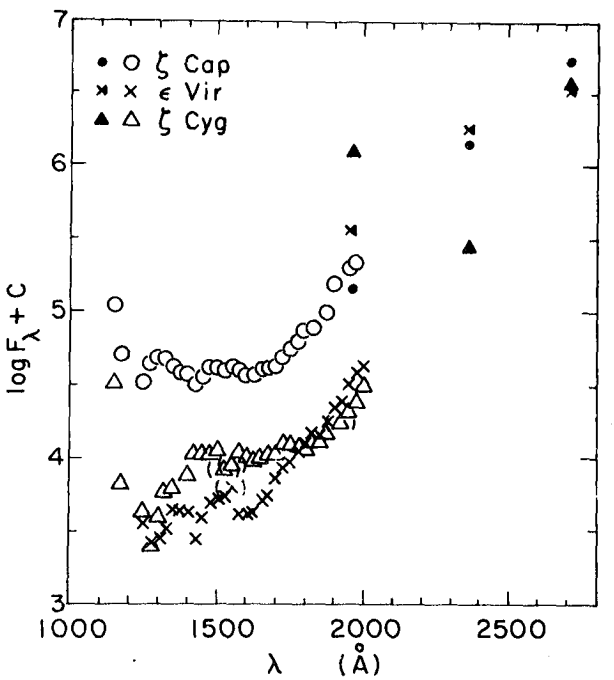

Figure 2: The energy distributions of the Barium star ζ Cap, the weak Barium star ζ Cyg and the standard star ε Vir, all normalized to the same visual magnitude. The short wavelength intensity increases with increasing Ba II anomaly.

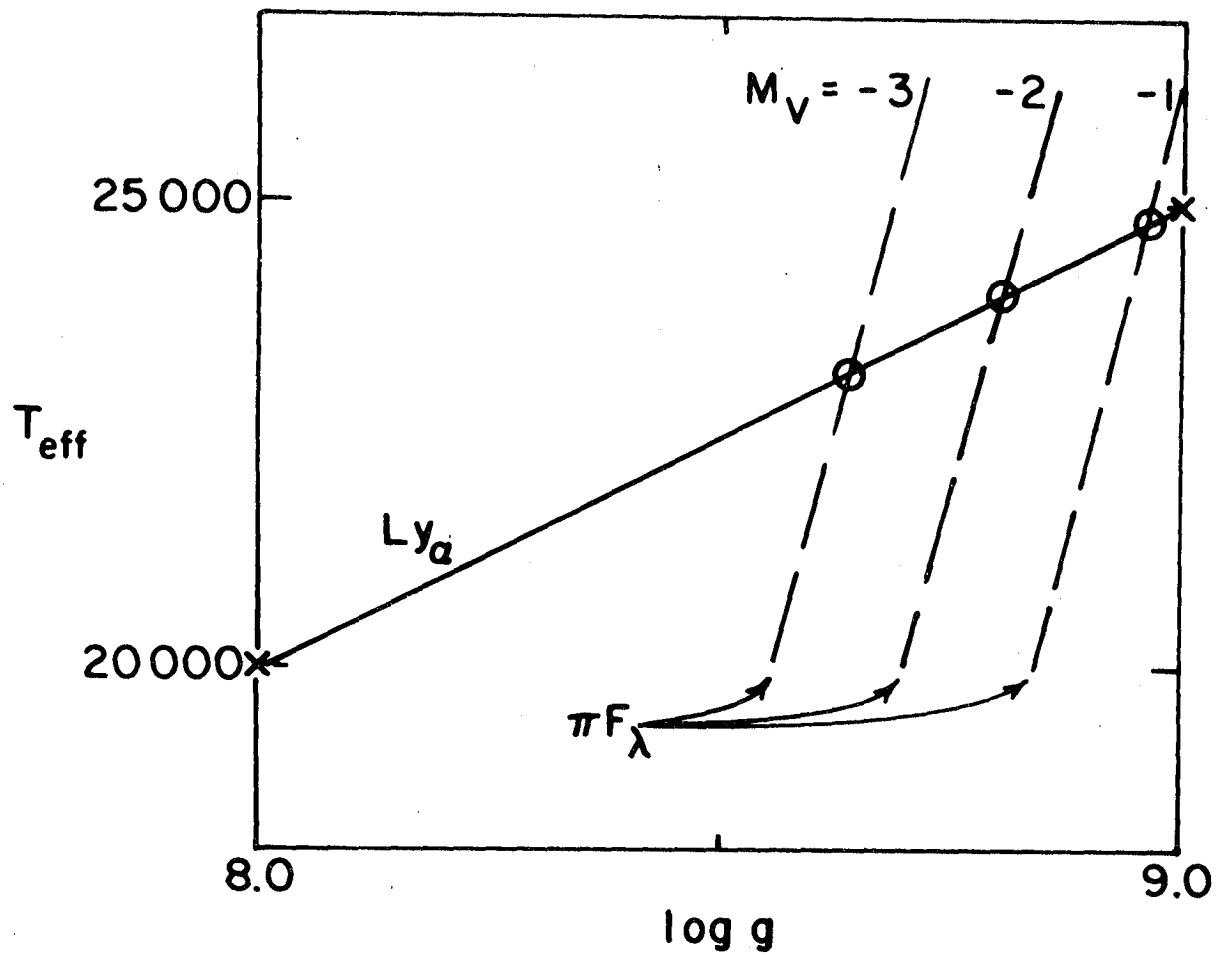

Figure 3: The T_{eff} log g plane showing the possible combinations of T_{eff} and log g giving the observed Ly α profile (solid line) for ζ Cap B and the relation between T_{eff} and log g leading to the observed absolute intensity at 1300Å(dashed lines). The different lines are obtained for different absolute magnitudes for ζ Cap A leading to different distances. The intersection of the appropriate dashed line with the solid line gives the value of log g and T_{eff} for ζ Cap B.

INGRESS OBSERVATIONS OF THE 1980 ECLIPSE OF THE SYMBIOTIC STAR CI CYGNI

Robert E. Stencel
Joint Institute for Laboratory Astrophysics - Univ. of Colo. & NBS

Andrew G. Michalitsianos
Laboratory for Astronomy and Solar Physics - Goddard Space Flight Center

Minas Kafatos
Department of Physics, George Mason University

Alexander A. Boyarchuk
Crimean Astrophysical Observatory, U.S.S.R. Academy of Sciences

INTRODUCTION

One of the major results from the IUE may prove to be the new knowledge gained by studies of the ultraviolet spectra of symbiotic stars. Symbiotics combine spectral features of a cool M giant-like photosphere with strong high excitation emission lines of nebular origin, superposed. An excellent pre-UV review has been given by Swings (1). The UV spectra are dominated by intense permitted and semi-forbidden emission lines and weak continua indicative of hot compact objects and accretion disks. Two symbiotics, AR Pav and CI Cyg are thought to be eclipsing binaries, and we have begun IUE observations during the predicted 1980 eclipse of CI Cygni.

SYSTEM PARAMETERS

Periodic albeit irregular light curve variations suggest that CI Cyg is an eclipsing binary, with the elements: minimum light = JD 2411902+855.25E. Boyarchuk has predicted ingress to begin about April 10, 1980 and egress to end about August 18, 1980, with a nearly 100 day totality. The visual magnitude range fluctuates between $+10^m$ and $+12^m$ with outbursts to $+9^m$ known. Light curves are described by Mattei (2) and Belyakina (3).

QUESTIONS TO BE ADDRESSED

Obviously the time variation of the UV line and continuum flux can be used to constrain the physical dimensions of the line-emitting regions and thereby used to discriminate among various excitation mechanisms. It may be possible to determine something about the origin and extent of mass transfer. Since the system inclination is known, information about the existence and nature of an accretion disk might be obtained, as well. These questions are posed in the light of recent IUE studies which will also be presented at this conference. In particular, Plavec (4) argues that a connection between Beta Lyr stars, W Ser stars and symbiotics (AR Pav) can be made in commonality as case B mass-transferring binaries (rates of -6 or more in the log) and accretion onto non-degenerate stars. IUE observations of RW Hya by Kafatos et al. (5) have been used to argue that tidal interaction on the cool object can greatly augment the intrinsic stellar wind and lead to the observed accretion effects. The visibility of UV continua from accretion disks among symbiotics may be a complicated function of densities and viewing angles.

We hope to be able to address several of these concerns with eclipse observations of CI Cyg.

PRE-INGRESS AND INGRESS OBSERVATIONS

At the time of this writing we have obtained spectra on March 16, and April 16 and 25. The March 16 spectra in SWP and LWR are remarkably similar to RW Hya (5) in showing numerous strong high excitation emission lines from species like permitted N V and C IV and semi-forbidden O IV, O III and N III, among others. In contrast to RW Hya where evidence for a 100,000 K continuum is seen, CI Cyg shows a weak Balmer continuum emission falling off towards higher frequencies. Also CI Cyg shows strong O III lines at 3047 and 3133 Å which are frequently seen in Miras and planetary nebulae but not strongly in RW Hya. These are Bowen fluoresced by He II Lyα. The measured line fluxes in CI Cyg are generally 2 to 10 percent of those in RW Hya. C IV 1550 for example had an integrated flux of about 2E-11 ergs/cm^2/s on March 16, 1980. We note that for reasonable assumptions about distance (cf. 5) for CI Cygni, we can compare fluxes in C IV against Mg II for symbiotics much as Ayres has done for normal cool stars (see paper by Ayres in these proceedings) and find symbiotics like CI Cyg and RW Hya lie three orders of magnitude above the C IV-Mg II flux correlation for normal cool stars. We interpret this to be a manifestation of different physical mechanisms involved: magneto-acoustic heating of the outer atmosphere for normal cool stars, versus photoionization-recombination for the symbiotics.

A preliminary comparison of the spectra obtained during ingress indicate a substantial decrease in the continuum at all wavelengths and a noticeable drop in the emission line flux from the higher excitation lines, particularly in the 1400 Å blend of Si IV and O IV. A lie at 2830 Å due to He I also appears to be decreasing in strength, while the O III lines at 3047 Å and 3133 Å may have slightly increased in strength. These changes are suggestive of a stratified nebula, where the highest excitation regions are centralized and of dimensions less than that of the M giant, of order 10^{12} cm. This region could represent the actual accretion disk. The O III lines may arise from a more extended region (Bowen fluoresced), perhaps comparable to the orbital separation, of order 10^{14} cm. It is not obvious that we have detected a hot companion star, given the weak cool continuum. Comparison with observations well out of eclipse and during a burst stage would be useful. If other observers would like to supplement the observing plan, collaboration would be welcomed.

REFERENCES

1. Swings, P., "Symbiotic Stars and Related Peculiar Objects" 1970 in Spectroscopic Astrophysics, G. Herbig, ed., Berkeley, U. of Calif. Press, p. 189.
2. Mattei, J., "The Symbiotic Star CI Cygni", 1977 J.R.A.S.C. 70, 325.
3. Belyakina, T. "Observations of CI Cygni in 1977-78", Info. Bull. Var. Stars, No. 1602.
4. Plavec, M., "IUE Observations of Long Period Eclipsing Binaries: Accretion onto Non-Degenerate Stars", 1980 U.C.L.A. Preprint No. 86.
5. Kafatos, M., A. Michalitsianos, and R. Hobbs, "IUE Observations of RW Hya", Astrophys. J., 1980 in press.

ULTRAVIOLET SPECTROSCOPY OF OLD NOVAE AND SYMBIOTIC STARS

David L. Lambert, Mark H. Slovak and Gregory A. Shields
University of Texas at Austin

Gary J. Ferland
Cambridge University

ABSTRACT

Low-dispersion, short-wavelength IUE spectra are presented for two old novae, DQ Herculis (1934) and V603 Aquilae (1918) = HD 174107, and for two symbiotic variables, AG Pegasi = HD 207757 and CI Cygni. The emission line spectra of the novae are relatively sparse, dominated by a strong C IV (λ1549) feature and showing weaker emissions arising from N V(λ1241), Si IV + O IV] (λλ1398, 1402), and He II (λ1640). The absence of intercombination lines suggest electron densities greater than 10^{10} cm^{-3}. The continua of the two novae are remarkably different, the appearance seemingly dictated by the inclination of the system. The symbiotic variables display a more variegated emission line spectrum, exhibiting features of O I (λ1304), N IV](λ1485), N III](λ1752), and C III] (λ1909). The continua for the quiescent symbiotics are stellar in appearance and change as a function of the system inclination. These results confirm the existence of hot companions in the symbiotic stars, lending support to the binary hypothesis for these variables. Model atmospheres are fit to the spectra to estimate the properties of the hot components.

INTRODUCTION

Ultraviolet spectra have been obtained for several old novae and various of the symbiotic stars in order to study the nature of these objects in a region inaccessible to ground-based observations. The ultraviolet data are being combined with optical spectra in order to provide absolute flux distributions extending into the near infrared.

In order to ascertain the steady-state post-eruptive properties of these active systems, the data were obtained while the stars were in their quiescent states. Hence, the observations can be compared directly with various of the steady-state models that have been proposed to explain the novae and nova-like variables.

The old novae are thought to be close binary systems (ref. 1) involved in active mass transfer via Roche lobe overflow of matter from a late type star onto a white dwarf. An accretion disk is formed around the white dwarf as a result of the mass transfer

process and is predicted to contribute an appreciable fraction of the ultraviolet luminosity (ref. 2). The old novae V603 Aql (1918) and DQ Her (1934) were examined and their spectra are discussed in the context of the binary model.

The exact nature of the symbiotic variables has been an unresolved puzzle for many years. The optical spectra are usually dominated by a late-type giant and a strong nebular line spectrum, obscuring any contribution from a hot companion. The IUE data obtained for various of the symbiotics, however, show clear evidence for the existence of a hot component in many of these stars, supporting the binary hypothesis discussed in reference 3. Data for the spectroscopic binary AG Peg and the eclipsing system CI Cyg are presented as examples.

OBSERVATIONS

The low resolution ($\Delta\lambda = 5 \times 10^{-10}$ m) spectra were obtained with the short wavelength prime (SWP) camera of the IUE satellite on June 29 and December 14, 1979. The exposures were taken through the $10^{\hat{}}$ x $20^{\hat{}}$ oval aperture and were untrailed with the exception of SWP 7407 (AG Peg).

The data have been converted to absolute fluxes using the calibration given in reference 4. Unfortunately, the June spectra were processed using an incorrect intensity transfer function (ITF). However, additional spectra of similar quality for V603 Aql (SWP 5921) and CI Cyg (SWP 5485) have been processed using both the incorrect ITF and a corrected version (ref. 5). The average correction error between the two was 2.3%. Since the uncertainty in the absolute flux calibration of the SWP spectra longward of L_α (λ1216) is estimated to be 10%, the results presented here would appear to be uneffected by the ITF problem.

The fluxes have been de-reddened using the reddening curve given in reference 6. The values of the color excess, E(B-V), used to de-redden the data are indicated in each of the figures. The color excesses are small for the novae, tending to be larger for the more luminous symbiotic stars.

DISCUSSION

THE OLD NOVAE

The IUE data for V603 Aql are compared with earlier OAO-2 and ANS satellite measurements in figure 1. The satellite data have been de-reddened assuming E(B-V) = 0.07 mag, as have the IUE fluxes. The systematic disagreement between the OAO-2 and IUE values shortward of λ1600 Å suggests real variability in the continuum of the hot component. The OAO-2 data were used (ref. 7) to derive ultraviolet colors and estimate a color temperature of 25,000 K. A hot model atmosphere (T_{eff} = 25,000K ; log g =4.5) (ref. 8) is compared to the IUE data in figure 1 as well as the predicted flux distribution for an optically thick accretion disk ($f_\lambda \propto \lambda^{-2.33}$). Also shown are values from a white dwarf model

(T_{eff} = 25,000 K ; log g = 8) (ref. 9). The model fluxes have been normalized to the stellar fluxes at λ1700 Å where the continuum appears free of emission lines.

The continuum of DQ Her can be seen in figure 2 and offers a startling contrast to that of V603 Aql. It is well represented by a flux distribution of the form $f_\lambda \propto \lambda^0$ = constant over the bandpass of the SWP camera (λλ1200-1900 Å). Despite the difference between the continua of the novae, however, the emission line spectra are qualitatively similar at least in the appearance of various of the lines. Note the strong N V (λλ1239, 1243) feature present in DQ Her which is absent from V603 Aql.

It is interesting to note that DQ Her is an eclipsing system seen at a relatively high inclination ($i \simeq 70^o$) whereas V603 Aql is viewed nearly pole-on ($i \simeq 15^o$). The difference in the appearance of the continua may thus reflect the differing aspects of these systems. Those binaries seen at high inclinations apparently must present a larger optical depth in the disk to the observer than do the lower inclination systems. This simple geometrical interpretation provides support for the models that posit the existence of optically thick accretion disks surrounding the hot white dwarf components.

THE SYMBIOTIC STARS

The IUE spectra of the symbiotic stars present a wealth of observational material. These data show a much richer and more diverse emission line spectrum than seen in the novae. Furthermore, the ultraviolet data provide direct confirmation, in many cases, of the existence of a hot companion. Spectra were obtained on two systems known to be binaries from optical studies. In figure 3 the low dispersion spectrum of AG Peg, a spectroscopic binary, is seen, and figure 4 presents a similar spectrum for the eclipsing system CI Cyg.

Satellite data also exist for AG Peg and are shown in figure 3 compared to the IUE fluxes after de-reddening using a value of E(B-V) = 0.12 mag. Despite the large uncertainties associated with the earlier measurements (∿34% at λ = 1330 Å), the continuum appears to have systematically decreased by approximately 20% since the epoch of the OAO-2 observations (May 1970). Such a decline appears to be the source of the steady 0.025 mag/year decrease seen in the optical light curve which would also imply a 20% decrease in flux.

Model atmospheres from reference 8 were fit to the continuum of AG Peg and serve to provide an estimate of the temperature of the hot component ($T_{eff} \simeq 40,000$ K). This value is in accord with the temperature estimated from the OAO-2 measurements, discussed in reference 10.

Both the continuum and the emission line spectrum of the eclipsing system CI Cyg (figure 4) provide a marked contrast to those of AG Peg. The emission lines are much narrower and generally weaker. Note the presence of the strong permitted nitrogen lines in AG Peg and their weaker appearance or even absence in

CI Cyg.

Further support for the hypothesis developed above relating system inclination to continuum appearance is provided from the comparison of these two systems. CI Cyg appears at a very high inclination showing flat-bottomed eclipses of variable depth. AG Peg, on the other hand, is seen at a lower inclination of approximately 36^{o}. Thus, the material (disk?) surrounding the high inclination systems would again appear to present a large optical depth to the line of sight. It is expected that spectra of the eclipsing nova T Aurigae and the other known eclipsing symbiotic star AR Pavonis would show similar effects.

CONCLUSIONS

IUE spectra have been presented for two old novae and for two of the symbiotic variables. Prominent emission line spectra are revealed as is a continuum whose appearance is effected by the system inclination. These data provide evidence for hot companions in the symbiotic stars, making plausible the binary model for these peculiar stars. It is also worthy to mention that recent IUE spectra of dwarf novae (ref. 11) provide additional support for the existence of optically thick accretion disks in active binary systems. The ultraviolet data of the eclipsing dwarf novae EX Hya and BV Cen appear flatter than for the non-eclipsing systems (e.g. VW Hyi), an effect which could be ascribed to the system inclination.

REFERENCES

1. Robinson, E. L.: The Structure of Cataclysmic Variables. Ann. Rev. Astr. Ap., vol. 14, 1976, pp. 119-142.

2. Herter, T; Lacasse, M. G.; Wesemael, F.; and Winget, D. E.: Theoretical Photometric and Spectroscopic Properties of Stellar Accretion Disks with Application to Cataclysmic Variables. Ap. J. Suppl., vol. 39, April 1979, pp. 513-535.

3. Boyarchuk, A. A.: Symbiotic Stars. Non-Periodic Phenomena in Variable Stars. Fourth Colloquium of Variable Stars, 1969, pp. 398-410.

4. Bohlin, R. C.; Holm, A. V.; Savage, B. D.; Snijders, M. A.; and Sparks, W. M: Photometric Calibration of the International Ultraviolet Explorer (IUE): Low Dispersion. NASA X-681-79-19, June 1979.

5. Cassatella, A.; Holm, A.V.; Ponz, D.; and Schiffer, F. H.: A Correction Algorithm for Low Dispersion SWP Spectra. NASA IUE Newsletter, No. 8, Feb. 1980, pp. 1-21.

6. Code, A. D.; Davis, J.; Bless, R. C.; and Brown, R. H.: Empirical Effective Temperatures and Bolometric Corrections for Early-Type Stars. Ap. J., vol. 203, Jan. 1976, pp. 417-434.

7. Gallagher, J. S.; and Holm, A. V.: Ultraviolet Detection of the Nova Variables V603 Aquilae and RR Pictoris. Ap. J. Lett., vol. 189, May 1974, pp. 123-126.

8. Kurucz, R. L.: Model Atmospheres for G, F, A, B, and O Stars. Ap. J. Suppl., vol. 40, May 1979, pp. 1-340.

9. Wesselius, P. R.; and Kooster, D.: Effective Temperatures of Hot White Dwarfs. Astr. Ap., vol. 70, Dec. 1978, pp. 745-750.

10. Gallagher, J. S.; Holm, A. V.; Anderson, C. M.; and Webbink, R. F.: Ultraviolet Photometry from the Orbiting Astronomical Observatory. XXXIII. The Symbiotic Star AG Pegasi. Ap. J., vol. 229, May 1979, pp. 994-1000.

11. Bath, G. T.; Pringle, J. E.; and Whelan, J. A. J.: Spectrophotometry of Dwarf Novae in the Wavelength Range 1250 - 7500 A. Mon. Not. R. Astr. Soc., vol. 190, Jan. 1980, pp. 185-194.

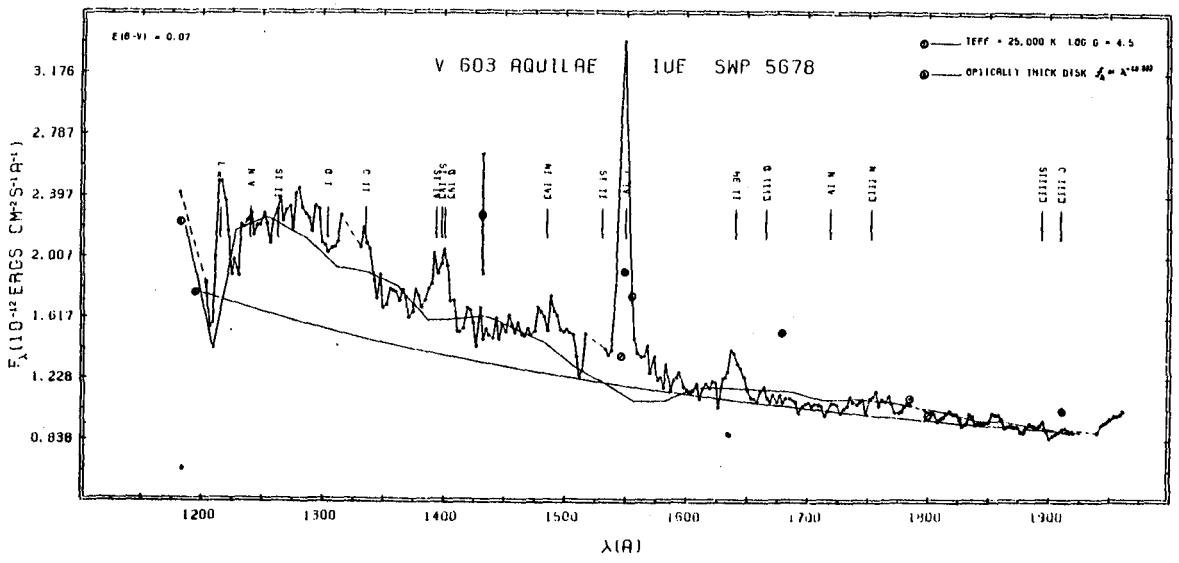

Figure 1 - The low-dispersion IUE spectrum for the old nova V603 Aql. The IUE fluxes are compared with the OAO-2 data (filled circles), the ANS data (open circles with dot), and the white dwarf model fluxes (circles with slash). Dashed regions of spectrum locate reseau contaminated portions. Also shown are the predicted fluxes of a stellar model atmosphere (①) and an optically thick accretion disk (②). See discussion in the text.

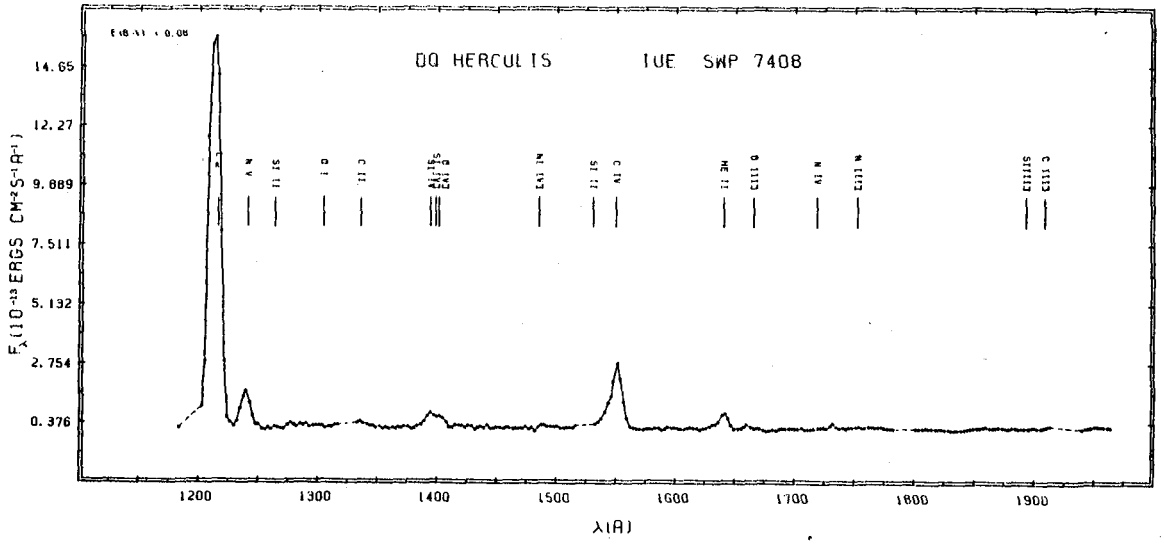

Figure 2 - As in figure 1 for the old nova DQ Her. The data have been de-reddened using a value of E(B-V) = 0.08 mag. The strong L_α feature is geocoronal in origin.

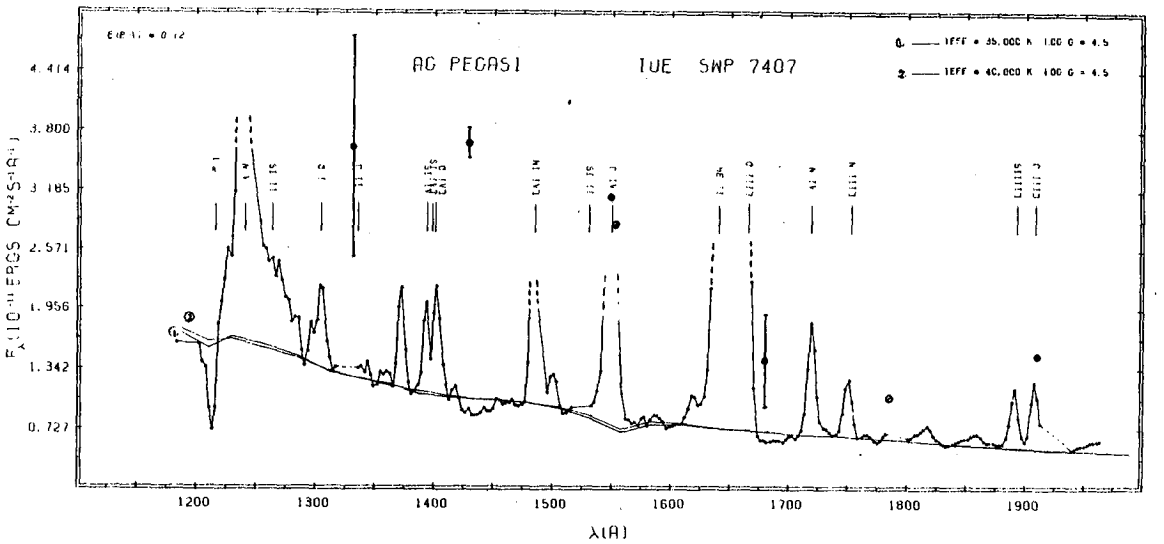

Figure 3 - Low-dispersion spectrum for the symbiotic variable AG Peg. The lines with dashed tops are saturated. OAO-2 data are represented by filled circles; ANS values by open circles with dot. Two model atmospheres are fit to the continuum: ① - T_{eff} = 35,000 K and ② - T_{eff} = 40,000 K.

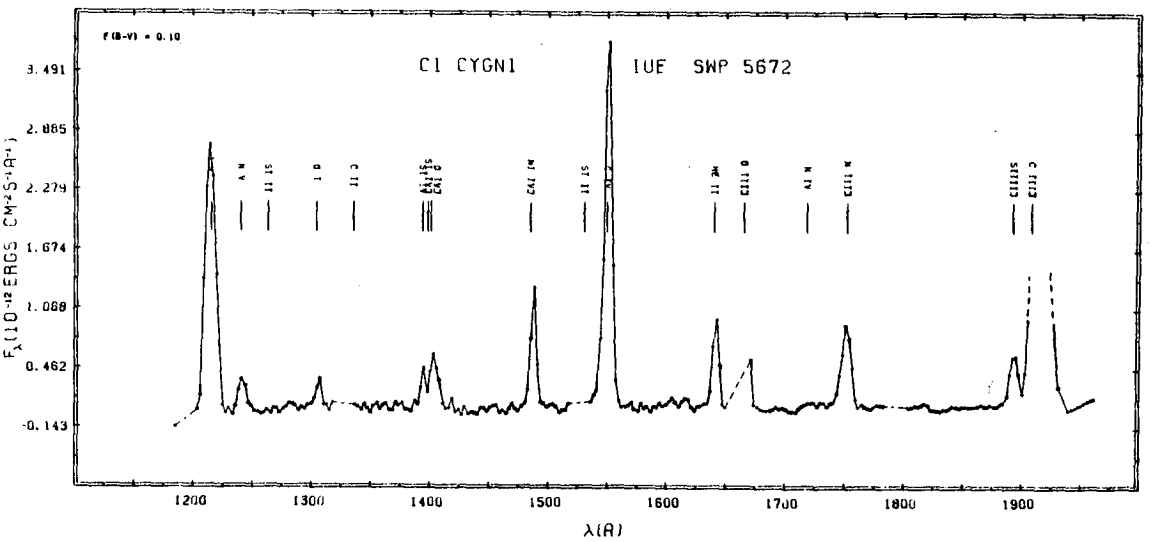

Figure 4 - As in figure 3 for the eclipsing symbiotic CI Cyg. The fluxes have been de-reddened using a value of E(B-V) = 0.10 mag.

IUE AND OTHER NEW OBSERVATIONS OF THE SLOW NOVA RR TEL

M.V. Penston, P. Benvenuti, A. Cassatella, A. Heck, P. Selvelli,
Astronomy Division, ESTEC
Villafranca Satellite Tracking Station,
European Space Agency,
Apartado 54065, Madrid, Spain

D. Ponz
Instituto Nacional de Tecnica Aeroespacial,
Villafranca Satellite Tracking Station,
Apartado 54065, Madrid, Spain

F. Macchetto
Astronomy Division, ESTEC
Space Science Dept., European Space Agency,
Postbus 299, Noordwijk, 2200 AG, The Netherlands

C. Jordan
Dept. of Theoretical Physics,
University of Oxford, U.K.

N. Cramer, F. Rufener
Observatoire de Geneve, Geneve,
CH-1290 Sauverny, Switzerland

J. Manfroid
Institut d'Astrophysique de l'Université de Liege,
B-4200 Cointe-Ougrée, Belgium

ABSTRACT

Ultraviolet spectra of RR Tel made with the International Ultraviolet Explorer satellite are reported. These cover the range 1150-3200 Å at both high and low dispersion through both large and small apertures. A range of exposure times yields a dynamic range of 1000 in line intensities. A line list of 431 lines is presented giving measured wavelength, intensity and full width at half maximum. Over three quarters of the lines are identified. There is a correlation of line width with ionization energy. Lines identified include common species from once to four times ionized. Lines seen are generally resonance, semi-forbidden or forbidden lines but some recombination lines are also seen for C, O and Ne. Many Fe II lines are seen - most are from odd levels near 5 ev to even low - lying levels but decays from even 10 ev levels are also seen. One third of the decays from the 5 ev levels are part of a cascade from higher levels. Population of the 10 ev levels may be due to Lα fluorescence. Diagnosis of densities and temperatures suggests stratification. Forbidden line wavelengths are used to refine intersystem separation of energy levels in some species.

Low dispersion data yield a continuum energy distribution. The strength of the $\lambda 2175$ feature and the He II Paschen line intensities yield $E_{B-V} = 0.10$ magnitude. The continuum energy distribution is not due to a simple combination of gaseous emission processes and a hot star or accretion disk but the very high ratio of the energy in the lines to that in the continuum of 3.3 argues such a source must be present.

New ground-based photometry finds variations of order 0.03 magnitudes r.m.s. from night to night and within a night. If due to the lines this, in combination with the emission measure, would interestingly constrain the distance but it is more likely the variation is seated in the continuum.

———— / ————

The full text of this paper will shortly be submitted to Monthly Notices of the Royal Astronomical Society. The line list is available on request from the authors.

ON THE NATURE OF THE NOVA-LIKE VARIABLE CD-42°14462

E. F. Guinan and E. M. Sion
Villanova University, Villanova, Pennsylvania 19085

ABSTRACT

Low-dispersion long and short wavelength IUE spectra of the nova-like system CD-42°14462 were obtained on August 24 U. T. 1979. The short wave spectrum exhibits absorption features due to C III (λ1175), Lα (λ1216), N V (λ1240), He II (λ1640), Si IV (λ1394), N IV (λ1785) with C IV (λ1550) as a P Cygni feature with blue-shifted absorption suggesting the presence of material leaving the system. Possible interpretations of this object are discussed.

INTRODUCTION

Nova-like variables seem to be related to cataclysmic variables but are not known to have suffered major outbursts such as those of dwarf novae, recurrent novae, classical novae or symbiotic variables.

The system CD-42°14462 (V3885 Sgr) (refs. 1, 2, 3, 4) is one such system which, optically, exhibits broad Balmer absorptions, weak He I absorption and Ca II with possible weak central emission in the H lines. Rapid flickering with periodicities near 30 seconds is presumably associated with a hot spot at the impact region of material with an accretion disk (refs. 5, 6).

Cowley et. al. noted its spectroscopic similarity with the nova-like system BD-7°3007. If one is viewing a single white dwarf, it is particularly puzzling to have the simultaneous presence of H, He I and Ca II. In normal white dwarf stars, Balmer H and He I lines are rarely observed together and when Ca II is present with only Balmer lines, the Balmer lines are usually narrower.

CD-42°14462 has recently been observed as an X-ray source by the Einstein satellite over the energy range 0.15 to 4.5 Kev (ref. 7). We report below on IUE observations of CD-42°14462 as part of a survey of nova-like variables at ultraviolet wavelengths.

OBSERVATIONS

We have obtained IUE low dispersion short (SWP 6280) and long (LWR 5450) wavelength spectra of the nova-like variable CD-42°14462. The exposure times with the large aperture were 8 minutes for both spectra. The short-wavelength spectrum was overexposed from 1250Å to approximately 1330Å and the long-wave spectrum was

overexposed in the interval 2450Å to 3000Å. The times of mid-exposure were August 24.7180 U.T. and August 24.7275 U.T. 1979 for the short- and long-wavelength spectra, respectively. In addition, using the Fine Error Sensor (FES) of the satellite, apparent magnitudes of $+10^{m}.35$ and $+10^{m}.34$ were measured. These apparent visual magnitudes are consistent with the measures of other investigators summarized in reference 2, and indicates a reasonably constant light level for the object. We display the short wave ($\lambda\lambda$1150Å - 1900Å) spectrum in figure 1.

The short-wavelength spectrum reveals the presence of the following absorption features: C III (λ1175), Lyα (λ1216), N V (λ1240), Si III (λ1300), Si IV (λ1393, 1402), He II (λ1640), N IV (λ1785) and possibly Al III (λ1850). In addition, a relatively strong C IV (λ1550) feature is observed in P Cygni profile with blue shifted absorption and essentially rest-frequency emission. The long-wave spectrum reveals the possible presence of N IV (λ2478), C IV (λ2493) and O V (λ2786) absorption features but otherwise appears featureless.

ANALYSIS AND DISCUSSION

Our continuum fluxes, plotted on a log F_ν vs. $1/\lambda$ (μ-1), are shown in figure 2, together with fluxes provided by J. L. Greenstein for a similar nova-like variable, BD-7°3007. On the same plot, fluxes from broad band photoelectric U, B, V, R, I photometry are shown from the observations of Wegner and Eggen for CD-42°14462 and multi-channel ground-based measurements of BD-7°3007 made by Greenstein (ref. 8). The absolute calibration of the U, B, V, R and I photometry was based upon the work of Hayes (ref. 9).

The spectrum of CD-42°14462 in figure 2 seems to be essentially flat from the far UV out to 5500Å but seems to turn downward longward of V with the lowest flux values being an I measurement near 0.9μ. Shown for comparison is a $F_\nu \alpha \nu 1/3$ flux distribution derived under local Black Body behavior for a viscous, steady state optically thick disk (ref. 10), a model stellar atmosphere (T_{eff} = 16,000°K; log g = 4.5) from Kurucz (ref. 11), and a steady state optically thick model accretion disk from the grid of Herter et al. (ref. 12), corresponding to a mass transfer rate $\dot{M} = 10^{-7} M_\odot$/yr and inclination i = 30°. The X-ray flux points log $F_\nu \simeq$ -30.1 ergs s^{-1} Hz^{-1} and log $F_\nu \simeq$ -28.4 ergs s^{-1} Hz^{-1} centered on ~5Å and 35Å, respectively due to Cordova (ref. 7) are off the scale of figure 2. The accretion disk model of Herter et al. (ref. 12) for the case shown in the figure predicts an X-ray flux of log F_ν = -25.6 ergs $cm^{-2}s^{-1}Hz^{-1}$ at 30Å.

The model accretion disk spectra shown in figure 2 are clearly discordant with overall observed fluxes. The $\nu^{1/3}$ distribution gives far better agreement than the models of Herter et al. (ref. 10) in the UV, but remarkably good agreement with the observed fluxes are achieved with the Kurucz stellar atmosphere at relatively low gravity. While we cannot completely rule out the presence of an accretion disk given the theoretical uncertainties in the models, the present data are best fitted with the Kurucz model atmosphere.

The hot components of other nova-like binaries have been fitted with hot stellar atmosphere models as reported by Slovak and Lambert for the old slow nova V603 Aquillae, and several symbiotic variables thought to have accretion disks but viewed at low inclination so that the disk is tilted out of the line of sight. Patterson* reported a cataclysmic variable, HT Cas, in which a white dwarf appears to dominate the light and seems to be responsible for the observed flickering.

Based upon our present data we cannot rule out any of the following three explanations of our overall continuum fluxes: (1) a hot optically thick accretion disk; (2) a cooler accretion disk ($T_{eff} \lesssim 25,000°K$) which mimics a stellar photospheric continuum; (3) a hot single star (no accretion disk) of uncertain surface gravity. A successful model of this system must account for the 0.2 day periodicity in the radial velocities found by Cowley et al. (ref. 4), the high-frequency oscillations reported in (ref. 5) and the X-ray fluxes reported by Cordova. A further constraint is imposed by the presence of the C IV P Cygni feature which almost certainly indicates systemic mass outflow of some type.

* Presented at the Fifth Workshop on Cataclysmic Variables, Austin, Texas, Mar. 1980.

REFERENCES

1. Bond, H.E., and Landolt, A.U. 1971, P.A.S.P., 83, p. 485.

2. Wegner, G. 1972, Ap. Letters, 12, p. 219.

3. Hesser, J.E., Lasker, B.M., and Osmer, P.S. 1972, Ap. J. (Letters), 176, L31.

4. Cowley, A.P., Crampton, D., and Hesser, J.E. 1977, Ap. J., 214, p. 471.

5. Hesser, J.E., Lasker, B.M., and Osmer, P.S. 1974, Ap. J., 189, p. 315.

6. Warner, B. 1973, M.N.R.A.S., 162, p. 189.

7. Cordova, F. 1980, preprint.

8. Greenstein, J.L. 1980, private communication.

9. Hayes, D.S. 1979, Dudley Obs. Report No. 14, p. 297.

10. Lynden-Bell, D. 1969, Nature, 233, p. 690.

11. Kurucz, R.L. 1979, Ap. J. Suppl., 40, p. 1.

12. Herter, T., Lacasse, M.G., Wesemael, F., and Winget, D.E. 1979, Ap. J. Suppl., 39, p. 513.

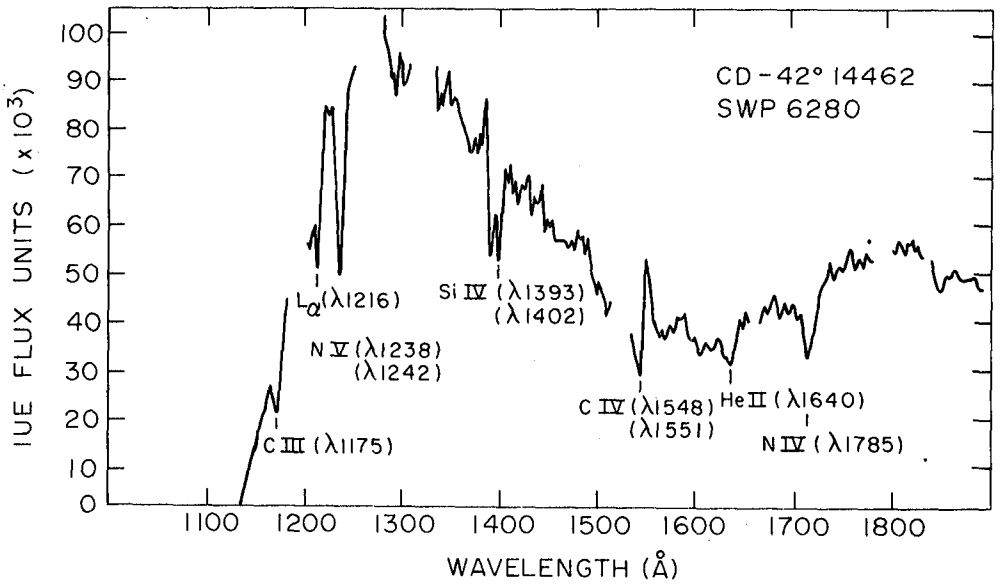

Figure 1: Short-wavelength IUE low-dispersion spectrum of CD-42°14462.

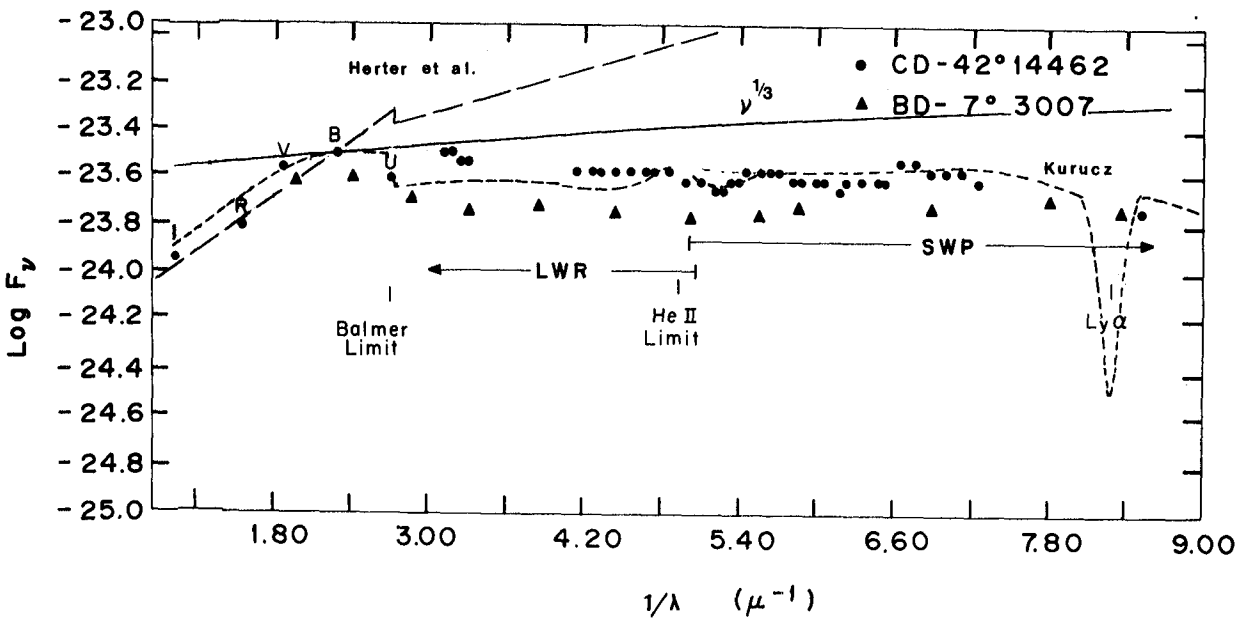

Figure 2: Flux plot of log F_ν vs. λ^{-1}. The small dash curve is a Kurucz model atmosphere for $T_{eff} = 16,000°K$; log g = 4.5, the large dash cruve is a Herter et al. accretion disk model ($\dot{M} = 10^{-7} M_\odot/yr$; i = 30°), and the solid curve is $F_\nu \propto \nu^{1/3}$. Optical fluxes are labelled with corresponding bandpass designations.

ORBITAL PHASE DEPENDENT IUE SPECTRA OF THE NOVA-LIKE BINARY TT ARIETIS

E. F. Guinan and E. M. Sion
Villanova University, Villanova, Pennsylvania 19085

ABSTRACT

We have obtained nine low-dispersion IUE spectra of the nova-like binary TT Ari over its 3^h17^m orbital period. Four short-wave spectra and five long-wave spectra exhibit marked changes in line strength and continuum shape with orbital phase. The short wave spectra show the presence, in absorption, of C III, Lyman α, Si III, N V, Si IV, C IV, He II, Al III, and N IV. C IV shows a P Cygni profile on two of the spectra. Implications of these spectra for the nature of nova-like variables will be discussed.

INTRODUCTION

The nova-like variable TT Ari (=BD + 14°341) was shown (ref. 1) to be a single line spectroscopic binary with orbital period P = 0.13755 days whose observed spectroscopic and photometric properties could be accounted for with the canonical model for cataclysmic variables; a low-mass red star losing mass through Roche lobe overflow to a disk surrounding a white dwarf primary. At the point of impact of the gas stream with the accretion disk, a hot spot is produced which also contributes to the light from the system.

Photometric studies have been reported (ref. 2, 3, 4) which show quasi-sinusoidal light variations with photometric period $P \simeq 0.1328$ days having an amplitude $\approx 0^m.2$ and quasi-periodic light variations with periods of $\approx 800^s$ and $\approx 40^s$ having amplitudes $0^m.1$ to $0^m.2$. Long term light variability ranging from $9^m.5$ to $11^m.8$ over a time interval of about a century are apparent from comparison with those magnitudes given in the BD catalogue to the value listed by Kukarkin et al. (ref. 5).

TT Ari has been observed as an X-ray source (ref. 6) by the Einstein satellite in the energy range 0.15 to 4.5 Kev. We report below on IUE spectra of TT Ari as a function of orbital phase which we have obtained as part of a survey of nova-like variables at ultraviolet wavelengths.

OBSERVATIONS

We have observed TT Ari through its orbit with the IUE satellite at low dispersion, both short and long wavelength spectra (1100Å to 3200Å). Table 1 lists the camera image number, aperture size, exposure time and time of mid-exposure expressed in universal time.

We have displayed the four short-wave spectra in figures 1-4. Absorption line features are present due to C III (λ1175), Lyα + He II (λ1216), N V (λ1240), O I + S III (λ1300), Si III (λ1394), C IV (λ1550), He II (λ1640) and Al III (λ1850). In SWP 6276 and SWP 6277 the Al III feature is not present. The long-wave spectra reveal few features that can be reliably considered real due to the noise level present. Not surprisingly, the contribution of the secondary star to the long-wave spectrum is not apparent, a fact in agreement with the optical spectra. We place an upper limit on the reddening $E(B-V) \sim 0.1$, based upon the lack of a detectable λ2200 absorption dip.

ANALYSIS AND DISCUSSION

The orbital phase coverage of our nine IUE spectra presents the opportunity to analyze variations in line strength, continuum flux levels and interfacing with the theoretical predictions of available binary models of cataclysmic variables. Using all of our spectra, the first ultraviolet light curve of the system is shown in figure 3. Ultraviolet fluxes at λ1800 and λ2400 are plotted versus time. In the same figure, we display a Fine Error Sensor (FES) light curve. The light variations shown in both the UV and FES light curves are consistent with the photometric period found previously (ref. 2). The shapes are also similar, but the amplitudes of the variation in both light curves are larger while the mean optical light level is lower than previous photometric studies by about $0^m.5$ (ref. 2). In figure 5, we plot the continuum fluxes for TT Ari taken from the SWP 6278 and LWR 5446 exposures near maximum light. The UBV fluxes in figure 5 are from the photometry in reference 2 where the magnitudes were normalized to value of $V_{max} = +11^m.90$ obtained from the FES measures. These were converted to absolute flux units with a calibration of Hayes (ref. 7). In the same figure we plot, for comparison, a $F_\nu \propto \nu^{1/3}$ flux distribution for a viscous steady state optically thick disk based upon local black body behavior, a model stellar atmosphere ($T_{eff} = 15,000$; $\log g = 4.5$) from Kurucz (ref. 8) and a steady state optically thick model accretion disk from the grid of Herter et al. (ref. 9) corresponding to a mass transfer rate $\dot{M} = 10^{-7} M\odot/yr$; $i = 30°$. It is apparent that the accretion disk fits are in rather large disagreement with the overall continuum. On the other hand, a Kurucz model atmosphere gives a reasonable fit to the data and implies an $T_{eff} \leq 20,000°K$. The lines exhibit an interesting phase behavior in the short-wave region. Spectra SWP 6275 and 6278 are near the same relative orbital phase (i.e. maximum light) and have essentially the same line features. Exposure SWP 6277 was obtained near minimum light and reveals weaker overall absorption lines and stronger emission in C IV, which has the appearance of a P Cygni profile. Spectrum SWP 6276 occurs at a relative phase intermediate between SWP 6275 and 6278. Cowley et al. (ref. 1) also find phase dependent changes in their optical spectra which they interpret as being caused by the changing aspect of the hot spot on the accretion disk of the primary, arising from orbital motion. They attribute the observed optical light variations to the same model. However, the presence of the P Cygni C IV feature strongly suggests some type of mass outflow from the system.

Our ultraviolet spectra raise several new puzzles about the nature of TT Arietis

and related objects. (1) Why are current disk models in disagreement with our continuum fluxes? Are the disk models unrealistic or is there an accretion disk present at all? If the latter is the case, all of the phenomena associated with a disk (e.g., rapid flickering, hot spot, etc.) must be discarded. (2) Are the strong absorptions arising from the disk, the stellar component or possibly the hot spot? What is the significance of the apparent phase dependence of the C IV P Cygni profile? Is it arising from a stream, a spherically outflowing stellar wind or from a disk? A resolution of some of these puzzles may be possible with a detailed analysis of the line strengths and shapes as a function of orbital phase at both maximum and minimum light. Would coverage of 2 or more consecutive orbits over an extended interval reveal the same phase dependent behavior as reported here? (3) If the interpretation of Cowley et al. (ref. 1) is correct why does the system not exhibit dwarf nova type outbursts? A more detailed analysis of this interesting system will be forthcoming.

REFERENCES

1. Cowley, A. P., Crampton, D., Hutchings, J. B., and Marlborough, J. M. 1975, Ap. J., 195, p. 413.

2. Smak, J., and Stepien, K. 1969, Nonperiodic Phenomena in Variable Stars, ed. L. Petre (Budapest: Academic Press), p. 335.

3. Sztajno, M. 1979, Inf. Bull. Var. Stars, No. 1710.

4. Mardirossian, F., Mezzetti, M., Pucillo, M., Santin, P., Sedmak, G., Cester, B., Giuricin, G., 1979, Inf. Bull, Var. Stars, No. 1622.

5. Kukarkin, B. V., Kholopov, R. N., Efremov, N. D., Kukarkina, N. P., Kurochkin, N. E., Medvedeva, G. I., Perova, N. B., Fedorovich, V. P., and Frolov, M. S. 1969, General Catalogue of Var. Stars (Moscow).

6. Cordova, F. 1980, preprint.

7. Hayes, D. S. 1979, Dudley Obs. Report No. 14, p. 297.

8. Lynden-Bell, D. 1969, Nature, 233, 690.

9. Kurucz, R. L. 1979, Ap. J. Suppl., 40, p. 1.

10. Herter, T., Lacasse, M. G., Wesemael, F., and Winget, D. E. 1979, Ap. J. Suppl., 39, p. 513.

TABLE I

IUE SPECTRA OF TT ARIETIS

Camera Number	Aperture	Exposure (min)	Time of Mid-Exposure AUG. 24.0 U.T. 1979
LWR 5445	Lg	15	24.4317
SWP 6275	Lg	10	24.4451
LWR 5446	Lg	8	24.4649
SWP 6276	Lg	9	24.4866
LWR 5447a	Lg	4	24.5051
LWR 5447	Sm	4	24.5266
SWP 6277	Lg	9	24.5363
LWR 5448	Lg	4	24.5558
SWP 6278	Lg	9	24.5786

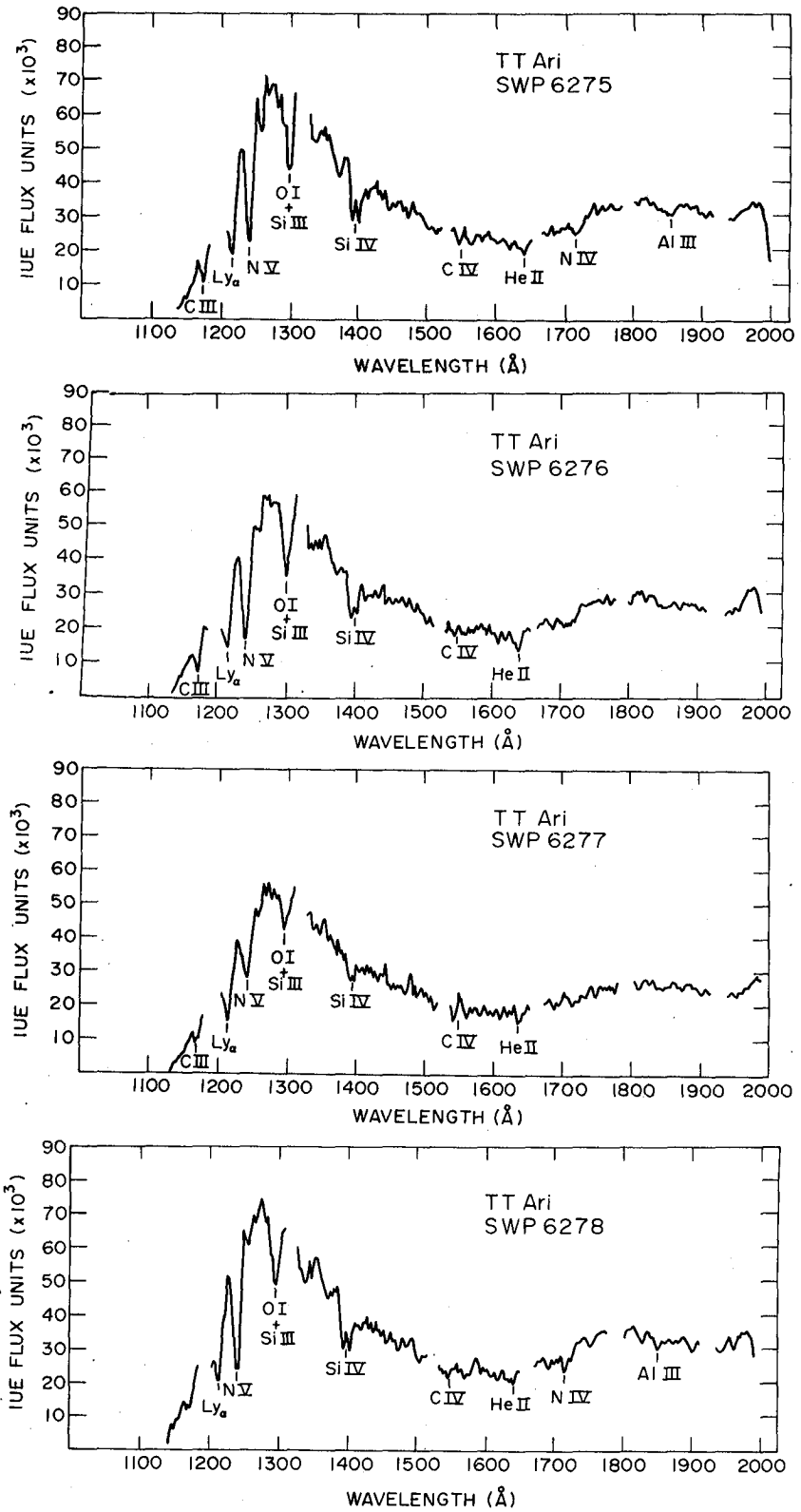

Figures 1-4: IUE flux plots of TT Arietis as a function of relative orbital phase plotted in IUE flux units vs. wavelength expressed in Å units.

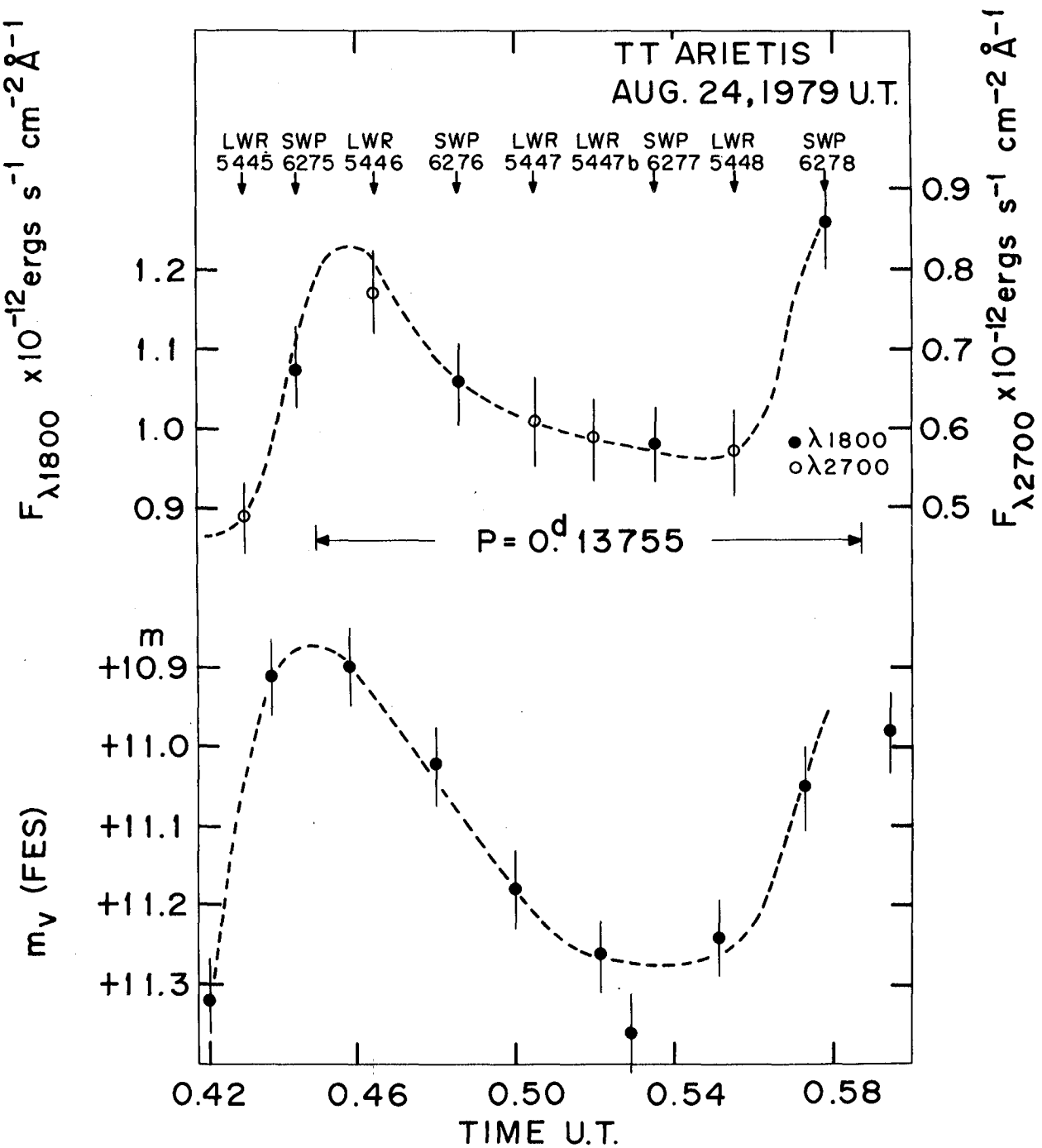

Figure 5:

Top panel of the figure shows a plot ot the λ1800 and λ2700 UV fluxes obtained over 100 Å bandpasses. The λ1800 and λ2700 fluxes were shifted in the figure to match at minimum light near Aug. 24.54 U.T. 1979. The times at which the various IUE spectra were obtained are also indicated in the figure. The apparent visual magnitude obtained with the FES on the satellite are also shown.

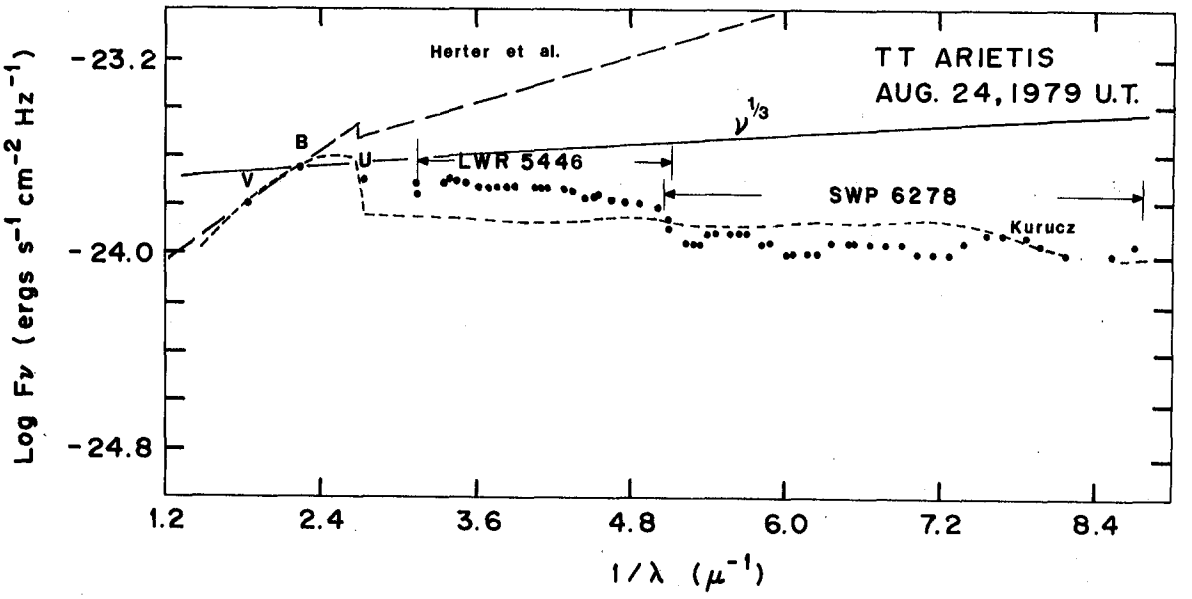

Figure 6:

Flux plot of log F_ν vs. λ^{-1}. The small dash curve is a Kurucz model atmosphere for T_{eff} = 16,000°K; log g = 4.5, the large dash curve is a Herter et al. accretion disk model, ($\dot{M} = 10^{-7} M\odot/yr$; i = 30°) and the solid curve is $F_\nu \propto \nu^{1/3}$. Optical fluxes are labelled with corresponding bandpass designations.

SEARCH FOR COLLIDING STELLAR WINDS IN PLASKETT'S STAR (HD 47129)

Sara R. Heap

Laboratory for Astronomy and Solar Physics
Goddard Space Flight Center
Greenbelt, MD 20771

ABSTRACT

High-dispersion spectra of Plaskett's star (HD 47129) were obtained with the short-wavelength spectrograph on IUE at five phases of the binary cycle. The unsaturated wind profiles, particularly those of Si IV λ1400, show complex, phase-dependent structure. Two interpretations for the structure are suggested, neither of which is entirely satisfactory: (1) the structure is a consequence of directed streams, and (2) the structure is a consequence of colliding winds from the primary and secondary.

INTRODUCTION

In the past 15 years, two observational discoveries from space have changed our way of thinking about OB stars. The first discovery, made by Morton (Ref. 1) and his colleagues at Princeton, was that OB giants have high-velocity winds. The second discovery, made by scientists using the Uhuru satellite (Ref. 2) was that some close binaries having an OB component emit x-rays. The interpretation of these observations is that the secondary is a compact object embedded in the wind of the OB giant, and x-rays are generated in the wake of the wind accreting onto the compact object. I don't think there is any doubt today that the massive x-ray binaries are associated with accretion by a compact object. Nevertheless, it is useful to think of other mechanisms of x-ray emission that do not involve a compact object. Prilutskii and Usov (Ref. 3) have, in fact, considered how x-rays might be generated in close binaries containing two O stars. They suggest that x-rays could be generated behind a shockfront formed where the wind of the primary collides either with the secondary itself, or with the wind of the secondary. It is this latter possibility -- the phenomenon of colliding winds -- that I wish to use as a framework for discussing Plaskett's star (HD 47129).

Let me first review the evidence that the two components of Plaskett's star do, in fact, have winds which may interact. Detailed studies of the visual spectrum (Ref. 4, 5, 6) indicate that Plaskett's star is a double-line spectroscopic binary whose components are both

O-giants. Table I summarizes some of the properties of the two components (Ref. 6). Although the spectral types are approximately the same (O7 I), their flux distributions differ, with the secondary appearing slightly cooler. In the red region of the spectrum, the primary and secondary are of approximately equal brightness, while in the blue spectral region, the primary is at least three times brighter. Spectra obtained with IUE indicate that in the ultraviolet, only the primary is visible, as indicated by the fact that "photospheric" lines like N IV λ1718 show radial-velocity variations which follow the radial-velocity curve of the primary (although shifted to shorter wavelengths by about 200 km/sec). The IUE observations also indicate that the primary has a wind typical of those of O giants with a terminal velocity of 2500 km/sec. Since the visual spectrum of the secondary is similar to that of the primary, and since the mass and radii of the two stars are similar (Ref. 6), I assume that the secondary also has a high-velocity wind.

Consequences of Colliding Stellar Winds

If this is the case, it seems worthwhile to develop the observable consequences of colliding stellar winds and to compare these predictions with observation. One potentially observable consequence of colliding stellar winds is, of course, the generation of x-rays. Cooke, Fabian and Pringle (Ref. 7) have predicted measurable x-ray luminosities of six binaries, including HD 47129, in which both stars are thought to be O stars undergoing mass-loss. Fabian, in fact, has observed Plaskett's star with HEAO-2, and I just found out yesterday the outcome of these observations: HD 47129 is an x-ray source with an x-ray luminosity of 6×10^{32} ergs per sec. This luminosity is two orders of magnitude below Cook et al.'s predictions. In fact, it is equivalent to x-ray luminosities of garden-variety single stars. Another potentially observable consequence of colliding winds is the alteration of the properties of the winds. The theory has not been developed in any quantitative manner, but it is not hard to see at least qualitatively how this alteration might go. In the absence of a companion, the O giant has an accelerating wind. The predominant species in the wind are ions like N V, Si IV, C IV which scatter stellar photons, thereby producing the P Cygni-type features typical of O-type ultraviolet spectra. Now consider how a companion with a wind modifies the situation (Figure 1). According to Prilutskii and Usov, a highly ionized cavity will form where the two winds collide. The presence of the cavity may be detectable through its effect primarily on the ionization law and secondarily, on the velocity law of the stellar wind. The ionization law describes how the number of ions capable of scattering varies with velocity in the wind. Because N^{+4}, Si^{+3}, C^{+3} are ionized to higher stages in the cavity, the P Cygni profiles of N V, Si IV, C IV are modified at the wavelengths corresponding to the velocities of the cavity. The velocity law describes how the velocity increases with distance. It may also be modified by the high-ionization cavity since the ions in this cavity have

TABLE I

PROPERTIES OF HD 47129
(taken from Ref. 6)

Period = 14.439601 days

$K = \begin{cases} 200 \text{ km/s (He II, Si IV, He I lines)} \\ 162 \text{ km/s } (H\gamma) \end{cases}$

$M_1 \approx M_2 \approx 55\ M_\odot$ or more

$R_1 \approx R_2 \approx 20\text{-}25\ R_\odot$

Distance between stars $\gtrsim 100\ R_\odot$

$\dot{M} \approx 2 \text{ to } 8 \times 10^{-6}\ M_\odot$ per year

no resonance transitions accessible to the stellar photons and hence, radiatively-driven acceleration is not possible in the cavity. The main effect, then, of the high-ionization cavity is the appearance of structure in a P Cygni profile. Furthermore, the appearance of structure should be phase-dependent: the profile should remain unaltered at phases 0.5 to 1.0 since the line of sight from the primary to the observer does not pass through the cavity, while it should be altered at phases 0.0 to 0.5.

IUE Observations

The IUE spectra show evidence for phase-dependent structure in some of the wind profiles, most notably Si IV and C IV. These two features are formed by scattering material over the full range of velocities, but because they are not fully saturated, they are still sensitive to anomalies in the ionization law. Figures 2 and 3 show the profiles of the Si IV and C IV wind features at four phases covering nearly half of the orbital cycle. (I should note that a good deal of care was taken in deriving the observed profiles so as to insure that the reduction process itself would not be a source of spurious structure. In particular, the interorder background was smoothed by a 31-point median filter followed by two 15-point running averages before it was used to obtain the net fluxes. In addition, the echelle ripple "constants" were derived for each profile by trial and error until the three orders containing a given profile overlay one another in the wavelength intervals where they overlapped. In no case did the constants used in the standard reduction procedure suffice!) For comparison, the top of each figure shows the profiles of these two features as calculated from the formulae and tables of Castor and Lamers (Ref. 8). Examination of Figures 2 and 3 shows the development of structure in the Si IV wind profile until at phase, $\phi = .47$, three sets of absorption features are visible, or alternatively, until two sets of "lack-of-absorption" features are visible. The radial velocities of these features are given in Table II. Although less dramatic, the C IV feature shows the development of "lack-of-absorption" midway in its profile at phase, $\phi = .64$.

The structure of these lines is open to several interpretations, none of which is entirely satisfactory. One, which follows along the lines of Struve, Sahade and Huang's interpretation of the visual spectrum, is that the wind of the primary contains directed streams which account for the sharp absorption components of the Si IV profile. If the velocity law for the components is the same as for the rest of the wind, then these streams extend out to 1.6 stellar radii. It is hard to understand how these streams could remain so contained with so little velocity dispersion out to such large distances. Another interpretation, which follows along the lines of the colliding wind hypothesis, is that the structure of the wind profiles is due to the "lack of absorption" caused by the erasure of Si^{+3} and C^{+3} in the high-ionization cavity. A simple model for the high-ionization cavity, such as that shown in

TABLE II

Measured Radial Velocities from SWP 4819 (ϕ = .37)

ID	Velocity (km/s)	Remarks
Si IV λ1393.755	-1550	Sharp
	-1190	Sharp
	-370	Broad
	+48	Sharp, interstellar
Si IV λ1402.769	-1570	Sharp
	-1140	Sharp
	-460	Broad
	+45	Sharp, interstellar

Figure 1, does not explain the observed phase-variations, but surely the geometry of the cavity must be more complicated than this simple model. The development of a more realistic model that includes the angular momentum of the system and possibly unequal rates of mass-loss from the two components would appear to be a fruitful line of research.

REFERENCES

1. Morton, D. C. 1967, Ap. J. 150, 535.

2. Giacconi, R. and Ruffini, R., Eds., Physics and Astrophysics of Black Holes and Neutron Stars, North-Holland, Amsterdam, 1978.

3. Prilutskii, O. F., and Usov, V. V. 1976, Soviet Ast. 20, 2.

4. Abhyankar, K. D. 1959, Ap. J. Suppl. 4, 157.

5. Struve, O., Sahade, J. and Huang, S.-S. 1958, Ap. J. 127, 148.

6. Hutchings, J. B. and Cowley, A. 1976, Ap. J. 206, 490.

7. Cooke, B. A., Fabian, A. C. and Pringle, J. E. 1978, Nature 273, 645.

8. Castor, J. I. and Lamers, H. J. G. L. M. 1979, Ap. J. Suppl. 39, 481.

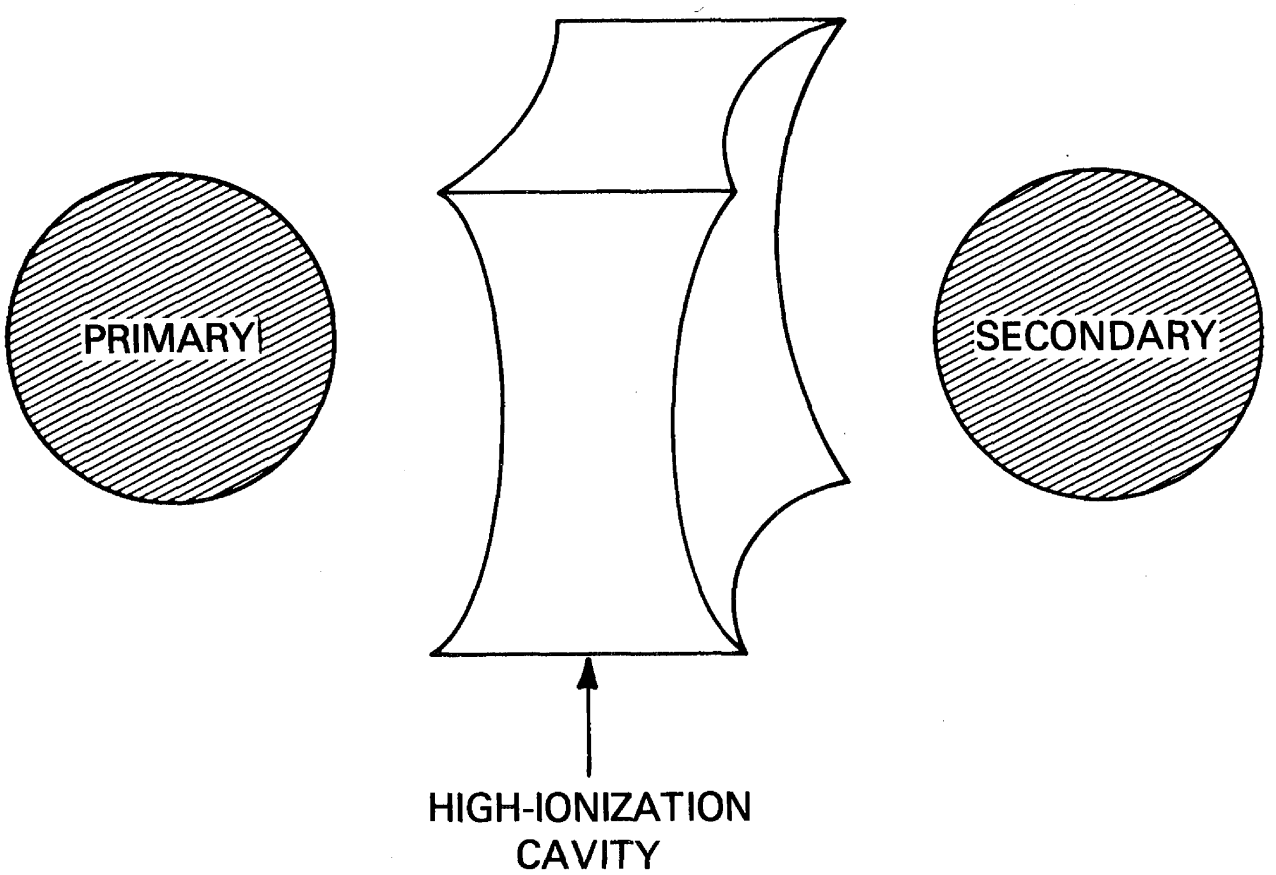

Figure 1

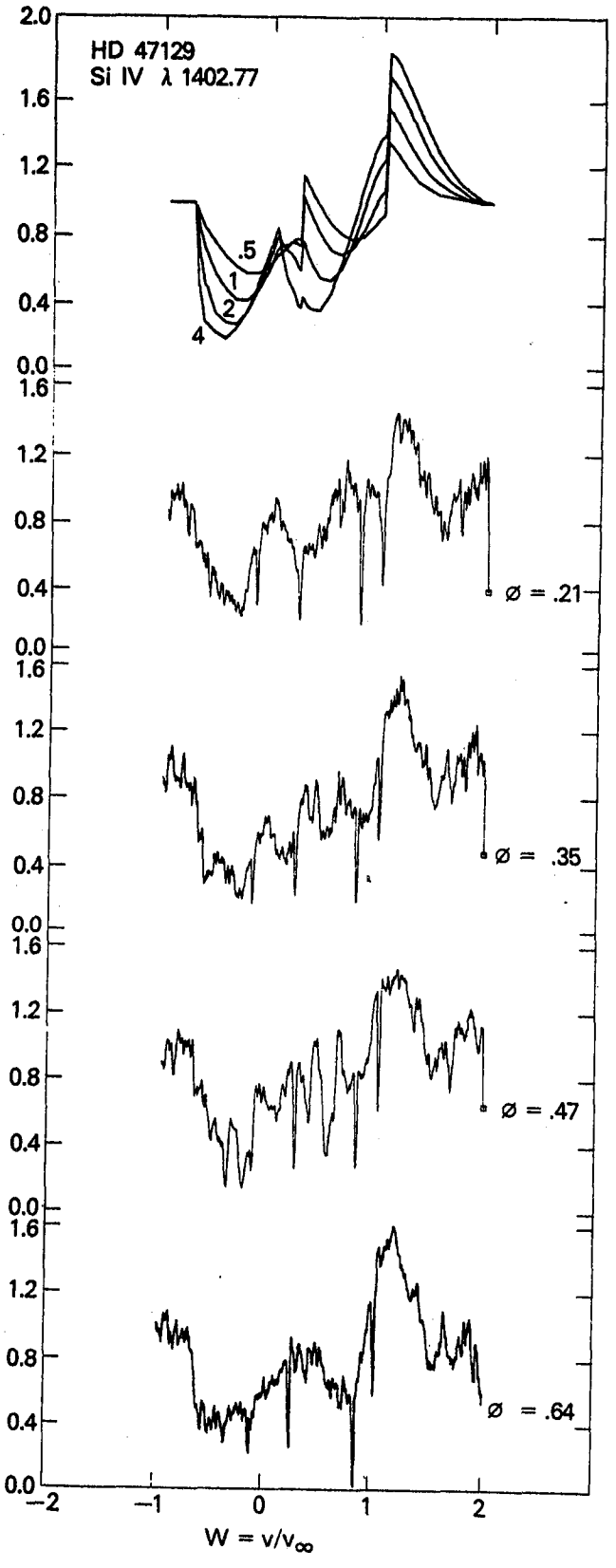

Figure 2

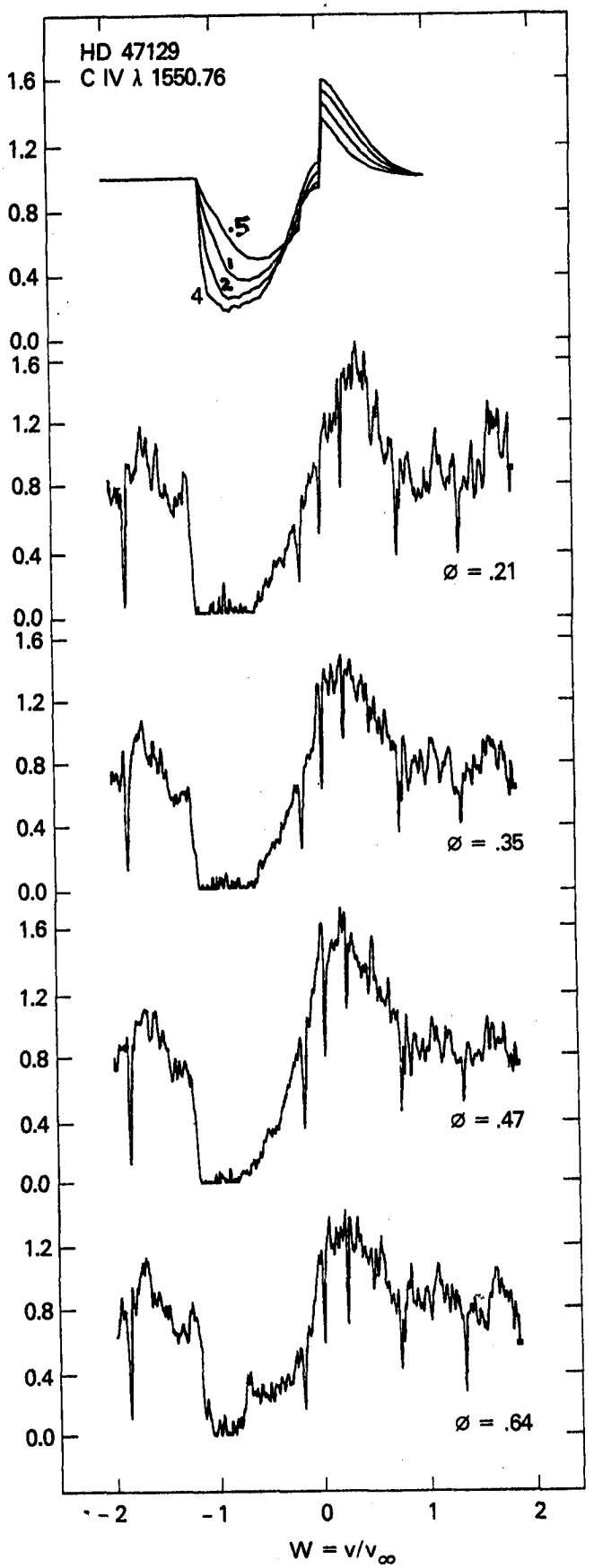

Figure 3

OBSERVATIONS OF CATACLYSMIC VARIABLES WITH IUE*

L. Hartmann and J. Raymond
Harvard-Smithsonian Center for Astrophysics
Cambridge, MA 02138

ABSTRACT

We report observations of the cataclysmic variables AN UMa, 2A0311-227, VV Pup, DQ Her, and GK Per made with IUE. We have been able to detect continuum emission in the short-wavelength (λ 1180-1950) region in DQ Her. This object exhibits a quasi-blackbody ($\sim \nu^2$) spectrum at short wavelengths; such blackbody components are a common property of the variables AM Her, SS Cyg, and U Gem, suggesting an underlying similarity in the activity of these diverse systems. "Flat" continuum components at longer wavelengths in general are not compatible with standard disk models. The emission line ratios in AE Aqr are anomalous, in that C IV is absent to a very low level relative to N V.

INTRODUCTION

Ultraviolet spectroscopy of cataclysmic variables is yielding a much different perspective on the nature of such objects than that obtained from optical and X-ray observations. In another paper (ref. 1) we have discussed the UV spectra of AM Her, SS Cyg and U Gem. Although these objects have quite different optical characteristics, they all exhibit blackbody components of UV emission with temperatures in the range 10 eV -40 EV. Here we examine the spectra of several other cataclysmic variables in order to study the ultraviolet emission through a wider range of stellar properties.

OBSERVATIONS

a) DQ Her

The object Nova DQ Her (1934) has been well studied photometrically and spectroscopically (refs. 2, 3, 4). Optically, it is a single-lined binary with a period of 4^h30^m. Periodic oscillations indicate that the white dwarf has a rotational period of 71 sec. Narrow emission lines arise from a nebular shell ~ 20" in diameter; He II λ4686 and high Balmer series lines follow the radial velocity variation of the hot object. These lines are doubled, with a separation ~ 650 km s^{-1} (ref. 4), interpretable in the standard way as emission from a rapidly rotating disk.

In Fig. 1 we show a 165 min. exposure on DQ Her taken through the large aperture at low dispersion. The spectrum is composed of a curving continuum upon which emission lines of N V, C IV, Si IV, He II, and C II are superimposed.

*Supported in part by NASA Grants NSG 5370 to the Harvard College Observatory and NAG-5-5 to the Smithsonian Astrophysical Obesrvatory.

The line ratios are very similar to those observed in AM Her. In addition, the continuum shapes are similar in DQ Her and AM Her. The ubiquitous blackbody emission appears as a Rayleigh-Jeans distribution rising for $\lambda < 1500$Å. The similar emission seen in AM Her, SS Cyg and U Gem was interpreted by Fabbiano *et al.* (ref. 1) as the result of nuclear burning of the accreted material.

Kraft (ref. 3) inferred the presence of an ultraviolet component with a blackbody temperature ~ 8 eV in an attempt to account for the λ4686 emission by photoionization. Our results indicate a temperature $\gtrsim$ 10 eV. However, we are unable to account for all of the λ1640 emission by recombination following photoionization by the blackbody component. As discussed by Fabbiano *et al.* (ref. 1), if the ν^{-2} component of the continuum and the λ1640 emission are both produced by optically thick cool gas illuminated by the black body, the λ1640 equivalent width is a simple function of black-body temperature. The maximum predicted equivalent width is $\lesssim$15Å, while the observed value is 40Å. Therefore either the emitting gas is optically thin to continuum radiation (ref. 5) or the λ1640 emission is produced by a mechanism other than recombination following photoionization by the blackbody component.

One clear difference of the DQ Her spectrum from that of AM Her is in the line widths. In AM Her the emission in He II λ1640 comes from a narrow component of 80 km s^{-1} width and a broad component ~ 600 km s^{-1} wide (ref. 6); this corresponds nicely with the optical observations of λ4686 (ref. 7). The optical profile of λ4686 in DQ Her is doublepeaked, with a separation of ~ 650 km s^{-1} between components (refs. 3, 4). The low-dispersion resolution of IUE is ~ 1000 km s^{-1} at λ1640, so that it is difficult to determine the expected line width. The λ1640 profile of DQ Her is marginally broader than that of AM Her, formally suggesting a line width ~ 800 km s^{-1}, which is consistent with the optical data within observational errors.

However, there is no question that the C IV, Si V, and N V profiles are much wider in DQ Her than in AM Her. From the C IV and N V widths we estimate a velocity width ~ 1400 km s^{-1}. Thus we have evidence of the manner in which the temperature of the disk decreases with increasing distance from the star.

The similarity of line strengths between AM Her and DQ Her, despite the fact that AM Her shows no evidence for a disk accretion pattern, demonstrates that the excitation of the ultraviolet emission is not controlled by the geometry of the flow.

We have also detected nebular emission from the expanding nova shell in C II λ1335 and C III] λ1909. The image of the 10" x 20" large aperture is barely visible on the photowrite image. From the line-by-line spectra we estimate fluxes of 4.7 and 1.2 x 10^{-14} erg cm^{-2} s^{-1} in λ1335 and λ1909 respectively from about one-half of the nebula. We do not detect the C I λ1656 emission predicted by Ferland and Turan (ref. 8), but the upper limit of ~ 2 x 10^{-14} erg cm^{-2} s^{-1} is within the two order of magnitude uncertainty of the prediction. The C II and C III emission probably arise from the relatively hot component of nebular gas which emits the [N II] and [O II] lines (ref. 9) rather than the cold, recombining gas, because recombination from the ground state of C III to the

$2s2p^2$ upper level of λ1335 would require a two-electron transition.

b) AN UMa and GK Per

AN UMa is an "AM Her"type system, i.e. a 1- to 3-hour binary consisting of a magnetic (10^7 - 10^8g) white dwarf accreting matter from a red dwarf. The SWP spectra of AN UMa, VV Pup and 2AO311-227 (the 3 AM Her types other than AM Her) all look remarkably similar when scaled with optical brightness.

The spectrum of AN UMa is shown in Fig. 2. While it has strong C IV, N V, and He II emission as in DQ Her, there appears to be little if any continuous emission. Rather, much of the spectrum appears to be composed of weak emission lines. This statement appears to be firm despite the low signal-to-noise ratio of the exposure on the basis of intercomparison of two separate exposures.

There is some evidence for an asymmetric profile of C IV in AN UMa as well as in DQ Her; with some extra emission on the short-wavelength side. What significance this asymmetry has is not known. The spectrum of 2AO311-227 is very similar to that of AN UMa.

In Fig. 3 we show the spectrum of the old nova GK Per (Nova Per 1901). Despite the weakness of the exposure, it is clear that the C IV emission is relatively weak viewed against the neighboring "pseudo-continuum" when compared with AN UMa. The emission structure appears to have similarities to AN UMa, particularly in a possible N V emission followed by an "absorption" dip ~ 1250-1270Å.

Of particular interest is the rough similarity of the GK Per spectrum to that of the hot UV stellar source in the center of the globular cluster NGC 6624 which has been identified with the bursting X-ray source (ref. 10). Although the spectrum is again quite weak, multiple long exposures indicate some evidence for the "absorption" dip at 1250- 1270,Åas well as a general lack of prominent emission lines.

The nature of the spectra in AN UMa and GK Per suggest an optically thin emitting region in the accretion disk. Our interpretation of the blackbody component as the result of nuclear burning on the white dwarf suggests that the difference in short-wavelength continuum is primarily due to the differences in how the accreted material arrives on the white dwarf surface.

c) AE Aquarii

The short wavelength spectrum of AE Aquarii is much different from those of the strong emission line objects discussed above in that N V and Si IV are extremely strong, while C IV is barely detected. One possible explanation is an abundance anomaly. Another is an emitting region extremely optically thick in the lines, as discussed for the Balmer lines by Williams (ref. 5). The relative intensities of N V and C IV can be explained if the lines are formed at temperatures of 16,000K and 10,00K respectively, as might be expected for cool gas illuminated by X-rays (ref. 11). The emitting area required is sensitive to the temperatures of formation, but it is consistent with reasonable sizes for an accretion disk.

REFERENCES

1. Fabbiano, G., Hartmann, L., Raymond, J., Steiner, J., and Branduardi- Raymont, G. 1980, submitted to *Ap J.*
2. Greenstein, J. L. and Kraft, R. P. 1959, *Ap. J.* 130, 99.
3. Kraft, R. P. 1959, *Ap. J.*, 130, 110.
4. ----1964, *Ap. J.*, 139, 457.
5. Williams, R. E. 1980, *Ap. J.*, 235, 939.
6. Raymond, J. C., Black, J. H., Davis, R. J., Dupree, A. K., Gursky, H., Hartmann, L. and Matilsky, T. A. 1979, *Ap. J. (Letters)*, 230, L95.
7. Greenstein, J. L., Sargent, W. L. W., Boroson, T. A. and Boksenberg, A. 1977, *Ap. J. (Letters)*, 218, L121.
8. Ferland, G. J. and Truran, J. W. 1980, preprint.
9. Williams, R. E., Woolf, E. K., Hege, E. K., Moore, R. L. and Kopriva, D. A. 1978, *Ap. J.*, 224, 171.
10. Dupree, A. K., Hartmann, L., Black, J. H., Davis, R. J., Matilsky, T. A., Raymond, J. C. and Gursky, H. 1979, *Ap. J. (Letters)*, 230, L89.
11. Hatchett, S., Buff, J. and McCray, R. 1976, *Ap. J.*, 206, 847.

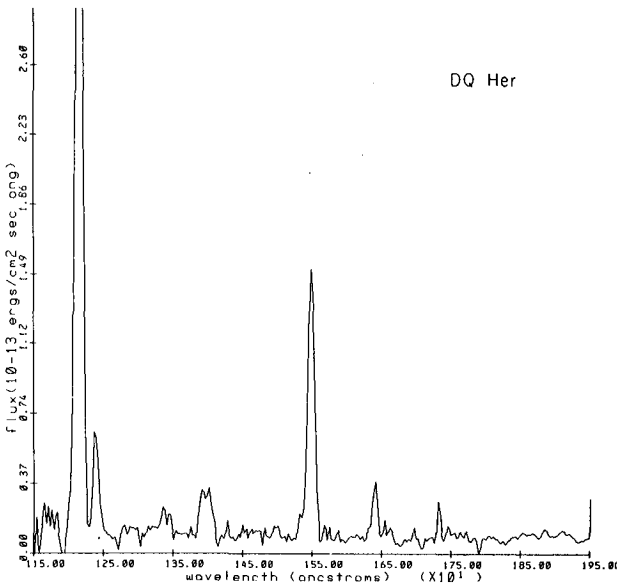

Figure 1

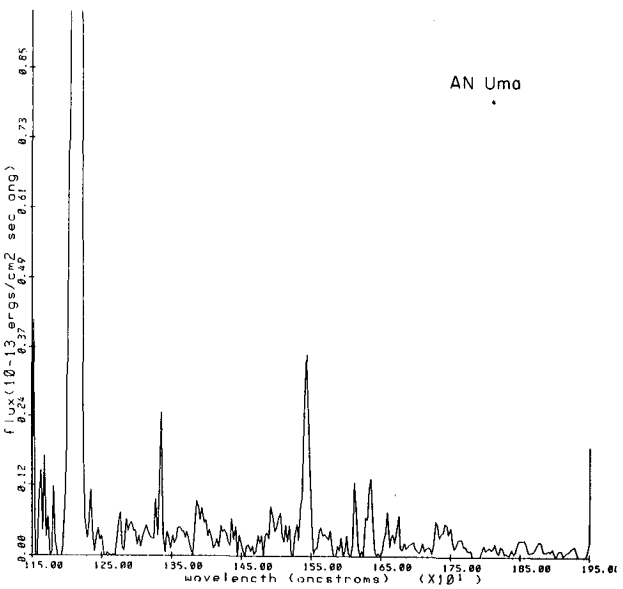

Figure 2

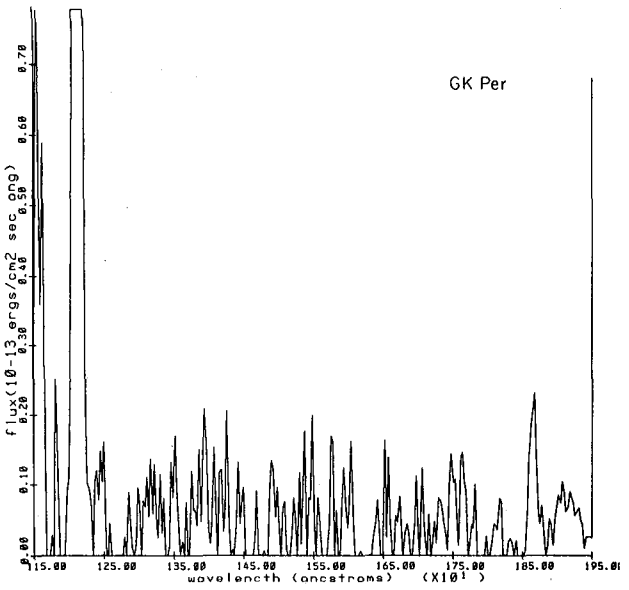
GK Per
flux(10-13 ergs/cm2 sec ang)
0.00
0.10
0.20
0.30
0.40
0.50
0.60
0.70
115.00
125.00
135.00
145.00
155.00
165.00
175.00
185.00
wavelength (angstroms) (X10¹)

Figure 3

COORDINATED IUE, EINSTEIN AND OPTICAL OBSERVATIONS OF ACCRETING DEGENERATE DWARFS*

G. Fabbiano, J.E. Steiner**, L. Hartmann and J. Raymond
Harvard-Smithsonian Center for Astrophysics

ABSTRACT

Three binary systems believed to be composed of a white dwarf and a late type star, AM Her, SS Cyg and U Gem, were observed simultaneously in the UV X-ray and optical wavelengths. AM Her was in its customary high state at the time of the observations, while SS Cyg and U Gem were in a low state. In all three cases, a significant UV black body component with $\underline{KT} \gtrsim 10$ eV was found. The flux in this component is in excess of the amount predicted by current scenarios of gravitational energy release.

We compare our observations of these objects with the data available in the literature, and we suggest an alternative scenario that would explain their general behavior.

INTRODUCTION

AM Her, U Gem, and SS Cyg are believed to be binary systems consisting of a late type star and of a more massive white dwarf. Optically they can be found in either a high emission state ($m_v \cong 12$, 8.1, 8.8 for AM Her, SS Cyg and U Gem respectively) or a low emission state ($m_v \cong 15$, 21.1, 14.4). SS Cyg and U Gem are optically quite similar, undergoing quasi-periodical outbursts lasting a few days. AM Her instead is found typically in the high emission state. These systems have all been detected in the X-rays. The mechanism of X-ray emission is generally believed to be radial accretion on the white dwarf. The three systems chosen for this study represent different kinds of accreting white dwarfs. AM Her has an intense magnetic field ($B \sim 10^8$G) (ref. 1) and because of this, it is believed to have no accretion disk and to be powered by an accreting column at the magnetic pole of the white dwarf. Optical spectroscopy shows that both SS Cyg and U Gem are associated with accretion disks. The X-ray behavior of SS Cyg has lead to an estimate of a magnetic field $B \sim 10^6$G associated with the white dwarf (ref. 2) No estimate of B has so far been produced for U Gem. The fact that

---

*Supported in part by NASA under contracts NAS8-30751 and NAS8-30453 and grants NAG 5-5 and NSG 5370.

**Also IAG-Universidade de Sao Paulo, Brazil under contract FAPESP(03) 79/0629.

the hard X-ray luminosity of U Gem is at least one order of magnitude smaller than that of SS Cyg suggests different magnetic field intensities and/or accretion rates in the two systems. The comparative study of these three accreting degenerate dwarfs should then give us information that can put interesting constraints on the theory for different values of the parameters of the systems.

In this paper, we report the results of coordinated observations in the optical/UV/X-rays of AM Her, U Gem and SS Cyg, and we compare our findings with the existing theoretical predictions. The simultaneity or quasi-simultaneity of our observations in the different energy bands allows us a straightforward, unambiguous comparison with the theory. For a more detailed discussion, see ref. 3.

OBSERVATIONS

A description of the X-ray instruments on board the Einstein Observatory may be found in ref. 4; for a description of the International Ultraviolet Explorer, see ref. 5.

AM HER

AM Her was observed with the 500 lines/mm Objective Grating Spectrometer in front of the High Resolution Imager (HRI) onboard the Einstein Observatory on March 17, 1979. The OGS allows us to obtain spectral information, which otherwise are not provided by the HRI. The soft X-ray spectrum of AM Her obtained from the OGS observations does not show any line contribution (Seward 1979, private communication). It is consistent with a black body radiation with KT ~ 30-40 eV (Heise 1980, private communication). The X-ray properties are summarized in Table I.

The short-wavelength spectra are spaced fairly uniformly over two orbital cycles. They confirm the suggestion of Raymond et al. (1979a) (ref. 6) that the UV continuum is the sum of two power law components. The $F_\nu \propto \nu^{-1}$ component is always present while the $F_\nu \propto \nu^2$ component disappears in phase with the X-ray eclipse. The UV continuum may be separated into the two components as shown by Raymond et al. (1979b) (ref. 7). The $F_\nu \propto \nu^2$ component may be interpreted as the Rayleigh-Jeans tail of the $\sim$ 30 eV black body which produces the soft X-ray emission.

U GEM

U Gem was observed on April 29, 1979 for 1,170s with the Imaging Proportional Counter (IPC) onboard the Einstein Observatory. This observation occurred 20 minutes after $\sim$ 8 hours of observation with the IUE satellite, during which six spectra of the source were taken. Each one of the IUE spectra was exposed from 40 to 60 minutes. U Gem was reported by the AAVSO to be in an optical low state at about m_v = 14.2 at the time of the X-ray and ultraviolet observations.

From a comparison of the hardness ratios of U Gem and SS Cyg, we find that the X-ray spectrum of U Gem at minimum appears to be softer than that of SS Cyg (KT ~ 20 keV). We define the hardness ratio as the ratio of the counts in the ($\gtrsim$ 1-4) keV band to those in the (< 1 keV) band. The IPC hardness ratio of U Gem is <.4 while that of SS Cyg is $\sim$ 1.7. The hardness ratio of SS Cyg has been calculated using unpublished IPC data taken in 1978 December, during an optical low state.

The (.5 - 4 keV) luminosity of U Gem is $1.3 \pm .2 \times 10^{30}$ erg s^{-1} for a distance of 76 pc (ref. 8). The X-ray observations show clear presence of variability. The X-ray intensity appears to decrease during the length of the observation; a feature involving a decrease of the intensity in a smaller time scale is also present. A χ^2 test shows that the data are definably incompatible with the hypothesis of constant intensity for time scales greater than 2 minutes.

The average of five short-wavelength IUE spectra is shown in Figure 4. In contrast to AM Her and SS Cyg (see below) the spectrum exhibits only absorption lines on a strong continuous background. There are no emission lines (the Lyα feature is very likely only geocoronal) while absorption lines of OI, CII, SiIV, CIV and HeII are present. A broad Lyα absorption line with a width $\Delta\lambda \sim 70$Å is also present.

Fig. 7 shows the composite spectrum of U Gem. A strong UV component can be seen with $f_{uv} \gtrsim 200\ (f_{opt} + f_x)$, assuming a UV temperature $\gtrsim$ 10 eV. For the distance found by Wade (1979) (ref. 8) the UV emitting area is between 3% and 15% of the canonical white dwarf projected surface. These facts, together with the facts that no strong and hard X-ray and no UV emission lines are seen, indicate that the UV component comes from the inner region of the disk (boundary layer) or from the accreting belt.

SS CYG

SS Cyg was observed simultaneously with the Einstein Observatory and the IUE satellite on May 17, 1979. The X-ray observation was done with the HRI/OGS (1000 lines/mm grating) in the focal plane of the telescope and lasted 9.9 hr. The total observing time, because of Earth occultation and other data gaps is 3.4 hr; of these about 2 hr are simultaneous with the observations in the ultraviolet. The IUE observations cover a total time of about 6 hr within the X-ray observing time. A total of nine low-dispersion long-wavelength spectra were taken, four of which are simultaneous to X-ray observations. SS Cyg was monitored by the AAVSO and appeared to be in an optical low state at the time of the Einstein and IUE observations, at a magnitude between 11.3 and 12.0. Szkody (1979, private communication) observed the source photometrically simultaneously with the Einstein and IUE observations.

The X-ray, UV and optical observations are summarized in Tables I and II. The MPC data are consistent with an exponential spectrum with kT = 10-30 keV and no significant low energy cut-off. The 2-6 keV intensity of SS Cyg is $(4.4 - 5.8) \times 10^{-11}$ erg cm^{-2} s^{-1}.

The average IUE spectrum of SS Cyg is shown in Figure 2. The emission lines are the same as the ones observed in AM Her, but the line/continuum ratios appear to be smaller. The main difference with the AM Her UV spectrum is in the presence of a broad Lyα absorption line. We measure a width for this line of $\Delta\lambda = (45 \pm 5)$Å.

The composite spectrum of SS Cyg during the May 17 observation is plotted in Figure 6. Here again, as in the case of AM Her, the UV data can be interpreted in terms of two components: a $\nu^{-1.3}$ power law that extends through the optical points and a ν^2 component that is predominant at the short wavelengths and could be representative of the Rayleigh-Jeans end of a black body spectrum.

The similarity between the AM Her and SS Cyg UV spectra suggests that SS Cyg, like AM Her, has magnetic funneling. This is consistent also with the hard X-ray emission at minimum. In maximum, however, the picture (fig. 3) is more like U Gem, which, we suppose, has an accreting disk. This difference can be explained by the higher accretion rate at maximum, when the Alfvèn radius is of the order of the star radius.

DISCUSSION

Despite previous work that indicates that AM Her, U Gem and SS Cyg have substantially different accretion patterns, they possess one outstanding similarity. All of these cataclysmic variables have an UV short wavelength component of their continuum spectrum which follows a $\sim \nu^2$ power law. This component had already been noticed in the spectrum of AM Her (ref. 6); our new observations show that it is also present in SS Cyg and in U Gem in quiescence. As discussed by Raymond et al. (1979a)(ref. 6), if this feature represents the Rayleigh-Jeans end of a black body with temperatures of the order of 20-30 eV (see also ref. 9), the UV and soft X-ray luminosity of AM Her would be far greater than its hard X-ray luminosity. As is apparent from our data (Figure 5, 6 and 7 and Table 2), the same is true in the case of SS Cyg and U Gem. This property disagrees with models of emission purely from gravitational accretion, both with and without magnetic fields (ref. 10, 11). A possible resolution of this problem is the action of nuclear burning. Kippenhahn and Thomas (1978) (ref. 12) have shown that it is possible to have localized burning in dwarf novae. They also suggested that the different geometry could alter the condition for unstable burning which plays a crucial role in current nova theories (ref. 13, 14). Moreover, the possibility of stable slow burning involving the p-p reaction instead of CNO burning is currently being investigated (Starrfield 1980, private communication). The results so far are very encouraging although detailed dynamical calculations applied to the particular dwarf novae configuration have not yet been performed. The action of nuclear burning on the X-ray flux in a radially symmetric accreting white dwarf has been investigated by Katz (1977) (ref. 15) and more recently by Weast et al. (1979) (ref. 16).

Our findings can be resumed as follows:

1) We have discovered the presence of a strong excess UV radiation in SS Cyg and U Gem. For U Gem we show that this radiation, for the most likely parameters for the system (ref. 8), is likely to originate from the boundary layer of the accretion disk. The luminosity of the UV component is 200 times larger than the combined optical and X-ray emissions. This is inconsistent with the traditional picture of gravitational accretion. We suggest that such a large UV flux might originate from nuclear burning (refs. 12, 16) (Sparks 1980, private communication) at the surface of the white dwarf in the vicinity of the disk boundary layer. A possible black body component of the UV flux similar to the one in U Gem is seen also in AM Her (confirming previous observations by Raymond et al. 1979a)(ref. 6) and in SS Cyg. Although the UV excess in these two systems is not as high as the one seen in U Gem, it is not possible to explain it in terms of the current theoretical framework (refs. 10, 17). In both cases the UV emitting area is of the same order of the X-ray emitting area, and in AM Her, in particular, the black body UV flux is eclipsed in phase with the X-ray flux. We suggest that nuclear burning of the accreted material might also happen in SS Cyg and AM Her and be responsible for the excess.

2) If nuclear burning is responsible for the UV black body excess, we find that AM Her, SS Cyg, and U Gem can be explained within a scenario of accretion in different magnetic regimes. A strong magnetic field ($\sim 10^8$G) in AM Her would be responsible for polar radial accretion, as suggested by many authors (see review of Chiappetti et al. 1980, ref. 18 and references therein). A re-examination of the data collected on SS Cyg both at maximum and at minimum, together with our new observations, shows the presence of a magnetic field $\sim 10^5 - 10^6$G, as suggested by Ricketts et al. (1979)(ref. 2). SS Cyg at minimum looks remarkably similar to AM Her, consistent with a picture of polar magnetic accretion. But the magnetic field is not so intense as to inhibit completely the formation of a disk, as shown by the observations of Walker and Chincarini (1968) (ref. 19). The increased accretion at maximum causes the magnetosphere to move closer to the white dwarf with the consequent building up of a disk. In U Gem instead, the magnetic field is so low as to make polar accretion impossible even at a minimum, as shown by the lack of emission lines in the UV.

TABLE 1
X-RAY OBSERVATIONS

	Start and Stop Times 1979 (UT)	Instrument	Energy Band (keV)	Flux (erg $cm^{-2}s^{-1}$)	D (pc)	L_x(erg s^{-1})
AM Her	$76^d\ 23^h\ 23^m\ 2^s$ $77^d\ 1^h\ 43^m\ 40^s$	HRI/OGS (500) MPC	.1 - 4.5 2 - 6	3.2×10^{-10} ± 15% (ON time) 1.0×10^{-11} ± 15% (eclipse) $(6.6 \pm .2) \times 10^{-11}$ (ON time) * (eclipse)	100	3.6×10^{32}
U Gem	$119^d\ 1^h\ 34^m\ 16^s$ $2^h\ 20^m\ 41^s$	IPC MPC	.5 - 4.5 2 - 6	$(2.0 \pm .2) \times 10^{-12}$ $<2.5 \times 10^{-11}$ (3σ)	76 (2)	1.3×10^{30} $<1.6 \times 10^{31}$ (3σ)
SS Cyg	$137^d\ 7^h\ 19^m\ 53^s$ $17^h\ 14^m\ 29^s$	HRI/OGS (1000) MPC	.4 - 2	3.5×10^{-11} ± 20% $(4.4 - 5.8) \times 10^{-11}$	120 (1)	5.7×10^{31} 8.3×10^{31}

*no eclipse data are available for MPC spectral analysis
(1) Kiplinger 1979 (ref. 20).
(2) Wade 1979 (ref. 8).

TABLE 2

	L_{opt} [a]	L_{BB} [a]	L_{HX} [a]	T_{BB}(eV)	T_{HX}(keV)
AM Her	6×10^{32}	$\sim 2.3 \times 10^{34}$	7.5×10^{31}	~ 28	> 30
SS Cyg	$\sim 1 \times 10^{33}$	$\geq 3.0 \times 10^{33}$	2.1×10^{32}	10-12	10-30
U Gem	$\sim 9 \times 10^{30}$	$\geq 2.3 \times 10^{33}$	1.3×10^{30}	≥ 10	

[a] In units of ergs s^{-1}; distance determinations are discussed in the text. The L_{HX} refer to the total hard X-ray emission.

REFERENCES

1. Tapia, S. 1977, Ap.J. (Letters), 212, L125.

2. Ricketts, M.J., King, A.R., and Raine, D.J., 1979, M.N.R.A.S., 186, 233.

3. Fabbiano, G., Hartmann, L., Raymond, J., Steiner, J. and Branduardi-Raymont, G. 1980 submitted to Ap.J.

4. Giacconi, R. et al. 1979, Ap.J., 230, 540.

5. Boggess et al. 1978a, Nature, 275, 372.

6. Raymond, J.C., Black, J.H., Davis, R.J., Dupree, A.K., Gursky, H., and Hartmann, L. 1979a, Ap.J. (Letters), 230, L95.

7. Raymond, J.C., Branduardi, G., Dupree, A.K., Fabbiano, G., and Hartmann, L. 1979b, IAU Montreal.

8. Wade, R.A. 1979, A.J., 84, 562.

9. Touhy, I.R., Lamb, F.K., Garmire, G.P., and Mason, K.O. 1978, Ap.J. (Letters), 226, L17.

10. Lamb, D.Q., and Masters, A.R. 1979, Ap.J. (Letters), submitted.

11. Kylafis, N.D., and Lamb, D.Q. 1979, Ap. J. (Letters), submitted.

12. Kippenhahn, R., and Thomas, H.L. 1978, Astr. Ap., 63, 265.

13. Giannone, P., and Weigert, A. 1967, Z. Astrophys., 67, 41.

14. Starrfield, S. 1971, M.N.R.A.S., 152, 307.

15. Katz, J.I. 1977, Ap.J., 215, 265.

16. Weast, G.J., Durinsen, R.H., Imamura, J.N., Kylafis, N.D., and Lamb, D.Q., 1979, "White Dwarfs and Variable Degenerate Stars" Proc. IAU Colloquium No. 53, ed. Van Horn, H.M., and Weidemann, V. (Univ. Rochester).

17. King, A.R., and Lasota, J.P. 1979, M.N.R.A.S., 188, 653.

18. Chiappetti, L., Tanzi, E.G., and Treves, A. 1980, preprint.

19. Walker, M.F., and Chincarini, G. 1968, Ap.J., 154, 157.

20. Kiplinger, A.L. 1979, Ap.J., 234, 997.

21. Swank, J., Lampton, M., Boldt, E., Holt, S., and Serlemitsos, P. 1977, Ap. J. (Letters), 216, L71.

22. Szkody, P. 1976, Ap.J., 207, 824.

23. Heap, S.R., et al. 1978, Nature, 275, 385.

24. Cordova, F.A., Nugent, J.J., Klein, S.R., and Garmire, G.P., 1980a, M.N.R.A.S., 190, 87.

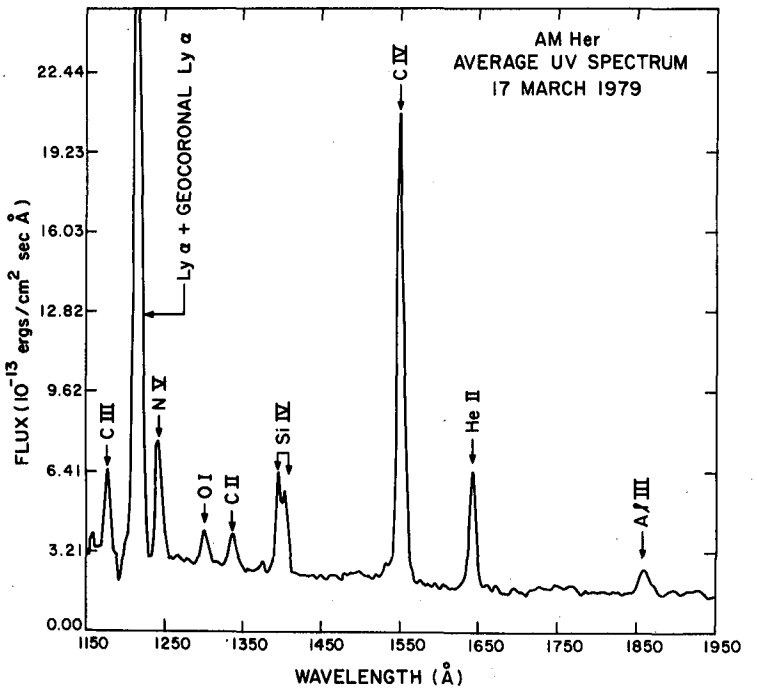

Figure 1. Average short wavelength UV spectrum of AM Her during the 1979 March 17 observations.

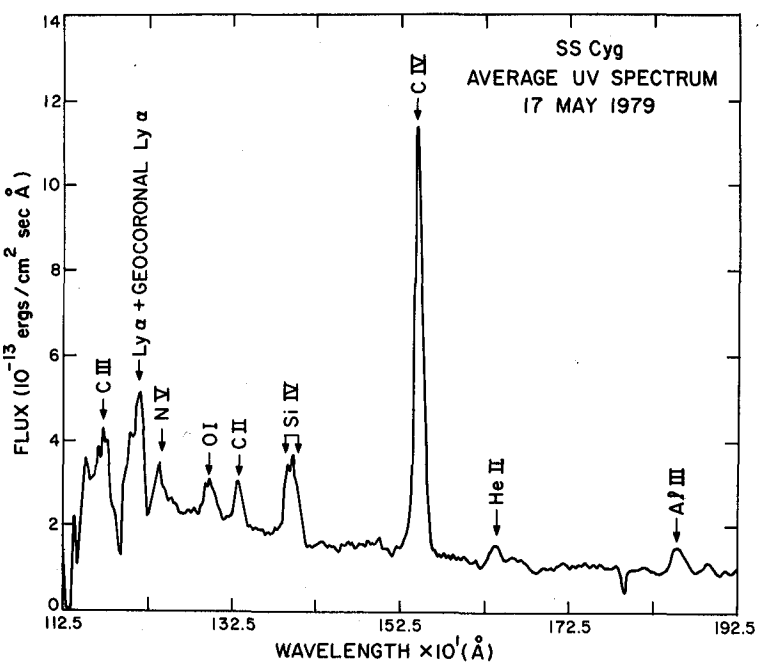

Figure 2. Average short wavelength UV spectrum of SS Cyg during the 1979 May 17 observations. SS Cyg was in quiescence at the time of the observations. Notice the similarity with the UV spectrum of AM Her (Fig. 1).

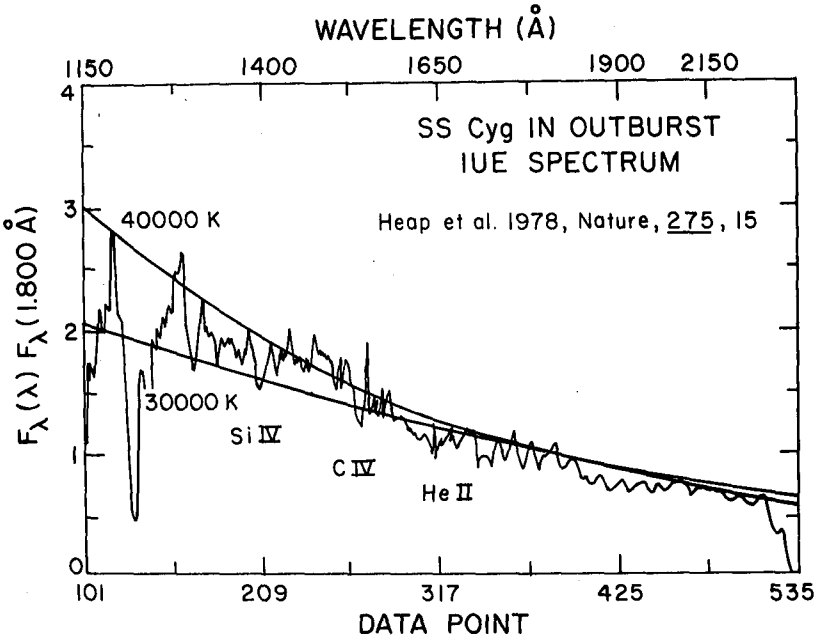

Figure 3. UV spectrum of SS Cyg in outburst.

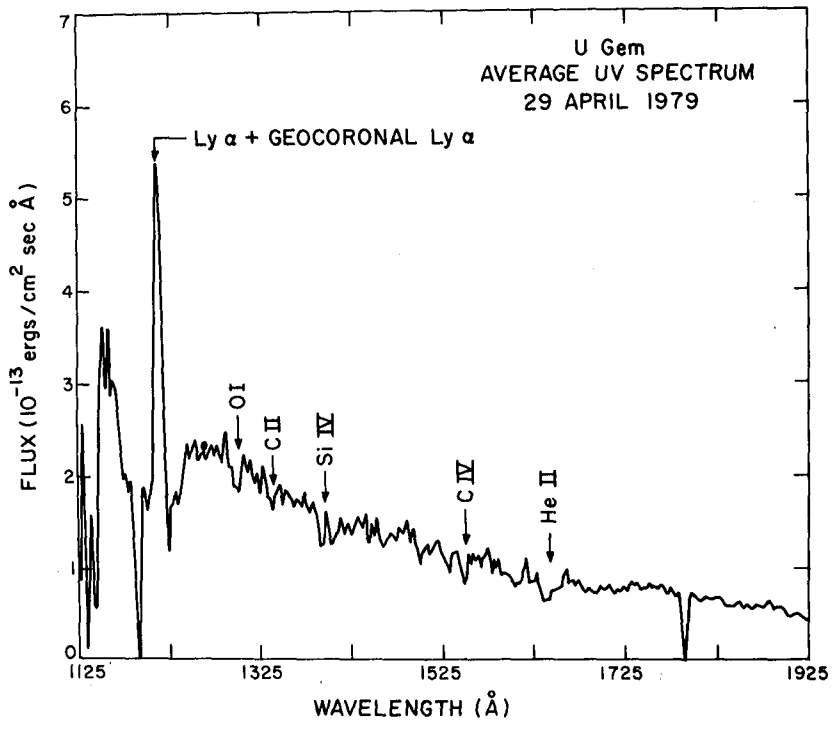

Figure 4. Average short wavelength UV spectrum of U Gem during the 1979 April 29 observations.

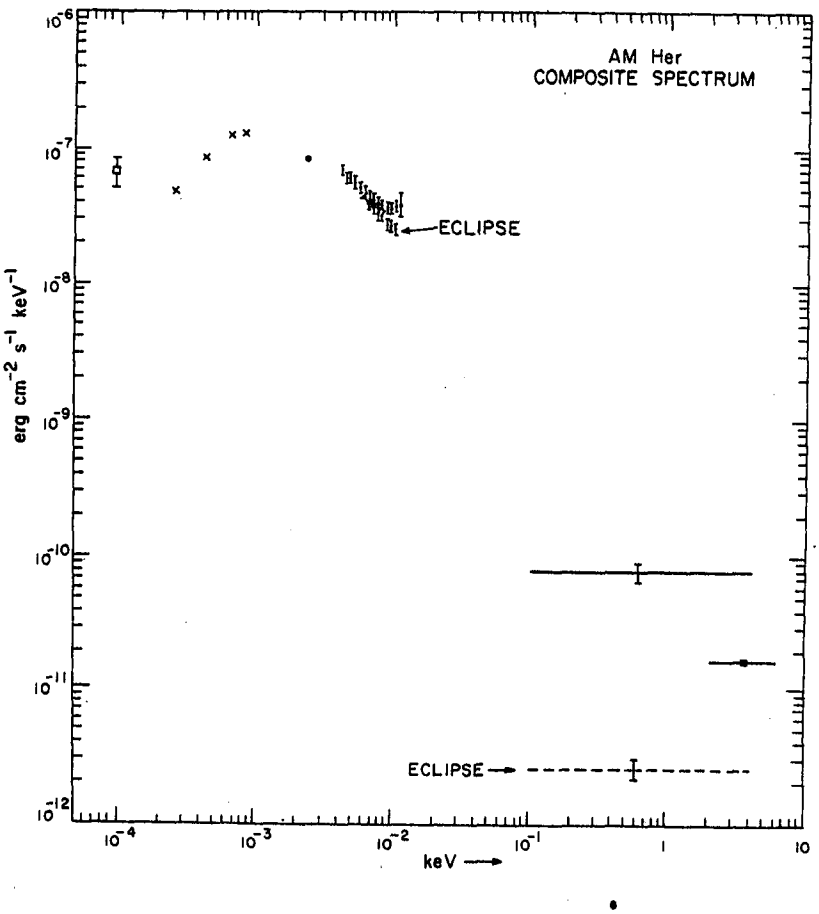

Figure 5. Composite spectrum of AM Her in high state. The optical, UV and X-ray points were obtained during the 1979 March 17 simultaneous observations. The optical point (dot) has been given to us by the AAVSO. The infrared points are the measurements of Merrill (crosses) and Rieke (square) as reported by Swank et al. (1977) (ref. 21).

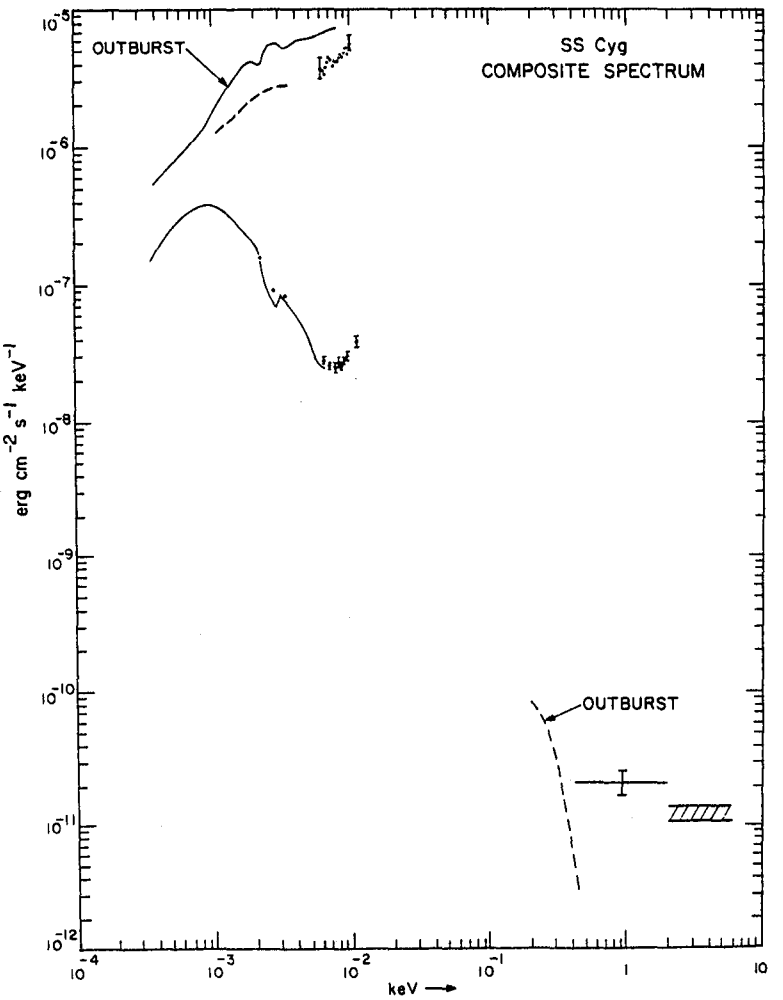

Figure 6. Composite spectrum of SS Cyg both in quiescence and in outburst. The U, B, V points (dots) in the spectrum in quiescence are the photometric measurements of Szkody (1980, private communication) simultaneous to the IUE (dots with error bars) and Einstein (lines) measurements of the 1979 May 17. The lower energy X-ray measurement is the HRI/OGS observation; the higher energy measurement represents the MPC data. The double line represents the range of variability of SS Cyg during the MPC observations. The continuous line that covers the IR through optical range is from the spectrophotometric measurements of Kiplinger (1979) (ref. 20). In the spectrum during outburst, the continuous line is again from Kiplinger (1979) (ref. 20) and the dotted line underneath it represents the Szkody (1976) (ref. 22) photometric measurements. Both these lines have been normalized to the UV data (Head et al. 1978) (ref. 23) during which the visual magnitude of the source was 9.5, one magnitude fainter than at maximum. The X-ray data are from Cordova et al. (1980) (ref. 24).

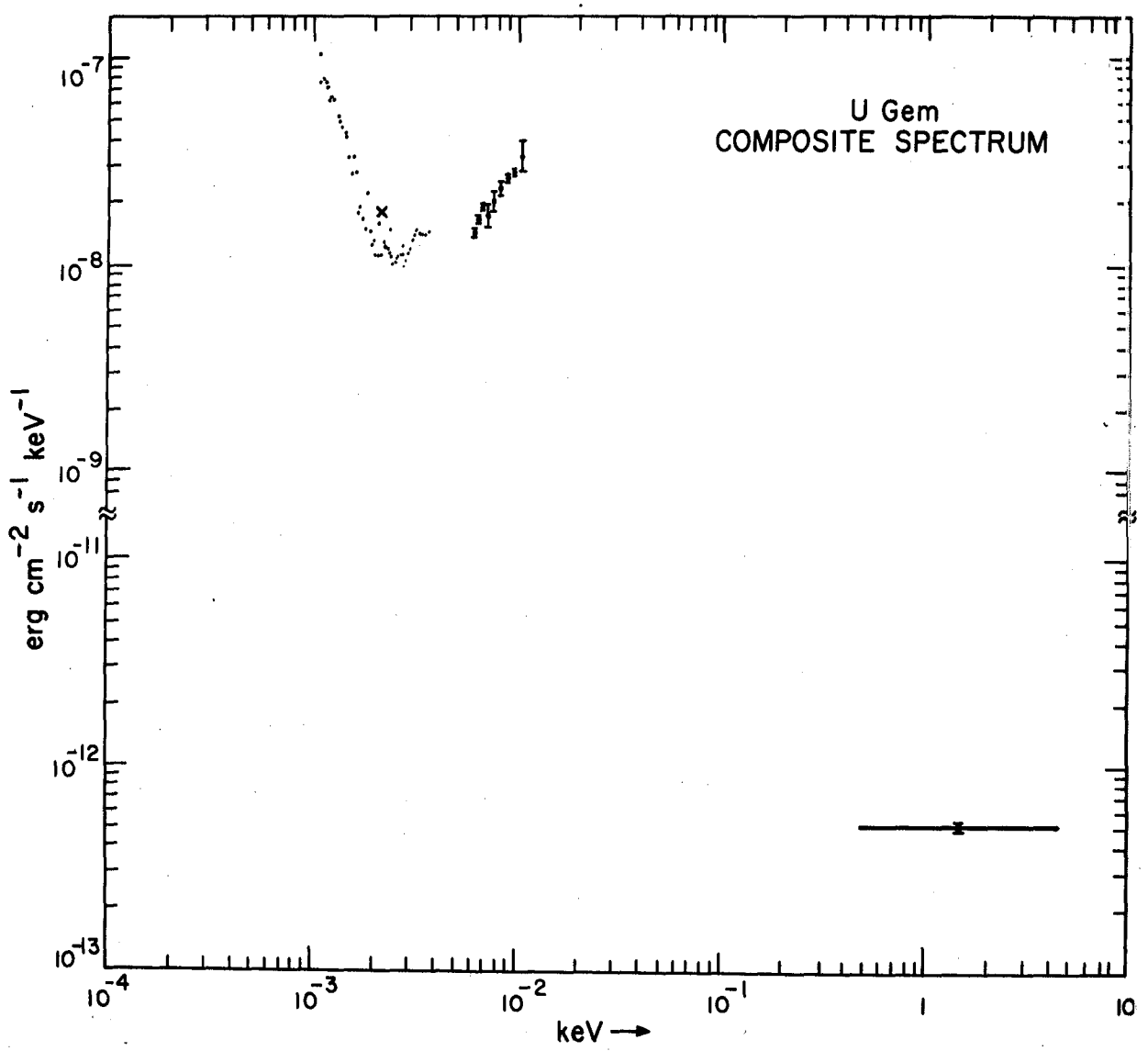

Figure 7. Composite spectrum of U Gem at minimum. The UV and X-ray points are relative to the quasi-simultaneous observations of 1979 April 29. The cross indicates the visual flux of U Gem at the time of the IUE and Einstein observations, as reported by the AAVSO. The dots cover the IR and optical observations of Wade et al. (1979)(ref. 8).

CYCLOTRON EMISSION FROM AM HERCULIS[1]

G. Chanmugam[2]
Joint Institute for Laboratory Astrophysics
University of Colorado and National Bureau of Standards

ABSTRACT

The cyclotron absorption coefficients, in the ordinary and extraordinary modes, are calculated for the shock heated region of AM Her. The equations of radiative transfer are solved and the intensity of the emitted UV radiation determined as a function of angle. The average spectrum is shown to have deviations from the previously predicted Rayleigh-Jeans spectrum and the magnetic field of AM Her is deduced to be roughly 5×10^7 gauss.

INTRODUCTION

The AM Herculis binaries are believed to contain a magnetic white dwarf, accreting matter from a companion star (refs. 1-3). The polarized light observed has been interpreted as being due to cyclotron emission, at the fundamental cyclotron frequency $\omega_c = eB/mc$, in a magnetic field $B \approx 2\times10^8$ gauss. It has been suggested that the matter accreting along the field lines forms a shock heated region (height $h \sim 10^6$) cm above the magnetic pole (refs. 4,5). This region was predicted to be a source of strong optically thick cyclotron emission peaking in the ultraviolet. However, the observed flux is much weaker (ref. 6). The theoretical estimates for the self-absorbed cyclotron emission were made using the angle-averaged cyclotron absorption coefficient (refs. 4,5,7). Recent estimates (ref. 8), made using the total cyclotron absorption coefficient and taking angular effects into account, suggest that the Rayleigh-Jeans spectrum would not be filled and that as a result the UV flux would be less than was previously predicted (refs. 4,5). In this paper the absorption coefficients $\alpha_{\pm}(\omega,\theta)$ for the ordinary (+) and extraordinary (-) modes are separately determined and the total intensity of the emitted radiation deduced as a function of frequency ω and the angle θ between the direction of the radiation and the magnetic field.

[1]Supported by NSF Grant AST-76-06807-A01.

[2]JILA Visiting Fellow, on leave from Dept. Physics and Astronomy, Louisiana State University, Baton Rouge, LA 70803.

CYCLOTRON RADIATION

The cyclotron absorption coefficients $\alpha_{\pm}(\omega,\theta)$ have been calculated, for a three-dimensional relativistic Maxwell distribution (as in ref. 8) for the electrons, by a modification (ref. 9) of methods previously used (refs. 10, 11). For the shock heated region of AM Her the Faraday rotation angle $\psi \approx \Lambda(\omega_c/\omega)^2/2\pi$ is $>> 1$, since the dimensionless parameter $\Lambda \equiv \omega_p{}^2 h/\omega_c c \sim 10^6$ (see eq. (3)), where ω_p is the plasma frequency and $\omega/\omega_c \sim 10$. In this case, the transfer equations for the intensities in the two modes decouple and (assuming Kirchhoff's law) take the form (ref. 10)

$$\frac{dI_{\pm}(\omega,\theta)}{dz} + \alpha_{\pm}(\omega,\theta)\cdot I_{\pm}(\omega,\theta) = \alpha_{\pm}(\omega,\theta) I_{RJ} \quad , \tag{1}$$

where $I_{RJ} = \omega^2 kT/8\pi^3 c^2$ is the Rayleigh-Jeans intensity per polarization mode. For a homogeneous plasma, the solutions are:

$$I_{\pm} = I_{RJ}[1 - \exp(-\alpha_{\pm} L)] \tag{2}$$

where L is the path length of the radiation through the source. The total intensity is then given by $I = I_+ + I_-$.

RESULTS

The shock heated region is treated as a uniform plasma slab which is perpendicular to the magnetic field so that the path length of the radiation is $L=h/\cos\theta$. The temperature of the slab is taken to be kT = 20 keV, as may be inferred from the hard X-ray observations (ref. 12), while the dimensionless parameter Λ is given by (refs. 4,8)

$$\Lambda \approx 1.6 \times 10^6 \left(\frac{M/M_{\odot}}{R/5\times10^8 \text{ cm}}\right)^{3/2} \frac{10^8 \text{ gauss}}{B} \quad , \tag{3}$$

where M is the mass of the white dwarf and R its radius.

The intensity of the emitted radiation is plotted as a function of cos θ for several harmonics in figure 1. Consider the radiation at $\omega/\omega_c = 12$. For $\cos\theta \approx 0$, the plasma is optically thick for both modes and hence the intensity is that of a black body (flat curve). For increasing values of cos θ the plasma first becomes optically thin in the ordinary mode (at $\cos\theta \approx 0.2$) and then in the extraordinary mode (at $\cos\theta \approx 0.4$) giving rise to the decrease in intensity. For lower harmonics the radiation is optically thick for a greater range of cos θ and conversely for higher harmonics. During an orbital cycle of AM Her, the viewing angle θ varies.

The total flux $F(\omega)$ from the plasma slab may be compared to the total Rayleigh-Jeans flux $B_{RJ}(\omega)$, if emitted as a black body:

$$\frac{F(\omega)}{B_{RJ}(\omega)} = \frac{\int_0^1 I(\cos\theta)\cos\theta\, d(\cos\theta)}{\int_0^1 2I_{RJ}\cos\theta\, d(\cos\theta)} \qquad (4)$$

In figure 2, $F(\omega)$ is plotted as a function of ω/ω_c, for several values of Λ. An important result is that $F(\omega)$ deviates from the Rayleigh-Jeans flux for $\omega/\omega_c \gtrsim 6$. If the angle-averaged absorption coefficient is used the flux would follow the Rayleigh-Jeans curve up to a frequency ω^* and be optically thin for $\omega > \omega^*$. The value of ω^* is $\approx 12\ \omega_c$ for $\Lambda = 1.0 \times 10^6$ (ref. 4). For $\omega \gtrsim \omega^*$ also, the angle-averaged results give fluxes higher than $F(\omega)$: by a factor ≈ 3 for $\omega \approx 14\ \omega_c$ and a factor ≈ 6 for $\omega/\omega_c \approx 30$. The values of $F(\omega)$ are in good agreement, for $\omega/\omega_c \lesssim 12$, with those obtained using the total cyclotron absorption coefficient (ref. 8), however for $\omega/\omega_c \gtrsim 12$, $F(\omega)$ is higher (e.g. by a factor of almost 2 for $\Lambda = 1.0 \times 10^6$, $\omega/\omega_c = 14$). This is because of the neglect of optically thin emission for small angles in ref. 8, an approximation which is good at low frequencies.

Raymond et al. (ref. 6) find that the UV continuum consists of a black body (kT = 25-30 eV) component, which also produces the soft X-rays (ref. 13), and a flat uneclipsed component produced by the X-ray heated secondary or by the accreting gas further up the accretion column. They do not however observe the optically thick cyclotron emission from the hot (kT $\approx$ 20 keV) shock heated region which had been predicted (refs. 4,5). The smallest value for the predicted cyclotron emission consistent with the soft X-ray flux is 20 times the observed value at 1500 Å. This discrepancy could be removed if the mass of the white dwarf ($M \approx 0.6\ M_\odot$) and the magnetic field ($B \approx 3 \times 10^7$ gauss) are lower than had been previously assumed (ref. 14). If angular effects are taken into account, as in this paper, a higher field $B \approx 5 \times 10^7$ gauss (with the same mass $M \approx 0.6\ M_\odot$, so that $\Lambda \approx 6.5 \times 10^5$) would suffice, since $\lambda = 1500$ Å would correspond to $\omega/\omega_c \approx 14$ (figure 2).

Recent UV observations of AM Her by Tanzi et al. (ref. 15) confirm the low UV flux observed by Raymond et al. (ref. 6). The former however find that the spectrum from 1150 to 3200 Å is well fitted by a power law $F(\lambda) \propto \lambda^{-2}$, i.e., $F(\omega) \approx$ constant. These observations are in better agreement with our results than those of ref. 6. The reasons for the differences in the observations are not entirely clear, but may be due to: (a) the observations not being carried out at the same time, (b) the neglect of reddening in ref. 6 and (c) the fit to the UV flux in ref. 15 being made without distinguishing between the eclipsed and uneclipsed flux or subtracting out the soft X-ray component.

In conclusion it is suggested that the magnetic field in AM Her is $B \approx 5 \times 10^7$ gauss which is a factor of about 4 below the usually adopted value. This lower value is consistent with estimates for the field strength made in understanding the optical polarization observations (ref. 9). The UV flux from the shock heated region is predicted to deviate from the Rayleigh-Jeans spectrum.

REFERENCES

1. Tapia, S.: Astrophys. J. (Letters), 212, L125, 1977.

2. Chanmugam, G.; and Wagner, R. L.: Astrophys. J. (Letters), 213, L13, 1977.

3. Stockman, H. S.; Schmidt, G. D.; Angel, J. R. P.; Liebert, J.; Tapia, S.; and Beaver, E. A.: Astrophys. J., 217, 815, 1977.

4. Masters, A. R.: The Binary System Containing the Pulsar PSR 1913+16 and Ultraviolet and X-radiation from Accreting Magnetic White Dwarfs. Ph.D. Thesis, Univ. of Illinois at Urbana, 1978.

5. Lamb, D. Q.; and Masters, A. R.: Astrophys. J. (Letters), 234, L117, 1979.

6. Raymond, J. C.; Black, J. H.; Davis, R. J.; Dupree, A. K.; Gursky, H.; Hartmann, L.; and Matilsky, T. A.: Astrophys. J. (Letters), 230, L95, 1979.

7. Chanmugam, G.; and Wagner, R. L.: Astrophys. J., 232, 895, 1979.

8. Chanmugam, G.: Astrophys. J., 1980, in press.

9. Chanmugam, G.; and Dulk, G. A.: Astrophys. J., to be submitted.

10. Ramaty, R.: Astrophys. J., 158, 753, 1969.

11. Dulk, G. A.; Melrose, D. B.; and White, S. M.: Astrophys. J., 234, 1137, 1979.

12. Swank, J. H.; Lampton, M.; Boldt, E.; Holt, S.; and Serlemitsos, P.: Astrophys. J. (Letters), 216, L71, 1977.

13. Tuohy, I. R.; Lamb, F. K.; Garmire, G. P.; and Mason, K. O.: Astrophys. J. (Letters), 226, L17, 1978.

14. Lamb, D. Q.: In Compact Galactic X-ray Sources, Eds. F. K. Lamb and D. Pines (Univ. of Illinois at Urbana), p. 27.

15. Tanzi, E. G.; Tarenghi, M.; Treves, A.; Howarth, J. D.; Willis, A. J.; and Wilson, R.: Astron. Astrophys., in press.

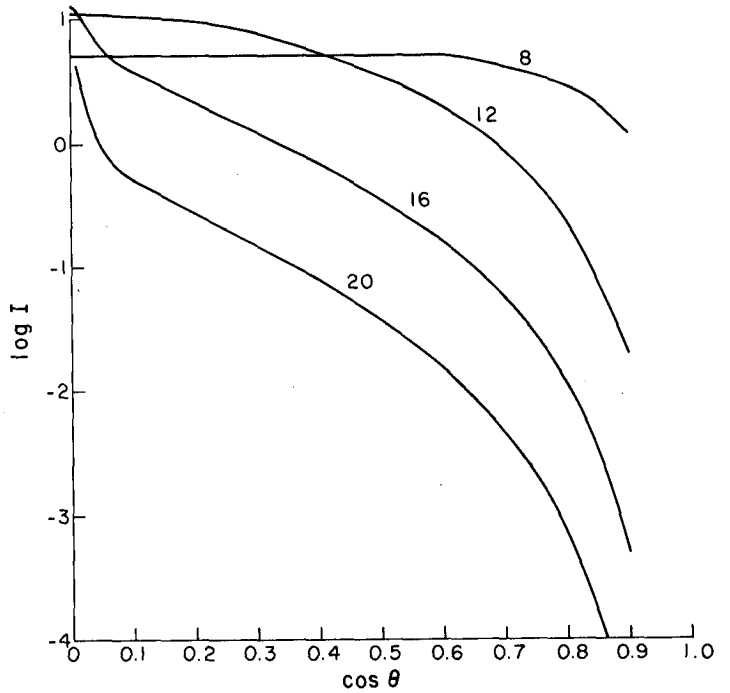

Fig. 1. Plot of the log of the intensity I vs. cos θ for $\Lambda = 10^6$, $h = 10^6$ cm, kT = 20 keV and ω/ω_c = 8, 12, 16 and 20.

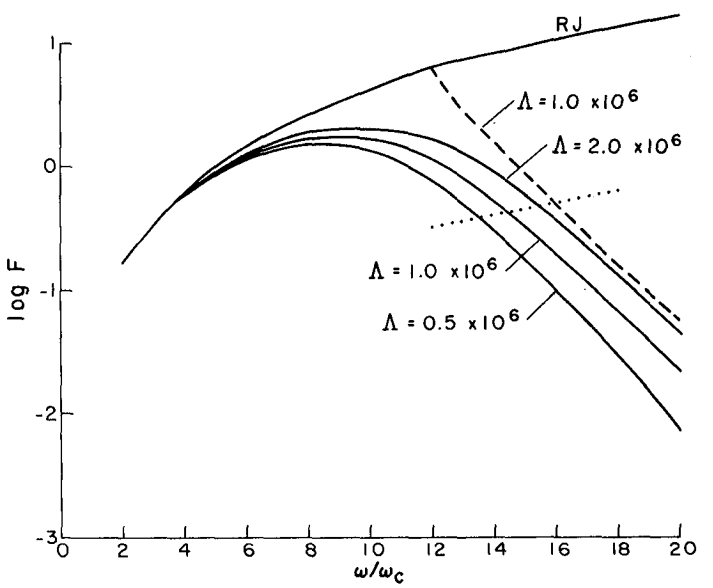

Fig. 2. Plot of the log of the flux F(ω), in arbitrary units, vs. ω/ω_c for kT = 20 keV and $\Lambda = 0.5 \times 10^6$ cm, 1.0×10^6 cm and 2.0×10^6 cm. The curve RJ is the Rayleigh-Jeans flux, dashed curve is due to Masters (ref. 4) while the dotted curve corresponds to 0.05 times the Rayleigh-Jeans flux (cf. ref. 6).

OBSERVATIONS OF SUPERNOVA 1979c IN M 100

Nino Panagia

Istituto di Radioastronomia CNR
Bologna, Italy

ABSTRACT

The IUE observations of supernova 1979c in M 100 are presented and discussed. The main results are:

1) The bulk of the energy is in the form of continuous emission which is radiated by the main SN envelope.
2) The absorption features originate mostly in both the disks and the haloes of our Galaxy and M 100.
3) The emission lines are produced in a highly ionized shell which has a radius greater than twice the radius of the main envelope and consists of compressed circumstellar material in which the abundance ratio N/C is about 30 times higher than solar.

INTRODUCTION

On April 19, 1979 Johnson (Ref. 1) discovered a bright supernova (denoted as 1979c, $m_B \simeq 12^m$) in the spiral galaxy M 100 (= NGC 4321).

The behavior of the light curve and the optical spectrum have indicated this SN to be a Type II (Ref. 2).

In the framework of a joint ESA-SRC target-of-opportunity program, on April 22, 1979 a series of low resolution spectra were taken in both short and long wavelength ranges. Observations were repeated at several subsequent epochs (April 24 and 27, May 1, 7 and 18, June 4, 15 and 28, and August 4).

In addition, simultaneous observations in the visual, radio and X-ray domains were also made resulting in a rather complete coverage and a thorough follow-up of the SN explosion and its time evolution. Detailed account of the first six weeks observations can be found in an article presently in the press (Ref. 3)

Here, I will present and briefly discuss the IUE observations with some reference to the optical results.

THE CONTINUUM AND THE TOTAL LUMINOSITY

The UV spectrum of the SN taken on April 22 is shown in Fig. 1. The bulk of the energy is radiated in the form of continuous emission which runs smoothly from 1600 to 3200 Å corresponding to a color temperature of $T_c \simeq 11000$ K.

The emission lines are estimated to contribute less than $\sim$ 15% of the total flux.

As seen in Fig. 2, which presents the observations made during the first four weeks, the continuum decreases steadily and becomes steeper with time, corresponding to a decrease of the color temperature from about 11000 K on April 22 to $\sim$ 7400 K on May 7. Starting in mid-May the decline in the UV bands becomes shallower and becomes similar to that observed in the optical range. This suggests an almost constant photospheric temperature after the middle of May.

Integrating over the whole optical and UV spectrum of April 22, after correction for extinction, the total flux is estimated to be $F_{tot} = 7.9 \times 10^{-10}$ erg $cm^{-2}s^{-1}$. Adopting a distance of 16 Mpc for M 100, the absolute luminosity on April 22, 1979 is L (April 22) = 2.4×10^{43} erg $s^{-1} = 6.3 \times 10^{9} L_{\odot}$. By integrating the observed spectra over time and frequency the total radiative energy released by the Supernova explosion has been estimated to be E_{rad} (1979c) = 7×10^{49} erg.

THE ABSORPTION LINES

Superimposed on the continuum are many absorption and emission features. In absorption one can easily identify (cf. Fig. 1 and 2) lines of low ionization ions such as CI, CII, OI, NaI, MgII, SiII, SII, as well as some resonance transitions of highly ionized species (e.g. SiIV, CIV, AlIII).

The absorptions extend from approximately zero velocity up to velocities of about 1600 km s^{-1} and can be produced in the interstellar media of both M 100 and our own Galaxy. The interstellar origin of all these absorption features is confirmed by the constancy of their widths and strengths in spectra taken at different epochs (cf. Fig. 2).

The velocity dispersion implied by the absorption features due to neutral and once ionized atoms observed between 1250 and 1350 Å is found to be in the range of 14-26 km s^{-1}. This estimate agrees very well with the more direct determination by Penston & Blades (Ref. 4) of 15 (+11, -6) km s^{-1} obtained from measurements of the absorption of the Ca II 3934-68 and Na I 5890-96 doublets.

Similarly, the absorption lines of highly ionized atoms imply the presence, in both galaxies, of a medium where the gas is highly ionized and the velocity dispersion is 50 km s^{-1} at least. Evidence for the presence of such a halo in our Galaxy has been found in the direction of 3C 273 and towards some high z stars (Ref. 5) as well as towards stars of the LMC (Ref. 6).

THE EMISSION LINES

The strongest emission features present in the April 22 spectrum can be identified with resonant transition of N V (1238.8-42 Å), Si IV (1393.7 - 1402.7 Å), C IV (1548.2-50.8 Å) and the intercombination transitions of N IV]

1486 Å, N III] 1750 Å, C III] 1909 Å. The intercombination lines of O III] 1663 Å and of O IV] 1406 Å, cannot be discerned in the spectrum. The He II 1640 Å line is neither clearly present in this spectrum nor in those taken at later epochs. On the other hand, in the spectrum one can clearly see the line 1718.5 Å of N IV which corresponds to a permitted transition between excited levels ($2p\ ^1p^0$-$2p^2\ ^1S$). This immediately tells us that nitrogen must be present largely in the form of N IV in order to produce such a strong line.

As seen in Fig. 2, the spectrum appears to contain several other lines which are somewhat weaker. However, they are severely blended with each other so that the identification of individual lines and a quantitative estimate of their intensities is impossible.

The same crowding of lines makes it difficult to properly determine the profile of the major features and to measure their intensities to accuracies better than, say, 30%. Nevertheless, by studying the spectrum observed on April 22 as well as those obtained at later epochs (cf. Fig. 2) the following is apparent:

1) The line profiles are sharply peaked at a velocity displacement of 1800 ± 300 km s^{-1} with respect to the laboratory wavelength. This velocity is only marginally higher than the radial velocity of M 100 and confirms that the emission lines originate in the SN envelope.
2) The wings of the individual emission features extend to no more than 4000 km s^{-1}.
3) The emission profiles appear to be symmetric with respect to the emission peak.

The peaked profiles indicate that the lines are formed in an expanding envelope in which a velocity gradient exists and the maximum expansion velocity is $v_{max}(UV) \simeq 4000$ km s^{-1}.

The symmetric extension of the line wings to the red and to the blue indicates that the UV emitting layers are far enough from the SN "photosphere" that any occultation of the receding part of the shell is negligible. From simple geometric arguments the average distance of the UV emitting shell from the SN surface can be estimated to be at least 2 photospheric radii (i.e. R (UV shell) $\geq 2.5 \times 10^{15}$ cm). Therefore, the UV emission line layers must be well separated from those which produce the continuous spectrum, i.e. the SN photosphere. Moreover, inspection of Fig. 2 shows that the line-to-continuum ratio increases with time. This is further confirmation that they evolve independently and, thus, are formed in different zones.

On the other hand, the optical lines display very asymmetric profiles (Ref. 3), with the blue portion being twice as extended as the red one. This indicates that the optical lines are formed in the main envelope which has been ejected in the SN explosion. Also the MgII λ2800 Å line presents similar characteristics in both profile and time evolution. Thus, this line too originates in the top layers of the SN photosphere.

The UV shell is likely to consist of gas originally ejected by the stellar

progenitor, a red supergiant, as a more or less continuous wind. The wind material must have subsequently been compressed and accelerated as a result of the SN explosion, possibly by the radiation pressure of an initial soft X-ray burst (Ref. 7). The UV shell mass can be estimated to be approximately $M(\text{UV shell}) \simeq 10^{-2} M_{\odot}$. This may be the result of steady mass loss of $\dot{M} \simeq 10^{-4}\ M_{\odot}$/year. From the intensities of the emission lines of C and N, as well as the upper limits to the O lines, it is estimated that the number abundance ratios of N/C and O/C are 7 and <4, respectively. This corresponds to a strong overabundance of nitrogen relative to both carbon and oxygen by a factor of 10-30. The high enrichment of N and/or the possible depletion of C and O are indicative of nuclear processing through CNO cycle. This can have occurred in an H-burning shell during the red giant phase of the progenitor star. Subsequently the material has been brought up to the surface and ejected from the star in the form of stationary wind. It is clear, then, that the anomalous CNO abundances found in the UV shell provide further evidence for the accumulation of circumstellar material prior to the SN explosion.

REFERENCES

1. Johnson, G.E.: 1979, IAU *Circular* No 3348.

2. Ciatti, F. et al.: 1979, IAU *Circular* No 3361 & 3371.

3. Panagia, N. et al.: 1980, *Mon.Not.Roy.Astr.Soc.*, in press.

4. Penston, M.V. & Blades, J.C.: 1980, *Mon.Not.Roy.Astr.Soc.* 190, 51P-57P.

5. Ulrich, M.H. et al.: 1980, *Astron.Astrophys.*, in press.

6. Savage, B.D. & de Boer, K.S.: 1980, *Astrophys.J.*, in press.

7. Klein, R.I. & Chevalier, R.A.:1978, *Astrophys.J.(Letters)* 223, L109-L112.

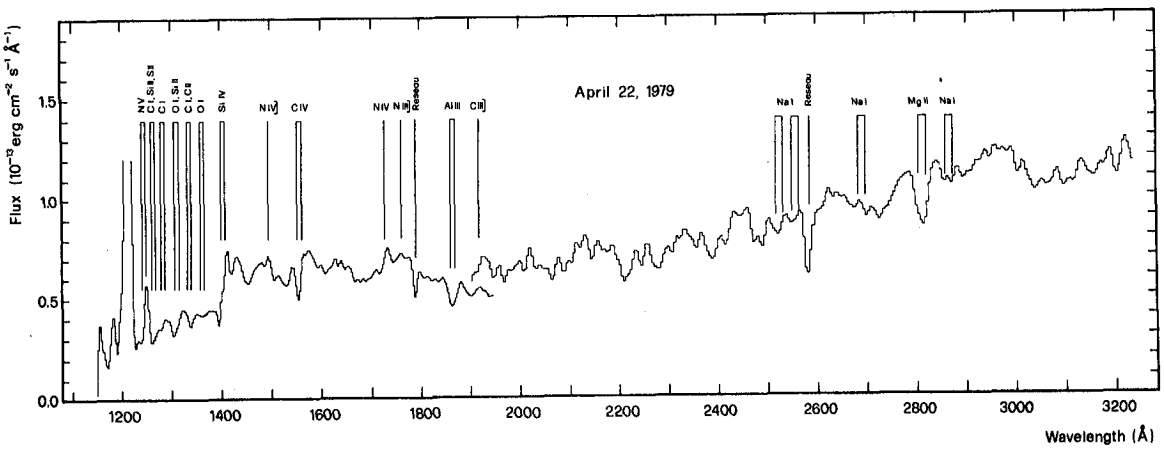

Figure 1. Ultraviolet spectrum of the supernova taken on April 22.3, 1979. The identifications of some relevant features either in absorption or in emission are given. The average wavelengths for components at zero velocity and at the M 100 radial velocity (z = 0.0054) are shown for absorption features. Only the redshifted wavelength is indicated for emission lines.

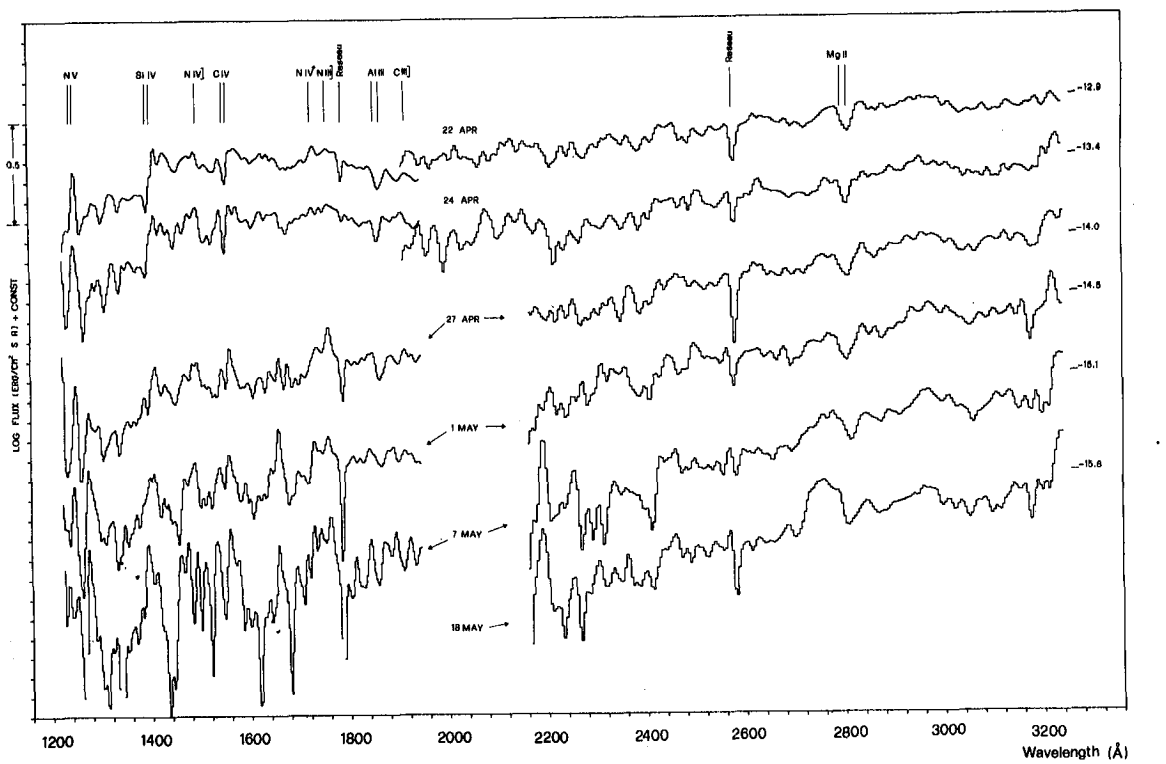

Figure 2. Evolution of the ultraviolet spectrum from April 22 to May 18. Note the increasing prominence of the far UV lines with time. Also noteworthy, is the development of the Mg II λ2800 Å line.

Horizontal Branch Stars, and Galactic and Magellanic Cloud Globular Clusters

Klaas S. de Boer

Washburn Observatory
University of Wisconsin, Madison WI 53706

Seven blue horizontal branch stars in the field have been observed, and a few HB stars have been isolated in globular clusters. Energy distributions are compared to assess possible differences, also in comparison with model atmospheres. Observed energy distributions of HB stars in NGC 6397 are used to estimate the total number of HB stars which produced the integrated fluxes as observed by ANS. Preliminary results are given for colors of globular clusters observed in the Magellanic Clouds and for their extent, based on the Washburn IUE extraction.

Since the observations of galactic globular clusters by the OAO-2 (Welch and Code 1980) and by the ANS (van Albada, de Boer and Dickens 1979, 1980) there is need for basic data on those constituents of globular clusters which provide most of the ultraviolet light. Neither of the two satellites had observed blue horizontal branch (BHB) stars in the field for their own sake, except for HD 109995 by OAO-2 (see Koornneef et al. 1980) and a few possible BHB stars by ANS (de Boer and Wesselius 1980).

IUE provided the opportunity to fill this gap. In addition, with its high spatial resolution it seemed to be possible to isolate BHB stars in galactic globular clusters, while an extension of the data base to Magellanic Cloud globular clusters is of general interest (Freeman 1979).

Blue Horizontal Branch Stars in the Field of the Galaxy

Seven BHB stars have been observed at low dispersion in the wavelength range 1150-3200Å. Most of the stars have an energy distribution in the UV which drops rapidly to <10% of the 1500-2000Å flux near 1330Å and none of the stars shows detectable flux shortward of Lα. In Fig. 1 the spectrum is shown for HD 86986. The fluxes are from the Washburn extraction which was adapted to correct the ITF error (see de Boer, Koornneef and Meade 1980, henceforth

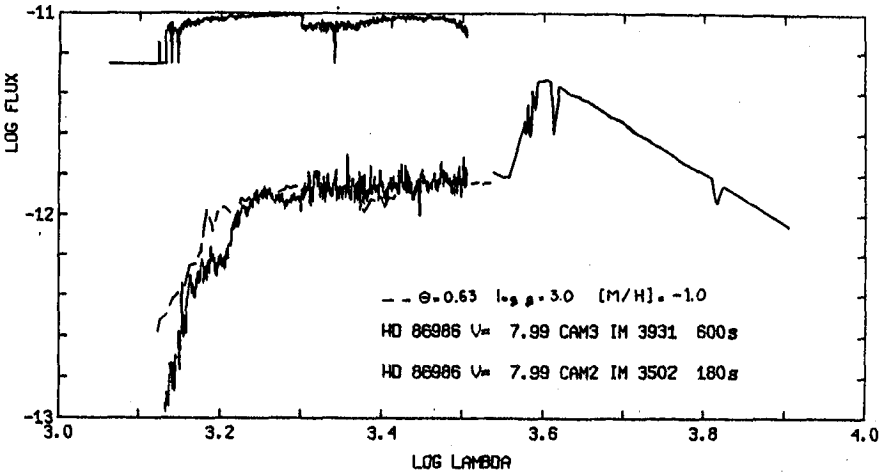

Fig. 1: Absolute flux of a field blue horizontal branch star. The uncertainty of the flux is plotted at the top in the same units as the spectrum (based on the Washburn extraction routine, see de Boer, Koornneef, and Meade 1980). Visual data are from Christensen (1978). Dashed lines near the UV spectrum are from a Kurucz model as labelled. Since the star has spectroscopically [M/H] ≈ -1.5, a better fit would be obtained with T ≈ 7800 K.

BKM). The large and small aperture spectra have been combined with weighting according to the error found in the Washburn extraction (BKM). The absolute calibration used is the one given by Bohlin et al. (1980) and the connection between SWP and LWR spectrum is made at 1992Å. From stromgren photometry and spectrum scans one obtains that HD 86986 has $T_{eff} \approx 8000$ K, log g ≈ 3.05, [M/H] ≈ -1.5 (Kodaira, Greenstein and Oke 1969; Hayes and Philip 1979). The UV, at $\lambda\lambda < 1600$, is very sensitive for temperature effects. Comparison with the Kurucz (1979) models indicates that a fair fit is obtained with a model with T_{eff} one or two hundred degrees below 8000 K. Models at 8000 K also give a lower UV flux for metallicities more near solar, but then strong lines near 2400Å are indicated, while these are very weak in the observed stellar spectrum.

BHB Stars in Globular Clusters

NGC 6397 is a relatively open cluster, and is bright in the UV in spite of E(B-V) ≈ 0.2. Both characteristics make it possible to isolate BHB stars with IUE. Up to now 3 stars have been observed, star no. 56 and 210 (Graham and Doremus 1968) and a star very near the nucleus of the cluster. The BHB stars in NGC 6397 are much bluer than the known field HB stars. GD 56 has T_{eff} = 12000 K and log g = 3.15 (Newell, Rodgers and Searle 1969).

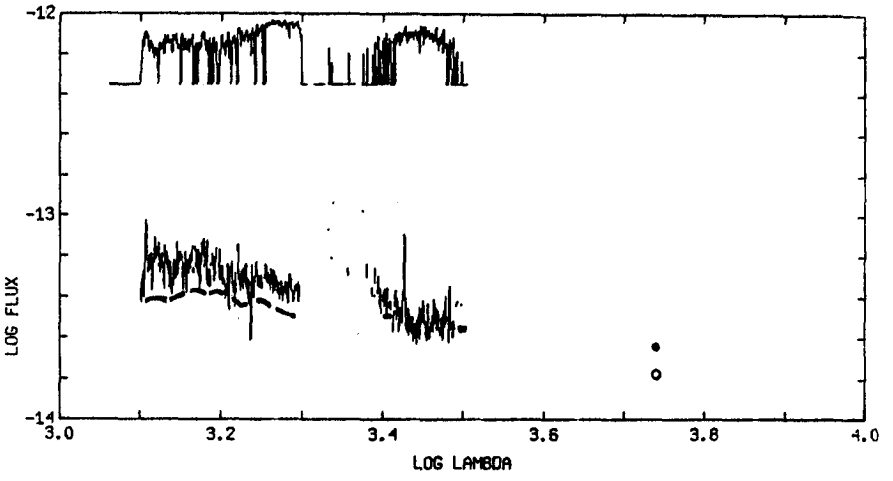

Fig. 2: Absolute reddening corrected flux for the BHB stars 56 with m_V = 13.95 (full spectrum and error plotted as in Fig. 1) and 210 with m_V = 13.63 (dashed line and filled circle at V) in NGC 6397.

The absolute flux at 1550Å of GD 56, log F_{1550} = -14.0, can be used in relation with the photometric flux from ANS log F_{1550} = -12.97 erg $cm^{-2}s^{-1}$ A^{-1} (van Albada, de Boer, Dickens 1980). Hence, in the ANS field of view of 2'.5 x 2'.5, 10 BHB stars have been sampled. Together with visual photometry this allows the determination of the total number of BHB stars in NGC 6397.

Globular Clusters in the Magellanic Clouds

The earlier UV photometric satellites OAO-2 and ANS had insufficient spatial resolution and sensitivity to isolate and measure globular clusters outside our galaxy. With IUE long integration times are possible and a few

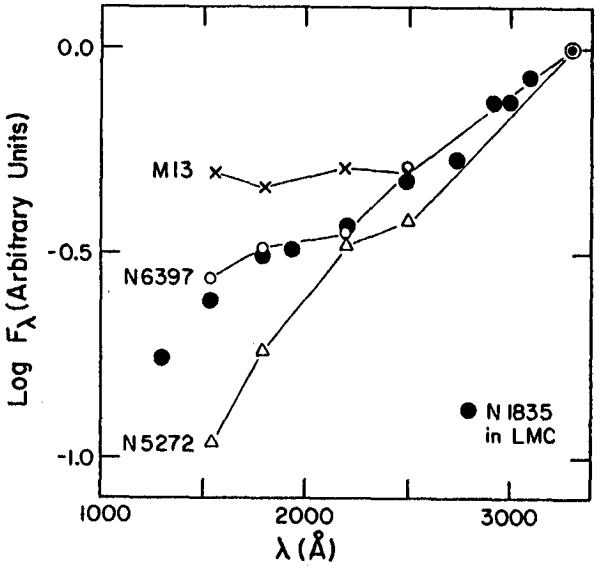

Fig. 3: UV energy distribution of the globular cluster NGC 1835 in the LMC, and for comparison 3 galactic globular clusters observed by ANS (van Albada, de Boer, Dickens 1980) adjusted to the IUE calibration following Bohlin et al. (1980). Fluxes with arbitrary relative shift.

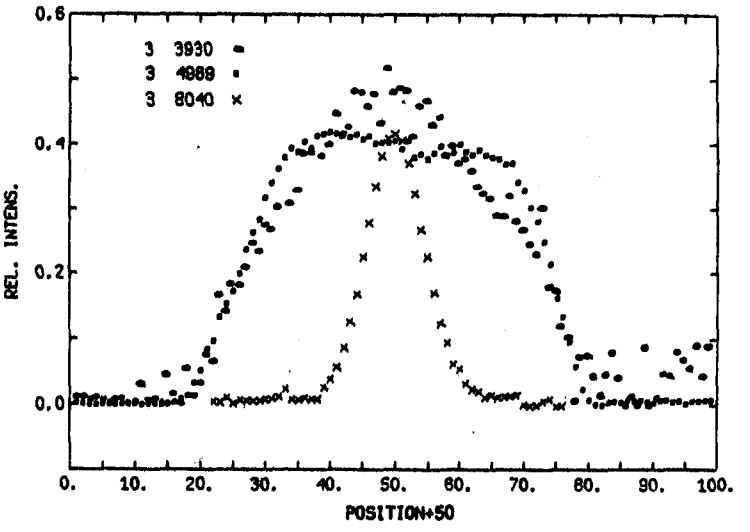

Fig. 4: Response of the large aperture in SWP (positionally adjusted coadded fits of 350 diagonals between 1580 and 2000Å; see BKM) for three different objects. Image 3-8040: star 56 in NGC 6397; image 3-2989: even illumination from diffuse light near the Trapezium; image 3-3930: NGC 1835 in the LMC. Further analysis of such responses can yield information on the spatial structure of LMC globular clusters.

clusters in the Magellanic Clouds have been observed. This program is still in progress and only preliminary results are given.

In Fig. 3 we show the UV energy distribution for NGC 1835, in comparison with three galactic globular clusters. The latter three have been selected from (van Albada, de Boer and Dickens 1980) group EB: M13, with extremely blue HB; group B: NGC 6397, with blue HB; group I: NGC 5272 with only moderately populated horizontal branch. NGC 1835 seems to have a UV brightness like a normal blue HB globular cluster.

The Washburn Extraction Routine (see BKM) can also be used to infer spatial information from the large aperture data. Fig. 4 shows as an example the spatial intensity distribution for a few different objects. Several of the globular clusters in the LMC are still so extended that two displaced large aperture IUE observations are required to get proper spatial information.

References

Bohlin, R.C., Holm, A.V., Savage, B.D., Snijders, M.A.J., Sparks, W.M. 1980, A & A, in press.
Böhm-Vitense, E. 1980, Ap.J., submitted.
Christensen, C.G. 1978, A.J., 83, 224.
de Boer, K.S., Code, A.D. 1980, in prep.
de Boer, K.S., Koornneef, J., Meade, M.R. 1980, this symposium. (BKM)
de Boer, K.S., Wesselius, P.R. 1980, A.J., submitted.
Freeman, K.C. 1979, in Scientific Research with the Space Telescope, p. 139, NASA CP-2111, Ed. M.S. Longair and J.W. Warner.
Graham, J.A., Doremus, C. 1968, A.J., 73, 226.
Hayes, D.S., Philip, A.G.D. 1979, P.A.S.P., 91, 71.
Kodaira, K., Greenstein, J.L., Oke, J.B. 1969, Ap.J., 155, 525.
Koornneef, J., Meade, M.R., Wesselius, P.R., Code, A.D., van Duinen, R.J. 1980, Wisconsin Astrophysics 101, "Picture Gallery".
Kurucz, R.L. 1979, Ap.J. Suppl. Ser., 40, 1.
Newell, E.B., Rodgers, A.W., Searle, L. 1969, Ap.J., 156, 597.
van Albada, T.S., de Boer, K.S., Dickens, R.J. 1979, A & Ap., 75, L 11.
van Albada, T.S., de Boer, K.S., Dickens, R.J. 1980, M.N.R.A.S., to be submitted.
Welch, G.A., Code, A.D. 1980, Ap.J., 236, 798.

Wallerstein: What is the nature of the companion of the hydrogen-poor star υSgr?

Plavec: It is a normal O9 star with no emission lines.

Stencel: What is the connection between W Ser and the symbiotic stars? Are the symbiotics extreme because of their larger mass exchange rates?

Plavec: I don't think that symbiotics have extreme rates of mass loss. In fact, it seems that in some of them, it is the hot star that is losing mass now, by a massive stellar wind, although we must suspect that over a long period of time, the cool component is the loser. I think that the basic characteristic of the symbiotics may be the subdwarf character of the hot star. This makes them related to central stars of planetary nebulae as well as to cataclysmic variables (since the hot star may well be surrounded by a disk). The nature of the relation is, unfortunately, obscure. Yet it seems that the symbiotic stars are trying to tell us something very important about helium subdwarfs in binary systems.

Plavec: 1. The absence of the traveling wave in HR 5110 may be due to the low luminosity of the secondary. 2. The origin and character of the emission lines could be studied with advantage: (1) by observing primary and secondary eclipses of suitable systems; (2) by studying the line pupils in the high-dispersion mode. Has it been done?

Simon: 1. At infrared wavelengths longward of 2 μm, the secondary contributes approximately 30% of the total light of the system. However, I find no evidence in JHKLM photometry obtained at Kitt Peak in February and March for variability $> 0.^{m}1$. A very low amplitude wave might still escape detection, even at 5 μm. 2. The observations suggested by Dr. Plavec are scheduled for later this year.

Hartmann: I have a question about the flare model for UX Ari. As I understand it, the evidence for mass motions in the flux tubes/ loops comes from the Mg II profiles. However, the flux tubes are at 10^{7}K. How is the Mg II emission related to the flux tubes?

Simon: It is possible that the Mg II emission comes from the splashdown points. More detailed observations are required for better modelling.

Penston: D. Allen and I have also been working on this star and we agree with many of your conclusions. There is one item which we do not understand and which you did not mention. This is the weakness of the O IV] lines. The broad component is absent unlike other three-times-ionized ions and the narrow components are the same strength as the S IV] lines!

Keyes: We see the same thing in our August 1978 spectrum.

Linsky: Would you comment on the very strong and broad N V emission?

Keyes: The N V emission lines do not show nebular emission components but have a ξ Cygni character indicating a maximum expansion velocity of 1500-2000 km s^{-1}.

Roman: In view of the similarity of the companions of ξ Cap and αCMa, is there also a relation between the spectral peculiarities of the primaries?

Böhm-Vitense: We do not understand the source of the x-rays. I think they are due to mass accretion by the white dwarf. The material may have come originally from Sirius A. This, of course, is only speculation presently. There appears to be circumstellar material in ξ Cap. Of course Sirius A looks like a hot metallic line star but the abundance anomalies, I think, are different from those observed for Ba II stars.

R. Green: Does the white dwarf companion to ξ Cygni seem to have a comparably large mass to that of the companion to ξ Cap?

Böhm-Vitense: The signal for ξ Cygni is less than for ξ Cap. We think ξ Cygni also has a companion, but we cannot be sure, we are still analyzing the data. If there is a white dwarf companion, it must be cooler, we estimate about 14000 to 15000K. The mass also comes out to be about 1 $M_{\odot}$.

Stencel: Wilson (1976 Ap. J.) has noted chromospheric pecularities for BaII stars as a class. Do you note Mg II and SWP differences?

Böhm-Vitense: Yes, ξ Cap has very strong Mg II emission lines with deep central reversals which have lower central intensities than k_1 and h_{ii}. It probably indicates circumstellar material. The emission lines are much stronger than in the comparison star ε Vir.

Stencel: Which nuclear process could provide the slow neutrons for barium production?

Wilson: There are different processes discussed in the literature; none of them looks very convincing to me. However, the overabundance of the process elements is observed. So we have to accept that there must be such a process available.

Savedoff: Can you estimate the separation of the ζ Cap system? I have been trying to model internal effects in 2-dimensional stellar models and estimate that horizontal thermal or density fluctuations of 10^{-20} suffice to drive mixing in 10^6 years. The peculiar abundances could result from gravitationally-induced meridional circulation rather than accretion from the outside.

Böhm-Vitense: ζ Cap is not among the stars McClure has studied. We have neither velocities nor periods. For similar stars, periods of the order 0.5 to 1 year have been found.

Sparks: Are there any features which would indicate a hot spot in the spectra of your old novae?

Slovak: Unfortunately, we don't have high-dispersion IUE data for any of the old novae, and so we cannot make a detailed line-by-line comparison. From the low-dispersion spectra, the emission lines do not appear to have significantly different widths (e.g., N V compared to He II) or other characteristics which would allow their origin to be ascribed to the "hot spot" as opposed to the disk in general.

Stencel: What correlations have you noted between continuum slopes and emission line widths? Can you speculate about the origin of the line broadening in your inclination-activity model?

Slovak: Though the analysis comparing emission line widths versus continuum slope has not been performed in detail, there appear to be no obvious correlations. Compare the spectrum of AG Dra (very hot component present, narrow emission lines) to that of AG Peg (a hot component of T_{eff} = 30,000K° - 40,000K°, broad WR emission lines). The line broadening may be related to activity of the hot component or possibly excitations effects. This still remains to be examined.

Michalitsianos: What are the general properties of symbiotic stars in the near- and far-infrared?

Slovak: The spectrum of AG Pegasi, displayed by Keyes, is typical of the near-infrared nature of most symbiotic stars. The continuum is generally that of a late-type giant (M0-M6 II), superposed on which is an emission line spectrum exhibiting He I, He II and Balmer lines in emission. The far-infrared properties of symbiotic stars have been explored by broad band (J,H,K,L, and M) photometric studies. Many exhibit a non-variable stellar-like continuum (S-type), whereas others show as variable, dusty infrared behavior (D-type).

Keyes: It is interesting to note that the UV spectral similarity you show for CI Cygni and AX Per is continued into the visible region. Both are rather high-excitation objects having displayed [Fe VII]. Another system rather similar to these is Z And. It might be useful to look closely in the UV at these 3 systems for similarities and contrasts.

Slovak: We have obtained IUE spectra, in April 1980, for Z And. and can confirm the resemblance to AX Persei and CI Cygni. The emission line spectrum is similar and there is no marked evidence for a hot continuum in the raw data.

Aller: From spectrophotometry (1972) Keyes and I concluded that RR Fel required a model with a large variation in temperature and density. No specific model would ever work. These magnificent data should go a long way in constructing a picture for this star. Congratulations!

Penston: We certainly confirm the stratification as we find that both line width and density vary with excitation potential.

Michalitsianos: Is RR Tel associated with soft x-ray emission?

Penston: I don't know.

Ahmad: The phase lag between the observations and the model of stellar winds might be accounted for if the winds are actually streaming out along magnetic field lines, which is what we would actually expect, rather than simply expanding radially.

Slovak: How are you sure that you have detected emission from the shell around DQ Herculis? Does shell emission fill the large aperture in the three hour exposure?

Hartmann: We observe faint C II and C III emission from an extended source. The emission does not appear to fill the large aperture uniformly, although it is difficult to tell from the weakness of the signal.

Chanmugam: Is there any evidence of an eclipse in 2A0311-227?

Raymond: We have one spectrum of short enough exposure time to separate out the eclipse, but it is too noisy to be useful.

Wallerstein: When you refer to a black body source that is a small fraction (10-15%) of that expected for a white dwarf, did you use a model for a 0.6 $M_\odot$ white dwarf? These accreting WD's may have a larger mass and hence a smaller radius.

Fabbiano: For SS Cygni the mass of the white dwarf is 1.05 $M_\odot$ and we used the corresponding radius for that mass.

Slovak: I would like to emphasize the point I made in my talk, concerning the inclination effects on the appearance of the continuum of these close binary systems involved in accretion disks. I cite, for example, the recent paper by Bath et al. (1980)* where the data for the dwarf novae (eclipsing systems: EX Hya and BV Cen) compared to non-eclipsing system: VW Hyi show the flattening of the continuum, ascribable to a large optical depth in the high-inclination systems.

Raymond: Does the transparency along the field account for the primary minimum in V in AM Her?

Chanmugam: Yes. The detailed calculations of ref. 9 confirm the earlier suggestion (ref. 7).

Michalitsianos: Is there circular polarization as well as the linear polarization that you have spoken of in AM Her? Do you derive the magnetic field intensity in this system from the circular polarization component?

---

* Bath, G. T., Pringle, J. E. and Whelan, J. A. J., 1980, M.N.R.A.S., 190, 1985.

Chanmugam: The polarization (both linear and circular) are discussed in ref. 9 and can be understood if the optical polarized radiation is at roughly the 5th cyclotron harmonic (i.e., $B \approx 4 \times 10^7$ gauss).

Michalitsianos: Don't you feel that a mass loss rate of $\dot{M} \approx 10^{-4}\ M_\odot Yr^{-1}$ is excessive from M supergiants?

Panagia: The quoted mass loss rate of $\dot{M} \approx 10^{-4} M_\odot/yr$ is in fact an upper limit. I think that a value two or three times smaller may well account for the UV shell mass. On the other hand, it is quite possible that the high mass loss rate indicated by the UV_2 shell corresponds to a paroxysmic episode of short duration, say about 10^2 years or so.

Heap: Could you say how you derived your N/C ratio? What lines did you use?

Panagia: The lines used to derive the N/C ratio are C IV 1550, C III] 1909_4 N IV] 1486 and N III] 1750. The adopted temperature was around 2×10^4 K but the results are quite insensitive to the exact value of T_e because the excitation energies are rather similar for all the transitions for corresponding ions of carbon and nitrogen. Therefore, the uncertainty in the ratio N/C should be lower than a factor of 2.

Aller: In the LMC there is a very blue cluster which resembles a globular cluster. The spectrum and energy scan resemble an A star (IAU symposium on galaxy Magellanic Clouds). Unfortunately, I don't remember the NGC number but this cluster was brighter than NGC 1831 and would be well worth examining with IUE.

de Boer: They are not on my observing list but I plan to add them soon or devote a separate observing program to such clusters.

Weaver: Does your viewgraph which shows the relative response of the spectrograph across the large aperture ($\perp$ to dispersion) represent an average over the entire spectrum? Is the relative response always higher towards the center of the camera face?

de Boer: It is the response over half of the spectrum (long half of SWP) and I have no information yet on systematics. It seems to me from what I did last week that LWR and SWP have opposite slope of the flat top.

V. NEBULAE AND INTERSTELLAR MEDIUM

OBSERVATIONS OF THE INTERSTELLAR MEDIUM WITH IUE

Edward B. Jenkins
Princeton University Observatory

IUE'S POTENTIAL FOR INTERSTELLAR MATTER RESEARCH

Over nearly eight years of operation, the Copernicus satellite has brought forth far-reaching conclusions on the composition and physical state of the interstellar medium. The many milestones of research from this orbiting telescope and spectrometer have demonstrated the unique value of ultraviolet absorption lines, far beyond some early, enthusiastic projections (e.g. ref. 1), since this region of the spectrum is especially rich in strong transitions from the lowest electronic levels of astrophysically important substances. In a complementary way, the IUE instrument has continued the tradition of disclosing new insights on the properties of low density regions in space.

In reviewing IUE's promise for exploring new frontiers, it is helpful to examine the strengths and weaknesses of this instrument relative to its predecessor, the one on board Copernicus. Since IUE records a spectrum with an image sensor instead of a scanning photomultiplier, it can integrate the signals from all spectral elements simultaneously and obtain information from stellar sources about 6 magnitudes fainter than those recorded by Copernicus (in spite of the latter's much larger collecting area). This increase in sensitivity means much to astronomers who wish to study the intrinsic properties of sources in the sky which emit UV radiation, since the classes of objects open to examination has broadened enormously, as this IUE symposium will attest. However, the observer dealing with the interstellar medium also realizes a gain, inasmuch as he or she can see to considerably greater distances or probe denser clouds where the absorption by grains is substantial.

On the other hand, we must acknowledge some important limitations of IUE for analyzing interstellar lines. Because there are small-scale photometric irregularities, it is generally conceded that the minimum detectable equivalent width is about 20 mÅ (Copernicus often registered lines at the 1 mÅ level). For a line to have a measurement of acceptable accuracy, it must have a strength of several times this threshold. However, the saturation of this line must be small, say less than a factor of 2, for a column density derivation to have even modest reliability. This condition is satisfied only if the velocity dispersion b for the gas is greater than about 8 km s^{-1}, which is often not the case for the more common interstellar species in individual absorbing regions. While saturated lines and the resulting uncertainties in their interpretation are a universal problem for astronomers, we must not be too harsh and categorically deny that useful work can be done in such instances. For example, one may compare the abundances of several species if their absorption lines are seen to have comparable strength and there is good reason to believe their velocity profiles are nearly identical. In this circumstance, we acknowledge that we have no information about what is happening in the saturated cores of the lines, but we do have the opportunity to compare

abundances of material in the outer wings of the velocity profile. Also, quite apart from equivalent widths, valuable information on the kinematics of interstellar gases in specially interesting contexts can be derived from ordinary measurements of the lines' radial velocity centroids.

HIGHLY IONIZED GAS

The appearance of sharp Si IV and C IV doublet absorptions in the IUE high dispersion stellar spectra of distant stars has attracted much attention. Initially, these lines were seen in the spectrum of the X-ray binary system HD153919 (4U1700-37) during the satellite's commissioning phase (refs. 2 and 3). At the time, it was suggested that X-rays from the binary system were responsible for ionizing the atoms in the ambient medium, since the Si IV and C IV absorption lines seemed extraordinarily strong. Now that a large number of stars have been observed with IUE, we realize that the highly ionized atoms in front of this source are not at all unusual; many of the ordinary O and B type stars show lines of comparable strength.

Throughout the history of high dispersion stellar spectroscopy, a recurrent controversy about the appearance of narrow absorption lines is whether they arise from some circumstellar accumulation of material or, alternatively, from the general medium between the stars. We can trace questions of this sort even back to the period following Hartmann's pioneering discovery of the stationary Ca II lines in the spectroscopic binary δ Ori in 1904 (ref. 4). It was not until about five years later that enough evidence from many binaries (ref. 5) could convince the skeptics that the Ca II lines indeed arose from the general reaches of space. Challenges on the general interstellar origin of some absorption lines also occurred during the era of the Copernicus satellite (refs. 6 and 7), to be answered by detailed case analyses (e.g., ref. 8) or by extensive statistical conclusions (refs. 9 and 10). The issue remains alive today, as we can see from the divergent viewpoints expressed by research groups interpreting their IUE recordings of the narrow Si IV and C IV lines. These features are found within their broader stellar counterparts and in most instances are well distinguished. Black et al. (ref. 11) have argued that the line widths are in accord with the expected values from material within an H II region which is photoionized by relatively energetic photons from the hot star. In contrast, from the perspective of Bruhweiler et al. (ref. 12) such lines may be produced in a hot phase of collisionally ionized interstellar material, which they labeled as "semitorrid" to differentiate it from the much hotter interstellar gas responsible for O VI absorption (refs. 13 and 14) and diffuse soft X-ray emission (ref. 15). Convincing evidence that Si IV and C IV lines can originate from general regions of space was presented by Savage and deBoer (ref. 16), who observed absorptions near zero velocity against a star in the LMC — a system with a radial velocity of approximately +250 km s^{-1}.

Neither of the conflicting interpretations seem to have serious flaws, and indeed both viewpoints may be correct. To support their respective conclusions, however, Black et al. and Bruhweiler et al. have had to rely on circumstantial relationships seen within fairly limited data bases. In this review, we will try to resolve the question by gathering all of the Si IV and

C IV data available at present and explore their relationships with various relevant parameters. We are no longer hampered by an insufficiency of independent observations, but we should be prepared to deal with spurious correlations arising from biased target star selections and the inclusion of data which are near the threshold of measurement. Our problems may be compounded when we commit the sin of mixing the data from different investigators, each of whom had categorically different types of coverage (stellar types and distance) and may have measured their lines in slightly different ways. Fortunately, the difficulties arising from selection effects and marginal detections are ameliorated by considering the complementary outputs from both the Copernicus and IUE satellites. The former is sensitive to very weak absorptions in nearby stars, while the latter can register the spectra of much fainter and more distant stars with their correspondingly higher column densities.

Table 1 summarizes the principal sources of Si IV and C IV data which are utilized for the studies which follow below. It must be emphasized that there are probably significant errors in some of the results. Many values are from preliminary analyses, others from reductions with a defective IUE intensity transfer function (ITF), while still others refer to target stars whose distances (or intrinsic characteristics) are poorly known. While individual points in the plots which follow may not be very trustworthy, the overall trends should, with some qualifications, be reasonably fair representations. To avoid inconsistencies and questionable assumptions, all of the column densities were rederived using the doublet-ratio method on the original measurements, rather than using the authors' quoted values for N(Si IV) or N(C IV). For doublet ratios less than 1.3, a lower limit corresponding to a factor of two saturation for the weaker line was assigned.

Support for the hypothesis that the observed Si IV and C IV arise primarily from the star's ionizing photons might be seen in a positive (but decidedly nonlinear) correlation of column density versus the star's effective temperature T_e*. Figure 1 shows these relationships for Si IV and C IV; one would be hard pressed to say that there is a convincing trend here. The column densities are adjusted by each star's radius to the 2/3 power to compensate for different sizes of the respective radiation-bounded Stromgren spheres of a given internal density. We might argue that the scatter could be blamed on wide variations of the density of the ambient gas in the different cases. Another test, which should be less sensitive to changes in density, is to determine if the ratio of C IV to Si IV varies with T_e*. We would expect this ratio to increase with T_e* since C III has a higher ionization potential than that of Si III. Figure 2, however, seems not to be at all encouraging in this regard.

Before we abandon the notion that photoionization from stars may be important sources of Si IV and C IV, we should remember that a good fraction of the chosen stars reside within OB associations. In such cases, the radiation field may be dominated by stars other than the target, such as possibly hotter but less conspicuous members of the group. Perhaps one could see more meaningful correlations if one classified the results according to association's distribution of stellar types or the conspicuousness of its H II region, rather than just the properties of the target stars.

We now turn to the hypothesis that the high stages of ionization arise primarily from widely distributed material at a high temperature. There are strong observational precedents (refs. 14 and 15) and sound theoretical reasons (ref. 21) which support the existence of very hot phases. Figure 3 shows how the column densities relate with the stars' distances. The wide dynamic range for distances and column densities for the Si IV plot results from our combining the Copernicus and IUE data. The lines of C IV were not measured in most of the Copernicus data base because the corrections for scattered light were too uncertain. Over the limited range of parameters for the C IV data, there seems to be no convincing dependence of column density with distance, but the Si IV results show an embarassingly strong relationship, with a best-fitting slope greater than unity, albeit the scatter at any given distance is large. It seems reasonable to suggest that Si IV is widely distributed but in a very irregular manner. Perhaps within 500 pc of the sun the density is significantly less than normal.

Figure 4 allows us to explore whether or not there is a relationship between the equivalent column density perpendicular to the galactic plane $N|\sin b|$ and the star's distance from the plane z. There is a hint of a turnover above 200 pc for the Si IV data. A deficiency of C IV at high z is less apparent, but the points above 1 kpc fall below a line of unit slope which passes through the middle of the low z points.

Further insight on the behavior of Si IV and C IV away from the galactic plane has been given by Savage and deBoer (refs. 16 and 22). They ranged the distance of the gas by assuming its radial velocity was dominated by corotation with the material in the plane of the galaxy. Their derived scale heights for C IV and Si IV absorption of approximately 2 and 4 kpc toward HD38282 and HD36402, respectively, seem generally consistent with what one would expect for hot gas in hydrostatic equilibrium above the plane. Of course, if a galactic wind or fountain of the type proposed by Shapiro and Field (ref. 23) is operating, the theoretical situation becomes more complicated and the distance cues from radial velocities become invalid (e.g. see ref. 24). The results of Bromage, Gabriel and Sciama (private communication via last-minute telex) for high latitude stars give a scale height for C IV of approximately 3 kpc, in accord with determinations toward the LMC.

If we proceed on the assumption that nearly all of the Si IV and C IV outline the presence of collisionally ionized interstellar gases, it is clear from the calculations of ionization equilibria (ref. 25) that the peaks in the relative fractions of 3-times ionized silicon and carbon occur at temperatures well below that of O VI ($\log T \sim 5.5$) or the characteristic temperatures for the observed diffuse X-ray emission ($\log T \sim 6$). We should not be surprised to find that the hot phases of interstellar gases exist over a broad range of temperatures. Indeed, we would be hard pressed to express why any particular temperature would be favored, since there are no abrupt changes in atomic properties (e.g. cooling functions) as there are, for instance, in an ordinary H II region near 10^4K (ref. 25). Viewed superficially, the relative absence of NV in the IUE spectra might indicate a lack of material near $\log T = 5.3$, between the O VI peak and those of Si IV or C IV. However, as the following discussion will demonstrate, the lower abundance of N V is consistent with

plausible physical explanations.

If interstellar gases are shock heated to a very high temperature by randomly arriving blast waves from supernovae (ref. 21) and allowed to cool radiatively, we would expect to find an overall temperature distribution for the material dn_e/dT which is proportional to the inverse of the cooling function Λ, if the cooling is isochoric. The relative ion abundances would then be evaluated by integrating over temperature the product of this distribution function, the appropriate ionization fraction curve and the element's overall abundance (assumed to be cosmic). For Λ and the ion fractions, we must use time dependent calculations which recognize that as a gas cools radiatively, there is a significant lag in the recombination from higher to lower stages of ionization.

Table 2 gives the relative fractions of Si IV, C IV and N V for the radiative cooling case, normalized to that of O VI. As it cools, the gas spends most of the time at log $T > 5.5$, and then it plunges fairly rapidly below this temperature. While the material spends relatively little time at the Si IV and C IV temperatures, the abundances of these ions are enhanced by a pronounced shoulder on the low temperature side of the time-dependent curves caused by dielectric recombination from higher stages. An interesting speculation is that the large variations in recorded densities of Si IV and C IV seen in Figure 3, significantly greater than those of O VI (ref. 10), are caused by the highly transitory aspect of the lower temperature cooling, making our ability to see the gas much more chancy. For isobaric cooling the decrease is slower at higher temperatures, and the low temperature plunge is more abrupt. This effect, coupled with time-dependent ion fraction curves which are closer to the steady-state ones, would result in significantly lower Si IV and C IV abundances.

An alternative to consider is that evaporation of cool clouds (ref. 26) is more important than radiative cooling, and that the ions we observe reside within the interface between the cloud's cool interior and the surrounding hot medium. In a different context (interstellar bubbles around stars losing mass), Weaver et al. (ref. 27) have calculated the time-dependent ion fractions for gas which is being heated within such an interface. These ratios are very close to those for the radiative cooling (see Table 2).

To arrive at a global value for the average densities of Si IV and C IV from the data sources listed in Table 1 is not a straightforward task, because over half of the data consist of upper or lower limits. One solution, however, is to assume that the actual distribution of column densities is fairly well-behaved and that a distance-weighted median is a good measure to adopt. Table 2 lists these medians for the Si IV and C IV data sources in Table 1. Put differently, over the total path length covered by all observations, half of the distance had lower densities and half had larger. Because most of the upper and lower limits are below and above these densities, respectively, the results would be virtually unchanged if we had actual measured values instead. One aspect of these determinations which is probably unfair is that there may be over-representation of the anomalously low-density volume within several hundred pc. of the sun. The N V density listed in the table is based on the fact that, except for the survey by Black et al.(ref.11),

the absorption lines are usually not detected and in a few cases only marginally seen. The O VI densities are from the summary by Jenkins (ref. 10).

The observed relative abundances of O VI, N V and C IV seem to fit the expected ratios rather well. On the other hand, the amount of Si IV present seems to be well above the expectations. Perhaps starlight ionization is an important contributor of additional Si IV. An alternative explanation may be that the ion fraction computed by Shapiro and Moore (ref. 25) on the low temperature side of the Si IV peak is significantly underestimated. Baulinas and Butler (ref. 28) have shown that charge exchanges with ionized helium atoms can be an important additional source of ionization for Si III (their calculations, however, depict only the steady-state solutions).

VENTURES OUT OF THE GALACTIC PLANE

A significant triumph of the IUE mission has been the instrument's ability to record spectra of sources fainter than those indicated by prelaunch projections for limiting magnitudes. Observers of the interstellar medium have been able to capitalize on this advantage by bridging the vast regions of space between the plane of our galaxy and the two Magellanic Clouds. At present count, thirteen early-type stars having V magnitudes between 10.5 and 12.5 have been observed at high resolution by IUE (refs. 22 and 29). As mentioned earlier, these observations gave us the most straightforward proof that Si IV and C IV exist in general regions of space and not just in the vicinity of very hot stars. If one is willing to accept the assumptions on how radial velocities scale with distance, the distribution of gas along the line of sight is mapped by the extension of absorption from zero to moderately high positive velocities, an effect which shows qualitative differences over the different ranges of ionization (and inherent line strengths).

In their spectra of stars in the Large Magellanic Cloud (LMC), Gondhalekar et al. (ref. 29) and Savage and deBoer (ref. 22) have identified discrete absorbing regions having radial velocities of about 80 km s^{-1} and 130 km s^{-1}, midway between the gas in the plane and that associated with the LMC. For their best example, HD36402, Savage and deBoer were able to measure the column density of Fe II in the material at intermediate velocity, because this ion had many transitions with widely different f-values and the velocity dispersion was large. They could also assign lower limits for the abundances of O I, Mg II, Al II and Si II. From an upper limit for N(HI) based on a lack of 21-cm emission in the same direction, Savage and deBoer concluded that these heavy elements are no less than a factor of ten below solar abundances. They were quick to add, however, that this conclusion may be invalid if the ions are associated primarily with ionized, rather than neutral hydrogen. One point does seem clear: material processed through stellar interiors may be found at large distances from the plane provided, of course, that we are not being fooled by the presence of high velocity clouds which are relatively local.

A group of observers analyzing the low resolution spectra of 3C273 (ref. 30) confirmed that along a direction quite different from that of the LMC the absorption by C IV in our halo is also quite strong. Using 21 cm profiles in the same direction to model the velocity structure of neutral halo material,

they too found that the heavy element abundances were not far below the cosmic ratios. Once again, the validity of this conclusion rests upon there not being much ionized hydrogen present (or extended wings of high velocity H I below the 21-cm detection threshold). Interstellar lines at low resolution for a supernova in M100 (ref. 30) were used to derive a velocity dispersion of about 20 km s^{-1} for neutral and once ionized atoms in our (and M100's) disk and halo material and 50 km s^{-1} for the highly ionized species. Because these lines were very strongly saturated, no abundances could be derived.

Material in the general vicinity of stars rapidly losing mass in the 30 Doradus complex (in the LMC) has been investigated by deBoer, et al. (ref. 32). They find absorption lines associated with H I regions at a velocity of +290 km s^{-1}. This neutral material is presumably part of a large, quiescent complex of gas surrounding the system. Lines from dense H II region material, such as those from O I, C II and Si II in states of fine structure excitation, are shifted by -40 km s^{-1} with respect to the neutral gas (i.e. they appear at +250 km s^{-1}). Such an outflow from the stellar system could result from either the rapidly moving stellar winds, an ionization front, or disturbances generated by past supernova activity. Even larger velocity shifts are seen for the highly ionized material, which is likely to be part of a hot corona around the LMC system (ref. 33). The relative abundances of Si II and O I in the H I gas near the LMC seem consistent with that in our galaxy, but the uncertainties are large. From their low resolution recording of Lα absorption, deBoer et al. estimated a ratio of gas to reddening of 1.9 x 10^{22} atoms cm^{-2} mag^{-1} for the material near 30 Doradus, after subtracting off estimates for the amount of foreground H I and reddening in the galactic plane. This figure is about 4 times that found toward stars in the plane surveyed by the Copernicus satellite (ref. 34).

HIGH VELOCITY GAS

New observations and theoretical treatments over the past decade have expanded our awareness of the widespread propagation through the interstellar medium of mechanical disturbances created by supernova explosions and high speed mass-loss winds from early-type stars (ref. 35). Rapidly moving gases which collide with the quiescent material form shocks which in turn cause significant heating and ionization. When interstellar absorption lines are shifted by at least 50 km s^{-1}, they are well enough separated from the strong lines of undisturbed gas to be studied with the IUE spectrograph. The velocity dispersion of the post-shock material is usually rather large, which helps to reduce the difficulties arising from curves of growth which are too flat.

Gondhalekar and Phillips (ref. 36) have investigated the high velocity material seen in front of one star behind the supernova remnant IC443 and another behind Shajn 147. From their column density measurements and an upper limit for the 21-cm emission they claim the depletions of Fe, Mg, Al, Si and Ca to be no more than a factor of 10 below the cosmic values. Actually, this conclusion would be invalid if these lines arose from ionized material, but the uniformity of their formal numbers from element to element suggests that the depletions are indeed rather modest. This conclusion is in accord with an earlier study of the Vela remnant using the Copernicus satellite (ref. 37).

Giaretta et al. (ref. 38) have measured abundances and derived physical conditions in high velocity clouds in front of four stars not near any particular known supernova remnant. A study of emission lines from the Cygnus Loop by Raymond et al. (ref. 39) gives results which are consistent with a shock velocity of about 130 km s^{-1}, but with a deficiency of recombined material indicated by a higher than expected ratio of [O III] to Hβ emission. They suggest that either they are viewing a recently shocked cloud which has not yet had time to recombine or the shock is just beginning to enter the snowplow phase. By studying the strengths of C IV, C III and C II emission lines relative to those of other elements in the Cygnus Loop, Benvenuti et al. (ref. 40) concluded that the depletion of carbon is largest in the immediate post-shock region containing C IV and becomes progressively smaller when the gas works its way downstream, presumably because graphite grains are evaporating in the hot material. Corrections for the effects of line saturation and the departures from steady flow, however, may modify this conclusion (ref. 39).

OTHER AREAS OF INVESTIGATION

We must not overlook IUE's value in contributing to our understanding of non-atomic species in the interstellar medium. Unfortunately, the short end of the wavelength coverage of IUE just misses the molecular hydrogen electronic transitions (the Lyman bands, and at shorter wavelengths still, the Werner system). But another important molecule, carbon monoxide, has its fourth positive system situated right in the middle of the short wavelength camera's coverage. This system is ideal for study, since the different vibrational members give us a very wide range of line strengths to observe. Black has reported on the CO column densities toward 12 stars (ref. 41), and much like the early Copernicus observations (ref. 42), finds no easily identifiable lines from other molecules. Tarafdar et al. (ref. 43) have tentatively identified the presence of circumstellar CO toward the star 9 Cep.

The behavior of the interstellar extinction in the ultraviolet by dust is an important diagnostic for studying the size and composition of the particles. Often there are large differences in the shape of the extinction curve from one region to the next (ref. 44). Results for eight reddened stars in the LMC seem to indicate that, with the exception of one star, the extinction curves turn up more rapidly at the short wavelength end than for stars in our part of the galaxy (ref. 45). This behavior is consistent with the notion that there are greater numbers of small particles in the dust mixture near the LMC stars.

Finally, we should not lose our awareness of IUE's potential for studying the very local regions of space. "Reversals" caused by interstellar gases can be seen in the chromospheric emission of cool stars at Lα (ref. 46) or Mg II (ref. 47), and if studied systematically, could help us to better understand the distribution of material within a few tens of parsecs.

This research was supported by NASA grant NSG-5248. The author is indebted to W. Taylor and D.G. York for communicating their results well in advance of publication.

REFERENCES

1. Spitzer, L. and Zabriskie, F.R.: Pub. Astr. Soc. Pacific, vol. 71, 1959, p. 412.

2. Grewing, M., Boksenberg, A., Seaton, M.J., Snijders, M.A.J., Wilson, R., Boggess, A., Bohlin, R.C., Perry, P.M., Schiffer, I.H. III, Gondhalekar, P.M., Macchetto, F., Savage, B.D., Jenkins, E.B., Johnson, H.M., Perinotto, M., and Whittet, D.C.B.: Nature, vol. 275, 1978, p. 24.

3. Dupree, A.K., Davis, R.J., Gursky, H., Hartmann, L.W., Raymond, J.C., Boggess, A., Holm, A., Kondo, Y., Wu, C.C., Machetto, F., Sandford, M.C.W., Willis, A.J., Wilson, R., Ciatti, F., Hutchings, J.B., Johnson, H.M., Jugaku, J., Morton, D.C., Treves, A., van den Heuvel, E.P.J.: Nature, vol. 275, 1978, p. 30.

4. Hartmann, J.: Ap.J., vol. 19, 1904, p. 268.

5. Slipher, V.M.: Lowell Obs. Bull., 1909, no. 51.

6. Steigman, G., Strittmatter, P.A. and Williams, R.E.: Ap.J., vol. 198, 1975, p. 575.

7. Castor, J., McCray, R. and Weaver, R.: Ap.J.(Letters), vol. 200, 1975, p. L107.

8. Morton, D.C. and Bhavsar, S.P.: Ap.J., vol. 228, 1979, p. 147.

9. Jenkins, E.B.: Comments Astr., vol. 7, 1978, p. 121.

10. Jenkins, E.B.: Ap.J., vol. 220, 1978, p. 107.

11. Black, J.H., Dupree, A.K., Hartmann, L.W., and Raymond, J.C.: Ap.J. (in press, July 15 issue) 1980.

12. Bruhweiler, F.C., Kondo, Y., and McCluskey, G.E.: Ap.J.(Letters), vol. 229, 1979, p. L39.

13. York, D.G.: Ap.J.(Letters), vol. 193, 1974, p. L127.

14. Jenkins, E.B. and Meloy, D.A.: Ap.J.(Letters), vol. 193, 1974, p. L121.

15. Williamson, F.O., Sanders, W.T., Kraushaar, W.L., McCammon, D., Borken, R. and Bunner, A.N.: Ap.J.(Letters), vol. 193, 1974, p. L133.

16. Savage, B.D. and deBoer, K.S.: Ap.J.(Letters), vol. 230, 1979, p. L77.

17. Bruhweiler, F.C., Kondo, Y. and McCluskey, G.E.: Ap.J., vol 237 (in press, April 1 issue) 1980.

18. Morton, D.C.: Ap.J., vol. 197, 1975, p. 85.

19. Morton, D.C. and Hu, E.M.: Ap.J., vol. 202, 1975, p. 638.

20. Morton, D.C.: Ap.J., vol. 222, 1978, p. 863.

21. McKee, C.F. and Ostriker, J.P.: Ap.J., vol. 218, 1977, p. 148.

22. Savage, B.D. and deBoer, K.S.: Submitted to Ap.J., 1980.

23. Shapiro, P.R. and Field, G.B.: Ap.J., vol. 205, 1976, p. 762.

24. Bregman, J.N.: Ap.J., vol. 236, 1980, p. 577.

25. Shapiro, P.R. and Moore, R.T.: Ap.J., vol. 207, 1976, p. 460.

26. McKee, C.F. and Cowie, L.L.: Ap.J., vol. 215, 1977, p. 213.

27. Weaver, R., McCray, R., Castor, J., Shapiro, P. and Moore, R.: Ap.J., vol. 218, 1977, p. 377.

28. Baliunas, S.L. and Butler, S.E.: Ap.J.(Letters), vol. 235, 1980, p.L45.

29. Gondhalekar, P.M., Willis, A.J., Morgan, D.H. and Nandy, K.: Proc. 2nd European IUE Conf., 1980.

30. Ulrich, M.H., Boksenberg, A., Bromage, G., Carswell, R., Elvius, A., Gabriel, A., Gondhalekar, P.M., Lind, J., Lindgren, L., Longair, M.S., Penston, M.V., Perryman, M.A.C., Pettini, M., Perola, G.C., Rees, M., Sciama, D., Snijders, M.A.J., Tanzi, E., Tarenghi, M., Wilson, R.: MNRAS, in press, 1980.

31. Panagia, N., Vettolani, G., Boksenberg, A., Ciatti, F., Ortolani, S., Rafanelli, P., Rosino, L., Gordon, C., Reimers, D., Hempe, K., Benvenuti, P., Clavel, J., Hack, A., Penston, M.V., Macchetto, F., Strickland, D.J., Bergeron, J., Tarenghi, M., Marano, B., Palumbo, G.G.C., Parmar, A.N., Pollard, G.S.W., Sanford, P.W., Sargent, W.L.W., Sramek, R.A., Weiler, K.W., Matzik, P.: MNRAS, in press, 1980.

32. deBoer, K.S., Koornneef, J. and Savage, B.D.: Ap.J., vol. 236, 1980, p. 769.

33. deBoer, K.S. and Savage, B.D.: Ap.J.vol. 238, in press, 1980.

34. Bohlin, R.C., Savage, B.D. and Drake, J.F.: Ap.J., vol. 224, 1980, p. 132.

35. McCray, R. and Snow, T.P.: Ann. Rev. Astr. and Ap., vol. 17, 1979, p. 213.

36. Gondhalekar, P.M. and Phillips, A.P.: Proc. 2nd European IUE Conf., 1980.

37. Jenkins, E.B., Silk, J., and Wallerstein, G. Ap.J.(Suppl.), vol.32, 1976, p. 681

38. Giaretta, D., Bates, B., Bankhead, R.E.L., Brown-Kerr, W., and McQuoid, J.A.: Proc. 2nd Eur. IUE Conf., 1980.

39. Raymond, J.C., Black, J.H., Dupree, A.K., Hartmann, L. and Wolff, R.S.: Ap.J. in press, 1980.

40. Benvenuti, P., D'Odorico, S. and Dopita, M.A.: Nature, vol. 277, 1979, p. 99.

41. Black, J.H.: Proc. IAU Symp. 87 on Interstellar Molecules, 1979.

42. Jenkins, E.B., Drake, J.F., Morton, D.C., Rogerson, J.B., Spitzer, L., and York, D.G.: Ap.J.(Letters), vol. 181, 1973, p. L122.

43. Tarafdar, S.P., Krishna Swamy, K.S., Vardya, M.S.: MNRAS, submitted 1980.

44. Savage, B.D. and Mathis, J.S.: Ann. Rev. Astr. and Ap., vol. 17, 1979, p. 73.

45. Nandy, K., Morgan, D.H., Willis, A.J., Wilson, R., Gondhalekar, P.M. and Houziaux, L.: Nature, vol. 283, 1980, p. 725.

46. Linsky, J.L., Ayres, T.R., Basri, G.S., Morrison, N.D., Boggess, A., Schiffer, F.H., Holm, A., Cassatella, A., Heck, A., Macchetto, F., Dupree, A.K., Jordan, C., and Wing, R.F.: Nature, vol. 275, 1978, p. 19.

47. Böhm-Vitense, E.: preprint 1980.

TABLE 1

Source	No. of stars	Remarks
Bruhweiler, et al. (ref. 17)	17	All targets were binary systems. Flawed ITF used.
Black, et al. (ref. 11)	12	Distances typically 1 kpc. Flawed ITF used.
Taylor and York (private communication of preliminary results)	46	Distances typically somewhat greater than 1 kpc, mostly in the galactic plane. Good ITF used.
Jenkins (special workup for this review)	22	High latitude, distant stars. Good ITF used.
	40	From Copernicus archives. Most stars are closer than 1 kpc.
Miscellaneous sources of Copernicus data (refs. 18, 19, 20, and 8)	3	ζ Oph, γ Ara, ζ Pup, and γ Vel.

TABLE 2 -RELATIVE ION ABUNDANCES

	Si IV	C IV	N V	O VI
Prediction for Isochoric Radiative Cooling	0.018	0.28	0.078	1.00*
Prediction for Evaporation Interfaces	0.010	0.16	0.063	1.00*
Observed representative densities (cm^{-3}):				
a) near the galactic plane (from data sources in Table 1)	3.6×10^{-9}	6.9×10^{-9}	$\lesssim 1.2 \times 10^{-9}$	2.0×10^{-8}†
b) away from the galactic plane (ref. 22)	1×10^{-9}	3×10^{-9}	$\lesssim 1 \times 10^{-9}$	---

* O VI set to 1.00; other ions are expressed relative to O VI.

† from ref. 10, corrected to $z = 100$ pc.

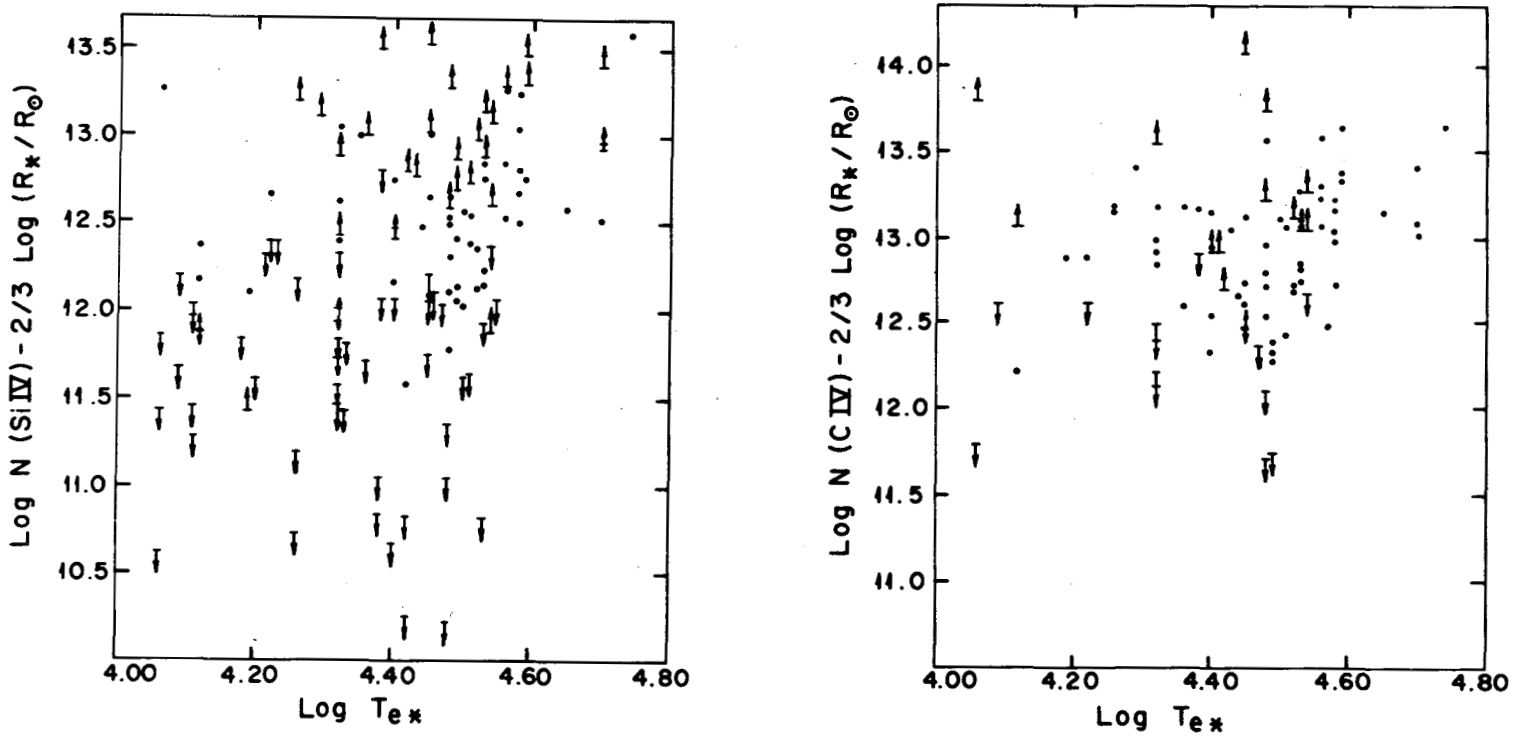

Figure 1. Logarithmic plots of column densities, adjusted for varying Stromgren Sphere sizes, versus the effective temperatures of the target stars.

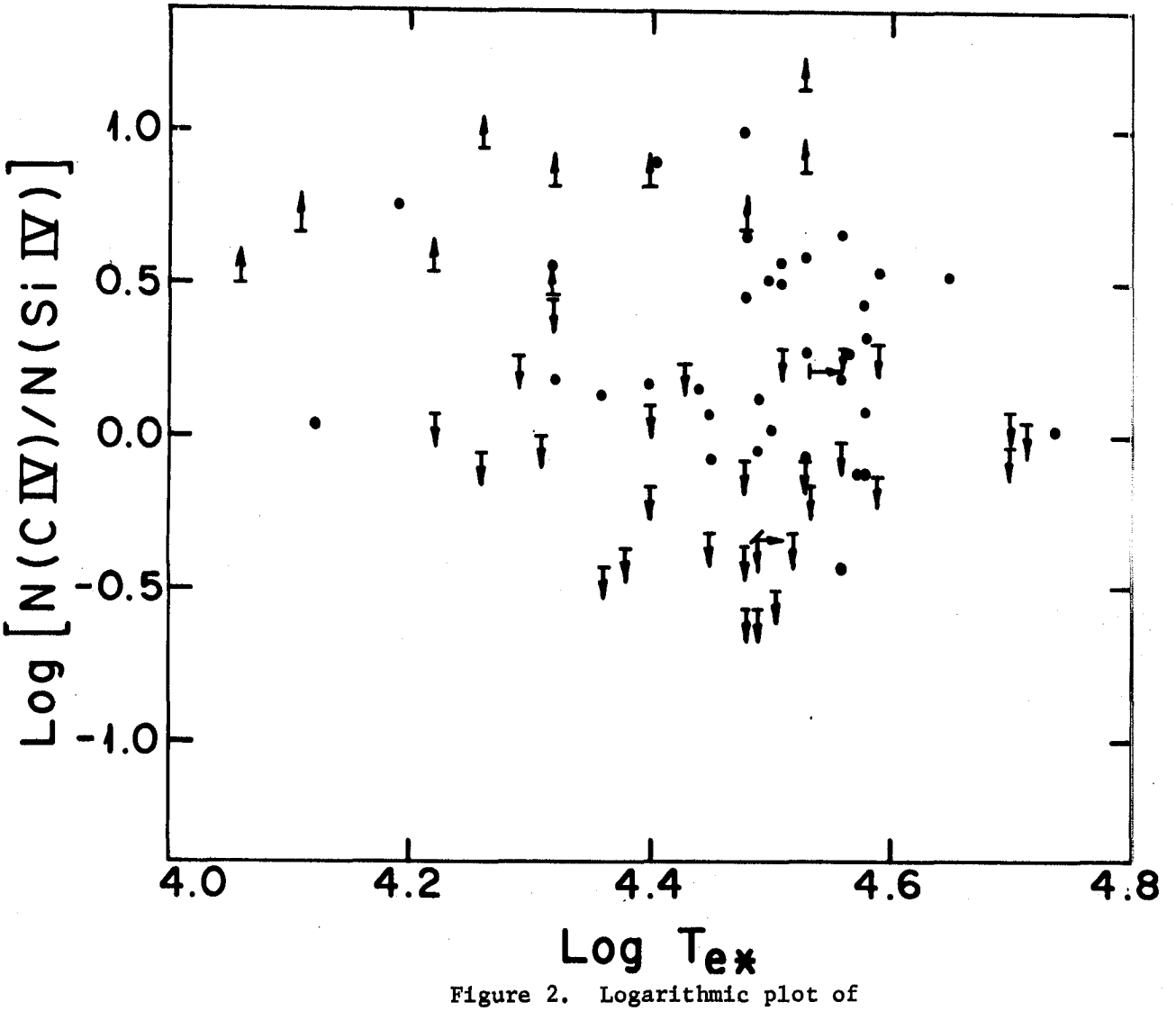

Figure 2. Logarithmic plot of the ratio of C IV to Si IV column densities versus the effective temperatures of the target stars.

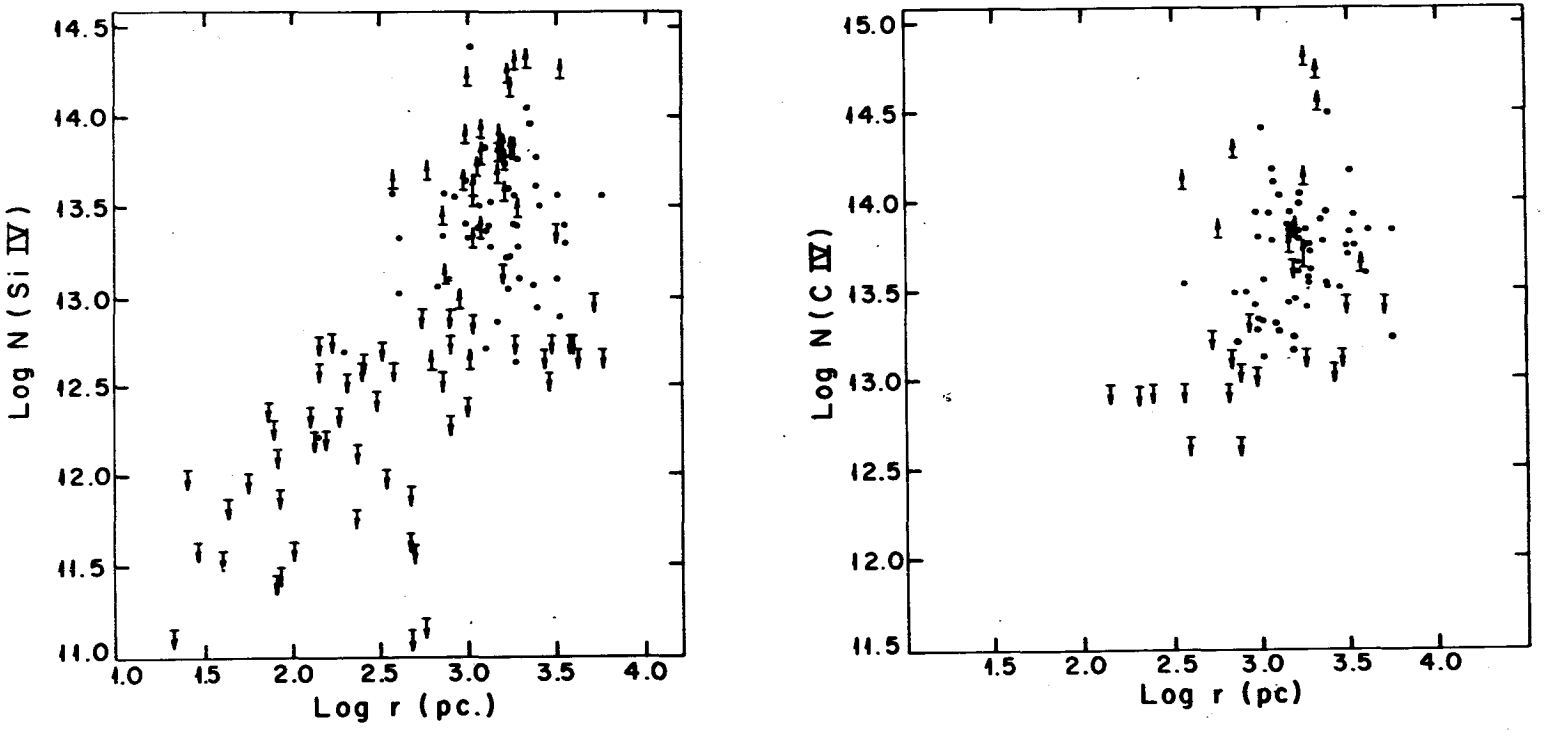

Figure 3. Logarithmic plots of column densities versus distances to the stars.

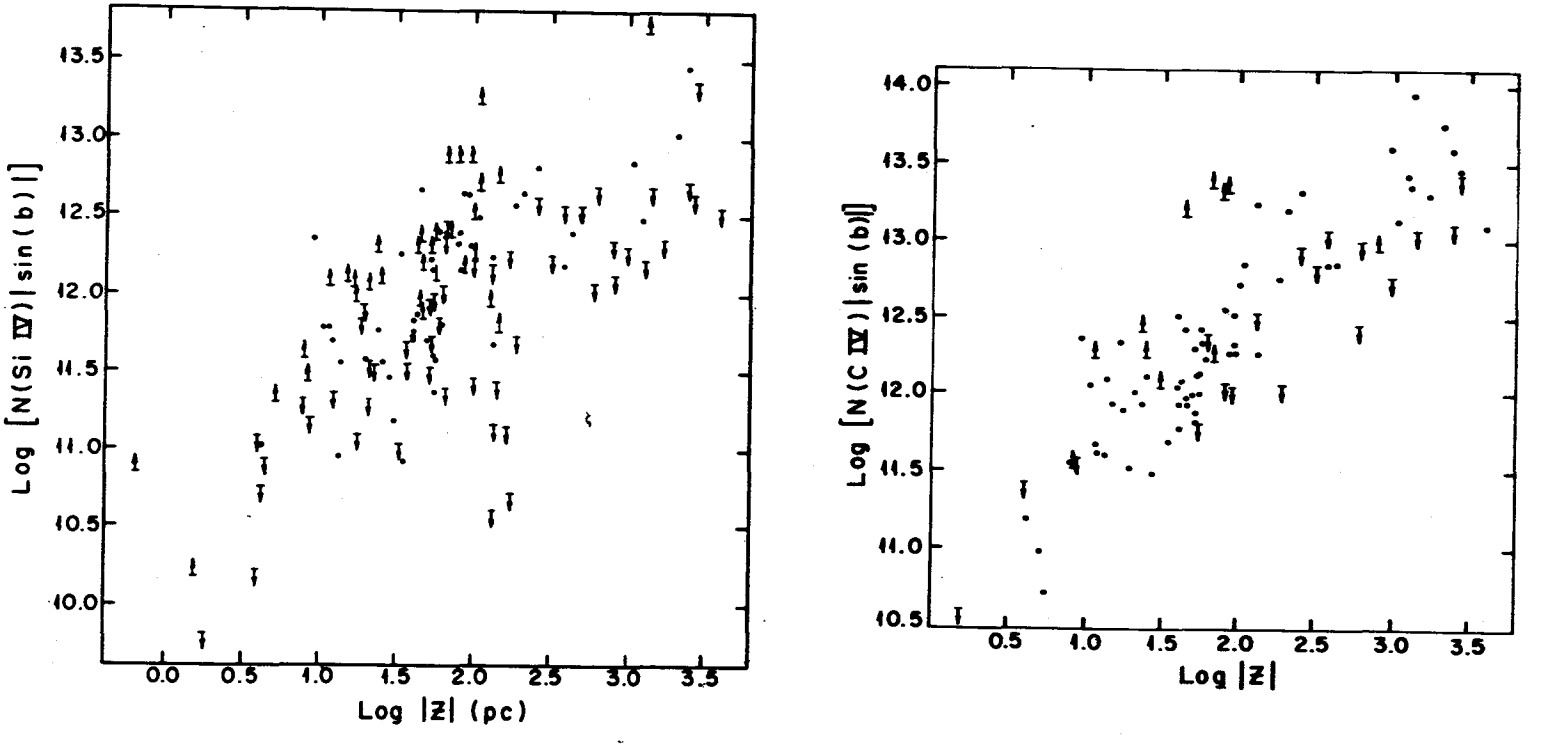

Figure 4. Logarithmic plots of equivalent column densities perpendicular to the galactic plane versus distance of the stars from the plane.

NEW INSIGHTS INTO THE PHYSICAL STATE OF GASEOUS NEBULAE

Manuel Peimbert
Instituto de Astronomía
Universidad Nacional Autónoma de México

ABSTRACT

The impact of our knowledge of H II regions, planetary nebulae and supernova remnants due to IUE is briefly examined. Some of the more relevant aspects related to the physical conditions of gaseous nebulae are reviewed. The analysis of IUE data is under process and already significant results have been obtained on the following properties of gaseous nebulae: a) density and temperature distribution, b) ionization structure, c) chemical composition, d) internal dust, and e) shock velocity for supernova remnants. The CNO abundances of planetary nebulae are compared with stellar evolution models.

INTRODUCTION

To understand the nature of gaseous nebulae it is necessary to study their physical properties; the most important are: density and temperature distributions, ionization structure, chemical composition, dust presence and mass motions. From a profound knowledge of gaseous nebulae, it is possible to derive accurate chemical compositions to study such important problems as stellar and galactic chemical evolution. The three types of gaseous nebulae that will be considered in this review are: H II regions, planetary nebulae (PN) and supernova remnants (SNR).

There are at least four areas in which ultraviolet observations are paramount for our understanding of gaseous nebulae: a) the determination of the ionization structure from the detection of ions without strong optical emission lines such as CII, CIII, CIV, NIII, NIV, NV, OIV, OV, SiII, SiIII, SiIV and MgII, b) the determination of the density structure from the ratio of emission lines such as 1907/1909 of CIII and 2422/2425 of NeIV, c) the determination of the temperature structure by comparing the line intensity of the same ion originating from three different energy levels like λλ1663, 4363 and 5007 of OIII which for an electron density $N_e<10^4$ cm^{-3} permits us to determine the electron temperature, T_e, and the mean square temperature variation over the observed volume, t^2, d) the presence of internal dust from the optical thickness of resonance lines like 1548 and 1551 of CIV and from the gaseous abundances of certain elements that might be partially locked up in grains like Mg, Si and C.

Excellent review papers on the possibilities for UV research of gaseous nebulae and on PN results derived from IUE data are presented elsewhere (ref. 1,2).

H II REGIONS

There have been three determinations of abundances of the Orion nebula based on IUE data (ref. 3,4,5). The three groups find a C/O ratio similar to the solar one (see table I) implying that the amount of carbon locked up in grains inside the Orion nebula is not substantial.

Perinotto and Patriarchi (ref. 3) obtain log $Mg^+/H^+ \leq -6.7$ for the Orion nebula; to estimate Mg/H they make use of the value $Mg^+/Mg = 0.15$ derived from a model of IC 418 by Harrington et al. (ref. 8) and conclude that their observed upper limit corresponds to a Mg/H value an order of magnitude smaller than the solar value implying that most of the Mg is locked up in grains. The Mg ionization correction factor should be verified due to its very large value and to the higher ionization degree of the Orion nebula relative to that of IC 418; furthermore from the models by Köppen (ref. 9) for objects like IC 418 and the Orion nebula with $33000 \leq T^* \leq 40000$ °K and $1 < (R^*/R_\odot)(N_e^{1/2}/100) < 10$ it is obtained that $0.008 \leq Mg^+/Mg \leq 0.04$. The possibility of resonance line scattering reducing the Mg 2800 line intensity should also be considered.

By comparing the C^{++} 1907+1909 intensity with that of C^+ 4267 it is found that $t^2 = 0.016$ for the Orion nebula (ref. 4).

Rosa (ref. 10) has observed two extragalactic H II regions, NGC 604 and NGC 5471, which show a continuum energy distribution with stellar absorption and emission lines. In addition NGC 5471 shows strong C^{++} 1907+1909 emission of nebular origin.

From the work of Bohlin et al. (ref. 5), Perinotto and Patriarchi (ref.11) and others, it is found that most of the continuum observed in galactic H II regions is due to dust-scattered light from the ionizing O and B stars. From these data the dust-scattering efficiency and albedo as a function of wavelength have been estimated. The results depend on the model adopted for the spatial distribution of the dust and stars, therefore more observations and better models are needed to decide among several possibilities.

The relatively low temperatures and high dust content of H II regions with solar abundances makes the detection of UV emission lines very difficult and consequently the determination of their chemical abundances. Alternatively, extragalactic metal-poor H II regions have higher electron temperatures which produce emission lines relatively brighter than the stellar dust-scattered continua. Metal-poor H II regions that can be observed without their ionizing stars, like those in the Magellanic Clouds, are particularly good for the study of emission lines.

The determination of the electron density, N_e, from UV lines is particularly important for the study of the regions of high degree of ionization. From the ratio 1907 [CIII] to 1909 CIII] and the computations by Nussbaumer and Schild (ref. 12) the N_e values of several PN have been obtained (ref. 13, 14). From the [Ne IV] 2422/2425 ratio the N_e value has been obtained for NGC 7662 (ref. 15).

There is no good method to determine directly from visual data T_e for the region where helium is twice ionized. This can be done by combining IUE data with visual observations or by using only IUE data. From the [NeIV] 1602/(2422+2425) and 2422/2425 ratios it is possible to obtain N_e and T_e. The [N_eIV] 1602/(2422+2425) ratio has already been measured in NGC 3918 (ref. 16). By comparing λ4267 of CII and λλ1907+1909 of CIII it has been found that t^2= 0.02 for IC 418 (ref. 4); while from λλ1663,4363 and 5007 of OIII it has been found that t^2= 0.00 for the regions where the OIII lines originate.

The most important result derived so far on PN from IUE data is a set of CNO abundances that are presented in table II. The O/H ratios are very similar to those derived from visual data. The UV carbon abundances are mainly based on C^{++} and C^{+} ionic concentrations and ionization structure models; for CIV 1548, 1551 the dust-free models predict higher intensities than observed (ref. 2, 16), the difference is most likely due to the presence of internal dust that absorbs the resonance line radiation. The UV carbon determinations are of higher accuracy than those based on the λ4267 CII lines (ref. 18) due to the larger number of observed ions and to the faintness of the λ4267 lines which typically have been overestimated by factors ranging from 1.5 to 2.5 (ref. 4). The UV nitrogen abundances in Table II are based on N^{++}, N^{+++} and N^{++++} ionic concentrations while the visual determinations are based only on N^{+}, which for many PN is only a trace ion; therefore the UV results are more reliable. It can be seen from Table II that the difference between the IUE and visual N/O determinations increases with degree of ionization which implies that the visual method breaks down by underestimating the N/O ratio in objects of high ionization degree.

The C abundances in Table II include only the gaseous component in the PN shell, and since part of the C might be locked up in grains inside the nebula, correspond to lower limits to the total values. For NGC 7027 it has been estimated that the amount of carbon locked up in grains is similar to that listed in Table II (ref. 24). In Table II the abundances of the sun and the Orion nebula are presented for comparison. It is clear from this table that, even without considering the amount of C in the form of dust, C and N have been substantially enriched during the evolution of their central stars. Renzini and Voli (ref. 25), based on the work by Iben's group, have computed the evolution of the surface abundances of He, C, N and O in intermediate mass stars from the main sequence phase up to the ejection of the PN. In figures 1 and 2 we compare the models with the observations of Table II. For C/O the models agree reasonably well with the observations. Alternatively for N/O not only PN of Type I (ref. 26) with high He/H values present large N/O values but also other PN of Type II like NGC 7027, NGC 6886 and IC 2448, which originated

from stars with $M/M_{\odot} \leq 2.4$ (ref. 27), present N/O values larger than predicted, possibly indicating that the stellar evolution models should include turbulent diffusion and meridional circulation (ref. 25).

The intensity ratio of the NV, CIV and MgII resonance doublets (λλ1239/1243, 1548/1551, 2796/2803) is expected to be equal to 2, the ratio of the respective collision strengths in dust-free nebulae. In all the reported cases the ratios are smaller than 2 (ref. 13,14) indicating dust presence. Moreover the ionization structure models without dust predict a higher intensity than observed for the CIV doublet (see above) possibly indicating that the doublet has been attenuated by internal dust. Pequignot and Stasinska (ref. 28) have found that the observed MgII doublet in NGC 7027 is a factor of 10 smaller than the value predicted by their dust-free models, they have estimated that a fraction of this difference is due to internal dust attenuation and that the rest is due to a substantial amount of Mg embedded in dust grains. From the Mg doublet ratio and a model containing dust it will be possible to quantitatively evaluate these two effects.

SUPERNOVA REMNANTS

Most of the SNR lines in the UV originate in regions where $4\times10^4 < T_e < 4\times10^5$ °K this temperature range corresponds to the gap left by the visual and X-ray observations. The UV is particularly well suited to derive accurate shock velocities, v_s, for cases where $v_s \sim 100$ km s^{-1}. From the value of v_s, the emission line intensities and models available, it is possible to determine the chemical composition of the SNR.

From IUE observations of the Cygnus Loop v_s values in the 100-130 km s^{-1} range have been obtained (ref. 29,30,31). By combining these observations with shock models and neglecting radiative transfer models due to the presence of dust it is found that λλ1548+1551 CIV, 1907+1909 [CIII] + CIII] and 2326 CII] are too weak by factors of 10, 2.5 and 1.5 (ref. 29,30) and by 10, 1.6 and 1.4 (ref. 31) respectively; it has been suggested that these observations can be explained by progressive destruction of graphite grains. Benvenuti et al. (ref. 30) find that λ1335 CII is too weak by about an order of magnitude while Raymond et al. (ref. 31), from the 1335/2326 ratio, find that the optical depth in the resonance lines due to dust reduces the λ1335 flux by a factor of ten. As mentioned before, resonance line scattering reduces the CIV line intensities in PN and it is highly probable that in SNR a similar situation prevails which would make the C underabundance in the Cygnus Loop marginal. Considering that C is depleted by about an order of magnitude in the interstellar medium this result would imply that substantial destruction of graphite grains occurs in shocks with $v_s \sim 130$ km s^{-1}. Raymond et al.(ref. 31) present some evidence in favor of a depletion of ∿3 in Si.

The Crab nebula is the only young SNR observable with the IUE; this SNR has not been significantly contaminated by the interstellar medium, therefore its chemical composition still corresponds to that of the SN. Davidson et al. (ref. 32) from preliminary IUE results obtain for the Crab nebula that $N(C)/N(O)<3$. By considering that in this object $O/O_{\odot} \sim 1/3$ (ref. 33) the C/O upper

limit implies that, contrary to expectations, at least this SN did not produce much carbon.

REFERENCES

1. Osterbrock, D.E.: Physical Characteristics of Ionized Gaseous Nebulae, in Scientific Research with the Space Telescope, NASA CP-2111, 1979, pp. 99-121.

2. Nussbaumer, H.: Observations of Planetary Nebulae. 2nd European Meeting on IUE, Tubingen, in press.

3. Perinotto, M.; and Patriarchi, P.: The Abundance of C and Mg in the Orion Nebula. Ap. J., Vol. 235, 1980, pp. L13-L16.

4. Torres-Peimbert, S.; Peimbert, M.; and Daltabuit, E.: IUE and Visual Observations of the Orion Nebula and IC 418: The C Abundance. Ap. J., 1980, in press.

5. Bohlin, R.C.; Hill, J.K.; Stecher, T.P.; and Witt, A.N.: Long-Slit Spectroscopy in the Rocket UV of the Orion Nebula. Ap. J., 1980, in press.

6. Lambert, D.L.: The Abundances of the Elements in the Solar Photosphere-VIII: Revised Abundances of C, N and O. M.N.R.A.S., Vol. 182, 1978, pp. 249-272.

7. Lambert, D.L.; and Luck, R.E.: The Abundances of the Elements in the Solar Photosphere-IX: Na to Ca. M.N.R.A.S., Vol. 183, 1978, pp. 79-100.

8. Harrington, J.P.; Lutz, J.H.; Seaton, M.J.; and Stickland, D.J.: UV spectra of PN. I. The Abundance of C in IC 418. M.N.R.A.S., 1980, in press.

9. Köppen, J.: Photoionization Models for Gaseous Nebulae. III. Third Period Elements. Astron. Astrophys. Suppl. Ser., Vol. 39, 1980, pp. 77-81.

10. Rosa, M.: IUE UV Spectra of Giant Extragalactic H II Regions. Astron. Astrophys. Letters, 1980, in press.

11. Perinotto, M.; and Patriarchi, P.: IUE Observations of the Continuous Spectrum of the Orion Nebula. Ap. J., 1980, in press.

12. Nussbaumer, H.; and Schild, H.: CIII Observable with IUE. Astron. Astrophys. Vol. 75, 1979, pp.L17-L19.

13. Flower, D.R.; Nussbaumer, H.; and Schild, H.: The EUV Spectra of Young PN. Astron. Astrophys., Vol. 72, 1979, pp. L1-L3.

14. Köppen, J.; and Wehrse, R.: High Dispersion EUV Observations of PN. Astron. Astrophys., 1980, in press.

15. Lutz, J.H.; and Seaton, M.J.: The NeIV ^2D-^5S Lines in the PN NGC 7662. M.N.R.A.S., Vol. 187, 1979, pp. 1p-7p.

16. Torres-Peimbert, S.; Peña, M.; and Daltabuit, E.: The High-Excitation PN NGC 3918 and IC 2448, 1980, this Symposium.

17. Aller, L.H.; and Keyes, C.D.: IUE Observations of Seven High-Excitation PN. Proc. Natl. Acad. Sci. USA, 1980, in press.

18. Torres-Peimbert, S.; and Peimbert, M.: Photoelectric Photometry and Physical Conditions of PN. Rev. Mexicana Astron. Astrof., Vol. 2, 1977, pp. 181-207.

19. Kaler, J.B.: The Enrichment of N and He in PN. Ap. J., Vol. 228, 1979, pp. 163-178.

20. Perinotto, M.; Panagia, N.; and Benvenuti, P.: Physical Conditions and Abundances of CNO Elements in NGC 7027. Astron. Astrophys., 1980, in press.

21. Harrington, J.P.; Lutz, H.J.; and Seaton, M.J.: in The First Year of IUE, ed. A.J. Willis, University College London, 1979, p. 199.

22. Flower, D.R.: UV Spectra of PN II. The Young PN IC 4997. M.N.R.A.S., 1980, in preparation.

23. Peimbert, M.; and Torres-Peimbert, S.: Chemical Composition of the Orion Nebula. M.N.R.A.S., Vol. 179, 1977, pp. 217-234.

24. Panagia, N.; Bussoletti, E.; and Blanco, A.: in CNO Isotopes in Astrophysics. ed. J. Audouze, D. Reidel Publ.,1977, p. 45.

25. Renzini, A.; and Voli, M.: Advanced Evolutionary Stages of Intermediate-Mass Stars I. Evolution of Surface Compositions. Astron. Astrophys., 1980, in press.

26. Peimbert, M.: in PN Observations and Theory , ed. Y. Terzian, D. Reidel Publ., 1978, pp. 215-224.

27. Peimbert, M.; and Serrano, A.: On the H and N Enrichment of the Interstellar Medium by PN. Rev. Mexicana Astron. Astrof., 1980, in press.

28. Péquignot, D.; and Stasińska, G.: An Abundance Gradient for Gaseous Mg in the PN NGC 7027. Astron. Astrophys., Vol. 81, 1980, pp. 121-127.

29. Benvenuti, P.; D'Odorico, S.; and Dopita, M.A.: UV Spectrum of SNR Reveals C Depletion of the Interstellar Medium. Nature, Vol. 277, 1979, pp. 99-102.

30. Benvenuti, P.; Dopita, M.; and D'Odorico, S.: Far UV Spectrophotometry of SNR Observations and Astrophysical Interpretation. Ap. J., 1980, in press.

31. Raymond, J.C.; Black, J.H.; Dupree, A.K.; Hartmann, L.; and Wolff, R.S.: UV Observations of the Cygnus Loop. Ap. J., 1980, in press.

32. Davidson, K.; Gull, T.; Stecher, T.; Maran, S.; Kafatos, M.; and Trimble, V.: IUE Observations of the Crab Nebula. 1980, in preparation.

33. Davidson, K.: Emission-Line Spectra of Condensations in the Crab Nebula. Ap. J., Vol. 228, 1979, pp. 179-190.

TABLE I.- ORION NEBULA - CHEMICAL ABUNDANCES[a]

Object	O/H (optical)	C/H (UV)	Mg^+/H^+ (UV)	Mg/H	t^2	Ref.
Orion	....	8.40	≤5.3	....	0.00	3
"	8.65	8.57	....	....	0.02	4
"	8.52	8.35	....	....	0.00	4
"	8.52	8.48	....	....	0.00	5
Sun	8.92	8.76	....	7.62	....	6,7

[a] Given in 12+log N(X)/N(H).

TABLE II.- PLANETARY NEBULAE - CHEMICAL ABUNDANCES

Object	O/H[a] (UV)	C/O[b] (UV)	N/O[b] (UV)	(C+N)/O[b] (UV)	N/O[b] (visual)	He/H[c] (visual)	Ref.
NGC 2392	8.74	-0.39	-0.33	-0.06	-0.29	0.091	17,18,19
NGC 2440	8.72	-0.20	+0.08	+0.26	+0.33	0.135	17,18,19
NGC 2867	8.65	+0.19	-0.55	+0.26	-0.52	0.112	17,19
NGC 3918	8.78	+0.20	-0.39	+0.30	-0.60	0.113	16,18
NGC 6302	8.79	+0.43	+0.25	+0.65	-0.15	0.191	17,19
NGC 6741	8.84	+0.26:	-0.14:	+0.41	-0.13	0.123	17,19
NGC 6886	8.72	+0.18:	+0.08:	+0.43	-0.53	0.102	17,19
NGC 7027	8.62	+0.49	-0.10	+0.59	-0.37	0.113	20,18,19
NGC 7662	8.58	-0.07	-0.54	+0.06	-0.88	0.094	21,18
IC 418	8.60	+0.26	....	....	....	....	8
IC 418	8.70	+0.33	....	....	....	....	4
IC 2448	8.46	+0.10	-0.27:	+0.25	-1.08	0.111	16,18
IC 4997	8.04	-0.40	....	....	....	....	22
Me 2-1	8.86	+0.05	-0.74	+0.12	....	....	17
PN[d]	8.70	+0.14	-0.24	+0.30	-0.42	0.119	
Orion	8.65	-0.08	....	-0.03	-0.97	0.100	23
Sun	8.92	-0.25	-0.93	-0.17	-0.93	....	6

[a] Given in 12+log N(O)/N(H). [b] Given in log N(X)/N(Y). [c] Given in N(He)/N(H).
[d] Average of this table without IC 4997 .

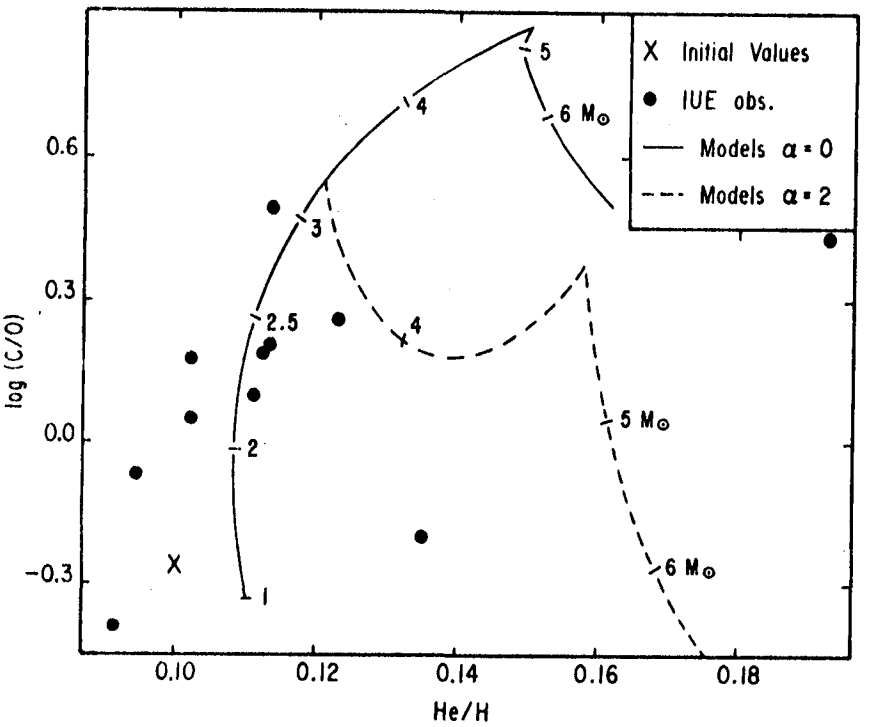

Figure 1. The model values (Renzini and Voli, ref. 25) correspond to the surface abundances at the time of the PN ejection. Along each sequence the values of the initial stellar mass are reported. The parameter α is the ratio of the mixing length to the pressure scale height, and α= 0 simply means that hot-bottom nuclear burning has been omitted.

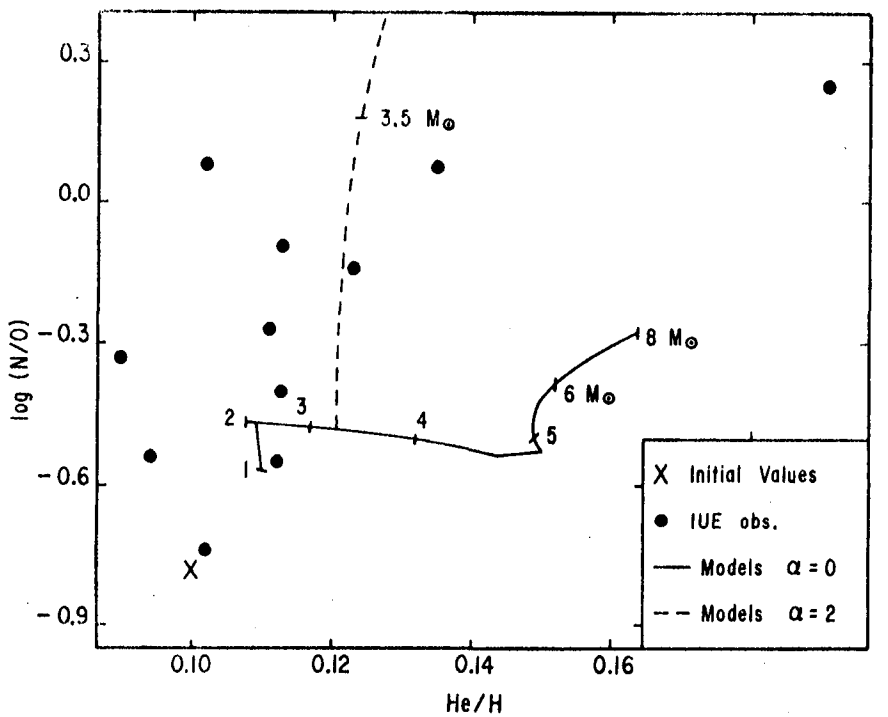

Figure 2. Same as Figure 1.

INTERSTELLAR ABUNDANCE DETERMINATION USING IUE DATA

Charles Joseph and Theodore P. Snow, Jr.
Laboratory for Atmospheric and Space Physics
University of Colorado at Boulder

INTRODUCTION

Analysis of the silicon interstellar abundances have been made for more heavily reddened lines-of-sight than were accessible to the Copernicus satellite. Silicon has rarely had accurate column densities determined from Copernicus data because the available lines all lie on the flat portion of the curve of growth for stars with $0.10 \lesssim E(B-V) \leq 0.35$. With IUE it is possible to reach color excesses of $E(B-V) \sim 0.5$-0.7, and in addition obtain data on the weak SiII line at 1808 Å, so that a wide range of oscillator strengths is available. The lower resolving power of the IUE, though, causes some difficulties in that several of the SiII lines are blended with strong lines of other species.

Data on the lines of sight analyzed so far have suggested that some of the absorption lines fall on the damped portion of the curve of growth, implying that silicon may not be as highly depleted as expected. The possibility cannot be ruled out at this time, however, that a curve of growth could be adopted with a higher b-value, so that none of the SiII lines are on the damped part, in which case substantial depletion would be inferred. The ambiguity is due in part to the recent discovery that some of the SiII lines have been assigned incorrect oscillator strength in the literature, and one line in particular (λ1526 Å) has an F-value which is too small. Work is currently under way by Shull and Snow using Copernicus to obtain correct values for these lines, which should then enable the correct determination of the silicon column density.

DATA REDUCTION

The column densities for silicon were determined from standard curve-of-growth analyses which exploit the relationship between absorption line equivalent widths and the column density of the absorbing particles. These results were then compared with column densities of HI, reduced according to the technique described by Bohlin (1975). The spectra used in this study are from recent observations by P. Conti, and are not subject to the Intensity Transfer Problems of earlier data. High-resolution IUE data were used in all cases.

The analysis was carried out on the interactive data system at the University of Colorado using a package of programs designed for interstellar abundance determinations (described in a separate paper, this Volume). The results discussed in this paper were obtained from the interstellar line spectra of the stars HD151804 (Spect. Class O9f, V=5.22, E(B-V)=0.41) and HD167659 (Spect. Class O8, V=7.39, E(B-V)=0.51), although the results were similar to those derived for a number of additional stars, to be described in a later paper.

The observed SiII lines used in the analysis have wavelengths at 1193, 1260, 1304, 1526, 1808 and 2334 Å, with the first two being of marginal use because they are blended with lines of Si and FeII respectively. When possible, an estimate of the contribution to the equivalent widths for each of the blended lines has been made from separate curve-of-growth analyses for CI and FeII. The SiII 2334 Å line, a forbidden intercombination line, is too weak in the current observations to produce a detectable absorption feature, and thus only provides an upper limit of its equivalent width. The remaining three lines consistently have small error bars associated with their equivalent widths and once the oscillator strengths are corrected should provide an unambiguous fit to a curve-of-growth.

The results of the analysis are as follows: The total hydrogen column density is 15.6E20 (Bohlin, et al., 1978) in the direction of HD151804 and is 25E20 in the direction of HD167659. Assuming that in each case some of the absorption lines do lie on the damped portion of the curve of growth, then the log of the silicon column densities are 16.8 for HD151804 and 16.7 for HD167659. Adopting the value of N/N_H=3.55E-05 as the solar abundance ratio of silicon, then depletion factors of 0.88 for HD151804 and of 1.79 for HD167659 are implied. These results however could be subject to change.

COMMENTS

The data indicates, although not conclusively, that silicon is probably more abundant than estimated from curve-of-growth analyses in which the SiII lines were assumed to follow the curve derived for other species. In an earlier case, (Snow, 1977), similar results were suggested. Likewise, de Boer (1979, 1980) has recently shown that oxygen may be typically more abundant than estimated from Copernicus data, where the OI lines all fell on the flat portion of the curve. Also, the absence of the SiII line at 1526 Å in most previous analyses probably caused systematic errors in the direction of decreased column density. In Morton's 1974 paper, Interstellar Absorption Lines in the Spectrum of Zeta Ophiuchi, the 1526 Å line was measured, but was inadvertently left off the graph. At any rate, detailed analyses for several lines-of-sight, to be published elsewhere, will be presented once the correct oscillator strengths are established.

REFERENCES

1. Bohlin, R.C.: Ap. J., 200, 402.

2. Joseph, C.L.: Analysis of IUE Spectra Using the Interactive Data Language. The Universe in Ultraviolet Wavelengths. NASA CP- , 19 (Paper of this Compilation).

3. Bohlin, R.C., Savage, B.D., and Drake, J.F.: Ap. J., 200, 402.

4. Snow, T.P.: Ap. J., 216 724.

5. de Boer, K.S.: Ap. J., 229, 132.

6. de Boer, K.S.: Ap. J., in press.

COMPARISONS BETWEEN OPTICAL AND ULTRAVIOLET INTERSTELLAR LINES FORMED IN THE CARINA NEBULA (NGC 3372)

James E. Hesser
Dominion Astrophysical Observatory
Herzberg Institute of Astrophysics

Nolan R. Walborn
Cerro Tololo Inter-American Observatory

ABSTRACT

Discovery of complex Ca II H and K interstellar line profiles towards stars embedded in the giant H II region surrounding Eta Carinæ (ref. 1) led us to undertake a reconnaissance of the richer ultraviolet (UV) interstellar line spectrum. Single IUE spectra were secured for those stars exhibiting the greatest variety of structure in the optical interstellar lines, namely, HD 93130, 93160, 93162, 93204, 93205, 93206 and HDE 303308. While subject to confirmatory observations and future analysis, our initial appraisal of the spectra suggest that: (1) longwards of Lyman Alpha many of the interstellar lines, including an unidentified one, in the spectrum of Zeta Oph (ref. 2) seem to be present in the Carina Nebula spectra; (2) interstellar line structure varies widely in both velocity and intensity throughout the region, as well as along a given line of sight as the species change; (3) new high velocity components of UV lines appear to extend the total range of velocities in the nebular interstellar lines to about 400 km/s; and (4) lines of the high excitation species Si IV and C IV are strong and also structured in velocity space.

INTRODUCTION

Optical observations at 9 Å/mm with the CTIO coudé spectrograph (ref. 1) revealed that a marked decrease in the strength of the interstellar calcium lines between stars in the inner and outer portions of the Carina Nebula arises from complex structure within or associated with that giant H II region. This phenomenon apparently represents a fourth type of interstellar line structure. Among the six components identified in the optical study, a total velocity range of about 330 km/s was found (fig. 1). Only in the Vela Supernova Remnant (SNR) has comparable velocity structure been observed (refs. 3-5). Subsequent CTIO coude spectra of HD 92740, 93206 and 93250 in the blue at 4.5 Å/mm and in the visual at 9 Å/mm revealed additional components in Ca II and structure in the Na D lines. In recent years one of us (NRW) has been carrying out an extensive survey of the optical interstellar lines with the improved resolution of the CTIO 4-m echelle spectrograph. The wealth of new and complementary information available from the interstellar lines accessible to IUE makes extension of the observations to the UV seem particularly worthwhile at this time. In this brief report we shall describe some salient features arising from an initial appraisal of the IUE spectra, with the caveat that proper morphological and physical analyses may require additional observations to achieve a sufficient signal-to-noise ratio.

OBSERVATIONS

Some relevant parameters for our small aperture, high-resolution data secured in September 1979 are summarized in Table I. Reductions used wavelength calibrations recorded during the Carina observations. We have also made use of a spectrum obtained by Dr. P. Conti for HD 93131 (LWR 1527).

RESULTS

1. Examination of the 10 Å/in plots provided by the IUE Observatory shows that when resolution, S/N and exposure levels are taken into consideration most interstellar lines stronger than about 15 mÅ, including the unidentified one at 1317.14 Å, in the Copernicus spectra of Zeta Oph (ref. 2) can be plausibly identified in our spectra. Both velocity and intensity aspects of the profiles are, however, quite different from those of Zeta Oph.

2. Complex velocity structure similar, but not necessarily identical, to that of Ca II K is seen in lines of C I*, C II, O I, Mg I, Mg II and Fe II.

3. Profiles of C I**, O I**, Si II*, S II, Cl I, Mn II, Ni II and Zn II generally seem to be unresolved or, at least, much simpler than those of the Ca II H and K lines. For instance, the Cl I 1347.24 Å line (f=0.112, W_λ(Zeta Oph) = 20.3 mÅ; when available these data from ref. 2 for Zeta Oph - ZO - will be given), although weak, is present in all our spectra, where it generally has a full width at half depth of about 0.12 Å. The line appears symmetrical and unresolved with the possible exception of towards HDE 303308, where there is a weak suggestion of a component at -43 km/s.

4. Good correspondence between the principal velocity components in the Ca II K-line and those in the Mg I 2852.127 Å line (f=1.90, W_λ(ZO)=218 mÅ) is seen upon comparison of figs. 1 and 2. In fig. 2 components at about -190, -95, -30, +60, and +100 km/s are identifiable. As with the H and K lines the velocity and intensity structure vary greatly from star to star. It is particularly interesting to compare line profiles of HD 93204 and 93205 in the figures; these two stars are separated by 20 arcsec on the sky, corresponding to a projected linear separation of 0.25 pc. (Note that velocities mentioned herein are approximate and based upon measurement on the figures relative to an adopted central position of the maximum absorption dip. Also, horizontal alignment of the profiles has been made about the presumed zero velocity component.)

5. The Mg II 2795.528 Å (f=0.592, W_λ(ZO)=312 mÅ) line profiles shown in fig. 3 are so badly saturated and, presumably, blended in the center that information on components within 80 km/s of zero velocity is lost. However, high velocity components are visible at about -185, -85, +90, and +190 km/s. The newly discovered component at +190 km/s in HD 93160 and 93162, if correctly identified, raises the total range of velocities in the Carina Nebula interstellar absorption lines to about 400 km/s. Comparable interstellar line velocities (a range of 270, or possibly, 550 km/s) are known only for portions of the Vela SNR (ref. 3-5), an object of considerably different appearance than NGC 3372. Velocity structure over 60 km/s is also known along lines of sight towards the giant H II region 30 Doradus in the Large Magellanic Cloud (ref. 1,6,7).

6. Profiles of the Mn II 2576.107 Å (f=0.288, W_λ(ZO)=138 mÅ) line, fig. 4, show, with the possible exception of HD 93162, only positive velocity components (+65, +135, +175 km/s). The structural differences between the low-excitation lines in figs.2-4 are readily apparent.

7. As an example of high-excitation lines, fig. 5 shows the C IV 1550.774 Å (f=0.097) and C IV 1548.202 Å(f=0.194, W_λ(ZO)$\lesssim$ 12: mÅ) lines, which are very strong in the Carina Nebula and show some velocity structure.

8. The Al III lines, 1854.716 Å (f=0.539, W_λ(ZO)=57:mÅ) and 1862.790 Å (f= 0.288, W_λ(ZO)=34:mÅ)are identical in appearance. Shoulders indicative of an unresolved component around +30 km/s appear in HD 93204, 93205, HDE 303308 and, possibly, HD 93130, while one near -30 km/s is suspected in HD 93162.

9. No evidence for interstellar molecules has been noted.

Our first appraisal of the velocity and intensity structure of the UV interstellar lines along various lines of sight to the Carina Nebula dramatically confirms and extends the complexity first noticed in the Ca II H and K lines. Excitation conditions in the interstellar medium within this giant H II region vary greatly on very small scales and, not surprisingly, differ markedly from those towards Zeta Oph. The new UV observations appear to have extended the total range of velocities spanned by interstellar lines in the Carina Nebula to about 400 km/s. Only some paths through the Vela SNR are known to show comparable interstellar line velocity structure; 30 Doradus in the LMC may be the site of similar, perhaps less extreme, behavior, however. Einstein satellite X-ray observations by Seward, et al. (ref. 8) have recently demonstrated that the weak Carina Nebula X-ray emission is actually composed of both diffuse emission and many weak sources associated with its numerous early O stars. Their observations rule out the Carina Source being a single, conventional SNR, although they suggest that emission originating in a hot gas due to stellar winds or due to supernova(e) which occurred 10^6-10^7 years ago could account for the diffuse X-ray component. It is clear that studies of the rich interstellar line spectra in both the UV and optical regions will provide numerous invaluable insights into the origin and current state of the enigmatic nebula surrounding Eta Carinae.

We gratefully acknowledge the excellent support of the IUE staff during the observations and the programs provided by S. Roundtree and J.B. Hutchings.

REFERENCES

1. Walborn, N.R. and Hesser, J.E.: Complex Interstellar Calcium Line Structure in the Carina Nebula. Ap.J., vol. 199, 1975,pp. 535-543.
2. Morton, D.C.: Interstellar Absorption Lines in the Spectrum of Zeta Ophiuchi. Ap.J., vol. 197,1975, pp.85-115.
3. Wallerstein, G. and Silk, J.: Interstellar Gas in the Direction of the Vela Pulsar. Ap.J., vol. 170, 1971, pp. 289-296.
4. Jenkins, E.B., Silk, J., and Wallerstein, G.: Interaction of the Vela Supernova Remnant with the Cloudy Interstellar Medium. Ap.J.Letters, vol. 209, 1976, pp. L87-L91.
5. _____: Ultraviolet Absorption Lines Associated with the Vela Supernova Remnant. Ap.J.Suppl., vol.32, 1976, pp. 681-714.

6. Blades, J.C.: High Resolution Observations of Interstellar Ca II and Na I in the 30 Doradus Nebula. Mon. Not. R.A.S., vol. 190, 1980, pp. 33-42.
7. Walborn, N.R.: Interstellar and Nebular Lines toward the 30 Doradus Central Object. Ap.J.Letters., vol. 235, 1980, pp. L101-L103.
8. Seward, F.D., et al.: X-rays from Eta Carinae and the Surrounding Nebula. Ap.J. Letters, vol. 234, 1979, pp. L55-L58.

TABLE I. - OBSERVATIONS OF CARINA NEBULA STARS

HD NUMBER	SPECTRAL TYPE	V	B-V	E(B-V)	EXPOSURE INFORMATION LWR(Exp. Time)	SWP(Exp. Time)
Group A: NW of Eta						
93160	O6III(f)	7.81	0.17	0.49	5666 (60 min)	
Group B: Nearest Eta						
93204	O5V((f))	8.42	0.10	0.42	5669 (120)	6597 (150)
93205	O3V	7.75	0.05	0.37	5647 (45)	6611 (60)
93162	WN6-A	8.10	0.42	0.62	5667 (90)	6609 (240)
303308	O3V((f))	8.17	0.13	0.45	5649 (100)	6596 (200)
Group C: SW of Eta						
93130	O6III(f)	8.06	0.22	0.54	5646 (75)	6594 (100)
93206	O9.7Ib(n)	6.24	0.13	0.42	5670 (15)	6612 (25)
Group D: Outer Boundaries						
93131	WN6-A	6.48	-0.02	0.25	1527 (7)	

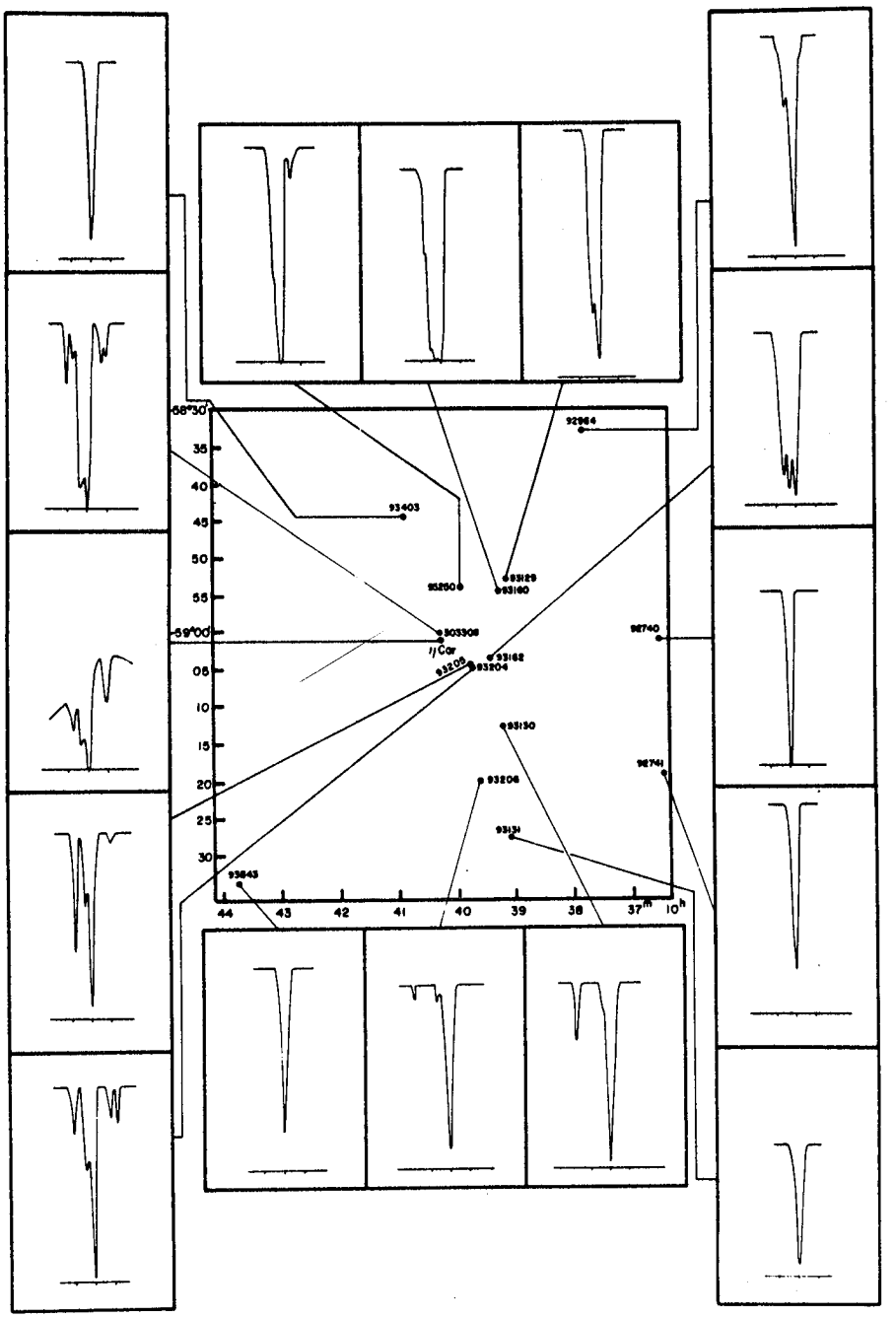

Fig. 1. The central part of this figure, which is from ref. 1, gives the distribution on the sky of the stars observed in the original CTIO coudé survey. The stars are identified by their HD or HDE numbers. The map is surrounded by the individual intensity profiles of the interstellar Ca II K line for each star. The vertical fiducial marks on the horizontal zero intensity line beneath each profile denote 0 and ± 100 km/s (heliocentric) velocity.

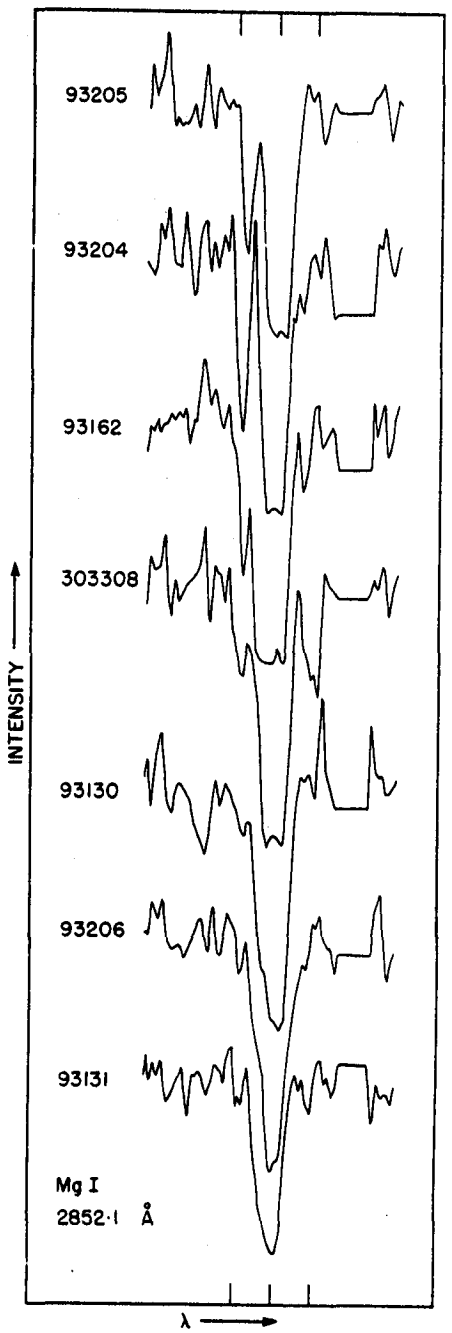

Fig. 2: Profiles of the Mg I 2852.127 Å line in seven Carina Nebula stars. For this, as well as the remaining figures, 6.0 Å of each spectrum are plotted. The fiducial marks on the abscissae indicate 0 and ± 100 km/s, although, as explained in the text, the zero point is somewhat arbitrary.

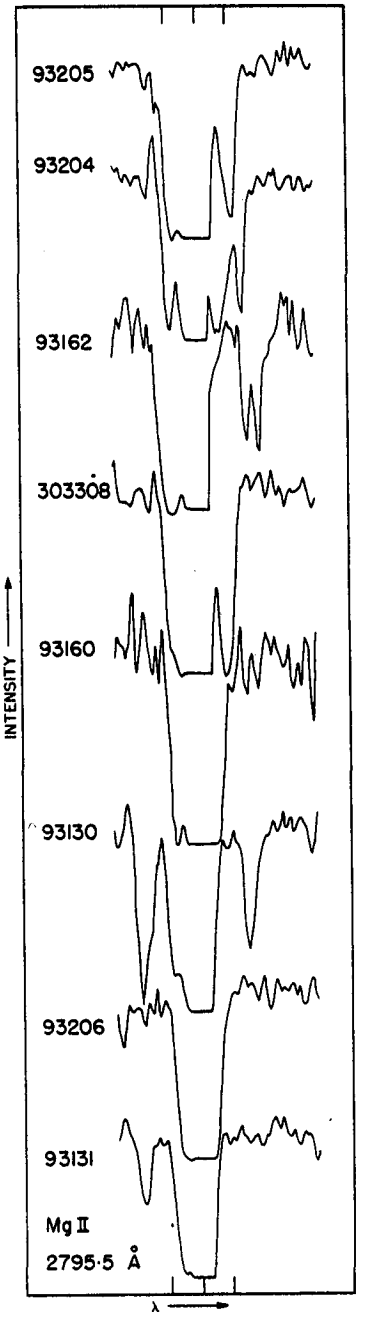

Fig. 3. Line profiles for the Mg II 2795.528 Å line; otherwise as in Fig. 2.

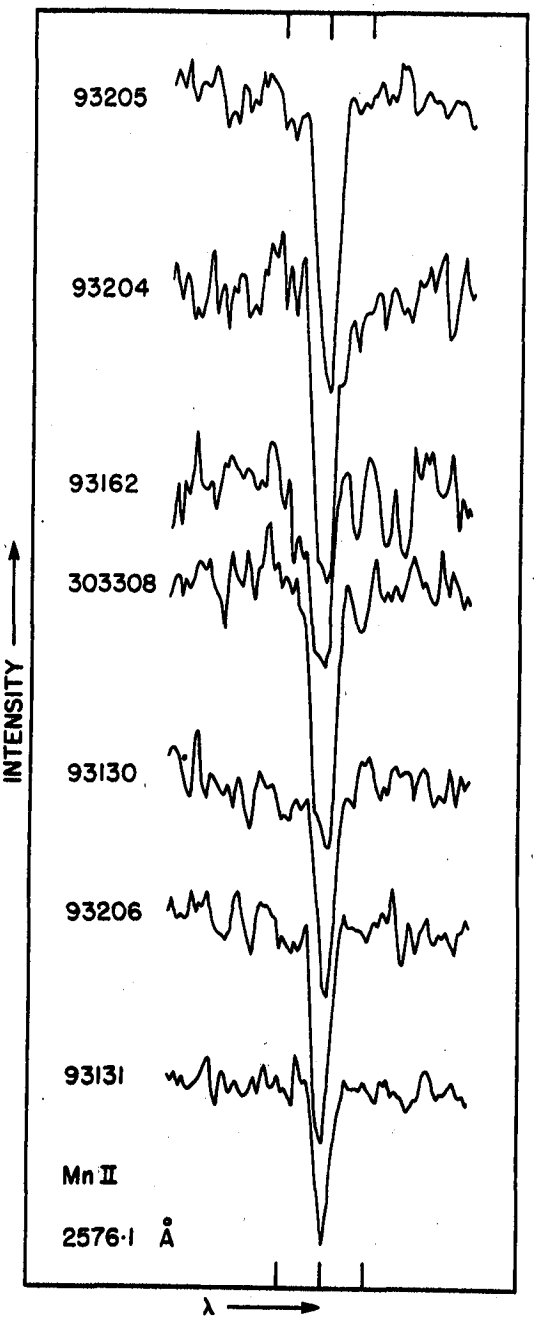

Fig. 4. Line profiles for the Mn II 2576.107 Å line; otherwise as in Fig. 2.

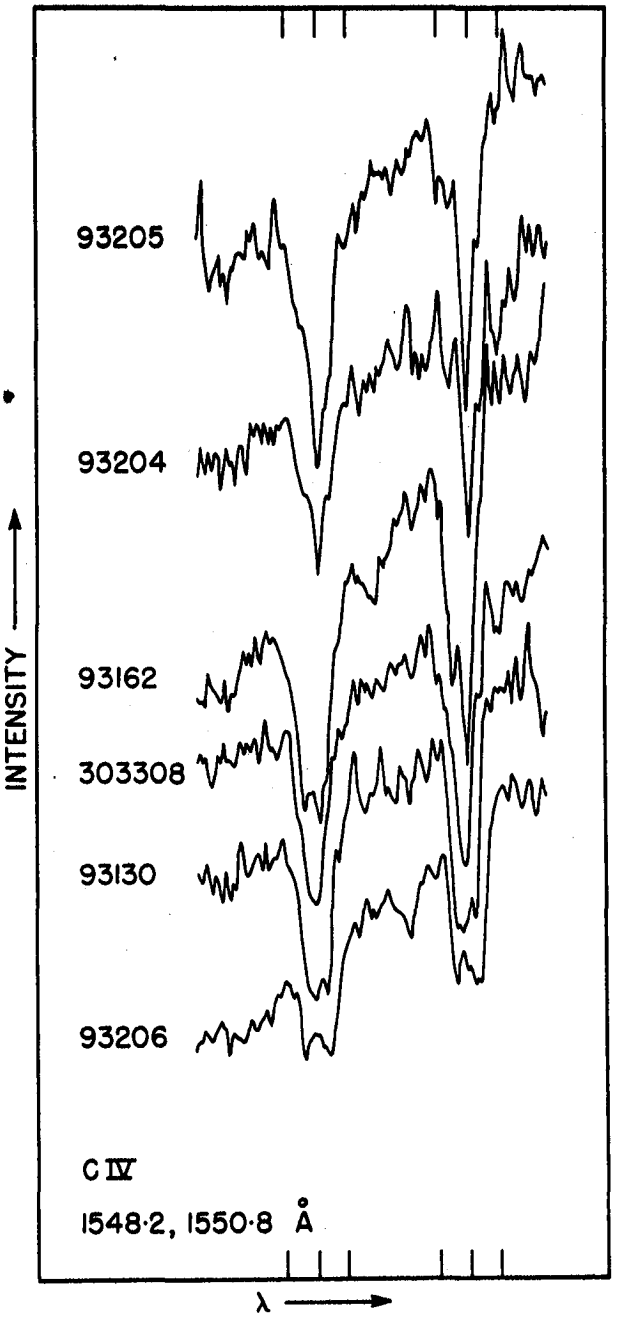

Fig. 5. Line profiles for the C IV 1548.202 Å and 1550.774 Å lines; otherwise as in Fig. 2.

A SEARCH FOR INTERSTELLAR MOLECULES IN THE SPECTRA OF HIGHLY REDDENED STARS*

D. Lien,[1] D. Buhl,[2] R.M. Crutcher,[1] B. Donn,[2]
A.M. Smith,[3] L.E. Snyder,[1] L.J. Stief[2]

ABSTRACT

The dark cloud in the line of sight towards X Persei has been searched for the molecular species OH, CH_2, HCl, CO and C_2 using the IUE satellite. We have detected CO, with a column density of $5 \times 10^{15} cm^{-2}$ and $1 \times 10^{14} cm^{-2}$ for ^{12}CO and ^{13}CO, respectively. We have placed upper limits on the log of the column densities of OH, CH_2 and HCl of 14.0, 12.8, and 12.3, respectively. Radio observations toward X Persei give a factor of 4 greater column density in CO, and a velocity width in the cloud containing the CO of 2 km/s, FWHM. Log N(OH) = 13.8 from radio data, which is consistent with our upper limit. We also have apparently detected the $F^1\pi_u - X^1\Sigma_g^+$ transition of C_2 at 1341Å. The equivalent widths of the C II lines are great enough to place them on the damping portion of the curve of growth. The derived column density of carbon implies a C/H ratio of 2/3 the solar value.

INTRODUCTION

Most molecules of astrophysical interest have electronic transitions in the spectral region covered by the International Ultraviolet Explorer Satellite (IUE). Because of this, we have undertaken the analysis of high dispersion spectra of ten stars embedded in or behind dark interstellar clouds which are known to contain strong lines of CH and CH^+ from optical studies (ref 1). These stars were observed in October, 1978, January, 1979, and March, 1980. The initial data reduction was done using the GSFC PDP 11/40 Forth Reduction System, set up by D. Klinglesmith. From this preliminary overview of all the data, we decided to analyze in detail only one star, and then return to the others. With this in mind, we spent the March 1980 observing run observing the chosen star in order to build up the total signal-to-noise ratio of the stacked data. This star, to which all further discussion is directed, is X Persei (HD 24534).

X Persei is a 6th magnitude O or B emission star. It has recently been identified with the X-ray source 3U 0352 + 30 (ref 2), and has a Vsini of about 500 km/s (ref 3). The broad stellar lines are easily distinguishable from the narrow interstellar lines. There is no indication in any of our data for a stellar wind or super-surface emission features.

* Supported in part by NASA under contract NSG 5278 to the University of Illinois

1. Department of Astronomy, University of Illinois
2. Laboratory for Extraterrestrial Physics, GSFC
3. Laboratory for Astronomy and Solar Physics, GSFC

Copernicus observations (ref 2) of the atomic and diatomic hydrogen lines give the total hydrogen column density toward X Persei as 2.4 x $10^{21}cm^{-2}$, with a fractional abundance of H_2 of 0.9, and an associated kinetic temperature derived from the first two rotational levels of H_2 of 71°K.

DATA REDUCTION

There are two main problems associated with the identification and subsequent analysis of weak interstellar lines: the noise and the background.

As the system stands, the ITF should remove all systematic tube defects, and hence all remaining noise should be random. Due to Pixel-ITF mismatching and possible time-dependent spots, this is not the case. In order to detect such non-random noise, we have found that sequential observations of the same star in the same camera should be taken with the star positioned at alternate ends of the large aperture for each exposure. This places a given spectral feature at different physical locations on the tube face for each exposure. The plotted results then show a wavelength shift between exposures, whereas any non-random noise feature will appear at the same wavelength. An example of this effect is shown in Figure 1. With this procedure, tube defects cannot be interpreted as weak lines.

When the gross spectrum is divided by the extracted background, a noisy straight line results. This implies that there are data mixed in with the background (e.g. order overlap). To correct for this problem, we assume that the background is of the form $B_T = C + (B_0 - C)f$, where B_0 is the observed background at a given wavelength, B_T is the "true" background at that point, and C and f are empirically derived constants. An example of this is shown in Figure 2, where B_0, B_T and C are shown, and f = 0.6. We chose this value of C because at the edge of the order there are very little data, hence that value of the background probably represents the component due to thermal noise and any reading induced noise. A best-fit value for f is found by varying the value of f and subtracting B_T from the gross spectrum until the equivalent widths of the same line in two different orders are equal. Thus C is a constant for each order, and f is a constant for the spectrum. We find that f = 0.6 reproduces equivalent widths between orders within 5%, and between exposures within 10%.

After the proper background for each spectrum has been subtracted from the gross spectrum for a given order, spectra are stacked after shifting each to the same radial velocity, at the wavelength of interest. All equivalent widths and line profiles are extracted from this stack. For X Persei, there are 6 spectra, shifted and stacked as described above.

RESULTS

Radio observations of the CO 1-0 rotational transition obtained by one of us (RMC) have been analyzed assuming LTE. We find $T_{01} = 5°K$, a velocity width of 2 km/s FWHM, and a ^{13}CO column density of 4.2 x $10^{14}cm^{-2}$. Assuming a $^{12}CO/^{13}CO$ ratio of 40 gives the column density of ^{12}CO as 1.8 x $10^{16}cm^{-2}$. Subsequent analysis in this section will assume a velocity width of 2 km/s,

and a rotation temperature for CO of 5^{o} K. This may not be a valid assumption when comparisons between atomic and molecular column densities are made; however, it is adequate as a first approximation.

We have observed the v" = 0 progression of the Fourth Positive system of CO through v' = 12 for ^{12}CO. Observations of the 1-0 rotational transition and the 2-0 vibrational band of the A-X system are shown in figure 3 for ^{12}CO and ^{13}CO. We have done an initial analysis of the system assuming that only the first four rotational levels are populated, at a rotation temperature of 5^{o}K. For each frequency over the band, we then calculate the optical depth contributed at that frequency by each of the nine transitions from the four levels, assuming that a Voigt profile describes the line. Under these assumptions, we find the column density of ^{12}CO to be about 5 x $10^{15}cm^{-2}$, and the column density of ^{13}CO to be about 1 x $10^{14}cm^{-2}$. These values compare favorably with the column densities derived from radio observations; reasons for the small differences may be due to the assumption of a thermal population of the rotational levels (which strongly affects the saturation of the UV CO lines), and the larger beamwidth of the radio measurement. It seems reasonable that the cloud is completely in front of the star.

We have made a detailed search for OH (1222Å), HCL (1290Å), and CH_2 (1416Å), and report that none of these molecules were detected above the 5 mÅ level. This puts upper limits on the logarithm of the column densities for these molecules at 14.0 (.004), 12.3 (.16), and 12.8 (.05), respectively. The numbers in parentheses are the oscillator strengths (ref 5,6,7). These limits are derived assuming that the molecular line is optically thin.

One of us (RMC) has detected the 1667 MHz radio OH line toward X Persei. He finds log N(OH)=13.8, which is consistent with our upper limit.

We have apparently detected the $F^{1}\pi_{u} - X^{1}\Sigma^{+}$ system of C_2 (ref 8), of which we have observed the 0-0 vibrational band at 1341 Å. The D-X system in the ultraviolet has previously been reported (ref 9). Since C_2 does not have a permanent electric dipole moment, transitions between rotational levels are forbidden; hence, there is expected to be a thermal population of the ground state rotational levels. The resultant profile due to the convolution of lines arising from these rotational levels with the response of the IUE spectrograph should show the transition as a broad profile, with a possible separation of the bands. This is about what we observe, as shown in Figure 4. We are in the process of modeling the C_2 line in much the same way as described for the CO lines.

The C II doublet at 1334Å, 1335Å is important not only as an indicator of the total hydrogen density (ref. 4), but also the abundance of this dominant species can provide some information about the composition of the dust. The equivalent widths of the two lines toward X Persei are 267 and 172 mÅ, for the 1334Å and 1335Å lines, respectively. For a velocity parameter, b, of 5 km/s or less, this puts the 1334Å line on the damping part of the curve of growth, thus making it independent of the exact velocity dispersion, providing it is less than about 5 km/s. This implies a column density of C (assuming most carbon is C II) of 5.6 x $10^{17}cm^{-2}$. For a total hydrogen

column density of 2.4×10^{21}, this implies a C/H ratio of 2.3×10^{-4} or about 2/3 the solar value. Formal errors have not been worked out, but errors in the exact placement on the curve of growth do not change by more than ±.15 in dex. The kinetic temperature based on the relative populations of the fine structure levels of C II is 55°K, which agrees favorably with the kinetic temperature of 71°K derived from the relative populations of the J = 0 and J = 1 levels of H_2. This implies that collisions dominate the de-excitation of the excited fine structure level of C II, and puts the brunt of the cooling on H_2 and other molecules.

SUMMARY

We have observed a total of ten stars with both the SWP and LWR cameras of the IUE in both high and low dispersion. We have chosen one star, X Persei (HD 24534, 6.0 BE), to analyze in detail.

Our ultraviolet observations of the column densities of CO match those derived from the radio to within a factor of 4, with the difference probably due to the larger beam size of the radio measurement and the assumption of a thermal population in the rotational levels of CO.

We give upper limits to the log column densities for OH, HCl, and CH_2 of 14.0, 12.3 and 12.8, respectively, and report the identification of the $F^1\pi_u - X^1\Sigma_g^+$ system of C_2. We find the carbon abundance to be about solar, with a possible depletion of about a factor of 2. We feel that with the proper precautions concerning both noise and correct background, the IUE can effectively be used for some studies of interstellar molecules.

REFERENCES

1. Cohen, J.G., Ap.J. 186, 149, 1973.
2. Mason, K.O., White, N.E., Sanford, P.W., Hawkins, F.K., Drake, J.F., and York, D.G., MNRAS 176, 193, 1976.
3. Hutchings, J.B., Cowley, A.O., Crampton, D., and Redman, R.O., Ap.J. 191, L101, 1974.
4. Morton, D.C., Ap.J. 197, 85, 1975.
5. Crutcher, R.M. and Watson, W.D., Ap.J. 203, L123, 1976.
6. Smith, P.L., Yoshino, K., and Parkinson, W.H., preprint, 1979 .
7. Snow, T.P. Ap.J. Letters, 201, L21, 1975.
8. Ballik, B. and Ramsay, R., Ap.J. 137, 61, 1963.
9. Snow, T.P., Ap.J. Letters, 220, L93, 1978.

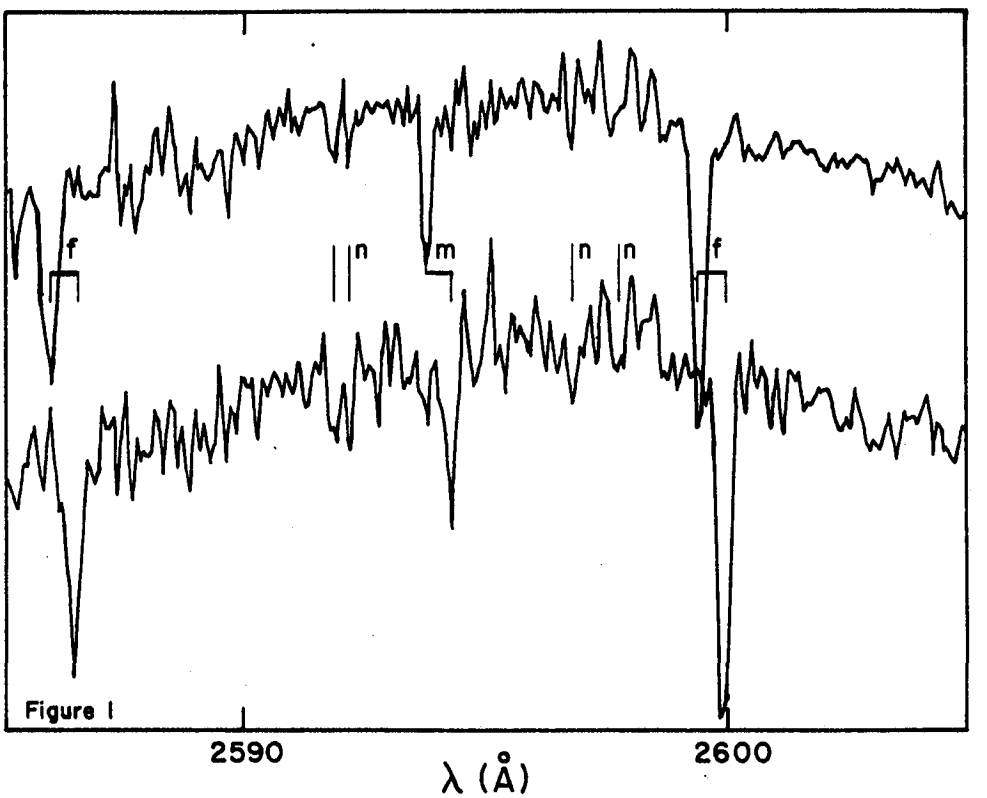

1. During sequential observations of the same star, if the star is shifted in the large aperture, spectral lines shift, but systematic noise does not; f indicates lines due to FeII, m indicates lines due to MnII, and n indicates systematic noise features on the tube.

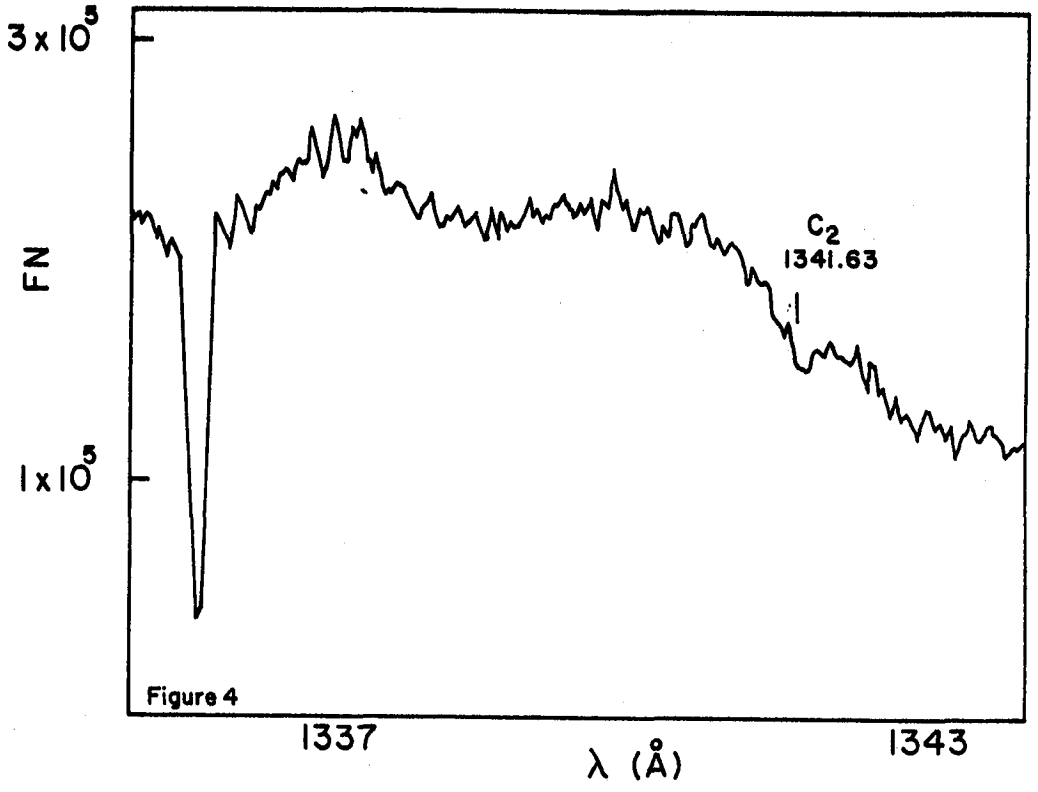

2. An example of the gross spectrum and the background subtraction technique used; B_0 is the IUE extracted spectrum, and B_T is the "true" background, as indicated by the equation. After the computation of B_T, it is smoothed by a median smoothing routine.

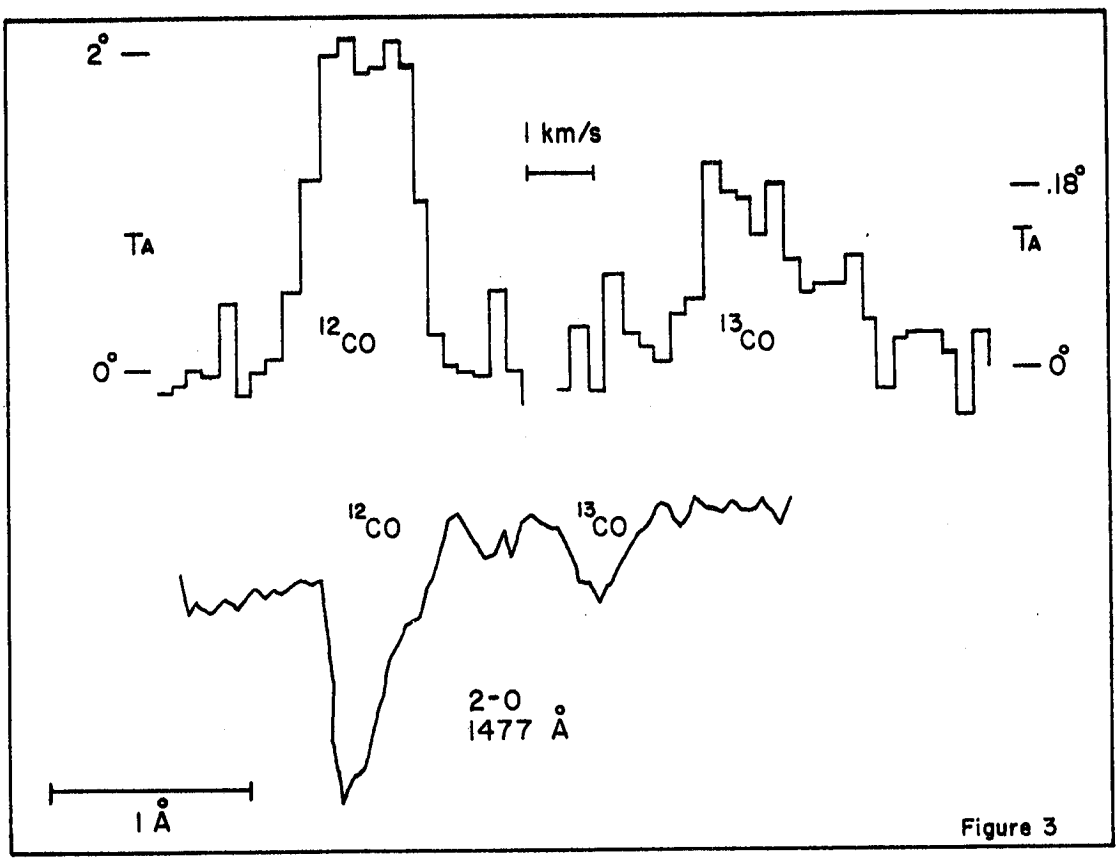

3. Radio and optical observations of CO. The radio observations are of the 1-0 rotational transition, and the UV CO are due to the 2-0 vibrational band of the Fourth Positive electronic system.

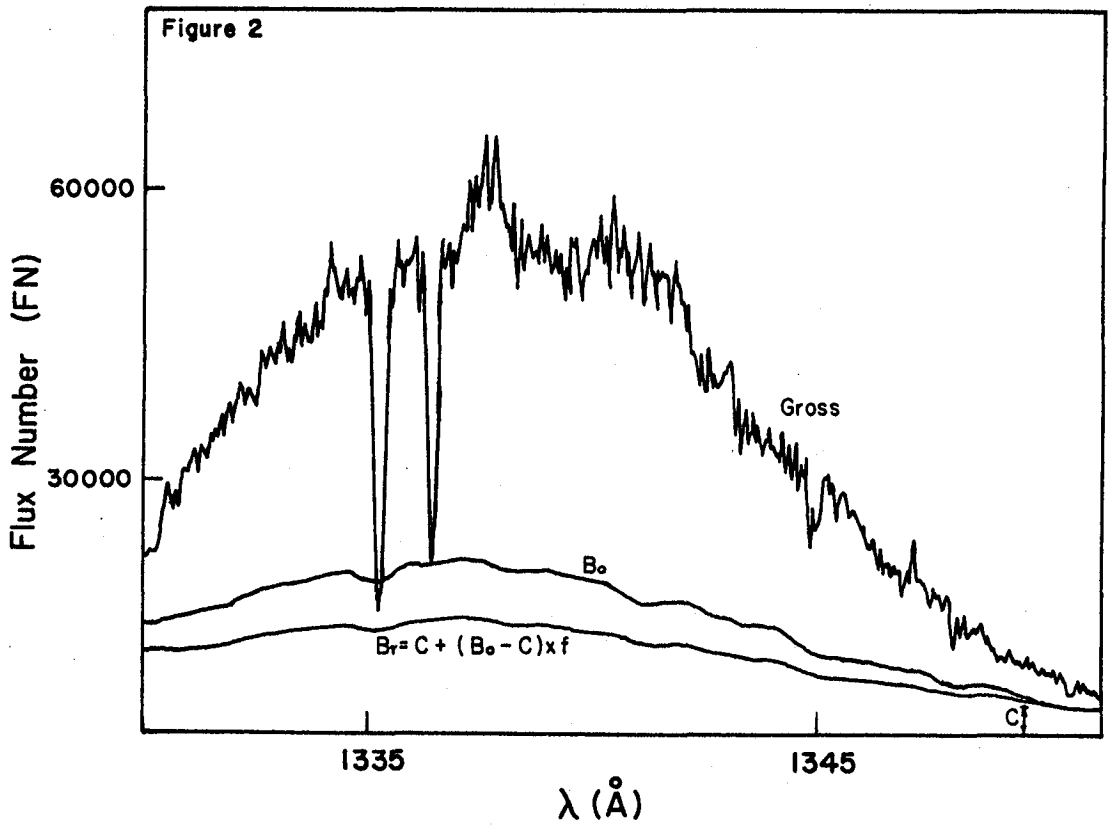

4. The $F^1\pi_u - X^1\Sigma_g^+$ system of C_2, showing the 0-0 vibrational band at 1341.63Å (band origin). The strong feature at the left is the 1335Å line of CII which originates from the excited fine structure level of the ion.

A COMPRESSED CLOUD IN THE VELA SUPERNOVA REMNANT

Edward B. Jenkins
Princeton University Observatory

George Wallerstein and E. Myccky Leep
University of Washington

Joseph Silk
University of California, Berkeley

INTRODUCTION

Our previous interstellar line survey, carried out with the Copernicus satellite, was limited to selected lines in only four bright stars (ref. 1). Nevertheless, our data revealed the presence of numerous absorbing, primarily ionized gaseous sheets and filaments, that had evidently been shocked, compressed, and accelerated by interaction with the SNR.

The significance of the interaction of supernovae with interstellar clouds was first stressed by Öpik (ref. 2), who suggested that star formation would be initiated. More recent studies have supported this viewpoint, although the direct evidence for triggering of star formation by supernovae is very tenuous. Herbst and Assousa (ref. 3,4) emphasized the location of young stellar associations at the edges of expanding shells of gas: such shells are not necessarily old SNR, however. A more direct connection was sought by Wootten (ref. 5) who found evidence for compression by a factor $\sim$10, heating, and enhanced line broadening in molecular clouds near the SNR W44 and W28.

Another connection between a supernova and star formation has been inferred from the presence of excess ^{26}Mg in certain inclusions in the Allende meteorite, taken to indicate that the unstable isotope ^{26}Al was injected into the protosolar nebula within $\sim 10^6$ yr of the nucleosynthesis of the ^{26}Al in a nearby supernova (ref. 6). Such circumstantial evidence suggests that interaction with the supernova may both have enriched and initiated the collapse of the interstellar cloud destined to form the sun and the solar system.

Finally, recent models of spiral structure have utilized supernova-induced star formation as a means of enabling star formation to be self-propagating in the galactic disk (ref. 7,8). To justify this type of theoretical work, one would like to know whether there is any evidence for the extreme compression of ambient gas near a SNR that is required to initiate star formation.

In an attempt to shed light on these issues and to further elucidate the nature of the interstellar medium in the vicinity of the Vela SNR, we have undertaken an extensive study with the IUE of interstellar absorption lines toward 35 stars in the vicinity of the Vela SNR. Observations of interstellar absorption, in particular of CI, towards one of these stars, HD 72350 (type B4 III), are of sufficient interest that we report here a preliminary analysis of this data before the entire survey has been reduced.

OBSERVATIONS

In June 1979 we obtained high resolution IUE spectra of 35 stars in the field of the Vela Supernova Remnant. From the video displays of the short wavelength echelle spectra it was clear that HD 72350 showed multiplet structures in all of the C I transitions which were especially prominent, indicating that the excited fine-structure levels are heavily populated. Two additional short-wavelength exposures of this star were recorded in September 1979 to verify this result and improve the net signal-to-noise ratio.

Column densities of various species were derived using curves of growth based on Voigt profiles. For unresolved blends of two or more transitions from C I, special curves of growth were calculated to derive the total equivalent width of the partially overlapping components. Table 1 lists the derived column densities as a function of the velocity dispersion parameter b, averaged from all but the weakest lines. We calculated the standard error of the results for cases where we measured three or more lines, and these dispersions are shown in parentheses after the respective entries. For our study of cloud compression, our primary objective is to derive column densities of neutral carbon atoms, i.e. (N(CI), N(CI*) and N(CI**), in the three levels of fine structure excitation, $^3P_0$, $^3P_1$ and $^3P_2$, respectively. From the standard errors in Table 2, we see that the best internal consistency for the column densities occurs for $b \geq 10$ km s^{-1}. Within the range $10 \leq b \leq 20$ km s^{-1}, the total column density of neutral carbon varies by a factor of three, but the ratios of C I, C I* and C I** populations are relatively insensitive to the choice of b. Our inability to detect the weaker transitions indicates that the absorptions we have measured do not have heavily saturated cores. In particular, our detection limit for λ1276.48 forces us to conclude that log N(CI) < 14.7 for any b greater than 4 km s^{-1}, if log fλ for this transition is about 0.8 (this line strength is based on a preliminary analysis of C I absorption data recorded by ref. 10; see also ref. 11). Hence, we are confident that the conspicuousness of the excited lines is attributable to a strong excitation of carbon rather than a large difference in line saturations.

If we assume log N(H) = 20.8 from the star's B-V color excess of 0.14 (ref. 12) and the general gas to reddening ratio of 4.8 x 10^{21} atoms cm^{-2} mag^{-1} (ref. 13), we find that the relative abundances of N I and O I are consistent with the cosmic abundance ratio if b ranges between 10 and 12 km s^{-1}. From earlier research works on ultraviolet interstellar data, we know that velocity dispersions of atoms in a stage of ionization below the dominant one for H I regions generally exhibit a lower b than those species in their dominant stages (e.g. see Figure 2 of ref. 14), so our N I and O I b values should exemplify only an upper limit for the b of C I. Doublet ratios for the Ca II and Na I absorptions in the visible yield b values of 10 and 5 km s^{-1}, respectively (ref. 9). The value for sodium appears to be too low perhaps because the equivalent widths were not very accurate; 8 km s^{-1} would be acceptable, but a larger b value implies the D lines are virtually unsaturated which is inconsistent with the observed line strength ratio. From the above considerations, we feel that it is reasonable to assume that the most probable value of b for C I is 12 km s^{-1}.

TABLE 1.-COLUMN DENSITIES (LOG NL) FOR LIGHT ELEMENTS IN THE H I REGION IN FRONT OF HD 72350

Element	No. of Lines	log NL for various b-values 8	10	12	15	20	Notes
CI	3	15.3(0.4)	14.8(0.2)	14.6(0.2)	14.4(0.2)	14.4(0.2)	
CI*	9	15.5(0.5)	15.1(0.3)	14.8(0.2)	14.7(0.2)	14.6(0.2)	
CI**	8	14.8(0.2)	14.6(0.1)	14.5(0.1)	14.4(0.1)	14.3(0.1)	
CI(total)	22	15.8	15.4	15.1	15.0	14.9	1
NI	3	17.6(0.3)	17.1(0.4)	16.3(0.4)	15.5(0.3)	15.0(0.2)	
OI	1	18.0	17.7	17.2	16.2	15.4	
OI*	1	<13.9	<13.9	<13.8	<13.8	<13.8	
Mg I	2	13.3	13.2	13.2	13.2	13.2	
CO	5	14.2(0.1)	14.2(0.1)	14.2(0.1)	14.2(0.1)	14.2(0.1)	
Na I	2	12.8	12.4	12.3	12.3	12.3	2
Ca II	2	13.2	12.9	12.8	12.7	12.7	2

Notes: 1-Includes two blends of CI* and CI** features.
2-From optical spectra (ref. 9).

THE NEUTRAL CARBON ABSORPTION LINE REGION

CAN THE CI ABSORPTION BE CIRCUMSTELLAR?

Prior to discussing the implications of the CI populations in Table 2 we must demonstrate that the observed cloud is not a circumstellar feature whose CI levels are pumped by radiation from HD 72350. Radiation from B4 III star is capable of ionizing CI. We first have shown that there is a negligible amount of CI recombination in the CII zone. Moreover, a sufficiently great column density is needed to shield CI near HD 72350 from the carbon ionizing photons that there can only be a negligible amount of CI at high pressure ($p/k >> 10^3$ cm^{-3} K) near the star. Finally, the stellar radiation field is not sufficiently intense to radiatively pump the CI without requiring an excessive large column density of shielding CII.

PROPERTIES OF THE C I CLOUD

Since we have shown that the cloud containing the CI is not circumstellar, we can adopt the perspective that it is normal interstellar material subjected to unusual physical conditions. From the fine-structure population ratios $f_1 \equiv CI^*/CI_{total}$ and $f_2 \equiv CI^{**}/CI_{total}$ we may arrive at permitted combinations of pressure and temperature using the diagrams for collisional equilibria in H I regions given by ref. 15. Figure 1 shows the combinations of pressure and temperature which are consistent with our population ratios, allowing for reasonable errors in column densities.

However, there are two additional constraints, shown in the figure, which we may impose on the conditions. First, we can require that a solution for the ionization equilibrium between CI and CII (ref. 15) not give a computed

value N(CI) less than the observed value assuming log N(H) = 20.8, a cosmic abundance ratio for C/H, and an ionization rate $\Gamma_C = 2 \times 10^{-10}$ s^{-1} for the general interstellar medium. (This argument is only a limiting case because the computed value could greatly exceed the observed N(CI)/N(H) if much of the reddening was not associated with the CI region.) This constraint may be even stronger than shown here, since there is a good chance that Γ_C in the Vela region is higher than the usual interstellar value and some of the free carbon atoms are depleted onto grains.

The second constraint comes from our upper limit for N(OI*). If we solve for the collisional equilibrium for the O I fine structure levels, assume a cosmic abundance ratio for C/O, and compute the total carbon density from the ionization equilibrium (see above), we obtain log T < 2.1. This result is independent of log p/k because the computed ratios OI*/OI and C/CI both scale approximately linearly with pressure.

DISCUSSION

From Fig. 1 we see that the temperature of the cloud lies between 25 and 100°K and P/K is greater than 10^4, and could be 10^6 or larger. The minimum density is about 250 hydrogen atoms/cm^3, and the density could easily be 3×10^3 or substantially higher. Such conditions could be realized by compression of pre-existing clouds by a supernova shock moving at about 400 km s^{-1} through the intercloud medium. Such a shock could compress the gas by a factor 300 so the shocked cloud could have had an initial density of order 10 cm^{-3}. The origin of shock clouds within the Vela B association poses an interesting problem. They are likely to be material left over from the formation of stars that have recently reached the main-sequence of the association.

REFERENCES

1. Jenkins, E. B., Silk, J., and Wallerstein, G. Ap. J. Suppl. 32, 681, 1976.

2. Öpik, E. J. Irish Astron. J., 2, 219, 1953.

3. Herbst, W. and Assousa, G. E. Ap. J. 217, 473, 1977.

4. Herbst, W. and Assousa, G. E. In Protostars and Planets, ed. by T. Gehrels (Tucson: University of Arizona Press), p. 368, 1978.

5. Wootten, H. A. Ap. J. 216, 440, 1977.

6. Lee, T., Papanastassion, D. A., and Wasserburg, G. W. Geophys. Res. Lett., 3, 41, 1976.

7. Mueller, M. W. and Arnett, W. D. Ap. J., 210, 670, 1976.

8. Gerola, H. and Seiden, P. E. Ap. J. 223, 129, 1978.

9. Wallerstein, G., Silk, J. and Jenkins, E. B. Ap. J. (in press) 15 Sept. 1980.

10. Jenkins, E. B., Jura, M. and Lowenstein, M. (in preparation).

11. de Boer, K. S. and Morton, D. C. Astron. and Astrophys. 71, 141, 1979.

12. Ferro, A. A. and Gerrison, R. F. Rev. Mex. de Astron. y Astrophys. 4, 351, 1979.

13. Bohlin, R. C., Savage, B. D. and Drake, J. F. Ap. J. 224, 132, 1978.

14. Spitzer, L. Jr. and Jenkins. Ann. Rev. of Astron. and Astrophys. 13, 133, 1975.

15. Jenkins, E. B. and Shaya, E. J. Ap. J. 231, 55, 1979.

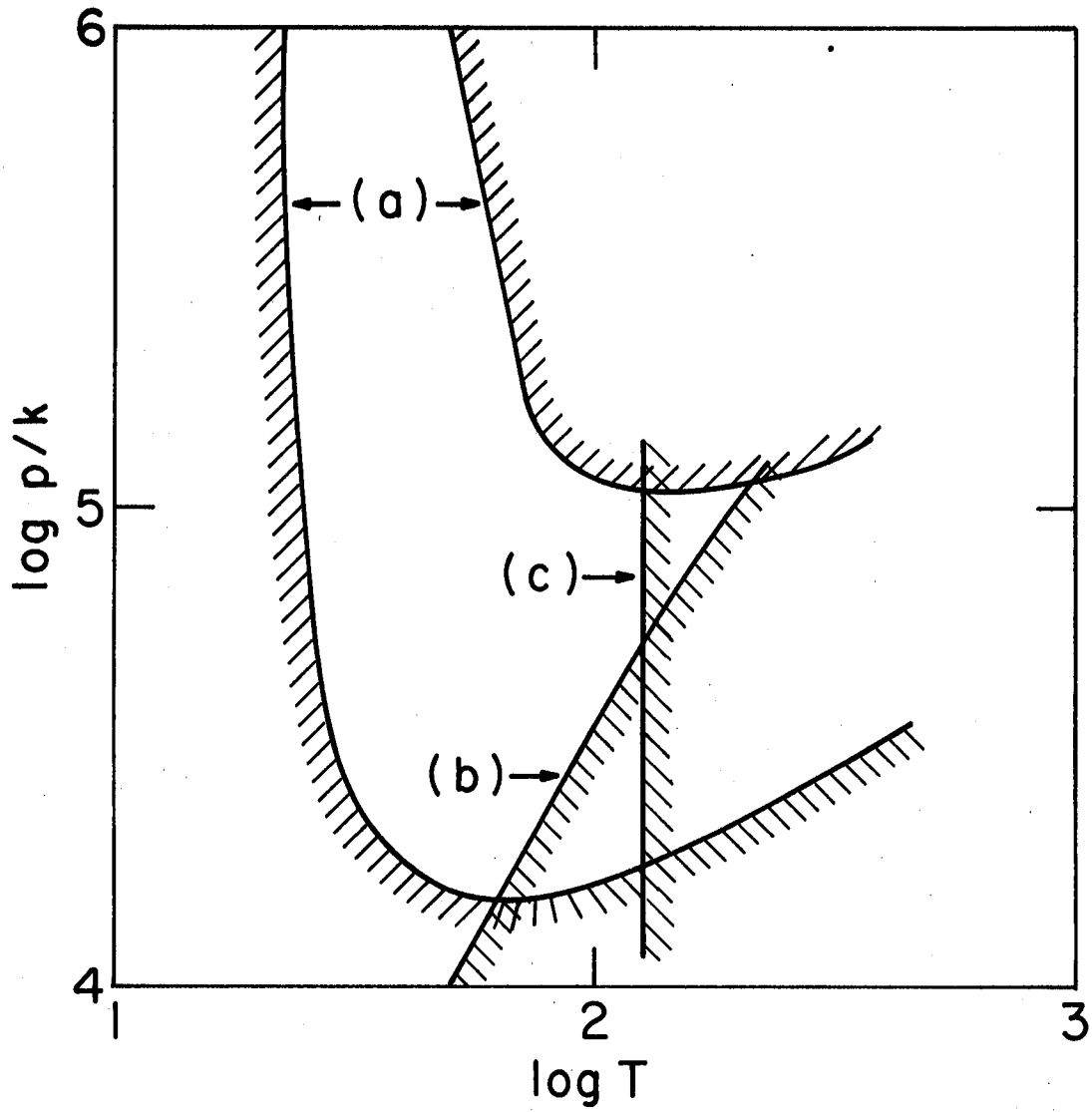

Fig. 1. Allowed pressures and temperatures for the CI cloud. Excluded areas are the shaded side of the lines. Lines marked (a) are from CI fine-structure excitation. Line (b) is from the relative abundance and ionization equilibrium of carbon. Line (c) is from the absence of observed absorption from OI*.

IUE OBSERVATIONS OF SUPERNOVA REMNANTS*

J.C. Raymond

Harvard-Smithsonian Center for Astrophysics

ABSTRACT

We discuss the UV emission spectra of several filaments in the Cygnus Loop and the Vela Supernova Remnant, including several which are anomalously bright in the optical O III lines. The effects of internal and interstellar resonance line scattering are estimated. Shock velocities, elemental abundances, and in some cases filament ages are given.

INTRODUCTION

Detailed discussions of IUE spectra of supernova remnants have been given by Benvenuti, D'Odorico and Dopita and Benvenuti, Dopita and D'Odorico (refs. 1,2). Raymond et al (ref. 3) considered long and short wavelength spectra of a bright filament in the Cygnus Loop which had been studied optically by Miller (ref. 4; his position 3). Here we compare that spectrum with two other filaments for which we have long exposures in both the long and short wavelength cameras.

Miller's position 3 is anomalously bright in the [O III] optical lines compared with models (refs. 5-7) and with most of the other bright optical filaments. Raymond et al.(ref. 3) inferred for this filament 1) a shock velocity of about 130 $km\ s^{-1}$, significantly faster than had been estimated from optical spectra; 2) weakening of the resonance lines of C II and C IV by up to a factor of ten by resonant scattering, either intrinsic to the filament or in the interstellar gas along the line of sight; 3) carbon and silicon only slightly depleted ($\approx$ a factor of 1.5) compared with oxygen; and 4) departure from steady-flow, in the sense that the recombination region is incomplete, implying an age for the filament of $\approx$ 200 yrs.

CONCLUSIONS

Table 1 compares the IUE spectrum of Miller's position 3 with the spectrum of another Cygnus Loop filament and that of a filament in the Vela Supernova Remnant. The Cygnus Loop filament has been studied optically by R. Fesen and R. Kirshner and called position "yellow". Its optical spectrum resembles those of

* Supported in part by NASA grants NSG 5370 to the Harvard College Observatory and NAG-5-5 to the Smithsonian Astrophysical Observatory.

Miller's positions 1 and 2. The filament selected for study in the Vela Supernova Remnant was a sharp, bright [O III] filament near the center of the remnant chosen from interference filter photographs provided by T. Gull. It is probably similar to Miller's position 3 in its relatively great [O III] / Hβ ratio. The fluxes listed in Table 1 for the Cygnus Loop have been corrected for reddening E(B-V) = 0.08 (refs. 8,9). Reddening is not obviously required by the optical spectra of the Vela Supernova Remnant (refs. 10,11), and no reddening correction was made, but we cannot exclude the possibility of significant extinction in the UV.

The emission in the bright lines at Miller's position 3 appears to be uniform over the large aperture, so interpretation in terms of a single velocity shock is at least reasonable. The other two spectra reported here show clear structure within the large aperture, and full interpretation will require separation of two or three spatial regions in each. Thus we will not attempt a serious fit of these spectra to individual shock models, but instead give a general comparison with Miller's position 3.

The three spectra are basically quite similar in the lines present. The outstanding difference between the two Cygnus Loop spectra is the strong Mg II emission at position "yellow" and the lack of Mg II at position 3. This confirms the hypothesis that the recombination zone, where Mg II emission is expected to arise, is almost absent at position 3, while more of a steady-flow shock has developed at "yellow". While this is expected from the optical spectra, there is a conceivable alternative explanation. It is possible that the Doppler velocities of the two filaments are such that the Mg II lines from position 3 coincide with the strong interstellar Mg II absorption, while those at "yellow" do not. A hit at the position of C II λ1335 prevents more than a lower limit to the factor by which resonant scattering reduces that line. The C IV / O III] ratio is larger at "yellow" by a factor of two, giving some indication that resonant scattering may be less severe. Either less severe scattering or a slightly higher shock velocity may account for the greater strength of N V at position "yellow", but the likelihood of a mixture of shock velocities makes even this uncertain.

In the coming year we will be studying the interstellar absorption lines in the vicinity of the Cygnus Loop and the Doppler velocities of the filaments under study in order to distinguish between interstellar resonant scattering and intrinsic scattering. In the latter case, resonance line photons tend to be scattered out the faces of a sheet of gas; the choice of bright optical filaments for study tends to select sheets of gas seen on edge, so the resonance lines appear to be weak relative to forbidden and intercombination lines. If the resonance line scattering is intrinsic, the ratio C II / C II] yields a column density, and consequently a density estimate.

The Vela SNR filament is much like position 3 of the Cygnus Loop in that the low temperature lines, C II and Mg II are relatively weak, again indicating a departure from steady flow. The weakness of N V indicates a slightly smaller shock velocity. The N III] and N IV] lines are rather strong compared with O III]. Since there is no optical evidence for an unusual abundance ratio (refs. 10,11), it seems likely that this is a result of the mixture of shock velocities. The C II / C II] ratio is only about a factor of 2 below those predicted by the models. The interstellar C II absorption has been studied extensively (ref. 12), and it seems that a Doppler shift of around 50 $km\ s^{-1}$ is needed to shift the emission lines away from the interstellar absorption.

One comparison of interest between the Cygnus Loop and Vela SNR is the relative abundances of carbon and silicon, since these elements are most strongly affected by grain depletion. Jenkins, Silk and Wallerstein (ref. 12) concluded from *Copernicus* observations of absorption lines that there was no significant depletion in shocks associated with the Vela SNR. The IUE spectra seem to indicate depletion of carbon and silicon by about a factor of 1.5 in both remnants as compared with the ratios of these elements to oxygen given by Allen (ref. 13), but further observational and theoretical study is required to confirm this result.

References

1. Benvenuti, P., D'Odorico, S., and Dopita, M. 1979, Nature, 277, 99.

2. Benvenuti, P., Dopita, M., and D'Odorico, S. 1980, Ap. J., in press.

3. Raymond, J.C., Black, J.H., Dupree, A.K., Hartmann, L., and Wolff, R.S. 1980, Ap. J., in press.

4. Miller, J.S. 1974, Ap. J., 189, 239.

5. Cox, D.P. 1972, Ap. J. 178, 143.

6. Raymond, J.C. 1979, Ap. J. (Supplement), 39, 1.

7. Shull, J.M., and McKee, C.F. 1979, Ap. J., 227, 131.

8. Parker, R.A.R. 1967, Ap. J., 149, 363.

9. Bless, R., and Savage, B. 1972, Ap. J., 171, 293.

10. Dopita, M.A., Mathewson, D.A., and Ford, V.L. 1977, Ap. J., 214, 179.

11. Osterbrock, D.E., and Dufour, R.J. 1973, Ap. J., 185, 441.

12. Jenkins, E.B., Silk, J., and Wallerstein, G. 1976, Ap. J. (Supplement), 32, 681.

13. Allen, C.W. *Astrophysical Quantities*, 3rd ed., (University of London, 1973).

LINE EMISSION

Relative to λ 1666

ION	λ	Cygnus Loop		Vela SNR
		Miller 3	"Yellow"	
N V	1240	19	42	11*
C II	1335	10*	62**	23
O V	1371	6*	-	-
O IV / Si IV	1400	73	115	148
N IV	1485	11	-	55
C IV	1550	108	266	205
He II	1640	27	38	40
O III	1666	100	100	100
N III	1745	52**	63	76
Si II	1818	6*	-	-
Si III	1890	27	128	73
C III	1909	181	424	293
C II	2325	102	240	74
Ne IV	2420	37	23*	47
O II	2470	21*	23*	20*
Mg II	2800	-	40	-
I(1666)†	-	2.5(-4)	5.4(-5)	3.9(-5)

* Estimated uncertainty greater than 30%

** Particle noise contributes up to 50% of this value.

† Ergs cm $^{-2}$ s^{-1} sr^{-1}.

SURFACE MAPPING OF SELECTED REGIONS IN THE ORION NEBULA

P. M. Perry, B. E. Turnrose, C. A. Harvel,
R. W. Thompson, A. D. Mallama

Computer Sciences Corporation
Astronomy Department

ABSTRACT

Low-dispersion, large-aperture, ultraviolet spectra ($\lambda\lambda$ 1135-3255Å) of selected regions in the Orion Nebula were obtained with the International Ultraviolet Explorer (IUE) scientific instrument. Spectra obtained at 35 contiguous locations defining a mosaic within the nebula were used to generate monochromatic images of high spatial resolution at the wavelengths of the ultraviolet emission lines CIII] λ1909, CII] λ2326, and [OII] λ2470. Image-processing techniques were utilized to generate and analyze these ultraviolet surface maps. The imagery at the three wavelengths studied shows definite differences in the spatial distribution of emission from the CII] CIII] and [OII] ions. Ways of using the imagery to determine ionization structure and C/O abundance ratios throughout the regions observed are being developed, in addition to means of analyzing the extensive continuum measurements in terms of dust-scattering characteristics.

INTRODUCTION

The central (Huygenian) region of the Orion Nebula (NGC 1976) possesses a wealth of fine structural detail which can only be studied with high-resolution instruments. Many studies have been carried out on visual images of the central region but, until recently, it was not feasible to obtain images of sufficiently high resolution in the far UV. Existing UV imagery (e.g., ref. 1), although of considerable scientific value, displays only large-scale surface detail.

The launching of the IUE has provided a unique opportunity to extend the high-resolution study of the surface features of the Orion nebula into the far UV. Even though the IUE scientific instrument described by ref. 2 is primarily designed to operate as a conventional spectrograph, its high degree of attitude stability and pointing accuracy, together with an extended sky coverage (10 by 20 arcseconds) using the large entrance aperture, give it the capability--when used in the mode to be presently described --of obtaining high spatial resolution images in the far UV. The observational technique involves the acquisition of low-dispersion spectra through the large aperture in both the long- and short-wavelength spectrographs. Contiguous image segments, defined by the size of the aperture, are obtained in a raster pattern covering the program area. As in a slitless spectrograph, each image segment is simultaneously accumulated at all wavelengths. The image processing operations to be described then reconstruct monochromatic images of the nebula in the wavelengths of the UV emission lines from a mosaic of the individual segments.

The following section of this paper describes the specific observational procedure used to obtain the images. The next section details the processing techniques employed in obtaining a preliminary set of "raw" mosaics, and then describes methods to be employed to further remove instrumental signature and improve the image reconstruction integrity. These raw mosaics are presented in the last section which contains a preliminary discussion of their significance and the use of the data obtained by this program in several scientific areas.

OBSERVATIONS

During the period from April 23 to April 28, 1979, a series of 69 large-aperture, low-dispersion images were taken covering a total of 35 contiguous overlapping areas in the central (Huygenian) region of the nebula. This area extends from just south of θ^2Ori A in a northwesterly direction across the bright bar towards θ^1Ori C (see Figures 1 and 2, and Table I). For all but one of these areas, both a long- and a short-wavelength camera exposure were obtained.

Figures 1 and 2 and Table I define the 35 areas used to form the mosaic and locate the mosaic as a whole within the nebula. Figure 1 shows the contiguous area observed outlined on a visual photograph of the central part of the nebula. Figure 2 shows the placement, orientation, and extent of each of the 35 areas observed; Table I gives the RA and DEC of each area, as well as the image number of the observation with each camera and the exposure time used. At the time of these observations, the spacecraft was oriented such that the long axis of the large aperture ran very nearly north-south.

As can be seen in Table I, exposure times for LWR and SWP were about 15 and 10 minutes, respectively. When possible, the exposure time for an area was estimated from the exposure time and exposure level of previously observed adjacent areas. In one case (area 32), the position of the area was changed to move it away from a bright star (θ^2A) after an adjacent area (area 33) was saturated by scattered light from the star.

Pointing of the spacecraft was maintained to an accuracy of 3 arcseconds or better (this is less than the spatial resolution of the system) by setting on θ^2Ori C (assumed 1950.0 coordinates: RA = $5^h33^m\ 04.^s0$, DEC = $-5^\circ27'\ 09".0$), offsetting to the RA and DEC of the target area, and then quickly acquiring θ^2Ori C as a guide star. The spacecraft gyros were trimmed to minimize drift during the maneuver. In those cases where an observation of the same area was immediately made using the other camera, the spacecraft was maneuvered to place the area in the large aperture of the other camera without going back to the set star. After each observation or set (LWR, SWP) of observations, the spacecraft was offset back to θ^2Ori C using the inverse of the offsets used to get to the target area. The difference between the expected FES location of the set star and its actual location was obtained in order to estimate the combined offset and drift error during the observation--this error was less than 3 arcseconds in all cases and usually around 1.5 arcseconds.

PROCESSING TECHNIQUES

The 35 observations described in the preceding section were first processed in the standard fashion at the IUE Image Processing Center (ref. 3). An example of a raw LWR image of the nebula is given in Figure 3, which illustrates the appearance of the CII]λ2326 and [OII]λ2470 lines against the continuum radiation. Each observation yields a two-dimensional array of fluxes arranged by wavelength and spatial position perpendicular to dispersion; this is the so-called line-by-line or spatially resolved spectrum which is used herein as the starting point for our special processing. Since the imagery to be reconstructed here is monochromatic, the wavelength dimension also translates into position; i.e., there is spatial resolution along the dispersion direction. Thus, from the line-by-line spectra of each observation, we can derive a two-dimensional image segment of that portion of the nebula subtended by the large aperture, for each of the UV emission lines observed. The purpose of our tailored processing is to assemble these segments into a set of monochromatic mosaics of the nebula, and to remove residual instrumental effects as well as any effects due to the particulars of the observations. For each of the mosaics, the following procedures are used.

A data array is dimensioned (51 x 69) to cover the program region (Figures 1 and 2) with a basic resolution of one IUE line-by-line spectrum sample. The celestial coordinates of the observations are read from the IUE image header, verified with handkept observing logs, and converted to the corresponding relative coordinates of our data matrix. At the same time, the exposure time is read from the IUE header and stored in core for later use.

The wavelengths in the line-by-line spectra are then read, and the locations of the emission lines of interest and suitable continuum background regions are noted. Then the fluxes are read from the appropriate locations. The image segment derived from this data is 5 line-by-line samples wide in the dispersion direction and 11 line-by-line samples high in the perpendicular direction. This corresponds closely to the 10 x 20 arcsecond dimensions of IUE's large aperture. (Remember that each line-by-line sample is $\sqrt{2}$ IUE pixels, or 2.16 arcseconds, on a side). Next, the background fluxes are interpolated within each line-by-line pseudo order and subtracted from the emission line fluxes. The resulting data are then normalized to a constant exposure time. The normalized fluxes are added to the data matrix, and an increment is added to the corresponding elements of a counter matrix.

When all the data have been so processed, the data matrix is divided by the counter matrix (in order to properly average the fluxes in grid elements where the observations were overlapped). Then the data are normalized to a maximum value of 30,000 for use by a COMTAL display device*, a header is added, and the resulting file is copied to tape.

The procedures described above result in preliminary mosaic imagery. Ways of further correcting and improving such data are currently under development. The effective transmission function, or vignetting function, for each element within the large aperture is being measured on unsaturated exposures of the geocoronal Lyman alpha line. SWP mosaics will be corrected for this function, and the possibility of relating that correction to LWR data will be

*Provided by the Laboratory for Astronomy and Solar Physics, GSFC.

investigated. Also, the possibility of using bilinear interpolation to render a more exact correspondence between the placement of the large aperture and the derived grid elements is being studied.

DISCUSSION

Figure 4 compares a visual image of the program region of the Orion nebula with the three preliminary UV mosaics which have been generated from the present data, using the emission lines CIII] λ 1909 (SWP), CII] λ 2326 (LWR), and [OII] λ 2470 (LWR). Note that the bright filamentary bar identified with an ionization front is visible in all three mosaics. The emission line from the singly ionized species (CII] and [OII]) is concentrated near the ionization front, whereas the emission from doubly ionized carbon is spread more throughout the principal HII region. The bar in the [OII] imagery appears to show a region of diminished intensity near the western end. In both CII] and [OII] there is detectable emission south of the bar, including fairly strong emission in the isolated region (to the east of the principal program area) which includes the compact optical object referred to as "cloudlet C" by Táylor and Münch (ref. 5). The cloudlet is a relatively low excitation object since no CIII] emission is seen. The general lack of CIII] emission south of the bar is another feature evident from the preliminary mosaic, even though the CIII imagery has the lowest signal-to-noise ratio because of the faintness of the λ1909 emission. Since that line is even weaker in the LWR spectra, only SWP spectra were used in generating the λ1909 mosaic. The SWP fluxes were corrected for ITF error using the Three Agency correction algorithm SWPFIX (ref. 4).

The data as they now stand indicate that several promising avenues of research are feasible. The imagery will be calibrated absolutely to obtain emission line intensities as a function of position with a resolution of about 4-5 arcseconds. Such intensity maps, perhaps corrected for density fluctuations by dividing through by an Hα image*, will be used to compare the ionization structure measured by the spatial distribution of the CII], CIII], and [OII] UV emission to the results of optical studies. The preliminary UV results compare favorably with optical measurements indicating that the higher ionization states are found chiefly within the principal inner HII region (see, for example, ref. 6). These data may also be compared to the less extensive UV measurements of Torres-Peimbert, et al. (ref. 7), and Bohlin, et al. (ref. 8). In particular, the present data will be used according to the considerations of refs. 7, 8, and 9 to measure the C/O abundance ratio as a function of position and compare it to the earlier results which find either solar values (ref. 7) or twice solar values (ref. 8) for C/O in Orion.

The measurements of the nebular continuum which are accumulated in the present program at all wavelengths from λ1150 Å to 3200 Å are of considerable interest in their own right in characterizing the properties of dust scattering as a function of position in the nebula. The grid of continuum measurements obtained here will ultimately be presented in a form suitable for dust studies. In this regard, we intend particularly to map the strength of the 2200 Å extinction feature in the bar, cloudlet C, and two other Taylor-Münch cloudlets (ref. 5) also observed.

*R. J. Dufour, private communication (1980)

REFERENCES

1. Carruthers, G. R., and Opal, C.: Ap.J, vol. 217, 1977, p. 95.

2. Boggess, A., et al., The IUE Spacecraft and Instrumentation, Nature, vol. 275, Oct. 1978, p. 2.

3. Klinglesmith, D. A., Perry, P. M., and Turnrose, B. E.: The International Ultraviolet Explorer Spectral Image Processing System, Proceedings of the Society of Photo-Optical Instrumentation Engineers, vol. 172, 1979, p. 279.

4. Cassatella, A., et al., A Correction Algorithm for Low Disperson SWP Spectra, NASA IUE Newsletter No. 8, 1979.

5. Taylor, K., and Münch, G.: Astron. Astrophys., vol. 70, 1978, p. 359.

6. Balick, B., Gammon, R. H., and Hjellming, R. M.: Pub. A.S.P., vol. 86, 1974, p. 616.

7. Torres-Peimbert, S., Peimbert, M., and Daltabuit, E.: IUE and Visual Observations of the Orion Nebula and IC 418: The Carbon Abundance (preprint), 1979.

8. Bohlin, R. D., Hill, J. K., Stecher, T. P., and Witt, A. N.: Long-Slit Spectroscopy in the Rocket Ultraviolet of the Orion Nebula, Ap. J. (in press).

9. Dufour, R. J., Talbot, R. J., Jr., and Shields, G. A.: The Carbon Abundance in Two HII Regions of the Small Magellanic Cloud. The Universe in Ultraviolet Wavelengths: The First Two Years of IUE. NASA CP 2171, 1980: this compilation.

TABLE I - LOG OF OBSERVATIONS

	RA			DEC			SWP		LWR	
AREA#	h	m	s	deg	m	s	IMAGE#	EXP*	IMAGE#	EXP*
1	5	32	50.87	-5	25	28.0	5068	10.0	4401	15.0
2			51.40			28.0	5061	10.0	4394	11.25
3			51.93			28.0	5053	10.0	4386	15.0
4			51.13			44.0	5069	10.0		
5			51.67			44.0	5060	10.0	4393	15.0
6			52.20			44.0	5052	10.0	4385	15.0
7			52.73			44.0	5065	10.0	4398	15.0
8			51.93		26	00.0	5059	10.0	4392	15.0
9			52.47			00.0	4997	8.0	4334	12.0
10			53.00			00.0	5051	10.0	4384	15.0
11			53.53			00.0	5050	10.0	4383	15.0
12			52.20			16.0	5058	10.0	4391	15.0
13			52.73			16.0	5054	10.0	4387	15.0
14			53.27			16.0	5036	10.0	4364	15.0
15			53.80			16.0	5034	10.0	4362	15.0
16			54.33			16.0	5066	10.0	4399	15.0
17			54.87			16.0	5067	10.0	4400	15.0
18			52.47			32.0	5057	10.0	4390	15.0
19			53.00			32.0	5055	10.0	4388	15.0
20			53.53			32.0	5035	10.0	4363	15.0
21			54.07			32.0	5033	8.0	4361	12.0
22			54.60			32.0	4996	8.0	4333	12.0
23			56.73			29.0	5049	9.0	4359	12.0
24			52.73			48.0	5056	10.0	4389	15.0
25			53.27			48.0	5032	8.0	4360	12.0
26			53.80			48.0	5031	8.0	4344	9.0
27			54.33			48.0	5000	8.0	4336	12.0
28			54.87			48.0	4999	2.0	4335	2.5
29			52.47		27	04.0	not observed			
30			54.07			04.0	5007	8.0	4342	12.0
31			54.60			04.0	5003	8.0	4339	12.0
32			55.13			09.0	5002	6.0	4338	9.0
33			55.67			04.0	5001	2.0	4337	3.0
34			54.87			15.0	5006	10.0	4342	15.0
35			55.40			20.0	5005	8.0	4341	15.0
36			55.93			20.0	5004	6.0	4340	9.0

*All exposures given in minutes.

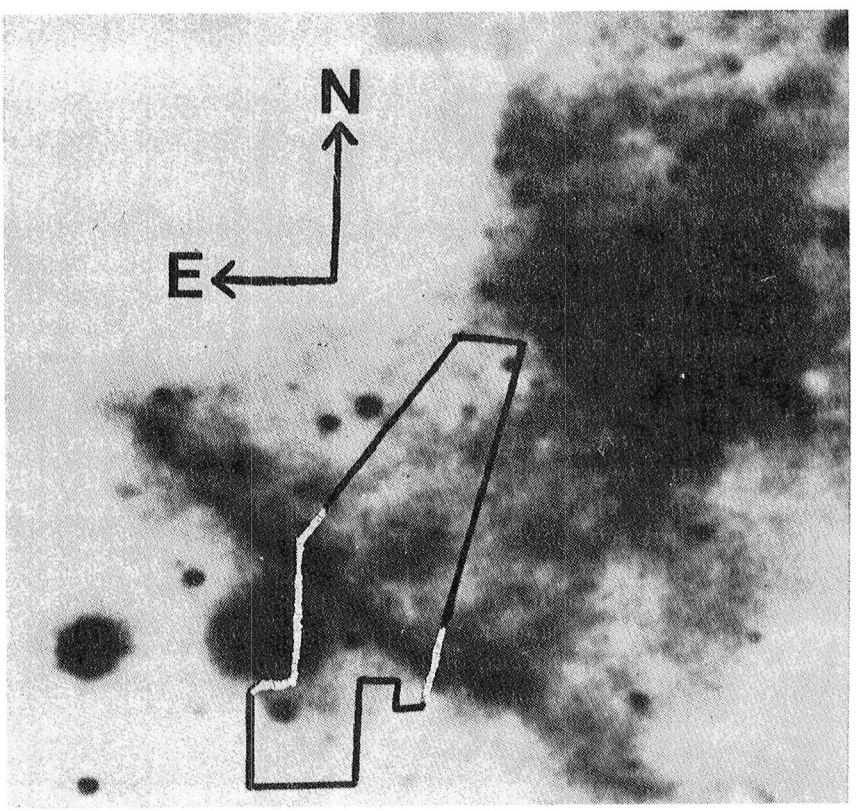

Figure 1 — [OI]λ6300 photograph of the central region of the Orion Nebula (courtesy T. R. Gull, GSFC) with UV survey area outlined.

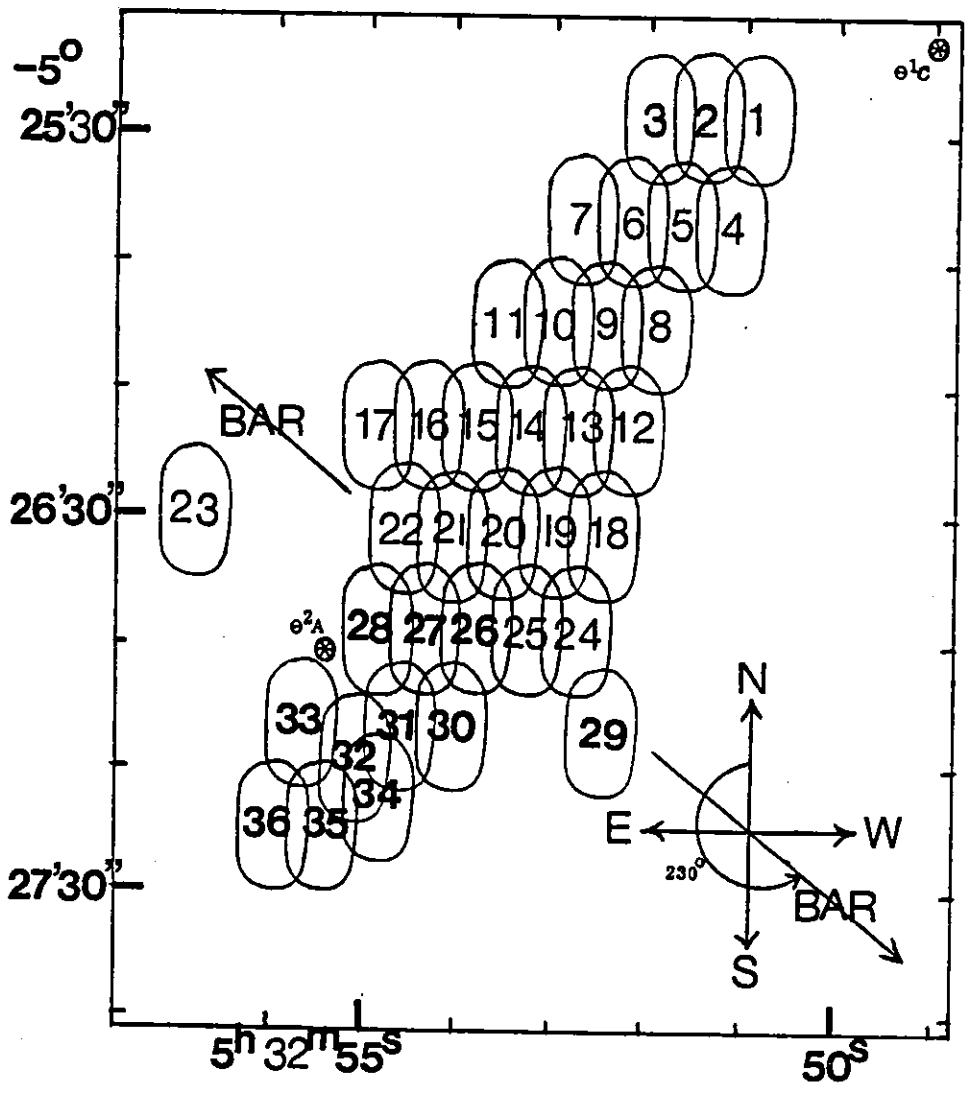

Figure 2 — Schematic drawing showing placement and orientation of survey apertures.

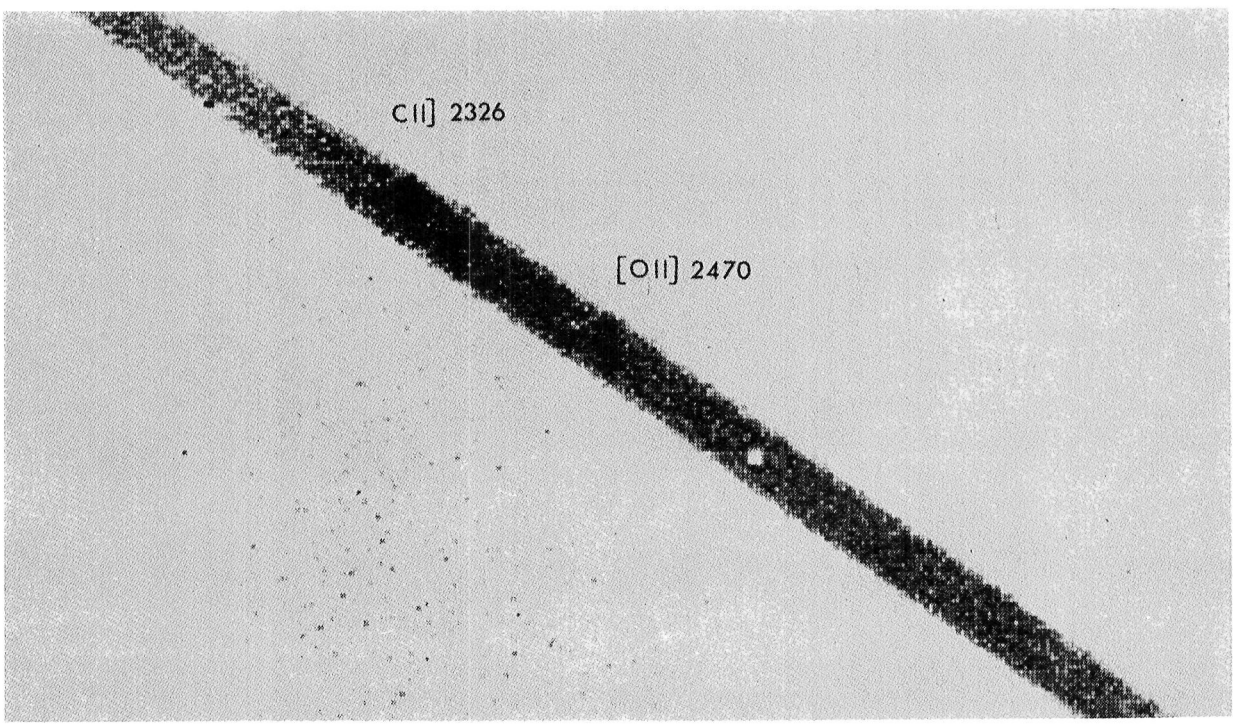

Figure 3 — Enlargement of raw image (LWR 4389, area 24) showing the CII] λ2326 and [OII]λ2470 emission lines against the continuum radiation.

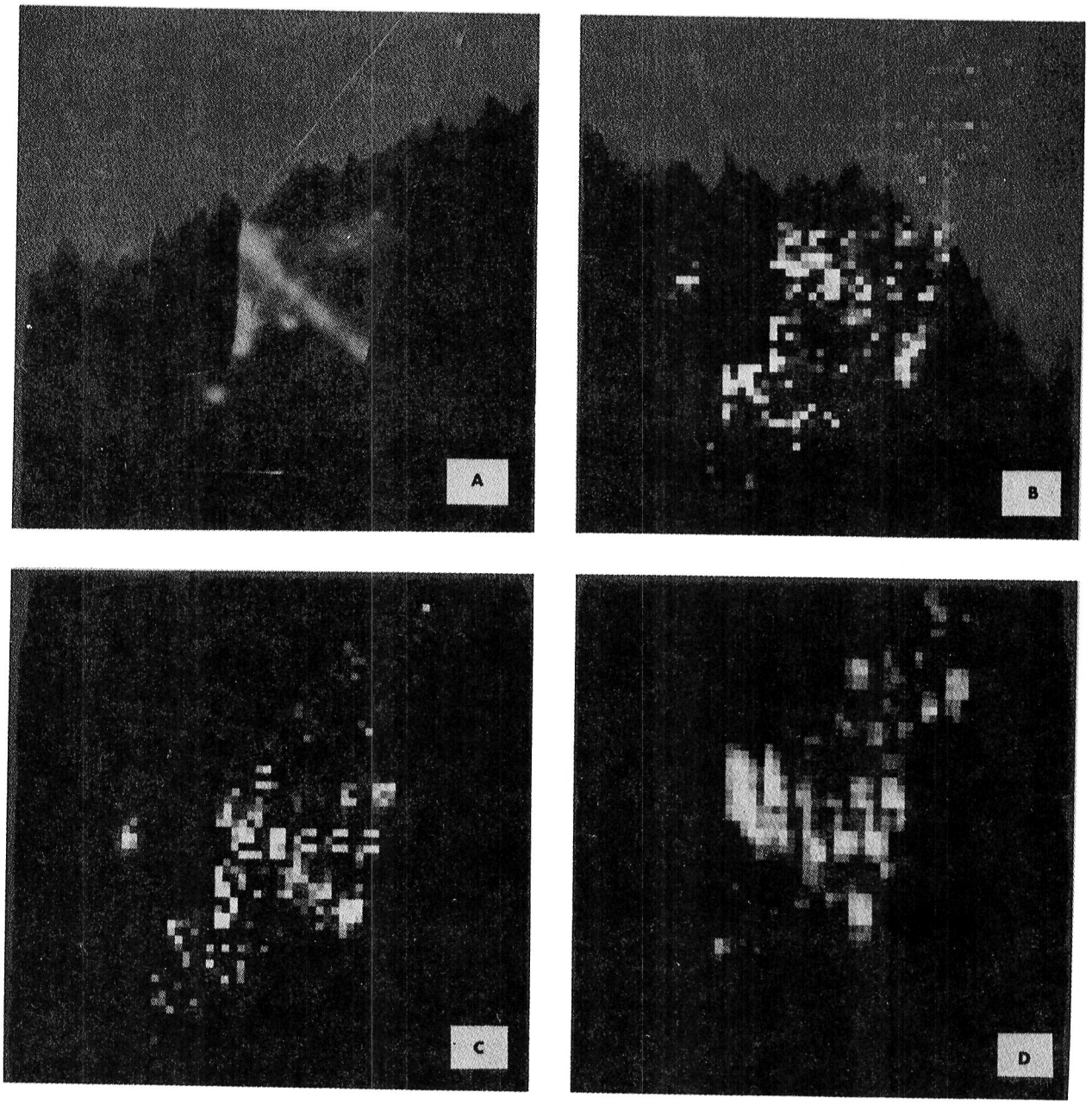

Figure 4 — Comparison of survey region in visual and UV wavelengths:

a. [OI]λ6300

b. [OII]λ2470

c. CII]λ2326

d. CIII]λ1909

Note that the brightness of each UV mosaic is scaled so that the highest intensity in that mosaic is white and zero or negative intensity is black. Relative intensities between the three mosaics cannot be inferred from these photographs.

ULTRAVIOLET ABSORPTION BY INTERSTELLAR GAS AT LARGE DISTANCES FROM THE GALACTIC PLANE

Blair D. Savage and Klaas S. de Boer

University of Wisconsin, Madison, WI 53706, U.S.A.

During the past two years we have acquired a total of 18 high dispersion spectra of 6 stars in the LMC, 3 in the SMC, and 2 foreground galactic stars. The LMC stars observed are HD 36402, HD 268605, Sk, 18-67, HD 38268, HD 38282, and HD 269357. The SMC stars observed are Sk 80, Sk 108, and HD 5980. Various investigations undertaken with these spectra have resulted in the following publications:

1. "Observational Evidence for a Hot Gaseous Galactic Corona" Savage, B.D. and de Boer, K.S. 1979, *Ap.J. Letters*, 230, L77.

2. "Ultraviolet Absorption by Interstellar Gas Near 30 Doradus" de Boer, K.S., Koornneef, J., and Savage, B.D. 1980, *Ap.J.*, (March 15).

3. "Evidence for Hot Gaseous Coronae Around the Magellanic Clouds" de Boer, K.S., and Savage, B.D. 1980, *Ap.J.*, (May 15).

4. "Ultraviolet Absorption by Interstellar Gas At Large Distances from the Galactic Plane" Savage, B.D., and de Boer, K.S., *Ap.J.*, (submitted).

Paper 4 contains a reasonably complete discussion of the Milky Way absorption features toward the 9 Magellanic cloud stars. Preprints of this paper are available on request; the abstract is given below:

Abstract from "Ultraviolet Absorption by Interstellar Gas at Large Distances from the Galactic Plane", Savage and de Boer, *Ap.J.*, (submitted):

We have analyzed 18 high-dispersion IUE spectra of 6 stars in the LMC, 3 stars in the SMC, and 2 foreground stars. Fourteen spectra cover the wavelengths λλ 1150-2000Å and 4 cover λλ 1900-3200Å. The velocity resolution is $\sim$ 25 km s^{-1}. All the Magellanic Cloud star spectra exhibit exceedingly strong interstellar absorption lines due to a wide range of ionization stages at galactic velocities and at velocities associated with the LMC or SMC. In this paper the analysis is restricted to the Milky Way absorption features. Toward the LMC stars, the strong interstellar lines have a positive velocity extension to $v_{LSR} \sim 150$ km s^{-1}, which exceeds by $\sim$ 100 km s^{-1} the extension recorded toward the SMC stars. The most straightforward interpretation of these velocity extensions is obtained by assuming that gas at large distances away from the plane of the galaxy participates in the rotation of the galaxy as found in the galactic disk. This then indicates that we have detected absorption by gas as far as perhaps 10 to 15 kpc below the plane of the galaxy. Toward many of the LMC stars the low ion stage lines exhibit a component structure with strong features near 60 and 130 km s^{-1}. The presence

of O I absorption at these velocities implies that a portion of the gas is neutral even though it is not detected in existing 21-cm emission data. A curve of growth analysis provides some information on the composition of the low-ion high-velocity gas. Solar abundances are consistent with the uncertain abundance estimates, although there is the possibility that the N/O ratio is less than solar. The high-ionization lines of Si IV and C IV are strong toward all the Magellanic Cloud stars while N V is not detected. These data provide definitive proof that highly ionized species exist in the general interstellar medium of our galaxy away from local stellar environments. The weakness of the high-ion lines toward the foreground galactic stars implies that the strong absorption toward the extragalactic stars is primarily produced by gas beyond $r \sim 0.9$ kpc. For this halo gas we obtain toward the LMC $\log N(\text{C IV}) \sim 14.0$, $\log N(\text{Si IV}) \sim 13.5$, and $\log N(\text{N V}) < 13.5$. Toward the SMC the N V limit is the same but the C IV and Si IV column densities are at least a factor of 2 larger. If the high-ion gas is produced by equilibrium "coronal ionization" the implied temperatures are in the range 0.7 to 1.4×10^5 K. The high-ion line profiles contain less component structure than the low ion profiles, suggesting a smoother high-ion gas distribution. While the low-ion gas might represent condensed material in a galactic fountain model, it is not obvious where within this model the high-ion gas fits since the fountain, if it exists, is presumably driven by gas with much higher temperatures. If the high-ion gas is primarily formed in "cloud coronae" one might expect to find a better correspondence between the low- and high-ion line profiles than is observed. Perhaps the high-ion gas represents a type of "transition region" between gas in the plane of the galaxy and a hotter exterior zone that cannot be studied with IUE data. Assuming solar abundances, the amount of halo gas detected represents ~ 2 percent of that found in the galactic disk.

ELECTRON DENSITIES FOR SIX PLANETARY NEBULAE AND HM SGE DERIVED FROM THE C III] λ1907/1909 RATIO

WALTER A. FEIBELMAN
Laboratory for Astronomy and Solar Physics, Goddard Space Flight Center

ABSTRACT

Electron densities for IC 418, NGC 6572, IC 1297, NGC 3242, NGC 6818, NGC 3211, and HM Sge derived from high-dispersion IUE C III] spectrograms are consistently higher than those derived from either surface brightness measurements of forbidden line intensity ratios in the visible. The nebulae were selected for a range of excitation classes from 3 to 9. Line splitting due to expansion velocities is observed for three objects. The great width of the λ1909 C III] line in HM Sge suggests large expansion velocities.

The results described are part of an ongoing observational program of planetary nebulae in collaboration with A. Boggess, R. W. Hobbs, and C. W. McCracken.

INTRODUCTION

The usefulness of the C III] λ1907/λ1909 ratio as a diagnostic tool for determining electron densities in planetary nebulae has been recognized for some time (Osterbrock 1970; Loulergue and Nussbaumer 1976). Observations of 24 planetary nebulae by means of the International Ultraviolet Explorer (IUE) satellite have shown that in the low resolution (∿7Å) mode C III] λ1909 is usually the strongest emission feature (Boggess, Feibelman and McCracken 1980). The high-dispersion spectrographs of IUE easily resolve the pair of C III] lines. The instruments have been described in detail elsewhere (Boggess et al. 1978). We report results on six planetary nebulae and HM Sge observed in the high-resolution (0.1Å) mode to determine the λ1907/λ1909 ratios from them.

DATA AND DISCUSSION

Loulergue and Nussbaumer (1976) have pointed out that in the regime of $N_e < 10^6$ cm^{-3}, characteristic of planetary nebulae, the magnetic quadrupole transition $2s^2\ ^1S_0 - 2s\ 2p\ ^3P_2^0$ at λ1906.68 has an emissivity comparable to the intercombination transition $2s^2\ ^1S_0 - 2s\ 2p\ ^3P_1^0$ at λ1908.73. Subsequently, Nussbaumer and Schild (1979) published new curves for the relative emission strengths of the λ1906.68/λ1908.73 ratio, based on improved data for the collision strengths. These curves for the ratio of the C III] pair versus log N_e permit one to derive electron densities from the IUE high-resolution data.

The planetary nebulae IC 418, NGC 6572, IC 1297, NGC 3242, NGC 6818, NGC 3211, and HM Sge (which is suspected of being a proto-planetary in its early stages of development) have been observed in the high-resolution mode and the C III] λ1907/λ1909 ratios have been determined. Dates of observation and exposure times for the nebulae are summarized in Table 1. All spectrograms were obtained through the large aperture centered on the nuclei. The

results are shown in Table 2, where the electron densities derived from these ratios in conjunction with the curves of Nussbaumer and Schild (1979) are listed in the last column. Also shown in Table 2 are values of electron densities given by Aller (1965) based on Hβ surface brightness data, and densities derived by Aller and Walker (1970) from forbidden line intensity ratios. For all planetaries listed in Table 2, ranging in excitation class from 3 to 9, the lowest electron densities are the ones derived from the Hβ data, while the highest were obtained from the present IUE data based on the C III] ratios.

Relatively little is known about IC 1297 from ground-based observations. Its excitation class is estimated here to be in the range of 7 - 8, and the electron temperature is assumed to be 11,000K. Observations of IC 1297 are needed to verify these assumptions. The high-resolution spectrograms of NGC 3242, and a lesser degree those of NGC 3211 and NGC 6818, show splitting of the C III] lines due to Doppler velocities. The remainder of the planetaries do not show this effect. For NGC 3242 an expansion velocity of 39 km/sec is obtained, which is in very good agreement with the average value of 39.8 km/sec given by Wilson (1950). Examples of the split lines for NGC 3242 and the single lines for NGC 6572 are shown in Fig. 1 and Fig. 2.

Flower, Nussbaumer, and Schild (1979) obtained a value of 0.02 for the C III] λ1907/λ1909 ratio for HM Sge observed in 1978, implying log $N_e \geq 6$, corresponding to log $N_e \approx 6.5$ when derived from the updated curves by Nussbaumer and Schild (1979). On June 2, 1979, we obtained a 180 minute exposure of HM Sge which had a better S/N ratio than the relatively short (40 min) exposure by Flower et al. (1979). The weak λ1907 component is superimposed on the very extended blue wing of the strong, asymmetric λ1909 component, shown in Fig. 3, making a precise determination of the λ1907/λ1909 ratio difficult. An upper limit of the electron density can be set as log $N_e \approx 10^6$, derived from $R \approx 0.04$. The presence of a narrow spike in the λ1909 line profile suggests the possibility that the emission plasma consists of two separate components.

The great width of the λ1909 line in HM Sge yields a large expansion velocity. Flower et al. (1979) give a value of >118 km/sec, but the present data yield only ≈63 km/sec. The maximum velocity may be a more significant quantity to consider because of the asymmetry of the line profile. Wallerstein (1978) found v_{max} = 1700 km/sec for Hα + He II derived from the full width at the base of the line in HM Sge on September 2, 1977, but also listed on a wide range of lesser velocities for other ions. The present IUE data result in v_{max} = 353 km/sec and 375 km/sec derived from the C III] λ1909 and Mg II λ2798, λ2803 resonance lines, respectively.

CONCLUSIONS

Electron densities, based on the C III] λ1907/ λ1909 intensity ratios for six planetary nebulae are consistently higher than those derived from surface brightness or forbidden line intensity ratios in the visible. The nebular expansion velocity of 39 km/sec for NGC 3242 is in good agreement with ground-based observations by Wilson (1950). HM Sge has an expansion

velocity and electron density substantially greater than those of typical planetary nebulae, and the complex structure in the λ1909 line profile suggests the existence of more than one emission region in the line of sight. It remains to be determined whether these shells will evolve into a classical planetary nebula structure.

The assistance of the IUE Observatory staff and their expertise in the acquisition of the observational material is gratefully acknowledged. Special thanks go to Drs. D. Klinglesmith and R. Fahey for the development of the computer programs used in the data reduction.

REFERENCES

1. Osterbrock, D. E.: Astrophysical Journal, 160, 25, 1975.

2. Loulergue, M.; Nussbaumer, H.: Astronomy and Astrophysics, 51, 163, 1976.

3. Boggess, A.; Feibelman, W. A.; McCracken, C. W.: in preparation, 1980.

4. Boggess, A.; et al.: NATURE, 275, 377, 1978.

5. Nussbaumer, H.; Schild, H.: Astronomy and Astrophysics, 75, L17, 1979.

6. Aller, L. H.: Landolt Bornstein Numerical Table, VI, 1, 566, Springer New York.

7. Aller, L. H.: Astrophysical Journal, 161, 917, 1970.

8. Wilson, O. C.: Astrophysical Journal, 111, 279, 1950.

9. Flower, D. R.; Nussbaumer, H.; Schild, H.: Astronomy and Astrophysics, 72, L1, 1979.

10. Wallerstein, G.: Publication of the Astronomical Society of the Pacific, 90, 36, 1978.

11. Torres-Peimbert, S.; Peimbert, M.: Rev. Mex Astr. Astrofis., 2, 181, 1978.

TABLE I.- HIGH-DISPERSION OBSERVATIONS OF PLANETARY NEBULAE

Object	Date	IUE Image Number	Exposure (min)
IC 418	18 Dec 1978	LWR 3200	40
NGC 3211	18 Dec 1978	LWR 3204	90
NGC 3242	18 Dec 1978	LWR 3206	60
NGC 6818	7 April 1979	LWR 4211	150
IC 1297	7 April 1979	LWR 4212	120
NGC 6572	7 April 1979	LWR 4213	100
HM Sge	20 Dec 1978	LWR 3219	28
HM Sge	2 June 1979	SWP 5429	180

TABLE II.-ELECTRON DENSITIES FOR PLANETARY NEBULAE

Nebula	Excitation Class (Ref. a)	T_e (x10^{-4}) (Ref. a & c)	C III] λ1907/λ1909 Ratio	log N_e		
				Ref. a	Ref. b	This work
IC 418	3	0.91 (c)	0.93	4.27	4.22	4.4
NGC 6572	5	1.08 (a)	0.80	4.14	4.00	4.5
IC 1297	(7-8)	-	(1.0)	-	-	4.4*
NGC 3242	7	1.10 (a)	1.09	3.87	3.90	4.2
NGC 6818	9	1.80 (a)	1.19	3.75	3.84	4.1
NGC 3211	9	1.37 (c)	1.11	3.44	-	4.1
HM Sge	-	-	0.04	-	-	6.0#

Ref. a: Aller (1965; N_e derived from Hβ data.

Ref. b: Aller and Walker (1970); N_e derived from forbidden lines.

Ref. c: Torres-Peimbert and Peimbert (1977); N_e derived from [O III] data.

Notes:

Excitation class for IC 1297 not listed in Ref. a. The value shown is estimated.

* = assuming T_e = 11,000K. # = assuming T_e = 12,000K.

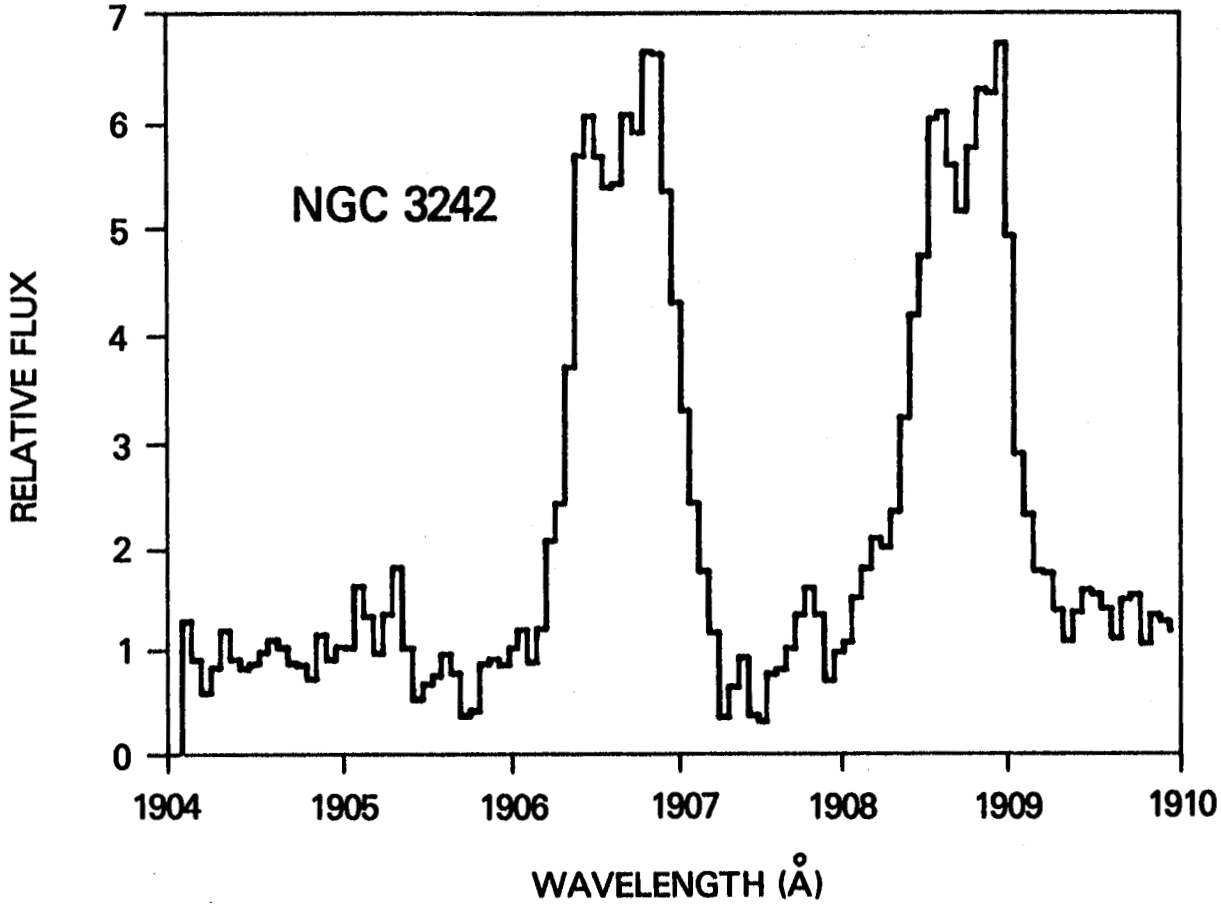

Fig. 1 - Section of IUE echelle spectrogram showing the C III] λ1906.68 and 1908.73 lines for NGC 3242.

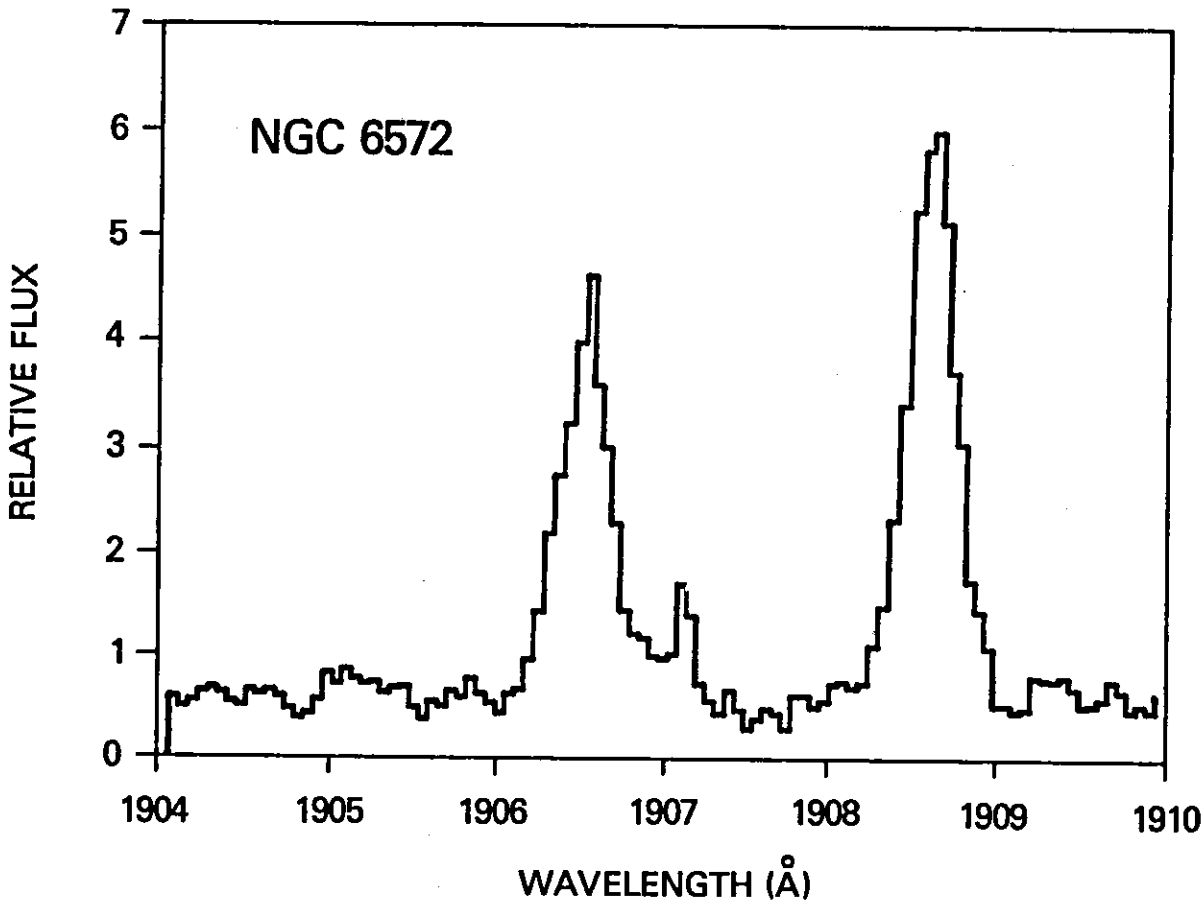

Fig. 2 - Same as Fig. 1, for NGC 6572

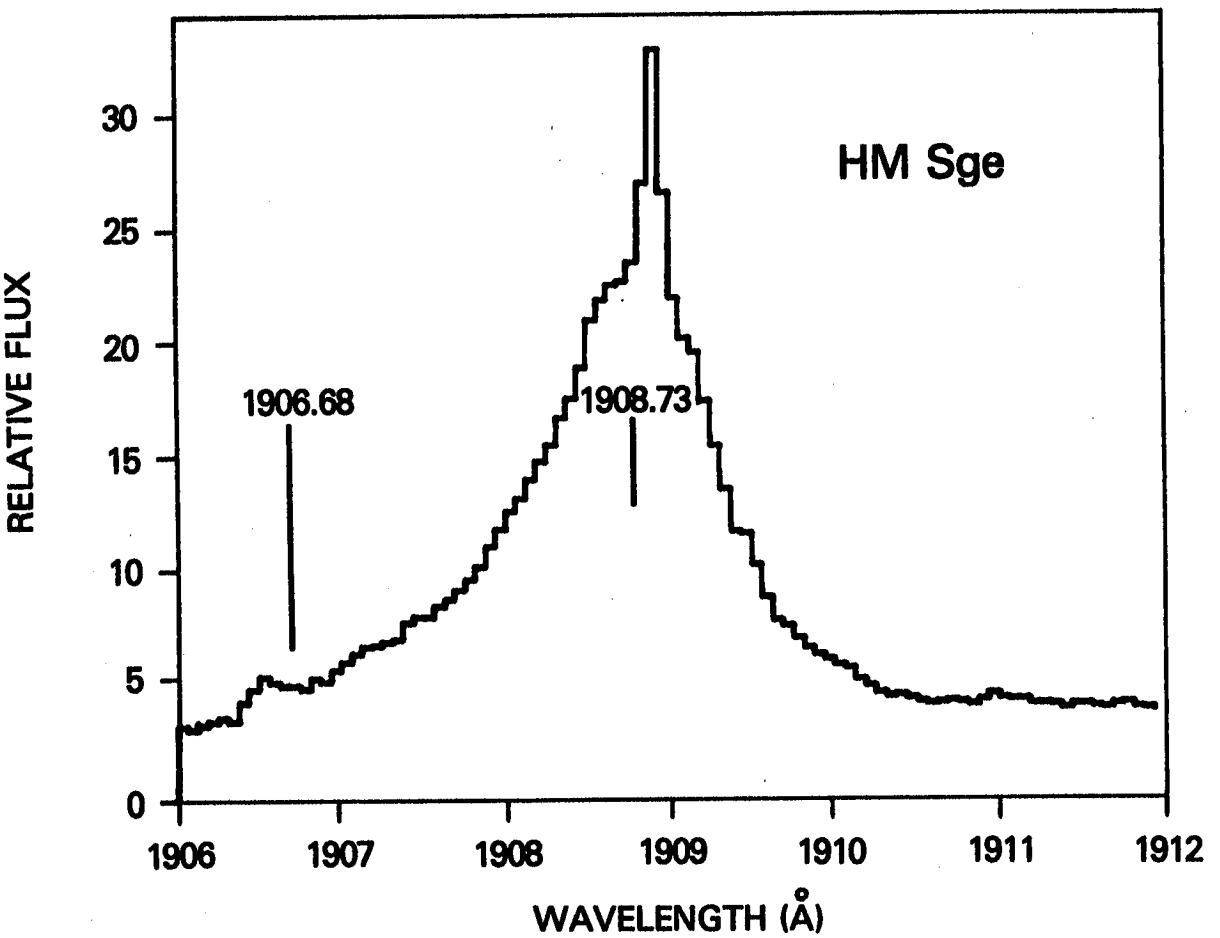

Fig. 3 - Same as Fig. 1, for HM Sge. The FWHM for the 1908.73 line is 0.8Å. The total width is ≈ 4.75Å.

SILICON AND MAGNESIUM IN PLANETARY NEBULAE

J.P. Harrington
Astronomy Program, U. of Maryland

P.A. Marionni*
Electro-Optics Branch, GSFC

ABSTRACT

The IUE satellite spectra of some planetary nebulae show features due to silicon and magnesium: Si III] λλ 1883, 1892; Si IV λλ 1394, 1403; Mg II λλ 2796, 2804 and [Mg V] λλ 2784, 2929. With the aid of modeling techniques, we can find the corresponding elemental abundances, which have not hitherto been known for planetary nebulae. In addition to previous observations of NGC 7662 and IC 418, we now have data for NGC 2440, Hu 1-2, IC 2003 and IC 2165. Silicon appears depleted by up to an order of magnitude relative to the sun. Large variations of magnesium abundance are found, which are likely to reflect differing degrees of depletion due to grain formation. Such observations may offer new insight into the formation of interstellar grains.

INTRODUCTION

It is known that elements such as Mg, Al, Si, Ca and Fe, which form refractory compounds, are strongly depleted in the interstellar medium, presumably by the formation of grains (ref.1). We would like to know if such depletions occur in planetary nebulae, for this would be direct evidence of grains within the ionized gas and the pattern of depletion could provide information about the formation and composition of the dust. Shields (ref. 2) has shown that Fe is depleted in a number of planetary nebulae; otherwise little is known about the abundance of refractory elements in these objects.

OBSERVATIONS

SILICON

Lines of Si III] λ1882.7, λ1892.0 and Si IV λ1393.8, λ1402.8 are seen in the IUE spectra of planetaries. The Si III] lines are close to the strong C III] λ1906.7, λ1908.7 doublet, while the Si IV lines are intermeshed with the O IV] λ1397.2, 1399.8, 1401.2, 1404.8, 1407.4 quintet. A high-dispersion spectrum of NGC 7662 (SWP 4106 - 400 min.) obtained by Dr. S.R. Heap clearly shows the individual components of Si III], Si IV and O IV]. For most nebulae, the Si lines are too faint to observe at high-dispersion, so we must rely on low-dispersion data. Low-dispersion observations of NGC 7662 with the small aperture (which gives somewhat better resolution than the large aperture) show the Si III] λ1883 and Si IV λ1394 lines (ref. 3). (The Si III] λ1883/λ1892 ratio, like C III] λ1907/λ1909, is density-sensitive, with a low density limit of about 1.5. In NGC 7662 this ratio is seen at high-

*NRC/NAS Resident Research Associate

dispersion to be greater than unity; thus for objects where we only observe the λ1883 line we have assumed the low-density ratio.) We have measured the flux in Si III λ1883 in four additional nebulae with the large slot in low dispersion. The results are presented in Table 1. For NGC 2440, the photowrite shows the spatially extended image of the λ1883 line.

Si IV is usually substantially weaker than O IV]. When the Si IV contribution to the blend becomes comparable to O IV], the feature shows a distinct blueward shift, since the λ1394 line is twice the intensity of λ1403. This effect is observed in Hu 1-2, the nebula with the largest Si III] intensity.

MAGNESIUM

The Mg II λ2796.4, λ2803.5 doublet is a strong feature in a few planetaries, e.g. IC 418 (ref. 4). It has also been observed in the high-excitation object NGC 7027 (ref. 5). We observe faint Mg II emission in IC 2165 and NGC 2440. In the latter case, the lines are also seen at high dispersion (LWR 6257).

Lines of [Mg V] at λ2783.9 and λ2929.2 were identified in NGC 7027 (ref. 5). The λ2784/λ2929 intensity ratio should be 3.6. We see the [Mg V] λ2784 line very clearly in our high-dispersion spectrum of NGC 2440 and there is also a feature of the expected intensity at λ2929. The [Mg V] lines have the same width as the other nebular lines.

We have measured the [Mg V] λ2784 flux in the low dispersion spectra of three objects: NGC 2440, IC 2165 and Hu 1-2. In IC 2165 there is clear stratification: the [Mg V] image is almost stellar while the Mg II image is very extended. This is also seen when the spectrum is traced with different slit heights.

INTERPRETATION

MODELS

We have constructed preliminary models of three nebulae. Details of the atomic data adopted and of the numerical procedures employed will be given elsewhere (ref. 6). It should be noted that the photoionization cross section of Mg^+ (ref. 7) is unusually small (0.28 Mb at threshold; cf. 6.3 Mb for H^o). This leads to a higher fractional abundance of Mg^+ than for other singly ionized species. The Si^{+2} and Si^{+3} photoionization cross sections we use (ref. 8, 9) are also many times smaller than the quantum defect values sometimes employed (e.g., ref. 10).

In Table 2 model predictions for IC 2165 and NGC 2440 are compared with observations. The model for IC 2003 is given elsewhere in this volume (ref. 11), where the CNO abundances of the three nebulae are discussed. All models employ blackbody stellar fluxes and simple density distributions. The defining parameters for the models of IC 2003, IC 2165 and NGC 2440, respectively, are as follows: Stellar temperature: 100,000 K; 135,000 K; 180,000 K. Stellar luminosity: 1.3×10^4 $L_\odot$; 2.6×10^3 $L_\odot$; 1.9×10^3 $L_\odot$.

Adopted distance: 7.6 kpc; 2.8 kpc; 2.3 kpc. Inner and outer radii: 0.06-.12 pc; 0.007-0.055 pc; 0.022- 0.122 pc. Filling factor: 0.043; 0.5; 0.14. Hydrogen density of filled volume: constant at 10^4 cm^{-3}; constant at 7.2×10^3 cm^{-3}; $n_H \propto r^{-1}$, decreasing from 1.4×10^4 cm^{-3} to 2.75×10^3 cm^{-3}. He/H ratio: 0.13; 0.13; 0.154.

We attempted to fit the [O III] λ5007/λ4363 temperature sensitive ratio and to match the overall ionization structure even if a fit to the total flux in some of the emission lines could not be achieved. We can use these models as a basis for the interpretation of the Si and Mg features.

SILICON

The silicon abundances in our models were adjusted to match the observed Si III] λ1883 intensity. Table 1 shows the resultant Si/O ratios. The solar value of Si/O is 0.052 (ref. 12, 13). Thus silicon would appear to be depleted by up to an order of magnitude in these nebulae. We do not yet have a model of Hu 1-2, but it is likely that the Si depletion for this object is less than for the others.

It can be seen from Table 2 that the Si IV intensities which result from our adopted abundances are consistent with the observational result that O IV] is the dominant contributor to the λ1400 blend. Because the collisional excitation rate for the Si^{+3} ion is 36 times larger than that of the O^{+3} ion, a Si/O ratio near solar would lead to the domination of this feature by Si IV; this is not observed even in Hu 1-2.

MAGNESIUM

Because of the small photoionization cross section for Mg^+ and the large collisional cross section for Mg II $^2S-^2P^o$ ($\Omega \sim 17$), we would expect Mg II λ2800 to be prominent in the UV spectra of planetary nebulae unless Mg is strongly depleted. In IC 418, λ2800 is strong and an approximately solar Mg/H ratio has been derived for this object (ref. 4). On the other hand, in the Orion nebula (which is of similar excitation), λ2800 is not seen. This implies an order of magnitude depletion of Mg (ref. 14). A depletion is also implied by the absence of Mg II λ2800 in high excitation planetaries; e.g. NGC 7662 (ref. 15,6). The fact that Mg II λ2800 is not observed in most of the nebulae examined by Boggess, Feibelman and McCraken (ref. 16) implies that the depletion is widespread.

The situation becomes more complex, however, when we consider planetaries in which [Mg V] is observed. An analysis of NGC 7027 by Péquignot and Stasińska (ref. 17) showed that no single Mg abundance could simultaneously reproduce the intensities of both [Mg V] λ2784 and Mg II λ2800. They were led to propose an abundance gradient, with Mg/H near solar in the inner region of the object and strongly depleted in the outer region.

We find just the same situation in IC 2165 and NGC 2440. The Mg abundances of the models in Table 2 have been adjusted to match the observed Mg II λ2800 fluxes. The resultant Mg/H ratios are 10^{-6} for IC 2165 and 8×10^{-7} for NGC 2440, compared to the solar Mg/H ratio of 4.2×10^{-5} (ref. 13).

However, if we were to adjust Mg/H to match the [Mg V] λ2784 line, the ratios would be 2.5×10^{-5} for IC 2165 and 3.5×10^{-5}, not significantly different from the solar value. (Compounding the difficulty is the fact that the models, even with the low abundances adopted, produce a Mg I] λ4571 intensity much greater than observed. There might be charge-transfer effects which would prevent the existence of as much Mg^0 in the ionized gas as the models predict, however.)

Péquignot and Stasinska propose that the carbon-rich nature of NGC 7027 is responsible for locking up the O in CO at the time of grain formation, so the Mg condenses as a metal rather than some more refractory compound, and thus can later evaporate in the inner regions of the nebula. This scheme might also be invoked for IC 2165, but in the case of NGC 2440, we find that C/O < 1 (ref. 11).

In any case, unless our ideas of the ionization structure for Mg are completely in error, further study of this "Mg II-[Mg V] anomaly" in planetary nebulae promises us insights into the formation and/or destruction of grains in differing chemical environments.

REFERENCES

(1) Spitzer, L., Jr.: Physical Processes in the Interstellar Medium. John Wiley and Sons, New York, 1978, p.6, p.204.

(2) Shields, G.A.: Gas-Phase Abundances of Iron and Carbon in Planetary Nebulae. Astrophys. J., vol. 219, no. 2, Jan. 15, 1978, pp.559-564.

(3) Harrington, J.P.; Lutz, J.H.; and Seaton, M.J.: IUE Observataions of the Planetary Nebulae NGC 7662. In: The First Year of IUE: Proceedings of the Symposium, London, England, April 4-6, 1979. London, University College, 1979, pp. 199-207.

(4) Harrington, J.P.; Lutz, J.H.; Seaton, M.J.; and Stickland, D.J.: Ultraviolet Spectra of Planetary Nebulae - I. The Abundance of Carbon in IC 418. Monthly Notices Roy. Astr. Soc., vol, 191, no. 1, April 1980, pp. 13-22.

(5) Grewing, M.; Boksenberg, A.; Seaton, M.J.; Snijders, M.A.J.: Wilson, R.; Boggess, A.; Bohlin, R.C.; Perry, P.M.; Schiffer, I.H.,III; Gondhalekar, P.M.; Macchetto, F.; Savage, B.D.; Jenkins, E.B.; Johnson, H.M.; Perinoto, M.; and Whittet, D.C.B.: IUE Observations of the Interstellar Medium. Nature, vol. 275, no. 5679, 5 October 1978, pp. 394-400.

(6) Harrington, J.P.; Lutz, J.H.; and Seaton, M.J.: Ultraviolet Spectra of Planetary Nebulae - II. NGC 7662. Monthly Notices Roy. Astro. Soc., to be submitted.

(7) Black, J.H.; Weisheit, J.C.; and Laviana, E.: Oscillator Strengths and Ground-State Photoionizaton Cross-Sections for Mg^+ and Ca^+. Astrophys. J., vol. 177, no. 2, 15 October 1972, pp. 567-572.

(8) Reilman, R.F; and Manson, S.T.: Photoabsorption Cross Sections for Positive Atomic Ions with $Z \leq 30$. Astrophys. J. Supplement Series, vol. 40, no. 4, August 1979, pp. 815-880.

(9) Shevelko, V.P.: Oscillator Strengths and Photoionization Cross Sections of Alkali-like Ions. Opt. Spectrosc., vol. 36, no. 1, January 1974, pp. 7-9.

(10) Köppen, J.: Photoionization Models for Gaseous Nebulae: III. Third Period Elements. Astron. Astrophys. Suppl. Ser., vol. 39, no. 1, January 1980, pp. 77-81.
(11) Marionni, P.A.; and Harrington, J.P.: Elemental Abundances in High Excitation Planetary Nebulae, 1980, this Symposium.
(12) Lambert, D.L.: The Abundances of Carbon, Nitrogen and Oxygen. Monthly Notices Roy. Astron. Soc., vol. 182, no. 1, January 1978, pp. 249-272.
(13) Lambert, D.L.; and Luck, R.E.: The Abundances of the Elements in the Solar Photosphere - IX: Na to Ca. Monthly Notices Roy. Astron. Soc., vol. 183, no. 1, April 1978, pp. 79-100.
(14) Perinotto, M.: and Patriarchi, P.: The Abundances of Carbon and Magnesium in the Orion Nebula. Astrophys. J. Letters, vol. 235, no. 1, 1 January 1980, pp. L12-L16.
(15) Péquignot, D.: Charge Transfer Reactions: II. A Photoionizaton Model of the Planetary Nebula NGC 7662. Astron. Astrophys., vol. 83, no. 1/2, March 1980, pp. 52-57.
(16) Boggess, A.; Feibelman, W.A.; and McCracken, C.W.: An Atlas of Emission Line Fluxes for Twenty-Four Planetary Nebulae in the 1150-3200Å Region. 1980, this Symposium.
(17) Péquignot, D.; and Stasińska, G.: An Abundance Gradient for Gaseous Magnesium in the Planetary Nebula NGC 7027. Astron. Astrophys. vol., 81, no. 1/2, January 1980, pp. 121-127.
(18) Torres-Peimbert, S.; and Peimbert, M.: Photoelectric Photometry and Physical Conditions of Planetary Nebulae. Rev. Mex. Astr. Astrofis., vol. 2, no. 3, Aug. 1977, pp. 181-207.
(19) Kaler, J.B; Czyzak, S.J.; and Aller, L.H.: Spectrophotometric Studies of Gaseous Nebulae. X. The Small High-Excitation Planetary Nebula IC 2165. Astrophys. J., vol. 153, no. 1, July 1968, pp. 43-48.
(20) Aller, L.H.; Czyzak, S.J.; and Kaler, J.B.: Spectrophotometric Studies of Gaseous Nebulae. VIII. The Irregular Planetary Nebula NGC 2440. Astrophys. J., vol. 151, no. 1, Jan. 1968, pp. 187-195.
(21) Aller, L.H.; and Walker, M.F.: The Spectra of Thirty-Three Gaseous Nebulae in the Yellow-Green Region Obtained with an Electronic Camera. Astrophys. J., vol. 161, no. 3, Sept. 1970, pp. 917-945.

TABLE 1 -- Si III] λ1883 FLUXES AND Si/O RATIOS

	IC 2003	IC 2165	NGC 2440	Hu 1 - 2
F(Si III] λ1883) erg/cm^2/s	4.10^{-14}	4.10^{-14}	$1.7x10^{-13}$	$6.x10^{-14}$
I(Si III] λ1883,92)[a]	3.0	3.2	5.8	11.
(Si/O) Abundance Ratio	0.006	0.006	0.005	--

[a] Relative to I(Hβ) = 100, corrected for reddening (ref. 11); I(λ1883)/I(λ1892) = 1.5 assumed.

TABLE 2. LINE INTENSITIES: OBSERVATIONS AND MODEL PREDICTIONS.

LINE	IC 2165 OBS.#	IC 2165 MODEL	IC 2165 t_{ion}*	NGC 2440 OBS.‡	NGC 2440 MODEL	NGC 2440 t_{ion}*
λ1241 N V	45.	40.	1.81	100.	95.	1.61
λ1394,03 Si IV		4.3	1.50		5.6	1.55
λ1401,5 O IV]	39.	18.3	1.68	54.	28.4	1.58
λ1406,17 S IV]		1.7	1.50		1.2	1.55
λ1485 N IV]	47.	50.	1.57	220.	170.	1.57
λ1549 C IV	970.	960.	1.55	500.	585.	1.57
λ1640 He II	260.	290.	1.73	350.	480.	1.56
λ1664 O III]	33.	35.	1.42	42.	42.	1.41
λ1750 N III]	37.	29.	1.42	170.	170.	1.44
λ1883,92 SiIII]	3.2	3.2	1.47	5.8	5.8	1.52
λ1908 C III]	850.	725.	1.43	750.	660.	1.40
λ2328 C II]	81.	33.	1.40	97.	80.	1.15
λ2424 [Ne IV]	110.	83.	1.62	160.	160.	1.49
λ2470 [O II]	--	--	--	17.	22.	1.20
λ2784 [Mg V]	5.2	0.21	1.87	8.3	0.19	1.60
λ2800 Mg II	6.4	6.2	1.40	3.9	3.8	1.21
λ3426 [Ne V]	63:	65	1.78	140:	134.	1.57
λ3727 [O II]	62.	55.	1.38	230.	310.	1.20
λ3869 [Ne III]	110.	150.	1.41	140.	140.	1.26
λ4267 C II	0.46	0.15	1.43	0.38	0.18	1.40
λ4363 [O III]	22.	18.	1.42	28.	22.	1.41
λ4571 Mg I]	0.6	5.1	1.39	0.2	5.4	1.18
λ4686 He II	42.	40.	1.73	58.	68.	1.56
λ4861 Hβ	100.	100.	1.51	100.	100.	1.46
λ5007 [O III]	1190.	920.	1.42	1500.	1200.	1.41
λ5200 [N I]	--	--	--	13.	30.	1.00
λ5755 [N II]	0.5:	2.1	1.38	17.	31.	1.19
λ5876 He I	11.	11.6	1.42	11.3	13.6	1.31
λ6300 [O I]	3.2	0.6	1.37	24.	29.	1.05
λ6312 [S III]	1.7	2.0	1.41	2.3	1.9	1.38
λ6584 [N II]	45.	54.	1.38	970.	1200.	1.19
λ6723 [S II]	6.	5.3	1.39	29.	28.	1.16
λ7325 [O II]	6.	8.9	1.38	16.	27.	1.20

#The UV observations are discussed in ref. 11. The optical data is from ref. 18 and 19. Intensities have been corrected for reddening (ref. 11).

‡Optical data from ref. 18, 20 and 21.

*Model temperature weighted by $N_e N_{ion}$, in units of 10^4 K. See ref. 11.

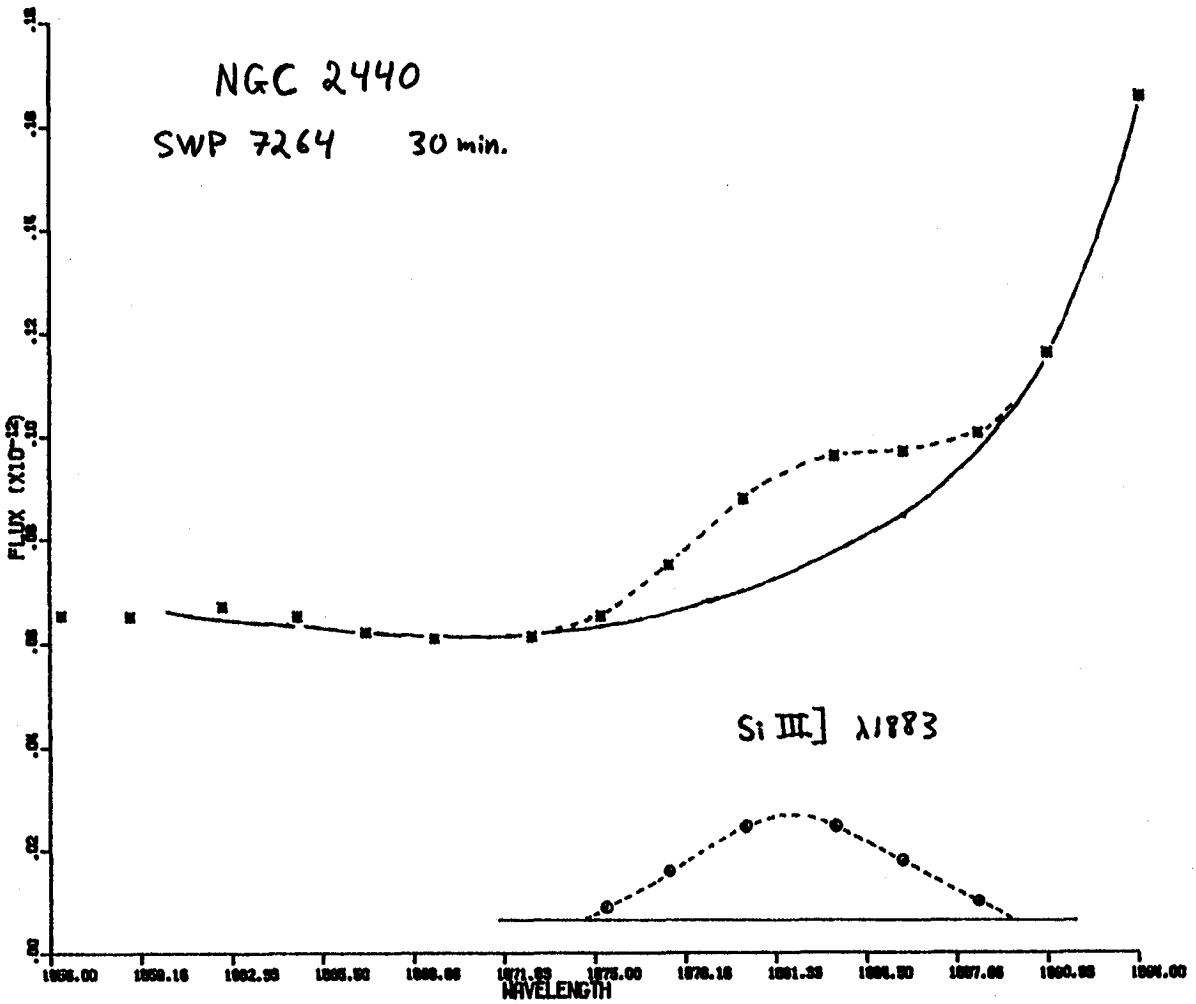

Fig. 1 - The Si III] λ1883 feature on the wing of C III] λ1909 in NGC 2440.

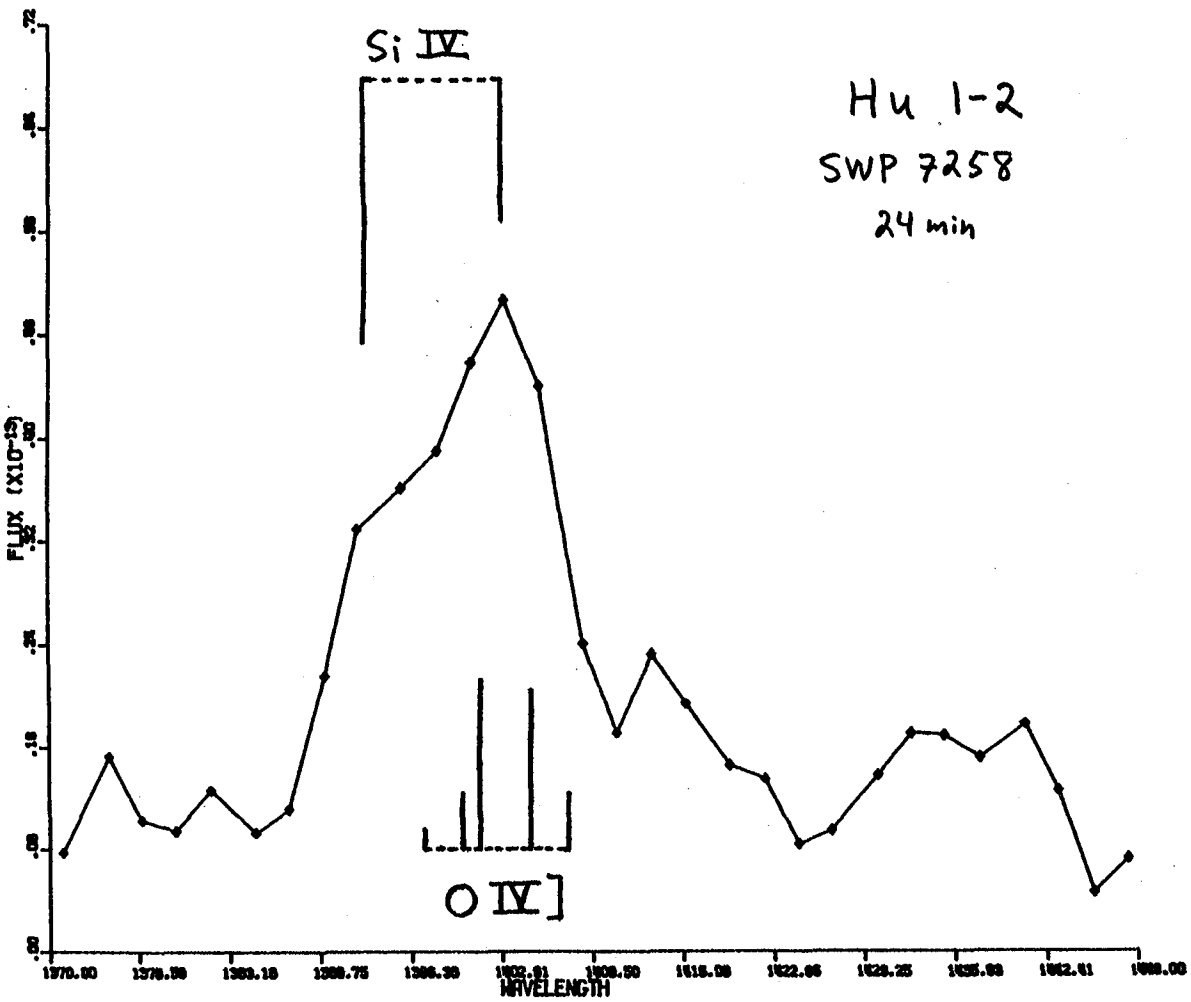

Fig. 2 - The λ1400 Si IV - O IV] blend in Hu 1-2. The length of the vertical lines indicates the theoretical relative intensity of the line component.

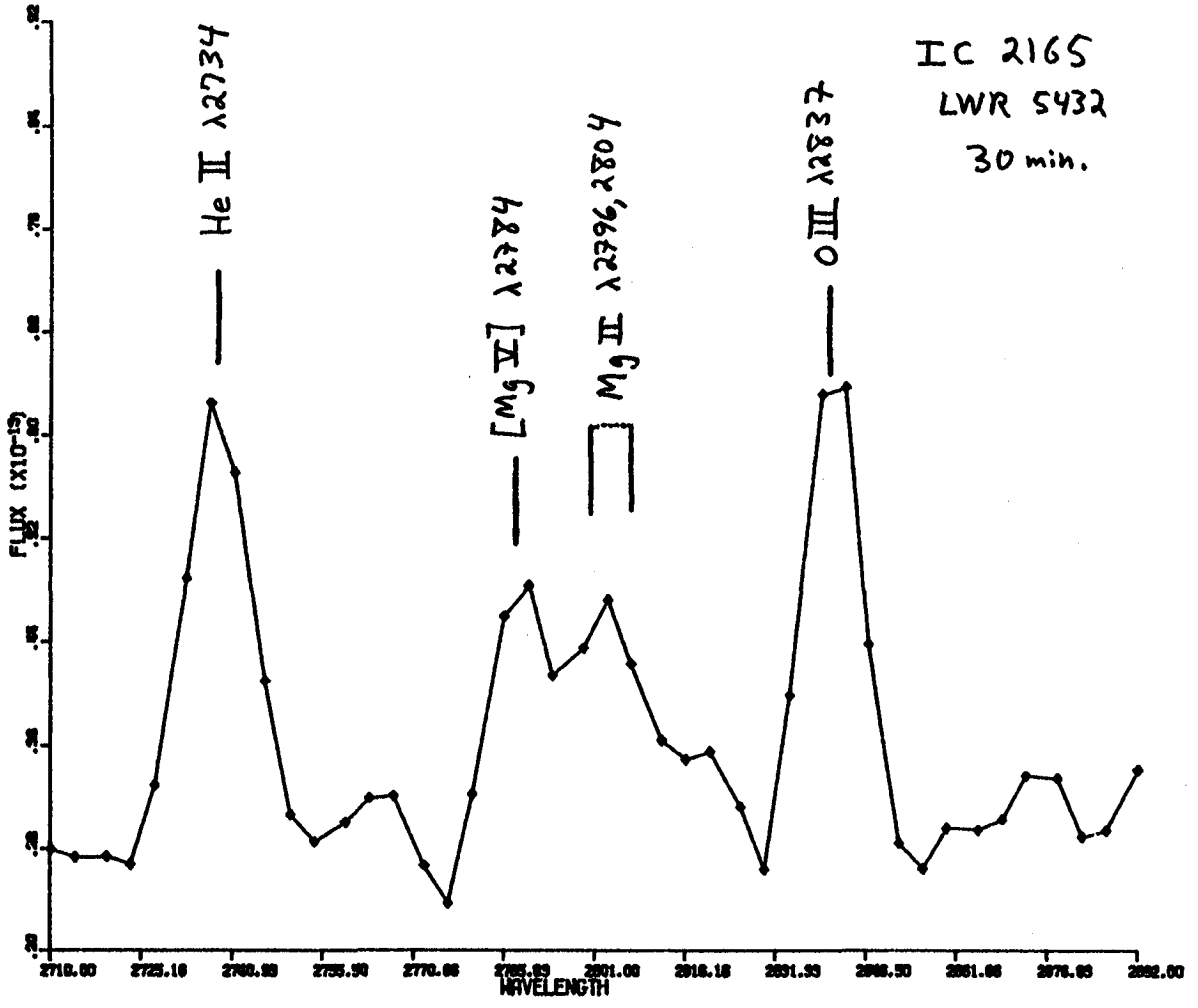

Fig. 3 - The Mg lines in IC 2165 at low resolution.

ELEMENTAL ABUNDANCES IN HIGH-EXCITATION PLANETARY NEBULAE

P.A. Marionni*
Electro-Optics Branch, GSFC

J.P. Harrington
Astronomy Program, U. of Md.

ABSTRACT

The IUE satellite has been used to obtain low dispersion spectra of the high excitation planetary nebulae IC 351, IC 2003, NGC 2022, IC 2165, NGC 2440, Hu 1-2, and IC 5217. Numerical modeling has been undertaken to determine the chemical composition of these objects with particular emphasis on obtaining elemental carbon and nitrogen abundances. Preliminary results for several nebulae suggest large variations in the C/N ratio from object to object.

INTRODUCTION

Ultraviolet (UV) observations can aid in the assessment of elemental carbon and nitrogen abundances in planetary nebulae (cf. ref. 1). Presented here are low dispersion UV observations of seven high excitation nebulae. Three approaches of varying degrees of complexity are used to infer carbon to nitrogen abundances (C/N) for some of the objects observed.

OBSERVATIONS AND DATA REDUCTION

Our IUE observations were performed in 1979 August and November. Selection criteria for the objects studied were a) nebulae of high excitation; b) except for Hu 1-2, nebulae included in the study of Torres-Peimbert and Peimbert (ref. 2); and c) except for NGC 2440 and to some extent NGC 2022, nebulae with angular sizes comparable to or less than the large entrance aperture. All spectra presented here were taken with the large entrance aperture, low dispersion configuration, using both the long wavelength redundant (LWR) and short wavelength prime (SWP) cameras.

Data reduction consisted of examination and extraction of spectra from the 55-line spatially resolved files provided to guest IUE observers. Integration of emission line features over effective slit heights commensurate with the angular extents of individual nebulae somewhat enhanced our signal to noise ratio. A spurious feature ~7-10 Å longward (on lines 21 through 23-24) of the NIII] λ1751 Å emission line has been removed from our data. A median smoothing of the background was employed. Conversion to an absolute flux scale was accomplished via interpolation of a tabulated IUE standard calibration (ref. 3).

Our results are contained in Table I. For each object the observed emission line intensities, $F(\lambda)$, have been corrected for interstellar extinction to the dimensionless quantities $I_c(\lambda)$ using the expression $\log[I_c(\lambda)] = 2 + cf(\lambda) +$

*NRC/NAS Resident Research Associate

log $(F(\lambda)/F(H\beta)]$. Here c is the logarithmic extinction coefficient, $f(\lambda)$ is based on the prescription of Seaton (ref. 4), and $F(H\beta)$ is the observed HI flux at λ4861 Å taken from various sources. The use of the intensity ratio F(HeII λ4686 Å/F(HeII λ1640 Å) in deriving interstellar reddening depends upon the portion of a given nebula observed in both the optical and ultraviolet and the validity of the UV extinction law in the direction of that object. Because of uncertainties in these quantities, additional criteria (mainly available radio data, optical studies, the 2200 Å interstellar feature, and, where measurable, the UV continuum of the central source of excitation) have been used in the determination of extinction coefficients.

Except for IC 2003, where $c = 0.37 \pm 0.05$, errors in c, if $f(\lambda)$ is assumed correct, may be as large as 0.2, and these extinction estimates are presented only to facilitate further analysis. In the case of NGC 2440, 45% of the object is estimated to have been overlaid by the entrance aperture.

A better than 10% consistency error in the ratio of strong lines, and $\lesssim$25% repeatability error is estimated for our SWP data. For all weak lines, and for all LWR data excepting the [NeIV] λ2422 Å feature, our assessment of the continuum level was the limiting factor to our accuracy, with probable errors up to 50% for the weakest features.

ANALYSIS

The interpretations of UV spectra from high-excitation nebulae are characterized by several major difficulties, and are thus implicitly model-dependent. First, rates of collisional excitation of UV transitions are extremely sensitive to temperature variations which can exist in high-excitation nebulae. Second, charge transfer processes become more important in determining specific ionization structures, since the neutral fraction of hydrogen is correspondingly higher for the lower mean photoionization efficiencies from higher temperature excitation sources. Recent calculations of a charge transfer rate involving OIV + HI $\rightleftarrows$ OIII + HII (ref. 5) so change the structure of previously calculated models that, due to lack of time, we have employed a refined Landau-Zener approximation (ref. 6) to this rate. We thus do not attempt to derive oxygen abundances on the basis of UV lines, and our thermal structures may be in error. Finally, the ions CIII, CIV, NIII, and NIV can coexist both in high temperature regions where the thermal structure is dominated by their own cooling (HeIII zones) and regions of lower temperature dominated by [OIII] forbidden line cooling; thus UV emission lines predominantly represent those ions in regions of high temperature.

The following analysis depends upon many atomic rates, which we cannot reference due to space limitations. References to these and the specific computational methods used will appear elsewhere (ref. 7). It should be noted, however, that the electron collisional cross sections used in the analysis of the NIII] λ1751 Å and CIII] λ1909 Å lines are those of Jackson (ref. 8) and Dufton et al. (ref. 9).

Visual inspection of the dominant UV emission lines of carbon and nitrogen in Table I suggests large variations in C/N ratios, if the ionic distributions of CIII and NIII and/or CIV and NIV are similar. More quantitatively, Shields (ref.

10), in a discussion of quasar spectra, has pointed out that the emission line ratios I_c(CIII] λ1909 Å)/I_c(NIII] λ1751 Å) and to a lesser extent I_c(CIV λ1549 Å)/I_c(NIV] λ1487 Å) are relatively insensitive to the details of specific ionizing distributions. Both from direct comparison of the collisional excitation rates involved, and the results of all our attempts to construct detailed numerical models for the objects in this study, the relationship C/N ~ .15 I(λ1909)/I(λ1751) and C/N ~ .15 I(λ1549)/I(λ1487) should usually be accurate to within a factor of two over the range of effective stellar temperatures 90,000 K to 200,000 K, nebular electron densities 2×10^3 - 2×10^4, and C/N .5 to 5. Plane-parallel (ref.11) and extended (ref.12) model atmosphere flux distributions as well as blackbodies have been considered in the models used to test these relations. This relation will break down when a significant fraction of the observed nebular volume is in higher stages of ionization. The application of this "ratio" method to the observations is presented in Table II.

An alternative method of deriving C/N ratios is to treat the transitions responsible for the dominant UV emission lines CIII] λ1909 Å, CIV λ1549 Å, NIII] λ1487 Å and NV] λ1240 Å as simple two-level atomic systems, collisionally populated at specific electron temperatures. Computational models in conjunction with optical observations may be developed to derive an average electron temperature, t_{ion}, weighted by the ionic abundances of each ion and the electron density integrated over the nebular volume. This differs little from classical approaches to deriving elemental abundances from emission line intensities, but the constraint on thermal equilibrium is addressed. The t_{ion} may be applied in conjunction with observed UV line intensities to find the absolute ionic abundances directly. Examples of temperature distributions for NGC 2440 and NGC 2165 are presented elsewhere (ref. 13) and in Table III. Application of this method to our UV data toward deriving elemental C and N abundances is presented in Table II.

Finally, detailed computations for a given nebula may be undertaken. Models of NGC 2440 and NGC 2165 are given elsewhere in this volume (ref. 13). The results of a calculation for IC 2003 are displayed in Table III, and C/N abundance ratios and adopted abundances for all preliminary models are presented in Table II. Simple blackbodies and constant density distributions have limitations; but one is at least able to reach a terminal state. We find that under these limitations, further variations in relative C and N abundances unfavorably redistribute the emergent intensities in these lines and lead to less acceptable thermal structures. More realistic density variations could be addressed by radio synthesis via the VLA, or, for objects of greater angular extent, optical monochromatic images.

The three methods we have used to address the problem of C/N abundance variations, when applied to the same set of UV and optical observations and analyzed via the same atomic data, are seen to yield reasonably consistent results. While the absolute abundances derived from UV lines may be regarded with some reserve because of their extreme sensitivity to the assumed electron temperature, we would emphasize that the ratios of UV lines are much less sensitive. The difference between NGC 2440 and Hu 1-2 on the one hand, and IC 2003 and IC 2165 on the other, must surely reflect real composition variations.

REFERENCES

1. Peimbert, M.: New Insights Into the Physical State of Gaseous Nebulae. The Universe at Ultraviolet Wavelengths. The First Two Years of IUE. NASA CP-2171, 1980: this compilation.

2. Torres-Peimbert, S.; and Peimbert, M.: Photoelectric Photometry and Physical Conditions of Planetary Nebulae. Rev. Mexicana Astr. Astrofisica, Vol. 2, 1977, pp. 181-207.

3. Bohlin, R.C.; Holm, A.V.; Savage, B.D.; Snijders, M.A.J.; and Sparks, W.: Photometric Calibration of the International Ultraviolet Explorer. NASA X-681-79-19, 1979, pp. 1-27.

4. Seaton, M.J.: Interstellar Extinction in the UV. M.N.R.A.S., Vol. 187, 1979, pp. 73P-76P.

5. Butler, S.E.; Heil, T.G.; and Dalgarno, A.: Charge Transfer of Multiply-Charged Ions with Hydrogen and Helium: Quantal Calculations. Center for Astrophysics Preprint Series, no. 1281, 1980.

6. Butler, S.E.; and Dalgarno, A.: Charge Transfer of Multiply-Charged Ions with Hydrogen and Helium: Landau-Zener Calculations. Center for Astrophysics Preprint Series, no. 1281, 1980.

7. Harrington, J.P.; Lutz, J.H.; and Seaton, M.J.: Ultraviolet Spectra of Planetary Nebulae - II. NGC 7662. M.N.R.A.S., 1980, to be submitted.

8. Jackson, A.R.G.: Excitation of CII] λ 2326, OIII] λ 1664 and Other Semi-Forbidden Lines in Quasars. M.N.R.A.S., Vol. 165, 1973, pp. 53-60.

9. Dufton, P.L.: Berrington, K.A.; Burke, P.G.; and Kingston, A.E.: The Interpretation of CIII and OV Emission Line Ratios in the Sun. Astr. Ap., 1978, Vol. 62, pp. 111-120.

10. Shields, G.A.: The Abundance of Nitrogen in QSOs. Ap.J., Vol. 204, 1976, pp. 330-336.

11. Hummer, D.G.; and Mihalas, D.: Model Atmospheres for the Central Stars of Planetary Nebulae. M.N.R.A.S., Vol. 147, 1970, pp. 339-354.

12. Cassinelli, J.P.: The Continuous Energy Distribution from Stars with Hot Extended Atmospheres. Ap. Letters, Vol. 8, 1971, pp. 105-109.

13. Harrington, J.P.; and Marionni, P.A.: Silicon and Magnesium Abundances in Planetary Nebulae. The Universe at Ultraviolet Wavelengths. The First Two Years of IUE. NASA CP-2171, 1980: this compilation.

14. Barker, T.: Spectrophotometry of Planetary Nebulae II. Chemical Abundances. Ap.J., Vol. 220, 1978, pp. 193-209.

15. Aller, L.H.; and Czyzak, S.J.: Spectrophotometric Studies of Gaseous Nebulae. XVI. The Moderately High Excitation Planetaries IC 2003, NGC 2022, and CD-23°12238, Ap.J., Vol. 160, 1970, pp. 929-938.

TABLE I. - OBSERVED UV EMISSION LINE INTENSITIES [#]
(corrected for interstellar extinction)

λ Å	Ion	f(λ) [*]	IC 351[a]	IC 2003[b]	NGC 2022[c,†]	IC 2165[d]	NGC 2440[e]	Hu 1-2[f]	IC 5217[g]
1240	NV	1.640	--	--	--	45.	100.	190.	38.:
1335	CII	1.417	--	--	--	--	8.4:	--	6.:
1400	OIV],SiIV	1.307	--	17.	110.:	39.	54.	52.	--
1487	NIV]	1.229	9.:	17.:	--	47.	220.	200.	14.:
1549	CIV	1.183	190.	320.	820.	970.	500.	540.	54.
1640	HeII	1.136	180.	330.	610.	260.	350.	460.	54.
1664	OIII]	1.128	--	20.	--	33.	42.	39.	26.
1751	NIII]	1.119	18.	16.	--	37.	170.	180.	9.5:
1909	CIII]	1.229	200.	320.	410.	850.	750.	398.	110.
1909	CIII]	1.229	--	350.	410.	830.	757.	560.:	140.:
2328	CII]	1.348	--	5.:	--	81.	97.	63.	40.:
2422	[NeIV]	1.120	--	45.	210.	110.	160.	150.	7.5:
2471	[OII]	1.023	--	--	--	--	17.	--	--
2512	HeII	0.954	--	--	--	12.	19.	--	--
2734	HeII	0.700	--	13.:	--	11.	17.	21.	4.1:
2784	[MgV]	0.659	--	--	--	5.2	8.3	17.	--
2800	MgII	0.646	--	--	--	6.4	3.9	--	1.7:
2837	OIII	0.619	--	9.:	--	9.1	7.5	6.7	2.7
3048	OIII	0.494	--	71.	30.:	8.5	13.7	30.	6.3
3204	HeII	0.424	--	--	17.:	79.	86.	37.	12.
C			0.35	0.37	0.60	0.64	0.4	0.70	0.55
F(Hβ) (10^{-12} ergs cm^{-2} s^{-1})			3.8	6.31	6.6	12.6	0.45 x 33.1	6.3	6.92

* ref. 4; † High Background; (:) uncertain; # Relative to $I_c(H\beta) = 100$.
a) SWP 6264, 6259; b) SWP 7260, 7261, LWR 6255; c) SWP 6260, 6261, LWR 5431; d) SWP 7259, 6262, LWR 5432; e) SWP 7262, 7264, LWR 6256, 6258; f) SWP 7258, LWR 6254; g) SWP 6257, 7257, LWR 5429.

TABLE II. - ABSOLUTE AND RELATIVE ELEMENTAL ABUNDANCES

	Method	IC 351	IC 2003	IC 2165	NGC 2440	Hu 1-2
C/N	CIII]/NIII] Ratio	1.7	3.0	3.4	0.66	0.33
C/N	CIV/NIV] Ratio	3.2:	2.8:	3.1	0.34	0.41
C/N	t_{ion}	--	3.6	3.7	0.62	0.70
C/N	Model	--	4.0	4.0	0.60	--
C/H	t_{ion}	--	3.2(-4)	2.7(-4)	2.3(-4)	--
C/H	Model	--	4.0(-4)	2.7(-4)	2.9(-4)	--
N/H	t_{ion}	--	8.9(-5)	7.3(-5)	3.7(-4)	--
N/H	Model	--	1.0(-4)	6.7(-5)	4.8(-4)	--
O/H	Model	--	3.3(-4)	1.7(-4)	3.6(-4)	--

TABLE III. - OBSERVATIONAL FLUXES AND MODEL PREDICTIONS FOR IC 2003

λ Å	Ion	f(λ)*	t_{ion} (10^4 K)	$I_c(\lambda)$	Model Fluxes
1400	OIV]	1.307	1.36	17.[a]	11.4
	SiIV]		1.27		4.1
1487	NIV]	1.229	1.30	17.:[a]	19.
1549	CIV	1.183	1.40	310.[b]	443.
1640	HeII	1.136	1.34	330.[b]	344.
1664	OIII]	1.128	1.21	20[a],24[b]	24.
1751	NIII]	1.119	1.22	16[a],21[b]	19.
1909	CIII]	1.229	1.22	321.[b]	464.
1909	CIII]	1.229	1.22	350.[c]	464.
2328	CII]	1.348	1.19	5.[c]	16.
2424	[NeIV]	1.120	1.32	45.[c]	48.
2734	HeII	0.700	1.34	13.:[c]	11.
3726,29	[OII]	0.315	1.18	34.[d]	21.
3869	[NeIII]	0.270	1.20	91.[d]	74.
4267	CII	0.155	1.22	1.5[e]	0.25
4363	[OIII]	0.130	1.21	16.:[d]	17.
4471	HeI	0.105	1.20	3.9[d]	4.1
4686	HeII	0.045	1.34	53.[d]	50.
4861	HI	0.000	1.24	100.	100.
5007	[OIII]	-0.300	1.21	1083.[d]	1250.
5755	[NII]	-0.190	1.18	0.82[d]	0.55
5876	HeI	-0.210	1.20	10.6[d]	11.0
6306	[OI]	-0.285	1.16	3.6[d]	4.3
	[SIII]		1.21		
6583	[NII]	-0.340	1.18	17.[d]	17.
7325	[OII]	-0.435	1.18	3.6[d]	3.9

* refs. 4,2; (:) uncertain.
a) SWP 7261-90m; b) SWP 7260-30m; c) LWR 6255-45m; d) ref. 14; e) ref. 15.

THE HIGH-EXCITATION PLANETARY NEBULAE

NGC 3918 AND IC 2448

S. Torres-Peimbert, M. Peña and E. Daltabuit
Instituto de Astronomía
Universidad Nacional Autónoma de México

ABSTRACT

We present IUE observations of NGC 3918 and IC 2448. Combining these observations with data in the optical range and computed model structures we derive the chemical composition for these objects. For NGC 3918 we obtain log C= -3.02, log N= -3.61 and log O= -3.22; while for IC 2448 we obtain log C= -3.44, log N= -3.81 and log O= -3.54.

INTRODUCTION

These planetary nebulae are ideally suited for observations with IUE since they have high surface brightness and small angular size.

They have been observed in the visual range by Torres-Peimbert and Peimbert (ref. 1). They derive for NGC 3918 N(He)/N(H)= .112, log N= -3.72, log O= -3.10 and log Ne= -3.84 and for IC 2448 N(He)/N(H)= .111, log N= -4.49, log O= -3.39 and log Ne= -4.08 under the assumption of t^2= 0.035.

OBSERVATIONS

For NGC 3918 we have the following large aperture exposures: SWP 1906 (7 min), SWP 3191 (20 min), SWP 3192 (10 min), LWR 1767 (12 min), LWR 2753 (20 min), LWR 2754 (10 min), LWR 2809 (6 min) and the following small aperture exposures: SWP 1906 (20 min), SWP 3216 (15 min), LWR 2809 (12 min). For IC 2448 we only have available the large aperture exposures: SWP 3194 (30 min) and LWR 2756 (30 min).

We have applied the mean calibration correction (ref. 2) to the observed fluxes to derive absolute fluxes. We present in Figure 1 composite large aperture spectra of these objects.

In Table II we present the derived intrinsic fluxes for all emission lines, $I(\lambda)$, the observed fluxes F(1641) and $F(H\beta)$ and the reddening correction at $H\beta$, $C(H\beta)$. To obtain the intrinsic fluxes we have used the relation log $I(\lambda)/I(H\beta)$= log $F(\lambda)/F(H\beta)+C(H\beta)f(\lambda)$. We have derived the reddening correction

by assuming that: 1) the fluxes relative to Hβ in the visual range are the same for the observed region as for the entire nebula, 2) the reddening law, f(λ), behaves as the expression given by Seaton (ref. 3) and 3) the intensity ratio of the HeII recombination lines I(1641)/I(4686) is 6.6 (ref. 4).

The internal errors in the measurements, as estimated from the different exposures, are ≤15% for NGC 3918, and presumably similar for IC 2448. For IC 2448 the listed flux for λ1549 is only an upper limit, since the line was saturated.

MODEL IONIZATION STRUCTURES

We have computed model ionization structures that will be described in detail elsewhere. The models predict line intensities for C, N, O, Ne, Mg, Si and S. For comparison we present a few representative models in Table III.

To try to fit NGC 3918 we computed models for an exciting star of T_*= 150,000 (from ref. 5). We have tried unsuccessfully to adjust both I(5007) and I(1909) simultaneously by varying density distribution and chemical abundances. The resonant lines of CIV, NV and MgII appear systematically too bright in our models. This effect has been noted by other authors (refs. 6 and 7) who explain it by dust absorption. In order to adjust the lines of low ionization, it is necessary to assume that the nebula is density bounded.

For our models of IC 2448 we have adopted an exciting star of T_*=125,000. We encounter the same problems in our attempt to adjust I(5007) and I(1909) and have found it necessary to assume a density bound nebula to improve the fit for ions of low stages of ionization. For this object we do not have observations of the faint lines and thus have less restrictions for our model.

IONIC ABUNDANCES

For NGC 3918 from the ratio I(1666)/I(5007) of O^{++} we obtain the same temperature as from I(4363)/I(5007). We also are able to derive a temperature of 13800 °K from the I(1602)/I(2423) ratio of Ne^{+3}; however none of our models predict the temperature of the highly ionized region to be drastically different for the O^{++} region.

To derive ionic abundances we adopted an empirical scheme of dividing the nebulae in three regions: those of low, medium and high stages of ionization. For elements in low stages of ionization we have assumed the observed T(NII) to be applicable. Our models do not predict such a sharp decrease in temperature in the outer shells and thus the derived abundances are probably overestimated, but these ions are not dominant in either nebula. For the elements in the intermediate stages we have used T(OIII) as derived from observations (ref. 1); and for the higher stages of ionization we have used temperatures 600 K higher than T(OIII), since our models predict this temperature variation. We have assumed t^2= 0.0 for our derivation of the ionic abun-

dances. The results are listed in Table II. For both objects, the O^{++} abundances derived from λ5007 and λ1666 are in excellent agreement and give us confidence in the adopted reddening.

All ionic abundances derived from ultraviolet lines are highly dependent on temperatures, and we typically expect errors of ±0.10 dex in the ionic determinations for errors of ±300 °K.

DISCUSSION

We have derived total abundances from the ionic ones. In the case of NGC 3918, for oxygen and nitrogen we have added all the ionic abundances in a straightforward way. For carbon we have taken into account only I(1909) and from comparison with our models we have adopted a ratio of relative volumes of carbon to oxygen $x(C^{++})/x(O^{++})= 0.74$. In the case of IC 2448 we have added O^{+} and O^{++}, and have corrected by a factor $i_{cf}= He/(He^{+})$, which is in agreement with our models. For nitrogen we have adopted an intermediate value between those derived from the comparison of our models and N^{+2} and N^{+4}. For carbon we have assumed that the resonance line I(1549) has been depleted by a factor of 2 due to dust and have added all other ions. Comparison with our models shows that the carbon abundance is probably underestimated. The total abundances relative to hydrogen in NGC 3918 are log O= -3.22, log N= -3.61 and log C= -3.02; in IC 2448 are log O= -3.54, log N= -3.81 and log C= -3.44.

We are grateful to M. Peimbert for fruitful discussions.

REFERENCES

1. Torres-Peimbert, S. and Peimbert, M.: Photoelectric Photometry and Physical Conditions of Planetary Nebulae. Rev. Mexicana Astron. Astrof. Vol. 2, No. 3, Aug. 1977, pp. 181-207.

2. Bohlin, R.C. and Snijders, M.A.J.: Photometric Calibration of the IUE. NASA Newsletter No. 2, Nov. 1978.

3. Seaton, M.J.: Interstellar Extinction in the UV. M.N.R.A.S., Vol. 187, No. 3, June 1979, pp. 73p-76p.

4. Seaton, M.J.: Calculated Intensities of HeII Recombination Lines in the Ultraviolet. M.N.R.A.S., Vol. 185, No. 1, Oct. 1978, pp. 5p-8p.

5. Hummer, D.G. and Mihalas, D.: Surface Fluxes for Model Atmospheres for the Central Stars of Planetary Nebulae. JILA Report No. 101, June 1970.

6. Pequinot, D., Aldrovandi, S.M.V., and Stasinska, G.: Charge Transfer Reactions. A Consistent Model of the Planetary Nebula NGC 7027. Astron. and Astroph., Vol. 63, 1978, pp. 313-324.

7. Bohlin, R.C., Marionni, P.A., and Stecher, T.P.: The Rocket Ultraviolet Spectrum of the Planetary Nebula NGC 7027. Ap. J., Vol. 202, 1975, pp. 415-420.

TABLE I .- UNREDDENED FLUXES RELATIVE TO Hβ[a)]

λ	Ion	I(λ)/I(Hβ) NGC 3918	I(λ)/I(Hβ) IC 2448
1215	HI	<-0.51	-0.41
1240	NV	-0.54	-0.25
1401	OIV] +SIV+SiIV	-0.46	....
1488	NIV]	-0.43	≤1.00
1549	CIV	+0.64	+0.37
1575	[NeV]	....	-1.01
1602	[NeIV]	-1.17	....
1641	HeII	+0.43	+0.40
1666	OIII]	-0.55	-0.63
1749	NIII]	-0.63	≤-0.82
1909	CIII]	+0.69	≥+0.58
2298	....	....	-0.75
2326	CII] + [OIII]	-0.38	-0.99
2386	NeII	-1.57	....
2423	[NeIV]	+0.11	-0.63
2471	[OII]	-0.98	....
2512	HeII	-1.33	....
2734	HeII	-1.03	-1.12
2800	MgII	<-1.34	<-1.10
2837	OIII	-0.98	-1.17
3023+47	OIII	-0.73	-1.06
3133	OIII	-0.04	-0.26
3204	HeII	-0.66	-0.83
log F(1641)	....	-10.05	-10.69
log F(Hβ)	....	-10.03	-10.84
C(Hβ)	....	+ 0.40	+ 0.22

a) Log I(λ)/I(Hβ).

TABLE II.- TEMPERATURE, DENSITY AND IONIC ABUNDANCES[a)]

		NGC 3918	IC 2448
T(NII)		8900	9400[b)]
T(OIII)		12100	12500
T(NeIV)		13800	13100[b)]
N_e(SII)		9000	12000
N_e(rms)		4600	1700
C^+	2326	-3.84	-4.62
C^{++}	1909	-3.52	$\geq$-3.72
C^{+3}	1549	-3.82	-4.20
N^+	6584	-4.68	-6.17
N^{++}	1749	-4.11	$\leq$4.40
N^{+3}	1488	-4.00	$\leq$4.71
N^{+4}	1240	-4.21	-4.05
O^+	3727	-4.06	-5.08
O^{++}	5007	-3.54	-3.71
O^{++}	1666	-3.55	-3.72
O^{+3}	1401	-3.46:	....
Ne^{++}	3869	-4.28	-4.38
Ne^{+3}	2423	-4.09	-4.90
S^+	6717+31	-6.30	-7.51:
S^{++}	6311	-4.99	....
S^{+3}	1393	-4.50:	....
Ar^{++}	7136	-5.97	-6.51:

a) Given in log $N(X^{+m})/N(H^+)$.

b) Adopted.

TABLE III.- COMPARISON OF MODELS WITH OBSERVATIONS.
LINE INTENSITIES, TEMPERATURES AND RELATIVE VOLUMES. a)

		NGC 3918				IC 2448		
		Obs.	N1	N2	N3	Obs.	I1	I2
HeI	4471	3.8	3.1	3.0	3.1	4.0	3.3	3.0
HeII	4686	44.0	41.8	44.0	43.1	38.0	34.7	41.2
CII]	2326	41.0	122.0	34.7	133.0	10.0	9.1	12.0
CIII]	1909	490.0	1070.0	567.0	1170.0	≥380.0	411.0	460.0
CIV	1549	450.0	2540.0	1950.0	1970.0	230.0	1010.0	885.0
[NI]	5200	0.5	0.0	0.0	0.1	.....	0.0	0.0
[NII]	6584	66.0	45.0	24.9	60.7	2.5	10.5	14.2
NIII]	1749	23.0	56.6	60.1	59.4	≤ 15.0	51.5	57.3
NIV]	1488	37.0	71.0	112.0	54.0	.....	65.7	55.2
NV	1240	29.0	174.0	296.0	104.0	56.0	8.3	6.1
[OI]	6300	3.8	13.0	4.7	15.2	.....	0.0	0.1
[OII]	3727	61.0	277.0	222.0	349.0	6.3	28.3	39.9
[OIII]	5007	1570.0	1590.0	2210.0	1630.0	1060.0	1400.0	1290.0
OIV]	1401	<35.0	18.8	39.9	16.4	.....	40.5	14.2
$T(C^{+})$		....	12600	12830	11890	....	13240	13260
$T(C^{++})$		....	12680	12940	12050	....	13340	13330
$T(C^{+3})$		....	13530	14180	12930	....	13540	13480
$T(N^{+})$		8900	12590	12820	11900	....	13250	13270
$T(O^{+})$		....	12620	12830	11840	....	13110	13130
$T(O^{++})$		12100	12700	12970	12100	12500	13250	13260
$x(C^{+})$		....	0.035	0.017	0.041	....	0.008	0.010
$x(C^{++})$		....	0.363	0.329	0.441	....	0.383	0.432
$x(C^{+3})$		....	0.386	0.415	0.340	....	0.574	0.525
$x(N^{+})$		....	0.015	0.008	0.018	....	0.005	0.007
$x(N^{++})$		....	0.438	0.395	0.520	....	0.481	0.541
$x(N^{+3})$		....	0.295	0.318	0.255	....	0.477	0.420
$x(O^{+})$		.155	0.111	0.066	0.137	.030	0.018	0.020
$x(O^{++})$		.513	0.447	0.461	0.421	.676	0.653	0.602
$x(O^{+3})$		....	0.195	0.213	0.228	....	0.300	0.349
N_H (cm^{-3})		4600	5000	5000	5000	1700	4000	2000
ε b)		.26	1.0	1.0	0.5	.02	1.0	1.0
log O/H		-3.22	-3.30	-3.20	-3.20	-3.54	-3.54	-3.54
log C/O		+0.20	+0.40	0.00	+0.40	+0.10	+0.10	+0.10
log N/O		-0.39	-0.20	-0.30	-0.20	-0.27	-0.16	-0.16
R_i (pc) c)		....	.001	.001	.001	....	.001	.107
R_o (pc)		.05	.068	.067	.084	.13	.074	.116
R_* ($R_\odot$) d)		....	0.10	0.10	0.10	....	0.10	0.10
T_* (10^3°K)		....	150	150	150	....	125	125

a) Relative to Hβ, where I(Hβ)= 100,
$T(X^{+m}) \equiv \int N_e N(X^{+m}) dV / \int N_e N(X) dV$.
$x(X^{+m}) \equiv \int N_e N(X^{+m}) dV / \int N_e N(X) dV$.

b) ε is the filling factor.

c) R_i, R_o are inner and outer radii.

d) R_*, T_* are central stars parameters.

ANALYSIS OF HIGH EXCITATION PLANETARY NEBULAE

L. H. Aller and C. D. Keyes
Astronomy Department, University of California, Los Angeles

ABSTRACT

Combination of extensive ground-based spectroscopic observation of high excitation planetary with IUE data permit determination not only of improved diagnostics but also better abundances for elements such as C and N that are well-represented in the ultraviolet spectra, and also C, Ar and metals Na, Ca and K whose lines appear in the λ3200-8100Å region. We summarize here some of the principal results from a cooperative program being carried out in collaboration with S. J. Czyzak of Ohio State, G. Shields of the University of Texas, and B. J. O'Mara and J. E. Ross of the University of Queensland.

INTRODUCTION

In our preliminary survey (ref.1), short-wave IUE data were affected by image-processing difficulties that introduced systematic errors. These errors have now been eliminated. Table 1 lists the measured intensities. Successive columns list approximate wavelengths, identifications, and for each nebula (except NGC 6741 and 6886) the logarithm of the flux in ergs $cm^{-2}sec^{-1}$ as received at the top of the earth's atmosphere. Quality is indicated by a, b, c, d, e. Lines indicated by a or b are fairly strong; their accidental errors should be of the order of 10%. Lines of quality c may have errors amounting to 25 - 35%, while those of quality d are seriously affected by noise; errors here can easily amount to 50 - 100%. We use e to indicate that the feature is believed to be present; the tabulated intensity is to be understood as essentially an upper limit. Thus ionic concentrations estimated from lines of quality d are very uncertain; those from e quality lines are upper limits. See Figs. 1,2,3

In principle, objects of small angular size that fit into the large slot present no difficulties for determination of interstellar extinction. Following Seaton (ref.2) one may compare the HeII intensity ratio I(λ1640)/I(λ4686). Although NGC 2440 has some outlying ansae, most of its radiation is accepted. The nebular angular sizes of NGC 2392 and 6302 exceed that of the slot. For NGC 6302 we find an extinction constant C = 1.44 from the HeII λ1640/λ2734 intensity ratio as compared with 1.41 from a comparison of radio and optical data (ref.3). For NGC 2392, C = 0.15 is in accord with the 1640/2734 ratio when account is taken of the λ2734 intensity measurement.

The availability of extensive ground-based data covering a wide gamut of ionization stages (ref.4 and unpublished data for NGC 2867, NGC 2440, NGC 6741, NGC 6302, and Me 2-1) has made possible a more thorough investigation of these objects than otherwise possible. For example, lines of [C&II], [C&III], [C&IV], [ArIII], [ArIV], and [ArV] but especially [NeIII], [NeIV] λ4724, 25, and [NeV] help bridge the gap from domains of low to those of high excitation. Strata producing these lines overlap those responsible for lines of CIII, CIV, NIII, NIV, NV, and OIV observed with the IUE. If a reasonable estimate of the electron density can be found, we can use the [NeIV] auroral/nebular line

ratio to estimate the electron temperature in these hotter, inner regions (eqn.4 of ref. 1).

In our earlier analysis (ref.1) we obtained diagnostics from optical region lines and calculated ionic concentrations from both optical and UV data. We found the ionization correction factors (ICF's) by interpolation in a grid of theoretical models based on Cassinelli's (ref.5) stellar fluxes and a fixed chemical composition. These grid models give a correct general excitation level but did not represent specific line intensities closely.

Our new method is to calculate individualized spherically symmetrical models for each nebula. We iterate an appropriate grid model, modifying the stellar energy distribution and truncation of the nebular radius to fit the observed intensity ratios for HeI/HeII, [OIII]/[OII], and [NeV]/[NeIII]. Lastly individual elemental abundances are adjusted to reproduce the observed optical region line intensities. This objective could be achieved for transitions of ions of He, N, O, and Ne observed with ground-based equipment but our present models are less satisfactory for the forbidden line of S, Cℓ and Ar. Curiously, if the lines of [ArIV] and [ArV] are represented, λ7135 of [ArIII] is too strong. The effect is exactly opposite to that found for our models of low-excitation nebulae. Inclusion of latest available charge exchange cross-sections, recombination coefficients, etc., has had a profound effect on our new series of models.

Spherically symmetrical shells or constant density models cannot predict successfully all nebular line intensities. By representing certain excitation ratios we hope that the general ionization pattern is adequately predicted. We then use the models to derive the ICF's and to estimate the electron temperature in the hotter inner regions. The [NeIV] aur/neb ratios support these estimates, although because of the high excitation potentials, the hottest portions of Ne^{+++} zones tend to be favored. We can derive the chemical composition by a best fit of the predicted intensities or by calculating ionic concentrations in the usual way and then using the models to derive the ICF's. We prefer the latter method, although both procedures agree reasonably well for most elements. The discordances tend to be larger for the clumpy nebulae, NGC 2392 and NGC 2440, particularly for nitrogen when the model representation was based on fitting the [NII] lines.

Although a reasonably good representation is found for visual region lines, agreement is less satisfactory in the ultraviolet. Many lines are weak and accidental errors are large which makes comparison difficult. The predicted NV 1239/41 intensities exceed the observed values which suggests the models predict too high a level of ionization for nitrogen. The predicted CIII/CIV intensity ratio always exceeds the observed one, presumably because of optical depth effects (ref.6). The predicted OIV 1403/09 intensity, however, tends to be less than the observed one. Theoretical predictions of the OIII 1661/66 feature tend to agree with the observed values, thus providing an independent check on the calibration and on the interstellar extinction. Although theoretical and observed [NeIV] aur/neb ratios tend to agree, when differences occur, they suggest that the electron temperature exceeds model predictions. Curiously, although a condition of acceptance of a model is that the [NeIII]/[NeV] line ratios are correctly represented, predicted [NeIV]

intensities are too weak. Possibly a modification of the assumed stellar energy flux or an improvement in the cross-sections would remove this discordance.

The theoretical models suffer from simplistic assumptions about geometry and density. Obviously, they are poor approximations for NGC 2440 and NGC 2392; no such model can predict even approximately a satisfactory spectrum for NGC 6302. For this nebula, only approximate ICF's can be found.

Table 2 compares abundance estimates with those of a previous survey based exclusively on ground-based data (ref.7) and solar values (ref.8). Shields, Czyzak, and Aller are carrying out an analysis of NGC 2440 in which the straightjacket of a constant density structure is no longer imposed. (For consistency we treat NGC 2440 here on the same basis as the other nebulae). Note that low carbon abundances are found in the clumpy planetaries, NGC 2392, 2440, and especially 6302 which are not well represented in the constant density approximation. All of these nebulae appear to be nitrogen rich. Perhaps high-excitation planetaries originate exclusively from relatively massive stars in which nitrogen building has been prominent. Furthermore, the relatively small departures of the abundances of S, C, Ar, and K from solar values suggest that these nebulae, particularly, came from stars that did not differ greatly from a solar-type composition.

Becker and Iben (ref.9) have calculated asymptotic giant branch evolution of intermediate mass stars. They discuss abundance modifications for stars of different mass and composition for the first dredge-up phase on the red giant branch and for the second dredge-up phase on the asymptotic giant branch. The depletion of C and O and the enrichment of He and N depends on mass and initial composition, being the more marked the greater the mass and the initial He and/or heavy metal content. For massive (5-11 solar mass) progenitor stars, our observed abundance modifications agree qualitatively with their results (cf. their table 6) but the predicted helium enhancement is greater than the observed. Probably few planetaries have progenitor stars as massive as five solar masses.

Alternately, following Scalo, Despain, and Ulrich (ref.10) we can consider highly evolved stars with double shells which develop high temperatures ($50 - 80 \times 10^6$ ^{o}K) at the bottom of their convective envelopes between shell flashes. Near the upper end of this temperature range, full CNO processing can occur; carbon will be destroyed, and nitrogen will be enhanced. Helium will not be produced in excessive amounts. Stars down to a lower limit of 1.5 solar masses can be involved.

In summary, use of IUE data helps enormously in our understanding of the spectra of gaseous nebulae and enables us to handle the problem of chemical compositions more accurately. Curiously, in a number of instances the simple extrapolation methods suggested by Seaton, Peimbert and Costero, and others for N, O, and Ne seem to work rather well.

TABLE 1.-LOGARITHM OF INTENSITIES OF NEBULAR LINES

λ	Iden	NGC 2392	NGC 2440	NGC 2867	Me 2-1	NGC 6302
1239/41	NV	-11.96b	-11.45a	-12.5:e	-12.1 e	-12.09b
1335	CII	-11.98 c		-12.15d	-12.45e	
1391	SiIV					
1403, 1409	OIV	-11.53b	-11.60b	-12.64d	-11.79 c	-12.38b
1487	NIV	-11.49b	-10.95a	-11.90c	-11.99d	-11.66a
1548/50	CIV	-11.06a	-10.56a	-10.81a	-10.62a	-11.65a
1640	HeII	-10.72a	-10.57a	-10.79b	-10.90a	-11.80a
1661/66	OIII	-11.34b	-11.52a	-11.98c	-12.06e	-12.33b
1747	NIV	-11.23a	-11.08a	-12.06c	-12.21d	-11.68a
1892	SiIII	-11.48c	-11.76b			-12.70c
1906/09	CIII	-10.69b	-10.37a	-10.38a	-10.80a	-11.83a
2326/28	CII	-11.76c	-11.46a	-11.25a	-12.10c	
2422	[NeIV]	-11.17b	-11.06a	-11.71b	-11.26a	-11.87a
2470	OII		-11.84c	-12.16d		-12.64d
2511	HeII		-11.88c	-12.1 e	-12.30c	-12.73d
2734	HeII	-12.08c	-11.87c	-12.13c	-12.27c	-12.66c
2798/2800	MgII			-12.12d		
2830	HeI		-12.05c	-12.14c	-12.62d	-12.75d
3024	OIII			-12.4:c		-12.8:d
3047	OIII		-12.14d	-12.05c	-12.42d	-12.32d
3133	OIII	-11.71b	-11.04c	-11.16a	-12.39a	-11.52b
3187	HeI			-11.96c		
3204	HeII		-11.45b	-11.76c	-11.89b	-11.92c

TABLE 2.-SUMMARY OF ABUNDANCE ESTIMATES

	NGC 2392	NGC 2440	NGC 2867	Me 2-1	NGC 6302	NGC 6741	NGC 6886	mean	mean ref.7	Solar ref.8
He	10.96	11.08	11.05	11.01	11.27	11.04	11.01	11.03	11.02	11.08
C	8.35	8.37	9.03	8.88	8.04	9.01	8.83	8.77	9.10	8.62
N	8.32	8.78	8.13	8.23	8.96	8.4	8.8	8.58	7.97	7.94
O	8.56	8.61	8.65	8.73	8.71	8.74	8.63	8.67	8.66	8.84
Ne	7.69	8.03	7.91	8.20	8.02	8.34	8.21	8.11	8.02	8.1
Na		6.26					6.29	6.27	6.23	6.28
S	6.78	6.43	6.75	7.13	6.81	6.91	6.48	6.82	6.97	7.2
Cℓ	5.11	5.28	5.20	5.29	5.56	5.36	5.39	5.34	5.26	5.5
Ar	6.12	6.47	6.25	6.41	6.93	6.63	6.51	6.55	6.38	6.0
K	4.75	4.64		5.38	5.48	4.68	5.18	5.15	4.90	5.16
Ca	4.80	4.90		5.03	5.37	5.38	4.87	5.12	5.10	6.35
Extinct. Coeff.	0.15	0.67	0.52	0.28	1.44	1.30	1.09			

Extinct. Coeff. = $\log[F_T(H\beta)/F_o(H\beta)]$

where $F_o(H\beta)$ = observed Hβ flux.

$F_T(H\beta)$ = Hβ flux corrected for interstellar extinction.

REFERENCES

1. Aller, L. H. and Keyes, C. D.: International Ultraviolet Explorer Satellite Observations of Seven High Excitation Planetary Nebulae. Proceedings Nat'l. Acad. Sciences USA, vol. 77, 1980, pp. 1231-1234.

2. Seaton, M. J.: Extinction of NGC 7027. Mon. Not. Roy. Astr. Soc., vol. 187, 1979, pp. 785-791; 73-76P.

3. Milne, D. K. and Aller, L. H.: Radio Observations at 5GHz of Southern Planetary Nebulae. Astron. & Astrophys., vol. 38, 1975, pp. 183-187.

4. Aller, L. H. and Czyzak, S. J.: A Spectroscopic Study of Moderately Bright Planetary Nebulae. Astron. & Astrophys., vol. 62, 1979, pp. 397-437.

5. Cassinelli, J. P.: Extended Model Atmospheres for Central Stars of Planetary Nebulae. Astrophys. J., vol. 165, 1971, pp. 265-284.

6. Bohlin, R. C.; Harrington, P. C.; and Stecher, T. R.: Rocket Ultraviolet Spectrum and Models of the Planetary Nebula NGC 7662. Ap.J., vol. 219, 1978, pp. 575-584.

7. Aller, L. H.: Chemical Composition of Planetary and Diffuse Nebulae. Proceedings Astron. Soc. Australia, vol. 3, 1978, pp. 213-219.

8. Ross, J. E. and Aller, L. H.: The Chemical Composition of the Sun. Science, vol. 191, 1976, pp. 1223-1229.

9. Becker, Stephen Allan and Iben, Icko: The Asymptotic Giant Branch Evolution of Intermediate-Mass Stars as a Function of Mass and Composition. I. Ap.J., vol. 232, 1979, pp. 831-853.

10. Scalo, John M.; Despain, Keith H.; and Ulrich, Roger K.: Studies of Evolved Stars. V. Nucleosynthesis in Hot-Bottom Convective Envelopes. Ap.J., vol. 196, 1975, pp. 805-817.

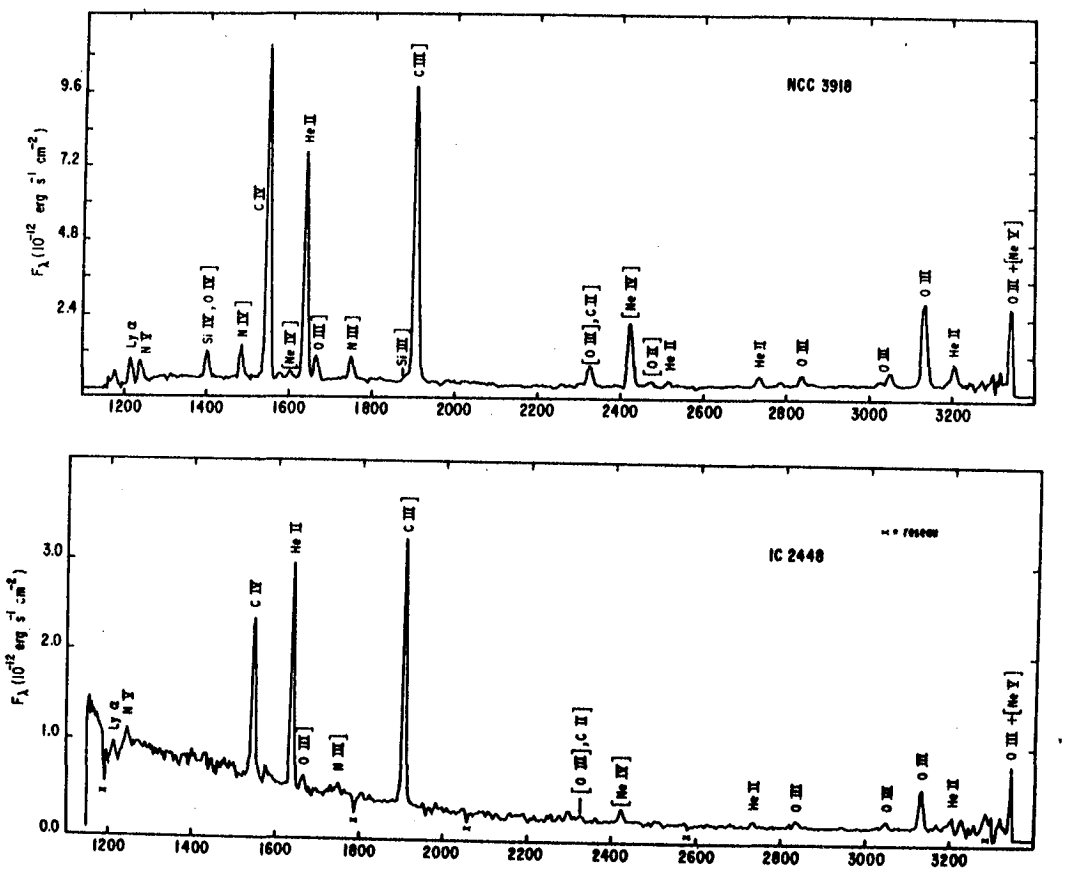

Figure 1. Calibrated IUE spectra. (a) For NGC 3918 we have added SWP 1906 and SWP 3192 for $\lambda < 1950$ A and all available large aperture spectrograms for longer wavelengths. (b) For IC 2448 we have combined SWP 3194 and LWR 2756.

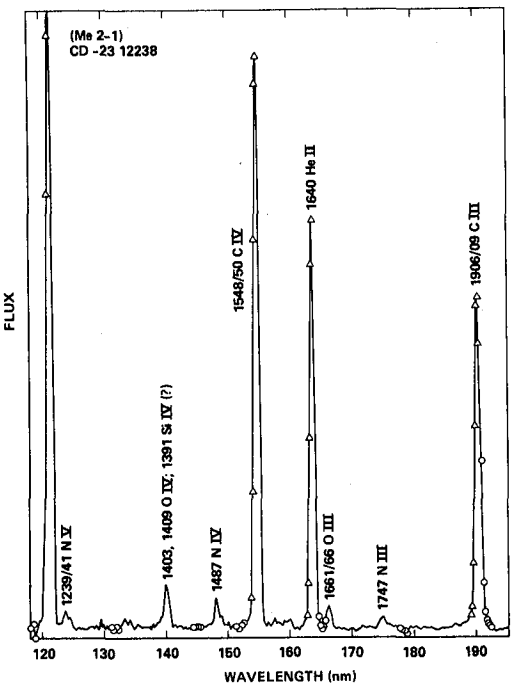

Fig. 1 Far Ultraviolet Spectrum of CD-2312238

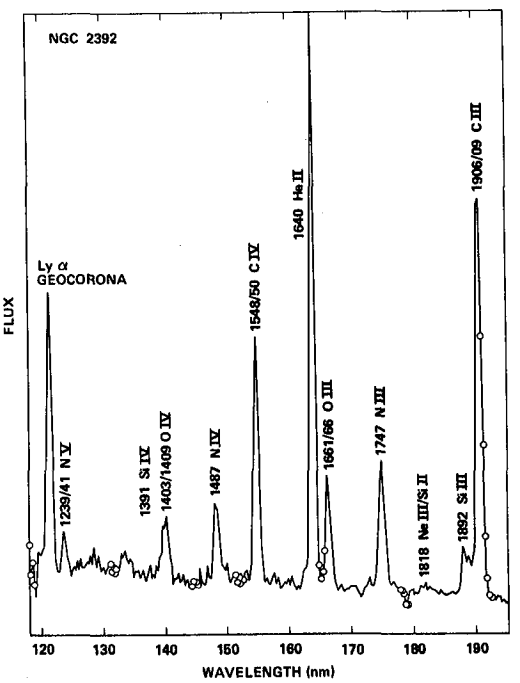

Fig. 2. Far Ultraviolet Spectrum of NGC2392

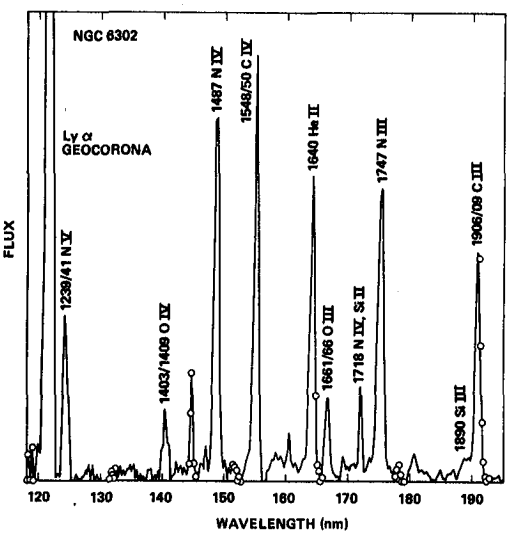

Fig. 3. Far Ultraviolet Spectrum of NGC6302

DISCOVERY OF THE MOLECULAR HYDROGEN ION (H_2^+) IN THE PLANETARY NEBULAE

Sara R. Heap and Theodore P. Stecher

Laboratory for Astronomy and Solar Physics
NASA-Goddard Space Flight Center
Greenbelt, MD 20771

ABSTRACT

Low-dispersion spectra of fifteen planetaries and hot subdwarfs were obtained with the SWP camera on IUE and continuous flux distributions corrected for interstellar extinction were derived. Several planetaries, particularly the young planetaries of high surface-brightness, show anomalous flux distributions. The most anomalous case is NGC 6210. We suggest that these anomalies may be explained as absorption by H_2^+ in the nebula. For the case of NGC 6210, we derive a column density, $N(H_2^+) = 8 \times 10^{16}$ cm^{-2}.

OBSERVATIONS

During the first year of observation with the IUE, we made a survey of planetary nebulae with the short-wavelength spectrograph, mainly for the purpose of investigating winds in the central stars, but in the process, we derived continuous flux distributions for these objects. The results of this survey are that planetaries have flux distributions like what you would expect from hot central stars (i.e., fluxes increasing steadily toward shorter wavelengths), but a couple of planetaries had odd flux distributions.

Figure 1 shows the flux distribution for a typical case, NGC 1535, and for the most anomalous case, NGC 6210. The fluxes in the figure are absolute fluxes corrected for interstellar reddening and normalized arbitrarily so that $F_\lambda(1950\text{Å}) = 1$. We use NGC 1535 as a standard of comparison with NGC 6210, because the two central stars appear to have almost identical properties. The visual spectra indicate that both are early O stars with higher-than-main sequence gravities (Refs. 1, 2). As you can see from Figure 1, the ultraviolet line spectra of the two stars are also strikingly similar: in both, N V 1240 is a very strong P Cygni feature, while C IV λ1550 is weaker and fully in emission; and in both, the subordinate line of OV λ1371 is also a strong P Cygni line. What is markedly different between the two spectra is their continuous flux distributions: the flux of NGC 1535 increases steadily toward shorter wavelengths, as you would expect for a hot star, but the flux of NGC 6210 drops off from its extrapolated values at wavelengths shorter than about 1500Å. Clearly, there is some source of absorption at the shorter wavelengths.

It is difficult to explain this difference as the effect of interstellar extinction, since several lines of evidence indicate that both NGC 1535 and NGC 6210 have similar, low amounts of reddening. The ratio of nebular radio flux density to Hβ flux yields a color excess, E(B-V) = 0.09 for NGC 1535 and E(B-V) = 0.06 for NGC 6210 (Ref. 3). The Ca II K line is weak in both visual spectra. In the case of NGC 6210, we obtained an LWR spectrum and found that the λ2200 extinction bump is consistent with a color excess, E(B-V) = 0.06.

INTERPRETATION

The two questions we have to ask, then, are (1) what is absorbing far-UV flux from the central star of NGC 6210, and (2) where does the absorbing material originate? The first question is relatively easy to answer because the flux deficiency looks just like the signature of the molecular hydrogen ion, H_2^+. This identification is supported by a quantitative comparison of the observations with the theoretical absorption properties of H_2^+. Figure 2 shows this comparison. The jagged line is the ratio of the relative fluxes of the two planetaries, while the smooth curve is the run of H_2^+ absorption, $e^{-\tau}$, for H_2^+ in the ground vibrational state, based on cross-sections calculated by Dunn (Ref. 4) and a column density of 8×10^{16} per cm^2.

The other question, where does the absorption come from, is also not difficult to answer because there are not too many places left to look. As I mentioned earlier, the spectra of the central stars of NGC 1535 and NGC 6210 are similar, and the amount of reddening of these two objects is also similar, so we can rule out the stellar atmosphere and the interstellar medium as the place in which the H_2^+ originates. There is just one place left to look, and that is the nebula itself.

Does this interpretation make sense? Should we expect H_2^+ in planetary nebulae? The answer, as Black (Ref. 5) has pointed out, is no, if you are considering a steady-state nebula. But NGC 6210 is a young nebula, still optically thick in H I (Ref. 6), so let us consider evolving nebulae, as illustrated in Figure 3. It is generally believed that planetary nebulae are the former envelopes of red giants. These envelopes were sloughed off due to the mechanical force of radiation pressure exerted on the gas and dust (Refs. 7, 8). Since the envelopes of red giants are basically composed of molecular hydrogen, and since the formation of the nebula is believed to be a cold flow, we can expect a planetary nebula to be initially composed of H_2. The loss of the red giant envelope, however, exposes the hot, inner stellar core, and radiation from the core, which is now seen as a central star, then proceeds to ionize the nebula. As the ionization front advances through the expanding nebula, it forms a thin shell of H_2^+:

$$H_2 + h\nu \rightarrow H_2^+ + e.$$

The H_2^+ generated by photo-ionization will be distributed among various vibrational states, but what we observe is absorption by H_2^+ from the ground vibrational state. We haven't done the necessary calculations, but it seems plausible that most of the H_2^+ generated by photo-ionization relaxes to the ground state as the result of collisions. Ground-state H_2^+ is destroyed by the inner edge of the H_2^+ shell by photo-dissociation:

$$H_2^+ + h\nu \rightarrow H^+ + H,$$

(It is this process that produces the absorption that we observe in NGC 6210) and by dissociative recombination,

$$H_2^+ + e \rightarrow H + H.$$

Supporting circumstantial evidence on H_2^+ shells in young planetary nebulae comes from the success rate of finding molecular hydrogen in planetary nebulae. In a survey of nine planetaries, Beckwith et al. (Ref. 9) found H_2 emission in five, four of which were young, high-density nebulae or their progenitors. All five nebulae with detectable H_2 showed [O I] as does NGC 6210.

We believe our detection of H_2^+ in NGC 6210 is significant not only because it represents a first detection of H_2^+ in planetary nebulae, but also because it should help to clarify our picture of nebular evolution.

REFERENCES

1. Heap, S. R. 1977, Ap. J. 215, 609.
2. Heap, S. R. 1977, Ap. J. 215, 864.
3. Kaler, J. B. 1976, Ap. J. Suppl. 31, 517.
4. Dunn, G. 1968, J.I.L.A. Report No. 92.
5. Black, J. H. 1978, Ap. J. 222, 125.
6. Seaton, M. J. 1966, M.N.R.A.S. 132, 113.
7. Wickramsinghe, N. C., Donn, B. D. and Stecher, T. P. 1966, Ap. J. 146, 590.
8. Kutter, S. G., Savedoff, M. and Schuerman, D. 1969, Ap. Space Sci. 3, 182.
9. Beckwith, S., Persson, S. E., .and Gatley, I. 1978, Ap. J. 219, L33.

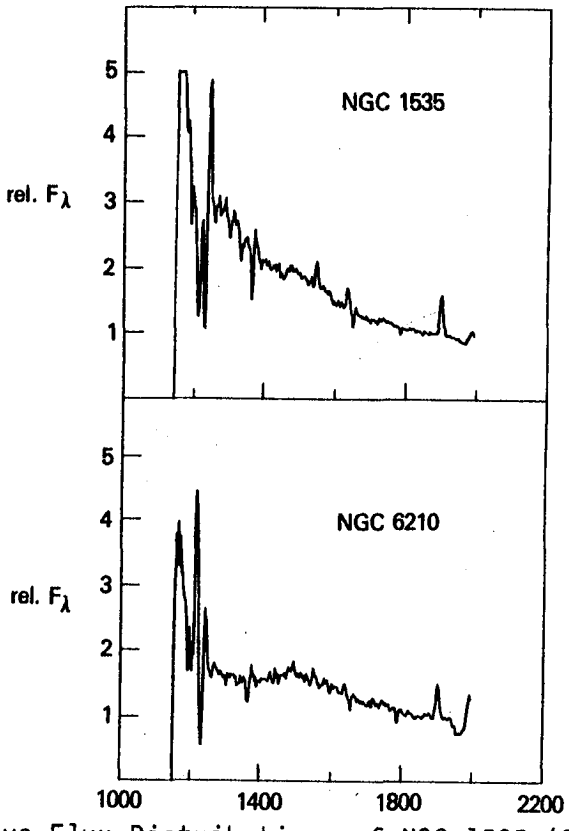

Figure 1. Relative Flux Distributions of NGC 1535 (SWP 3374) and NGC 6210 (SWP 3327). The raw fluxes contain ITF errors, but the effect of these errors should be small. The absolute fluxes were corrected for interstellar extinction on the assumption that E(B-V) = 0.06 for NGC 6210 and E(B-V) = 0.09 for NGC 1535.

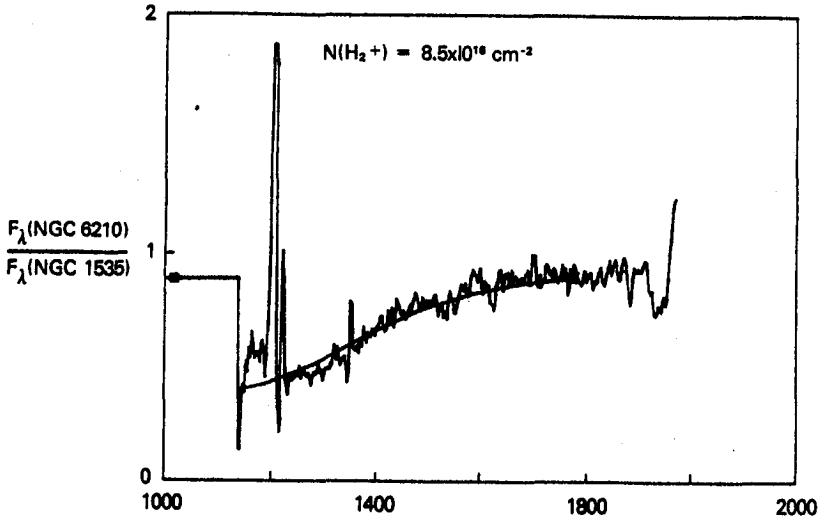

Figure 2. Comparison of the Observed Flux Ratio with Predicted Absorption by H_2^+. The jagged line is the ratio of the relative fluxes shown in Figure 1. The smooth curve is exp $(-N\sigma_\lambda)$.

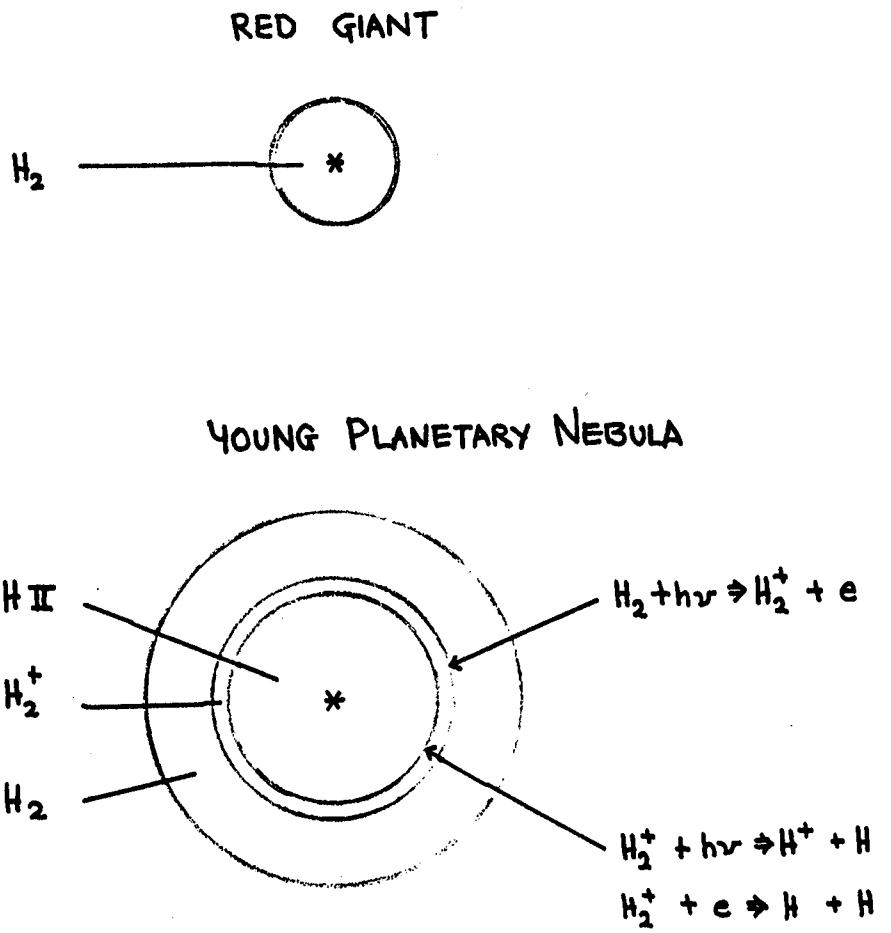

Figure 3. Evolutionary Scheme for Planetary Nebulae.

AN ATLAS OF EMISSION LINE FLUXES OF PLANETARY NEBULAE IN THE 1150-3200Å REGION

A. Boggess, W. A. Feibelman and C. W. McCracken
Laboratory for Astronomy and Solar Physics
Goddard Space Flight Center

ABSTRACT

Emission line fluxes in units of 10^{-12} erg $cm^{-2}sec^{-1}$ for 28 planetary nebulae are presented. The nebulae were chosen to cover a wide range of excitation classes, apparent diameters, location in the sky, and types of central stars. All objects were observed in the low-dispersion mode of the IUE spectrographs, using the large entrance aperture.

INTRODUCTION

Ultraviolet observations have an important role to play in the study and interpretation of planetary nebulae. The range from 1200 to 3200Å contains lines of carbon, nitrogen, oxygen and silicon in ionization stages difficult to observe from the ground. In addition, forbidden lines from ions such as three and four times ionized neon and argon provide opportunities for probing the high temperature regions of these objects. The first spectra obtained of planetaries throughout this range were those of NGC7027 and NGC7662, by Bohlin and his collaborators using sounding rockets (1, 2). However, it has only been with the advent of the IUE that such data could be obtained routinely for a large number of nebulae to $m_v \approx 12$. With this in mind, a systematic program of observing planetary nebulae has been conducted during the first two years of IUE operations in order to provide data on these objects covering a wide range of excitation class, apparent diameter, and spectral type of the central star. The results presented here are from low dispersion observations of 28 planetary nebulae. Intensities of the emission lines in these objects are given in the accompanying tables. Plots of the actual calibrated spectra will be published elsewhere.

OBSERVATIONS

All the planetary nebulae listed in the accompanying tables have been observed in the low-dispersion mode, corresponding to a resolution of about 7Å, through the 10"x20" large apertures, with the nebulae centered in the aperture. Thus the resulting data correspond essentially to slitless spectra of the nebulae and their central stars. The majority of the objects (about 75%) are small enough so that the measured fluxes represent those of the entire nebula. Many of the nebulae have been observed more than once to extend the dynamic range of the data, and in these cases the fluxes tabulated are from the spectrogram yielding the best signal-to-noise ratio for the line in question.

The fluxes have been generated from the net extracted spectra and corrected, when necessary, for ITF errors. The data have been converted to absolute units using the calibration curve of Bohlin, et al. (3). All the spectra were processed for "extended source extraction" in order to measure the total emission in the entrance aperture, even when the nebula was known to be small or semi-stellar. As a test, a few of these small objects were processed in both "extended source" and "point source" extraction and the results were identical, as one would expect. For those objects that exceed the entrance aperture dimension, allowances have to be made to convert the measured fluxes into actual percentages of the entire flux emitted by the nebula and the position angle may have to be considered, too.

The tabulated emission line fluxes are believed to have internal accuracies of ±10%, except for those values shown in brackets where the accuracy may be on the order of ±20%. This lower accuracy is usually due to weaker lines with low S/N ratio or because of high-radiation backgrounds during the time of observation. To these errors, one must add the uncertainty of the IUE absolute calibration, which is estimated to be about 10%. No corrections for interstellar extinction have been applied. The presence of geocoronal Ly-α on all spectra prevents any measurements of nebular features within ~ 15Å of Ly-α.

Although determinations of intensity ratios of doublets for establishing electron densities or electron temperatures, line profiles, expansion velocities and line splitting will require high-dispersion spectrograms of the objects studied so far, there are nevertheless some preliminary conclusions that can be drawn from the low-resolution spectra. The sampling of 28 objects is sufficiently large to make some general statements: 1) There are remarkable differences among the UV spectra even between objects of similar excitation class and extinction. 2) All nebulae show CIII] λ1907-09 and this feature can be used as an indicator in surveys for nebular emission objects. 3) Objects that are classified as low-excitation nebulae in the visible generally show the emission lines of CIII], [OII] and MgII. 4) HeII may be present in both low- and high-excitation nebulae, and a few planetaries show mixtures of both very high- and low-excitation lines. 5) Those classified as high-excitation objects show NV, [NeIV], and [MgV] lines.

RESULTS

In the accompanying tables the nebulae have been grouped roughly according to excitation class. The tables give excitation classes and nebular diameters from Lang (4) and spectral types of central stars from Aller (5). All entries give the measured emission line fluxes in units of 10^{-12} erg cm^{-2} sec^{-1}. Fluxes of lower accuracy are shown in brackets. Letter entries in the tables are defined as follows:

a = absorption line
b = blended lines
p = emission component of P-Cygni feature
s = a few pixels saturated
WR = broad emission feature of Wolf-Rayet type
z = line is probably present.

REFERENCES

1. Bohlin, R. C., Marionni, P. A., Stecher, T. P.: Ap. J. 202, p. 415, 1975.

2. Bohlin, R. C., Harrington, J. P., and Stecher, T. P.: Ap. J. 219 p. 575, 1978.

3. Bohlin, R. C., Holm, A. V., Savage, B. D., Snijders, M. A. J., and Sparks, W. M.: A. & A. (in press) 1980.

4. Lang, K. R.: "Astrophysical Formulae", Springer, New York, 1974.

5. Aller, L. H.: Mem. Soc. Roy. Sci., Liege, IX, p. 271, 1976.

Table 1

Emission Line Fluxes for Low Excitation Planetary Nebulae

		BD 30°3639	IC418	IC2149	IC3568
Diameter (arcsec)		3.0	12.4	8.6	18
Excitation Class		1	3	4	5
Central Star		WC9	07fp	07.5fp	05f
1239/41	NV	7.71	-	-	-
1309	SiII	9.60	-	-	-
1335	CII	6.64	(21.85)	-	-
1403/09	OIV]	4.57	-	-	-
1487	NIV]	5.14	-	3.93	-
1548/50	CIV	a	16.64p	3.05p	3.42p
1640	HeII	5.23	-	-	-
1661/66	OIII]	2.91	-	-	-
1674	?	3.80	-	-	-
1747	NIII	5.78	-	-	-
1892	SiIII	4.23	-	-	-
1907/09	CIII]	44.63	29.92	4.94	7.11
2297	CIII	28.59	-	-	-
2325/29	CII], [OIII]	20.37	82.52	2.08	-
2470	[OII]	-	27.50	1.19	-
2798	MgII	-	29.75s	-	-
2830	HeI	12.78	-	-	-
3047	OIII	-	1.23	-	-
3095	?	-	6.64	-	-
3133	OIII	-	6.64	-	-
3188	HeI, OIII	-	-	z	(0.27)

Table 2

Emission Line Fluxes From Moderately High Excitation Planetary Nebulae

		J320	IC4846	NGC6891	Hu 2 - 1	NGC7026
Diameter (arcsec)		6.4	2.0	12.6	-	11.2
Excitation Class		5	5	5	-	6
Central Star		-	-	07f	-	OVI
1309	SiII	-	-	-	(0.15)	(0.04)
1371	OV	-	-	-	-	0.30
1487	NIV]	(0.55)	-	(1.67)	-	0.12
1548	CIV	5.41	-	3.86p	a	0.83
1640	HeII	1.88	-	-	-	0.67
1661/66	OIII]	-	-	-	-	-
1718	NIV,SiII]	-	-	(0.41)	-	-
1747	NIII	-	-	-	(0.19)	-
1892	SiIII	0.20	-	-	-	-
1907/09	CIII]	7.76	0.47	3.12	1.77	0.49
2325/29	CII], [OIII]	1.07	(0.43)	-	1.94	-
2423/26	[NeIV]	0.52	-	-	-	-
2470	[OII]	-	(0.70)	-	(0.98)	-
2734	HeII	(0.30)	(0.90)	-	-	-
2946	HeI	(0.22)	-	-	-	-
3047	OIII	0.49	(0.39)	-	z	-
3133	OIII	2.32	-	(0.84)	-	1.17
3188	HeI,OIII	-	(0.17)	(0.88)	2.21	-

Table 3

Emission Line Fluxes for Moderately High Excitation Planetary Nebulae

		NGC6572	IC4997	NGC6565	NGC6644	NGC3132
Diameter (arcsec)		16.4	1.6	9.0	2.6	(56)
Excitation Class		5	5	6	6	6p
Central Star		Of+WR	Of+WR	-	-	A+sdO
1239/41	NV	(2.33)	0.56	0.29	-	-
1309	SiII	0.82	(0.93)	-	-	-
1335	CII	z	0.29	-	0.31	-
1371	OV	1.91	-	(0.81)	-	-
1403/09	[OIV]	(1.03)	0.09	-	-	-
1487	[NIV]	z	0.15	-	-	-
1548/50	CIV	2.66p	3.51	0.78	9.50	-
1575	[NeV]	-	-	0.44	-	-
1640	HeII	1.57	0.34	2.04	2.39	6.62
1661/66	[OIII]	0.95	5.11	-	0.89	0.74
1718	NIV, [SiII]	2.03	-	-	-	z
1747	NIII	1.32	2.16	0.48	-	0.75
1817	[NeIII] ,SiII	-	0.23	-	-	-
1892	SiIII	(0.72)	0.33	-	-	-
1907/09	[CIII]	50.52s	17.67	2.55	12.31s	4.21
2252	HeII	-	0.26	-	-	-
2325/29	[CII], [OIII]	10.47	2.35	0.98	1.71	-
2423/26	[NeIV]	-	-	(0.37)	0.71	-
2470	[OII]	5.62	1.59	(0.49)	0.60	-
2511	HeII	-	z	-	-	-
2734	HeII	-	z	-	-	(0.58)
2798/03	MgII	-	1.90	-	1.66s	-
2830	HeI	1.84s	0.33	-	0.24	(0.33)
2852	MgI	-	z	-	-	-
2946	HeI	(0.70)	0.38	-	-	-
3047	OIII	-	(0.18)	(0.33)	-	-
3133	OIII	-	-	1.12	2.65	2.27
3188	HeI,OIII	2.33	-	-	(0.98)	-
3204	HeII	-	(1.96)	-	-	-

Table 4

Emission Line Fluxes for High Excitation Planetary Nebulae

		NGC1535	J900	NGC3242	IC1297	HM Sge*	NGC7009
Diameter (arcsec)		18.4	9.4	(40)	-	-	26.8
Excitation Class		7	7	7	-	-	7p
Central Star		07	em?	cont?	-	-	cont.
1239/41	NV	29.71	(0.23)	5.63	-	0.87	21.91
1286	?	(2.98)	-	-	-	-	-
1309	SiII	(3.46)	-	-	-	-	-
1335	CII	-	(0.24)	-	-	(0.09)	-
1371	OV	7.82	-	(1.06)	2.41	0.35	4.98p
1391	SiIV	-	-	-	-	0.25	-
1403/09	OIV]	(3.43)	(0.18)	-	0.68	0.31	-
1487	NIV]	-	0.51	(3.85)	z	1.15	z
1548/50	CIV	10.74	5.23	-	7.62	5.02	10.86
1575	[NeV]	z	-	-	0.42	(0.12)	4.36
1640	HeII	14.30	1.68	118.30	14.98	3.44b,WR	43.00
1661/66	OIII]	z	(0.24)	-	1.38	2.66b	3.68
1718	NIV,SiII]	-	-	-	-	2.07b,WR	-
1747	NIII	7.84	-	-	1.30	5.15b	1.29
1817	[NeIII] ,SiII	-	-	-	-	0.57	-
1892	SiIII	-	(1.10)	-	0.41b	3.04b	-
1907/09	CIII]	8.26	7.51	98.13	7.02b	10.09b	25.70
2101	CIII	-	-	(0.93)	-	-	-
2252	HeII	-	-	0.87	-	-	-
2297	CIII	-	-	5.19	-	-	2.60
2325/29	CII], [OIII]	-	1.07	2.01	0.90	1.67	1.93
2423/26	[NeIV]	-	0.52	9.15	0.70	0.36	1.93
2470	[OII]	-	-	-	-	0.22	-
2511	HeII	-	-	0.85	z	-	(0.64)
2734	HeII	-	0.30	2.45	0.52	0.20	1.73
2784	[MgV]	-	-	-	(0.71)	-	-
2798/03	MgII	-	-	-	-	7.16	-
2830	HeI	1.18	-	3.33	0.77	1.75	3.68
2946	HeI	-	-	-	-	-	1.17
3024	OIII	-	-	2.65b	-	-	(0.97)b
3047	OIII	-	0.50	6.04b	0.47	0.19	3.99b
3133	OIII	3.81	2.30	36.18s	4.41	0.43	24.81
3188	HeI,OIII	-	-	-	(1.18)	-	3.21b
3204	HeII	-	z	6.41	-	z	3.56b

*The fluxes of HM Sge are for the first set of observations, 6 June 1978. Considerable changes have occurred during the past two years and will be described elsewhere.

Table 5

Emission Line Fluxes for Very High Excitation Planetary Nebulae

		IC2165	NGC3211	NGC6818	NGC7027	Hu 1 - 2
Diameter (arcsec)		8.0	13.8	18.4	14.2	5
Excitation Class		9	8	9	10p	10
Central Star		cont?	?	cont.	-	-
1239/41	NV	0.44	0.46	0.47	(0.71)	0.71
1309	SiII	-	-	-	1.21	-
1335	CII	-	0.17	-	z	-
1391	SiIV	-	-	(1.54)	-	-
1403/09	OIV]	0.82	1.74	-	-	0.54
1487	NIV]	1.02	1.72	2.22	0.65	1.85
1548/50	CIV	21.95	4.42	7.05	17.06	5.49
1575	[NeV]	-	-	z	-	-
1640	HeII	6.71	14.90	21.88s	3.47	5.55
1661/66	OIII]	0.62	1.12	1.78	z	-
1747	NIII	0.63	1.07	1.51	-	1.53
1817	[NeIII], SiII	0.18	-	-	-	-
1892	SiIII	z b	z b	0.67	z b	-
1907/09	CIII]	21.84bs	28.83b	35.92	9.64b	3.95
2252	HeII	1.00	-	-	1.03	-
2297	CIII	-	-	0.21	-	-
2325/29	CII], [OIII]	1.36	1.21	2.11	1.90	0.43
2423/26	[NeIV]	2.70s	5.44s	8.37	1.02	2.26
2470	[OII]	-	-	-	0.53	-
2511	HeII	0.28	0.29	0.57	-	0.22
2734	HeII	1.31	0.96	1.23	0.49	0.36
2784	[MgV]	0.37	0.27	0.50	2.29b	-
2830	HeI	0.86	0.34	0.72	0.40b	-
2929	MgII	-	-	0.11	0.27	-
3024	OIII	0.36	-	0.54	0.67	-
3047	OIII	1.80	0.80	1.20b	1.17	0.37
3133	OIII	9.83s	4.23	8.33	11.03	0.87
3204	HeII	2.40	(2.12)	3.30	1.61	(1.00)

THE CARBON ABUNDANCE IN TWO H II REGIONS OF THE SMALL MAGELLANIC CLOUD

Reginald J. Dufour and Raymond J. Talbot, Jr.
Rice University

Gregory A. Shields
University of Texas at Austin

ABSTRACT

Observations of the ultraviolet spectra of two locations in the H II region NGC 346 and of the entire H II region IC 1644 in the Small Magellanic Cloud (SMC) were made using the International Ultraviolet Explorer (IUE) satellite. From measurements of the C III] λ1909 lines, the abundance of carbon in the nebulae was derived using theoretical model analysis combined with ground-based spectrophotometry of other emission lines. The abundance of C relative to H in the SMC was found to be lower by -0.9 dex compared with the Sun and lower by -0.8 dex compared with the Orion Nebula. This C deficiency is similar to that of O, Ne, S, and Ar in the SMC, but not as great as found for N (≈ - 1.2 dex). Therefore, it is concluded that the sites and history of C nucleosynthesis in galaxies is similar to that of O, Ne, S, and Ar, in contrast to that of N, which appears to be more complex, perhaps because of a mixture of secondary primary sources or a significant contribution from intermediate-mass long-lived stars.

INTRODUCTION

The Large and Small Magellanic Clouds (LMC and SMC) provide a unique opportunity to study in detail the structure and composition of two galaxies representing an earlier epoch in the chemical evolution of galaxies compared with our own. Recent ground-based spectroscopic studies of H II regions in the Clouds by the Peimberts (refs., 1,2), Aller et al. (refs. 3,4), Pagel et al. (ref. 5), and Dufour (refs, 6.7), show that [O/H] is -0.5 in the LMC and -0.9 in the SMC (where the bracketed ratio represents the difference of the logarithm of the abundance ratio between the galaxy and the sun). Nitrogen shows the greatest deficiency of all elements studied (He, N, O, Ne, S, and Ar) with [N/H] ≈ -1.1 in the LMC and [N/H] ≈ -1.4 in the SMC. Also, helium is slightly deficient in H II regions in the Clouds compared with similar nebulae in the Galaxy.

While spectrophotometric studies of H II regions in the Magellanic Clouds with ground-based telescopes have resulted in the accurate determination of the abundances of a number of elements of astrophysical importance, others, such as carbon, can only be readily observed in the ultraviolet. Therefore, we have initiated observations of the ultraviolet spectra in the λλ1135-3255 Å range of several H II regions in the LMC and SMC with the International Ultraviolet Explorer (IUE) satellite. In this note we report the first results of observations of two H II regions in the SMC.

OBSERVATIONS AND RESULTS

The spectra of two H II regions in the SMC, NGC 346 and IC 1644, were obtained in May 1979 with the Short Wavelength Prime (SWP) and Long Wavelength Redundant (LWR) cameras of the IUE at low dispersion. The SWP observations covered the λλ1135-2085 region with a spectral purity of 30 Å. The 10 x 20 arc second elliptical aperture was used in all of the observations. Emphasis was placed on the SWP observations in order to measure the C III] λ1909 and C IV λ1549 lines necessary for determining the carbon abundance.

The nebula NGC 346 is the most prominent H II region in the SMC located in the northeast area of the main body of stars. It is listed as N66 in Henize's (ref. 8) catalog of LMC and SMC emission nebulae. Since the nebula has a significant apparent size, 490 x 580 arc seconds, two locations were observed: N66A--a bright knot located in the southern part of the nebula, and N66NW--a smooth star-free area located in the northwest lobe of the nebula. These two locations were chosen primarily because there exists published ground-based photoelectric spectrophotometry of them (refs. 2, 7).

The nebula IC 1644 is a small (~ 10 arc second diameter) H II sphere of high surface brightness located southeast of the SMC bar in the Shapley's "wing" feature. It is listed as N81 in Henize's catalog. Dufour et al. (refs. 7, 9) have published photoelectric and photographic spectrophotometry for all significant emission lines in the λλ3727-7136 spectral region of N81 from ground-based observations.

Generally two or more integrations of each location were obtained with the SWP and LWR cameras. A log of the observations is given in Table I. The observations of NGC 346/N66A and NGC 346/N66NW regions were obtained during the US1 shift and have low particle background. The IC 1644/N81 observations were obtained during the US2 shift and have very high particle noise backgrounds. In addition, the underlying stellar continuum is considerable for NGC 346/N66A and particularly so for IC 1644/N81. Because of the high particle background and stellar continuum encountered in the IC 1644/N81 observations, only two 10-minute SWP integrations were usable for quantitative measurements of the five obtained.

The photometrically and geometrically corrected spectra on the GO tapes prepared by NASA/GSFC were analyzed using interactive picture processing systems at Rice University and at NASA/JSC in Houston. SWP spectra processed with the incorrect Intensity Transfer Function were corrected with the three-agency 4th file method. The resulting 55 line x 602 word spectra background arrays where then analyzed using a FORTH interactive spectral analysis system originally developed by F.H. Schiffer, III at NASA/JSC. This permitted us to use a variety of smoothing, background subtraction, and spectral extraction techniques optimized for each observation. The only prominent lines (other than Ly α predominantly from the geocorona) detected in the nebulae were the C III] λ1909 pair unresolved on our own spectra; as was Mg II λλ2796,2804, which might have been expected to be detectable on some of the LWR spectra.

Measurements of the C III] λ1909 strengths were made using an interactive Tektronixs cursor routine to set continuum levels and integrate areas. Several measurements of each line were made in an attempt to evaluate the magnitude of possible errors due to the prejudice of the operator in setting the continuum level, estimating the line width, etc. Comparison of the line strengths measured on two different spectra of a given object provided an

estimate of the instrumental errors. The areas in instrumental units (FN) were converted to the observed flux in ergs sec^{-1} cm^{-2} using the large aperture SWP calibration for low dispersion derived by Bohlin et al. (ref. 10). These were corrected for interstellar extinction (which is rather small for the SMC) using the UV extinction curve of Savage and Mathis (ref. 11) along with published extinctions for the nebulae from ground-based observations of the $H\alpha/H\beta$ ratios. The 1909 reddening-corrected fluxes were then scaled to the Hβ fluxes observed for each region by previous investigations. For the two regions in NGC 346 we used the ratio of the areas of the IUE and ground-based entrance apertures; while for the smaller nebula IC 1644 we assumed that it was entirely within both the IUE and ground-based apertures.

The line intensities for C III] λ1909 derived from our observations along with those of other important diagnostic lines observed from the ground are presented in Table II. We also present estimated upper limits to the C IV λ1549 and Mg II λ2800 lines derived from the IUE spectra. We give estimated errors for the λ1909 intensities based primarily on the uncertainties in the measurements of the line profiles. The actual errors for λ1909 may be two or three times larger, due to the uncertainties in scaling the IUE λ1909 fluxes to the ground-based $H\beta$ fluxes as well as uncertainties in the absolute calibration of the IUE SWP spectra. The ground-based observations were made with photoelectric scanners and have probable errors of the order of 10 percent. Other relevant data about the nebulae are presented in the tables also.

ANALYSIS AND DISCUSSION

Elemental abundances for H, He, C, N, O, Ne, S, and Ar in the nebulae were derived by Shields using a nebula modeling code similar to that used in previous studies of H II regions in M101 (ref. 12) and M83 (ref. 13). Since all three nebulae have rather similar spectra, we used a single model differential analysis approach. A "standard model" was calculated to match the spectrum of NGC 346/N66A (T^*_{eff} = 45,000°K) and used to derive the temperature fluctuations for various ions compared with $T(O^{++})$ obtained via the [O III] λλ5007/4363 ratio. The computed fluctuations were used with the observed [O III] temperatures and line strengths to calculate various ionic abundances for those ions with observed lines. Elemental abundances were then inferred from these ionic abundances using ionization corrections for ions without observed lines from the standard model. The final results are presented in Table III.

Using the estimated upper limits to the strengths of the C IV λ1549 lines for NGC 346/N66A in the model, we found that about 92 percent of the carbon in the H^+ zone was in the form of C^{++}. Consequently, the corrections for C^+ and C^{+++} in the SMC nebulae are small, so the fact that we did not observe C IV should not significantly affect the accuracy of the C abundances derived. Based on model and observational uncertainties in $T(O^{++})$ alone, we estimate that the uncertainty in the C abundance for the various nebulae is about 0.1 dex. The good, but possibly fortuitous, agreement of the C abundances between the three nebulae suggests that the accuracy by which the C abundance is now known in the SMC is better than ± 0.2 in the logarithm. Since this model is also the first theoretical model analysis of an H II region in the SMC, it is gratifying to note that the other abundances calculated agree very well with those of previous investigations for which the analyses were based on standard nebular diagnostic formulae.

On the right side of table 3 we give the logarithmic differences between the SMC mean abundances and those determined for the Sun (ref. 14 for C,N, and O; ref. 15 for He, Ne, Mg, S, and Ar) and for the Orion Nebula (ref. 16). It is clear from inspection of the table that the C/O ratio in the SMC is essentially identical to that found for the Sun and the Orion Nebula. The abundance deficiency of C relative to H in the SMC compared with the Sun and Orion is clearly more similar to that of the elements O, Ne, S, and Ar than to that of N, which is substantially more deficient than the others. Therefore, we conclude that the nucleosynthesis of C follows closely that of O, Ne, S, and Ar as predicted by theoretical nucleosynthesis models(refs. 17,18) . The large variation of N/O while C/O remains constant implies that the stellar sources of N do not contribute a large fraction of the C.

It is of interest to compare this result with the recent study of abundances in several high excitation planetary nebulae with the IUE by Aller and Keyes (ref. 19). Several of the nebulae studied were overabundant in N by factors of 5-10 compared to solar and Orion values. None of these N-rich nebulae showed significant enhancements in the C abundance. These results and ours suggest that the site(s) of C nucleosynthesis is the same as that of O, Ne, S, and Ar. The processes, presumably from intermediate mass stars (ref. 20), which subsequently enrich galaxies with N later in their evolution apparently do not significantly affect the relative abundances of C, O, Ne, S, and Ar.

We also note in ending that the Mg abundance found for the two locations in NGC 346 using our estimated upper limit is at least 1.4 dex lower than the solar value. Unless the nucleosynthesis of Mg is similar to that of N in the SMC, which is unlikely, the low abundance of Mg is apparently due to its depletion by dust in the H II regions. The magnitude of this depletion is then rather surprising, when one notes that the dust content of the SMC is very low compared with the LMC and our galaxy.

REFERENCES

1. Peimbert, M. and Torres-Peimbert, S., 1974. Astrophys. J., 193, 327.
2. Peimbert, M. and Torres-Peimbert, S., 1976. Astrophys. J., 203, 581.
3. Aller, L.H., Czyazk, S.J., Keyes, C.D., and Boeshaar, G., 1974. Proc. Nat'l. Acad. Sci. USA, 71, 4496.
4. Aller, L.H., Keyes, C.D., and Czyzak, S.J., 1979. Proc. Nat'l. Acad. Sci. USA, 76, 1525.
5. Pagel, B.E.J., Edmunds, M.G., Fosbury, R.A.E., and Webster, B.L., 1978. Mon. Not. R. Astr. Soc., 184, 569.
6. Dufour, R.J., 1975. Astrophys. J., 195, 315.
7. Dufour, R.J., and Harlow, W.V., 1977. Astrophys. J., 216, 706.
8. Henize, K.G., 1956. Astrophys. J. Suppl., 2, 315.
9. Dufour, R.J., and Killen, R.M., 1977. Astrophys. J., 211, 68.
10. Bohlin, R.C., Holm, A.V., Savage, B.D., Snijders, M.A.J., and Sparks, W.M., 1980. Astron. and Astrophys., in press.
11. Savage, B.D., and Mathis, J.S., 1979. Ann. Rev. Astron. and Astrophys., 17, 73.
12. Shields, G.A., and Searle, L., 1978. Astrophys. J., 222, 821.
13. Dufour, R.J., Talbot, R.J., Jr., Jensen, E.B., and Shields, G.A., 1980. Astrophys. J., 236, 119.
14. Lambert, D.L., 1978. Mon. Not. R. Astr. Soc., 182, 249.

15. Cameron, A.G.W., 1973, in Explosive Nucleosynthesis, eds., D.N. Schramm and W.D. Arnett, Univ. of Texas Press: Austin, p.3
16. Peimbert, M., and Torres-Peimbert, S., 1977. Mon. Not. R. Astr. Soc., 179, 217.
17. Talbot, R.J., Jr., and Arnett, W.D., 1973. Astrophys. J., 186, 51.
18. Arnett, W.D., 1978. Astrophys. J., 219, 1008.
19. Aller, L.H., and Keyes, C.D., 1979. UCLA Astron. and Astrophys. Preprint No. 82.
20. Edmunds, M.G., and Pagel, B.E.J., 1979. Mon. Not. R. Astr. Soc., 185, 77P.

TABLE I -- IUE OBSERVATIONS LOG

Nebula	SWP Exposures (min)	LWR Exposures (min)
NGC 346/N66A	30,120	30
NGC 346/N66NW	120,180	30,30
IC 1644/N81	10,10,15*	20,20,20
	20*, 60*	30*

*Not usable due to saturated pixels + high background

TABLE II - LINE INTENSITIES FOR SMC H II REGIONS

λ(A)	ION	NGC346 N66A	NGC 346 N66NW	IC 1644 N81
1548,1551	C IV	<20	<15	<30
1907,1909	C III]	123.±19.*	120.±10.*	162.±32.*
2796,2804	Mg II	<20:	<20.	-
3726,3729	[O II]	95.5	108.	128.
3869	[Ne III]	44.7	35.0	37.8
4340	Hγ	46.8	46.6	45.5
4363	[O III]	7.08	6.07	6.44
4471	He I	---	3.33	3.50
4861	Hβ	100.	100.	100.
4959	[O III]	---	172.	177.
5007	[O III]	513.	501.	525.
5876	He I	10.2	11.0	11.9
6312	[S III]	2.6:	1.8	---
6563	Hα	282.	286.	286.
6584	[N II]	4.37	6.38	6.30
6678	He I	2.95	3.51	3.08
6716	[S II]	6.76	} 14.4	6.0
6730	[S II]	4.47		5.4
7136	[Ar III]	9.77	--	6.7:
7320,7330	[O II]	2.34	___	
	C(Hβ)	0.17	0.07	0.04
	log I(Hβ)	-11.41	- 11.12	-11.02
	reference (optical)	1	7	7, 9

*Errors quoted for λ1909 are based on comparative statistics between two observations; actual errors due to absolute calibration of IUE and zero point transfers may be two or three times larger.

TABLE III -- MODEL ABUNDANCE RESULTS

	(1) NGC 346 / N66A	(2) NGC 346 / N66NW	(3) IC 1644 / N81	(4) MEAN / SMC	(5) SUN (refs. 14, 15)	(6) ORION (ref. 16)	(7) (4) - (5)	(8) (4) - (6)
He	10.91	10.92	10.94	10.92	---	11.00	---	-0.08
C	7.64	7.76	7.85	7.75	8.67	8.52	-0.92	-0.77
N	6.49	6.69	6.68	6.62	7.99	7.76	-1.37	-1.14
O	8.00	8.06	8.06	8.04	8.92	8.75	-0.88	-0.71
Ne	7.23	7.20	7.20	7.21	8.03	7.90	-0.82	-0.69
Mg	<6.1	<6.1	---	<6.1	7.52	---	<1.4	---
S	6.4:	6.6:	6.6:	6.6:	7.20	7.41	-0.6	-0.8
Ar	5.80	---	5.66	5.73	6.57	6.7:	-0.84	-1.0
C/N	1.15	1.07	1.17	1.13	0.68	0.76	0.45	0.37
C/O	-0.36	-0.30	-0.21	-0.29	-0.25	-0.23	-0.04	-0.06

SUPERBUBBLES

Theodore R. Gull
Laboratory for Astronomy and Solar Physics
NASA/Goddard Space Flight Center

Frederick C. Bruhweiler
Computer Sciences Corporation

Minas Kafatos
George Mason University

Sabatino Sofia
Laboratory for Astronomy and Solar Physics
NASA/Goddard Space Flight Center

ABSTRACT

Individual massive stars with $M_{bol} < -6$ have huge stellar winds that create interstellar bubbles. Stars with masses greater than $8M_\odot$ ($4M_\odot$?) are considered supernova progenitors. These massive stars are numerous in OB associations where few supernova remnants are detected. Model calculations describing the evolution of an association show: 1) that large, hot cavities are formed by pushing the ambient gas into neutral shells; 2) that the shell radii change with galactocentric radius, 3) that only thirty percent of the interstellar medium is in the form of supercavities and 4) that a consequence is that only a small fraction of supernovae form supernova remnants. These results have strong bearing on interpretation of interstellar studies being done by IUE and by HEAO-B.

INTRODUCTION

The previous talk (ref. 1) described the observable interstellar bubble being driven by an O star, HD148937. Other talks (ref. 2,3) discussed IUE observations of supernova remnants which presumably had massive stars as progenitors. We know that O and B stars form as associations throughout the galactic plane. If individual stars can dramatically alter the interstellar medium, we are led to wonder what an OB association would do. The model calculations discussed here described the bulk properties of how the surrounding interstellar medium is changed as an OB association evolved. The resultant structure of the interstellar medium can be studied by IUE and HEAO-B and indeed such studies are underway at present.

THE BASIS FOR CONSIDERING SUPERBUBBLES

Our interest in the structure of the interstellar medium has been whetted by a recent emission line survey of the Milky Way (ref. 4). It presents a photographic record of nearby dust clouds and ionized hydrogen regions with a rough excitation classification being possible by singly-ionized sulfur imagery and by doubly-ionized oxygen imagery. Several new supernova remnants (ref. 5, 6) were discovered from this data. Many interstellar bubbles in the form of bowshocks (ref. 7), arcs and shells (ref. 8 and 9) were newly detected. However, ionization structure around OB

associations varied considerably. We were led to ask how a supernova remnant, formed within an OB association, would be detected. The answer proved non-trivial, but opened up the realization that OB associations play a major role in determining structure of the interstellar medium.

Supernova remnants within our galaxy present an enigma: there do not seem to be enough. Based upon statistics of supernova events within similar galaxies, we should expect one every thirty years (ref. 10). If we assume that pulsars are stellar remnants left over from supernova events, then pulsar statistics imply a supernova every ten years (ref. 11). We might expect that for every supernova there should exist, for a finite time, a supernova remnant generated by the ejecta propagating through the interstellar medium. Yet the supernova rate derived from statistics of supernova remnants is about one every eighty years (ref. 12).

Related to this puzzle is the apparent lack of supernova remnants within OB associations. There simply is a lack of non-thermal radio emission plus associated filamentary optical shells within OB associations.

An intriguing clue comes from 21-cm studies (ref. 13), that large shells of neutral hydrogen having 100 to 2000 pc radii were scattered throughout the galactic plane. Because the associated kinetic energies exceeded the available energy of a supernova by a factor of 100, Heiles (ref. 13) postulated a type III supernova event. We find a more reasonable explanation is available based upon evolutionary products of an OB association.

AN EVOLUTIONARY MODEL OF OB ASSOCIATIONS

A simple model was devised based upon the kinematic properties of stellar winds plus supernovae in an OB association (ref. 14). The model could be divided into three phases: A. Bubble Phase, B. First Supernova Phase, and C. Late Supernova Phase. The bubble phase lasts for about 3×10^6 years during which the approximately thirty stars with $M_{bol} < -6$ push the interstellar medium away with the combined stellar winds. For a typical OB association these most massive stars have the following averaged properties: $\bar{M}_{bol} = -8.8$, $\dot{M} \sim 10^{-6} M_\odot$ yr^{-1}, $v_t \sim 2000$ km s^{-1}, where M_{bol} is the bolometric magnitude, $\dot{M}$ is the mass loss rate in solar masses, $M_\odot$, per year, and v_t is the terminal wind velocity. For an individual star an interstellar bubble is driven outward by the stellar wind. The bubble radius is (ref. 15):

$$R_B = 27\ n^{-1/5}\ L_{36}^{1/5}\ t_6^{3/5}\ \text{pc} \qquad (1)$$

with outward moving velocity of

$$V_B = 16\ n^{-1/5}\ L_{36}^{1/5}\ t_6^{-2/5}\ \text{km s}^{-1} \qquad (2)$$

where

$$L_{36} = \frac{1}{2}\ \dot{M}\ v_t\ 10^{36}\ \text{ergs s}^{-1} \qquad (3)$$

(n = ambient interstellar medium number density and t_6 = time in 10^6years).

The first supernova phase begins at about 3×10^6 years when the 30 most massive stars ($M \geq 15M_\odot$) become supernovae. The ejecta initially has little interstellar gas to shock until it has expanded to the shell radius ($\gtrsim$85 pc). Because the shell is mostly HI and H_2 gas and because the ejecta is very dilute when it shocks the shell, the temperature is not very high and the shell evolution is well described by the snowplow model for supernovae. The shell expands with time as:

$$R_S(t) = R_1^4 + 3\frac{M_1 V_1}{n\mu_H m_H \pi}(t-t_1)^{1/4} \qquad (4)$$

with

$$V_S(R_S) = R_S^{-3}\frac{3M_1V_1}{4\mu m_H n\pi}$$

This phase lasts until the shell stalls or until the second wave of supernovae occur.

The second supernova phase commences as stars down to $8M_\odot$ become supernovae. This occurs at $t \sim 10^7$ years and serves to maintain and/or enlarge the shell. Approximately 180 stars exceed $8M_\odot$ and contribute to the second phase. The shell radius becomes 170 to 700 pc before stalling. We note that <u>if</u> stars as low as $4M_\odot$ become supernovae, then the shell will continue to expand and be maintained longer.

The model calculations included number densities with scale heights and gravitational restoring forces depending upon the z-distance and for three galactocentric radii: 5 kpc, 10 kpc and 20 kpc. As the gravitational force only affects the bubble in the z-direction, bubble radii, etc. were calculated for parallel to the plane and perpendicular to the plane (Table 1). The radii perpendicular to the plane, being least affected by galactic rotation, are felt more reliable. We find that the bubble radius changes with galactocentric radius as calculated by our model (Figure 1).

Of about 50 hydrogen shells, we find only six to be associable with OB associations. This is not surprising as the larger bubbles would surround very evolved associations with remaining spectral types trending towards A. Moreover, interstellar extinction prevents detecting the more distant associations. Approximately thirty percent, not ninety percent, of the interstellar medium is superbubble interiors. This indeed will produce only arcs, or partial shells as shells break into adjacent shells, setting up hot, ionized tunnels.

MODELLING THE SUPERNOVA REMNANT OCCURRENCES

We realized that supernovae occurring within an interstellar bubble or superbubble would not create the classically detectable supernova remnants. Basically, a supernova remnant is the product of ejecta interacting with the ambient interstellar gas (ref. 16). Until the supernova ejecta ($\sim 5M_\odot$) has swept an equivalent amount of material, the ejecta is in free expansion.

By the time the supernova ejecta has expanded to encounter the shell boundary it is too diffuse and only a brief flash (like Barnard's Loop) is detected. Studies of detected supernova remnants both in the Milky Way and the Magellanic Clouds suggest supernova remnants are detectable only if the ambient density exceeds 0.1 cm^{-3}.

A compensating factor includes the knowledge that many runaway stars occur and some B stars diffuse from the association beyond the hot cavity into the neutral shell. About two-thirds of all stars are in binary systems. In a massive binary system, the more massive star explodes and tends to fling the less massive star away. The lower-massed star then becomes a runaway star. (Twenty percent of all OB stars appear to be runaways (ref. 17)). Those runaway OB stars that escape the hot cavity create the detectable supernova remnants.

Only a small fraction escape the supercavities. Since the shell radii are much smaller at 5 kpc, more escape the hot cavity than at 10 kpc. No OB stars escape the hot cavity at 20 kpc. Hence, the model demonstrates a very galactocentric distribution of supernova remnants. We also note that the OB stars that escape are on the lower mass portion of the OB star mass function. There indeed may be a narrow mass range of OB stars that produce detectable supernova remnants. Based upon thirty percent of the interstellar medium being supercavities, the following percentages of supernovae create detectable supernova remnants:

R gal = 5 kpc	15 percent to 30 percent
= 10 kpc	9 percent to 23 percent
= 20 kpc	0 percent

The distribution of supernova remnants is maximum near the galactic center and zero beyond 20 parsecs. Radio observations bear this out.

CLOSING COMMENTS

The superbubbles, along with hot supercavities around OB associations provide a model for comparing interstellar column densities, velocity components and degree of ionization. Perhaps the most important test regions are young OB associations, like Orion OB 1, where the first supernova events should have occurred. Very highly ionized gases should be interior, with rapidly expanding HII, HI and H_2 shell components.

We note that a Crab-like supernova remnant, namely ejecta still interacting with the expelled magnetic fields, will be detectable for several thousand years. With a 50,000 year interval between supernovae within a specific OB association, about six percent of the OB associations would have a detectable supernova remnant at any given time. However, very hot interiors with isothermal X-ray emission should occur for much longer times. We point out that the Carina Nebula has a diffuse component seen by HEAO-B (ref. 18) and suggest more detailed studies be done to check our models. We are already investigating several superbubbles in our galaxy using IUE and HEAO-B, and we are studying shell structures in the Magellanic Clouds using HEAO-B.

REFERENCES

1. Bruhweiler, F. C.; and Gull, T. R.: included in this volume, 1980.

2. Raymond, J.: included in this volume, 1980.

3. Davidson, K.; Gull, T. R.; Stecher, T. P.; Maran, S. P.; Kafatos, M.; and Trimble, V.: included in this volume, 1980.

4. Parker, R.; Gull, T.; and Kirshner, R.: An Emission Line Survey of the Milky Way. NASA SP-434, 1979.

5. Gull, T.; Kirshner, R.; and Parker, R.: Ap. J. Letters, 215, 69, 1977.

6. Blair, W.; Kirshner, R.; Gull, T.; Sawyer, D.; and Parker, R.: submitted to Ap. J.

7. Gull, T.; and Sofia, S.: Ap. J., 230, 782, 1979.

8. Heckathorn, J.; and Gull, T.: to appear in BAAS.

9. Chu, Y-H.; and Gull, T.: in preparation, 1980.

10. Tammann, G. A.: Supernovae and Supernova Remnants. Ed. C. B. Cosmavici, (Dordrecht:Reidel). 1974, p. 155.

11. Tayler, J. H.; and Manchester, R. N.: Ap. J., 215, 885, 1974.

12. Caswell, J. L.; and Lerche, I.: MNRAS, 187, 201, 1979.

13. Heiles, C.: Ap. J. 229, 533, 1979.

14. Bruhweiler, F.; Gull, T.; Kafatos, M.; and Sofia, S.: Ap. J. Letters, May 15, 1980.

15. Weaver, R.; McCray, R.; Castor, J.; Shapiro, P.; and Moore, R.: Ap. J. 218, 377, 1977.

16. Kafatos, M.; Sofia, S.; Bruhweiler, F.; and Gull, T.: submitted to Ap. J., 1980.

17. Cruz-Gonzalez, C.; Recillas-Cruz, E.; Costero, R.; Peimbert, M.; and Torres-Peimbert, S.: Revista Mexicana de Astron y Astrof, 1, 211, 1974.

18. Seward, F.; Forman, W.; Giacconi, R.; Griffiths, R.; Hernden, F.; Jones, C.; and Pye, J.: Ap. J. Letters, 234, L55, 1979.

TABLE . EXPANSION OF SHELLS AT SELECTED DISTANCES FROM THE GALACTIC NUCLEUS, R_{GAL}, IN THE GALACTIC PLANE

R_{gal} (kpc)	v(km s^{-1})	Parallel to the Plane			Perpendicular to the Plane		
		$t(10^6 yr)$*	R_s(pc)	$\bar{n}(cm^{-3})$	$t(10^6 yr)$*	R_s(pc)	$\bar{n}(cm^{-3})$§
		A. End of Bubble Phase					
5	17	3	85	3	3	85	3
10	21	3	106	1	3	105	1
20	33	3	168	0.1	3	168	0.1
		B. End of First Supernova Burst Phase ($M \geq 15M_\odot$)					
5	5	8.6	137	3	9	170+	0.44
10	5	11	185	1	10	207	0.37
20	5	19	357	0.1	17	384	0.054
		C. End of Second Supernova Burst Phase ($M \geq 8M_\odot$)					
5	-	14	179	3	-	170+	0.44
10	5	19	251	1	37	497	0.086
20	5	43	520	0.1	46	693	0.033

* t is the total characteristic time of the shell expansion through each phase.

\+ Expansion has exceeded R_{crit} and the shell size is now limited by gravitational deceleration (see text).

§ $\bar{n}$ is the average of the region between the initial z and final z for each phase and is derived as:

$$\bar{n} = \frac{\pi n_o \int_{z_1}^{z_2} z^2 e^{-z/h} dz}{4/3\pi(z_2^3 - z_1^3)}$$

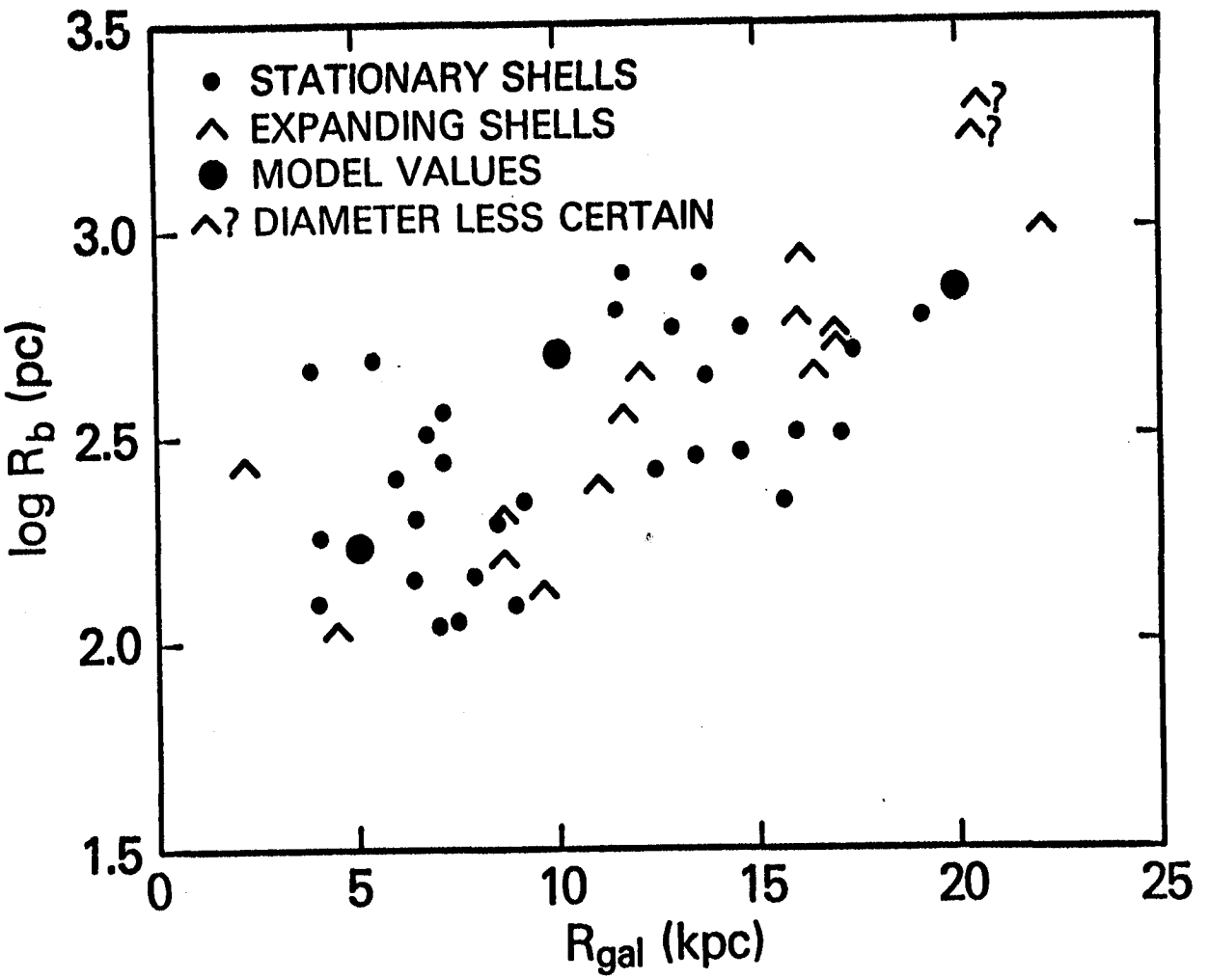
STATIONARY SHELLS
EXPANDING SHELLS
MODEL VALUES
DIAMETER LESS CERTAIN
log R_b (pc)
R_{gal} (kpc)
3.5
3.0
2.5
2.0
1.5
0
5
10
15
20
25

Figure 1

THE YOUNG Of STAR HD148937 AND ITS ASSOCIATED INTERSTELLAR BUBBLE - H II REGION

Frederick C. Bruhweiler
Computer Sciences Corporation

Theodore R. Gull
NASA/GSFC, Laboratory for Astronomy and Solar Physics

ABSTRACT

HD148937 and nebulosities surrounding the star are found to be closely inter-related. IUE spectroscopy of HD148937 shows the star to be a young Of star with low mass loss. Properties of the surrounding interstellar bubble and the H II region support the implied youth of HD148937.

DESCRIPTION OF NEBULOSITIES

The peculiar Of star HD148937 with its symmetrical S-shaped nebulae, NGC 6164 and 6165 plus the two gaseous shell structures enshrouding this star make it one of the most intriguing objects in the sky.

As photographs reveal, the outermost shell is very thin, dusty, and very nearly circular. This shell extends 44' to the northeast and 64' to the west of HD148937. The mottled appearance and the increase of dust to the east may indicate that the eastern rim of this shell is interacting with the nebula NGC 6188.

Enclosed within this thin shell is what appears to be an H II region. Narrow bandpass photography shows diffuse emission in Hα and [O III] λ5007 emanating from this interior region. The inner periphery of this H II region is marked by a thin filamentary arcuate structure traced out by well defined [O III] emission. This inner filamentary shell or 'halo' has a major axis of 20' and a minor axis of 15' (aligned with the major and minor axes of the inner nebulosities NGC 6164-5). The filamentary nature of this halo is identical to that seen in shock interfaces in supernova remnants. Inside this halo appears to be a real hole in the diffuse emission. The detectable emission in this region is limited to the well defined blobs defining NGC 6164-5.

The inner nebular complex NGC 6164-5 shows remarkable symmetry and has been considered a planetary nebula. However, Westerlund (1960) rejected this hypothesis based upon the luminosity of HD148937. The notable investigation of Pismis (1974), concluded that the symmetry of these blobs of gas were indeed strong evidence that they were ejected by the central star.

THE CENTRAL STAR: HD148937

The central star HD148937 has been identified as an extreme Of star classified as either O6f (Westerlund 1960) or O7f (Hutchings 1976). Westerlund by assuming membership in the ARA OB1 association derived

M_V = -6.2 corresponding to a distance of 1400 pc. However, Hutchings, based upon the Hα equivalent width, derived a more luminous $M_V = -7.2 \pm 0.4$.

Recently, from studies of IUE high-dispersion spectra, Hutchings and Rudloff (1980) find high mass-loss rates for extreme Of stars. Yet, the two extreme Of stars HD108 and HD148937 were exceptions and did not fit into this scheme. The UV resonance profiles of C IV and Si IV in these stars were unsaturated indicating mass-loss rates of $2 \times 10^{-7} M_\odot\ yr^{-1}$, a rate two orders of magnitude below what is expected from extreme Of stars. The reason for these low mass-loss rates remain unexplained. A clue may be found in that Hutchings and Rudloff refer to a private communication by Walborn who noted that these stars are quite different in their spectral morphology from other Of stars; an aspect also described by Westerlund (1960) in the case of HD148937.

The narrow bandpass photographs show very strong diffuse [O III] indicating a rather hot O star exciting NGC6188, the nebula immediately to the east of HD148937. Two O stars HD150135 (O6.4V) and HD150136 (O5III) fall on the sky where the most intense emission is observed.

In Table 1, the pertinent information for these stars is given. By adopting M_V = -5.0 for a typical O6.5V star (Panagia 1973) and assuming interaction of the large circular shell and NGC6188, we deduce a distance of 1200 for both HD150135 and HD148937. This in turn implies a M_V = -5.7 for HD148937. This is a luminosity much less than found by Hutchings (1976) and slightly lower than adopted by Westerlund (1960). Clearly the H II region around HD148937 is in the foreground to NGC6188 and likely interacting with it. As such, M_V = -5.7 represents an approximate upper limit to the luminosity of HD148937.

Examination of an IUE high-dispersion spectrum of HD148937 loaned to us by Peter Conti revealed that it closely mimicked UV spectra of O stars like the subdwarf HD48798 and the MK spectral standard 15 Mon (O7 V). One might add that by accepting that HD148937 is near the main sequence that the low mass-loss rate found for this star in the UV is no longer discrepant since mass-loss rates of main-sequence stars are much lower.

PHYSICAL CONDITIONS AND AGES OF NEBULOSITIES

In order to estimate the physical conditions in the outer nebula we adopt the approach of Lasker (1967, 1966) in describing H II regions. For this discussion the interstellar medium interior to the filamentary 'halo' can be ignored. Using the data from Panagia (1973) and taking radii of the H II region corresponding to the range of possible luminosities and distances of HD148937 (i.e. ZAMS to a star of M_V = -5.7) we can derive the parameters describing the physical conditions of the expanding H II region surrounding HD148937.

As a H II region expands into the interstellar medium at some point a compressed neutral shell forms just ahead of the ionization front. This best describes what we see in the outer nebula surrounding HD148937. In this case, the thin dust shell delineates the compressed neutral gas.

With the relative thickness of this dust shell ($1-ri/_{rs}$), and the physical dimensions in hand we can use the models and approximations of Lasker (1960, 1966) to estimate the physical conditions and age of this H II region. The results are given in Table 2 for values for a star with $M_V = -4.7$ (a star near the ZAMS) and for a star with $M_V = -5.7$. These results indicate that the H II region is quite young with an age on the order of 3×10^5 to 6×10^5 yrs.

If we consider that the inner shell or filamentary halo is due to an interstellar bubble, the snowplow approximation gives for the radius of the bubble (Weaver, McCray, and Castor 1977)

$$R = 27\ n_6^{-1/5}\ L_{36}^{1/5}\ t_6^{3/5}\ \text{pc.}$$

This was determined by scaling the mass-loss rate found by Hutchings and Rudloff to the lower luminosities found relevant here. Taking the angular dimensions of the inner halo structure, we find the range of deduced ages varying from 2.4×10^5 to 5×10^5 years for the less and more luminous cases at 790 and 1200pc respectively. These results compare favorably with the ages determined for the H II region for these same two cases.

CONCLUSION

The ages implied from the interstellar bubbles and the H II region imply a young age and are in relatively good agreement. In addition, the UV spectrum is very similar to other high gravity O stars. The evidence strongly favors the interpretation that HD148937 is an unevolved O star. The inner S-shaped nebulosity (NGC 6164-5) may in fact be due to instabilities which have occurred in a very young O star. The remarkable symmetry of this nebulosity has lead Pismis (1974) to suggest that this material was ejected from the polar regions of the central star.

The strong similarities of this nebulosity to planetary nebulae plus the fact that HD148937 is quite bright ($M_V = 6.71$) suggest that similar objects may be masquerading as planetary nebulae.

Table 1

HD148937 and the Exciting Stars of NGC 6188

star(HD#)	Sp. Type	V	A_V
148937	06-07V	6.71	1.98
150135	06.5V	6.89	1.47
150136+	05III	5.62	1.44

\+ possible binary

Table 2

Physical Conditions of the H II Region

	CASE A	CASE B
distance	790 pc	1200 pc
ionization radius	12 pc	18.5 pc
interior number densities	10 cm^{-3}	13.4 cm^{-3}
shell density	37-70 cm^{-3}	50-95 cm^{-3}
ambient number density	17-18 cm^{-3}	22.5-24
$1-(r_i/r_s)$	.05-.09	.05-.09
t_{char}	3.5×10^5 yr.	5×10^5 yr.
S_o	8-8.5 pc	12.5-13 pc

REFERENCES

Hutchings, J. B. 1976, Ap. J. 203, 438.

Hutchings, J. B. and von Rudloff, I. R. 1980, preprint.

Lasker, B. M. 1966, Ap. J. 143, 700.

Lasker, B. M. 1967, Ap. J. 149, 23.

Pismis, P. 1974, Revista Mexicana de Ast. y Ap. 1.

Weaver, R., McCray, R. and Castor, J. 1977, Ap. J. 218, 317.

Westerlund, B. 1960, Archiv fur Astr. 2, 467.

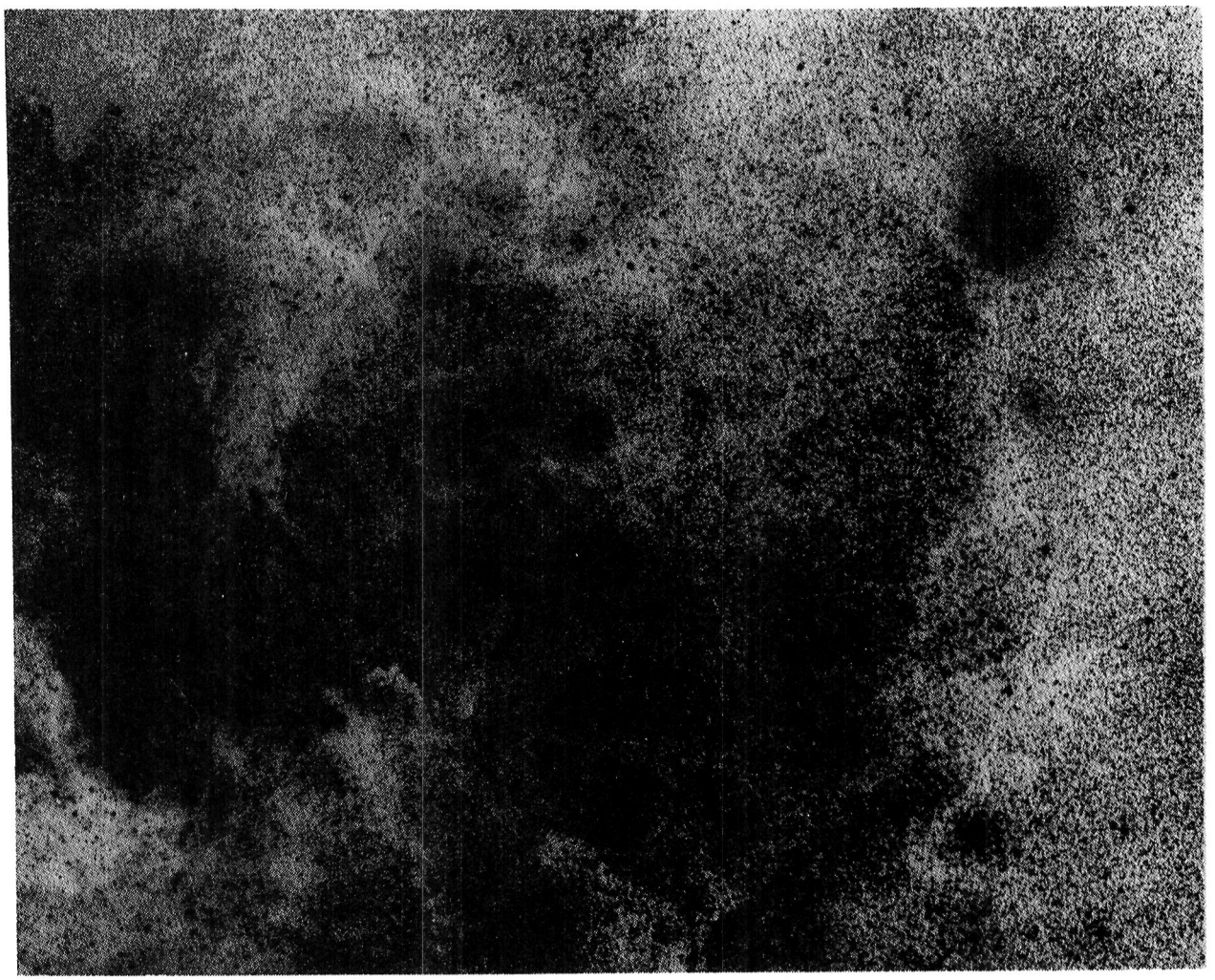

Figure 1 - The nebulosities surrounding HD148937 as imaged by the SRC Schmidt telescope using IIIaJ emulsion and GG395 filter. Innermost is the S-shaped nebulosity, NGC6154-5, centered upon HD148937. Faintly discernible is the hollow cavity immediately surrounding the star. The cavity is sharply bounded by filamentary structure initially detected as [O III] filaments. The H II region, extending two degrees, is faintly detected here but well-defined in Hα imagery. The H II region is bounded by a thin, dusty shell surrounding the entire structure. NGC 6188 is seen to the east.

PRELIMINARY REPORT ON IUE SPECTRA OF THE CRAB NEBULA

K. Davidson
Department of Astronomy
University of Minnesota

T. R. Gull, S. P. Maran, T. P. Stecher
Laboratory for Astronomy and Solar Physics
NASA-Goddard Space Flight Center

M. Kafatos
Department of Physics
George Mason University

V. L. Trimble
Department of Physics
University of California, Irvine

ABSTRACT

The Crab Nebula is marginally observable with the IUE. Observations of the optically brightest filamentary regions, made with IUE in August 1979, show the C IV λ1549, He II λ1640, and C III] λ1909 emission lines. The intensities of these lines have been compared with visual-wavelength data. It appears that carbon is not overabundant in the Crab; carbon/-oxygen is approximately "normal" and oxygen is slightly scarcer than "normal" as a fraction of the total mass.

INTRODUCTION

The Crab Nebula is the only young supernova remnant (i.e., one composed of supernova ejecta rather than of swept-up interstellar matter) which can be detected with the IUE. In August 1979, several IUE shifts were devoted to surveying a few spots in the nebula, using the large (10X20 arc sec) apertures, at low dispersion. The brightest spot found in this preliminary work will be further observed in 1980. The results of the 1979 work, described here, are preliminary. It appears that only near the brightest spot does the nebula produce ultraviolet emission line fluxes that are bright enough to be measured with the IUE. This is a region of superimposed "filaments" southwest of the pulsar, near the "bright filament" of Davidson (ref. 1) and "position 2" of Miller (ref. 2).

OBSERVATIONS

The present results are based on two exposures with the short-wave spectrograph, with integration times of 260 and 420 minutes, respectively (Figures 1 and 2). At the bright region that we observed, the C IV λ1549, He II λ1640, and C III] λ1909 lines appear to have been detected; radiation hits also affected the data shown in the Figures.

The He II λ1640 brightness is essential, because it allows comparison with relative line intensities in the visual wavelength region, thanks to the theoretical intrinsic relation (ref. 3) between the He II recombination lines,

$$I(\lambda 1640)/I(\lambda 4686) \approx 7.$$

No observations reported in refs. 1 and 2 were taken at positions that coincide exactly with the location in the nebula that was observed with IUE. However, for the purpose of the present preliminary analysis, we may average these previous results for the bright filamentary region. The lines that we take into account here are listed in Table I, where we have assumed a reddening for the Crab,

$$E_{B-V} = 0.5 \text{ mag}$$

from ref. 4. The adopted reddening was used to correct the visual line ratios, [O III]/Hβ/He II/He I, and separately to correct the ultraviolet line ratios, C III]/He II/C IV; then the previously-mentioned intrinsic ratio of the He II λ1640/λ4686 recombination lines was used to combine all of the relative intensities on the common scale of Table I.

The visual wavelength data of Table I were taken from refs. 1 and 2. Differences between these two references are less than 20 percent and probably real, due to the slightly different locations that were observed. The ultraviolet data (present work) in Table I must be regarded as very rough estimates, with errors as large as a factor of 1.5 quite possible.

DISCUSSION

Ultimately, appropriate photoionization calculations will be required to support a full analysis of the data in Table I and the further measurements to be obtained this year. In the meantime, some rough estimates will be instructive.

Theoretically, each blob or filament in the Crab Nebula is expected to have a stratified structure in photoionization equilibrium (ref. 5). An illustrative model is shown in Figure 3. The scheme shown in the figure is supported, to some extent, by temperature estimates from the lines of [S II] and [O III] (refs. 2 and 6). Zones B and C in the model are too cool to contribute significantly to the ultraviolet lines that we observed. Therefore, in this analysis, we consider only zone A. The [O III] λ4363/λ5007 temperature estimates generally give values around 14,000 - 15,000 K for this zone. (Actually these are averages, since there must be a temperature gradient within the zone.)

The intensity ratio of the He II λ4686/He I λ4471 recombination lines in the Crab Nebula shows that most of the helium in zone A is in the form of He^+, not He^{++}, in particular,

$$n(He^{++})/n(He^{+}) \sim 0.1.$$

This probably means that O^{3+} and C^{4+} are negligible compared with O^{++} and C^{3+}, respectively. Thus, in zone A we have C^{++}, C^{3+}, O^{+}, and O^{++}. It is very unlikely that more than 50 percent of the oxygen in zone A is O^{+}. Most likely, in zone A, at least 60 percent of the oxygen is O^{++} (see ref. 6). In the following discussion, we keep this in mind and consider only the C III], C IV, and [O III] lines.

Using conventional values for collision strengths (ref. 8),

$$\frac{I(\text{C III] } \lambda 1909)}{I([\text{O III}]\ \lambda\lambda 4959, 5007)} \approx 13\, e^{-\left(\frac{46{,}500\ K}{T}\right)} \frac{n(C^{++})}{n(O^{++})}$$

and

$$\frac{I(\text{C IV } \lambda 1549)}{I([\text{O III}]\ \lambda\lambda 4959, 5007)} \approx 50\, e^{-\left(\frac{64{,}400\ K}{T}\right)} \frac{n(C^{3+})}{n(O^{++})}$$

The line intensities reported in Table I then imply ionic abundance ratios for various representative temperatures, as listed in Table II. Note that the most likely temperature is around 15,000 K.

It seems clear that the carbon/oxygen ratio in the Crab is not very large. Also included in Table I are the observed relative line intensities in the high-excitation planetary nebula NGC 7662 (ref. 7), normalized to Hβ. The intensities of the lines observed in the Crab, which are attributed to zone A, are remarkably similar to those found in the planetary nebula. Since NGC 7662 was extensively modeled in ref. 7, an idea of the abundances in the Crab may also be obtained under the assumption that the physical conditions are similar. For NGC 7662, the carbon abundance was found to be solar and the C/O ratio was equal to unity, with the oxygen abundance less than solar. The temperature of the inner zone of NGC 7662, where the C IV line is formed, was 14,000 K. It is somewhat surprising that the C IV line is so strong in the Crab, since the C^{3+} ions are reduced by dielectronic recombination and by charge transfer on neutral hydrogen, which is much more abundant in the Crab. The inferred carbon/oxygen ratio in the Crab does not confirm the prediction of Arnett's (ref. 9) Case B, in which the supernova ejected all mass above the helium-burning shell, nor does it confirm the suspicion of Davidson (ref. 6). It is consistent with the Arnett Case A, in which all mass above the oxygen-burning shell is ejected. There are, however, a variety of models for the presupernova star and not all have been accompanied by explicit abundance predictions for the remnant nebula. Considering that some O^{+} must be present, but has been omitted from this analysis, it is probable that

$$\frac{n(\text{carbon})}{n(\text{oxygen})} \approx \left[\frac{n(C^{++}) + n(C^{3+})}{n(O^{+}) + n(O^{++})}\right] \quad \text{zone A}$$

$$\approx 1 \quad \text{within a factor of two}$$

It is important to recall that in the Crab Nebula, the abundance of oxygen by mass is lower than solar (ref. 6). Incidentally, note that the C IV/C III] ratio is considerably higher (perhaps by 3 to 5 times) than anticipated from the simplest photoionization calculations. It is too soon to say whether this indicates a serious difficulty for such calculations. It is unfortunate that the O III] λ1663 line cannot be measured as a check on this matter. The line is expected to be faint and its position corresponds to a reseau mark; a similar comment applies to N III near λ1750.

The interstellar absorption feature at λ2200 was observed in the continuum and will provide an independent determination of the extinction along the line of sight to the Crab Nebula. The extinction also can be independently determined from the ratio of the He II recombination lines, which is known from theory, once the absolute fluxes are available.

REFERENCES

1. Davidson, K. 1978, Ap. J., 220, 177.
2. Miller, J. S. 1978, Ap. J., 220, 490.
3. Seaton, M. J. 1978, M.N.R.A.S., 185, 5p.
4. Miller, J. S. 1973, Ap. J. (Lett.), 180, L83.
5. Davidson, K. 1973, Ap. J., 186, 223.
6. Davidson, K. 1979, Ap. J., 228, 179.
7. Bohlin, R. C., Harrington, J. P., and Stecher, T. P. 1978, Ap. J., 219, 575.
8. Osterbrock, D. E. 1974, Astrophysics of Gaseous Nebulae, San Francisco: W. H. Freeman and Co., p. 47.
9. Arnett, W. D. 1975, Ap. J., 195, 727.

TABLE I. SOME RELATIVE LINE INTENSITIES IN THE BRIGHT FILAMENTARY REGION OF THE CRAB NEBULA

(corrected for interstellar reddening)

Identification		Crab Nebula	NGC 7662
[O III]	4959, 5007	16.	15.5
Hβ	4861	1.0	1.0
He II	4686	0.7	0.4
He I	4471	0.3	0.03
C III]	1909	7.5	5.5
He II	1640	5.	3.0
C IV	1549	5.	7.3

Crab Nebula Data: Visual lines from refs. 1 and 2.
NGC 7662 Data: From ref. 7.

TABLE II. C/O IONIC ABUNDANCE RATIOS IN THE CRAB NEBULA ZONE A

T (K)	$\frac{n(C^{++})}{n(O^{++})}$	$\frac{n(C^{3+})}{n(O^{++})}$
12,000	1.74	1.29
14,000	1.00	0.60
16,000	0.66	0.34
18,000	0.48	0.22

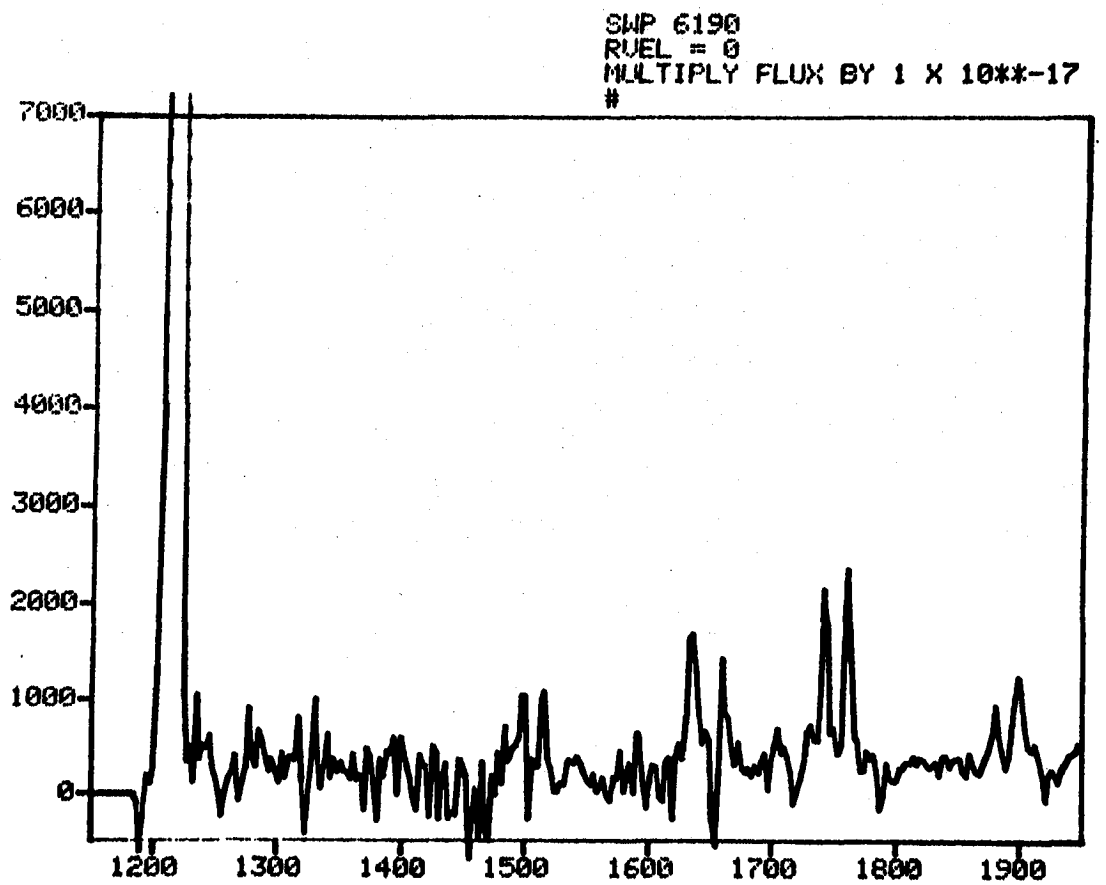

Figure 1. Results of 260-min exposure initiated at 02:51 G.M.T. on August 15, 1980.

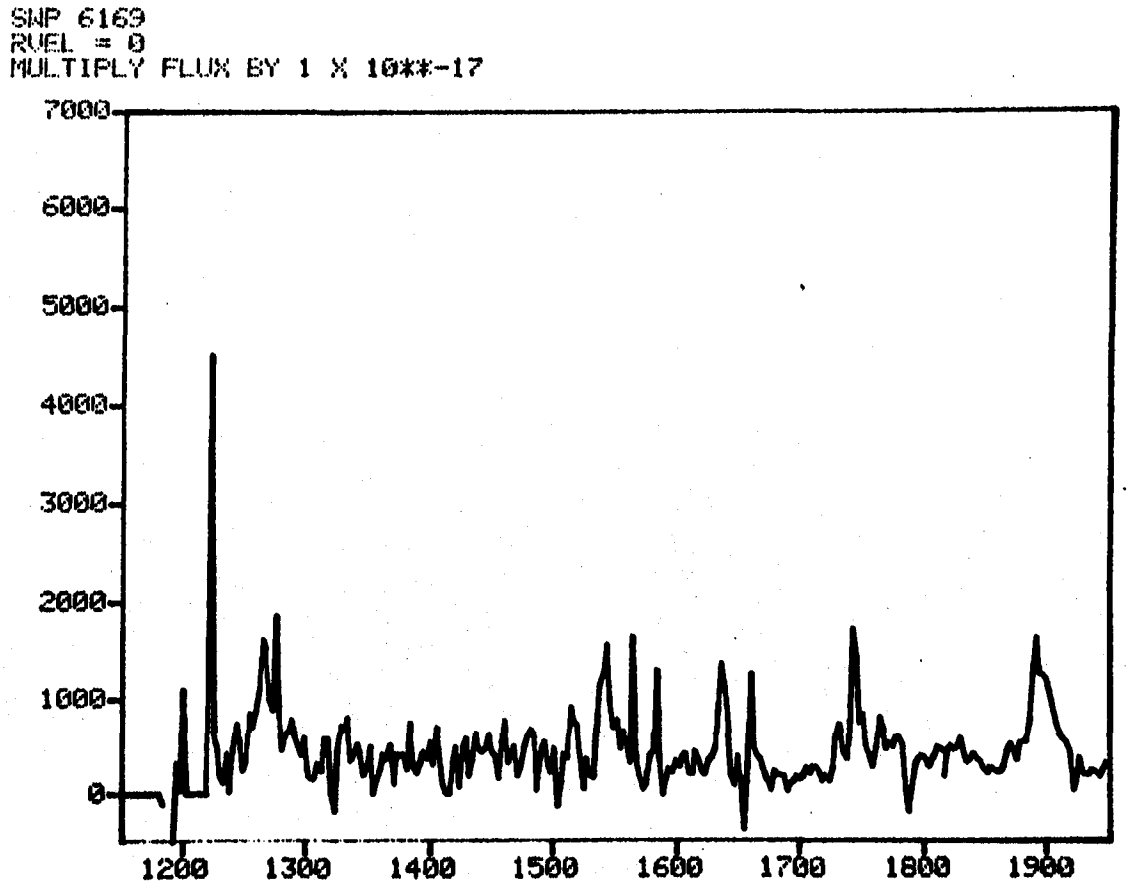

Figure 2. Results of 420-min exposure initiated at 02:55 G.M.T. on August 13, 1980.

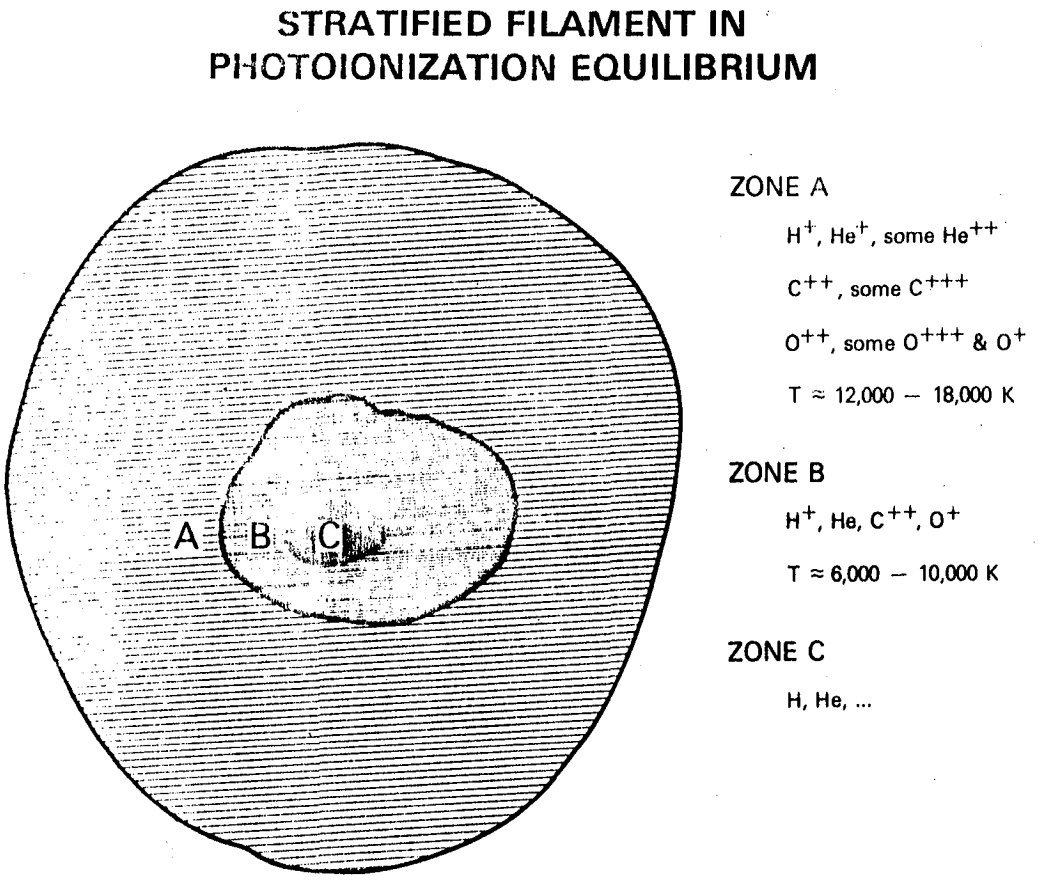

Figure 3. Schematic model for stratified filament in photoionization equilibrium in the Crab Nebula.

IUE OBSERVATIONS OF THE CRAB PULSAR

P. Benvenuti, L. Bianchi, A. Cassatella, J. Clavel, J. Darius,
A. Heck, H.V. Penston, Astronomy Division, ESTEC,
Villafranca Satellite Tracking Station,
ESA, Madrid, Spain

F. Macchetto, Astronomy Division, ESTEC, SSD,
ESA, Noordwijk, The Netherlands

P.L. Selvelli
Astronomical Observatory,
Trieste, Italy

J. Zamorano
Astrophysical Department
Universidad Complature
Madrid, Spain

ABSTRACT

The Crab Nebula Pulsar has been observed with IUE in the long and short wavelength ranges. The Pulsar was successfully detected in two long wavelength images as a brighter point-like spectrum above the nebular background. The detection failed in two short wavelength images which shows only a nebular continuum. The extracted spectra, after subtraction of the nebular contribution, were retained in bands of 50Å and averaged. There is no positive evidence of spectral features apart from the interstellar absorption at 2200Å. The spectrum is in excellent agreement with the optical data. An attempt to deredden the spectrum using the standard UV extinction curve (Ref. 1) and a visual extinction of $A_V = 1.6$ (Ref. 2) produced an unexpected flux excess in the 2200Å region. Using the nebular data in the short and long wavelength range and assuming a power law as a plausible description of the unreddened nebular emission, we have derived an extinction curve in the direction of the Crab Nebula. Our curve differs from the standard one, showing a narrower and blue shifted 2200Å bump.

We conclude that the UV spectrum of the Crab Pulsar can be interpreted, along with the near IR and visual one, as speculation radiation powered by electrons with a range of different energies.

However, before observing the spectral index of the spectrum, further investigation has to be carried on for a better determination of the UV interstellar extinction in the direction of the Crab Nebula.

REFERENCES

1. Santon, M.J. 1979, Mon. Not. R. Ast. Soc., 187, 730.
2. Miller, J.S. 1973, Astrophys. J. Letters, 180, L83.

Savage: Do you see damping wings in the strong Si II lines?

Joseph: Yes. The λ1193 and λ1260 lines are blended making them difficult to determine, but the λ1526 line does have damping wings which are possibly asymmetric.

Blades: In conjunction with M. J. Bailow (UCL) I have studied at very high resolution the interstellar Na I D lines in these Carina sight-lines. We used the 1.9 m Mt. Stomlo reflector at code focus with a photon counting detector which resulted in a velocity resolution of 1-3 km s^{-1} (FWHM). The interstellar Na I profiles are highly complex; in many cases the structure within the profiles is very similar to that shown in your Ca II K profiles. In addition, we find complex Na I profiles in sight-lines that are well away from the center of the nebula.

Hesser: Nolan Walbarn and I found evidence for D-line structure in three stars many years ago from CTIO coudé spectra; he has also been studying the D lines with the much improved resolution of the echelle spectrograph on the CTIO 4-m telescope. In the IUE data for Mg II 2796 Å in HD 93131 we also see evidence for multiple components where none were suspected in the original k-line survey. Nevertheless, the differences between lines seen towards the inner and outer portions of the nebula are dramatic, and suggest that the structure definitely originates within this giant H II region.

Peimbert: Which is the angular extent covered by the multiple line profiles?

Hesser: In our original optical search the complex profiles were limited to stars within about 15 arc min of η car. However, the discovery of new absorption line components in the very strong UV lines suggests that stars near the outer boundaries of the original survey should be re-examined for weak structure. A component in the Mg II 2796 Å line in the spectrum of HD 93131 suggests that multiple components, albeit weaker and fewer, may persist over a larger area. Also, it may be useful to recall that the nebular emission lines ([N II], [O III], Hα) are broad and double to distances as large as 2.5° from the center of the Carina Nebula, as shown by Malcolm Smith and collaborators.

Peimbert: Do you have other results for the C/H ratio based on other stars?

Lien: No; so far we have analyzed only one star in detail.

Penston: I was interested in what you said about the background. At VILSPA we have been working on a high dispersion calibration: this work also suggests that at the short-wavelength ends the background is indeed contaminated by the data. Consequently, we would favor the type of procedure you recommend. But I wonder if anyone else has any other comments--for example, when one compares the equivalent widths between Copernicus and IUE what does this say?

Lien: So far, the only other background subtraction technique I've encountered is assuming a gaussian overlap of orders. As to the comparison with Copernicus observations, it is something I plan to do in the future.

de Boer: Are you aware of the fact that SWP spectra which have IUE flux in the gross spectrum above 80000, suffer from nonlinearity in the ITF without being flagged as "saturated"?

Lien: Yes, and I have been careful not to stack in data for which this condition occurs.

de Boer: I also wonder about your background correction. There is only one way to find out whether your line goes down to the camera background or not: print out the flux numbers per pixel. In our LMC-SMC high dispersion spectra we do not need an additional background correction to the interorder level (de Boer and Savage 1980 Ap.J. 238 in press; Savage and de Boer 1980 this symposium). A more general remark on your C II lines: how much absorption do you expect from the foreground medium? That all by itself would add absorption width to the supposed b=2 kms CO cloud! I just do not believe the result as you present it.

Lien: Our lines are not resolved by the IUE, and so even lines on the saturated or low part of the damping part of the curve of growth will not reach zero flux level. The distance to the cloud in question is ~300 pc, and thus we feel that whatever is in front of it is negligible, in regard to the addition of "wings" to the line.

Jenkins: If I understood correctly, you have attempted to derive a column density for carbon using the 1335 C II lines assuming b=5 km s^{-1}. I don't see how your result can be at all reliable for lines as strong as you have shown, since they must be heavily saturated and well up on the flat part of the curve of growth.

Lien: The line is on the damping part of the curve of growth for b $\leq$ 5 km s^{-1}, and the CO velocity as seen in the ratio is 2 km s^{-1}, thus the column density is independent of the velocity, if it has the same velocity dispersion as the CO.

Raymond: To be compressed, the cloud must have been shocked to around 10^3 K. You have a density, the cooling time can be estimated. Is it compatible with the age of the remnant?

Wallerstein: Yes, the cooling time is compatible with the age of 10^4 years.

Stecher: What influence does ζ Pup and γ Vel have on your model if your cloud and the stars are at the same distance?

Wallerstein: Very little. Both stars are rather far away, ζ Pup is 10° away and γ Vel is 5° away. At our high densities the radiation field is not an important source of excitation.

Peimbert: What can be said about the Mg/H ratio for the region where you detected the λ2800 Mg^+ line?

Raymond: The Mg II lines are brighter compared with O III than predicted by the models by about a factor of 2. This is probably because the region observed is not a clean, single-velocity shock.

de Boer: Out to which distance did you have problems with scattered light from the Trapezium stars?

Perry: None of our survey areas were close enough to the Trapezium to cause any problem since the scattered light from the stars can be subtracted from our emission line data as long as the detector is not saturated.

Maran: Are you at a point in your analysis yet where you can say whether these data actually will give more information on the spatial distribution of physical parameters than is available from visible-light filtergrams?

Perry: Our efforts so far have been concentrated on generating the basic mosaics. We intend to pursue the several lines of analysis mentioned in the discussion section, notably the C/O abundance question and dust scattering/extinction properties, both of which are more sensitively addressed in the context of the UV data than in the visible.

Peimbert: Have you looked into the [Ne IV] λ2422/λ2425 ratio to check the discrepancy between the λ1907/λ1909 and the visually determined densities?

Feibelman: We now have data on a number of planetary nebulae for the [Ne IV] λ2422/λ2425 ratio but have not yet determined electron densities from them. We plan to do this in the near future.

Aller: I'd like to second Peimbert's suggestion about measuring the [Ne IV] nebular line ratio. These data when combined with the auroral λ4724,26 [Ne IV] transition give both N_e and T_e. Ar IV and some other ions also indicated an enhanced density in central requires of high excitation, but there is some fear that theoretical nebular line ratios in $3p^3$ configurations may be uncertain.

Feibelman: Yes, we plan to examine the [Ne IV] lines for both N_e and T_e. There may be stratification effects that play a role in [Ar IV].

Aller: There are measured Si II, Mg I, etc. lines in visible regime which might supply helpful additional information. It is curious that [Ca V] indicates a high degree of depletion for Ca from particle formation, yet you find [Mg V] indicating a situation of essentially no depletion!

Feibelman: Yes, there are the Si recombination lines in the visual but they are very faint and I do not know of any recombination rated calculations that would be necessary to make use of them. The Mg I] λ4751 line is included in our models, which for these two nebulae, predict this line to be stronger than observed. Because of the small photoionization cross section of Mg^0, a much larger fraction of Mg than H is neutral. Perhaps charge transfer would prevent this. It is interesting

that a model of IC 418 with a solar Mg abundance, which gives the right Mg II λ2800 intensity, also gives about the right Mg I] intensity. Not only is Mg different from Ca or Fe in that it is not depleted anywhere. One would like to know why this nebula is so different.

Peimbert: From your Mg V data it seems that you need to increase the high energy end of the stellar continuum in the models and by fitting the C III lines, and not the resonance C IV lines, you would find a higher carbon abundance.

Harrington: The ionization potential of Mg IV is so high that one could greatly increase the flux in that part of the spectrum without much impact on the bulk of the radiation at lower frequencies which ionizes C III to C IV. However, the ionization potential of Ne IV is not much lower than that of Mg IV and in fact our models fit the [Ne V] line intensities. Thus the problem does not seem to lie with the flux at very short wavelengths.

Savage: Do the nebulae you have observed have infrared excesses that might be attributed to dust?

Harrington: A number of them do if you look at the paper by Cohen and Barlow (1974). It is interesting that the ratio of IR luminosity to Lα luminosity given in this tabulation is often around 0.3, so that not all the Lα is being absorbed and converted to IR. This is relevant to the problem of how much of the radiation in UV resonance lines, like C IV λ1549, may be absorbed by internal dust. I think we should be cautious, because the optical depth in Lα is greater than that in other lines, so that if there is a lot of absorption for the other lines, we might expect almost all the Lα to be converted to IR. And there are planetaries like NGC 7662 that have very small IR excesses, and yet show evidence for depletion of refractory elements, and thus must contain some dust.

Panagia: I wonder whether you can find any indication that the observed C IV line intensities are systematically lower than the model predictions. Such an effect would imply the presence of internal dust as found for example in NGC 7027 (Perinotto, et al., 1980, A.&A., in press).

Marionni: The failure to reproduce correct I(λ1909) and I(λ1549) intensities, and more particularly their ratio, could well be due to internal dust absorption of the resonant λ1549 doublet. This was first suggested by the failure of simple models to interpret the UV emission from NGC 7027 (Bohlin, et al., Ap. J., 202, 1975). Since dielectronic recombination and charge-transfer will favor C III] emission at the expense of C IV if there are density enhancements in He^{++} zones, however, and we have not addressed such density structures here, it would be premature to attribute all problems to dust (see the talk by W. A. Feibelman, this symposium). You might, however, compare our unusually high-density and low-filling factor for IC 2003 with reality (cf. Barker, Ap. J., 219, 1978), and see that we've had to strain things to get the observed I(λ1909)/I(λ1549) from our models. Without increased density in regions of high temperature, yes, λ1549 always seems to be predicted too strong. Most of the objects we observed are not strong IR emitters.

Raymond: For objects this compact, can you be sure that features in the stellar spectrum, such as C IV, don't affect the apparent line fluxes?

Torres-Peimbert: From the spatially resolved spectra (and photowrites) it is possible to differentiate the stellar emission, and there don't seem to be any significant differences in the line profile. It can also be seen that C IV λ1549 and He II λ1641 are more centrally condensed than C III λ1909.

Dufour: How did you treat temperature fluctuations in your models? Did you notice any relationship between the C/O ratio and the magnitude of the O/H depletion in the nebulae?

Aller: The temperature fluctuations came out directly from the model. The C/O ratio is not closely correlated with O/H ratio; for the small sample the scatter is considerable; we will have to examine many more objects.

Peimbert: Have you compared the C^{++} abundance derived from the 1909 C III lines and the 4267 C II recombination line?

Aller: We have, and the results seem to be disappointing in the sense that the ionic concentration implied by the intensity of 4267 tends to be too large. This problem has to be solved because we can observe 4267 in faint objects such as SMC planetaries and we'd like to use it for abundance determinations. We have a restricted sample of high-excitation objects and it is necessary to study additional planetaries.

Marionni: What methods did you employ to relate UV line fluxes obtained from NGC 6302 to optical fluxes, given that the angular extent of the object is much greater than the 10" x 20" slit size available on IUE?

Aller: We used the ratio of 1640 and 2734 He II lines together with optical data to derive c = 1.44 which is in good agreement with some data by Dufour and Eason. The IDS data refer to the bright central core. We have some information about spatial variations from IPCS, but the optical and IUE data do not refer to exactly the same areas. The IPCS data suggest the effects are not larger.

Jenkins: Have you tried correlating O VI column densities with the probable positions of the bubbles?

Gull: We hope to do such in the very near future.

D'Odorico: Most galactic SNR detected at optical wavelengths are not associated with O, B stars. If the star responsible for the explosion is a runaway B star, would you expect to see the young association at a small angular distance from the remnant?

Gull: Young associations would produce supernovae from primarily O stars. These O stars would still be within the hot cavity when they become supernovae. The remnant-creating supernovae would come from B stars which either as runaways or evaporation from the association have escaped the low-density cavity.

Blades: Would you like to comment and enlarge upon your statement that interstellar absorption lines may be used as tracers of the structure of these superbubbles? In particular, do your models predict the level of ionization of interstellar species?

Gull: Much of the interior of young cavities may be 5×10^5 K at least part of the time. However, the old superbubbles, where no further supernovae occur within, would be substantially cooler where C IV, S IV, etc. should be traceable. Intervening super cavities should be separable by velocity components.

Savage: For such an important astronomical object it would be desirable to correct for ultraviolet extinction by using extinctive curves derived from stars in the general direction of the Crab Nebula. This would allow you to approximately compensate for the fact that the ultraviolet extinction curve does vary in shape from place to place in the galaxy.

Maran: I agree that this would be a useful project, although there are a variety of ways to estimate the extinction between the sun and the Crab Nebula.

Peimbert: What is the O/H enrichment expected under case A (if the enrichment of O/H is significant you can rule out case A from the optical observation of Davidson)?

Maran: According to Arnett (1975) there indeed is much more oxygen in Case A than in Case B.

VI. EXTRAGALACTIC OBJECTS

NEW INSIGHT INTO THE PHYSICAL STATE OF GALAXIES AND QUASARS

Richard F. Green
Steward Observatory, University of Arizona

Data from the International Ultraviolet Explorer satellite have revolutionized many concepts in extragalactic astronomy. These include the physical processes at work in the emitting gas characteristic of active objects, the nature of the continuum source itself in those objects, and the constituent hot stellar and gaseous components of normal galaxies. This review will not be exhaustive, but will concentrate on several problems of extragalactic research investigated with IUE.

NORMAL GALAXIES

The spectral energy distributions of normal galaxies contain information valuable for two related problems: population synthesis, for which optical spectra alone are not sufficient to deduce the parameters relevant to hot stars; and studies of high-redshift galaxies to determine both cosmological constants and galactic evolution.

Several of these difficult observations have been made with IUE, including the nuclei of M81 and M87 (ref. 1), M31 and M32 (ref. 2, 3), NGC 4472 (ref. 3), NGC 3379 (ref. 4), and NGC 1052 (ref. 5). The calibrated spectrophotometry from IUE shows good agreement with that of ANS, in particular for M31 and M81 (ref. 6), and in general for a large body of ANS galaxy observations (ref. 7).

All authors agree that the observations cannot be explained by a simple extension below 2500 Å of the spectrum representative of a pure old metal-rich population dominated by G and K stars. Simple spectral fitting suggests the presence of a population of type A0 for M81 (ref. 1) to early F for NGC 1052 (ref. 5). More sophisticated modeling for the bulge of M31 (ref. 3, 6) admits several possibilities. An acceptable fit is obtained from an old Population I (M67) cluster horizontal branch plus blue stragglers. Much better fits are derived for both long and short ultraviolet wavelengths from Population II, globular cluster horizontal branches. These stars would contribute 5 to 10% of the light in the V band and 75% of the light at 2000 Å. Several lines of evidence suggest that the UV light does not represent OB associations. It will be important to assess the contribution of hot stars between the red giant and white dwarf phases, such as planetary nebula nuclei, sdO and sdB stars. An important implication of these results is the large range in metallicity for elliptical systems, both in the presence of metal-poor stars and in the requirement of a metal-enhanced population to offset the dilution in optical absorption line strength produced by the redder Population II stars that must co-exist with the horizontal branch.

Ultraviolet observations of low-redshift galaxies may be used for comparison with optical observations of high-redshift galaxies. The two absorption breaks used for redshift determination, one primarily from MgII at 2800 Å and one primarily from FeII at 2640 Å, are both detected at their expected strengths (refs. 2, 3). In general, galaxies observed through fixed bandpasses will reach, as a function of increasing redshift, a maximum redward excursion in color, then become bluer again at higher redshifts. For spirals, this turning point is reached at $Z \sim 0.7$ in V-R, while for ellipticals it is found at $Z \sim 1.2$ (ref. 7). Since spirals have more ultraviolet flux relative to visual than ellipticals, beyond some redshift brightest cluster galaxies observed through a fixed bandpass will be giant spirals rather than giant ellipticals. The above predictions may now be compared with observations of high-redshift galaxies to learn about population evolution.

A significant result of IUE has been the discovery of a highly ionized halo around the Galaxy (refs. 8, 9) and around the Large and Small Magellanic Clouds (refs. 8, 10). C IV and Si IV have been detected in absorption with strengths implying column densities around 10^{14} cm^{-2} (refs. 8, 11). If the gas is in co-rotation, then the velocity structure of the absorption against stars in the Magellanic Clouds indicates that gas has been detected out to 10-15 kpc below the plane of the Galaxy. Electron collisional ionization models suggest temperatures around 10^5 K. This result has been confirmed by the discovery of C IV and Si IV in absorption at zero redshift against the quasar 3C 273 (refs. 12, 13, 14), showing that the highly ionized gas is globally distributed with comparable physical properties. N V has not been observed, placing a limit on the excitation temperature. The existence of this hot halo around our own (by definition, normal) galaxy strongly favors the interpretation of C IV and Si IV absorption systems, observed in the line of sight to high redshift quasars but at large velocity differences, as arising in the halos of intervening galaxies.

ACTIVE GALAXIES

Ultraviolet observations of active galaxies are valuable in revealing the presence of a hot star population, an ionizing non-thermal source, or resonance emission lines giving information on the physical state of ionized gas and the dynamics of the galactic system. Four individual cases are presented as examples of the kinds of problems investigated with IUE.

Extragalactic H II regions are either isolated systems or well-defined regions within a larger galaxy where active star formation is taking place. Observations of three of these faint objects with IUE (ref. 15), produced only upper limits in the Ly α emission flux in two of the cases, yielding a Ly α/Hβ flux ratio of less than 0.25. Ly α was detected in emission in the most metal-poor object with a flux ratio to Hβ of about 4, similar to that seen in quasars, but with a line width of ~ 150 km s^{-1}. A proposed explanation is the destruction of Ly α photons by dust in the more metal abundant objects, with concomitant reddening of the hot star continuum. The implication lies in the real difficulty in detecting primeval galaxies at high redshift, because they may be characterized by neither a strong ultraviolet continuum, nor strong ultraviolet emission lines.

NGC 1052 is an active elliptical galaxy with a compact nuclear radio source, strong optical emission lines, and a high M_{HI}/L_B. Observation with the short wavelength camera of IUE (ref. 5) shows no evidence of a non-thermal ionizing continuum. The only emission lines seen are C II] λ2326 and C III] λ1909, with no higher excitation lines. The observational picture is consistent with a shock heating model that brings the gas to around 10^4 K and cools it through the observed lower excitation UV and optical lines, although there is still some discrepancy in the predicted ultraviolet line intensities.

PKS 2158-380 is an example of a radio galaxy with extended optical emission lines, observed over a projected distance of 30 kpc. IUE spectra (ref. 16) show that the gas is in a high ionization state; the presence of He II λ1640 out to great distances suggests that the conditions are not like those of an H II region. The Ly α/Hβ flux ratio is consistent with the recombination value at the low density of $n_e < 300$ cm^{-3} found from optical [S II] line ratios beyond 4 kpc from the nucleus. A non-thermal spectrum of the form $f_\nu \propto \nu^{-1.3}$ is observed in the nucleus, and provides enough ionizing photons if the gas at 15 kpc radius can see them. The radio source is an asymmetric double with a position angle 50° different from the axis of rotation of the gas. The suggested morphology is that of a highly warped plane of gas, possibly produced by accretion onto a non-spherical potential with an axis different from any pre-existing symmetry axis.

The active galaxy and X-ray source NGC 7582 poses a problem: although strong optical emission lines are observed, the IUE spectra show a steep featureless continuum, with $f_\nu \propto \nu^{-3.4}$ (ref. 17). The 2200 Å depression yields a value for the extinction lower than that derived from the Balmer decrement, but the complete absence of ultraviolet emission lines favors the higher value. The evidence therefore suggests that the ratio of 2200 Å absorption strength to E_{B-V} may depart significantly from the average value in the case of this galaxy and by implication, possibly in others as well. This galaxy shows no Mg II emission, although on the basis of optical line strengths, it should have been detected at twice the quoted upper limit. The authors suggest that absorption must just cancel the emission.

QUASARS, SEYFERT GALAXIES AND BL LAC OBJECTS

These different manifestations of extreme activity in extragalactic objects are combined in order to discuss some common physical problems.

HYDROGEN EMISSION LINES AND THE PRESENCE OF DUST

A number of investigators have studied the ratio of Ly α/Hβ emission-line intensities in low-redshift quasars and Seyfert galaxies (refs. 1, 12, 13, 18, 19, 20, 21, 22, 23, 24). The combined result of all these measurements is that the ratio for broad emission lines is around 6, with a very small dispersion, while the simple approximation of optically thick radiative recombination predicts a value of about 40. The Hα/Hβ ratio and Pα/Hα ratio when measured (e.g., ref. 25) are more nearly consistent with the predictions of recombination theory.

The controversial question is whether selective extinction and reddening by dust is required to explain the observed line ratios, and, as a corollary, whether this dust is mixed into the broad-line emitting region or is intervening. For a lucid discussion of the problem and related ultraviolet observations, see ref. 26.

The presence of the λ2175 Å absorption feature at the emission-line redshift provides definite evidence for dust in some Seyfert galaxies. In 3C 120 (ref. 20), the inferred reddening of $E_{B-V} = 0.38$ is sufficient to account for the entire discrepancy from the recombination value. On the other hand, even though a substantial correction for dust is inferred for Mk 79 (ref. 20), I Zw 1 and NGC 7469 (ref. 24), it cannot account for enough "missing" Ly α photons.

Theoretically, dust is an attractive and efficient way to destroy resonantly trapped Ly α photons. Some observational evidence suggests that the He II λ1640/Ly α ratio is enhanced by a factor of two over the theoretical expectation (ref. 27), a result of the attenuation of Ly α by a small amount of internal dust. The problem is, that if enough dust were mixed into the broad-line region to produce the observed Ly α/Hβ ratio, He II and C IV would be strongly enhanced relative to Ly α, a result not observed (refs. 28, 29). The conclusion is therefore that the dust must be external to the broad-line region (ref. 30).

Two observational probes are suggested (ref. 30) to test for reddening by dust, neither of which is very sensitive to the details of temperature and density for conditions expected in the broad line emitting clouds. They are the recombination ratios of He II λ1640/λ4686 and O I λ1303/λ8446. The ratio for He II is observed to be 1.5 - 2 (e.g., ref. 26); this value corresponds to a differential extinction of $E_{B-V} \sim 0.3$, implying a factor of 6 to 8 correction in the Ly α/Hβ ratio. For 3C 273, a measurement of O I λ1303 yields $E_{B-V} = 0.26$ (ref. 26), while no λ1303 emission was detected in NGC 4151 (ref. 26). In several cases, the data are therefore consistent with a reddening by dust leading to a differential extinction of $E_{B-V} \sim 0.3$, an amount sufficient to account for the discrepancy between the observed Ly α/Hβ flux ratios and those predicted for optically-thick recombination.

Several lines of evidence, however, argue against dust as the sole responsible agent. The λ2175 Å absorption feature is seldom seen in quasar spectra at a strength comparable to that in 3C 120 or Mk79. As an example, the total correction for 3C 273 amounts to $E_{B-V} = 0.05$ at the source and $E_{B-V} = 0.04$ from the Galaxy (ref. 13). The discrepancy with the line ratio probes may lie in measuring difficulties, in establishing the true continuum level near the broad wings of Ly α and C IV λ1550. An attempt to separate the flux of strong line wings from the continuum in 3C 273 results in a measurement (ref. 13) of He II and O I ultraviolet line fluxes three times stronger than those quoted above, consistent with the low value of differential extinction inferred from the λ2175 feature. In addition, the data on Ly α/Hβ and Hα/Hβ flux ratios for 19 Seyfert galaxies (ref. 24) are not consistent with a narrow intrinsic range of emission-line ratios and variable reddening, and cannot be characterized by any single reddening sequence.

A general difficulty with dust is that the extinction is very sensitive to the amount of dust present. The Seyfert galaxy data (ref. 24), after correction for the differential extinction inferred from the λ2175 feature, show a scatter of only about a factor of two in the Ly α/Hβ ratios. Since a convincing argument has been made that much of the reddening must be external to the broad line region, a remarkably constant column density is required to produce the observed range of line ratios.

A different approach to the problem is to consider the energy budget. Selective destruction of Ly α radiation would lead to a significant excess of ionizing photons over the number of Ly α photons produced by recombination. The photon budget balancing depends slightly on the assumed continuum shape at the Lyman edge and strongly on the fraction of the sky covered by emission line clouds as seen from the continuum source. For 3C 273 (refs. 1, 12), if all the Lyman continuum photons out to 2 or 4 Rydbergs are converted to Balmer line emission plus Ly α, then Hβ is found to be deficient by a factor of 2-4 and Ly α by 10-20. Using the Hβ flux as a measure of the covering fraction, Ly α is then suppressed by about a factor of 5. If a statistical covering factor of 10% is used (ref. 23), then the Ly α flux is approximately consistent with its recombination value, and Hβ is enhanced by up to a factor of 5.

The enhancement of Hβ is favored in an analysis of the broad-lined radio galaxy, 3C 390.3 (ref. 22). It was cleanly decomposed into a broad emission-line component, with velocity width $\sim$ 5000 km s^{-1}, and a sharp line component with width $\sim$ 400 km s^{-1}. The Ly α/Hβ intensity ratio is consistent with Case B recombination for the sharp line component, whereas it is lower than that value by a factor of 16 for the broad line component. Interpreted in terms of a photoionization model including collisional excitation, Ly α is carrying its predicted share of the cooling, about 25%. The Balmer lines carry an unexpectedly large fraction, more than 30%; this fraction is comparable in the case of 3C 273.

Sophisticated line transfer calculations can reproduce the observed line intensity ratios without invoking dust. A thermal balance model treating photoionization and hydrogen excited-state population equilibrium (ref. 31) shows that ionization from excited states is significant in keeping the emitting cloud up to 1/3 ionized into high optical depths, with a consequent high electron density. At $\tau_{Ly\,\alpha} > 5 \times 10^6$, the Ly α line thermalizes by electron collisional de-excitation. It ceases to be an effective coolant, and the Balmer lines deep in the cloud are forced into that role. A careful treatment of the Ly α photon escape probability and frequency redistribution (ref. 32) yields the result that the Balmer lines and Paschen α arise from a region within in the cloud at $\tau_{Ly\text{-}c} \gtrsim 100$.

The perspective, then, is that there is evidence for dust, internal to the emitting clouds from the enhanced He II λ1640 emission relative to Ly α, and external from the λ2175 absorption feature. The narrow range in observed Ly α/Hβ intensities and the derived ionizing energy budgets suggest that the departure from simple recombination models is a line transfer effect through optically thick clouds, with a strong enhancement of Balmer line cooling.

THE FE II PROBLEM

A substantial fraction of low-redshift quasars and Seyfert galaxies show emission lines of permitted Fe II in the 4500 - 5200 Å region (refs. 33, 38). These lines arise from excitation of ground state and low-lying metastable levels to 5-6 eV levels, followed by radiative decay to 3 eV levels, with a branching ratio of about 100 to 1 favoring the ultraviolet resonance transitions. There is a marked similarity between Fe II and Mg II in both excitation potential and relative abundance, yet while the Mg II emission doublet at λ2800 is a benchmark in quasar spectra, only upper limits were at first provided by IUE for the Fe II multiplets in either absorption or emission (refs. 1, 12).

Three mechanisms have been proposed to explain the presence of the optical Fe II lines (ref. 34). Radiative recombination is the least likely, unless the Fe abundance is anomalously high. Resonance fluorescence of continuum photons is a possibility with the optically thick emission-line clouds trapping the ultraviolet resonance photons, while the optical photons leak out. The observational consequence would be that $\sim$ 90% of the quasars show the ultraviolet resonance lines in emission, while the 10% with an optically thick cloud in the line of sight would show absorption. The theoretical difficulty is that with a covering factor as small as 10%, a very large turbulent velocity is required in each cloud to absorb enough continuum photons. Recent improvements in the collisional cross-sections for Fe II, incorporating improved atomic data and a more elaborate atom (refs. 35, 36, 39), show that collisions could be very important in populating the upper levels.

To study the situation, three extreme iron-line Seyferts, I Zw 1, II Zw 136, and Mk 231 were observed with IUE (ref. 37). The Fe II ultraviolet multiplets were clearly detected; the best estimate for the ratio of optical to ultraviolet photons is $\sim$ 3 for I Zw 1, $\sim$ 2 for II Zw 136, and 1-2 for Mk 231. These results are consistent with the predictions for collisional excitation, with high optical depth in the ultraviolet lines. The previous difficulty in detecting the ultraviolet Fe II emission probably results from the fact that these 12 multiplets are broad and of low contrast; and are easily seen only in places like the "blue wing" of Mg II emission. The question remains as to why only some quasars and Seyfert galaxies show Fe II; it may provide a sensitive probe of optical depth or electron density when the physical conditions are better understood.

ABSORPTION SPECTRA OF QUASARS

Quasars are sources of continuum emission against which intervening material can be detected in absorption over very long lines of sight. They therefore act as probes of both the local conditions of associated gas and the intergalactic medium. Unfortunately, high-redshift quasars are faint objects for IUE, so only the strongest absorption systems can be detected.

The discovery of Lyman-edge absorption at the quasar emission redshift signifies the presence of one of the optically thick emission-line clouds in the line of sight. The fraction of any randomly selected sample of quasars

showing this absorption is an estimate of the covering factor, the fraction of the sky seen from the continuum source covered by optically thick material. None of a sample of seven high-redshift quasars observed with IUE (refs. 23, 44) showed Lyman edge absorption at the emission redshift. Ton 490 has a substantial Lyman edge absorption (ref. 40), but it may very likely be associated with a strong absorption system at 10,000 km s^{-1} shift to the violet. From a compilation of relevant IUE data (ref. 14), only one quasar out of 13 shows this Lyman-edge absorption, yielding a covering factor of $\sim$ 8%. This result is in good agreement with that from a sample of 30 very high-redshift quasars observed optically (ref. 41), a factor of $\sim$ 10%. As seen above, the determination of the fraction of continuum flux absorbed is critical to understanding the ionization structure and emission-line intensities of the quasar gas.

High-redshift quasars also provide a probe of the intergalactic medium and intervening gas associated with galaxies and clusters. In three cases (refs. 23, 42), flux has been detected below the He I ionization edge at λ504. The near-transparency of the intergalactic medium at these wavelengths requires that the helium neutral fraction be very low; collisional ionization models put a lower limit on the temperature of about 3×10^5 K (ref. 43). At least 75% of the high-redshift quasars observed with IUE (refs. 14, 23) show an optically thick Ly α - Ly edge absorption system along the line-of-sight, most with a velocity difference with respect to the emission redshift of order C. Follow-up optical observations (ref. 44) have revealed low excitation metal-lines plus weak C IV in these systems. Their line-of-sight density is $\sim$ 2 per unit redshift. With quasars as a probe, IUE observations can therefore sample the distribution of galaxies and associated halo gas at redshifts around 1.

THE CONTINUUM

BL Lac Objects

An obvious and essential property of BL Lac objects was revealed with the first IUE observations (ref. 1). The continuum flux is detected down to the wavelength limit of instrumental sensitivity as a continuation of the optical power law. No ultraviolet emission lines are detected, not even Ly α. Since the ionizing photons are present, the conclusion must be that the absence of emission lines is because of the absence of emitting gas. These objects therefore provide an uncontaminated look at the continuum source itself.

The combination of a power-law spectrum, detectable linear polarization of the optical light, and rapid time variability suggests a synchrotron origin for some of the continuum radiation in BL Lac objects (ref. 45). IUE observations in combination with measurements at many frequencies provide the critical sampling of the electromagnetic spectrum that will be necessary to discriminate among differing theoretical interpretations.

Mk 501 is one of the brighter BL Lac objects, and has been observed quasi-simultaneously at radio, infrared, optical, ultraviolet, and X-ray frequencies (ref. 46). The resulting spectrum shows a power law extending from ultraviolet to X-rays, steepening toward very hard X-rays. The flat

spectrum radio emission cannot be an extension of that power law. A crucial step in the analysis is the separation of the power law from the dominant contribution of the optical and infrared light by the galaxy surrounding the active nucleus. Qualitatively different conclusions can be drawn depending on the method used (ref. 47). By removing a standard galaxy energy distribution, the power-law is seen to flatten off in the near ultraviolet and visual.

This spectral flattening may be interpreted as a reflection of the radio spectral turn-over, with the optical, ultraviolet and soft X-rays produced by "self-Compton" scattering of the radio photons off the relativistic electrons. Quantitative model fitting suggests a magnetic field of $\sim 4 \times 10^{-4}$ G and a variability time scale of $\sim$ 7 years. The steepening toward hard X-rays would reflect a high energy cut-off in relativistic electrons at $\sim$ 4 GeV. These data cannot rule out other models, however, such as inverse Compton scattering off hot thermal electrons, or two separate synchrotron components, one for the radio and one for the optical-ultraviolet.

Further observations show that neither the spectral energy distribution of Mk 501 nor a limited range of model parameters characterize all BL Lac objects uniquely. On the basis of simultaneous, multi-frequency observations of 0735+178 (ref. 48), the self-Compton model predicts an emission region size greater than 2.2 light years, but variability has been observed on a time scale of a week. In addition, the object I Zw 187 (ref. 48) shows an X-ray excess of a factor of 10 over the extrapolation of the power-law continuum, and emits such a low radio power that a magnetic field in excess of 10 G is required for inverse Compton scattering to be responsible for the higher frequency radiation.

The variable power-law component in Seyfert galaxies and quasars may be closely related to the BL Lac phenomenon. Multifrequency monitoring of the variability of two such objects, the quasar III Zw 2 and the Seyfert galaxy Mk 509, (ref. 49), shows that, while they have varied only at the 10% level in the ultraviolet, optical, and infrared, they have undergone substantial variations, in phase, in the radio and in X-rays. Further time-resolved observations may prove valuable in defining the relationship among components of the continuum emission.

Quasars

The optical and ultraviolet spectral energy distributions of quasars are more complex than those of BL Lac objects because of the presence of gas. From continuum points selected to be free of the effects of emission lines, an average optical-ultraviolet spectrum can be characterized by $f_\nu \propto \nu^{-0.6}$ (ref. 50). IUE observations of high redshift quasars (refs. 23, 44) show that below $\sim$ 1000 Å, the flat spectrum breaks and assumes the form $f_\nu \propto \nu^{-2.5}$ down to at least 400 Å. This steep spectral slope is a property of the continuum itself, as opposed to an effect of absorption or reddening, and is confirmed by optical observations of quasars with $Z > 3$. One implication of this result is that an extrapolation of the optical power law will overestimate the ionizing flux at 2 Rydbergs by a factor of 2-4.

A compilation of the entire spectral energy distribution of 3C 273 is shown in the Figure (ref. 13). The dot-dash line connected to the solid line of IUE observations is an empirical extrapolation (not a measurement), based on the assumption that the far-ultraviolet energy distribution of 3C 273 is similar to that of high redshift quasars observed with IUE. The Figure gives the impression that there is an excess of flux in the ultraviolet. The 3000 Å "bump" and Ly α two-photon emission can account for only a small fraction of that light. One proposed interpretation is that the ultraviolet radiation is a "thermal" excess, reminiscent of that seen in accretion disk binary stars (e.g. ref. 51). If the excess flux in 3C 273 could be characterized by a single temperature, it would be $\sim 2 \times 10^4$ K (ref. 13). Accretion-disk binaries exhibit a range in temperatures from $1\text{-}3 \times 10^4$ K. The high redshift quasars so far observed, however, seem to show the break in spectral slope at the same wavelength to within ~ 200 Å. One possibility is that quasars have a closely regulated "thermal" emission mechanism near the continuum source. Another possibility to be considered is that a wavelength-defined effect may represent an atomic process not yet understood. Multi-frequency observations of other quasars will be valuable in addressing this question.

The results discussed here reflect the success of IUE in problems of extragalactic research and the promise of future space astronomy efforts.

REFERENCES

1. Boksenberg, A., et al. 1978, Nature, 275, 34.

2. Johnson, H. M. 1979, Ap. J. (Letters), 230, L137.

3. Bruzual A. G., and Spinrad, H. 1980, NASA CP-2171: this volume.

4. Cappacioli, M., Bertola, F., and Oke, J. B. 1980, (in preparation).

5. Fosbury, R. A. E., Snijders, M. A. J., Boksenberg, A., and Penston, M. V. 1980, preprint.

6. Wu C.-C., Faber, S. M., Gallagher, J. S., Peck, M., and Tinsley, B. M. 1980, Ap. J., 237, 290.

7. Coleman, G. D., Wu, C.-C., and Weedman, D. W. 1980, submitted to Ap. J. Suppl.

8. Savage, B. D. and de Boer, K. 1980, Wisconsin Astrophysics Preprint No. 109.

9. Savage, B. D. and de Boer, K. S. 1979, Ap. J. (Letters), 230, L77.

10. de Boer, K. S. and Savage, B. D. 1980, Ap. J., 238.

11. Jenkins, E. 1980, NASA CP-2171, this volume.

12. Boggess, A. et al. 1979, Ap. J. (Letters), 230, L131.

13. Ulrich, M. H. et al. 1980, M.N.R.A.S., in press.

14. Snijders, M. A. J. 1980, in Proceedings of the Tübingen Conference: The Second Year of IUE.

15. Meier, D. L. and Terlevich, R. 1980, preprint.

16. Foxbury, R. A. E. 1980, preprint.

17. Clavel, J. et al. 1980, M.N.R.A.S., in press.

18. Davidsen, A. F., Hartig, G. F. and Fastie, W. G. 1977, Nature, 269, 203.

19. Baldwin, J. A., Rees, M. J., Longair, M. S. and Perryman, M.A.C. 1978, Ap. J. (Letters), 226, L57.

20. Oke, J. B. and Zimmerman, B. A. 1979, Ap. J. (Letters), 231, L13.

21. Baldwin, J. A. et al. 1979, Proceedings of Conference: The First Year of IUE.

22. Ferland, G. J., Rees, M. J., Longair, M. S., and Perryman, M. A. C. 1979, M.N.R.A.S., 187, 65P.

23. Green, R. F. et al., 1980, Ap. J., in press.

24. Wu, C.-C., Boggess, A. and Gull, T. R. 1980, preprint.

25. Puetter, R. C., Smith, H. E., Soifer, B. T., Willner, S. P., and Pipher, J. L. 1978, Ap. J. (Letters), 226, L53.

26. Davidsen, A. F. 1979, in IAU Symposium No. 92, "Objects of High Redshift," Los Angeles.

27. Baldwin, J. and Netzer, H. 1979, Ap. J., 226, 1.

28. Ferland, G. and Netzer, H. 1979, Ap. J. 229, 274.

29. Shuder, J. M. and Mac Alpine, G. M. 1979, Ap. J., 230, 348.

30. Netzer, H. and Davidson, K. 1979, M.N.R.A.S., 187, 871.

31. Kwan, J. and Krolik, J. H. 1979, Ap. J. (Letters), 233, L91.

32. Canfield, R. C. and Puetter, R. C. 1980, preprint.

33. Green, R. F. and Schmidt, M. 1980, in preparation.

34. Phillips, M. M. 1978, Ap. J., 226, 736.

35. Collin-Souffrin, S., Joly, M., Heidmann, N. and Dumont, S. 1979, Astr. & Ap., 72, 293.

36. Jordan, C. 1979, Progress in Atomic Spectroscopy, B, 1453.

37. Snijders, M. A. J., Boksenberg, A., Haskell, J. D. J., Fosbury, R. A. E., and Penston, M. V. 1980, preprint.

38. Phillips, M. M. 1977, Ap. J. Suppl., 38, 187.

39. Netzer, H. 1980, Ap. J., 236, 406.

40. Gondhalekar, P. M. and Wilson, R. 1979, in Proceedings of Conference: The First Year of IUE.

41. Smith, M. G. et al. 1980, preprint.

42. Boggess, A., Wu, C.-C, Gondhalekar, P. M., and Wilson, R. 1979 in Proceedings of Conference: The First Year of IUE.

43. Sargent, W. L. W., Young, P. J., Boksenberg, A., and Tytler, D. 1980, Ap. J. Suppl., 42, 41.

44. Green, R. F. et al. 1980, in preparation.

45. Stein, W. A., O'Dell, S. L., and Strittmatter, P. A. 1976, Ann. Rev. of Astron. and Ap., 14, 173.

46. Kondo, Y. et al. 1980, preprint.

47. Snijders, M. A. J. et al. 1979, M.N.R.A.S., 189, 873.

48. Bregman, J. N., Glassgold, A. E., and Huggins, P. J. 1980, NASA CP-2171, this volume.

49. Huchra, J. P., Geller, M. J. and Morton, D. C. 1980, NASA CP-2171, this volume.

50. Richstone, D. O. and Schmidt, M. 1980, Ap. J., 235, 361.

51. Fabbiano, G., Steiner, J. E., Hartmann, L. and Raymond, J. 1980, NASA CP-2171, this volume.

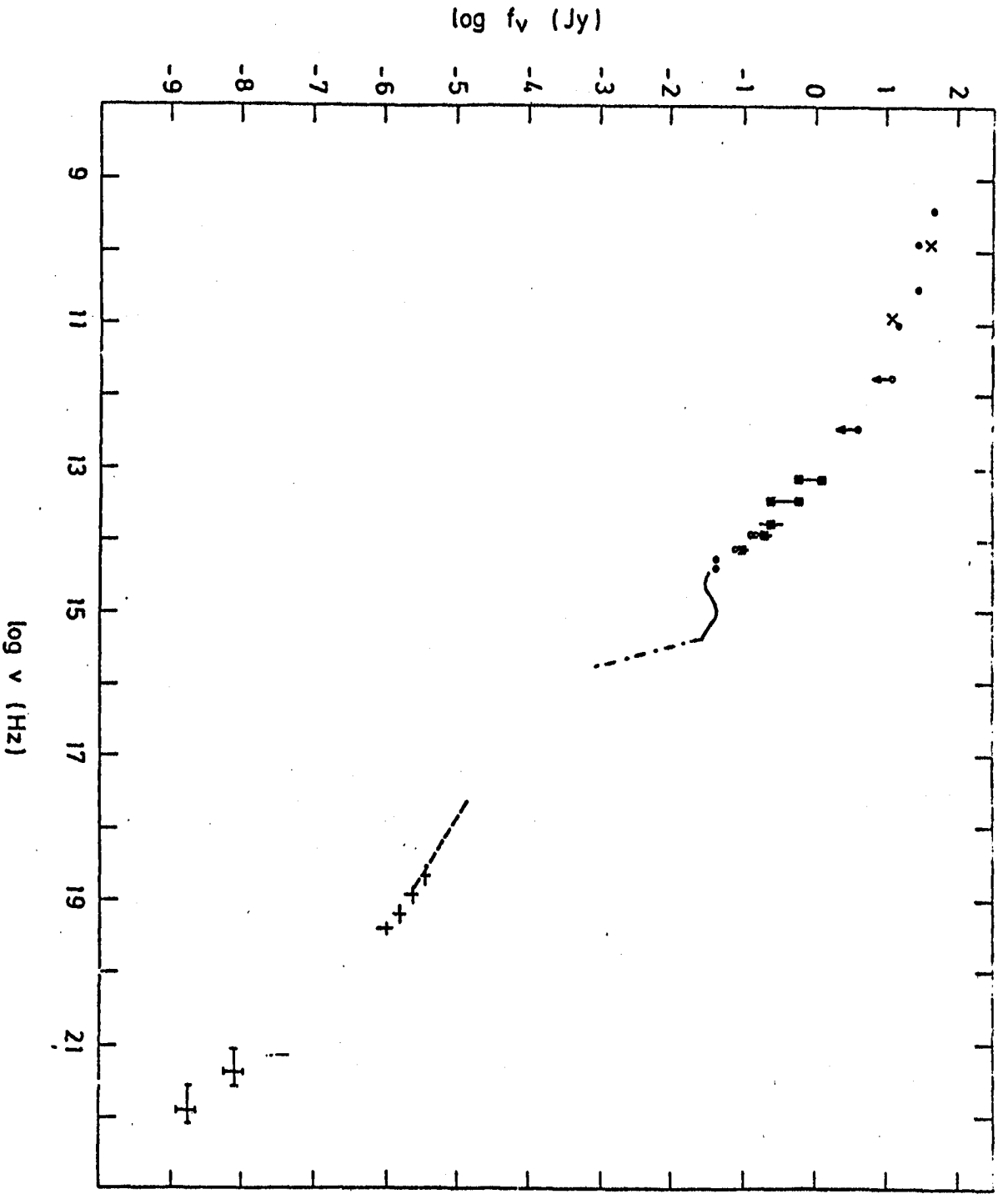

Figure 1

OBSERVATIONS OF THE NUCLEUS OF M100

N. Panagia and G. Vettolani
Istituto di Radioastronomia CNR
Bologna, Italy

G.G.C. Palumbo
Laboratorio TESRE-CNR
Bologna, Italy

P. Benvenuti
ESA, VILSPA
Madrid, Spain

F. Macchetto
ESA, ESTEC
Noordwijk, Netherlands

ABSTRACT

The IUE observations of the nucleus of M100 are presented and briefly discussed.

INTRODUCTION

M100 = NGC 4321 is a spiral galaxy in which a bright Type II Supernova (SN 1979c, m_B (max) $\simeq 12^m$) was discovered on April 19, 1979. Its spectral evolution has been followed with IUE for more than two months (refs. 1,2). At all epochs, the spectrum was dominated by continuous radiation on which emission and absorption features were superimposed. The equivalent width of most of the absorption features appeared not to vary with time suggesting that they originated in the interstellar media of M100 and our own galaxy. However, the possibility remained that the absorption lines be formed in the SN photosphere. Thus, the problem required some independent check for obtaining a definite solution.

This prompted us to observe the nucleus of the galaxy with IUE in order to discern bona fide interstellar features, which should be present in the spectra of both SN 1979c and the nucleus, from those originated in the SN photosphere which must be absent from the nucleus spectrum. Moreover, the nucleus of M100 in itself is worth being studied because in blue plates it presents interesting structure, namely, a central condensation (a core of $\sim$ 3") enveloped by a more diffuse region (a halo of $\sim$ 20") which contains additional 4 condensations around the central core (ref. 3). Also, radio observations with VLA have detected emission from a similarly extended area (ref. 4) and X-ray observations with the Einstein Observatory have revealed the presence of at least 2 condensations in the nuclear region (ref. 3).

OBSERVATIONS AND DISCUSSION

The observations were made on April 18, 1980 (LWR 7542, exposure time 197^m) and April 20, 1980 (SWP 8790, exposure time 420^m) at the ESA Satellite Tracking Station in Villafranca del Castillo, Madrid, Spain. Since the large slot (10" x 20") was employed for both observations, two of the condensations were observed at the same time. The spectra are displayed in Figure 1 and 2. The main results of a preliminary analysis can be summarized as follows:

1) The spectra of both components are dominated by continuous emission with approximate shapes $F_\nu \propto \nu^{-2}$ (upper component) and $F_\nu \propto \nu^{-1.5}$ (lower component). These imply relatively high color temperatures in the UV, of the order of 15 to 20 x 10^3K.

2) The line spectrum consists mostly of absorption features which are characteristic of the interstellar medium in both halos (e.g. Si IV 1400, C IV 1550, Al III 1850) and disks (e.g. Mg II 2800, C I 1260-1330, C II 1335, O I 1305, Si II 1260-1304, S II 1250-59) of M100 and our galaxy. This result confirms the interstellar origin of most absorption lines found in the SN 1979c spectra.

3) Emission lines, if present, are very weak. In fact, one may possibly identify the lines He II 1640 and O III] 1663 in both spectra. However, it is not clear whether they are real emissions or rather their appearance is mimicked by the shoulders of nearby absorption lines. Also, the possible presence of an emission component of the Mg II 2800 line in both spectra is indicated by the lower absorption observed in the red portion of the Mg II 2800 line just in correspondence to the radial velocity of M100.

REFERENCES

1. Panagia, N. et al., 1980, M.N.R.A.S., in press.
2. Panagia, N., 1980, this Conference.
3. Palumbo, G.G.C., Maccacaro, T., Marano, B., Panagia, N., Vettolani, G., and Zamorani, G., 1980, in preparation.
4. Weiler, K.W., Matzik, P., Sramek, R.A., Wielebinski, R., and Panagia, N., 1980, in preparation.

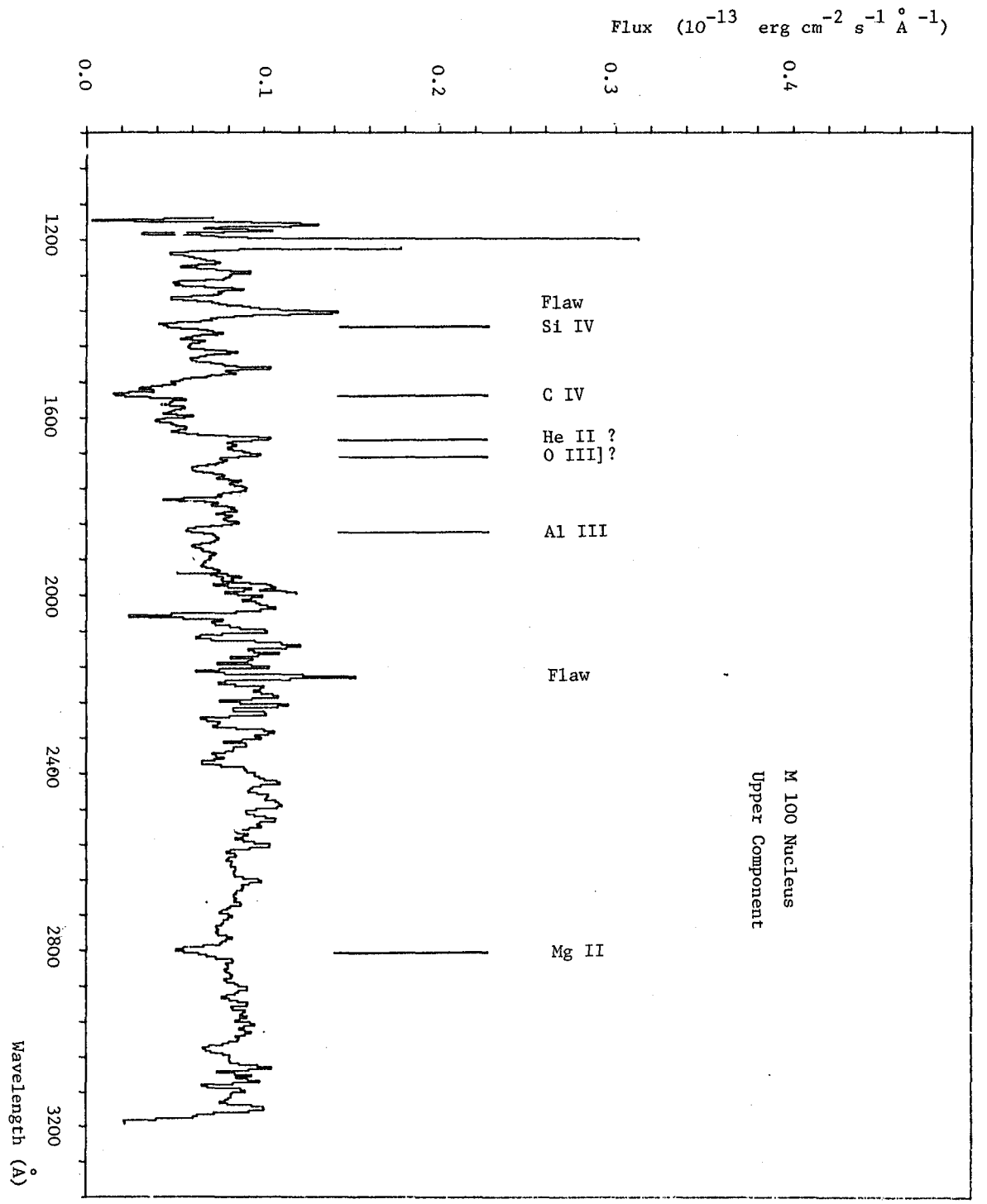
Flux (10^-13 erg cm^-2 s^-1 Å^-1)
0.0
0.1
0.2
0.3
0.4
1200
1600
2000
2400
2800
3200
Wavelength (Å)
Flaw
Si IV
C IV
He II ?
O III]?
Al III
Flaw
Mg II
M 100 Nucleus
Upper Component

Figure 1

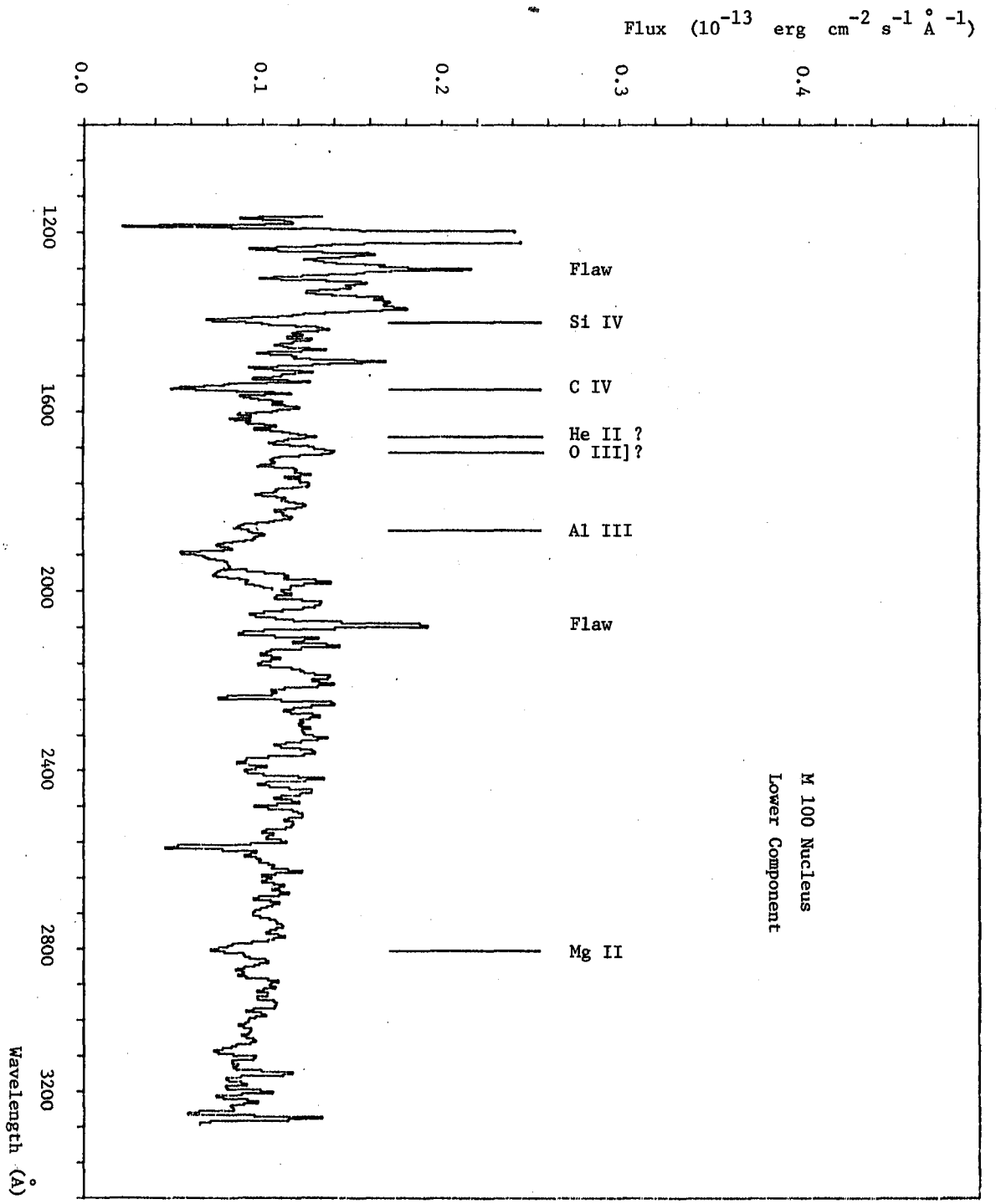
Flux (10^-13 erg cm^-2 s^-1 Å^-1)
0.0
0.1
0.2
0.3
0.4
1200
1600
2000
2400
2800
3200
Wavelength (Å)
Flaw
Si IV
C IV
He II ?
O III]?
Al III
Flaw
Mg II
M 100 Nucleus
Lower Component

Figure 2

IUE OBSERVATIONS OF THE NUCLEAR REGION OF M51

P. Benvenuti
ESA-IUE Observatory - MADRID

S. D'Odorico
European Southern Observatory - GENEVA

ABSTRACT

The nucleus of the Sc galaxy M51 = NGC 5194 has been observed with IUE in the long and short wavelength range. Visual inspection and cross-cuts perpendicular to the dispersion reveal the presence of a UV knot 10 arcsec south of the nucleus of the galaxy. Separate spectra of the nucleus and of the knot were extracted using the spatially resolved images.

The energy distribution of the nucleus fits the known blue and visual spectrum. Shortward of 2800Å, the nucleus and the knot have similar brightness. In the 1200-2000Å range both spectra are essentially flat. The UV knot has been identified with an Hα region at 500 pc from the center of the galaxy.

The CIII] λ1909Å and the [OII] λ2470 lines have been detected both in the nucleus and in the UV knot while upper limits have been set for the CIV λ1550Å and CII λ2325Å emissions. The UV line intensities have been used in conjunction with final line data to infer physical conditions and abundances of the emitting gas (Benvenuti and D'Odorico, 1980, in preparation).

It is known from population synthesis work based on final observations that the nucleus of M51 contains a predominantly old population. The UV data will now be used together with existing final observations in an attempt to solve the ambiguities of previous population synthesis work, in particular the nature of the stars responsible for the observed UV flux. The UV knot shows a spectrum with little contribution from yellow and red stars. At the same time the number of stars of spectral type earlier than AØ has to be small.

It has to be remarked that the presence of regions of completely different stellar populations at distances as small as 500 pc would create severe ambiguities in the interpretation of the spectra of galaxies at more than 20 Mpc, where such regions would not be resolved.

THE ULTRAVIOLET SPECTRA OF EARLY TYPE GALAXIES

G. Bruzual A. and H. Spinrad

Astronomy Department
University of California, Berkeley, California 94720

ABSTRACT

The average spectral energy distribution for a sample of bright elliptical galaxies is presented in the range λλ 2000 to 3200 Å. Spectral synthesis indicates that elliptical galaxies are most likely older than 9 Gyrs. The ultraviolet flux is consistent with a population of red horizontal branch stars, as those present in metal-rich globular clusters. Data for distant ($z \sim 1$) first-ranked cluster galaxies show indications of spectral evolution.

INTRODUCTION

Detailed knowledge of the ultraviolet spectra (λλ 2000-3200A) of early type galaxies is important for at least three reasons. First, it may provide clues about the presence of a hot stellar population which does not contribute appreciably at optical wavelengths. Second, spectral features identified in the spectra of nearby galaxies can be used as redshift indicators for distant galaxies (up to $z \sim 1$). And, third, combining this information with our notions of stellar evolution, some conclusions about the spectral evolution of galaxies can be derived. In particular, the stellar population present in first-ranked galaxies in distant clusters can be compared with that expected for galaxies of different morphological types at the corresponding age, and hence the correctness of the assumption of similarity of all first-ranked cluster galaxies can be tested.

OBSERVATIONS

Low resolution IUE spectra with moderate signal-to-noise ratio in the range from 2000 to 3200 Å are now available for several early type stellar systems. Table I gives galaxy identification and morphological type, exposure time and IUE observer for the sample used in this paper. Figure 1 shows the average spectral energy distribution, where each galaxy spectrum has been normalized at 2900 Å and weighted according to the exposure time.

The most conspicuous spectral features that can be seen in this spectrum are the Mg I (2852) and Mg II (2799) absorption lines and the spectral discontinuities at 2420, 2640, and 2900 Å, which result from the blends of many metallic lines. This spectrum is characteristic of a metal-rich stellar population, as can be seen from the IUE spectra of globular clusters (ref. 3). These features are prominent in spectral types A7 and F8 (ref. 4). No emission lines have been detected in this spectral range. The high frequency structure for $\lambda < 2300$ and $\lambda > 3200$ Å is due to the low signal-to-

noise ratio of the individual spectra at their edges, and does not represent reproducible spectral features. This has been checked by comparison with a ground based spectrum of M32 of high signal-to-noise ratio, down to λ 3200 Å. The apparent sharp absorption features at λλ 2400, 2580, and 3100 Å are due to reseau marks in the IUE camera.

INTERPRETATION

The quality of the present data is high enough to allow an interpretation of the spectrum in terms of the stellar population present in elliptical galaxies. As part of a separate investigation (refs. 5 and 6), evolutionary models for galaxy populations and spectra have been constructed. Elliptical galaxies are well represented by a model in which initial star formation takes place at a constant rate for a time interval of 1 Gyr, with an initial mass function similar to that observed in the solar neighborhood (x=1.35), and is zero afterwards. Evolutionary tracks for solar composition from Ciardullo and Demarque (ref. 7) are used to follow the subsequent evolution of the stellar population. The observed luminosity function for giants in the solar vicinity, as derived by Tinsley and Gunn (ref. 8), is used to complete the evolutionary tracks onto the giant branch. Standard stellar spectra for solar metallicity are used to construct the resulting galaxy spectrum with a resolution of 50 Å in the optical region. In the ultraviolet, OAO-2 (ref. 4) spectra for stellar types earlier than G5, and IUE spectra obtained by the authors for late type giants, complete the spectra with a resolution of 10 Å to 2000 Å.

The following results have been derived from these models.

(a) In the region from 2000 to 4000 Å the observed spectra are well reproduced by the model at an age of 5 Gyr. However, this model has B-V = 0.83, which is about 0.15 magnitude bluer than a typical giant elliptical. In addition, this young age implies formation redshifts for $q_o = 0$ of 0.34 ($H_o = 50$) or 1.04 ($H_o = 100$) which seem much too low for current views of massive galaxy formation. The predicted B-V at z = 0.46 is 1.26 ($H_o = 100$). This is too blue for the observed color of 1.4 (refs. 9 and 10). For a different interpretation, see ref. 11.

(b) In the region from 5000 to 8000 Å, the observed spectrum is not reproduced until an age of 8 to 9 Gyr. However, by this time, the model is deficient in ultraviolet light. We have interpreted this deficiency as due to the lack of horizontal branch stars in our model. To test this hypothesis we have added some light to the models from stars in the range F0 to F8, which resemble well the spectra of metal-rich globular clusters (ref. 3). The fraction of this light added to the models is arbitrary and depends on the age assumed for the galaxies. Table II shows the fraction of light inside the V-band for three different stellar groups at three possible galaxy ages. The fit to the observed spectrum from 2000 to 8000 Å is equally good for any of these models. Thus, it does not seem possible to derive the typical age of the population on spectral grounds solely. Assumptions about the evolution of the horizontal branch population, together with observed spectra of galaxies at z > 0.4 may provide clues about the most plausible age. This

is being explored in ref. 10.

c) Even though some light from giant stars hotter than those commonly seen in the solar neighborhood is required to reproduce the galaxy data, these stars are not hotter than F0 (T=7200, B-V=0.30). In the HR diagram these stars fall to the right of the RR Lyrae instability strip, and thus are characteristic of a red horizontal branch (ref. 12). This is not surprising, given the similarity of the galaxy spectra and those of metal-rich globular clusters (ref. 3). The number of horizontal branch stars required to reproduce the spectra is equivalent to a few percent of the total number of stars in the red giant branch. This ratio is given in the last line of Table II. Most likely these stars are more conspicuous in the elliptical galaxies than in the solar neighborhood because of the intrinsic differences between both populations and the larger volume sampled in the case of the galaxies.

SPECTRAL EVOLUTION

Figure 2 shows the observed spectral energy distribution for E galaxies at z = 0, 0.2, 0.5, and 1.1 in the rest frame of the galaxies (refs. 10 and 13). The galaxies at z=0.5 and 1.1 are bluer in the range λλ 2700 - 3800 Å than the average nearby elliptical. Similarly, the amplitude of the 4000 Å discontinuity is lower in the distant E galaxies than in nearby ones. This is expected from the normal evolution of the main sequence stars in these galaxies (ref. 5). The extent to which star formation could be taking place in these ellipticals at z > 0.5, as well as the relative importance of horizontal branch stars at the respective epoch is the subject of a separate investigation (ref. 10). Certainly, some luminous, red-color-selected E galaxies have had no active star formation over the last 5-7 Gyrs.

CONCLUSIONS

Our spectral synthesis models for the spectrum of elliptical galaxies in the range λλ 2000 to 8000 Å imply that these systems are most likely older than 8-9 Gyr. The flux in the region from 2000 to 3200 Å can be understood as being produced by stars in the red horizontal branch, similar to those observed in metal-rich globular clusters. In this respect we disagree with the recent results of O'Connell (ref. 11). Spectra of distant elliptical galaxies show slight indications of evolution, consistent with our ideas about stellar evolution.

REFERENCES

1. Johnson, H. M. 1979, *Ap. J. (Letters)*, 230, L137.
2. Cappacioli, M., Bertola, F., and Oke J. B. 1980, (in preparation).
3. Dupree, A. K., Hartmann, L., Black, J. H., Davis, R. J., Matilsky, T.A., Raymond, J. C., and Gursky, H. 1979, *Ap. J. (Letters)*, 230, L89.
4. Code, A. D., and Meade, M. R. 1979, *Ap. J. Suppl.*, 39, 195.
5. Bruzual A., G. 1980, Ph.D. Thesis, University of California, Berkeley (in preparation).
6. Bruzual A., G., and Kron, R. G. 1980, *Ap. J.* (in press).
7. Ciardullo, B., and Demarque, P. 1977, Trans. Astr. Obs. Yale Univ., 33.

8. Tinsley, B. M., and Gunn, J. E. 1976, *Ap. J.*, 203, 52.
9. Kristian, J., Sandage, A., and Westphal, J. A. 1978, *Ap. J.*, 221, 383.
10. Bruzual, A., G., and Spinrad, H. 1980 (in preparation).
11. O'Connell, R. W. 1980, *Ap. J.*, 236, 430.
12. Phillip, A. G. D., Cullen, M. F., and White, R. E. 1976, Dudley Obs. Reports, 11.
13. Spinrad, H., Stauffer, J., and Butcher, H. 1980 (in preparation).

TABLES

Table I. Galaxies observed with IUE

Galaxy**	Type	LWR exposure	Reference
M31 (nuc)	Sb	8.5 hrs	1,*
M32	dE2	5.5	*
NGC 3379	E1	7.0	2
NGC 4472	E2	10.5	*

* Data from authors.
** IUE aperture size was "large", an oval 10"x20" in dimension.

Table II. Fraction of Flux in the V-band

Model age (Gyr)	9	13	16
Turnoff	G5	G7	G9
[FO - F8] (HB)	0.05	0.09	0.13
Turnoff - M6V	0.44	0.37	0.34
Red Giants	0.51	0.54	0.53
N(HB)/N(RG)*	0.028	0.034	0.050

* Number ratio of horizontal branch to red giant stars.

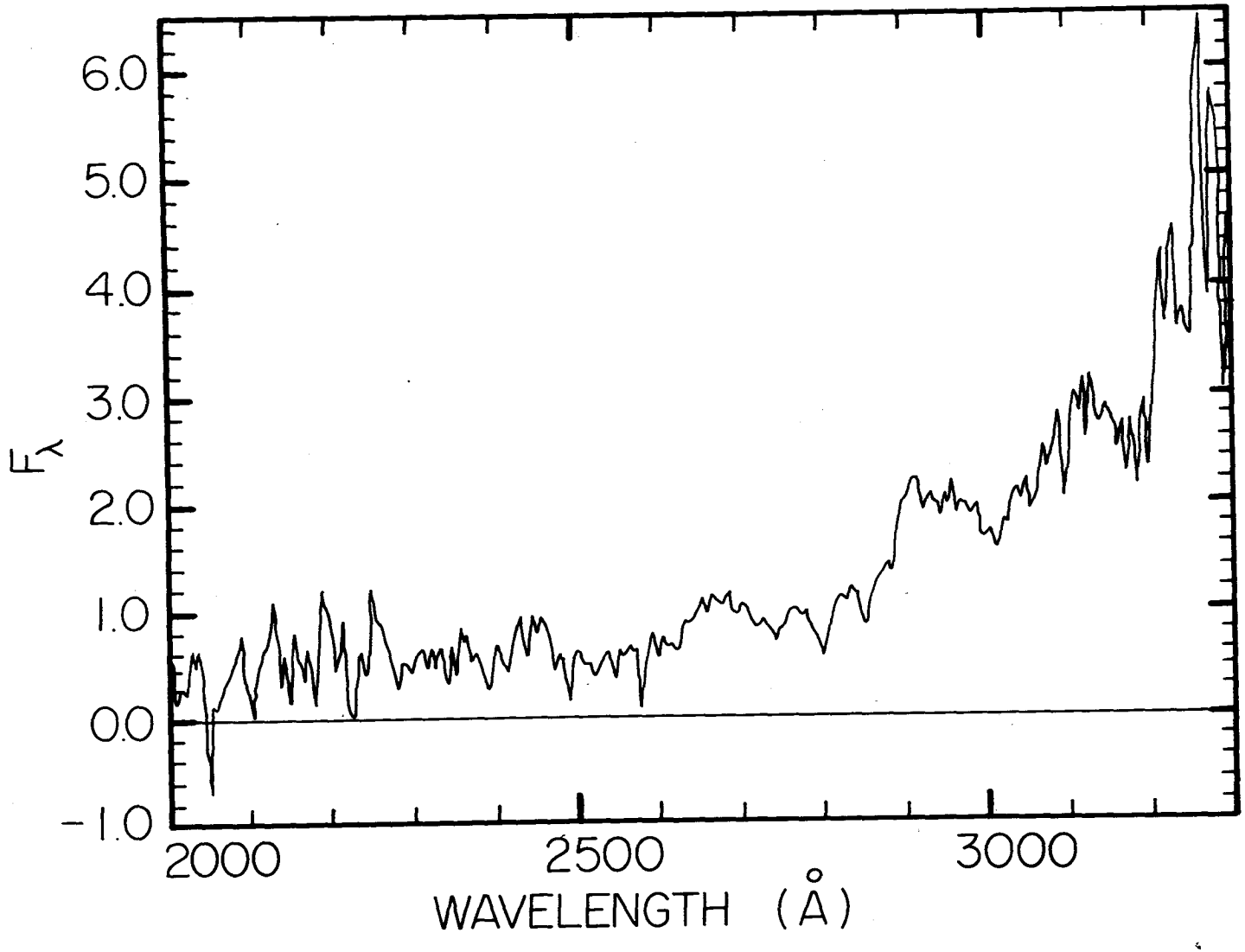

Figure 1. Average spectral energy distribution for galaxies listed in Table I. Each spectrum was normalized at 2900 Å and then weighted according to the exposure time. (See text for details).

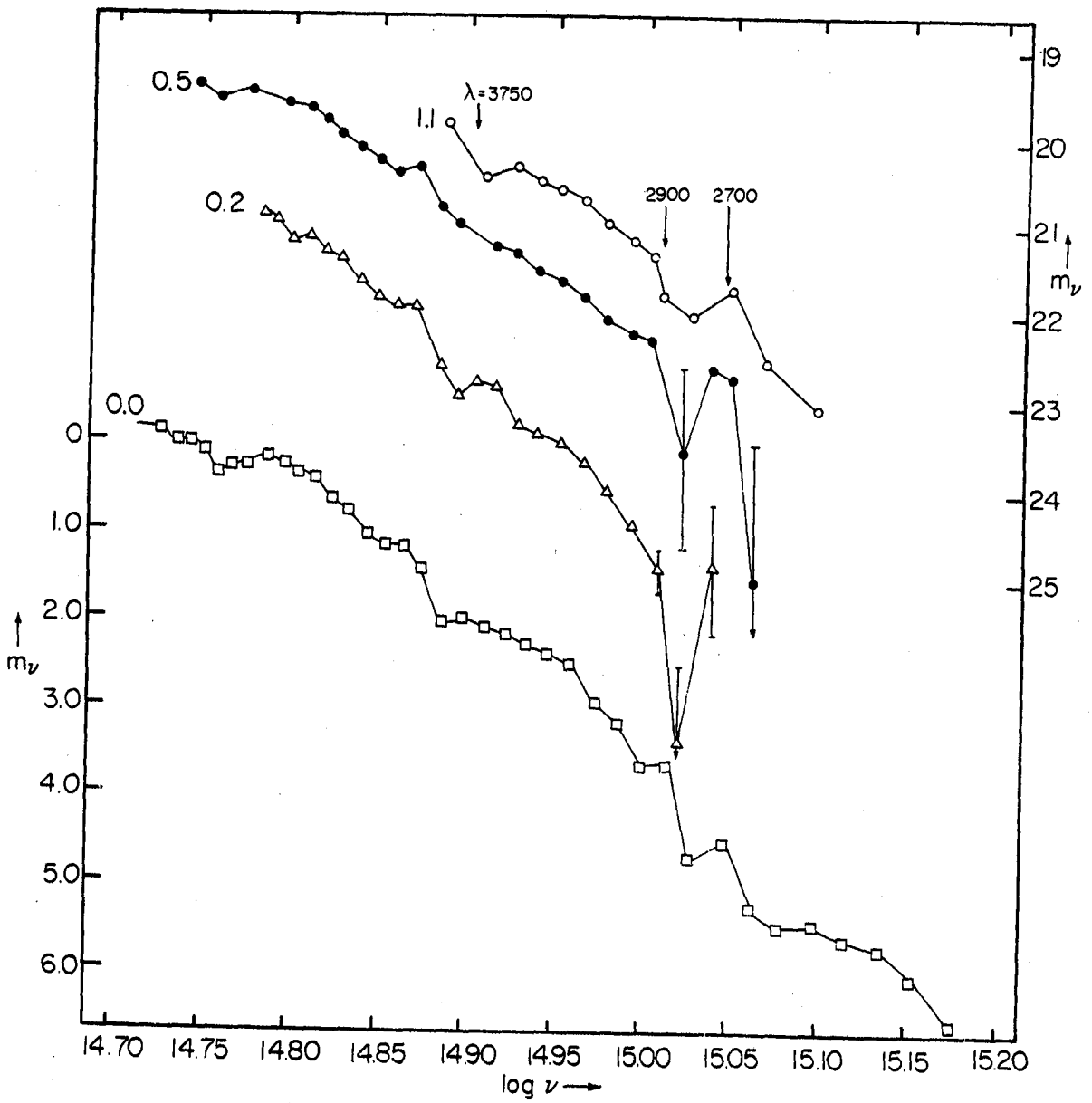

Figure 2. Observed spectral energy distribution for galaxies at z=0, 0.2, 0.5, and 1.1 in the rest frame of the galaxies. (See refs. 10 and 13 for details).

IUE OBSERVATIONS OF SEYFERT GALAXIES[1]

Chi-Chao Wu
Astronomy Dept., Computer Sciences Corporation

A. Boggess and T. R. Gull
Laboratory for Astronomy and Solar Physics
Goddard Space Flight Center

In this presentation we wish to discuss the following three topics:

- Lα / Hβ ratio
- Continuous energy distribution
- Line profile

THE Lα / Hβ RATIO

If the broad hydrogen lines in Seyfert galaxies and QSOs were produced by photo-ionization - recombination plus a small contribution from collisional excitation, the Lα / Hβ ratio would be about 40. However, the composite spectrum derived by combining ground observations of high and low redshift QSOs shows Lα / Hβ ~ 3(1). This result has subsequently been confirmed for a few individual QSOs such as 3C 273(2), PKS 0237-23(3) and B2 1225+31(4). With the IUE, it has become possible to measure the Lα fluxes for a large number of Seyfert galaxies. Since the fluxes of Balmer lines are already available from ground-based observations, we can derive the Lα /Hβ ratios for individual objects. In a recent paper (5) we presented the Lα fluxes for 19 objects. Fifteen of these objects were observed by ourselves, and published data were used for the remaining four. The Lα /Hβ ratios of type 1 Seyferts are also found to be about a factor of 10 lower than predicted by recombination theory. The results are summarized in Figure 1 where we plot the Lα /Hβ ratio against the Hα / Hβ ratio. Four reddening lines are also plotted in Figure 1. The origins of the reddening lines labeled A, B, C, and D correspond to Hα / Hβ = 2.8 and Lα / Hβ = 40, 20, 10, and 5 respectively. The standard extinction curve of Code et al. (6) was used to construct the reddening lines. Increments of 0.1 in E(B-V) are indicated by the tick marks along each reddening line. If simple recombination plus collision produce the emission in the broad line region (BLR) of Seyferts and QSOs, the observed points should concentrate at the origin of curve A; or, if there is dust along the line of sight, the observed points would lie along curve A. As indicated in Figure 1, there is no such concentration of points. In fact, the observed points do not cluster about any of the four reddening lines. Foreground reddening does not seem to play a major role in the low Lα / Hβ ratio because, among the 19 objects, only I ZW 1, 3C 120, MKN 79 and NGC 7469 show

[1] Partially supported by a NASA research contract NAS 5-25774

reasonably strong 2200 Å dust absorption features. On the average, these 4 objects do have higher Hα / Hβ ratios than most others. Another interesting point in Figure 1 is that the objects having the largest Lα / Hβ ratios are the type 2 Seyfert MKN 78 and the narrow line component of 3C 390.3. The broad component of 3C 390.3 has the low Lα / Hβ ratio typical of type 1 Seyferts (7). It seems that the low Lα / Hβ ratio is characteristic for the BLR and is probably caused by high density effects (see Ref. 8).

THE CONTINUOUS ENERGY DISTRIBUTION

In figure 2 we plot the continuous energy distribution of NGC 4151 and MKN 509 from the X-ray region to the infrared. Filled circles and triangles are observational data; solid and dashed lines are extrapolations. The X-ray fluxes are from the observations of Mushotzky et al. (9); the UV data (not corrected for reddening) are our own; the optical data are from de Bruyn and Sargent (10); and the IR data are from Rieke (11). For MKN 509 and some others, the spectrum may be turning over at 10.6 μm. But from 3.6 μm to 1200 Å, the data seem to indicate a single power law. The UV - IR power law is significantly steeper than the X-ray power law. This is true for 5 other Seyferts for which we have data from the X-rays to the UV and in a few cases to the IR. In some cases, the extrapolated optical (UV - IR) spectrum falls above the observed X-ray spectrum, suggesting a turnover in the UV, or alternatively a turn-up in the soft X-rays. This turnover may occur at about 1200 Å as found by Green et al. (12) for quasars. Photons in the spectral region between the Lyman limit and the soft X-rays are the major source of heating for the emitting region, and Figure 2 makes it apparent that simple extrapolation of the optical spectrum may grossly overestimate the amount of energy available for heating.

Shields and Mushotzky (13) have studied the effect of hard X-rays on the emission lines of Seyfert galaxies and QSOs. They find that hard X-ray photons enhance the strength of high excitation lines. This result is confirmed by the UV spectra. Strong X-ray Seyferts like MKN 509, ESO 141-G55, and MCG 2-58-22 have Lα / C IV ratios of about 2 or less, whereas UV spectra of weaker X-ray sources, like I Zw 1 and MKN 478, have Lα / CIV ratio of about 5.

THE LINE PROFILE

The CIV 1550 line is relatively free of contamination by other emission lines, so it is suitable for line profile studies. In Figure 3, we have plotted the observed CIV line of MKN 509 (stepped line). Superimposed on the observed data are the computed profiles: 1. Gaussian (continuous curve); 2. Logarithmic (circles); and 3. The first exponential integral function (triangles). It is clear, in this case at least, that the Gaussian profile does not describe the observed data very well. At wavelengths not far from the line center, the logarithmic and the first exponential integral function profiles are essentially identical. In the far wings the first exponential integral function fits the data better. Capriotti, Foltz, and Byard (14, 15) have derived expected profiles of lines emitted by different kinematical and dynamical models of the BLR. They find

that logarithmic profiles can be produced by a spherical ensemble of discrete emitting clouds with steady state radial inflow or outflow. A ballistic radial outflow model produces profiles described by the first exponential integral function. As shown in Figure 3, the CIV λ1550 profile of MKN 509 is best fitted by the first exponential integral function, indicating that the emitting clouds of the BLR are in ballistic outflow.

Our line profile fits were done independently for the blue portion and the red portion of the line. As indicated in Figure 3, when the blue side of the line (open circles) is reflected onto the red side, the red wing line profile (closed circles) is broader, in agreement with the Balmer line asymmetries found by Osterbrock (16). Capriotti, Foltz and Byard (11, 12) suggested that shielding of line photons by dust in the BLR or in the emitting clouds is the cause for this asymmetry. Anderson (17) on the other hand, proposed that the observed asymmetry is a result of gravitational redshift. Either mechanism could fit the asymmetry of the CIV profile.

REFERENCES

1. Baldwin, J. A. 1977, M. N. R. A. S., 178, 67p.
2. Boggess, A., et al. 1979, Ap. J., 230, L131.
3. Hyland, A. R., Becklin, E. E., and Neugebauer, G. 1978, Ap. J., 220, L73.
4. Soifer, B. T., Oke, J. B., Matthews, K., and Neugebauer, G. 1979., Ap. J., 227, L1.
5. Wu, C.-C., Boggess, A., and Gull, T. R., 1980, Ap. J., Nov. 15 issue.
6. Code, A. D., Davis, J., Bless, R. C., and Hanbury - Brown, R. 1976, Ap. J., 203, 417.
7. Ferland, G. J., Rees, M. J., Longair, M. S., and Perryman, M. A. C. 1979, M. N. R. A. S., 187, 65p.
8. Kwan, J., and Krolik, J. H. 1979, Ap. J., 233, L91.
9. Mushotzky, R. F., Marshall, F. E., Boldt, E. A., Holt, S. S., and Serlemitsos, P. J. 1980, Ap. J., 235, 377.
10. de Bruyn, A. G., and Sargent, W. L. W. 1978, A. J., 83, 1257.
11. Rieke, G. H. 1978, Ap. J., 226, 550.
12. Green, R. F., Pier, J. R., Schmidt, M., Estabrook, F. B., Lane, A. L., and Wahlquist, H. D. 1980, preprint.
13. Shields, G. A., and Mushotzky, R. F. 1979, Astr. Ap., 79, 56.
14. Capriotti, E., Foltz, C., and Byard, P. 1980a, preprint.
15. . 1980b, preprint.
16. Osterbrock, D. E. 1977, Ap. J., 215, 733.
17. Anderson, K. S. 1980, preprint.

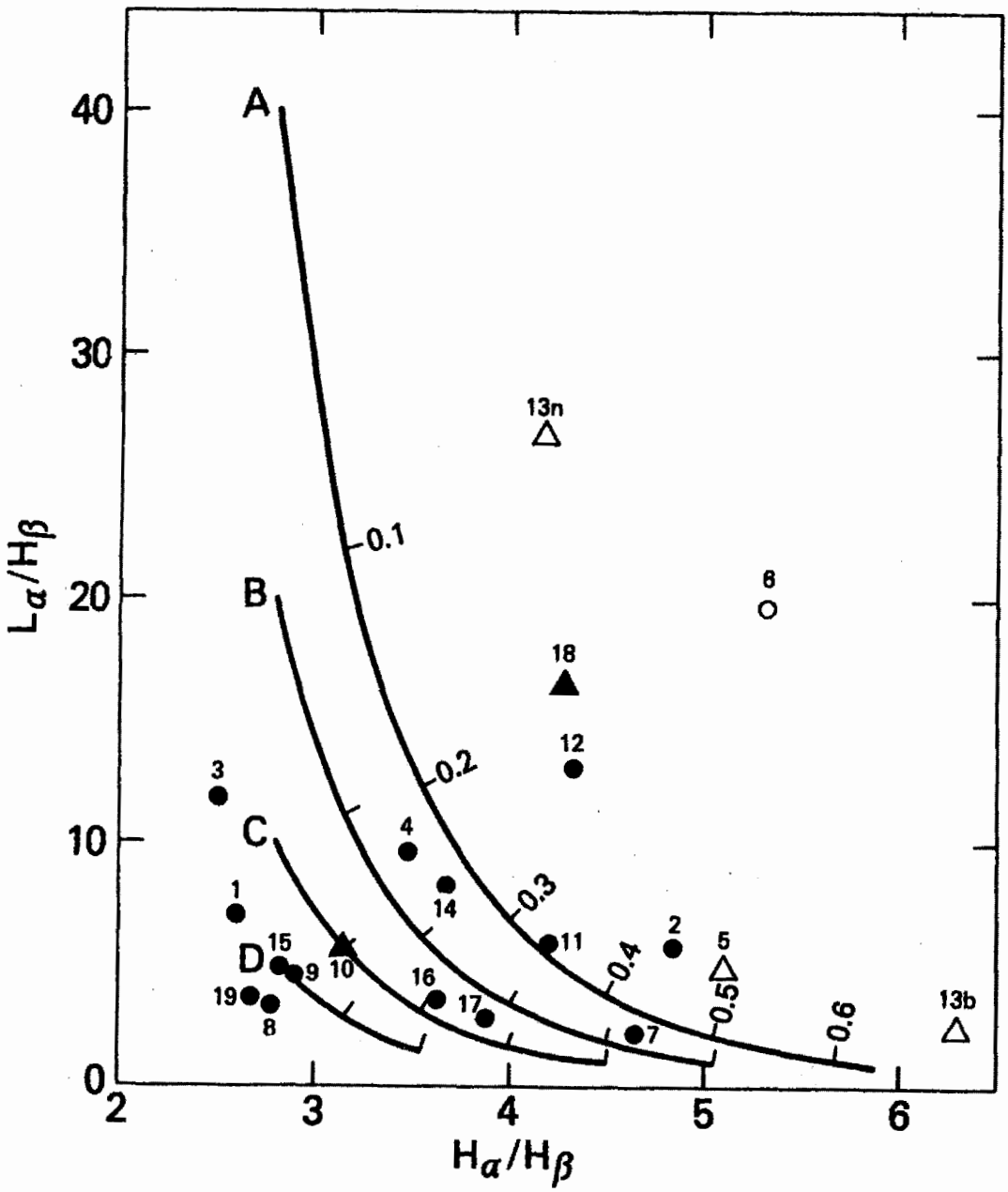

Fig. 1. The Lα / Hβ - Hα / Hβ diagram

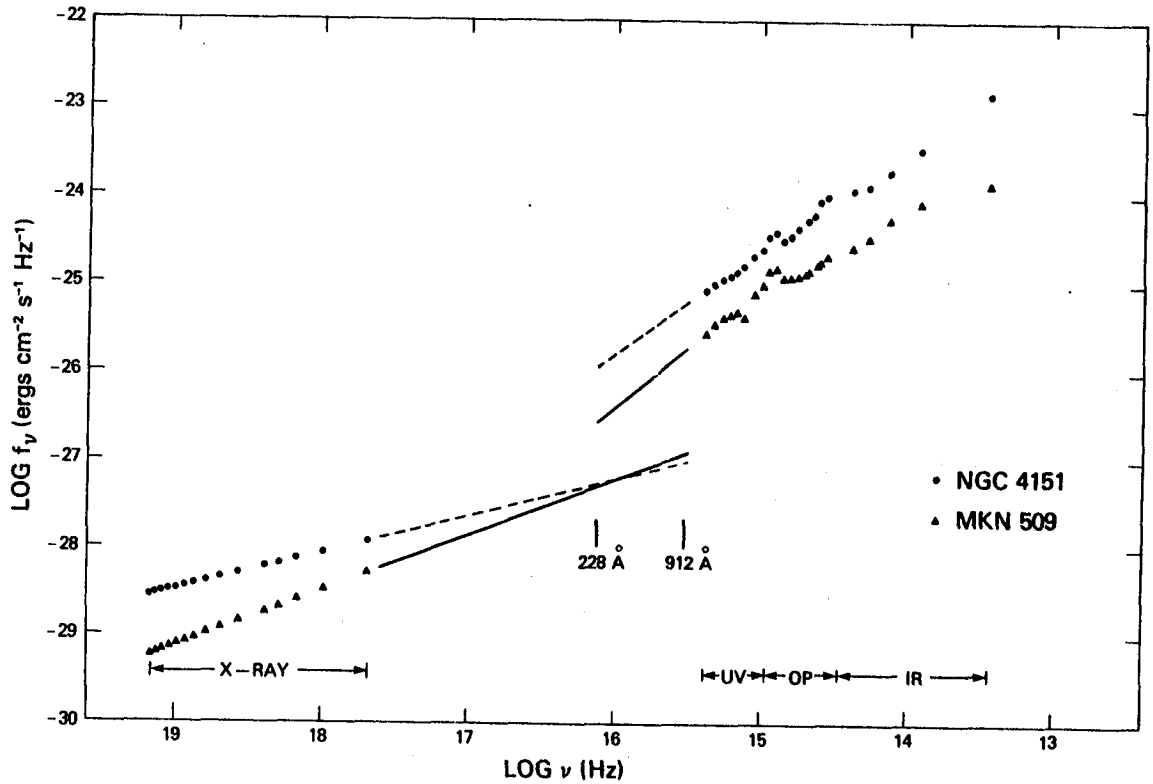

Fig. 2. The continuous energy distribution of Seyfert galaxies MKN 509 and NGC 4151.

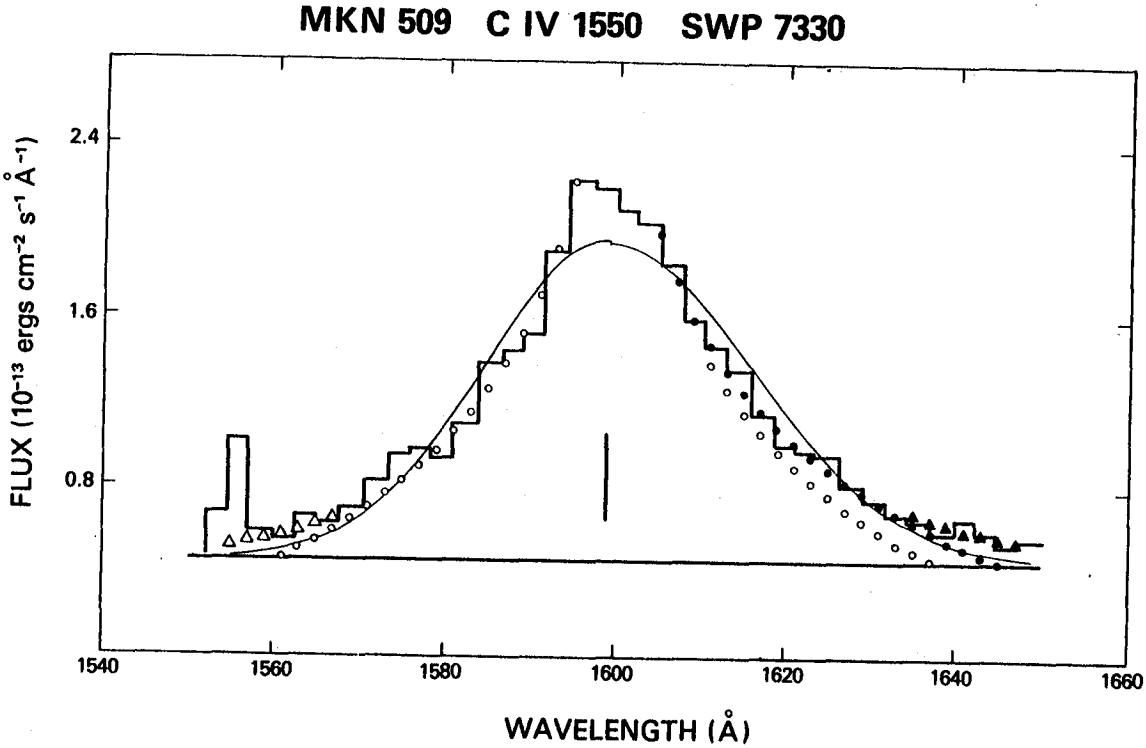

Fig. 3. The CIV λ1550 line of MKN 509.

THE UV VARIABILITY OF THE SEYFERT I GALAXIES III Zw 2 AND MARKARIAN 509

John Huchra and Margaret Geller
Harvard-Smithsonian Center for Astrophysics

Donald Morton
Anglo-Australian Observatory

III Zw 2 and Markarian 509 are classified as classical Seyfert I galaxies based on their broad emission line spectra and strong blue optical continuum[1]. The optical spectra of both galaxies are similar -- Balmer emission with a full-width-zero-intensity of $\sim$ 150 Å, weak Fe II emission and weak He emission[1]. The redshift of III Zw 2 is Z = 0.091, and its magnitude and colors are V = 15.6, U-B = -0.70 and B-V = 0.52. The redshift of Markarian 509 is Z = 0.034 and it has V $\cong$ 13.1, U-B = -0.98 and B-V = 0.22.

The two galaxies differ markedly in their radio properties. III Zw 2 is a strong source with a highly variable compact component[2,3] while MK 509 is a very weak source[4,5]. Both galaxies show significant variations in x-rays[6,7] and MK 509 has shown variations at optical wavelengths as well[8]. We have made simultaneous observations in the ultraviolet, optical and infrared in order to examine three fundamental aspects of the origin of the continuum emission: (1) are these thermal and nonthermal components, (2) how large is the emitting region, and (3) does the UV flux originate in the same region responsible for the optical, IR, radio and/or x-ray continuum emission?

The ultraviolet observations were made in the low dispersion mode through the large aperture of IUE. Exposure times for Mk 509 were 40 min in both short and long wavelength cameras; those for III Zw 2 were 3½ hours in the short wavelength camera. Mk 509 was observed in May, August and November of 1979. III Zw 2 was observed in May of 1978 and in May and August of 1979. The average short wavelength spectra are shown in figure 1; more detailed discussions of these spectra will be published later[9,10]. We measured UV fluxes in bandpasses of 70-200Å free of strong emission lines. Simultaneous optical data were obtained with a photon-counting reticon and the 1.5 m Tillinghast Reflector at Mt. Hopkins. Broad band IR photometry was obtained within 10 days of the UV measurements with the CFA InSb system on the 2.1 m at KPNO. We also accumulated all other published optical[11,12,13,14], IR[15,16,17,13] and x-ray[18] photometry. Additional unpublished x-ray[19] and radio[20] data were kindly made available by J. Delvaille and W. Dent and T. Balonek.

Although we do not have sufficient simultaneous coverage to discuss timescales and detailed spectral changes, we have enough information to

discuss amplitudes and long term trends. Two ways of characterizing the amplitude of variation are the ratio of the variance (σ) to the mean (μ) and the ratio of the maximum excursion (Max E) to the mean. These yield identical information if the deviations are characterized by a normal distribution; however Max E/μ is much more sensitive to the presence of a long tail in the distribution. It should be pointed out that it would be better to use the median rather than mean for these characterizations provided the median is well defined.

Table 1 gives estimates of σ/μ and Max E/μ derived from all the available data at the frequencies listed. n is the number of observations and $\bar{f}$ is the mean flux density in each band. Figure 2 shows the energy distributions from the x-ray to the radio. We also give an estimate of the observational error for a single observation (σ/μ has been corrected for σ obs) at each frequency. For the UV observations, the error in the observed flux -- calculated by examining the pixel to pixel deviations over our bandpasses -- is comparable to the measured calibration error in IUE[21]: both are $\sim$ 6%. The other errors are as quoted by the observers.

For III Zw 2, the amplitude of the variations in the UV-O-IR range is less than or of order 15% whereas in the x-ray and high frequency radio the variations exceed 50%. The amplitude of the variations in Mk 509 decreases steadily from the x-ray to the infrared.

Figure 3 shows the behavior of III Zw 2 in the x-ray through radio (high frequency) from May 1978 through Dec. 1979. The simultaneous outburst in the radio and x-rays is apparent, but no such variation is seen in the optical and IR. Although we do not have a UV measurement at the peak of the outburst, the UV data in 1979 follow the optical data well but do not follow the radio data.

For both objects, the overall energy distribution appears to be non-thermal. It has been suggested that the IR continuum in III Zw 2 is due to dust[17,15], however the optical and UC observations of III Zw and 2 and Mk 509 suggest that this is not the case. The Hα/Hβ/Hγ ratios in both objects indicate little reddening for the region of permitted line formation and the equivalent widths of the optical and UV lines do not vary. The IR-UV spectra of III Zw 2 and Mk 509 have the same shape. Both are reasonably well characterized by a powerlaw with an emission feature at 3000 Å (also often seen in quasars[12]). Finally, there is no evidence for the 2200 Å feature in the long wavelength spectrum of Mk 509. If the IR were re-radiated UV, we would expect to see this feature[22].

If the IR is not thermally reradiated UV flux, the low amplitude of variability in UV-IR indicates that the region in which this radiation originates is not the same as that in which the radio and X-rays are produced. The simultaneous appearance of bursts in the radio and X-ray implies that the X-radiation is inverse Compton scattered flux produced in the compact radio component.

We would like to thank Dr. M. Aaronson, J. Peters, and B. Wyatt for their help in obtaining simultaneous optical and infrared observations. We would also like to thank R. Mushotsky, J. Delvaille, T. Balonek and A. Wilson for useful discussions and communication of data prior to publication. Steve Preston provided valuable assistance in reducing the data at CFA.

REFERENCES

1. Osterbrock, D., 1977, Ap. J. 215, 733.
2. Huchtmeier, W. and Wright, A. 1973, Ap. Lett. 15, 209.
3. Wittels, J. J., Cotton, W. D., and Shapiro, I. I., 1978, Ap. J., L47-L48.
4. Wilson, A., and Meurs, E., 1980, private communication.
5. Willis, A., and Wilson, A., 1980, private communication.
6. Schnopper, et al., 1978, Ap. J. 222, L91.
7. Dower, R., et al., 1980, Ap. J. 235, 377.
8. Magnitskaya, O., and Saakyan, K., 1976, Astrofizica 12, 431.
9. Geller, M., Huchra, J., and Morton, D., 1980, to be published.
10. Huchra, J., and Geller, M., 1980, to be published.
11. de Bruyn, A., and Sargent, W. L. W., 1978, A. J. 83, 1257.
12. Neugebauer, G., et al., 1979, Ap. J. 230, 79.
13. Lebofsky, M., and Reike, G., 1980, Nature 284, 410.
14. Green, R., Williams, T., and Morton, D., 1978, Ap. J. 226, 729.
15. Reike, G., 1978, Ap. J. 226, 550.
16. Glass, I., 1979, M.N.R.A.S. 186, 29P.
17. Rieke, G., and Lebofsky, M., 1979, Ap. J. 227, 710.
18. Marshall, F., 1980, B.A.A.S. 11, 792.
19. Delvaille, J., 1980, private communication.
20. Dent, W., and Balonek, T., 1980, private communication.
21. Bohlin, R., et al., 1980, Astron. & Ap. in press.
22. Oke, J. B., and Zimmerman, B., 1979, Ap. J. 231, L13.

Table 1 (a) III Zw 2 Variability

Band	log ν (Hz)	n	σ/μ	Max E/μ	log $\bar{f}$ (ergs/cm^2/s/Hz)	σ_{obs}
2-6 Kev	18.0	7	0.50	1.66	-28.91	.20
1475 Å	15.31	2	—	—	-26.14	.10
1595 Å	15.27	3	0.12	0.22	-26.12	.10
1830 Å	15.21	3	0.12	0.22	-25.92	.10
3500 Å	14.94	6	0.13	0.46	-25.43	.10
4500 Å	14.83	9	0.15	0.42	-25.39	.05
5500 Å	14.74	8	0.12	0.44	-25.34	.05
7000 Å	14.63	7	0.12	0.44	-25.22	.05
1.25 μ	14.38	14	0.11	0.46	-25.02	.05
1.65 μ	14.26	12	0.13	0.45	-24.88	.05
2.20 μ	14.13	13	0.10	0.38	-24.61	.05
3.5 μ	13.93	4	(0.10)	0.29	-24.42	.10
10.1 μ	13.48	1	—	—	-24.36	.20
90 GHz	11.0	8	0.89	2.78	-22.65	.20
30 Ghz	10.5	8	0.33	0.91	-22.54	.10
15.5 GHz	10.2	21	0.17	0.64	-22.69	.07
7.9 GHz	9.9	11	0.21	0.66	-22.79	.05

Table 1 (b) MK 509 Variability

Band	log ν (Hz)	n	σ/μ	Max E/μ	log $\bar{f}$ (ergs/cm^2/s/Hz)	σ_{obs}
2-10 Kev.	18.16	4	(0.27)	(0.74)	-28.67	.15
1430 Å	15.32	3	0.21	0.40	-25.34	.10
1760 Å	15.23	3	0.19	0.35	-25.23	.10
2250 Å	15.12	3	0.16	0.31	-25.11	.10
2660 Å	15.05	3	0.11	0.20	-25.00	.10
3500 Å	14.93	1	—	—	-24.82	.10
4000 Å	14.89	2	—	—	-24.87	.05
4700 Å	14.81	4	0.11	0.25	-24.93	.03
5400 Å	14.75	4	0.06	0.11	-24.90	.03
5900 Å	14.71	4	0.07	0.16	-24.88	.03
7000 Å	14.63	3	0.10	0.23	-24.78	.05
1.25 μ	14.38	3	0.01	0.05	-24.53	.03
1.65 μ	14.26	3	0.01	0.02	-24.36	.03
2.20 μ	14.13	3	0.04	0.07	-24.18	.03
3.5 μ	13.93	4	(0.11)	—	-23.92	.15
10.1 μ	13.48	1	—	—	-23.85	
6 cm	9.70	1	—	—	-25.40	
21 cm	9.15	1	—	—	-24.90	

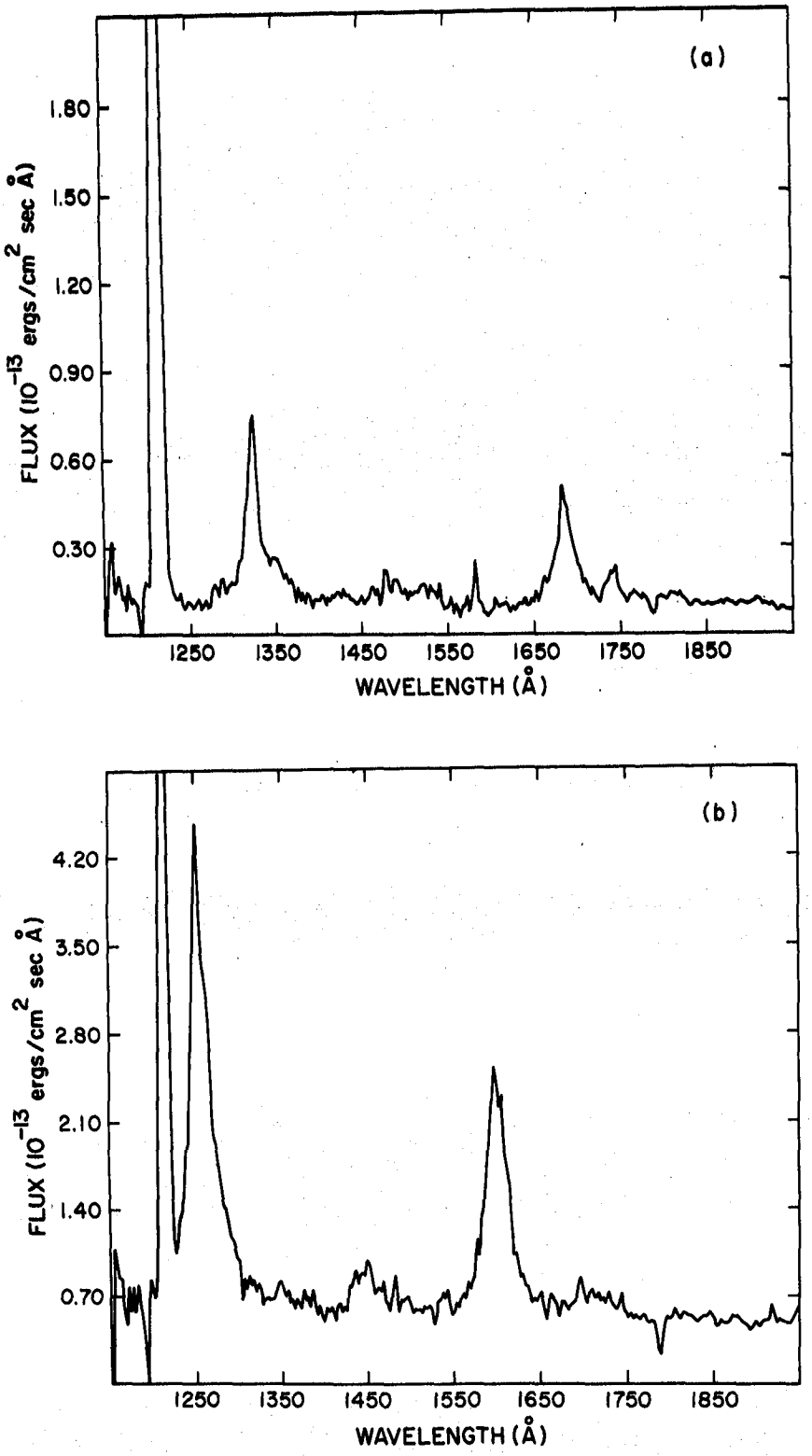

Fig. 1. IUE SWP spectra of (a) III Zw 2, and (b) Mk 509.

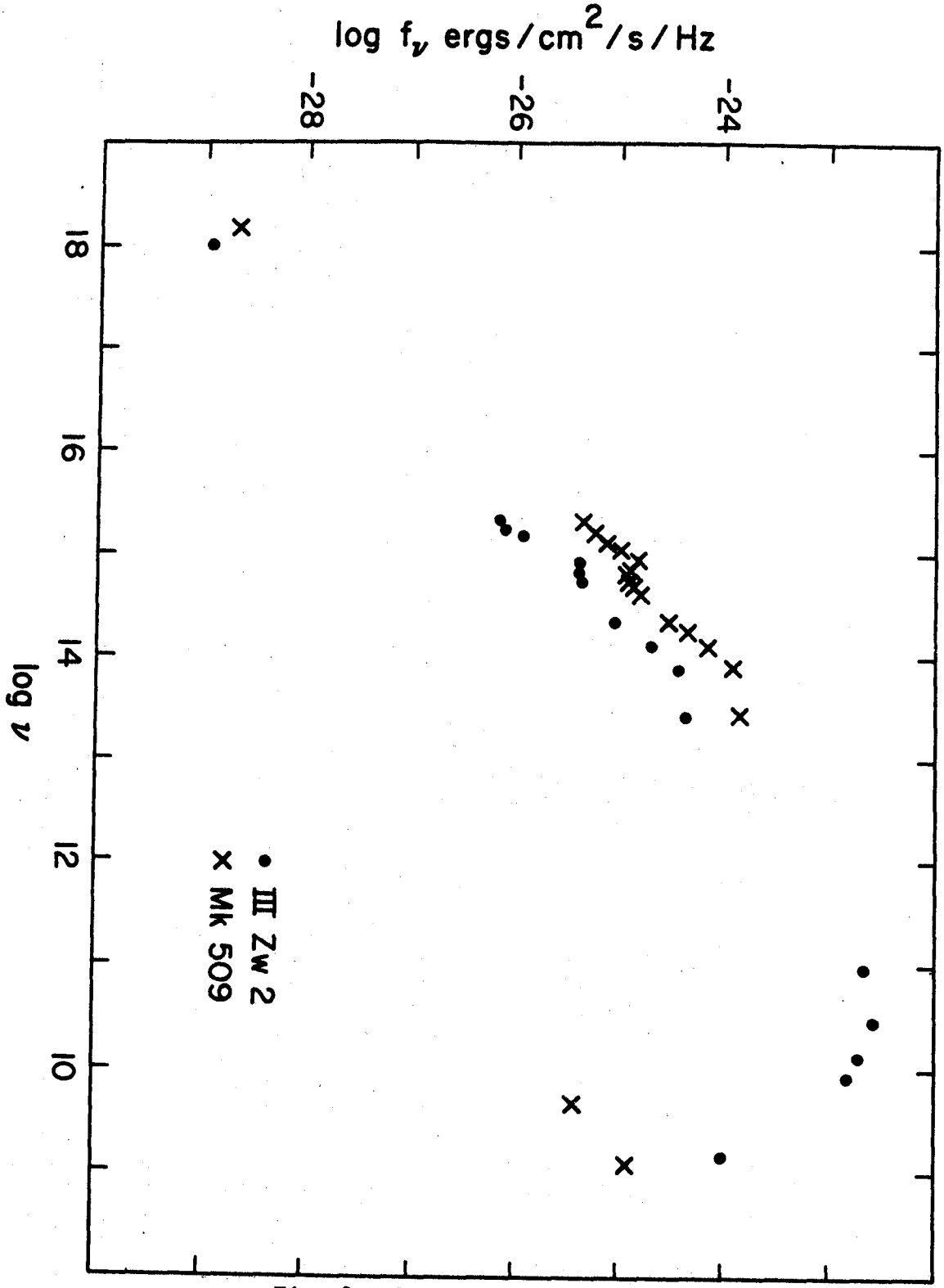

Fig. 2. Composite energy distributions - Radio through X-ray - for III Zw 2 and Mk 509.

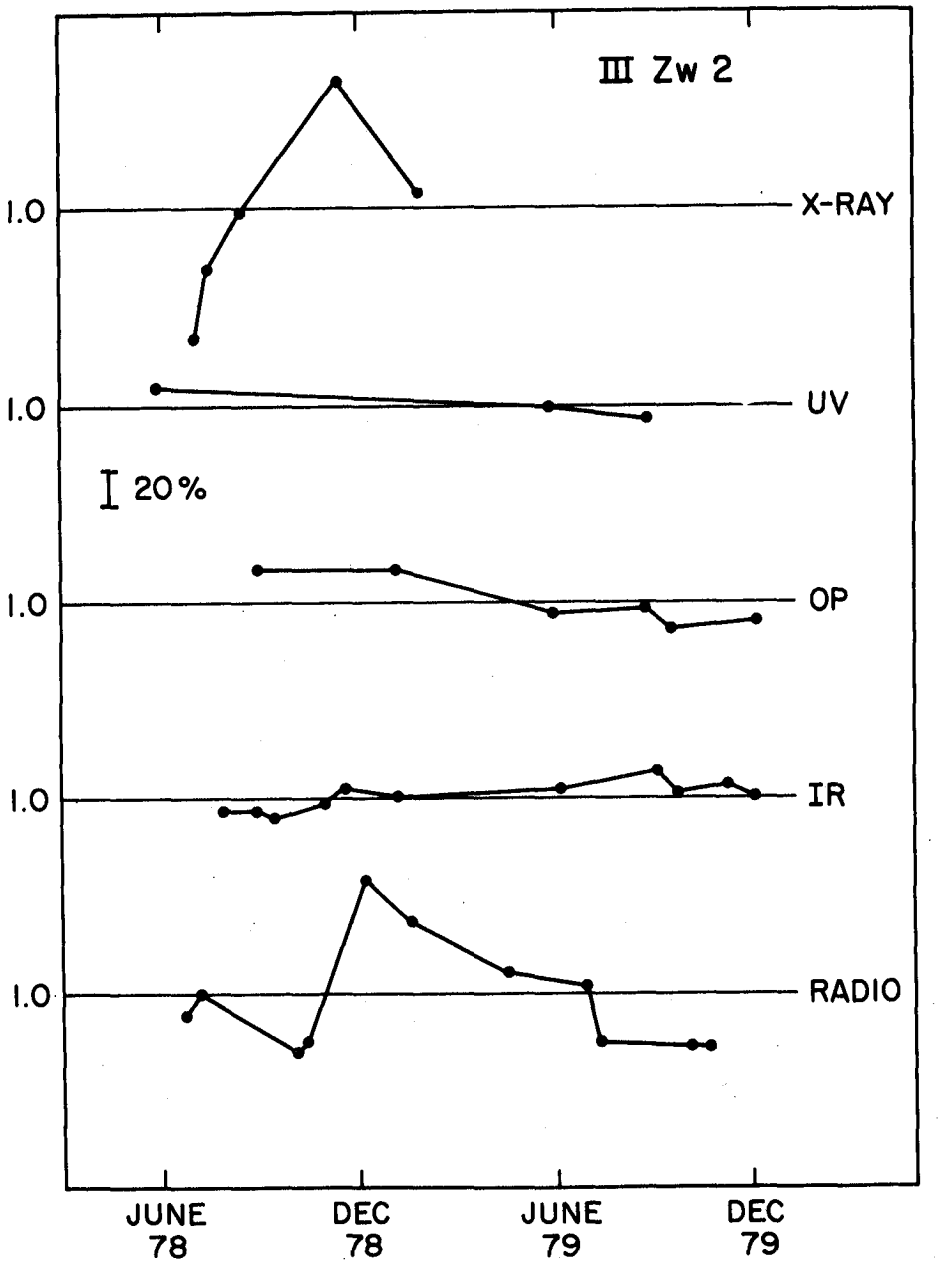

Fig. 3. X-ray, UV, optical, IR, and radio light curves for III Zw 2 plotted as deviations relative to the mean flux. Available data are shown for the time period June 1978 to December 1979. The lines between points are only meant to aid the eye and are not necessarily representative of the true light curve.

SIMULTANEOUS OBSERVATIONS OF ACTIVE GALACTIC NUCLEI WITH IUE

J.N. Bregman, A.E. Glassgold, and P.J. Huggins

New York University

ABSTRACT

IUE observations of four active nuclei have been coordinated with radio, infrared, and X-ray measurements to obtain simultaneous determinations of their continuous spectra. The results for the BL Lac objects 0735+178 and I Zw 187 indicate sufficient UV and X-ray fluxes to ionize any gas. Comparison of the X-ray measurements with the extrapolated optical-UV continuum show a definite X-ray excess for I Zw 187 but none for the other BL Lac object.

INTRODUCTION

We present continuum data on four active nuclei of quasar-like extragalactic objects, with frequency coverage from the radio to the X-ray band. Such measurements are an essential first step to the understanding of the mechanisms by which the central energy source produces the emitted radiation. In particular, the ability to measure the UV flux of these objects with IUE supplies crucial data for defining the characteristics of their continuous spectra. Some of the most interesting types of active nuclei, e.g. the BL Lac objects, present particular difficulties in that they vary on timescales as short as days or weeks. Our observations were planned so that simultaneous observations (within hours or days) could be made at all frequencies in order to obtain definitive spectra for these objectives.

OBSERVATIONS

Table 1 presents the four extragalactic objects observed in October 1979. The IUE observations were low dispersion, short and long wavelength (except for I Zw 187) spectra, taken with the large aperture. Near simultaneous observations were made at radio frequencies by H. Aller of the Univ. of Mich. (8 and 14 GHz), and by W. Dent of the Univ. of Mass. (32 and 90 GHz); at infrared wavelengths by R. Rudy of the Univ. of California at San Diego (H,J,K, and L); and at X-ray frequencies with the

Einstein Observatory by the Columbia Astrophysics Laboratory (0.3 - 4 kev). An estimate of the optical flux (V band) was also obtained at the IUE immediately before each exposure. All the measurements were made within two days of the IUE exposures, except for those at 32 and 90 GHz, which were made within seven days.

Table 1. IUE Observations

Object (Type)	V	z	D * (Mpc)	Camera	Exp (Min)	UV slope
0735+178 (BL Lac)	15	>0.424	>1020	SW	225	1.7
				LW	130	
I Zw 187 (BL Lac)	16	0.055	160	SW	285	1.6$
NGC 3516 (Seyfert)	13#	.0093	28	SW	100	2.3
				LW	75	
NGC 2782 (Hotspot)	13#	.0084	25	SW	165	1.4
				LW	105	

* based on H=100 km/s Mpc.
$ infrared-optical-ultraviolet slope
# extended underlying galaxy

The simultaneous multifrequency spectra are given in Figs 1-4. The ultraviolet data have been dereddened for the extinction in the Galaxy using the measurements of gas and dust given by Burstein and Heiles (1979), and the Seaton (1979) fit for the selective extinction.

RESULTS

The continuum spectra cover 8 decades in frequency from the radio region (9.9 GHz) to the kev X-ray band (up to 10(+18) Hz). Although the data are closely simultaneous, the two large gaps in coverage (submillimeter to far infrared, and extreme UV to soft X-ray) make suspect any attempt to draw a single continuum through all the data. Nevertheless, we can see that the BL Lac object 0735+178 is consistent with one smooth continuum, and that the

X-ray data can be fit reasonably well by an extrapolation of the infrared-optical-UV data. This extrapolation is a power law $F \sim \nu^{-\alpha}$ with $\alpha = 1.3$. The total integrated flux at the earth is 1.1 (-10) ergs/cm^{2}s, and the total luminosity is greater than 2.0 (+44) ergs/s, for q=1/2, and H=100 km/s Mpc. The other BL Lac object, I Zw 187, differs in several respects: (1) the total integrated flux is 4.2 (-11) ergs/cm^{2}s, and the total luminosity is 1.1 (+43) ergs/s, at least 20 times fainter than 0735+178; (2) the decrease from the radio to the optical is less, i.e. a factor of 100 instead of 1000; (3) the extrapolated infrared-optical-ultraviolet power law is steeper, $\alpha \simeq 1.7$; and (4) there is evidence for an X-ray excess, i.e. the observed X-ray flux is about 10 times greater than that extrapolated from lower frequencies. The Seyfert I galaxy NGC 3516 continues this trend: (1) the ratio of radio to optical flux is only about 10; (2) $\alpha \simeq 2.3$; and the X-ray excess is about 50. NGC 2782 presents some interesting contrasts which probably arise because it is not a quasar-like object. There is almost no change in flux between the radio and infrared region, and the X-ray flux is much less than what is expected when the UV continuum is extrapolated into the X-ray band.

DISCUSSION

Simultaneous UV and X-ray data allow the total flux of ionizing photons to be estimated more accurately than is possible from optical data alone. The BL Lac object 0735+178 is one of the few to have a large enough red shift ($z>0.424$) to shift the Lyman limit to the short wavelength band of the IUE. The fact that the continuum shows no dip or change of slope below the Lyman limit places an upper limit of about 10 (+18) cm on the amount of neutral hydrogen along the line of sight to 0735+178.

It is interesting to compare the optical-UV continua of the two BL Lacs reported here with the Red QSOs recently studied by Rieke et al. (1979) and by Smith and Spinrad (1980). Although the Red QSIs gave very steep spectra ($\alpha \geq 3$), they possess broad emission lines. The fact that the optical-UV continua of the two BL Lac objects are considerably less steep than those of the Red QSOs suggests that the 'lineless' property of BL Lac objects arises from a lack of gas rather than a lack of ionizing flux.

The ability to reliably extrapolate the infrared-optical-UV flux to higher frequencies is also important for an understanding of the continuum emission mechanism. The clear detection of an X-ray excess in I Zw 187 seems consistent with the inverse Compton process, in which radio frequency photons are raised to X-ray energies by scattering from relativistic electrons. By use of the model of Jones, O'Dell, and Stein (1974), the simultaneous data may be used to estimate the size and magnetic field strength of the emitting region. For I Zw 187 we estimate a magnetic field strength

of about 16 G and a size of about 0.0085 pc (10 light days) - approximately the size deduced from temporal flux variations. The data for 0735+178 yield a lower limit of 0.66 pc (2.2 light years) for the size of the continuum emitting region, which is discrepant with that determined from flux variations (1 light week). This disagreement suggests that some new ingredient must be added to the canonical model of the inverse Compton process for the case of 0735+178, such as relativistic flow (Blandford and Konigl, 1979).

REFERENCES

Blandford, R. and Konigl, A., 1979, Ap.J. 232, 34.
Burstein, D. and Heiles, C., 1978, Ap.J. 225, 40.
Jones, T.W., O'Dell, S.L., and Stein, W.A., 1974, Ap.J., 192,201.
Rieke, G.H., Lebofsky, M.J., and Kinman, T.D., 1979, Ap.J., 232, L151.
Seaton,, M.J., 1979, MNRAS, 187, 73p.
Smith, H.E., and Spinrad, H., 1980, Ap.J., 236, 419.

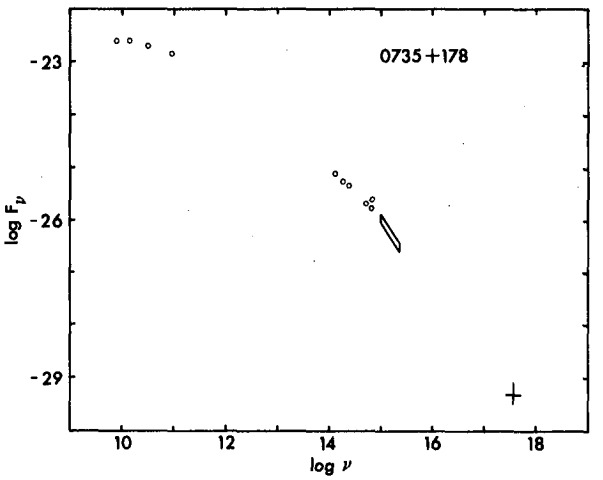

Figure 1

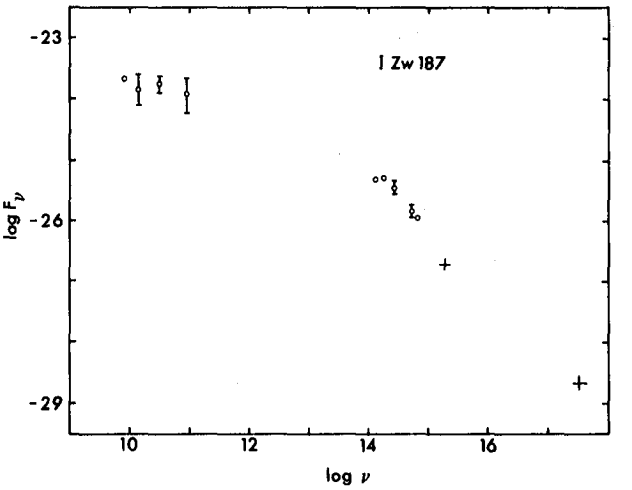

Figure 2

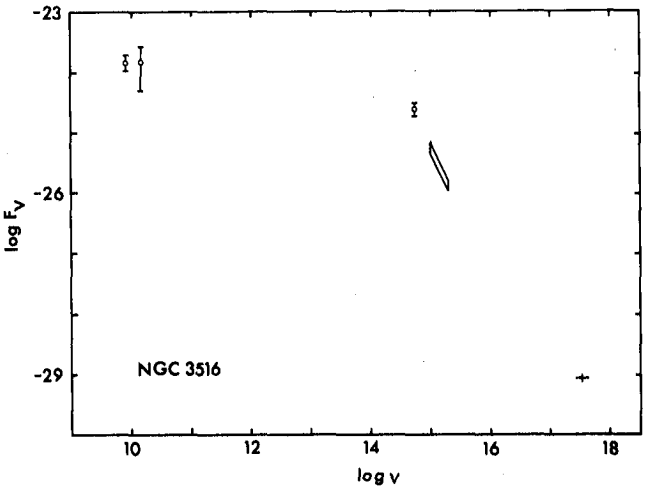

Figure 3

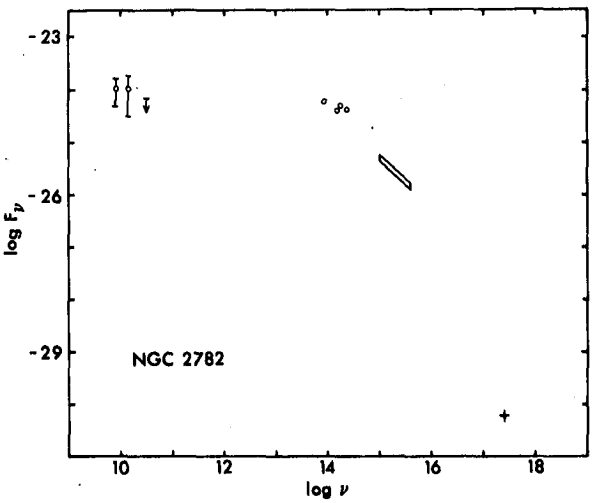

Figure 4

IUE OBSERVATIONS OF Fe II GALAXIES

M.V. Penston
Astronomy Division, ESTEC,
Villafranca Satellite Tracking Station,
European Space Agency,
Apartado 54065, Madrid, Spain

M.A.J. Snijders, A. Boksenberg, J.D.J. Haskell
Department of Physics & Astronomy,
University College London,
Gower Street, London WC1E 6BT

R.A.E. Fosbury
Royal Greenwich Observatory,
Herstmonceux Castle,
Hailsham, Sussex

ABSTRACT

Repeated observations of the Seyfert 1 galaxies I Zw 1 and II Zw 136, which have very strong Fe II emission lines in the optical region, were made at low resolution with the IUE Satellite. The ultraviolet spectra are very similar: both are variable and show broad emission features of Fe II (especially the UV multiplets 1, 33, 60, 62 and 63) as well as the emission lines usually strong in Seyferts and quasars e.g: Lyα, Mg II, C III], C IV and N V. The data strongly support the hypothesis that the optical Fe II emission lines are primarily due to collisional excitation and that resonance fluorescence makes only a minor contribution to the excitation of these lines.

INTRODUCTION

Fe II emission lines in the optical spectra of quasars and Seyfert galaxies were first discovered in 3C273 (ref. 1) and I Zw 1 (ref. 2) and are actually present in many objects (refs. 3, 4). Usually these lines are thought to be excited by either resonance fluorescence or collisional excitation (e.g. refs. 1, 4, 9). Both mechanisms involve excitation of Fe^+ atoms from 4 even-parity levels, the ground state and 3 low-lying metastable levels, to 6 odd levels at 5 to 6 eV, and subsequent cascade to even metastable levels around 3 eV. In Fig. 1 we show an Fe^+ energy level diagram with the strongest observed optical and ultraviolet (this paper) multiplets indicated.

The excitation can be through either collisional excitation by thermal electrons or absorption of UV continuum photons in the UV resonance lines, but in both cases large optical depths in the resonance lines are required for an efficient conversion of ultraviolet to visual photons. For the case of collisional excitation we would expect both the optical and the ultraviolet lines to be in emission. For resonance fluorescence the optical lines are in

emission but the ultraviolet lines could be either in absorption or emission depending on the geometrical situation. In principle, there are amply sufficient ultraviolet continuum photons available for the fluorescence mechanism; however the Fe II lines are formed in the broad line region which may cover only a small part of the continuum source and the absorption lines then must be very broad in order to intercept sufficient ultraviolet photons, requiring uncomfortably large turbulent velocities (ref. 5). Using better atomic data and more extensive model atoms it has been recently shown (refs. 5, 8) that the collisional theory can explain the observed optical Fe II lines. However attempts to observe the predicted Fe II ultraviolet emission lines in Seyfert nuclei have so far only resulted in upper limits to either absorption or emission lines (refs. 10, 12). In quasars, older work also resulted only in upper limits (e.g. ref. 13) but recently better data for several intermediate redshift objects show evidence for Fe II emission in the ultraviolet in the form of broad, low-contrast emission features (refs. 14, 15).

In this paper we present ultraviolet observations for two Seyfert galaxies, with very strong optical Fe II emission lines, which have been extensively studied in the optical. Optical studies of I Zw 1 show two redshift systems at Z = 0.0608 for low ionization lines, (ref. 16). The broad line component has relatively narrow features which greatly facilitate the study of the Fe II emission lines (refs. 2, 3-6, 16, 17). II Zw 136 has broader lines, FWHM about 2000 km sec^{-1} for I Zw 1, and a shallower spectral slope, $\alpha = 0.49$ compared with 1.33 for 1 Zw 1 (ref. 3), but in general the optical spectra of these two objects are similar (ref. 3, 4, 6). By studying these three objects simultaneously we might be able to obtain insight into the vexing problem of why some extragalactic objects show strong Fe II emission and others virtually none (refs. 4, 18). It has been suggested that Fe II emission line objects have a higher density and that the C III] 1908/C IV 1549 ratio might be lower than is normal (ref. 5). However, the available material on differences between line ratios for objects with and without Fe II optical emission is very uncertain and the separation for example of optical depth and density effects is problematical (ref. 5).

In section 2 we discuss the observations and data reduction, in section 3 we present the results for I Zw 1 and II Zw 136 and in section 4 we discuss and summarize the conclusions.

OBSERVATIONS AND DATA REDUCTION

All spectra were obtained using the IUE satellite in the low resolution mode and with the large apertures. A summary of the observations is given in Table 1. For both I Zw 1 and II Zw 136 the exposure times were determined by the strength of the strongest emission lines, Lyα and Mg II, and in the SWP images the continuum is rather faint. The last 2 SWP spectra of I Zw 1 were obtained near the end of a shift and these exposures had to be curtailed, so both are underexposed.

The SWP images were originally processed with the faulty ITF, but after subsequent correction of the ITF errors in the GPHOT image (ref. 19) we re-extracted the spectra directly from GPHOT image using improved software (ref. 19). For the LWR spectra we only reprocessed the background in order to remove particle events and image defects. An improved net spectrum was then obtained from the standard gross spectrum and the new background signal.

Only a relative wavelength scale is given, as the position of the source in the large aperture is unknown. Zero points for the absolute wavelength scales were obtained from the Lyα and Mg II emission lines in the case of I Zw 1 and II Zw 136.

Emission line strengths given in this preliminary report on these data are based on estimated continua and simply integrating the observed flux between suitable wavelength limits. The final results (ref. 20) will be based on profile fitting techniques where possible. For I Zw 1 part of the profile fitting has been done and we can accurately separate complex features like the Si II, Si III, Lyα, N V blend over $1180 < \lambda < 1250$, and estimate the strength of the individual components.

THE UV SPECTRA OF I ZW 1 AND II ZW 136

In Fig. 2 the mean long wavelength spectra of I Zw 1 and II Zw 136 are shown. For I Zw 1 rest wavelengths were calculated assuming $\lambda_o = \lambda/(1+0.0608)$, appropriate for the low ionization lines like Fe II and Mg II (ref. 7).

Comparison of the near UV spectra of Fe II Seyfert galaxies as shown in Fig. 2 with those of other Seyferts and quasars (ref. 10-12) shows two remarkable differences.

i) The Si III] λ_o 1892 intercombination line is greatly increased in strength with respect to C III] λ_o 1908. Normally Si III]/C III] is 0.1 to 0.2, in I Zw 1 Si III]/CIII] $\simeq$ 0.5. Clavel (private communication) has noticed the same effect in another Seyfert galaxy with strong optical and ultraviolet Fe II emission lines.

ii) The strong "blue wing" of the Mg II line previously noticed in some medium redshift quasars (ref. 21) is also present in I Zw 1 and II Zw 136 but here clearly is not due to Mg II alone. In particular, for I Zw 1, profile fitting shows that most of the "Mg II line wing" cannot be due to Mg II at all and that Fe II UV multiplets 62 and 63 provide a good identification.

Comparison between I Zw 1 and II Zw 136 shows that the Fe II multiplets are clearly stronger in I Zw 1, as in the optical region. Only 3 multiplets UV 33, UV 62 and UV 63 can be measured easily in both objects. Multiplets UV 2, 3, 34, 35 and 36 are rather weak and blended with C II] $\lambda \sim 2326$, [Ne IV] $\lambda_o \sim 2422$ and [O II] λ_o 2470 (the Ne IV lines fall virtually on top of the fiducial at 2580 Å but inspection of the original data shows that a substantial emission line is present in both objects at $\lambda_o \sim 2422$. The red

wing of multiplet UV 1 coincides with possible galactic Mg II $\lambda \sim 2798$, absorption, and in II Zw 136 the blue half of the UV 1 emission feature is absent. The latter could be a result of absorption in the object in the two resonance lines which arise from the ground state, $\lambda\lambda$ 2585 and 2600. From theoretical calculations including both fluorescence and collisional processes it appears that even in situations where collisional excitation is the dominant process, in forming the Fe II lines, some resonance fluorescence should take place (ref. 5). Some absorption could also be present in UV 2 and UV 3 and contribute to the apparent weakness of these multiplets.

In table 2 we list the observed emission line strength for both objects. In general, the emission lines do not show evidence for variability and only mean values are given; a possible exception are the weak, far UV lines of II Zw 136 and for these we give values at the two epochs. In December 1978 the weak lines in the SWP region appear to be substantially stronger than in May 1979. However the strong lines Lyα, N V and C IV do not show this effect and the "variability" could be due to errors in the estimated continuum level, which is difficult to determine in all these spectra. Even in the long wavelength spectra the results for the weak broad Fe II emission blends are sensitive to small errors in the adopted continuum. In particular, the results for UV 60 and UV 61, which in the observer's frame fall longward of 3000 Å, where the IUE sensitivity decreases rapidly, are of very low accuracy. At wavelengths $\lambda_o < 2100$ Å there exist additional as yet unidentified broad features. The C III], Si III] blend has very extended wings which could be due to Fe III emission, and the O IV], Si IV feature, $\lambda \sim 1400$, has extra emission in both the red and blue wings which appears present on all spectra. Finally, there are extensive weak emission blends for 1560 Å $< \lambda_o <$ 1800 Å which cannot be explained by the presence of the He II λ1640, O III] $\sim \lambda$1666 and N III] $\sim \lambda$1750 lines. These could be due to Fe II emission from levels above 7 eV, which are strong in solar spectra, RR Tel and Nova Cygni 1978 (ref. 22-24).

We include in table 2 the total optical Fe II emission line flux and the strength of Hβ. For the strongest optical Fe II lines there is good agreement between the measurements of different observers (refs. 3, 4, 16, 17) but for the total emission line strength the weaker features have to be included and here substantial differences do exist. For I Zw 1 we used only the most recent results (ref. 17); comparison between various Hβ measurements (refs. 6, 17) shows that the older data (ref. 6) substantially overestimated the Hβ line strength. For II Zw 136 the Hβ flux (ref. 6) could also be up to 30% too high. Comparison between recent measurements of Fe II lines in both objects indicates that the most extensive set of data (ref. 6) probably still underestimates the total Fe II emission. After comparing all available data we estimate

$$F(\text{Fe II, optical}) \sim 10.3 \times 10^{-13} \text{ erg cm}^{-2} \text{ s}^{-1}$$

for II Zw 136. The optical multiplets 1, 6 and 7, which arise from the metastable a^4P level, have been excluded from the total optical Fe II emission strength. Their role is probably comparable to the Fe II ultraviolet multi-

plets and they have been added to the total Fe II UV flux. Combining all Fe II UV data and applying approximate corrections for blends, e.g. [O II] λ_o 2470, or multiplets not measured (UV 60 and UV 61 for II Zw 136), we obtain for the ratio of optical to ultraviolet Fe II photons: 2.8 for I Zw 1 and 2.1 for II Zw 136. The line strengths for II Zw 136 are in rough agreement with recent collisional excitation models (ref. 5), which predict comparable strength for Hβ, C III], Mg II and the ultraviolet Fe II total line strength, but with at least a factor 2 uncertainty. The highest conversion efficiency of ultraviolet to optical photons is obtained in I Zw 1 and in this object the Fe II lines appear to be considerably stronger than so far predicted; especially the optical lines. These conversion efficiencies are only rough estimates and for individual levels the conversion efficiency can differ substantially; for example for level $z\,^6P^o$ the optical to UV photon ratio is $3.2\ ^{+4.4}_{-1.1}$ where the errors are based on the uncertainties in the UV flux alone.

Very high column densities are indicated by these ultraviolet to optical photon ratios (ref. 9).

Towards shorter wavelengths the continuum variability increases. The December 1978 spectrum of II Zw 136 is shown in Fig. 3 and the 2 mean spectra of I Zw 1 in Fig. 4. Just as in the optical, I Zw 1 has a steeper spectral slope than II Zw 136. The C IV lines in I Zw 1 are very weak but as C III], O IV] + Si IV and N V are normal this cannot be explained by simply a lack of ionizing UV photons. There is no evidence for an intrinsic λ2200 extinction feature in either of the two Seyfert galaxies, but a weak galactic extinction feature could be present in I Zw 1 ($E(B-V) < 0.03$).

SUMMARY

We have observed 2 Seyfert 1 galaxies which emit strong Fe II emission lines in the optical region. They have similar UV spectra, and only differ from normal Seyferts and QSOs (refs. 10-12, 25) in the presence of easily noticable Fe II UV emission lines. In both objects the conversion of UV to optical Fe II photons seems to be comparable: for every detected UV photon there are 1 to 3 optical photons, which implies very high optical depth in the UV lines (refs. 5, 8, 9). The present data appear in good agreement with theoretical predictions based on the collisional excitation theory (refs. 5, 8, 9). The apparent absence of UV Fe II emission in earlier work is possibly due to the nature of the UV emission lines, consisting of broad blends of low contrast against the continuum which can cover the whole region between λ2300 and λ2650 (Fig. 1 and ref. 14) and the region λ > 2700 Å. Some expected UV Fe II multiplets, e.g. UV 64 a ^4D to $z\,^4P^o$, are not discovered so far; these have rest wavelengths around λ3000 and the typical observed wavelengths at λ3200 in the minimum efficiency zone between the IUE and optical domains. Again this points to the need for better observations and highlights the inherent problems in measuring these often weak, broad features. So far only one obvious difference between Fe II and normal Seyfert galaxies has been discovered: the Si III] λ 1892 line appears much stronger than is normal. It has been stressed that theoretical predictions for Fe II lines should give

self-consistent results for other strong lines, and usually Lyα, Hβ, C III], C IV and Mg II are mentioned in this respect (refs. 5, 8). The present results suggest that Si III] should be included and that a check on Fe III, which has many strong lines in this wavelength region (ref. 26) in early type stars, could be useful.

ACKNOWLEDGEMENTS:

Two of us M.A.J.S. and A.B. wish to acknowledge financial support from the S.R.C.. It is a pleasure to thank the resident astronomers at VILSPA ground station for help in acquiring the data.

REFERENCES

1. Wampler, E.J. and Oke, J.B., 1967, Ap. J., 148, 695.

2. Sargent, W.L.W., 1968, Ap. J. Lett, 152, L 31.

3. Philips, M.M., 1977, Ap. J. Suppl, 38, 187.

4. Osterbrock, D.E., 1977, Ap. J., 215, 733.

5. Netzer, H., 1980, Ap. J., 236, 406.

6. Oke, J.B. and Shields, G.A., 1976, Ap. J., 207, 713.

7. Philips, M.M. 1978, Ap. J., 226, 736.

8. Collin-Souffrin, S., Joly, M., Heidmann, N. and Dumont, S., 1979, Astr. & Ap., 72, 293.

9. C. Jordan, 1979, Progress in Atomic Spectroscopy, part B, 1453.

10. Boksenberg, et al., 1978, Nature, 275, 404.

11. Oke, J.B. and Zimmerman, B, 1979, Ap. J. Lett., 231, L13.

12. Ulrich et al., 1980, M.N.R.A.S., in press.

13. Baldwin, J.A. and Netzer, H., 1978, Ap. J., 226, 1.

14. Wills, B.J., Netzer, H., Uomoto, A.K., and Wills, D., 1980, preprint.

15. Philips, M.M., 1980, preprint.

16. Philips, M.M., 1976, Ap. J., 208, 37.

17. Oke, J.B. and Lauer, T.R., 1979, Ap. J., 230, 360.

18. Davidson, K. and Netzer, H., 1979, Rev. Modern, Phys. 51, 715.

19. Snijders, M.A.J., 1980, SRC IUE Newsletter N° 5

20. Snijders, M.A.J., Boksenberg, A., Haskell, J.D.J., Penston, M.V. and Fosbury, R.A.E., 1980, to be submitted to M.N.R.A.S.

21. Grandi, S.A. and Philips, M.M., 1979, Ap. J., 232, 659.

22. Doschek, G.A., Feldman, U., Van Hoosier, M.E. and Bartoe, J.-D.F., 1976, Ap. J. Suppl., 31, 417.

23. Penston, M.V., et al., 1980, in preparation.

24. Stickland, D.J., Penn, C.J., Seaton, M.J., Snijders, M.A.J., Storey, P.J., and Kitchin, C.R., 1979, "The First Year of IUE", ed. A.J. Willis, p. 63.

25. Green, R.F., Pier, J.R., Schmidt, M., Estabrook, F.B., Lane, A.L., and Wahlquist, H.D., 1980, Ap. J., in press.

26. Viotti, R., 1976, M.N.R.A.S., 177, 617.

TABLE 1

OBJECT	DATE	IUE IMAGE NR.	EXPOSURE TIME (SEC)	REMARKS
I ZW 1	2.08.78	LWR 1955	210	
I ZW 1	5.08.78	SWP 2216	200	
I ZW 1	18.08.78	SWP 2333	155	
II ZW 136	18.12.78	SWP 3637	120	
II ZW 136	27.05.79	LWR 4610	180	
II ZW 136	29.05.79	LWR 4628	180	
II ZW 136	29.05.79	SWP 5389	100	
I ZW 1	31.05.79	SWP 5411	60	underexposed
I ZW 1	2.06.79	LWR 4673	180	
I ZW 1	2.06.79	SWP 5427	60	underexposed

TABLE 2 Emission Line Intensities

line	λ_o	F(10^{-13} erg cm^{-2}s^{-1}Å^{-1}) I ZW 1		II ZW 136	
				Dec 78	May 79
Hβ	4861	3.9 ± 0.3	(1)	5.6 ± 0.5	(2)
Fe II	optical	26.3	(1)	10?	(3)
				8.7	(2)
Fe II	UV 60	2.4 ± 1.2			
?	290 7.6 (4)	1.1 ± 0.5			present
Fe II	UV 61	1.4 ± 0.8			
O III	2837	0.8 ± 0.4			
Mg II	2798	6.0 ± 1.5			4.2 ± 0.6
Fe II	UV 62 + UV 63	3.2 ± 1.6			1.0 ± 0.4
Fe II	UV 1	1.9 ± 1.0			0.9 ± 0.6 (5)
Fe II	UV 33	1.6 ± 0.9			1.1 ± 0.3
Fe II + [O II]	UV 34 + 2470	1.2 ± 0.5	(6)		1.5 ± 0.6 (6)
[Ne IV]		present			present
Fe II + C II]	UV 2, UV 3, UV 35, UV 36, 2326	<3.1 ± 1.7			2.4 ± 1.0
Fe II	UV 6	1.0 ± 0.5	(7)		(7)
C III] + Si III]	1908 (8) + 1892	6.0 ± 1.2			6.6 ± 0.7
CIV + Si II	1549 + 1531	4.5 ± 1.5		12.1 ± 2.0	13.5 ± 2.5
OIV] + Si IV	1402 + 1393	4.0 ± 1.0		4.8 ± 1.0	2.9 ± 0.8
C II	1335	0.3 ± 0.2		1.1 ± 0.4	0.30 ± 0.15
O I	1304	0.7 ± 0.3		3.7 ± 1.2	1.2 ± 0.4
Si II	1263	1.5 ± 1.0		1.1 ± 0.4	1.5 ± 0.3
N V	1240	6.0 ± 1.5	(9)	4.9 ± 2.0	3.4 ± 1.5
Lyα	1216	16.0 ± 4.0	(9)	32.1 ± 3.0	31.4 ± 3.0
Si III	1206	3.1 ± 1.0	(9)		
Si II	1192	1.5 ± 0.5	(9)		

notes to table 2:

(1) ref. 22, (2) ref. 7, (3) see text, (4) calculated rest wavelength, comparision between I ZW 1 and II ZW 136 suggests that this is a low ionization feature (5) see text, (6) [OII] λ_o 2470 could contribute up to 50% of the total strength, (7) the reality of multiplet 6 of Fe II is questionable, (8) could include Fe III emission, (9) this four features have been separated using profile fitting methods.

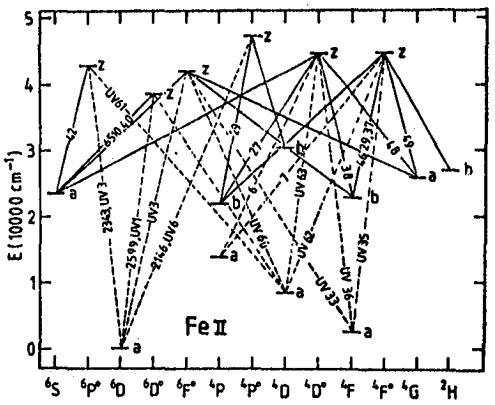

Fig. 1 Energy level diagram of Fe II with observed multiplets in the optical (——) and UV (– –) regions. For a few multiplets mean rest wavelength (Å) are shown and the multiplet numbers for most transitions are given.

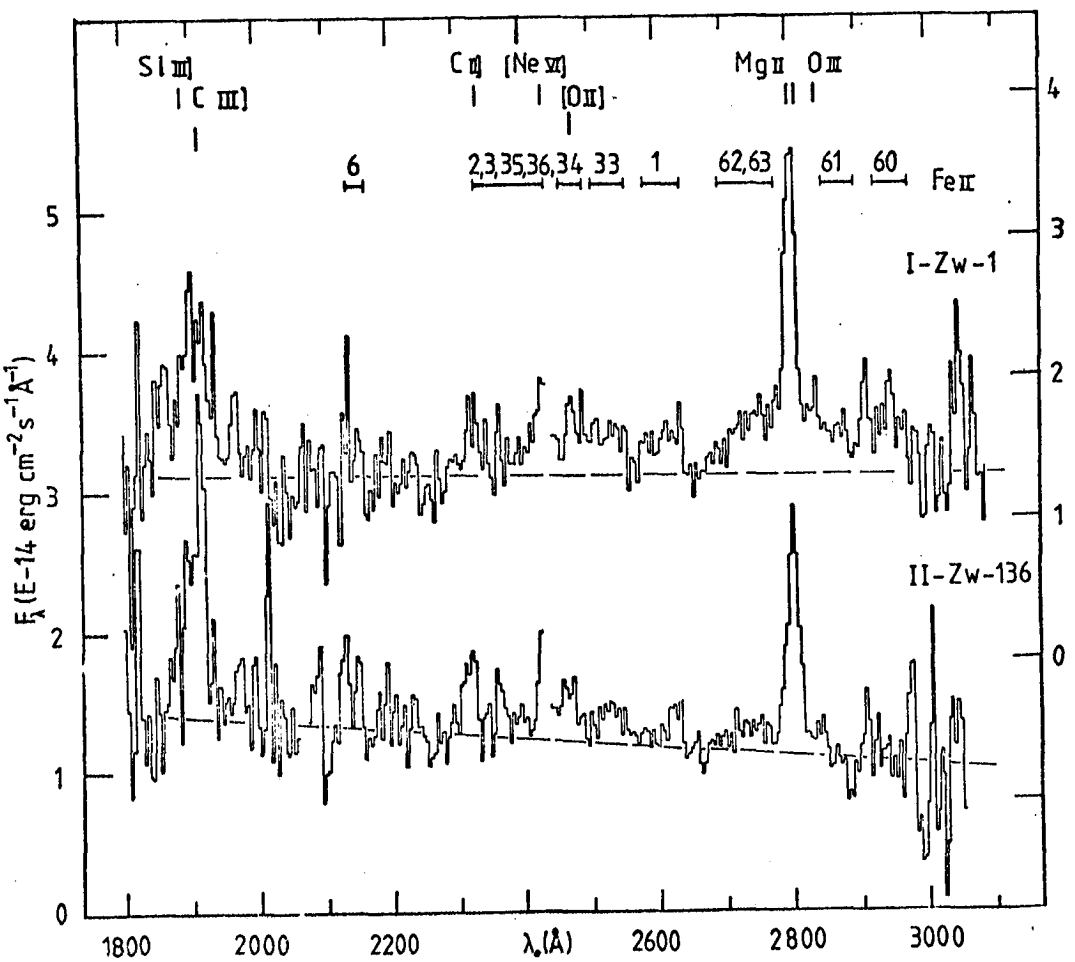

Fig. 2 Mean long wavelength spectra for I ZW 1 and II ZW 136.

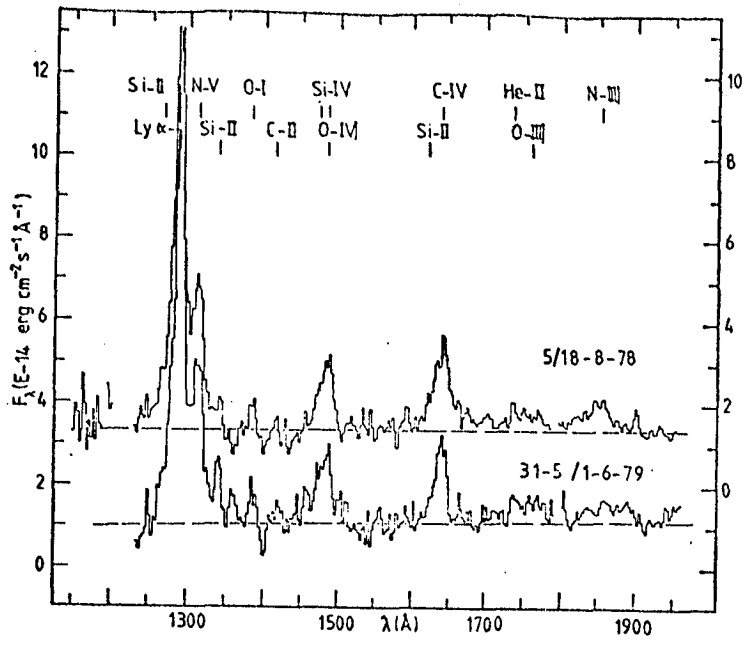

Fig. 3 Mean short wavelength spectra for I ZW 1.

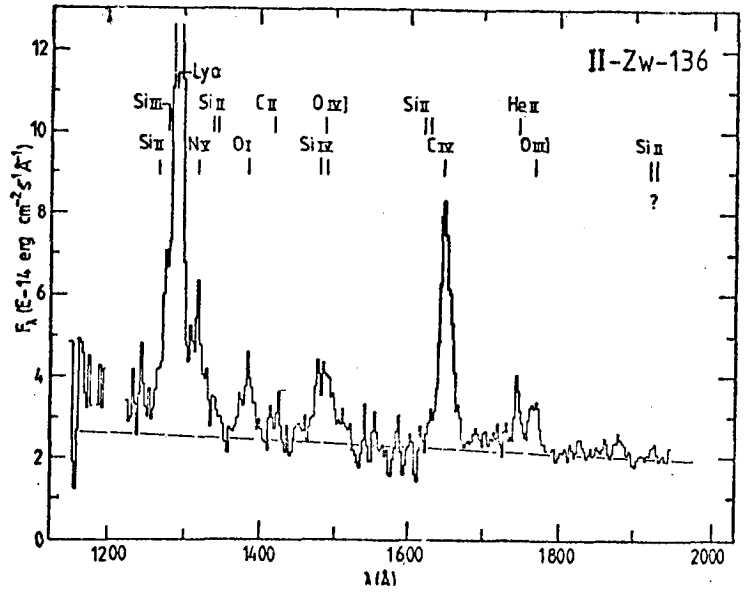

Fig. 4 One of the two short wavelength spectra for II ZW 136.

Wilson: IUE observations of 3C390.3 showed that the $L_\alpha/H\beta$ ratio for the narrow-line component was consistent with recombination theory and that it was the broad-line component which deviated. Is this a general result applicable to all quasars and Seyferts?

R. Green: Unfortunately, the narrow-line component is seldom easily separable from the broad-line one; 3C390.3 seems to be an extreme case. In the one other good case of well differentiated components that I know, 3C351, Green et al. found that the narrow component ratio of $L_\alpha/H\beta$ was consistent with the recombination value, while the broad-line ratio was again quite low, around 3.5 observed.

Weistrop: What is reference for the final 3C273 viewgraph?

R. Green: Ulrich et al. paper combining all European data on 3C273.

Bregman: What are the physical parameters that one deduces for Mrk 501 using theoretical models, and are these parameters (e.g., size) consistent with observation (e.g., size deduced from temporal flux variation).

R. Green: Kondo et al. derived the physical parameters from a synchrotron self-Compton model. They derive a magnetic field of 4×10^{-4}G, energy density in relativistic electrons of 10^{-2} erg cm^{-3}, and a lifetime for radiating particles of 7 years. There is no evidence for X-ray flux variability since the Uhuru observation, although there is evidence for spectrum variability, for which the theoretical time-scale is about 4 years. The physical size measured from VLBI was used for the models.

R. Green: With an old stellar population as the best fit, is the synthesis very sensitive to your assumed initial mass function?

Bruzual: No, the spectral energy distribution is independent of the critical mass functions. This is because low mass stars of all masses end up in the same region of the HR diagram where they become red giants. The initial mass function determines the rate at which the giant branch is populated, and hence, the rate of luminosity evolution, and also the so call "evolutionary correction".

Mushotsky: Can you comment on the effect of the IUE data on the "K" correction for distant slant elliptical galaxies and any implications for q_o.

Bruzual: The present data do not as yet sufficiently constrain evolution such that limits on q_o can be placed. Work in progress may throw some light into the subject (see answer to previous question and reference 10).

Peimbert: What was the metal composition used for the stars and which effects would you expect for different metallicities?

Bruzual: I have used solar metallicity only. Assuming a fraction of metal-poor stars as part of the normal population of the galaxy would

reduce the number of horizontal branch stars required to explain the UV spectrum. However, these stars do not seem to contribute at optical wavelengths.

Penston: I would imagine that your conclusions should be rather sensitive to the exact value of the reddening you assume for the galaxies you observe. Do you have any comment on this?

Bruzual: The only galaxies I have corrected for reddening were M31 and M32, with E(B-V) = 0.10. I assumed no reddening towards the other galaxies. I agree with your statement that slight differences in reddening will change (only slightly) our estimate for the number of horizontal branch stars.

Kafatos: What are the estimated ejection velocities of the clouds?

Wu: About 5,000 km s^{-1}.

Wallerstein: If the electron temperature is 12,000 K, why do we see [Fe VII]?

Penston: The [Fe VII] comes from a different region than that in which we derived the electron temperature.

Green, R.: Since Fe II and Mg II have nearly the same excitation potentials and abundances, does the same amount of flux emerge in all the iron multiplets taken together as in the Mg II resonance lines?

Penston: Basically, yes.

Steiner: Is Fe II in emission an evidence for the collisional excitation hypothesis? Resonance fluorescence can allow UV emission lines, depending on physical conditions and geometry.

Penston: I think it's generally agreed now that the covering factor as deduced from the paucity of cases where Lyman continuum absorption is seen at the emission redshift shows that not enough photons can be absorbed by the Fe II resonance lines to provide the observed level of emission.

VII. DATA REDUCTION

Washburn Extraction and Width of IUE Point Spread Function

Klaas S. de Boer, Jan Koornneef*, Marilyn R. Meade

Washburn Observatory of the University of Wisconsin
Madison, WI 53706, U.S.A.

*European Southern Observatory, Casilla 16317, Santiago 9, CHILE

We review the Washburn Extraction Routine for low dispersion IUE spectra. The shape of the point spread function (PSF) in low dispersion spectra is sufficiently well described by a gaussian function. The PSF is in large and small aperture essentially identical and we present values of σ. Several advantages of the extraction routine are mentioned.

Introduction

The Washburn IUE extraction routine (Koornneef and de Boer 1979, henceforth KB) has been used up to now only to extract low dispersion spectra. The routine basically fits an a priori known point spread function (PSF) to the intensity distribution perpendicular to the dispersion. In four iterations the routine finds the intensity I in the spectrum, the background B as the baseline of the input data, and the position x_o of the spectrum. We find that the PSF can be represented sufficiently close by a gaussian, hence in pixels at positions x, the intensities fit to

$$I(x) = B + \frac{I}{\sqrt{2\pi\sigma^2}} \exp\left\{-\frac{1}{2}\left(\frac{x - x_o}{\sigma}\right)^2\right\} ,$$

where σ is the dispersion of the gaussian function in units of $\sqrt{2}$ x (pixel length). Crivellari and Morossi (1980) also find a gaussian but they suggest that haloing in the camera can be accounted for by adding a 15% effect of a Lorentz profile. Our extraction is performed on a line of pixels diagonally through the image, hence deviating from perfect perpendicular by small angles, 6° for SWP, 8° for LWR (see Fig. 1).

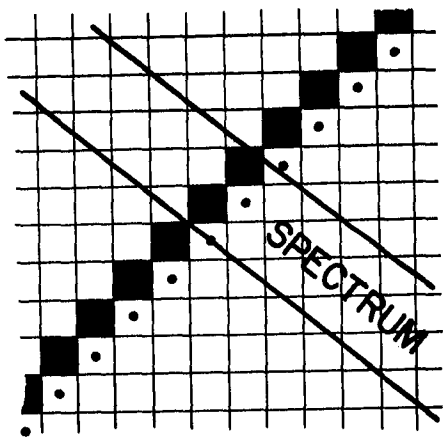

Fig. 1: Schematic view of pixel grid, spectrum and diagonals. Filled squares: set of pixels on one diagonal; dot-pixels: set for next diagonal in Washburn extraction.

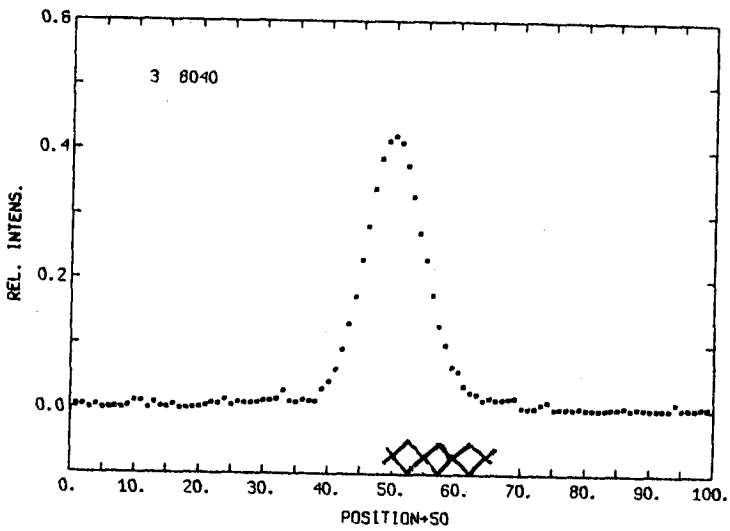

Fig. 2: The actual intensities of the pixels of each fit are coadded, after proper alignment of the centroid of the PSF, and normalization of the fitted PSF to unit area; the PSF is gaussian for point sources. This plot shows the sum of 350 extracted diagonals in SWP between 1580 and 2000Å, of a M_V = 14 BHB star in NGC 6397 (de Boer 1980). The very minor deviation from a gaussian in the lower wings is caused by the change of σ from $\approx$ 1.1 to $\approx$ 0.9 respectively (see fig. 4).

Based on a prescribed σ, we have extracted many images since the development of the routine. Coaddition of all the x-adjusted fits provides a check on the actual PSF. In LWR, the PSF is always gaussian. In SWP images reduced in 1979, the PSF turned out to be inexplicably asymmetric. We have reduced the spectra from images of that period which had the flaw in the SWP ITF, by redressing that error at the pixel level based on the data from Table 1 of Holm (1979a). These rereduced spectra now produce also a gaussian PSF in SWP.

Properties of the Point Spread Function (PSF)

In order to find what σ is in the spectra, we have carried out extractions with σ also as a free parameter. In that case, of course, the resulting I is meaningless. From the free-σ extraction we have calculated average σ's in 40Å and 50Å wide bands in SWP and LWR respectively, representing 34 diagonals in SWP and 27 diagonals in LWR. In the calculation of that average, σ's larger than 1.8 and smaller than 0.3 have been excluded, the large σ's because they cannot be real regarding the grand average of $\sigma = 0.98 \pm 0.03$ ($\sqrt{2}$ x pixel length); the small ones were excluded because they came from an accidentally high central pixel with low wing-pixels on the input diagonal.

Before extracting, extreme-valued pixels get low weight (see KB). In the provided geometric-photometric images all pixels have been offset by 2000 IUE flux numbers. Reseaux then have pixel-values < 1950 f.n.; these get low

weight. High pixels (saturated, > 32500 IUE f.n.) also get low weight. There is another set of pixels which gets low weight. KB showed that the ITF's applied to the raw images truncated at a certain value. Hence, in commissioning phase data in LWR no pixel had more than 20000 IUE f.n., resulting in unflagged "semi-saturation" in spectra which had not yet DN near 255. The ITF's employed since May 1978 are better but still have truncation. Holm (1979b) emphasized this more and gave actual DN's. The spectral ranges where this is important are:

λ	max f.n. per pixel (Turnrose 1978)	max trustable standard extracted intensity
≈ 1300	17740	≈ 85000 IUE flux
≈ 2800	25220	≈ 120000 IUE flux

where the maximum trustable intensities are adapted from KB allowing for smaller σ found presently. Such pixels also get low weight resulting in positively improved intensities from the extraction fit (see KB sec 5). Turnrose et al. (1980) described a numerical extrapolation to the ITF.

As reported by KB, the PSF was essentially equal for large and small aperture spectra. For the presently discussed 12 images for each camera, that ratio is close to unity indeed. Figure 3 shows how this ratio behaves with respect to wavelength.

KB reported that the PSF in SWP had σ = 1.05 constant, and in LWR had σ = 1.3 at 2000Å to σ = 0.9 at 3000Å. For later images, Koornneef derived that in SWP σ gradually decreased to shorter wavelengths, and that in LWR the change of σ along the spectrum was less pronounced. Figure 4 shows how, for characteristic images, σ changes along the spectrum. Apparently, the IUE

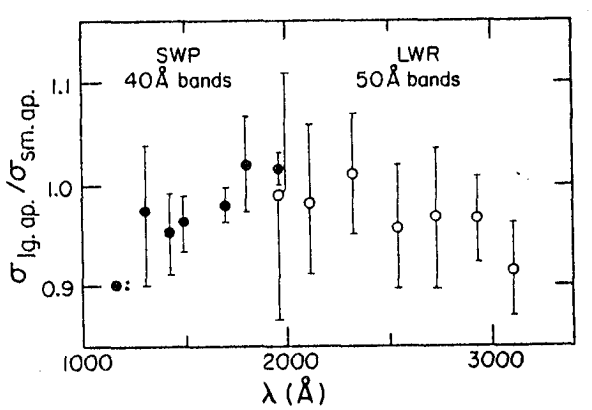

Fig. 3: Ratio $\sigma_{la.ap}/\sigma_{sm.ap.}$ for a gaussian Point Spread Function of IUE low dispersion point-source spectra in its relation to wavelength. Average for 12 images in each camera, with standard deviations given. In several SWP images the signal had vanished at 1180Å leading to a very uncertain ratio in this figure. Images were obtained between Sept. 1978 and Feb. 1980.

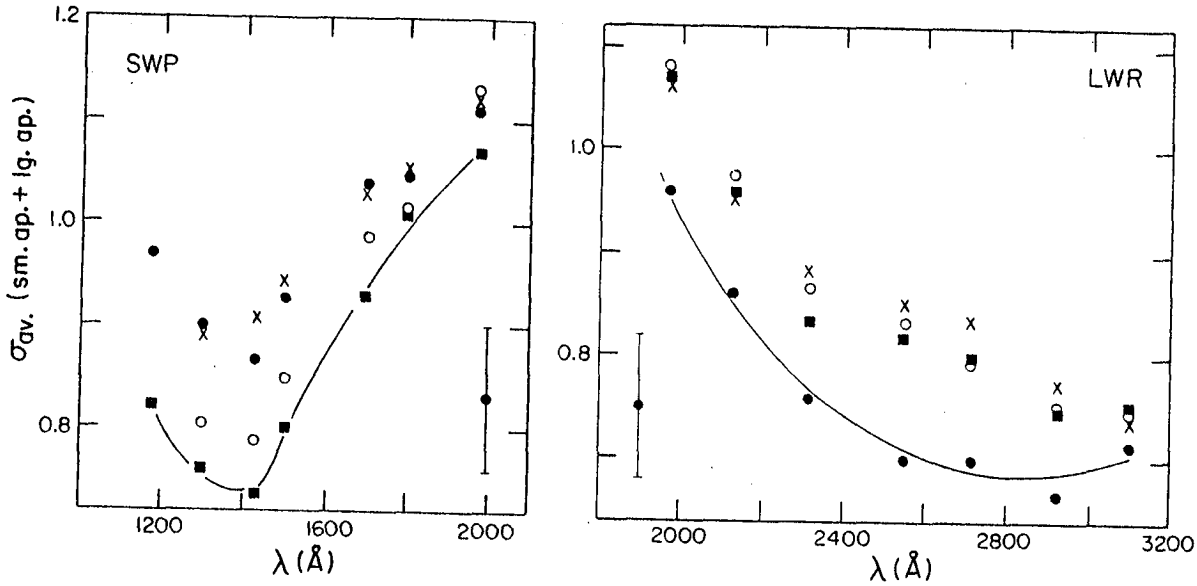

Fig. 4: Width σ of gaussian PSF in relation to wavelength, for 4 images in each camera. The thin lines are only meant to aid the eye. The point with error bar in the corner gives the characteristic size of the dispersion.

optical system has been brought into an optimized condition after a few months of operation. A plot of σ with image number (not shown) indicates large σ for early images, in time levelling off to values of σ as given presently.

Most likely, there is a correlation between σ, i.e. the level of σ, and the temperature in the satellite. Figure 5 shows for each camera the values σ at specified wavelengths in relation with the read head temperature THDA (Bohlin et al. 1980). No clear correlation is apparent.

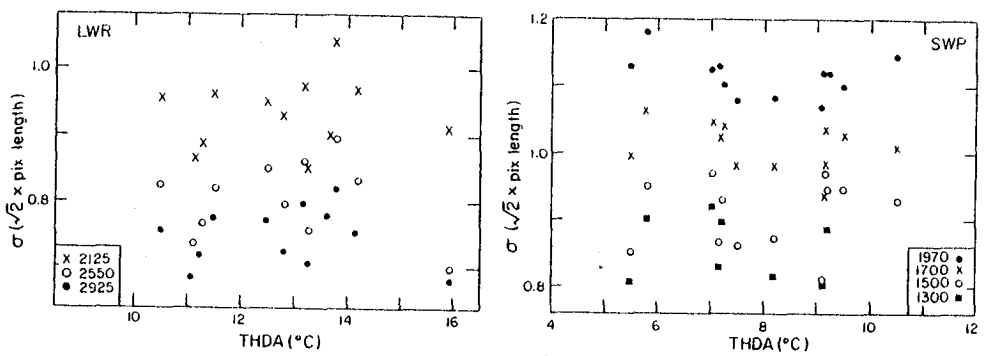

Fig. 5: For all 12 images, in each camera, we show how σ behaves with respect to the temperature THDA available on the scripts. No clear correlation is indicated. The figure can be used to judge the dispersion of the σ's.

Error Estimate

The Washburn routine fits a prescribed PSF to the data points on a line of pixels diagonally through the image. The best fit is found at the minimum of the sum of the deviations of all points. This minimum deviation is used as a quality indicator of the fit. The procedure is set up such that the final error is calculated from all the data points at full weight, hence saturated data points or points from truncated ITF's get "flagged" in proportion to their deviation from the adopted PSF. The error estimate is used as weighting factor in combining data from small with large aperture (if available) and so bad data (reseaux, saturation, etc.) are effectively replaced by good data, in addition to an overall improvement. The propagated errors are most important after calculating the ratio of two different spectra (extinction studies; Koornneef and Code 1980) in order to obtain a fair judgement of the limited spectral overlap between SWP and LWR spectra.

Spectral Resolution

The Washburn IUE extraction routine has a sampling rate twice as large as in the standard IUE extraction. We therefore may expect somewhat better spectral resolution. Often we resolve in low dispersion the strong interstellar Mg II in the direction of the Magellanic Clouds, and the stellar Si IV doublet.

Spatial Resolution

The main advantage of PSF fitting is that one may offer any spatial function to give the best fit. A first step has been made by Koornneef and Mathis (1980) who studied the spatial intensity distribution near 30 Doradus in the LMC. With such procedures also the shape of the UV light distribution of globular clusters in the LMC can be determined (de Boer 1980).

Bohlin, R.C., Holm, A.V., Savage, B.D., Snijders, M.A.J., Sparks, W.M. 1980, A & Ap., in press.
Crivellari, L., Morossi, C. 1980, 2nd year of IUE, ESA, in press.
de Boer, K.S. 1980, This symposium.
Holm, A.V. 1979a, NASA IUE Newsletter 7, at p. 30.
Holm, A.V. 1979b, NASA IUE Newsletter 7, at p. 34.
Koornneef, J., Code, A.D. 1980, Ap.J., to be submitted.
Koornneef, J., de Boer, K.S. 1979, NASA IUE Newsletter 5; and SRC IUE Newsletter 4, p. 41. (KB)
Koornneef, J., Mathis, J.S. 1980, Ap.J., submitted.
Turnrose, B., Harvel, C., Bohlin R.C. 1980, NASA IUE Newsletter 8, p. 32.

RESULTS OF BASIC IMPROVEMENTS TO THE EXTRACTION OF SPECTRA FROM IUE IMAGES

Don. J. Lindler
Andrulis Research Corporation

and

Ralph C. Bohlin
Laboratory for Astronomy and Solar Physics
Goddard Space Flight Center

ABSTRACT

Now that IUE is a mature operational satellite, the in-flight performance of the scientific instrument can be assessed. Since an additional 5 years of operations seem likely, the data reduction system is being optimized to realize the full capabilities of the observatory. Results of two methods of extracting spectra from IUE images are compared. The first method, which is presently implemented, performs a geometric correction of the image followed by a photometric correction. The spectral data are then extracted using a slit with an effective width and sampling interval of 2.4Å for the SWP camera and 3.7Å for the LWR camera in low dispersion. The second method performs the photometric correction without doing a geometric correction. The spectral data are then extracted from the photometrically corrected image by an extraction slit, which follows the spectral orders in the non-geometrically corrected space, with an effective width and sampling interval 1/2 that of the present method. In the first method, the non-linear data are subjected to resampling in the geometric correction procedure. Since the new method omits this resampling, and uses an effective slit one half as wide, the photometric integrity is preserved and the resolution is increased. For example, a pair of emission lines separated by two slit widths are blended in the first method but are clearly resolved in the second method. The noise in extracted spectra is increased by about 1.4, as expected on the basis of slit widths. However, the guest investigator will soon have the option of binning the data to reduce noise or co-adding multiple exposures to obtain a significantly improved resolution. The new magnetic tapes will remain essentially unchanged, except for longer record lengths necessitated by the increased number of spectral sample points.

PRESENT METHOD

The first processing step for each image is a geometric correction of the raw image performed by means of bilinear interpolation within a square grid of 169 fiducial marks (reseaux). This correction involves a resampling of the original image, resulting in some degradation of resolution. Since this resampling is done in the (non-linear) DN space of the raw image, some photo-

metric error is also introduced (ref. 1). The photometric correction of the image is effected by means of a pixel-by-pixel intensity transfer function. The spectral data and background data are then extracted with slit widths of 1.4 pixels. The background is smoothed with a triangular filter before subtraction to obtain the net spectrum.

NEW METHOD

In the new method the resampling of the raw image is avoided by performing the photometric correction without prior geometric correction. Using the square grid of 169 reseaux the correct ITF can be associated with each pixel. Normally the raw data pixel will have a position between four available ITF curves. Each of these ITF's is applied to the pixel DN value, and bilinear interpolation of the four values yields the flux value. To extract the spectrum from the photometrically corrected image it is necessary to use dispersion constants for a geometrically corrected image. This is done by computing the position of the points, shown in Figure 1, in "geomed" space and then using the information from the reseaux grid to compute the position in "ungeomed" space. The flux value assigned is the bilinear interpolation of the flux values of the four pixels around the ungeomed position. Neighboring points are added in the spatial direction giving a table of flux versus wavelength and spatial position. The gross and the background spectra are then obtained by summing the appropriate regions in the spatial direction (Figure 2). In the new method, points within a reseau are not used for background determinations. The background is then smoothed using a median filter (for removal of noise spikes) followed by a triangular filter.

RESOLUTION ENHANCEMENT

The most pronounced improvement of the new method is the increase in apparent resolution. Figure 3 shows a region of a platinum wavelength calibration spectrum extracted with the old and new method. The pair of spectral lines at about 2815Å is unresolved with the old method but is clearly resolved with the new method. The increased resolution is due to not resampling the image for geometrical correction and to using an extraction slit with an effective width one half as wide.

BACKGROUND SMOOTHING

In Figure 4 the comparison of the two background smoothing techniques is shown. Note that the reseau at about 1950Å has already been removed before smoothing in the new method. Remains of the reseau in the background of the old method still show after smoothing. The new method of smoothing does a much better job of removing blemishes and fine structure in the background without harming the general curvature.

NOISE

The noise levels for a point source and a trailed spectrum were established using 60% flood images. To achieve approximately the same flux as an astronomical source, a slit height of 2.5 lines (3.5 pixels) of extracted data was used for a point source, and of 10 lines was used to simulate a trailed spectrum. The noise statistics for the SWP and LWR images are shown in Figure 5 and 6 as a function of wavelength.

REFERENCES

1. Turnrose, B. and Harvel, C., International Ultraviolet Explorer Image Processing Information Manual.

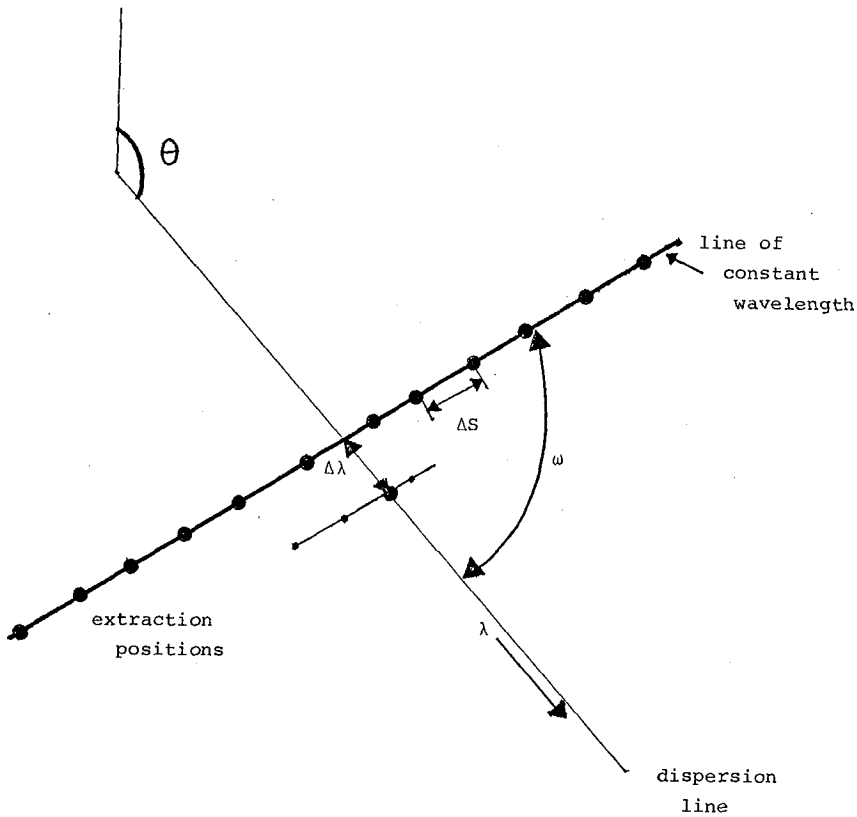

Figure 1 - Spatial information extraction.

ΔS - spacing of extraction positions in the spatial direction (.707 pixels)

Δλ - spacing in the wavelength direction

Θ - angle of the dispersion line

ω - angle of the line of constant wavelength from the dispersion line

● - extraction positions

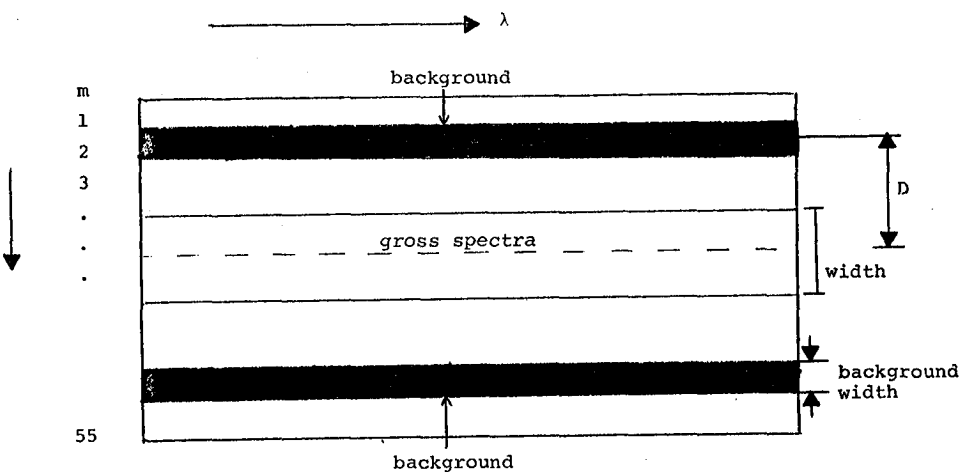

Figure 2 - Extraction of the gross and background spectra from the spatial information.

m - spatial position, i.e. line number of extracted data

D - distance of background extraction from the center of the dispersion line

WIDTH - width of the region to be summed vertically to obtain gross spectrum or background

Note that wavelength (λ) increases to the right.

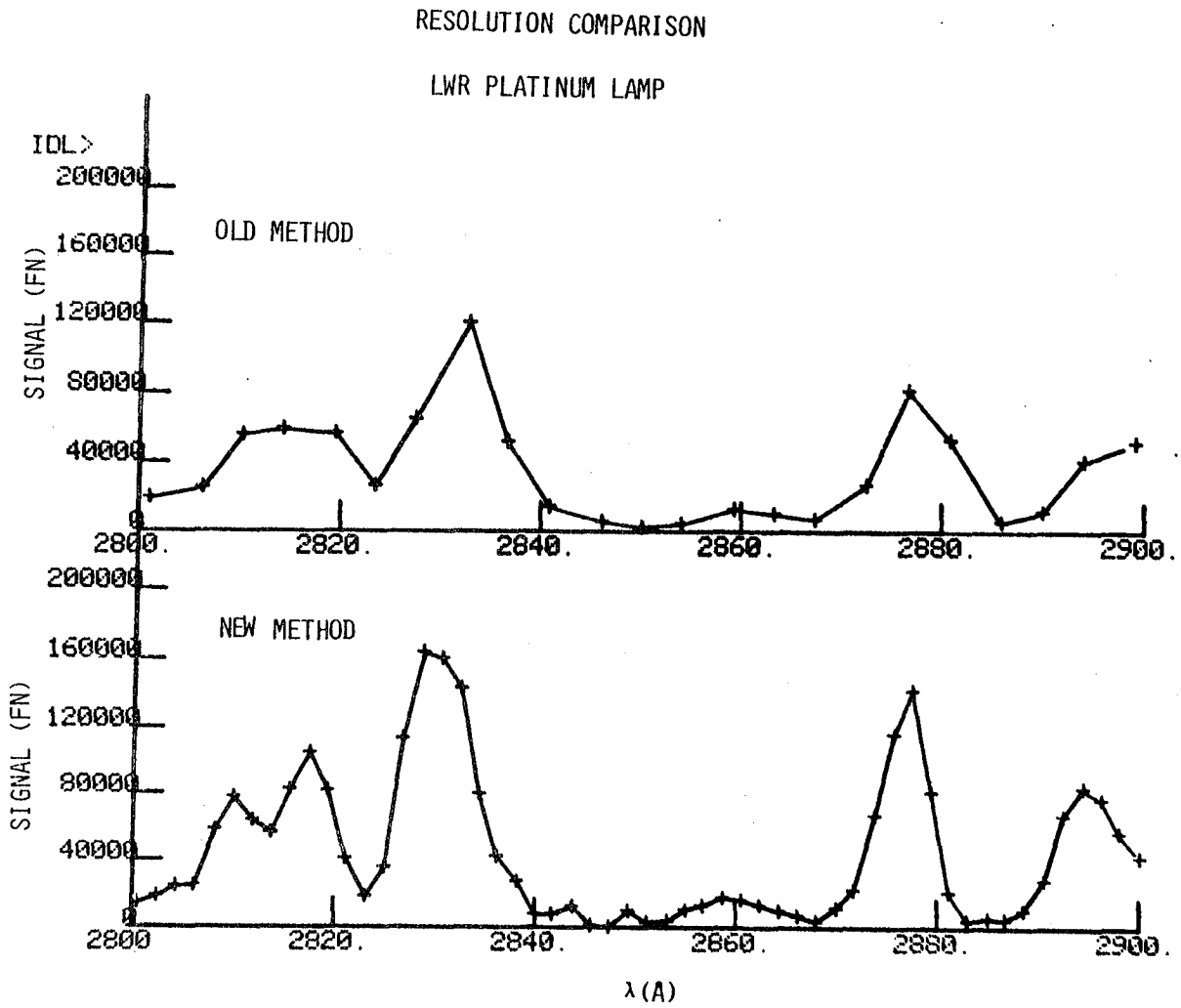

Figure 3 - Comparison of a portion of a LWR platinum lamp spectrum extracted with the new and old extraction methods. The symbol "+" marks extraction positions, i.e. data points that are on the guest observer data tapes.

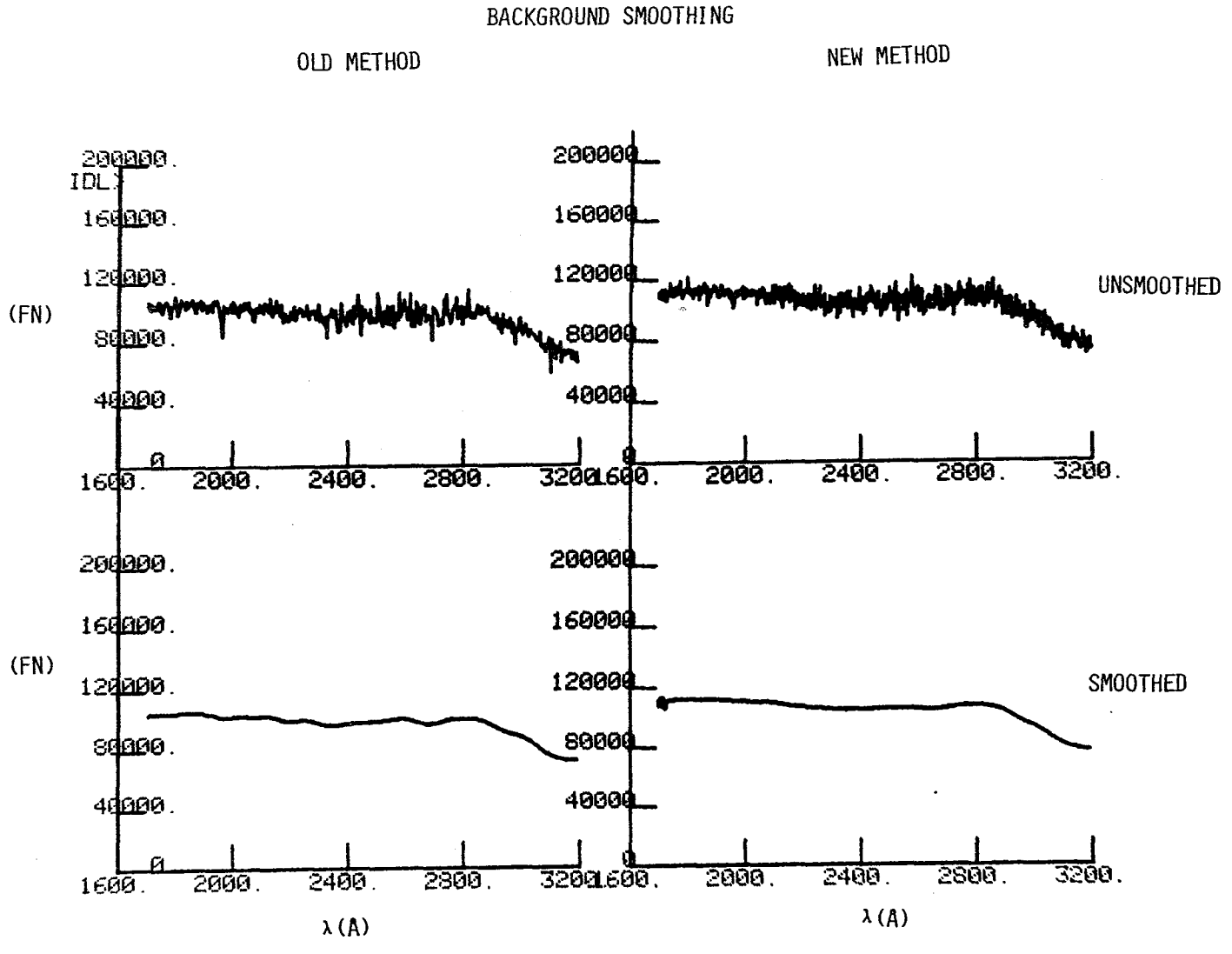

Figure 4 - Comparison of the treatment of the background data using the old and new techniques. The unsmoothed trace has the reseaux removed in the new method. The main difference in the two smoothed curves is the application of a median filter in the new method.

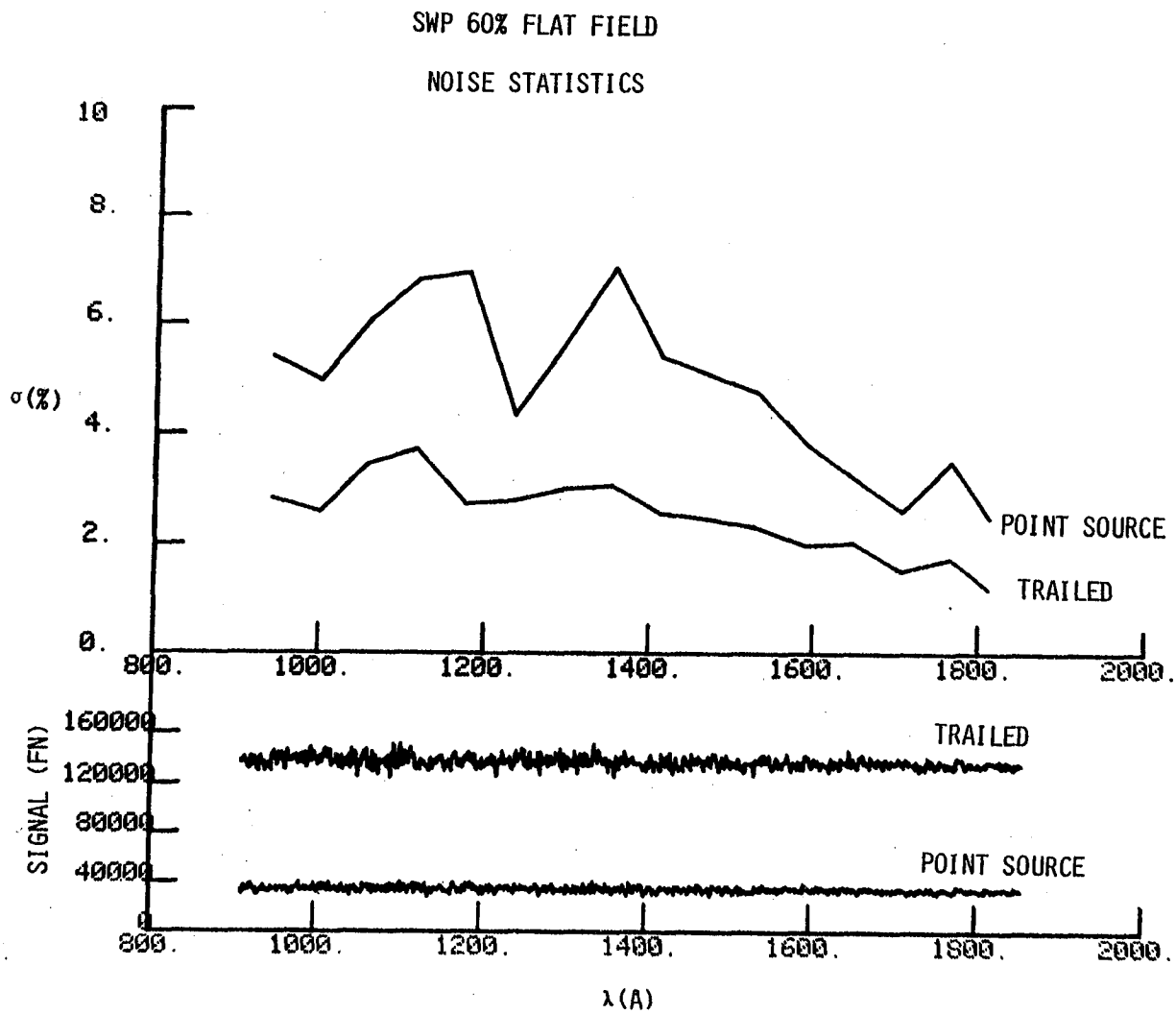

Figure 5 - Noise statistics of artificial spectra extracted from a SWP 60% flat field with extraction slits equal to the FWHM of the widths of trailed and point sources. The values of the 1σ noise statistics were the scatter among the individual 50 points of bins of the signal.

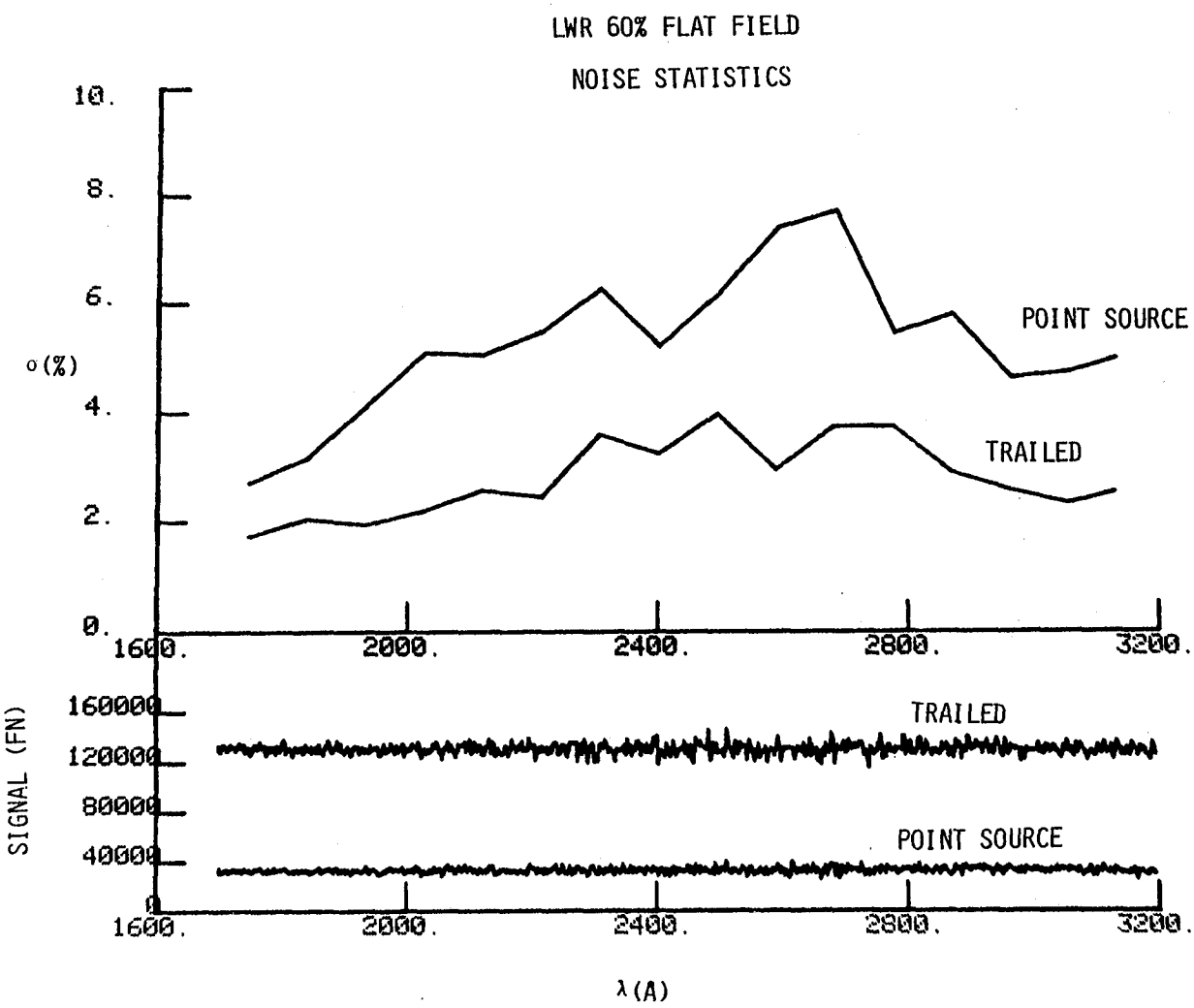

Figure 6 - Same as Figure 5 for the LWR camera.

EXTRACTING SPATIAL INFORMATION FROM LARGE APERTURE EXPOSURES OF DIFFUSE SOURCES

J. T. Clarke and H. W. Moos
Physics Dept., Johns Hopkins University, Balt., MD 21218

ABSTRACT

The spatial properties of large aperture exposures of diffuse emission can be used both to investigate spatial variations in the emission and to filter out camera noise in exposures of weak emission sources. Spatial imaging can be accomplished both parallel and perpendicular to dispersion with a resolution of 5-6 arc sec, and a narrow median filter running perpendicular to dispersion across a diffuse image selectively filters out point source features, such as reseaux marks and fast particle hits. Spatial information derived from observations of solar system objects will be presented.

INTRODUCTION

Since the IUE telescope has an image quality of 3 arc sec and a total instrumental resolution of 5-6 arc sec, it is possible to accomplish spatial imaging of diffuse sources within the 10 x 23 arc sec entrance aperture in a single exposure. Spatial asymmetries have been observed in planetary spectra in the directions both parallel and perpendicular to the dispersion line, and a relative sensitivity calibration of the instrumental response along the major axis of the aperture (perpendicular to dispersion) at H Lyα (1216 Å) has been obtained from exposures of diffuse geocoronal emission. It is seen that diffuse emission produces an image on the camera which is $\sim$ 20 arc sec full width at half maximum (FWHM) in the direction perpendicular to dispersion; by contrast, noise features such as radiation-induced spikes and reseaux marks are generally not greater than 6 arc sec FWHM. Running a narrow median filter across the data in this direction readily discriminates between these noise features and the diffuse emission. Details of the data reduction procedures which we have developed both for spatial imaging within the large aperture and for noise filtering in images of diffuse emission will be presented here, along with sample data showing:

i) spatial imaging in observations of geocoronal emission and Jovian aurora, and

ii) noise filtering in spectra of weak emissions from the Io torus.

SPATIAL IMAGING

Spatial imaging in exposures using the large entrance aperture with the SWP camera requires knowledge of the relative sensitivity of the instrument in the exposed region of the camera face. This is most easily accomplished by taking an exposure of a uniform diffuse source; at 1216 Å such a source exists in the geocoronal H Ly α emission. This section gives the result of adding 6 exposures of geocoronal Ly α background to obtain the relative sensitivity of the SWP camera along the major axis of the large aperture, i.e. perpendicular to dispersion.

This one-dimensional spatial imaging has been accomplished by integrating the flux with respect to wavelength around 1216 Å in each of the line-by-line spatially resolved spectra in the vicinity of the large aperture. The zero flux level was determined by an average of the flux level on either side of the Ly α emission. The estimated position of these lines is shown on the righthand side of Figure 1 (line 9 is the central dispersion line). The line and order numbers increase toward the center of the camera face.

The circles plotted on the left-hand side of Fig. 1 represent the sum of exposures SWP 4009-4014 (taken 24 January 1979), adding the wavelength-integrated fluxes at 1216 Å individually for each line number. These summed fluxes are listed in Table 1 in units of IUE flux numbers, and in arbitrary units which are normalized to one for the central dispersion line. Subsequent images of diffuse emission may be divided line-by-line by these numbers to correct for relative response in the aperture. A second sum of geocoronal exposures taken on 12 March 1980 showed the same profile to within 5% for the individual points, indicating no significant changes in the relative response of the camera over one year of operation. The X's plotted on the same graph show the peak flux in each line near 1650 Å in a short exposure of a stellar source, indicating an instrumental spatial FWHM of about 6 arc sec. For comparison, Koorneef and de Boer (IUE Newsletter no. 5) obtained 5.1 arc sec FWHM in a more accurate determination of the point source response. Given the size of the large aperture (10.3 x 23.0 arc sec) three point sources could be resolved in the length of the aperture, and some imaging is possible along the dispersion direction.

It should be pointed out that thermal shifts in the spacecraft may move the large aperture image slightly on the detector face, and the central dispersion line may be moved from side to side in the IUE data reduction procedure. Care should be taken to determine accurately which spatially-resolved spectrum corresponds to the center of the large aperture image before this calibration is applied. In addition, this calibration is strictly accurate only at 1216 Å.

As an example, Fig. 2 shows a 3-dimensional spectral-spatial image of IUE exposure SWP 5309 of the north polar region of Jupiter, taken with the large entrance aperture on 19 May 1979. The dispersion direction, along the X-axis, is marked in Å, the Y-axis represents flux, and the Z-axis gives spatial imaging along a line which is roughly north-south. H_2 Lyman band emissions are visible from the north pole at around 1570 Å and at 1608 Å, and to a lesser extent around 1250 Å.

NOISE FILTERING

In a series of long (7-8 hours) exposures of the Io plasma torus taken with the large aperture and the SWP camera, noise features were found to be comparable in intensity to the weak observed emission lines. This section describes three procedures employed in the reduction of these data to preferentially filter out the noise features:

i) Limiting the width of the artificial slit used in the extraction of the gross spectrum

ii) Running a 7-point median filter on the data perpendicular to dispersion

iii) Adding exposures

Methods (i) and (ii) capitalize on the fact that an emission line from an extended source is much broader perpendicular to dispersion than the noise features, which tend to appear as point sources above the pedestal level. Noise spikes are produced randomly by fast particle hits on the detector camera face; in addition, some noise features recur at the same position on the camera, presumably caused by chemical imbalance in the camera phosphor. At the curved edges of the large aperture the flux from a uniform diffuse source decreases (see preceding article); including only the central portion of the aperture in the gross spectrum thus improves the signal-to-noise ratio, and also bypasses a couple of reseaux marks. This was accomplished by adding the central 7 orders of the 55-line spatially resolved spectra (e.g. setting H = 7), and then normalizing the background flux accordingly.

To compensate for throwing away the flux from the curved edges of the aperture the fluxes are multiplied by the appropriate geometric factor (1.64): this is accurate only if the diffuse source is uniform in intensity.

A narrow median filter passed over the data perpendicular to the dispersion line would have the effect of erasing only features which are narrow compared to the size of the filter, i.e. a high-frequency filter. A 7-point median filter (14-15 arc sec) was found to distinguish well between point sources (FWHM of 5-6 arc sec) and diffuse emission (FWHM of 18-20 arc sec). This filter was run using the spatially-resolved spectra, so that the separation of "points" perpendicular to dispersion was 2.1 arc sec. The flux in a given order at a given wavelength was determined by the median of the fluxes at the same wavelength of 7 spatial orders, centered on the given order. The filter was thus a "running median". Fig. 3 shows the result of a 7-point running median on a sample profile which combines diffuse emission (taken from the geocoronal Ly α profile from the preceding article) and a point source noise spike (FWHM = 6 arc sec). The dashed line is the "before" picture, the solid line "after" the filter. The filter completely wipes out the noise spike, but may also truncate the diffuse emission by a few percent.

The well-known technique of adding spectra to improve signal-to-noise was applied to 3 spectra of comparable duration, after each of these spectra had been compiled using the previous two techniques. This spectrum, labelled "Sum", is shown in Fig. 4 along with one of the three separate spectra, as compiled under the standard IUE extended-source reduction. Although these techniques have been applied only to images of a diffuse source thus far, they should work equally well on trailed spectra of point sources.

TABLE 1

Line	IUE FN ($\times 10^3$) $\times$ Å	Relative Sensitivity
3	21	.04
4	175	.33
5	368	.69
6	465	.87
7	488	.91
8	516	.97
9	534	1.00
10	547	1.02
11	574	1.07
12	530	.99
13	438	.82
14	243	.45
15	94	.18

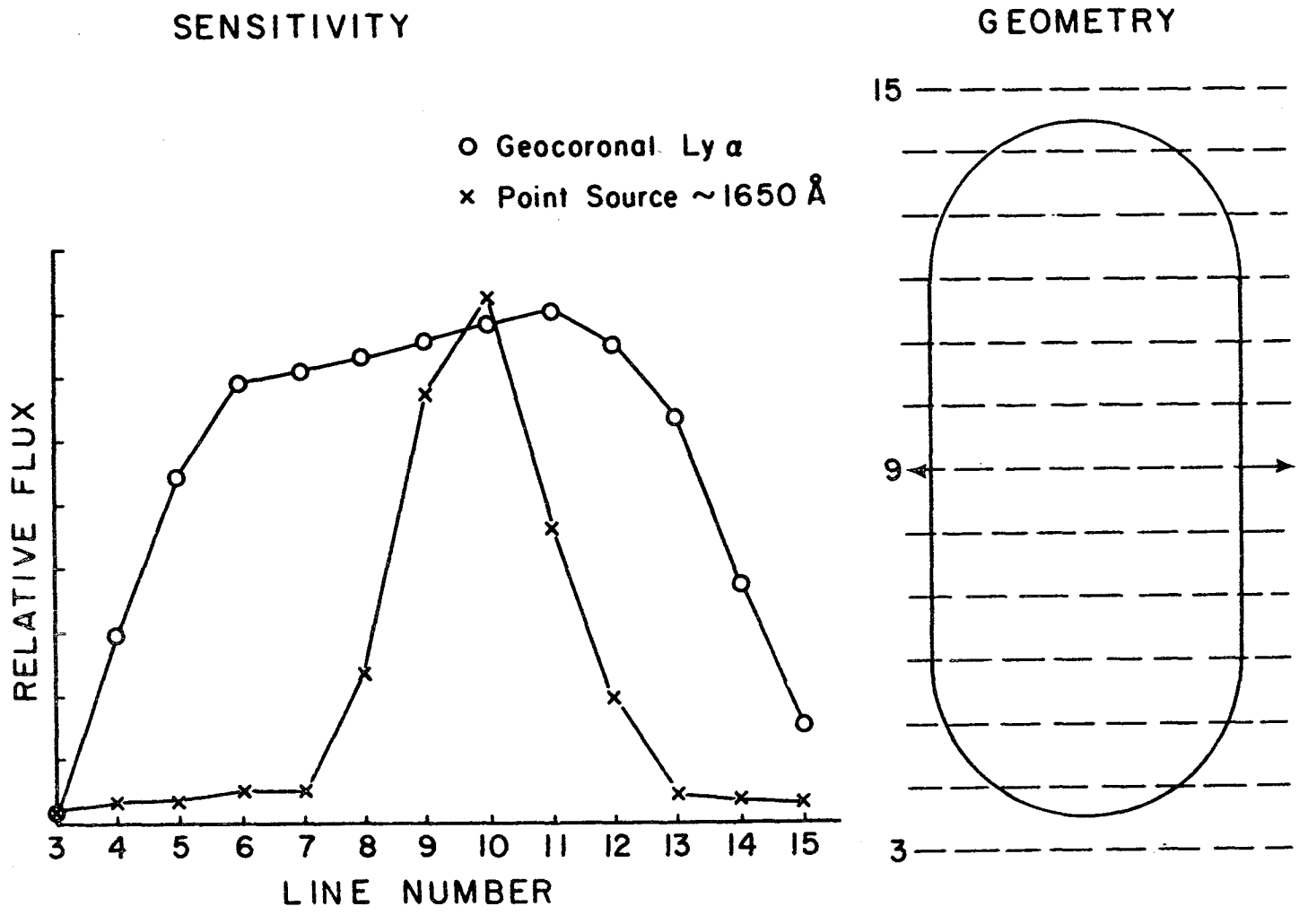
SENSITIVITY
GEOMETRY
o Geocoronal Ly α
× Point Source ~1650 Å
RELATIVE FLUX
3 4 5 6 7 8 9 10 11 12 13 14 15
LINE NUMBER
15
9
3

Figure 1

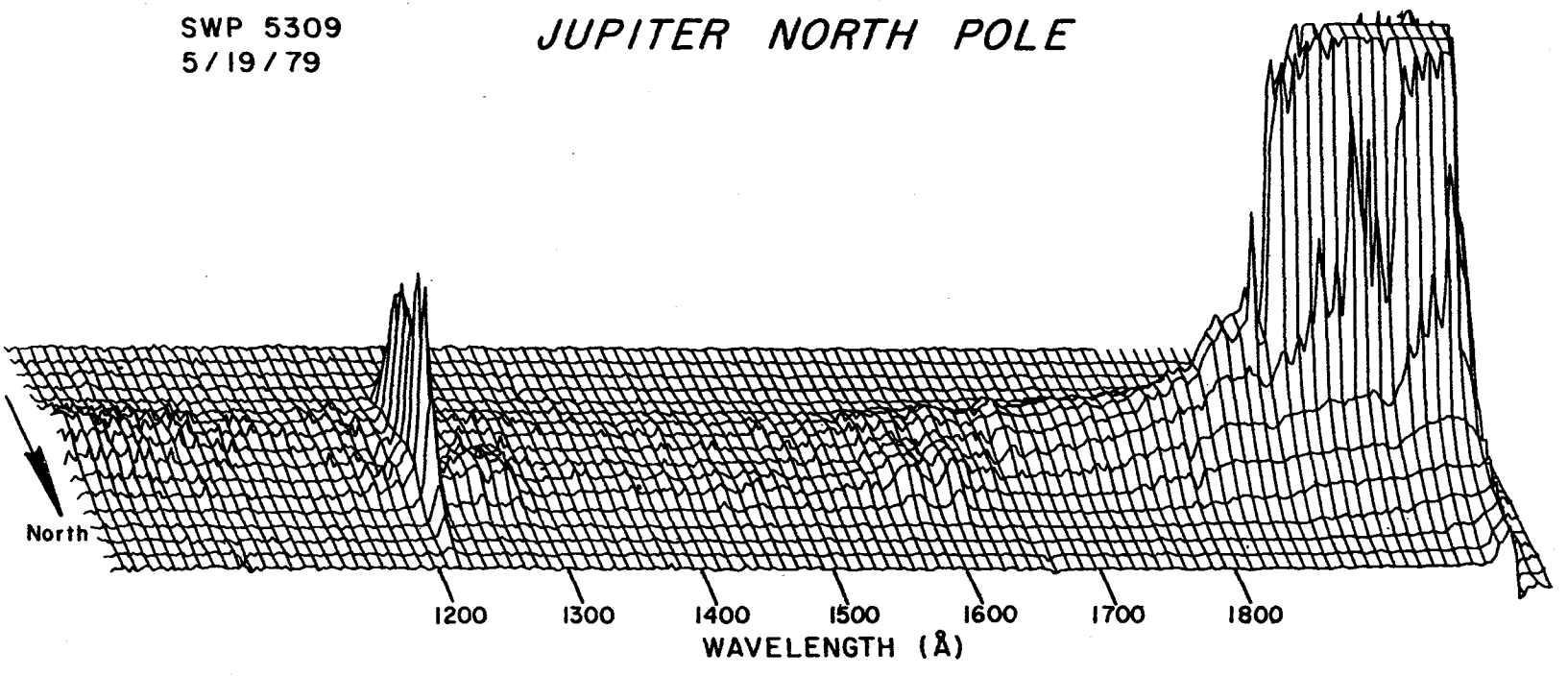
SWP 5309
5/19/79
JUPITER NORTH POLE
North
1200
1300
1400
1500
1600
1700
1800
WAVELENGTH (Å)

Figure 2

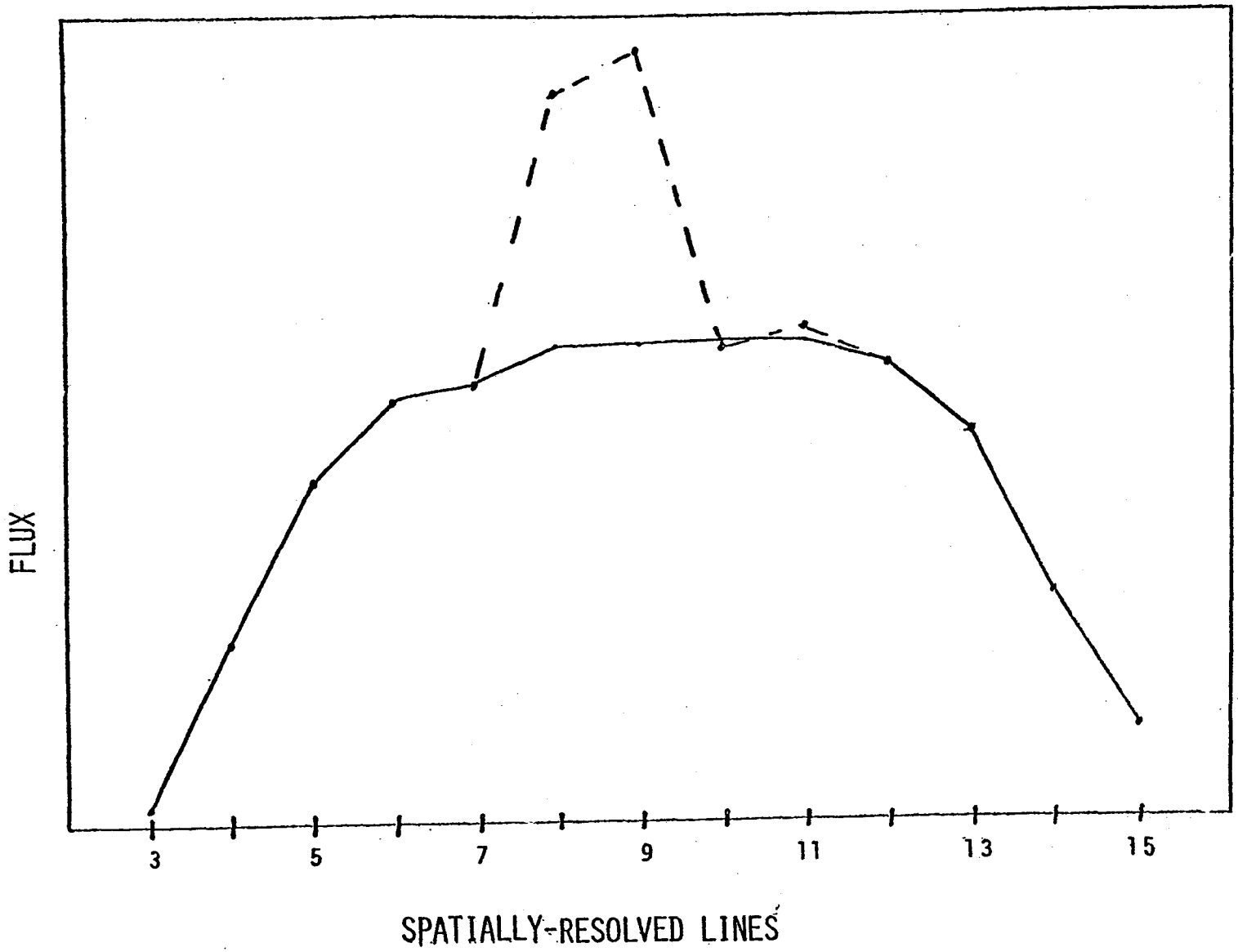

Figure 3

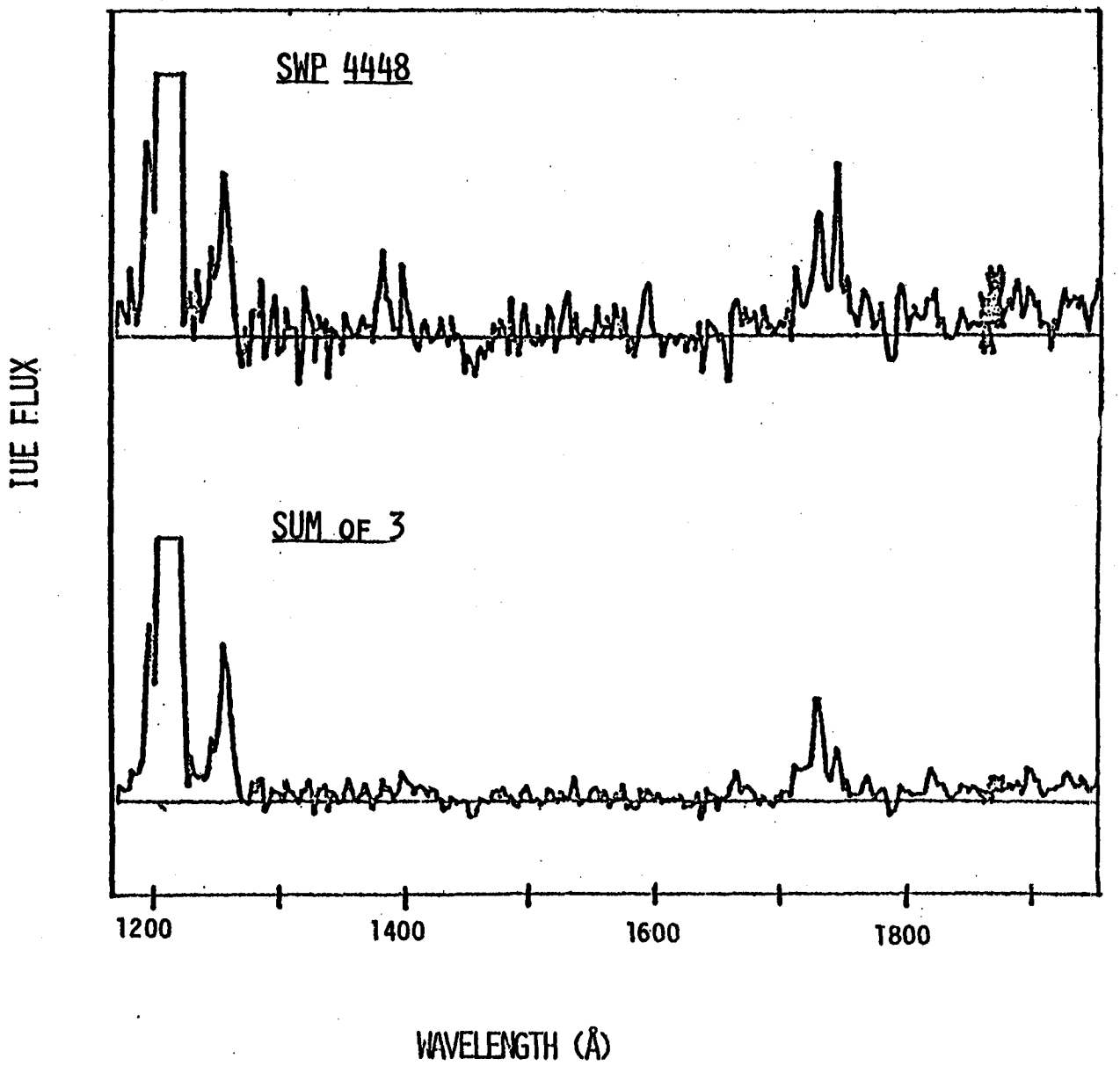

Figure 4

IMPROVEMENTS TO THE ACCURACY OF THE IUE WAVELENGTH SCALES IN HIGH DISPERSION*

Barry E. Turnrose, Christopher A. Harvel
Astronomy Department
Computer Sciences Corporation

Ralph C. Bohlin
NASA Goddard Space Flight Center

ABSTRACT

The data base of Pt-Ne emission lines used to calibrate the IUE high dispersion wavelength scales has been scrutinized to improve the internal consistency of the adopted laboratory wavelength values and provide a homogeneous, documented line list, which IUE Guest Observers may use to evaluate quantitatively those Pt-Ne spectra taken to calibrate their data. After deletion of incorrect or inappropriate data in the old data base (lines with incorrect wavelength assignments; lines which are too faint, too bright, or blended; lines which fall near reseau marks, etc.) and the addition of several new entries, a total of 172 Pt-Ne lines for the SWP camera and 164 Pt-Ne lines for the LWR camera are now used for routine wavelength calibration in the high dispersion mode. The internal one sigma scatter of the assigned wavelengths corresponds to 0.32 pixels along the dispersion direction for SWP (2.5 km s^{-1} velocity uncertainty) and 0.26 pixels along the dispersion direction for LWR (1.9 km s^{-1} velocity uncertainty). Thermal effects, which can introduce large systematic image shifts, are excluded from these uncertainties but are independently correctable, in principle.

In addition, new software has been written to calculate the wavelength corrections needed to reduce the extracted IUE high dispersion wavelengths to a heliocentric coordinate system. Two subroutines separately calculate the instantaneous velocity components due to the satellite motion about the earth (accurate to $\pm$ 0.25 km s^{-1}) and the earth's orbital motion about the sun (accurate to $\pm$ 0.01 km s^{-1}). The velocity corrections in the line of sight to the target will become part of the standard data reduction procedures under the new software system to be implemented this year.

INTERNAL ACCURACY

IUE wavelength scales are determined by Pt-Ne spectra from onboard hollow cathode lamps. A data base (or line library) of Pt-Ne emission lines and laboratory wavelengths for each spectrograph and dispersion mode is used in conjunction with measurements of the positions of the emission lines in the calibration images to define polynomial fits (ref. 1), which functionally relate pixel location to wavelength and

*Work performed Under Contract NAS-5-24350.

order number. These dispersion relations are subsequently used in the spectral extraction process to assign wavelengths, and so the accuracy of the line libraries is crucial to the accuracy of the IUE wavelength scales. Thermal effects, which can introduce large systematic image shifts, are another factor in the accuracy of the IUE wavelength scales. Such effects are in principle independently correctable and are discussed elsewhere in this volume (ref. 2).

Although the IUE wavelength scales in high dispersion suffer no known serious deficiencies, an analysis of the high dispersion line libraries for the LWR and SWP cameras was undertaken for several reasons. First, it was observed that many lines were chronically rejected from the solutions for the dispersion formulae; this was suggestive of erroneous or inappropriate data in the line libraries. Second, spot checks showed the data in the libraries to be inhomogeneous and largely undocumented. This, too, suggested that inappropriate data might be included in the line libraries. The removal of inappropriate data is important because of the danger that noise in the images could otherwise occasionally be erroneously identified as a non-existent line. Third, it was felt that the organization of the line libraries into a homogeneous, consistent, and documented line list would be of value to IUE users by allowing them quantitatively to evaluate those Pt-Ne spectra taken to evaluate the wavelength accuracy of their data. The details of the line library analysis to be discussed here have been presented in the NASA IUE Newsletter (ref. 3). In the remainder of this section, we briefly summarize the steps and the conclusions of the analysis.

All entries in the original high dispersion line libraries (219 lines in LWR, 243 lines in SWP) were checked against available published references to verify the laboratory wavelength assignments and document the ionic origin. Where necessary, library entries were modified to agree with the published references according to a hierarchical ordering of preferred references. Lines for which no published reference could be found were deleted from the libraries.

All of the "chronically rejected" lines (i.e., lines rejected more than 50% of the time in a sample of more than 20 separate solutions in each of the SWP and LWR cameras) were examined on photowrite prints including some early annotated large scale prints prepared by T. R. Gull of GSFC and on plots of spectra extracted from the calibration images. There were 65 such lines in SWP, and 57 such lines in LWR. Most could be understood as being inappropriate because they were too bright, too faint, blended, near reseau marks, off of the tube face, or having apparently incorrect wavelengths in the published references. In all such cases, the lines were deleted from the libraries. Only a small number of the frequently rejected lines (4 lines in SWP, 7 lines in LWR) could not be reasonably explained and were left in the libraries.

The current analysis did not make a systematic attempt to add new lines to the edited libraries. In several instances, however, new entries were made and their accuracy verified by testing on several different Pt-Ne images. In all, 5 new lines were added to the library for each camera.

Table I summarizes the evolution of the SWP and LWR high dispersion line libraries. In the row marked "No. of Chronically Rejected Lines," the numbers in parentheses indicate the number of lines always rejected. Further details on the lines deleted from the original libraries, as well as a complete and documented listing of the new libraries, may be found in ref. 3. The new line libraries defined in accordance with the changes summarized in Table I have been in use since 18 April 1980. Prior to implementation in production processing, they were tested to insure their validity and to determine whether any improvement in the overall scale or internal accuracy of high dispersion wavelength calibrations results from their use. No change in the scale or zero points of the dispersion relations obtained with the new libraries was observed to an accuracy of one tenth of a pixel. This is not a surprising result since the majority of the lines deleted in arriving at the new libraries were generally rejected from the solutions using the old libraries.

The new libraries do, however, yield solutions with somewhat higher internal accuracy as judged by the standard deviations of the emission line positions calculated from the fitted dispersion formulae, compared to the exact emission line positions found by a two dimensional cross-correlation search technique. These standard deviations are measured separately in the line direction, $\sigma(L)$, and the sample direction, $\sigma(S)$. Table II summarizes the behavior of wavelength solutions obtained using the old and new libraries for several different Pt-Ne images in each camera. Note that the dispersion relations using the new libraries consistently employ a large fraction of the total number of available lines in the final solutions. This implies that the major sources of systematic error in the library entries have probably been eliminated, lending further credence to the consistency of the final libraries. The typical one sigma scatter in a given direction of 0.32 pixels for SWP and 0.26 pixels for LWR corresponds to a one sigma velocity uncertainty of 2.5 km s^{-1} in SWP and 1.9 km s^{-1} in LWR. These values are largely due to the inherent inaccuracies in the IUE geometric correction and line-finding algorithms and should be close to the errors expected in an arbitrary spectrum of an astronomical source obtained in the small aperture. Any additional errors should be caused only by thermal shifts in the cameras and spectrographs, which are being analyzed for a future discussion in the NASA IUE Newsletter.

CORRECTION TO HELIOCENTRIC WAVELENGTHS

The resolving power ($R = \lambda/FWHM$) of the IUE spectrographs varies from 1.0×10^4 to 1.5×10^4 over the entire wavelength range covered (ref. 1). Therefore the IUE velocity resolution varies from 20 km s^{-1} to 30 km s^{-1}. If it is assumed that the centroid of a line can be determined to approximately 10% of its FWHM, then a measured radial velocity should be accurate to about 2 km s^{-1} (best case). The orbital velocity of the Earth about the Sun (~30 km s^{-1}) and the velocity of the spacecraft about the Earth (~4 km s^{-1} at perigee) are both larger than the best possible velocity determinations and their effect should be removed from the data.

Two subprograms have been written for IUESIPS , the International Ultraviolet Explorer Spectral Image Processing System, to calculate orbital velocities. One of these determines the velocity vector of the Earth at a given time using the orbital elements of the Earth and the time derivatives of these elements as given in ref. 4. The other program determines the velocity vector of the spacecraft about the Earth at a given time using all the orbital elements of the spacecraft for Nov. 22, 1979 except for the period, which is set to exactly one sidereal day. Since the orbit of the spacecraft is periodically adjusted to maintain a sidereal period and, moreover, an approximately fixed ground path, it is not necessary to update the orbital elements used by the program. This program is accurate to ± 0.25 km s^{-1} over the entire life of the spacecraft (launch to present). Both of these subprograms will be added to IUESIPS in the near future and a detailed description of them, including a FORTRAN listing, will be published in the NASA IUE Newsletter.

REFERENCES

1. Boggess, A., et al.: In-Flight Performance of the IUE. Nature, vol. 275, Oct. 1978, p. 377.

2. Thompson, R. W., Turnrose, B. E., and Bohlin, R. C.: Effects of Temperature Fluctuations on IUE Data Quality. The Universe in Ultraviolet Wavelengths: The First Two Years of IUE. NASA CP-2171, 1980: this compilation.

3. Turnrose, B. E., and Bohlin, R. C.: IUE Data Reduction XVI. High Dispersion Line Libraries. NASA IUE Newsletter, 1980.

4. American Ephemeris and Nautical Almanac.

TABLE I. - CHARACTERISTICS OF NEW AND OLD LINE LIBRARIES

	SWP	LWR
No. Lines in Old Library	243	219
No. Chronically Rejected Lines	65 (29)	57 (15)
No. Lines Deleted	76	60
No. Lines Added	5	5
No. Lines in New Library	172	164

TABLE II. - CHARACTERISTICS OF SOLUTIONS USING NEW AND OLD LINE LIBRARIES

Image No.	New Line Library			Old Line Library		
	σ(L) px.	σ(S) px.	Fraction of lines used	σ(L) px.	σ(S) px.	Fraction of lines used
SWP5419	.35	.31	.93	.40	.36	.72
SWP6349	.34	.29	.93	.38	.37	.74
SWP6699	.34	.30	.90	.40	.36	.74
SWP8266	.36	.29	.91	---	---	---
MEAN	.35	.30		.39	.36	
LWR4656	.26	.28	.95	.26	.28	.76
LWR5483	.27	.30	.93	.27	.34	.75
LWR5725	.26	.27	.93	.26	.30	.73
LWR7205	.26	.24	.93	---	---	---
MEAN	.26	.27		.26	.31	

ANALYSIS OF IUE SPECTRA USING THE INTERACTIVE DATA LANGUAGE

Charles L. Joseph
Laboratory for Atmospheric and Space Physics
University of Colorado at Boulder

INTRODUCTION

In recent years, the use of interactive computer languages have made a major impact on data handling. Today, programs written in interactive languages are widely used for analyzing spectra, for finding graphical solutions, and for color imaging. The ability to create complex programs to be executed in an interactive mode, rather than relying on individual single-line commands, has been the main cause of the increased effectiveness of these languages.

One language in particular, the Interactive Data Language (IDL), has been extensively used to analyze high-resolution spectra from the IUE. IDL is the third generation of interactive languages developed at the University of Colorado. Like other interactive languages, IDL is designed for use by the scientist rather than the professional programmer, allowing him to conceive of his data as simple entities and to operate on this data with minimal difficulty. A comprehensive treatment of the capabilities of the Interactive Data Language is beyond the scope of this paper. Instead, we shall confine our attention to a package of programs created to analyze interstellar absorption lines as an example of the graphical power of IDL.

AN APPLICATION OF IDL

The package of interactive programs, created to analyze the IUE high-resolution data on the interstellar medium, can be divided into three basic parts: identifying interstellar absorption lines, measuring their equivalent widths, and fitting the observed data to a theoretical curve-of-growth. This package has reduced the analysis time by at least an order of magnitude over traditional methods. While these programs lend speed and consistency to the analysis, all judgements are made by the operator thus preserving his responsibility in the reduction process. The power of this package of programs stems from the unique marriage between the scientist and the computer provided by the Interactive Data Language.

The first step in the reduction process is to identify absorption lines. Here, the operator easily selects a feature of interest by setting a graphical cross-hair (to be called cursors) on it and then striking a keyboard character. The cursors, which are internal to the computer terminal, are moved by rotating a thumbwheel potentiometer[1] and their location is read whenever a keyboard character is struck. The computer identifies the species producing the absorption line by comparing the observed wavelength with laboratory wavelengths in a finding table stored permanently in the computer. Once the operator is satisfied with the computer's selection, he can proceed to take the equivalent width of the line.

[1] Many terminals use a different type of control to move the cursors.

Using only a single button command, the second step is initiated with the region of the spectra containing the absorption line being automatically expanded. The operator using the cursors selects two points through which he thinks the continuum passes. Once the continuum is established, the computer calculates the equivalent width and automatically stores this information along with the wavelength, the species identification, and the oscillator strength, all taken from the finding list in the computer. The first two steps are repeated until all absorption lines to be analyzed are exhausted.

The ease and speed in using this package of programs is demonstrated in the transition to the last stage. The data which was automatically stored in the previous stage is also automatically retrieved in the final stage so that users need not use precious time instructing the computer to create or to read data files.

The final step is to compare the observed data with a theoretical curve-of-growth selected from a library of curves stored in the computer. This is a graphical technique in which the observed data points are shifted, as a group along the x-axis until the best fit to a theoretical curve is found. The operator accomplishes the shifting by again using cursors. He does this by locating one of the data points, recording its position, and indicating where that data point should be relocated. After several shifts the best fit is obtained and the column density determined.

Several other capabilities, such as an error analysis, have been incorporated into this package of programs for the purpose of completeness and versatility. The flexibility to edit previous work done on the system has been included as well. At each stage of the analysis, the operator is automatically supplied with formatted output so that he has a detailed record of the reduction process. Because of these and numerous other features, this package of programs successfully keeps the operator in total control of the reduction process while relieving him of most of the burden.

Single-button commands play an integral part in these programs because they help streamline the analysis and they help facilitate the ease in learning how to operate these programs. Input instructions to the computer are normally handled via five different single-button commands, but the programs can also be interrupted to enter extensive instructions. The programs are structured to guide a beginner through the analysis so that he does not have to rely on a clumsy manual. Having only five single-button commands makes this possible. Once the operator becomes sufficiently familiar with these programs, the extraneous printing is suppressed, which further increases the speed.

Finally, this package of programs has a block structure which was created to offer gross scale flexibility for current and future needs. These programs, for example, are designed for easy adaptation to accept spectra from future observing instruments with different wavelength coverages.

A FINAL COMMENT

As was stated earlier, the power of an interactive computer language rests in its ability to support complex programming. The previous section demonstrates an example where most of the instructions to the computer have been reduced to single button commands, where all necessary reference materials are stored permanently in the computer, and where all judgements are still reserved for the operator. This is the kind of programming that achieves the speed and consistency of automation while allowing the scientist to remain intimate with and in complete control of the reduction process. It is truly interactive.

PROBLEMS AND PROGRAMMING FOR ANALYSIS OF IUE HIGH RESOLUTION DATA FOR VARIABILITY

C. A. Grady
LASP, University of Colorado at Boulder

ASTRACT
Observations of variability in stellar winds provide an important probe of their dynamics. It is crucial however to know that any variability seen in a data set can be clearly attributed to the star and not to instrumental or data processing effects. In the course of analysis of IUE high resolution data of α Cam and other O, B and Wolf-Rayet stars several effects were found which cause spurious variability or spurious spectral features in our data. Programming has been developed to partially compensate for these effects using the Interactive Data Language (IDL) on the LASP PDP 11/34 at the University of Colorado. Use of an interactive language such as IDL is particularly suited to analysis of variability data as it permits use of efficient programs coupled with the judgement of the scientist at each stage of processing.

INTRODUCTION

In order to extract the scientifically interesting information from a data set, it is necessary to be certain that any features in the data represent the object under study, and not the instrument studying the object, or the way in which the data has been reduced. This is applicable both to single observations of an object, or to a series of observations whose purpose is to search for temporal variability. During analysis of IUE high-resolution spectra of several O, B, and Wolf-Rayet stars a number of effects were found which cause either spurious variability or spurious spectral features in the data. This can considerably complicate analysis and interpretation of spectra. Not all of these effects can be easily seen in a cursory examination of the data provided by VILSPA and GSFC.

SIGNATURES OF PROBLEMS

The problems we have uncovered at the University of Colorado (C.U.) are more important in the hot stars surveyed than the ITF problem, or other problems addressed to date. Some can be identified quite quickly. These include improper zero levels in the centers of saturated absorption features, such as interstellar lines or strong P Cygni profiles. (This is more of a complication for analysis than a real stumbling block, since the true zero level is inferred directly.) A more serious problem is poor matching between adjacent orders (see Fig. 1), which rules out immediate interpretation and analysis of extended spectral features such as P Cygni profiles.

More subtle effects may not be as obvious. These include distortions of line profiles, which in extreme cases can cause a saturated line to appear unsaturated, for example. In other cases spectral features clearly present in the gross spectrum may be masked in the net spectrum. Spurious absorption features may also be introduced into the spectrum (see Fig. 2). Clearly,

the absence of real spectral features, and the presence of spurious features can lead to significant misinterpretation of the data.

It is important to note that these problems are not peculiar to either VILSPA- or GSFC- processed data. They also can occur in data that has been processed with the new ITF as well as old ITF data. Data from some observing runs has up to 97% of the images affected. The problems are typically worst at the short wavelength end of the images, where the orders of the echellogram are most closely crowded together, but may affect the entire image. In many cases 50% of an image is rendered useless, which is an unfortunate waste of valuable observing time. These effects are not constant from exposure to exposure and can therefore introduce considerable spurious variability which can totally swamp any real variations present in a set of observations (see Fig. 3).

A PROBABLE CAUSE

Images having normal photowrites and gross spectra but showing these data problems have been found at C.U. to have background records which contain ghost spectral features and which are an appreciable fraction of the amplitude of the gross spectrum (up to 95%). This indicates that the gross and background scan lines have been misplaced perpendicular to the dispersion direction, with the background scan apparently obtained at a position very close to or within the stellar spectrum.

It is necessary to consider what physically might cause this misplacement. The IUE Image Processing Information Manual (Version 1.0) (1) notes that thermal effects in the spectrograph optical train can cause shifts of up to three pixels perpendicular to the dispersion direction in the geometrically and photometrically corrected image. The calibration exposures used in the automatic registration procedure are taken every two weeks normally, whereas thermal shifts are known to occur on time scales of a few hours.

Thus, if data are processed using the automatic registration procedure, the image may be incorrectly scanned for the gross spectrum and background. The gross appears to be less noticeably affected than the interorder scans, probably because use of a larger slit makes placement of the scan line less critical. Also, as the orders crowd together at short wavelengths in the echelle format, the problem becomes more severe. If the background scan line is to be placed on or very near to an order, a net spectrum results which bears very little resemblance to the true spectrum when the background scan is subtracted from the gross spectrum.

A PARTIAL SOLUTION

If any of these data problems appear in an image or set of images, it is essential to check the data in several ways. First, if the photowrite appears to be abnormal it is probably impossible to extract believable data from that image. If the photowrite seems normal, the problem may be related to improper extraction procedures and the gross spectrum and background record on the data tape should be examined order by order. If

the gross spectrum, when ripple-corrected, shows poor matching between adjacent orders, or other distortions, reprocessing at VILSPA or GSFC is recommended.

There are situations, however, in which data having some of the problems described here can be salvaged without a need for reprocessing. Programs have been developed for this purpose on the LASP PDP 11/34 at C.U. using Interactive Data Language (IDL). Use of an interactive language such as IDL is particularly suited to reprocessing work or variability analysis as it permits use of efficient programs coupled with the judgement of the scientist at each stage of processing.

Our basic technique, following a suggestion by Heap (private communication) has been to repeatedly smooth the background tracing provided by VILSPA or GSFC with a running boxcar average until no spectral features remain. This is then subtracted from the gross spectrum, and the resulting spectrum is ripple corrected. This approach only works if the background is not too badly behaved and if it is not comparable to the gross in amplitude. Using these programs, we have been able to identify variability in several OB stars with confidence that the variability is stellar (2).

SUMMARY

The types of data-processing errors uncovered at C.U. in IUE high-resolution data indicate that IUE data should be thoroughly examined before analysis is attempted on any spectrum. Use of an interactive language such as IDL and programming similar to that developed at C.U. can make this a routine and relatively painless process. By taking such precautions much greater confidence can be placed in the results of any analysis and interpretation of IUE data whether from single images or as part of a search for temporal variability.

REFERENCES

1. International Ultraviolet Explorer Image Processing Information Manual. Version 1.0, Jan. 1980.

2. Grady, C.A. and Snow, T.P. Jr.: IUE Observations of Variability in Winds from Hot Stars. The Universe in Ultraviolet Wavelengths: The First Two Years of IUE. NASA CP-2171, 1980: this compilation.

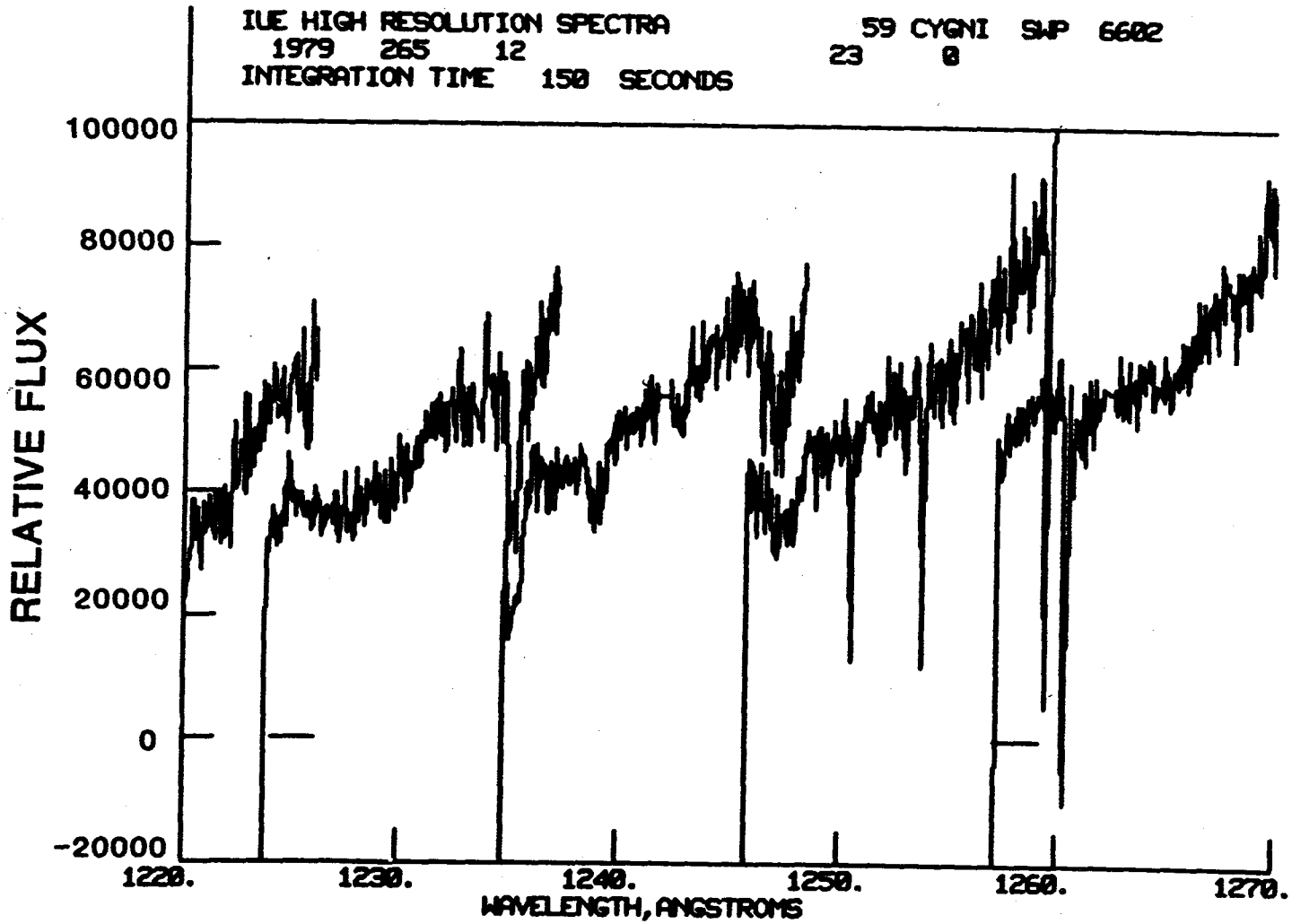

1. NV λ1240 P Cygni profile region in 59 Cygni showing poor matching between orders. This image was processed with the new ITF.

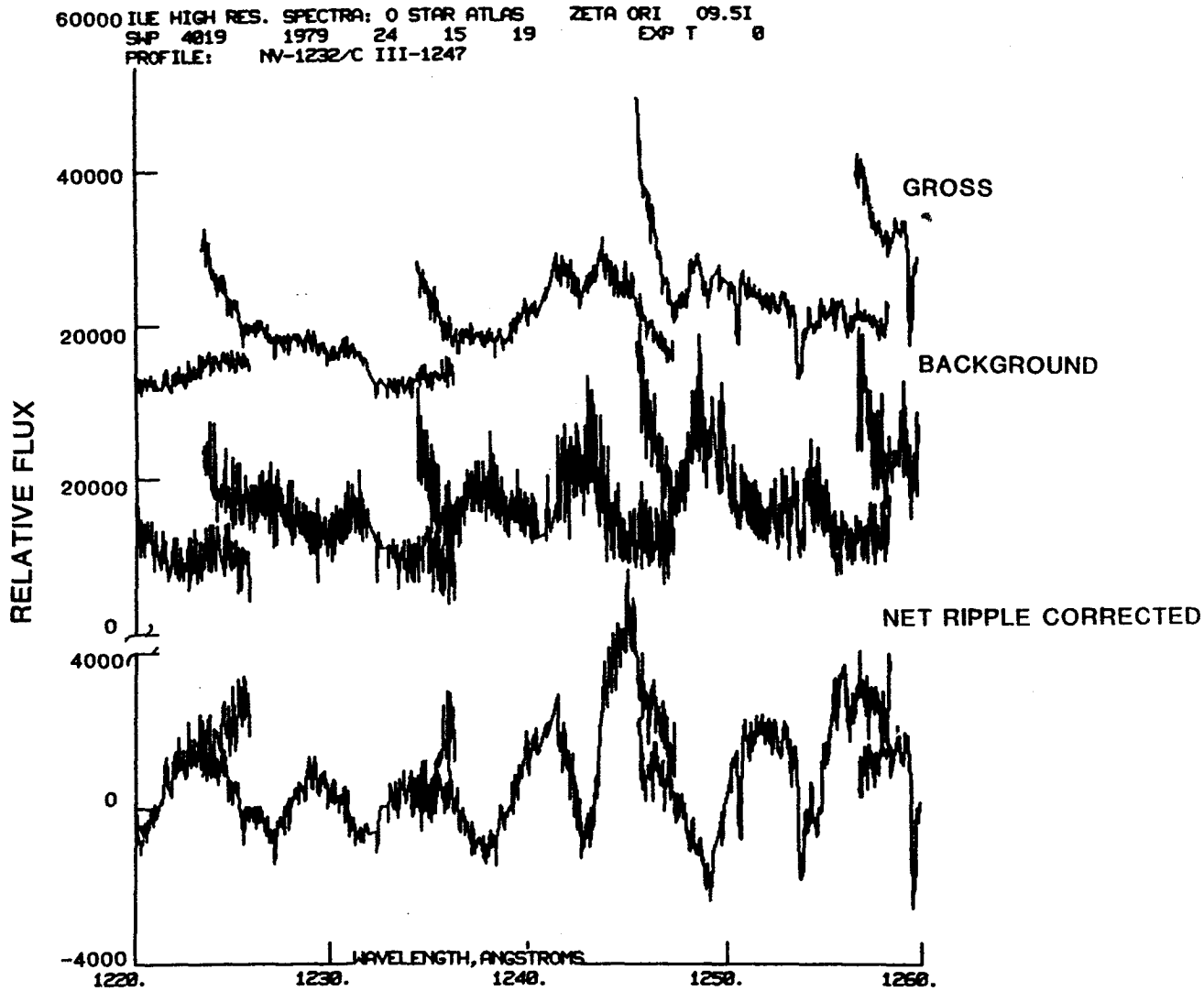

2. NV λ1240 region in ζ Ori. All tracings have been ripple corrected for ease in viewing. Top tracing: gross spectrum. Middle: background. Note that amplitude is about the same as for the gross. Bottom: net obtained by subtracting the background from the gross. Note spurious absorption features which have replaced the NV P Cygni profile.

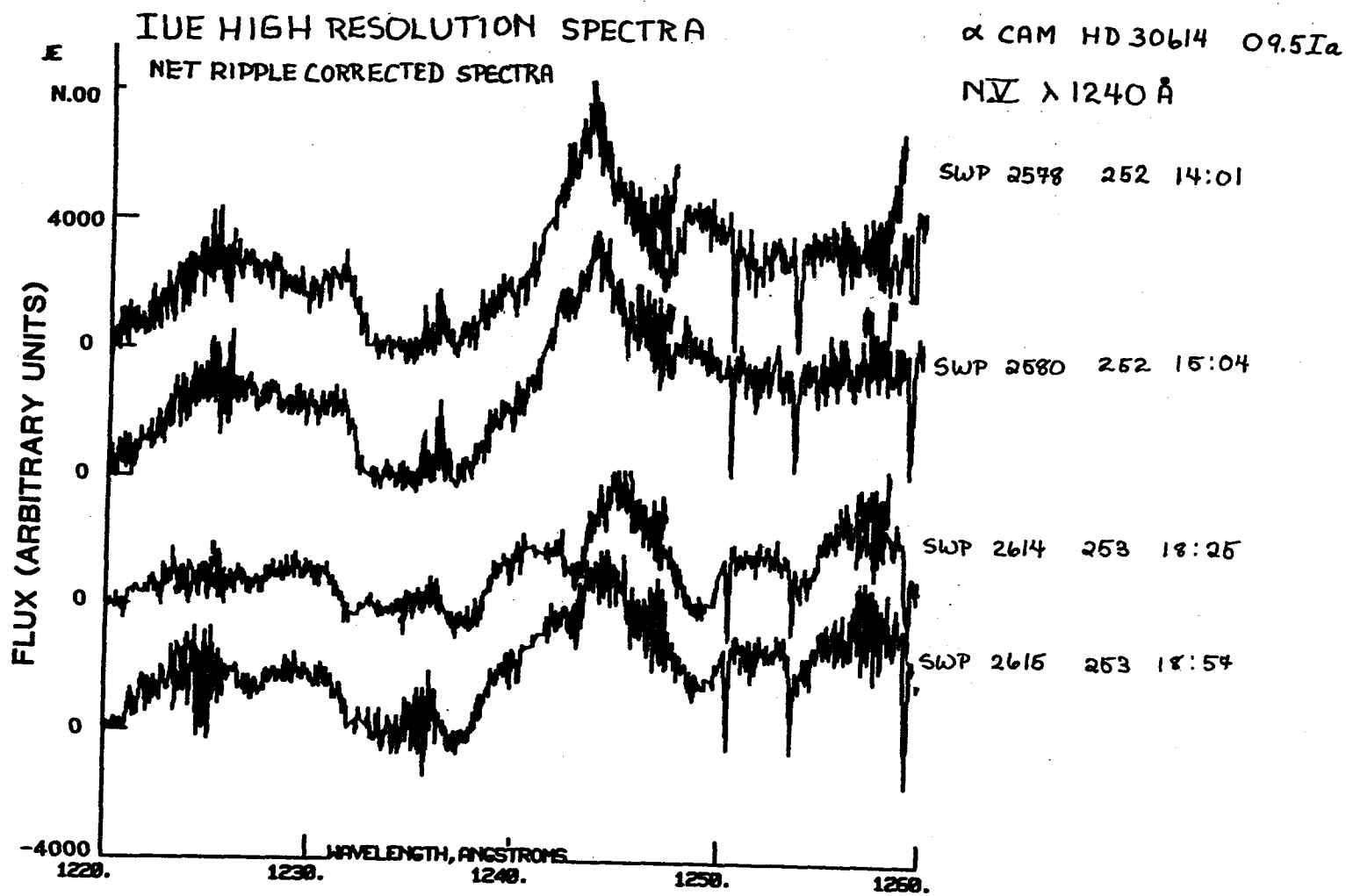

3. NV λ1240 in α Cam. These 4 tracings are the net ripple corrected spectra provided by VILSPA or GSFC. The gross spectra for these are essentially identical. Note the appearance and disappearance of CIII λ1247 absorption. Note also the considerable distortions in the P Cygni profile in SWP 2614, 2615. These changes are of the same order as <u>real</u> variations noted in OB stars, but in this case are completely spurious.

EFFECTS OF TEMPERATURE FLUCTUATIONS ON IUE DATA QUALITY*

Randall W. Thompson and Barry E. Turnrose
Computer Sciences Corporation
Astronomy Department

Ralph C. Bohlin
Laboratory for Astronomy and Solar Physics
Goddard Space Flight Center

ABSTRACT

Analysis of IUE calibration lamp images has shown that variation in the temperature of the scientific instrument causes shifts in the location of the spectral format with respect to the reseau grid on the detector and in the location of the reseaux themselves. In high dispersion, a camera head amplifier temperature difference of 6C corresponds to a shift of 4 pixels in the spectral format for LWR and 2 pixels for SWP along the dispersion direction. Shifts perpendicular to the dispersion (for the same temperature difference) are less than one pixel for both cameras. In low dispersion spectra, the shifts are similar but orthogonal to those described above with the larger motion lying in the direction perpendicular to the dispersion. In both dispersion modes, the observed shifts are apparently independent of wavelength. In high dispersion, the constant pixel shift mimics a constant velocity error.

Studies of reseau motion support earlier findings that decreases in temperature lead to an overall expansion of the grid of reseaux. For example in SWP, reseaux near the edge of the tube were found to move ~1.5 pixels with a temperature variation of 9 C.

Procedures are under development for utilizing these temperature correlations to correct the dispersion-relation and reseau-position files to the temperature of each target image and thereby achieve improved wavelength and photometric accuracy in reduced IUE spectra.

INTRODUCTION

Dispersion relations and reseau positions for IUE images have historically been determined and updated at approximately biweekly intervals from sets of standard calibration images consisting of Pt-Ne exposures superposed on tungsten-flood (TFLOOD) backgrounds. Since July 1978 reseau positions have been measured exclusively on the low dispersion Pt-Ne-plus-TFLOOD images to avoid the occasional contamination of reseaux caused by the presence of a high dispersion Pt-Ne spectrum. Approximately forty sets of reseau positions and dispersion constants have so far been accumulated in this manner for each camera and dispersion mode.

* Work performed under Contract NAS 5-24350

Although it has been known that the dispersion relations and reseau positions determined from the biweekly calibrations exhibit significant variation, and that this variation was suspected to be a direct consequence of thermal influences, there has heretofore been no detailed study quantitatively relating the observed variations in spectral position to measurable temperatures. The current work presents the first results of such an analysis: remarkable correlations of spectral position with camera head amplifier temperatures (THDA). It also presents results which confirm earlier studies suggesting that temperature changes induce a measurable expansion/contraction of the grid of reseau positions. In the sections to follow we discuss separately our studies of spectral format and reseau motion.

SPECTRAL FORMAT

The motion of IUE spectra with respect to the camera tube face has long been observed (ref. 1), and the standard IUESIPS (IUE Spectral Image Processing System) reduction procedures routinely incorporate a spectral registration step for each image which compensates for the component of spectral motion perpendicular to the dispersion direction. Because the component of spectral motion parallel to the dispersion direction cannot presently be removed without recourse to accurate spectral feature identification, there is no practicable means of correcting for this motion in a routine way on all spectra at the time of processing. In an attempt to better understand the nature of the spectral shifts in IUE images, and with the hope that such an understanding would lead to the means of correcting for the shifts, a study of the available calibration images acquired during the first two years of operation of IUE was undertaken. In this study, the fitted dispersion relations functionally relating pixel location to wavelength and order number (ref. 1) for the low and high dispersion modes in both the SWP and LWR cameras were used to trace the movement of particular wavelengths within the image line and sample grid from one calibration to the next. Initially displayed as line and sample coordinates vs time, these data illustrated that, for a given camera, changes in spectral location were the same in either dispersion mode. Further investigation showed that the spectral shifts appeared to correlate with several of the available temperatures monitored in the scientific instrument. In particular, the camera head amplifier temperature, THDA, was chosen as a convenient thermal parameter because its value at the time of image exposure and/or read is available directly from the Observatory Record sheets for many images, from printed listings of hourly camera snapshots (maintained by the IUE OCC) for many other images, and also from the science header on Guest Observer tapes for images acquired since 14 March 1979. Linear least squares regression analysis revealed remarkable correlations of the observed spectral motions with THDA. These correlations were remarkable not only because they revealed quantitative evidence for the thermal nature of the observed shifts, but also because THDA is a direct measurement of a camera temperature, and as such, is only an indirect measure of thermal conditions within the spectrographs themselves. The significant correlation of spectral motion with THDA indicates that THDA is in most instances a good measure of the thermal conditions giving rise to the spectral shifts, which presumably

originate within the spectrograph portion of the scientific instrument. (A notable exception to the correlation is discussed below). Since the reseau positions used to geometrically correct the Pt-Ne images in this analysis were measured directly on the low dispersion Pt-Ne-plus-TFLOOD images, and since no high dispersion Pt-Ne images were considered if they were obtained more than 3 hours earlier or later than the accompanying low dispersion image, none of the spectral shifts discussed here should be attributable to reseau motion.

The observed spectral shifts were transformed for each camera and dispersion mode into orthogonal components parallel and perpendicular to the dispersion direction. Such a coordinate system is convenient in particular because it reveals the magnitudes of the observed shifts along the direction for which compensation is currently not made. Figures 1-4 display the relative shifts parallel to the dispersion, plotted against THDA, for the four possible camera/dispersion mode combinations. A positive shift is a shift in the direction of increasing wavelength, and all shifts are shown relative to the mean of the displayed points. The straight lines in Figures 1-4 are the linear correlations of the shift and temperature calculated by least squares regression.

In Figures 1 and 2, the relative shifts and fitted straight lines for three distinct wavelengths are shown. Although there is a perceptible difference in the slope of the three fitted relations in each of these figures, it appears that the differences can be explained by the scatter of the data. We conclude that the thermal spectral shifts are constant pixel shifts within the accuracy of measurement $\sim \pm 0.3$px. Such a situation mimics a constant velocity shift in the extracted spectra of high dispersion images and is the likely cause of the velocity-like wavelength errors recently reported by Leckrone (ref. 2). In Figures 1 and 2 the fitted linear relation to the plotted data for the first wavelength listed is given in equation form at the lower right; in Figures 3 and 4 the equation pertains to the data plotted. In all four figures the error bars shown correspond to the least square fitting errors in pixels and to the quantization of the recorded temperature values.

Not shown here are the correlations of shifts perpendicular to the dispersion with THDA. As a point of interest, whereas the shifts parallel to the dispersion are greater than those perpendicular to the dispersion in high dispersion, the reverse is true in low dispersion because of the orthogonality of the low and high dispersion orders. Data on these shifts will be included in the complete documentation of this work being prepared for distribution in the NASA IUE NEWSLETTER.

It should be noted that the point in Figure 2 marked by an "X" was not included in the correlation computation. This datum was obtained with the spacecraft pointed close to the anti-sun direction, and in a configuration in which the spectrographs became hotter than the cameras. Such a condition apparently represents a limitation to the degree to which THDA can be used to predict spectral shifts. Although correlations with other available temperatures are being investigated, it is likely that extreme thermal configurations will always be difficult to model.

RESEAU MOTION

Independent of the motion of the spectral format on IUE images, the measured positions of reseau marks are known to change from one calibration image to the next due to a slight thermal sensitivity of the camera readout electronics. A separate study of the behavior of reseau positions as a function of temperature has been initiated in light of the successful correlation of spectral shifts with temperature described in the previous section. As with spectral shifts, a better understanding of the nature of the observed behavior might allow for corrections that could improve the quality of the reduced IUE data. In the case of reseaux, an improved geometric correction resulting from improved reseau positions would yield an improved photometric correction as well as improved spectral placement.

In analyzing the available body of data on reseau positions, it was deemed advantageous to utilize the available archives of UVFLOOD flat-field exposures rather than the standard set of low dispersion Pt-Ne-plus-TFLOOD exposures. This is because subtle complications in determining reseau positions can arise from the presence of the low dispersion Pt-Ne spectra on the TFLOOD flat fields, and such complications could mask the relatively subtle thermal effects under study. As a result, for the present study new measurements of reseaux on some 16 LWR and 20 SWP 60% UVFLOOD images acquired over the first two years of IUE operation were analyzed. The new measurements employed a cross-correlation template better matched to the large fiducial reseau, the addition of three more reseau positions in each camera near the tube edges, and the suppression of the standard smoothing of found reseau positions, which uses a polynomial curve fitting technique. Further details of all the above considerations are being prepared for the NASA IUE NEWSLETTER.

Figures 5 and 6 summarize the results of the temperature-dependence studies of reseaux so far conducted on in-flight images. These figures represent three separate sets of reseau measurements, each corresponding to a different THDA value. The diamond symbols indicate the positions of a low-temperature reseau set. From these positions, the displacements (magnified according to the scale indicated on the figures) are drawn to the location of all corresponding reseaux from two higher-temperature images. The actual THDA values are given in the figure captions.

Notice that reseau positions near the tube edge for SWP shift as much as ~ 1.5 pixels with a change in head amplifier temperature of 9 C. Both LWR and SWP exhibit a general eccentric contraction of the overall reseau grid with increasing temperature, in agreement with previous studies (ref. 3). Reseau studies are continuing in order to refine the initial results presented here.

DISCUSSION

Motivating both the spectral format and reseau motion studies is the desire to improve the quality of reduced IUE spectra. It is our intent to further codify

the temperature dependence of reseau behavior and then ultimately develop in IUESIPS the capability of utilizing mean dispersion constants and reseau positions which can be temperature-corrected on the basis of THDA values or read directly and decoded from the spacecraft snapshots of the image science headers. It is anticipated that significant improvements in photometric and wavelength accuracy over that currently achievable with biweekly calibrations and mean low resolution dispersion constants (ref. 4) could be realized with temperature-corrected calibrations. It should be noted in this regard, however, that ref. 3 states that the ultimate effectiveness of temperature-correction schemes for reseau positions depends on the magnitude of beam-pulling effects within the cameras (i.e., the influence of the distribution of illumination within the image on the placement of the camera read beam).

REFERENCES

1. Klinglesmith, D. A., Perry, P. M., and Turnrose, B. E.: The International Ultraviolet Explorer Spectral Image Processing System. Proceedings of the Society of Photo-Optical Instrumentation Engineers, vol. 172, 1979, p. 279.

2. Leckrone, D. L.: Systematic Errors in the SWP Wavelength Scale, NASA IUE NEWSLETTER (in press).

3. Oliver, M., Settle, J., Shuttleworth, T., and Sandford, M.: Report to the 3-Agency Committee on IUE Image Processing. IUE Technical Note No. 44, Appleton Laboratory, University College London, March 1979.

4. Turnrose, B. E., Bohlin, R. C., and Harvel, C. A.: IUE Data Reduction XI. Mean Dispersion Relations for Low Dispersion Spectra. NASA IUE NEWSLETTER No. 7, 1980.

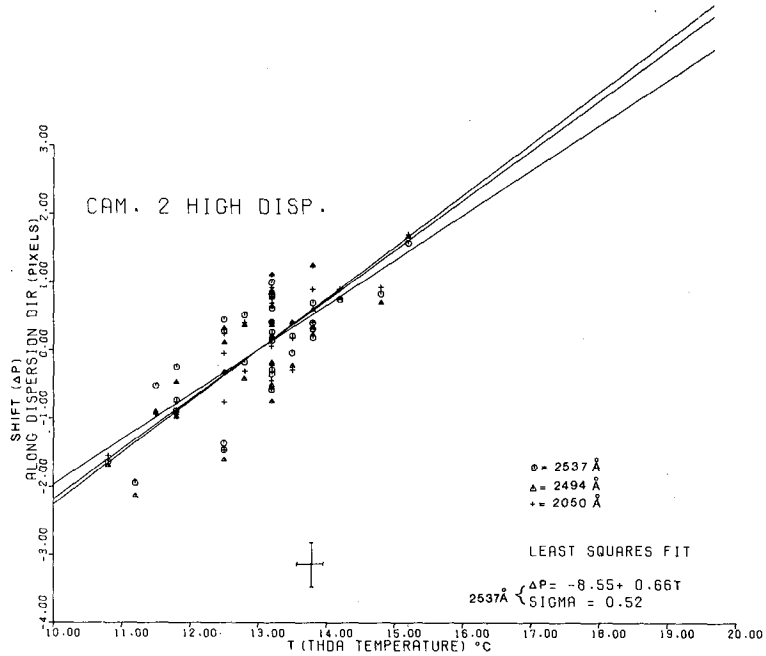

Figure 1 Camera 2 (LWR) high dispersion spectral format shifts along the dispersion relative to the mean as a function of camera head amplifier temperature. Data for 3 different wavelengths are plotted.

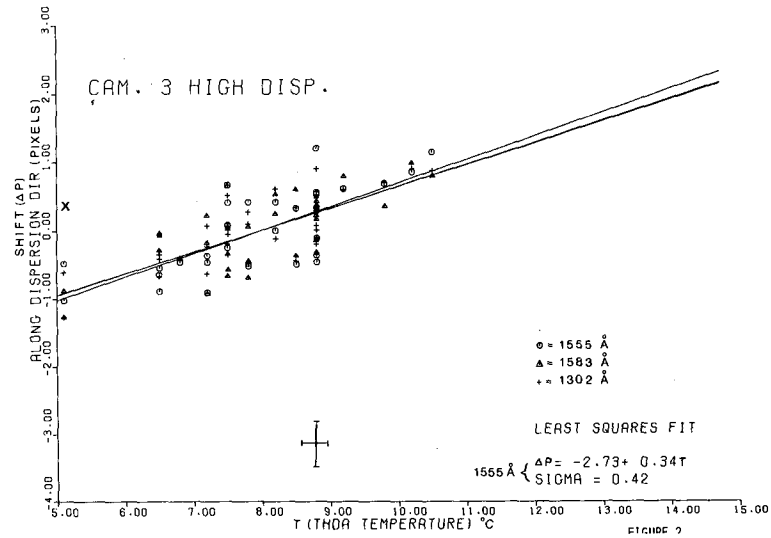

Figure 2 Camera 3 (SWP) high dispersion spectral format shifts along the dispersion relative to the mean as a function of head amplifier temperature. Data for 3 different wavelengths are plotted.

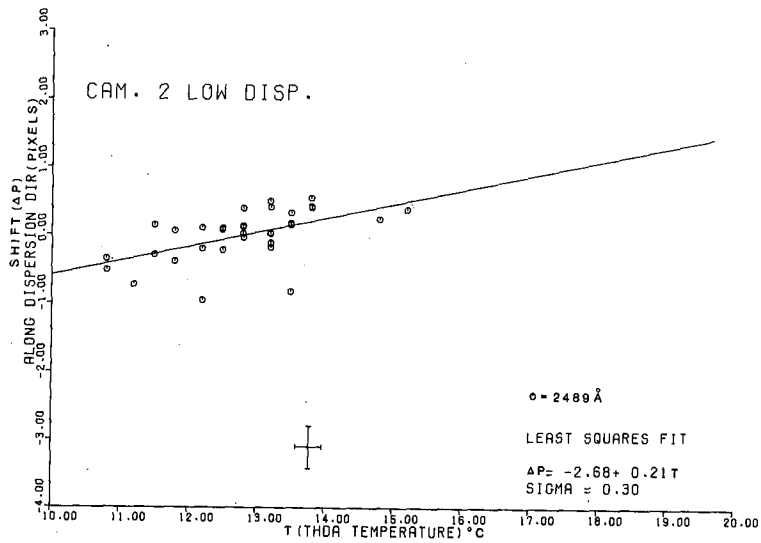

Figure 3 Camera 2 (LWR) low dispersion spectral format shifts along the dispersion relative to the mean as a function of head amplifier temperature.

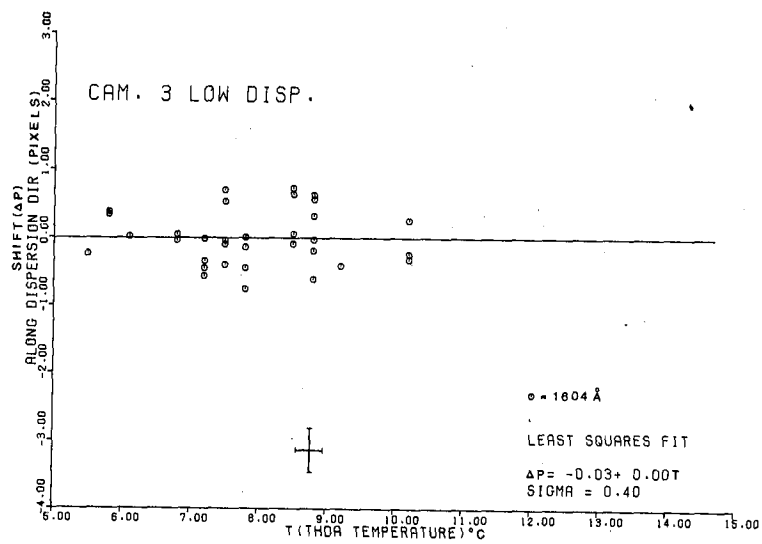

Figure 4 Camera 3 (SWP) low dispersion spectral format shifts along the dispersion relative to the mean as a function of head amplifier temperature.

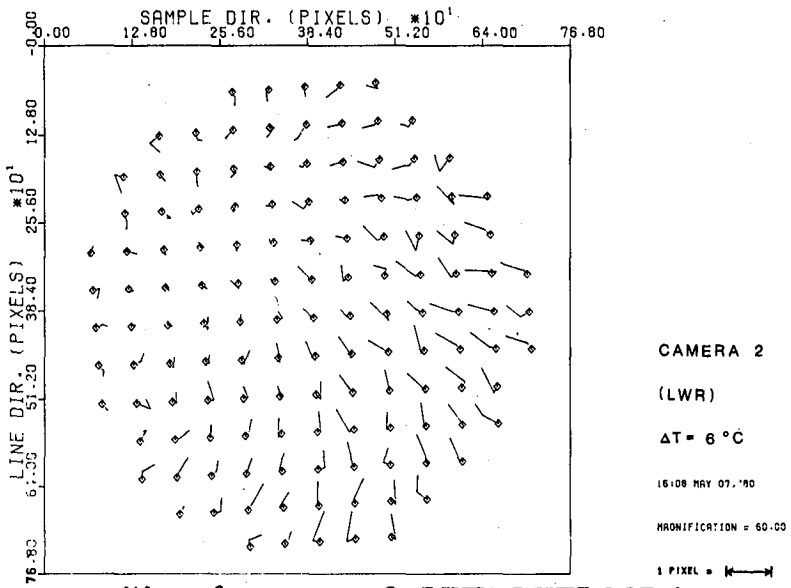

Figure 5 Reseau positions for camera 2 (LWR) UVFLOOD images at 3 different head amplifier temperatures. Diamond symbols are plotted at positions of reseaux for the lowest temperature (10.8 C). The lines are vectors representing the displacement of reseaux for the second and third temperatures (12.8 C and 16.9 C), relative to the first temperature and magnified by a factor of 60. The magnified displacement scale is shown graphically at the lower right.

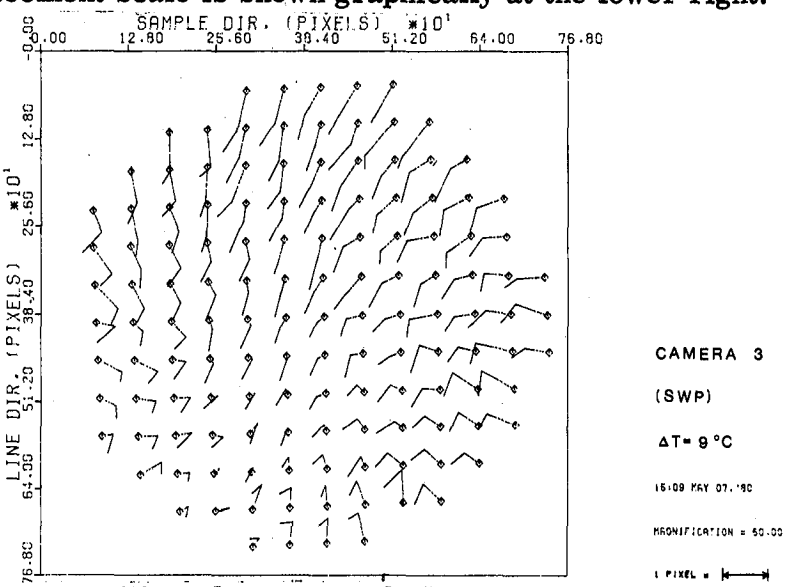

Figure 6 Reseau positions for camera 3 (SWP) UVFLOOD images at 3 different head amplifier temperatures. Diamond symbols are plotted at positions of reseaux for the lowest temperature (5.5 C). The lines are vectors representing the displacement of reseaux for the second and third temperatures (9.2 C and 14.2 C), relative to the first temperature and magnified by a factor of 60. The magnified displacement scale is shown graphically at the lower right.

Weaver: For large aperture exposures, will the artificial slit extraction be along the major axis of the aperture as opposed to being along the pixel diagonals as was formerly done or along the perpendicular to the dispersion line?

Will this change be reflected in the line-by-line spectra also? In other words, will "pseudo-pixels" of constant λ actually represent data of constant λ? (Previously they did not.)

Lindler: The low dispersion extraction will be along the direction of constant wavelength. For extended sources in the large aperture this will be in the direction along the major axis of the aperture. This will also be true for spatial line-by-line extractions. For trailed spectra, a separate scheme will again extract data points at the correct wavelength, but at the 90° trail angle instead of the actual slit angle applicable to extended nebulae objects. In high dispersion the extraction will be along diagonals.

Fischel: Do I understand that you use the space coordinate from the dispersion relation to determine where the pixel was in the ungeometrically corrected (low) image, and thus essentially use the nearest-neighbor approximation?

Lindler: The image position in a geometrically corrected image is computed using the dispersion velatrons.

Fischel: Then you really do the resampling? You just don't output the result separately?

Lindler: Yes.

Blades: You mention that your internal velocity accuracy is a few km s^{-1} now that you are using the new wavelength table. Have you made any external checks on the accuracy? For example, have you compared wavelengths of the same interstellar lines obtained from the IUE and Copernicus?

Turnrose: No, but I believe that other workers have looked at this and quote errors of $\pm$ 5 km s^{-1}

de Boer: In the Washburn Extraction Routine, the extracted intensities have equal spacing in wavelength because the gaussian fit done on all individual diagonals of the image gives the correct position of the spectrum.

Clarke: In the case of wavelength uncertainties, does the program give the user a choice of possible identifications for a given line?

Joseph: Yes. Also, it should be stressed that he must approve of the selection, even in cases where there is not any uncertainty, in order to proceed.

Lien: The main point is that if such a regional data center is set up, the programming should be set up such as to take into account the problems specific to the IUE, such as the non-linear wavelength scale, and summing or stacking data.

Holm: Does your system permit the user to reject the supplied programs and to develop his own programs to analyze the spectra?

Joseph: Yes. The system was designed with that purpose in mind.

Turnrose: In response to the question of A. V. Holm about performing spectral registration (perpendicular to dispersion) with the IUESIPS program DSPCON: Such registration is successful if the geometric correction is good; however, temperature changes result in differential motion across the image, thus making it impossible to exactly register all echelle orders simultaneously with the present techniques. Effects of this type may be responsible for some of the background-extraction problems which Ms. Grady has pointed out.

Fischel: We have noted the same effects here at GSFC, and have reached the same conclusions and used much the same techniques.

Leckrone: Have you had the opportunity to try out the new median filtering routine for background smoothing? If so, has this helped reduce the artifacts due to poor sampling of the background that you described?

Grady: We have yet to try this routine but will try it as soon as possible.

Fahey: Imagination is needed to create tests of true stellar variability as opposed to numerically induced effects. Some of the things I have done are: Correlate central depths with equivalent widths. Normalize varying equivalent widths to 0 to 1, measure deviations of the He I 3s-3p lines from their mean. Measure lines which appear on 2 orders (e.g., He I 2945A). Measure interstellar lines which had better not vary. Measure "nightly" variations (e.g., 7 SWP's on one shift).

Grady: We also have data taken on single shifts. The star in which we first identified the spacious variability was Cam which was observed nearly continuously for 3 days by T. P. Snow, Jr. and Henny Lamers from both VILSPA and GSFC. As a result we could see changes in the way the data was handled every 35 minutes.

Lien: Two questions: How much does the temperature change as a function of time? How does this affect the background extraction?

Thompson: 1) Depending on spacecraft orientation, temperature changes can be either rapid or relatively slow. Significant changes can occur on time scales of several hours; the range of THDA values for the calibration images used in this analysis is 5°C to 15°C (for SWP and 10°C to 17°C for LWR). Data on spacecraft temperature is routinely maintained by the IUE OCC, and excerpts from their tabulations will be included in the detailed writings to appear in the NASA IUE Newsletter. 2) If you

refer back to Figure 6 showing motion of SWP reseaux with temperature changes, you can see that the motion is differential across the tube face; i.e., up to 1.5 pixels at one portion of the tube and near zero at other portions. Note also that the largest component of the motion is roughly perpendicular to the SWP echelle orders in high dispersion. Consequently, an image at an arbitrary temperature will have orders which cannot necessarily be all registered with the dispersion relations used to extract the gross and background spectra. This can cause increased contamination of some background extractions. Furthermore, the differential reseau motion can cause small scale curves and kinks in the echelle orders, further affecting the spectral extraction.

Jenkins: Have you studied the dependence of the wavelength calibrations on the rate of change of temperature, in addition to just the actual temperatures?

Thompson: Unfortunately there is insufficient data to determine a relationship between wavelength calibration and the time derivative of camera temperature. However, we would expect that when temperatures are changing rapidly with time the camera temperature would no longer necessarily reflect conditions in the spectrograph and the correlation would break down. Also, if the temperatures varied significantly during the time of exposure the spectral features would probably be blurred to the extent indicated in figures 1-4.

Head amplifier temperatures were monitored 2 hours before and after each set of wavelength calibration exposures and in general the temperatures varied less than 1.5 C over the 4-hour interval. The largest variation observed was 6 C in 4 hours.

BIBLIOGRAPHIC DATA SHEET

1. Report No.	2. Government Accession No.	3. Recipient's Catalog No.
NASA CP-2171		

4. Title and Subtitle	5. Report Date
THE UNIVERSE AT ULTRAVIOLET WAVELENGTHS - THE FIRST TWO YEARS OF INTERNATIONAL ULTRAVIOLET EXPLORER	May 1981
	6. Performing Organization Code 680
7. Author(s) Robert D. Chapman, Editor	8. Performing Organization Report No.
9. Performing Organization Name and Address Goddard Space Flight Center Greenbelt, Maryland 20771	10. Work Unit No.
	11. Contract or Grant No.
	13. Type of Report and Period Covered Conference Publication
12. Sponsoring Agency Name and Address National Aeronautics and Space Administration Washington, D.C. 20546	14. Sponsoring Agency Code

15. Supplementary Notes

16. Abstract

This volume contains the papers presented at a symposium held at the Goddard Space Flight Center on May 7-9,1980, to celebrate the first two years of the International Ultraviolet Explorer (IUE). Almost one hundred papers document the contribution of IUE to all fields of astronomy: solar system studies, hot stars, cool stars, binary stars and highly evolved objects, nebulae and the interstellar medium, and extragalactic objects. The volume also contains papers on techniques for reduction of IUE data.

17. Key Words (Selected by Author(s))	18. Distribution Statement
International Ultraviolet Explorer, Ultraviolet Astronomy, Solar System, Stars, Binary Stars, Nebulae and Interstellar Medium, Galaxies	Unclassified- Unlimited Subject Category 90

19. Security Classif. (of this report)	20. Security Classif. (of this page)	21. No. of Pages	22. Price*
Unclassified	Unclassified	838	A99

*For sale by the National Technical Information Service, Springfield, Virginia 22161.

GSFC 25-44 (10/77)

*U.S. GOVERNMENT PRINTING OFFICE: 1981 735-006/8 1-3